



BIOLOGICAL INORGANIC CHEMISTRY

A New Introduction to Molecular
Structure and Function

2nd Edition



Robert R. Crichton

Biological Inorganic Chemistry

A New Introduction to Molecular Structure and Function

This page intentionally left blank

Biological Inorganic Chemistry

A New Introduction to Molecular
Structure and Function

Second Edition

Robert R. Crichton

ISCN,
Batiment Lavoisier,
Université Catholique de Louvain,
Louvain-la-Neuve,
Belgium



AMSTERDAM • BOSTON • HEIDELBERG • LONDON • NEW YORK • OXFORD • PARIS
SAN DIEGO • SAN FRANCISCO • SINGAPORE • SYDNEY • TOKYO

Elsevier

Radarweg 29, PO Box 211, 1000 AE Amsterdam, The Netherlands
The Boulevard, Langford Lane, Kidlington, Oxford OX5 1GB, UK

First edition 2008

Second edition 2012

Copyright © 2012 Elsevier B.V. All rights reserved

No part of this publication may be reproduced, stored in a retrieval system or transmitted in any form or by any means electronic, mechanical, photocopying, recording or otherwise without the prior written permission of the publisher

Permissions may be sought directly from Elsevier's Science & Technology Rights Department in Oxford, UK: phone (+44) (0) 1865 843830; fax (+44) (0) 1865 853333; email: permissions@elsevier.com. Alternatively you can submit your request online by visiting the Elsevier web site at <http://elsevier.com/locate/permissions>, and selecting *Obtaining permission to use Elsevier material*

Notice

No responsibility is assumed by the publisher for any injury and/or damage to persons or property as a matter of products liability, negligence or otherwise, or from any use or operation of any methods, products, instructions or ideas contained in the material herein. Because of rapid advances in the medical sciences, in particular, independent verification of diagnoses and drug dosages should be made

British Library Cataloguing in Publication Data

A catalogue record for this book is available from the British Library

Library of Congress Cataloging-in-Publication Data

A catalog record for this book is available from the Library of Congress

ISBN: 978-0-444-53782-9

For information on all Elsevier publications
visit our website at www.elsevierdirect.com

Printed and bound in China

12 13 11 10 9 8 7 6 5 4 3 2

Working together to grow
libraries in developing countries

www.elsevier.com | www.bookaid.org | www.sabre.org

ELSEVIER

BOOK AID
International

Sabre Foundation

Preface to the 2nd edition xi

- 1. An Overview of Metals and Selected Nonmetals in Biology 1**
 - Introduction 1
 - Why do We Need Anything Other Than C, H, N, and O (together with some P and S)? 2
 - What are the Essential Elements and the Essential Metal Ions? 3
 - An Idiosyncratic View of the Periodic Table 7
 - References 18
- 2. Basic Coordination Chemistry for Biologists 21**
 - Introduction 21
 - Types of Chemical Bonds 21
 - Ionic Bonding 21
 - Covalent Bonding 22
 - Hard and Soft Ligands 23
 - The Chelate Effect 24
 - Coordination Geometry 26
 - Redox Chemistry 28
 - Crystal Field Theory and Ligand Field Theory 29
 - References 34
- 3. Structural and Molecular Biology for Chemists 35**
 - Introduction 35
 - The Structural Building Blocks of Proteins 37
 - Primary, Secondary, Tertiary, and Quaternary Structure of Proteins 41
 - The Structural Building Blocks of Nucleic Acids 49
 - Secondary and Tertiary Structures of Nucleic Acids 50
 - Carbohydrates 53
 - Lipids and Biological Membranes 57
 - A Brief Overview of Molecular Biology 59
 - Replication 60
 - Transcription 62
 - Translation 62
 - Postscript 68
 - References 68
- 4. Biological Ligands for Metal Ions 69**
 - Introduction 69
 - Amino Acid Residues 69
 - Low-Molecular-Weight Inorganic Anions 72
 - Organic Cofactors 72

Insertion of Metal Ions into Metalloproteins	76
Chelatase – The Terminal Step in Tetrapyrrole Metallation	77
Iron–Sulfur Cluster Formation	79
More Complex Cofactors – MoCo, FeMoCo, P-clusters, H-clusters, and CuZ	80
Siderophores	86
References	89

5. An Overview of Intermediary Metabolism and Bioenergetics 91

Introduction	91
Redox Reactions in Metabolism	92
The Central Role of ATP in Metabolism	94
The Types of Reaction Catalysed by Enzymes of Intermediary Metabolism	96
An Overview of Catabolism	97
Selected Case Studies – Glycolysis and the Tricarboxylic Acid Cycle	100
An Overview of Anabolism	105
Selected Case Studies: Gluconeogenesis and Fatty Acid Biosynthesis	106
Bioenergetics – Generation of Phosphoryl Transfer Potential at the Expense of Proton Gradients	108
References	115

6. Methods to Study Metals in Biological Systems 117

Introduction	117
Magnetic Properties	119
Electron Paramagnetic Resonance (EPR) Spectroscopy	120
Mössbauer Spectroscopy	122
NMR Spectroscopy	124
Electronic and Vibrational Spectroscopies	125
Circular Dichroism and Magnetic Circular Dichroism	126
Resonance Raman Spectroscopy	126
Extended X-Ray Absorption Fine Structure (EXAFS)	127
X-Ray Diffraction	128
References	131

7. Metal Assimilation Pathways 133

Introduction	133
Inorganic Biogeochemistry	133
Metal Assimilation in Bacteria	137
Metal Assimilation in Fungi and Plants	144
Metal Assimilation in Mammals	151
References	153

8. Transport, Storage, and Homeostasis of Metal Ions 155

Introduction	155
Metal Storage and Homeostasis in Bacteria	155
Metal Transport, Storage, and Homeostasis in Plants and Fungi	161
Metal Transport, Storage, and Homeostasis in Mammals	170
References	175

9. Sodium and Potassium – Channels and Pumps 177

Introduction – Transport Across Membranes	177
Sodium <i>versus</i> Potassium	178
Potassium Channels	180

- Sodium Channels 184
- The Sodium–Potassium ATPase 184
- Active Transport Driven by Na^+ Gradients 187
- Sodium/Proton Exchangers 190
- Other Roles of Intracellular K^+ 191
- References 194

- 10. Magnesium–Phosphate Metabolism and Photoreceptors 197**
 - Introduction 197
 - Magnesium-Dependent Enzymes 198
 - Phosphoryl Group Transfer Kinases 199
 - Phosphoryl Group Transfer – Phosphatases 203
 - Stabilisation of Enolate Anions – The Enolase Superfamily 204
 - Enzymes of Nucleic Acid Metabolism 205
 - Magnesium and Photoreception 210
 - References 213

- 11. Calcium – Cellular Signalling 215**
 - Introduction – Comparison of Ca^{2+} and Mg^{2+} 215
 - The Discovery of a Role for Ca^{2+} Other than as a Structural Component 215
 - An Overview of Ca^{2+} Regulation and Signalling 216
 - Calcium Pumps 218
 - Intracellular Ca^{2+} Compartments 222
 - Ca^{2+} and Cell Signalling 225
 - References 228

- 12. Zinc – Lewis Acid and Gene Regulator 229**
 - Introduction 229
 - Mononuclear Zinc Enzymes 230
 - Carbonic Anhydrase 231
 - Metalloproteinases 232
 - Alcohol Dehydrogenases 237
 - Other Mononuclear Zinc Enzymes 237
 - Multinuclear and Cocatalytic Zinc Enzymes 238
 - Zinc Fingers DNA- and RNA-Binding Motifs 244
 - References 246

- 13. Iron: Essential for Almost All Life 247**
 - Introduction 247
 - Iron Chemistry 248
 - Iron and Oxygen 248
 - The Biological Importance of Iron 250
 - Biological Functions of Iron-Containing Proteins 250
 - Haemoproteins 251
 - Oxygen Transport 251
 - Activators of Molecular Oxygen 254
 - Electron Transport Proteins 259
 - Iron–Sulfur Proteins 262
 - Other Iron-Containing Proteins 267
 - Dinuclear Nonhaem Iron Enzymes 272
 - References 275

- 14. Copper – Coping with Dioxygen 279**
 - Introduction 279
 - Copper Chemistry and Biochemistry 279
 - Type 1 Blue Copper Proteins – Electron Transport 280
 - Copper-Containing Enzymes in Oxygen Activation and Reduction 282
 - Type 2 Copper Proteins 282
 - Mars and Venus – The Role of Copper in Iron Metabolism 295
 - References 296
- 15. Nickel and Cobalt: Evolutionary Relics 297**
 - Introduction 297
 - Nickel Enzymes 297
 - Methyl-coenzyme M Reductase 302
 - Cobalamine and Cobalt Proteins 303
 - B₁₂-dependent Isomerases 303
 - B₁₂-dependent Methyltransferases 306
 - Noncorrin Co-containing Enzymes 308
 - References 309
- 16. Manganese – Oxygen Generation and Detoxification 311**
 - Introduction: Mn Chemistry and Biochemistry 311
 - Photosynthetic Oxidation of Water – Oxygen Evolution 311
 - Mn²⁺ and Detoxification of Oxygen Free Radicals 314
 - Nonredox di-Mn Enzymes – Arginase 317
 - References 321
- 17. Molybdenum, Tungsten, Vanadium, and Chromium 323**
 - Introduction 323
 - Mo and W Chemistry and Biochemistry 323
 - Molybdenum Enzyme Families 324
 - The Xanthine Oxidase Family 325
 - The Sulfite Oxidases and DMSO Reductases 328
 - Tungsten Enzymes 329
 - Nitrogenases 331
 - Vanadium 337
 - Chromium 340
 - References 341
- 18. Non-metals in Biology 343**
 - Introduction 343
 - The Major Biogeochemical Cycles 343
 - Carbon, Hydrogen, Oxygen, and Phosphorus 344
 - The Nitrogen Cycle 348
 - Sulfur and Selenium 350
 - Chlorine and Iodine 353
 - References 358
- 19. Biomineralisation 359**
 - Introduction 359
 - Principles of Solid-State Biological Inorganic Chemistry 360
 - An Overview of the Major Classes of Biominerals 361

- Iron Deposition in Ferritin 361
- Formation of Magnetite in Magnetotactic Bacteria 368
- Calcium-Based Biominerals – Calcium Carbonates in Ascidians and Molluscs 370
- Silica-Based Biominerals 376

References 377

20. Metals in Brain 379

Introduction 379

The Brain and the Blood–Brain Barrier (BBB) 379

Sodium, Potassium, and Calcium Channels 384

Calcium and Signal Transduction 387

Zinc, Copper, and Iron 388

Copper 392

Iron 393

Concluding Remarks 394

References 394

21. Metals and Neurodegeneration 395

Introduction 395

Metal-based Neurodegeneration 395

Neurodegenerative Diseases Associated with Metals 401

Amyotrophic Lateral Sclerosis (ALS) 409

Creutzfeldt–Jakob and Other Prion Diseases 410

Disorders of Copper Metabolism – Wilson’s and Menkes Diseases and Aceruloplasminaemia 412

References 414

22. Metals in Medicine and Metals as Drugs 415

Introduction 415

Disorders of Metal Metabolism and Homeostasis 415

Metal-based Drugs 420

Cisplatin, an Anticancer Drug 421

Other Metals as Anti cancer Drugs 424

Metallotherapeutics with Lithium 425

Contrast Agents for Magnetic Resonance Imaging (MRI) 427

References 431

23. Metals in the Environment 433

Introduction Environmental Pollution and Heavy Metals 433

Aluminium 434

Cadmium 435

Mercury 439

Lead 440

Metals as Poisons 443

References 445

This page intentionally left blank

Preface to the 2nd Edition

The importance of metals in biology, the environment and medicine has become increasingly evident over the last twenty five years. The movement of the electrons in the electron transfer pathways of the photosynthetic organisms and in the respiratory chain of mitochondria, coupled to proton pumping to enable the synthesis of ATP, is carried out by iron- and copper-containing proteins (cytochromes, iron–sulphur proteins and plastocyanins). The water-splitting centre of green plants (photosystem II), which produces oxygen, is based on the sophisticated biological use of manganese chemistry. Metals like cadmium, manganese and lead in our environment represent a serious health hazard. Cadmium is present in substantial amounts in tobacco leaves, so that cigarette smokers on a packet a day can easily double their cadmium intake. Yet, while many metals are toxic, many key drugs are metal based – examples are Cis-platin and related anticancer drugs, and lithium carbonate, used in the treatment of bipolar disorder. Paramagnetic metal complexes are widely used as contrast agents for magnetic resonance imaging. Numerous trace metals are also required to ensure human health, and while metal deficiencies are well known (for example inadequate dietary iron causes anemia), it is evident that excessive levels of metals in the body can also be toxic.

It has been clear from the outset that the study of metals in biological systems can only be approached by a multidisciplinary approach, involving many branches of the physical and biological sciences. The study of the roles of metal ions in biological systems represents the exciting and rapidly growing interface between inorganic chemistry and the living world. It has been defined by chemists as bioinorganic chemistry, and by biochemists as inorganic biochemistry. From 1990–97 the European Science Foundation funded a programme on the Chemistry of Metals in Biological Systems.¹ This resulted, in the course of what turned out to be a monumentally important meeting held in the Tuscan town of San Miniato, in the launching of important initiatives around the international consensus name ‘Biological Inorganic Chemistry’. The outcome was the creation of the *Society of Biological Inorganic Chemistry (SBIC)* in 1995, with Dave Garner as its first President,² and the *Journal of Biological Inorganic Chemistry (JBIC)* in 1996 with Ivano Bertini as its first Editor. These then joined the already existing **ICBICs** (International Congress of Biological Inorganic Chemistry) and **EUROBICs** (European Congress of Biological Inorganic Chemistry), to form a series of acronyms, which all now use the stylized French word for a ballpoint pen ‘**bic**’ to designate the term biological inorganic chemistry. While I use the definition Biological Inorganic Chemistry in this book, I would like to indicate to the prospective reader that this text will deal to a much greater extent with the biochemical aspects of metals in living systems rather than with their inorganic chemistry.

The success of the first edition of ‘*Biological Inorganic Chemistry*’ stimulated both myself and Elsevier to produce a 2nd expanded edition, which I trust will serve a useful role for both students and teachers of this ever dynamic field. I have tried where possible to include up to the minute illustrations of the fundamental messages

1. The Steering Committee of this Programme, which I joined in 1992, was made up of Helmut Sigel (Basle, Switzerland) as chair, Ivano Bertini (Florence, Italy), who organized the San Miniato meeting; Sture Forsen (Lund, Sweden), Dave Garner (Manchester, UK), Carlos Gomez-Moreno (Zaragoza, Spain), Paco Gonzales-Vilchez (Seville, Spain), Imre Sovago (Debrecen, Hungary), Alfred Trautwein, Lübeck, Germany), Jens Ulstrup (Lyngby, Denmark), Cees Veeger (Wageningen, Holland), Raymond Weiss (Strasbourg, France), and Antonio Xavier (Oeiras, Portugal).

2. He was succeeded by Elizabeth C. Theil (1998–2000), Alfred X. Trautwein (2000–2002), Harry B. Gray (2002–2004), Fraser Armstrong (2004–2006), Bob Scott (2006–2008), Trevor Hambley (2008–2010), José Moura (2010–2012).

that I have tried to articulate as clearly and with as much enthusiasm as in the first edition. The organisation of the book has been structured around three parts — Basic Principles, Metals in Biology and Metals in Medicine and the Environment. Not only is the text updated and more intensively resourced, but I have included new Chapters on Non-metals in Biology, Metals in Brain Function, Metals and Neurodegeneration, Metals in Medicine and Metals as Drugs and Metals in the Environment, while a number of other Chapters have been significantly expanded.

I would like to thank again my long-term collaborator Professor Roberta Ward for her help with Chapters 20 and 21 and to FrédéricALLEMAND for drawing most of the Figures, as well as Adrian Shell and Louisa Hutchins at Elsevier, Oxford for their understanding and patience. I thank PerkinElmer Informatics (previously CambridgeSoft Inc.) for providing a copy of ChemOffice with ChemDraw, which I used to represent the structures and reactions shown in this book. I also thank all my colleagues who have encouraged me by their supportive comments on their utilisation of the First Edition, remain responsible for any errors or mistakes, and hope that this text which I enjoyed writing will give as much pleasure to its reader, and hopefully encourage some of them to embark on the exciting adventure which the study of metals in biological systems represents.

Louvain-la-Neuve, 20th November, 2011
Robert R. Crichton FRSC

An Overview of Metals and Selected Nonmetals in Biology

Introduction	1
Why do We Need Anything Other Than C, H, N, and O (together with some P and S)?	2
What are the Essential Elements and the Essential Metal Ions?	3
An Idiosyncratic View of the Periodic Table	7

INTRODUCTION

The extraordinarily important role of metals in biology, the environment, and medicine has become increasingly evident over the last twenty to thirty years. Iron- and copper-containing proteins (cytochromes, iron-sulfur proteins, and plastocyanins) are key players in electron transfer, both in the electron-transfer pathways of photosynthetic organisms and in the respiratory chain of mitochondria. Coupling electron transfer with proton pumping across membranes to establish proton gradients is a universal way of generating the currency of cellular free energy, ATP: this constitutes the process which we call oxidative phosphorylation. Photosystem II, which produces oxygen, protons, and electrons from water, which our renewable energy enthusiasts would dearly love to mimic, utilises sophisticated manganese chemistry. Metals like cadmium, manganese, and lead in our environment represent a serious toxic hazard. Even relatively unheard-of elements like polonium can seize the front pages of our national newspapers when their alpha radiation is used to poison a Soviet dissident in London. While many metals are toxic, some metals are used as drugs — cisplatin and related metal-based drugs are used to treat cancer, while lithium, in the form of lithium carbonate, is used in the treatment of manic depression. Modern medicine has increasingly developed noninvasive techniques, both for diagnosis and for therapy. Magnetic resonance imaging depends heavily on the use of paramagnetic metal complexes as contrast agents. A number of metals such as isotopes of cobalt, gallium, and technetium are used as radiopharmaceuticals to deliver sterilizing radiation to targets within the body. A small number of trace elements, like selenium, and the halogens, chlorine and iodine, are also required to ensure human health. While metal deficiencies are well known (for example, inadequate dietary iron causes anemia), it is evident that excessive levels, even of essential metals, can also be toxic — as we will see, this is the case for iron in excess.

It has been clear from the outset that the study of metals in biological systems can only be approached by a multidisciplinary approach, involving many branches of the physical and biological sciences. The study of the roles of metal ions in biological systems represents the exciting and rapidly growing interface between inorganic chemistry and the living world. It has been defined by chemists as bioinorganic chemistry, and by biochemists as inorganic biochemistry. As explained in the Preface, I prefer to use the definition ‘biological inorganic chemistry’ in this book, but would like to indicate to the prospective reader that this text will deal to a much greater extent with the biochemical aspects of metals and other inorganic elements in living systems rather than with their inorganic chemistry.

WHY DO WE NEED ANYTHING OTHER THAN C, H, N, AND O (TOGETHER WITH SOME P AND S)?

The word ‘*organic*’ itself can have a large number of meanings. The chemical definition is ‘applied to a class of compound substances which naturally exist as constituents of organised bodies (animals or plants), or are formed from compounds which so exist, such as *organic acids*, *bases*, *molecules*, *radicals*: they all contain or are derived from hydrocarbons’. Hence, organic chemistry is the chemistry of hydrocarbons and their derivatives, or more generally, ‘any chemical compound containing carbon’. However, in this latter definition, some simple compounds of carbon, like carbon dioxide, are sometimes classified as inorganic compounds. Of course, we quickly perceive that carbon alone does not suffice for life — we would not be able to do much with just the three elemental forms of carbon, graphite, diamond, and fullerenes¹ (the latter is illustrated below in Fig. 1.1 by the

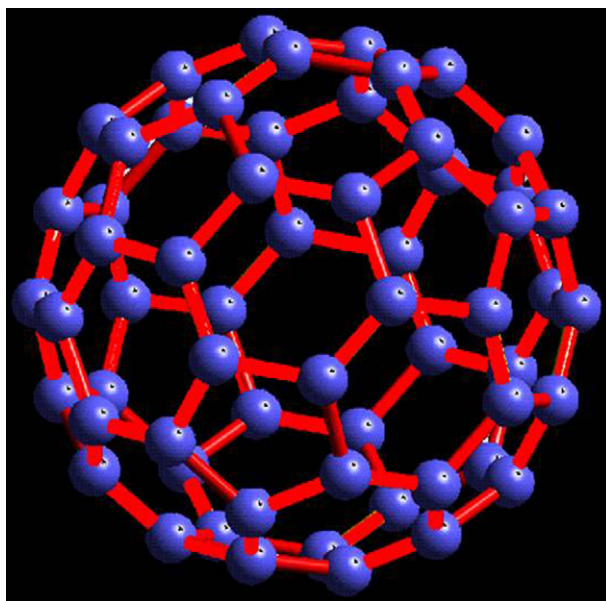


FIGURE 1.1 Buckminsterfullerene a 60 carbon ‘bucky ball’, made entirely and exclusively of carbon.

structure of **Buckminsterfullerene**, a spherical molecule with the formula C_{60} , so named in honor of the geodesic domes of Richard Buckminster Fuller, which they resemble). We also need hydrogen, oxygen, nitrogen, a non-negligible dose of phosphorus, as well as some sulfur.

It follows that, with the inclusion of oxygen, nitrogen, phosphorus, and sulfur, we escape from the relatively restricted sphere of hydrocarbons made up solely of carbon and hydrogen, and enter a brave new world of organic molecules — acids, aldehydes, ketones, alcohols, amines, sugars, amino acids, and lipids. From these organic building blocks, we can construct proteins, polysaccharides, fats, nucleic acids, even phospholipid bilayers (which together with proteins, constitute the structural leitmotif of biomembranes).

Yet, a living cell does not just require these organic building blocks, together with the biopolymers, and the biomembranes. The enormous negative charges that are generated along the polyphosphate backbone of nucleic acids need to be balanced with appropriate positively charged counter-ions. In order to generate ATP, our universal energy currency, we need to separate proton transport from electron transfer, and use the energy of proton

1. Fullerenes are molecules composed entirely of carbon, in the form of ellipsoids, spheres or tubes. Spherical fullerenes are called ‘bucky balls’.

gradients to drive ATP synthesis. While we can transfer electrons using organic molecules like flavins, redox metal ions like iron and copper are much better adapted to this. We need to find ways of amplifying signals, arriving at the cell membrane at nanomolar concentrations, but which result in millimolar intracellular responses. As we move from unicellular organisms to more complex multicellular organisms, we need to generate transmembrane electrical potentials so that we can transmit messages in the form of electrical signals, sometimes over quite long distances. For almost all of these purposes, large, cumbersome and bulky proteins are clearly not the answer. But, perhaps above all else, we must enable the proteins which we call enzymes to catalyse reactions, many of which would quite simply be impossible if we relied solely on organic molecules.

So, if these six elements alone do not enable life as we know it to exist, in its multiple and varied forms — what other elements do we require? Traditionally, whereas *organic chemistry* concerns compounds of biological origin, *inorganic chemistry* concerns the properties and behaviour of inorganic compounds, considered to be of mineral origin — inorganic chemistry in French was previously called ‘*chimie minérale*’ (mineral chemistry²). In more recent times, the boundaries between inorganic and organic have become more blurred — many inorganic compounds contain organic ligands, while, as mentioned earlier, some carbon-containing compounds are traditionally considered inorganic, and many organic compounds contain metals. As we will see in the next section, in the course of evolution, Nature has selected constituents not only from the organic world, but also from the inorganic world to construct living organisms. Many of these are metals, elements to the left of the periodic table, which readily lose their valence electrons to form cations.

There is an interesting historical illustration of this requirement for metals in catalysis. The celebrated German chemist Richard Willstätter (Chemistry Nobel Prize, 1915) proposed that enzymes were not proteins — in his view, the protein was only a carrier for the veritable catalytic centre (he called the protein “*nur ein träger Substanz*”). In 1929, James Sumner accidentally left a preparation of urease from jack bean (the enzyme which catalyses the decomposition of urea to ammonia and carbon dioxide) on a laboratory table overnight. The night was cold, and to his surprise, the following morning, he found that the protein had crystallised. Together with John Northrop, who crystallised pepsin and trypsin, the conclusive proof of the protein nature of enzymes was thereby established (they both received the Chemistry Nobel Prize in 1946). Although their discovery appeared to have disproved Willstätter’s theory, he was vindicated some 50 years later by the demonstration that urease is in fact a nickel-dependent enzyme, and that when the Ni is removed, urease loses its catalytic activity. Of course, with the benefit of hindsight, we can see that both viewpoints were correct. The protein is indeed a carrier for the Ni, but a carrier which provides the right coordination sphere³ to bind the Ni in the right conformation, as well as creating the right environment for the molecular recognition of the substrates, urea and water, and their binding in the right orientation to enable the di-metallic nickel site to carry out its catalysis (see Chapter 15 for more details).

WHAT ARE THE ESSENTIAL ELEMENTS AND THE ESSENTIAL METAL IONS?

Just six elements — oxygen, carbon, hydrogen, nitrogen, calcium, and phosphorus — make up almost 98.5% of the elemental composition of the human body by weight. Just 11 elements account for 99.9% of the human body (the additional five are potassium, sulfur, sodium, magnesium, and chlorine). However, as we will see shortly, we can identify between 22 and 30 elements which are required by some, if not all, living organisms. Many of these are metals: some of them, like sodium, potassium, calcium, and magnesium, are present in quite large concentrations, and are known as ‘bulk elements’. Indeed, these four cations constitute nearly 99% of the metal ion content of the human body. Others, like cobalt, copper, iron, manganese, molybdenum, and zinc, are known as ‘trace elements’, with dietary requirements that are much lower than the bulk elements; yet, they are no less indispensable for human life.

2. As illustrated by the avant-garde translation of the title of Steve Lippard and Jeremy Berg’s book ‘Principles of Bioinorganic Chemistry’ — ‘*Biochimie Minérale*’.

3. See the Glossary for explanations concerning specialised terms like this.

We now discuss just why these elements out of the entire periodic table have been selected. One thing is clear — they were not only selected as a function of their abundance and their availability in the universe as well as in the earth's crust, and the oceans (which constitute the major proportion of the earth's surface), but also on the basis of their suitability for the functions that they are called upon to play, in what is predominantly an aqueous environment.⁴

It therefore comes as no great surprise that within our solar system itself, all 11 of the principal elements found in man are in the top 20 in terms of abundance, with five of them figuring in the top ten — hydrogen, carbon, nitrogen, oxygen, and sulfur. When we consider the abundance of these 11 obviously essential elements in the earth's crust (Fig. 1.2), we find that no less than six of them (hydrogen, oxygen, and the four alkali and alkaline

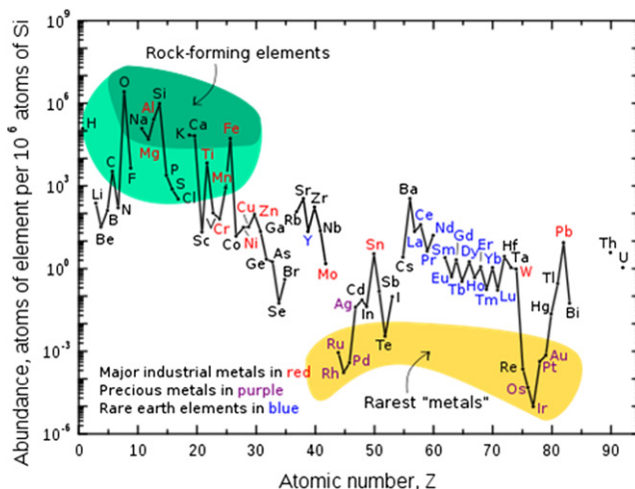


FIGURE 1.2 Abundance (atom fraction) of the chemical elements in Earth's upper continental crust as a function of atomic number.

earth metals cited above — sodium and potassium, magnesium, and calcium) are among the top ten (together with aluminium, silicon, titanium and, not surprisingly, iron, since the earth's core is predominantly constituted by iron, together with significant amounts of nickel). The remaining five are among the top 20.

But we have every reason to believe that life, as we know it, originated from the oceans, so we also need to consider the distribution of the eleven essential elements in this environment. This is, of course, influenced by the solubility of the corresponding element in salt water. So, it is no surprise that today we find very low concentrations of iron in the oceans (although, if the primitive atmosphere was, as we think, reducing, divalent ferrous iron would have been readily available in a soluble form). So, of our eleven key elements, how many are now found in the water of our oceans? Clearly, sodium and chlorine for starters, but hydrogen, oxygen, and carbon, together with magnesium, sulfur, calcium, potassium, and bromine, make the top 10. The only two which do not make it are nitrogen and phosphorus, and we know that they also exist in non-negligible amounts.

So, of the 11 principal elements that are found to be essential for human life, they are all omnipresent in the solar system, the earth's crust, and the oceans. Of course, they would have had to be '*bioavailable*' (a designation, which really means not just being in the right place at the right time, but being free to be assimilated by the biological system in question).

4. Another important distinction between organic chemistry and the chemistry of living organisms (biochemistry) is that the former is carried out almost entirely in nonaqueous media, whereas the latter occurs essentially in approximately 56 M H₂O.

However, as we mentioned earlier, there is a second, and absolutely indispensable criterion for selection — namely that the element must fulfil a *function* which is both an absolute requirement for life as it existed at that moment in time, and which cannot, or may not, be fulfilled by some other element. We can immediately see that the six elements involved in the earlier definition of organic chemistry are ideally placed to do their job, forming covalent bonds with tetravalent carbon. We will return to the case of chlorine later, but what of the four metal ions in the top eleven?

One interesting way to compare the suitability for function with the properties of a number of key selected metal ions is presented in Table 1.1. We list the strength of ligand binding (the affinity of the metal ion for any

TABLE 1.1 Correlations Between Ligand Binding, Mobility, and Function of some Biologically Relevant Metal Ions

Metal Ion	Binding	Mobility	Function
Na ⁺ , K ⁺	Weak	High	Charge carriers
Mg ²⁺ , Ca ²⁺	Moderate	Semi-mobile	Triggers, transfers structural
Zn ²⁺	Moderate/Strong	Intermediate	Lewis acid, transfers structural
Co, Cu, Fe, Mn, Mo*	Strong	Low	Redox catalysts Oxygen chemistry

*Charge not given, since this varies with oxidation state

atom, group, or molecule that is attached to the central metal ion), the mobility, and the functions of a number of important biologically relevant metal ions. What emerges immediately is that as the strength of binding of the metal ion to biological ligands decreases, the mobility of the metal ion increases, and it is therefore able to function much more effectively as a transporter of charge. Thus, Na⁺ and K⁺ (together with H⁺ and Cl[−]), which bind weakly to organic ligands, are ideally suited to generate ionic gradients across biological membranes, and to ensure the maintenance of osmotic balance. This is precisely what these two essential alkali metal ions do in biological systems, although, as we will see in Chapter 9, they also have other interesting additional roles. In contrast, Mg²⁺ and Ca²⁺, with intermediate binding strengths to organic ligands, can play important structural roles and, particularly in the case of Ca²⁺, serve as a charge carrier and a trigger for signal transmission within the cell. The various roles of these two alkaline earth cations are discussed respectively in Chapters 10 and 11.

The inclusion of the six transition metal ions — cobalt, copper, iron, manganese, molybdenum, and zinc — in Table 1.1 is no coincidence — we saw earlier that they are essential trace elements for man. So, together with the 11 bulk elements, we have now identified 17 of the ‘essential’ elements. Their relative positions in the Periodic Table are shown in Fig. 1.3, which presents the first six rows of the Periodic Table, colour-coded into families. Zn²⁺ has ligand-binding constants intermediate between those of Mg²⁺ and Ca²⁺ and those of the group of five other transition metals. Unlike them, zinc effectively does not have access to any other oxidation state than Zn²⁺ (the +1 state compounds are very unstable). Zn²⁺ not only plays a structural role, but can also fulfil a very important function as a Lewis acid (Chapter 12).

The other five transition metal ions, Co, Cu, Fe, Mn, and Mo, bind tightly to organic ligands and participate in innumerable redox reactions. Fe and Cu are constituents of a large number of proteins involved in electron-transfer chains. They also play an important role in oxygen-binding proteins involved in oxygen activation, as well as in oxygen transport and storage (Chapters 13 and 14). Co, together with another essential transition metal, Ni, was particularly important in the metabolism of small molecules like carbon monoxide, hydrogen, and methane, which were thought to be abundant in the reducing atmosphere of early evolution, and is still utilised by a number of microorganisms (Chapter 15). Although Co is an essential element for man, Ni proteins are virtually unheard of in

higher eukaryotes, with the obvious exception of the plant enzyme urease, which Sumner crystallised from jack bean. Mn plays an important role in the detoxification of oxygen free radicals, as well as in the water-splitting complex of oxygen-evolving photosynthetic organisms (Chapter 16). Mo, while relatively rare in the earth's crust, is the most abundant transition metal in seawater and is an important component of nitrogenase, the key enzyme of nitrogen-fixing organisms. However, on account of its facility to act as an interface between one- and two-electron redox systems, Mo has been widely incorporated into many redox enzymes. Microorganisms which do not require Mo use tungsten, W, Mo's homologue in the third row of the periodic table (Chapter 17).

After Mo, vanadium is the second most abundant transition metal in the ocean and is certainly beneficial and probably essential for man. It is used in the form of a V prosthetic group in V-dependent haloperoxidases, which utilise hydrogen peroxide to oxidise a halide ion into a reactive electrophilic intermediate. There has been extensive debate as to whether a final transition metal ion is an essential trace element, as was originally proposed over 50 years ago — it has been widely accepted as an essential element for over 30 years. We discuss Mo and W together with V and Cr in Chapter 17.

This leaves the halogen, chlorine, which, as the chloride anion, is abundant in nature and essential to many forms of life, including man. If we add V, Cr, Ni, and W to the list, we come to a total of 20.

The remaining candidates for the title of essential elements, in order of their position in the periodic table (Fig. 1.3), are boron, fluorine, silicon, arsenic, selenium, bromine, tin, and iodine.

The metalloid elements B, Si, and the nonmetal Se are essential elements for mammals, plants, and microorganisms. The chemistry and biology of B and Si, together with that of As, is dealt with later in this chapter, while that of Se is discussed together with S in Chapter 18. An interesting account of biochemical selenology can be found in Flohé, 2009.

Fluorine has been considered for many years as an essential element for man and is employed as an additive in toothpastes and often added to municipal water supplies to combat dental caries. Halogenated natural products are frequently reported metabolites in marine seaweeds. We know that many marine organisms and algae couple light-driven oxidative reactions with the halogenation of a large number of substrates. These reactions are catalysed by vanadium haloperoxidases (Chapter 17), most of which incorporate Br (some use Cl or I). We discuss F and Br later in this Chapter, as well as tin, which remains somewhat of an enigma. Even if it were to be shown to be essential for some species, we still do not have the slightest idea what the biological functions of Sn might be. The importance of iodine for man and other higher animals, as well as some invertebrates, is accounted for by its presence as an essential constituent of thyroid hormones, as we discuss further in Chapter 18, at the same time as chlorine.

AN IDIOSYNCRATIC VIEW OF THE PERIODIC TABLE

In Fig. 1.3, we presented a truncated version of the Periodic Table in which elements have been colour-coded into nine families — respectively the alkali metals (often known as the alkali earth metals), the alkaline earth metals, the transition metals, the other metals, the metalloids, the nonmetals, the halogens, the noble gases, and finally, with just lanthanum as its sole example, the rare earths. Now in Fig. 1.4, we present an idiosyncratic view of the Periodic Table, highlighting a few characteristic facets of a selected number of elements, and in what follows, we have tried to illustrate some of these. Those elements that have been dealt with above, or will be dealt with specifically in later chapters, and will not be discussed in any detail here. The presentation follows their order by group and by row in the periodic table. An equally idiosyncratic view of the Periodic Table can be found in the wonderful and memorable book by Primo Levi (Levi, 1985).

Element number 1, hydrogen H, although placed in group I, is clearly a nonmetal. It is the most abundant element in the universe, as well as being the lightest and the simplest (with just one proton and one electron), powering nuclear fusion to generate helium plus energy in the sun. H is also extremely important in biology. As we will see in later chapters, it can be incorporated into nonmetal covalent bonds with carbon, C—H and nitrogen, N—H. These bonds are kinetically very stable, even in the presence of dioxygen, and confer much of the enormous stability to organic molecules in biological systems. However, it can also participate in

Hydrogen H Essential												2 Helium He																					
Gradients of H ⁺ , across membranes are used for ATP synthesis												Lighter than air, good for filling balloons and making people's voices high pitched																					
3 Lithium Li	4 Beryllium Be Toxic											5 Boron B Essential	6 Carbon C Essential	7 Nitrogen N Essential	8 Oxygen O Essential	9 Fluorine F Essential	10 Neon Ne																
Treatment of manic depression with Li ₂ CO ₃	Aquamarine and emerald are precious forms of the mineral beryl, Be ₃ Al ₂ (SiO ₃) ₆											Cross-linking plant cell walls	Almost all molecules in living organisms	Essential component of proteins, nucleic acids, etc.	The oxygen paradox - essential for respiration, but toxic	Required for bone hardening and preventing dental caries	In a vacuum discharge tube, neon glows reddish orange																
11 Sodium Na Essential	12 Magnesium Mg Essential											13 Aluminium Al Toxic	14 Silicon Si Essential	15 Phosphorous P Essential	16 Sulphur S Essential	17 Chlorine Cl Essential	18 Argon Ar																
Sodium channels	Chlorophylls											Acid rain	Plants especially grasses and Diatoms	Cellular energy currency, ATP	Coenzyme A, Fe-S clusters	Chloride channels in cystic fibrosis	Heavier than air - good in glove boxes																
19 Potassium K Essential	20 Calcium Ca Essential	21 Scandium Sc	22 Titanium Ti	23 Vanadium V Essential	24 Chromium Cr Essential?	25 Manganese Mn Essential	26 Iron Fe Essential	27 Cobalt Co Essential	28 Nickel Ni Essential	29 Copper Cu Essential	30 Zinc Zn Essential	31 Gallium Ga	32 Germanium Ge	33 Arsenic As Essential ?Toxic	34 Selenium Se Essential	35 Bromine Br Essential ?	36																
Potassium channel	Intracellular signalling - calmodulin	Predicted to exist by Mendeleev. Discovered 1879 in Scandinavia	The space age element	Insulin-like effects, bromoperoxidases in seaweed	Promotes glucose tolerance by an, as yet, unknown mechanism	Oxygen evolving complex in Photosystem II	Haem in haemoglobin gives blood its red colour	Vitamin B12	Active site of hydrogenase	Cytochrome oxidases superoxide dismutases	Lewis acid, Zinc fingers in DNA-binding proteins	67 Ga (78% G emitter). Tumor imaging	Semi-conductors	Arsenite and arsenic trioxide (treatment of malignancies)	Glutathione peroxidase, key anti-oxidant enzyme	Stratospheric ozone-depleting refrigerants and extinguishing agents																	
37	38	39	40	41	42 Molybdenum Mo Essential	43 Ruthenium Ru	44	45	46 Palladium Pd	47 Silver	48 Cadmium Cd Toxic	49	50 Tin Sn Essential ?	51 Antimony Sb Toxic	52	53 Iodine I Essential	54																
					FeMoCo in nitrogenase	Anti-cancer Ru drugs			Pd-catalysts 2010 Chemistry Nobel Prize.	Antimicrobial agent	Ubiquitous toxic environmental pollutant		Alloyed with Cu in bronze and with Pb in pewter			Thyroid hormones, T3, T4																	
55	56	57-71	72	73	74 Tungsten W Essential	75 Osmium	76	77	78 Platinum Pt	79 Gold Au	80 Mercury Hg Toxic	81	82 Lead Pb Toxic	83	84 Polonium Po	85	86																
					Tungsten lamps	Densest element, EM stain			Cis-platin anticancer drug	Auranofin Therapy for rheumatoid arthritis	The Mad Hatter		Pawter wine cups -Decline and fall of the Roman Empire?		Death by alpha particle emission																		
																		57	58	59	60	61	62	63	64 Gadolinium Gd	65	66	67	68	69	70	71	
																									Gd-DTPA MRI contrast agent								

FIGURE 1.4 An idiosyncratic periodic table.

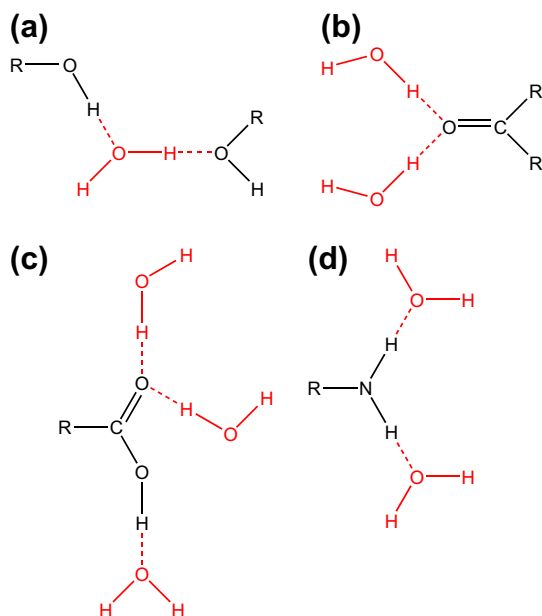


FIGURE 1.5 Hydrogen bonding between water and (a) hydroxyl groups, (b) keto groups (c) carboxyl groups and (d) amino groups.

noncovalent hydrogen bonds (Fig. 1.5), which, in the aqueous medium inhabited by living organisms, play a very important role in the structures, notably of proteins and nucleic acids (see Chapter 3). H can be transferred in an important number of biological redox reactions involving transfer of either one or two electron. It can participate in the generation of the proton gradients across biological membranes which are universally used for ATP synthesis.

The **alkali earth metals** form Group 1 of the periodic table, made up of lithium, sodium, potassium, rubidium, cesium, and francium (not shown in Fig. 1.3). Their name derives from the observation that their addition to water generates an alkaline solution. They are all low density, soft, and extremely reactive metals, which are rarely found in their metallic form. This group has properties which are closer and more alike than any other group of the periodic table. Since they desperately want to lose their solitary outer sphere electron, their reactions with almost any other species (including molecular oxygen) are violent and explosive.

On account of its lightness, Li is found, together with aluminium, in very strong, light alloys extensively used in the aerospace industry as well as in many top of the range alkali batteries. While Li is not required for life, it is used therapeutically for the treatment of bipolar disorder and schizophrenia, always taken orally at a total dose of up to 2 g/day in the form of lithium carbonate, which causes the least irritation to the stomach. Effective treatment requires attaining serum lithium concentrations of between 0.4 and 0.8 mM. The mechanisms of lithium action within the brain are not known in detail, but it is thought to attenuate two major signaling pathways in brain by competing with Mg^{2+} for binding sites on proteins (as we discuss in greater detail in Chapter 22).

Na^+ and K^+ are involved in ionic gradients and in osmotic regulation: cells maintain much higher intracellular concentrations of K^+ than Na^+ . Fig. 1.6 illustrates the selective binding sites for Na^+ , K^+ , Ca^{2+} , and Cl^- in transport proteins. The opening and closing of sodium and potassium ion channels create the electrochemical gradients across cell membranes which transmit nerve impulses and other information and regulate cellular function. The way in which biological systems manage to select the ions that are transported across membranes will be discussed in later chapters.

The three remaining alkali metals Rb, Cs, and Fr have no biological relevance, although, as we will see in Chapter 23, the radioactive isotope of Cs, Cs^{137} , was a major pollutant after the 1986 nuclear disaster at

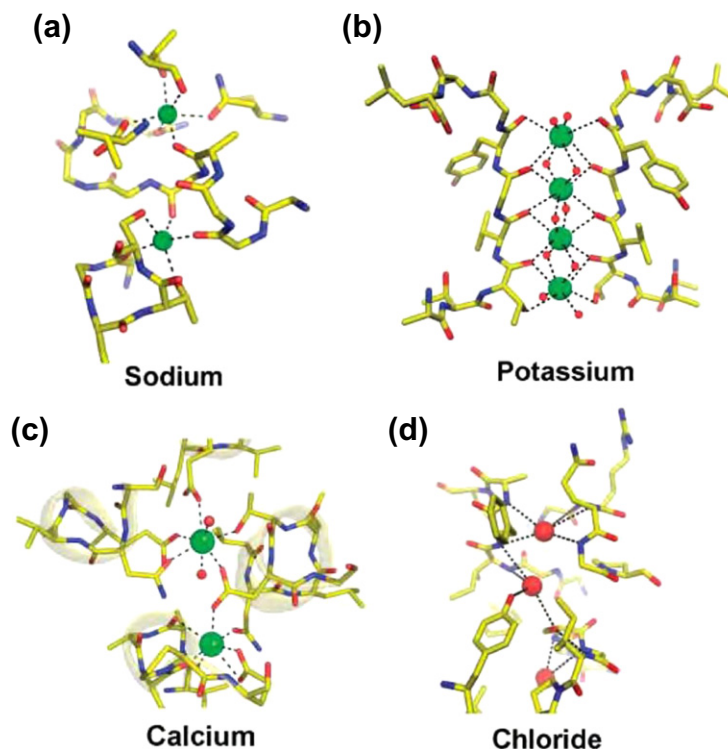


FIGURE 1.6 Selective binding sites in transport proteins for Na^+ , K^+ , Ca^{2+} , and Cl^- . (a) Two Na^+ binding sites in the LeuT Na^+ -dependent pump. (b) Four K^+ binding sites in the KcsA K^+ channel. (c) Two Ca^{2+} binding sites in the Ca^{2+} ATPase pump. (d) Two central Cl^- binding sites in a mutant CIC Cl^-/H^+ exchanger. (From Gouaux and MacKinnon, 2005.)

Chernobyl, and continues to represent an environmental hazard. Cs is also used in atomic clocks, accurate to one second every few hundred thousand years.

The alkaline earths, beryllium, magnesium, calcium, strontium, barium, and radium, together constitute Group 2 of the periodic table. They are usually found in relatively un-reactive forms, bound to oxygen: the free metals still have a tendency to lose their outer electrons, but less easily than the Group 1 elements, and are a little less reactive.

Be is extremely toxic in man, causing inflammation of the lungs and lung cancer. On account of its lightness, it is used in aircraft manufacture, and its silicate forms the beautiful green gemstones, emerald and aquamarine. Mg is essential, as is Ca. The role of Mg is intimately intertwined with phosphate, involved in many phosphoryl transfer reactions, as Mg-ATP in muscle contraction, in the stabilisation of nucleic acid structures, as well as in the catalytic activity of ribozymes (catalytic RNA molecules). It is also found as the metal centre in the light-absorbing pigments, chlorophylls, in photosynthetic organisms. Ca, a crucial second messenger signalling key changes in cellular metabolism, is also important in muscle activation, in the activation of many proteases, both intra- and extracellular, and as a major component of a range of bio-minerals, including bone (Chapter 19). Sr, Ba, and Ra have no biological importance. Sr gives the dramatic crimson colour to fireworks, and is used as an additive in the glass of TV sets and monitors. However, its radioisotope Sr^{90} can get absorbed into the bone in place of Ca. The insoluble sulfate of Ba is used for 'barium meals' in order to take X-ray pictures of the digestion of food by the stomach. Traces of Ra (and polonium) were isolated from pitchblende uranium ore by Pierre and Marie Curie in 1898 (one ton of pitchblende typically yields about one seventh of a gram of radium). Marie Curie received the Nobel Prize for chemistry on December 10, 1911, 'for services to the advancement of chemistry by the discovery of the elements radium and polonium'. She was the first woman to win the Nobel Prize, and the first person ever to

be awarded two. One of the four stated aims of the 2011 international year of chemistry is to celebrate the centenary of her prize.⁵ Fig. 1.7 shows her in the company of no less than seven other Nobel Prize winners at the First Solvay Conference on Physics held at the Hotel Metropole in Brussels in 1911.

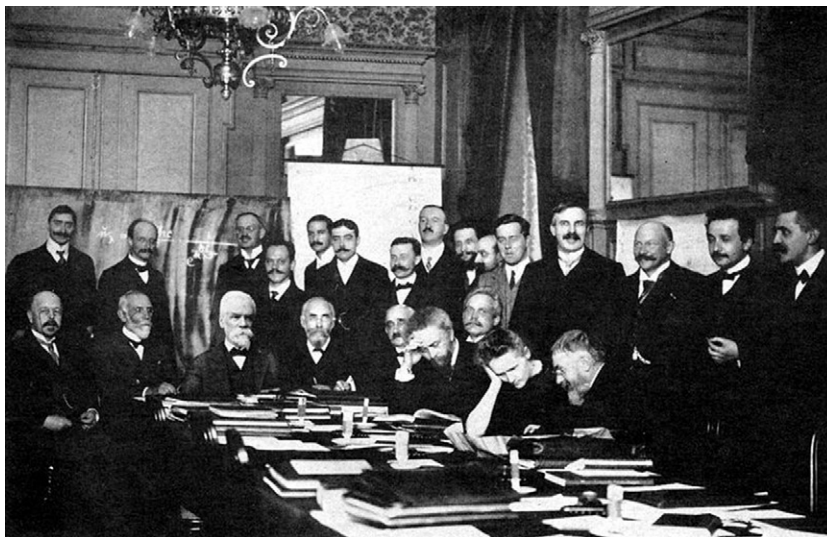


FIGURE 1.7 Photograph of participants at the 1911 Solvay Conference, Hotel Metropole, Brussels. Seated (L to R): Walther Nernst*, Marcel Brillouin, Ernest Solvay, Hendrik Lorenz*, Emil Warburg, Jean-Baptiste Perrin*, Wilhelm Stein, Marie Curie*, Henry Poincaré. Standing (L to R) Robert Goldschmidt, Max Planck*, Heinrich Rubens, Arnold Sommerfeld, Frederick Lindemann, Maurice de Broglie, Martin Knudsen, Friedrich Hasenöhl, Georges Hostelet, Eduard Herzen, James Hopwood Jeans, Ernest Rutherford*, Heike Kamerlingh Onnes*, Albert Einstein*, Paul Langevin. *Nobel Prize winners.

The elements of Groups 3–12, which occupy the central block of the periodic table, are usually referred to as the **transition metals** or the d-block elements. IUPAC⁶ defines a transition metal as “an element whose atom has an incomplete d sub-shell, or which can give rise to cations with an incomplete d sub-shell.” According to this definition, *in senso stricto*, the group 12 elements, Zn, Cd, and Hg are not transition metals. The elements of groups 4–11 are now generally recognised as transition metals, as are Sc and Y in group 3.

When, in 1869, Mendeleev proposed his celebrated classification of the elements, he found it necessary to leave a blank at the position now occupied by Sc. He did however predict some of its properties, and when it was discovered a few years later (1879) in Scandinavia, the agreement of its properties with his predictions contributed greatly to the general scientific acceptance of the periodic table. Neither Sc nor its 5th period homologue Y, are of any biological importance. The third group 3 element in Fig. 1.3, lanthanum, La, is the first of the 15 so called lanthanides. Together with Sc and Y, they are defined by IUPAC as the rare earth metals (Sc and Y are considered rare earth elements since they tend to occur in the same mineral deposits as the lanthanides and have similar chemical properties). Some of the rare earth metals find extensive use in green technologies, especially in wind turbines and hybrid cars. Each megawatt of power generated by a wind turbine requires one ton of rare earth permanent magnets — notably neodymium, dysprosium, and terbium. Each Toyota Prius car is reported to have

5. Marie Curie, her husband, Pierre, and Henry Becquerel had shared the 1903 Physics Nobel Prize for their work on radiation. She received the 1911 prize after the tragic death of Pierre, run over and killed by a horse-drawn vehicle while crossing the rain-swept cobbled Rue Dauphine near the Sorbonne on 19th April, 1906. Marie was given Pierre's chair at the Sorbonne, becoming the first female professor in France.

6. IUPAC, the International Union of Pure and Applied Chemistry.

1 kg of neodymium in its motor and 10–15 kg of lanthanum in its battery. Today, 97% of world production of the world's rare earth supply comes from China, and the Chinese authorities have made it clear that they intend to reduce export quotas for rare earths to protect them from over-exploitation. Many mines from alternative sources in countries like Australia, Brazil, Canada, South Africa, Greenland, and the United States were closed when China undercut world prices in the 1990s, and it will take a few years to restart production. It is estimated that in several years, worldwide demand for rare earths will exceed supply by 40,000 tons annually.⁷ Gadolinium, like the rest of the lanthanides, is a nonessential element. It is widely used as a contrast agent for magnetic resonance imaging (Fig. 1.8),⁸ because of its high paramagnetism (it has seven unpaired electrons) and favourable properties

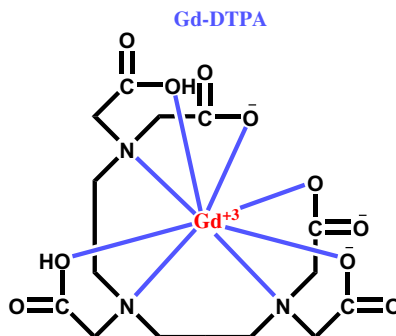


FIGURE 1.8 The structure of the MRI contrast agent Gd-DTPA (diethylene triamine penta-acetic acid).

of electronic relaxation. This dramatically changes the water proton relaxation rates and adds an important amount of additional physiological information to the anatomical resolution of the noncontrasted image.

Whereas Ti is very abundant in the earth's crust, it is not an essential element, unlike the remainder of the biologically very important first row of transition metals. It is often referred to as the 'space age metal', on account of its use in strong lightweight alloys for the aerospace industry, as well as in medical prostheses, orthopedic implants, mobile phones, etc., and it also has therapeutic potential in a number of antitumour drugs. Of the other two members, neither Zr nor Hf (the latter named *Hafnia* after the Latin name for Copenhagen) has any biological importance.

The most important industrial application of V is as a catalyst for the production of sulfuric acid. It is probably a micronutrient in mammals including humans, although its precise role is unknown, and V compounds have been shown to have an insulin-like effect. V is known to be essential as a constituent of haloperoxidases, particularly in some marine organisms, as well as in some nitrogen-fixing organisms where it replaces Mo in nitrogenase. We discuss V along with the enigmatic Cr in Chapter 17. The names tantalum, Ta, and niobium, Nb, are derived from the names in Greek mythology of Tantalus, and his daughter Niobe.

The incorporation of chromium makes steel highly resistant to corrosion (stainless steel), and together with chromium electroplating represents the highest-volume uses of Cr. There have been persistent reports that Cr(III) is required in trace amounts for sugar and lipid metabolism, although whether its complete removal from the diet causes Cr deficiency has been recently questioned (Di Bona et al., 2010). Despite doubts about its essential nature, Cr remains extremely popular as a nutritional supplement, weight-loss and muscle-development agent, second only to Ca-containing products among mineral supplements. Mo, as we discussed above, is an essential element for most organisms, but is replaced by tungsten, W, in the corresponding enzymes of organisms which do not use

7. According to a recent report, not only rare earths cause supply concerns, but so also do helium, phosphorus, and copper together with the platinum group elements (Critical raw materials for the EU, 2010).

8. Magnetic resonance imaging is one of the recent noninvasive techniques which have transformed medical diagnosis in the last few decades.

Mo (typically thermophilic Bacteria and hyperthermophilic Archae⁹). W also replaced osmium and tantalum (and before that, carbon) in the electric lamps of the early twentieth century, which gradually replaced gas lamps. Tungsten lamps, made of tightly coiled helices of finely drawn tungsten wire, in bulbs filled with argon, would provide, according to Edison's vision, 'light for the masses', thereby conquering the fear of darkness. As Oliver Sacks delightfully recounts in his wonderful book 'Uncle Tungsten', the history of chemical discovery has been inseparable from the quest for light (Sacks, 2001, p. 337).

The next six transition metals, Mn, Fe, Co, Ni, Cu, and Zn, are all essential and are discussed in detail in later chapters. While it is important as an oxygen atom donor, the most significant contribution to biology of Mn, the first of the group 7 elements, is the catalytic cluster involved in the photosynthetic oxidation of water in plants, and, at a much earlier point in geological time, in cyanobacteria (Chapter 16). This reaction generates oxygen, which, of course, changed the whole pattern of the evolution of planet Earth. Perhaps the greatest pollution event in the history of our planet, this progressively moved us from an essentially reducing atmosphere to the oxidative world that we now know. There were, of course, advantages — respiration is almost 20 times more effective at producing ATP than fermentation, but with that came the disadvantages associated with the generation of highly reactive, and toxic oxygen species (often designated the oxygen paradox). Neither of the other two group 7 elements have biological roles. Technetium (Tc), like Sc, filled a gap in Mendeleev's periodic table, and many of its properties were predicted by him before its discovery only in 1937. Tc has no stable isotopes — all of its isotopes are radioactive. Almost all Tc is produced artificially (only minute amounts are found in nature), and since it was the first of the predominantly artificial elements, it was given the name technetium (from the Greek *τεχνητός*, — *artificial*). The short-lived isotope of Tc, technetium-99 m (half-life 52.5 min), renders invaluable service in nuclear medicine as a tracer for in vivo imaging by positron emission tomography. Rhenium, Re, is one of the rarest elements in the Earth's crust, and is among the most expensive industrial metals (over 6000\$/kg in 2009). Jet engines, which contain up to 6% of Re, represent its largest use, with industrial catalysts the next most important.

The oxygen paradox, referred to in the previous paragraph, results from the capacity of iron and copper to generate toxic reactive oxygen species, notably the hydroxyl radical through the well-known Fenton reaction. The many and diverse roles that Fe can play will be presented in more detail in Chapter 13. They include oxygen carriers, enzymes that activate and insert oxygen into a wide variety of substrates, electron-transfer proteins (both haem-containing cytochromes and iron-sulfur proteins), as well as iron-storage and transport proteins, to name but a few. With very few exceptions, Fe is essential for almost all living organisms, most probably because of its role in the generation of the amino acid radicals required for the conversion of ribonucleotides to deoxyribonucleotides, essential for DNA synthesis, by Fe-dependent ribonucleotide reductases. Ru, like Rh and Pd (see below), has important applications in industrial catalysis. Organometallic ruthenium complexes are highly efficient catalysts for olefin metathesis with important applications in organic and pharmaceutical chemistry, while other ruthenium complexes are increasingly being used in solar energy technologies. More recently, Ru-based drugs have been developed as anticancer agents. Osmium is the densest natural element, and its tetroxide is widely used for staining biological tissue for electron microscopy.

Co, although present at much lower levels in mammals than Zn, Fe or Cu, is nonetheless indispensable in a number of important vitamin B₁₂-dependent enzymes, including the ribonucleotide reductases of organisms, like *Lactobacilli*,¹⁰ which do not have access to iron. The ribonucleotide reductases of these organisms use a cobalt-based cofactor, related to vitamin B₁₂. Co is also used in a number of other enzymes, some of which catalyse complex isomerisation reactions. Neither Rh nor Ir, the other members of group 10, has any biological implications. As much as 80% of the world production of rhodium goes into catalytic converters, which convert up to 90% of harmful gases from auto exhaust (hydrocarbons, carbon monoxide, and nitrogen oxide) into less harmful substances (nitrogen, carbon dioxide, and water vapour).

9. The three primary kingdoms of cells are Eukaryotes, Bacteria, and Archae.

10. So called since they are found in milk, where the iron-binding protein lactoferrin, sequesters iron so tightly that it is no longer available for microbial requirements.

Ni, like Co, seems to be much more extensively utilised by anaerobic bacteria, in reactions involving chemicals like CH_4 , CO, and H_2 , the metabolism of which was important before the appearance of dioxygen. In higher organisms, notably plants, the only Ni-containing enzyme is urease. Since humans, in common with most terrestrial vertebrates, excrete excess nitrogen from the metabolism of their proteins and constituent amino acids in the form of urea — they are ureotelic — they do not produce this urea-hydrolysing enzyme. Over half of the supply of palladium and its congener platinum goes into catalytic converters. Palladium is also found in many electronic devices and in fuel cell technology. A large number of carbon–carbon bond forming reactions in organic chemistry (such as the Heck and Suzuki coupling) are facilitated by catalysis with palladium compounds, and in 2010, palladium-catalysed organic reactions were recognised by the Nobel Prize in chemistry. Pt, initially in the form of the *cis* isomer of $\text{Pt}(\text{NH}_3)_2\text{Cl}_2$, used under the name of cisplatin, has been hugely successful in the treatment of testicular and ovarian cancers. Since the appearance of *cis-platin* resistant tumours, new Pt anti-tumour drugs have been developed. The precise mode of action of *cis-platin* is discussed in detail in Chapter 20, together with a number of other striking examples of metals as drugs.

One direct consequence of the appearance of dioxygen was that new redox systems and enzymes were required which could operate at much higher redox potentials than previously. As we will see in Chapter 14, copper proved to be particularly suited to this role, and, like Fe, is frequently encountered in reactions involving dioxygen. Ag and Au are known as precious metals, although, unlike Au, Ag forms a black tarnish of silver sulfide in contact with air. Its bromides and iodides are used in photographic film. Over the last six millennia, Ag has been used to prevent microbial infections, which is particularly important in the treatment of burn wounds, making it the most important antimicrobial agent available before the introduction of antibiotics. However, the last few years have seen the emergence of silver nanoparticles which are being heralded as an excellent candidate for therapeutic purposes. Gold might seem to be a surprising (and at first sight costly) therapeutic agent. Nonetheless, gold therapy for rheumatoid arthritis, notably using the orally active derivative Auranofin (Fig. 1.9), which can be

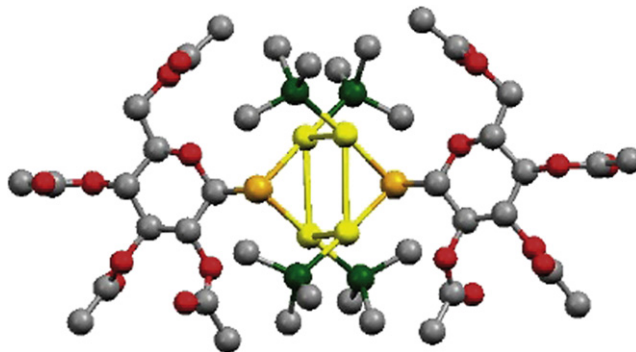


FIGURE 1.9 The orally active anti-rheumatoid arthritis drug Auranofin®.

administered at doses of 3–6 mg/day without necessitating regular visits to the doctor, represents a ‘second-generation’ drug in the treatment of this painful condition.

As we will see in Chapter 12, zinc shares with the alkaline earths the property of belonging to one block of the periodic table while having many of the properties characteristic of another. In the case of zinc and the other two elements in its block, cadmium and mercury, they resemble the three heavy elements of the boron group. Zn, in addition to its use as a Lewis acid in enzyme catalysis, plays a structural role stabilizing protein molecules. It is also involved in a characteristic motif, termed a Zn finger, in a number of eukaryotic DNA-binding proteins, which regulate the transcription of DNA into RNA. The other two elements in group 12, cadmium and mercury, are both extremely toxic, as will be discussed in Chapter 23. Cd is the cause of Itai-itai disease, while Hg is the cause of “hatter’s shakes.” Mercurous nitrate was employed in hat-making to render the felt used in the production of ‘top

hats' more rigid. Prolonged exposure to the mercury vapours caused mercury poisoning. Victims developed severe and uncontrollable muscular tremors and twitching limbs, called "hatter's shakes"; other symptoms included distorted vision and confused speech. Advanced cases developed hallucinations and other psychotic symptoms. This may well explain the expression 'mad as a hatter', illustrated classically in Lewis Carroll's alluring description of the Mad Hatter's Tea Party (Fig. 1.10) in 'Alice in Wonderland'.



FIGURE 1.10 The Mad Hatter's Tea Party. (From Lewis Carroll's *Alice in Wonderland*.)

The elements of groups 13–16 fall into three categories (Fig. 1.3), the metalloids, the other metals, and the nonmetals. The important biological role of some of the nonmetals, oxygen, nitrogen, phosphorus, sulfur, and selenium together with the halogens, chlorine and iodine, will be discussed in Chapter 18.

The metalloids boron (B), silicon (Si), germanium (Ge), arsenic (As), antimony (Sb), and tellurium (Te) are located along a diagonal line separating the metals from the nonmetals¹¹ (Fig. 1.11). Whereas some metalloids have beneficial and essential roles in biological systems (B, Si), others are highly toxic (As, Sb). All organisms, therefore, face the challenge of dealing with the presence of metalloids either in terms of the need to acquire sufficient amounts for effective metabolism, or conversely the need to extrude them to prevent toxicity. Major intrinsic proteins (MIPs) are a family of selective membrane channels which facilitate diffusion of water and small uncharged solutes. Recently, in bacteria, fungi, protozoa, mammals, and plants, specific members of the MIP family of solute channels have been shown to facilitate the diffusion of reduced and noncharged polyhydroxylated forms of various metalloids (Fig. 1.11).

The essential role of boron in plants was first described more than 80 years ago, and there is increasing evidence that boron is also an essential element in yeast and mammals, including man. During the past decade, it has been shown that the principal function of boron in plant cell walls is to crosslink rhamnogalacturonan molecules, an abundant and crucial structural component in plants, which means there is a high demand for B in plants. B is widely distributed in the earth's crust ($5\text{--}100\text{ mg kg}^{-1}$) and mainly occurs as boric acid $[\text{B}(\text{OH})_3]$. At increasing pH, this weak Lewis acid forms the charged borate anion $[\text{B}(\text{OH})_4]^-$, which has physico-chemical similarity to bicarbonate. Recently, molecular genetics experiments using *Arabidopsis thaliana* have identified two types of boron transporters, a boric acid channel, NIP5;1, and a boric acid/borate exporter, BOR1. Both

11. Polonium, with chemical resemblance to bismuth and tellurium, is often considered as a metal.

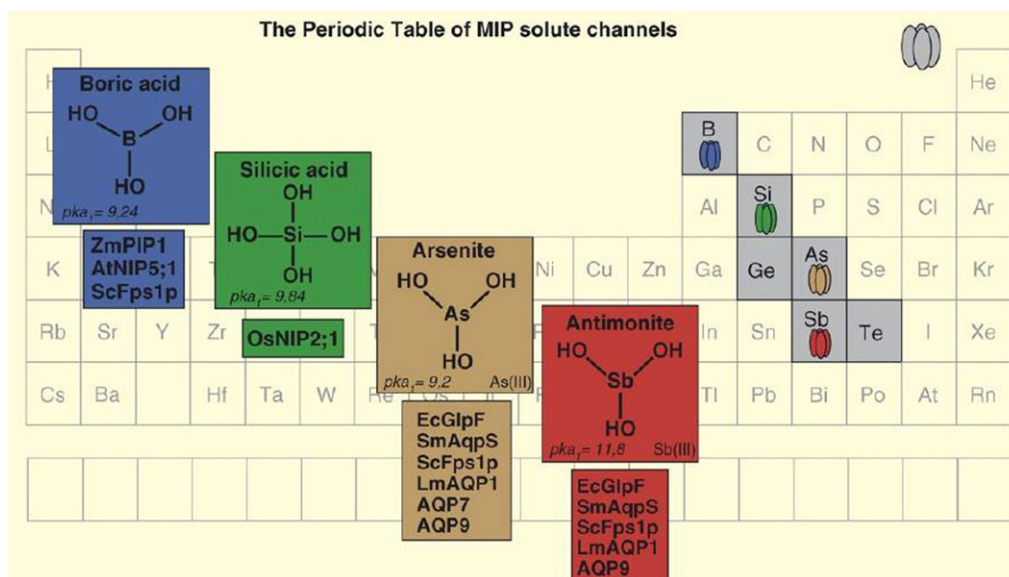


FIGURE 1.11 Transport systems of metalloids. The metalloid element group is highlighted in grey. Poly hydroxylated uncharged species of some metalloids are channelled by some MIPs, and the chemical structures and first pK_a values are displayed for four of them — boric acid, silicic acid, arsenite, and antimonite. The MIPs that facilitate their transport are listed below each structure. Abbreviations: At, *A. thaliana* (rock cress); Ec, *E. coli*; Lm, *L. major* (Lieshmania); Os, *O. Sativa* (rice); Sc, *S. cerevisiae* and Sm, *S. melloti* (both yeasts); Zm, *Z. mays* (maize). AQP7 and AQPs are mammalian homologues; AQP aquaporin. (From Bienert, Schüssler, & Jahn, 2008. Copyright 2008 with permission from Elsevier.)

proteins were shown to be required for plant growth under boron limitation. In addition, BOR1 homologues are required for boron homeostasis in mammalian cells and boron-toxicity tolerance in yeast and plants (Takano, Miwa, & Fujiwara, 2008). Among the higher animals that require B are zebra, fish, and frogs. The critical experiment showing that B is essential for a mammal to complete the life cycle, or defining a biochemical role for B's necessity for life, is lacking. However, B-deprived experimental animals and human beings, when compared with controls fed nutritional amounts of B, show detrimental effects in bone growth and bone maintenance, brain function, and inflammatory response regulation.

Silicon, the second most abundant element in the Earth's crust after oxygen, is an essential element for mammals, where it is thought to be important for the development of bone and connective tissue. Although silicon was first reported to be an essential nutrient some 35 years ago, it is only in the last few years that we have begun to understand just why it is so important for mammals. This recent research confirms that silicon stimulates the formation of collagen, the protein that gives bones their strength and flexibility, joint cartilage its cushioning ability, and the scaffold upon which bone mineralisation occurs. In contrast, it is found as a major element in plants, particularly in grasses, and in many unicellular organisms such as diatoms (an order of microscopic unicellular algae with siliceous cell walls). Silicon exerts beneficial effects on plant growth and production, and in higher plants, Si can account for up to 10% of the dry weight of shoots. Roots take up silicon in the form of silicic acid, and recently both influx and efflux transporters for silicic acid of the MIP family have been identified in grasses, including rice, barley, and maize.

MIP proteins have also been identified as uptake channels for arsenic and antimony, which shows how these toxic elements could enter the food chain. However, very recently (Wolfe-Simon et al., 2010), scientists from NASA have discovered a bacteria from samples taken from the toxic and briny Mono Lake in California which completely swaps phosphorus for arsenic, and can incorporate As into its DNA. The discovery not only offers

insights into the evolution of life, but might help to resolve problems of As-contaminated drinking water. If MIPs are entry pathways for metalloid-based cytotoxic drugs, the possibility also exists of taking advantage of different substrate specificities and uptake pathways between MIPs of drug-target cells and those of patient cells to direct metalloid-based drugs to their therapeutic targets. Arsenic is highly toxic in man, and much speculation has surrounded As poisoning as the cause of death of Napoleon Bonaparte, on account of the levels of As in the Emperor's hair (perhaps derived from fungal activity on a green pigment present in the wallpaper of his apartments in St. Helena).

An interesting interaction between selenium and arsenic has emerged, which suggests that Se could play a pivotal role in detoxifying As in the mammalian bloodstream. Asc protects rats from the liver damage caused by seleniferous wheat, and it has been shown that the mutual detoxification of the individually highly toxic arsenite and selenite requires the endogenous tripeptide, glutathione, which in vivo, in a nonenzymic manner, forms an As–Se compound, seleno-bis(S-glutathionyl) arsinium ion (Fig. 1.12) in red blood cells, which is subsequently excreted in the bile (Prince et al., 2007).

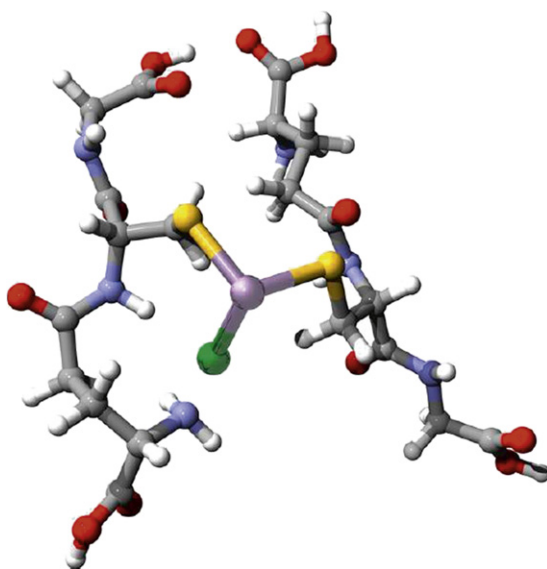


FIGURE 1.12 Structure calculated for one conformer of the seleno-bis(S-glutathionyl) arsinium ion. Se is in green, As in mauve, S in yellow, O in red, N in blue, C in grey, and H in red. (From Prince et al., 2007. Copyright 2007, with permission from Elsevier.)

Of the remaining metalloids, germanium is a semiconductor which is used extensively in fibre optics. Polonium was discovered by Pierre and Marie Curie, and named after her native land, which at that time did not exist as an independent country (it was under Russian, Prussian, and Austrian partition). We have already referred earlier to the murder of Alexander Litvinenko by lethal polonium-210-induced acute radiation syndrome.

Al, while extremely abundant in the earth's crust, is not used by living organisms. It has long been known to be a neurotoxin, although its involvement as a cause of Alzheimer's disease now seems highly unlikely. It is clear that acid rain, due to sulfur dioxide and nitrogen oxide emissions, notably from coal-fired power stations, increases both the solubility and the bioavailability of aluminium. Its toxicity is also discussed in Chapter 23. Gallium is nonessential, but on account of the similarity between Ga^{3+} and Fe^{3+} , it binds to iron transport and storage proteins like transferrin and ferritin. The radioactive isotope of gallium, ^{67}Ga , concentrates to a large extent in many tumours and at sites of inflammation and infection, and since many tumours overexpress the transferrin receptor, it can be used for tumour imaging.

In group 14, Tin, Sn, is thought to be an essential trace element for some species, although its precise role remains unknown. After the discovery of the antitumour activity of cisplatin, many other metal-based organo-metallic compounds were synthesised and screened for their potential therapeutic properties, and some promising organotin compounds have been found. Tin is, of course, an important component of a number of alloys, together with copper in bronze (the Bronze age began about 3500 BC), and with lead in pewter. Lead, Pb, is highly toxic, causing saturnism,¹² particularly among young children in socially deprived inner cities. The toxicity of environmental Pb finds its molecular explanation in the extraordinary high affinity of Pb (binding constant of 10^{15} M) for the key Zn-dependent enzyme of haem biosynthesis, protoporphobilinogen synthase.

Fluorine (F) has a well-established beneficial action in human beings. Most of the body's fluorine is contained in bones and teeth. F is an essential hardening component of bones and fluorine is also beneficial in imparting caries resistance to the enamel of teeth. The mechanisms through which F has beneficial effects are through making the hydroxyapatite of tooth enamel and dentin less soluble and, thus, more resistant to acid attack, and altering calcium, magnesium, and/or phosphorus metabolism, and tissue deposition and/or use. Animal studies suggest that F increases bone strength, reaching peak strength when it contains 1200 $\mu\text{g F/g}$, followed by a decline at higher concentrations, which eventually leads to impaired bone quality. However, fluoride cannot be considered an essential nutrient because the critical experiment showing F is essential to complete the life cycle, or defining a biochemical role for F necessary for life, is lacking. Further, excess F stains the teeth with mottled spots, characterised by a more porous dental enamel — this is known as dental fluorosis. The addition of F in drinking water to retard dental caries particularly in children has been criticised on the grounds of potential toxicity, but the concentrations used are many orders of magnitudes below that which would be required to inhibit many key enzymes.

Bromine is thought to be essential for plants and animals, although no known biological role has been established. It has flame-extinguishing characteristics and is used in fireproofing agents and to make flame resistant plastics. Bromoperoxidases will be discussed in detail in Chapter 17.

Iodine is an essential element with an important role in mammals in the regulation of metabolism, through the action of the two related hormones produced by the thyroid gland, triiodothyronine (T_3) and thyroxine (T_4). Iodine, which is relatively scarce, is actively concentrated in the thyroid gland where both T_3 and T_4 are produced.

Helium, like the other members of **noble gases**, is an inert gas, often used in balloons on account of its low density and, when inhaled, results in a comic transposition of the human voice to a significantly higher register — not a realistic way to mimic counter-tenors, but very effective in well-loved cartoon characters. As we mentioned earlier, world supplies of He are running out. Neon¹³ has the property of emitting light in a tube filled with the gas when an electric discharge is applied. Argon, in contrast to He, is heavier than air, thus making it the ideal medium in which to work anaerobically (keep everything at the bottom of your argon-flushed glove-box!).

This concludes this brief introduction in which I have tried not to say too much about elements that we will encounter in greater detail later on, but to give some indications of the multiple roles, for good as well as for ill, of a number of other metal ions which play an important role in living organisms.

REFERENCES

- Bienert, G. P., Schüssler, M. D., & Jahn, T. P. (2008). Metalloids: essential, beneficial or toxic? Major intrinsic proteins sort it out. *Trends in Biochemical Sciences*, 33, 20–26.
- Di Bona, K. R., Love, S., Rhodes, N. R., McAdory, D., Sinha, S. H., Kern, N., et al. (2010). Chromium is not an essential trace element for mammals: effects of a “low-chromium” diet. *The Journal of Biological Inorganic Chemistry*, 16, 381–390.

12. Chronic lead poisoning: Saturn was the alchemist's name for lead. The metal, Pb (Latin *plumbum*) was used in domestic plumbing from Roman times, on account of its being soft and malleable. It may have been responsible for the decline of the Roman Empire, not from the plumbing, but rather through the use of pewter drinking vessels. It is unlikely that modern-day plumbers ever use it (they prefer other metals or plastics). The attraction of Pb for young children is that it has a very sweet taste.

13. neon is derived from the Greek “neos, meaning” new.

- Gouaux, E., & MacKinnon, R. (2005). Principles of selective ion transport in channels and pumps. *Science*, 310, 1461–1465.
- Flohé, L. (2009). The labour pains of biochemical selenology: the history of selenoprotein biosynthesis. *Biochimica et Biophysica Acta*, 1790, 1389–1403.
- Levi, P. (1985). *The periodic table*. London: Michael Joseph. p. 233.
- Sacks, O. (2001). *Uncle tungsten. Memories of a chemical boyhood*. London: Picador.
- Takano, J., Miwa, K., & Fujiwara, T. (2008). Boron transport mechanisms: collaboration of channels and transporters. *Trends in Plant Science*, 13, 451–457.
- Wolfe-Simon, F., et al. (2010). A bacterium that can grow by using arsenic instead of phosphorus. *Science*. 2 Dec, 2010.

This page intentionally left blank

Basic Coordination Chemistry for Biologists

Introduction	21
Types of Chemical Bonds	21
Hard and Soft Ligands	23
Coordination Geometry	26
Redox Chemistry	28

INTRODUCTION

Biological inorganic chemistry is by its nature an interdisciplinary subject with linguistic and conceptual problems that render it difficult for students who have a background uniquely in either biology or chemistry. The major problem for the student with a background in biology is the understanding of the concepts inherent in the interactions of chemical species (charged or uncharged) with each other. Such concepts involve electronic structure and considerations of symmetry which in turn affect the bonding between them. In this chapter, we will lay out the basics of such concepts with particular reference to the interactions of metal ions with organic molecules.

The electron in its simplest description can be considered as a negatively charged cloud that occupies a definite but arbitrarily defined region of space relative to the nucleus. Such regions are called orbitals¹ and can contain a maximum of 2 electrons of opposing spin. The *s* orbitals are spherical. The *p* orbitals are dumb-bell shaped and there are three of them, each one lying across a Cartesian *xyz*-axes system. The *d* orbitals (apart from the d_{z^2}) are four-lobed and their orientation along a Cartesian *xyz*-axes system is shown in Figure 2.1. The *f* orbitals are seven in number but their shape and orientation are beyond the scope of this book.

TYPES OF CHEMICAL BONDS

Atoms within the same molecule or between different molecules interact and are held together by bonds formed by electrons. The number of bonds that an atom can form is usually determined by its valency — the number of unpaired electrons in its outer shell (the valency shell). Bonding results in each atom achieving the noble gas configuration.²

Ionic Bonding

Electronegativity is the tendency of an atom to attract electrons in a molecule. Large differences in electronegativity between atoms in a given molecule often cause the complete transfer of an electron from the unfilled outer

1. Strictly speaking, an orbital is not a physical reality but refers to a particular solution of complicated wave equations associated with the theoretical description of atoms and they are referred to by the initial letter of the terms describing the spectral lines: sharp, principal, diffuse, and fundamental.

2. The noble gases of Group VIII of the Periodic Table (Figure 1.3) all contain eight electrons in their outer shell.

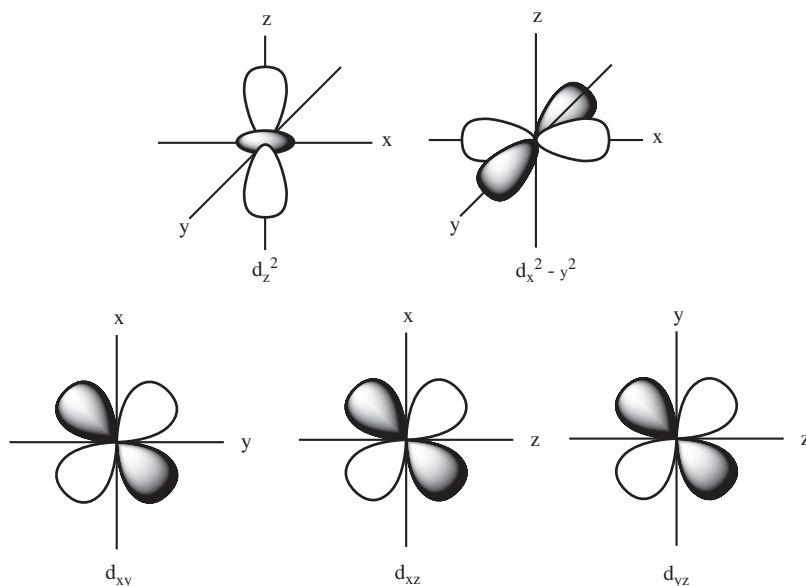


FIGURE 2.1 Graphic representation of the five d orbitals along a Cartesian xyz -axes system.

shell of one atom to the unfilled shell of another. The resulting charged species (ions) are held together by electrostatic forces. Such bonds are highly polarised and are referred to as ionic bonds. Ionic bonding is the simplest type of chemical bonding encountered. NaCl, can be written as $[\text{Na}^+ \text{Cl}^-]$, the sodium atom giving up one electron to resemble the stable neon atom, while the chlorine atom acquires an extra electron to resemble the stable argon atom. MgCl_2 [$\text{Mg}^{2+} \text{Cl}_2^-$] and CoBr_3 [$\text{Co}^{3+} \text{Br}_3^-$] are other examples of ionic compounds.

Covalent Bonding

Orbital overlap, i.e., mutual sharing of one or more electrons, can occur when two atoms are in close proximity to each other. The bonding resulting from such overlap is referred to as covalent bonding. Most frequently, for a significant overlap and hence a more stable bond, either both atoms have half-filled valency orbitals as in the H_2 molecule or one atom has a filled valency orbital not used for bonding and the other one a vacant valency orbital. Pure covalent bonding occurs in compounds containing atoms of the same element like H_2 . Most compounds, however, contain atoms of different elements, which have different electronegativities and, hence commonest type of bonding lies somewhere between purely ionic and purely covalent as in HCl.

Coordinate bonds are a special case of covalent bonds where the electrons for sharing are supplied by one atom. There is often a fractional positive charge on the donor atom and a fractional negative charge on the acceptor atom. $\text{CoBr}_3 \cdot 3\text{NH}_3$ (Figure 2.2) exhibits this type of bonding and hence traditionally it is referred to as a coordination compound.

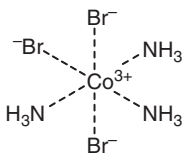


FIGURE 2.2 Structure of the coordination complex $\text{CoBr}_3 \cdot 3\text{NH}_3$.

Coordination³ compounds consist of a central atom or ion, like Co^{3+} , surrounded by electron-rich groups (ligands), like NH_3 . The ligands are directly bound (coordinated to) to the central atom or ion, they are usually between 2 and 9 in number and may be single atoms, ions, or molecules. The ligands directly bound to the metal are said to be in the inner coordination sphere, and the counter-ions that balance out the charge are said to be outer sphere ions. Coordination compounds are usually referred to as complexes, they can be charged or uncharged and their structure is defined by the coordination number (the number of ligand atoms bonded to the central atom) and their coordination geometry (the geometrical arrangement of the ligands and the symmetry of the entire complex). The central ion can be in any oxidation state, which remains unchanged in the coordination complex. We shall endeavour in what follows to explain some of the concepts of coordination chemistry and their relevance to biological inorganic chemistry.

HARD AND SOFT LIGANDS

In 1923, the American chemist G.N. Lewis provided a broad definition of acids and bases which covered acid–base reactions not involving the traditional proton transfer: an acid is an electron pair acceptor (Lewis acid) and a base is an electron pair donor (Lewis base). The concept was extended to metal–ligand interactions with the ligand acting as donor, or Lewis base, and the metal ion as acceptor, or Lewis acid.

The metal ions can be empirically sorted into two groups on the basis of their preference for various ligands: the large and polarisable ions which prefer large, polarisable ligands and the smaller, compact, and less polarisable ones which prefer compact, less polarisable ligands. Such a correlation, coupled to the broader definition of acid–base, led to the concept of “hard” and “soft” acids and bases which can be useful in classifying and to some extent predicting the strength of metal–ligand bonds, and hence the stability of complexes.

The general characteristics of each group are summarised in Table 2.1 along with a classification of metal ions and ligands of importance in biological inorganic chemistry. In general, “hard” acids prefer “hard”

TABLE 2.1 Classification of Biologically Important Metal Ions and Ligands According to the ‘Hard–Soft Acid–Base’ Concept and their General Characteristics

Acid/Acceptor (Metal ions)		Base/Donor (LIGANDS)
Hard	High charge density Small ionic radius No easily excited outer shell electrons Na^+ , K^+ , Mg^{2+} , Ca^{2+} , Cr^{3+} , Fe^{3+} , Co^{3+}	Low polarisability High electronegativity Vacant, high-energy orbitals Hard to oxidise H_2O , OH^- , CO_2^- , CO_3^{2-} , NO_3^- , PO_4^{3-} , ROPO_3^{2-} PO_4^{3-} , ROPO_3^{2-} , $(\text{RO})_2\text{PO}_2^-$, ROH , RO^- , R_2O , NH_3 , RNH_2 , Cl^-
Intermediate	Fe^{2+} , Co^{2+} , Ni^{2+} , Cu^{2+} , Zn^{2+}	NO_2^- , SO_3^{2-} , Br^- , N_3^- , imidazole
Soft	Low charge density Large ionic radius Easily excited outer shell electrons Cu^+	High polarisability Low electronegativity Low energy vacant orbitals Easily oxidised RSH , RS^- , CN^- , CO

3. Although there is no real reason for treating coordination compounds separately from molecular ones, the historic convention will be used here for reasons of convenience.

ligands, whereas “intermediate” and “soft” acids form more stable complexes with “soft” bases. Hard–hard interactions will be primarily ionic in nature whereas soft–soft interactions will be governed by ‘orbital’ interactions.

A number of more specific ligand–metal ion interactions are hidden within Table 2.1. For example, Mg^{2+} is often associated with phosphate ligands (Chapter 10); Ca^{2+} is most commonly coordinated by carboxylate ligands as in proteolytic enzymes of the blood coagulation cascade where Ca^{2+} is often bound to γ -carboxyglutamate residues; and Cu^{2+} is often bound to histidine residues. Nonbiological metal ions which are of importance in medicine or as environmental pollutants can also use the same ligands. Thus, Al^{3+} and Ga^{3+} fall into the ‘hard’ category, while Cd^{2+} , Pt^{2+} , Pt^{4+} , Hg^{2+} , and Pb^{2+} are classified as ‘soft’.

Ligands are also classified electronically (according to the number of electrons donated to the central atom) and structurally (by the number of connections they make to the central atom). The structural classification of the ligands refers to their denticity, i.e., the number of donor atoms from each molecule. A ligand attached by one atom is described as monodentate, by two bidentate, by three tridentate, and so on. Multidentate ligands bound directly to one atom are known as chelating agents and a central metal atom bound to one or more ligands is called a chelate.

The Chelate Effect

Metal ions dissolved in water are effectively complexed to water molecules. Displacing the set of water ligands, partially or entirely by another set in such aqua metal ions, results in forming what is more conventionally known as complexes. Displacement of water molecules by multidentate ligands results in more stable complexes than similar systems with none or fewer chelates.

Such enhanced stability, referred to as the chelate effect, is due to a favourable entropic contribution irrespective of the associated enthalpy changes. The large increase in entropy is the result of the net increase in the number of unbound molecules, i.e., released nonchelating ligands, usually water, from the coordination sphere of the metal ion. The chelate effect decreases in magnitude with increasing size of the chelate ring. The complexing capacity of chelators is best expressed by using the pM^4 where M is the central metal ion. The term allows for comparisons between ligands of different denticity. The larger the value of pM for a particular ligand, the more stable is the metal complex.

Chelation is important in medicine. Treatment of the hereditary disease thalassaemia⁵ requires regular blood transfusion and the excess iron can be removed by the hexadentate chelator desferrioxamine (Desferal[®], DFO) with pFe of the order of 27 and depicted in Figure 2.3. DFO loses three protons when it binds to Fe^{3+} . This illustrates an important aspect of coordination chemistry, namely that the positive charge on the metal ion stabilises the acid anion (i.e., the conjugate base) of protonated ligands. The same thing is true for other biological ligands, such as water, alcohols, carboxylic acids, imidazole, phenols, phosphoric acid, and thiols. In the particular case of water, deprotonation to form a hydroxy ligand is presumed to be involved in a number of metalloenzyme-catalysed hydrolytic reactions, e.g., the role of Zn^{2+} in carbonic anhydrase (Chapter 12).

Another important class of natural chelator molecules is the corrins and porphyrins (Figure 2.4). They are thermodynamically very stable and have four nearly coplanar pyrrole rings, the nitrogen atoms of which can accommodate a number of different metal ions in different oxidation states like Fe^{2+} in haem, Mg^{2+} in chlorophyll, and Co^{3+} in vitamin B₁₂.

4. This has been defined by Ken Raymond as the negative logarithm of the concentration of the free or uncomplexed metal ion $\text{M}_{\text{aq}}^{n+}$ ($\text{pM}^{n+} = -\log [\text{M}_{\text{aq}}^{n+}]$) and it is calculated from the formation constant for a total ligand concentration of 10^{-5} M and $[\text{M}_{\text{aq}}^{n+}]_{\text{tot}}$ of 10^{-6} M under standard conditions (i.e., pH 7.4 and 25 °C).

5. The blood of the patients with thalassaemia contains an abnormal form of haemoglobin.

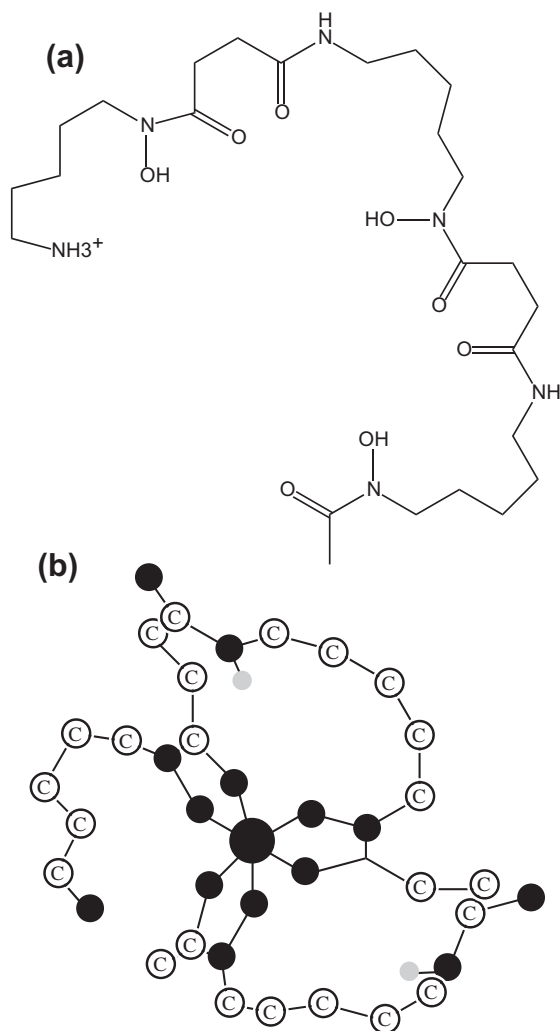


FIGURE 2.3 (a) The metal chelator desferrioxamine (DFO) and (b) its complex with iron.

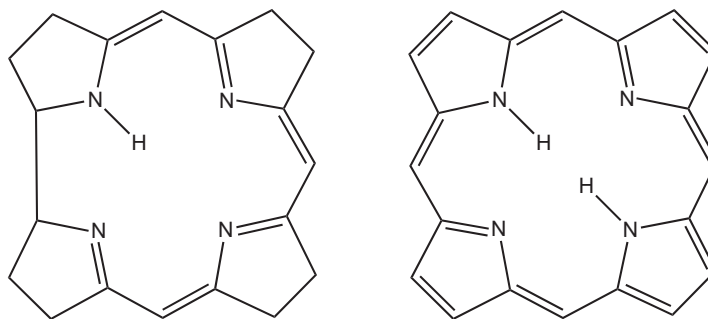


FIGURE 2.4 The structures of corrin (left) and porphyrin (right).

The chelate effect in proteins is also important, since the three-dimensional structure of the protein can impose a particular coordination geometry on the metal ion. This determines the ligands available for coordination, their stereochemistry, and the local environment, through local hydrophobicity/hydrophilicity, hydrogen bonding by nearby residues with bound and nonbound residues in the metal ion's coordination sphere, etc. A good example is illustrated by the Zn^{2+} -binding site of Cu/Zn superoxide dismutase, which has an affinity for Zn^{2+} such that the nonmetallated protein can extract Zn^{2+} from solution into the site, and can displace Cu^{2+} from the Zn^{2+} -site when the di- Cu^{2+} protein is treated with excess Zn^{2+} .

COORDINATION GEOMETRY

The shape of a molecule, i.e., its geometry, is generally defined by the bonds within the molecule which are disposed in a 3-d array. The different pairs of electrons involved in bonding are attracted by two nuclei and they will tend to stay as far from each other as possible to minimize electrostatic repulsions. The shape of a molecule can be predicted on the basis of the number of electron pairs in the valence shell of the central atom. Two pairs result in a linear arrangement, three a triangular one, and four occupy the vertices of a tetrahedron. Five pairs give two possible arrangements, the stable trigonal bipyramid and the less stable square pyramid. The predicted stable geometries are shown in Table 2.2.

TABLE 2.2 Predicted Arrangements of Electron Pairs in the Valence Shell of the Central Atom

Number of pairs	Predicted stable geometry
2	Linear
3	Equilateral triangle
4	Tetrahedron
5	Trigonal bipyramid
	Square pyramid (less stable)
6	Octahedron

Hence, diatomic molecules are linear and so are triatomic ones in the absence of unshared pairs (lone pairs). However, deviations from linearity are observed when lone pairs are present. Lone pairs are attracted by one nucleus instead of two (as in the case of the shared pairs) and hence occupy more space than shared pairs. For example, the water molecule is a 'bent' molecule with a bond angle $\text{H}-\text{O}-\text{H}$ less than 180° due to the repulsions between the two lone pairs of the oxygen atom.


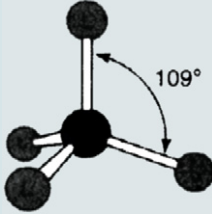
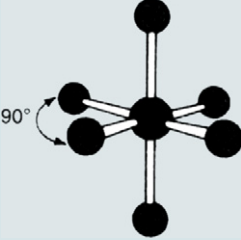
The charge cloud model gives reasonable predictions concerning the shapes of molecules. However, it does not account for the positions of the nonbonding electron pairs (lone pairs) in the molecules. A limitation of such treatment is apparent in the implication that the valency of an element is equal to the number of unpaired electrons in the valency shell. For example, oxygen has 2 unpaired electrons and hence a valency of 2. However, carbon has 2 unpaired electrons but a valency of 4 instead of the expected 2. This higher than expected valency can be explained by the reorganisation of the valence orbitals into new ones possessing a spatial orientation other than the ones discussed above, i.e., the atomic orbitals combine to give new orbitals of different shape and orientation: the hybrid orbitals. A summary of the types of hybridisation and the geometry of the resulting hybrid orbitals is shown in Table 2.3.

TABLE 2.3 The Most Commonly Encountered Types of Hybridisation

Overlapping orbitals	Name of hybrid	Geometry	Example
One <i>s</i> and three <i>p</i>	sp^3	Tetrahedral	Carbon
One <i>s</i> and two <i>p</i>	sp^2	Trigonal	Boron
One <i>s</i> and one <i>p</i>	sp	Linear	Beryllium
One <i>s</i> , three <i>p</i> and one <i>d</i>	sp^3d	Trigonal bi-pyramid	Platinum
One <i>s</i> , three <i>p</i> and two <i>d</i>	sp^3d^2	Octahedral	Titanium

The geometry of the coordination compounds can be similarly predicted based on the coordination number of the central atom. Coordination number 2 and 3 are both relatively rare and give linear and planar or pyramidal geometries, respectively. The most important coordination numbers are 4, 5, and 6 with the latter being the most important one as nearly all cations form 6-coordinate complexes. Table 2.4 shows the geometries corresponding to the commonest coordination numbers in biological systems.

TABLE 2.4 Common Geometries for 4- and 6-Coordinate Metal Ions with Examples for Each Case

Coordination number	Geometry of coordination compound	Example
4	 <p>Square</p>  <p>Tetrahedral</p>	$[\text{Cu}(\text{NH}_3)_4]^{2+}$ (square planar) CuCl_4 (tetrahedral)
6	 <p>Octahedron</p>	Fe^{3+} -DFO

REDOX CHEMISTRY

The nature of the ligand donor atom and the stereochemistry at the metal ion can have a profound effect on the redox potential of redox-active metal ions. What, we may ask, is the redox potential? In the sense that they involve group transfer, redox reactions (more correctly oxidation–reduction reactions) are like other types of chemical reactions. Whereas, for example, in hydrolytic reactions a functional group is transferred to water, in oxidation–reduction reactions, electrons are transferred from **electron donors** (reductants) to **electron acceptors** (oxidants). Thus, in the reaction



Cu^+ , the reductant, is oxidised to Cu^{2+} , while the oxidant Fe^3 is reduced to Fe^{2+} .

We can divide redox reactions into two half-reactions or **redox pairs**, in which one partner, the electron acceptor, or oxidant, is reduced, whereas its conjugate electron donor, or reductant, is oxidised:



The sum of the two half-reactions (2) and (3) is the whole reaction (1). These particular half-reactions occur in the terminal oxidase of the mitochondrial electron transport chain, mediated by cytochrome c oxidase, and its mechanism is described in greater detail in Chapters 13 and 14.

The number of electrons transferred need not be one, and indeed, for many biochemical processes, are frequently two. A **conjugate redox pair** is analogous to a **conjugate acid–base pair** (HA and A^-); however, unlike the latter, the two half-reactions of a redox reaction, like (2) and (3) above, can be physically separated in an electrochemical cell. In the example shown in Figure 2.5, the half-cell undergoing oxidation passes the electrons

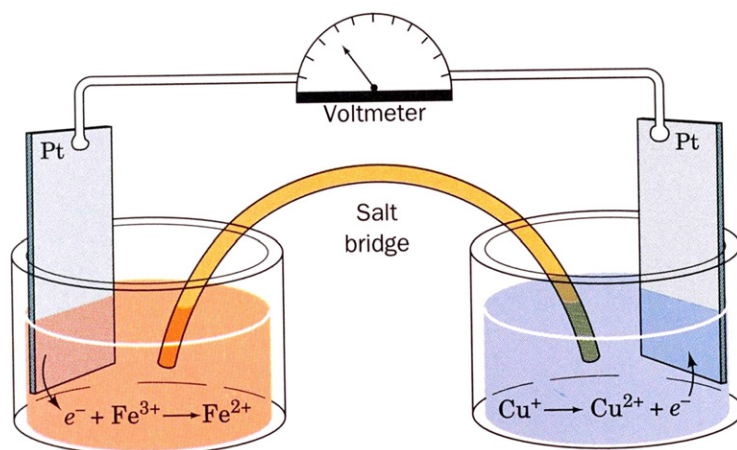


FIGURE 2.5 An example of an electrochemical cell. The half-undergoing oxidation ($\text{Cu}^+ \rightleftharpoons \text{Cu}^{2+} + e^-$) passes the liberated electrons through the wire to the half-cell undergoing reduction ($\text{Fe}^{3+} + e^- \rightleftharpoons \text{Fe}^{2+}$). Electroneutrality in the two half-cells is maintained by transfer of ions through the electrolyte-containing salt bridge. (from Voet & Voet, 2004. Copyright 2004 with permission John Wiley and Sons.)

as an electrical current in the wire connecting their two electrodes. A salt bridge is required to complete the circuit, maintaining electroneutrality in the two half-cells by the transfer of ions.

The standard reduction potential E_0' can be defined as the electromotive force (in volts) measured in a half-cell containing 1 M oxidant and 1 M reductant at 25 °C and pH 7.0, in equilibrium with a reference half-cell which can accept the electrons.

If we consider the general case illustrated in (5)



the equation which relates the standard redox potential to the observed redox potential was originally formulated by Walther Nernst⁶ in 1881 (illustrated for equation (4)):

$$E_h = E_0 + RT/nF \ln [\text{Ox}_1]/[\text{Red}_1] \quad (5)$$

By convention, standard reduction potentials are defined with reference to the half-reaction of the standard hydrogen electrode at pH 0, 25 °C, and 1 atmosphere of hydrogen gas which is in contact with a platinum electrode (6):



This is arbitrarily assigned a standard reduction potential $E'_0 = 0.0$ V. At the biochemical standard state of pH 7, the hydrogen half-cell has an $E'_0 = -0.421$ V.

Figure 2.6 presents a biological redox scale at pH 7.0. The standard redox potentials of the redox pairs such as $\text{Cu}^{2+}/\text{Cu}^+$ and $\text{Fe}^{3+}/\text{Fe}^{2+}$ can be altered by as much as 1 V by varying the nature of their ligands and their geometry.

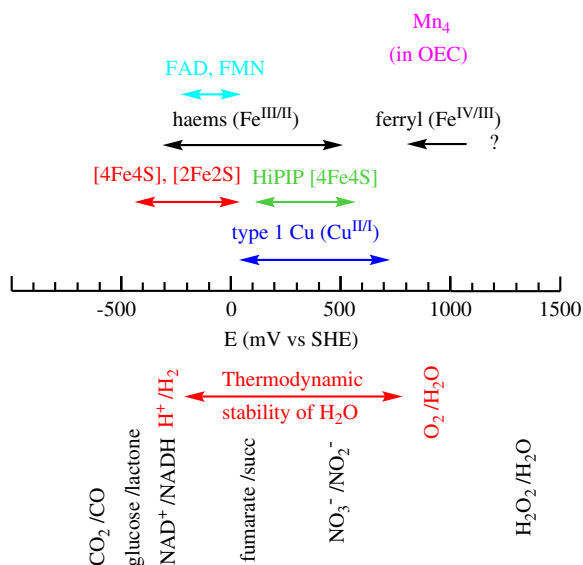


FIGURE 2.6 The biological redox spectrum at pH 7.

Crystal Field Theory and Ligand Field Theory

The crystal field theory (CFT) was developed for crystalline solids by the physicist Hans Bethe in 1929. The model takes into account the distance separating the positively and negatively charged ions and treats the ions simply as point charges with the attractive and repulsive interactions between them as purely electrostatic/ionic

6. Who went on to get the Nobel prize in Chemistry in 1920, and together with Arrhenius and Ostwald was one of the founding fathers of physical chemistry.

ones. In the case of neutral ligands, such as water and ammonia, dipolar charge separations are considered. The central point in this theory is the effect of the symmetry of the arrangement of ligands on the energy of the d orbitals of a central metal atom. Imagine a cube with a metal ion occupying its centre and a Cartesian system of xyz -axes going through it. There are five d orbitals for the metal ion: two aligned along the principle axes hence referred to as d_{z^2} and $d_{x^2-y^2}$ and three distributed between the axes and hence referred to as d_{xy} , d_{xz} , d_{yz} . In the absence of any ligand, the d orbitals are all of equal energy. We describe such orbitals as degenerate. Imagine now negatively charged ligands approaching the cube along the xyz -axes. For an octahedral compound that means six ligands moving toward the centres of the faces of the cube. The ligands have a negative field around them which will be at a maximum along the direction of the approach, that is, the xyz -axes. For s and p electrons, this is of little consequence but for any d electrons this is of great importance. Not only will such electrons be repelled, but those in the orbits along one of the Cartesian axes will experience a greater repulsion than those in an orbit between the axes, since such electrons will be pointing toward where the ligand negative field is at its maximum value. Such unevenness in the repulsion will lift the degeneracy of the orbitals and will create preferences for occupation along the orbitals of the lowest energy: the electrons will occupy the orbitals in between the xyz -axes, i.e., the d_{xy} , d_{yz} , and d_{xz} rather than the orbitals along the axes, i.e., d_{z^2} and $d_{x^2-y^2}$, which lie along the direction of approach of the ligands. In other words, the field associated with the ligands splits the previously homogenous spherical field of the central ion into two groups of different energy level: the e_g group of the d_{z^2} and $d_{x^2-y^2}$ orbitals of relatively high energy and the t_{2g} group of the d_{xy} , d_{xz} , d_{yz} orbitals of relatively low energy. The notation/symbol used for each subset of orbitals indicates its symmetry: e is used for doubly degenerate orbitals, t for triply degenerate ones. The energy splitting is shown schematically in Figure 2.7.

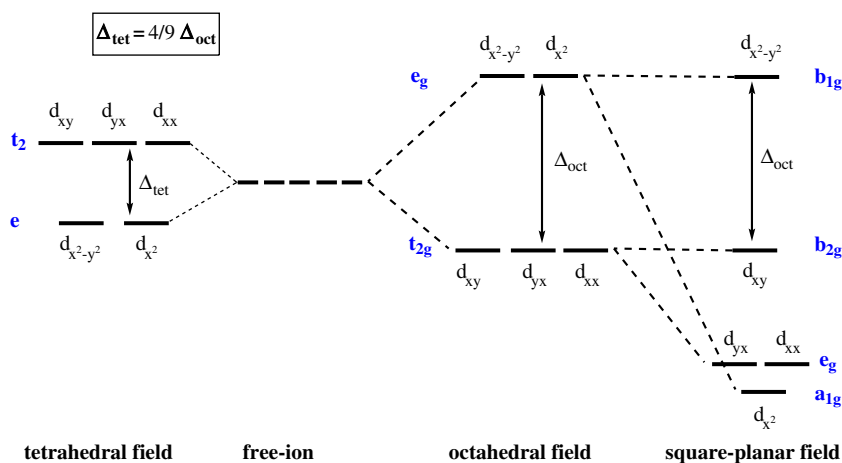


FIGURE 2.7 Crystal field d orbital splitting diagrams for common geometries.

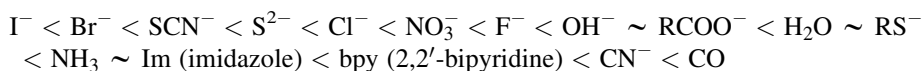
The above treatment considers the ligands in an octahedral geometry (i.e., with the ligands placed at the centre of the faces of the cube). The square planar case is simply an extension of the octahedral where two ligands are removed from the z -axis. The repulsion of electrons in the d_{z^2} and $d_{x^2-y^2}$ orbitals will not be the same and the result is a square planar shape.

Consider now the cube and the ligands fitting into a tetrahedral geometry (i.e., the ligands are placed at four corners of the cube). The energy of the d orbitals which point towards the edges should now be raised in energy higher than those which point towards the faces. The tetrahedral ligand field splitting is exactly the opposite to that of the octahedral field.

A splitting of magnitude Δ^7 is produced and it depends on both the nature of the metal ion and of the ligand. In the case of the octahedral field, each electron placed in one of the t_{2g} orbitals is stabilised by a total of $-2/5\Delta$, while electrons placed in the higher energy e_g orbitals are destabilised by a total of $3/5\Delta$. The splitting for a tetrahedral complex, Δ_{tet} is less than for an octahedral one and algebraic analysis shows that Δ_{tet} is about $4/9\Delta_{oct}$.

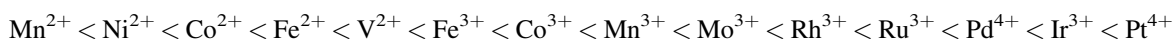
Two factors will determine how electrons redistribute themselves among the d orbitals: (a) the tendency for electrons to repel each other results in the half-filling of the d orbitals by single electrons before electron pairing occurs and (b) the orbitals of low energy will be filled before higher energy orbitals are occupied. The difference in energy Δ will determine which of those two factors will become important. A strong ligand field will result in a large Δ which in turn will lead to the low energy t_{2g} orbitals being occupied in preference to the e_g orbitals leaving the e_g vacant and hence available for bonding. The resultant electronic configuration of the central ion is then known as spin-paired. A weak ligand field will result in half-filled orbitals and the spin-free configuration.

Different ligands will cause different separation of the d orbitals. This is evident in the multitudes of colors available for a given metal ion when the ligand or stereochemistry varies. The ability of the ligands to cause a large splitting of the energy between the orbitals is independent of the metal ion, its oxidation state, and the geometry of the molecule. The ranking of the ligands in order of their ability to cause large orbital separations gives rise to spectrochemical series, a shortened version of which is the following:



Thus, iodide is a weak field ligand and gives small ligand field splitting, while carbon monoxide gives a strong field and a large Δ . The energy difference Δ over this range of ligands increases by a factor of about two. It must be noted that this series must be used as a simple and useful rule and not taken as universally accepted, as it has been built on experimental data for metal ions in common oxidation states.

Metals can also be arranged according to a spectrochemical series:



When CFT is applied to metal ions of a symmetrical spherical charge, such as the alkali metal ions K^+ and Na^+ , the energy calculations show that large cations of low charge should form few coordination compounds. Transition metal cations, however, contain electrons in orbitals which are not spherically symmetric and which affect bond energies and properties of the metal concerned. The weakness of the CFT is further highlighted by the spectrochemical series. One would expect negatively charged ligands to give stronger crystal fields than neutral ones if only pure electrostatic repulsions were in operation. The position of the negatively charged halide ions as weak field ligands therefore seems odd, as does the fact that hydroxide ion is a weaker field ligand than its parent acid water, despite having the same donor ion. CFT is incapable of explaining the differences in magnetic and spectral properties of coordinated metal ions compared to the free metal ion, and indeed in explaining why these properties depend on the nature of the ligand. For example, $[FeF_6^{3-}]$ has magnetic properties corresponding to five unpaired electrons, whereas those of $[Fe(CN)_6]^{3-}$ correspond to only one unpaired electron.

Such discrepancies between empirical observations and theory eventually prescribed a need to describe the bonding in complexes of various symmetries not only taking into account the electrostatic interactions but also the overlap interactions of the molecular orbitals. This theory is referred to as the ligand field theory (LFT). Consider

7. This is referred to as the crystal field splitting in CFT measuring the magnitude of the electrostatic interaction or the ligand field stabilisation energy in LFT measuring the strength of the ligand field. In this book, we shall simply refer to it as the energy difference or 'splitting'.

the shapes of the s , p , and d orbitals as shown in Figure 2.1 and the same symmetry arrangements as in CFT but with the additional use of the molecular orbital theory (MOT) of chemical bonding. MOT combines the approximate energies and wave functions of all of the component atomic orbitals to obtain the best approximations for the energies and wave functions of the molecule. In other words, it makes use of covalency in the metal–ligand interactions.

During the formation of a molecule, the atomic orbitals of the individual nuclei interact. Such interactions may be constructive or destructive depending on whether their wave functions add or subtract in the region of overlap. Which orbitals can overlap effectively is dictated by symmetry considerations and only orbitals of matching symmetry may interact. A constructive interaction will result in the formation of two types of bonding molecular orbital: the σ and the π molecular orbitals⁸ with a build-up of electron density between the two nuclei. Destructive interactions will give rise to antibonding orbitals called σ^* and π^* with an associated decrease in electron density. The bonds associated with σ and π orbitals are called respectively σ and π bonds. In simplistic terms direct, ‘head-on’ overlap of two suitably orientated orbitals result in a σ -bond with uniform distribution of charge density around the axis of the bond whereas ‘side-ways’ overlap will give rise to a π -bond with distribution of the charge density above and below a plane crossing the axis of the bond. The electrons involved in the latter type of bonding are spread out over a greater volume than those involved in the former type. A π -bond will hence be more readily polarised than a σ -bond and such bonds are said to be delocalised as sideways overlap occurs between all orbitals in the vertical plane and all those in the horizontal plane. This is the case of alkynes and nitriles, both possessing two sets of π -bonds perpendicular to each other. Delocalisation gives additional stability to a molecule as the increase in the volume of the space occupied by the electrons involved lowers the potential energy of the system.

The bonds involved in coordination complexes can then be described as σ -bonds (any lone pair donation from a ligand to the metal) and π -bonds (any donation of electron density from filled metal orbitals to vacant π orbitals of the ligand or from the p orbitals of the ligand to the metal d orbitals). In the octahedral environment of a central metal atom with six surrounding ligands, the s , p_x , p_y , p_z , d_{z^2} , and $d_{x^2-y^2}$ valence shell orbitals of the central metal atom have lobes lying along the metal–ligand bond directions and hence are suitable for σ bonding. The orientation of the d_{xy} , d_{xz} , and d_{yz} makes such orbitals appropriate only for π -bonding. It is assumed that each ligand possesses one σ orbital.⁹ Each of the metal orbitals will be combined with its matching symmetry of the ligand system to give a bonding (maximum positive overlap) and an antibonding (maximum negative overlap) molecular orbital. The simplified MO diagram¹⁰ for the formation of a sigma-bonded octahedral ML_6 complex is shown in Figure 2.8.

If a molecular orbital is closer in energy to one of the atomic orbitals used to construct it than to the other one, it shall have more the character of the first one than the second one. Hence, the electrons occupying the six bonding σ molecular orbitals will be largely “ligand” electrons with some metal ion character. Electrons occupying the antibonding orbitals will be mainly “metal” electrons. During the complex formation the metal d electrons will go either only to t_{2g} or to both t_{2g} and e_g^* . In the absence of any π bonding any electrons in the t_{2g} (which could contribute to π -bonding) will be purely metal electrons and the level is essentially nonbonding, whereas the e_g^* levels participate in σ -bonding with the ligand. In other words, the central portion of the diagram closely resembles the t_{2g} and e_g orbitals derived from crystal field theory (Figure 2.7), with one difference: the e_g orbital is now e_g^* .

In terms of crystal field theory, the larger gap between t_{2g} and e_g^* energy levels in strong field ligands is essentially a consequence of the raising of the e_g^* energy levels by electrostatic interactions between the ligand and the d electrons of the metal. However, the molecular orbital model shows how the difference in energy Δ could also be increased, by lowering the energy of the t_{2g} orbitals. Figure 2.9 shows the situation when π bonding

8. Pronounced as *sigma* and *pi* from the Greek letters.

9. If the ligands possess also π -orbitals these have to be taken into account.

10. a_{1g} , e_g , t_{1u} encountered in the diagram are symmetry symbols for the associated orbitals: a_{1g} represents a single orbital which has the full symmetry of the molecular system; e_g and t_{1u} represent a set of two and three orbitals, respectively, which are equivalent within the individual set apart from their orientation in space. Subscripts g and u indicate whether the orbital is centrosymmetric or anticosymmetric.

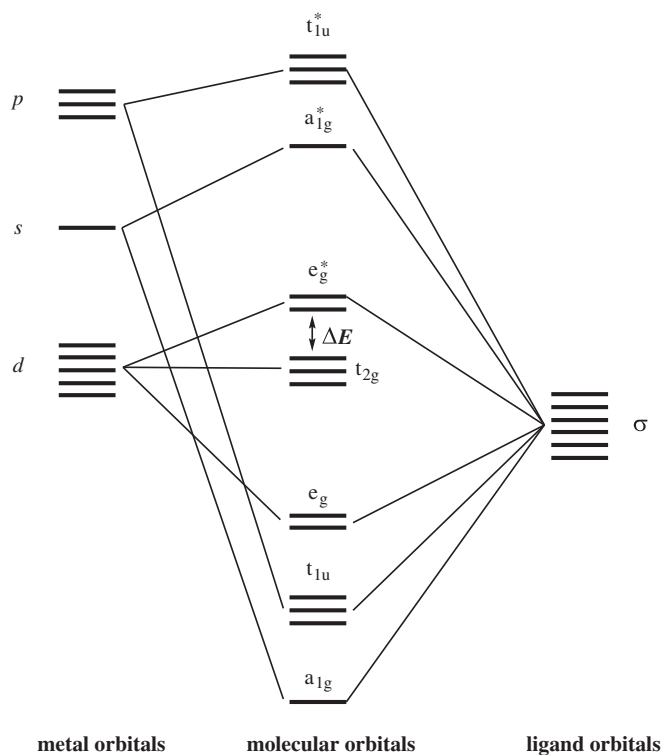


FIGURE 2.8 Simplified MO energy level diagram for the formation of a sigma-bonded octahedral ML_6 complex in which there are no π -bonding interactions between metal and ligand. (From Mackay & Mackay, 1989.)

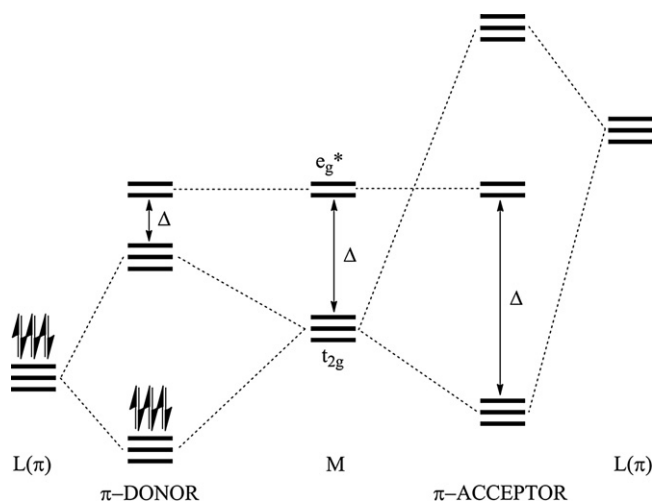


FIGURE 2.9 The ways in which π -bonding interactions with a ligand can influence the value of the energy difference, Δ for an octahedral complex. High-energy, poorly populated π -orbitals in the ligand increase the splitting (i.e., are π -acceptors), whereas filled, low-energy π -orbitals decrease the splitting (they are π -donors).

interactions between the metal t_{2g} orbitals and the p orbitals of the ligand are considered. π bonds are generally weaker than σ -bonds so the effect is to modify rather than dramatically alter the description. Two orbitals from each ligand are combined to give a total of 12 which are subdivided into four sets with three ligand group orbitals in each set. The metal t_{2g} orbitals are the most suitable for interaction. There are two cases to be considered: (a) the metal t_{2g} orbitals are vacant and the ligand π orbitals are full and at a lower energy than the metal t_{2g} . In this case, there is a decrease in the magnitude of Δ . The electron density will be transferred from the ligand to the metal (the ligand is now a **π donor**); (b) the metal t_{2g} orbitals are filled, and the ligand π orbitals unfilled and at higher energy than the metal t_{2g} . This causes an increase in Δ and the transfer of electron density will now be from the metal to the ligand (the ligand is now a π acceptor). This explains in a satisfactory way the position of CO and CN^- in the spectrochemical series: because they have vacant orbitals of π -symmetry. This additional π -bonding is responsible for the stabilisation of the low oxidation states of metals by strong field ligands as the high electron density on such metal ions can be delocalised onto the ligands. In contrast, weak field ligands, like F^- and OH^- are π donors, and would be expected to stabilise high oxidation states. The essential take-home message is that the metal ion has its properties influenced by the ligands, and vice versa.

REFERENCES

- Constable, E. C. (1996). *Metals and ligand reactivity*. Chapter 1. VCH Weinheim. pp. 1–21.
- Cotton, F. A., & Wilkinson, G. (1980). *Advanced inorganic chemistry: A comprehensive text* (4th ed.). New York, Chichester: John Wiley and Sons. pp. 1396.
- Huheey, J. E., Keiter, E. A., & Keiter, R. L. (1993). *Inorganic chemistry: Principles of structure and reactivity* (4th ed.). Benjamin Cummings.
- Kirchner, B., Wennmohs, F., Ye, S., & Neese, F. (2007). Theoretical bioinorganic chemistry: the electronic structure makes a difference. *Current Opinion in Chemical Biology*, 11, 134–141.
- Mackay, K. M., & Mackay, R. A. (1989). *Introduction to modern inorganic chemistry* (4th ed.). Glasgow and London: Blackie. pp. 402.
- Neese, F. (2003). Quantum chemical calculations of spectroscopic properties of metalloproteins and model compounds: EPR and Mössbauer properties. *Current Opinion in Chemical Biology*, 7, 125–135.

Structural and Molecular Biology for Chemists

Introduction	35
The Structural Building Blocks of Proteins	37
Primary, Secondary, Tertiary, and Quaternary Structure of Proteins	41
Secondary and Tertiary Structures of Nucleic Acids	50

INTRODUCTION

In the previous chapter we introduced readers from a more biological background to some notions of inorganic chemistry and, in this chapter, we explain to readers from a more chemical and physical background the fundamental concepts of structural and molecular biology, which will be necessary to follow our path through the diverse roles of metals in biological systems. For more information concerning the content of this Chapter see Branden and Tooze, 1991; Berg et al., 2002; Campbell et al., 2005; Creighton, 1993; Fersht, 1999; Voet and Voet, 2004.

Our introduction to structural and molecular biology begins with a sharp reminder that life must function in an aqueous environment. We believe that terrestrial life originated in some kind of primordial sea, and, as the fossil record suggests, it is only quite recently that it ventured onto dry land. It might puzzle a few readers as to how it came about that this aquatic life managed to survive during periods of extensive glaciation. There is a very simple explanation — liquid water, unlike most liquids, expands on freezing — the density of ice is 0.9167 g/cm^3 at 0°C , and is lower than that of water, which has a maximum density of 1.000 at 4°C .¹ This means that water freezes from the top down, allowing aqueous life to remain viable underneath the ice. Water is a polar solvent: the large difference in electronegativity between O and H means that the O—H bond has 33% ionic character, reflected in the dipole moment of water (1.85 Debye units). An immediate consequence of this is that H_2O molecules associate through hydrogen bonds. In the highly ordered structure of ice, each water molecule is hydrogen bonded to four neighbours in a tetrahedral arrangement (Figure 3.1). Even at the physiological temperature of 37°C , water molecules still form an extensive network of hydrogen bonds, accounting for the highly cohesive nature of liquid water. In common with the other two kinds of noncovalent bonds, electrostatic interactions, and van der Waal's interactions, hydrogen bonds are transient. Like the lights on a Christmas tree flickering on and off, continually being formed and broken, switching partners, these weak noncovalent forces play essential roles in biology. Whether it is the folding of proteins into elegant predetermined three-dimensional forms, the faithful replication of huge DNA molecules, the specific molecular recognition of substrates by enzymes, or of signalling molecules by their receptors, these myriad weak interactions are at the heart of the biological action. All biological structures

1. Which is why cold rooms are maintained at this temperature.

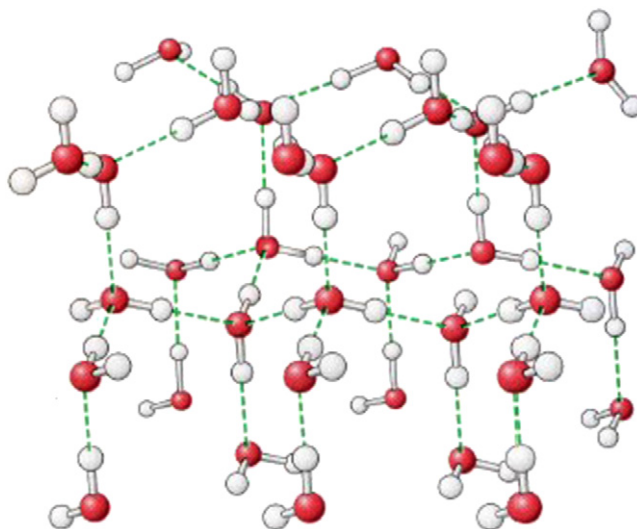


FIGURE 3.1 Structure of ice. Hydrogen bonds (dashed lines) are formed between water molecules.

and processes depend on the interplay of noncovalent interactions as well as covalent ones. Water is an excellent solvent for polar molecules, and will of course weaken electrostatic forces and hydrogen bonding between polar molecules by competing for their mutual attractions. So, in the presence of water, a hydrogen bond between a carbonyl group and the NH of an amide can be replaced, as shown in Figure 3.2: the H of water could either

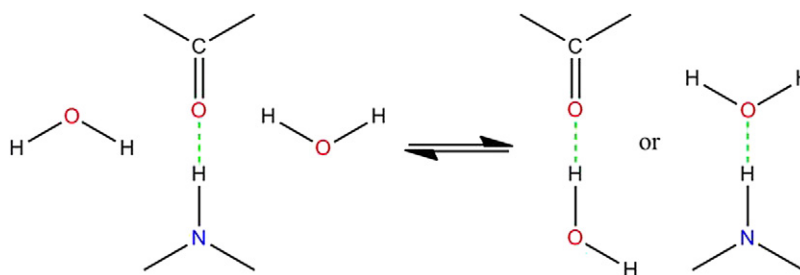


FIGURE 3.2 The effect of water on hydrogen bonding between a carbonyl group and the NH of an amide.

replace the amide N or else the O of water could replace the O of the carbonyl. As a consequence, such hydrogen bonds, which play an important role in protein and nucleic acid structures, can only be formed if water is excluded. The fact that water weakens interactions between polar molecules leads us to the important conclusion that we can circumvent this problem by creating water-free environments within biological macromolecules. This is reinforced by yet another consideration, this time concerning nonpolar molecules, illustrated in Figure 3.3. Water is a very poor solvent for nonpolar molecules compared to most organic solvents. Nonpolar molecules cannot participate in the hydrogen bonding which is so important in liquid water. As a consequence, the water molecules around them become more ordered (i.e., lower in entropy) than water molecules in the bulk solution. When two such nonpolar molecules come together, some of their surrounding water molecules are released and can return to the bulk solution. So, nonpolar molecules have a spontaneous tendency to prefer nonpolar environments. By aggregating together in water, they release the water molecules around them, increasing the entropy of water, and

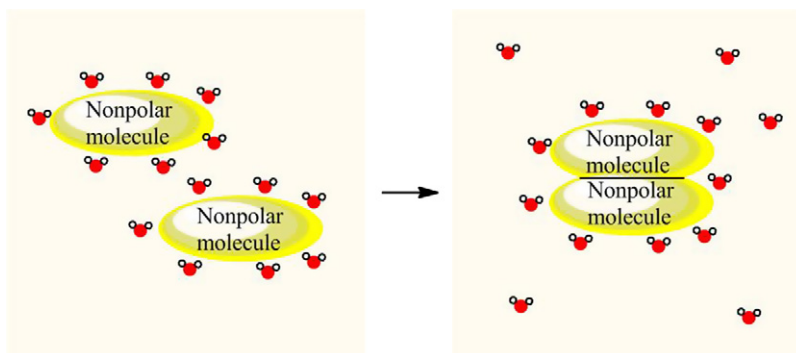


FIGURE 3.3 The hydrophobic effect. The aggregation of nonpolar groups in water leads to an increase in entropy owing to the release of water molecules into bulk water.

thereby satisfying the second law of thermodynamics.² This hydrophobic effect is the driving force behind a great many biochemical processes including protein folding, nucleic acid structure, and the formation of biological membranes.

THE STRUCTURAL BUILDING BLOCKS OF PROTEINS

Proteins are formed from α -amino acids which, with the exception of proline, have a primary amino group and a carboxylate group on the same carbon (proline is an α -imino acid, with a secondary amino group). With the exception of glycine, they all have the L (or R) configuration,³ and are joined by peptide (amide) bonds (Figure 3.4) to form polypeptide chains. Since, at pH 7, they are present as dipolar ions, it follows that proteins

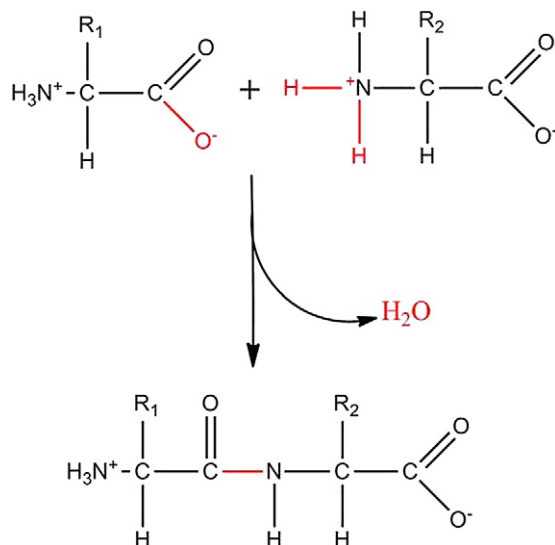


FIGURE 3.4 The zwitterionic structure of two α -amino acids, and the condensation reaction to form a dipeptide, linked by a peptide bond.

2. Which can be summarised as the statement that disorder increases spontaneously, well illustrated by the state of the desk of an author in search of inspiration.

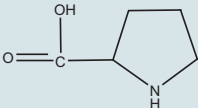
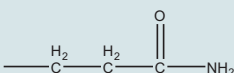
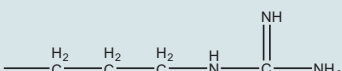
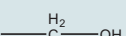
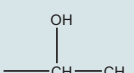
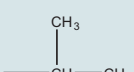
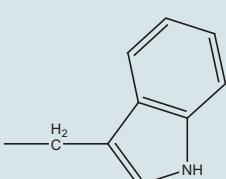
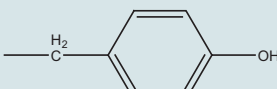
3. With four different groups attached to the tetrahedral α -carbon, α -amino acids are chiral. Only L-amino acids are found as constituents of proteins. For most amino acids the L-isomer has the S (rather than R) absolute configuration.

will have a positively charged amino terminal group, and a negatively charged carboxyl terminal group. There are just 20 amino acids which are routinely found in proteins. This finds its explanation, as we will see later in the chapter, because these are the amino acids for which there are aminoacyl-tRNA synthetases. These enzymes can selectively charge each of these 20 amino acids onto their cognate tRNAs. In a small number of proteins there is a 21st amino acid, selenocysteine, and we will see in Chapter 18 how the codon TGA, which usually means “stop”, can encode selenocysteine. In Table 3.1, the 20 protein amino acids are represented by

TABLE 3.1 Protein Amino Acids

Name of amino acid	Structure of R-group	Properties	pK of R-group
Alanine	A —CH_3	Hydrophobic	
Cysteine	C $\text{—CH}_2\text{—SH}$	Polar, forms disulfide bridges	8.37
Aspartate	D $\text{—CH}_2\text{—C(=O)—O}^-$	Polar, charged	3.90
Glutamate	E $\text{—CH}_2\text{—CH}_2\text{—C(=O)—O}^-$	Polar, charged	4.07
Phenylalanine	F $\text{—CH}_2\text{—C}_6\text{H}_5$	Hydrophobic	
Glycine	G —H	Highly flexible	
Histidine	H $\text{—CH}_2\text{—C}_4\text{H}_3\text{N}_2$	Hydrophobic/polar donor/acceptor of H^+	6.04
Isoleucine	I $\text{—CH(CH}_3\text{)—CH}_2\text{—CH}_3$	Hydrophobic, sterically hindered β -carbon	
Lysine	K $\text{—CH}_2\text{—CH}_2\text{—CH}_2\text{—CH}_2\text{—NH}_2$	Polar, flexible side chain	10.54
Leucine	L $\text{—CH}_2\text{—CH(CH}_3\text{)—CH}_3$	Hydrophobic	
Methionine	M $\text{—CH}_2\text{—CH}_2\text{—S—CH}_3$	Hydrophobic	
Asparagine	N $\text{—CH}_2\text{—C(=O)—NH}_2$	Polar, uncharged	

TABLE 3.1 Protein Amino Acids—Cont'd

Name of amino acid	Structure of R-group	Properties	pK of R-group
Proline	P 	Imino acid, can form <i>cis</i> -peptide bonds	
Glutamine	Q 	Polar, uncharged	
Arginine	R 	Polar, charged	12.48
Serine	S 	Polar, uncharged	
Threonine	T 	Polar, uncharged, rather hydrophobic	
Valine	V 	Hydrophobic, sterically hindered β -carbon	
Tryptophan	W 	Hydrophobic, very bulky	
Tyrosine	Y 	Polar, but almost as hydrophobic, as phenylalanine	10.46

their three-letter and one-letter code, the structure of their R group and, where appropriate, the pK_a of the R group is given. This basic assembly kit can be divided into amino acids which have nonpolar, uncharged, and generally hydrophobic side chains; those which have polar, but uncharged, side chains; and those which have polar, charged side chains.

The amino acids with nonpolar, aliphatic side chains, Ala, Ile, Leu, Met, and Val, are sufficiently hydrophobic that they are most often buried in the generally hydrophobic core of non-membrane-embedded proteins. Note that Ile and Val have particularly sterically hindered β -carbons. Of the aromatic amino acids, His, with a pK of around 6, will mostly be in the uncharged form at physiological pH values (therefore more often hydrophobic than polar), and will be a likely choice for reactions which involve proton transfer. Phe and Trp are clearly hydrophobic. Despite having a polar hydroxyl group, if we consider the free energy required to transfer

Tyr from water to an organic solvent, it is not very different from Phe, so we should not be surprised to find it in hydrophobic environments. Gly is an unusual amino acid, with only a hydrogen atom as side chain, and peptide bonds involving Gly residues can take up all sorts of conformations. Pro, which does not have a proton when in a peptide bond, clearly, is hydrophobic, cannot participate in hydrogen bonding, and has the unique capacity among the protein amino acids to be able to form cis-peptide bonds (there is a cis/trans prolyl isomerase to restore the trans form).

Of the polar, uncharged residues, as pointed out above, Tyr is not particularly polar, although it can participate in hydrogen bonding through its phenol group. The other hydroxylated amino acids, Ser and Thr, and the amides Asn and Gln can be at surface positions interacting with water, or in the interior, where they may participate in hydrogen bonding with other polar residues. A word of caution concerning Ser — there are an important number of enzymes — collectively known as serine proteases and esterases — in which a particular local environment renders the oxygen of the serine residue extremely nucleophilic. This is, however, the exception rather than the rule, and in most contexts the Ser hydroxyl group is no more reactive than that of ethanol.

Finally, special mention must be made of Cys, which, when present alone, can be considered to belong to the polar uncharged group described above. It can, however, when correctly positioned within the three-dimensional structure of a protein, form disulfide bridges with another Cys residue (Figure 3.5). These are the only covalent bonds, apart from the peptide bond, of course, that are usually found in proteins.⁴

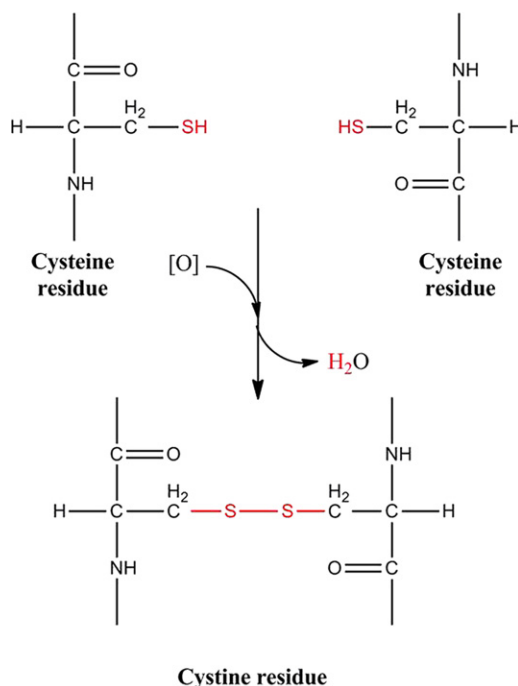


FIGURE 3.5 Disulfide formation between two cysteine residues. The product of the oxidation reaction, stable to acid hydrolysis is called cystine.

4. Some proteins, like collagen and elastin, have covalent cross-links between their fibres, which are formed after their synthesis (post-translational modification).

The charge properties of a protein will be determined by the five amino acids with potentially charged R-groups. At pH 7, Glu and Asp will have a negative charge, Lys and Arg a positive charge, while His residues will be about 10% positively charged.⁵ These polar, charged residues, Asp, Glu, Lys, Arg, and the protonated form of His, will often be found at the surface of proteins, where they may not only interact with the polar layers of ordered water molecules surrounding the protein, but may also participate in hydrogen bonds and salt bridges with other polar/charged residues.

PRIMARY, SECONDARY, TERTIARY, AND QUATERNARY STRUCTURE OF PROTEINS

We can distinguish several levels of structural organisation in proteins. These are usually described as primary, secondary, tertiary, and quaternary, as shown in the well-known illustration of Irving Geis (Figure 3.6). The primary structure is quite simply the linear amino acid sequence of the polypeptide chain.

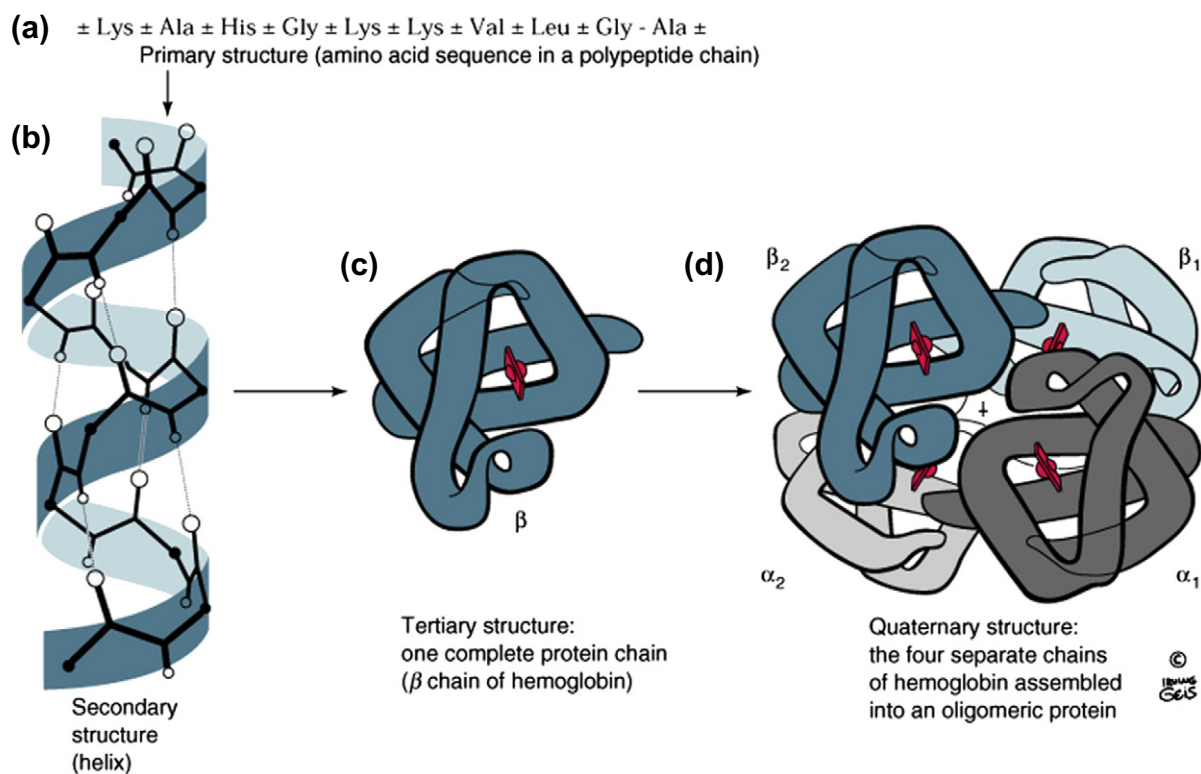


Figure copyrighted by Irving Geis.
Copyright 1999 John Wiley and Sons, Inc. All rights reserved.

FIGURE 3.6 Structural organisation of proteins. (From Voet & Voet, 2004. Reproduced with permission from John Wiley & Sons, Inc.)

We know, from the classic experiments of Christian B. Anfinsen (Anfinsen, 1973), that the amino acid sequence inherently contains all the information required for the overall three-dimensional structure of the protein (but, we still do not yet know how to predict the latter accurately from the former). The secondary

5. Assuming that the pKs are not influenced by their environment in the protein (which they often are).

structure of the protein consists of local regular structures stabilised by hydrogen bonds involving the amide backbone of the polypeptide chain, such as α -helices, β -pleated sheets, and reverse turns. The tertiary structure is formed by the packing of such structural elements into one or more compact globular units, often referred to as either supersecondary structures or domains. This compact structure is described by the three-dimensional localisation of all atoms of the protein's amino acid sequence, both main chain and side chains. This often brings together amino acid residues which are far apart in the primary structure to form a functional region, known as the active site. Some proteins, like haemoglobin, illustrated in Figure 3.6, contain several polypeptide chains, each with their individual tertiary structure, arranged together in a quaternary structure.

When Linus Pauling and Robert Corey carried out their pioneering X-ray crystallographic studies on a number of amino acids and dipeptides in the 1930s and 40s, they arrived at three very important conclusions and constraints: (i) the most important constraint was that all six atoms of the amide (or peptide) group lie in the same plane. Pauling had predicted planar peptide bonds because of resonance of electrons between the double bond of the carbonyl group and the amide C–N bond of the peptide bond, which results in partial double bond character in the C–N bond and partial single-bond character of the C=O bond, (ii) the peptide bond is usually trans, and (iii) the maximum amount of hydrogen bonding potential is realised between amide functions. Since the peptide units are essentially rigid structures, linked by covalent bonds at the α -carbons, the only degree of freedom that they have are the rotations around these bonds – defined by the angles **phi** (ϕ) around the N–C $_{\alpha}$ bond and **psi** (ψ) around the C $_{\alpha}$ –C' bond (Figure 3.7a). If we can define the angles ϕ and ψ for each amino acid, we can describe the conformation of the main chain of the protein.

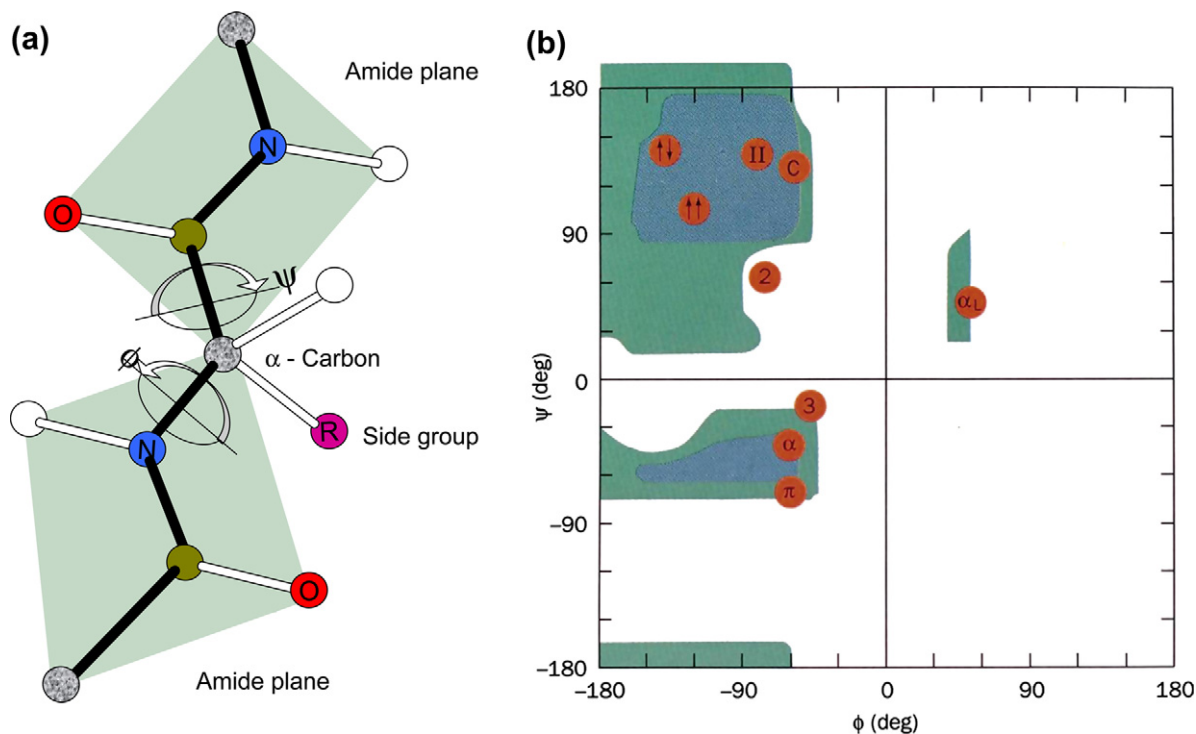


FIGURE 3.7 (a) Diagram of a polypeptide chain with the peptide units represented as rigid structures showing the conformational angles ϕ and ψ (Adapted from Voet & Voet, 2004.) by conventional mathematical signs for parallel and antiparallel as in Figure 3.7b. (b) a Ramachandran plot, showing the sterically allowed angles for ϕ and ψ . The regular conformations of polypeptides are α_R , right-handed α -helix; α_L , left-handed α -helix; \circ , antiparallel β -sheet; \bullet , parallel β -sheet; R, right-handed 3_{10} helix; π , right-handed π -helix; Δ , polyPro.

The Indian biophysicist G.N. Ramachandran made calculations of the allowed values of ϕ and ψ , which would avoid steric collisions either between atoms in different peptide groups or between a peptide unit and the side chains attached to C_α . The representation of the allowed values of ϕ and ψ in Figure 3.7b is called a Ramachandran plot, and it is clear that only a few regions of the diagram are sterically allowed. The areas corresponding to right-handed α -helices, β -strands, and left-handed α -helices are indicated, as are a number of other secondary structures. Observed values for all amino acid residues, except glycine in well refined X-ray structures of proteins which have been determined to high resolution and the observed values for Gly residues in these same proteins, are shown in the two panels of Figure 3.8. This underlines the remark made earlier that Gly plays a

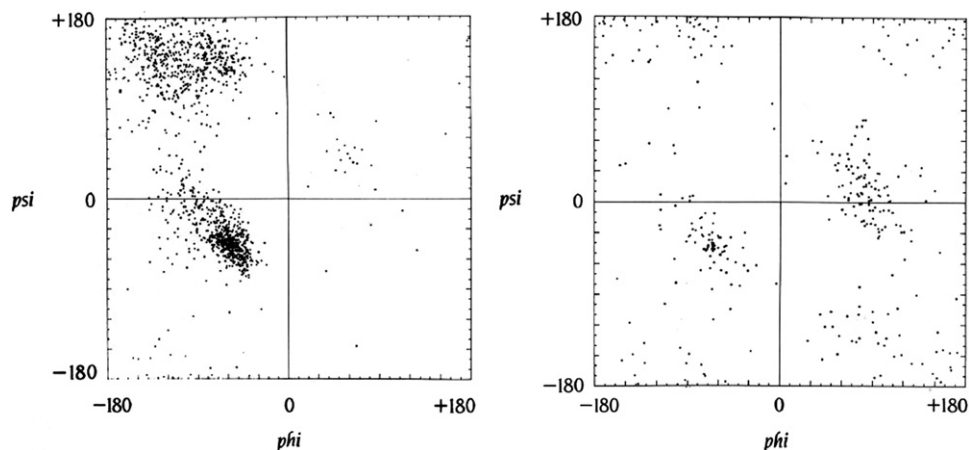


FIGURE 3.8 (a) Observed values for ϕ and ψ angles in protein structures for all residues except Gly (b) observed values for Gly. (From Branden & Tooze, 1991. Reproduced with permission from Garland Publishing, Inc.)

structurally important role, by allowing unusual main chain conformations. This may explain why a high proportion of Gly residues in homologous protein sequences are conserved.

The simplest way to create a local ordered structure within a polypeptide chain made up of amide linkages would be to form hydrogen bonds between residues which are close to one another in the amino acid sequence. As seen from Figure 3.9, this would involve either the second, third, fourth, or fifth NH group from the $C=O$ of the first amino acid residue. In the 2.2₇ ribbon description, 2.2 refers to the number of residues per turn and the subscript 7 to the number of atoms between the main chain carbonyl oxygen and the amide

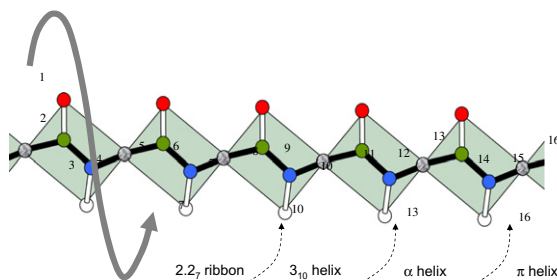


FIGURE 3.9 The hydrogen-bonding pattern of several polypeptide helices. The polypeptide chain is helically wound such that the $N-H$ group on residue n forms a hydrogen bond with the $C=O$ bond on residues $n - 2$, $n - 3$, $n - 4$ or $n - 5$.

hydrogen with which it forms the first hydrogen bond. In this description, the α -helix is a 3.6_{13} helix and the π -helix a 4.4_{16} helix.

On the basis of the observations described above, together with model-building studies, Pauling and Corey proposed two important structures, which they predicted would be found in proteins, namely the α -helix and β -pleated sheets (Eisenberg, 2003).⁶ In April 1948, when he was visiting professor in Oxford, confined to bed by a cold, Linus Pauling got fed up with reading detective stories. He called for paper, pencil, and ruler, and drew the way he thought a polypeptide chain would look on a sheet of paper. Then, by folding it through the alpha carbon atoms and bending it to form hydrogen bonds, he discovered the α -helix, where the ribbon hydrogen bonds dropped into place as straight lines of the right length (Judson, 1979). The α -helix has 3.6 residues per turn, with hydrogen bonds between the C=O of residue n and the NH of residue $n + 4$ (Figure 3.10), corresponding to the

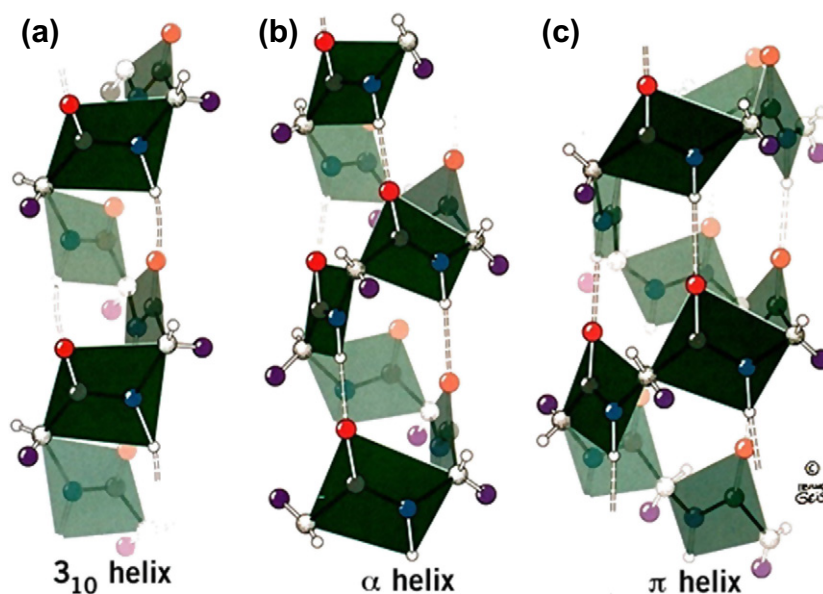


FIGURE 3.10 Comparison of the three helices which are found in proteins. (a) The 3_{10} helix, which has 3.0 peptide units per turn and a pitch of 0.6 nm, making it thinner and more elongated than the α -helix. (b) The α -helix, which has 3.6 peptide units per turn and a pitch of 0.54 nm. (c) The π -helix, which has 4.4 residues per turn and a pitch of 0.52 nm, making it wider and shorter than the α -helix. (From Voet & Voet, 2004. Reproduced with permission from John Wiley and Sons, Inc.)

allowed ϕ and ψ angles of 60° and -50° respectively. Although Pro cannot participate in hydrogen bonding, Pro residues do turn up in any of the first four positions in the first turn of α -helices (since the first hydrogen bond is between the C=O of the first and the NH of the fifth residue). When Pro does occur elsewhere in a helix, it usually produces a bend in the helix. Since the peptide unit has a dipole moment (due to the different polarity of NH and C=O groups), it follows that α -helices have a significant dipole moment, with a partial positive charge at the amino end and a partial negative charge at the carboxyl terminus. α -Helices can contain from 5 to over 40 residues, with an average length of around 10 residues. Two other helical structures are also found in proteins, the 3_{10} helix and the π -helix (Figure 3.10). The 3_{10} helix accounts for about 4% of amino acid secondary structures in proteins, compared to about 31% for the α -helix. It is often found as a single turn at the C-terminus of α -helices, enabling

6. To get an extraordinary insight into this discovery see Max Perutz's wonderful essay with the same title in his book "I wish I'd made you angry earlier" (Perutz, 2002).

the polypeptide chain to change direction. The right-handed π -helix with 4.4 residues per turn is of particular interest in metalloproteins, including the ferritin superfamily, nitrogenases, and the metal-inserting ferrocyclases of metalloporphyrin synthesis. In the π -helix, the N—H group of an amino acid forms a hydrogen bond with the C=O group of the amino acid *five* residues earlier; this repeated $i + 5 \rightarrow i$ hydrogen bonding defines the π -helix. π -helices appear to be derived by evolution from the insertion of a single residue into an α -helix. This newly discovered evolutionary origin explains not only why π -helices have been so rarely detected up to now, despite occurring in 15% of known proteins, but also why they tend to be associated with function (Cooley et al., 2010; Fodje and Al-Karadaghi, 2002).

The second structural element to be proposed by Pauling and Corey was the β -pleated sheet (Figure 3.11). These sheets are made up of β -strands, typically from 5 to 10 residues long, in an almost fully extended

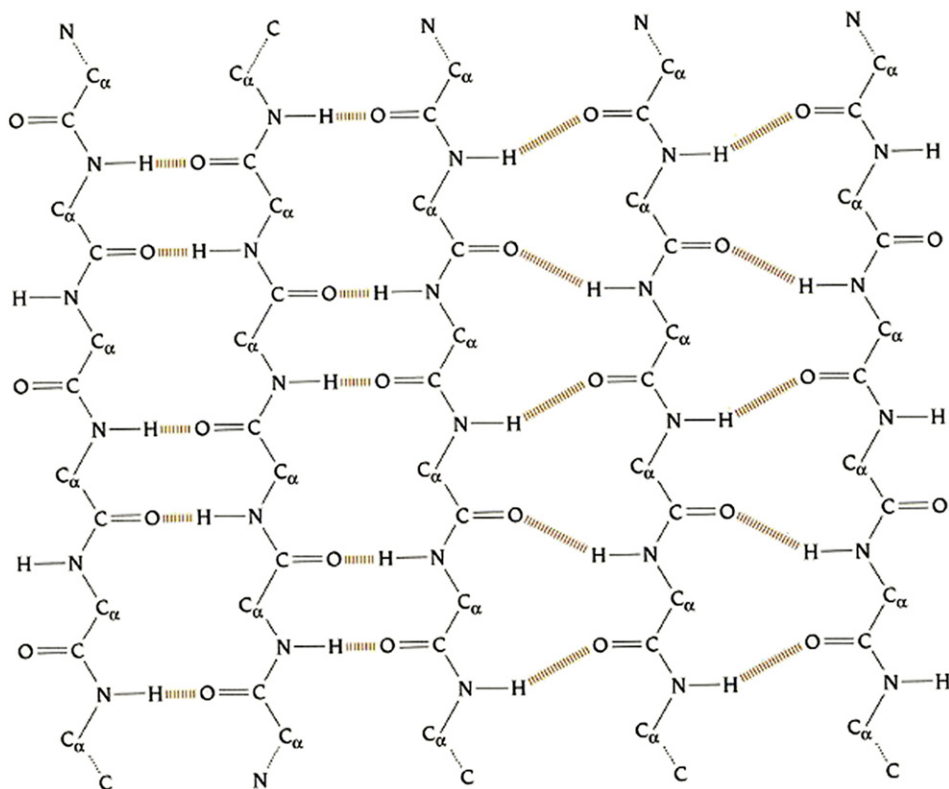


FIGURE 3.11 The hydrogen bonds between the β -strands in the mixed β -sheet of thioredoxin from *E. coli*. (From Branden and Tooze, 1991. Reproduced with permission from Garland Publishing, Inc.)

conformation, aligned alongside one another with hydrogen bonds formed between the C=O bonds of one strand and the NH of the other, and vice versa. The β -sheets are pleated (i.e., they undulate) with the C α atoms alternatively a little above, or a little below the plane of the β -sheet, which means that the side chains project alternatively above and below the plane. β -Strands can interact to form two types of pleated sheets:

- (i) Parallel β -pleated sheets (Figure 3.11), in which the polypeptide chains run in the same direction, have less stable hydrogen bonds than antiparallel β -sheets. This is reflected in the finding that parallel β -sheets of less than five strands are rare. However, the C α carbon atoms are all at the same distance, decreasing the

restrictions on the amino acid sequences which can take up this secondary structure. In contrast to antiparallel β -pleated sheets, which often involve contiguous amino acid sequences, parallel β -pleated sheets require a substantial number of amino acids to link the two parallel β -strands, and this is frequently furnished by an α -helix. The resulting β - α - β motif constitutes one of the frequently encountered supersecondary structures found in many proteins.

- (ii) Antiparallel β -pleated sheets (Figure 3.11), in which the polypeptide chains run in opposite directions. The hydrogen bonds are well oriented, but the C_α carbons occupy two distinct positions, one relatively close, one much further apart. This places important restrictions on the amino acid residues which can occupy the former positions (the principal protein of silk, fibroin, has a repetitive sequence GAGA(S) with the Gly residues in the close positions, and the Ala (or Ser) in the more distant ones⁷). Adjacent antiparallel β -sheets can be joined by hairpin loops (often referred to as β -bends) with a hydrogen bond between the $C=O$ of the first amino acid and the NH of the fourth, like 3_{10} helix turns, allowing the peptide to turn through 180° .

Because a single β -pleated sheet only exploits 50% of the potential hydrogen-bonding capacity of its partners, many strands, typically ranging from 4 or 5 to more than 10, come together to form a network of β -sheets. These β -sheets can be entirely parallel, exclusively antiparallel, or a mixture of both (Figure 3.11).

The association of secondary structures can give rise to so-called supersecondary structures, often referred to as folds, which frequently constitute compactly folded domains in globular proteins. They are presented in Figure 3.12

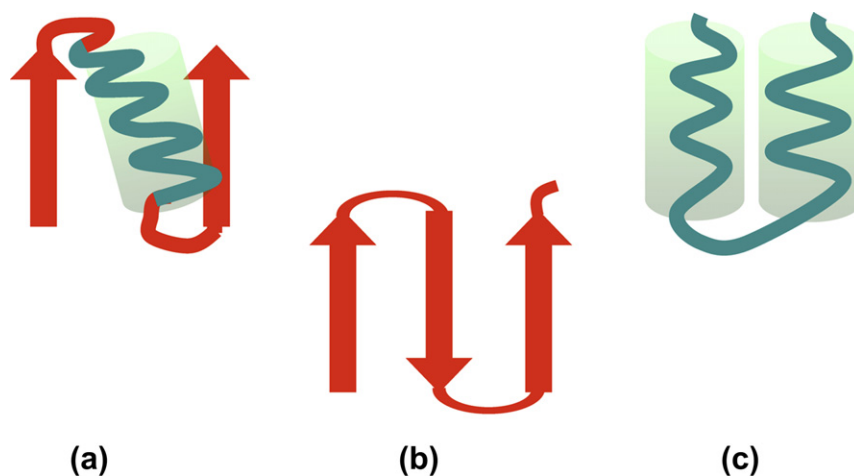


FIGURE 3.12 Supersecondary structures found in proteins: (a) β - α - β motif; (b) antiparallel β -sheets connected by hairpin loops; and (c) α - α motif.

and involve three motifs: (a) the β - α - β motif, in which an α -helix acts as a linker between two parallel β sheets, (b) antiparallel β sheets, often linked by the β -turns mentioned above, and (c) the α - α motifs, in which two α -helices are packed in an antiparallel fashion, with a short connecting loop. Examples of these three structural domains are illustrated in Figures 3.13–3.15. The schematic representation of the main chains of proteins introduced by Jane Richardson (Richardson, 1981) is used, with the polypeptide backbone represented by ribbons, α -helices as coils, and β -sheets as arrows pointing towards the C-terminus, joined by loops, usually on the outer surface of the protein. This enables the characteristic folds of proteins to be more easily identified than when all of the side chains are included.

7. When a gallant young man inadvertently puts his foot on the ball gown of his elegantly dressed partner, the ripping sound corresponds, in part at least, to the rupture of millions of hydrogen bonds.

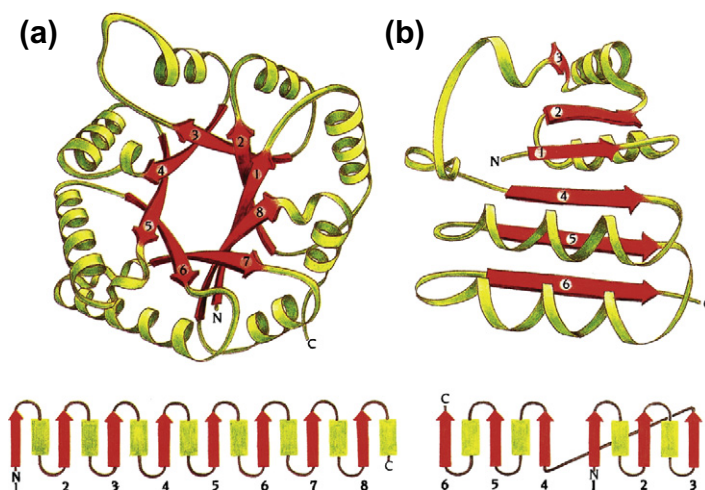


FIGURE 3.13 (a) Triose phosphate isomerase (TIM) has a β - α - β structure made up of 8 $\beta\alpha$ motifs terminating in a final α -helix, which form a barrel-like structure. (b) An open twisted β -sheet with helices on both sides, such as the coenzyme-binding domain of many dehydrogenases. (From Branden & Tooze, 1991. Reproduced with permission from Garland Publishing, Inc.)

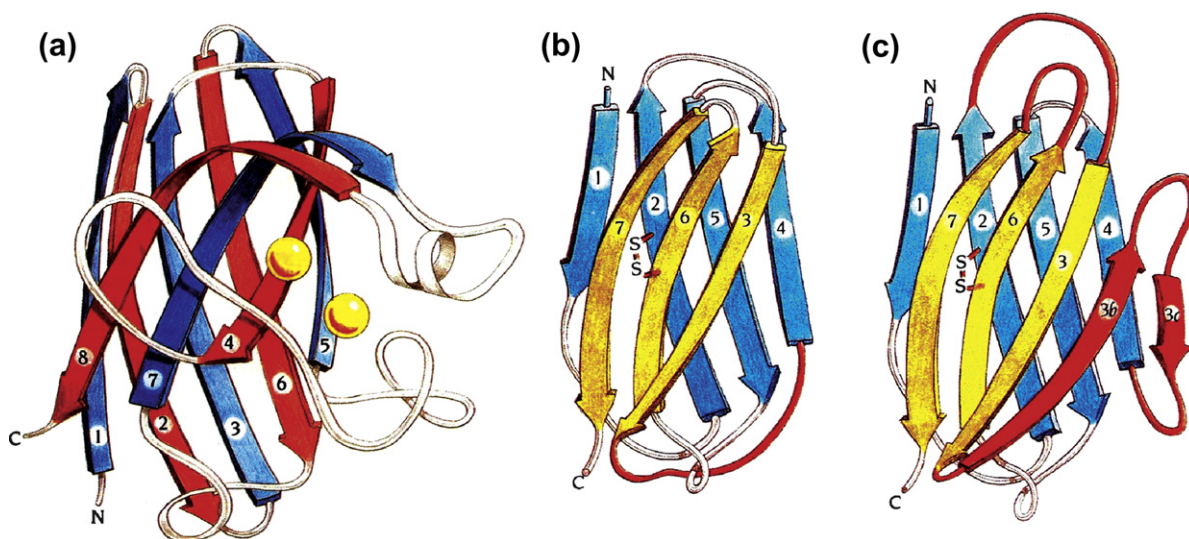


FIGURE 3.14 (a) The Cu-Zn superoxide dismutase is made up of eight antiparallel β -strands; both the constant (b) and variable (c) domains of immunoglobulins are made up of seven antiparallel β -strands with the same topology: the variable domain contains two additional β -strands. (From Branden & Tooze, 1991. Reproduced with permission from Garland Publishing, Inc.)

Triose phosphate isomerase (TIM), a 247-residue enzyme of the glycolytic pathway (Chapter 5), is an example of the first of the two main classes of α/β proteins, made up of β - α - β motifs. It consists of a core of eight twisted parallel β -strands, arranged close together to form a cylindrical structure, known as a β -barrel viewed in Figure 3.13a from the top. The β -strands are connected by α -helices, located on the outside of the β -barrel. This domain structure is often referred to as the TIM barrel, since it was first found in triose phosphate isomerase. In the topological representation at the bottom of the figure, the α -helices are represented by rectangles and the β -sheets as

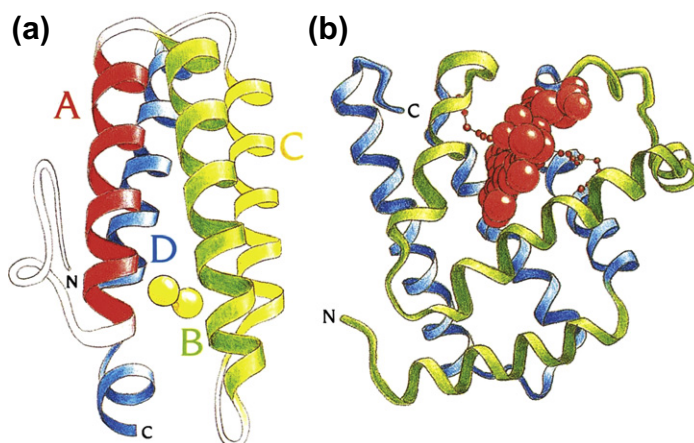


FIGURE 3.15 (a) Four helix bundle domain proteins, illustrated by myohaemerythrin. The oxygen-binding site is located at the di-iron centre within the hydrophobic core of the helical bundle. (b) The globin fold, represented here by myoglobin. (From *Branden & Tooze, 1991*. Reproduced with permission from Garland Publishing, Inc.)

arrows. The second class of α/β proteins contain an open twisted β -sheet surrounded by α -helices on both sides of the β -sheet. A typical example (Figure 3.13b) is the nucleotide-binding domain found in a number of dehydrogenases and kinases.

The second family of protein supersecondary structures, the antiparallel β -structures, represent a very diverse range of function, including enzymes, transport proteins, antibodies, and virus coat proteins. Their cores are built up of a number of β -strands, which can vary from four or five to over ten, arranged in such a way that they form two groups of β -sheets which are joined together and packed against each other to form a β -sandwich. The enzyme superoxide dismutase (Figure 3.14a) is made up of eight such antiparallel β -strands, arranged in such a way that they form two groups of β -sheets (colour-coded blue and red) which form the β -sandwich. When two such twisted β -sheets are packed together, they form a barrel-like structure. The immunoglobulins are a family of molecules which function in the molecular recognition of foreign antigens. Though they are made up of a large number of domains, most of them (12 out of 13 in immunoglobulin G, IgG) have the ancestral immunoglobulin fold (Figure 3.14b). In the constant domains of immunoglobulins, this consists of seven β -strands, with four strands forming one β -sheet and three strands forming a second sheet. The sheets are closely packed against each other and are joined by a disulfide bond between them. The variable domains (Figure 3.14c) have a very similar structure to the constant domains, but have nine β -strands instead of seven. The two additional strands are inserted in the loop region between strands 3 and 4 and are functionally important in that they contain one of the hypervariable regions (in red), which is placed close to the other two hypervariable domains. These three hypervariable regions together constitute the part of the immunoglobulin molecule, which determines its specificity in the recognition of antigens.

The simplest way to pack a pair of adjacent helices is to place them antiparallel to one another connected by a short loop. A frequently encountered domain structure in proteins is a bundle of four parallel and antiparallel helices with their long axes aligned around a central hydrophobic core. The helices are arranged in such a way that helices that are adjacent in the amino acid sequence are also adjacent in the three-dimensional structure. Side chains from all four helices are buried in the middle of the bundle, where they form a hydrophobic core. This is illustrated by myohaemerythrin (Figure 3.15a), a nonhaem oxygen transport protein found in marine worms.

Another important helical domain is the globin fold, found in the first protein for which the three-dimensional structure was determined, the oxygen storage protein, myoglobin (Figure 3.15b), from the muscle of the sperm

whale. The four globin chains of haemoglobin have a very similar three-dimensional structure to myoglobin. It later became apparent that oxygen-binding hemoproteins from invertebrate insect larvae (*Chironomus thummi*) and from the lamprey, a blood-sucking eel-like cyclostome (a subclass of jawless parasitic fish), also have the globin fold. The pairwise arrangements of the bundle of eight α -helices in the globin fold are quite different from that found in the four helix bundle domains. The helices, which vary in length from 7 (helix C) to 28 (helix H) residues, wrap around the core of the molecule, with its haem-binding pocket, such that most adjacent helices in the 3-D structure are not adjacent in the amino acid sequence.

The Structural Building Blocks of Nucleic Acids

Nucleic acids are made up of three components — nitrogen-rich bases of the pyrimidine and purine families, illustrated in [Figure 3.16](#) by the DNA bases adenine and guanine, and thymine and cytosine respectively, which are

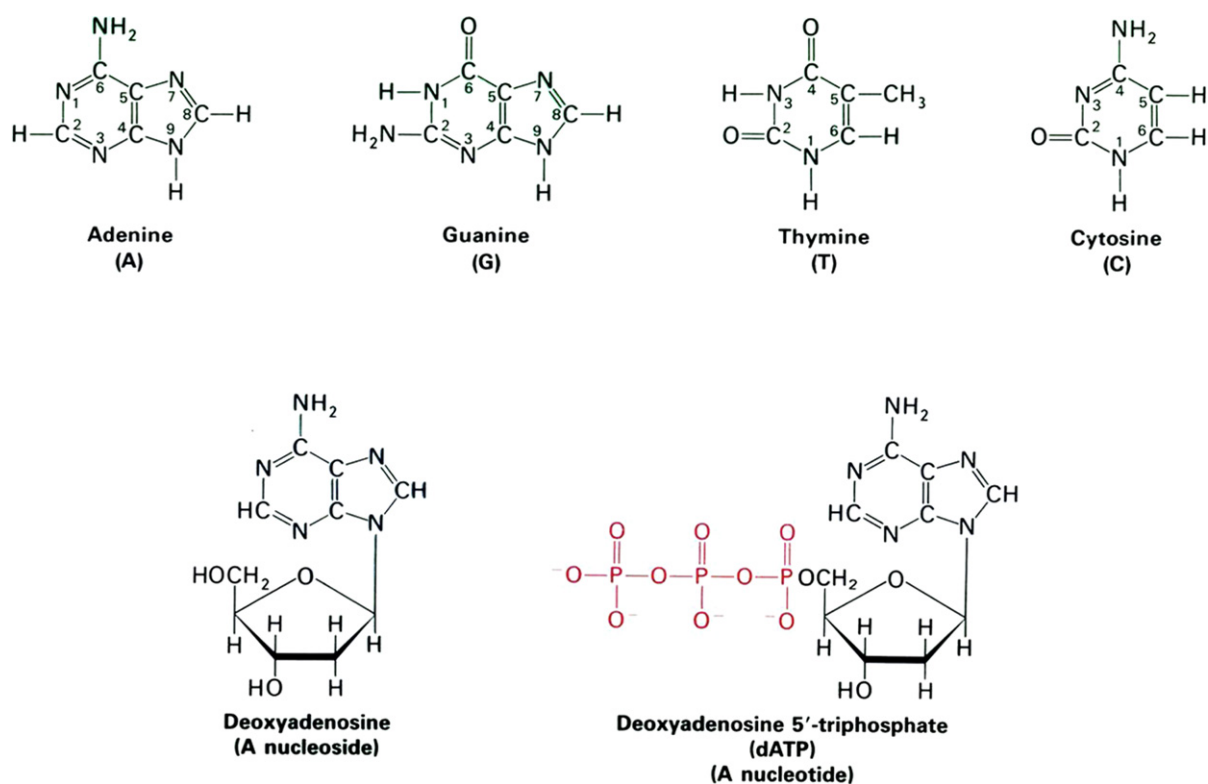


FIGURE 3.16 The structures of the four bases (A, G, T and C) found in DNA and of a nucleoside (deoxyadenosine) and a nucleotide (deoxyadenosine-5'-triphosphate).

linked in an N-glycosidic bond to a sugar (either ribose or deoxyribose in RNA and DNA respectively) and phosphate groups, which link the sugar residues. The combination of a nucleobase with a sugar generates a nucleoside — hence, adenine becomes deoxyadenosine when bound to deoxyribose, while a nucleobase plus a sugar plus one or more phosphate residues (usually on the 5'-hydroxyl of the ribose or deoxyribose) constitutes a nucleotide (in the example given, deoxyadenosine 5'-triphosphate).

In RNA, the base thymine (T) found in DNA is replaced by uracil, which is similar in structure to T, but lacks the methyl group. The nucleotides in nucleic acids are linked by phosphodiester bonds between the 3'-hydroxyl of one nucleoside and the 5'-hydroxyl of the sugar of its neighbour in the sequence, as was first shown by Alexander Todd⁸ in 1952 (Figure 3.17).

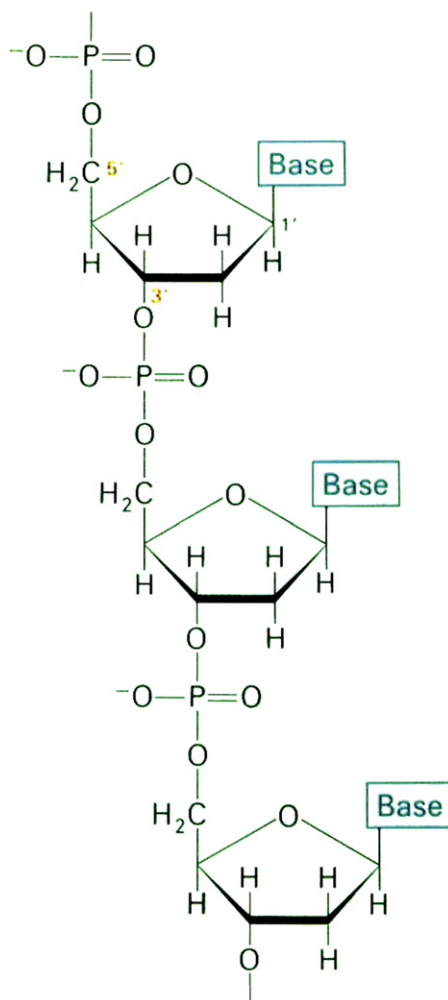


FIGURE 3.17 The structure of part of a molecule of DNA. The deoxyribose residues are linked by phosphodiester bonds between the 3'OH of one nucleoside and the 5'OH of the next.

SECONDARY AND TERTIARY STRUCTURES OF NUCLEIC ACIDS

An enormous kick-start to modern molecular biology was given by the seminal 1953 Nature paper of Francis Crick and Jim Watson on the double helical structure of DNA. It was based on two important observations.

8. Sir Alexander Todd, who won the 1957 Chemistry Nobel Prize was a former pupil of Allan Glen's school in Glasgow, where I also got my secondary education. He not only established the chemical structure of nucleic acids, but we owe to him our knowledge of the structures of FAD, ADP and ATP.

Firstly, the determination of the base composition of DNA from a number of sources had shown that while the overall base composition varied widely, there was always the same amount of A as of T, and the same amount of G as of C. Secondly, high-quality X-ray photographs of DNA fibres were consistent with a helical structure composed of either two or three polynucleotide chains. The major physiological form of the DNA double helix is the B-DNA described by the X-ray pictures of Rosalind Franklin,⁹ with 10 base pairs per turn (Figure 3.18),

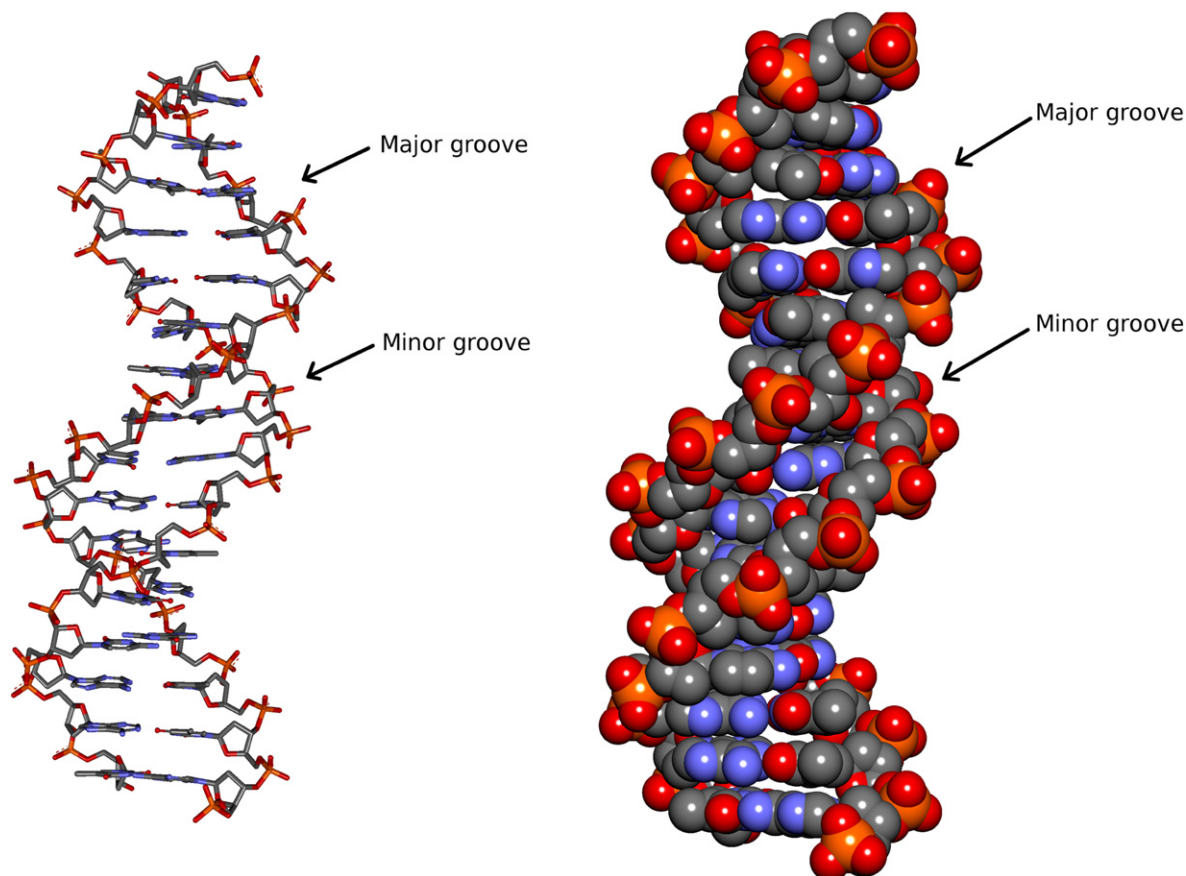


FIGURE 3.18 The B-form of the DNA double helix viewed along the helix axis in a ball and stick representation (left) and in a space-filling representation (right). The major and minor grooves are indicated.

each pair of bases separated by 0.34nm and by a helical twist of 36° per base pair, resulting in extensive interactions between the bases (often referred to as stacking). The purine and pyrimidine bases project into the interior of the helix, forming hydrogen bonds between A and T and between G and C (Figure 3.19), such that the helix has a solid core. The deoxyribose-phosphate backbone winds about the outside of the molecule, with the two sugar-phosphate chains running antiparallel to one another. As will become apparent later, when we consider regulation of genetic expression, this sugar-phosphate backbone constitutes the potential binding sites for proteins which, through their binding to DNA, will influence the expression of its genetic material. We can

9. Rosalind Fanklin took the X-ray photographs of DNA which were used by Watson and Crick in their prediction of the structure of DNA. She died of ovarian cancer in 1958.

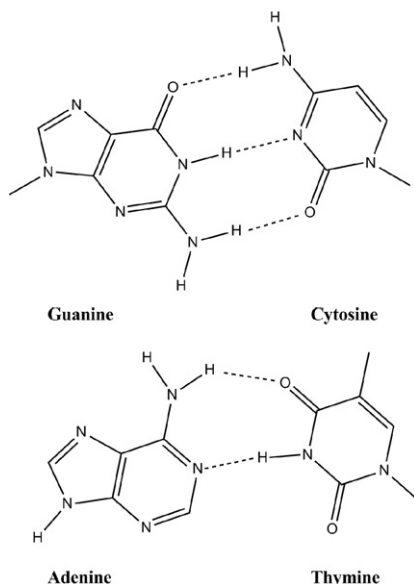


FIGURE 3.19 The classic Watson–Crick base pairing between A and T, and between G and C in DNA.

clearly distinguish (Figure 3.18) a much broader side of the DNA double helix, the so-called major groove, from the less accessible minor groove.

The DNA double helix is stabilised both by hydrophobic interactions between the bases (base stacking) and by hydrogen bonds between the A–T and G–C base pairs, and it can be reversibly dissociated into the individual strands by heating. This process is termed melting, and the melting temperature (T_m) is defined as the temperature at which half the helical structure is lost. The importance of hydrogen bonding in stabilising the double helical structure is underlined by the observation that G–C-rich DNA has a much higher T_m than A–T-rich DNA (G–C base pairs have three hydrogen bonds whereas A–T pairs have two).

While RNA molecules do not have the double-stranded structure usually found in DNA, many RNA molecules have stem-loop structures in which the antiparallel strands are connected by a 5–7 residue loop. Rather like the β -turn in proteins, this allows the polynucleotide chain to change direction by 180° . However, in addition to the classic base pairs (with U replacing T), a number of non-Watson–Crick base pairs are also found. This is particularly well illustrated by the structure of the first RNA molecule to have its three-dimensional structure determined – the transfer RNA encoding Phe (tRNA^{Phe}), which is presented in Figure 3.20. The striking feature of this structure is the optimisation of hydrogen-bonding interactions, many of them non-Watson–Crick, which ensures that the molecule attains the maximum degree of hydrogen bonding between bases. It is interesting to note that the anticodon (G_mAA) which interacts with the mRNA to correctly position Phe for incorporation into the appropriate protein is situated in the three-dimensional structure 8nm away from the Phe residue, bound to the 3'-OH of the tRNA (highlighted in red in the figure).

Whereas DNA is mostly located in the nucleus of cells in higher organisms (with some also in mitochondria and in plant chloroplasts), RNA has a much broader cellular distribution. RNA comes in three major and distinct forms, each of which plays a crucial role in protein biosynthesis in the ribosome, the intracellular organelle which is the site of protein biosynthesis. Ribosomal RNA (rRNA) represents two-thirds of the mass of the ribosome, messenger RNA (mRNA) encodes the information for the amino acid sequence of proteins, while transfer RNAs (tRNAs) serve as adaptor molecules, allowing the four-letter code of nucleic acids to be translated into the 20-letter code of proteins. The tRNA molecules contain a substantial number of modified bases, which are introduced by specific enzymes.

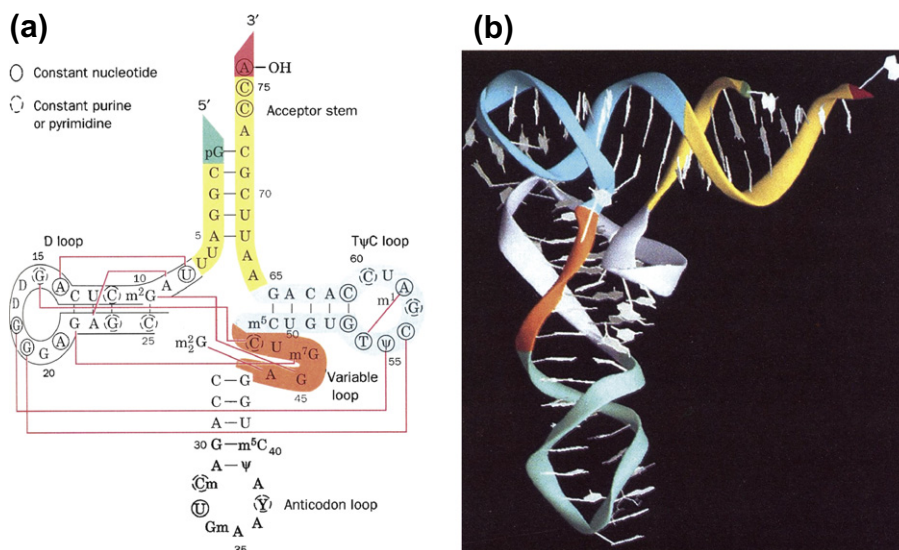


FIGURE 3.20 The structure of yeast tRNA^{Phe} (a) the cloverleaf form of the base sequence: tertiary base-pairing interactions are represented by thin red lines connecting the participating bases. Bases that are conserved in all tRNAs are circled by solid and dashed lines respectively. The different parts of the structure are colour-coded. (b) The X-ray structure showing how the different base-paired stems are arranged to form an L-shaped molecule. The sugar-phosphate backbone is represented as a ribbon with the same colour scheme as in (a). (From Voet & Voet, 2004. Reproduced with permission from John Wiley and Sons, Inc.)

Carbohydrates

Carbohydrates, so-called because they have the empirical formula $C_nH_{2n}O_n$, make up an important class of biomolecules. They are extensively used in the form of simple sugars (monosaccharides) in intermediary metabolism (Chapter 5), in polymer form (polysaccharides) as storage forms of both carbon and energy (such as polymers of glucose in the starch of plants and the glycogen of animals), and as structural elements (polymers of glucose in the cellulose of plant cell walls, and of N-acetylglucosamine in the chitin of invertebrate shells), or even attached to proteins and lipids in highly specific structure involved in biological recognition (like the blood group determinants).

We begin by describing very briefly the main classes of monosaccharides, together with some of the stereochemical properties which give them their particularity with regard to molecular recognition. If we stick with the definition of monosaccharides as $(CH_2O)_n$, it is clear that we need n to be at least 3 (three carbon ‘oses’, or sugars called trioses), and we must have one of the carbons at the level of oxidation of an aldehyde or ketone — as illustrated (Figure 3.21) by the structure of the two trioses, glyceraldehyde (an aldose), and dihydroxyacetone (a ketose). These two molecules are isomers of one another, and can be interconverted by enzymes called isomerases. We note an important point in addition, namely, that the hydroxyl group on the central carbon of glyceraldehyde can be either on the right or on the left side of the central carbon chain. In fact, most sugars (with the exception of the sugar acid ascorbic acid, better known as vitamin C) have the hydroxyl furthest away from their potential reducing function (the aldehyde or ketone group) to the right, and are therefore called D-sugars. We will not fatigue the reader with the niceties of the structures of the different aldo- and keto-tetroses, pentoses, hexoses, etc., but simply illustrate a few more, all of which play an important role in metabolism, often in a phosphorylated form — D-ribose, D-galactose, and D-glucose (aldoses and D-fructose (ketose)). We illustrate our next important point with glucose (an aldohexose), which can exist in a cyclic form by ring closure between the aldehyde function and the hydroxyl function on carbon 5 — this forms what is called a hemiacetal, and when the

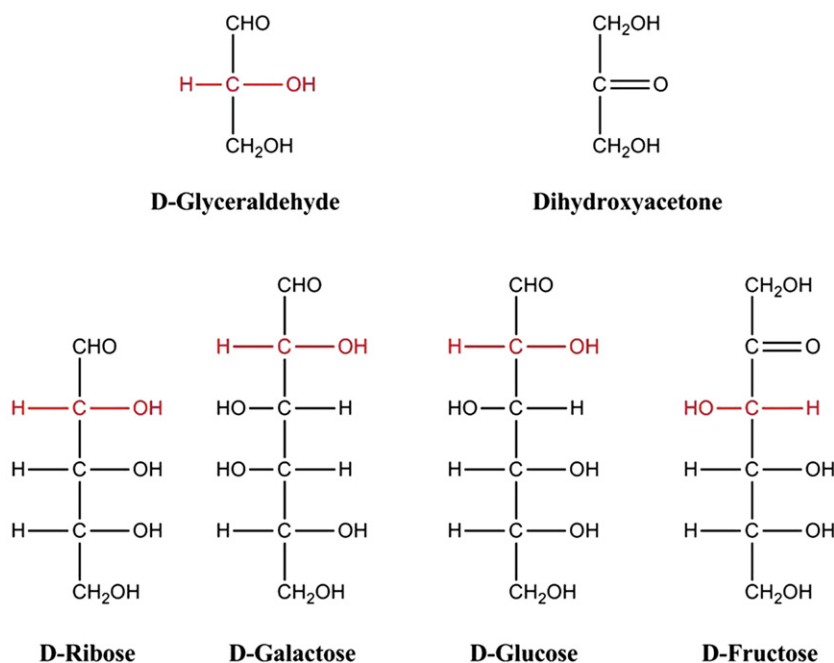


FIGURE 3.21 The trioses D-glyceraldehyde (aldose) and dihydroxyacetone (ketose), the pentose D-ribose, the hexoses D-galactose and D-glucose (aldoses), and the ketohexose D-fructose in their open chain forms. The configuration of the asymmetrical hydroxyl group on the carbon the furthest away from the aldehyde or ketone group determines the assignment of D- or L-configuration.

same thing happens with a ketone, as in fructose, we form a hemiketal (Figure 3.22). The name is less important than the consequence — the product now has an asymmetric carbon atom such that that carbon 1 of glucose in the cyclic form can have its hydroxyl group either below the plane of the ring (α -D-glucose) or above it (β -D-glucose). These two forms are known as anomers, and carbon 1 is the anomeric carbon. This has profound effects, as we will see shortly, when we form links between two sugar residues (contrast the vastly different physical properties of starch and cellulose). Of the sugars represented in Figure 3.21, ribose, fructose, and galactose can, and will, like glucose, form cyclic forms which are the most stable structures in aqueous solution. Finally, we must distinguish between glucose and galactose, which have a different configuration of the hydroxyl group on carbon 4 — these are epimers. Many of the monosaccharides described here will be found in metabolic pathways, often phosphorylated. Other biologically important sugar derivatives include deoxy sugars, like β -D-2-deoxyribose in DNA, and amino sugars, like N-acetylglucosamine, where the hydroxyl on carbon 2 is replaced by an acetylated amino group, as in chitin.

When two sugars are linked together, a glycosidic bond is formed between them (Figure 3.23), which is illustrated by the very Belgian disaccharide,¹⁰ maltose derived from starch hydrolysis. Here, the two glucose molecules are linked by an α -glycosidic linkage (α -1–4) between the aldehyde group of one glucose molecule and the hydroxyl of carbon 4 of the other, in its α -configuration. Contrast this with cellobiose, the principal

10. A map of France dating from the late 1800s, which I bought a few years ago, had a small part of Belgium intruding at the northern extremities, described as ‘kingdom of beer drinkers’. The major substrate for beer production is the disaccharide maltose, produced by partial hydrolysis of starch in the preparation of the malt, prior to addition of the yeast which then ferments the sugars to ethanol. Since Belgian beers are a major cultural and economic heritage (and in my humble opinion among some of the best in the world), maltose is a good candidate for the national sugar.

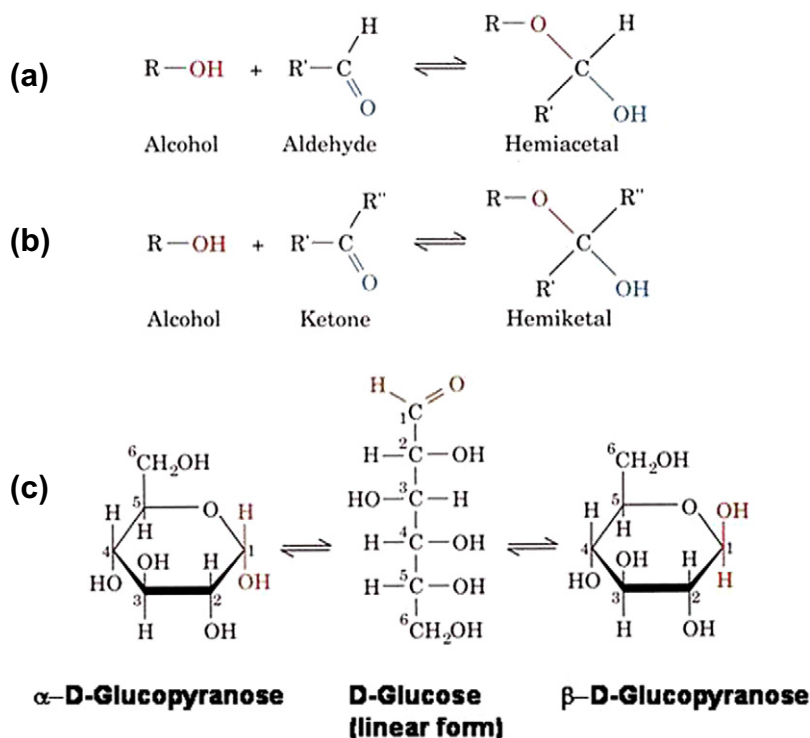


FIGURE 3.22 The reaction of alcohols with aldehydes (a) and ketones (b) to form hemiacetals and hemiketals. (c) The reaction between the alcohol on carbon 5 and the aldehyde of glucose forms two hemiacetals, α -D-glucopyranose and β -D-glucopyranose (pyranose by comparison with pyran, the simplest compound containing this six-membered ring).

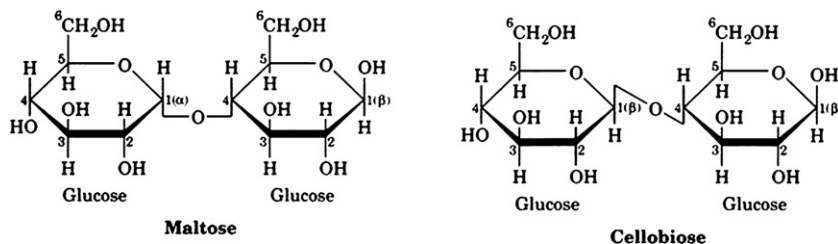


FIGURE 3.23 The structures of the disaccharides maltose and cellobiose, derived from the hydrolysis of starch and cellulose, respectively.

disaccharide derived from hydrolysis of cellulose, which has a β -1–4 linkage between the two glucose molecules (Figure 3.23).

There are two main classes of polysaccharides — those which are used as stores of energy and carbon like glycogen and starch, and structural polysaccharides like cellulose. Starch, the principal-storage polysaccharide of plants, is a mixture of the linear α (1–4)-linked polyglucose α -amylose, and amylopectin which, although having mostly amylose-like α (1–4)-linkages, also has α (1–6)-branches every 24–30 glucose residues. Glycogen, the storage polysaccharide of animals, is found predominantly as hydrated cytoplasmic granules in tissues like liver and muscle, which contain up to 120,000 glucose units. It has a structure similar to amylopectin, but with

$\alpha(1-6)$ -ramifications every 8–14 residues (Figure 3.24), which allows its rapid degradation to simultaneously release glucose units from the end of each branch point.

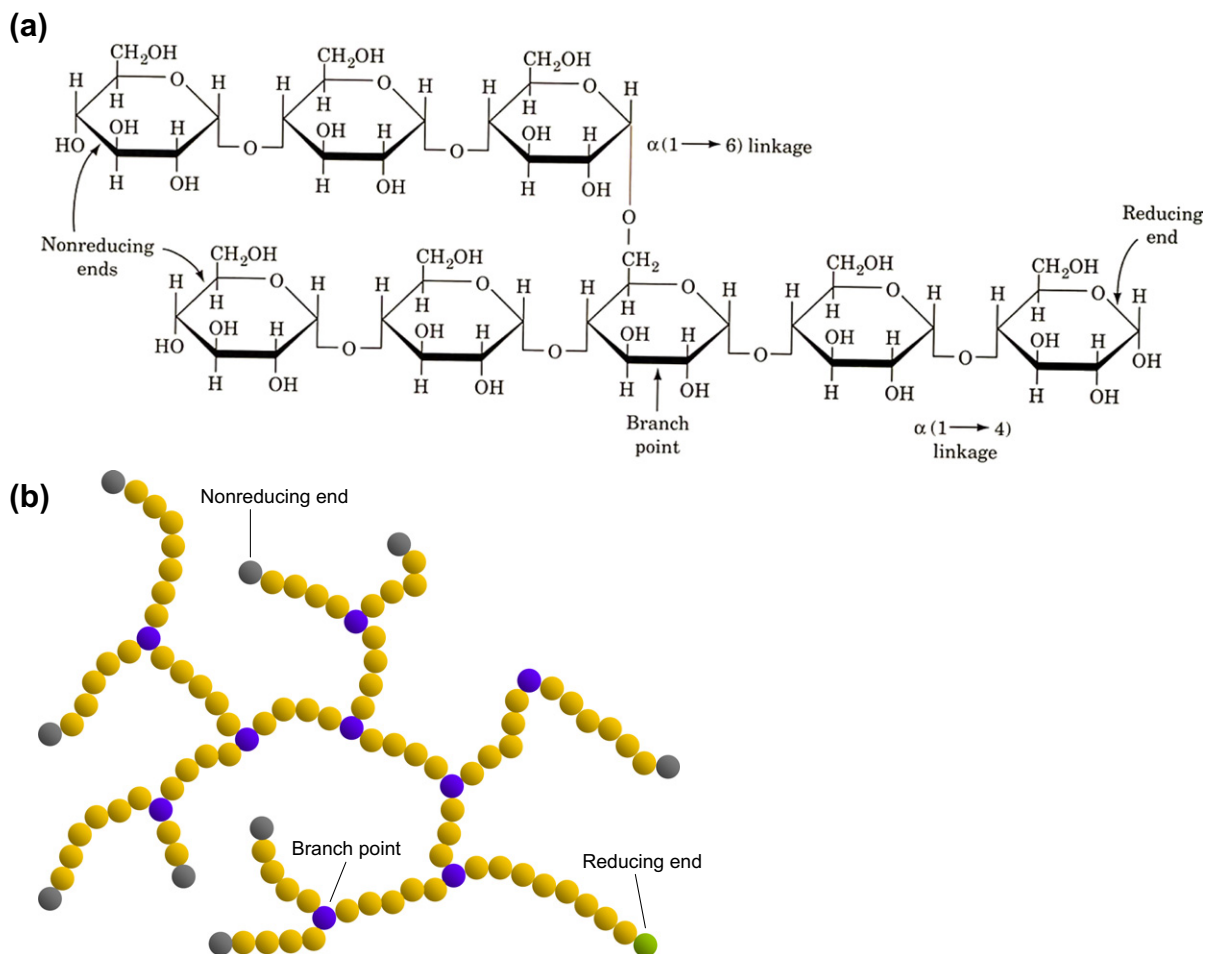


FIGURE 3.24 (a) Molecular structure of glycogen (the polyglucose chain in the actual molecule are, of course, much longer); (b) Schematic diagram showing the branched structure: note that while there is only one reducing end, there are multiple nonreducing ends from which glucose units can be released.

Cellulose represents the major structural component of plant cell walls — around 10^{15} kg of cellulose, half of the carbon in the biosphere, is synthesised (and degraded) annually. In contrast to the storage polysaccharides, it is a glucose polymer linked exclusively by $\beta(1-4)$ glycosidic bonds, typically with up to 15,000 glucose residues. In contrast (Figure 3.25) to the extensively $\alpha(1-4)$ structure of starch and glycogen, which have bent structures, more accessible to hydration (as in the glycogen storage granules mentioned earlier), the $\beta(1-4)$ linkages of cellulose favour long straight chains. These can form fibrils of parallel chains, which interact with one another through a hydrogen-bonding network. So, a simple change in the configuration of a glycosidic bond can produce spectacular differences between a hydrated granular store of energy and a major component of vegetable cell walls, which, for example in trees, must ensure a considerable role in load bearing. When we turn to the shell of crustaceans like the lobster, which have a polymer composed of N-acetylglucosamine in a $\beta(1-4)$ linkage, the changes in the properties are remarkable.

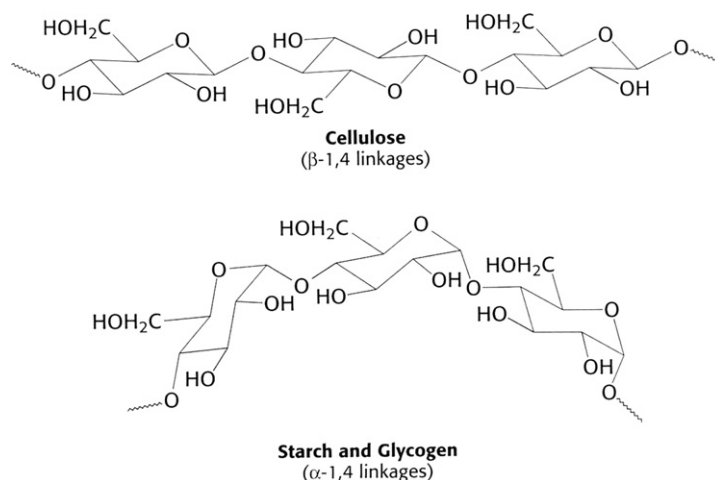


FIGURE 3.25 An illustration of how the configuration of glycosidic bonds determine polysaccharide structure and function. The β -1—4 linkages in cellulose favour straight chains, optimal for structural purposes, whereas the α -1—4 linkages are favourable to bent structures, better adapted to storage in a hydrated form.

Lipids and Biological Membranes

Lipids¹¹ are fat-soluble molecules, unlike the other biological macromolecules we have described up to now, which are all water-soluble — in addition, they are **not** macromolecules, but of relatively low molecular weight. With the exception of a class of lipids (for reasons of Commissions of Nomenclature¹² known as simple lipids, despite the organic complexity of their structures — they include steroids, isoprenoids, etc.), they are complex lipids. By definition, they are saponifiable; in other words, upon treatment with an alkali, they produce a soap, containing an alcohol, classically glycerol, and other products, usually fatty acids. Fatty acids typically have an even number of carbon atoms (reflecting their synthesis from acetyl CoA, Chapter 5), often 16 or 18 and may be saturated, like stearic acid (mp 69.6 °C) or have one (or more) double bonds, like oleic acid (mp 13.4 °C) (Figure 3.26a). However, the important message to get across here is that the properties of the lipid will be determined by the nature of the fatty acids that it contains. A simple example from everyday life is the difference between lard (animal fat) and olive oil. Lard, at 20 °C is solid, yet olive oil at the same temperature, is liquid — why? Both are triglycerides (Figure 3.26b), but whereas the former consists of glycerol esterified to three molecules of saturated fatty acids (typically stearic acid), in the latter, glycerol is esterified to three molecules of oleic acid, with a single double bond. Triglycerides are a very efficient reservoir of energy resources, not only because they can produce twice as much energy/g than carbohydrates or proteins, but also because they can be stored in an anhydrous form. This is in marked contrast to glycogen, which binds about twice its weight in water. Animals have cells which are specialised in the synthesis and storage of triglycerides, adipocytes, with the fat globules occupying almost the entire cell.

Having established that the simplest ‘complex’ lipid is a triglyceride, we pass to the biological properties of phospholipids which combine the fat-soluble properties of the triglyceride with the addition of a polar, charged group on one of the glycerol hydroxyl functions (Figure 3.26c). Several alcohols are found in phospholipids, but we consider here the glycerophospholipids. The polar head group is made up of a phosphate group, attached to

11. From Greek *lipos* — fat.

12. There are two classes of sins — those of omission and of commission. When it comes to scientific nomenclature, these are clearly sins of Commission!

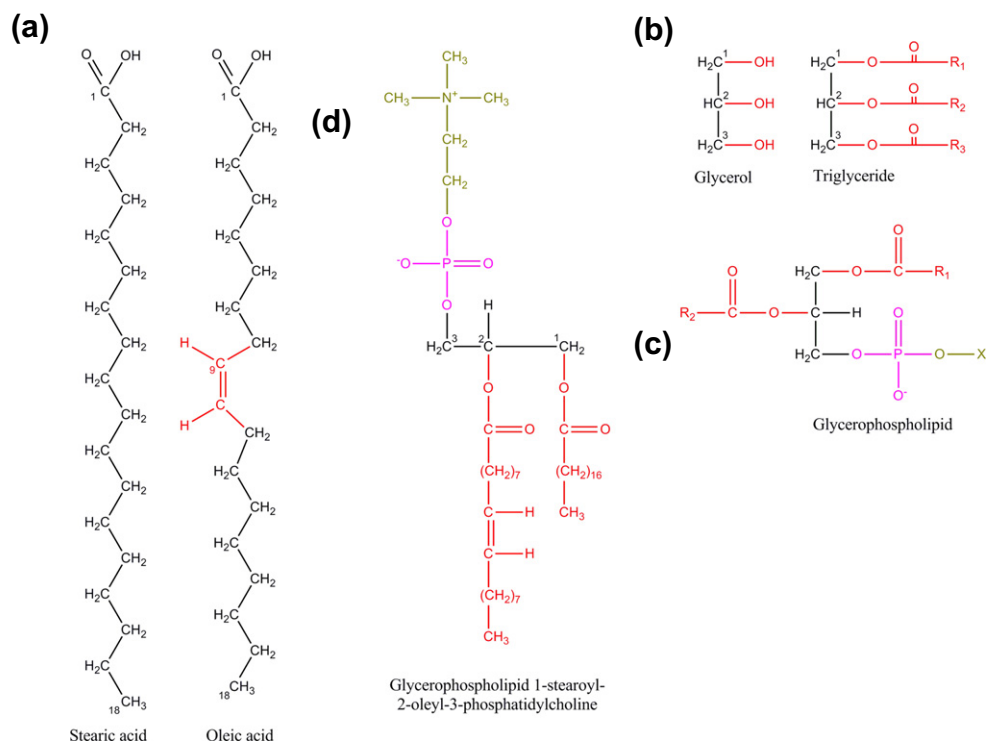


FIGURE 3.26 (a) Stearic and oleic acid, (b) glycerol and a triglyceride, (c) the general structure of a glycerophospholipid, and (d) the glycerophospholipid 1-stearoyl-2-oleyl-3-phosphatidylcholine.

a diglyceride (this constitutes a phosphatidic acid) to which a polar alcohol is esterified. The alcohol may be ethanolamine, choline (as in Figure 3.26d), serine, inositol, etc., and the resulting families of phospholipids are called phosphatidyl ethanolamine, phosphatidyl choline, etc. What we have is an **amphiphilic** molecule, which will bury its hydrophobic component in a nonaqueous environment and maintain its polar head group in contact with water. Such molecules will spontaneously form monomolecular layers on the surface of water and will readily form bimolecular layers in aqueous solution. An important feature of lipid bilayers is that they have an inherent capacity to close on themselves, leaving no hydrocarbon chains exposed, forming compartments and are self-sealing, because a hole in the lipid bilayer would be energetically very unfavourable. This is the basis for biological membranes in which the amphiphilic phospholipids form a double bilayer of hydrophobic fatty acid side chains, excluding water within the bilayer, but yet exposing the polar head groups on either side of the bilayer to the aqueous milieu. The driving force for the self-assembly of lipid bilayers is what we often call the ‘hydrophobic effect’, i.e., predominantly nonpolar parts of biological molecules seek environments in which they are close to other similar molecules, forming a hydrophobic core. Hydrophobic interactions, as we have seen, also play a dominant role in the folding of proteins, creating their hydrophobic cores, and in the stacking of bases in nucleic acids.

However, lipid bilayers are impermeable to ions and most polar molecules, with the exception of water, so they cannot, on their own, confer the multiple dynamic processes which we see in the function of biological membranes. All of this comes from proteins, inserted into the essentially inert backbone of the phospholipid bilayer (Figure 3.27), which mediate the multiple functions which we associate with biological membranes, such as molecular recognition by receptors, transport via pumps and channels, energy transduction, enzymes, and many more. Biomembranes are noncovalent assemblies of proteins and lipids, which can best be described as a fluid matrix, in which lipid (and protein molecules) can diffuse rapidly in the plane of the membrane, but not across it.

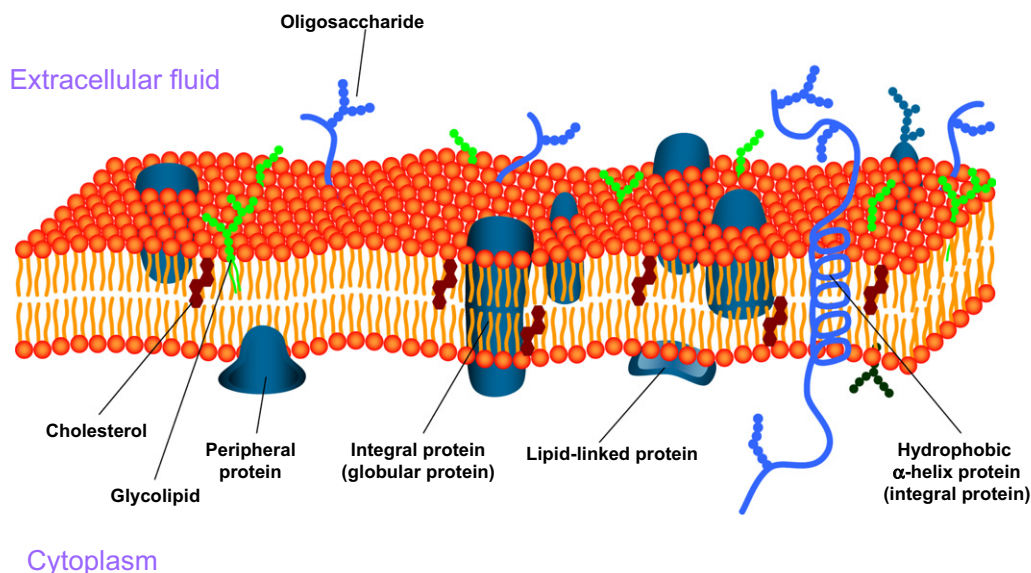


FIGURE 3.27 Schematic diagram of a plasma membrane. (Adapted from Voet & Voet, 2004.)

Biological membranes can therefore be considered as two-dimensional solutions of oriented lipids into which proteins are selectively inserted, either as integral membrane proteins, which traverse the entire bilipid layer, or as peripheral proteins, associated with one face of the membrane, where they may be bound covalently by a glycolipid linkage. Biological membranes are asymmetric: in the case of the plasma membrane, it will often have carbohydrates in the form of oligosaccharides or glycolipids exposed at the outer side of the membrane. Finally, we should point out that, in animal cells, the part of the protein which traverses the hydrophobic phospholipid membrane, is frequently a hydrophobic α -helix, some 20–30 residues long.

A Brief Overview of Molecular Biology

For historical reasons, that part of biochemistry which deals with the two-dimensional transfer of genetic information, from the four-letter code of DNA and RNA to the 20-letter code of proteins, has often been referred to as molecular biology.¹³ There is little doubt that the recent advances in genome sequencing and the extensive use of gene arrays to detect changes in gene expression have heightened the popular impression that molecular biology in this narrow definition can solve all of the problems. It cannot, and will not, without the much more time and labour-consuming tasks of purifying and characterising the proteins which the genome encodes. Unfortunately, the information contained in the DNA sequence of a gene does not allow us to predict its structure (unless it happens to be homologous to another protein of known structure), far less its biological function. Nonetheless, the tools of molecular biology are sufficiently important for the practice of modern biochemistry that we need to know about them. We begin by what has often been termed the central dogma of molecular biology. The replication of DNA generates two identical daughter molecules. Transcription incorporates some of the information contained therein into RNA, and the ribosome then converts this into the amino acid sequence of the corresponding protein by a process called translation.

13. A brief look at the contents page of any recent issue of the *Journal of Molecular Biology* (founded by John Kendrew, protein crystallographer and winner of the Nobel prize for Chemistry together with Max Perutz for the 3-dimensional structures of myoglobin and haemoglobin) will clearly establish that this is not so!

Replication

At the end of their classic 1953 paper, Watson and Crick wrote ‘It has not escaped our notice that the specific pairing we have postulated immediately suggests a possible copying mechanism for the genetic material’ (Watson and Crick, 1953). This may seem, with hindsight, fairly obvious. There is little doubt that DNA polymerases, the enzymes which synthesise DNA, do place the correct base in the daughter strand of newly synthesised DNA (Figure 3.28) by classic Watson–Crick base-pairing. DNA polymerase assembles the new DNA chain directly on

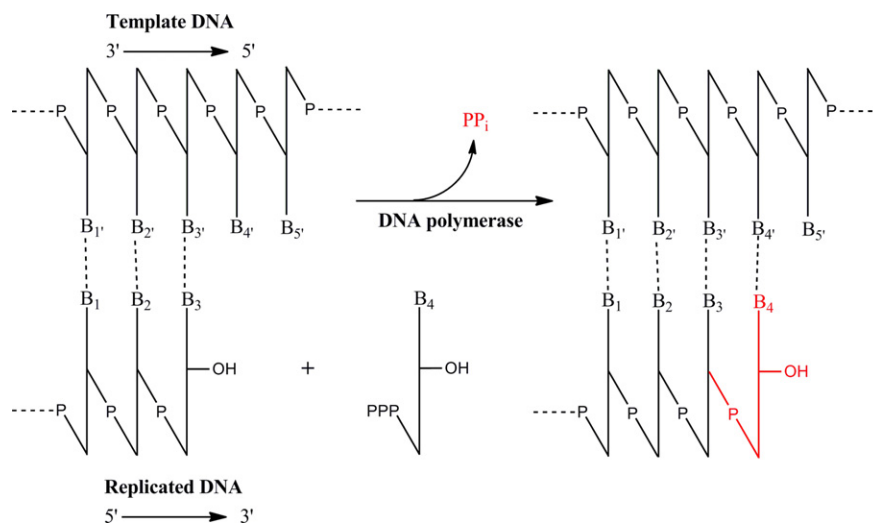
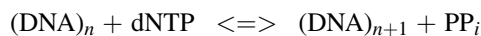


FIGURE 3.28 The global reaction catalysed by DNA polymerase.

a preexisting DNA template, using a primer strand with a free 3'-hydroxyl group. The reaction involves a nucleophilic attack by the 3'-hydroxyl group of the primer on the α -P atom of the deoxynucleoside triphosphate. Formation of the phosphodiester bridge is accompanied by the release of pyrophosphate



Like all enzymes with nucleoside triphosphate substrates, DNA and RNA polymerases are metalloenzymes and typically require two metal ions (usually Mg^{2+}). As we illustrate in Figure 3.29, one metal ion binds both the α -phosphoryl group of the nucleoside triphosphate (NTP) and the 3'-hydroxyl group of the primer, whereas the other coordinates only with the 3'-hydroxyl group. The two metal ions are bridged by the carboxylate groups of two aspartate residues which hold the metal ions in the correct orientation. The metal ion bound to the primer activates the 3'-hydroxyl group, facilitating its attack on the α -phosphoryl group of the NTP in the active site. Both metal ions help to stabilise the negative charge on the pentacoordinate transition state, illustrated in Figure 3.29b for RNA polymerase, while the metal ion bound to dNTP stabilises the negative charge on the pyrophosphate product.

However to make things a whole lot more complicated, the two strands of the DNA molecule are antiparallel, yet only one site of replication is visible by low-resolution techniques, like electron microscopy during the replication of double-stranded DNA, at what is known as the replication fork (Figure 3.30a). There is no way that DNA polymerase can synthesise one strand of DNA in the way which is illustrated in Figs 3.28/3.29 and simultaneously synthesise the other strand in the opposite direction, (which logically would have a 5'-phosphate at its

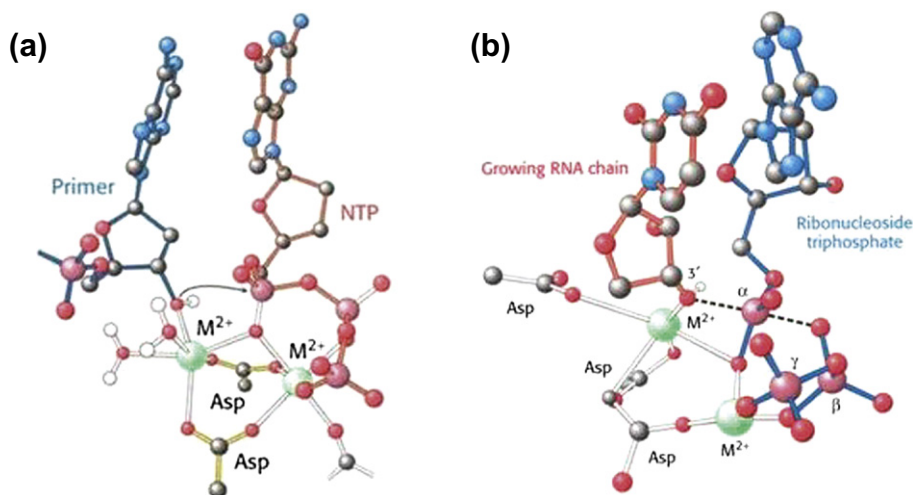


FIGURE 3.29 (a) DNA polymerase catalysed phosphodiester bond formation typically requires two metal ions, usually Mg^{2+} . (b) A model of the transition state for phosphodiester-bond formation in RNA polymerase. (From Berg, Tymoczko & Stryer, 2002. Reproduced with permission from W.H. Freeman and Co.)

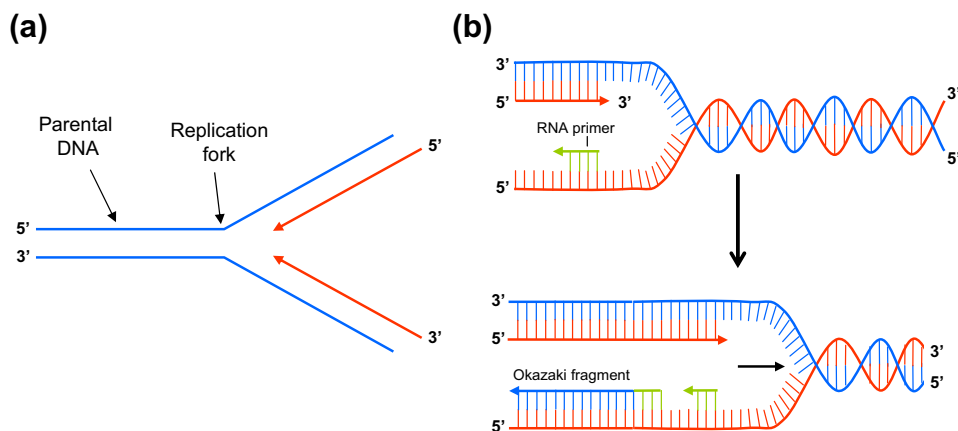


FIGURE 3.30 (a) DNA replication at low resolution (as seen for example by electron microscopy). Only one replication fork is visible and it appears that both strands of the parental DNA replicate continuously in the same direction, which cannot be the case, since the two strands of parental DNA are antiparallel. (b) The problem is solved by the priming of DNA synthesis with short RNA primers, whose 3'-hydroxyl can be used by DNA polymerase, producing Okazaki fragments, while on the other strand, DNA synthesis is continuous.

terminus rather than what the enzyme actually requires, namely a 3'-hydroxyl). This problem is solved by the semi-discontinuous replication of DNA, in which both daughter strands are synthesised in the required $5' \rightarrow 3'$ direction. However, this requires the introduction on the strand which lacks a 3'-hydroxyl, of short RNA primers (synthesised by yet another protein, primase), whose 3'-hydroxyl can then be used to synthesise DNA in the opposite direction to that of DNA replication on the other, so-called 'leading strand', which always has a 3'-hydroxyl available for the polymerase, so that DNA is synthesised continuously (Figure 3.30b). On the 'lagging strand', DNA synthesis

on the 3'-hydroxyl of the short RNA primer produces short DNA fragments, each starting from an RNA primer, called Okazaki¹⁴ fragments (in eukaryotes, these consist of only 100–200 nucleotides, while in prokaryotes, they are much longer). The primer RNA is then excised, and replaced by DNA through a second DNA polymerase, which can remove RNA from one Okazaki fragment while replacing it by DNA on a neighbouring fragment. Once their RNA has been replaced by DNA, the Okazaki fragments on the lagging strand are joined together by a DNA ligase.

Transcription

Whereas in the process of replication, DNA polymerase replicates the entire DNA molecule, in the process of transcription, RNA polymerases synthesise an RNA molecule which has a sequence complementary to a small fragment of one of the two strands of DNA (the coding strand). The reaction which they catalyse, illustrated by a model of the transition state for RNA polymerase (Figure 3.29b), is similar to that catalysed by DNA polymerase. However, unlike DNA polymerase which has but one site on the entire DNA molecule to initiate DNA synthesis, RNA polymerases search the DNA for initiation sites (called promoters) – the 4.8×10^6 base-pair genome of *E. coli* has about 2000 promoters. RNA polymerases rely upon protein subunits called σ (sigma) factors to recognise promoter sites by gliding rapidly along the DNA duplex until they find a promoter, binding to it, and initiating RNA synthesis. The σ -factor is then released, allowing the core polymerase to continue synthesising until it encounters a termination signal, whereupon it releases the newly synthesised RNA, binds to a σ factor, and goes off in search of a new promoter.

Often, RNA molecules undergo 'maturation' after their synthesis by the polymerase, referred to as post-transcriptional processing, involving both excision of nucleotides and chemical modification. For example, tRNAs undergo extensive processing (Figure 3.31). In the case of the tRNA^{Tyr} of yeast, this includes the excision of a 19-residue 5'-terminal sequence and a 14-nucleotide intervening sequence from the primary transcript, addition of a –CCA to the 3'-terminus, and extensive modification of a number of bases to form the mature tRNA. This includes transformation of uridines into pseudouridine (ψ), dihydrouridine (D), and thymine. Yet another series of post-transcriptional modifications, of great importance in eukaryote mRNAs (Figure 3.32), includes the addition of a 5' cap, which defines the start site for translation of the mRNA (see next section), addition of a 3' poly(A) tail and splicing. Genes of eukaryotes, unlike prokaryotes, have their coding sequences (exons) interspersed with noncoding intervening sequences (introns). The lengths of the introns typically represent four to ten times that of the exons. Thus, the primary transcripts of eukaryotic mRNAs must not only have caps and tails attached, but the noncoding introns must be excised and the exons joined up to form the mature mRNA, corresponding to the amino acid sequence of the protein. This process is known as gene splicing and clearly must be carried out with absolute precision – a one-nucleotide error in splicing would shift the reading frame of the mRNA and lead to an entirely different amino acid sequence. The splicing of eukaryotic mRNAs requires the cooperation of a number of small nuclear RNAs and proteins which form a large complex called a spliceosome.

Translation

Translation, the biosynthesis of proteins, involves passing from the four-letter code of mRNA into the 20-letter code of proteins. It is clear that with 20 different amino acids in proteins, for translation to occur, we require a triplet code, with three nucleic acid bases (codons) encoding for one amino acid. This means that the genetic code, as it is called, consists of 64 codons. It is therefore degenerate, i.e., most amino acids have more than one codon. The genetic code is read, not by specific recognition of codons by individual amino acids themselves, but rather by the selective binding of amino acids to adaptor molecules, as first postulated by Francis Crick in 1955 (Figure 3.33). These adaptors, called transfer RNAs (tRNAs), then recognise the corresponding codon on the

14. Reiji Okazaki showed that when replicating *E. coli* are labelled for short periods of time with precursors of DNA, some of the newly synthesised DNA is recovered as small fragments of 1000 to 2000 nucleotides long, which are subsequently incorporated into double-stranded DNA.

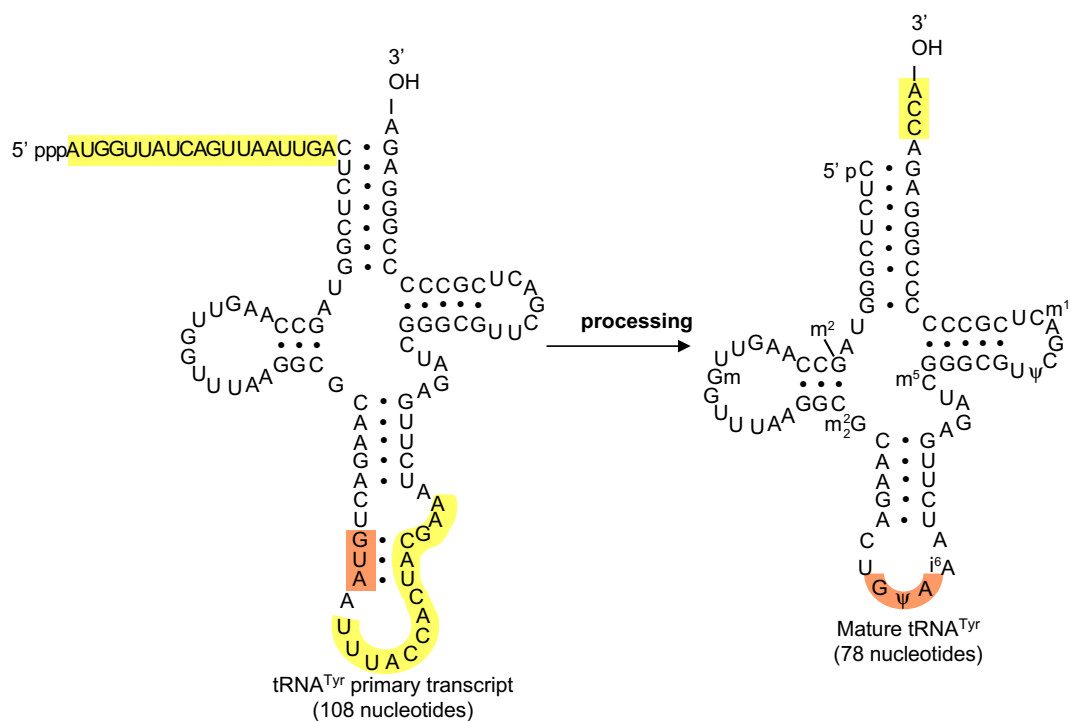


FIGURE 3.31 The post-transcriptional processing of yeast tRNA^{Tyr}.

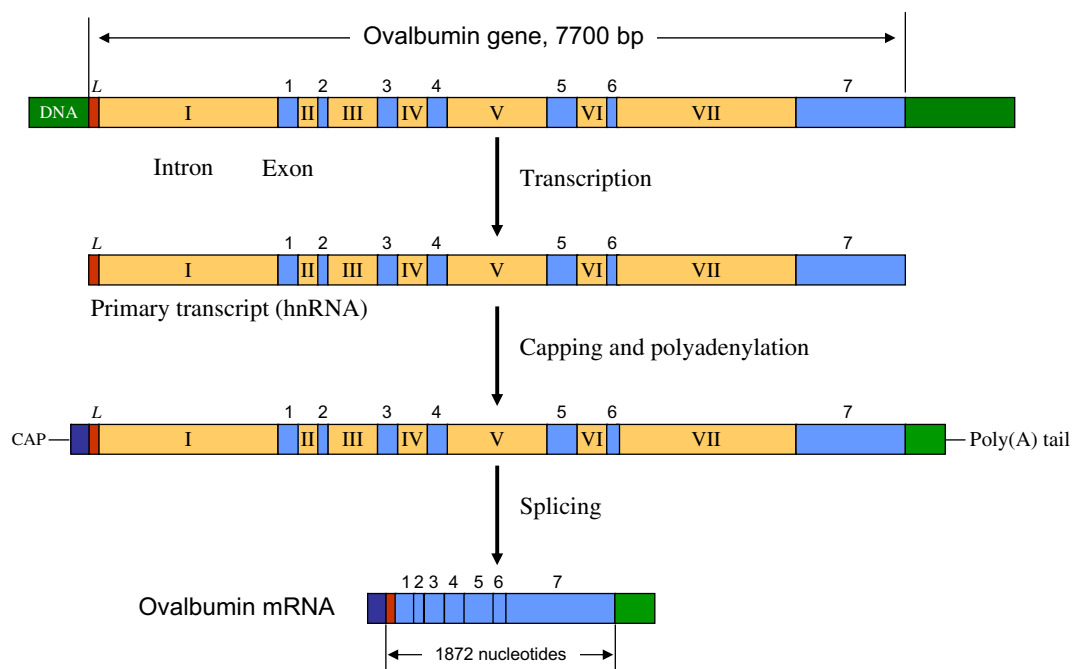


FIGURE 3.32 The steps involved in the maturation of eukaryotic mRNA, illustrated for the chicken ovalbumin gene.

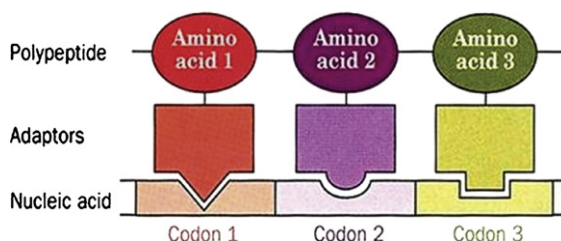


FIGURE 3.33 The adaptor hypothesis. (Adapted from Voet & Voet, 2004.)

mRNA by base pairing between the codon and a three-base anticodon on the tRNA molecule. The key step in determining the specificity of protein biosynthesis is the loading of the amino acids onto their corresponding tRNA by enzymes called aminoacyl tRNA synthetases. This is a two-step process involving the formation of an enzyme-bound aminoacyl-adenylate between the amino acid and a molecule of ATP, followed by the transfer of the amino acid to the terminal 2'- or 3'-hydroxyl of its tRNA to form the aminoacyl-tRNA (Figure 3.34). The importance of

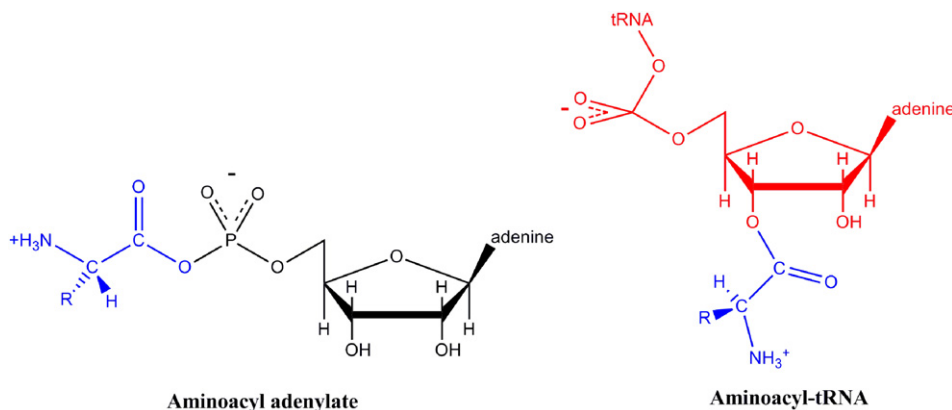


FIGURE 3.34 Structures of an aminoacyl-adenylate and of an aminoacyl-tRNA.

this reaction is underlined by the classic experiment in which cysteine, loaded on tRNA^{Cys}, was reductively converted to alanine using Raney nickel, and it was shown that Cys residues in rabbit haemoglobin synthesised using this Ala-tRNA^{Cys} were systematically replaced by Ala, confirming that the coding properties of this hybrid tRNA are determined by the tRNA, not by the amino acid which is bound (Chapeville et al., 1962).

An aminoacyl-tRNA synthetase exists for each of the 20 amino acids, and is highly specific for its amino acid – the wrong amino acid is introduced into a protein on average only once in every 10⁴–10⁵ reactions. This is, in part, due to the presence of two physically distinct domains within many synthetases (Figure 3.35a). The catalytic domain (acylation site) carries out the initial recognition of the amino acid, and transfers it to its cognate tRNA, whereas the editing domain eliminates the wrong amino acid by hydrolysing either the aminoacyl-adenylate or the aminoacyl-tRNA. We can illustrate this by the case of threonyl-tRNA synthetase, which must distinguish between Thr, Val (with a methyl group in place of a hydroxyl), and Ser (with a hydroxyl group but lacking the methyl group). The catalytic site avoids Val by using a zinc ion, bound to the enzyme by two His and one Cys residue. The zinc ion can also coordinate Thr through its side-chain hydroxyl group and its amino group (Figure 3.35b): the hydroxyl group also forms hydrogen bonds to an adjacent Asp residue. Val cannot bind in this way through its methyl group and is therefore not adenylated and transferred to tRNA^{Thr}. Ser can, however, be

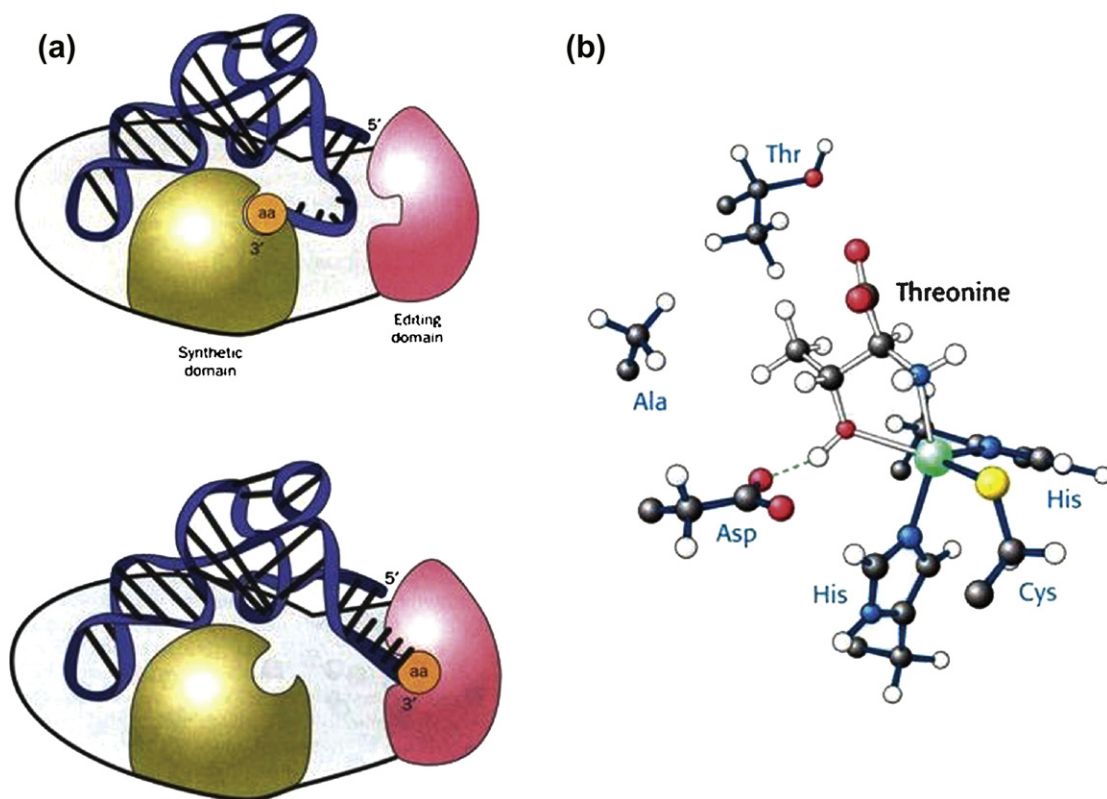


FIGURE 3.35 (a) A cartoon comparing the positions of the 3'-end of an aminoacyl-tRNA in its synthetic (top) and editing (bottom) modes. (From Voet & Voet, 2004) (b) The amino acid-binding site of threonyl-tRNA synthetase showing the amino acid bound to a zinc atom through its amino and hydroxyl groups (From Berg *et al.*, 2002. Reproduced with permission from W.H. Freeman and Co.)

coupled to tRNA^{Thr} , albeit at a 10^{-2} – 10^{-3} rate less than Thr. What enables the error rate to be reduced further is that when the $\text{Ser-tRNA}^{\text{Thr}}$ is transferred to the editing site, more than 20 Å from the acylation site, it is hydrolysed releasing Ser and free tRNA, whereas $\text{Thr-tRNA}^{\text{Thr}}$ is not. This double sieve of acylation and editing sites ensures the observed high fidelity of charging of tRNAs, with the former typically discriminating against amino acids that are larger, and the hydrolytic editing site cleaving activated complexes that contain an amino acid smaller than the correct one.

How, in turn, does the synthetase recognise its specific tRNA? From extensive mutagenesis studies, it appears that the aminoacyl-tRNA synthetases recognise particular regions of the tRNA molecule, most often in their anticodon loops and/or in their acceptor stems.

Once the amino acid has been bound to its tRNA, it can pass to the next phase of protein synthesis, involving its interaction with mRNA, which takes place on the ribosome, a molecular machine of enormous complexity. The ribosome of *E. coli* is a ribonucleoprotein assembly of molecular weight 2,700 kD, and sedimentation constant of 70S.¹⁵ It is made up of roughly two-thirds RNA and one-third protein, and can be separated into a small (30S) and a large (50S) subunit. The 30S subunit contains 21 proteins and one 16S RNA molecule, while the large subunit

15. Sedimentation coefficients are expressed in Svedbergs (S), after the Swedish biochemist The Svedberg who developed the ultracentrifuge in the 1920s. While S values are indicative of molecular weight, they are not additive — the 70S ribosome is made up of one 50S and one 30S subunit!

has 34 different proteins and two RNA molecules, one 23S and one 5S. Despite its size and complexity, the structure of both ribosomal subunits has been determined to atomic resolution (Figure 3.36), and very recently, the

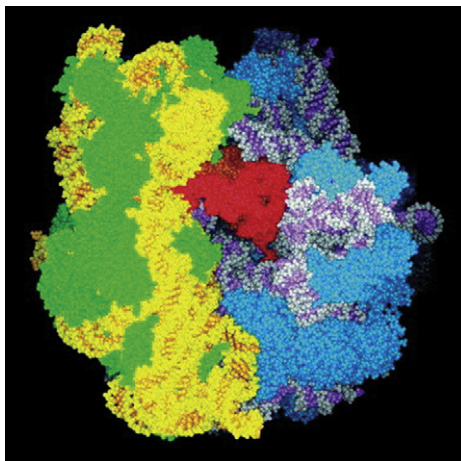


FIGURE 3.36 A space-filling model of the 70S ribosome: the three RNA molecules, 5S, 16S and 23S are respectively in white, yellow and purple respectively; ribosomal proteins of the large and small subunit are in blue and green respectively; the tRNA in the A-site, with its 3'-end extending into the peptidyl-transferase cavity is in red and the P-site tRNA is in yellow. (From Moore, & Steitz, 2005. Copyright 2005 with permission from Elsevier.)

atomic structure of the 70S ribosome has been determined at 2.8 Å resolution. For more information on protein synthesis and ribosomes see Moore and Steitz, 2005; Rodnina et al., 2007; Selmer et al., 2006; Yonath, 2005.

We know that there are three tRNA-binding sites which bridge the small and large subunits, two of them bound to the mRNA by anticodon–codon base pairs. These sites are called the A (aminoacyl) and the P (peptidyl) sites. The third site, as we will see later, binds an empty tRNA and is designated E (exit). A number of protein factors are involved in the three stages of ribosomal protein synthesis – initiation, elongation, and termination. In bacteria, protein synthesis starts with the binding of the 30S subunit to the mRNA. This is followed by binding of the initiator tRNA (charged with N-formylMet) to the start codon AUG on the mRNA and completed by binding of the 50S subunit to form the 70S ribosome. With the initiator tRNA (or subsequently a peptidyl-tRNA) in the P site, the elongation cycle can begin with the binding of the corresponding aminoacyl-tRNA to its codon on the mRNA in the A site of both subunits (Figure 3.37). The next step is peptide-bond formation, which does not require energy. The amino group of the aminoacyl-tRNA attacks the carbonyl of the ester linkage of the peptidyl-tRNA to form a tetrahedral intermediate, which collapses, with the formation of the peptide bond and release of the deacylated tRNA (Figure 3.38). The peptide chain is now attached to the tRNA in the A site of the 30S subunit, whereas both this tRNA and its attached peptide are now in the P site of the 50S subunit. In order for translation to proceed, the mRNA must be moved so that the codon for the next aminoacyl-tRNA can enter the A site. This translocation step, involving the protein elongation factor G, is driven by the hydrolysis of GTP. The mRNA advances by one codon, placing the peptidyl-tRNA once again entirely in the P site. It is important to note that throughout the entire elongation cycle, the peptide chain remains in the P site of the 50S subunit, at the entrance to a tunnel¹⁶ which communicates with the exterior of the 50S subunit. The empty tRNA is now in the exit site, and can dissociate from it to complete the cycle. Elongation continues until the A site is occupied by one of the three

16. This exit tunnel through the 50S subunit was first revealed by three-dimensional image reconstruction twenty-five years ago (Yonath et al., 1987) by two giants of ribosome research, Ada Yonath and the late Heinz-Günther Wittmann (in whose laboratory in Berlin I spent a very fruitful stay 1970–73).

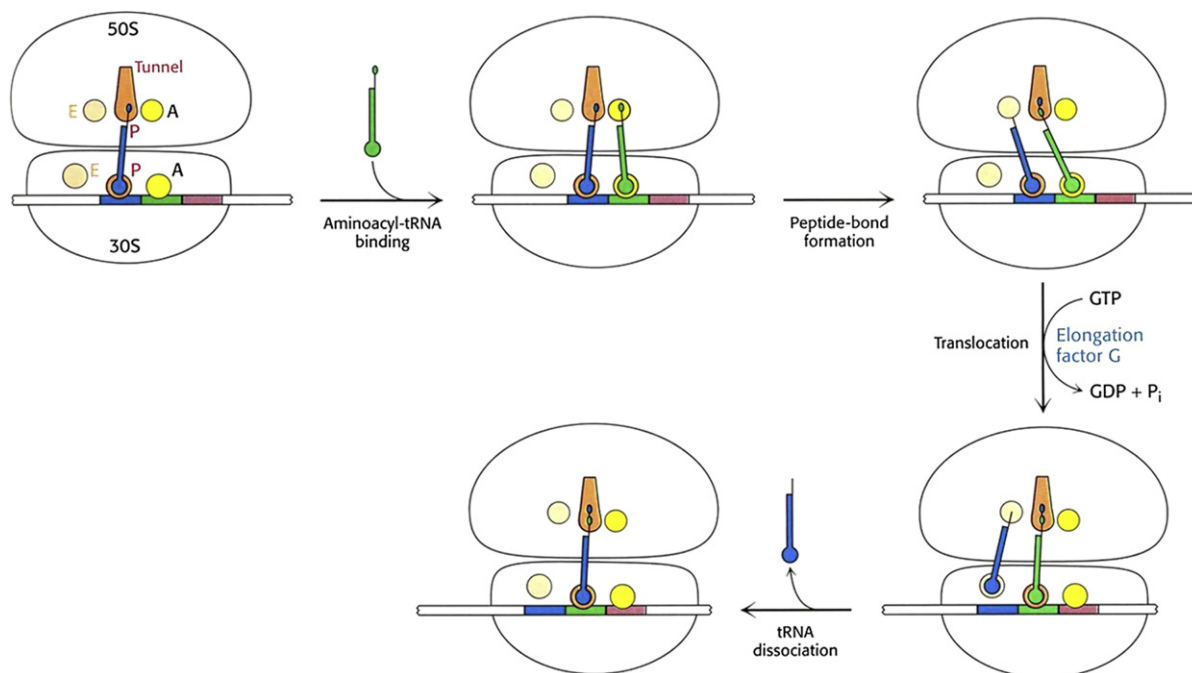


FIGURE 3.37 Mechanism of protein synthesis. (From Berg *et al.*, 2002. Reproduced with permission from W.H. Freeman and Co.)

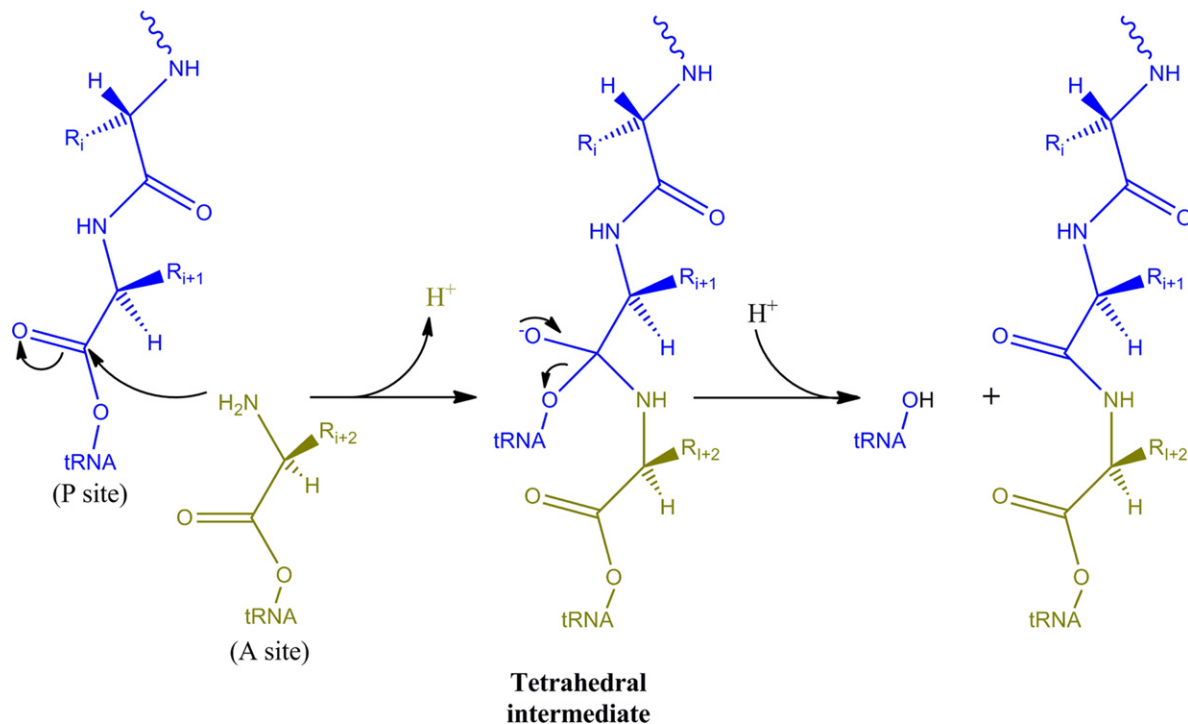


FIGURE 3.38 Peptide-bond formation. (For more details see Rodnina, Beringer, & Wintermeyer, 2007; Yonath, 2005.)

stop codons. Since there are no tRNAs with corresponding anticodons, chain termination occurs, with release of the completed polypeptide.

The peptidyl transferase centre of the ribosome is located in the 50S subunit, in a protein-free environment (there is no protein within 15 Å of the active site) supporting biochemical evidence that the ribosomal RNA, rather than the ribosomal proteins, plays a key role in the catalysis of peptide bond formation. This confirms that the ribosome is the largest known RNA catalyst (ribozyme), and to date, the only one with synthetic activity. Adjacent to the peptidyl transferase centre is the entrance to the protein exit tunnel, through which the growing polypeptide chain moves out of the ribosome.

Protein biosynthesis by eukaryotic ribosomes, which are larger and more complex than those of bacteria, is very similar in its basic outline to that of bacteria. The major difference is in the initiation of translation, which involves recognition of the 5'-cap on the mature mRNA, mentioned earlier, by the small ribosomal subunit.

Postscript

It is clear that in this brief overview of molecular biology, we have not covered a number of important areas, which have an important impact on the study of metalloproteins. These include molecular cloning and recombinant DNA technology, which allow proteins to be overexpressed and individual amino acids to be mutated to any other of the 19 protein amino acids: genome and proteome analysis, which enable the sequences of all of the genes of entire organisms to be determined, and the quantification, localisation, interactions, and, where possible, activities and identification of all of the proteins in an organism, respectively: DNA repair; control of transcription and translation; post-translational modification of proteins; regulation of eukaryotic gene expression; and enhancers and silencers of gene expression. Fuller information can be found in one of the excellent textbooks of biochemistry included in the bibliography. But, since this is a textbook about metals in biology, and not about biochemistry and molecular biology, brevity was required.

REFERENCES

- Anfinsen, C. B. (1973). Principles that govern the folding of protein chains. *Science*, 181, 223–230.
- Branden, C., & Tooze, J. (1991). *Introduction to protein structure*. New York and London: Garland Publishing, Inc. 302.
- Berg, J. M., Tymoczko, J. L., & Stryer, L. (2002). *Biochemistry* (5th ed.). New York: W.H. Freeman and Co. 974.
- Campbell, P. N., Smith, A. D., & Peters, T. J. (2005). *Biochemistry illustrated biochemistry and molecular biology in the post-genomic era* (5th ed.). London and Oxford: Elsevier. 242.
- Chapeville, F., Lipmann, F., G. von Ehrenstein, B Weisblum, Ray, W. J., Jr., & Benzer, S. (1962). On the role of soluble ribonucleic acid in coding for amino acids. *Proceedings of the National Academy of Sciences of the United States of America*, 48, 1086–1092.
- Creighton, T. E. (1993). *Proteins structures and molecular properties* (2nd ed.). New York: W.H. Freeman and Co. 507.
- Eisenberg, D. (2003). The discovery of the α -helix and the β -sheet, the principal structural features of proteins. *Proceedings of the National Academy of Sciences of the United States of America*, 100, 11207–11210.
- Fersht, A. (1999). *Structure and mechanism in protein science a guide to enzyme catalysis and protein folding*. New York: W.H. Freeman and Co. 631.
- Judson, H. F. (1979). *The eighth day of creation*. New York: Simon and Shuster.
- Moore, P. B., & Steitz, T. A. (2005). The ribosome revealed. *TIBS*, 30, 281–283.
- Perutz, M. F. (2002). *I wish I'd made you angry earlier. Essays on science, scientists and humanity*. Oxford University Press. 354.
- Rodnina, M. V., Beringer, M., & Wintermeyer, W. (2007). How ribosomes make peptide bonds. *TIBS*, 32, 20–26.
- Selmer, M., Dunham, C. M., Murphy, F. V., Weixlbaumer, A., Petry, S., Kelley, A. C., et al. (2006). Structure of the 70S ribosome complexed with mRNA and tRNA. *Science*, 313, 1935–1943.
- Voet, D., & Voet, J. G. (2004). *Biochemistry* (3rd ed.). Hoboken: John Wiley and Sons. 1591.
- Watson, J. D., & Crick, F. H. C. (1953). Genetical implications of the structure of deoxyribonucleic acid. *Nature*, 171, 964–967.
- Yonath, A. (2005). *Ribosomal crystallography: Peptide bond formation, chaperone assistance and antibiotics activity*.
- Yonath, A., Leonard, K. R., & Wittmann, H. G. (1987). A tunnel in the large ribosomal subunit revealed by three-dimensional image reconstruction. *Science*, 236, 813–816.

Biological Ligands for Metal Ions

Introduction	69
Insertion of Metal Ions into Metalloproteins	76
Chelatase – The Terminal Step in Tetrapyrrole Metallation	77
Iron–Sulfur Cluster Formation	79
More Complex Cofactors – MoCo, FeMoCo, P-clusters, H-clusters, and CuZ	80
Siderophores	86

INTRODUCTION

In Chapter 2, we explained the basic notions involved in the coordination chemistry of metal ions. We now consider potential ligands, which could be involved in binding metals in metalloproteins. We already defined ligand binding as the affinity of the metal ion for any atom, group, or molecule that is attached to the central metal ion. We can divide them into three categories:

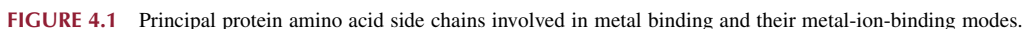
- naturally occurring amino acids in the protein itself, and amino acids within the protein which have been chemically modified:
- low-molecular-weight inorganic anions
- organic cofactors

As was pointed out in Chapter 2, biologically important metal ions and their ligands can be classified according to the hard-soft theory of acids and bases (Table 2.1). While there are exceptions, most metal ions bind to donor ligands as a function of preferences based on this concept, with hard acids (metal ions, like Na^+ , K^+ , Ca^{2+} , Mg^{2+} , and Fe^{3+}) binding preferentially to hard bases (ligands, like O), and soft acids (like Cu^+) to soft bases (like S and N).

Amino Acid Residues

Of the 20 amino acids present in proteins (Chapter 3), only a relatively small number are potential metal ligands. The ligand groups, which are encountered most often are the thiolate of Cys, the imidazole of His, the carboxylates of Glu and Asp, and the phenolate of Tyr (Fig. 4.1). Less frequently, we encounter the thioether group of Met, the amino group of Lys and the guanidino group of Arg, and the amide groups of Asn and Gln. Metal ions can also bind to peptide bonds, through the carbonyl or the deprotonated amide nitrogen, and to the terminal amino and carboxyl groups of the protein.

Cysteine can bind to either one or two metal ions, and is frequently found as a ligand to iron (e.g., in Fe–S clusters) and to Cu^+ (e.g., in copper chaperones which transfer copper to specific copper-binding proteins). Histidine can bind metal ions in two positions, and has a strong preference for Cu^{2+} . The



carboxylate oxygens of aspartate (and its homologue, glutamate, which is not included in Fig. 4.1) are preferential ligands for the alkali and alkaline earth metals like Ca^{2+} . They can bind a single metal ion in either a mono- or bi-dentate (chelating) mode, or bind two metal ions in a bidentate, bridging mode. Fe^{3+} also shows a strong affinity for the oxygen donor atoms of carboxylates as well as the phenoxide of tyrosine. Like cysteine, the sulfur of methionine is often found bound to iron, e.g., in electron-transfer hemoproteins like cytochrome c.

A number of proteins of the blood clotting (coagulation) cascade (including prothrombin, and a number of other clotting factors) undergo post-translational modification¹ in a reaction catalysed by a vitamin K-dependent carboxylase, which transforms specific Glu residues into γ -carboxyglutamic acid, Gla (Fig. 4.1). In the reaction (Fig. 4.2), the dihydroquinone (reduced) form of vitamin K, KH_2 , is oxidised to the epoxide form, KO, by O_2 . The

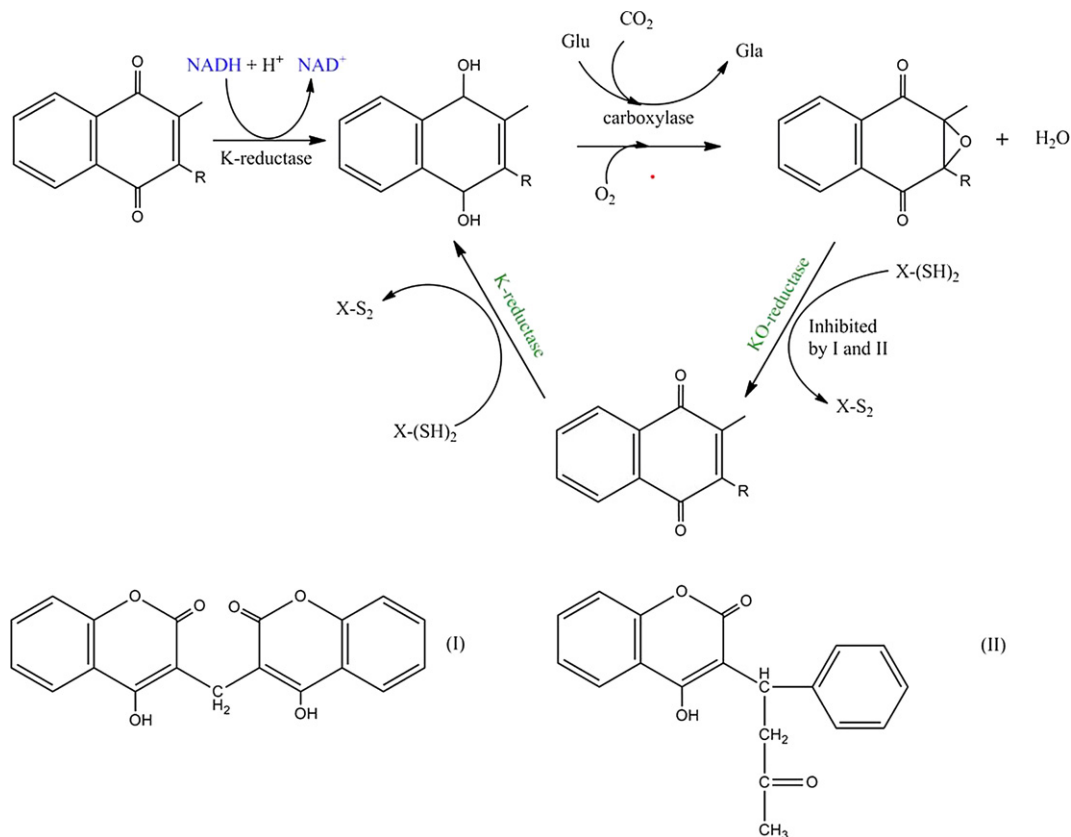


FIGURE 4.2 The vitamin K cycle as it functions in protein glutamyl carboxylation reaction. The conversion of protein-bound glutamic acid into γ -carboxyglutamic acid is catalysed by a carboxylase. During the carboxylation reaction vitamin K hydroquinone (KH_2) is converted to vitamin K epoxide (KO). $\text{X}-(\text{SH})_2$ and $\text{X}-\text{S}_2$ represent, respectively, the reduced and oxidised forms of thioredoxin. The NADH-dependent and dithiol-dependent vitamin K reductases are different enzymes. Both the dithiol-dependent K- and KO-reductases are inhibited by dicoumarol (I) and warfarin (II).

epoxide, KO, is then converted back to the KH_2 form by two reductases, which require dithiols, like thioredoxin, as cofactor.

γ -Carboxyglutamic acid is a much better chelator of Ca^{2+} than glutamate itself, enabling prothrombin to bind Ca^{2+} , which anchors it to the membranes of blood platelets released after injury. This then positions prothrombin in close proximity to other proteases of the blood clotting cascade, initiating the sequence of events which leads to clot formation. Both of the dithiol-dependent K- and KO-reductases are inhibited by dicoumarol (I) and warfarin

1. Enzyme-catalysed modification of the protein after the protein has been released from the ribosome (the protein synthesis assembly machinery).

(II). These vitamin K antagonists are used therapeutically as anticoagulants,² because they block conversion of the vitamin K epoxide back to the vitamin K hydroquinone (Fig. 4.2).

We will encounter yet another post-translationally modified amino acid later in this chapter, namely the C-terminal thiocarboxylate used as sulfur donor in the biosynthesis of the universally distributed MoCo cofactor.

Low-Molecular-Weight Inorganic Anions

A number of low-molecular-weight inorganic ligands are involved in metal binding in metalloproteins. These include HCO_3^- and PO_4^{3-} , as ligands to Fe^{3+} in proteins involved in iron transport, in association with amino acid residues of the protein. We will discuss the role of CN^- and CO as ligands to Fe in bacterial hydrogenases, where they are part of more complex metal centres in a later section.

Many pathogenic bacteria, such as *Neisseria* and *Haemophilus*, are able to capture iron directly from the iron-binding proteins transferrin and lactoferrin of their mammalian hosts. It is quite ironic, not to put it too subtly, that iron is then transported through the periplasm to the cytoplasmic membrane of these nasty bugs, by the ferric ion-binding protein, FbpA, which is a member of the same superfamily as transferrin and lactoferrin! Transferrins, lactoferrins, and FbpA all belong to a superfamily of proteins, which function by a so-called ‘Venus fly trap’ mechanism.³ They are made up of two domains. Fe^{3+} binds in a cleft between the two domains, which close together upon binding of iron and the appropriate anion (HCO_3^- or PO_4^{3-}). In FbpA, the Fe^{3+} ion is octahedrally coordinated by two oxygens from Tyr195 and Tyr196, an imidazole nitrogen from His9, a carboxylate oxygen from Glu57, an oxygen atom from an exogenous phosphate, and an oxygen atom from a water molecule (Fig. 4.3a). In transferrin, the Fe^{3+} is coordinated by similar residues (Tyr92, Tyr192, and His253), except that Asp60 replaces Glu and the octahedral coordination is completed with a bidentate (bi)carbonate as the synergistic anion (Fig. 4.3b). Whereas in FbpA, the two Tyr residues in its binding site are adjacent to one another in the amino acid sequence, in transferrin the two Tyr residues are located on different domains and play a role in the closing motion of the iron-binding protein lobes.

Organic Cofactors

As we will see in subsequent chapters, many metalloproteins have their metal centres located in organic cofactors, like the tetrapyrrole porphyrins and corrins, in metal clusters like the Fe–S clusters in iron–sulfur proteins, or in even more complex cofactors, like the FeMo-cofactor of nitrogenase. We discuss their structures briefly here before moving on in a selected number of cases to the way in which metal insertion into the cofactor is engineered.

Co, Fe, Mg, and Ni are inserted into the tetrapyrrole nucleus of corrins and porphyrins (Fig. 4.4) to form vitamin B₁₂ and other cobalamine cofactors, haem, chlorophyll, and coenzyme F₄₃₀ respectively. We discuss briefly later in this chapter how metals are incorporated into porphyrins and corrins to form haem and other metallated tetrapyrroles. The important and varied functions of hemoproteins in oxygen transport and storage, in oxygen activation, and electron transport are discussed in greater detail in Chapter 13. The isomerases, methyl transferases, and class II ribonucleotide reductases, which employ cobalamine cofactors, are discussed in Chapter 15, where we also discuss the unusual Ni-corrin coenzyme F₄₃₀ cofactor involved in the final step of methane production. The verdant color of chlorophyll, harbinger of spring, as plants, trees, and shrubs, recover from the dead of winter, not only visually revitalises us, but also harnesses the energy of the sun to generate energy and to fix CO₂, as we explain in greater detail in Chapter 10.

2. Why these anticoagulants are lethal to rodents but not to man is not clear, but may reflect the relative dose — what is nontoxic to a 70 kg human could well be so for a 200–300 g rat (underlining the dictum of Paracelsus that ‘the dose makes the poison’).

3. The Venus fly trap is a carnivorous swamp flower of the sundew family, native to the Carolinas: it has leaves with two hinged blades which snap shut to trap insects.

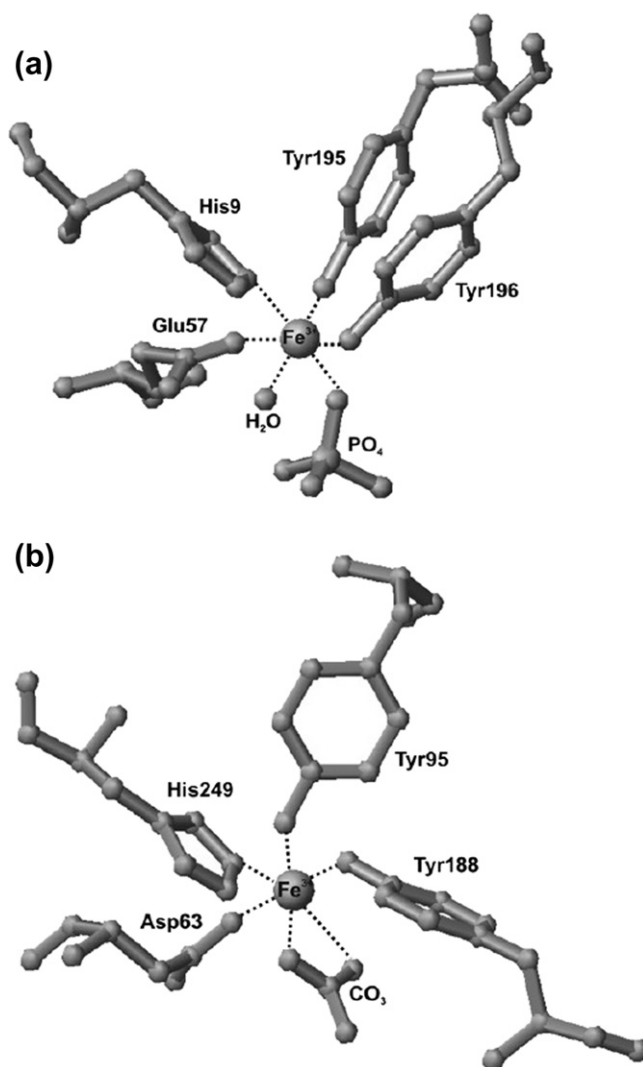


FIGURE 4.3 The Fe^{3+} -binding sites of (a) *Neisseria meningitidis* FbpA and (b) the N-lobe of human transferrin. In each protein, the Fe^{3+} ion is coordinated by similar ligands. In FbpA, two oxygens from Tyr195 and Tyr196, an imidazole nitrogen from His9, a carboxylate oxygen from Glu57, an oxygen atom from an exogenous phosphate, and an oxygen atom from a water molecule coordinate Fe^{3+} . In transferrin, the Fe^{3+} is coordinated by similar residues (Tyr92, Tyr192, His253) except that Asp60 replaces Glu and a bidentate (bi)carbonate completes the octahedral geometry preferred by Fe^{3+} . (From Krewulak & Vogel, 2007. Copyright 2007, with permission from Elsevier.)

For the first billion years of evolution, the environment was anaerobic, which meant that both iron and sulfur were abundant, and so proteins containing iron–sulfur (Fe–S) clusters were probably among the first catalysts that Nature had available to it. They are distributed in virtually all living organisms, but their recognition as a distinct class of metalloproteins only occurred after the discovery of their characteristic EPR (Electron Paramagnetic Resonance) spectra in the oxidised state in the 1960s. These proteins have iron atoms bound to sulfur, either in the form of thiol groups of cysteine residues of the protein, or as both inorganic sulfide and cysteine thiols as ligands. The biochemical utility of these Fe–S clusters resides not only in their possibility to easily transfer electrons, but also in their tendency to bind the electron-rich oxygen and nitrogen atoms of organic substrates.

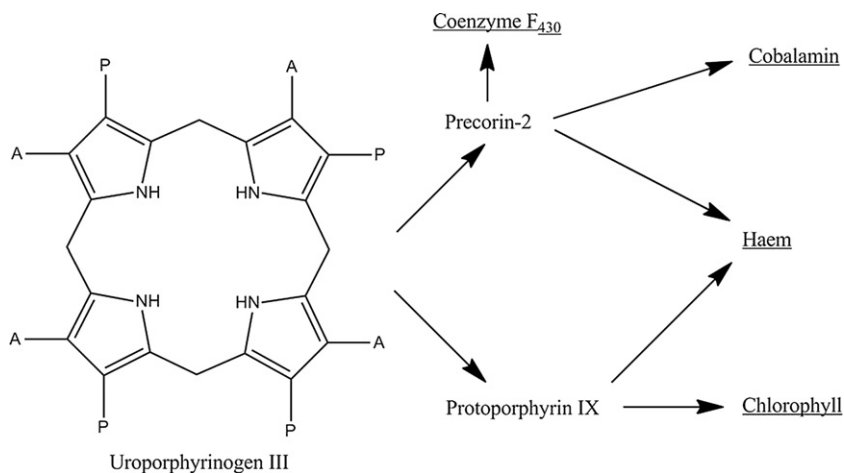


FIGURE 4.4 The structures of corrin (left) and porphyrin (right).

Iron–sulfur proteins (Rao and Holm, 2004), contain four basic core structures which have been characterised crystallographically both in model compounds and in iron–sulfur proteins. These are (Fig. 4.5): (a) rubredoxins, found

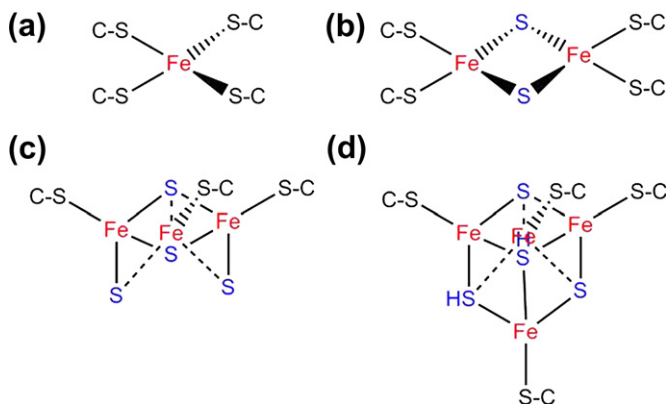


FIGURE 4.5 Structures of the four common iron–sulfur centres (C–Cys). (a) Rubredoxin; (b) rhombic two iron–two sulfide [$\text{Fe}_2\text{--S}_2$] cluster; (c) cuboidal three-iron–four sulfide [$\text{Fe}_3\text{--S}_4$] cluster; and (d) cubane four iron–four sulfide [$\text{Fe}_4\text{--S}_4$] cluster.

in bacteria, where the [Fe–S] cluster consists of a single Fe atom liganded to four Cys residues – the iron atom can be in the +2 or +3 valence state; (b) rhombic two iron–two sulfide [$\text{Fe}_2\text{--S}_2$] clusters – typical stable cluster oxidation states are +1 and +2 (the charges of the coordinating cysteine residues are not considered); (c) cuboidal three-iron–four sulfide [$\text{Fe}_3\text{--S}_4$] clusters – stable oxidation states are 0 and +1; and (d) cubane four iron–four sulfide [$\text{Fe}_4\text{--S}_4$] clusters – stable oxidation states are +1 and +2 for ferredoxin-type clusters and +2 and +3 for “Hipip”⁴ clusters. Electrons can be delocalised, such that the valences of individual iron atoms lie between ferrous and ferric forms. Low-molecular-weight proteins containing the first and the last three types are referred to as rubredoxins (Rd) and ferredoxins (Fd), respectively. The protein ligands are frequently Cys residues, but a number of others are found, notably His, which replaces two of the thiol ligands in the high-potential [$\text{Fe}_2\text{--S}_2$] Rieske proteins of the respiratory chain.

When compared to haem and iron–sulfur clusters, there are a number of much more complex organic cofactors which are found in metalloproteins (Rees, 2002). An albeit selective gallery is presented in Fig. 4.6. They include the Mo-cofactor found in a great number of Mo-dependent enzymes, the FeMo-cofactor and the

4. Hipip – high-potential iron–sulfur protein.

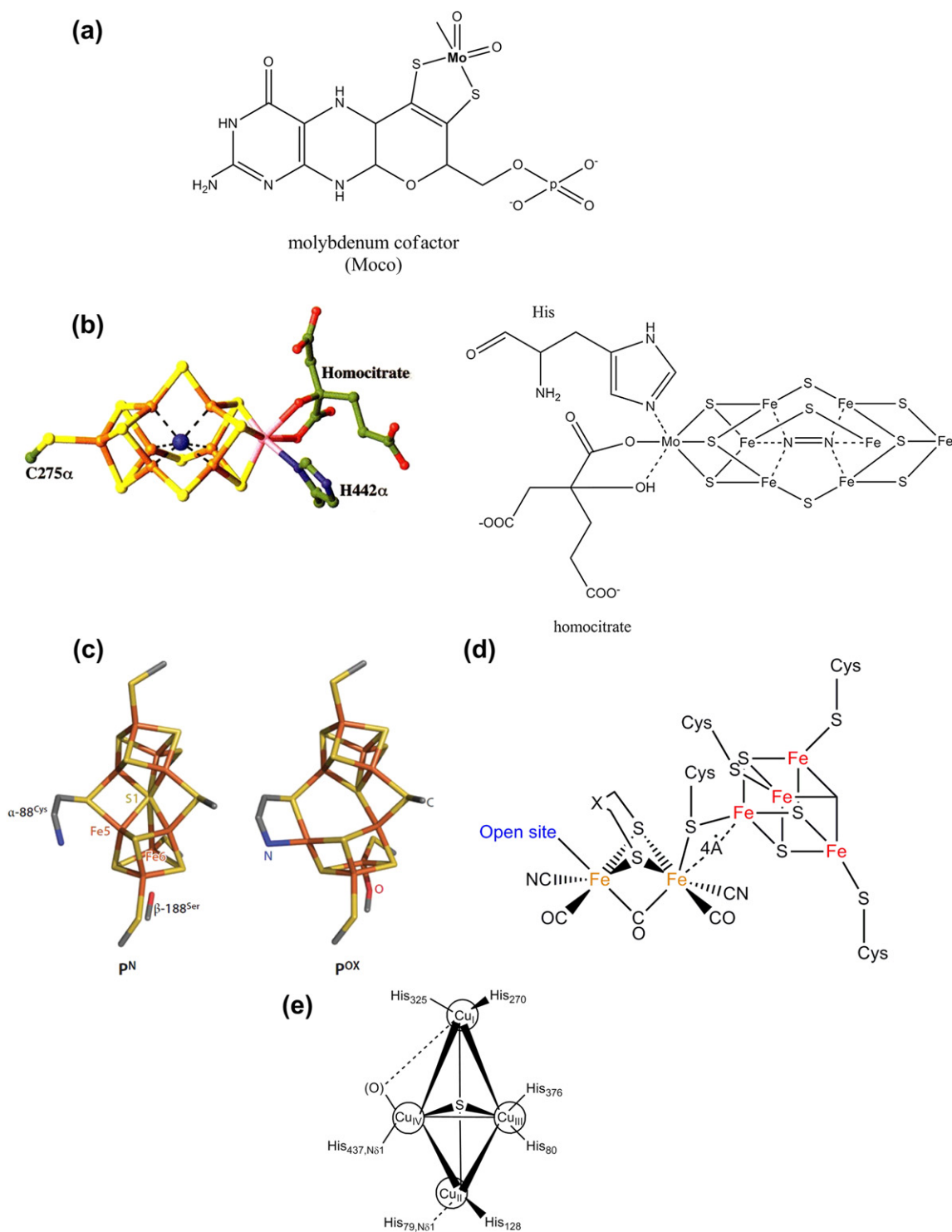


FIGURE 4.6 A selective gallery of more complex organic cofactors which are found in metalloproteins. (a) The Moco cofactor; (b) the FeMo-cofactor, (c) the P-cluster of nitrogenase, (d) the H-cluster of microbial hydrogenases, and (e) the Cu₂ cluster of microbial nitrous oxidases.

P-cluster of nitrogenases, the three types of metal clusters found in microbial hydrogenases, the unusual common structural features of which include CO ligands, and the Cu_2 cluster of microbial nitrous oxidases. The biosynthesis of some of these cofactors is discussed later in this chapter.

The unique case of microbial siderophores, which are low-molecular-weight iron chelators, will be discussed right at the end of this chapter.

INSERTION OF METAL IONS INTO METALLOPROTEINS

At this point, we might ask what might seem like an obvious question. Are the metal sites, which we have discussed above pre-formed (i.e., does the binding site already exist when the protein is synthesised), or does metal binding result in a major change in the conformation of the protein? In FbpA and the transferrins which we encountered earlier, there is clear evidence for a conformational change between an ‘open’ (metal-free) and a ‘closed’ (metal-bound) form of the protein. Fe binding and release is proposed to function via a ‘Venus fly trap’ mechanism where large-scale movements of the two domains result in the opening or closing of the iron-binding site which lies between them, as we discuss in greater detail in Chapter 8.

As we will also see in Chapter 8, free copper levels are extremely low within cells because the copper is bound to a family of metallochaperones⁵ which are subsequently involved in the incorporation of copper into copper-containing proteins. The mechanism proposed for copper insertion into the Cu/Zn superoxide dismutase, SOD1, is presented in Fig. 4.7, and appears to use an already-preformed Cu-binding site. The copper chaperone CCS acquires copper as Cu^+ from a copper transporter and then docks with the reduced dithiol form of SOD1 (steps I and II)

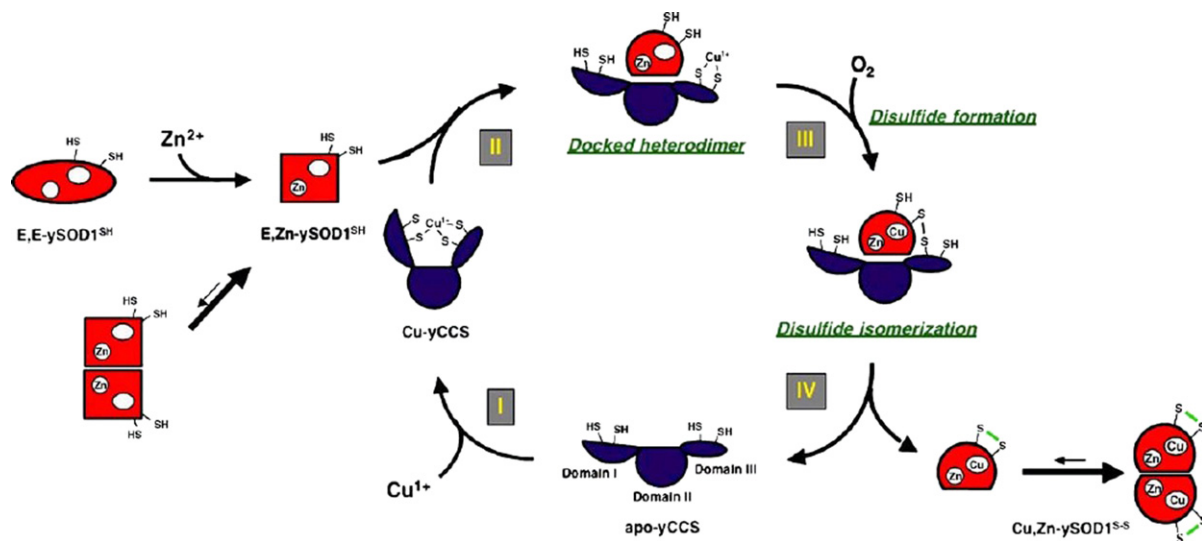


FIGURE 4.7 Proposed mechanism of copper insertion into SOD1 by its metallochaperone, CCS. The copper chaperone acquires copper through unknown routes and then docks with a disulfide reduced form of SOD1 (steps I and II). This complex is inert to further reaction unless exposed to oxygen or superoxide (step III), at which point a disulfide-linked heterodimeric intermediate forms. This complex undergoes disulfide isomerisation to an intramolecular disulfide in SOD1 (step IV). Copper is transferred at some point after introduction of oxygen and the mature monomer is proposed to be released from CCS. (From Culotta, Yang, & O'Halloran, 2006. Copyright 2006, with permission from Elsevier.)

5. Chaperones were persons who, for the sake of propriety, accompanied young unmarried ladies in public, as guide and protector.

and II) to give a heterodimer. When exposed to oxygen or superoxide (step III), a disulfide is formed within the heterodimer, which subsequently undergoes disulfide isomerisation to an intramolecular disulfide in SOD1 (step IV). At some point after the introduction of oxygen, copper is transferred from the chaperone to the SOD1. The mature monomeric SOD1 is then released from the CCS chaperone and dimerizes to its active form.

We discuss briefly now how metals are incorporated into porphyrins and corrins to form haem and other metallated tetrapyrroles, and how Fe–S clusters are synthesised.

CHELATASE – THE TERMINAL STEP IN TETRAPYRROLE METALLATION

Tetrapyrroles are organic molecules that contain four five-membered heterocyclic (pyrrole) rings, linked in a cyclic or linear array. Haem, chlorophyll, cobalamin (vitamin B₁₂), siroHaem,⁶ and coenzyme F₄₃₀ belong to a family of prosthetic groups that are characterised by their tetrapyrrole-derived nature and contain a central, complexed metal ion: Fe²⁺ in haem and siroHaem, Mg²⁺ in chlorophyll and bacteriochlorophyll, Co²⁺ in cobalamin, and Ni²⁺ in coenzyme F₄₃₀. They are all derived from a common tetrapyrrole precursor, uroporphyrinogen III (Fig. 4.8). The insertion of each of these metal ions involves a group of enzymes called chelataases, of which the best characterised is ferrochelatase, which inserts Fe²⁺ into protoporphyrin IX in the terminal step of

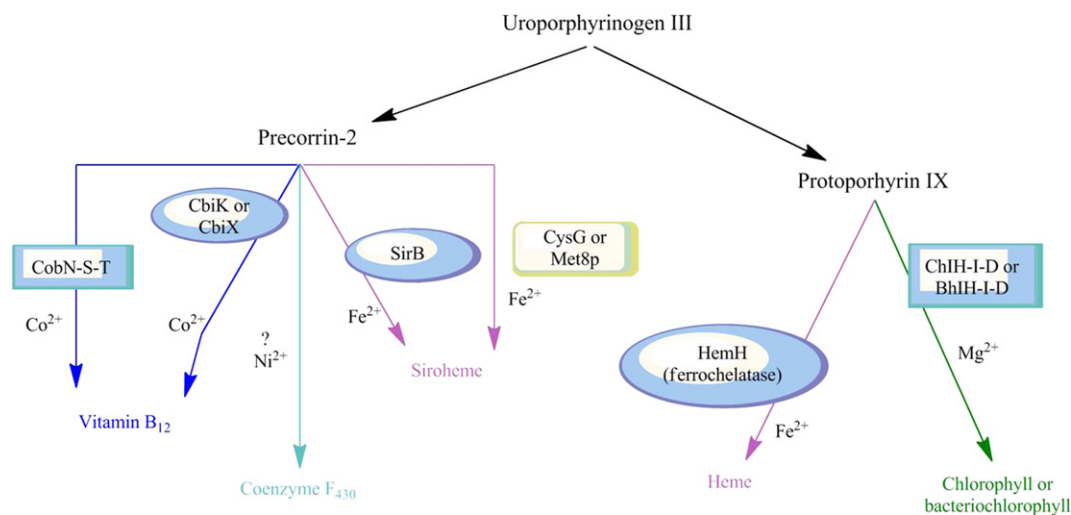


FIGURE 4.8 The tetrapyrrole biosynthetic pathways. Chelataases selectively insert Fe²⁺ to form haem, Mg²⁺ to form chlorophyll, Co²⁺ to form cobalamin, and, in methane-producing bacteria, Ni²⁺ to form coenzyme F₄₃₀.

the haem biosynthetic pathway. The different chelataases are thought to have similar mechanisms, which involve as the first step the distortion of the tetrapyrrole porphyrin upon binding to the enzyme to give a saddled structure (Fig. 4.9a) in which two opposite pyrrole rings are slightly tilted upwards while the other two pyrrole rings are tilted slightly downwards. In Fig. 4.9a, the two unprotonated nitrogen atoms of the pyrrole rings point upward, while the two protonated nitrogens point downward with respect to the porphyrin ring. Subsequent to the distortion of the porphyrin ring, the first metal–porphyrin bond is formed (Fig. 4.9b), followed by other ligand exchange steps leading to formation of a complex in which the iron atom is sitting on top of the porphyrin, with two of its nitrogen atoms coordinated to the metal while the other two are still protonated. This is followed by the

6. Sirohaem is a tetrahydroporphyrin which has adjacent reduced pyrrole rings and is present in bacterial sulfite and nitrite reductases.

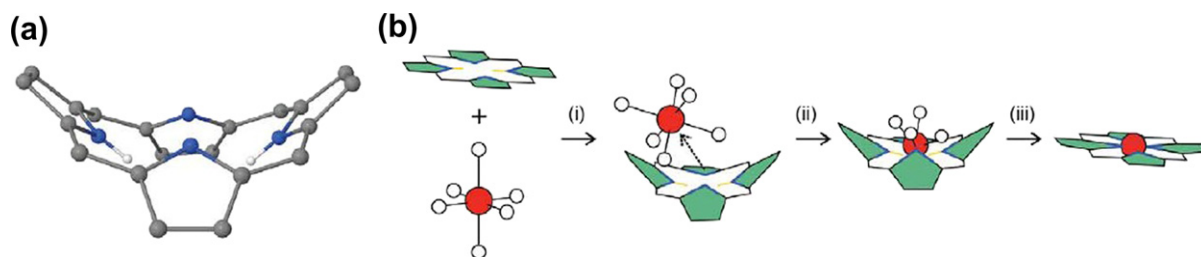


FIGURE 4.9 Mechanism of porphyrin metallation. **(a)** Out-of-plane saddling deformation used to describe a nonplanar distortion of the porphyrin macrocycle in which two opposite pyrrole rings with unprotonated nitrogen atoms (blue spheres) point upwards, and the other two pyrrole rings with protonated nitrogen atoms (blue and white spheres) point downwards. **(b)** Steps in the reaction mechanism for incorporation of the metal ion (red) into porphyrin (pyrrole rings, green; unprotonated pyrrole nitrogen atoms, blue; protonated pyrrole nitrogen atoms with protons, yellow) include (i) deformation of the porphyrin ring; (ii) formation of the first metal–porphyrin bond, followed by other ligand-exchange steps leading to formation of a ‘sitting-atop’ complex (in which two pyrroline nitrogen atoms coordinate to the metal ion and two protons remain on the pyrrole nitrogen atoms); and (iii) sequential deprotonation of the two pyrrole nitrogen atoms coupled with formation of the metallated porphyrin. (From Al-Karadaghi *et al.*, 2006. Copyright 2006, with permission from Elsevier.)

sequential deprotonation of the two pyrrole nitrogen atoms coupled with formation of the metallated porphyrin. The saddling of the porphyrin is an out-of-plane deformation, which exposes both of the protons and the lone pairs of the nitrogen atoms of the porphyrin molecule in an appropriate arrangement for metal insertion.

The structure of several ferrochelatases has been determined, and it is clear that the porphyrin rings B, C, and D are held in a very tight grip by conserved amino acids, whereas the A ring is distorted. Two metal-ion-binding sites have been identified, one located at the surface of the molecule, occupied by a fully hydrated Mg^{2+} ion, and the other located in the porphyrin-binding cleft, close to the distorted porphyrin ring A, with its nitrogen pointing towards His183 and Glu264 (Fig. 4.10). It has been proposed that the metal ion on the outermost site, by ligand exchange with a series of acidic residues arranged along the helical edge of a π -helix,⁷ would be shuttled to the inner site, there to be exchanged with the pyrrole nitrogens, resulting in insertion of the metal ion into the

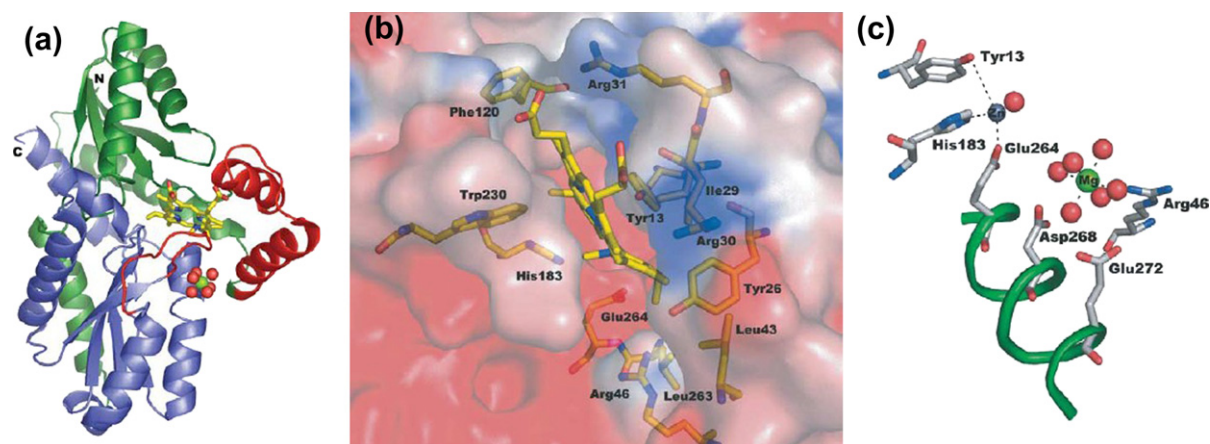


FIGURE 4.10 Porphyrin and metal-ion-binding sites in ferrochelatase. **(a)** Structure of *B. subtilis* ferrochelatase in complex with the transition-state inhibitor *N*-methylmesoporphyrin (*N*-MeMP). **(b)** Interaction of *N*-MeMP with amino acids in the substrate-binding cleft of *B. subtilis* ferrochelatase. **(c)** Two metal-binding sites in *B. subtilis* ferrochelatase. The two sites are shown with a Zn^{2+} ion (grey sphere) and a fully hydrated Mg^{2+} ion (green sphere). (From Al-Karadaghi *et al.*, 2006. Copyright 2006, with permission from Elsevier.)

7. For more information concerning this unusual type of helix, see Chapter 377.

porphyrin. The two sites, occupied respectively by a Zn^{2+} ion and a fully hydrated Mg^{2+} ion, are $\sim 7 \text{ \AA}$ apart. Two of the ligands to the Zn^{2+} ion in the outer site, His183 and Glu264, are invariant in all ferrochelatases. The side chains of Glu272, Asp268, and Glu272 are aligned along the π -helix, in a line connecting the two metal sites. Only a π -helix can provide such an alignment of side chains. This is reminiscent of several other metalloproteins, like nitrogenase and the ferritin superfamily, in which residues in π -helices function to coordinate metal ions involved in enzymatic activity.

An interesting question is why does a particular chelatase introduce just one particular divalent transition metal ion rather than any one of a number of others? It might be because that particular M^{2+} is present in that biological compartment (e.g., in the case of haem synthesis, Fe^{2+}) and present at much larger concentrations than any other. Clues have begun to appear, however, from experiments in which site-directed mutagenesis of specific amino acid residues in the proposed metal-ion-binding site of the chelatase has changed the specificity of the metal ion, which is inserted into the porphyrin.

IRON–SULFUR CLUSTER FORMATION

Numerous Fe/S proteins are known in each of the three kingdoms of living organisms, i.e., in Eubacteria, Archaeobacteria, and Eukaryotes, and their multiple functions in electron transport and catalysis are reviewed in Chapter 13. In contrast to most other cofactors, Fe/S clusters are essentially inorganic in nature, consisting simply of iron cations (Fe^{2+} or Fe^{3+}) and inorganic sulfide anions (S^{2-}). Our understanding of the way in which these clusters are assembled has evolved rapidly in the last few years and we summarise our current understanding of the eukaryotic mitochondrial iron–sulfur cluster (ISC) assembly machinery here. The mitochondrial ISC assembly system is strikingly similar to that in bacteria, and it is now clear that mitochondria play a prime role in Fe/S protein biogenesis, since they are not only responsible for maturation of Fe/S proteins inside but also outside of the organelle. The current view of Fe/S protein biogenesis in eukaryotes (Fig. 4.11) involves the interplay of three complex multiprotein systems, referred to as ISC assembly, ISC export, and CIA (cytosolic iron–sulfur protein assembly machinery).

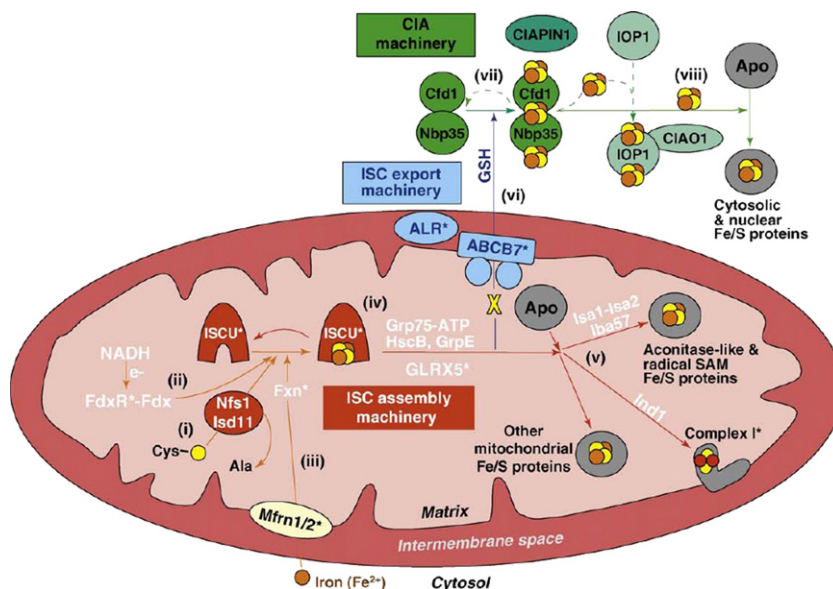


FIGURE 4.11 A current working model of Fe/S protein biogenesis in eukaryotes. Fe/S protein biogenesis is a complex process involving three different machineries. The figure depicts the names used for human components, yet in many parts builds on the mechanisms derived from functional studies in yeast. (From Sheftel, Stehling, & Lill, 2010. Copyright 2010, with permission from Elsevier.)

A current working model for ISC biogenesis in eukaryotes is illustrated in Fig. 4.11. The names used are those of the human components. The biogenesis involves the transient *de novo* synthesis of an ISC, with the sulfur atom derived from cysteine via the pyridoxal phosphate (PLP)-dependent cysteine desulfurase, Nfs1 in complex with Isd11. In this reaction, the sulfur atom of free cysteine is transferred to a conserved cysteine of Nfs1 to form a persulfide as a reaction intermediate. The sulfur is then transferred directly to the scaffold protein complex ISCU, a necessary process to avoid the potential unregulated release of toxic sulfide. The reduction of sulfur to sulfide requires electrons derived from NADH (Nicotinamide Adenine Dinucleotide, in its reduced form) via an electron-transfer chain involving the ferredoxin reductase (FdxR) and the [2Fe–2S] ferredoxin (Fdx). Iron enters the mitochondria through the carrier protein mitoferrin (Mfrn1/2) and, in a process involving the iron chaperone protein, frataxin (Fxn), is combined with sulfide on the mitochondrial Fe/S scaffold ISCU. The Fe/S cluster transiently bound to ISCU is then transferred to mitochondrial apoproteins in an ATP-dependent process. This requires a chaperone system (consisting of the Hsp70 chaperone Grp75, HscB, and GrpE) and the monothiol glutaredoxin GLRX5. Additional proteins, Isa1, Isa2, and Iba57, play specific roles in delivering Fe/S clusters to a subset of Fe/S proteins that includes aconitase-like and radical S-adenosyl methionine (SAM) Fe/S proteins, whereas Ind1 is involved in the assembly of Fe/S clusters in respiratory complex I (see Chapter 5). For cytosolic and nuclear Fe/S proteins, an unknown intermediate (X) is synthesised by the ISC assembly machinery and transported out of the mitochondria by the inner membrane ABC transporter⁸ ABCB7. The process seems to require both the sulfhydryl oxidase ALR and glutathione (GSH). In the cytosol, a transiently bound Fe/S cluster is formed on a scaffold complex consisting of the P-loop NTPases Cfd1 and Nbp35. The Fe/S clusters are then transferred and inserted into extramitochondrial apoproteins in a reaction involving IOP1 and CIAO1.

MORE COMPLEX COFACTORS – MOCO, FEMOCO, P-CLUSTERS, H-CLUSTERS, AND CUZ

Our understanding of metal incorporation into metalloporphyrins and Fe–S clusters, which are widely distributed in a great many metalloproteins has advanced greatly in recent years. However, it has also become apparent that there are a growing number of more complex cofactors, some of them with a more specific distribution. The transition metal molybdenum (Mo) is found as an essential part of the active site in a wide range of metalloenzymes in bacteria, fungi, algae, plants, and animals. However, the metal itself is biologically inactive unless it is incorporated into a special molybdenum cofactor (MoCo), which incorporates a dithiolene group (Fig. 4.6a) and is required by a number of enzymes, such as nitrate reductase, sulfite oxidase, xanthine dehydrogenase, and aldehyde oxidase. In all organisms studied to date, MoCo is synthesised by a highly conserved biosynthetic pathway (Fig. 4.12), which can be divided into five steps involving the biosynthetic intermediates precursor cyclic pyranopterin monophosphate (cPMP), MPT (Metal Binding Pterin), adenylated MPT, and MoCo. The six enzyme activities involved in MoCo biosynthesis (and their corresponding genes) have been widely identified. As is common in the biosynthesis of other flavins and pterins, MoCo synthesis starts from guanosine triphosphate (GTP), and involves the circularisation of GTP to the precursor cyclic pyranopterin monophosphate (cPMP). This reaction is catalysed by two proteins, one a radical SAM⁹ enzyme and the second protein involved in pyrophosphate release. The former has two oxygen-sensitive [4Fe–4S] clusters, one of which is involved in radical SAM generation while the other is crucial for substrate binding. Thereafter, three enzymes are responsible for formation of the dithiolene group in the metal-binding pterin molybdopterin (MTP). Two sulfur atoms are incorporated into cPMP by the heterotetrameric (two large subunits and two small subunits) enzyme MPT synthase to yield MTP, with its characteristic dithiolate function. The small subunit carries a sulfur atom as a thiocarbonate at its C-terminal Gly residue, which is deeply buried in the large subunit to form the active site. Unusually, in human MTP synthase both subunits are encoded by a bicistronic mRNA.

8. Membrane transport proteins having the ABC molecular domain (ATP-binding cassette), characteristic of a large superfamily of proteins that hydrolyse ATP and transport a diverse array of small molecules across membranes.

9. Radical SAM (S-adenosyl methionine) enzymes utilise iron–sulfur clusters and SAM to initiate a diverse set of radical-mediated reactions.

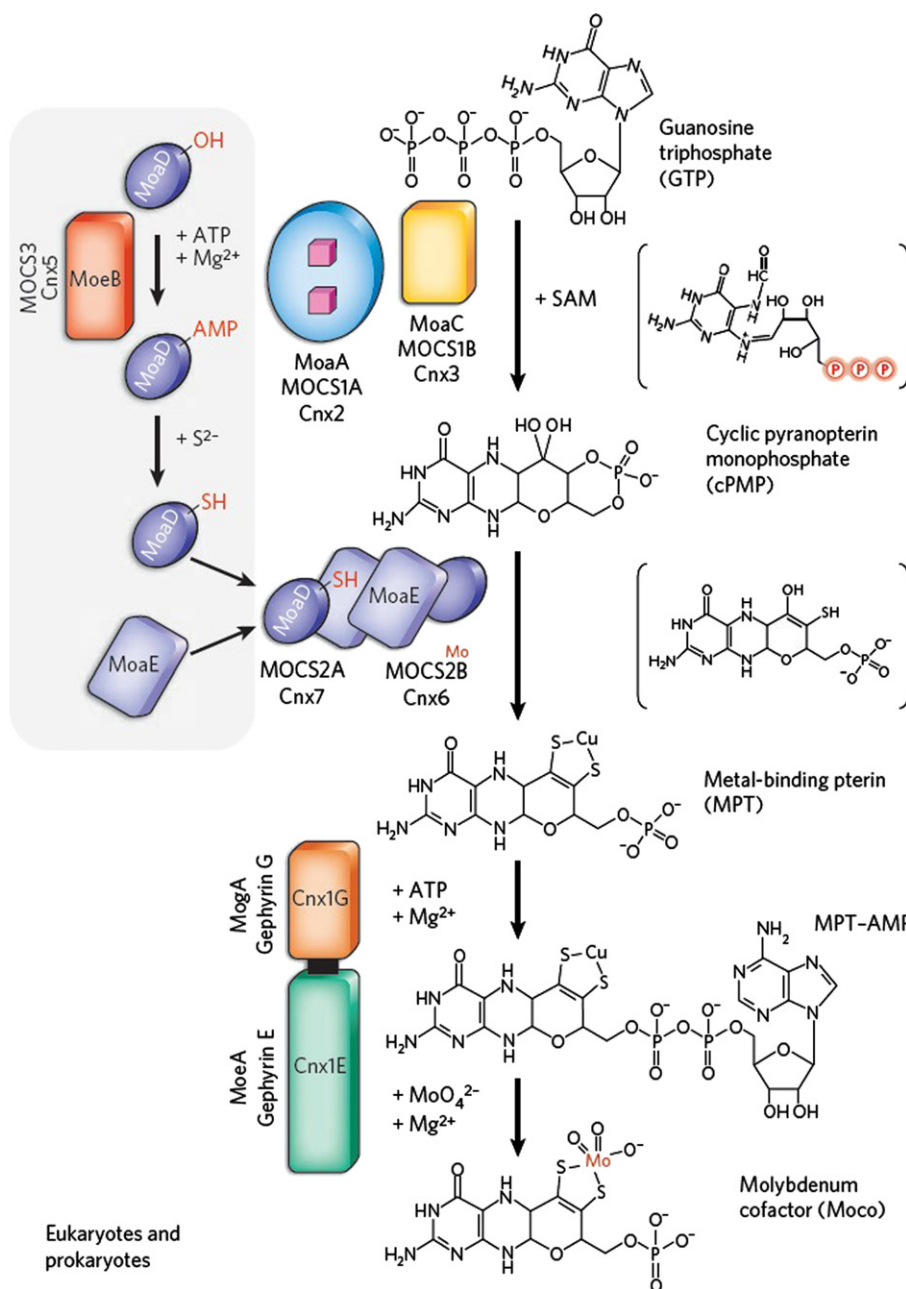


FIGURE 4.12 The basic steps of Moco biosynthesis, starting from GTP. The pathway is based on data derived from *E. coli*, plants and humans. Proposed (first step) or partially characterised (second step) intermediates are indicated in parenthesis. Homologous proteins from *E. coli* ('Mo' nomenclature) humans ('MOCS' nomenclature except gephyrin) and plants ('Cnx' nomenclature) are shown for comparison. The separate pathway for regenerating MTP synthase is grouped within the grey box (for simplicity, only the MoeB protein is shown). Eukaryotes express fusion proteins that contain a MoeB domain and a common rhodanese-like domain involved in sulfur transfer to the small subunit of MTP synthase. (From Schwarz, Mendel, & Ribbe, 2009. Copyright 2009, with permission from Elsevier.)

In a separate pathway, MTP synthase is regenerated (grouped within a grey box in Fig. 4.12) by transferring sulfur to the small subunit. In *Escherichia coli*, MoeB catalyses the adenylation of the carboxyl of the C-terminal Gly residue of MoeD, in a reaction very similar to that catalysed by the E1 enzyme that activates ubiquitin in the ubiquitin/proteasome pathway referred to earlier. The AMP-activated MoeD is then sulfurated by sulfide transfer from an unknown donor. It is assumed that Cu is inserted directly after dithiolate formation. In the last two steps, adenylylated MPT is formed from Mg-ATP, and, finally, in the presence of molybdate (MoO_4^{2-}), bound MPT-AMP is hydrolysed, Cu is released and Mo is transferred to the MPT dithiolate, and the MoCo cofactor is released.

Since MoCo is labile and oxygen-sensitive, which makes it highly unstable, it needs to be transported and stored bound to a MoCo carrier protein (MCP), or else rapidly incorporated into Mo-dependent enzymes

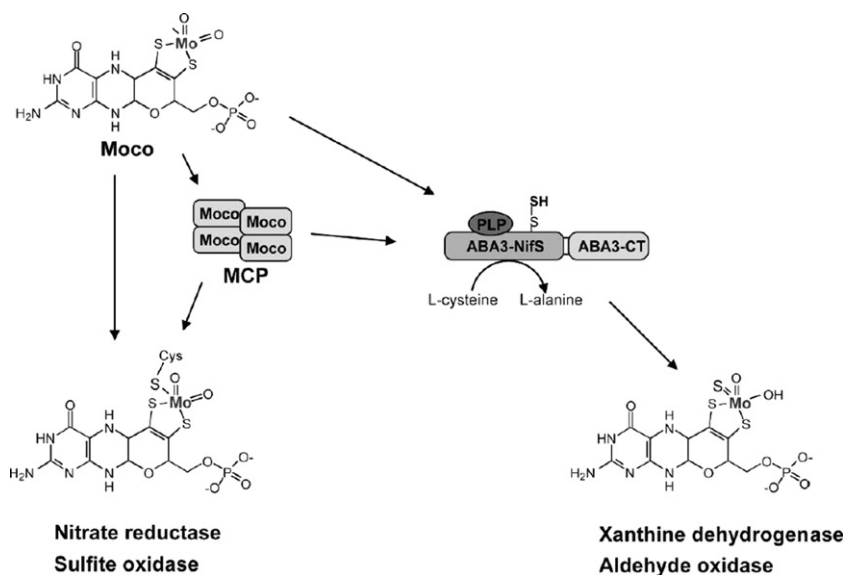


FIGURE 4.13 Mature Moco can be either bound to a Moco carrier protein (MCP), to NR and SO, or to the ABA3 protein. ABA3 generates a protein-bound persulfide, which is the source of the terminal sulfur ligand of Moco in enzymes of the XDH/AO family. (Adapted from Mendel, Smith, Marquet, & Warren, 2007.)

(Fig. 4.13). The active form of MoCo requires a third sulfur ligand, which, in the case of nitrate reductase (NR) and sulfite oxidase (SO), is supplied by a cysteine residue of the apo-protein. For xanthine dehydrogenase (XDH), and aldehyde oxidase (AO), the third sulfur ligand is derived from cysteine and is generated as a persulfide by a PLP-dependent cysteine desulfurase, analogous to that found in Fe—S cluster formation. This is then transferred to MoCo, and occupies a similar position to the terminal sulfur in NR and SO.¹⁰ It is interesting to note that the formation of active Mo-enzymes depends not only on the availability of Mo, but also requires both Fe and Cu.

Nitrogen fixation is carried out by a small number of microorganisms, called diazotrophs, some of which (of the genus *Rhizobium*) function symbiotically¹¹ in the root nodules of nitrogen-fixing legumes (like peas, clover). The reduction of the triple bond of dinitrogen to ammonia is carried out by nitrogenases (discussed in detail in

10. There is yet a third class of Mo-dependent enzymes, the dimethyl sulfoxide reductases (DMSOR), which use a dimeric form of the sulfated MoCo as their cofactor — more of this in Chapter 17.

11. A long-term association between individuals belonging to two different species: often used in the sense of beneficial associations to both partners.

Chapter 17), which are typically composed of two proteins, the **Fe-protein**, a homodimer with one [4Fe–4S] cluster bridged between the subunits and one ATP-binding site in each subunit, and the **MoFe-protein**. The **MoFe-protein**, an $\alpha_2\beta_2$ heterotetramer, contains two complex metallo-clusters, each containing a total of eight metal ions: the **P-cluster** is an [8Fe–7S] cluster located between the [4Fe–4S] cluster of the Fe protein and the FeMo cofactor, whereas the Fe–Mo cofactor is a [Mo–7Fe–9S–X–homocitrate] cluster (where X is C, N or O), buried within each α -subunit. The flow of electrons is from the [4Fe–4S] cluster to the P-cluster and then to the Fe–Mo cofactor.

The **P-cluster** (Fig. 4.6C) can be considered as two [Fe₄S₄] clusters, which have a common bridging μ_6 sulfide ion at one corner. The P clusters undergo structural rearrangements between the oxidised (p^{ox}) and the resting state (dithionite reduced, p^{N}), in which all of the Fe atoms are in the ferrous state. In the reduced form, the bridging sulfite ion forms the eighth corner of each of the two cubane-like structures, coordinated to two iron atoms of each [4Fe–3S] unit. Two cysteine thiols serve as bridging ligands, each coordinating one Fe atom from each cluster – these are the same four Fe atoms that are also coordinated to the central sulfide ion. In the two-electron oxidised cluster (**b**), two of the Fe atoms that were bridged to the central sulfide have moved away from it, leaving it tetracoordinate. The two Fe atoms in question remain four-coordinate, through coordination to the amide nitrogen of Cys 87 α and the side-chain hydroxyl of Ser 186 β . The P-cluster is the only known [Fe–S] cluster to contain serine-O (β -subunit, Ser188) and amide-N (α -subunit, Cys88), as well as typical cysteine-S ligands. The geometry of the P-cluster suggests that it is likely to be assembled by the fusion of two [Fe₄S₄]-like subclusters. This reaction mechanism is well established in synthetic inorganic chemistry, and P-cluster topologs have been recently synthesised. Fig. 4.14 presents structural models for the cluster species in a FeMoco-deficient form of the MoFe protein before (*a*) and after (*b*) P-cluster maturation.

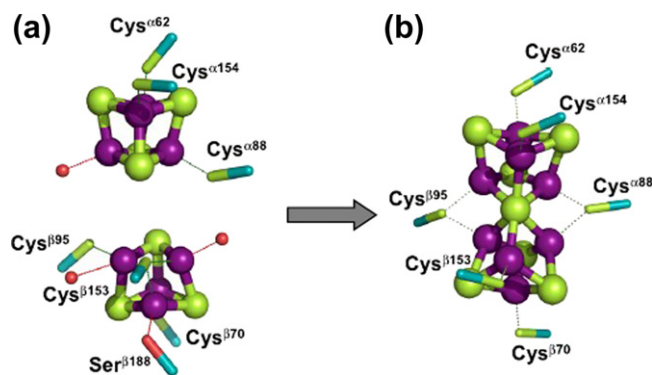


FIGURE 4.14 Structural models for the P cluster species in a FeMoco deficient form of the MoFe protein before (*a*) and after (*b*) P-cluster maturation. The precursor model (*a*) comprises two individual subclusters, a [Fe₄S₄] cluster (*Upper*) and a [Fe₄S₄]-like cluster (*Lower*), with a bridging cysteine in place of a core sulfide; whereas the P-cluster model (*b*) is nearly identical to the mature [Fe₈S₇] structure in the $\Delta nifB$ MoFe protein (Fe, purple; S, green). The possible protein ligands are indicated; additional ligands comprising light atoms (N or O) are represented by red spheres. (From Lee *et al.*, 2009. Copyright 2009 National Academy of Sciences, USA.)

The **FeMo-cofactor** (Fig. 4.6b) can be considered as being structurally similar to the P cluster, consisting of one [Fe₄–S₃X] cubane and one [MoFe₃–S₃X] cubane, sharing a single atom X at a corner common to both cubanes. The two cubanes are additionally bridged by three sulfide ions. Alternatively, the cofactor could be described as a [Fe₆–S₉] core (with the iron atoms symmetrically coordinated to the central atom X), which is capped at each end of the core. The cofactor is bound to the protein by one Cys and one His residue at either end of the structure, and the Mo ion is coordinated approximately octahedrally by three sulfide ions from the cofactor itself, the terminal imidazole nitrogen of the histidine residue of the protein, and two oxygens from a molecule of the unusual tricarboxylic acid homocitrate, which is an essential component of the cofactor. The complexity of the

enzyme systems required to synthesise both the P cluster and the FeMoco cluster, together with the proteins required for their insertion into functionally active nitrogenase, has combined to render the biotechnological dreams of cloning nitrogen fixation into other crop plants an illusion.

The first diazotroph to have its entire nitrogen fixation (*nif*) genes analysed was *Klebsiella pneumoniae*, and the *nif* gene cluster in chromosome K from this organism is shown in Fig. 4.15. Although this is much simpler than in

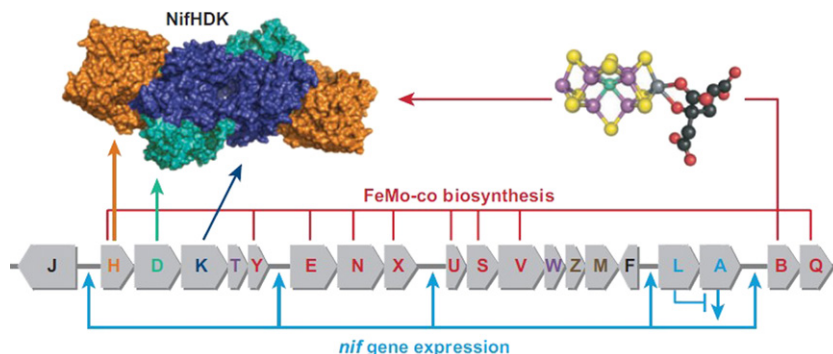


FIGURE 4.15 Nitrogen fixation (*nif*) gene cluster of *Klebsiella pneumoniae*. Genes encoding the nitrogenase component proteins, *nifHDK*, are shown on the left. Genes whose products are involved in nitrogen fixation are color-coded according to their functions. (Adapted from Rubio & Ludden, 2008.)

other model organisms used to study nitrogen fixation like *Azotobacter vinelandii*, its 23-kb sequence nonetheless comprises 20 genes, organised in several transcriptional units.¹² Genes encoding the three protein components of nitrogenase *nifHDK* are shown on the left, with the same colors as the corresponding proteins in the nitrogenase molecule above. Genes whose products are involved in nitrogen fixation are color-coded according to their functions.

Now that we have a clearer idea of the exact functions of many of the genes, and thanks to recent characterisation of a number of assembly-related intermediates, we are beginning to have a better understanding of the biosynthesis of FeMoco. The proteins involved can be functionally divided into three classes: molecular scaffolds (NifU, NifB, and NifEN¹³) on which the FeMoco is progressively assembled, metallocluster carrier proteins (NifX and NifY) which transport FeMoco precursors between assembly sites in the pathway, and enzymes (NifS, NifQ, and NifV) which provide sulfur, molybdenum, and homocitrate as substrates for cofactor synthesis. The role of NifH remains controversial. The biosynthetic pathway is outlined in Fig. 4.16. FeMoco assembly is probably initiated by NifS and NifU, which mobilise iron and sulfur. NifS is a PLP-dependent cysteine desulfurase, generating a protein-bound cysteine persulfide, which is donated to NifU for the formation of [Fe₂S₂] and [Fe₄S₄] clusters (stages 1 and 2). These are then used as building blocks for the formation of a large Fe–S core on NifB (stage 3). Although the precise role of NifB is unknown, it contains the characteristic CX₃CX₂C signature motif at its N-terminus, typical of the radical SAM superfamily, which binds an essential [Fe₄S₄] cluster. The function of the cluster is to provide the electron for the reduction of SAM, which then undergoes cleavage to methionine and the highly reactive 5-deoxyadenosine radical. It is not impossible that NifB might link two [Fe₄S₄] cubanes by inserting a sulfur atom along with the central X atom to construct a full Fe–S core which could later be rearranged into the final core structure of FeMoco. This core would then be processed into a Mo-free precursor (stage 4), which can then be converted to the mature FeMoco on NifEN by Fe-protein-mediated insertion of Mo and

12. Whereas *K. pneumoniae* fixes N₂ under strictly anaerobic conditions, *A. vinelandii* combines N₂ fixation with a robustly and strictly aerobic metabolism.

13. Throughout, the rest of the book genes are in italics, e.g., NifA, whereas the proteins themselves are in regular type, e.g., NifA.

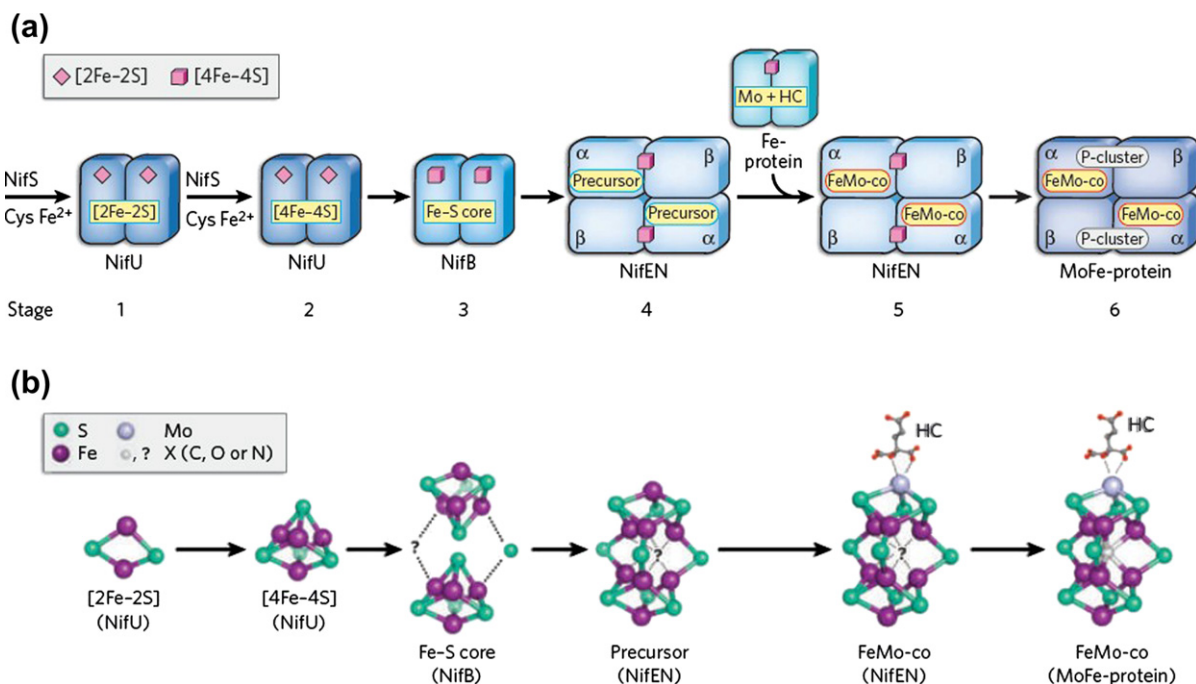


FIGURE 4.16 Biosynthesis of FeMoco. **a**, Sequence of events during FeMoco assembly. The biosynthetic flow of FeMoco is NifU–NifS \rightarrow NifB \rightarrow NifEN \rightarrow MoFe-protein. The permanent metal centres of the scaffold proteins are coloured pink; the transient cluster intermediates are colored yellow. HC, homocitrate. **b**, Structures of intermediates during FeMo-co assembly. Shown are the cluster types that have been identified (on NifU, NifEN, and MoFe-protein) or proposed (for NifB). Hypothetically, NifB could bridge two $[4\text{Fe}-4\text{S}]$ clusters by inserting a sulfur atom along with the central atom, X, thereby generating a Fe–S scaffold that could be rearranged into a precursor closely resembling the core structure of the mature FeMo-co. In the case of the NifEN-associated precursor, only the 8Fe model is shown. The potential presence of X in the intermediates of FeMo-co biosynthesis is indicated by a question mark. (From Schwarz *et al.*, 2009. Copyright 2009, with permission from Elsevier.)

homocitrate (stage 5). It seems likely that the FeMoco is assembled by having the complete Fe–S core structure in place before insertion of the Mo. After the completion of FeMoco assembly on NifEN, FeMoco is delivered to its final location in the MoFe-protein (stage 6).

Yet another organic cofactor of extraordinary complexity is the H-cluster of $[\text{FeFe}]$ hydrogenases (Fig. 4.6d), which catalyses the reduction of protons to hydrogen. The mature cofactor consists of a $[\text{Fe}_4\text{S}_4]$ cluster bridged by a cysteine thiolate sulfur atom to a 2Fe subcluster, which has CO, CN, and dithiolate ligands (Nicolet *et al.*, 2002). The unusual coordination of cyanide and carbon monoxide ligands to the 2Fe subcluster was established by spectroscopic methods, since the electron density of carbon, nitrogen, and oxygen cannot easily be differentiated by X-ray crystallography. The 2Fe subcluster is thought to be assembled on the scaffold protein HydF in a process requiring two radical SAM enzymes, HydE and HydG. The H-cluster is assembled in a stepwise fashion, first, by insertion of a $[\text{Fe}_4\text{S}_4]$ cluster into the structural gene *apo-HydA* (Fig. 4.17). The 2Fe subcluster of the H cluster is synthesised on HydF from a $[2\text{Fe}-2\text{S}]$ cluster framework in a process requiring HydE, HydG, and GTP* and transferred from HydF to HydA. The diatomic ligands CN and CO of the 2Fe cluster are derived from tyrosine, which is cleaved to form *p*-cresol and dehydroglycine (Fig. 4.17). The latter, by an as yet unknown mechanism, generates CN and CO. The origins of the dithiolate bridge and the role of HydE remain to be elucidated. The nature of the bridgehead atom (C, N, or O) in the 1,3-dithiolate ligand could not be determined unequivocally from the X-ray data, and is therefore shown as X in the Figure 4.17.

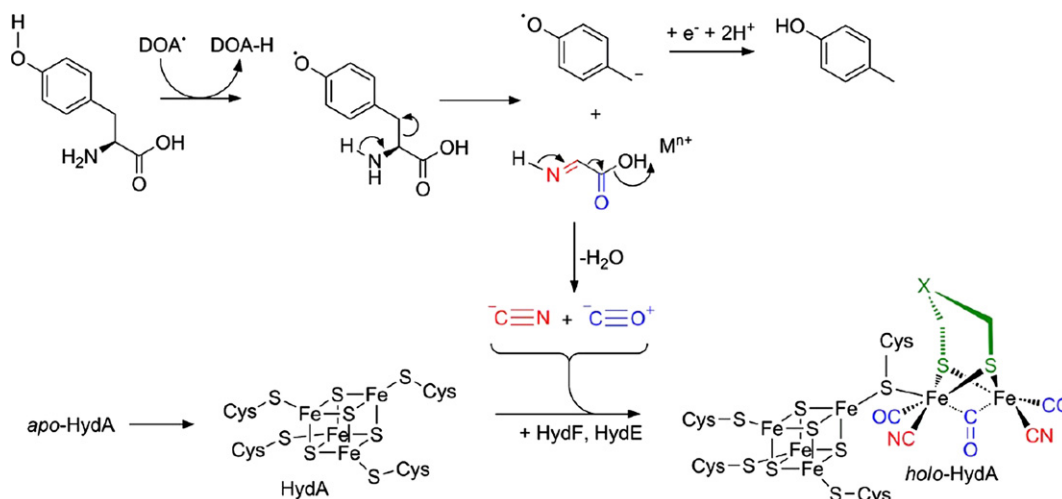


FIGURE 4.17 The role of HydG in [FeFe]-hydrogenase cofactor assembly. M^{n+} represents catalysis by either an active site acid ($M = \text{H}$, $n = 1$) or a metal ion (for example, Fe^{2+} or Fe^{3+} that may form part of a second iron–sulfur cluster in HydG). (From Roach, 2010. Copyright 2010, with permission from Elsevier.)

Finally, in this gallery of extraordinary ligands, we have the Cu_Z cluster of nitrous oxide reductase. This enzyme is found in denitrifying bacteria where it catalyses the final step in the nitrogen cycle, the reduction of nitrous oxide (N_2O) to dinitrogen, thereby returning fixed nitrogen to the atmosphere. Nitrous oxide reductase contains two types of copper centres, Cu_A and Cu_Z . The Cu_A centre (which is described in Chapter 14) serves as an electron-transfer centre, while the Cu_Z centre is associated with the active site of nitrous oxide reduction. The Cu_Z site comprises four copper ions arranged in a tetranuclear cluster bound to a central sulfide (Fig. 4.6e) with a bridging oxygen between Cu_1 and Cu_4 . Seven histidine residues complete the coordination of the cluster, three of the Cu atoms bound to two His residues while Cu_4 is liganded by a single His ligand. It has been suggested that Cu_4 is the binding site for N_2O , since it has only one His ligand and coordinates the bridging oxygen species. In addition to the structural gene for the N_2O reductase protein, a number of other gene products are required for cofactor assembly and insertion, which have been well characterised.

SIDEROPHORES

In Chapter 2, we mentioned the Fe(III) chelator, desferrioxamine B, which is a member of a large class of iron-binding molecules called siderophores. Siderophores are iron-complexing molecules, of low molecular weight (typically less than 1000), which are synthesised by bacteria and fungi and serve to allow the microbial cell to take up iron from its environment (described in Chapter 7). All of the natural siderophores are designed to selectively chelate Fe(III), which, under aerobic conditions, is the predominant form of iron in the environment. This means that they usually contain hard O-donor atoms as ligands and form thermodynamically extremely stable octahedral (hexacoordinate) complexes with Fe(III). They can be classified into several groups according to their chemical structures: hydroxamates, catecholates, carboxylates, as well as polydentate phenolate/nitrogen heterocycle/carboxylate combinations. More than five hundred siderophores have been structurally characterised. A few examples are given in Fig. 4.18. Ferrichrome (pFe = 25.2),¹⁴ first isolated from the smut mold *Ustilago* in 1952, the best characterised of the hydroxamate siderophores (desferrioxamine B also belongs to this family), has a cyclic hexapeptide backbone to which are attached three molecules of N-acyl-N-hydroxy-L-ornithine.

14. pFe as defined in Chapter 2.

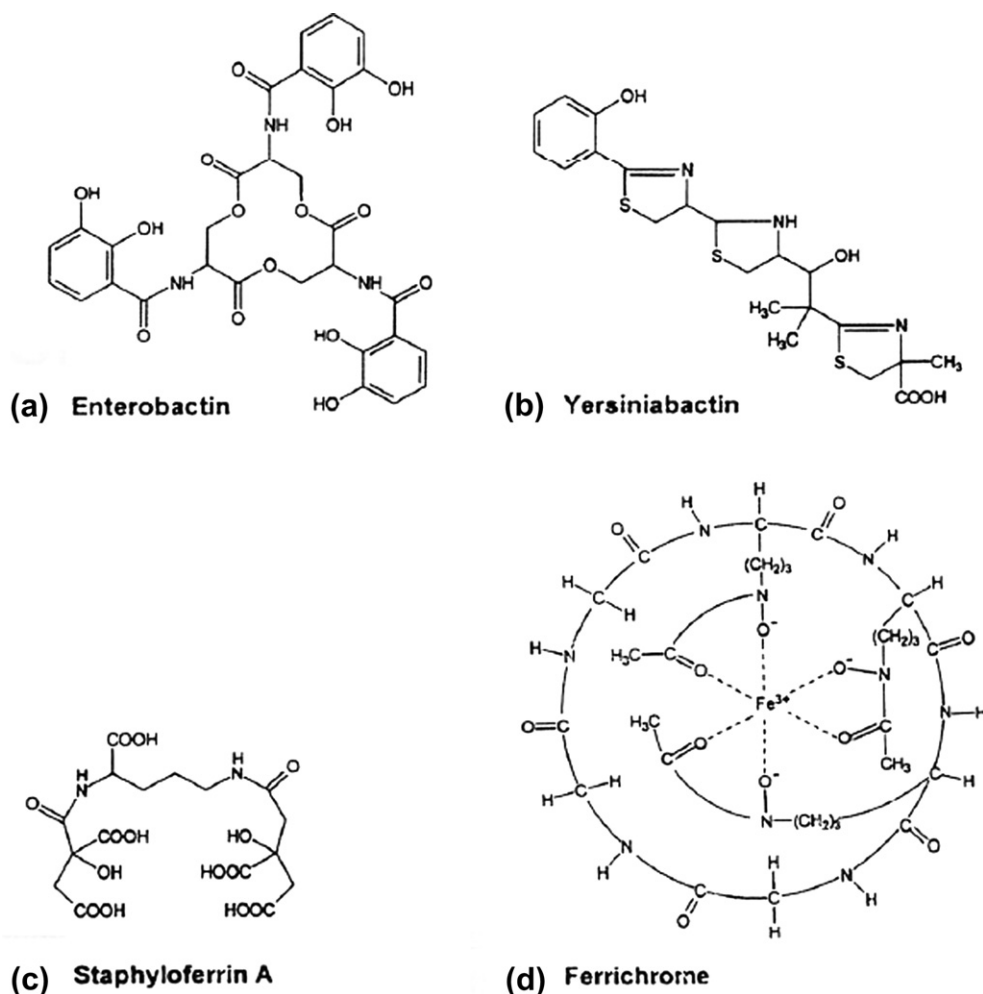


FIGURE 4.18 Chemical structures of selected siderophores to illustrate the four major structural classes (a) Enterobactin (b) Yersiniabactin (c) Staphyloferrin (d) ferrichrome.

Enterobactin ($pFe = 35.5$), the prototype of the catecholate siderophores, is the principal siderophore produced by *Escherichia coli* (Raymond et al., 2003). It is a cyclic triester of dihydroxybenzoyl-serine. When enterobactin binds iron, the six deprotonated hydroxyl groups of the dihydroxybenzoyl (or catecholate) functions wrap around the metal ion in the centre of the molecule (Fig. 4.19). Staphyloferrin A, the iron-transporting siderophore of *Staphylococci*, contains a D-ornithine backbone to which two citric acid residues are linked, which are involved in Fe(III) binding. Yersiniabactin is an example of a heterocyclic siderophore, from the highly pathological *Yersinia* family.¹⁵ In ferric-yersiniabactin, the iron atom is coordinated by the three nitrogens, and three negatively charged oxygen atoms, arranged in a distorted octahedral arrangement (Miller et al., 2003).

The importance of iron for a bacteria like *E. coli* can be illustrated by the fact that 14 genes alone are required for enterobactin-mediated iron uptake, including those for its synthesis, export, transport of the ferric-enterobactin back into the cell and iron release. In total, *E. coli* has at least eight uptake systems for iron, encoded by some 50 genes.

15. This family of charmers includes *Y. pestis*, the causative agent of the plague.

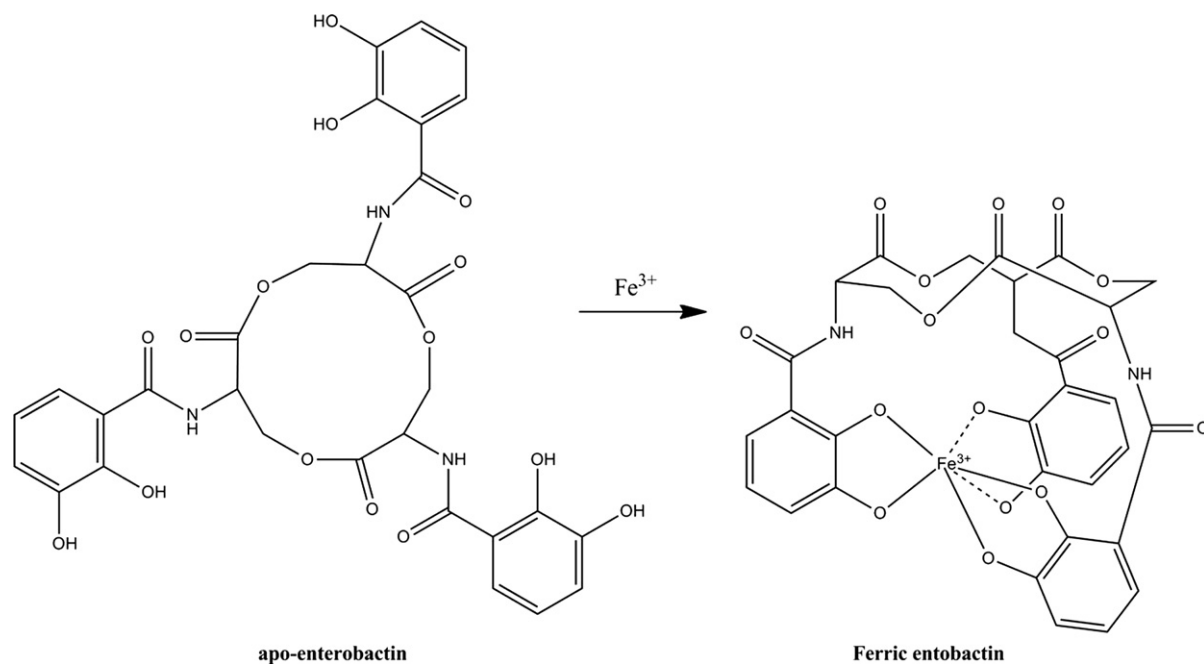


FIGURE 4.19 Iron incorporation into apo-enterobactin.

Because they often function as virulence factors, the enzymes involved in siderophore biosynthesis are potential targets for developing antimicrobial strategies. The mechanisms of siderophore biosynthesis follow the same fundamental biosynthetic logic involving similar protein machinery, which we describe in greater detail in Chapter 5 for fatty acid biosynthesis. It is also used in the microbial biosynthesis of many important natural products polyketides and peptides (including many antibiotics). Essentially, as is illustrated in Fig. 4.20, for enterobactin, it involves

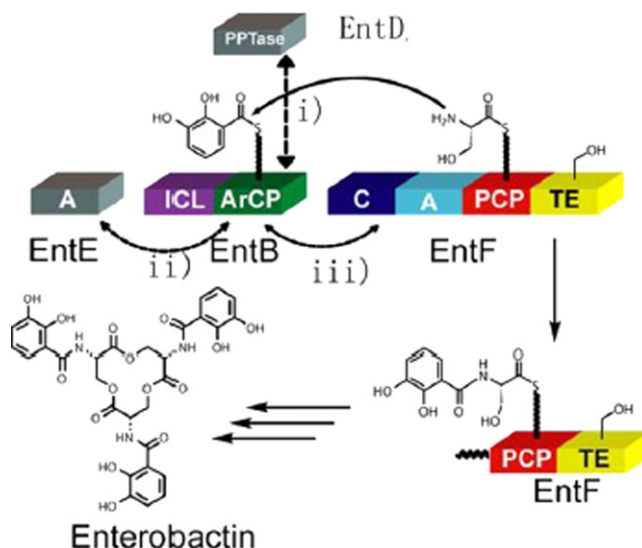


FIGURE 4.20 Enterobactin biosynthesis scheme. The endogenous phospho-pantotheinyl transferase is EntD. Protein–protein interactions between the EntBArCP aryl carrier protein domain and the other protein components during enterobactin biosynthesis are indicated by double-headed arrows. The ArCP must be recognised by the PPTase (EntD (i), EntE (ii), and the EntF C domain (iii)). (Modified from Zhou, Lai, & Walsh, 2007.)

a central carrier protein onto which the precursors are loaded, which undergo a series of elongation steps on a multimodular protein assembly line. The enterobactin synthetase consists of four proteins (EntBDEF) and is synthesised from 2,3-dihydroxybenzoic acid (DHB). DHB is activated by EntE and transferred to the carrier protein domain of EntB. The four-domain EntF protein together with EntE and EntB then carry out the stages of chain initiation, elongation, and termination, which, after the hydrolysis of three molecules of DHB-serine, leads to release of the final cyclized product by the thioesterase domain of EntF.

REFERENCES

- Al-Karadaghi, S., Franco, R., Hansson, M., Shelnutt, J. A., Isaya, G., & Ferreira, G. C. (2006). Chelataes: distort to select? *Trends in Biochemical Sciences*, 31, 135–142.
- Chu, B. C., Garcia-Herrero, A., Johanson, T. H., Krewulak, K. D., Lau, C. K., Peacock, R. S., et al. (2010). Siderophore uptake in bacteria and the battle for iron with the host; a bird's eye view. *Biometals*, 23, 601–611.
- Culotta, V. C., Yang, M., & O'Halloran, T. V. O. (2006). Activation of superoxide dismutases: putting the metal to the pedal. *Biochimica et Biophysica Acta*, 1763, 747–758.
- Krewulak, K. D., & Vogel, H. J. (2008). Structural biology of bacterial iron uptake. *Biochim. Biophys. Acta*, 1778, 1781–1804.
- Lee, C. C., Blank, M. A., Fay, A. W., Yoshizawa, J. M., Hu, Y., Hodgson, K. O., et al. (2009). Stepwise formation of P-cluster in nitrogenase MoFe protein. *Proceedings of the National Academy of Sciences of the United States of America*, 106, 18474–18478.
- Mendel, R. R., Smith, A. G., Marquet, A., & Warren, M. J. (2007). Metal and cofactor insertion. *Natural Product Reports*, 24, 963–971.
- Miller, M. C., Parkin, S., Fetherston, J. D., Perry, R. D., & Demoll, E. (2006). Crystal structure of ferric-yersiniabactin, a virulence factor of *Yersinia pestis*. *Journal of Inorganic Biochemistry*, 100, 1495–1500.
- Nicolet, Y., Cavazza, C., & Fontecilla-Camps, J.-C. (2002). Fe-only hydrogenases: structure, function and evolution. *Journal of Inorganic Biochemistry*, 91, 1–8.
- Rao, P. V., & Holm, R. H. (2004). Synthetic analogues of the active sites of iron-sulfur proteins. *Chemical Reviews*, 104, 527–559.
- Raymond, K. N., Dertz, E. A., & Kim, S. S. (2003). Enterobactin: an archetype for microbial iron transport. *Proceedings of the National Academy of Sciences of the United States of America*, 100, 3584–3588.
- Rees, D. C. (2002). Great metaloclusters in enzymology. *Annual Review of Biochemistry*, 71, 221–246.
- Roach, P. L. (2010). Radicals from S-adenosylmethionine and their application to biosynthesis. *Current Opinion in Chemical Biology*. 2010 Dec 13. (Epub ahead of print).
- Rubio, L. M., & Ludden, P. W. (2008). Biosynthesis of the iron-molybdenum cofactor of nitrogenase. *Annual Review of Microbiology*, 62, 93–111.
- Schwarz, G., Mendel, R. R., & Ribbe, M. W. (2009). Molybdenum cofactors, enzymes and pathways. *Nature*, 460, 839–847.
- Sheftel, A., Stehling, O., & Lill, R. (2010). Iron-sulfur proteins in health and disease. *Trends in Endocrinology and Metabolism*, 21, 302–314.
- Zhou, Z., Lai, J. R., & Walsh, C. T. (2007). Directed evolution of aryl carrier proteins in the enterobactin synthetase. *Proceedings of the National Academy of Sciences of the United States of America*, 104, 11621–11626.

This page intentionally left blank

An Overview of Intermediary Metabolism and Bioenergetics

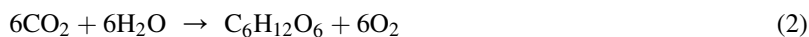
Introduction	91
Redox Reactions in Metabolism	92
The Central Role of ATP in Metabolism	94
The Types of Reaction Catalysed by Enzymes of Intermediary Metabolism	96
An Overview of Catabolism	97
Selected Case Studies – Glycolysis and the Tricarboxylic Acid Cycle	100
An Overview of Anabolism	105
Selected Case Studies: Gluconeogenesis and Fatty Acid Biosynthesis	106
Bioenergetics – Generation of Phosphoryl Transfer Potential at the Expense of Proton Gradients	108

INTRODUCTION

What, we may ask, is intermediary metabolism? It is the sum of all of the reactions which are involved in the transformation of the substances which are assimilated by an organism from its environment: their transformation, on the one hand, into energy and their use, on the other, to ensure the biosynthesis of molecules necessary for the function of the organism, like the proteins, nucleic acids, membrane, oligo- and polysaccharides, and storage and membrane lipids that we described in Chapter 4 (For more information concerning the content of this Chapter see Berg et al., 2002; Campbell et al., 2005; Devlin, 2005; Voet and Voet, 2004). The former, essentially degradative process is often referred to as **catabolism** (Figure 5.1) – transforming more complex and more reduced metabolites into simpler, more oxidised products accompanied by the generation of ATP and reducing power in the form of NADPH. A good example is the transformation of glucose (represented here by its empirical formula) to carbon dioxide and water by the combination of glycolysis and the tricarboxylic acid cycle:



In contrast, **anabolism**, often referred to as biosynthesis, consumes energy, rather than producing it, typically taking more oxidised molecules and transforming them into more complex, more highly reduced end products. The reverse process to that described in Equation (1), carried out by many photosynthetic organisms, involves the fixation of atmospheric CO_2 to form glucose, catalysed by the enzymes which constitute the Calvin¹ cycle:



Two important implications of the reactions described in Equations (1) and (2) are: (i) that redox reactions play an important role in metabolic transformations, with the cofactors nicotinamide adenine dinucleotide (NAD^+)

1. After the Californian biochemist Melvin Calvin, who received the Nobel prize for his discovery that the first product of CO_2 fixation was phosphoglycerate, and went on to establish the cycle.

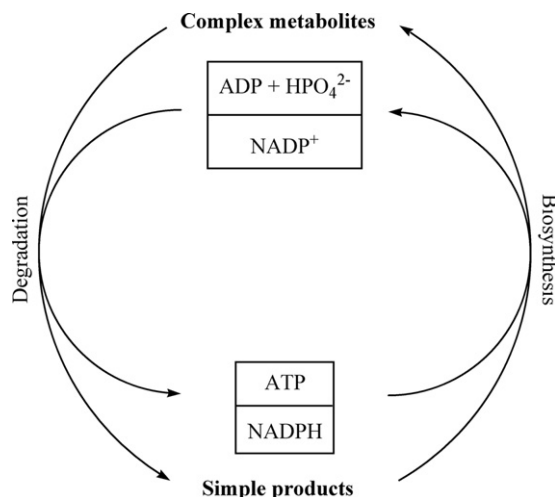


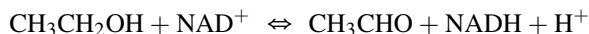
FIGURE 5.1 Energy (as ATP) and reducing power (in the form of NADPH) for biosynthesis (*anabolism*) are derived from degradation (*catabolism*) of complex metabolites.

often acting as electron acceptor in catabolic pathways and reduced nicotinamide adenine dinucleotide phosphate (NADPH) as electron donor in anabolism, and (ii) that energy which is generated by catabolism is then used in biosyntheses (almost always in the form of adenosine triphosphate, ATP).

The ways in which energy in the form of ATP is produced and is utilised constitutes bioenergetics, and will be discussed in greater detail at the end of this Chapter. However, before turning to a selection of metabolic pathways, we outline some fundamental notions concerning redox reactions followed by a brief description of the central role of ATP in metabolism as an acceptor and donor of phosphoryl groups, and finally a summary of the types of reactions that we will encounter as we wend our way along a sample of some of the pathways of intermediary metabolism.

REDOX REACTIONS IN METABOLISM

Since many of the transformations undergone by metabolites involve changes in oxidation state, it is understandable that cofactors have been developed to act as electron acceptors/donors. Two of the most important are NAD^+ and NADP^+ (Figure 5.2). Nicotinamide adenine dinucleotide (NAD^+) can accept what is essentially two electrons and a proton (a hydride ion) from a substrate like ethanol in a reaction catalysed by alcohol dehydrogenase, to give the oxidised product, acetaldehyde, and the reduced cofactor NADH plus a proton:



Whereas redox reactions on metal centres usually only involve electron transfers, many oxidation/reduction reactions in intermediary metabolism, as in the case above, involve not only electron transfer, but hydrogen transfer as well — hence the frequently used denomination ‘dehydrogenase’. Note that most of these dehydrogenase reactions are reversible. Redox reactions in biosynthetic pathways usually use NADPH as their source of electrons. In addition to NAD^+ and NADP^+ , which intervene in redox reactions involving oxygen functions, other cofactors like riboflavin (in the form of flavin mononucleotide, FMN, and flavin adenine dinucleotide, FAD) (Figure 5.3) participate in the conversion of $[-\text{CH}_2-\text{CH}_2-]$ to $[-\text{CH}=\text{CH}-]$, as well as in electron transfer chains. In addition, a number of other redox factors are found, e.g., lipoate in α -ketoacid dehydrogenases, and ubiquinone and its derivatives, in electron transfer chains.

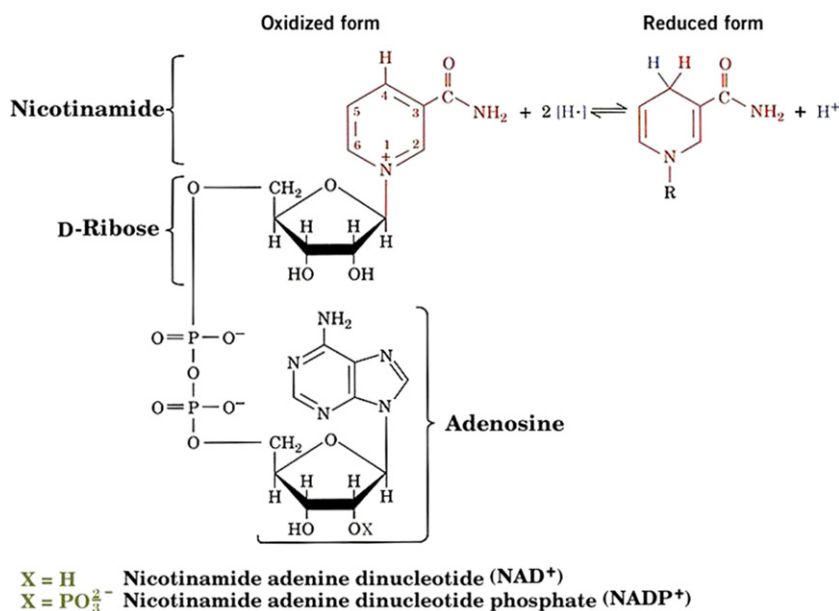


FIGURE 5.2 The structure of NAD^+ and $NADP^+$ and the role of the nicotinamide moiety as an electron acceptor.

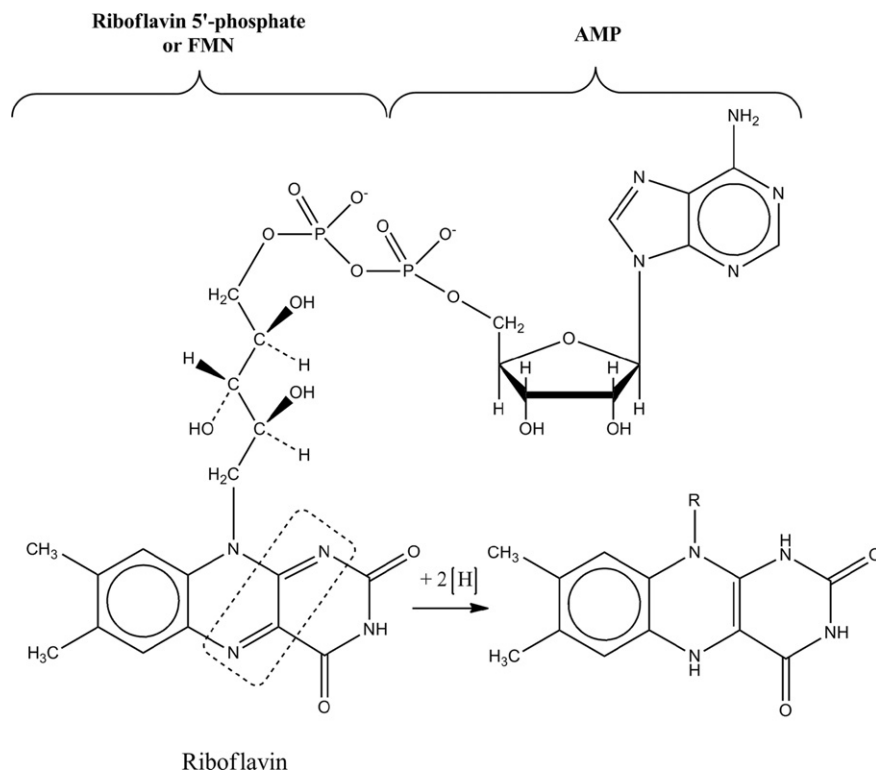


FIGURE 5.3 The flavin coenzymes FAD and FMN. Whereas FMN consists simply of riboflavin monophosphate, FAD has an AMP unit joined to riboflavin monophosphate. Note that in contrast to NAD^+ , flavins can be half-reduced to the stable radical $FADH$ or fully reduced to the dihydroflavin shown.

THE CENTRAL ROLE OF ATP IN METABOLISM

We can situate the importance of ATP in intermediary metabolism by some anecdotal information. The average ATP molecule is hydrolysed within minutes of its synthesis (its turnover is very rapid). At rest, the average human consumes around 40 kg of ATP per day, while during vigorous exercise, this may rise to around 0.5 kg/min! The hydrolysis of ATP (Figure 5.4) to ADP and P_i is accompanied by a relatively large free energy change² (~ 50 kJ/mole), as is that of

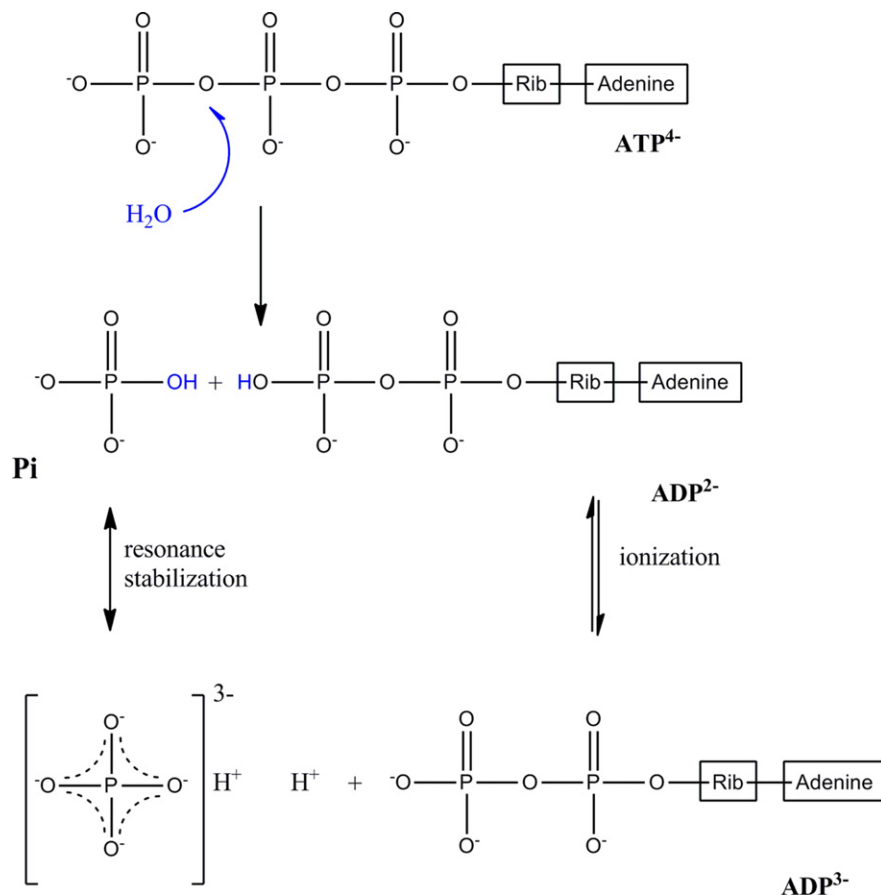


FIGURE 5.4 The chemical basis of the large free energy change associated with ATP hydrolysis. Hydrolysis is accompanied by relief of the electrostatic repulsion between the negative charges on ATP by charge separation; the resulting phosphate anion is stabilised by resonance, while the other product, ADP^{2+} releases a proton into a medium where $[H^+]$ is very low ($\sim 10^{-7}$ M).

ADP to AMP and P_i . In contrast, the hydrolysis of AMP to adenosine and phosphate generates very little free energy change. In biochemical terms, the importance of ATP as the energetic currency of the cell depends on the capacity of the couple ATP/ADP to accept phosphoryl groups from high-energy donors and to donate phosphoryl groups to low energy acceptors. Thus, to give an example from the glycolysis pathway described below, ATP can donate its

2. Where possible we have used the free energies ΔG calculated from *in vivo* concentrations of metabolites rather than the standard free energies ΔG° , which do not take account of local concentrations of reactants and products.

phosphoryl group to glucose to generate glucose-6-phosphate and ADP. We can consider this as the sum of two reactions, one energetically unfavourable, the other extremely favourable (Figure 5.5). This can be readily understood,

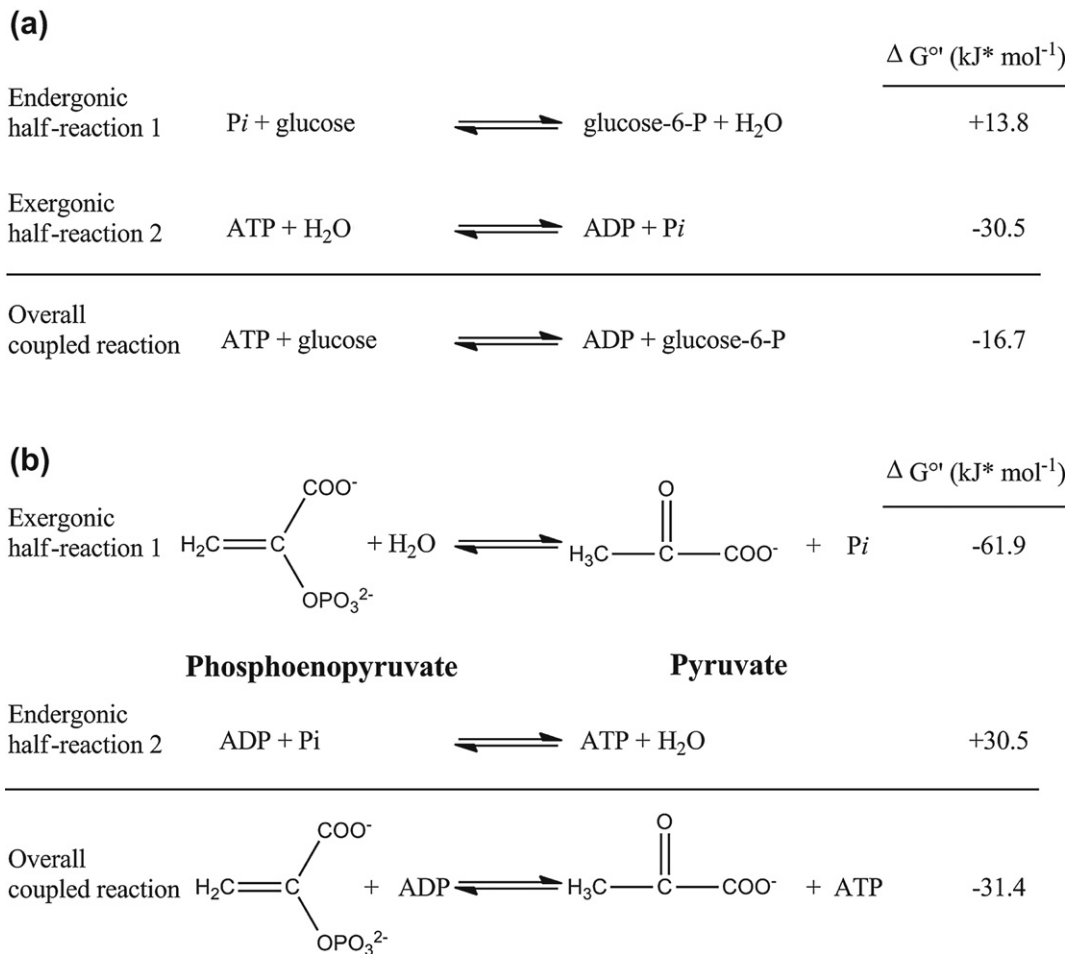
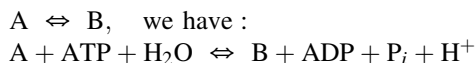


FIGURE 5.5 The coupled reaction in which ATP supplies the phosphoryl group for glucose-6-phosphate synthesis: in contrast, phosphoenolpyruvate has a phosphoryl transfer potential sufficiently elevated to enable it to donate its phosphoryl group to ADP, generating ATP.

since the free energy change for hydrolysis of glucose-6-phosphate is significantly lower than that of ATP. In contrast, the phosphoenolpyruvate molecule can readily transfer its phosphoryl group to ADP, thereby generating ATP. This is the essence of the central role of ATP as the energetic currency of the cell, accepting phosphoryl groups from potential donors, like phosphoenolpyruvate, and donating them to potential acceptors, like glucose. Another important feature of ATP is that the hydrolysis of ATP can be used in a coupled reaction, e.g., instead of



the coupled reaction will change the equilibrium ratio of products to reactants by around 10⁸, which will make very unfavourable reactions become energetically extremely favourable (indeed coupling one or more reactions to the hydrolysis of n ATP molecules will increase the equilibrium ratio by a factor of 10^{8 n}).

THE TYPES OF REACTION CATALYSED BY ENZYMES OF INTERMEDIARY METABOLISM

While intermediary metabolism encompasses a vast number of transformations, in reality there are only a few types of reactions which are used. The first class are the redox reactions described above. A second class are nucleophilic displacements (Figure 5.6), often referred to as group transfer reactions: the most commonly

Nucleophilic Displacement

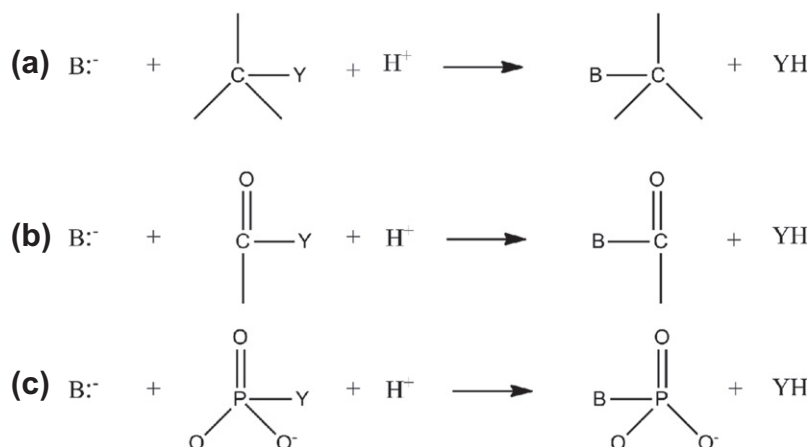
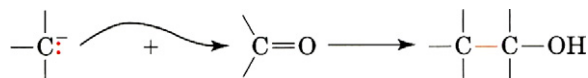


FIGURE 5.6 Nucleophilic displacement reactions involving glycosyl (a), acyl (b) or phosphoryl (c) group transfers.

transferred groups are glycosyl groups (a), acyl groups (b) and phosphoryl groups (c). Other group transfer reaction (Table 5.1), which we have already encountered, include phosphoryl transfer, using ATP or other nucleoside di- or triphosphates and electron transfer (described above for nicotinamide and riboflavin derivatives). Other examples include transfer of acyl and aldehyde groups, CO_2 , one-carbon units, sugars, and phosphatidate. Elimination reactions (Figure 5.7) often result in the formation of carbon–carbon double bonds, isomerisations involve intramolecular shifts of hydrogen atoms to change the position of a double bond, as in the aldose–ketose isomerisation involving an enediolate anion intermediate, while rearrangements break and reform carbon–carbon bonds, as illustrated for the side-chain displacement involved in the biosynthesis of the branched chain amino acids valine and isoleucine. Finally, we have reactions which involve generation of resonance-stabilised nucleophilic carbanions (enolate anions), followed by their addition to an electrophilic carbon (such as the carbonyl carbon atoms of aldehydes, ketones, esters, and CO_2), resulting in the formation of carbon–carbon bonds:



These carbanions can be formed (Figure 5.8) by proton abstraction from ketones resulting in aldol condensations, by proton abstraction from acetyl CoA, leading to Claisen ester condensation, and by decarboxylation of β -keto acids leading to a resonance-stabilised enolate, which can likewise add to an electrophilic centre. It should be noted that the reverse of decarboxylation also leads to formation of a carbon–carbon bond (this is again a group transfer reaction involving biotin as the carrier of the activated CO_2 to be transferred).

TABLE 5.1 Types of Group Transfer reaction Involved in Intermediary Metabolism with the Donor of the Group to be Transferred (left) and the Type of Group Transferred (right)

ATP	Phosphoryl
NADH* and NADPH*	Electrons
FADH ₂ * and FMNH ₂ *	Electrons
Coenzyme A*	Acyl
Lipoamide*	Acyl
Thiamine pyrophosphate*	Aldehyde
Biotin*	CO ₂
Tetrahydrofolate*	One-carbon units
SAdenosylmethionine	Methyl
UDP-glucose	Glucose
CDP-diacylglycerol	Phosphatidate
*Contains a derivative of a B vitamin	

Group transfer reactions often involve vitamins,³ which humans need to obtain in their diet, since we are incapable of realising their synthesis. These include nicotinamide (derived from the vitamin nicotinic acid), and riboflavin (vitamin B₂) derivatives, required for electron transfer reactions, biotin for the transfer of CO₂, pantothenate for acyl group transfer, thiamine (vitamin B₁, as thiamine pyrophosphate) for transfer of aldehyde groups, folic acid (as tetrahydrofolate) for exchange of one-carbon fragments. Lipoic acid (not a vitamin) is both an acyl and an electron carrier. In addition, vitamins like pyridoxine (vitamin B₆, as pyridoxal phosphate), vitamin B₁₂, and vitamin C (ascorbic acid) participate as cofactors in an important number of metabolic reactions.

AN OVERVIEW OF CATABOLISM

As we pointed out in Figure 5.1, there are two broad strands to intermediary metabolism, those in which energy is produced and reducing power generated (catabolism) and those in which energy is consumed and reducing power utilised (anabolism).

In catabolism (Figure 5.9), complex macromolecules, such as proteins and storage polysaccharides (glycogen in animals, starch in plants) and fat stores in the form of triglycerides, are first hydrolysed to their basic components — respectively amino acids, monosaccharides, essentially glucose, and glycerol plus fatty acids. In the second phase, these molecules are transformed into a series of molecules which will feed the final, and central core of catabolism, namely the tricarboxylic acid cycle. Glucose is converted into pyruvate by the glycolysis pathway, described in greater detail below. Of the twenty amino acids found in proteins, all must first be divested of their amino group, which is usually converted to ammonium ions (which in many higher organisms, including man, must be detoxified by conversion to urea). The resulting carbon skeletons are then transformed into either

3. Defined, classically, as things you get ill with when you don't have them! (i.e., — which we are incapable of synthesising ourselves).

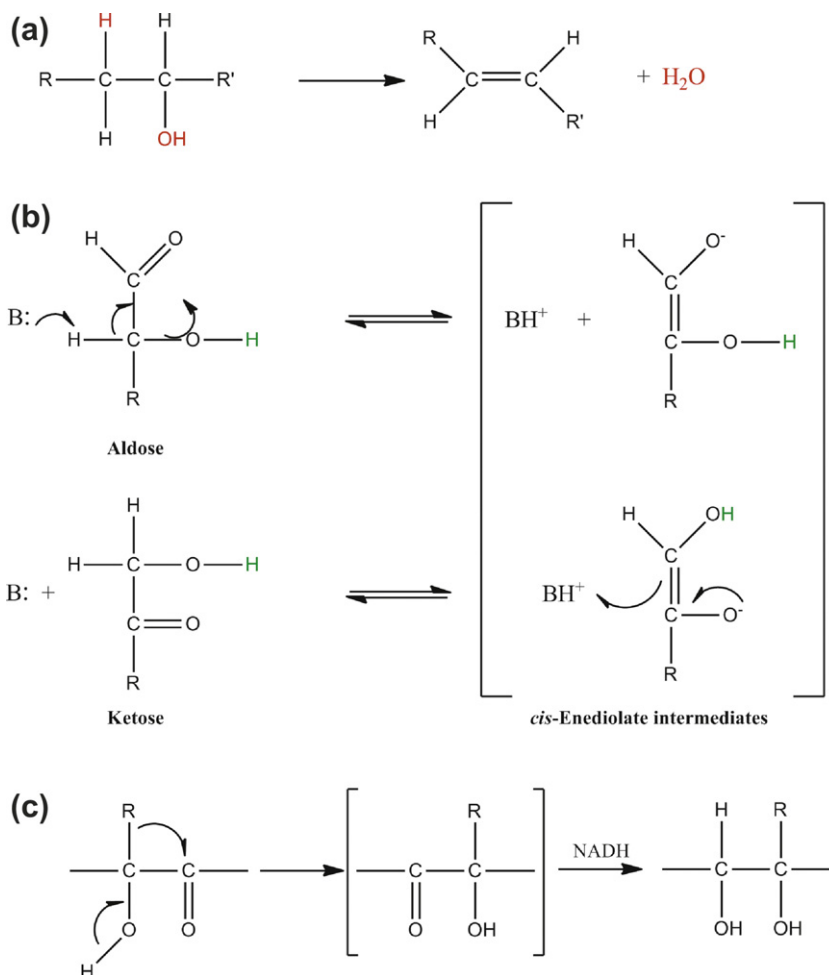


FIGURE 5.7 Examples of (a) elimination, (b) isomerisation (aldose/ketose), and (c) a complex rearrangement of the pinacol/pinacolone type found in the biosynthesis of valine and isoleucine.

pyruvate, acetyl CoA, or one of the constituents of the tricarboxylic acid cycle. In the case of triglycerides, glycerol can enter the glycolytic pathway directly, while the long chain fatty acids are transformed by β -oxidation into acetyl CoA. The oxidation of amino acids and fatty acids is centralised within the mitochondria, where all of the enzymes involved in the tricarboxylic acid cycle are also localised.

As was indicated in (1), in addition to CO_2 , the other final product of glucose oxidation is H_2O , which is produced by the four-electron reduction of dioxygen together with 4H^+ to give two molecules of water. The reducing equivalents come from the dehydrogenase reactions of catabolism in the form of NADH and FADH_2 . Their electrons are then transferred through a series of electron acceptors to the terminal oxidase of the so-called respiratory chain, cytochrome c oxidase. As the electrons pass down this electron-transport chain, they generate a proton gradient which, as we will see shortly, is used to drive the proton-translocating ATP synthase. This aspect of mitochondrial function is usually referred to as oxidative phosphorylation.

We will return to an overview of anabolic pathways shortly, but first we want to examine in more detail two important catabolic pathways, glycolysis and the tricarboxylic acid cycle.

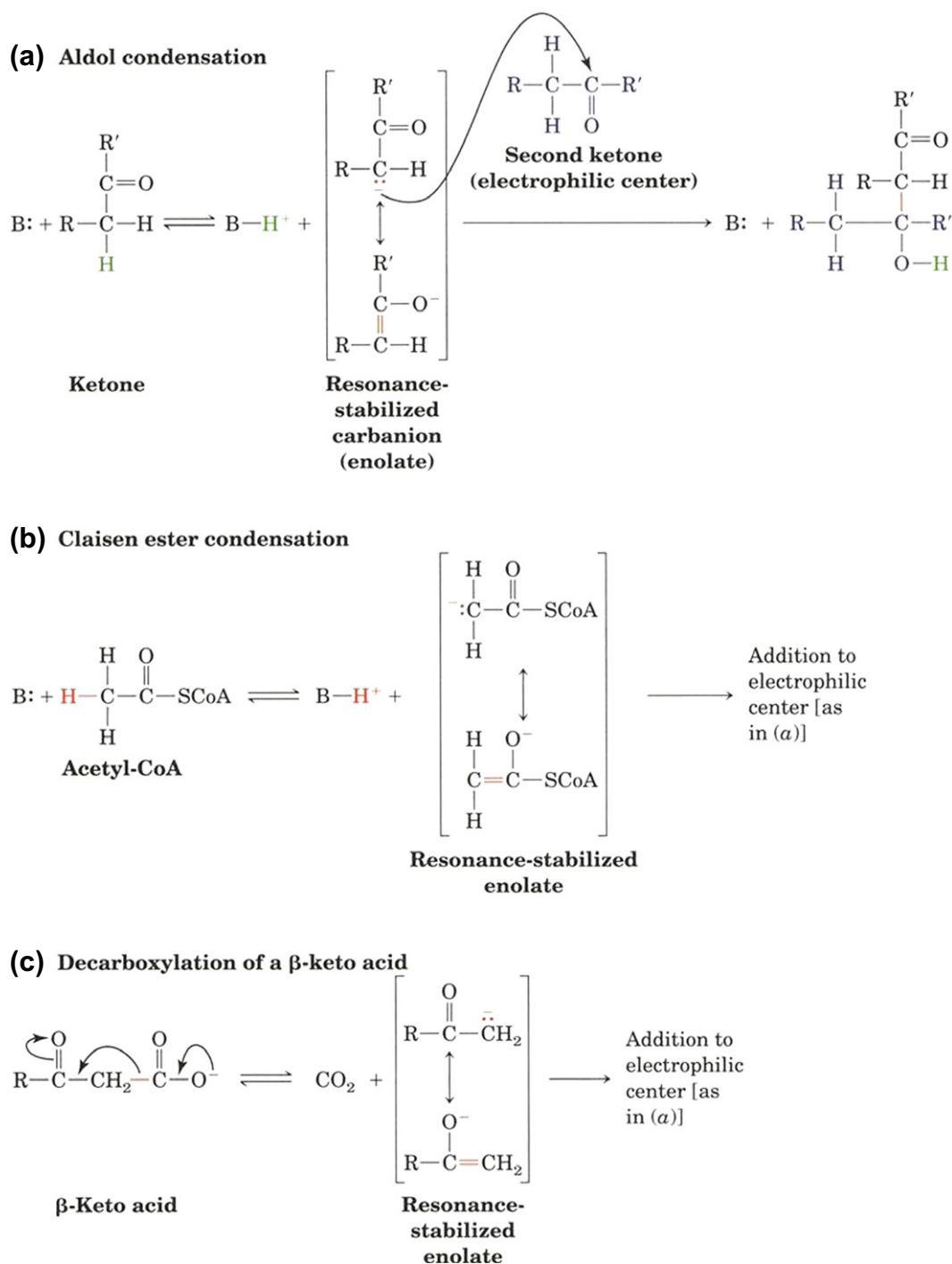


FIGURE 5.8 Examples of formation and cleavage of carbon–carbon bonds (a) aldol condensation, (b) Claisen ester condensation, (c) decarboxylation of a β-keto acid. (Adapted from Voet & Voet, 2004.)

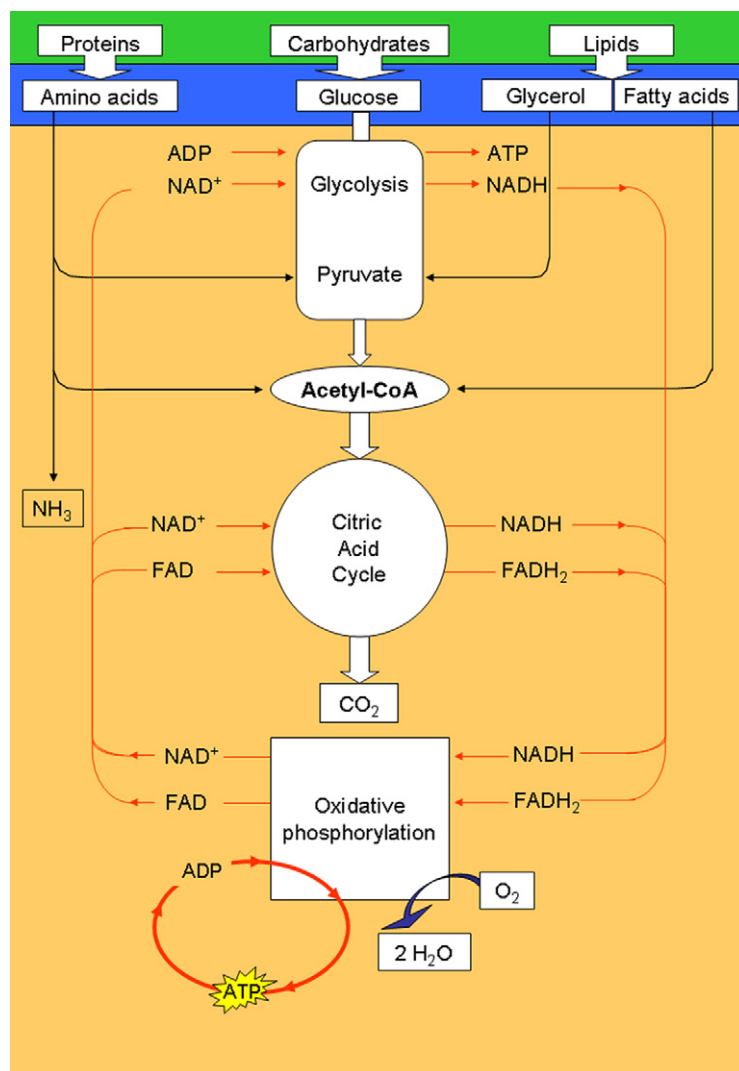


FIGURE 5.9 An overview of catabolism.

SELECTED CASE STUDIES – GLYCOLYSIS AND THE TRICARBOXYLIC ACID CYCLE

Glycolysis⁴ is an almost universal pathway for glucose catabolism, widely distributed in living organisms which converts glucose into two molecules of pyruvate with the net production of 2 molecules of ATP and 2 molecules of NADH. It consists of a sequence of ten reactions (Figure 5.10), the first five of which transform one molecule of glucose into two molecules of triose phosphate, and consume 2 molecules of ATP. The five subsequent reactions transform two molecules of glyceraldehyde-3-phosphate into two molecules of pyruvate with production of 4 molecules of ATP and 2 of NADH. Of the ten reactions, six are phosphoryl transfers (1,3,6,7,8,10), two are sugar isomerisations (2,5), one is an aldol cleavage (4), one is an NAD^+ -dependent redox reaction involving the

4. From Greek *glyk* – sweet and *lysis* – splitting.

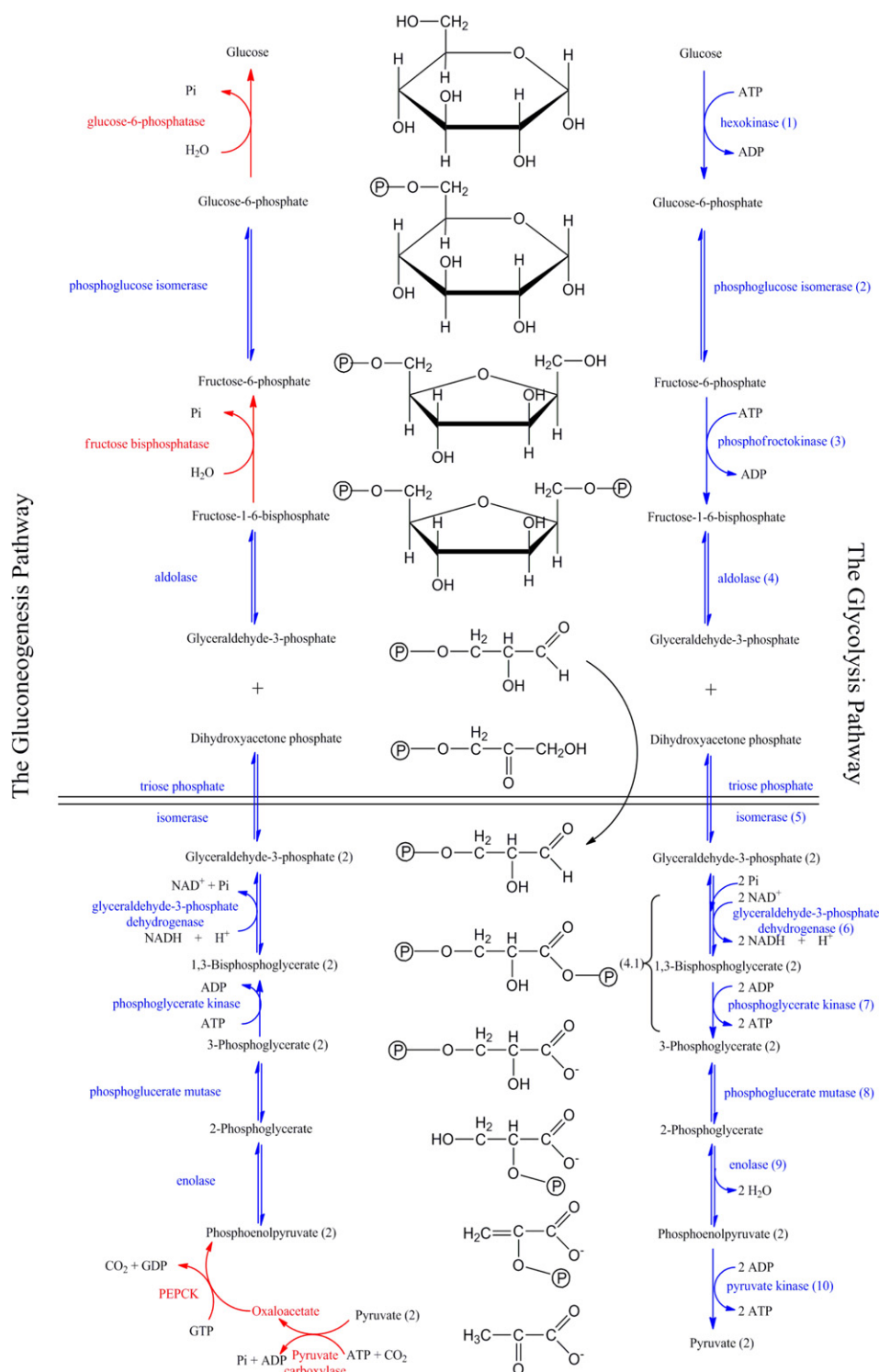


FIGURE 5.10 The pathways of glycolysis and gluconeogenesis.

conversion of a thiohemiacetal to an acyl thioester (6), which is accompanied by a phosphoryl transfer, and one is an elimination reaction (dehydration) resulting in formation of a double bond (9).

The glycolytic pathway is characteristic of many catabolic processes, where you have to invest some energy at the start before getting more energy back out of the system. As we saw in Figure 5.5, the reaction catalysed by hexokinase (1) uses the energy of ATP hydrolysis to drive phosphorylation of glucose, which ensures not only that the resulting glucose-6-phosphate is not re-exported from the cell (it costs ATP hydrolysis to bring glucose into the cell in the first place), but also that glucose is thereby activated for its subsequent degradation. In free energy terms, this reaction is essentially irreversible ($\Delta G -27.2$ kJ/mol), given the intracellular concentrations of the substrates and products. Following its isomerisation (2) to the corresponding ketose (fructose-6-phosphate), a second essentially irreversible phosphoryl transfer ($\Delta G -25.9$ kJ/mol), catalysed by the key regulatory enzyme of the glycolytic pathway, phosphofructokinase, results in formation of fructose-1,6-bisphosphate. This is subjected to an aldol cleavage⁵ generating two triose phosphates, dihydroxyacetone-phosphate (derived from carbons 1–3 of glucose) and glyceraldehyde-3-phosphate (from carbons 4–6). Only one of these products of aldol cleavage, glyceraldehyde-3-phosphate proceeds further along the glycolysis pathway. The isomerization of these two triose phosphates, catalysed by triose phosphate isomerase (5), completes the first half of glycolysis. Triose phosphate isomerase has attained catalytic perfection (Knowles, 1991) – the rate of reaction between enzyme and substrate is diffusion controlled, and all encounters between the enzyme and its substrate lead to reaction.

In the second half of the glycolytic pathway, the investment of energy in the first half is repaid by net generation of energy in the form of 4 ATP and 2 NADH molecules. Glyceraldehyde-3-phosphate dehydrogenase (6) catalyses the NAD^+ -dependent oxidation of the aldehyde, glyceraldehyde-3-phosphate GAP, which binds to the thiol of an active-site cysteine residue forming a thiohemiacetal, to the corresponding acid (as an enzyme-bound acyl thioester). This undergoes attack by inorganic phosphate, P_i , forming the acyl phosphate product, 1,3-bisphosphoglycerate (Figure 5.11). This reaction is a good example of coupling an energetically favourable reaction (oxidation of a thiohemiacetal) with an energetically unfavourable reaction (formation of an acyl phosphate). The product of the reaction, 1,3-bisphosphoglycerate, then transfers its phosphoryl group to ADP (7), thereby recuperating the investment of 2 ATP molecules in the first phase of glycolysis. The product, 3-phosphoglycerate, then undergoes phosphoryl transfer (8). This involves reaction with a phosphoenzyme to produce a 2,3-bisphosphoglycerate intermediate, which decomposes to form 2-phosphoglycerate, regenerating the phosphoenzyme. Dehydration of 2-phosphoglycerate (9) by the Mg^{2+} -dependent enzyme enolase (described in greater detail in Chapter 10) leads to the “high-energy” compound, phosphoenolpyruvate. As we saw earlier (Figure 5.5), it can transfer its phosphoryl group to ADP (10) producing another 2 ATP molecules per molecule of glucose oxidised, and represents the third essentially irreversible reaction of the glycolytic pathway ($\Delta G -13.9$ kJ/mol).

The second metabolic pathway which we have chosen to describe is the tricarboxylic acid cycle, often referred to as the Krebs cycle.⁶ This represents the biochemical hub of intermediary metabolism, not only in the oxidative catabolism of carbohydrates, lipids, and amino acids in aerobic eukaryotes and prokaryotes, but also as a source of numerous biosynthetic precursors. Pyruvate, formed in the cytosol by glycolysis, is transported into the matrix of the mitochondria where it is converted to acetyl CoA by the multi-enzyme complex, pyruvate dehydrogenase. Acetyl CoA is also produced by the mitochondrial β -oxidation of fatty acids and by the oxidative metabolism of a number of amino acids. The first reaction of the cycle (Figure 5.12) involves the condensation of acetyl Co and oxaloacetate to form citrate (1), a Claisen ester condensation. Citrate is then converted to the more easily oxidised secondary alcohol, isocitrate (2), by the iron–sulfur centre of the enzyme aconitase (described in Chapter 13). This reaction involves successive dehydration of citrate, producing enzyme-bound cis-aconitate, followed by rehydration, to give isocitrate. In this reaction, the enzyme distinguishes between the two external carboxyl groups

5. This reaction is one of the best examples of the importance of considering ΔG values rather than ΔG° : the latter is $+23.9$ kJ/mol, whereas in the cell ΔG is -1.3 kJ/mol. This reflects the actual concentrations of the metabolites within the cell.

6. Hans Krebs proposed the cycle in 1937 on the basis of experiments on minced pigeon muscle. He received the Nobel prize for medicine and physiology (jointly with Fritz Lipmann) in 1952.

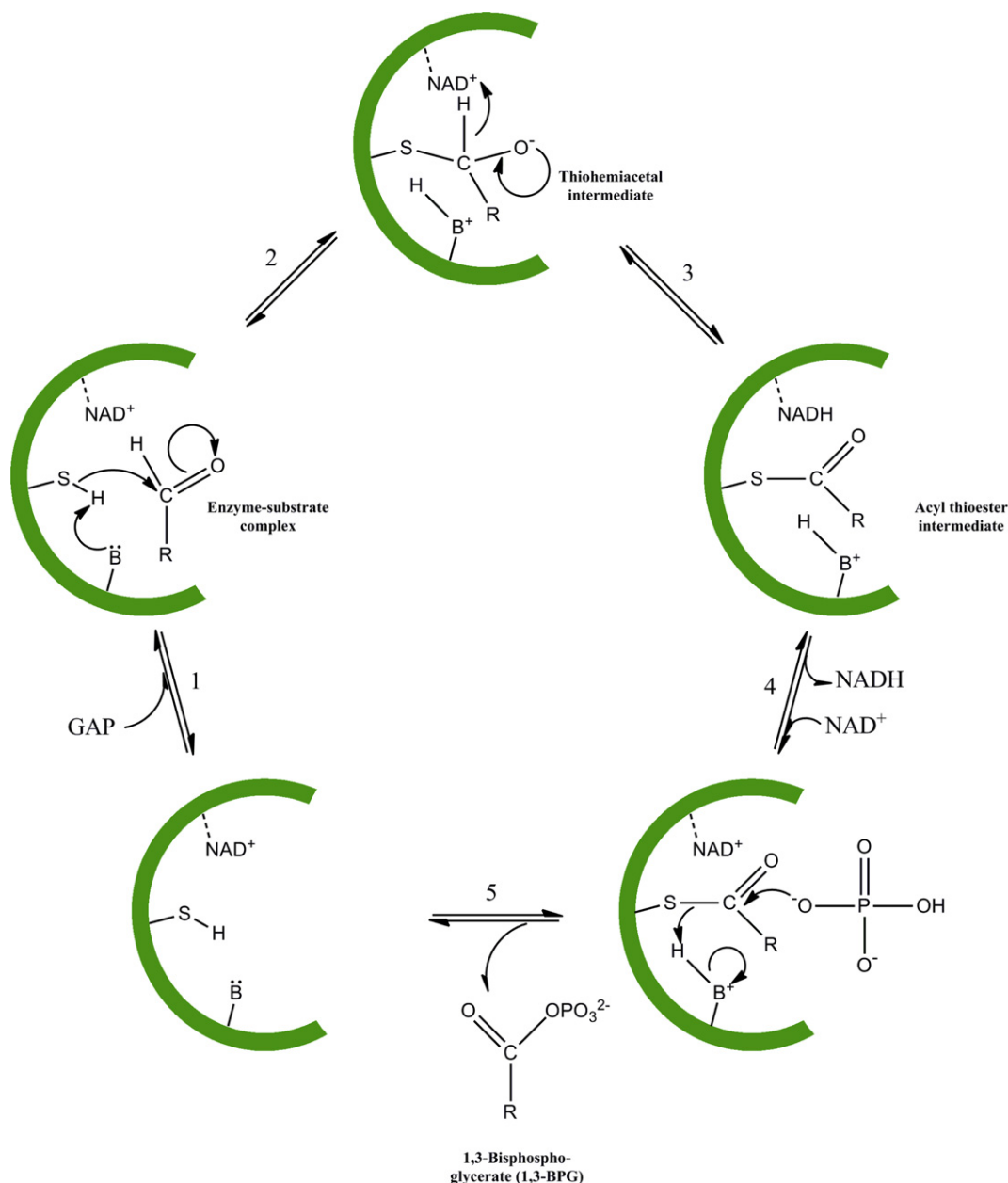


FIGURE 5.11 Mechanism of the glyceraldehyde-3-phosphate dehydrogenase reaction. (Adapted from Voet & Voet, 2004.)

of the pro-chiral citrate molecule. The hydroxyl group of isocitrate is then oxidised to give an enzyme-bound α -keto acid which readily decarboxylates to α -ketoglutarate and CO₂ (3). In a second oxidative decarboxylation reaction, entirely analogous to the conversion of pyruvate to acetyl CoA, α -ketoglutarate is converted to succinyl CoA, CO₂, and NADH (4). The “high-energy” of the thioester bond in succinyl CoA is conserved (5) by conversion of GDP to GTP (since nucleoside di- and triphosphates are interconvertible, this is equivalent to

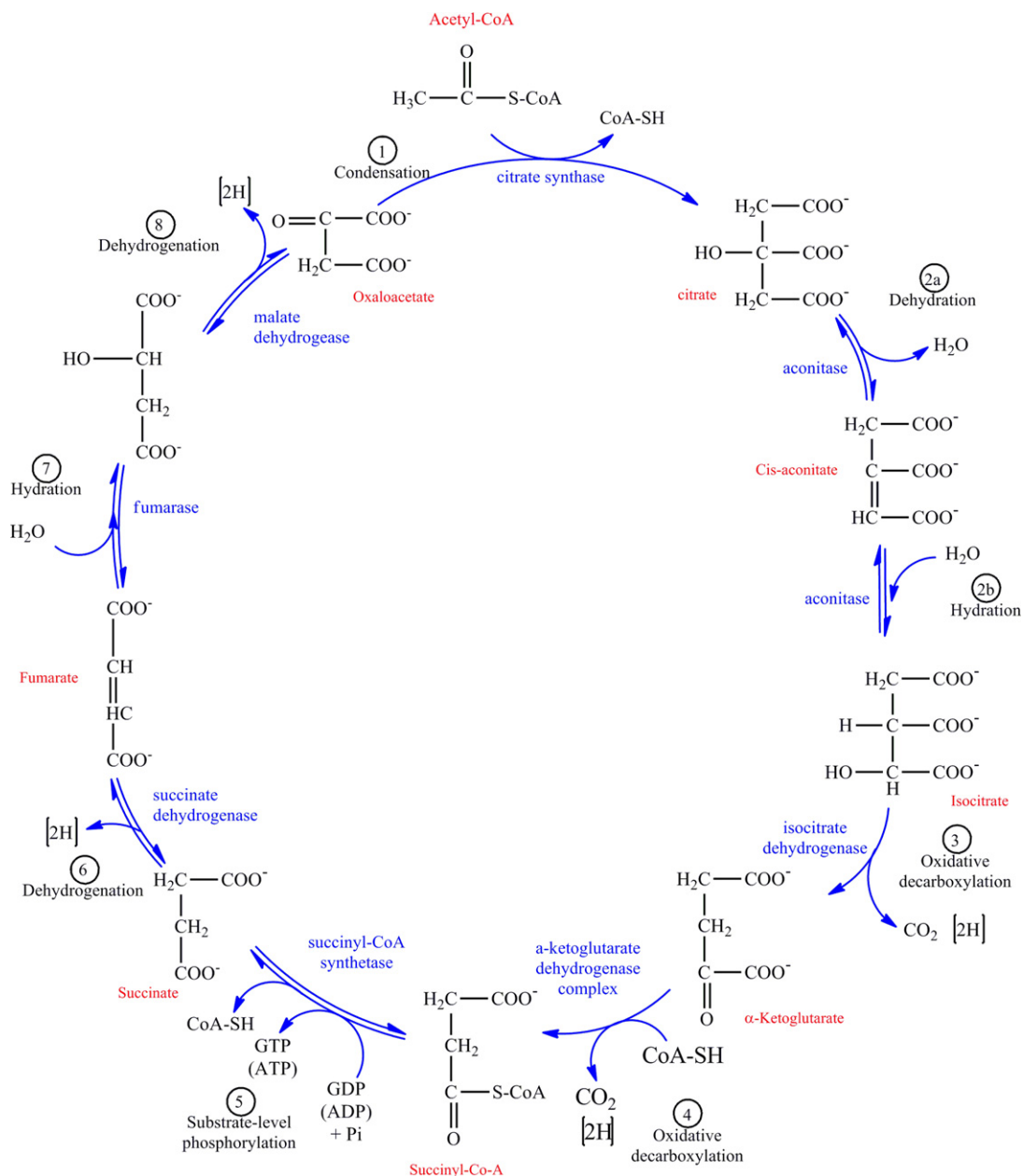


FIGURE 5.12 The reactions of the tricarboxylic acid cycle.

conversion of ADP to ATP). The central single bond between the methylene carbons of succinate is then oxidised to a trans double bond (6) in a reaction catalysed by the FAD-dependent enzyme, succinate dehydrogenase. Addition of water to fumarate catalysed by fumarase generates malate (7), which, in a final NAD^+ -dependent oxidation, is converted to oxaloacetate (8), thus completing the cycle. The sequence of reactions (6–8) is also used in the β -oxidation of fatty acids.

The global outcome of the Krebs cycle is that one molecule of acetyl CoA is converted to 3 molecules of NADH, 2 of CO_2 , 1 of GTP, and 1 of FADH_2 . The reducing equivalents will be used, as we will see later, to generate ATP.

AN OVERVIEW OF ANABOLISM

As was pointed out in the introduction, the opposite of catabolism, anabolism involves the biosynthesis of more complex and generally more highly reduced molecules, from the simpler and more oxidised molecules generated in the course of catabolism. These biosynthetic pathways require both energy in the form of ATP and reducing power in the form of NADPH. Whereas most of the NADH is funnelled through the mitochondrial respiratory chain for use in ATP synthesis, catabolism can also produce reducing equivalents in the form of NADPH (mostly through a variant of glucose catabolism, the pentose phosphate pathway). Photosynthetic organisms can generate both NADPH and ATP using light energy.

The tricarboxylic acid cycle plays a key role, in centralising the oxidative metabolism of intermediates from catabolic pathways. However, the tricarboxylic acid cycle not only enables the oxidation of acetyl CoA but it also supplies a number of molecules which are used in biosynthetic pathways. Figure 5.13 shows the positions at which

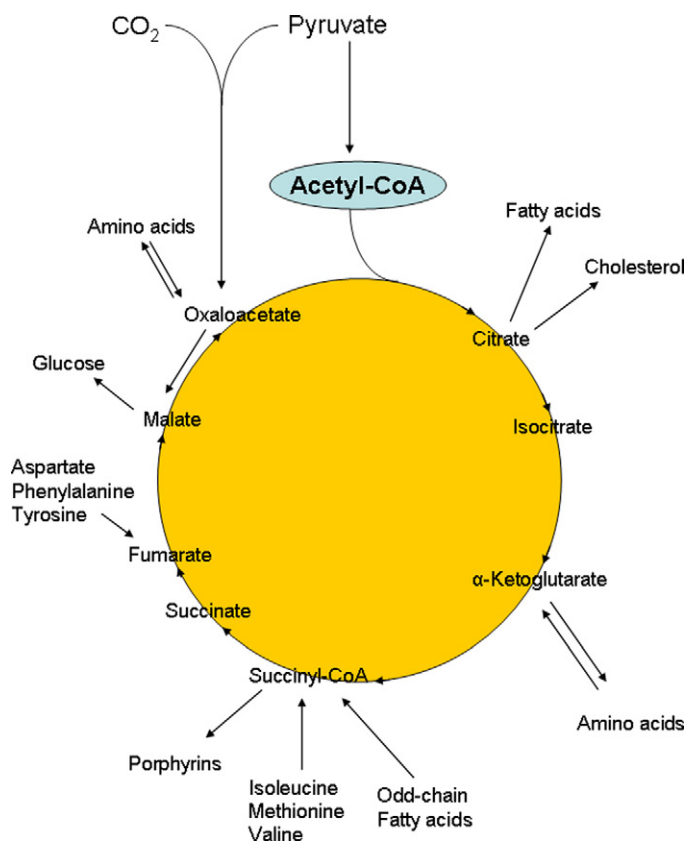


FIGURE 5.13 The tricarboxylic acid cycle plays a central role in supplying intermediates for biosynthetic pathways as well as receiving intermediates from catabolic pathways. (Adapted from Voet & Voet, 2004.)

intermediates are drawn off for use in anabolic pathways. α -keto acids, like oxaloacetate and α -ketoglutarate, can undergo transfer of an amino group with an amino acid (aminotransferase) to give aspartate and glutamate,

respectively. Both of these amino acids are used extensively in the biosynthesis of other amino acids and in nucleotide biosynthesis. Succinyl CoA is used together with glycine in the synthesis of porphyrins, while citrate is the starting point of both fatty acid and cholesterol biosynthesis. However, all of these biosynthetic pathways require free energy, so cycle intermediates which have been siphoned off must be replaced. These so-called anaplerotic reactions (filling up, Greek, *ana*, up + *plerotikos*, to fill) are also illustrated in Figure 5.13.

It is clear that, to avoid metabolic chaos, biosynthetic pathways cannot use the same enzyme machinery as the corresponding catabolic ones. Sometimes, as in the synthesis of glucose from pyruvate (gluconeogenesis), this implies the use of alternative enzymes for only a few specific steps in the pathway, sometimes, as in the biosynthesis of fatty acids, the pathway is localised in a different cellular compartment from the catabolic pathway, and uses different enzymes. We now discuss each of these pathways in turn.

SELECTED CASE STUDIES: GLUCONEOGENESIS AND FATTY ACID BIOSYNTHESIS

Glucose is extremely important in metabolism, both as a fuel and as a precursor of essential structural carbohydrates and other biomolecules. The brain, like red blood cells, is almost completely dependent on glucose as an energy source. However, the capacity of the liver to store glycogen (the body's reserve of glucose) is only sufficient to supply the brain with glucose for about half a day under conditions of fasting or starvation. Under these conditions, the needs for glucose must be met by gluconeogenesis, the synthesis of glucose from non-carbohydrate precursors. These include lactate and pyruvate, produced by glycolysis, but also citric acid cycle intermediates themselves as well as all but two of the twenty protein amino acids. All of these molecules have in common that they can be converted to oxaloacetate, the starting material for gluconeogenesis. There is no pathway for the net conversion of acetyl CoA into oxaloacetate in animals. Since most fatty acids are oxidised completely to acetyl CoA, they cannot serve as glucose precursors either.⁷

As illustrated in Figure 5.10, seven of the ten enzymes of the glycolytic pathway are used in gluconeogenesis, and the three which are not, as we might expect, are those which catalyse essentially irreversible steps in glycolysis. The first two, hexokinase and phosphofructokinase, which use ATP in the glycolytic pathway are replaced by hydrolytic reactions catalysed, respectively, by glucose-6-phosphatase⁸ and fructose-1,6-bisphosphatase, which remove the phosphoryl groups as inorganic phosphate. The conversion of pyruvate to phosphoenolpyruvate is more complex, first because the reaction is energetically extremely unfavourable, and second because the pyruvate, required for gluconeogenesis is localised within the mitochondrial matrix, whereas the enzymes of the glycolytic pathway are in the cytosol. The solution (Figure 5.14) involves the energy-dependent

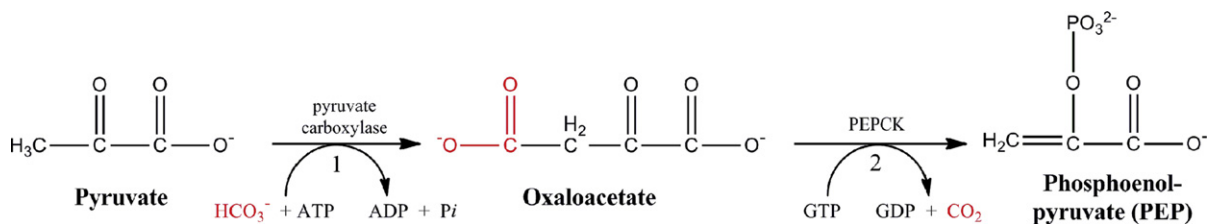


FIGURE 5.14 Conversion of pyruvate to oxaloacetate and then to phosphoenolpyruvate.

carboxylation of pyruvate within the mitochondria by pyruvate carboxylase, to form oxaloacetate. Oxaloacetate is then exported to the cytosol, either as malate or as aspartate, as described below. In the cytosol, it is converted to phosphoenolpyruvate again in an energy-dependent process, this time involving GTP (Figure 5.14), by the enzyme

7. Hence, the old, yet true, dictum that you can make fat from sugar, but you cannot make sugar from fat.

8. Glucose-6-phosphatase is found only in liver and kidney, and allows these tissues to supply glucose to other organs of the body, like the brain, which have little or no reserves of carbohydrates.

phosphoenolpyruvate carboxykinase (PEPCK). In some species PEPCK is almost equally distributed between the mitochondria and the cytosol, so that some PEP required for gluconeogenesis can be generated in the mitochondria and exported directly to the cytosol by a specific transport system (Figure 5.15). However, oxaloacetate

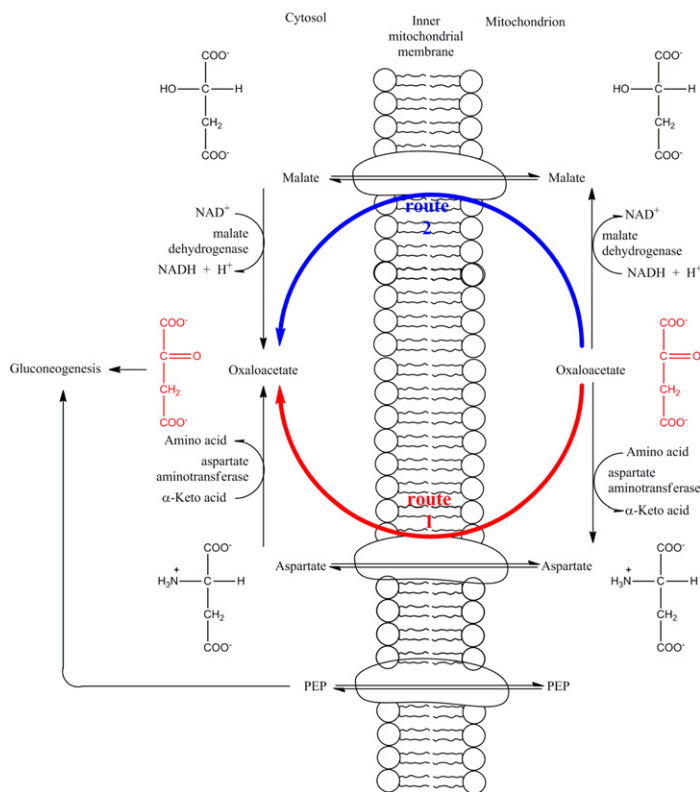


FIGURE 5.15 Transport of oxaloacetate and PEP from the mitochondria to the cytosol.

cannot cross the inner mitochondrial membrane directly, and must be converted to either aspartate by the action of aspartate transaminase (Route 1) or to malate, by malate dehydrogenase (Route 2) (Figure 5.15). Route 2, often called the malate shuttle, involves mitochondrial oxidation of $NADH$ followed by cytosolic reduction of NAD^+ thereby allowing reducing equivalents as $NADH$ to be transferred from the mitochondria to the cytosol, where they are required for gluconeogenesis.

We already mentioned that the enzymes involved in the β -oxidation of fatty acids are located in the mitochondria. The source of two-carbon fragments for the biosynthesis of both fatty acids and isoprenoids like cholesterol is acetyl CoA, which is generated by oxidative metabolism in the mitochondria. Acetyl CoA cannot escape from the mitochondria, but it can be exported to the cytosol as citrate, where it is reconverted to oxaloacetate and acetyl CoA. Fatty acid (and cholesterol) biosynthesis takes place in the cytosol, and requires bicarbonate, which is incorporated into acetyl CoA to form malonyl CoA by acetyl CoA carboxylase. The biosynthesis of fatty acids, mostly the C_{16} palmitate (Chapter 4), requires one molecule of acetyl CoA and seven molecules of malonyl CoA. In animals, the seven enzymatic reactions which are required for fatty acid synthesis are present in a single multifunctional protein complex, known as fatty acid synthase.⁹ The synthase also contains an acyl-carrier protein

9. This is not the only example of Nature inventing the assembly line a long time before Henry Ford — both pyruvate dehydrogenase and α -ketoglutarate dehydrogenase mentioned earlier in the chapter are also multi-enzyme complexes.

(ACP), to which the growing fatty acids are esterified. ACP, like Coenzyme A, has a phosphopantothenate group which forms thioesters with acyl groups. The phosphopantothenate phosphoryl group is esterified to a serine OH group in ACP, whereas in CoA it is esterified to AMP (Figure 5.16). However, in fatty acid biosynthesis it acts as a flexible link transporting the substrate between the different enzymatic domains of the fatty acid synthase.

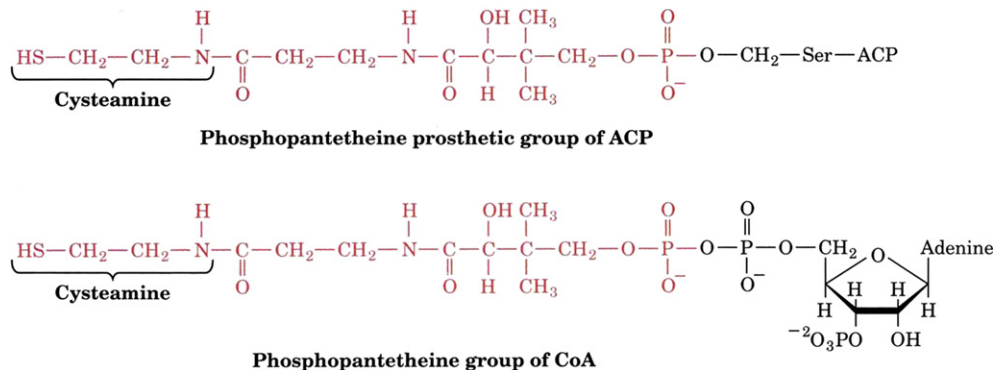


FIGURE 5.16 The phosphopantetheine group in acyl-carrier protein (ACP) and in CoA.

In the successive steps of fatty acid synthesis (Figure 5.17), acetyl CoA is transferred to ACP by malonyl/acetyl-CoA-ACP transacylase (MAT), and then to the thiol group of β -ketoacyl-ACP synthase (KS, indicated in the figure as E). Malonyl-ACP is formed from malonyl CoA in an analogous fashion to acetyl CoA by the action of MAT. The condensation reaction between the acetyl group and the β -carbon of malonyl-ACP is catalysed by KS accompanied by decarboxylation with formation of acetoacetyl-ACP and release of the Cys-SH of the active site of KS. The next three steps involve reduction, dehydration, and further reduction convert acetoacetyl-ACP to butyryl-ACP, and represent the direct opposite to the β -oxidation that we saw in the Krebs cycle (succinate to oxaloacetate) which is also found in fatty acid oxidation (oxidation/hydration/oxidation). However, in the biosynthetic pathway NADPH is the electron donor, whereas in the two redox steps of β -oxidation the electron acceptors are, respectively, FAD and NAD⁺. The condensation reaction, two reduction steps and dehydration are repeated a further six times, resulting in palmitoyl-ACP. At this stage, the thioester bond is hydrolysed by palmitoylthioesterase releasing palmitate, the final product and regenerating the synthase for another round of biosynthesis.

BIOENERGETICS – GENERATION OF PHOSPHORYL TRANSFER POTENTIAL AT THE EXPENSE OF PROTON GRADIENTS

In our brief discussion of intermediary metabolism, we did not mention that there is an alternative to full-blown respiratory oxidative catabolism, what Louis Pasteur described as ‘la vie sans air’. Many organisms can live without oxygen, albeit producing much less ATP per molecule of substrate oxidised than in respiration. They achieve this by compensating, for example, in glycolysis the reduction of NAD⁺ to NADH by a compensatory reduction of another organic molecule. Two examples are the reduction of pyruvate to lactate in muscle tissue during exercise, and the reduction of acetaldehyde (derived from the decarboxylation of pyruvate) to ethanol by yeasts. These fermentations, as they are called, can result in a vast number of interesting end products, both culinary (beer, wine, most alcoholic beverages,¹⁰ cheese, yoghurt, sauerkraut, etc.) as well as many industrial and medical applications.

10. Virtually any source of glucose can undergo alcoholic fermentation – 100 g of potatoes in an oxygen-free atmosphere at 22 °C will give 600 mg of ethanol in 8 days – the product is pretty unpalatable, but distillation can change that!

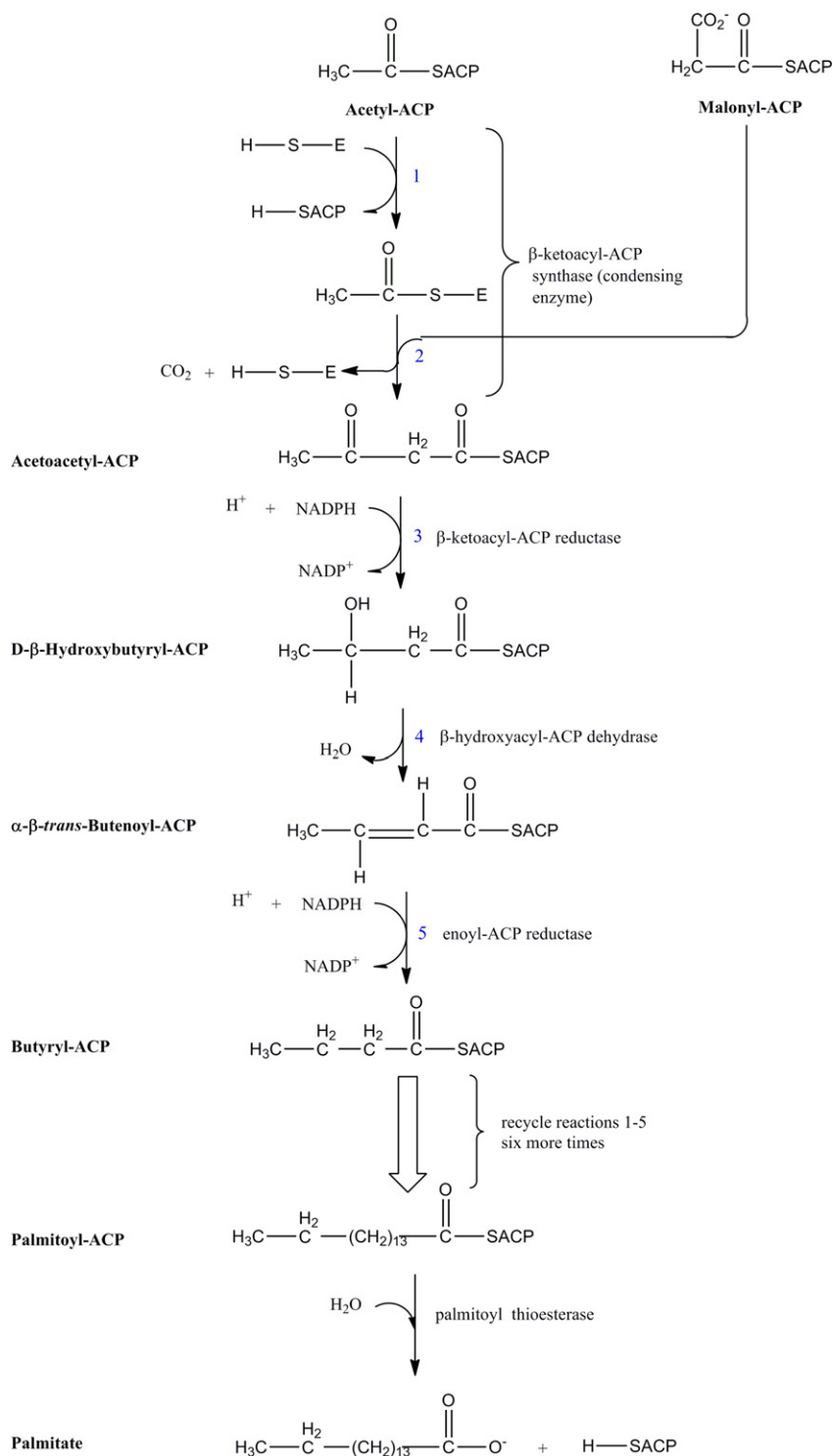


FIGURE 5.17 Fatty acid biosynthesis.

However, the overwhelming attraction of respiration is the greatly increased yield of ATP — fermentation of one molecule of glucose to lactate or ethanol yields just 2 ATP molecules, whereas full oxidation of glucose to CO₂ and water yields between 36 and 38! So far we have only seen what the biochemist calls ‘substrate-level’ phosphorylation — ATP production in the course of metabolic processes. To achieve the yields of ATP production we find in respiration, we need to harness the potential energy of the reducing equivalents — NADH and FADH₂ by transferring their electrons to an electron acceptor with a much higher redox potential — and in the mitochondrion this is dioxygen.

The standard redox potential E'_o (standard conditions for the biochemist are 1 M oxidant, 1 M reductant, 10⁻⁷ M [H⁺], i.e., pH 7 and 25 °C) for most biological redox couples are known. Remember that in this context E'_o refers to the partial reaction written as:

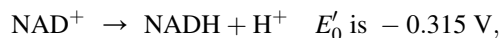


In addition, the standard free energy change $\Delta G^{\circ'}$ is related to the change in standard redox potential E'_o by

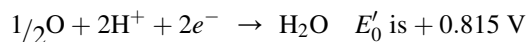
$$\Delta G^{\circ'} = nF\Delta E'_o$$

where n is the number of electrons transferred, F is the *faraday*, a constant equal to 96.48 kJ/mol/V, and $\Delta E'_o$ is the difference between the two standard redox potentials in volts.

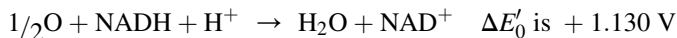
The driving force of oxidative phosphorylation is the difference between the electron transfer potential of NADH or FADH₂ relative to that of O₂. For the redox couple:



while for the couple:¹¹



so that for the reaction:



we can calculate that $\Delta G^{\circ'} = -220.1$ KJ/mol. For comparison, the $\Delta G^{\circ'}$ for ATP hydrolysis is -31.4 kJ/mol, so we should be able to make a few ATP molecules with this potential bonanza of energy. However, there are two important conditions — first, we cannot simply dissipate all of the potential energy difference in one ‘big bang’, but pass the electrons through a series of transporters which have progressively increasing redox potentials, and second we must use a system coupled to electron transfer which will allow us to make ATP synthesis turn — and that involves generating a proton gradient across the internal mitochondrial membrane.

The first condition is met by having a series of four protein complexes, inserted into the mitochondrial inner membrane, each made up of a number of electron (and sometimes proton) acceptors of increasing redox potential. Three of them (Complexes I, III, and IV) are presented in cartoon form in [Figure 5.18](#). Complex I, referred to more prosaically as NADH-Coenzyme Q oxidoreductase, transfers electrons stepwise from NADH, through a flavo-protein (containing FMN as cofactor) to a series of iron–sulfur clusters (of which more in Chapter 13) and ultimately to coenzyme Q, a lipid-soluble quinone, which transfers its electrons to Complex III. The $\Delta E'_o$ for the couple NADH/CoQ is 0.36 V, corresponding to a $\Delta G^{\circ'}$ of -69.5 kJ/mol, and in the process of electron transfer, protons are exported into the intermembrane space (between the mitochondrial inner and outer membranes).

Complex II (which is not shown in the Figure) contains succinate dehydrogenase, the FAD-dependent Krebs cycle enzyme, and like complex I, transfers its electrons through iron–sulfur centres and a *b*-type cytochrome

11. It is clearly absurd to talk about ‘half’ oxygen molecules given the strength of the O=O double bond. However, for more pedestrian reasons of considering the transfer of two electrons from NADH or FMNH₂, through a long series of transporters all the way to the end of the line at molecular oxygen, we would request our more chemically based readers to grant us this small indulgence.

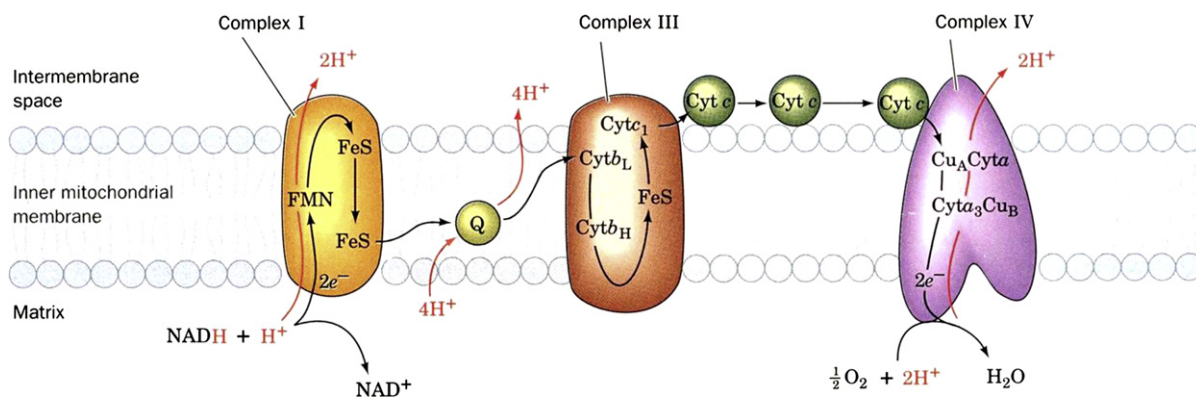


FIGURE 5.18 The mitochondrial electron-transport chain. (From Voet & Voet, 2004: pp. 1591.)

(more of these haem iron proteins in Chapter 13) to coenzyme Q. However, here the $\Delta E'_o$ is only 0.085 V, corresponding to a $\Delta G^{\circ'}$ of -16.4 kJ/mol, which is not sufficient to allow proton pumping.

Complex III (Coenzyme Q: Cytochrome *c* Oxidoreductase) transfers electrons from coenzyme Q to cytochrome *c*, through a sequence of cytochromes and iron–sulfur cofactors. Here, the $\Delta E'_o$ for the couple CoQ/cytochrome *c* is 0.19 V, corresponding to a $\Delta G^{\circ'}$ of -36.7 kJ/mol, again enough to power the synthesis of an ATP molecule and to ensure that protons are pumped across the inner mitochondrial membrane.

Finally, Complex IV, Cytochrome *c* Oxidase, takes the electrons coming from four molecules of cytochrome *c*, a small, water-soluble haem protein, moving outside of the membrane in the intermembrane space and carries out the four-electron reduction of a molecule of dioxygen to two molecules of water. The $\Delta E'_o$ for the couple cytochrome *c*/O₂ is by far the highest of the four complexes, 0.58 V, corresponding to a $\Delta G^{\circ'}$ of -112 kJ/mol, and there is certainly proton pumping, which must involve conformational changes since, in this Complex, unlike the three others, there are only one-electron cytochromes and copper atoms, with no obvious proton exchanges possible (more information about cytochrome *c* oxidase in Chapters 13 and 14).

We now turn our attention to how the gradient of protons pumped by Complexes I, III, and IV across the inner mitochondrial membrane into the intermembrane space, together with the associated membrane potential, is used to turn the molecular rotor which ensures ATP synthesis. Without entering into the detail, we can calculate that the ΔG for pumping a proton from the mitochondrial matrix to the intermembrane space is 21.5 kJ/mol. Since the estimated ΔG (the real *in vivo* free energy) for synthesis of an ATP molecule is between +40 and +50 kJ/mol, we can estimate that at least two protons (most likely three) need to be pumped per ATP generated. From experimental data we know that two electrons descending the respiratory chain from NADH (i.e., via Complexes I, III, and IV) to oxygen will produce 3 ATP molecules. By comparison two electrons entering via FADH₂ and passing through Complexes II, III, and IV to oxygen will result in formation of only 2 ATP molecules.

If, during electron transfer along the respiratory chain, protons are translocated from the matrix to the intermembrane space, how, we may ask, is this proton gradient used to synthesise ATP? Where better to start than with the enzyme itself, the proton-translocating ATP synthase (Figure 5.19) (Capaldi & Aggeler, 2002). It is composed of two parts: one called F₀ which is inserted into the inner mitochondrial membrane and contains the proton translocation channel; the second, F₁, consists of a stalk, which connects with the F₀ component, to which a roughly oval-shaped ball is attached.¹² F₁ consists of five types of subunit (stoichiometry $\alpha_3\beta_3\gamma\delta\epsilon$), two of which, the α and β subunits make up the bulk of F₁. Both bind nucleotides, although only the β subunits are directly involved in

12. I much prefer the description of F₁ as a ball on a stick, rather than, as sometimes found in textbooks, a lollipop.

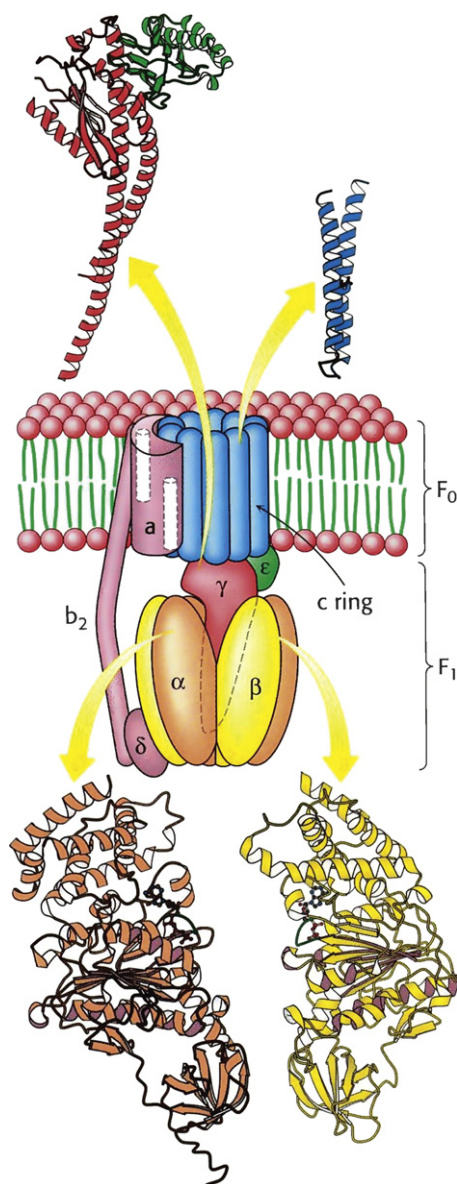


FIGURE 5.19 Structure of ATP synthase. (From *Berg, Tymoczko, & Stryer, 2002: pp. 974.*)

catalysis of ATP synthesis. The central stalk consists of the γ and ϵ subunits, and the γ subunit has a long α -helical coiled coil which extends into the centre of the $\alpha_3\beta_3$ hexamer. Crucially for the mechanism, this breaks the symmetry of the $\alpha_3\beta_3$ hexamer, such that each of the catalytic β subunits interacts with a different face of γ .

On the basis of binding studies, Paul Boyer proposed a binding change mechanism for proton-driven synthesis of ATP by the enzyme (Figure 5.20), which implied that the enzyme (in particular the three β subunits) could exist in three different forms, one which binds ATP with such high affinity (the tight, T form) that it converts bound ADP and P_i to ATP — however, it is incapable of releasing the ATP. At the same time, a second subunit will be in the loose, L, conformation, which can bind ADP and P_i , but cannot release them, while the

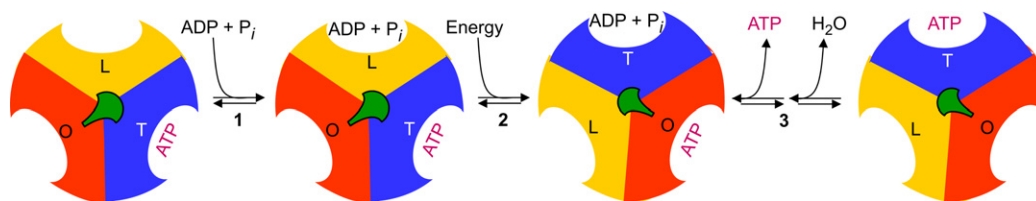


FIGURE 5.20 Energy-dependent binding change mechanism for ATP synthesis by proton-translocating ATP synthase. F_1 has three conformationally distinct interacting $\alpha\beta$ protomers: O, the open conformation, has very low affinity for ligands and is inactive; L has loose binding for ligands and is catalytically inactive; T has tight binding for ligands and is catalytically active. ATP synthesis proceeds in three steps. (1) Binding of ADP and P_i to site L. (2) Energy-dependent conformational change converts binding site L to T, T to O and O to L. (3) Synthesis of ATP at site T and release of ATP from site O. After two further cycles of this reaction cycle the enzyme returns to its initial state. The energy that drives the conformational change is transmitted to the catalytic $\alpha_3\beta_3$ assembly via rotation of the $\gamma\epsilon$ assembly, represented here by the centrally located asymmetric object (green). (Adapted from Voet & Voet, 2004.)

third subunit is in the open, O conformation. This third subunit can exist in two states — one in which, similar to the T or L forms, a nucleotide is bound, and a second in which it has a more open conformation and releases the bound nucleotide. John Walker and his group were in fact able to crystallise the bovine heart F_1 -ATP synthase with each of the three catalytic subunits in one of the three conformational states (Figure 5.21), confirming the

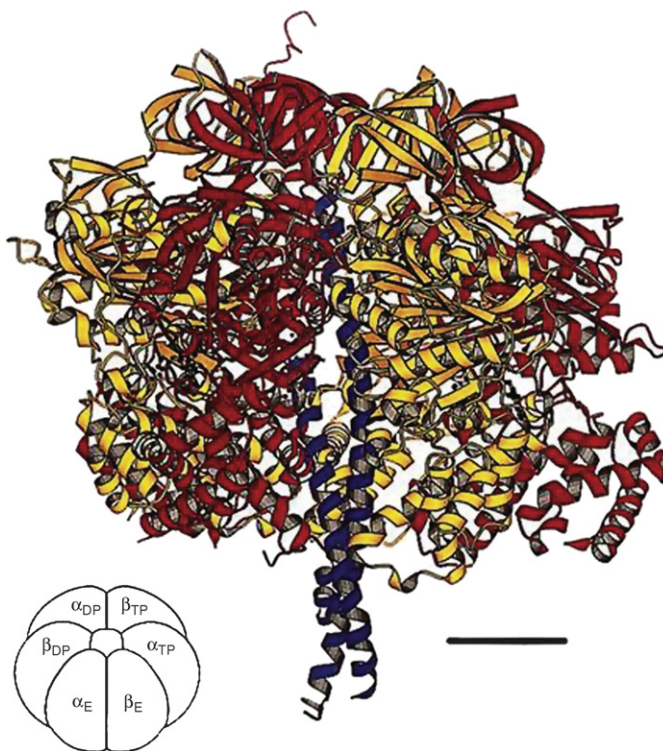


FIGURE 5.21 The X-ray structure of the F_1 -ATP synthase from bovine heart mitochondria. The α , β , and γ subunits are in red, yellow, and blue respectively. The inset (bottom left) shows the orientation of the subunits in this view. The bar is 20 Å long. (From Abrahams, Leslie, Lutter, & Walker, 1994.)

predictions of the Boyer mechanism.¹³ The structure supports a catalytic mechanism in intact ATP synthase in which the three catalytic subunits are in different states of the catalytic cycle at any instant. As indicated in the insert, the front of the three β subunits is in the O (here E for empty) form, that to the left has dinucleotide bound (L) and that on the right is in the T form. This convincingly demonstrates that ATP synthase functions by rotational catalysis.

What drives the interconversion of the three states is the rotation of the γ subunit. As the proton flux causes rotation of the γ subunit, say by 120° , the three β subunits will change position and conformational state. So, the subunit which had ATP tightly bound will adopt the open conformation, and ATP will be released. The loosely bound ADP and P_i will find itself in the tight conformation, and its high affinity for ATP will drive ATP synthesis. Finally, the subunit previously in the open form, will adopt the L form, and bind ADP and P_i . The most elegant proof that the ATP synthase is a rotary molecular motor comes from studies in which the $\alpha_3\beta_3$ hexamer was fixed to a Ni- surface (using a short sequence of His residues attached to the end of the protein chain – a His tag) with the γ subunit pointing upward and attached to a fluorescently labelled actin filament (Figure 5.22).

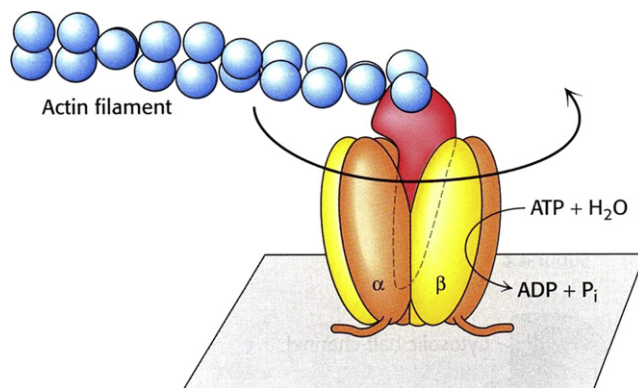


FIGURE 5.22 Direct observation of ATP-driven rotation in ATP synthase. The $\alpha_3\beta_3$ hexamer is fixed to a surface with the γ subunit pointing upward and linked to a fluorescently labeled actin filament. Addition of ATP results in rotation of the γ subunit, which can be observed with a fluorescence microscope. (From Berg *et al.*, 2002: pp. 974.)

Addition of ATP (to stimulate the reverse reaction of ATP synthesis) resulted in a rotation of 120° for each equivalent of ATP added.

One final conceptual question remains. How does the flow of protons through F_0 drive the rotation of the γ subunit? It is suggested that the **c** subunit (Figure 5.19), which has an aspartate residue (Asp 61) in the middle of a pair of helices which traverse the membrane, plays a key role. There are channels in the **a** subunit, which surrounds the central ring of **c** subunits, but which do not cross the membrane, but rather go more or less half way across from each side of the membrane (Figure 5.23). Suppose further that two residues of Asp 61 of two subunits **c** are in contact with the two half-channels of the **a** subunit. One has picked up a proton from the high concentration of protons on the cytosolic (intermembrane space) of the mitochondria, and will be in its protonated (neutral) form. The other, coming from the half-channel on the matrix side, which is proton deficient, will be in its charged, nonprotonated form. Rotation of the **c** ring by 360° will now align the protonated Asp 61 with the matrix half-channel, whereas the unprotonated Asp 61 of the second will be confronted by the proton-rich cytosolic half-channel (25 times higher $[H^+]$ concentration than in the matrix). The net result is vectorial proton migration across the inner mitochondrial membrane as a consequence of rotation of the **c** ring.

13. Boyer and Walker received the 1997 Nobel prize for Chemistry together with Jens Skou, who discovered the Na^+/K^+ ATPase (of which more in Chapter 9).

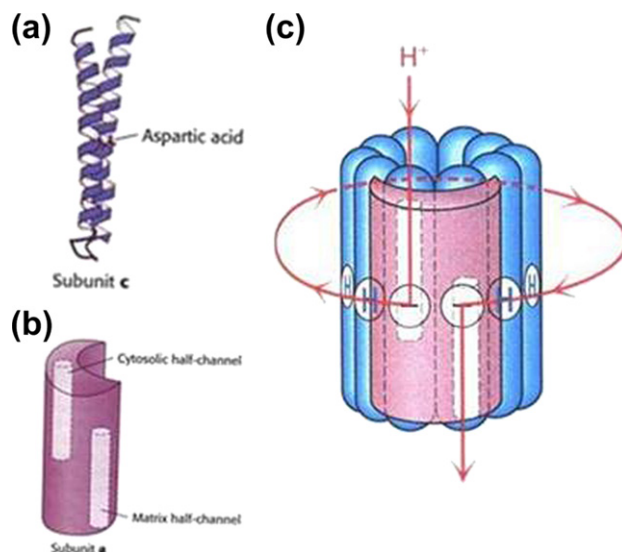


FIGURE 5.23 Components of the proton-translocating unit of ATP synthase (a, b) and the proton path through the membrane (c). Each proton enters the cytosolic half-channel, follows a complete rotation of the c ring, and exits through the other half-channel into the matrix. (From *Berg et al.*, 2002: pp. 974.)

REFERENCES

- Abrahams, K. P., Leslie, A. G., Lutter, R., & Walker, J. E. (1994). Structure at 2.8 Å resolution of F₁-ATPase from bovine heart mitochondria. *Nature*, 370, 621–628.
- Berg, J. M., Tymoczko, J. L., & Stryer, L. (2002). *Biochemistry* (5th ed.). New York: W.H. Freeman and Co.
- Campbell, P. N., Smith, A. D., & Peters, T. J. (2005). *Biochemistry illustrated niochemistry and molecular biology in the post-genomic era* (5th ed.). London and Oxford: Elsevier. pp. 242.
- Capaldi, R., & Aggeler, R. (2002). Mechanism of F₁F₀-type ATP synthase, a biological rotary motor. *TIBS*, 27, 154–160.
- Devlin, T. M. (2005). *Textbook of Biochemistry with clinical correlations* (6th ed.). Hoboken: John Wiley and Sons. pp. 1208.
- Knowles, J. R. (1991). Enzyme catalysis: not different, just better. *Nature*, 350, 121–124.
- Voet, D., & Voet, J. G. (2004). *Biochemistry* (3rd ed.). Hoboken: John Wiley and Sons.

This page intentionally left blank

Methods to Study Metals in Biological Systems

Introduction	117
Magnetic Properties	119
Electron Paramagnetic Resonance (EPR) Spectroscopy	120
Mössbauer Spectroscopy	122
NMR Spectroscopy	124
Electronic and Vibrational Spectroscopies	125
Circular Dichroism and Magnetic Circular Dichroism	126
Resonance Raman Spectroscopy	126
Extended X-Ray Absorption Fine Structure (EXAFS)	127
X-Ray Diffraction	128

INTRODUCTION

The study of metals in biological systems requires techniques, some of them highly specific, some limited to specific characteristics of the metal ion in question, some of more general applicability. Thus, Mössbauer spectroscopy in biological systems is restricted to iron-containing systems because the only element with a Mössbauer nucleus available is ^{57}Fe . The EPR spectroscopic techniques will only be of application if the metal centre has an unpaired electron. In contrast, provided that suitable crystals can be obtained, X-ray diffraction allows the determination of the three-dimensional structure of metalloproteins and their metal centres.

It is not our intention to describe the techniques in any detail, but rather to indicate what information can be derived from the application of the method in question (and also what cannot). This is motivated in this second edition by the imminent entry into production of a companion volume to the present one ‘Practical Approaches to Biological Inorganic Chemistry’ (Crichton and Louro, 2012). More detailed information on some of these techniques can be found in Arnesano et al., 2005; Banci et al., 2006; Bertini et al., 2005; Campbell & Dwek, 1984; Que, 2000; Ubbink et al., 2002.

Two important practical generalisations should be made at the outset. The first is that there is little sense in using sophisticated physico-chemical techniques to analyse impure biological samples, and reciprocally that highly purified biological materials should not be subjected to poor analytical techniques. The second, perhaps even more important, is that in general, the more techniques you can use on a biological sample the better, since there are virtually no situations in which one single method will reply to all of your questions. A classical example is illustrated by bacterial hydrogenases which have an unusual coordination geometry around the metal centre, involving CO and CN ligands. Although high-resolution X-ray structures were available, the impossibility of distinguishing between the electron density of C, O, and N meant that the ultimate resolution of the structure relied on spectroscopic techniques as well as protein crystallography.

Table 6.1 summarises the parameters which can be obtained with each of the techniques and the information that the method should (hopefully) supply.

TABLE 6.1 Spectroscopic Methods – An Overview

Method	Parameters	Information content
Magnetic susceptibility	Molecular <i>g</i> -value, axial and rhombic zero-field splitting, exchange interaction	Number of unpaired electrons/ground spin state; defines antiferromagnetic and ferromagnetic interactions; quantitates ground sublevel splittings
Mössbauer spectroscopy	Quadrupole coupling, isomer shift	For ^{57}Fe sites: oxidation and spin state; chemical environment
Electron paramagnetic resonance (EPR)	Quadrupole tensor, nuclear Zeeman splitting, <i>g</i> values, coupling constants, relaxation times	Usually for odd electron metal sites: probes ground-state wave function at high resolution
Electron-nuclear double resonance (ENDOR)		Combines sensitivity of EPR and high resolution of NMR to probe ligand superhyperfine interactions
Nuclear magnetic resonance (NMR)	Chemical shift, nuclear coupling constants, relaxation times	For paramagnetic proteins: enhanced chemical shift resolution, contact and dipolar shifts, spin delocalisation, magnetic coupling from temperature dependence of shifts.
Vibrational spectroscopy (Raman and IR)	Energies (with isotope perturbation), intensities and polarisations	Identification of ligands coordinated to a metal centre
Electronic absorption spectroscopy (ABS)	Energies, intensities, and band shapes	Direct probe of ligand field and charge transfer excited states
Magnetic circular dichroism (MCD)	Same as ABS plus circular polarisation induced by applied magnetic field and magnetic susceptibility	Greater sensitivity than ABS in observing weak transitions and greater resolution due to differences in circular polarisation; complimentary selection rules aiding in assignment of electronic transitions
Circular dichroism (CD)	Same as ABS plus circular polarisation due to asymmetric nature of metal site	Allows detection of transitions not readily observable in absorption
Resonance Raman spectroscopy	Intensity profiles, depolarisation ratios	Allows study of chromophoric active sites in biological molecules at low concentration; can provide information on metal–ligand bonding
Extended X-ray absorption fine structure (EXAFS)	Energies, intensities, and polarisations	Identity of ligand atoms: distance of ligand atoms from metal: number of scattering ligands of a given type
X-ray diffraction	Atomic coordinates at a given resolution	Identity of ligands to metal centre (but distances more precise by EXAFS)

Spectroscopic techniques have the advantage over protein crystallography in that not only are crystals not required, but they can allow time-resolved measurements to be made which can detect short-lived intermediates. However, to obtain structural information, the observed spectroscopic data must be fitted to molecular structures. This can be done with reference structures which model the spectroscopic properties of the metalloprotein site. These could be synthetic low-molecular-weight complexes of known molecular structure, or known high-resolution metalloprotein structures obtained by X-ray crystallography or high-field NMR. Yet another promising approach is the use of quantum chemical calculations of spectroscopic properties of metalloproteins and model compounds to elucidate their geometrical and electronic structures (Neese, 2003).

MAGNETIC PROPERTIES

A brief consideration of the magnetic properties of metal ions will help us enormously in understanding some of the techniques that we will study later. We begin by defining diamagnetic and paramagnetic molecules. The former, with closed shells of electrons, have no inherent magnetic properties and, when weighed in the presence or absence of a magnetic field, will show a small decrease in weight (due to repulsion by the magnetic field). In contrast, paramagnetic molecules show a net attraction to the magnetic field, and a much larger increase in weight. An unpaired electron corresponds to an electric current and, by virtue of its spin and its orbital motion, to a magnetic field. Because transition metals are of great importance in biology, we are particularly interested in the magnetic properties of their unpaired electrons, and the information we can derive from studying these properties. Magnetic susceptibilities may be measured by direct methods for small molecule models of metalloprotein cores and from them magnetic moments (expressed in Bohr magnetons) can be readily calculated. The diamagnetic contribution of the rest of the protein molecule and its associated bound water content makes this difficult to apply to metalloproteins. However, the higher sensitivity of SQUID (superconducting quantum interference device) susceptometers and other magnetometers makes direct determination of magnetic properties of metalloproteins possible. Since the magnetic susceptibility of most molecules varies with temperature, the magnetic moment and hence the number of unpaired electrons can be derived from temperature-dependent studies. EPR and NMR can also be used to deduce these parameters.

For paramagnetic molecules the magnetic moment has two sources, spin and orbital contributions. For transition metal ions (with the exception of Co^{2+} and Co^{3+}) where there is only a small orbital contribution, the magnetic moment reflects the spin-only term, and expected spin-only magnetic moments in octahedral arrangements for d electrons in biologically relevant transition metals¹ are given in Table 6.2. For the first three

TABLE 6.2 Spin-Only Magnetic Moments for Octahedral Arrangements

Number of d electrons	Magnetic moment (Bohr magnetons)	
	High-spin	Low-spin
2 (V^{3+})		2.83
3 (V^{2+} , Cr^{3+})		3.81
4 (Mn^{3+} , Cr^{2+})	4.93	2.83
5 (Mn^{2+} , Fe^{3+})	5.92	1.73
6 (Fe^{2+} , Co^{3+})	4.90	0.00
7 (Co^{2+})	3.87	1.73
8 (Ni^{2+})		2.83
9 (Cu^{2+})		1.73
10 (Cu^+)		0.00

d electrons there is no ambiguity concerning their location, since they are in the three t_{2g} sets of orbitals (Table 6.3). For d^4 , two alternative configurations are possible; the fourth electron may remain parallel to the other three and enter the higher-energy e_g level or it may pair up with one of the electrons already present in the t_{2g} level (which will produce maximum crystal field stabilisation). The first is known as the **high-spin** state, while the

1. Therefore titanium with one d electron is not included.

TABLE 6.3 Electronic Configurations in Octahedral Configuration

Number of <i>d</i> electrons	Electron configuration				
	t_{2g}	t_{2g}	t_{2g}	e_g	e_g
1	↑				
2	↑	↑			
3	↑	↑	↑		
4 high-spin	↑	↑	↑	↑	
4 low-spin	↑↓	↑	↑		
5 high-spin	↑	↑	↑	↑	↑
5 low-spin	↑↓	↑↓	↑		
6 high-spin	↑↓	↑	↑	↑	↑
6 low-spin	↑↓	↑↓	↑↓		
7 high-spin	↑↓	↑↓	↑	↑	↑
7 low-spin	↑↓	↑↓	↑↓	↑	
8	↑↓	↑↓	↑↓	↑	↑
9	↑↓	↑↓	↑↓	↑↓	↑
10	↑↓	↑↓	↑↓	↑↓	↑↓

arrangement with the paired electrons is the **low-spin** (or strong field) state. Alternative electronic configurations are also possible for d^5 , d^6 , and d^7 ions in octahedral complexes.

When bridging ligands connect two or more magnetic centres, their electron spins can either cancel each other out or reinforce one another — this constitutes antiferromagnetic and ferromagnetic coupling, respectively. This phenomenon is frequently encountered in biological inorganic chemistry, particularly the former, and we will encounter a good example in the case of the iron core stored within the interior of the protein core of the iron-storage protein, ferritin (Chapter 19).

ELECTRON PARAMAGNETIC RESONANCE (EPR) SPECTROSCOPY

The bioinorganic chemistry of V, Mn, Fe, Co, Ni, Cu, Mo, W, as well as of a number of nonbiological transition elements, is permeated by their paramagnetism, and EPR spectroscopy is a particularly useful tool for their analysis (Hagen, 2006). It can be used with frozen dilute solutions of metalloproteins, and is quite sensitive (high-spin ferric ions can be detected in the μM range), and it has the potential to establish the stoichiometries of complex mixtures of paramagnets. EPR detects unpaired electrons in a sample by their absorption of energy from continuous microwave irradiation (X-band, *ca.* 9–10 Hz) when the sample is placed in a strong magnetic field (around 0.3 Tesla). In standard EPR practice, the EPR absorption is detected by varying the magnetic field at constant microwave frequency, because in order to get the resonance condition, the wavelength of the microwave frequency must be tuned to the dimensions of the resonator cavity. EPR spectra are usually represented as the first derivative of the measured absorption spectrum and are characterised by the four main parameters: intensity, linewidth, *g*-value (which defines position), and multiplet structure.

What type of information can we obtain from metalloprotein EPR? Examination of the EPR spectrum should permit: (i) the identification of the type of bonding involved, based on its central hyperfine interaction, the oxidation state of the metal ion, and possibly the type of metallo-ligand centre (for example distinguishing between a 3Fe rather than a 4Fe cluster); (ii) quantification of the concentration of the paramagnet; (iii) structural characterisation, which is an extension of (i), involving the identification of ligands based on ligand hyperfine interaction of atoms in their first coordination sphere; (iv) functional characterisation, such as determining the saturation binding of a metal ion to a specific site on the protein or using EPR spectroscopy to determine the reduction potential of a prosthetic group in the protein. Resonances can be split into multiplet structures by the interaction of the electron spins with nuclear spins: this gives rise to what are called hyperfine interactions. To gain more detailed information on ligand identification and to increase resolving power, it may be necessary to apply advanced EPR techniques such as ENDOR (electron-nuclear double resonance spectroscopy) and ESEEM (electron spin echo envelope modulation).

Figure 6.1a shows the EPR spectra of horse spleen apoferritin which had been incubated with haemin. The signal at $g = 6$ is typical of high-spin haem iron (III); a small peak at $g = 4.3$ is also present, typical of free

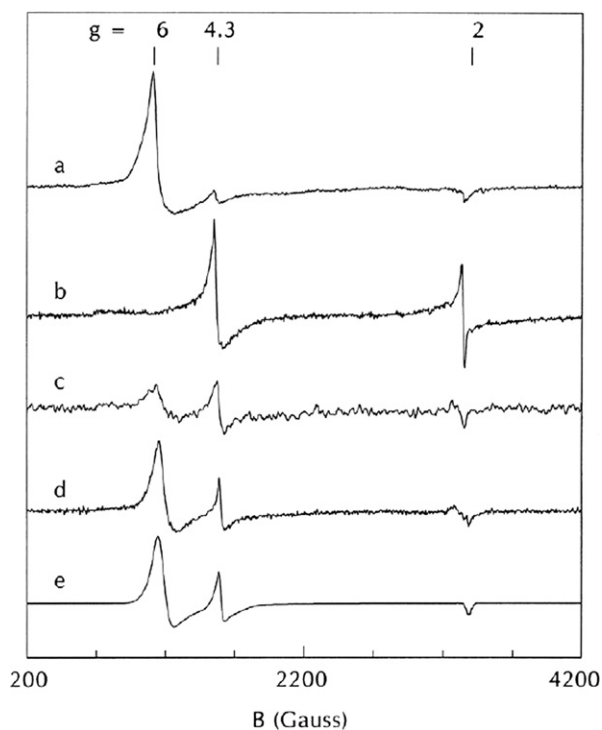


FIGURE 6.1 (a) EPR spectrum of horse spleen apoferritin incubated with haemin (8 haemin molecules/molecule of apoferritin) at pH 8; (b) EPR spectrum of horse spleen apoferritin +20 iron atoms/molecule of apoferritin at pH 4; (c) EPR spectrum of horse spleen apoferritin incubated with haemin (8 haemin molecules/molecule of apoferritin) in sodium phosphate buffer, 0.1 M, pH 8, dialysed against sodium acetate buffer, 0.1 M, pH 5.3, crystallised with ammonium sulfate and cadmium sulfate and the crystals then re-dissolved in water; (d) EPR spectrum of horse spleen apoferritin incubated with haemin (8 molecules of haemin/molecule of apoferritin) in sodium phosphate buffer, 0.1 M, pH 8, dialysed against sodium acetate buffer 0.1 M, pH 5.3; (e) the signal 3d was simulated as an effective $S = 1/2$ system with g-strain. The intensity was corrected for the Boltzmann population over the three doublets of the $S = 5/2$ system assuming a zero-field splitting $D \approx 2 \text{ cm}^{-1}$ i.e., 34% population of the middle doublet for a temperature of 16 K. Similarly, the intensity of the $g = 6$ signal from the lowest Kramers doublet of an axial $S = 5/2$ system was corrected assuming $D \approx 10 \text{ cm}^{-1}$, i.e., 84% population of the $m_S = \pm 1/2$ doublet at 16 K. For all spectra, frequency: 9.41 GHz, temperature: 16 K. (From *Carette et al.*, 2006. Copyright 2006 with permission from Elsevier.)

high-spin nonhaem Fe(III), often found in biological systems. In contrast, the EPR spectrum of apoferritin incubated with Fe^{2+} (Figure 6.1b) presents a signal at $g = 4.3$ corresponding to high-spin nonhaem Fe(III) and another at $g = 1.94$ representative of mixed-valence iron clusters similar to those encountered in di-iron proteins such as ribonucleotide reductase, methane monooxygenase, etc. (see Chapter 13 for more details). Figures 6.1c and d show the process of demetalation in which the haemin gradually loses its iron, the $g = 6$ signal decreasing and being replaced by that at $g = 4.3$. In Figure 6.1e, the signal of Figure 6.1d was simulated as an effective $S = 1/2$ system with g -strain. The intensity was corrected for the Boltzmann population over the three doublets of the $S = 5/2$ system assuming a zero-field splitting $D \approx 2 \text{ cm}^{-1}$ i.e., 34% population of the middle doublet for a temperature of 16 K. Similarly, the intensity of the $g = 6$ signal from the lowest Kramers doublet of an axial $S = 5/2$ system was corrected assuming $D \approx 10 \text{ cm}^{-1}$, i.e., 84% population of the $m_S = \pm 1/2$ doublet at 16 K (Carette et al., 2006).

MÖSSBAUER SPECTROSCOPY

Mössbauer spectroscopy probes high-energy transitions in the atomic nucleus and is based on the phenomenon of Recoil-free γ -ray resonance absorption. The effect was discovered by Rudolf Mössbauer in 1957, one year before he received his doctorate from the Technical University of Munich.² Under normal conditions, atomic nuclei recoil when they emit or absorb gamma rays and the wavelength varies with the amount of recoil. Mössbauer found that at a sufficiently low temperature, a significant fraction of the nuclei embedded in a crystal lattice may emit or absorb gamma rays without any recoil. The strictly monochromatic γ -radiation emitted from the excited nucleus of a suitable isotope during a radioactive decay pathway can therefore be absorbed by the same isotope in the sample (biological applications are essentially restricted to ^{57}Fe ; the natural abundance of ^{57}Fe is 2%, unless isotope enrichment is used). The interest of the method lies in the fact that, if the energy transitions occur within the nucleus itself, their magnitude depends on the density and arrangement of extranuclear electrons, i.e., on the chemical state of the atoms. The extremely small perturbation (10^{-8} eV) caused by the difference of chemical state between emitter and absorber can be easily offset and measured by Doppler modulation. The gamma-ray energy is varied by mechanically moving the source relative to the sample (usually by a few millimeters/second). This causes a Doppler shift³ in the frequency of the emitted radiation (higher frequency if the source moves towards the sample, lower if it moves away from it). The counts of γ -rays transmitted at each Doppler velocity are averaged many times to improve the signal-to-noise ratio, and in the resulting spectra, gamma-ray intensity is plotted as a function of the source velocity, lower if it moves away from it), and the spectra are collected over a wide range of temperature from 4.2 K to over 300 K. The Mössbauer signal is influenced by the nuclear charge, the nature of the surrounding ligands, and the symmetry of the ligand field. The observed isomer shift, δ , in mm/sec gives information about the metal oxidation and spin states and the nature of the ligands coordinated to the iron. From a structural point of view, the quadrupole splitting, ΔE_Q , is dependent on electric field gradients at the nucleus and reflects the asymmetry of the electric field surrounding the metal centre.

Figure 6.2 shows the Mössbauer spectrum of human haemosiderin (the lysosomal breakdown product of the iron-storage protein, ferritin) and its precursor prehaemosiderin and of haemosiderin from an iron-loaded rat and horse. The variable temperature spectra for haemosiderin (Figure 6.2a) show three components of haemosiderin mineralisation. Both the ferrihydrite-like and goethite-like materials give sextet spectra at 4.2 K. The doublet component in the centre of the 4.2 K spectrum is due to amorphous ferric oxide. At 1.3 K, this component becomes a sextet and is contained within the overall six-line pattern. Both the ferrihydrite-like and goethite-like materials exhibit superparamagnetic behaviour, which leads to both their spectral components becoming doublets as the temperature is raised. However, the mean temperature at which this transition occurs is much higher in the

2. Mössbauer received the Nobel prize in physics in 1962.

3. The well known effect whereby the pitch of the sound of a moving object (train, plane, etc.) gets higher as it approaches and becomes progressively lower as it recedes.

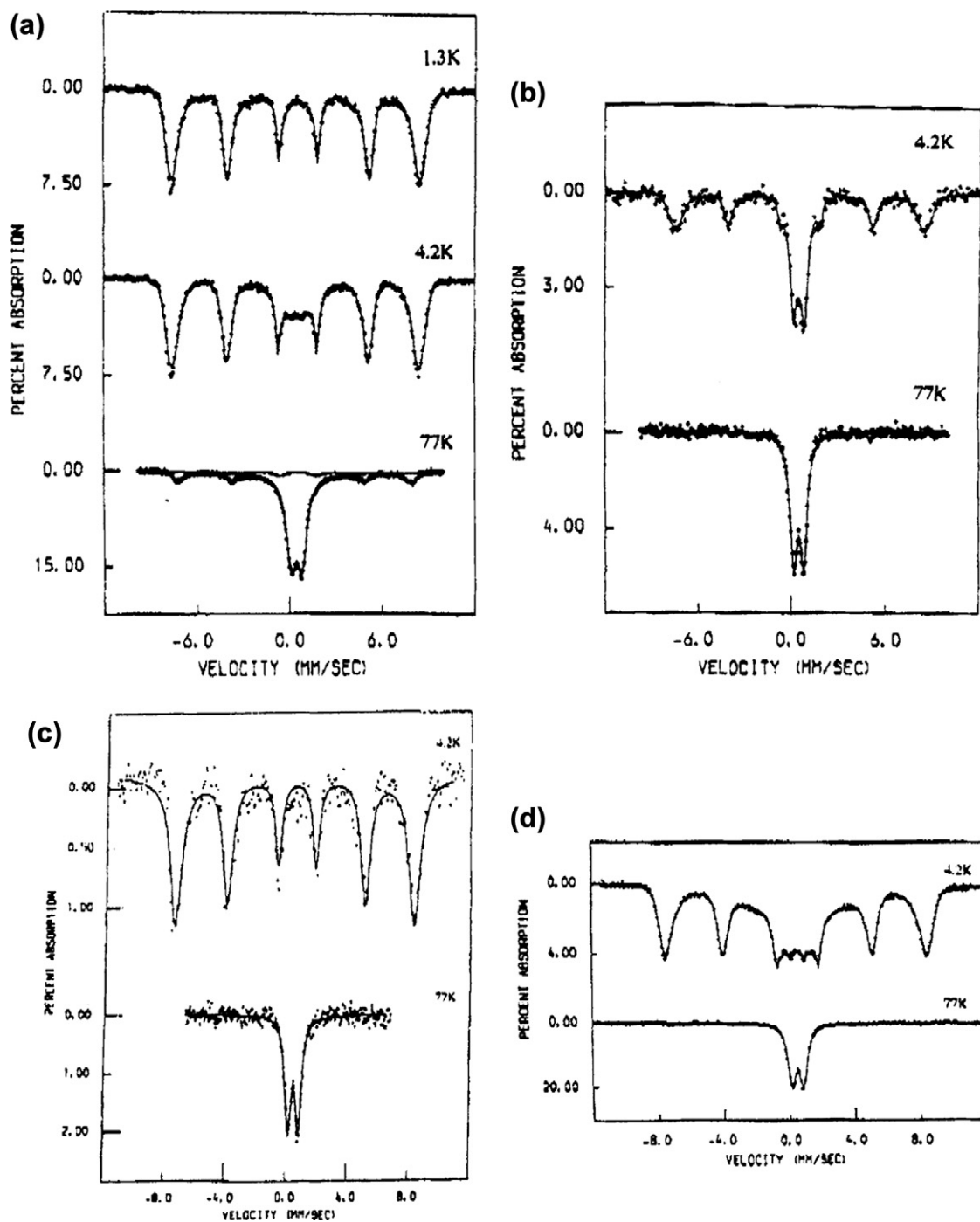


FIGURE 6.2 Mössbauer spectra of human haemosiderin (a), prehaemosiderin (b), haemosiderin from iron-loaded rats (c), and horse haemosiderin (d). (From Ward *et al.*, 1994. Copyright 1994 with permission from John Wiley and Sons.)

case of the component associated with the goethite-like material. This leads to a sextet component in the 77 K spectrum which is characteristic of the presence of the goethite-like mineralisation product and is clearly shown in the 77 K spectrum of Figure 6.2a. In Figure 6.2b, the lack of any sextet in the 77 K spectrum shows the absence of goethite-like material in the ferritin, while the intense doublet in the centre of the 4.2 K spectrum indicates a substantial quantity of the amorphous ferric oxide. Figure 6.2c, with a pure doublet at 77 K and a pure sextet at 4.2 K, indicates that the haemosiderin isolated from the iron-loaded rat has only ferrihydrite-like cores, while in the case of the horse haemosiderin (Figure 6.2d) there is also a minority proportion of amorphous cores corresponding to the central doublet in the 4.2 K spectrum.

NMR SPECTROSCOPY

Nuclear magnetic resonance (NMR) is a widely utilised technique which detects the reorientation of nuclear spins in a magnetic field. It can potentially be used to determine the three-dimensional structure of the protein itself, as well as supplying information on kinetics and dynamics, ligand binding, and determination of pK values of individual amino acid residues, on electronic structure and magnetic properties, to mention only some of the applications. In addition, it can be selectively applied to specific nuclei — ^1H , ^{13}C , ^{15}N , ^{19}F (often substituted for H as a probe of local structure), and ^{31}P , the latter not only for the study of nucleic acids but also for the study of phosphorylated metabolites within cells. The theory underlying an NMR experiment is very similar to that for EPR, but the setup is very different for technical reasons. In EPR, the promotion of molecules from their ground state to an excited state by microwave radiation is detected by the corresponding **absorption** of energy. In contrast, NMR relies on a **relaxation** process — the radiofrequency radiation raises molecules to their excited state and the experiment then monitors their return (relaxation) to their ground state. The most frequently used method in NMR is to apply a pulse of radiofrequency to the sample and then detect the transient signal as the nuclear spins return to their ground state. The transient signal then undergoes a Fourier transformation to give the NMR spectrum. From NMR experiments, four parameters can be derived — the chemical shift (δ), which like the g -value in EPR defines the field position of the NMR signal (in this case with respect to a reference marker added to the sample), the intensity (I), the relaxation times, and the coupling constant. Modern NMR instruments can resolve resonances for most of the protons in even large molecules, not just because the magnets themselves now produce very high fields (up to 900 MHz) but also because of the development of multidimensional NMR techniques.⁴ Because dipolar interactions with neighbouring spins depend on distance, structural information can be deduced. The 2-D NMR techniques, notably of *correlation spectroscopy* (COSY) and *nuclear Overhauser effect spectroscopy* (NOESY), allow the proximity of atoms within a macromolecule to be determined. This is based on the fact that with COSY, protons that are attached to adjacent atoms can be studied, while NOESY spectra can detect two protons that are located closer than about 0.5 nm to each other, because they will perturb each other's spin — even when they are far removed from each other in the amino acid sequence of the protein.

The full assignment of the hundreds of different resonances in the NMR spectrum and measurement of a great number of interproton distances and torsional angles can allow the complete three-dimensional structures of medium-sized proteins to be determined in solution.⁵

Until a decade ago, metalloproteins containing paramagnetic metal ions were not thought to be suitable for the application of NMR techniques because the presence of paramagnetic centres destroys the resolution of the spectrum. However, the loss of resolution is less severe when the paramagnetic centre exhibits fast electronic relaxation. The application of advanced pulse techniques and data handling methods can overcome the limitations that paramagnetism presented previously. The presence of paramagnetism in a protein allows structural and

4. Multidimensional NMR was pioneered by Richard Ernst (Nobel prize for chemistry, 1991) and its application to structure determination of biological macromolecules, already heroically undertaken with all the limitations of one-dimensional NMR, was further developed and refined by Klaus Wüthrich (Nobel prize for chemistry, 2002).

5. At typically a concentration of around 10^{-3} M, which for a protein of molecular weight 20 kD represents a concentration of 20 mg/ml.

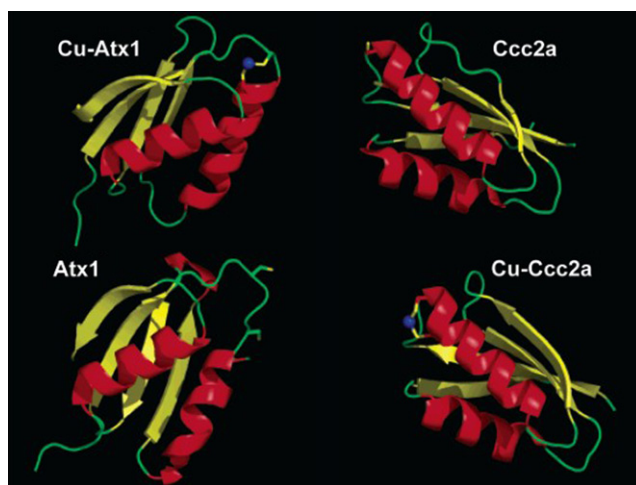


FIGURE 6.3 AtxA and Ccc2 exchanging a Cu(I) ion. (From *Fragai, Luchinat and Parigi, et al., 2006*. Copyright 2006 with permission from the American Chemical Society.)

mechanistic information by means of NMR that have no equivalent in the NMR study of diamagnetic proteins. Indeed, the replacement of diamagnetic and NMR-silent metal ions by suitable paramagnetic metal ions can be deliberately introduced into proteins to provide structural and mechanistic information not obtainable otherwise. A good example is the incorporation of lanthanides in Ca^{2+} -binding sites of proteins.

It has become clear that proteins are not rigid objects, but that they can sample a rather wide range of different conformations. NMR is a particularly appropriate technique to estimate the time scale of these conformational changes, from seconds to picoseconds, providing information both on conformational heterogeneity and on the time scale of motions associated with it. This is illustrated in [Figure 6.3](#) for the transfer of a copper(I) ion from the copper chaperone Atx1 to the soluble domain of the Ccc2 ATPase, where in the adduct between the two proteins, a copper-bridged intermediate is formed. In Atx1, the two metal-binding cysteines move from a buried location in the copper(I)-loaded protein to become solvent-exposed after copper release. In contrast, the structure of Ccc2a remains almost invariant upon binding of copper(I), indicating that the metal-binding site in the apo-form of Ccc2a is more pre-organised than in ApoAtx1.

ELECTRONIC AND VIBRATIONAL SPECTROSCOPIES

Transitions between different electronic states result in absorption of energy in the ultraviolet, visible, and, for many transition metal complexes, the near infrared region of the electro-magnetic spectrum. Spectroscopic methods which probe these electronic transitions can, in favorable conditions, provide detailed information on the electronic and magnetic properties of both the metal ion and its ligands.

Electronic spectra of metalloproteins find their origins in: (i) internal ligand absorption bands, such as $\pi \rightarrow \pi^*$ electronic transitions in porphyrins; (ii) transitions associated entirely with metal orbitals ($d-d$ transitions); (iii) charge transfer bands between the ligand and the metal, such as the $S \rightarrow \text{Fe(II)}$ and $S \rightarrow \text{Cu(II)}$ charge transfer bands seen in the optical spectra of Fe/S proteins and blue copper proteins, respectively. [Figure 6.4a](#) presents the characteristic spectrum of cytochrome *c*, one of the electron transport haemoproteins of the mitochondrial electron transport chain. In the reduced form, this consists of four absorption bands, the γ (Soret) band and three others, designated α , β , and δ , while in the oxidised form the spectrum is characteristically different. The three α bands of cytochromes *a*, *b* and *c* in beef heart mitochondria can be clearly distinguished ([Figure 6.4b](#)).

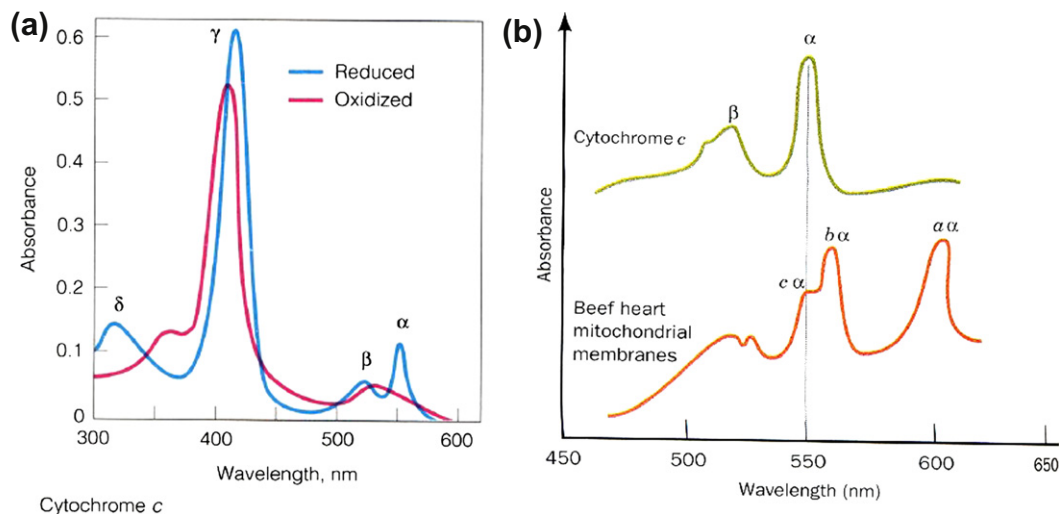


FIGURE 6.4 (a) Visible absorption spectrum of cytochrome c in its reduced and oxidised states. (b) The three separate α -bands in the visible spectrum of beef heart mitochondria (below) indicating the presence of cytochromes a, b, and c, with the spectrum of cytochrome c (above) as reference.

CIRCULAR DICHROISM AND MAGNETIC CIRCULAR DICHROISM

Because proteins are made up of chiral amino acids (Chapter 4), they can discriminate between right and left circularly polarised light (lcp and rcp, respectively). The different absorption of lcp and rcp light (reflected by different extinction coefficients) is termed circular dichroism (CD). CD is particularly useful for metals bound within proteins and can often detect and resolve electronic transitions that are not so accessible by classical absorption spectroscopy. This is because some of the d–d transitions which are observed in small molecule inorganic complexes by electronic absorption spectroscopy cannot be observed in the absorption spectra of metalloproteins. These ligand field transitions can be intense in the CD spectrum, and potentially give much more information, as illustrated for reduced *Chromatium vinosum* high-potential iron (Figure 6.5). In addition, CD is a useful tool for obtaining information about the secondary structure of proteins. Since α -helices, β -sheets, and random coils all have characteristic CD spectra, the relative amounts of these different secondary structures can be evaluated. In the presence of a molecular field, even nonchiral molecules exhibit CD spectra, which can be measured by the technique called magnetic circular dichroism (MCD). The intensity developed by spin–orbit coupling between excited states and between ground states and excited states can be exploited, particularly at low temperature, which generates more intense metal-centred d–d transitions in low-temperature MCD relative to absorption spectra. Although the theoretical analysis of MCD spectra is usually complex, it can be a powerful fingerprint for the identification of bound ligands. An example is the use of MCD to identify the presence of a thiolate ligand coordinated to low-spin ferric haem iron in cytochrome P-450s.

RESONANCE RAMAN SPECTROSCOPY

As in Raman spectroscopy, resonance Raman spectroscopy gives information about molecular vibrational frequencies. These frequencies are in the range of 10^{12} – 10^{14} Hz and correspond to radiation in the infrared region of the electro-magnetic spectrum. In resonance Raman spectroscopy, the energy of an incoming laser beam is tuned to be near to an electronic transition (in resonance); vibrational modes associated with the particular transition exhibit a greatly increased Raman scattering intensity, usually overwhelming Raman signals from all other transitions. In haemoproteins, such as haemoglobin, tuning the laser to near the charge transfer electronic

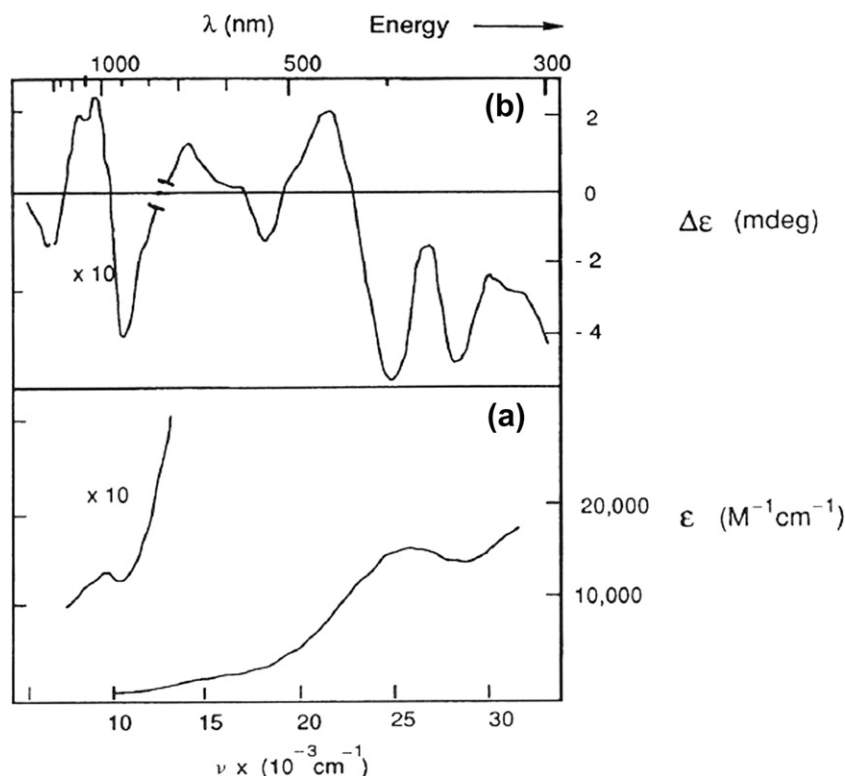


FIGURE 6.5 Absorption spectrum (a) and CD spectrum (b) of the Fe_4S_4 cluster of a high-potential iron protein (HiPIP- from *Chromatium* sp.). (From Cowan, 1997. Copyright 1997 with permission from John Wiley and Sons.)

transition of the iron centre gives a spectrum which only reflects the stretching and bending modes associated with the terapyrrole iron. Resonance Raman spectroscopy reduces the complexity of the spectrum, allowing us to look at only a few vibrational modes at a time. Its main advantage over classical Raman spectroscopy is the large increase in the intensity of the peaks (by a factor of as much as 10^6), allowing spectra to be obtained with sample concentrations as low as 10^{-8} M.

EXTENDED X-RAY ABSORPTION FINE STRUCTURE (EXAFS)

The availability of easily tunable high-flux X-ray beams from synchrotron radiation has led to the development of new types of X-ray spectroscopy. One technique of particular interest for metalloproteins is extended X-ray absorption fine structure (EXAFS) (Strange and Feiters, 2008). Here, the absorption of X-rays by a solid or liquid sample is measured as a function of wavelength at energies just above the absorption transition of a particular metal atom (the absorber). At energies just above the sharp absorption threshold, a pattern of rapid oscillations is observed, which represents an interference effect from the neighbouring atoms of the absorber. A Fourier transform of the oscillations can be analysed to give, in favourable cases, information on the number, types, and distances of neighbouring atoms. This usually requires parallel studies on model compounds of known structure and, for many metal centres in proteins, can give extremely accurate structural information, without the requirement for an ordered sample (see the next section on X-ray diffraction). Geometric information derived from fitting EXAFS data to a model structure can be reliable to ± 0.01 Å.

The ferroxidase site in reduced bacterioferritin from *Desulfovibrio desulfuricans* (DdBfr) with iron–ligand distances in angstroms is shown in Figure 6.6a as determined by crystallography and, in Figure 6.6b, adjusted to

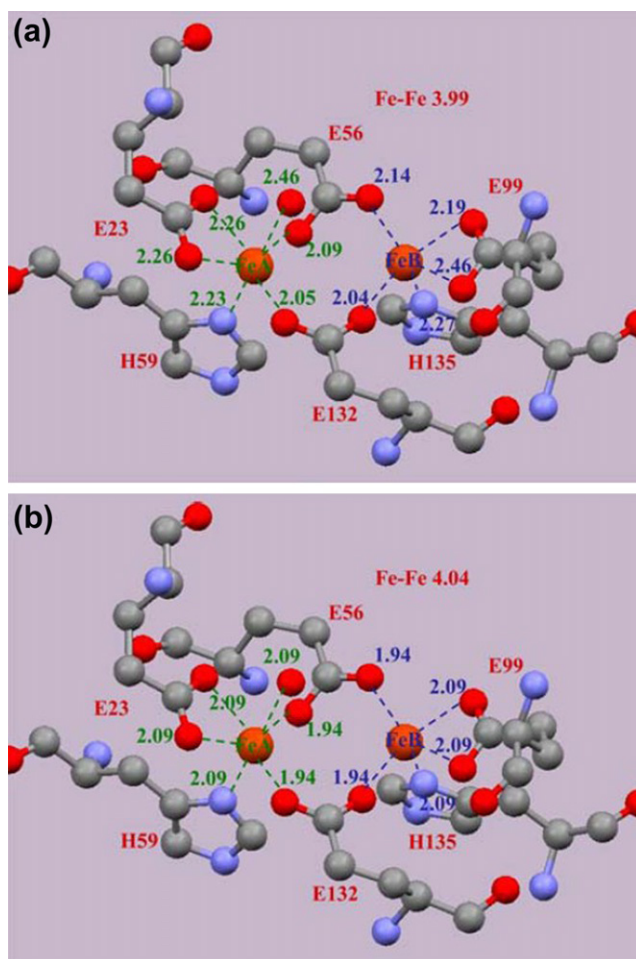


FIGURE 6.6 Ferroxidase site in reduced Bacterioferritin from *Desulfovibrio desulfuricans* with iron–ligand distances in ångströms: (a) as determined by crystallography, (b) adjusted to give agreement with the EXAFS. Grey, carbon; red, oxygen; blue, nitrogen; orange, iron; hydrogens are omitted for clarity. Green and blue distance values refer to Fe_A (left iron ion) and Fe_B (right), respectively. (From Toussaint *et al.*, 2009. Copyright 2009 with permission from Springer.)

give agreement with the EXAFS data (Toussaint *et al.*, 2009). The iron–ligand distances are shorter than in the crystallographic study, and the iron ion in the reduced state has an ionic radius which is significantly larger than that measured in the oxidized state, consistent with reduction from Fe(III) to Fe(II).

X-RAY DIFFRACTION

Protein crystallography had its beginnings in 1934, when J.D. Bernal and Dorothy Crowfoot (Hodgkin) showed that crystals of pepsin gave an X-ray diffraction pattern, made up of sharp reflections which showed that the protein had an ordered structure, with most of its 5000 atoms occupying clearly defined positions. Since then, protein crystallography has advanced to become one of the most important techniques for structure determination of macromolecules, with thousands of structures being determined every year. The principal reasons for this explosion of X-ray crystallographic prowess are: (i) more coherent protocols for protein crystallisation; (ii) cryo-crystallography; (iii) the use of brighter and tunable synchrotron-generated X-ray beams (which can enable

reliable data collection on crystals which would have been considered too small for study some years ago); (iv) better data collection facilities; and (v) the quasi-generalised use of multiple anomalous dispersion (notably by replacement of methionine residues in the protein by selenomethionine residues) to resolve the 'phase problem' (Ealick, 2000).

Structure determination of proteins requires the availability of an ordered sample in the form of a single crystal. Since protein crystals typically contain large amounts of water, to prevent them from drying, and thereby losing their regular ordered structure, they must be kept moist in the presence of the liquid of crystallisation during data collection. This is usually achieved by mounting the wet crystals in small glass capillaries, which are placed in a narrow beam of monochromatic X-rays. The crystal is then rotated in order to produce a diffraction photograph. While we can record the intensities and hence the amplitudes of the X-rays diffracted by the crystal, we cannot translate them into atomic structure without knowledge of both the amplitudes of the scattered beams

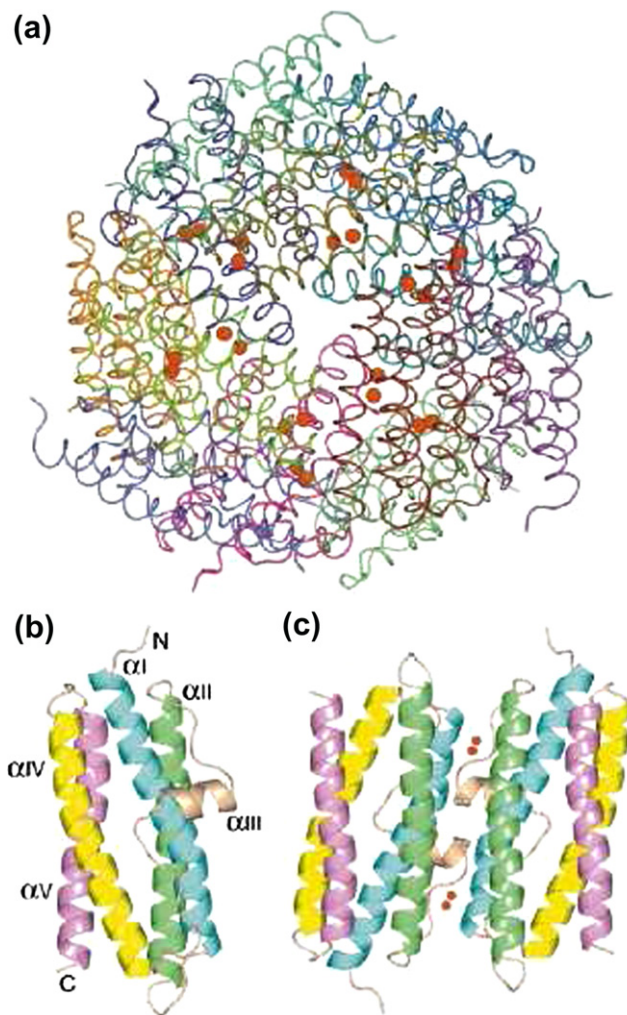


FIGURE 6.7 The structure of *Bacillus brevis* Dps dodecamer. (a) The *BbDps* dodecamer. The 12 subunits are shown by the ribbon representation of their C $^{\alpha}$ traces. The 24 iron ions at the ferroxidase centres inside the protein shell are shown as red spheres. (b) Ribbon diagram of the *BbDps* monomer. Helices αI – αV are shown in different colours. (c) A *BbDps* dimer. The iron ions in the two ferroxidase centres at the dimer interface are shown as red spheres. The helices are coloured as in (b). (From Ren *et al.*, 2003. Copyright 2003 with permission from Elsevier.)

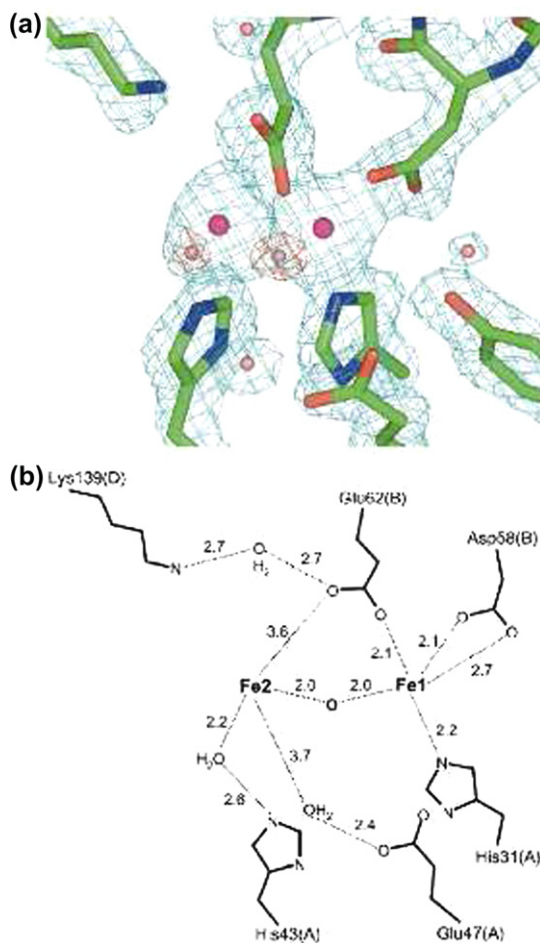


FIGURE 6.8 The di-nuclear ferroxidase centre *Bacillus brevis* Dps dodecamer. (a) Electron densities at one of the di-nuclear ferroxidase centres at the dimer interface. The $(2F_o - F_c)$ map is coloured in light blue and contoured at the 1.4σ level. The two iron ions have the highest density values in the map, which are 12.7σ and 7.2σ . The existence of two water molecules at the di-iron site is revealed by the superimposed $(F_o - F_c)$ map, which is coloured in red and contoured at the 4.0σ level. The iron ions and water molecules are shown as spheres, coloured in magenta and light orange, respectively. (b) A drawing of the coordination of the iron ions at the di-nuclear centre. The coordination is indicated by dotted lines and distances (in Å). (From Ren *et al.*, 2003. Copyright 2003 with permission from Elsevier.)

and their experimentally inaccessible phase constants. The phase problem was first resolved by J. Monteath Robertson⁶ for the (then) complex organic compound phthalocyanin, by isomorphous replacement in which comparison of the molecule with either H, Ni or Cu at its centre allowed him to find phase constants and absolute structures. This approach, multiple isomorphous replacement (MIR), was extended to protein crystals by the preparation of derivatives in which a heavy atom is bound specifically and uniformly to molecules within the crystal. MIR techniques further require that the heavy atom derivatisation does not introduce additional changes in the molecular structure or change the crystallographic parameters. MIR has now been replaced by multiple anomalous scattering⁷ (MAD). MAD exploits the potential of using more than one wavelength along with the

6. Gardiner professor of chemistry in the University of Glasow, whose lectures I attended as an undergraduate in the early 1960s.

7. Anomalous scattering occurs when the frequency of the X-rays used falls near the absorption edge of one or more atoms in the sample, eg., transition metals, often found in metalloproteins, and other atoms such as selenium.

known position of anomalous scattering atoms to resolve the phase ambiguity. Most MAD phasing experiments use proteins in which methionine residues have been replaced by selenomethionine. From a practical point of view, such experiments can only be carried out at synchrotron beamlines, and since all of the data are collected on the same sample, systematic sources of error are eliminated and resulting phase angles are more accurate.

The 12-subunit DNA-binding proteins from starved cells (Dps proteins) are yet another form of iron-storage protein found in bacteria (see Chapter 8). Initial crystallographic studies on the Dps protein of *E. coli* led to the claim that Dps proteins did not have a ferroxidase centre. Figure 6.7 shows the structure of *Bacillus brevis* Dps, which confirmed that a di-iron ferroxidase centre certainly does exist (Ren, Tibbelin, Kajino, Asami, & Ladenstein, 2003). The ferroxidase centre possesses unique features among all the di-iron proteins identified so far. Dps does not have a single di-iron site within the four-helix bundle of the subunit. Instead, two neighbouring dinuclear iron-binding sites are present at the dimer interface inside the dodecamer (Figure 6.7c), related by the local 2-fold axis. They are located in a shallow groove formed by helices α I and α II from one subunit and their symmetry-related counterparts from the other subunit. One might consider that these helices at the dimer interface form a special four-helix bundle, which accommodates not one but two di-iron sites. The ligands to the pentahedral Fe 1 (Figure 6.8) come from two subunits, while the more loosely coordinated Fe 2 has only one direct protein ligand, the bridging carboxylate Glu 62 (B) with additional water-mediated contacts to Glu 47 (A) and His 43 (A).

REFERENCES

- Arnesano, F., Banci, L., & Piccioli, M. (2005). NMR structures of paramagnetic proteins. *Quarterly Reviews of Biophysics*, 38, 167–219.
- Banci, L., Bertini, I., Cantini, F., Felli, I. C., Gonnelli, L., Hadjiladis, N., et al. (2006). The Atx1-Ccc2 complex is a metal-mediated protein-protein interaction. *Nature Chemical Biology*, 2, 367–368.
- Bertini, I., Luchinat, C., Parigi, G., & Pierattelli, R. (2005). NMR spectroscopy of paramagnetic metalloproteins. *Chembiochem*, 6, 1536–1549.
- Campbell, I. D., & Dwek, R. A. (1984). *Biological spectroscopy*. Menlo Park, Calif.: Benjamin/Cummings Publishing Co., Inc. pp. 404.
- Carette, N., Hagen, W., Bertrand, L., de Val, N., Vertommen, D., Roland, F., et al. (2006). Optical and EPR spectroscopic studies of demetallation of hemin by L-chain apoferritins. *Journal of Inorganic Biochemistry*, 100, 1426–1435.
- Crichton, R. R. & Louro, R. O. (Eds.), (2012). *Practical approaches to biological inorganic chemistry*. Elsevier.
- Ealick, S. E. (2000). Advances in multiple wavelength anomalous diffraction crystallography. *Current Opinion in Chemical Biology*, 4, 495–499.
- Fragai, M., Luchinat, C., & Parigi, G. (2006). “Four-dimensional” protein structures: examples from metalloproteins. *Accounts of Chemical Research*, 39, 909–917.
- Hagen, W. R. (2006). EPR spectroscopy as a probe of metal centres in biological systems. *Dalton Transactions*, 37, 4415–4434.
- Neese, F. (2003). Quantum chemical calculations of spectroscopic properties of metalloproteins and model compounds: EPR and Mössbauer properties. *Current Opinion in Chemical Biology*, 7, 125–135.
- Que, L., Jr. (2000). *Physical methods in bioinorganic chemistry: Spectroscopy and magnetism*. Sausalito, Ca: University Science Books. pp. 59–120.
- Ren, B., Tibbelin, G., Kajino, T., Asami, O., & Ladenstein, R. (2003). The multi-layered structure of Dps with a novel di-nuclear ferroxidase center. *Journal of Molecular Biology*, 329, 467–477.
- Strange, R. W., & Feiters, M. C. (2008). Biological X-ray absorption spectroscopy (BioXAS): a valuable tool for the study of trace elements in the life sciences. *Current Opinion in Structural Biology*, 18, 609–616.
- Toussaint, L., Cuyper, M. G., Bertrand, L., Hue, L., Romão, C. V., Saraiva, L. M., et al. (2009). Comparative Fe and Zn K-edge X-ray absorption spectroscopic study of the ferroxidase centres of human H-chain ferritin and bacterioferritin from *Desulfovibrio desulfuricans*. *Journal of Biological Inorganic Chemistry*, 14, 35–49.
- Ubbink, M., Worrall, J. A. R., Canters, G. W., Groenen, E. J. J., & Huber, R. (2002). Paramagnetic resonance of biological metal centers. *Annual Review of Biophysics and Biomolecular Structure*, 31, 393–422.
- Ward, R. J., Ramsey, M., Dickson, D. P., Hunt, C., Douglas, T., Mann, S., et al. (1994). Further characterisation of forms of haemosiderin in iron-overloaded tissues. *European Journal of Biochemistry*, 225, 187–194.

This page intentionally left blank

Metal Assimilation Pathways

Introduction	133
Inorganic Biogeochemistry	133
Metal Assimilation in Bacteria	137
Metal Assimilation in Fungi and Plants	144
Metal Assimilation in Mammals	151

INTRODUCTION

After outlining the roles of metals in biology, their coordination chemistry, structural and molecular biology, and involvement in metabolism and bioenergetics as well as considering their biological ligands and the plethora physicochemical array of techniques available for their study in biological systems, we complete these introductory chapters by a consideration of how the metal ions essential for living organisms are assimilated from their surroundings. Clearly, this poses three distinct types of problems illustrated by three different kinds of organisms. For single-celled microorganisms, they must acquire the metal ions they require from their immediate environment. If they are motile, and in a liquid milieu they can ‘swim around’ in search of their food, but find it they must. If they are multicellular organisms, but are rooted to the spot in the soil, like most members of the plant family are, they must find their source of nutrition in the soil, wherever they can extend their roots. And finally, if they are multicellular mobile animals they can forage for their food, fish or hunt for it and kill it, or in the case of humans, buy it at the supermarket before eating it. They can also take advantage of preprocessing of their nutritional supply by the organisms from which they have acquired it — this is after all how we obtain the vitamins that we cannot synthesize ourselves. We recognise that this is a reductionist simplification, but it serves conveniently to situate the three model systems that we will consider here, because the mechanisms of metal assimilation are often significantly different. Supplementary material can be found in Cobine et al., 2006; Crichton, 2009; Hantke, 2001; Kosman, 2003; Palmer and Guerinot, 2009; Petris, 2004; Solioz and Stoyanov, 2003).

We therefore discuss in succession the assimilation of metal ions by bacteria, by plants, and fungi, and finally by mammals, with a particular focus on man. In most cases, we consider systems involved in iron uptake and then those involving copper and zinc. This is based on the simple logic that these are the three metals for which the assimilation systems are the best characterized. We begin with a brief outline of inorganic biogeochemistry and then discuss a few other metals where sufficient information is available. The specific cases of Na^+ , K^+ , and Ca^+ will be dealt with in Chapters 9 and 11. We remind the reader that uptake systems for the essential metalloids B and Si and their toxic homologues As and Sn were already discussed in Chapter 1.

INORGANIC BIOGEOCHEMISTRY

Biogeochemistry is a complex field which encompasses the study of the processes (biological, chemical, geological, and physical) that govern the composition of our natural environment. A particular focus of

biogeochemistry is the study of the cycles within the biosphere of chemical elements, such as carbon, nitrogen, phosphorus, and sulfur, which will be discussed in more detail in Chapter 18. Marine phytoplankton, including cyanobacteria, play an essential role in many of these biogeochemical cycles. More than 100 million tonnes of CO_2 fixation, which corresponds to more than 50% of the global total, is contributed by the photosynthesis of these organisms. The photosynthetic apparatus, in both bacteria and plants, has a very high requirement for a range of metal ions, including iron for the electron transport cytochromes and FeS proteins, Cu in the electron transporter plastocyanin, Mg in chlorophylls, Mn in the O_2 evolving complex, and Zn for carbon fixation and for CO_2 acquisition via carbonic anhydrase.

The role of Fe as a limiting nutrient has been well established in the last decade in the so-called high-nutrient low chlorophyll regions of the oceans. A series of massive iron seeding experiments carried out to test the ‘iron hypothesis’ advanced by [Martin and Fitzwater \(1988\)](#) have unequivocally shown that iron supply limits plankton production in one third of the world’s oceans, despite the perennially high surface concentration of macronutrients ([Fig. 7.1](#)). The dynamics of phytoplankton blooms are limited by iron supply, which



FIGURE 7.1 World map showing the locations of the ten major iron addition experiments completed thus far. (*Adapted from Vraspir & Butler, 2009.*)

in turn affects the biogeochemical cycles of carbon, nitrogen, silicon, and sulfur. In the Southern Ocean Iron Experiment (1.7 tonnes of iron sulfate dropped in the sea), the results showed that one atom of iron could bring down between 10,000 to 100,000 atoms of carbon out of the atmosphere by encouraging phytoplankton growth. It has been suggested ([Shi, Xu, Hopkinson & Morel, 2010](#)) that dissolution in the ocean of additional

CO₂, generated by the activity of man,¹ results in an increase in the partial pressure of CO₂, a decrease in pH, and a decrease in HCO₃⁻ concentration. This could change ocean chemistry to reduce the bioavailability of iron, increasing Fe stress of phytoplankton populations in some parts of the ocean. Whether massive iron fertilization of the oceans could absorb this buildup of CO₂, which is associated with global warming according to many people, is still highly controversial, in view of the unknown potential effects on marine ecosystems.

It seems that two cyanobacteria, *Prochlorococcus* and *Synechococcus*, on their own, account for some 20–40% of global CO₂ fixation, despite only accounting for 1% of the photosynthetic biomass. Cyanobacteria are also the only photosynthetic organisms capable of nitrogen fixation, deriving their energy and major constituents out of only air: sunlight, CO₂, and N₂. These blue-coloured bacteria are found in almost every conceivable environment, from oceans to fresh water to bare rocks to soil. Present in Precambrian fossils, they are probably among the oldest living organisms, and were responsible 2.75 billion years ago for generating a new pollutant, **molecular oxygen**, through photosynthesis-driven cleavage of water. In the surface waters, sunlight progressively changed the predominantly reducing atmosphere into one in which oxidised Fe(III) was much less bioavailable than the previously highly soluble Fe(II). In contrast, as a consequence of the oxidation of sulfide to sulfate, Cu and Zn became much more available (whereas the Zn proteome represents only 5–6% of the entire proteome in prokaryotes, it represents 9% of the total proteome in eukaryotes).

It has been suggested that in certain parts of the oceans where dissolved zinc levels are extremely low, the limited availability of Zn might also limit CO₂ fixation. This is because the Mg²⁺-dependent enzyme which fixes CO₂, RuBisCO (ribulose-1,5-bisphosphate carboxylase/oxygenase), is a notoriously inefficient enzyme, with a low affinity for its substrate, CO₂. It therefore requires high concentrations of CO₂, and while cyanobacteria have evolved extremely effective mechanisms for uptake of CO₂, which is then converted to HCO₃⁻, they need to regenerate CO₂ from HCO₃⁻ in the vicinity of RuBisCO, and this requires the Zn²⁺-dependent enzyme, carbonic anhydrase. This was the first Zn²⁺-dependent enzyme to be discovered (Chapter 12) and virtually all carbonic anhydrases discovered to date² have a catalytic Zn²⁺ ion, bound to one His and two Cys residues.

Clearly, marine organisms, including not only phytoplankton but also bacterioplankton, fungi, and macroalgae, require metal ions in order to survive and thrive in the ocean. Their bioavailability may well be controlled to a large extent by their chemistry and speciation in the oceans. One strategy to facilitate uptake of metal ions would be the production of organic ligands. It has become clear that quite a number of trace metal ions including cobalt, copper, iron, nickel, and zinc are complexed in seawater by biogenic ligands which appear to be metal specific. We have already encountered the low-molecular-weight iron-binding siderophores in Chapter 4, and we will describe the way in which they are taken up by bacteria below. Two structural classes of siderophores have been identified and characterised from marine bacteria. They are (i) siderophores which are amphiphilic with variations in the chain lengths of the fatty acids attached (Fig. 7.2) and (ii) siderophores which have an α -hydroxy carboxylic moiety, which is photoreactive when coordinated to Fe(III) (Fig. 7.3). Complex formation with organic ligands dominates the chemical speciation of a number of other trace metals in seawater, including Co, Cu, and Zn. In most cases, the nature of the ligands and the organisms producing them remain unknown. Phytochelatins (see later in the chapter) and the tripeptide glutathione, from which they are synthesised, have been isolated from eukaryotic phytoplankton, and may be directly involved in the transport of Cu.

An important aspect of the inorganic biogeochemistry of anaerobic involves microorganisms which enzymatically reduce a variety of metals in metabolic processes that are not related to metal assimilation. These microorganisms can obtain the energy to support their growth by coupling the oxidation of hydrogen, nitrate,

1. I more than hesitate to use the word anthropogenic to describe this!

2. The marine diatom *Thalassiosira weissflogii* has a Cd²⁺-containing carbonic anhydrase.

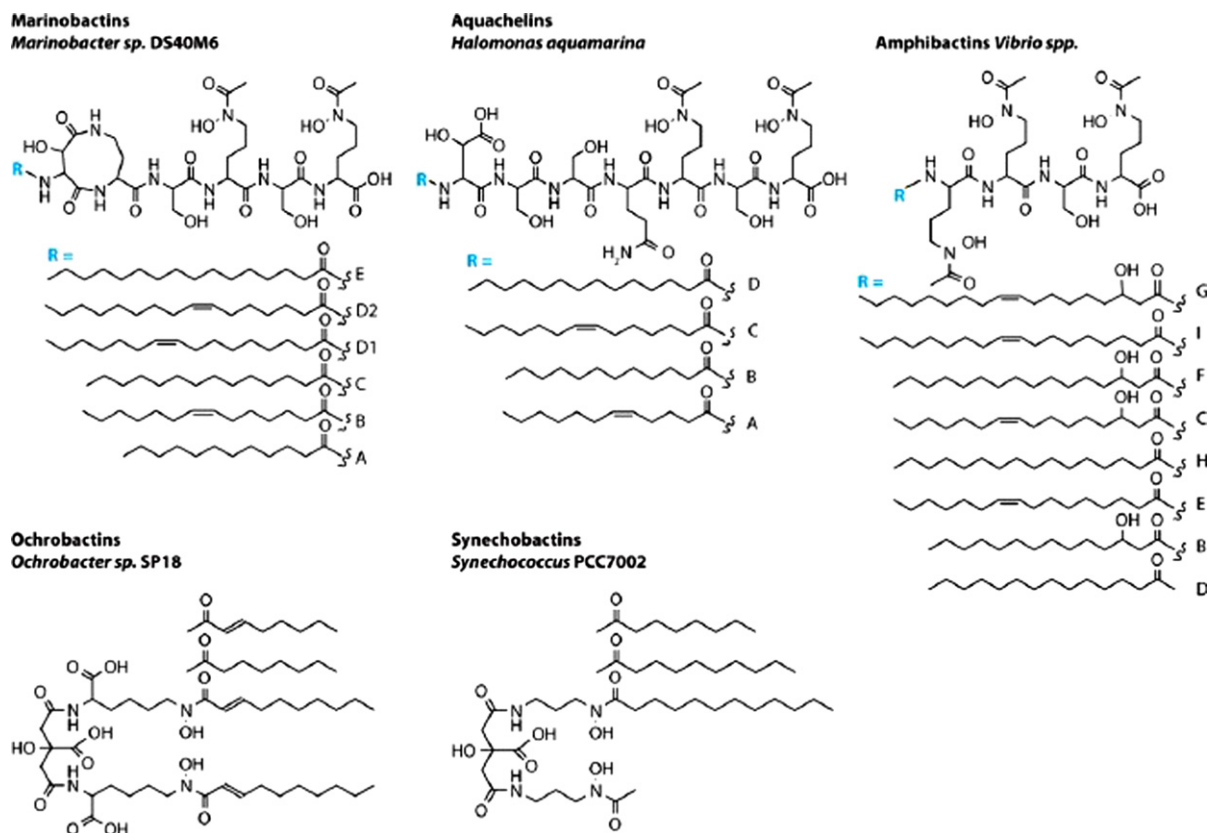


FIGURE 7.2 Amphoteric marine siderophores, including marinobactins, aquachelins, amphibactins, ochrobactins, and synechobactins. (Adapted from *Vraspir & Butler, 2009. NIH Public Access.*)

oxygen, and a number of organic compounds to the reduction of Fe(III) or Mn(IV). This dissimilatory³ Fe(III) and Mn(IV) reduction influences the organic as well as the inorganic geochemistry of anaerobic aquatic sediments and groundwater. Microorganisms capable of conserving energy from metal reduction are widely dispersed throughout the Bacteria and Archaea kingdoms. However, they face the dilemma that the most prevalent forms of Fe(III) or Mn(IV) in the majority of environments are the insoluble oxides. Electron transfer from the inner membrane to the outer membrane in *Geobacter* and *Shewanella* species appears to involve an electron transport chain of inner membrane, periplasmic, and outer membrane multihaem c-type cytochromes (Fig. 7.4). In *Shewanella oneidensis*, multihaem decahaem c-Cyts CymA and MtrA are believed to transfer electrons from the inner membrane quinone/quinol pool through the periplasm to the outer membrane. The c-Cyts MtrC and OmcA at the extracellular face of the outer membrane can directly reduce solid metal oxides. Likewise, outer membrane multihaem c-Cyts OmcE and OmcS of *Geobacter sulfurreducens* are thought to transfer electrons from outer membrane to type IV pili that are hypothesised to relay the electrons to solid metal (hydr)oxides. These multihaem c-Cyts play critical roles in *S. oneidensis* and *G. sulfurreducens*-mediated dissimilatory reduction of solid metal oxides by facilitating ET across the bacterial cell envelope.

3. A word which is not recognised in English or American dictionaries: it clearly was invented to indicate the opposite of assimilation - nothing to do with dissimulation!

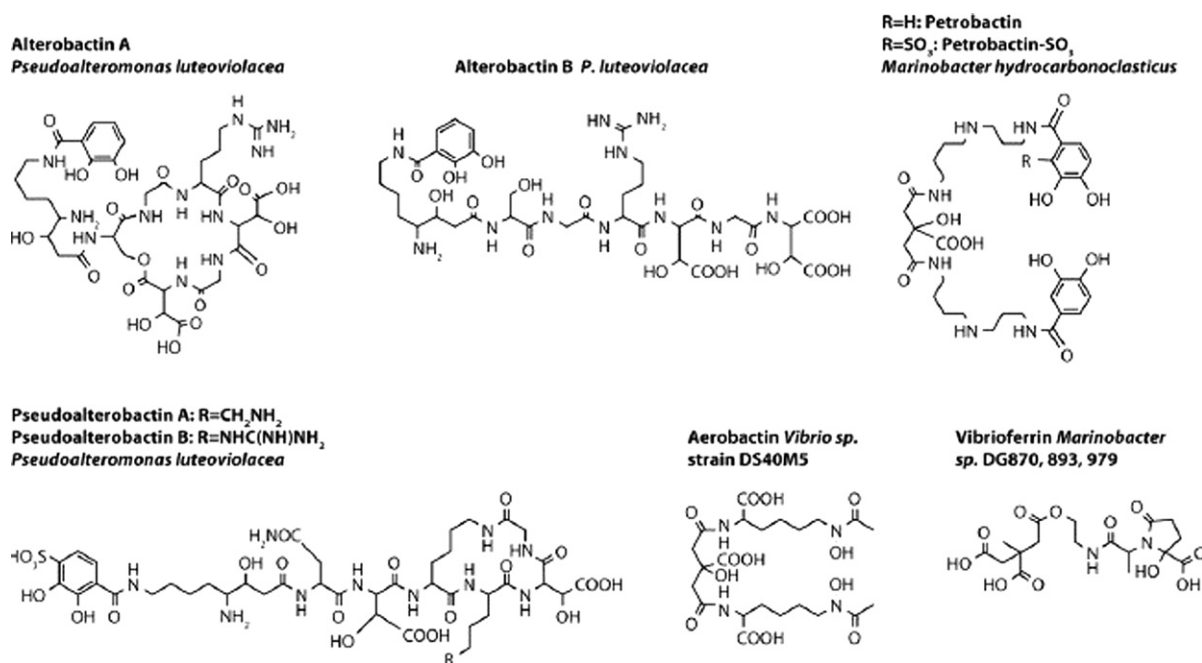


FIGURE 7.3 Other marine siderophores, including alterobactins, pseudoalterobactins, aerobactin, petrobactins, and vibriobactins. (Adapted from Vraspir & Butler, 2009. NIH Public Access.)

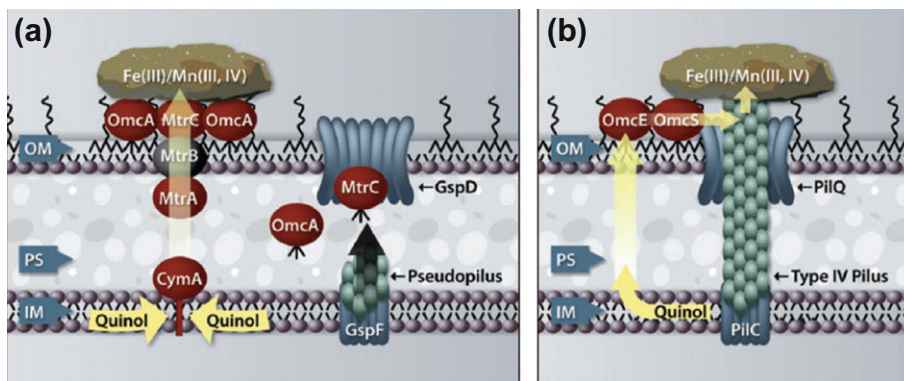


FIGURE 7.4 Proposed models depicting electron transfer pathways for *Shewanella oneidensis* MR-1 (a) and *Geobacter sulfurreducens* (b) during dissimilatory reduction of solid metal (hydr)oxides. (From Shi, Squirer, Zachara & Fredrickson, 2007.)

METAL ASSIMILATION IN BACTERIA

Bacteria are surrounded by rigid cell walls which give them their characteristic shapes, and enable them to live in hypotonic environments without swelling and lysing their plasma membranes. The so-called Gram-negative bacteria,⁴ which we will mostly deal with here, have a thin cell wall surrounding their plasma membrane, covered by an additional outer membrane. This defines four compartments — the outer membrane, the periplasm, the plasma membrane, and the cytosol. This means that, for charged or even hydrated metal ions to enter the

4. This classification is based on whether or not the bacteria take up the Gram stain, devised by Christian Gram in 1884.

cytoplasm of these bacteria they must cross two membranes and the periplasmic space. As we will see in what follows, this requires quite a number of transport proteins. In contrast, Gram-positive bacteria have a very thick cell wall confronting the external environment, and their unique outer membrane plays a role which is similar to that of the plasma membrane in Gram-negative bacteria.

While we tend to talk about transition metals as trace elements, in terms of their actual concentration within individual bacterial cells, they are found at concentrations which are several orders of magnitude higher than the concentration in a typical bacterial growth medium. Thus, in *Escherichia coli*, Fe and Zn are present at around 2×10^5 atoms/cell, which corresponds to around 0.1 mM, while intracellular Cu, Mn, Mo, and Se levels are around 10 μ M.

The impact of genome-sequencing projects on our understanding about metal-assimilation pathways has been enormous, particularly among organisms with genomes that are not too large, nor too complex. The first complete genomes to be sequenced were those of small RNA and DNA viruses. Today, the complete genome sequence of over 1500 bacteria have been determined, and for the family of Cyanobacteria, the complete genomic sequence of around 40 members of the family are known. This of course means that once a metal assimilation gene has been identified, its presence and presumed functionality can be assigned to other family members. In a similar manner, identification of a gene with homology to a known transport protein in any other bacterial species can lead to the putative identification of the corresponding pathway in other bacteria. Clearly, there is one small codicil — the presence of the gene does not establish that it is expressed — that requires the much more exacting task of showing that the gene product (i.e., the protein) is indeed present.

In what follows, we discuss uptake, i.e., assimilation of metal ions from the environment into the organism itself. Later, in Chapter 8, we consider metal transport, storage, and homeostasis within organisms and cells.

1. Iron

Because of both the low solubility of ferric iron (at pH 7 the free Fe^{3+} concentration is around 10^{-9} M) and the large amounts of iron required for their growth, bacteria have developed a large variety of iron uptake systems. These probably reflect the type of iron sources present in their particular environment at a given time. Most of the abundant nutrients required for Gram-negative bacteria diffuse across the outer membrane passively through transmembrane channels made up of porins, to pass into the periplasm. However, scarce metals like iron and cobalt (e.g., vitamin B12 in the GI tract of humans in the case of the common colon bacteria *E. coli*) need to be transported actively across each layer of the cell envelope.⁵ In the case of iron, as we briefly described in **Chapter 4**, this is achieved by synthesising and secreting into their surrounding environment highly specific Fe^{3+} -complexing compounds, termed siderophores, which are taken up by specific transport systems. They may also use ambient iron sources, such as Fe^{3+} -loaded siderophores from other bacteria and fungi. *E. coli* produces endogenously only one siderophore, enterobactin, the biosynthesis of which we described in **Chapter 4**. However, it has outer-membrane receptors for the uptake of a number of exogenous ferric hydroxamate siderophores, like ferrichrome and ferrioxamine, which it is itself incapable of synthesising, as well as the periplasmic transporter FhuB and the inner membrane ABC transporter FhuCD, necessary for their uptake.⁶ It also has an uptake system which enables it to acquire iron from ferric citrate, despite the fact that ferric citrate is neither a carbon nor an energy source for *E. coli*, as well as a specific uptake system for Fe^{2+} , which allows it to grow anaerobically.

Many highly pathogenic bacteria can also acquire iron from the haem of their mammalian hosts, by secreting proteins called haemophores which release haem from haemoglobin to specific transport proteins in the outer membrane. Yet other pathogens can use iron bound to transferrin and to lactoferrin. The list of pathogenic microorganisms which are able to use the mammalian host's iron transport systems reads like a roll call from Hell's kitchen of human bacterial diseases — *Haemophilus influenzae* (a wide range of clinical diseases, but, surprisingly not influenza!), *Neisseria meningitidis* (meningitis), *Neisseria gonorrhoeae* (gonorrhea), *Pseudomonas aeruginosa* (an opportunistic

5. If a bacterial cell waited for simple diffusion of 10^{-9} M Fe^{3+} through porins, it would die instantaneously!

6. The yeast *Saccharomyces cerevisiae* goes one better — it itself synthesises no siderophores, but has no less than four plasma membrane facilitators for uptake and internalization of several ferric siderophores.

pathogen, which exploits any break in host defenses), *Serratia marcescens* (urinary tract and wound infections), *Vibrio cholera* (cholera), *Yersinia pestis* (plague), and *Yersinia enterocolytica* (gastroenteritis), to mention but a few!

Iron uptake from transferrin, siderophores, and haem by Gram-negative bacteria is represented schematically in Fig. 7.5. All three iron uptake pathways require an outer-membrane receptor, a periplasmic-binding protein (PBP), and an inner-membrane ATP-binding cassette (ABC) transporter. Whereas Fe^{3+} -siderophores and haem

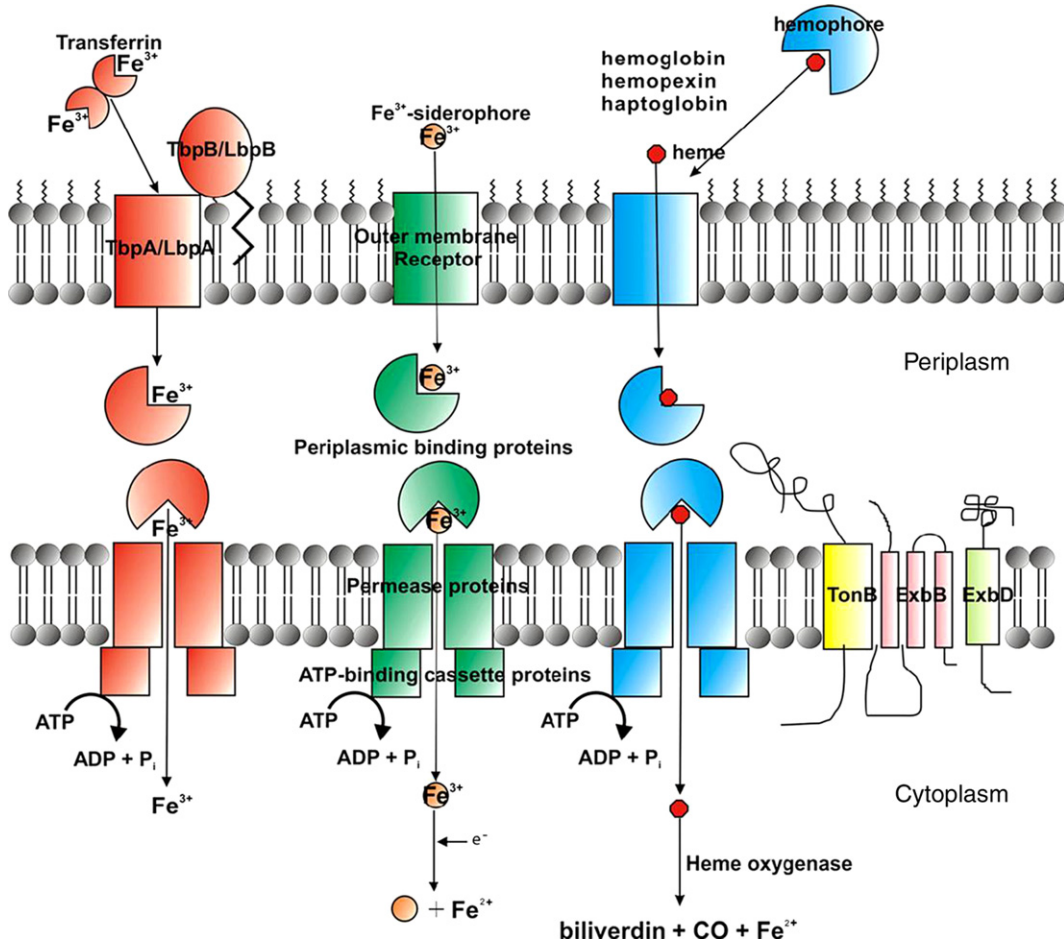


FIGURE 7.5 Schematic representation of iron uptake in Gram-negative bacteria. There are numerous iron uptake pathways in Gram-negative bacteria which include iron uptake from transferrin, siderophores, or haem. All of these uptake pathways require an outer-membrane receptor, a PBP, and an inner-membrane ABC transporter. Not all bacteria have all three systems; but some have more than one type. Transport through the outer-membrane receptor requires the action of the TonB system (TonB, ExbB, and ExbD). (From Krewulak & Vogel, 2008. Reproduced with permission from Elsevier.)

are transported across the outer membrane by their receptors, the iron is stripped from transferrin and lactoferrin at the outer membrane by their respective receptor complexes, the TbpA/TbpB and LbpA/LbpB proteins, attached to the outer membrane by an N-terminal lipid anchor. It is thought that one of them, perhaps TbpB acts as a primary binding protein for iron-saturated transferrin, facilitating its binding to TbpA. Both TbpA and LbpA are integral membrane proteins, which are predicted to have large surface loops that bind transferrin and lactoferrin, respectively, forcing the separation of the two domains surrounding the iron-binding sites and releasing the Fe^{3+} . However, to date, the structures of TbpA/TbpB and LbpA/LbpB have not been determined.

All outer-membrane transporters (OMTs) involved in iron uptake are made up of a 22-stranded β -barrel, which is occluded by an independently folded mixed α - β globular 'cork' domain of around 160 amino acid residues. This is illustrated for a vitamin B12 receptor and the ferric siderophore receptors for citrate, enterobactin, ferrichrome, pyochelin, and pyoverdine from *E. coli* and *P. aeruginosa* in Fig. 7.6. The ferric siderophore sits on top of the 'cork' domain, as can be seen in Fig. 7.7 for FecA. The binding of the ligand induces a conformational

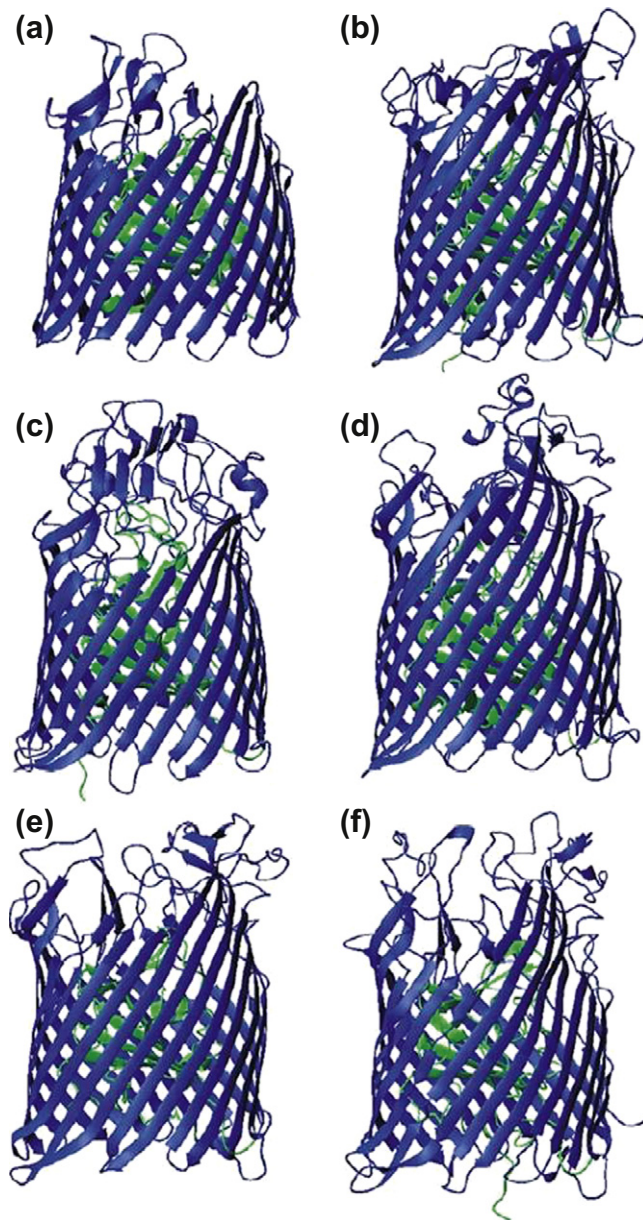


FIGURE 7.6 Outer-membrane siderophore receptors from *Escherichia coli* and *Pseudomonas aeruginosa*. Ribbon representations of the (a) vitamin B₁₂ (BtuB), (b) *E. coli* ferric-citrate (FecA), (c) ferric-enterobactin (FepA), (d) ferric-hydroxamate (FhuA), (e) *P. aeruginosa* pyochelin (FptA), and (f) *P. aeruginosa* pyoverdine (FpvA) receptors. The mixed α - β globular (cork) domain is coloured green while the 22-strand β -barrel is coloured blue. (From Krewulak & Vogel, 2008. Reproduced with permission from Elsevier.)

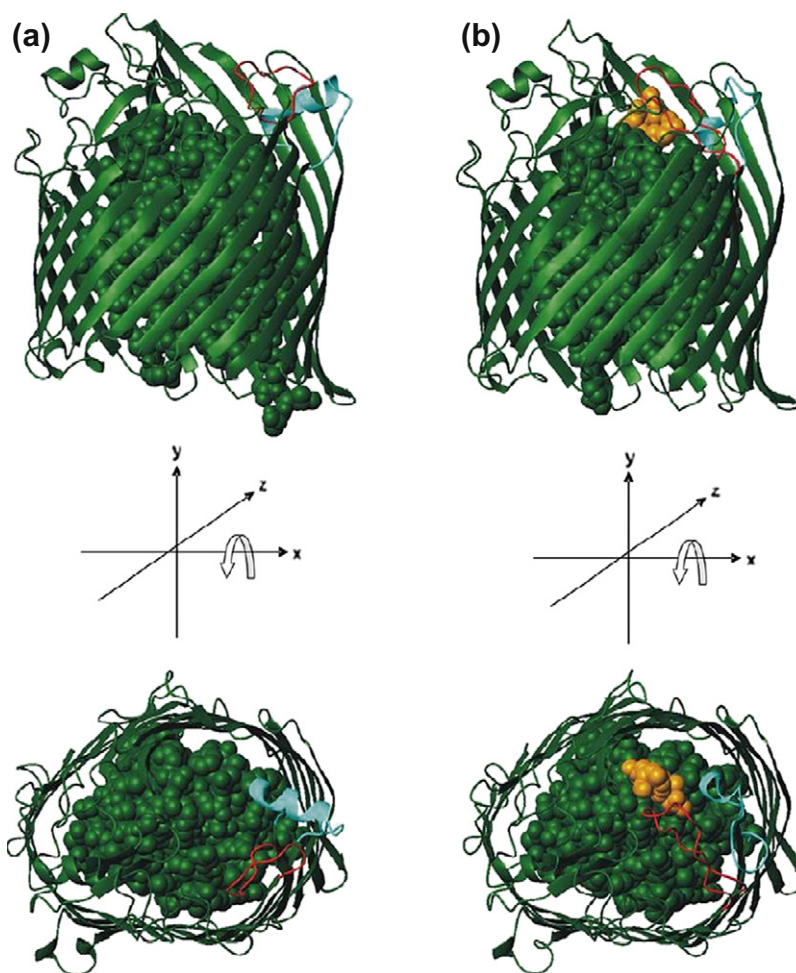


FIGURE 7.7 Ribbon representations of the crystal structures of (a) ligand-free and (b) FecA bound to ferric citrate. The 22- β strand barrel is depicted in ribbon format and the N-terminal cork domain is in space-filling format. The binding of ferric citrate (coloured orange) induces a conformational change in the extracellular loops L7 (cyan) and L8 (red) such that the solvent accessibility of ferric citrate is reduced. (From Krewulak & Vogel, 2008. Reproduced with permission from Elsevier.)

change in two extracellular loops, reducing the accessibility of ferric citrate. In order for the ferric siderophore to move into the periplasmic space, the cork has to be at least partially displaced from the interior of the beta-barrel. However, the outer membrane has neither an established ion gradient nor a source of ATP to provide energy for this process. The energy is provided by the TonB protein,⁷ together with the ExbB and ExbD proteins which are anchored in the cytoplasmic membrane. In a still not well-understood manner, they harvest the energy of the proton motive force of the cytoplasmic membrane. We know that the highly conserved C-terminal region of TonB interacts directly with the OMT, as is illustrated in Fig. 7.8 for the ferric enterobactin OMT, FepA.

Once the Fe^{3+} -siderophore, haem, or Fe^{3+} have been delivered into the periplasm by the OMTs and TonB, they are transported by periplasmic-binding proteins across the periplasmic space. We already mentioned that the

7. So called because, together with the Ton A protein (now designated FhuA), they were originally identified as two membrane proteins required for uptake and internalization of the T1 bacteriophage (yet another ironic twist of iron biology).

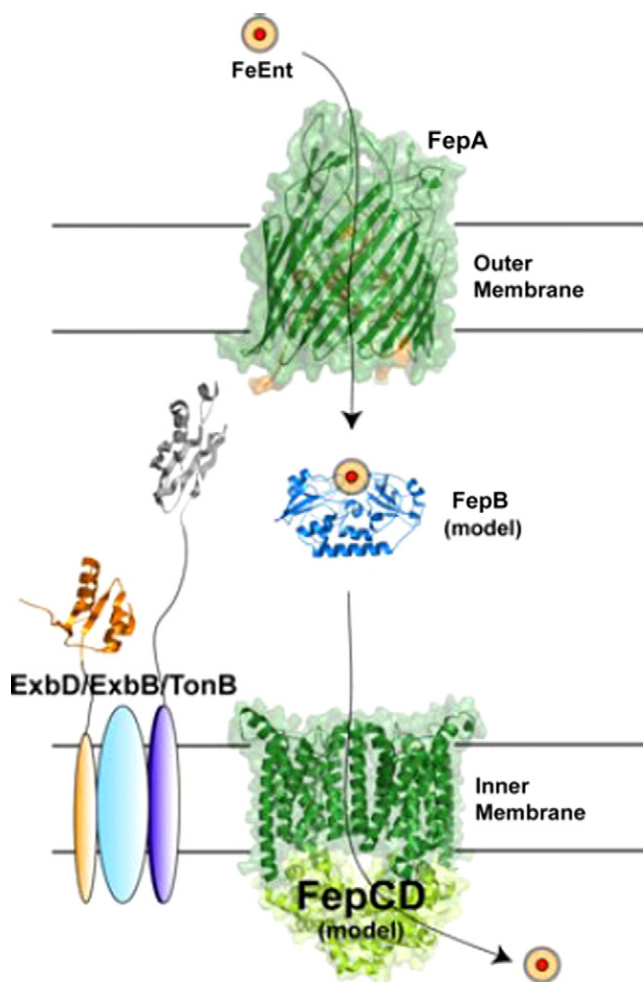


FIGURE 7.8 A representation of the siderophore uptake pathway in *E. coli* using ferric-enterobactin (FeEnt) transport as an example (see text for details). (From *Chu et al., 2010*. Reproduced with permission from Springer.)

bacterial Fe^{3+} -PBPs are members of the transferrin superfamily, as indeed are the periplasmic proteins involved in the transport of amino acids or phosphate, for example (Chapter 4). However, the siderophore PBPs belong to an entirely different and unique class of PBPs, with the two lobes of the protein organised in a quite different manner, as illustrated in Fig. 7.8 for the ferric enterobactin PMP, FepB. The siderophore-bound PBP then docks into the periplasmic face of their corresponding ABC transporter in the plasma membrane, which releases them into the cytoplasm at the expense of ATP hydrolysis. In microorganisms which are at least partial aerobes, under anoxic or reducing conditions, Fe^{2+} diffuses freely through the porins of the outer membrane and is transported by a system which is different from the Fe^{3+} transport systems.

Transport systems for iron from siderophores, haem, or transferrin in Gram-positive bacteria, which lack an outer membrane, closely resemble the ABC transport systems found in the inner membrane of Gram-negative bacteria. Iron uptake involves a membrane-anchored binding protein, which resembles the PBP of Gram-negative organisms, and a membrane-associated ABC transporter (Fig. 7.9).

In the cytosol, iron must be released from its siderophore or from haem. Since the coordination chemistry of siderophores, with their preponderance of hard oxygen ligands, is designed to complex Fe^{3+} , one might

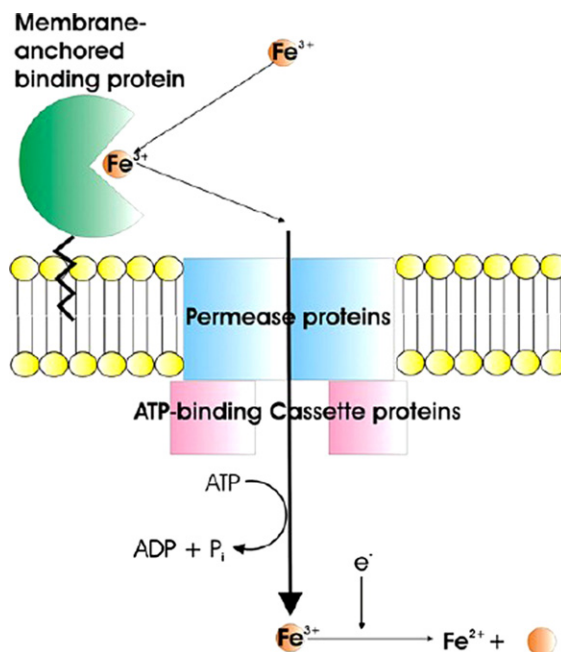


FIGURE 7.9 Schematic representation of iron uptake in Gram-positive bacteria, which unlike Gram-negative bacteria, lack an outer membrane. Therefore, the uptake of iron from haem, siderophore, or transferrin involves a membrane-anchored binding protein and a membrane-associated ABC transporter. (From Krewulak & Vogel, 2008. Reproduced with permission from Elsevier.)

reasonably assume that reduction of the Fe^{3+} to Fe^{2+} would represent a logical mechanism for iron release in the cytosol. The reduction of Fe^{3+} would decrease the binding constant substantially, resulting in a weak Fe^{2+} -chelate complex from which Fe^{2+} can dissociate relatively easily. A number of enzymes with ferric reductase activity have been identified in bacteria, but none appear to be specific for individual ferric siderophores, and it seems that the ferrireductases are in reality flavin reductases. The reduced flavins are generated by electrons supplied by NAD(P)H, presumably because the redox potential of the NAD(P)⁺/NAD(P)H couple is not able to reduce the ferric chelates directly. In the case of Fe^{3+} -enterobactin, an esterase, encoded by the *fes* gene, localised within the operon for enterobactin biosynthesis and uptake, is required for iron release. Whether the esterase is itself a ferric reductase remains unclear.

For pathogenic bacteria which can utilise haem as a source of iron, cytosolic iron release is carried out by a bacterial haem oxygenase, the enzyme involved in haem catabolism in many different organisms.

2. Copper and Zinc

Because of their importance in many enzymes, bacteria have had to develop uptake systems for both copper and zinc. Copper uptake (and homeostasis, which is discussed in Chapter 8) has been extensively studied in the Gram-positive bacteria *Enterococcus hirae*. At the membrane, a reductase, indicated as R in Fig. 7.10, reduces Cu^{2+} to Cu^{+} which is taken up by CopA when copper is limiting. In contrast, when copper is in excess, CopB extrudes excess copper. Both CopA and CopB belong to the P1 subclass of P-type ATPases, which includes the proteins involved in the disorders of copper metabolism in humans, Menkes's, and Wilson's disease (discussed in Chapter 14).

Methanotrophs are Gram-negative bacteria which utilise methane as their sole source of carbon and energy. They play an important role in controlling emissions of CH_4 , the second most important greenhouse gas after CO_2 . Almost all methanotrophs use a copper-dependent methane monooxygenase in the first step of carbon

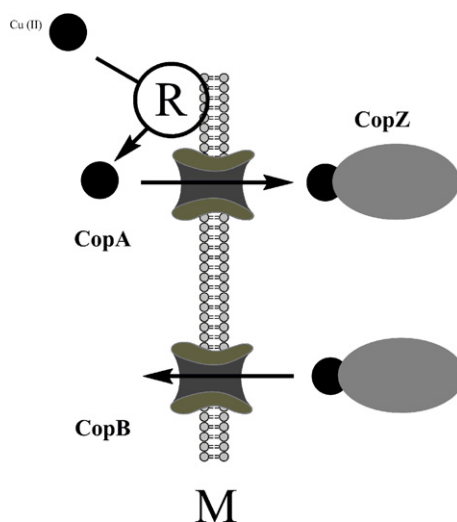


FIGURE 7.10 Copper uptake in *E. hirae*.

assimilation, converting methane to methanol. In order to meet their very high requirement for copper, they synthesise and release a high-affinity copper-binding compound, called methanobactin. The crystal structure of methanobactin has been determined, and is given in Fig. 7.11 together with a schematic representation, which underlines its oligopeptide character, reminiscent of many siderophores. While it is not yet established how Cu-methanobactin is internalised by methanotrophs, by analogy with ferric siderophores, it is likely that a TonB-dependent pathway similar to that described above, is involved. This type of uptake mechanism is utilised for the uptake of Co-containing cobalamine, as we saw, and in *Helicobacter pylori*⁸ a similar TonB-dependent system is involved in Ni uptake.

Likewise, for zinc, bacteria have developed active uptake systems. In many bacteria, the high-affinity Zn^{2+} uptake system uses an ABC transporter of the cluster 9 family, which mostly transports zinc and manganese, and is found in nearly all bacterial species. First identified in cyanobacteria and pathogenic streptococci, but also found in *E. coli*, the system is encoded by three genes *znuABC* and consists of a substrate-binding protein (SBP) (in Gram-negative organisms this corresponds to a periplasmic-binding protein or PBP) ZnuA, a membrane permease ZnuB, and an ATPase ZnuC. While the crystal structures of several SBPs have been determined, it is still not clear how these proteins discriminate between zinc and manganese binding. Low-affinity transporters of the ZIP family, described later in this chapter, such as ZupT, have also been shown to be involved in bacterial zinc uptake.

METAL ASSIMILATION IN FUNGI AND PLANTS

1. Iron

We have taken the liberty of assimilating fungi with plants not because we think they are more like vegetables than animals, but because many recent exciting findings on transition metal uptake in yeast have important implications for what is going on in higher eukaryotes such as plants and animals. The budding yeasts of the genus *Saccharomyces* are used as extremely attractive, simple-model organisms for the study of eukaryotic cell biology. *Saccharomyces cerevisiae*, used commercially in bread making and the production of alcoholic beverages and of industrial alcohol, continues to serve as the paradigm for studies of fungal iron metabolism. This is easily

8. The bacteria responsible for many gastric ulcers.

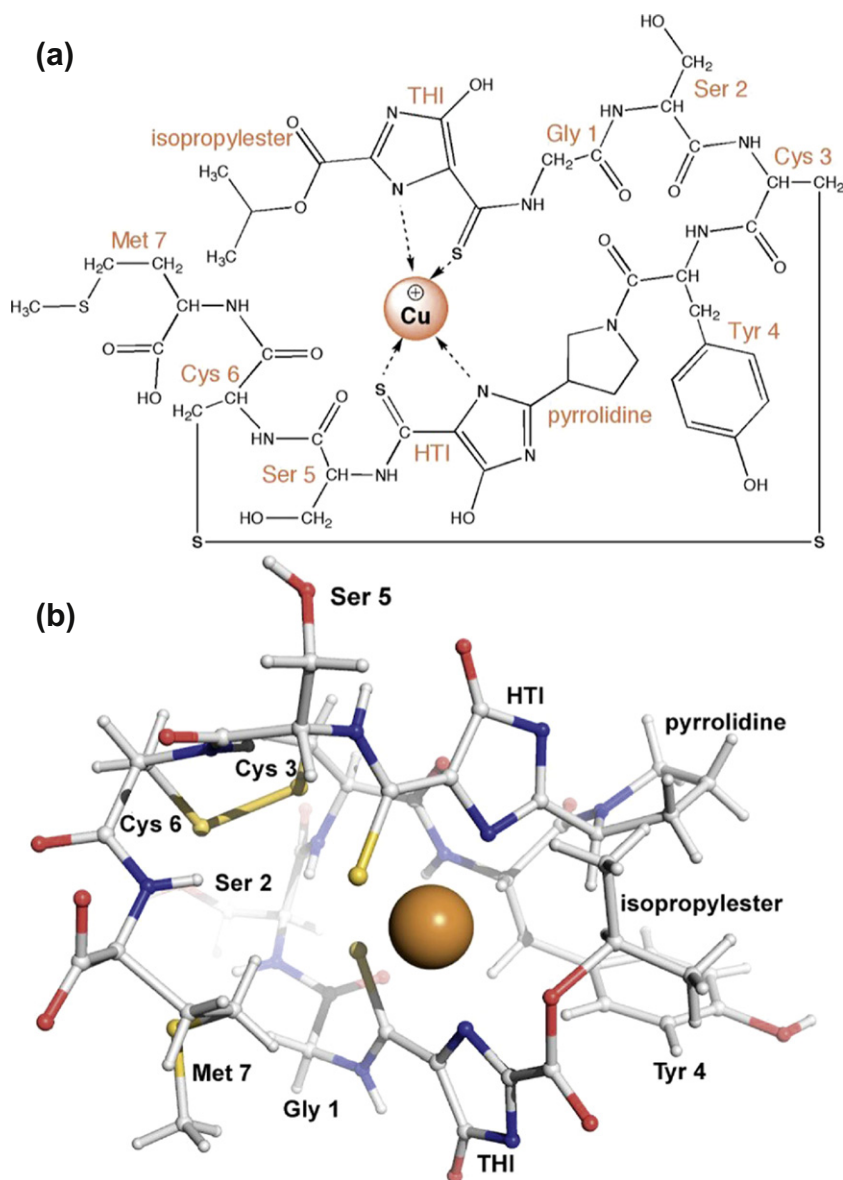


FIGURE 7.11 Structure of Cu-methanobactin from *M. trichosporium*. (a) Schematic diagram. (b) Ball-and-stick representation of crystal structure. The copper ion is shown as a brown sphere. (From Balasubramanian & Rosenzweig, 2008. Copyright 2008, American Chemical Society.)

explained — short generation time and ease of production of large amounts of biomass relatively inexpensively on defined media, not to mention the fact that it was the first complete eukaryote genome to be sequenced. Its genome is small (6,043 genes), and unlike mammals, and it is comparatively easy to inactivate specific yeast genes. And finally, it turns out that not only do many of the mechanisms involved in iron uptake and metabolism in higher eukaryotes have homologous systems in yeast, but that many of the genes involved in iron acquisition in yeast have homologous genes in higher eukaryotes which are frequently able to rescue yeast mutants defective in iron acquisition and metabolism.

Figure 7.12 summarises the iron uptake systems of *Saccharomyces cerevisiae*. There are essentially three mechanisms involved, which are described in detail below. In two of these, after reduction to Fe^{2+} at the plasma

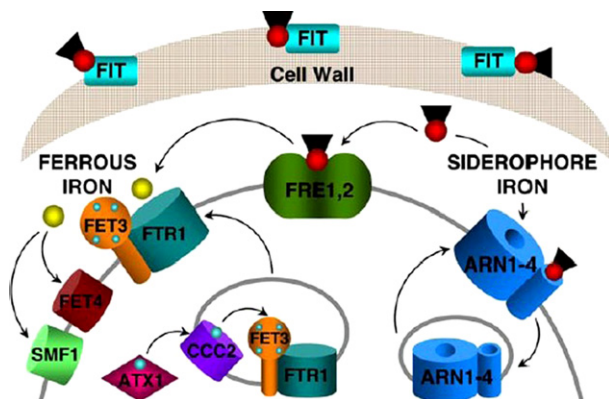


FIGURE 7.12 Iron uptake systems of *S. cerevisiae*. The FIT mannoproteins of the cell wall facilitate retention of siderophore–iron in the cell wall, but are not required for siderophore uptake. Many siderophores likely cross the cell wall through non-specific pores. Siderophore-bound iron can be reduced and released from the siderophore by the FRE reductases. Ferric iron salts and low-affinity chelates are also reduced by the FRE reductases prior to uptake. Reduced iron can then be taken up through either the high-affinity ferrous iron transporter (the FET3 and FTR1 complex) or through low-affinity transporters (FET4 and SMF1). FET3 acquires copper intracellularly through the activities of the copper chaperone ATX1 and the copper transporter CCC2. Intact siderophore–iron chelates can be taken up via members of the ARN transporter family. The ARN transporter binds the ferric siderophore, and the transporter–siderophore complex undergoes endocytosis prior to translocation of the ferric siderophore chelate across the membrane. (From Philpott, 2006. Copyright 2006, with permission from Elsevier.)

membrane, iron is taken up by one of two possible mechanisms, a high-affinity pathway involving re-oxidation of the Fe^{2+} (the ferroxidase pathway), or a low-affinity pathway, involving direct transport of Fe^{2+} . In addition, non-reductive transport systems able to directly mediate uptake of iron from iron-siderophore complexes, either secreted by the fungi themselves, or produced by other organisms in their environment, can come into play. These different systems operate under different conditions of environmental and growth requirements.

The plasma membrane of yeast is surrounded by a porous cell wall that protects the cell from osmotic lysis and excludes larger macromolecules. Before iron can be taken up across the plasma membrane, it must cross the cell wall, a dynamic structure, made up of a lattice of glucans and chitin, and an outer layer of mannoproteins. In *S. cerevisiae*, iron depletion induces very high levels of expression of a family of mannoproteins, Fit1p, Fit2p, and Fit3p (*Facilitator of iron transport*), which enhances iron uptake from ferric siderophores. They may facilitate retention of siderophore ferric siderophores in the cell wall, but they are not required for siderophore access. The cell wall is also important in the uptake of haem by pathogenic fungi, like *Candida albicans*.⁹ It is likely that many siderophores cross the cell wall through non-specific pores.

Most fungi produce (or at least encode in their genomes) one or more integral membrane reductases, which are usually relatively unspecific for the metal ion reduced. In *S. cerevisiae*, the most abundant of these FRE1 exhibits comparable activity with Fe^{3+} and Cu^{2+} and can use a variety of one-electron acceptors. This membrane-spanning haem protein is homologous to the gp91(PHOX) protein of the NADPH oxidase complex of human phagocytic cells. FRE1 is therefore thought to be a transmembrane flavocytochrome b_{558} electron transfer protein, with NADPH- and FAD-binding domains at its cytosolic face, and a pair of intramembrane haemes which transfer electrons one at a time to Fe^{3+} at the external surface of the cell. *S. cerevisiae* has a second reductase, FRE2 which also seems to be involved in reduction of both Cu^{2+} and Fe^{3+} .

9. Responsible for a large number of oral and vaginal mucosal infections, as well as systemic infections, particularly when cellular immunity is compromised.

The high-affinity pathway involves oxidation of Fe^{2+} to Fe^{3+} by the ferroxidase FET3 and subsequent transport of Fe^{3+} across the plasma membrane by the permease FTR1. FET3p is a member of the family of multicopper oxidases, which include ascorbate oxidase, laccase, and ceruloplasmin (see Chapter 14), and does not become functional until it is loaded with copper intracellularly through the activities of the copper chaperone ATX1p and the copper transporter CCC2p. It appears that Fe^{3+} produced by FET3 is transferred directly to FTR1, and does not equilibrate with the bulk phase, as is illustrated in Fig. 7.13. This is almost certainly achieved by the classic metabolite-channeling¹⁰ mechanism, a common feature of multifunctional enzymes.

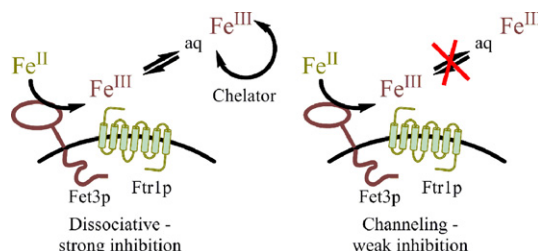


FIGURE 7.13 Cartoon representing the effect of iron chelators in dissociative and channeling models of transfer of Fe(III) from Fet3p to Ftr1p. (Adapted from Kwok *et al.*, 2006.)

In the low-affinity pathway, Fe^{2+} is transported directly into the cell through divalent metal ion transporters, which like the reductases are not specific to Fe^{2+} but can also transport Mn^{2+} , Ni^{2+} , and Cu^{2+} . One such family of transporters in *S. cerevisiae*, the Smf1 proteins are orthologues of the DCT1 (or Nramp2) divalent cation transporters found in mammalian cells (see below). Transport of Fe^{2+} by both Smf1 and DCT1 is coupled to the transport of H^+ , with a stoichiometry of one H^+ for one Fe^{2+} . Another ferrous iron transporter, characterised in *S. cerevisiae* but not in other fungi, is the Fet4 protein, which like the Smf proteins has a low-substrate specificity, and though of low affinity probably represents the principal iron uptake pathway for baker's yeast at high iron levels in the culture medium.

In common with most prokaryotes, many fungi have siderophore-dependent iron uptake systems. The ferri-chrome-type siderophores are often employed, although other types of siderophore are also used. Indeed, even if, like the quintessential scavenger baker's yeast (*Saccharomyces cerevisiae*), they produce no siderophores of their own, they nonetheless have several distinct facilitators for the uptake of ferric siderophores, including ferric enterobactin, which is produced by many bacteria, but not by fungi.

Just as the number of fungal genome sequences continues to grow, so progress in genome sequencing of plants has advanced rapidly. After the initial success of the determination of the complete genome of *Arabidopsis thaliana*, the publication of the second fully sequenced and annotated plant genome, that of rice, constitutes a major scientific achievement. The complete sequence of the first of the large cereal genomes, maize, has now been completed together with those of soybean, sorghum, and wine grapes, to mention a few. They will shortly be joined by those of barley and wheat, together with the mainstay of classical plant science, the tomato as well as potato. This should allow the identification of candidate genes which might play a role in iron uptake, transport, and regulation of iron homeostasis by analogy with fungal and mammalian systems, and allow us to unravel in greater detail the complexities of plant genome organisation and diversity.

Iron is important in plants not only because of its role in fundamental processes such as photosynthesis, respiration, nitrogen fixation, and DNA synthesis, but also because of its involvement in key enzymes of plant hormone synthesis, such as lipoxygenases and ethylene-forming enzymes. Despite the fact that iron represents 4–5% of the total solid mineral composition of soils, it is generally present in soils in a poorly soluble form, and

10. The process of direct transfer of an intermediate between the active sites of two enzymes that catalyse sequential reactions in a biosynthetic pathway.

its bioavailability is further decreased at the neutral and alkaline pH values found in semi-arid, calcareous (calcium carbonate-rich) soils.

Plant iron uptake can be divided into two distinct families, with quite distinct strategies. **Strategy I** plants reduce Fe^{2+} to Fe^{3+} outside of the roots, and then take up the Fe^{2+} . In contrast, **Strategy II** plants solubilise Fe^{3+} by excreting Fe^{3+} phytosiderophores, which are taken up by specific transporters and the iron is then reduced to Fe^{2+} in the symplasm of the root cell (Fig. 7.14). In **Strategy I** plants, (dicotyledons such as *Arabidopsis*,¹¹ pea,

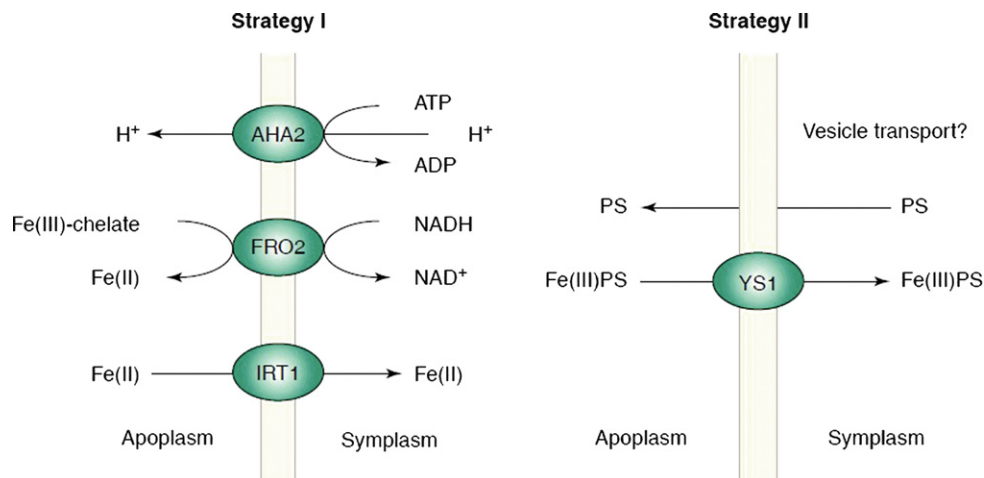


FIGURE 7.14 Mechanisms of iron uptake by higher plants. In strategy I plants (e.g., *Arabidopsis*, pea and tomato), Fe(III) chelates are reduced before the Fe(II) ion is transported across the plasma membrane. Strategy II plants (e.g., barley, maize, and rice) release siderophores capable of solubilising external Fe(III) and then transport the Fe(III) siderophore complex into the cell. AHA2 is a P-type H^+ -ATPase, FRO2 is the Fe(III) chelate reductase, IRT1 is a Fe(II) transporter, and YS1 is the transporter of the phytosiderophore (PS)–Fe complex. (Adapted from Schmidt, 2003. Copyright 2003, with permission from Elsevier.)

and tomato), iron mobilization is achieved by the combined action of a proton-extruding H^+ -ATPase, AHA, and a ferric chelate reductase, FRO2, both of which are induced by iron deficiency. An iron transporter of the ZIP family, named IRT1, seems to be the principal transporter of ferrous iron in *Arabidopsis*, and orthologues of IRT1 have also been characterised in tomato and rice.

In **Strategy II** plants, monocotyledon grasses, which include barley, maize, and rice, high-affinity Fe(III) chelators (phytosiderophores, PS) are synthesised by the plants themselves and excreted into the environment around their roots in order to complex and solubilise the ferric iron in the soil. Transporters specific for the Fe(III)-siderophore complex then take the complex into the cytosol, where the iron is released from the phytosiderophore by an as-yet-undefined mechanism. The best characterised of these transporters is YS1 (yellow stripe 1) or YSL1 (yellow stripe-like), so named after the phenotypic appearance of a maize mutant deficient in phytosiderophore uptake. However, unlike the bacterial or fungal siderophores, phytosiderophores (Fig. 7.15) of the mugeneic acid family are synthesised from L-methionine via nicotianamine. Whereas the Strategy II grasses produce and excrete the mugeneic acid family of siderophores, nicotianamine is found in both Strategy I and Strategy II plants, where there is much evidence that it is involved in the intercellular transport of iron as the Fe-nicotianamine chelate.

However, evidence has begun to accumulate that grasses can also take up iron as Fe^{2+} . It is established that the Fe^{2+} transporter IRT1 is upregulated in iron-deficient rice, and that rice can still take up Fe^{2+} even when the synthesis of nicotianamine, the precursor of phytosiderophores, is compromised. Now, it has been shown that introducing

11. Thale cress, a small flowering plant, member of the brassica family which includes mustard and cabbage, and is a model organism for studying plant biology.

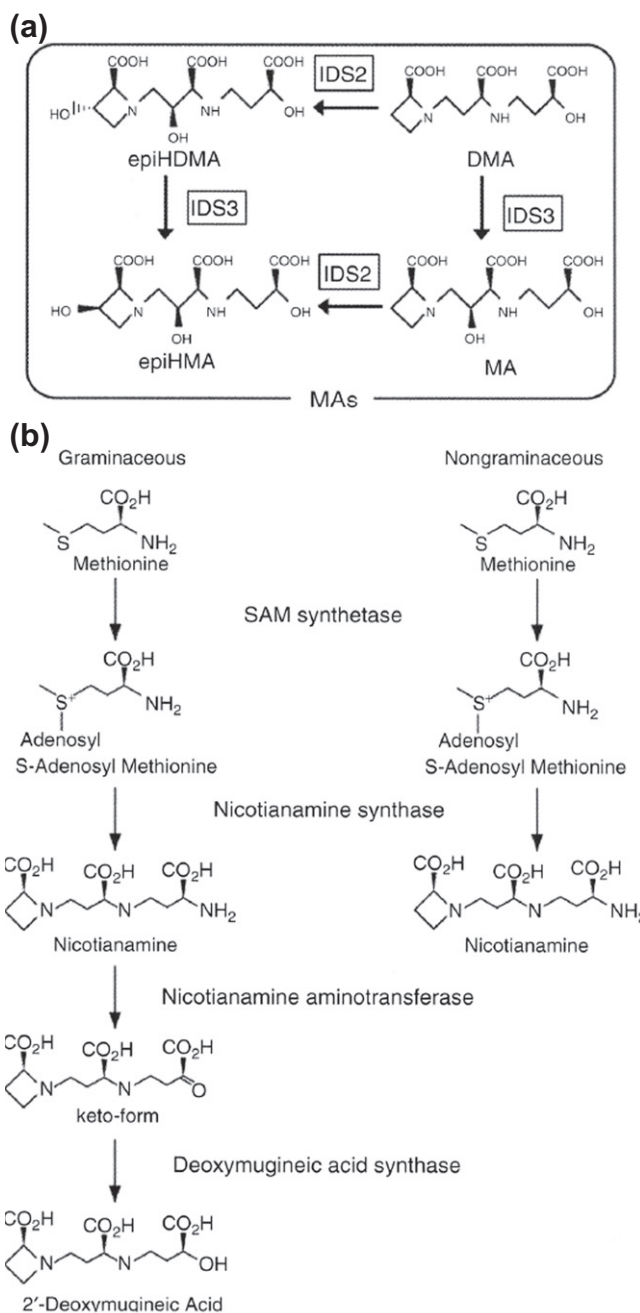


FIGURE 7.15 (a) Outline of biosynthesis of nicotianamine in graminaceous and non-graminaceous plants and its conversion to deoxymugineic acid (DMA) in graminaceous plants. (b) Conversion of DMA to other phytosiderophores.

a ferric chelate reductase gene from yeast, which had been selected for enhanced activity at alkaline pH into rice, increases the yield by 8-fold when the transgenic plants are grown in calcareous soils (Guerinot, 2007). When we consider that one-third of the world's soils are alkaline, these results could have a major impact on rice production.

2. Copper and Zinc

Genetic studies in the yeast *S. cerevisiae* identified two proteins involved in high-affinity copper uptake at the plasma membrane, CTR1 and CTR3. After reduction of Cu^{2+} by the same reductases, FRE1 and FRE3 described above for iron, these proteins transport Cu^+ . In yeast a third member of the CTR family, CTR2 localises to the vacuole and is proposed to mobilise copper stored in the vacuolar compartment to the cytoplasm when extracellular copper is limited. There is also a low affinity copper uptake system through FET4 and SMF1 permeases.

Zinc uptake in fungi is carried out to a large extent by the ZIP (Zrt-, Irt-like Protein) family of metal ion transporters. The family name comes from the yeast Zrt1 protein and the *Arabidopsis thaliana* Irt1 protein. These were the first identified members of a family of Zn transporters, which are found at all phylogenetic levels, including bacteria, fungi, plants, and mammals. The mammalian members of the family are given the systematic designation “SLC39” (Eide, 2004). Without any known exception, the members of the ZIP family transport zinc and/or other metal ions from the extracellular space, or from the lumen of cellular organelles, into the cytoplasm. This, together with their transmembrane topography, distinguishes them from the CDF (cation diffusion facilitator)/Znt family: the mammalian members of the family have been named Znt and given the systematic designation “SLC30” (Palmiter & Huang, 2004). As we will see when we consider zinc homeostasis in Chapter 8, this family transports zinc from the cytoplasm into the lumen of extracellular organelles or to the outside of the cell. Thus, CDF proteins work in the opposite direction to ZIP proteins.

Most ZIP proteins have eight predicted transmembrane domains (Fig. 7.16) and similar predicted topologies with both the N- and C-termini located on the extracytoplasmic face of the membrane with a His-rich domain

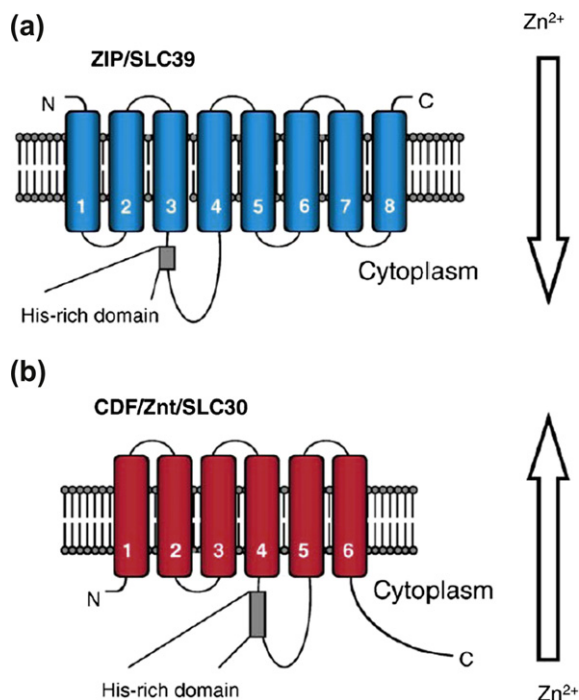


FIGURE 7.16 Predicted membrane topologies for the ZIP/SLC39 and CDF/Znt/SLC30 families of metal ion transporters (a) ZIP/SLC39 (b) CDF/Znt/SLC30. (From Eide, 2006. Copyright 2006 with permission from Elsevier.)

frequently in the long cytoplasmic loop between transmembrane domains 3 and 4. In contrast, most CDF transporters have six predicted transmembrane domains, a His-rich domain in the loop between domains 4 and 5; but here the N- and C-termini are on the cytoplasmic side of the membrane.

In the yeast *S. cerevisiae*, at least four different transporters are involved in zinc uptake. The most important of these is the ZIP family member ZRT1, which is required for growth under low zinc concentrations. ZRT1 has a high affinity for zinc with an apparent K_m for free Zn^{2+} of 10 nM. A second ZIP protein, ZRT2, with a lower affinity for zinc (apparent $K_m \sim 100$ nM) probably plays a role under less severe zinc limitation. In addition to the two ZIP proteins, two other lower affinity systems also operate. One is the FET4 protein, which we saw earlier is also involved in the low affinity uptake of iron and copper.

In dicotyledon plants, like *Arabidopsis*, acidification of the soil would result in an increase in the solubility of both zinc and copper. Cu is taken up by the Cu^+ transporter COPT1, the *Arabidopsis* orthologue of the yeast copper transporter CTR1 and is probably reduced by FRO2, which is also responsible for iron reduction. Zn is most likely taken up by members of the ZIP family, some of which are root specific, while others are found in both roots and shoots.

In monocotyledon plants, there is no suggested role for phytosiderophores in Cu uptake, and as in dicotyledons, it is probably taken up as Cu^+ by COPT1. In addition, plants of this group may also take up Cu as Cu^{2+} via a member of the ZIP family. ZIP2 and ZIP4 are upregulated by Cu deficiency. In contrast, there is good evidence for the involvement of mugeneic acids in absorbing Zn from the soil.

METAL ASSIMILATION IN MAMMALS

Since in mammals, metals need first to be assimilated from dietary sources in the intestinal tract and subsequently transported to the cells of the different organs of the body through the bloodstream, we will restrict ourselves in this section to the transport of metal ions across the enterocytes of the upper part of the small intestine (essentially the duodenum), where essentially all of the uptake of dietary constituents, whether they be metal ions, carbohydrates, fats, amino acids, vitamins, etc., takes place. We will then briefly review the mechanisms by which metal ions are transported across the plasma membrane of mammalian cells and enter the cytoplasm, as we did for bacteria, fungi, and plants. The specific molecules involved in extracellular metal ion transport in the circulation will be dealt with in Chapter 8.

1. Iron

Within the intestinal tract of mammals, dietary iron is essentially in two forms, haem iron and non-haem, ferric, iron. Haem iron is generally more readily absorbed than non-haem iron, reflecting no doubt the origins of many mammals (including man) as hunters. Non-haem iron from sources such as vegetables, tend to be a poor source of iron, because of the presence of phosphates, phytates, and polyphenols, which form stable, insoluble ferric complexes and decrease absorption. Haem iron is taken up by an as yet elusive specific transporter, and Fe^{2+} is then released into the intracellular iron pool by haem oxygenase, which degrades haem to Fe^{2+} , porphobilinogen, and CO (Fig. 7.17). Non-haem dietary iron is taken up in a manner reminiscent of the low affinity iron uptake pathway in yeast. Fe(III) is reduced to Fe(II) by a ferric reductase (Dcytb) at the apical membrane and the Fe(II) is transported into the intestinal cell by DMT1, a proton-coupled divalent cation transporter. Within the intestinal cell, iron enters a low-molecular-weight pool: some of it may be stored in ferritin, while some of it can cross to the basolateral membrane. There it can be transferred to the circulation by a transmembrane transporter protein, ferroportin. In the circulation, serum iron is transported as diferric-transferrin (Tf), described below and in Chapter 8. It has been suggested that iron incorporation into apotransferrin might be facilitated by the oxidation of Fe^{2+} to Fe^{3+} . Two candidates for this ferroxidase activity have been proposed (Fig. 7.17) — ceruloplasmin (CP), the principal copper-containing protein of serum, or hephaestin, a member of the family of multicopper oxidases (which includes ceruloplasmin), which appears to be bound to the basolateral membrane.

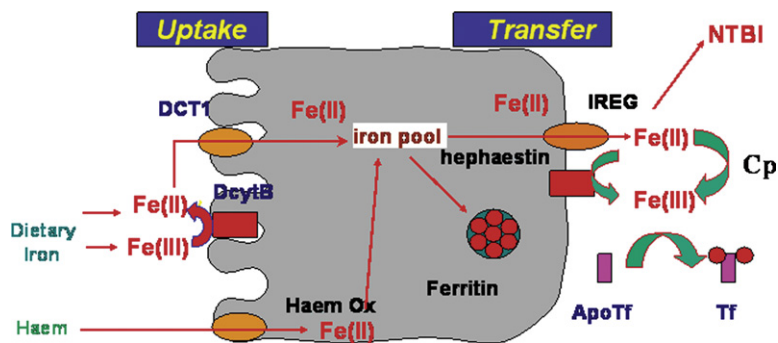


FIGURE 7.17 Schematic representation of iron absorption in normal subjects. Iron is taken up from the gastrointestinal tract either as haem or non-haem iron. The former is degraded to release Fe(II) by haem oxygenase, whereas the latter is reduced by DcytB and transported across the apical membrane by DCT-1. Within the enterocyte, the iron pool can equilibrate with the intracellular storage protein ferritin. At the basolateral membrane, iron is transported out of the cell by IREG-1; its incorporation into apotransferrin may be aided by the ferroxidase activity of hephaestin. DcytB, Duodenal cytochrome b; DCT1, divalent cation transporter protein 1; IREG-1, iron-regulated transporter-1; Haem ox, haem oxygenase; Cp, ceruloplasmin; Tf, transferrin; NTBI, non-transferrin-bound iron.

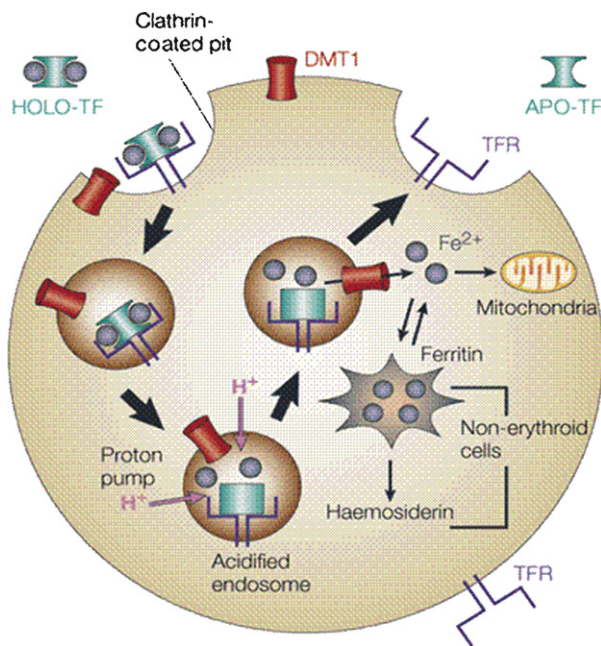


FIGURE 7.18 The transferrin to cell cycle. HOLO-TF diferric transferrin; TFR, transferrin receptor; DMT1, divalent metal transporter.

Serum iron is delivered to cells via the transferrin to cell cycle (Fig. 7.18). The diferric-transferrin molecule binds to its receptor and the complex is invaginated into clathrin-coated pits, which fuse with the target membranes of endosomes delivering the vesicle contents into the interior of the endosome. The pH of the endosome is reduced to around 5–6 by the action of an ATP-dependent proton pump, and at this pH iron is released from transferrin bound to its receptor as Fe^{3+} , presumably by protonation of the bound carbonate. The divalent cation (metal) transporter DMT1 is thought to assure the transport of iron out of the endosome into the cytoplasm, presumably after reduction of Fe^{3+} to Fe^{2+} . The cytoplasmic iron can then be transferred to the mitochondria for use in haem and iron–sulfur cluster synthesis, or stored in ferritin (Chapter 8). Unlike most other protein ligands taken up by

receptor-mediated endocytosis, apotransferrin retains a high affinity for its receptor at acidic pH values, and is recycled back to the plasma membrane, where it dissociates from its receptor and goes off into the circulation in search of further iron. This sequence of events constitutes the transferrin to cell cycle, which ensures iron uptake by cells that have transferrin receptors.

2. Copper and zinc

Copper uptake across the gastrointestinal tract is poorly understood — most probably utilising the divalent cation transporter DMT1. At the cellular level, Cu is imported across the plasma membrane of mammalian cells as Cu^+ , by members of the CTR family. The CTR family of proteins have been found in yeast and plants, as we saw, but also in humans and other mammals. They contain several methionine-rich motifs at their N-terminus, and conserved cysteine and histidine residues at their C-terminus. Unusually, CTR proteins can mediate the uptake of platinum anticancer drugs into mammalian cells (see Chapter 22).

The ZIP family are involved in Zn transport into the cytosol, mostly across the plasma membrane. Although the human genome encodes 14 ZIP-related proteins, ZIP4 appears to mediate Zn uptake. It's involvement in dietary Zn uptake into intestinal enterocytes is well established, and mutations in ZIP4 have been found in patients with acrodermatitis enteropathica, a recessive disorder of Zn absorption which results in Zn deficiency. DMT1 is probably also involved in the transport of dietary zinc across the brush border membrane of the intestine.

REFERENCES

- Balasubramanian, R., & Rosenzweig, A. C. (2008). Copper methanobactin: a molecule whose time has come. *Current Opinion in Chemical Biology*, 12, 245–249.
- Chu, B. C., Garcia-Herrero, A., Johanson, T. H., Krewulak, K. D., Lau, C. K., Peacock, R. S., et al. (2010). Siderophore uptake in bacteria and the battle for iron with the host; a bird's eye view. *Biometals*, 23, 601–611.
- Cobine, P. A., Pierrel, F., & Winge, D. R. (2006). Copper trafficking to the mitochondrion and assembly of copper metalloenzymes. *Biochimica et Biophysica Acta*, 1763, 759–772.
- Crichton, R. R. (2009). *Inorganic biochemistry of iron metabolism: from molecular mechanisms to clinical consequences* (3rd ed.). Chichester: John Wiley and Sons. pp 461.
- Eide, D. J. (2004). The SLC39 family of metal ion transporters. *Pflügers Archiv — European Journal of Physiology*, 447, 796–800.
- Eide, D. J. (2006). Zinc transporters and the cellular trafficking of zinc. *Biochimica et Biophysica Acta*, 1763, 711–722.
- Guerinot, M. L. (2007). It's elementary: enhancing Fe^{3+} reduction improves rice yields. *Proceedings of the National Academy of Sciences USA*, 104, 7311–7312.
- Hantke, K. (2001). Bacterial zinc transporters and regulators. *Biometals*, 14, 139–249.
- Kosman, D. J. (2003). Molecular mechanisms of iron uptake in fungi. *Molecular Microbiology*, 47, 1185–1197.
- Krewulak, K. D., & Vogel, H. J. (2008). Structural biology of bacterial iron uptake. *Biochimica et Biophysica Acta*, 1778, 1781–1804.
- Kwok, E. Y., Severance, S., & Kosman, D. J. (2006). Evidence for iron channeling in the Fet3p-Ftr1p high-affinity iron uptake complex in the yeast plasma membrane. *Biochemistry*, 45, 6317–6327.
- Martin, J. H., & Fitzwater, S. E. (1988). Iron deficiency limits phytoplankton growth in the north-east Pacific subarctic. *Nature*, 331, 341–343.
- Palmer, C. M., & Guerinot, M. (2009). Facing the challenges of Cu, Fe and Zn homeostasis in plants. *Nature Chemical Biology*, 5, 333–340.
- Palmiter, R. D., & Huang, L. (2004). Efflux and compartmentalisation of zinc by members of the SLC30 family of solute carriers. *Pflüger's Arch.*, 447, 744–751.
- Petrus, M. J. (2004). The SLC31 (Ctr) copper transporter family. *Pflügers Archiv — European Journal of Physiology*, 447, 796–800.
- Philpott, C. C. (2006). Iron uptake in fungi: a system for every source. *Biochimica et Biophysica Acta*, 1763, 636–645.
- Schmidt, W. (2003). Iron solutions: acquisition strategies and signalling pathways in plants. *Trends in Plant Science*, 8, 188–193.
- Shi, D., Xu, Y., Hopkinson, B. M., & Morel, F. M. M. (2010). Effect of ocean acidification on iron availability to marine phytoplankton. *Science*, 327, 676–679.
- Shi, L., Squier, T. C., Zachara, J. M., & Fredrickson, J. K. (2007). Respiration of metal (hydr)oxides by *Shewanella* and *Geobacter*: a key role for multihaem c-type cytochromes. *Molecular Microbiology*, 65, 12–20.
- Solioz, M., & Stoyanov, J. V. (2003). Copper homeostasis in *Enterococcus hirae*. *FEMS Microbiology Reviews*, 27, 183–195.
- Vraspir, J. M., & Butler, A. (2009). Chemistry of marine ligands and siderophores. *Annual Review of Marine Science*, 1, 43–63.

This page intentionally left blank

Transport, Storage, and Homeostasis of Metal Ions

Introduction	155
Metal Storage and Homeostasis in Bacteria	155
Metal Transport, Storage, and Homeostasis in Plants and Fungi	161
Metal Transport, Storage, and Homeostasis in Mammals	170

INTRODUCTION

As in Chapter 7, we consider successively the transport, storage, and metal ion homeostasis of iron, copper, and zinc in bacteria, fungi and plants, and in animals. Since the assimilation of metals in unicellular bacteria and eukaryotes like yeast does not require their transport to other cell types, we confine our discussion only to storage and homeostasis. However, for plants and mammals, we consider transport of metals which have been assimilated from the soil by the roots and from the intestinal tract from ingested foodstuff to other cell types in the organism. The storage proteins ferritin and metallothionein are widely distributed in bacteria, plants, and animals, although ferritin appears to be absent from yeast. Whereas homeostatic mechanisms often operate at the level of transcription in prokaryotes and unicellular eukaryotes, cellular iron homeostasis operates at the level of translation of stable mRNAs (for further details see [Boal & Rosenzweig, 2009](#); [Crichton, 2009](#); [Eide, 2006](#); [Sutak et al., 2008](#); [Vaulont et al., 2005](#)).

METAL STORAGE AND HOMEOSTASIS IN BACTERIA

1. Iron

Once iron has been assimilated within the bacterial cell, it is made available for intracellular functions. Iron from siderophores, ferric citrate, and from lactoferrin and transferrin is directly available, whereas haem iron must be released by the action of haem oxygenase. This pool of ferrous iron can be used for intracellular functions, however, in many bacteria, iron can be incorporated into a number of iron storage proteins, constituting an intracellular reserve which accumulates iron when it is in excess for future use under conditions of iron deficiency. Three types of potential iron storage proteins are found in bacteria, characterised by a similar molecular architecture of a roughly spherical protein shell surrounding a central cavity within which a mineral core of iron can be deposited. These are the 24-subunit ferritins (Ftns, which are also found in eukaryotes) and haem-containing bacterioferritins, Bfns, found in eubacteria, and the 12-subunit Dps proteins (DNA-binding proteins from starved cells), present only in prokaryotes ([Fig. 8.1](#)). That Dps proteins should be considered as iron storage proteins is a matter of debate. Their principal role seems to be to protect bacterial DNA against oxidative stress, notably due to H_2O_2 , by binding non-specifically and preventing free Fe^{2+} from catalysing Fenton chemistry. Although they form evolutionarily distinct families, they have many structural and functional similarities. They are composed of

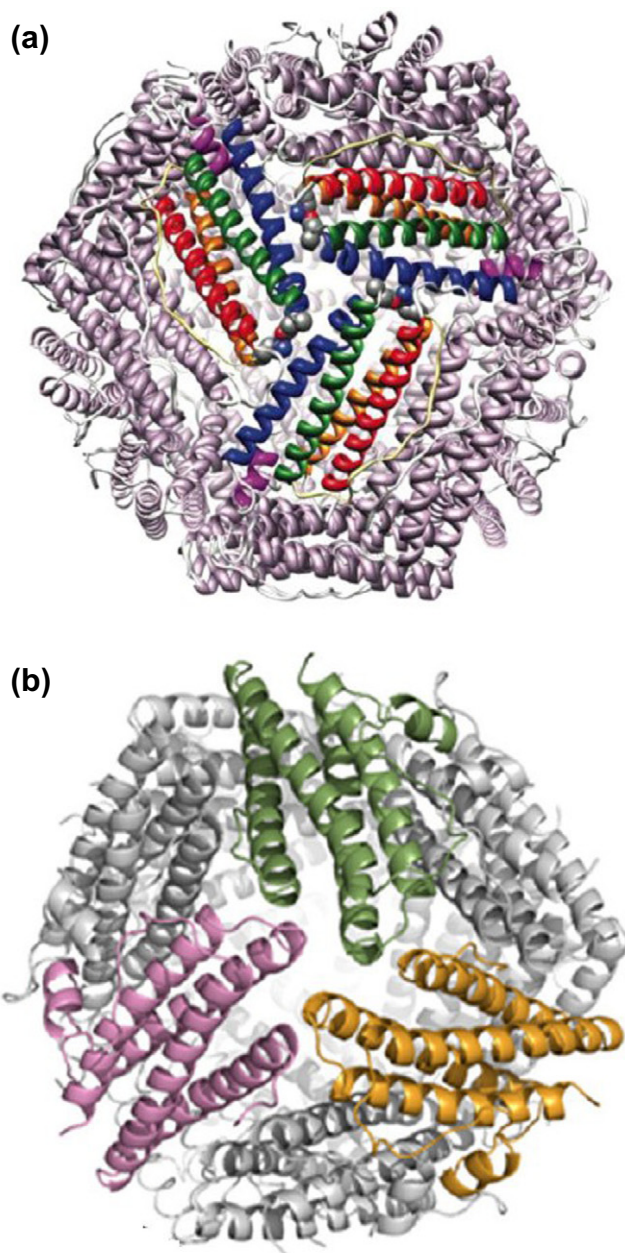


FIGURE 8.1 (a) Structural organisation of a ferritin protein (From *Watt, Hilton, & Graff, 2010*. Reproduced with permission from Elsevier). (b) Structural organisation of a Dps protein. (From *Chiancone & Ceci, 2010*. Reproduced with permission from Elsevier.)

either 24 (ferritins and bacterioferritins) or 12 (Dps proteins) similar if not identical subunits. Their subunits are folded in a central bundle of four α -helices, which assemble to form a roughly spherical protein shell surrounding a central cavity within which iron is stored (up to 4,500 iron atoms per 24mer in ferritins and bacterioferritins and around 500 in the smaller Dps protein 12mer).

Iron is stored in these proteins in the ferric form, but is taken up as Fe^{2+} , which is oxidised by ferroxidase sites (a more detailed account of iron incorporation into ferritins is given in Chapter 19). As we point out in Chapter 13, ferritins are members of the much larger di-iron protein family. After oxidation, the Fe^{3+} migrates to the interior cavity of the protein to form an amorphous ferric phosphate core. Whereas the ferritins in bacteria appear to fulfil the classical role of iron storage proteins, the physiological role of bacterioferritins is less clear. In *Escherichia coli*, it seems unlikely that bacterioferritin plays a major role in iron storage.

For many years, it was thought that iron homeostasis in *E. coli* and many other bacteria was regulated exclusively in response to iron availability by the Fur (Ferric Uptake Regulator) protein. In the presence of Fe^{2+} , this homodimer functions as a negative regulator of genes involved in iron acquisition — including not only expression and utilisation of siderophores, but also their biosynthesis (Fig. 8.2). Fur also controls the iron-regulated expression of bacterial virulence determinants.

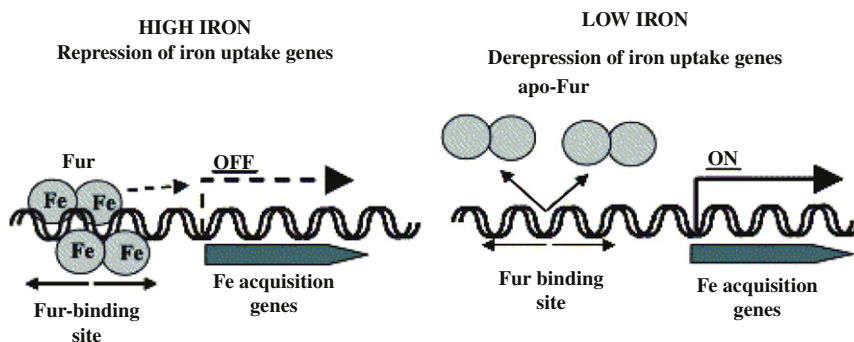


FIGURE 8.2 Schematic representation of Fur-mediated gene expression. (Adapted from Andrews et al., 2003.)

However, in Gram-positive bacteria with a high GC content in their DNA (such as *Mycobacterium* and *Streptomyces*), the DtxR protein (diphtheria toxin regulator) is responsible for global iron regulation, and can be considered as a functionally analogous iron sensor. The crystal structure of the Fur protein from the opportunistic pathogen *Pseudomonas aeruginosa*, and of DtxR from *Corynebacterium diphtheriae*, has been determined (Fig. 8.3). Though Fur and DtxRs have little or no sequence similarity, their α -helical DNA-binding domains are similar, and in both DtxR and Fur, two dimers bind to a single operator that is at least 27 base pairs long. A model of the interaction of *P. aeruginosa* Fur with DNA is also illustrated in Fig. 8.3.

Fur is itself part of the family of gene-regulatory proteins throughout many bacterial species. The major subclass is mainly involved, like Fur in *E. coli*, in the control of iron homeostasis, but it can also function in acid tolerance and protection against oxidative stress. One class of the Fur family, Zur, is involved in the regulation of zinc uptake (see below).

However, a puzzle in iron regulation, until recently, has been that, despite being a negative repressor, Fe^{2+} -Fur is found to be a positive regulator for a number of genes. In *E. coli*, these include the tricarboxylic cycle enzymes aconitase, fumarase, and succinate dehydrogenase, both of the ferritins, FtnA, and Bfr, and the Fe-superoxide dismutase, sodB. The explanation has come from the discovery of the family of small, non-coding RNAs, present in all organisms, which mostly function as regulators of translation and messenger RNA stability. One of these, RyhB, a 90 nucleotide RNA, downregulates a set of iron storage and iron-using proteins when iron is limiting (Fig. 8.4). Further, *ryhB* is itself negatively regulated by Fe^{2+} -Fur. RyhB RNA levels are inversely correlated with the mRNA levels of the *sdhCDAB* operon, which codes for succinate dehydrogenase and the five other proteins which had been found to be upregulated by Fe^{2+} -Fur. When Fe^{2+} -Fur is active, transcription of RyhB RNA is repressed, and in the absence of RyhB, the mRNAs for the proteins are upregulated and no longer degraded. This means (Fig. 8.4) that when iron is abundant, active Fur not only switches off iron acquisition genes, but by

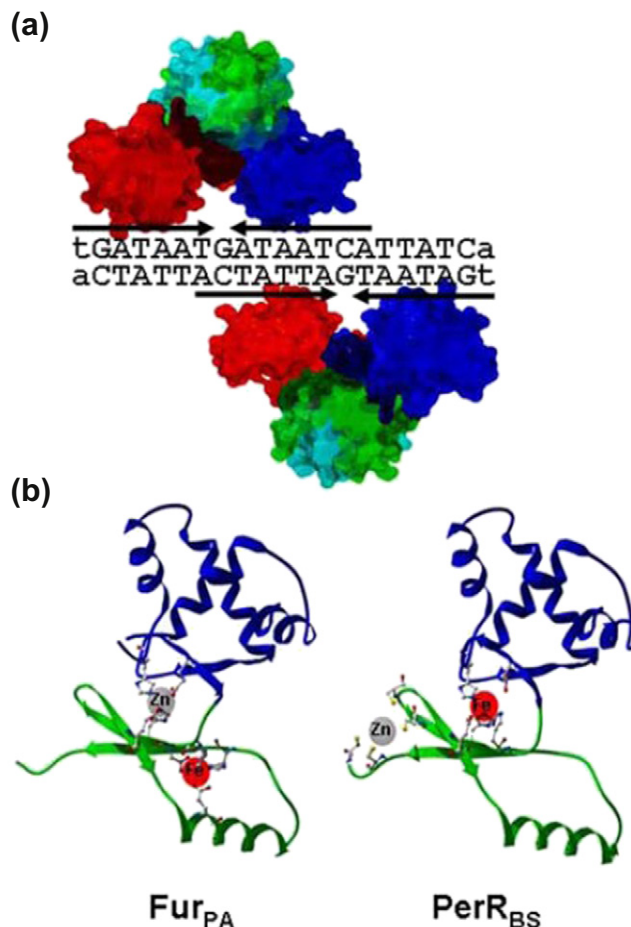


FIGURE 8.3 Interaction of Fur family proteins with DNA and metal ions. (a) Model of the interaction of Fur_{PA} with DNA. The N-terminal DNA-binding domains are in red and blue, with the C-terminal dimerisation domains in green. The classical Fur box is defined as a 19-bp inverted repeat sequence (capitals), originally assumed to bind one dimer. (b) Comparison of proposed metal-binding sites in Fur_{PA} and PerR_{BS}. (From Lee & Helmann, 2007. Reproduced with permission from Springer.)

switching off *ryhB* as well, iron storage genes are switched on. Conversely, in iron penury, inactive Fur allows the genes for iron acquisition to be switched on, and those for iron storage to be switched off. We will see later in the chapter that a similar up- and downregulation of iron uptake and storage pathways, albeit at the level of translation rather than transcription, operates in animals.

2. Copper and Zinc

Both copper and zinc appear to be stored in many bacteria in cysteine-rich proteins, called metallothioneins, which will be discussed from a structural point of view later in the chapter. The expression of these metal-sequestering, low-molecular-weight, cysteine-rich proteins, is often induced by both monovalent Cu(I) and divalent Zn(II), as well as by the non-biologically necessary, but potentially toxic, Ag(I) and Cd(II).

Because of their importance in the activity of many enzymes, bacteria have had to develop efficient uptake systems for copper and zinc. However, since both of these metals are toxic in excess, their intracellular content must be tightly regulated. Copper uptake homeostasis has been most extensively studied in the Gram-positive

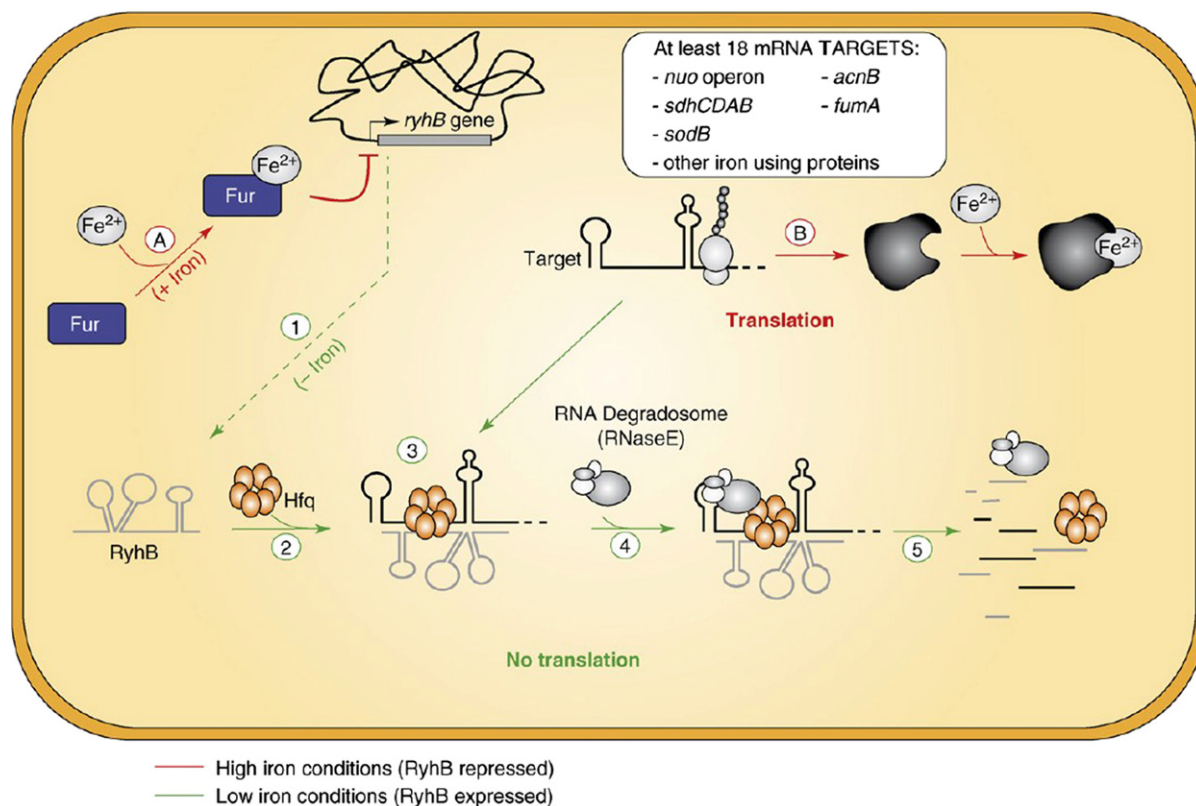


FIGURE 8.4 Mechanism of RyhB during iron starvation. (A) In conditions of sufficient iron, the activated protein Fur represses RyhB transcription and (B) the translation of non-essential iron-using proteins is possible. When iron becomes scarce, (1) Fur becomes inactive and RyhB is rapidly expressed. (2) RyhB is stabilised by the RNA chaperone Hfq. (3) The sRNA RyhB pairs with an mRNA target in an antisense manner, which blocks translation. (4) The multi-protein complex RNA degradosome recognises the sRNA–mRNA target complex and degrades both RNAs simultaneously. (From Massé, Salvail, Desnoyers, & Arguin, 2007. Reproduced with permission from Elsevier.)

bacterium *Enterococcus hirae*. The four genes involved, *copY*, *copZ*, *copA*, and *copB* are arranged in the *cop* operon. As mentioned in Chapter 7, the proteins CopA and CopB are copper-transporting ATPases, *copY* is a copper-responsive repressor, and *copZ* is a chaperone which is used in intracellular copper metabolism (more of copper chaperones later in the chapter). The *cop* operon enables *E. hirae* to grow in copper-limiting conditions, as well as in copper concentrations up to 8 mM. Under low-copper conditions, CopA allows Cu acquisition, while CopB extrudes excess Cu and also Ag. Fig. 8.5 shows a model for copper homeostasis in *E. hirae*. Copper enters the cell via CopA or by nonspecific leakage. Excess cytoplasmic copper binds to CopZ, which can then donate Cu^+ to CopB for export and to the CopY repressor to induce the *cop* operon. In low-copper conditions, two CopY dimers in the zinc form are bound to the two *cop* boxes in front of the *cop* operon. When CopZ donates Cu^+ to CopY, one Zn^{2+} per CopY monomer is replaced by two Cu^+ , with concomitant release of CopY from the promoter and induction of transcription of the downstream genes. Copper is reduced to the cuprous form, Cu(I) , by an as-yet-uncharacterised reductase before being imported into the cell by CopA, whence it is carried in the cytoplasm by the specific metallochaperone, CopZ. Copper is then transferred from CopZ to the dimeric Zn-containing repressor CopY, displacing the Zn and releasing the CopY from the promoter. This allows transcription of the four *cop* genes to proceed. Under high-copper conditions, excess CopZ is degraded by a copper-activated protease.

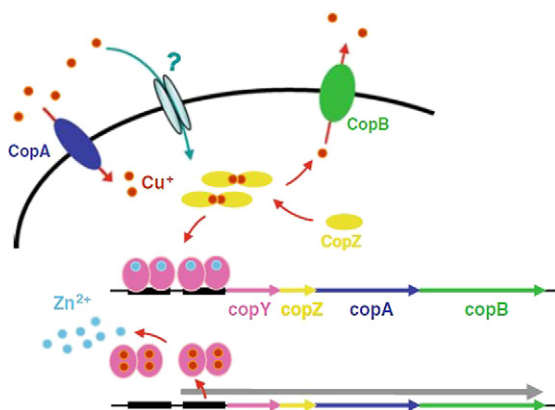


FIGURE 8.5 Copper homeostasis in *Enterococcus hirae*. Copper homeostasis in *Lactococcus lactis*. How copper enters the cell is unknown. Excess cytoplasmic copper binds to CopZ, which can then donate Cu^+ to either the copper ATPases for export or the CopR repressor to induce transcription. In low-copper conditions, a CopR dimer in the zinc form is bound to the *cop* box in front of the *copRZA* operon and the *copB* gene. When CopZ donates Cu^+ to CopR, one Zn^{2+} per CopR monomer is replaced by two Cu^+ , with concomitant release of CopR from the promoters and induction of transcription of the downstream genes. CopA then accomplishes copper export from the cytoplasm. The function of CopB is unknown. (From Solioz, Abicht, Mermoud, & Mancini, 2010. Copyright 2010 with permission from Springer Verlag.)

Bacterial copper proteins are found only in the plasma membrane (Gram-positive bacteria) or in the plasma membrane and the periplasm (Gram-negative bacteria), not in the bacterial cytoplasm. However, cyanobacteria do have copper proteins in their cytoplasm. These important photosynthetic bacteria require copper for plastocyanin, which plays a critical role in the photosynthetic electron transport chain. Both plastocyanin and cytochrome *c* oxidase are found in the thylakoid compartments within the cytoplasm. In *Synechocystis*, the Cu(I) $\text{P}_{1\text{B}}$ -ATPase CtaA imports Cu(I) . A second ATPase, PacS, imports Cu(I) into the thylakoid, and the Atx1-like copper chaperone ScAtx1 is believed to deliver Cu(I) from CtaA to PacS (Fig. 8.6).

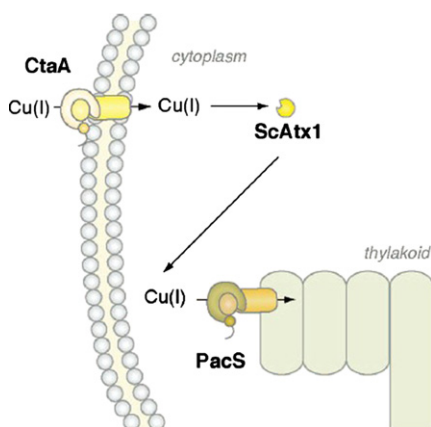


FIGURE 8.6 Copper trafficking pathways in the cyanobacterium *Synechocystis*.

In many bacterial species, zinc storage is apparently not a major mechanism in attaining homeostasis, the exception being cyanobacteria, which detoxify and store zinc in a metallothionein. A more common way of ridding the cell of excess zinc is by exporting it. The importance of this is clearly illustrated by the highly Zn^{2+} -resistant bacterium, *Ralstonia metallidurans*, isolated from a decantation tank in a zinc factory, and which has a minimal inhibitory Zn^{2+}

concentration of 12 mM. In general, the systems that provide zinc homeostasis involve (i) metal-handling proteins involved in metal uptake or efflux and (ii) metal sensors, which regulate the abundance of the respective metal-handling proteins. The known genes involved in Zn handling and sensing in *Cyanobacteria* are indicated in Fig. 8.7 (Blindauer, 2008). Zn(II) enters and leaves the periplasm by nonspecific porin proteins. It is imported into the cytosol

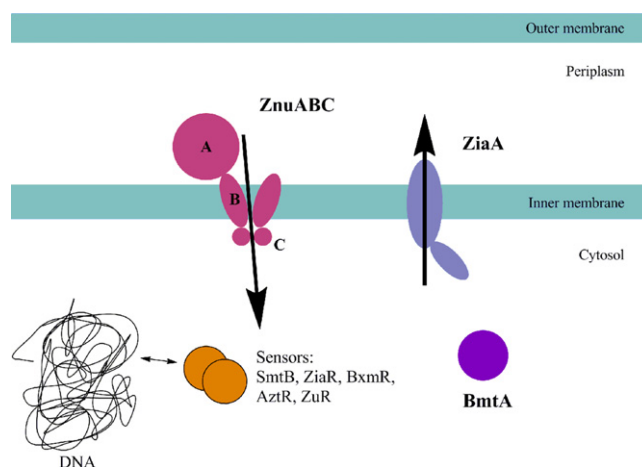


FIGURE 8.7 Summary of known zinc-handling genes in *Cyanobacteria*.

by the ABC transporter ZnuABC (also known as ZntABC), which is responsible for high-affinity Zn uptake. Its expression under zinc-starvation conditions is regulated by Zur. Zn(II) is pumped out of the cytosol by the ATPase ZiaA. BmtAs, bacterial metallothioneins, sequester Zn (and Cd) inside the cell. The majority of prokaryotic Zn sensors are either (i) members of the ‘winged helix’ SmtB/ArsR-related heavy metal-dependent transcriptional repressors, (ii) related to ZntR, or (iii) orthologues of Fur, which also contain a winged-helix DNA binding motif. Most of the high-affinity zinc uptake systems are regulated by Zur proteins, a subgroup of the Fur family. In addition, other members of the Fur family Mur and Nur are implicated in regulation of the uptake of Mn and Ni.

METAL TRANSPORT, STORAGE, AND HOMEOSTASIS IN PLANTS AND FUNGI

While unicellular fungi do not require metal transport systems, multicellular fungi and plants most certainly do, and we consider their transport in plants, and then consider how metal ions are sequestered in storage compartments before addressing their homeostasis. Once again, we consider in turn these processes for iron, copper, and zinc. Since iron metabolism has been most intensively studied in *Saccharomyces cerevisiae*, of all the fungi, we will focus our attention on iron homeostatic mechanisms; however, as the reader will see shortly, copper and zinc homeostasis have many similarities.

1. Iron, copper, and zinc transport and storage in plants

The acquisition of iron, copper, and zinc in plant roots has been described in Chapter 7. Once within the root epidermal cell, the iron must be transported through the roots to the xylem and thence to the leaves, and this intercellular metal transport is illustrated for dicots in Fig. 8.8 and for monocots in Fig. 8.9. In dicots, Fe, Zn, and Cu are taken up into the symplast by transporters in the epidermis. Reduction of Fe and possibly of Cu by FRO2 and acidification of the soil by an *Arabidopsis* H⁺ ATPase contribute to increased metal uptake. Metals can then travel through the symplastic space to the vasculature. Transport into the xylem is still not fully characterised. In the case of Fe, it is probably as citrate, and the citrate transporter FRD3 has been shown to efflux citrate into the xylem and is required for Fe transport to the shoot. Zn and Cu are thought to be effluxed into the xylem by

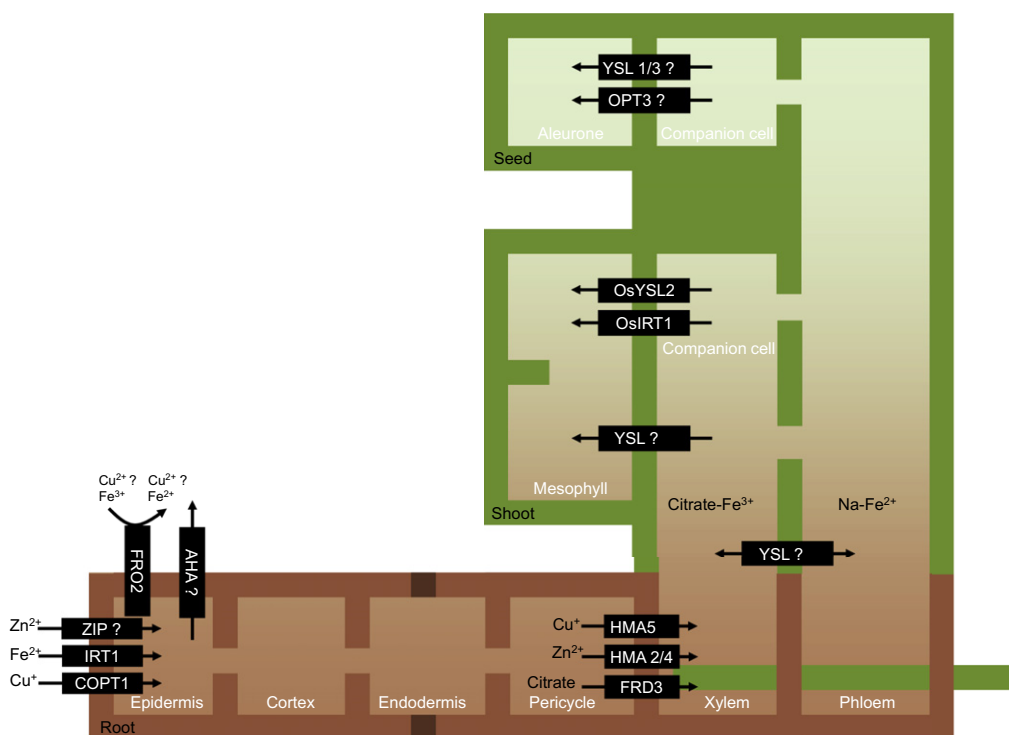


FIGURE 8.8 Fe, Zn, and Cu are taken up into the symplast by transporters in the epidermis. Reduction of Fe and possibly Cu by FRO2 and acidification of the soil by an *Arabidopsis* H^+ ATPase contribute to increased metal uptake. Metals can then travel through the symplastic space to the vasculature, bypassing the waxy Casparian strip (dark brown boxes) on the endodermis. Transport into the xylem is still not fully characterised but is thought to involve members of the HMA family and the citrate effluxer FRD3. In the xylem, metals are carried to the shoot through the transpiration stream where they are unloaded into the shoot, most likely by a member of the YSL family. YSLs may also translocate metals to the phloem, where they can then be delivered to the seed. (Adapted from Palmer & Gueriot, 2009.)

members of the HMA family. In the xylem, metals are carried to the shoot through the transpiration stream where they are unloaded into the shoot, most likely by a member of the YSL family. YSLs may also translocate metals to the phloem, where they can be transported as nicotianamine (NA) chelates and delivered to the seed.

In monocots, Fe and Zn are taken up as phytosiderophore chelates by YSL transporters in the epidermis. Fe can also be taken up by OsIRT1. Metals move through the symplastic space to the vasculature. The citrate effluxer FRDL1 is important for loading of citrate into the xylem and subsequent Fe transport to the shoot through the transpiration stream. YSL transporters also may play a role in unloading the xylem into the shoot and the phloem. Fe is unloaded from the phloem by OsYSL2 and OsIRT1 into shoot and seed tissue.

The photoreduction of xylem-transported ferric carboxylates, like citrate, is thought to be an important driving force in the reduction of iron in shoots: thereafter, the distribution of iron to the leaves is probably mediated again by the NA-iron complex (Fig. 8.9).

Once metals have been transported to their target tissue, they need to be distributed within the subcellular compartments where they are required, and need to be safely stored when they are in excess. Nearly 90% of Fe in plants is located in the chloroplasts, where it is required in the electron transfer chain, and in the synthesis of chlorophylls, haem, and Fe–S clusters. Fe, Cu, and Zn are also required in chloroplasts as cofactors for superoxide dismutases to protect against damage by reactive oxygen species during chloroplast development, and Cu is also required in other enzymes including the essential Cu protein plastocyanin. Pathways of intracellular metal transport in plant cells are illustrated in Fig. 8.10. Transport into the chloroplast is best characterised for Cu,

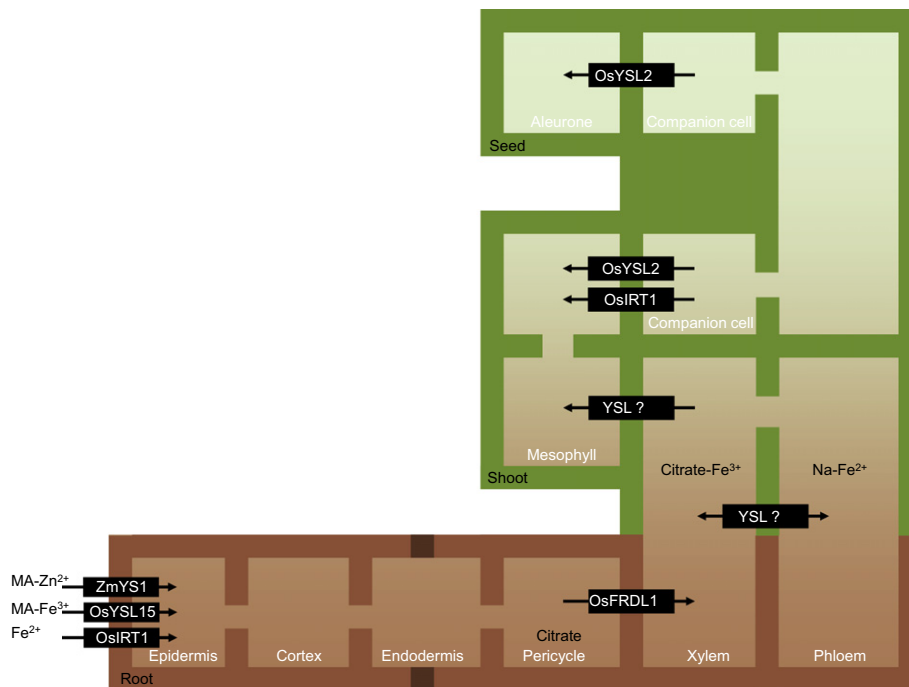


FIGURE 8.9 Fe and Zn are taken up as phytosiderophore chelates by YSL transporters in the epidermis. Fe can also be taken up by OsIRT1. Metals move through the symplastic space to the vasculature, bypassing the waxy Casparian strip on the endodermis. The citrate effluxer FRDL1 is important for loading of citrate into the xylem and subsequent Fe transport to the shoot through the transpiration stream. YSL transporters also may play a role in unloading the xylem into the shoot and the phloem. Fe is unloaded from the phloem by OsYSL2 and OsIRT1 into shoot and seed tissue. The dark brown boxes represent the Casparian strip. MA, mugineic acid; NA, nicotianamine. (Adapted from Palmer & Guerinot, 2009.)

which is transported into the chloroplast by HMA1, PAA1, and possibly PIC1. PAA2 is thought to transport Cu across the thylakoid membrane. Transport of Fe into the chloroplast is known to require reduction by FRO7 and may involve transport by PIC1. Fe and Cu must be transported into the mitochondria, but very little is known, although ATM3 is well established as an Fe—S exporter. In seeds, the vacuole plays an important part in storage of essential metals. Fe is transported into the vacuole by VIT1, Zn is transported into the vacuole by MTP1 (or MTP3) and HMA3, and Fe is remobilised from the vacuole by NRAMP3 or NRAMP4.

Plants contain phytoferritins, which accumulate in non-green plastids¹ in conditions of iron loading. They are targeted to the plastids by a putative transit peptide at their N-terminal extremity, and possess the specific residues for ferroxidase activity and iron nucleation, found in mammalian H-type or L-type ferritin subunits. We already mentioned the presence of metallothioneins in photosynthetic cyanobacteria, and it comes as no surprise that metallothioneins as well as phytochelatin are found in plants where they probably function by protecting from toxic metals.

2. Iron, copper, and zinc homeostasis in plants (Grotz & Guerinot, 2006)

In *Arabidopsis*, the basic helix-loop-helix (BHLH) transcription factor, FIT, orthologous to tomato FER protein regulates iron-deficiency responses. The expression of FIT in the *fer* mutant of tomato rescues the ability of the

1. Plastids are members of a family of organelles found in the cytoplasm of eukaryotic cells, all of which contain DNA and are bounded by a double membrane.

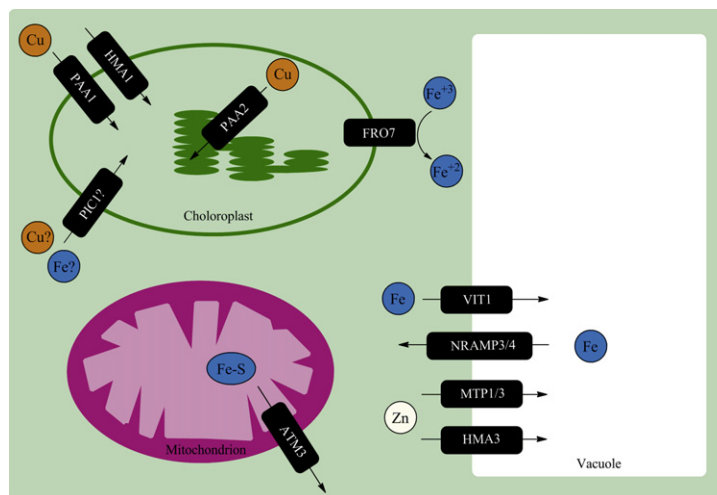


FIGURE 8.10 Fe is transported into the vacuole by VIT1, Zn is transported into the vacuole by MTP1 (or MTP3) and HMA3, and Fe is remobilised from the vacuole by NRAMP3 or NRAMP4. Transport into the chloroplast is best characterised for Cu, which is transported into the chloroplast by HMA1, PAA1 and possibly PIC1. PAA2 is thought to transport Cu across the thylakoid membrane. Transport of Fe into the chloroplast is known to require reduction by FRO7 and may involve transport by PIC1. Very little is known about transport in and out of the mitochondria, though ATM3 is well established as an Fe-S exporter. (Adapted from Palmer & Guerinot, 2009.)

plants to induce the iron-deficiency response. Like FER, FIT1 is root specific; it is however induced under Fe-deficient conditions. In *fit* mutants, the Fe²⁺ transporter IRT1 is absent, and the mRNAs for the reductase FRO2 and the Fe(III) chelate reductase activity are both absent. It appears that additional members of the BHLH family act as binding partners in concert with FIT in the iron-deficiency response, as outlined in Fig. 8.11. IRT1 and

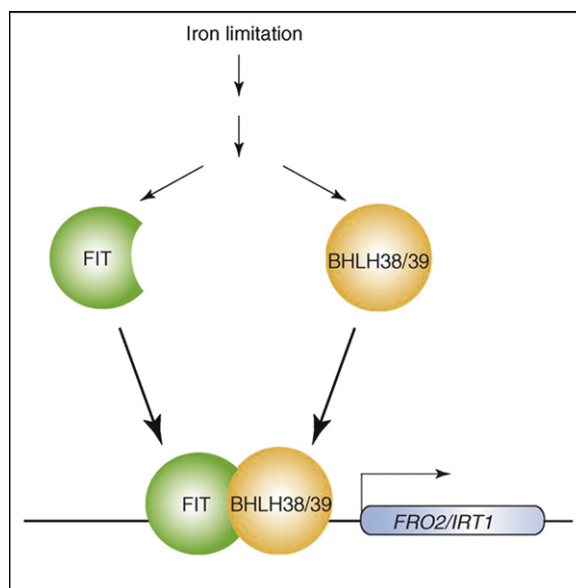


FIGURE 8.11 Model for the induction of *FRO2* and *IRT1* by FIT and BHLH38/BHLH39. Expression of FIT, BHLH38, and BHLH39 is increased under iron limitation. FIT heterodimerizes with either BHLH38 or BHLH39 to induce transcription of *FRO2* and *IRT1* in the outer layers of roots. (Adapted from Walker & Connolly, 2008.)

FRO2 are also regulated post-transcriptionally, most likely by ubiquitination in the presence of iron, followed by endocytosis and degradation in the vacuole, in a similar manner to ZRT1 in the presence of zinc.

A model for the regulation of iron-deficiency responses in strategy I plants (Fig. 8.12) involves a regulatory circuit consisting of two parts (a) a shoot–root loop and (b) a root–shoot loop. In the root–shoot part of the

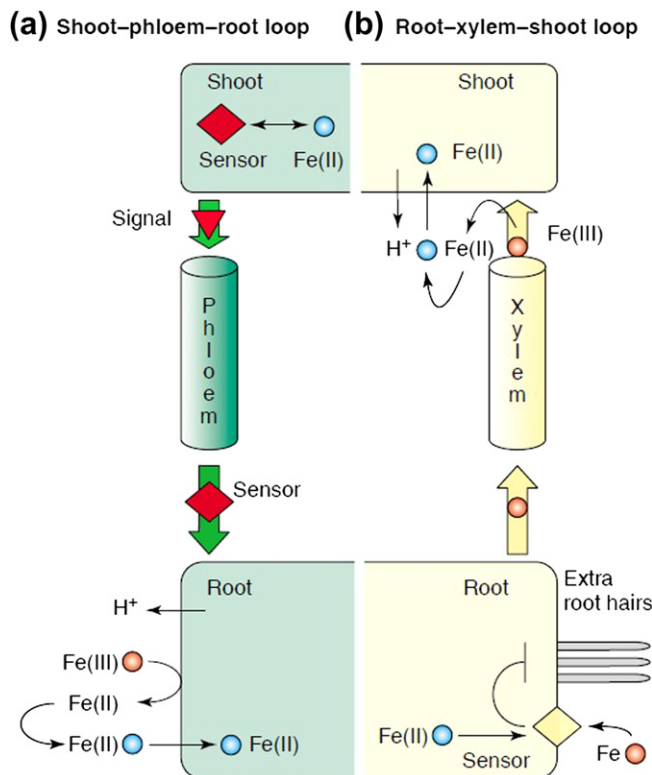


FIGURE 8.12 Model for the regulation of the iron-deficiency responses in strategy I plants. A regulatory circuit consisting of two parts, (a) a shoot–root loop and (b) a root–shoot loop, appears to control a set of responses; cross talk between these loops allows fine tuning and foraging of iron when iron sources are spatially heterogeneous. (Adapted from Schmidt, 2003.)

circuit, differentiation of root epidermal cells is controlled by iron availability, either within the root cell or in the rhizosphere (the immediate external environment of the root). Development of extra numbers of root hairs² (which would increase iron uptake) is repressed by iron in the vicinity of the roots. Iron taken up and translocated to the leaves in the xylem regulates the uptake of iron into the leaf cells. When the iron levels in the leaf declines, this is detected by a sensor, and a signal molecule is synthesised which conveys this information to the root via the phloem. The effect of this signal is to increase the transfer of electrons, the net proton excretion, and the activity of the Fe^{2+} -transporter, resulting in increased iron uptake by the root cells. It is likely that more than one sensor is involved in this process. The outcome of the interaction between the two signaling cascades is to positively or negatively regulate the uptake of iron.

In strategy II monocots, the key transcriptional regulator of genes involved in phytosiderophore synthesis and iron uptake is the BHLH protein, IRO2. A model of the regulatory network has been established. In response

2. Initiation and elongation of the root hairs is defined by a set of some 606 genes, describing the ‘root-hair morphogenesis transcriptome’.

to Fe-deficiency signals, two iron sensors, IDEF1 and IDEF2, bind to IDE1 and IDE2 motifs present in the promoter of the *IRO2* gene and activate *IRO2* expression. *IRO2* can then set in motion the expression of genes which have an *IRO2*-binding motif. This most likely includes the genes for two additional transcription factors which have *IRO2*-binding motifs. This cascade of signal transduction ultimately results in the plant responses of increased phyto siderophore synthesis, including overexpression of genes involved in biosynthesis of their precursor methionine, and of iron uptake genes.

Phytoferritin transcription is induced by iron excess and repressed by iron deficiency in leaves as well as in roots in several plant species. In the case of maize, there are two ferritin genes which are differentially regulated by two independent signaling pathways, one involving an oxidative step and one dependent on the plant growth hormone, abscissic acid.

The response of *A. thaliana* to Cu deficiency in roots and vegetative tissue is well established (Fig. 8.13). When Cu is limiting, cytosolic and plastid Cu/Zn SODs are downregulated and FeSOD is upregulated. The reverse is

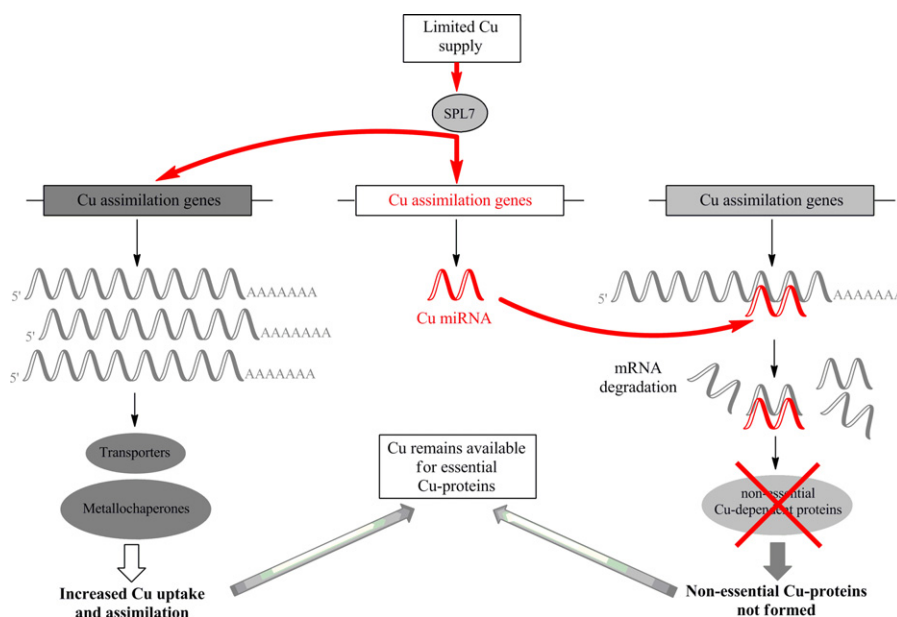


FIGURE 8.13 Model for SPL7 and Cu-microRNA-mediated responses to low Cu availability in *A. thaliana*. (Adapted from Pilon, Cohu, Ravet, Abdel-Ghany, & Gaymard, 2009.)

observed in Cu supplementation. A microRNA, miR398, targets the mRNAs that encode the Cu/Zn SODs. Strong oxidative stress reduces the expression of miR398, resulting in increased Cu/Zn SOD activity. The master Cu homeostasis regulator is SPL7. Low cellular Cu activates SPL7-mediated transcription of genes involved in copper uptake and assimilation as well as the four Cu-microRNAs (miR397, miR398, miR408, and miR857). The Cu-microRNAs in turn mediate the RISC (RNA-induced silencing complex)-dependent cleavage of transcripts that encode non-essential Cu proteins. These microRNAs also target Cu proteins (laccases and plastocyanin). Thus, at least four microRNAs, called the Cu-microRNAs, are regulated by Cu availability (Fig. 8.13). It is proposed that induction of the Cu-microRNAs and, therefore, a reduction in Cu protein expression during Cu-limited conditions would allow for preferential allocation of limited Cu to the most essential Cu proteins such as plastocyanin, which is absolutely required for photoautotrophic growth in plants.

Transcriptional control is also involved in Zn homeostasis in *A. thaliana* and the ZIP transporters IRT1 and IRT2 are both upregulated in Zn deficiency.

3. Iron, copper, and zinc transport and storage in fungi

As we saw in Chapter 7, during reductive uptake of iron by *Saccharomyces cerevisiae*, extracellular ferric complexes are reduced and the ferrous iron that is released is taken up by the low-affinity divalent metal permease (FET4) or the high-affinity oxidase—permease system (FET3—FTR1), which was outlined in Fig. 7.1. Copper participates in the biogenesis of FET3 in a late Golgi compartment via the copper chaperone CCC2. Iron can also be taken up from ferric siderophore complexes. Iron is clearly required in substantial amounts for haem and Fe—S biosynthesis, as we described in Chapter 4. Many proteins which contain haem and Fe/S are located in the mitochondria, making the mitochondria a focal point for the coordination of intracellular iron metabolism (Fig. 8.14). Iron is imported as Fe^{2+}

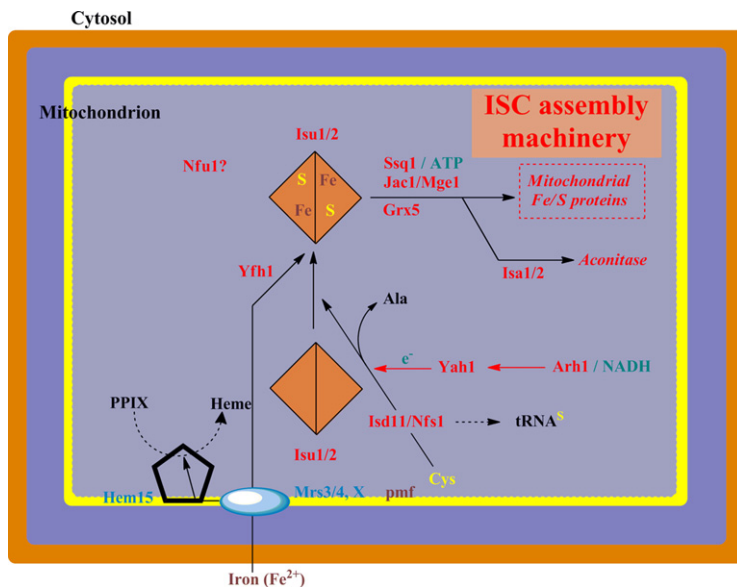


FIGURE 8.14 A model for the mechanism of Fe/S protein biogenesis in mitochondria. (From Lill *et al.*, 2006. Copyright 2006 With permission from Elsevier.)

across the mitochondrial inner membrane in a membrane potential-dependent manner facilitated by the mitochondrial carrier proteins MRS3 and MRS4, together with other unknown proteins (X). It is then used for haem synthesis from protoporphyrin IX (PPIX) by ferrochelatase (Hem15) and for the biogenesis of Fe/S proteins. The latter process starts with the release of sulfur from cysteine by the Nfs1/Isd11 cysteine desulfurase complex and the formation of a transient Fe/S cluster on the Isu1/2 scaffold proteins. The electron (e^-) transfer chain $\text{NADH} \rightarrow$ ferredoxin reductase $\text{Arh1} \rightarrow$ ferredoxin Yah1 and the putative iron donor Yfh1 (frataxin) are needed for transient Fe/S cluster synthesis on Isu1/2. YFH1 may also serve a similar chaperone function in the terminal step of haem biosynthesis supplying iron to ferrochelatase. The structure of frataxin and its role in the human neurological disease, Friedreich's ataxia, are discussed in Chapter 21. Yeast strains with a deletion in gene *YFH1* accumulate excess iron in the mitochondria, and undergo mitochondrial oxidative damage. To date, no ferritin-like iron storage protein, like those found in bacteria, plants, animals, and almost every other living organism, has been reported in asco- and basidiomycetes. Indeed, scrutiny of the *S cerevisiae* genome reveals no protein with convincing homology to consensus sequences for ferritins. Intracellular iron is stored in the vacuole, which in yeast is a dynamic storage depot associated with the handling in addition to Fe, of Cu, Zn, Mn, Mg, and Ca. Iron can be mobilised by a similar reductive mechanism to that used in the high-affinity uptake pathway at the plasma membrane, involving homologous proteins — the reductase, FRE6, and the oxidase/permease, FET5, and FTH1(?)

We have already described the plasma membrane systems employed in yeast for copper uptake in Chapter 7. We describe briefly here the chaperone proteins involved in the intracellular transport and delivery of copper to target proteins (Fig. 8.15), which were first described in *S. cerevisiae*. The first of the copper chaperones to be identified was

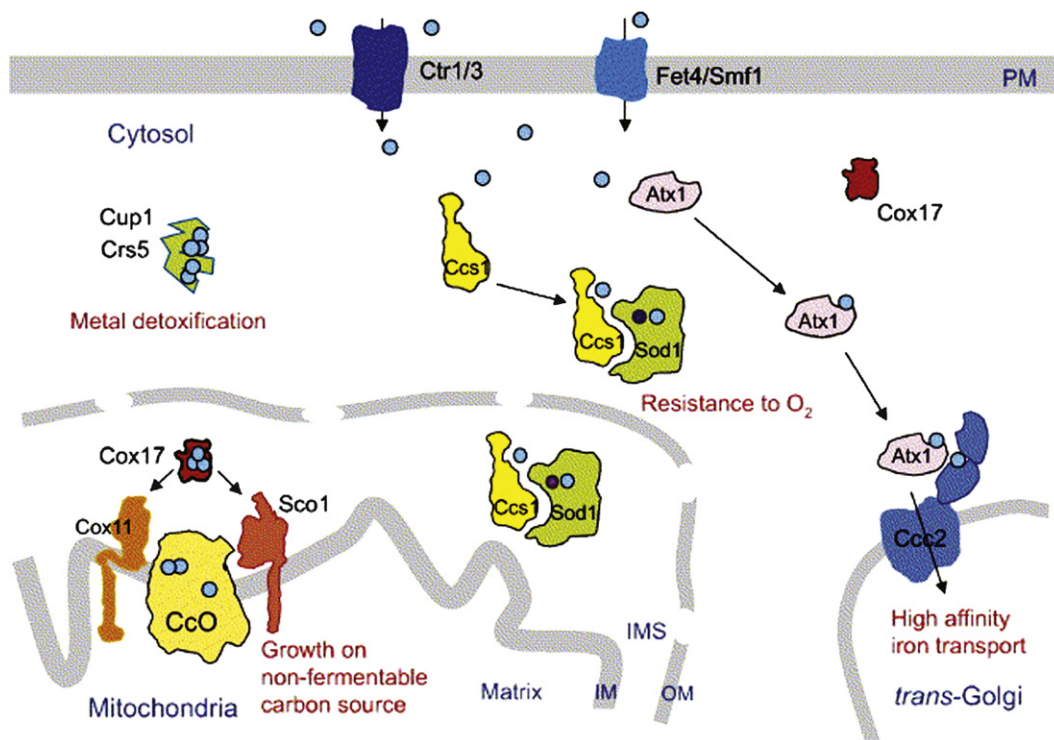


FIGURE 8.15 Copper homeostasis in *Saccharomyces cerevisiae*. (From Cobine, Pierrel, & Winge, 2006. Copyright 2006, with permission from Elsevier.)

the yeast Atx1 protein, which delivers copper to CCC2, a P-type ATPase on the Golgi membrane, which transports copper into the lumen of the secretory pathway where it can be incorporated into newly synthesised cuproproteins like the plasma membrane FET3 oxidase. As we will see a little later in this chapter, CCC2 corresponds to the human P-type ATPases which are mutated in Menkes and Wilson's diseases. A second chaperone, CCS1, provides Cu(I) for activation of the Cu, Zn superoxide dismutase, Sod1, in both the yeast cytoplasm and the intermembrane space (IMS) between the inner and outer mitochondrial membranes. The mechanism by which it functions was described in Chapter 4. Finally, in much the most complex of the three chaperone pathways, COX17, present in both the cytosol and IMS, transports copper to the mitochondria for incorporation into the important terminal oxidase of the respiratory pathway, cytochrome *c* oxidase (CcO), which is discussed in detail in Chapter 14. COX17 delivers copper to the co-chaperones COX 11, for insertion into the Cu_B site of CcO and SCO1, for insertion into the Cu_A site of CcO.

As we saw in Chapter 7, there are several plasma membrane zinc uptake transporters in yeast. Within the cell, a number of other proteins are involved in zinc transport within the cell. *S. cerevisiae* is unusual in that it does not appear to have any plasma membrane zinc efflux transporters. This is to a large extent compensated by the capacity of the vacuole to serve as a major site of zinc sequestration and detoxification, enabling wild-type cells to tolerate exogenous zinc concentrations as high as 5 mM. The zinc stored in the vacuole can attain millimolar levels, and can be mobilised under zinc-deficient conditions for use by the cell. Vacuolar zinc uptake is mediated by two members of the cation diffusion facility CDF family, Zrc1 and Cot1 (Fig. 8.16).

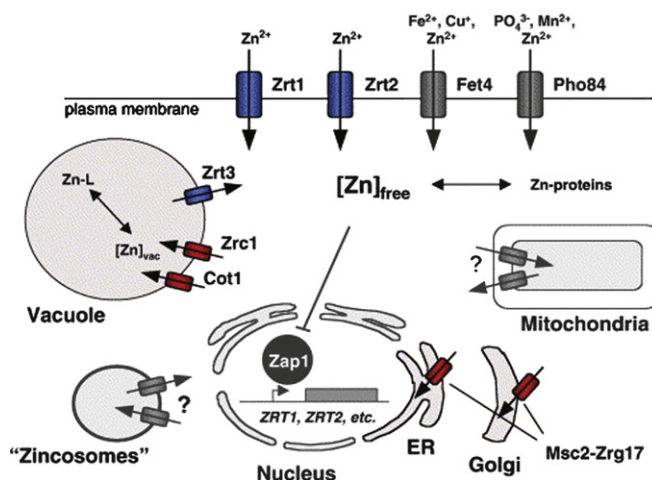


FIGURE 8.16 An overview of zinc transport and trafficking in the yeast *S. cerevisiae*. ZIP family transporters are shown in blue and CDF family transporters are shown in red. Hypothetical transporters or known proteins from other families of transporters are shown in gray. The Zap1 transcriptional activator, shown in black, is responsible for the upregulation of many target genes in zinc-limited cells. Zn^{2+} in the vacuole is likely bound by some ligand (L) to facilitate storage. (From Eide, 2006. Copyright 2006, with permission from Elsevier.)

Zrc1 is a $\text{Zn}^{2+}/\text{H}^{+}$ antiport,³ allowing the zinc accumulation in the vacuole to be driven by the proton concentration gradient generated by the vacuolar H^{+} -ATPase. The Cot1 protein may function in the same way. The release of zinc to the cytosol is mediated by the Zip family member Zrt3. Within the vacuole, zinc may be bound to organic anions. Vesicular storage sites for zinc may also exist in mammalian cells, where they have been designated “zincosomes”, and such membrane-bound vesicles have also been observed in zinc-treated yeast. There are almost certainly zinc transporters to supply the metal to mitochondria, and in the secretory pathway, involving both the Golgi apparatus and the endoplasmic reticulum, there are also zinc transporters, notably the Msc2/Zrg17 complex.

4. Iron, copper, and zinc homeostasis in fungi

As we saw earlier (Chapter 7), *S. cerevisiae* has a variety of genes coding for proteins which are involved in iron acquisition at the cell surface, and many of them are transcriptionally induced in response to low iron. The high-affinity transport system (Fet3, Ftr1) contains a ferroxidase, which requires copper as a cofactor, and as a consequence, genes that are involved in the trafficking and transport of copper to this Fet3 protein (Atx1 and Ccc2, described later) are also regulated at the transcriptional level by iron. It is clear that high-affinity iron uptake is seriously compromised by low levels of extracellular copper. Iron-dependent gene regulation in *S. cerevisiae* is mediated by two transcription factors, Aft1 and Aft2 (‘Activator of Ferrous Transport’). Under iron-limiting conditions, Aft1 activates transcription of a specific set of genes involved in iron uptake, mobilisation of stored iron, and metabolic adaption which occur under iron-limitation conditions. These include seventeen genes involved directly or indirectly in iron uptake at the plasma membrane. Among these are both reductases Fre1 and 2, the high-affinity (Fet3, Ftr1) and low-affinity (Fet4) systems for free iron uptake, as well as the family of transporters (Arn1 to Arn4) which cycle between the cell surface and an endosomal compartment, mediating ferric siderophore uptake. It also regulates the expression of a number of other genes, including other cell surface reductases, a mitochondrial iron transporter (Mrs4), and proteins involved in the biosynthesis of iron–sulfur clusters (Isu1 and Isu2), and the three cell wall mannoproteins, FIT1, FIT2, and FIT3, which enhance retention of ferric siderophores. Aft2 regulates the expression of an overlapping set of genes.

3. An antiport simultaneously transports two molecules (or in this case, ions) simultaneously in opposite directions.

In fungi, copper homeostasis involves, as in mammals, some degree of post-transcriptional control of copper transporters. However, we consider here transcriptional regulation of genes involved in copper acquisition, mobilisation, and sequestration. A number of them have been characterised — the two most important copper-responsive transcription factors in *S. cerevisiae* are Mac1, which activates gene expression in response to copper deficiency, and Ace1, which activates gene expression in response to elevated copper. Mac1 protects cells from copper deficiency by activating expression of the high-affinity copper uptake systems CTR1 and CTR3 (Fig. 8.15) as well as the cell surface reductase FRE1. Mac1 is also required for the post-translational degradation of Ctr1 under conditions of copper excess. However, the principal resistance to copper excess is the Ace1-dependent induction of the *CUP1* gene (Fig. 8.15). *CUP1* encodes a small cysteine-rich copper-binding metallothionein, which protects the cells by sequestering copper, thereby preventing its toxicity. Ace also regulates the expression of a second metallothionein gene (*CRS5*) and the copper–zinc superoxide dismutase gene (*SOD1*).

Zinc homeostasis in general parallels copper homeostasis, involving both transcriptional and post-translational regulatory mechanisms. In *S. cerevisiae*, the high-affinity zinc uptake gene *ZRT1* increases in response to zinc limitation, whereas in zinc repletion *ZRT1* undergoes zinc-induced endocytosis and is degraded in the vacuole. The ZAP1 zinc-responsive transcription factor increases the expression of the three uptake systems encoded by the *ZRT1*, *ZRT2*, and *FET4* genes (Fig. 8.16), but does not affect the Pho84 phosphate transporter, which may also transport Zn. It also stimulates the release of zinc from the vacuole by activation of the *ZRT3* vacuolar efflux system. ZAP1 also increases the expression of *ZRC1*, a gene which modulates zinc influx into the vacuole.

METAL TRANSPORT, STORAGE, AND HOMEOSTASIS IN MAMMALS

Finally, we deal with metal storage, transport, and homeostasis in mammals. We have already described iron uptake from the gastrointestinal tract and the transferrin to cell cycle which delivers most of the iron to mammalian cells. We will focus our attention here on cellular transport and utilisation of iron and its storage in ferritin. The transport and storage of copper and zinc will then be discussed. We then conclude with an account of metal homeostasis, first treating the question at the cellular level and finally addressing the way in which mammals regulate their dietary iron, copper, and zinc absorption in order to prevent either metal-ion deficiency or excess. As we will see, in man this is a non-trivial problem on account of our severely limited capacity to excrete iron, making the control of dietary iron absorption a matter of capital importance.

1. Iron transport and storage in mammals

Most mammalian cells take up iron transported in serum by transferrin, an 80 kD bilobal protein with two identical iron-binding sites, one in each half of the molecule. The coordination of the iron atom involves four protein ligands and a carbonate anion, as we described in Chapter 4, and the transferrin to cell cycle for delivering iron was outlined in Chapter 7. Iron release from the extremely stable diferric transferrin bound to its receptor is facilitated by the acidic pH prevailing in the endosome and by the fact that the receptor imposes a conformation on the bound transferrin that is essentially that of the open apotransferrin form.

Figure 8.17 reminds us of the transferrin cell cycle, but also indicates some of the intracellular fates of iron once it has been released and transported out of the endosomal compartment by the divalent metal-ion transporter, DMT1, after reduction by a ferrireductase, STEAP3. The iron in the cytosol constitutes the so-called labile iron pool, possibly bound among other ligands to an as-yet-unidentified chaperone. Iron can be stored in ferritin, transferred to the mitochondria via the mitochondrial transport carriers mitoferrin (Mfrn) 1 and 2, used for other cellular functions, or exported into the plasma from the basolateral membrane of duodenal enterocytes, from macrophages, hepatocytes, and a limited number of other cell types. This involves the protein known as IREG1 or ferroportin described already in Chapter 7. We will discuss ferroportin in more detail in the next section on iron homeostasis, since it is the target of hepcidin, a recently described iron regulatory peptide.

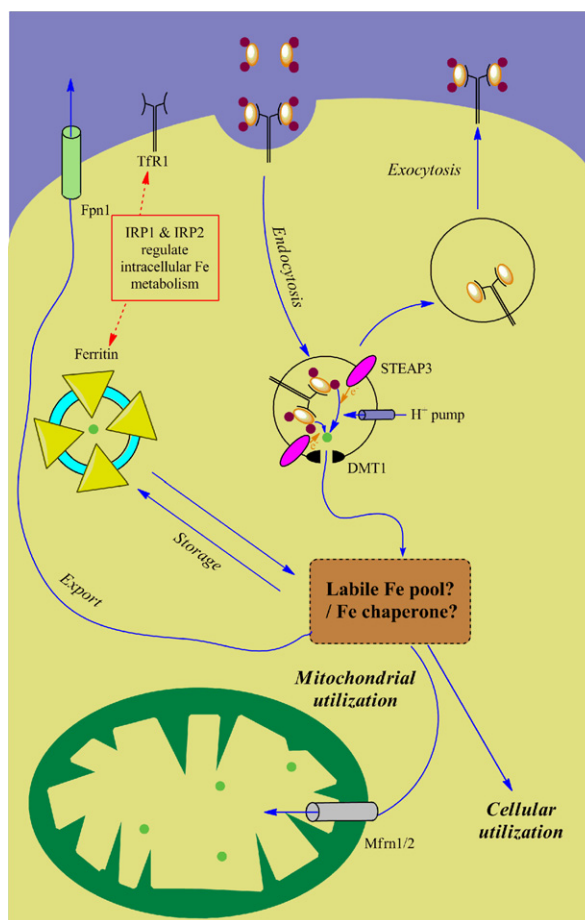


FIGURE 8.17 Schematics of cellular iron uptake and utilisation. (Adapted from Richardson *et al.*, 2010.)

About a quarter of total body iron is stored in macrophages and hepatocytes as a reserve which can be readily mobilised for red blood cell formation (erythropoiesis). This storage iron is mostly in the form of ferritin like bacterioferritin, a 24-subunit protein in the form of a spherical protein shell enclosing a cavity within which up to 4500 atoms of iron can be stored, essentially as the mineral ferrihydrite. Despite the water insolubility of ferrihydrite, it is kept in solution within the protein shell, such that one can easily prepare mammalian ferritin solutions which contain 1 M ferric iron (i.e., 56 mg/ml!). Mammalian ferritins, unlike most bacterial and plant ferritins, have the particularity that they are heteropolymers, made up of two subunit types, H and L. Whereas H-subunits have a ferroxidase activity, catalysing the oxidation of two Fe^{2+} atoms to Fe^{3+} , L subunits appear to be involved in the nucleation of the mineral iron core: once this has formed an initial critical mass, further iron oxidation and deposition in the biomineral takes place on the surface of the ferrihydrite crystallite itself (for a more detailed discussion, see Chapter 19).

2. Iron homeostasis in mammals

The regulation of cellular iron homeostasis is to a large degree controlled at the level of the translation of the mRNAs of proteins involved in cellular iron metabolism (Rouault, 2006; Wallander *et al.*, 2006). The key players in this post-transcriptional regulation are two iron regulatory proteins (IRP1 and IRP2), which function as

cytosolic iron sensors. In conditions of iron deficiency, IRPs bind with high-affinity ($K_D \sim 20\text{--}100\text{ pM}$) to stem loops, known as iron regulatory elements (IREs), in mRNAs encoding the regulated proteins (Fig. 8.18). When the

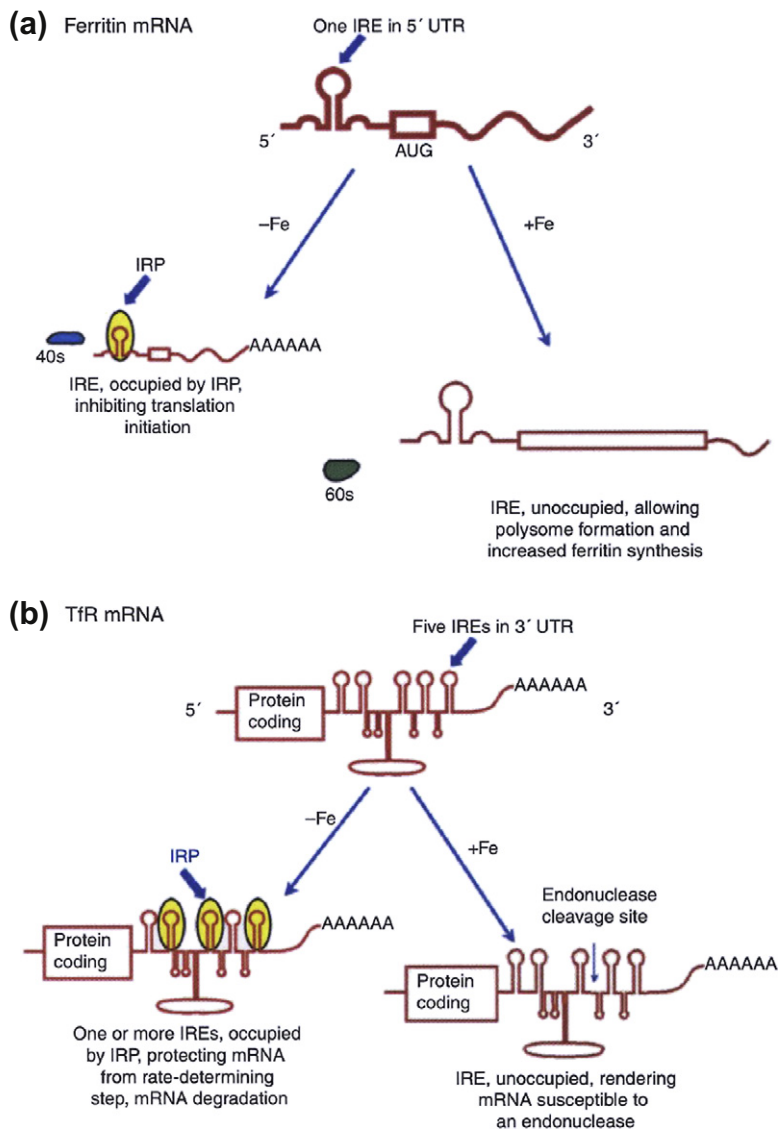


FIGURE 8.18 Outline of translational regulation of mRNAs of a number of proteins involved in iron metabolism in low and high iron (a) Ferritin mRNA (b) TfR mRNA. IRPs bind to IREs located in either the 5'- or 3'-UTRs of specific mRNAs. During low iron conditions, IRP1 and IRP2 bind with high affinity to 5' IREs and to the five 3' IREs in TfR mRNA, resulting in the translational repression of 5' IRE-containing mRNAs and the stabilisation of the TfR mRNA. During high iron conditions, IRPs lose their affinity for IREs, increasing translation of 5' IRE-containing mRNAs and mediating degradation of the TfR mRNA. Increased iron levels result in the conversion of the IRP1 RNA binding form into the $[4\text{Fe-4S}]$ cluster c-acon form, while increased iron and/or haem levels mediate IRP2 proteasomal degradation. (From Crichton, 2009. Copyright 2009 John Wiley and Sons.)

IREs are in the 5'-untranslated region of the mRNA, as is the case for ferritin and ferroportin, binding of IRPs prevents initiation of translation. In contrast, in the case of the transferrin receptor and DMT1, where the IREs are

in the 3'-untranslated region, binding of the IRPs to the mRNAs protects them against degradation by nucleases. This results in increased iron uptake and blockage of iron storage and export. When iron is abundant, the IRPs are no longer active in binding, allowing ferritin and ferroportin mRNAs to be translated and resulting in the downregulation of transferrin receptor and DMT1 synthesis as a result of the nuclease-catalysed degradation of their mRNAs. Under these conditions, IRP1 acquires aconitase activity, associated with the incorporation of a 4Fe4S cluster, whereas IRP2 is condemned, after ubiquitination, to degradation in the proteasome.

Systemic iron homeostasis in mammals depends on the regulation of dietary iron absorption by the enterocytes of the duodenum and the recycling of iron by macrophages recovered from the breakdown of the haemoglobin from senescent red blood cells. In hereditary disorders of iron loading, known collectively as haemochromatosis, iron is deposited in parenchymal cells, transferrin saturation increases, and as the iron load increases, serious damage results to many tissues, notably liver, endocrine tissues like pancreas, and heart. Hereditary haemochromatosis can be divided into three classes – classical haemochromatosis, juvenile haemochromatosis, and ferroportin disease. Classical haemochromatosis is associated with mutations in *HFE*, a gene which encodes a protein of the major histocompatibility complex, although in rare cases another gene can be involved, the *TFR2* gene which codes for a homologue of the major transferrin receptor gene, *TFR1*. Juvenile haemochromatosis is a rare form of hereditary haemochromatosis, characterised by early and severe onset of symptoms, particularly cardiac and endocrine defects. Most patients have mutations in the recently cloned *HJV* gene (haemojuvelin), which is expressed in muscle, liver, and heart, but whose function is still unknown. A very small subset of juvenile haemochromatosis patients have mutations in the *HAMP* gene, which codes for the prepro form of hepcidin, a peptide synthesised by the liver, which is a major regulator of iron metabolism. Hepcidin is positively regulated by iron and negatively regulated by iron deficiency and hypoxia: it limits intestinal iron absorption and iron release by macrophages. Ferroportin disease, the third class of hereditary haemochromatosis, is caused by pathogenic mutations in the gene encoding the iron exporter, ferroportin.

We now have an increasingly detailed understanding of how systemic iron homeostasis is regulated. The first index of iron loading, increased transferrin saturation, leads to increased levels of Fe₂-Tf, which is detected by the liver via a complex pathway involving *HFE*, *TFR2*, and *HJV*, the proteins of three of the genes known to be mutated in haemochromatosis. Hepatocytes respond to this signal by increased expression of the *HAMP* gene, resulting in increased secretion of the regulatory peptide, hepcidin. Circulating hepcidin blocks dietary iron uptake by the duodenal enterocytes and iron recycling from macrophages, in both cases through internalization of ferroportin, which blocks iron export (Fig. 8.19). The outcome of this is to decrease serum iron levels, leading logically to the feedback response of downregulating hepcidin synthesis and secretion. This once again allows ferroportin to be displayed on the surface of enterocytes and macrophages, allowing them once again to export iron into the circulation. In classical and juvenile haemochromatosis, mutations in *HFE*, *TFR2*, and *HJV* lead to downregulation of hepcidin synthesis, decreased levels of circulating hepcidin, and ferroportin hyperactivity. The latter accounts for the increased iron absorption and uncontrolled release of iron from macrophages, defects characteristic of hereditary haemochromatosis.

3. Copper and zinc transport and storage in mammals

Contrary to popular belief, ceruloplasmin,⁴ the principal copper-containing protein in plasma, is not involved in copper transport. This is clearly underlined by the clinical observation that patients with aceruloplasminaemia (i.e., lacking ceruloplasmin in their blood) have perfectly normal copper metabolism and homeostasis. Copper is transported in plasma mostly by serum albumin with smaller amounts bound to low-molecular-weight ligands like histidine. Likewise, zinc is mostly transported in plasma bound to proteins (albumin and α_2 -macroglobulin).

4. Ceruloplasmin, akin to Pirandello's *Six Characters in Search of an Author*, has long been a protein in search of a function. It is certainly involved in tissue iron mobilisation, since systemic iron loading is found in the tissues of patients with aceruloplasminaemia and other mutations of the ceruloplasmin gene.

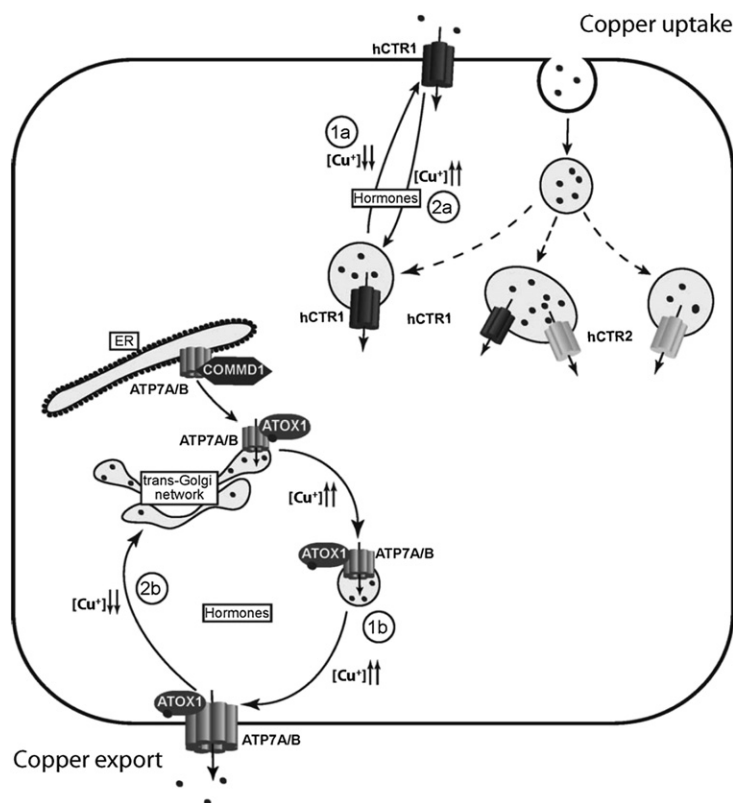


FIGURE 8.20 Regulation of cellular copper transport. (From van den Berghe & Klomp, 2010. Reproduced with permission from Springer Verlag.)

while in zinc-replete medium, they are largely present in intracellular organelles. In addition, zinc homeostasis is controlled at the transcriptional level by the zinc-responsive transcription factor MTF1, which protects cells against zinc toxicity by increasing the expression of zinc-binding metallothionein genes and also acting on a number of other zinc transporters. MTF1 can also be induced by copper, but this requires the presence of zinc-saturated metallothionein.

REFERENCES

- Andrews, S. C., Robinson, A. K., & Rodriguez-Quinones, F. (2003). Bacterial iron homeostasis. *FEMS Microbiol. Rev*, 27, 215–237.
- Blindauer, C. A. (2008). Zinc-handling in cyanobacteria: an update. *Chemistry & Biodiversity*, 5, 1990–2013.
- Boal, A. K., & Rosenzweig, A. C. (2009). Structural biology of copper trafficking. *Chemical Reviews*, 109, 4760–4779.
- Chiancone, E., & Ceci, P. (2010). The multifaceted capacity of Dps proteins to combat bacterial stress conditions: detoxification of iron and hydrogen peroxide and DNA binding. *Biochimica et Biophysica Acta*, 1800, 798–805.
- Cobine, P. A., Pierrel, F., & Winge, D. R. (2006). Copper trafficking to the mitochondrion and assembly of copper metalloenzymes. *Biochimica et Biophysica Acta*, 1763, 759–772.
- Crichton, R. R. (2009). *Inorganic biochemistry of iron metabolism: From molecular mechanisms to clinical consequences* (3rd ed.). Chichester: John Wiley and Sons.
- Eide, D. J. (2006). Zinc transporters and the cellular trafficking of zinc. *Biochimica et Biophysica Acta*, 1763, 711–722.
- Grotz, N., & Guerinot, M. L. (2006). Molecular aspects of Cu, Fe and Zn homeostasis in plants. *Biochimica et Biophysica Acta*, 1763, 595–608.

- Lee, J. W., & Helmann, J. D. (2007). Functional specialization within the Fur family of metalloregulators. *Biometals*, 20, 485–499.
- Lill, R., Dutkiewicz, R., Elsässer, H. P., Hausmann, A., Netz, D. J., Pierik, A. J., et al. (2006). Mechanisms of iron-sulfur protein maturation in mitochondria, cytosol and nucleus of eukaryotes. *Biochimica et Biophysica Acta*, 1763, 652–667.
- Massé, E., Salvail, H., Desnoyers, G., & Arguin, M. (2007). Small RNAs controlling iron metabolism. *Current Opinion in Microbiology*, 10, 140–145.
- Palmer, C. M., & Gueriot, M. L. (2009). Facing the challenges of Cu, Fe and Zn homeostasis in plants. *Nature Chemical Biology*, 5, 333–340.
- Pilon, M., Cohu, C. M., Ravet, K., Abdel-Ghany, S. E., & Gaymard, F. (2009). Essential transition metal homeostasis in plants. *Current Opinion in Plant Biology*, 12, 347–357.
- Richardson, D. R., Lane, D. J., Becker, E. M., Huang, M. L., Whitnall, M., Rahmanto, Y. S., Sheftel, A. D., & Ponka, P. (2010). Mitochondrial iron trafficking and the integration of iron metabolism between the mitochondrion and cytosol. *Proc Natl Acad Sci U S A*, 107, 10775–10782.
- Rouault, T. A. (2006). The role of iron regulatory proteins in mammalian iron homeostasis and disease. *Nature Chemical Biology*, 2, 406–414.
- Schmidt, W. (2003). Iron solutions: acquisition strategies and signaling pathways in plants. *Trends in Plant Science*, 8, 188–193.
- Solioz, M., Abicht, H. K., Mermod, M., & Mancini, S. (2010). Response of gram-positive bacteria to copper stress. *The Journal of Biological Inorganic Chemistry*, 15, 3–14.
- Sutak, R., Lesuisse, E., Tachezy, J., & Richardson, D. R. (2008). Crusade for iron: iron uptake in unicellular eukaryotes and its significance for virulence. *Trends in Microbiology*, 16, 261–268.
- van den Berghe, P. V., & Klomp, L. W. (2010). Posttranslational regulation of copper transporters. *Journal of Biological Inorganic Chemistry*, 15, 37–46.
- Vaulont, S., Lou, D.-Q., Viatte, L., & Kahn, A. (2005). Of mice and men: the iron age. *The Journal of Clinical Investigation*, 115, 2079–2082.
- Walker, E. L., & Connolly, E. L. (2008). Time to pump iron: iron-deficiency-signalling mechanisms of higher plants. *Current Opinion in Plant Biology*, 11, 530–535.
- Wallerand, M. L., Leibold, E. A., & Eisenstein, R. S. (2006). Molecular control of vertebrate iron homeostasis by iron regulatory proteins. *Biochimica et Biophysica Acta*, 1763, 668–689.
- Watt, R. K., Hilton, R. J., & Graff, D. M. (2010). Oxido-reduction is not the only mechanism allowing ions to traverse the ferritin protein shell. *Biochimica et Biophysica Acta*, 1800, 745–759.

Sodium and Potassium – Channels and Pumps

Introduction – Transport Across Membranes	177
Sodium <i>versus</i> Potassium	178
Potassium Channels	180
Sodium Channels	184
The Sodium–Potassium ATPase	184
Active Transport Driven by Na^+ Gradients	187
Sodium/Proton Exchangers	190
Other Roles of Intracellular K^+	191

INTRODUCTION – TRANSPORT ACROSS MEMBRANES

Before examining the important roles of the alkali metals sodium and potassium, we should briefly review how ions are transported across membranes. As we pointed out in Chapter 3, the phospholipid bilayer of biological membranes is essentially impermeable to polar molecules and to ions – the permeabilities of Na^+ and K^+ are of the order of 10^{-12} cm/sec – the corresponding value for H_2O is around 10^{-2} . So, simple diffusion would not suffice to explain the msec transmission of nerve impulses. Transport across membranes is conferred by two classes of membrane proteins, namely channels and pumps. Channels allow ions to flow down a concentration gradient by a process known as passive transport or facilitated diffusion. Of course, channels cannot remain open all of the time, and so they are usually **gated**, which simply means that, like regular garden gates, they usually remain shut, and can only be opened, either by the binding of a ligand (**ligand-gated**) or by changes in the membrane potential (**voltage-gated**). **Ligand-gated** channels, like the acetylcholine receptors in post-synaptic membranes, are opened by the binding of the neurotransmitter acetylcholine, whereas the **voltage-gated** sodium and potassium channels, which mediate the action potentials in neuronal axons described below, are opened by membrane depolarisation.

In contrast, pumps use energy, in the form of ATP or light, to drive the unfavourable uphill transport of ions or molecules against a concentration gradient; in other words, they are involved in active transport. There are two types of ATP-driven pumps, so-called P-type ATPases and ABC (ATP-binding cassette) transporters, both of which use conformational changes induced by ATP binding and its subsequent hydrolysis to transport ions across the membrane. The $(\text{Na}^+/\text{K}^+)\text{-ATPase}$ described below is one of the P-type ATPases, which achieves uphill exchange of cytoplasmic Na^+ ions for extracellular K^+ ions using ATP-mediated phosphorylation, followed by autodephosphorylation, to drive conformational changes that allow access to the binding sites of the pump from only one side of the membrane at a time. Another mechanism of active transport, which uses the electrochemical gradient of one ion to drive the counter-transport of another, will be illustrated by the Na^+/H^+ exchanger, crucial among other things for the control of intracellular pH. Yet another example, discussed in Chapter 11, is the $\text{Na}^+/\text{Ca}^{2+}$ exchanger, which plays an important role in removing Ca^{2+} from cells.

SODIUM VERSUS POTASSIUM

Sodium and potassium are relatively abundant in the earth's crust, although sodium is much more prevalent in seawater. The Na^+ and K^+ content in the average man represent about 1.4 g/kg and 2.0 g/kg, making them among the most important of metal ions in terms of concentration. However, their distribution is quite different. Whereas in most mammalian cells, 98% of K^+ is intracellular, for Na^+ the situation is the reverse. This concentration differential ensures a number of major biological processes, such as cellular osmotic balance, signal transduction, and neurotransmission. It is maintained by the $(\text{Na}^+ - \text{K}^+) - \text{ATPase}$, which we will discuss below. However, despite the presence of only 2% of total body K^+ outside of cells, this extracellular K^+ concentration plays a major role in maintaining the cellular membrane resting potential. Fluxes of these alkali metal ions play a crucial role in the transmission of nervous impulses both within the brain and from the brain to other parts of the body (Chapter 20). The opening and closing of gated ion channels (**gated channels**), which are closed in the resting state, and which open in response to changes in membrane potential, generate electrochemical gradients across the plasma membranes of neurons. A nerve impulse is constituted by a wave of transient depolarisation/re-polarisation of membranes which traverses the nerve cell, and is designated an action potential. **Hodgkin and Huxley (1952)** demonstrated that a microelectrode implanted into an axon (the long process emanating from the body of a nerve cell) can record an action potential (**Figure 9.1(a)**). In the first ~ 0.5 ms, the membrane potential increases from around -60 mV to about $+30$ mV, followed by a rapid repolarisation, which overshoots the resting potential (hyperpolarisation) before slowly recovering. The action potential results from a rapid and transient increase in Na^+ permeability followed by a more prolonged increase in K^+ permeability (**Figure 9.1(b)**). The opening and closing of these gated Na^+ and K^+ ion channels in the axonal membranes create the action potentials (essentially electrochemical gradients) across these membranes, which allows information transfer and also regulates cellular function.

The regulation of the flow of ions across cell membranes is absolutely essential for the functioning of living cells. Because of the hydrophobicity of cellular membranes (as we saw earlier) the energetically driven preference of ionic species such as Na^+ , K^+ , Cl^- , H^+ , and Ca^{2+} to cross, never mind to find themselves preferentially on one side or other of a biological membrane, would be impossible. Without ionic gradients, which maintain high concentrations of K^+ within the cell and low concentrations of Na^+ , cells would not be able to carry out their normal metabolic activities. This means, in simplistic terms, that some molecular machines must be able to distinguish between Na^+ and K^+ ions (presumably unhydrated, since the degree of hydration could make for difficulties in discrimination). So, before even beginning a discussion of 'active' transport proteins, whether ion pumps or ion exchangers, we ask the question how do potential transporters distinguish between these two closely related cations?

We begin by a reminder that studies over the last 50 years of synthetic and naturally occurring ion-binding small molecules (host/guest chemistry with ions) have established the basic rules of ion selectivity within small molecules. Two major factors are important in ion selectivity – the atomic composition and the stereochemistry (e.g., the size) of the binding site. Using synthetic chemistry, molecules have been created of a given class with selectivity favouring Li^+ (radius 0.60 Å), Na^+ (radius 0.95 Å), K^+ (radius 1.33 Å), and Rb^+ (radius 1.48 Å) by simply adjusting the cavity size to match the ion (**Dietrich, 1985**).¹

Now that we have high-resolution crystal structures of membrane transport proteins, we can begin to understand how ion selectivity is accomplished. In **Figure 9.2** the Na^+ -selective binding sites in the Na^+ -dependent leucine transporter LeuT and the K^+ -selective binding sites in the K^+ channel provide a direct comparison of selectivity for Na^+ - and K^+ .

LeuT transports leucine and Na^+ across the cell membrane using the energy of the Na^+ gradient to pump leucine into the cell. The structure (**Figure 9.2(a)**) shows a leucine and two Na^+ ions bound deep inside the protein,

1. The author remarked that this was particularly easy for the alkali metals of group **1A** because the differences in ionic radius are greatest (0.35 Å).

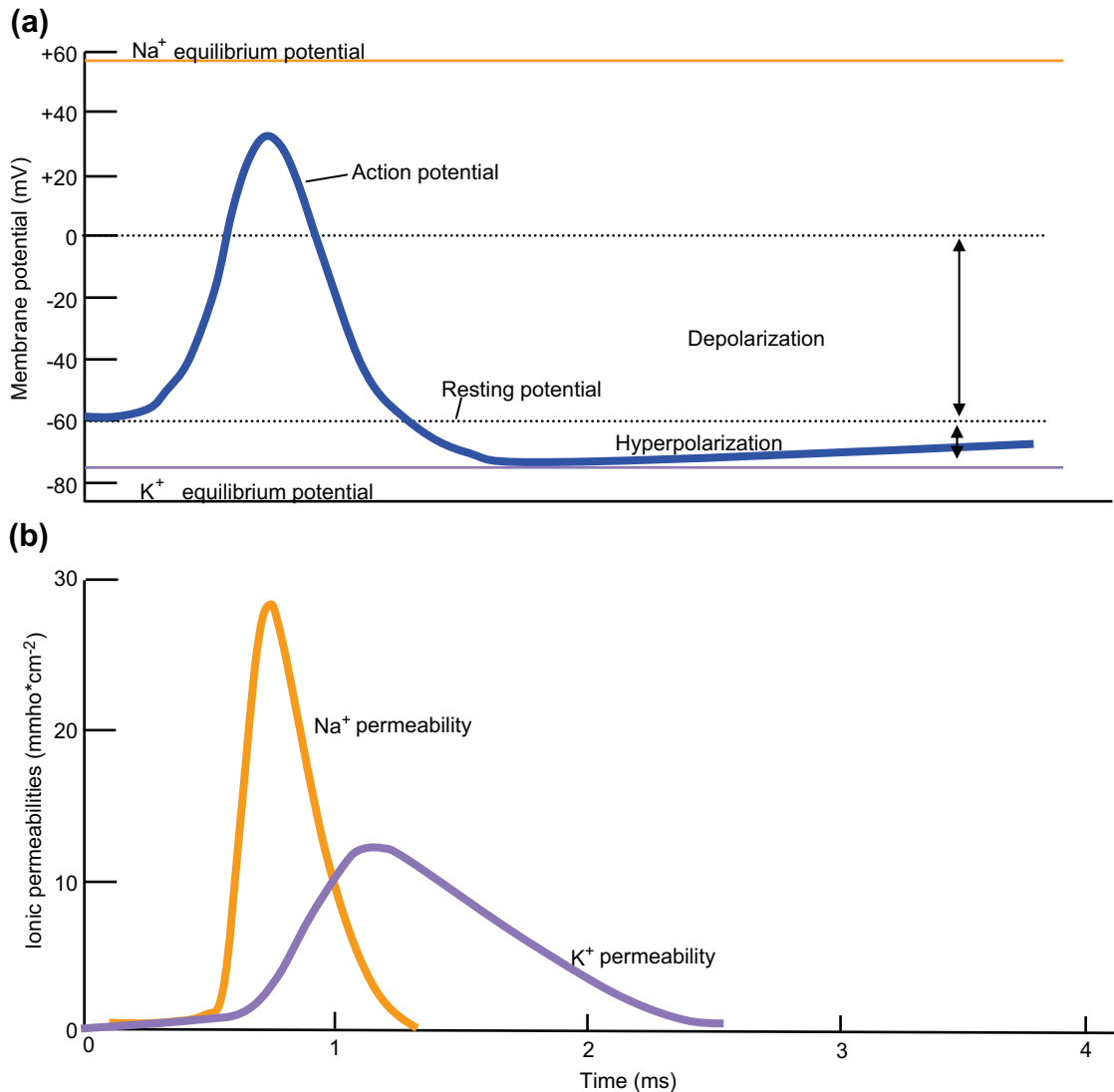


FIGURE 9.1 Time course of an action potential.

partway across the membrane. The Na⁺ ions are completely dehydrated. One of the sites has six oxygen atoms in direct contact with the ion, five of which have only a partial negative charge and one has a full negative charge on a carboxylate group. The second site contains five oxygen atoms all of which have only a partial negative charge. Two important features of these binding sites are (i) the binding sites consist of oxygen atoms in direct contact with Na⁺ — a formal negative charge can occur (site 1) but is not essential (site 2) — and (ii) the size of the binding site cavity formed by the oxygen atoms is a good match to the Na⁺ ion, with a mean Na⁺—O distance for both sites combined of 2.28 Å.

We will describe the K⁺ channels which conduct K⁺ ions selectively across the cell membrane, down the electrochemical gradient in greater detail below. The K⁺ channel (Figure 9.2(b)) contains four K⁺-binding sites in a row, forming a selectivity filter. In each of these sites, the K⁺ ion is dehydrated and interacts with eight

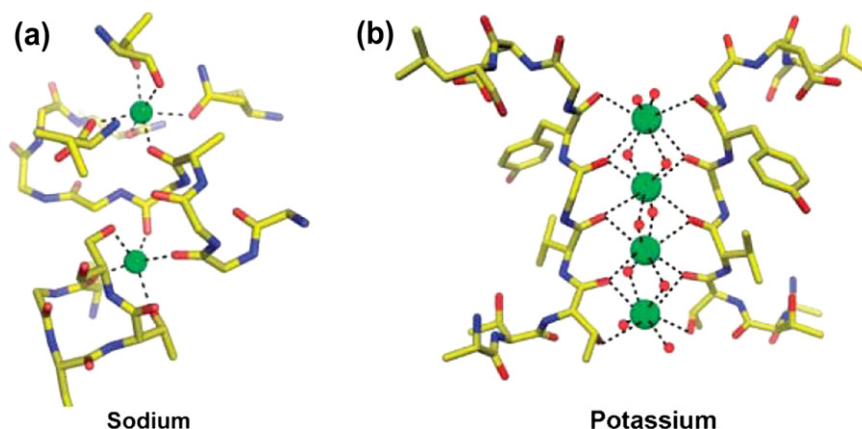


FIGURE 9.2 Na^+ - and K^+ -selective binding sites in transport proteins. (a) Two Na^+ binding sites in the LeuT Na^+ -dependent pump (PDB code 2A65). (b) Four K^+ binding sites in the KcsA K^+ channel (PDB code 1K4C). (From Gouaux & MacKinnon, 2005. Reproduced with permission from John Wiley & Sons.)

partial-charge-bearing oxygen atoms. The size of the cavity formed by the selectivity filter sites is a good match to the K^+ ion, with a mean $\text{K}^+\text{--O}$ distance of 2.84 Å. The greater number of oxygen atoms forming the K^+ -binding sites (eight oxygen atoms) compared to that of the Na^+ sites (five or six oxygen atoms) is a simple geometric consequence of the larger radius of K^+ , which allows a greater number of oxygen atoms to surround the ion.

What the comparison of LeuT and the K^+ channel tells us about alkali metal ion selectivity in transport proteins is the following. The Na^+ and K^+ sites both contain oxygen atoms, mostly the kind with partial negative charges. This agrees well with the rules learned from host/guest chemistry with ions. There is a tendency for Na^+ sites to contain one formal charge, attributable to the smaller radius and higher charge density of the Na^+ ion, although a formal charge is not essential. What appears as the most important factor distinguishing Na^+ and K^+ sites is the size of the cavity formed by the binding site. This suggests that the essence of alkali metal cation selectivity is similar to that in ion binding by small molecules: The protein selects for a particular ion, Na^+ or K^+ , by providing an oxygen-lined-binding site of the appropriate cavity size.

POTASSIUM CHANNELS

K^+ channels selectively transport K^+ across membranes, hyperpolarise cells, set membrane potentials, and control the duration of action potentials, among a myriad of other functions. They use diverse forms of gating, but they all have very similar ion permeabilities. All K^+ channels show a selectivity sequence of $\text{K}^+ \sim \text{Rb}^+ > \text{Cs}^+$, whereas the transport of the smallest alkali metal ions Na^+ and Li^+ is very slow – typically the permeability for K^+ is at least 10^4 that of Na^+ . The determination of the X-ray structure of the K^+ ion channel has allowed us to understand how it selectively filters completely dehydrated K^+ ions, but not the smaller Na^+ ions. Not only does this molecular filter select the ions to be transported, but also the electrostatic repulsion between K^+ ions, which pass through this molecular filter in Indian file, provides the force to drive the K^+ ions rapidly through the channel at a rate of $10^7\text{--}10^8$ per second (reviewed in Doyle et al., 1998; MacKinnon, 2004).²

The first voltage-gated potassium channel to be identified was the gene encoding the *Shaker* mutation³ in the fruit fly *Drosophila*. Figure 9.3 presents the first pictures of the tetrameric Shaker K^+ channel with

2. The 2003 Nobel prize for chemistry was awarded to Rod MacKinnon for his pioneering work in this area.

3. These mutant fruit flies shake violently when anaesthetised with ether.

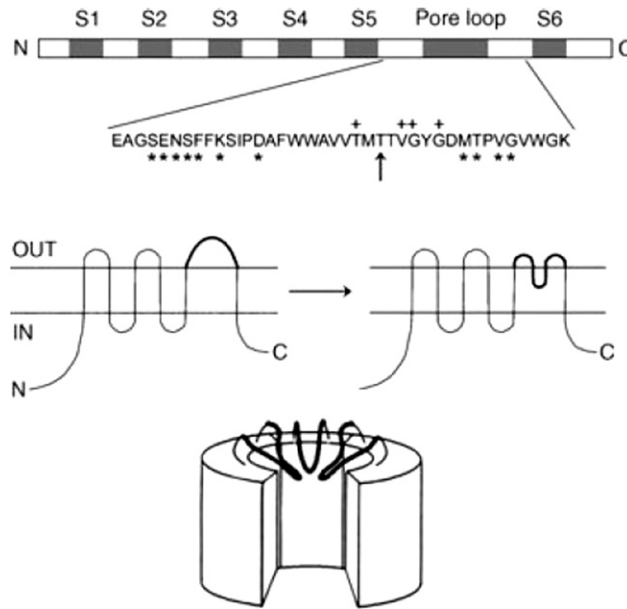


FIGURE 9.3 One of the first pictures of a tetrameric K^+ channel with a selectivity filter made of pore loops. A linear representation of a Shaker K^+ channel subunit on top shows shaded hydrophobic segments S1–S6 and a region designated the pore loop. A partial amino acid sequence from the Shaker K^+ channel pore loop highlights amino acids shown to interact with extracellular scorpion toxins (\square), intracellular tetraethylammonium (\uparrow), and K^+ ions (+). The pore loop was proposed to reach into the membrane (middle) and form a selectivity filter at the centre of four subunits (bottom). (From MacKinnon, 2004. Reproduced with permission from John Wiley & Sons.)

a selectivity filter made of pore loops. A linear representation of a Shaker K^+ channel subunit on top shows shaded hydrophobic segments S1–S6 and a region designated the pore loop. A partial amino acid sequence from the Shaker K^+ channel pore loop highlights amino acids shown to interact with the extracellular inhibitor scorpion toxins (\square), the intracellular tetraethylammonium (\uparrow), and K^+ ions (+). The pore loop was proposed to reach into the membrane (middle) and form a selectivity filter at the centre of four subunits (bottom).

The first structure determination of a K^+ channel was the bacterial K^+ channel KcsA from *Streptomyces lividans*, which has a simple topology with only two membrane-spanning segments per subunit, corresponding to the Shaker K^+ channel without the S1–S4 segments. Currently, we have the structures of a number of K^+ channel-pH-dependent bacterial K^+ channels, voltage-gated and calcium-gated K^+ channels from bacteria, and voltage-gated mammalian K^+ channels. What is most striking is that they all have a similar architecture. They are all tetramers with four-fold symmetry about the central K^+ -conducting pore. Based on hydrophobicity analysis there are two closely related families of K^+ channels, those containing two membrane-spanning segments per subunit, such as KcsA, and those containing six, like the *Drosophila* and the vertebrate voltage-gated K^+ channels. In the latter case, the last two transmembrane helices, S5 and S6, together with the P-loop which connects them, constitute the pore itself. Several other families of ion channels have similar architectures, including the calcium-activated K^+ channels. The two membrane-spanning families include the inwardly rectifying K^+ channels, and some bacterial K^+ channels. They are made up of four subunits, each of which has only two transmembrane segments. The analogous M1 and M2 segments and pore loop form the complete transmembrane structure of the two transmembrane K^+ channels. Sequence homology is very high between the two families in the channel region, particularly in the pore region itself. K^+ channels allow some other monovalent cations through (but not Na^+), do not allow the passage of anions, and are blocked by divalent cations.

The KcsA K^+ channel has what is often referred to as an ‘inverted tepee’⁴ structural arrangement, nearly 45 Å long, and made up of three distinct regions of variable width. On the cytoplasmic side (Figure 9.4), it starts with

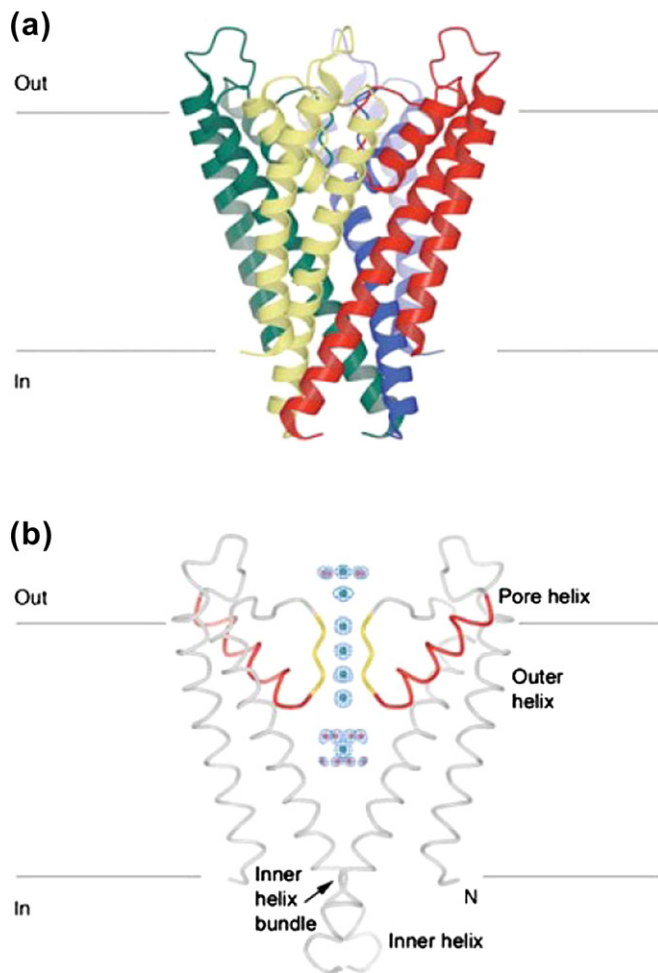


FIGURE 9.4 (a) A ribbon representation of the KcsA K^+ channel with its four subunits coloured differently. The channel is oriented with the extracellular solution on top. (b) The KcsA K^+ channel with front and back subunits removed. The pore helices are shown in red and selectivity filter in yellow; the electron density along the ion pathway is shown in a blue mesh. The outer and inner helices correspond to S5 and S6 in Figure 9.3. (From Mackinnon, 2004. Reproduced with permission from John Wiley & Sons.)

a channel (the internal pore), 0.6 nm wide by 1.8 nm long, which has four negatively charged side chains at its entrance (perhaps a precaution to prevent anions entering the channel). The central cavity is wider, ~1 nm in diameter and contains around 50 water molecules, enabling a hydrated K^+ ion to move through the hydrophobic interior of the membrane. The third part exposed to the extracellular solution, termed the selectivity filter, constituted by the P loops, is only about 0.3 nm wide, such that only an unhydrated K^+ ion can pass through. The selectivity filter, 1.2 nm in length, consists of four K^+ -binding sites in a row. Each of these sites can bind a dehydrated K^+ ion, which interacts with eight carbonyl oxygens (main chain carbonyl or side-chain hydroxyl atoms) of a highly conserved TVGYG amino acid sequence (Figure 9.5). Mutations in this sequence lead

4. The wigwam of American Indians.

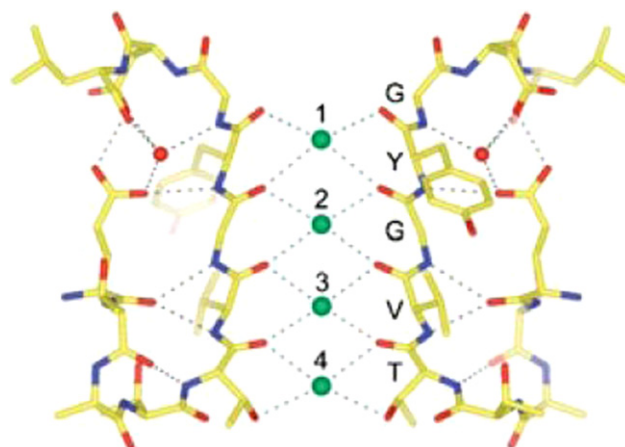


FIGURE 9.5 Detailed structure of the K^+ -selectivity filter (two subunits). Oxygen atoms (red) coordinate K^+ ions (green spheres) at positions 1–4 from the extracellular side. Single letter amino acid code identifies select amino acids of the signature sequence (yellow: carbon, blue: nitrogen, and red: oxygen). Green and gray dashed lines show $O \cdots K^+$ and hydrogen-bonding interactions, respectively. (From MacKinnon, 2004. Reproduced with permission from John Wiley & Sons.)

to disruption of the ability of the channel to distinguish between K^+ ions and Na^+ ions. From the relative electron density of the sites, it is clear that each site is occupied by K^+ only half of the time; in other words, that at any given time only two of the binding sites are occupied, with water molecules in the intermediate sites. Thus, two K^+ ions permanently occupy the sites 1 and 3 or 2 and 4, with a water molecule sandwiched between them

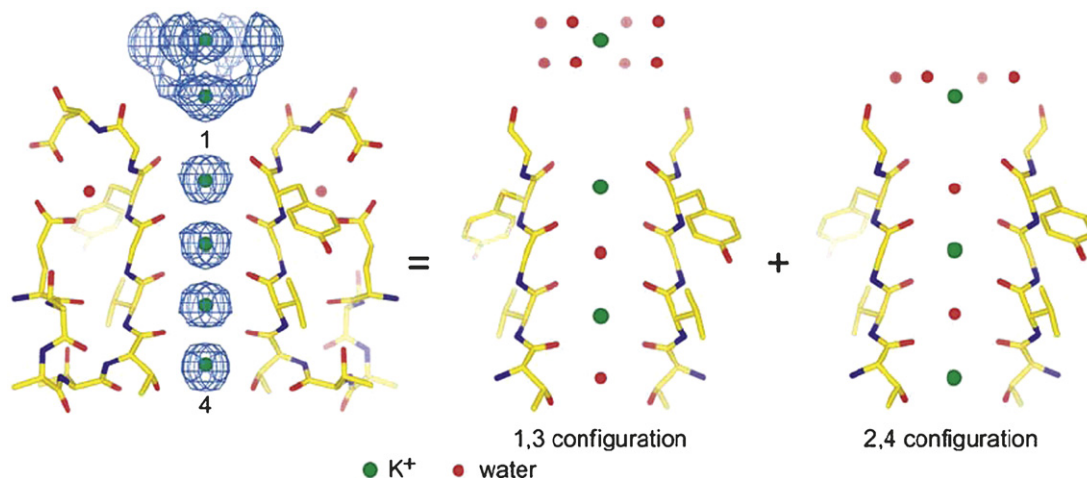


FIGURE 9.6 Two K^+ ions in the selectivity filter are hypothesised to exist predominantly in the two specific configurations 1,3 and 2,4. (From MacKinnon, 2004. Reproduced with permission from John Wiley & Sons.)

(Figure 9.6). The X-ray structures also give support to a previously suggested ‘knock-on’ mechanism whereby K^+ ions can traverse the channel. Additional K^+ ions coordinated by eight water molecules are observed at the extracellular mouth of the channel and in the central cavity. When one of these ions enters either end of the filter, it displaces the equilibrium of the two K^+ ions already resident, with the consequence that the column of K^+ ions moves along until one of the ions is ejected, and the new K^+ ion takes its place in the filter.

We saw earlier how the 3-D structure of a two transmembrane bacterial K^+ channel, KcsA, analogous to the inwardly rectifying K^+ channels, reveals an ‘inverted tepee’ arrangement around a central pore, with the narrow outer mouth of the pore formed by the pore loop (Figure 9.7). Information on how the pore might be opened comes

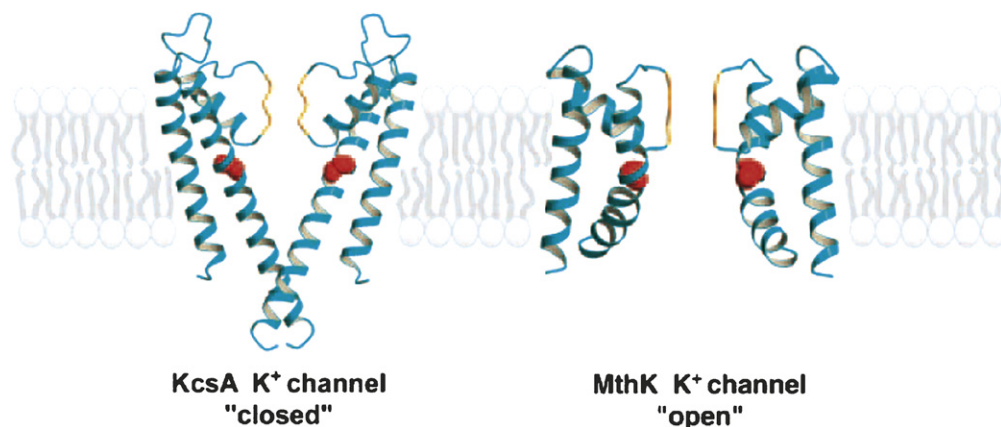


FIGURE 9.7 Structures of potassium channels in open and closed conformations. The selectivity filter is orange, and the conserved glycine residue, which is thought to be critical for the bending of the M2 helix in the open conformation, is in red. (From Yu, Yarov-Yarovoy, Gutman, & Catterall, 2005. Reproduced with permission of Blackwell Publishing Ltd.)

from the structure of a bacterial 2TM calcium-activated K^+ channel, MthK (Figure 9.7), analysed in its calcium-bound, presumably open, form. The M2 helices are bent at a highly conserved glycine residue, and this bend appears to open the intracellular mouth of the pore sufficiently to allow permeation of ions.

SODIUM CHANNELS

The sodium channels (Catterall, 2000) consist of a highly processed α subunit (260 kDa), associated with auxiliary β subunits. The pore-forming α -subunit is sufficient for functional expression, but the kinetics and voltage dependence of channel gating are modified by the β subunits. The transmembrane organisation is shown in Figure 9.8. The α -subunit is organised in four homologous domains (I–IV), each consisting of six transmembrane α helices (S1–S6) and an additional pore loop located between the S5 and S6 helices, each similar to the individual subunits of the 6TM K^+ channels. The pore loops line the outer, narrow entry to the pore, while the S5 and S6 helices line the inner, wider exit from the pore. The S4 segments in each domain contain positively charged amino acids in every third position. These residues serve as gating charges and move across the membrane to initiate channel activation in response to depolarisation of the membrane. A short intracellular loop connecting the domains III and IV serves as the inactivation gate, folding into the channel structure and blocking the pore from the inside during sustained depolarisation of the membrane. It contains an Ile–Phe–Met–Thr (IFMT) motif, which is crucial for inactivation. The circles in the re-entrant loops in each of the four domains represent the amino acids that form the ion selectivity filter: the outer rings have the sequence EEDD and the inner rings DEKA.

THE SODIUM–POTASSIUM ATPASE

Mammalian cells maintain a lower concentration of Na^+ (around 12 mM) and a higher concentration of K^+ (around 140 mM) than in the surrounding extracellular medium (respectively 145 mM and 4 mM). The Na^+ – K^+ –ATPase which maintains high intracellular K^+ and low intracellular Na^+ is localised in the plasma membrane, and belongs to the family of P-type ATPases. Other members of the family in eukaryotes are the sarcoplasmic

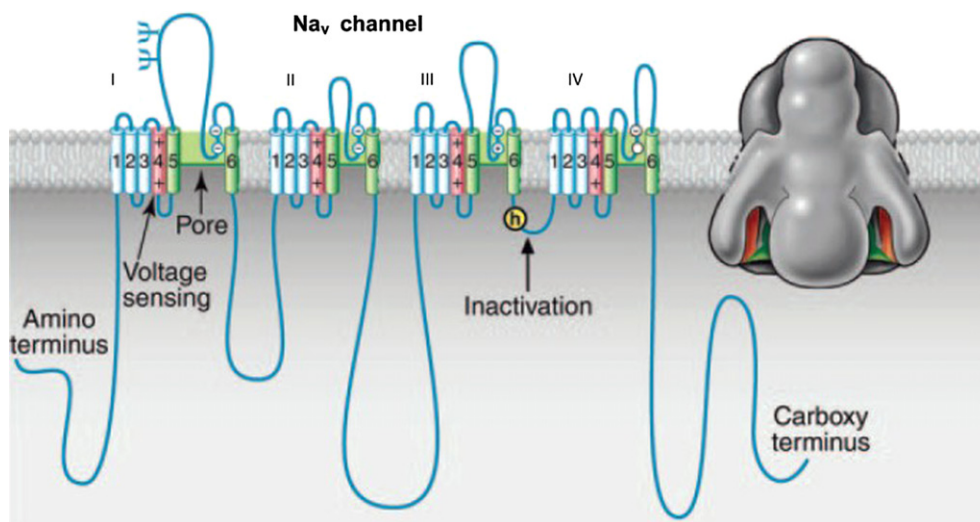
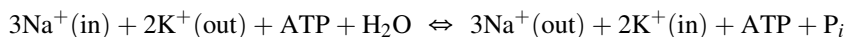


FIGURE 9.8 Transmembrane organisation of sodium channel α -subunit. Right 3-D structure of the α -subunit at 0.2 nm resolution. (From Yu *et al.*, 2005. Reproduced with permission of Blackwell Publishing Ltd.)

reticulum and plasma membrane Ca^{2+} ATPases, gastric H^+ , K^+ -ATPases, and, in plants, the H^+ -ATPases. The overall reaction catalysed is



This results in the extrusion of three positive charges for every two which enter the cell, resulting in a transmembrane potential of 50–70 mV, and has enormous physiological significance. More than one-third of the ATP utilised by resting mammalian cells is used to maintain the intracellular $\text{Na}^+ - \text{K}^+$ gradient (in nerve cells this can rise to up to 70%), which controls cell volume, allows neurons and muscle cells to be electrically excitable, and also drives the active transport of sugars and of amino acids (see later).

The $\text{Na}^+ - \text{K}^+$ -ATPase achieves the thermodynamically unfavourable uphill exchange of cytoplasmic Na^+ ions for extracellular K^+ ions by using ATP-mediated phosphorylation, followed by autodephosphorylation, to power conformational changes that allow ion access to the binding sites of the pump from only one side of the membrane at a time. How this is achieved is still not entirely clear, but a number of experimental observations can be put together to provide a plausible mechanism. Key among these is that the ATPase is phosphorylated by ATP in the presence of Na^+ , and that the resulting aspartyl phosphate residue is only dephosphorylated in the presence of K^+ . This immediately suggests, as outlined in Figure 9.9, that the enzyme may exist in two distinct conformations, E_1 and E_2 , which differ not only in their conformation but also in their catalytic activity and their ligand specificity. Indeed, this cation exchange is accomplished by conformational changes linked to phosphorylation and dephosphorylation of the pump, which permit strictly alternating access to its binding sites. This is from the extracellular side in the phosphorylated state in the $E_2\text{-P}$ state, but from the cytoplasm in the dephosphorylated state (E_1). The E_1 form faces toward the inside of the plasma membrane, has a high-affinity site for Na^+ , and reacts with ATP to form the “high-energy” aspartyl phosphate intermediate $E_1 \sim \text{P.3Na}^+$. In relaxing to its “low-energy” conformation $E_2\text{-P}$, the bound Na^+ is released. The outward-facing $E_2\text{-P}$, which has a high affinity for K^+ , binds 2K^+ , and the aspartyl phosphate group is hydrolysed to give $E_2.2\text{K}^+$. This form then changes conformation to the E_1 form, releasing its 2K^+ inside the cell, and allowing the cycle to recommence. The outcome of this is to couple ATP hydrolysis with the vectorial transport of Na^+ and K^+ across the plasma membrane. The inhibition of the $(\text{Na}^+ - \text{K}^+) \text{-ATPase}$ by cardiac glycosides such as digitalis (an extract of foxglove leaves), which blocks the

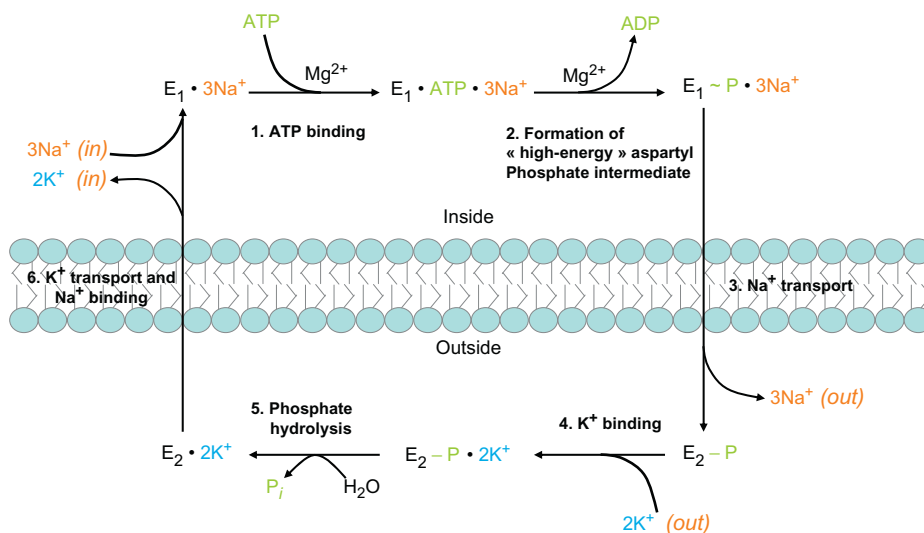


FIGURE 9.9 A model for the active transport of Na^+ and K^+ by the $\text{Na}^+-\text{K}^+-\text{ATPase}$. (Adapted from Voet & Voet, 2004.)

dephosphorylation of the $\text{E}_2\text{-P}$ form of the enzyme, is the basis for a number of steroid drugs which are commonly prescribed for the treatment of congestive heart failure.

The structures of a number of P-type ATPases, including the $\text{Na}^+-\text{K}^+-\text{ATPase}$, have been determined. They have a common overall domain organisation of the main catalytic (α -) subunit (Figure 9.10): six to twelve

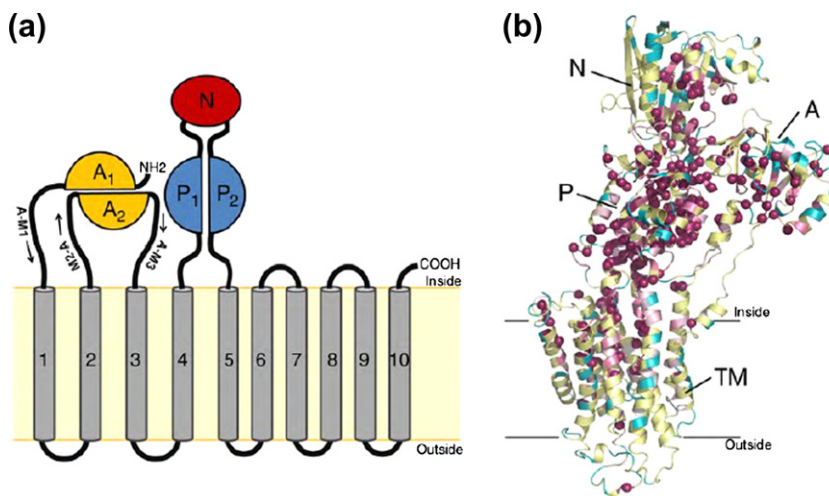


FIGURE 9.10 PDB structures and conservation of P-type ATPases. (a) Topology diagram of a typical P-type ATPase α -subunit with 10 TM helices. (b) Sequence conservation among human P-type ATPases. Highly conserved residues (magenta spheres) cluster in the P-domain. (From Bubltz *et al.*, 2010. Reproduced with permission from Elsevier.)

α -helices which make up the ion transport domain and three cytoplasmic domains, the N-domain (nucleotide binding), P-domain (phosphorylation), and A-domain (actuator), which confer the ATP hydrolysing activity. The N-domain positions the γ -phosphoryl of ATP for nucleophilic attack, a conserved Asp in the P-domain accepts the phosphoryl group and forms a high-energy aspartyl-phosphate, while a Glu residue in the A domain positions a water molecule for subsequent hydrolysis, which leads to release of the phosphoryl group. The overall structures

and ion-binding site architecture of four P-type ATPases, rabbit sarcoplasmic reticulum Ca^{2+} -ATPase (SERCA), pig Na^{+} - K^{+} -ATPase, human K^{+} , H^{+} -ATPase (modeled on the Na^{+} - K^{+} -ATPase structure), and plant H^{+} -ATPase are presented in Figure 9.11.

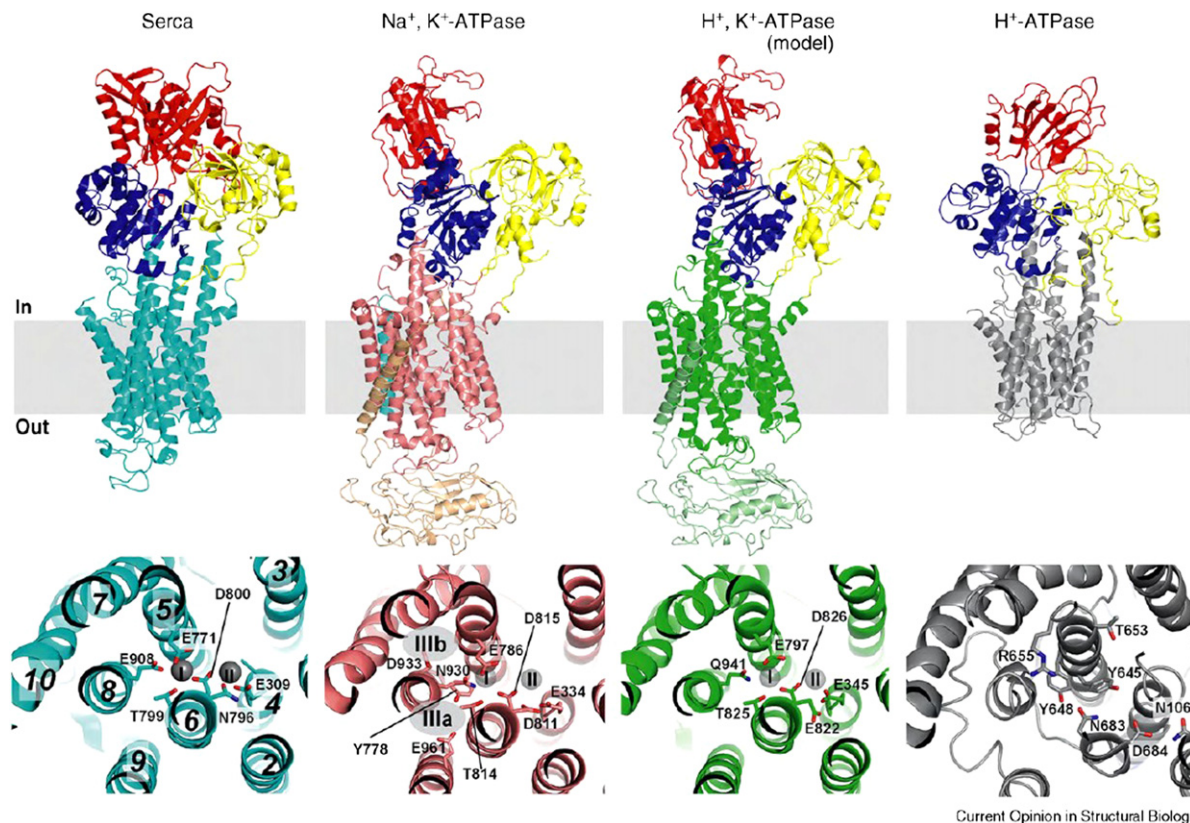


FIGURE 9.11 Overall structures and ion-binding site architectures of P-type ATPases. The upper panel depicts rabbit SERCA (E1 PDB entry 1T5S), pig Na^{+} - K^{+} -ATPase ($E_2\text{:P}_i$, PDB entry 3KDP), a homology model of the human gastric H^{+} , K^{+} -ATPase based on the Na^{+} - K^{+} -ATPase structure (3KDP), and plant H^{+} -ATPase AHA2 (E1, PDB entry 3B8C). N-, P-, and A-domains are coloured red, blue, and yellow, respectively; the β -subunit and γ -subunit of Na^{+} - K^{+} -ATPase wheat and cyan, respectively, and the β -subunit of H^{+} , K^{+} -ATPase pale green. The ion-binding sites are viewed approximately perpendicular to the membrane plane from the extracytoplasmic side, in the E1 state (human Na^{+} - K^{+} -ATPase and H^{+} , K^{+} -ATPase modeled on SERCA E1 (1T5S)). Ion liganding residues are shown as sticks, transmembrane helices and calcium ions in SERCA are indicated by numbers and grey spheres, respectively, and the sites superposed as transparent spheres onto the Na^{+} - K^{+} -ATPase and H^{+} , K^{+} -ATPase models. Putative binding sites for the third sodium ion in the Na^{+} - K^{+} -ATPase are indicated as gray ellipses. (From *Bublitz, Poulsen, Morth, & Nissen, 2010. Reproduced with permission from Elsevier.*)

ACTIVE TRANSPORT DRIVEN BY Na^{+} GRADIENTS

Many transmembrane transporter proteins, termed secondary transporters, use the discharge of an ionic gradient to power the ‘uphill’ translocation of a solute molecule across membranes. Coupling solute movement to ion transport enables these secondary transporters to concentrate solutes by a factor of 10^6 with a solute flux 10^5 faster than by simple diffusion. We have already encountered the co-transport of leucine and Na^{+} by LeuT, but there are many other examples. Sugars and amino acids can be transported into cells by Na^{+} -dependent symports. Dietary glucose is concentrated in the epithelial cells of the small intestine by a Na^{+} -dependent symport, and is then

transported out of the cells into the circulation by a passive glucose uniport situated on the capillary side of the cell (Figure 9.12). For this system to continue functioning, ATP hydrolysis, which maintains the intra-cellular Na^+ concentration through the (Na^+-K^+) -ATPase, is absolutely required.

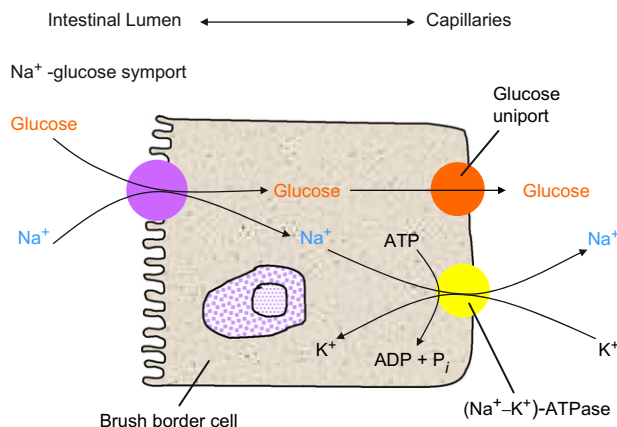


FIGURE 9.12 Epithelial brush border cells of the small intestine concentrate glucose from the intestinal lumen in symport with Na^+ : this is driven by the Na^+-K^+ -ATPase located on the capillary side of the cell. The glucose is then exported out of the brush border cell by a passive uniport system. (Adapted from Voet & Voet, 2004.)

Glutamate transporters, also referred to as excitatory amino acid transporters (EAATs), clear synaptically released glutamate from the extracellular space, thus ensuring the precise control of excitatory synaptic transmission. In addition, excessive extracellular concentrations of glutamate can be neurotoxic and the efficient removal of glutamate limits pathological conditions associated with excitotoxic cell death. The transport cycle and stoichiometry of EAATs, of which five mammalian isoforms have been characterised, is presented in Figure 9.13.

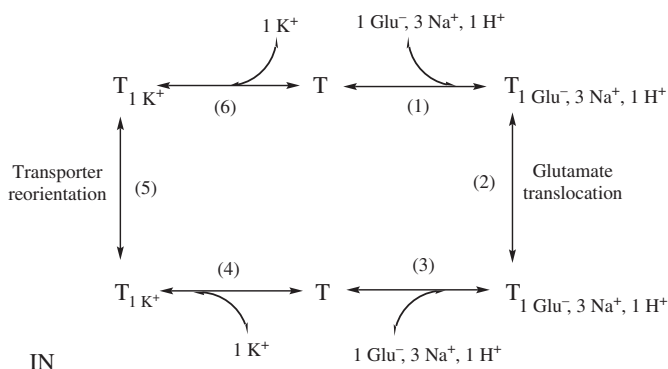


FIGURE 9.13 Transport cycle and stoichiometry of excitatory amino acid transporters (EAATs). Simplified state diagram of the EAAT transport cycle. After glutamate and coupled ions (step 1) bind to the transporter (T), they are translocated (step 2) and released into the cell cytosol (step 3). Next K^+ binds from the intracellular side (step 4) and reorients the substrate-free transporter (step 5). K^+ is released outside the cell (step 6). (From Jiang & Amara, 2011. Reproduced with permission from Elsevier.)

After glutamate and coupled ions bind to the transporter, they are translocated and released into the cell cytosol. Next, K^+ binds from the intracellular side and reorients the substrate-free transporter, and finally K^+ is released outside the cell.

Secondary active transporters, including EAATs, are thought to function through an alternating access mechanism, in which the substrate-binding site is alternatively accessible from the extracellular and intracellular sides through a process that depends on one or more conformational changes. The determination of a number of crystal structures of the archeal glutamate transporter orthologue Glt_{Ph} from *Pyrococcus horikoshii* has enabled us to form a general picture of how EAATs transport glutamate. Glt_{Ph} exists as a trimer comprised of three identical subunits in the crystal. Each protomer contains eight TM domains and two re-entrant loops (Figure 9.14). The first six TM domains (TM1–6)

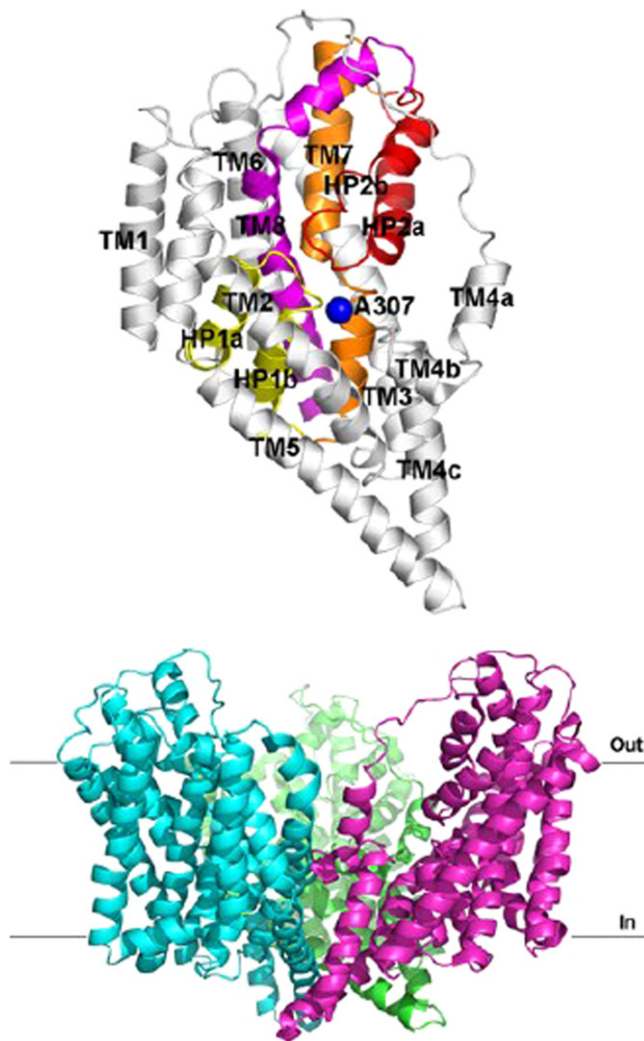


FIGURE 9.14 (D) Cartoon representation of the Glt_{Ph} protomer viewed in the plane of the membrane. Transmembrane domain s1-6 coloured in gray form a scaffold that holds the core translocation domain comprised of HP1 (yellow), TM7 (orange), HP2 (red), and TM8 (magenta). Residue A307 in Glt_{Ph} is shown as a blue sphere in the Glt_{Ph} protomer (D). (E) View of a Glt_{Ph} trimer parallel to the membrane. Subunits in the trimer are coloured in green, magenta, or cyan. (From Jiang & Amara, 2011. Reproduced with permission from Elsevier.)

form a scaffold surrounding a C-terminal core domain that contains structural elements required for the transport mechanisms. This C-terminal translocation core domain includes two opposite-facing helical hairpins (HP1 and HP2), which have been proposed to act as the inner and outer doors of the transporter, a seventh TM helix interrupted by

a β -linker and an amphipathic helix, TM8, in the crystal. The first Glt_{ph} structure to be determined with the substrate bound (PDB ID 1XFH) represents an occluded state, in which both inner and outer gates are closed (Figure 9.15(b)).

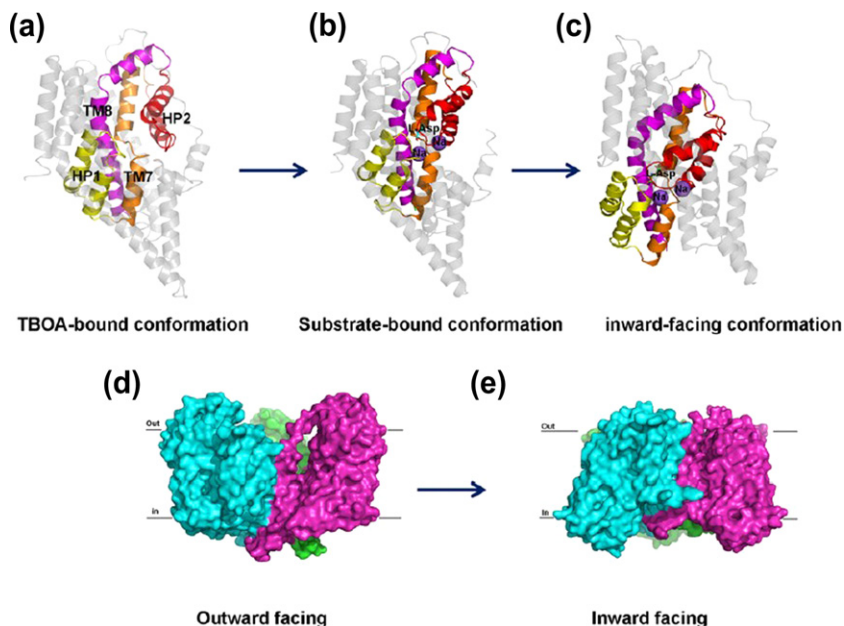


FIGURE 9.15 Mechanisms of substrate transport. (a) The TBOA-bound Glt_{ph} structure (PDB ID 2NWW) showing HP2 displaced from the substrate-binding site (TBOA is removed from the structure for clarity). (b) The substrate-bound Glt_{ph} structure (PDB ID 2NWX) showing the closed HP2 with two sodium ions and the bound substrate, L-aspartate. (c) The inward-facing Glt_{ph} structure (PDB ID 3KBC) in which the whole C-terminal domain moves toward the cytoplasm. (d) Surface representation of the outward-facing Glt_{ph} before the core domain moves into the cytoplasm. (e) Surface representation of the inward-facing Glt_{ph}. The three protomers are coloured in green, magenta, or cyan. The illustrations are based on the Glt_{ph} crystal structures 2NWW, 2NWX, and 3KBC, and made using the software Pymol (Schrödinger, LLC). (From Jiang & Amara, 2011. Reproduced with permission from Elsevier.)

Two other structures have been determined. A second structure (PDB ID 2NWW), referred to as the TBOA-bound conformation, was crystallised in the presence of the competitive inhibitor, DL-threo-benzyloxyaspartate (TBOA). The overall structural features of the TBOA-bound Glt_{ph} are very similar to those of the substrate-bound carrier (PDB ID 1XFH) except that the HP2 region is displaced away from the substrate-binding site (Figure 9.15(a)). A third Glt_{ph} structure (PDB ID 3KBC) was recently resolved, referred to as the inward-facing conformation, in which the C-terminal core domain moves inward approximately 18 Å toward the cytoplasm (Figure 9.15(c)).

The model which emerges is the following. In the outward-facing carrier, HP2 opens up spontaneously to expose the binding site. After glutamate and co-transported ions bind, HP2 closes and seals the substrate-binding site, and the transporter is in an occluded, outward-facing conformation (Figure 9.15). The whole core domain then moves towards the cytosol which permits the opening of the internal gate, presumably HP1, and the transporter is in an occluded, inward-facing conformation (Figure 9.15). Finally, K⁺ binds to and facilitates reorientation of the carrier back to an outward-facing state.

SODIUM/PROTON EXCHANGERS

The carrier-mediated transport of sodium in exchange for protons across membranes is a virtually universal phenomenon in biology, from bacteria to man. It is carried out by a family of Na⁺/H⁺ exchangers which is often referred to as antiporters. They are classified as secondary active transporters, since the driving force is the

electrochemical gradient of one of the ions, which drives the counter-transport of the other. They play a varied number of functions throughout biological systems, and in eukaryotes are vital for cellular homeostasis and play key roles in cancer and heart disease. As one example (Figure 9.16), the mammalian epithelial brush border Na/H

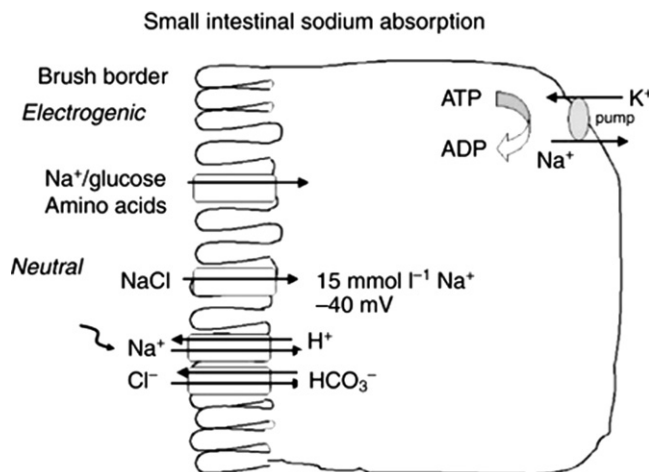


FIGURE 9.16 Na absorption in the mammalian small intestine. Neutral Na⁺ absorption requires Na⁺/H⁺ exchangers.

exchanger NHE3 is active under basal conditions and functions as part of neutral NaCl absorption in the intestine and renal proximal tubule, where it accounts for the majority of total Na absorbed. Higher eukaryotic genomes have between seven and nine Na⁺/H⁺ exchanger-like proteins. The first to be characterised, NHE1, is ubiquitous and localises to the plasma membrane of most mammalian cells: it is also found at the basolateral membrane of intestinal enterocytes. Based on computer modelling, like all of the other Na⁺/H⁺ exchangers, it is predicted (Figure 9.17) to have 12 membrane-spanning segments at the N-terminus (around 500 amino acid residues), with a more hydrophilic C-terminus which is intracellular and has multiple sites for phosphorylation by protein kinases and binding of other regulatory factors. Using the crystal structure of the *E. coli* Na⁺/H⁺ antiporter (Figure 9.17), the 3-dimensional structure of human Na⁺/H⁺ exchanger (HNE1) has been predicted.

OTHER ROLES OF INTRACELLULAR K⁺

Quite a number of enzymes are known to be activated by K⁺ — a good example is the glycolytic enzyme, pyruvate kinase, where the role of the metal is thought to be to orient the phosphoenolpyruvate in the substrate-binding pocket. The more active role of Mg²⁺ in this enzyme is discussed in Chapter 10. Since the intracellular concentrations of K⁺ and of Mg²⁺ are high they dominate metal binding to nucleic acids, with the divalent Mg²⁺ binding more strongly to the polyanionic sugar-phosphate backbone, on account of its higher charge. Metal binding reduces electrostatic repulsion between phosphates, stabilising both base pairing and base stacking; this is underlined by the increase in melting temperature of the DNA in the presence of metal ions. Much of the intracellular K⁺ and Mg²⁺ is found bound to the RNA in ribosomes.

The chromosomes of eukaryotes are linear, and replication of the free ends of these linear DNA molecules presents particular problems. The sequencing of the ends of chromosomes revealed that they consist of telomeres, hundreds of tandem repeats of a hexanucleotide sequence, which in all vertebrates is d(TTAGGG). These G-rich telomeric sequences can fold into a G-quadruplex, a DNA secondary structure consisting of stacked G-tetrad planes, or G-quartets (Figure 9.18), connected by a network of Hoogsteen hydrogen bonds: the cavity in the centre

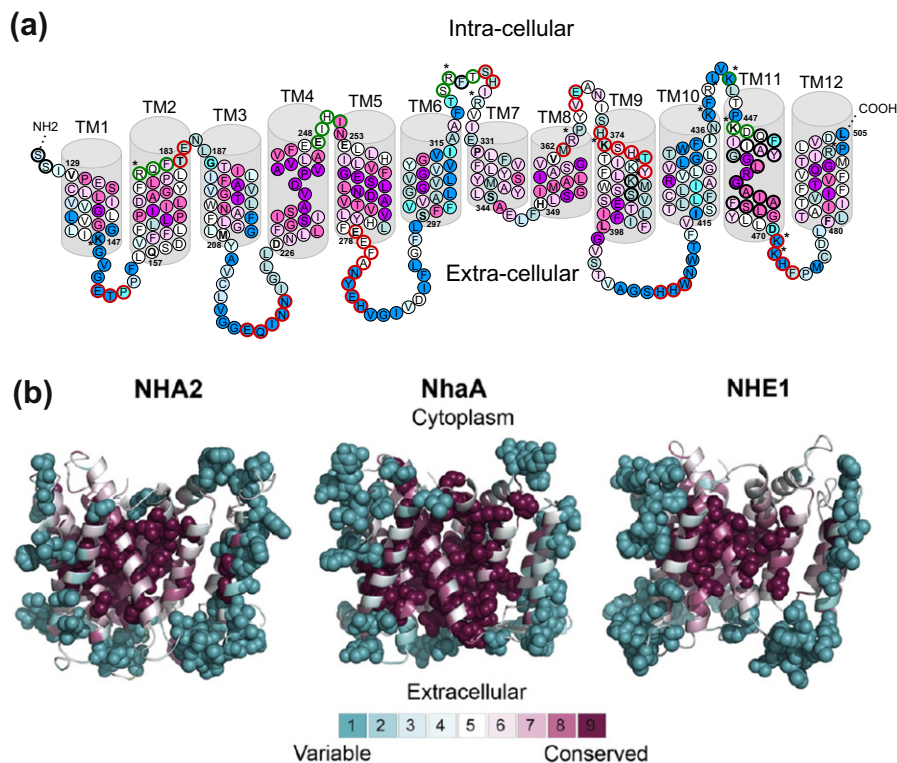


FIGURE 9.17 The evolutionary conservation profiles of EcNhaA, NHA2 and NHE1 (a) The membrane topology of NHE1 (residues 126–505). The residues are coloured according to their conservation grades. (b) The evolutionary conservation profiles of NHA2, NhaA, and NHE1 mapped on the crystal structure of NhaA. (Adapted from Landau *et al.*, 2007 (a), and (b) from Schushan *et al.*, 2010. Reproduced with permission from Elsevier.)

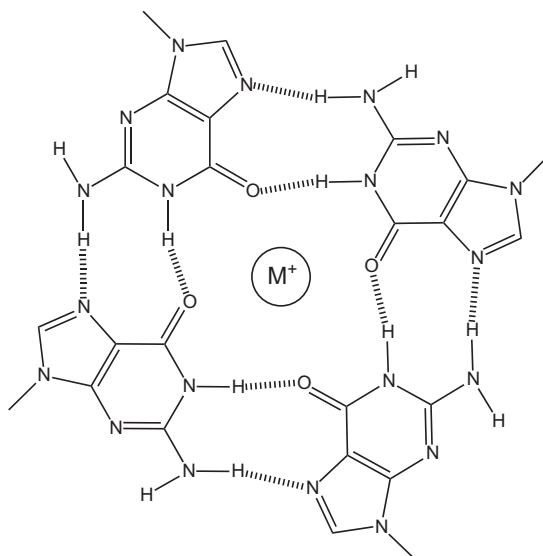


FIGURE 9.18 The structure of a G-quartet. (From Wozki & Schmidt, 2002.)

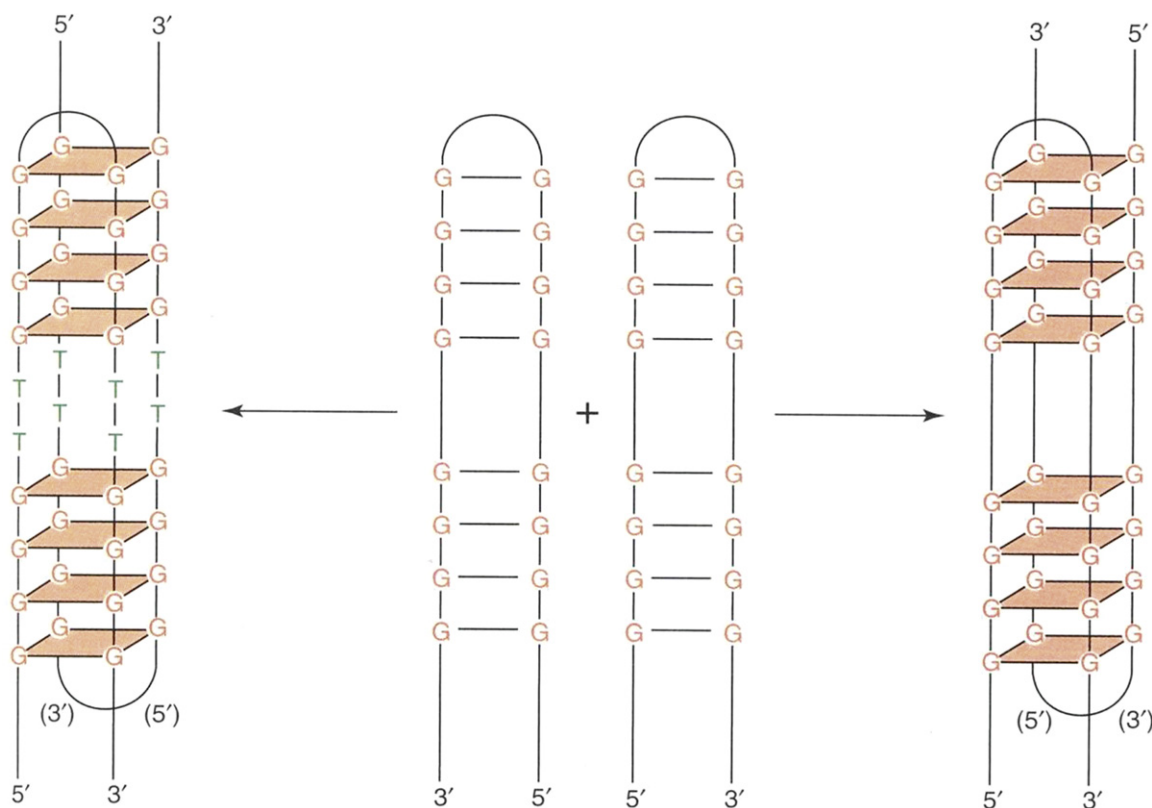


FIGURE 9.19 G-quadruplex DNA. (From Wozki & Schmidt, 2002.)

can accommodate monovalent cations such as Na^+ and K^+ , with coordination of the four O-6 oxygens. The quartets can stack upon each other to form a multilayer structure (Figure 9.19). The repetitive G-rich sequences found at the ends of eukaryotic chromosomes (telomeres) can form several isomeric antiparallel arrangements where the tetraplex involves intramolecular folding, when one polynucleotide supplies two or more strands to the complex.

The formation and stabilisation of the DNA G-quadruplex in the human telomeric tandem repeats of the sequence d(TTAGGG) inhibit the activity of telomerase, a cancer-specific reverse transcriptase which is activated in 80–90% of tumours, making it an important target for therapeutic intervention. Clearly, knowledge of the intact human telomeric G-quadruplex structure under physiological conditions is a prerequisite for rational, structure-based drug design. The folding structure of the human telomeric sequence in K^+ solution has recently been determined by NMR (Figure 9.20), demonstrating a novel intramolecular G-quadruplex folding topology, which is quite different from that reported previously for the 22-nucleotide Tel22 in Na^+ solution, and is the predominant conformation for the extended 26-nucleotide sequence Tel26 in K^+ solution, whether Na^+ is present or not. The addition of K^+ readily converts the Na^+ -form conformation to the K^+ -form hybrid-type G-quadruplex. The hybrid-type G-quadruplex topology suggests a straightforward secondary structure folding pathway with effective packing for the extended human telomeric DNA. Furthermore, since this hybrid-type telomeric G-quadruplex is likely to be that which is found under physiological conditions, its distinct folding topology makes it an attractive target for specific targeting by small-molecular-weight drugs which, by stabilising the telomeric G-quadruplexes, could represent an important cancer therapeutic strategy.

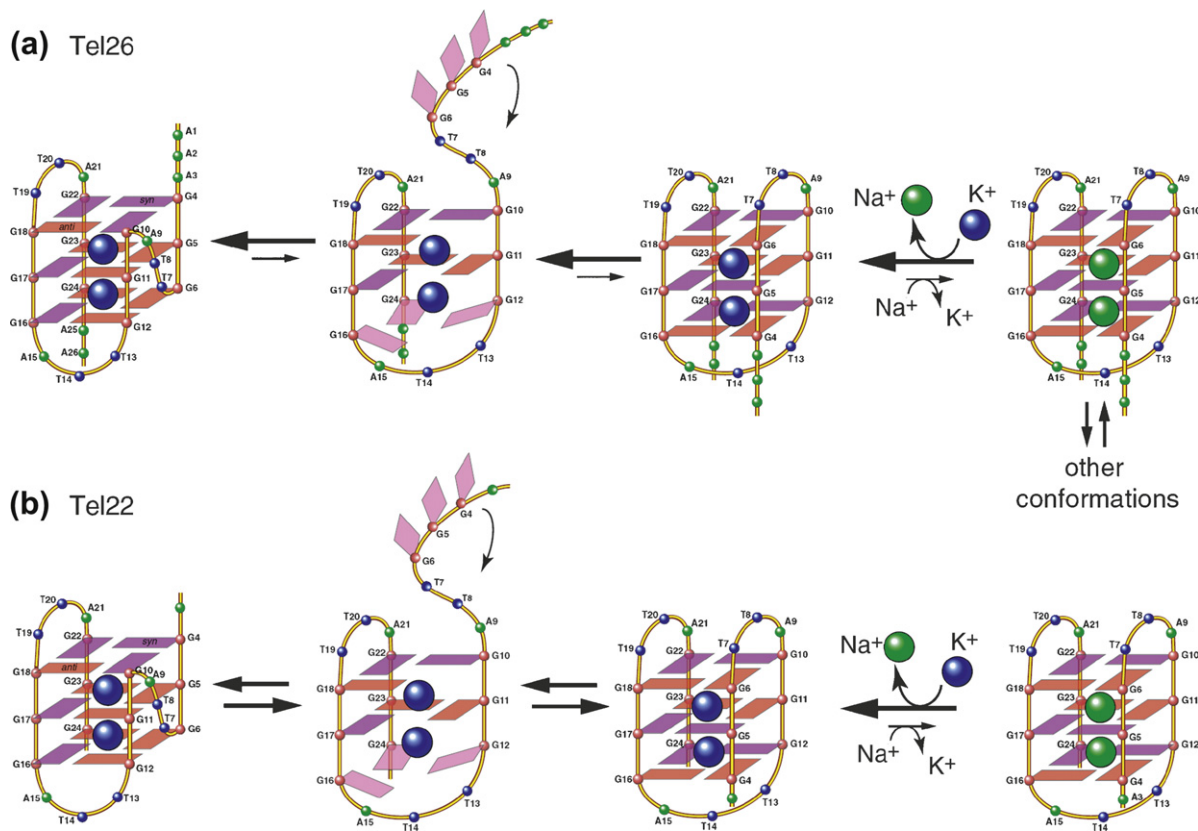


FIGURE 9.20 Schematic diagram of interconversions between the Na^+ and K^+ forms of telomeric G-quadruplexes. (From Ambrus *et al.*, 2006.)

REFERENCES

- Ambrus, A., Chen, D., Dai, J., Bialis, T., Jones, R. A., & Yang, D. (2006). Human telomeric sequence forms a hybrid-type intramolecular G-quadruplex structure with mixed parallel/antiparallel strands in potassium solution. *Nucleic Acids Research*, *34*, 2723–2735.
- Bublitz, M., Poulsen, H., Morth, J. P., & Nissen, P. (2010). In and out of the cation pumps: P-type ATPase structure revisited. *Current Opinion in Structural Biology*, *20*, 431–439.
- Catterall, W. A. (2000). From ionic currents to molecular mechanisms: the structure and function of voltage-gated sodium channels. *Neuron*, *26*, 13–25.
- Dietrich, B. (1985). Coordination chemistry of alkali and alkaline-earth cations with macrocyclic ligands, cations with macrocyclic ligands. *The Journal of Chemical Education*, *62*, 954–964.
- Doyle, D. A., Cabral, J. M., Pfuetzner, R. A., Kuo, A., Gulbis, J. M., Cohen, S. L., *et al.* (1998). The structure of the potassium channel: molecular basis of K^+ conduction and selectivity. *Science*, *280*, 69–77.
- Gouaux, E., & MacKinnon. (2005). Principles of selective ion transport in channels and pumps. *Science*, *310*, 1461–1465.
- Hodgkin, A. L., & Huxley, A. F. (1952). A quantitative description of membrane current and its application to conduction and excitation in nerve. *The Journal of Physiology*, *117*, 500–544.
- Jiang, J., & Amara, S. G. (2011). New views of glutamate transporter structure and function: advances and challenges. *Neuropharmacol*, *60*, 172–181.

- Landau, M., Herz, K., Padan, E., & Ben-Tal, N. (2007). “<http://www.ncbi.nlm.nih.gov/pubmed/17981808>” Model structure of the Na⁺/H⁺ exchanger 1 (NHE1): functional and clinical implications. *J Biol Chem*, 282, 37854–37863.
- MacKinnon, R. (2004). Potassium channels and the atomic basis of selective ion conduction (Nobel Lecture). *Angewandte Chemie International Edition*, 43, 4265–4277.
- Schushan, M., Xiang, M., Bogomiakov, P., Padan, E., Rao, R., & Ben-Tal, N. (2010). Model-guided mutagenesis drives functional studies of human NHA2, implicated in hypertension. *J Mol Biol*, 396, 1181–1196.
- Voet, D., & Voet, J. G. (2004). *Biochemistry* (3rd ed.). Hoboken: John Wiley and Sons.
- Yu, F. H., Yarov-Yarovoy, V., Gutman, G. A., & Catterall, W. A. (2005). Overview of molecular relationships in the voltage-gated ion channel superfamily. *Pharmacological Reviews*, 57, 387–395.
- Wozki, S. A., & Schmidt, F. J. (2002). DNA and RNA: composition and structure. In T. M. Devlin (Ed.), *Textbook of biochemistry with clinical correlations* (5th ed.). (pp. 45–92).

This page intentionally left blank

Magnesium–Phosphate Metabolism and Photoreceptors

Introduction	197
Magnesium-Dependent Enzymes	198
Phosphoryl Group Transfer Kinases	199
Phosphoryl Group Transfer – Phosphatases	203
Stabilisation of Enolate Anions – The Enolase Superfamily	204
Enzymes of Nucleic Acid Metabolism	205
Magnesium and Photoreception	210

INTRODUCTION

Mg^{2+} is one of the most abundant elements in the earth's crust and in the human body, and the most abundant divalent cation within cells. Around 50% of total Mg^{2+} resides in bone, the remainder essentially within cells; 50% of cytosolic Mg^{2+} is bound to ATP, and most of the rest, together with K^+ , is bound to ribosomes. The intracellular concentration of free Mg^{2+} is around 0.5 mM. Less than 0.5% of the total body Mg^{2+} is in plasma, where its concentration is maintained within fairly strict limits.

Mg^{2+} has properties which make it quite unique among biological cations. Inspection of Table 10.1 reveals that of the four common biological cations, the ionic radius of Mg^{2+} is much smaller than the others, whereas its

TABLE 10.1 Properties of Common Biological Cations

Cation	Ionic Radius (Å)	Hydrated Radius (Å)	Ionic Volume (Å ³)	Hydrated Volume (Å ³)	Exchange Rate (s ⁻¹)	Transport Number
Na^+	0.95	2.75	3.6	88.3	8×10^8	7–13
K^+	1.38	2.32	11.0	52.5	10^9	4–6
Mg^{2+}	0.65	4.76	1.2	453	10^5	12–14
Ca^{2+}	0.99	2.95	4.1	108	3×10^8	8–12

(from Maguire & Cowan, 2002).

hydrated radius is the largest of all four. This means that the volume of the hydrated Mg^{2+} cation is 400 times larger than its ionic volume (since the radius enters into the equation to the third power), compared to values around 25 times for Na^+ and Ca^{2+} , and a mere 5 times for K^+ .

Other factors that play an important role in determining the biological role of Mg^{2+} are its coordination number and coordination geometry, its solvent exchange rates, and its transport number.¹ Like Na^+ , Mg^{2+} is invariably hexa-coordinate, whereas both K^+ and Ca^{2+} can adjust easily to 6, 7, or 8 coordination. Thus, Ca^{2+} can accommodate a more flexible geometry, compared to the octahedral geometry of the obligatory hexacoordinate cations, resulting in deviations from the expected bond angle of 90° by up to 40° , compared with less than half that for Mg^{2+} . Likewise, bond lengths for oxy-ligands can vary by as much as 0.5 \AA for Ca^{2+} , whereas the corresponding values for Mg^{2+} vary by only 0.2 \AA .

In contrast to the other three cations, Mg^{2+} has a much slower exchange rate of water in its hydration sphere (Table 10.1). Mg^{2+} often participates in structures, for example, in ATP binding catalytic pockets of kinases and other phosphoryl transferase enzymes, where the metal is bound to four or five ligands from the protein and the ATP. This leaves one or two coordination positions vacant for occupation by water molecules, which can be positioned in a particular geometry by the Mg^{2+} to participate in the catalytic mechanism of the enzyme. This capacity is an example of outer sphere activation of a substrate by a metal ion (Figure 10.1) as distinct from the

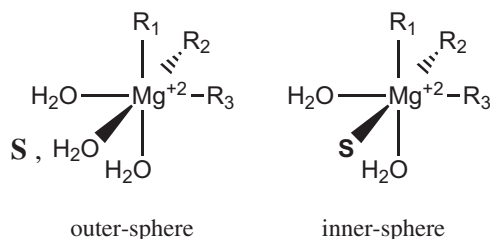


FIGURE 10.1 Comparison of inner- and outer-sphere modes of activation, where S is the substrate. (Adapted from Cowan, 2002.)

more usual inner-sphere activation. Unlike the other alkaline earth and transition metal ions, essentially on account of its small ionic radius and consequent high electron density, Mg^{2+} tends to bind the smaller water molecules rather than bulkier ligands in the inner coordination sphere. Many Mg^{2+} -binding sites in proteins have only 3, 4, or even less direct binding contacts to the protein, leaving several sites in the inner coordination sphere occupied by water, or in the phosphoryl transferases, by nucleoside di- or tri-phosphates.

In addition, the high charge density on Mg^{2+} ensures that it is an excellent Lewis acid in reactions notably involving phosphoryl transfers and hydrolysis of phosphoesters. Typically, Mg^{2+} functions as a Lewis acid, either by activating a bound nucleophile to a more reactive anionic form (e.g., water to hydroxide anion) or by stabilising an intermediate.

MAGNESIUM-DEPENDENT ENZYMES

Many enzymes involved in the pathways of intermediary metabolism are Mg^{2+} dependent, as are a great many of the enzymes involved in nucleic acid metabolism. Of the ten enzymes involved in the glycolytic pathway (Chapter 5), five are Mg^{2+} dependent. This comes as no surprise since four of the five (hexokinase, phosphofructokinase, phosphoglycerate kinase, and pyruvate kinase) involve phosphoryl transfers. The fifth, enolase, forms a complex with Mg^{2+} before the 2-phosphoglycerate substrate is bound. The inhibition of glycolysis by fluoride results from binding of F^- , in the presence of phosphate, to the catalytic Mg^{2+} , thus blocking substrate binding and inactivating the enzyme. As we could anticipate from its being the most abundant cytosolic divalent cation, Mg^{2+} binds strongly to nucleoside di- and tri-phosphates such as ATP and ADP, and is therefore directly involved in almost all reactions involving these molecules.

1. The transport number estimates the average number of solvent molecules associated with a cation sufficiently tightly to migrate with the cation in solution.

As pointed out above, Mg^{2+} binding to the enzyme can either be directly through protein side chains or peptide carbonyls (inner sphere) or by indirect interactions through metal-bound water molecules (outer sphere). Mg^{2+} -dependent enzymes can be divided into two general classes. First, there are those in which the enzyme binds the magnesium–substrate complex, and usually the enzyme has little or only weak interaction with the Mg^{2+} , its principal binding being to the substrate. Second, there are enzymes to which Mg^{2+} binds directly, altering the structure of the enzyme and/or playing a catalytic role.

Mg^{2+} binding to enzymes is relatively weak (K_a not more than 10^5 M^{-1}) such that the enzyme is often isolated in the metal-free form, and Mg^{2+} must be added to the *in vitro* enzyme assay system. As pointed out earlier, the intracellular free Mg^{2+} concentration is about $5 \times 10^{-3} \text{ M}$, so that most Mg^{2+} -dependent enzymes have adequate local concentrations of Mg^{2+} for their activity. Two factors which make Mg^{2+} biochemistry difficult to carry out are that the metal is, like Zn^{2+} , spectroscopically silent, and second that, since 1990 the only practically useful isotope ^{28}Mg , with high energy β and γ emission and a half-life of 21.3 h, has become outrageously expensive (\$30,000 per mCi), such that it is no longer used for transport studies. These practical problems may, in part, be resolved by substituting Mn^{2+} for Mg^{2+} to carry out spectroscopic studies, and to use substitute isotopes such as $^{63}\text{Ni}^{2+}$ for transport studies.

PHOSPHORYL GROUP TRANSFER KINASES

Phosphoryl group transfer reactions either add or remove phosphoryl groups to or from cellular metabolites and macromolecules, and play a major role in biochemistry. Phosphoryl transfer is the most common enzymatic function coded by the yeast genome, and in addition to its importance in intermediary metabolism (Chapter 5) the reaction is catalysed by a large number of central regulatory enzymes which often are part of signalling cascades, such as protein kinases, protein phosphatases, ATPases, and GTPases.

Kinases are Nature's tools for introducing phosphoryl groups into organic molecules, whether they are metabolites such as glucose and fructose-6-phosphate in the glycolysis pathway or proteins which are part of signalling cascades, such as that which activates glycogenolysis and simultaneously inhibits glycogen synthesis via phosphorylation of protein side chains (serine residues in this particular case). The donor of the phosphoryl group is usually Mg^{2+} –ATP.

The resting adult human brain consumes around 80 mg of glucose and 50 ml of O_2 per minute, and once the glucose has been transported across the plasma membrane it is rapidly phosphorylated by hexokinase, the first enzyme of the glycolytic pathway. Hexokinase catalyses the transfer of a phosphoryl group from Mg^{2+} –ATP to glucose to form glucose-6-phosphate and Mg^{2+} –ADP. It is a member of a superfamily of proteins with a common characteristic $\beta\beta\alpha\beta\alpha$ -fold, which is repeated in both the N-terminal and the C-terminal domains. The members have a common ATPase domain, and include kinases, which phosphorylate not only sugars but also glycerol, acetate, and other carboxylic acids. As illustrated by glucose binding to hexokinase (Figure 10.2), catalysis by these enzymes is known to be accompanied by a large conformational change, which is associated

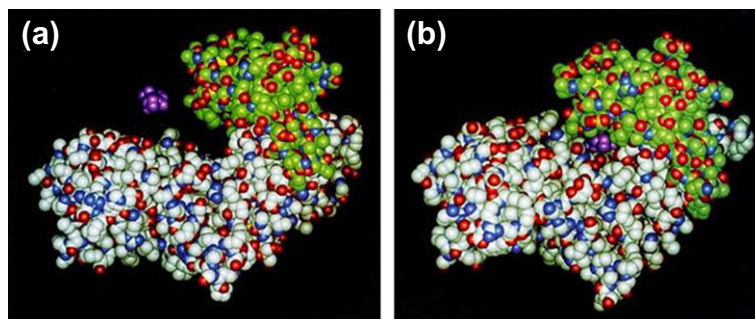


FIGURE 10.2 (a) yeast hexokinase; (b) in its complex with glucose. (From Voet & Voet, 2004: pp. 1591. Copyright 2004 with permission from John Wiley and Sons, Inc.)

with interdomain motion. The two lobes of the active site cleft swing together from an open to a closed conformation by about 8 Å. This also has the consequence of excluding water from the active site, which may explain why phosphoryl transfer to glucose is 4×10^4 times faster than to water.

Another characteristic of this kinase family, as has been shown by Jeremy Knowles (Knowles, 1980) using ATP-made chiral in its γ -phosphoryl group, is that phosphoryl group transfer occurs with inversion of configuration. This is taken to be indicative of a direct, in-line transfer of the phosphoryl group from substrate to product by the addition of a nucleophile to the phosphorus atom yielding a trigonal bipyramidal intermediate, the apices of which are occupied by the attacking and leaving groups (Figure 10.3).

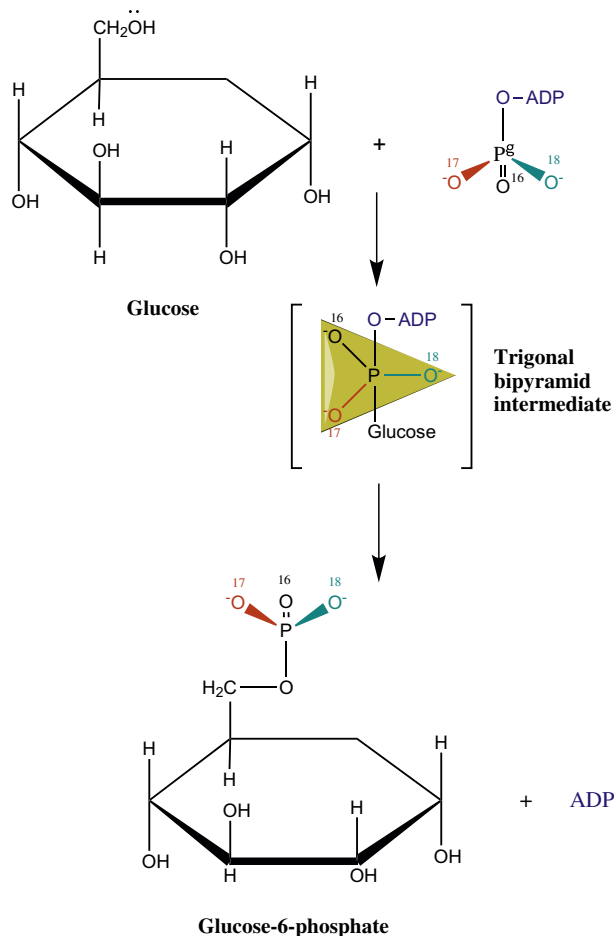


FIGURE 10.3 In the phosphoryl transfer reaction catalysed by hexokinase, the γ -phosphoryl group of ATP inversion of configuration. (Adapted from Voet & Voet, 2004: pp. 1591.)

Hexokinase forms a ternary complex with glucose and Mg^{2+} -ATP before the reaction takes place, which, as a result of the domain closure, places ATP in close proximity to the C6 hydroxyl group of glucose (Figure 10.4). By complexing the phosphate groups of ATP, Mg^{2+} is thought to shield their negative charges, making the γ -phosphorus atom more accessible to nucleophilic attack by the C6—OH group of the glucose molecule. However, it also seems that, as in many of the other members of the superfamily, the Mg^{2+} ion not only binds

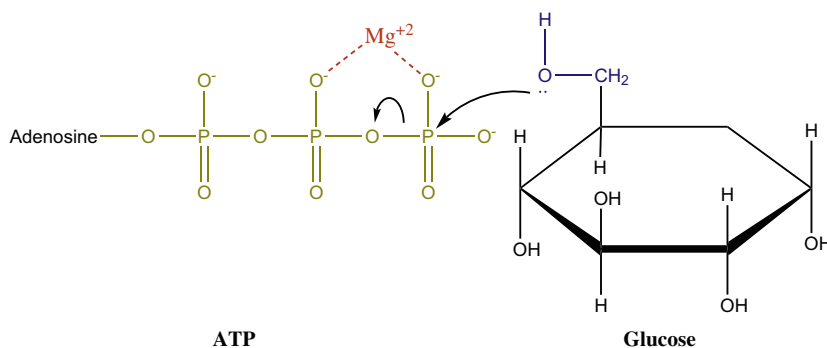


FIGURE 10.4 Nucleophilic attack of the C6–OH group of glucose on the γ -phosphate of Mg^{2+} –ATP complex. (Adapted from Voet & Voet, 2004: pp. 1591.)

directly to the oxygen atoms of the β - and γ -phosphoryl groups, but also binds through a water molecule to the carboxylate of a well-conserved Asp residue. This Asp acts as a general base responsible for deprotonating the hydroxyl on the sugar which will be phosphorylated. This is illustrated for the rhamnulose kinase from *E. coli* (Figure 10.5), which catalyses the transfer of the γ -phosphoryl group from ATP to the 1-hydroxyl group of

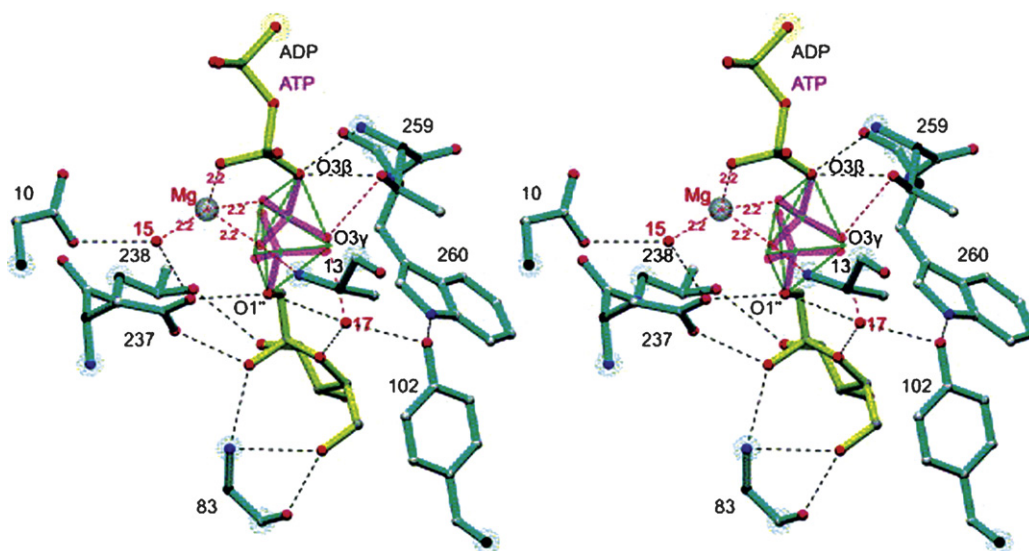


FIGURE 10.5 Stereoview of the reaction running through a bipyramidal pentavalent phosphorus atom. The γ -phosphoryl group before and after the transfer is in a transparent mode. A putative Mg^{2+} was placed at the expected position between Asp10 and the β and γ -phosphoryl groups. (From Grueninger & Schultz, 2006. Copyright 2006 with permission from Elsevier.)

L-fructose. The γ -phosphoryl group of the ATP can be positioned in such a way that the three oxygen atoms are on the corners of a trigonal bipyramid between O3 β of ADP and the O1'' atom of β -L-fructose. Moreover, the required Mg^{2+} can be modelled between the β - and γ -phosphoryl groups and the well-conserved Asp10, as shown in Figure 10.5. The putative Mg^{2+} binds directly to the phosphate oxygen atoms and through a water molecule to the carboxylate group. Since Mg^{2+} prefers an octahedral coordination sphere, it requires a water structure different from that observed in holo rhamnulose kinase.

In contrast to the kinases that phosphorylate metabolites, there are a number of families of protein kinases that phosphorylate Ser, Thr, and Tyr residues in specific target proteins, usually as part of a signal amplification cascade in response to an extracellular stimulus. We consider briefly here the family of mitogen-activated protein kinases (MAPKs) which function as mediators of many different cellular signals. MAPKs function as the terminal component of a signalling cascade, which in mammals, following an initial extracellular stimulus, amplifies the signal through at least 14 MAP kinase kinase kinases (MKKKs); these, in their turn, activate 7 MAP kinase kinases (MKKs), which then activate 12 MAPKs (Figure 10.6). At each step of the cascade, the signal is amplified

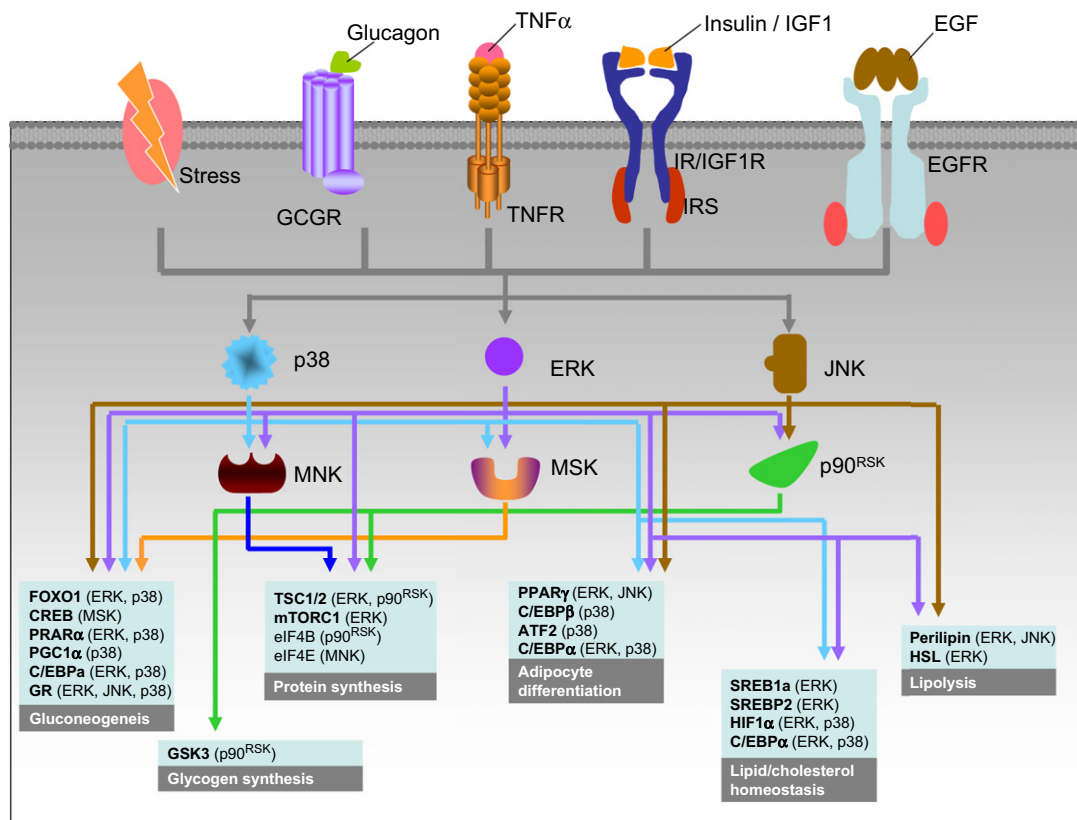


FIGURE 10.6 Schematic representation of the mitogen-activated protein kinase (MAP) cascades in mammalian cells.

several fold. Each MAP kinase cascade consists of an MAPKKK, an MAPKK, and an MAPK. Various external stimuli may activate one or more MAPKKK, which in turn may activate one or more MKKs. However, the MKKs are relatively specific for their target MAPKs. The activated MAPKs then phosphorylate specific translation factors, which regulate the synthesis of target mRNAs (e.g., Elk-1, Ets1, p53, NFAT4, and Max) as well as specific kinases (e.g., p90^{RSK}, S6 kinase, and MAPKAP kinase). The resulting transcription factors and kinases then induce cellular responses, such as growth, differentiation, and apoptosis. While it is clearly established that these kinases require Mg²⁺, in the form of the Mg²⁺–ATP complex, in a great many cases they also seem to require a second magnesium ion. It is not clear in the absence of any a priori chemical necessity, what the function of the second magnesium might be. As often happens when biochemists have no clear idea of what is going on, conformational change of the enzyme protein is invoked.

PHOSPHORYL GROUP TRANSFER – PHOSPHATASES

In contrast to kinases, phosphatases catalyse the removal of phosphoryl groups, again either from phosphorylated metabolites like glucose-6-phosphate or fructose-1,6-bisphosphate in the central metabolic pathways or from proteins which have been phosphorylated by protein kinases. Unlike the kinases, they catalyse a hydrolytic reaction in which the phosphoryl group is transferred to water. We consider here as an illustration phosphatases and the phosphoglucomutases of the haloacid dehalogenase² (HAD) superfamily of phosphotransferases. However, although this still involves nucleophilic catalysis, instead of an in-line mechanism with a penta-coordinate transition state, we have formation of a covalent aspartylphosphate enzyme intermediate (Figure 10.7a)

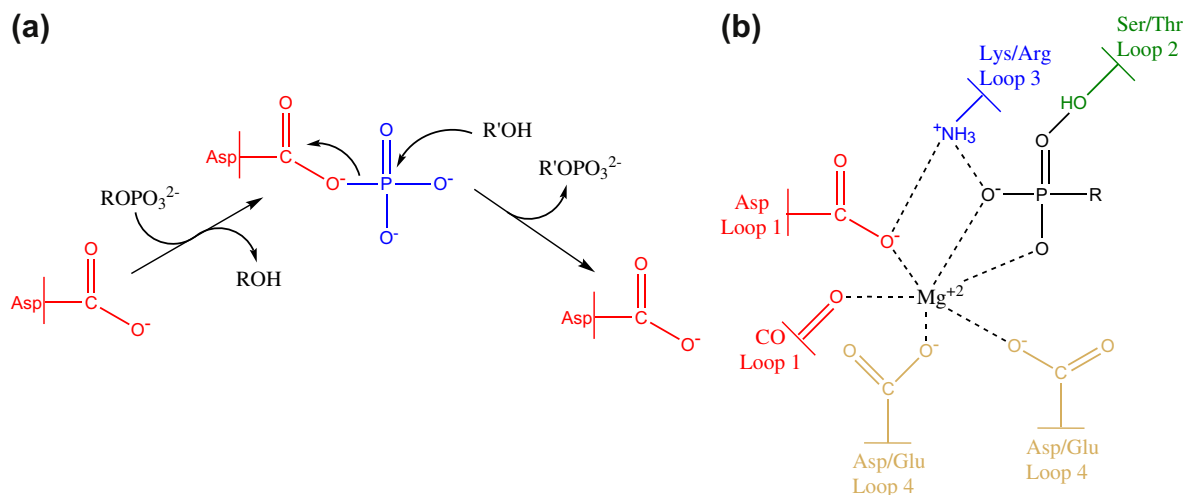


FIGURE 10.7 (a) In HAD enzymes Asp mediates phosphoryl-group transfer to a variety of acceptors, including H₂O (b) the catalytic scaffold around the essential Mg²⁺ ion. (Adapted from Allen & Dunaway-Mariano, 2004.)

The Mg²⁺, which is essential for the reaction, binds both to the nucleophilic Asp and to the phosphorylated substrate, providing orientation and charge shielding for nucleophilic attack (Figure 10.7b). The aspartylphosphate has a high energy of hydrolysis, which drives phosphoryl transfer to water, the predominant acceptor of phosphoryl groups. In the phosphatases, hydrolysis of the aspartylphosphate intermediate is facilitated by a general base which typically contributes a rate enhancement of 10²–10⁴. In contrast, in the ATPases the rate of dephosphorylation of the aspartylphosphate is greatly reduced by the use of a Thr residue which contributes only 30-fold to the rate enhancement. And in the phosphoglucomutase reaction, in which glucose-1-phosphate is converted to glucose-6-phosphate by two phosphoryl transfer reactions with formation of a glucose-1,6-bisphosphate intermediate (Figure 10.8), the rate of hydrolysis of the aspartylphosphate is reduced even further. This is probably achieved by the sugar phosphate itself positioning the base catalyst necessary for phosphoryl transfer, whereas a water molecule cannot do so. The structural and functional role of the divalent cation in the active centre of phosphatases is well illustrated by the case of human phosphoserine phosphatase. When the essential Mg²⁺ is replaced by Ca²⁺, the enzyme is inactivated. Figure 10.9(a) shows the active site of a bacterial phosphoserine phosphatase with a Mg²⁺ and phosphoserine in the active site, while Figure 10.9(b) shows human phosphoserine phosphatase with a Ca²⁺ ion bound and the modelled substrate in the active site. The hepta-coordinate Ca²⁺ binds to both side-chain oxygen atoms of the catalytic Asp 20, unlike the hexa-coordinate Mg²⁺,

2. Although named after a dehalogenase, of the more than 3000 sequenced proteins of the HAD family, the vast majority are phosphoryl transferases.

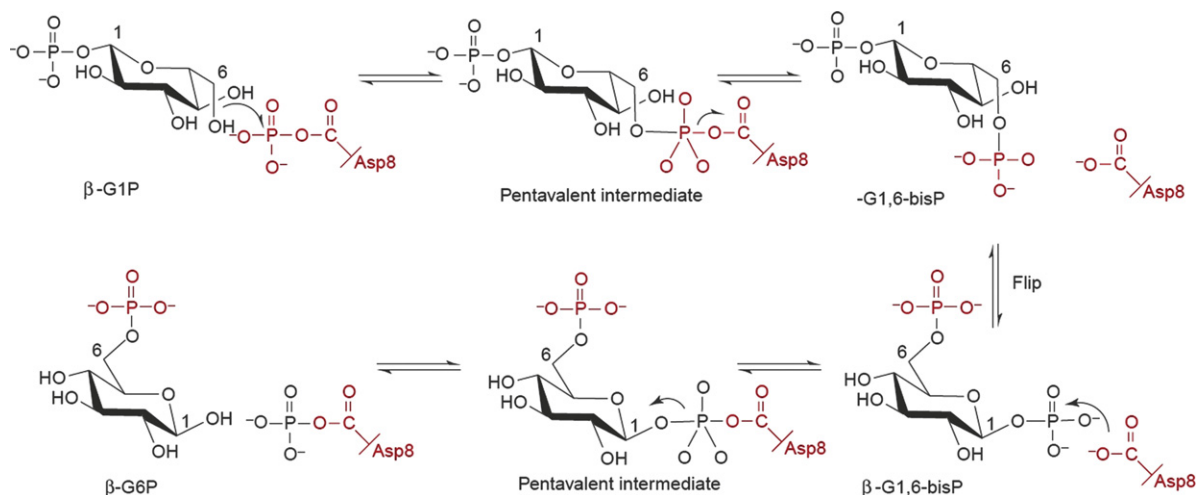


FIGURE 10.8 The phosphoglucomutase reaction proceeds via two phosphoryl transfer reactions. (Adapted from Allen & Dunaway-Mariano, 2004.)

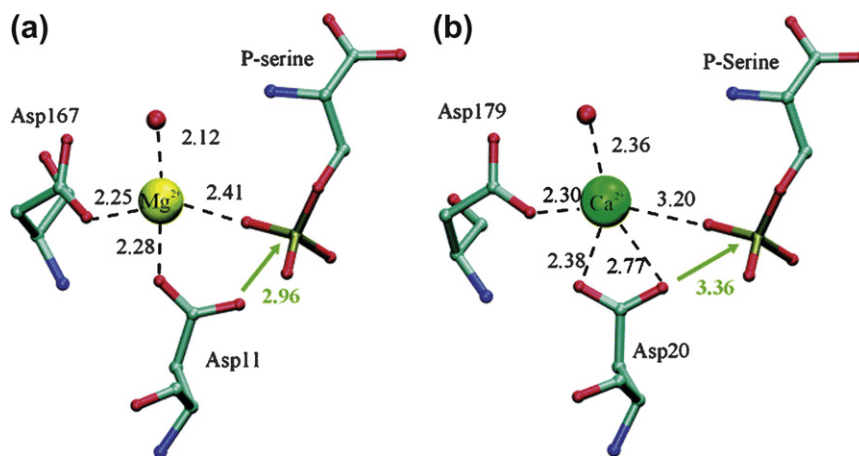


FIGURE 10.9 Active site of *Methanococcus* phosphoserine phosphatase with Mg^{2+} and phosphoserine in the active site (a) and of human phosphoserine phosphatase with Ca^{2+} bound and the modelled substrate in the active site (b). (From Peeraer et al., 2004. Copyright 2004 with permission from John Wiley and Sons, Inc.)

which ligates only one oxygen atom (Figure 10.9). This prevents the nucleophilic attack by one of the Asp 20 side-chain oxygens on the phosphorus atom of the substrate, accounting for the inhibition (Peeraer, Rabijns, Collet, Van Scaftingen, & De Ranter, 2004).

STABILISATION OF ENOLATE ANIONS – THE ENOLASE SUPERFAMILY

Yet another example of a family of Mg^{2+} -dependent enzymes is the enolase superfamily which catalyse a series of mechanistically diverse and different overall reactions. However, they all share a partial reaction in which an active site base of the enzyme abstracts the α -proton of a carboxylate substrate to generate an enolate anion intermediate which is stabilised by coordination to the essential Mg^{2+} ion. This intermediate then is directed to different products in the different active sites (Figure 10.10). The three ‘founder’ members of this family are the mandelate racemase

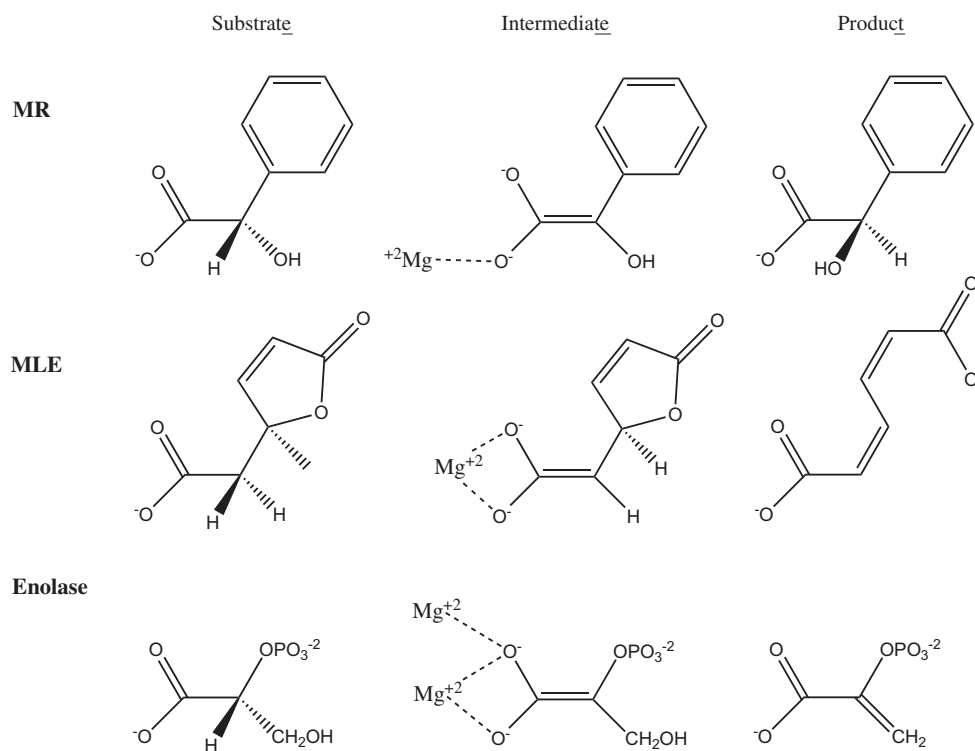


FIGURE 10.10 The substrates, enolate anion intermediates, and products of the MR; MLE and enolase reactions. (Adapted from Gerlt, Babbitt, & Rayment, 2005.)

(MR) and the muconate lactonising enzyme (MLE) of *Pseudomonas putida* and enolase, the fifth glycolytic enzyme referred to above. The three-dimensional structures of all three enzymes are remarkably superposable (Figure 10.11). All three have a two-domain structure, with the active sites located at the interface between flexible loops in the capping domain and the C-terminal barrel domain. The capping domain is formed by segments from the N- and C-termini of the polypeptide chain, while the barrel domain is formed from ends of the β -strands of the modified TIM-barrel domain. Whereas the TIM molecule (Figure 3.7) has $[(\beta/\alpha)_8\beta]$, the enolase superfamily instead has $[(\beta/\alpha)_7\beta]$. All members of the superfamily contain ligands (nearly always Glu or Asp) for the essential Mg^{2+} , located at the ends of the third, fourth, and fifth β -strands, which is illustrated for enolase in Figure 10.12.

In enolase, the substrate, 2-phosphoglycerate (2-PGA) is coordinated to two Mg^{2+} ions, one of which is liganded to the three conserved carboxylate residues (Asp 246, Glu 295, and Asp 320). Currently, more than 600 enolase sequences have been identified in the databases, and all are thought to be isofunctional, catalyzing the conversion of 2-PGA to phosphoenolpyruvate. In the MLE subclass of the superfamily, at least three reactions are known to be catalysed – in addition to the lactonisation of muconate, succinylbenzoate synthase, and L-Ala-D/L-Glu epimerase reactions are observed within the ~ 300 members. The MR subclass catalyses at least five reactions, mandelate racemisation and 4 sugar dehydratases. As in the MLE subclass, of the ~ 400 members identified, only $\sim 50\%$ of these are functionally assigned.

ENZYMES OF NUCLEIC ACID METABOLISM

Clearly, since DNA and RNA molecules are polynucleotides, composed of an invariant sugar-phosphate backbone, it comes as no surprise that many of the enzymes involved in their metabolism require Mg^{2+} ions. We do not

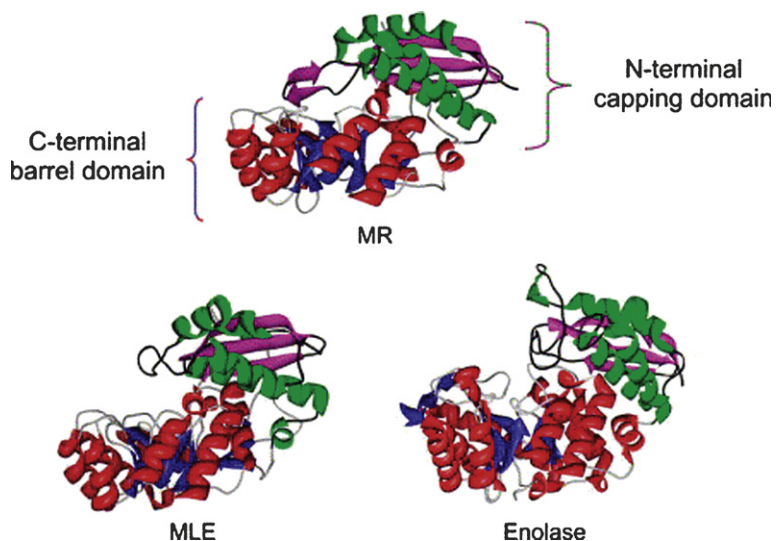


FIGURE 10.11 Comparison of the structures of MR, MLE, and enolase showing the two homologous domains which illustrate divergent evolution. (From Gerlt *et al.*, 2005. Reproduced with permission from Elsevier.)

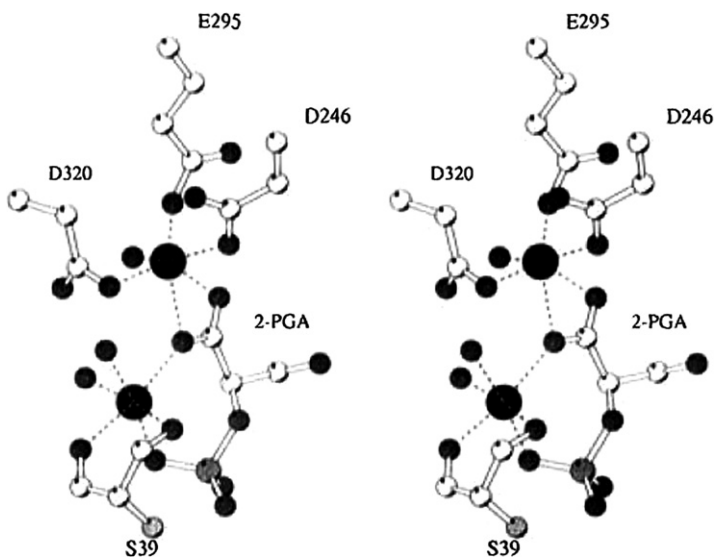


FIGURE 10.12 Stereoview of the coordination of the two Mg^{2+} ions in the enolase-(Mg^{2+})₂-2-PGA complex. (From Larsen, Wedeking, Rayment, & Reed, 1996. Copyright (1996) American Chemical Society.)

consider here how this very large number of enzymes achieve their structure or sequence specificity, although the sensitivity of ligand geometry and electrostatic environment of Mg^{2+} ions is proposed to greatly enhance substrate recognition and catalytic specificity (for a review, see Yang, Lee, & Nowotny, 2006), but rather consider the role of the metal ions. However, it is salutary to recall a few examples of their specificity. Restriction endonucleases each typically recognise a specific six-base-pair sequence, and the more than 3000 type II restriction endonucleases recognise over 200 different sequences — how is this sequence specificity achieved? Endonucleases

such as Rnase H remove the RNA primer strand from the RNA–DNA hybrid in Okasaki fragments during DNA replication, yet they do not cleave either double-stranded DNA or RNA. DNA and RNA polymerases, even without their elaborate proofreading function, insert the wrong nucleotide only every 10^3 – 10^4 bases, despite the relatively small free energy difference of only ~ 2 kcal/mol between Watson–Crick and mismatched base pairs.

Nucleic acid metabolism is dominated by phosphoryl transfer reactions (Figure 10.13). These include the reactions involved in DNA and RNA biosynthesis, catalysed by DNA and RNA polymerases. In these reactions,

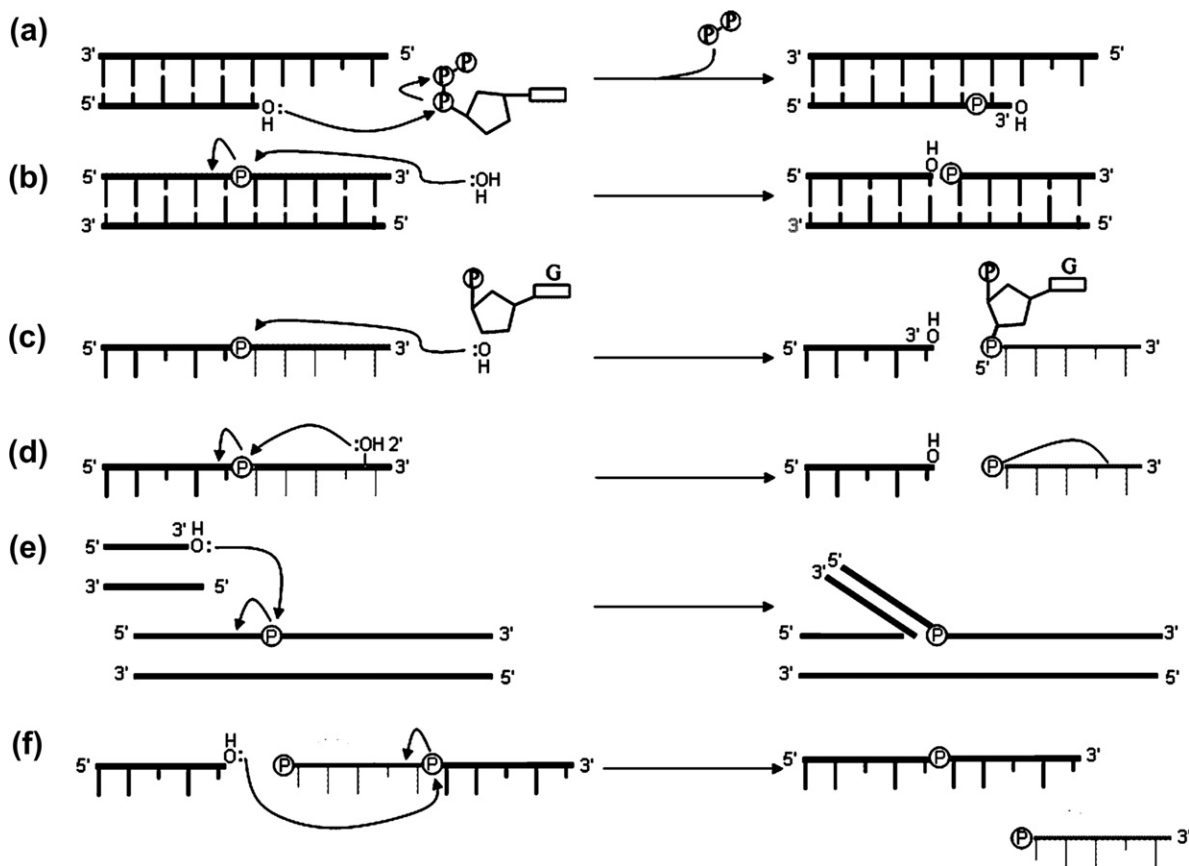


FIGURE 10.13 Phosphoryl transfer reactions. The figure shows (a) nucleotide polymerisation, (b) nucleic acid hydrolysis, (c) first cleavage of an exon–intron junction by group I ribozyme (d) and by a group II ribozyme, (e) strand transfer during transposition, and (f) exon ligation during RNA splicing. (Adapted from Yang *et al.*, 2006.)

the hydroxyl group at the 3' end of an RNA or DNA strand attacks the α -phosphate of an incoming (deoxy) ribonucleotide triphosphate [d]NTP to form a new phosphodiester bond, releasing a molecule of pyrophosphate (Figure 10.13(a)). A similar phosphoryl transfer occurs in DNA and RNA cleavage, except that the phosphate being attacked is the backbone of a nucleic acid, and the nucleophile is either a water molecule or a sugar hydroxyl. When a water molecule is the nucleophile, the cleavage products are a 5' phosphate and a 3' hydroxyl (Figure 10.13(b)). When the 2' or 3' hydroxyl group of a ribonucleotide is the nucleophile, as in RNA splicing, catalysed by the group I and group II self-splicing ribozymes, the 5' end product is covalently linked to the ribonucleotide (Figures 10.13(c) and (d)). If the nucleophile is the terminal 3' hydroxyl of a DNA or RNA strand,

this can result in strand transfer, as in DNA transposition³ (Figure 10.13(f)) or in exon ligation, involved in RNA splicing (Figure 10.13(g)).

The discovery of self-splicing introns showed that RNA can catalyse chemical reactions. Yet, unlike proteins, RNA has no functional groups with pKa values and chemical properties similar to those considered to be important in protein-based enzymes. Steitz and Steitz (1993) postulated that two metal ions were essential for catalysis by ribozymes using a mechanism similar to DNA cleavage, in which a free 3' OH is produced. Based on the X-ray structures of alkaline phosphatase and of the exonuclease fragment of DNA polymerase, they proposed that two divalent cations, almost certainly Mg^{2+} , bound to conserved carboxylate residues were essential for catalysis. In all phosphoryl transfer reactions, the first step is deprotonation and activation of a nucleophile, either a water molecule or a sugar hydroxyl group (Figure 10.14(a)). This is followed by formation of

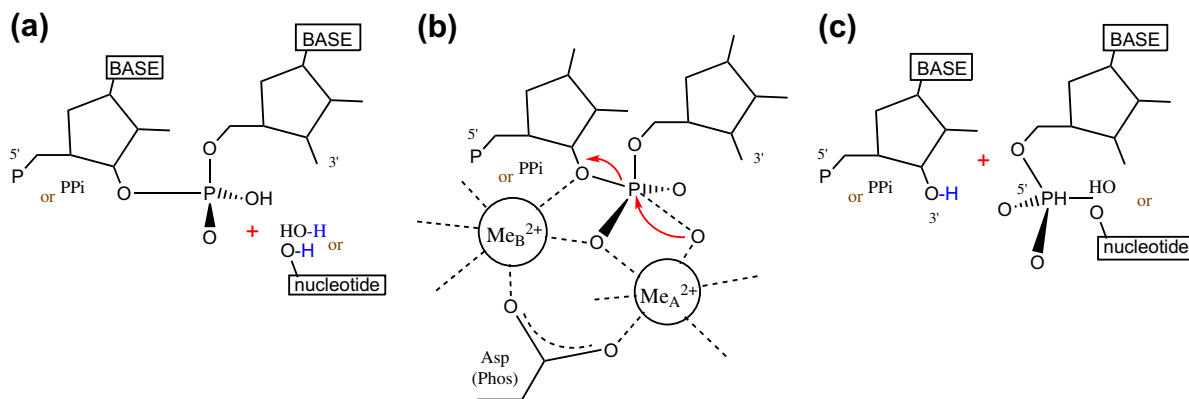


FIGURE 10.14 Diagram of two-metal-ion-dependent phosphoryl transfer reaction. (a) Substrates. The scissile phosphate can belong to a nucleic acid or nucleotide. A water molecule or sugar hydroxyl group needs to be deprotonated (shown in blue) and activated to become a nucleophile. (b) Pentacovalent intermediate. The two metal ions are always coordinated by a nonbridging oxygen of the scissile phosphate and a conserved Asp, which may be substituted by a phosphate (phos) in ribozymes. (c) Products. A new phosphoryl bond is formed between the nucleophile and scissile phosphate with the phosphate configuration inverted, and the 3' leaving group is reprotonated. (Adapted from Yang *et al.*, 2006.)

a pentacovalent phosphate intermediate (Figure 10.14(b)), in which the two metal ions are always coordinated by a nonbridging oxygen of the scissile phosphate and a conserved Asp, which may be substituted by a phosphate (Phos) in ribozymes. The final step is the formation of a new phosphoryl bond between the nucleophile and the scissile phosphate with the phosphate configuration inverted, and reprotonation of the 3' leaving group (Figure 10.14(c)).

High-resolution structural studies (Nowotny & Yang, 2006) on reaction intermediate and product complexes of ribonuclease H, representing different stages of the reaction, are schematically outlined in Figure 10.15. Upon binding of an RNA/DNA hybrid, the two metal ions find their appropriate binding sites 4.0 Å apart in the active site and are positioned for catalysis. Metal ion A is coordinated in octahedral geometry, orienting and activating the water molecule for nucleophilic attack. Metal ion B, which is irregularly coordinated, may destabilise the enzyme–substrate complex. In the next stage, movement of the two metal ions toward each other brings the nucleophile close to the phosphorus atom to form the pentacovalent transition state. The closer than 4 Å separation between the two divalent cations (3.5 Å) may efficiently neutralise the developing negative charge in the transition state, which is then converted to the products, and the 5'-phosphate and 3'-OH dissociate. The release of the

3. DNA transposases are required in site-specific DNA recombination, moving transposable elements around in DNA molecules of bacteria and other organisms.

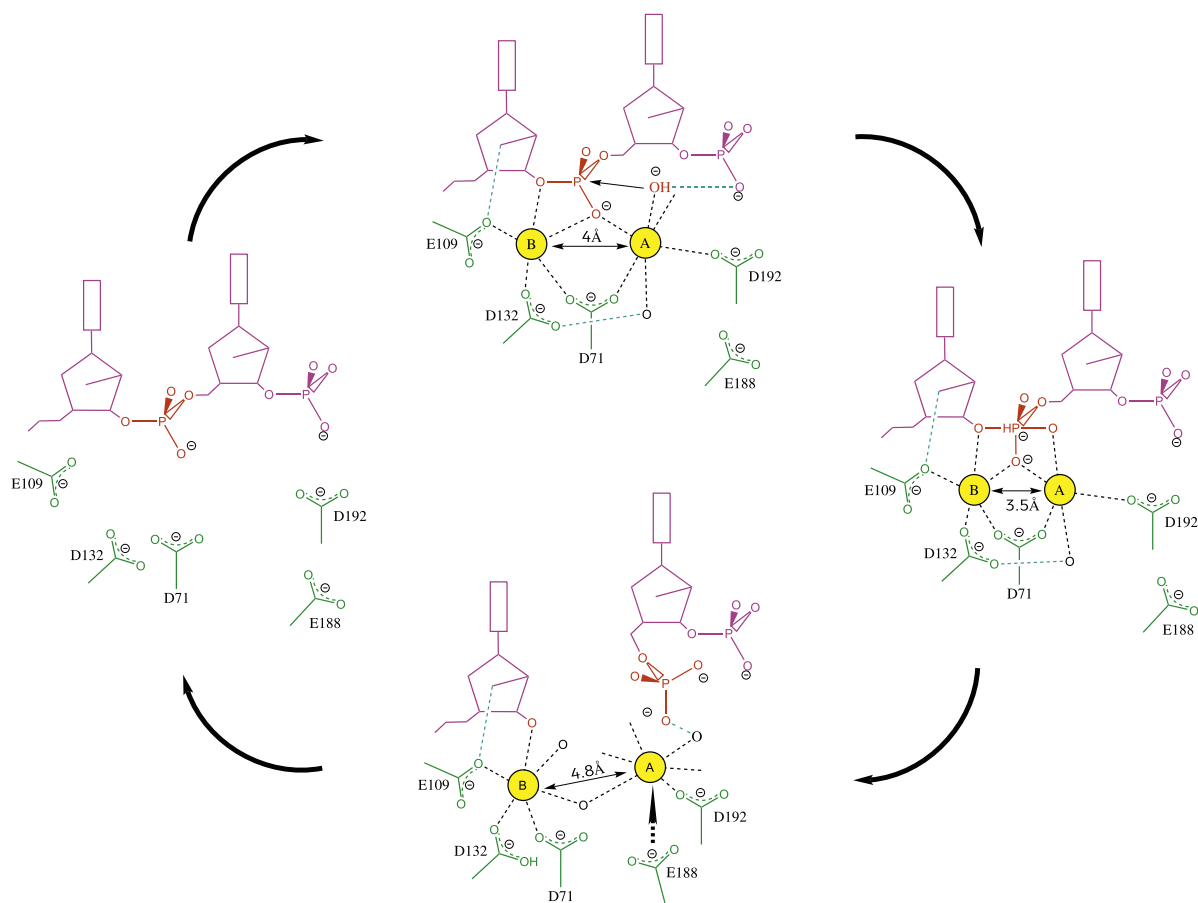


FIGURE 10.15 Schematic representation of the reaction steps proposed for RNase H. The substrate RNA is shown in pink and products in purple. Coordination of metal ions is highlighted in dark blue, and scissile phosphate in red. Selected hydrogen bonds are shown as blue lines. Black circles represent water molecules. The distance between the two metal ions is indicated in the enzyme–substrate, enzyme–intermediate, and enzyme–product complexes. (Adapted from Nowotny & Yang, 2006.)

5'-phosphate group allows metal ion B to relax and attain a regular octahedral coordination with two new ligands from water molecules.

In the classic two-metal polymerase/phosphodiesterase reactions, one ion activates a catalytic water or ribose hydroxyl for nucleophilic attack, while the second coordinates the leaving group: both metal ions stabilise the pentavalent transition state. Recent structural studies (Schmidt, Burgin, Deweese, Osherooff, & Berger, 2010: pp. 974) have led to a novel variation of the classic two-metal mechanism for DNA cleavage by topoisomerases.⁴ The proposed cleavage mechanism is indicated in Figure 10.16. Metal A and Arg781 stabilise the transition state, whereas metal B and His736 anchor the (–1) phosphate.

Yet another superfamily, the nucleotidyl-transferase family, also utilises the two-metal-ion-dependent catalysis: the members include transposases, retrovirus integrases, and Holliday junction resolvases.⁵ Whereas, in the nucleases, the Mg^{2+} ions are asymmetrically coordinated, and play distinct roles, in respectively activating the

4. These important enzymes are responsible for DNA supercoiling

5. It would simply befuddle the reader to explain what these enzymes do – suffice it to know that they cut and paste DNA fragments with as much exquisite specificity, as we hopefully do with our word processors!

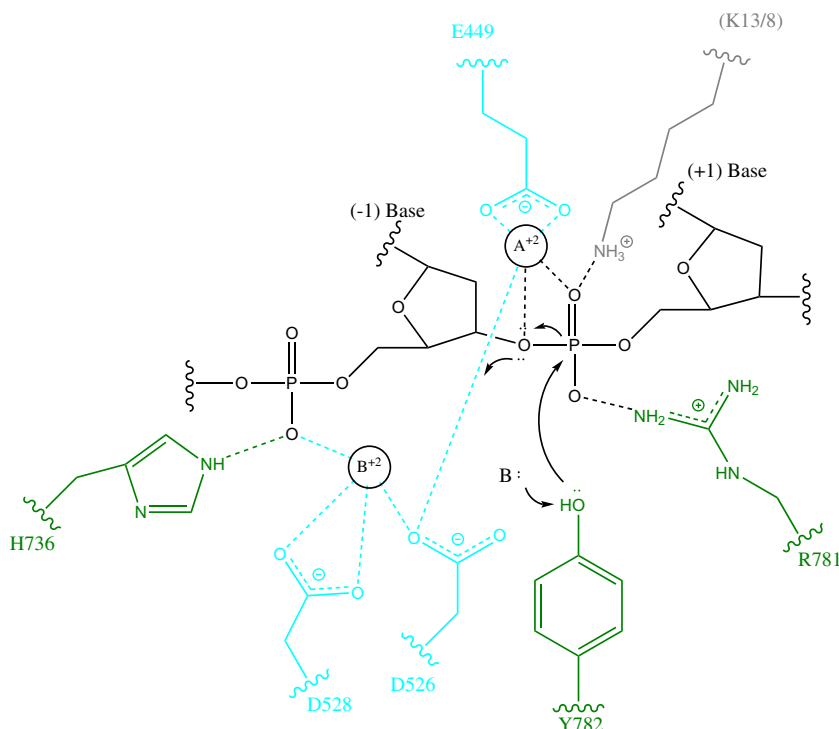
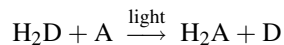


FIGURE 10.16 DNA cleavage by type IA and II topoisomerases. (Adapted from Schmidt *et al.*, 2010.)

nucleophile and stabilising the transition state, in the transposases, they are symmetrically coordinated and exchange roles to alternatively activate a water molecule and a 3'-OH for successive strand cleavage and transfer.

MAGNESIUM AND PHOTORECEPTION

We conclude this brief overview of the biological chemistry of Mg^{2+} by introducing the green pigment that gives us all so much joy in springtime, chlorophyll. Not only does it give the verdant colour to our trees and garden plants, but it also harnesses solar energy to ensure not only CO_2 fixation, but also a plethora of other important metabolic functions. Contrary to popular belief that photosynthesis corresponds to the fixation of CO_2 accompanied by the evolution of molecular O_2 , in reality more than 50% of photosynthetic organisms are strict anaerobes. The effective reaction carried out by photosynthetic organism uses the energy of solar photons to oxidise an electron donor, H_2D (which is H_2O in green plants), to supply electrons to an electron acceptor, A (usually NADP^+), generating the oxidised donor, D (O_2 in green plants), and the reduced acceptor, AH_2 (NADPH), according to the general equation



The principal photosynthetic photoreceptor is chlorophyll, a cyclic tetrapyrrole, which is formed, like haeme, from protoporphyrin IX. However, it has a cyclopentenone ring (V) fused to the pyrrole ring III, variable modifications of the substituents of rings I and II, esterification of the propionyl side chain of ring IV by a tetraisoprenoid alcohol, has one of its pyrrole rings reduced (ring IV in eukaryotic and oxygen-evolving cyanobacteria, ring II and IV in other photosynthetic bacteria), and, most importantly, the central metal ion is Mg^{2+} instead of Fe^{2+} (Figure 10.17). Chlorophylls are very effective photoreceptors, since they contain an extensive network of alternating single and double bonds (they are polyenes). They have very strong absorption bands in the

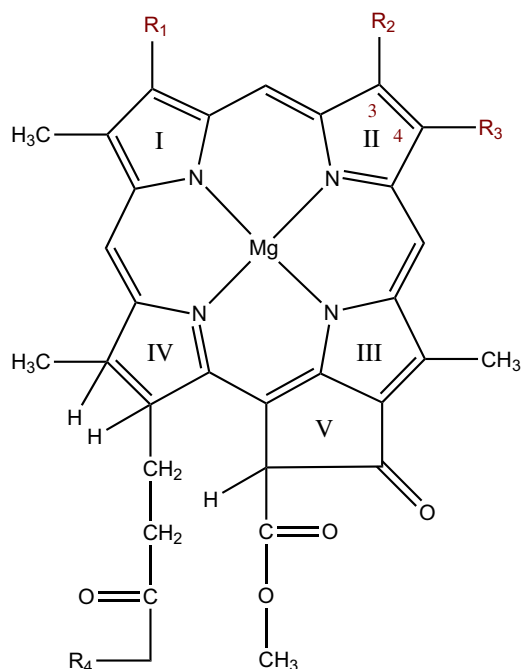


FIGURE 10.17 The chlorophyll a and b molecules have vinyl, ethyl, and phytyl side chains as R_1 , R_3 , and R_4 respectively: In chlorophyll a R_2 is a methyl group but is replaced by a formyl group in chlorophyll b. (Adapted from Voet & Voet, 2004: pp. 1591.)

visible region of the spectrum, where the sun's radiation is also maximal. The peak molecular extinction coefficient of the various chlorophylls is in excess of $10^5 \text{ M}^{-1} \text{ cm}^{-1}$ among the highest known for organic molecules.

Why, we may ask, does nature use Mg^{2+} as the metal in solar energy capture? Perhaps, as has been suggested by Frausto da Silva and Williams (2001), the reasons are first that Mg^{2+} does not have the redox properties of other metal ions such as Mn, Co, Fe, Ni, and Cu when inserted into a porphyrin, and it does not enhance fluorescence as much as the corresponding Zn porphyrin would.

If the light-harvesting system relied only on the special pair of chlorophyll molecules, which constitute the reaction centre, it would be inefficient for two reasons. First, chlorophyll molecules absorb only on the blue and red regions of the spectrum, so that light in the middle of the visible region, from 450–650 nm, which constitutes the peak of the solar spectrum, would be lost. Second, on account of the low density of reaction centres, many of the photons arriving on the photosystem would be unused. Accessory pigments, both additional chlorophyll molecules, and other classes of molecules, such as carotenoids⁶ and the linear tetrapyrrole phycobilins, which together constitute the reaction centre antenna, absorb energy and funnel it to the reaction centres. The phycobilins are particularly important in harvesting the yellow and green light which reaches the ecological niche of the blue-green (cyanobacteria) and red marine algae. The excited state of the special pair of chlorophyll molecules is lower in energy than those of the other antenna pigment molecules (Figure 10.18).

What happens when the energy of a photon of light absorbed by one of the accessory pigments is transferred to a chlorophyll molecule in the reaction centre? The light energy excites an electron from its ground-state level to an excited level, and can be moved from the initial chlorophyll molecule to a suitable nearby electron acceptor. This results in photoinduced charge separation, a positive charge being formed on the chlorophyll molecule and a negative charge on the acceptor. This is beautifully illustrated in the structure of the bacterial photosynthetic

6. Which are not only responsible for the orange colour of carrots, but for the spectacular autumn colours of deciduous trees as well.

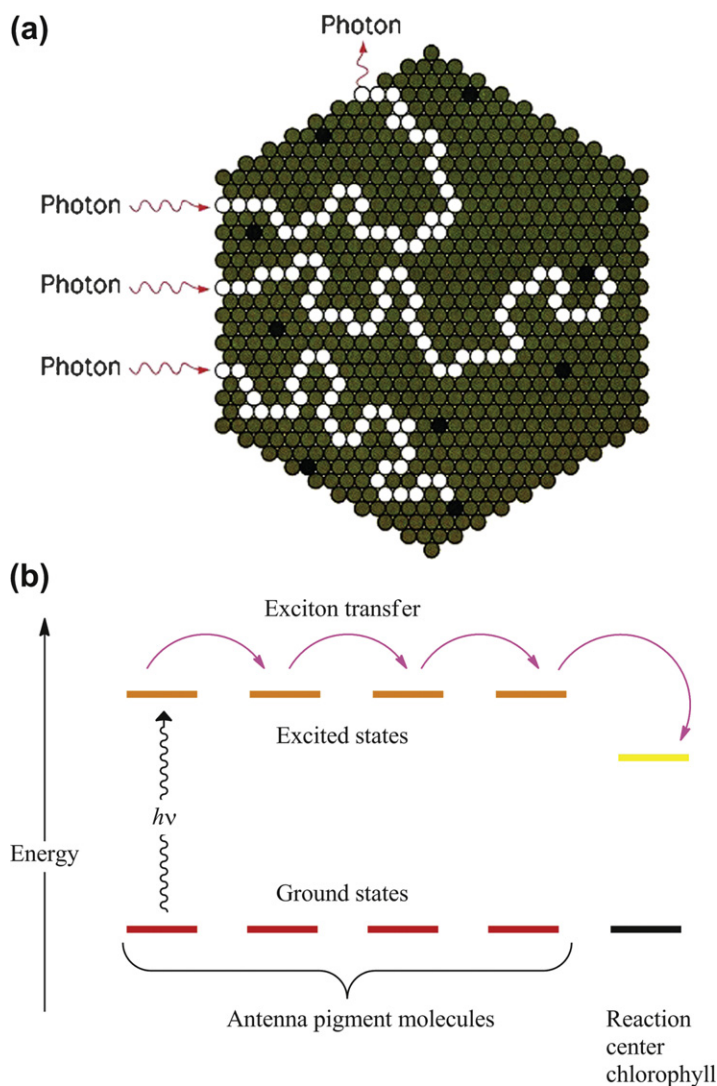


FIGURE 10.18 Solar energy transfer from accessory pigments to the reaction centre; (a) The photon absorption by a component of the antenna complex transfers to a reaction centre chlorophyll, or, less frequently is reemitted as fluorescence. (b) the electron ends up on the reaction centre chlorophyll because its lowest excited state has a lower energy than that of the other antenna pigment molecules. (Adapted from Voet & Voet, 2004.)

reaction centre from the bacterium *Rhodospseudomonas viridis* (Figure 10.19).⁷ The two bacteriochlorophyll molecules of the reaction centre, which constitute the special pair referred to above, are incorporated into a nearly perfect two-fold symmetry axis of two similar polypeptide chains, L (red) and M (blue). The two chlorophyll molecules are almost parallel, with a $\text{Mg}^{2+}-\text{Mg}^{2+}$ distance of $\sim 7 \text{ \AA}$, and are each in a predominantly hydrophobic region of the protein with a His side chain as fifth ligand to the metal ion. An additional polypeptide chain,

7. This was the first transmembrane protein to have its structure described in detail by Deisenhofer, Huber, and Michel in 1984. They received the Nobel prize for chemistry four years later.

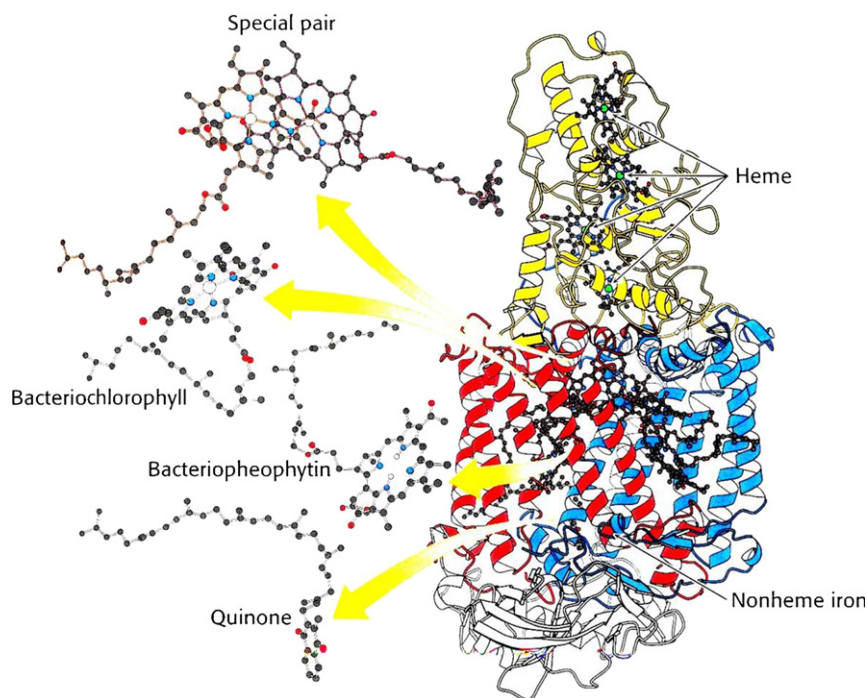


FIGURE 10.19 The core of the bacterial photosynthetic reaction centre. (From Berg, Tymoczko, & Stryer, 2001. Reproduced with permission from W.H. Freeman and Co.)

designated H (white) and a cytochrome subunit (yellow), which subsequently restores the electron deficit in the special pair, complete the structure.

Once the special pair has absorbed a photon of solar energy, the excited electron is rapidly removed from the vicinity of the reaction centre to prevent any back reactions. The path it takes is as follows: within 3 ps (3×10^{-12} s) it has passed to the bacteriopheophytin (a chlorophyll molecule which has two protons instead of Mg^{2+} at its centre), without apparently becoming closely associated with the nearby accessory bacteriochlorophyll molecule. Some 200 ps later, it is transferred to the quinone. Within the next 100 μs the special pair has been reduced (by electrons coming from an electron transport chain which terminates with the cytochrome situated just above it), eliminating the positive charge, while the excited electron migrates to a second quinone molecule.

REFERENCES

- Allen, K. N., & Dunaway-Mariano, D. (2004). Phosphoryl group transfer: evolution of a catalytic scaffold. *TIBS*, 29, 495–503.
- Berg, J. M., Tymoczko, J. L., & Stryer, L. (2001). *Biochemistry* (5th ed.). New York: Freeman.
- Cowan, J. A. (2002). Structural and catalytic chemistry of magnesium-dependent enzymes. *BioMetals*, 15, 225–235.
- Frausto da Silva, J. J. R., & Williams, R. J. P. (2001). *The biological chemistry of the elements* (2nd ed.). Oxford University Press. p. 270.
- Gerlt, J. A., Babbitt, P. C., & Rayment, I. (2005). Divergent evolution in the enolase superfamily: the interplay of mechanism and specificity. *Archives of Biochemistry and Biophysics*, 433, 59–70.
- Grueninger, D., & Schultz, G. E. (2006). Structure and Reaction Mechanism of L-Rhamnulose Kinase from *Escherichia coli*. *Journal of Molecular Biology*, 359, 787–797.
- Knowles, J. R. (1980). Enzyme-catalysed phosphoryl transfer reactions. *The Annual Review of Biochemistry*, 49, 877–919.

- Larsen, T. M., Wedeking, J. E., Rayment, I., & Reed, G. H. (1996). A carboxylate oxygen of the substrate bridges the magnesium ions at the active site of enolase: structure of the yeast enzyme complexed with the equilibrium mixture of 2-phosphoglycerate and phosphoenolpyruvate at 1.8 Å Resolution. *Biochemistry*, 30, 4349–4358.
- Maguire, M. E., & Cowan, J. A. (2002). Magnesium chemistry and biochemistry. *BioMetals*, 15, 203–210.
- Nowotny, M., & Yang, W. (2006). Stepwise analyses of metal ions in RNase H catalysis from substrate destabilization to product release. *EMBO Journal*, 25, 1924–1933.
- Peeraer, Y., Rabijs, A., Collet, J.-F., Van Scaftingen, E., & De Ranter, C. (2004). How calcium inhibits the magnesium-dependent enzyme human phosphoserine phosphatase. *European Journal of Biochemistry*, 271, 3421–3427.
- Schmidt, B. H., Burgin, A. B., Deweese, J. E., Osheroff, N., & Berger, J. M. (2010). A novel and unified two-metal mechanism for DNA cleavage by type II and IA topoisomerases. *Nature*, 465, 641–644.
- Steitz, T. A., & Steitz, J. A. (1993). A general two-metal-ion mechanism for catalytic RNA. *Proceedings of the National Academy of Sciences of the United States of America*, 90, 698–6502.
- Voet, D., & Voet, J. G. (2004). *Biochemistry* (3rd ed.). New York, Chichester: John Wiley and Sons.
- Yang, W., Lee, J. Y., & Nowotny. (2006). Making and breaking nucleic acids: two-Mg²⁺-ion catalysis and substrate specificity. *Molecular Cell*, 22, 5–13.

Calcium – Cellular Signalling

Introduction – Comparison of Ca^{2+} and Mg^{2+}	215
The Discovery of a Role for Ca^{2+} Other than as a Structural Component	215
An Overview of Ca^{2+} Regulation and Signalling	216
Ca^{2+} and Cell Signalling	225

INTRODUCTION – COMPARISON OF Ca^{2+} AND Mg^{2+}

How does Nature achieve the high degree of selective binding of Ca^{2+} by biological ligands compared to Mg^{2+} ? The differences in structure, thermodynamic stability, and reaction rates all stem from the difference in their ionic radii (Mg^{2+} , 0.6 Å; Ca^{2+} , 0.95 Å) measured in an octahedral oxygen donor environment. The Mg^{2+} ion is strictly octahedral with Mg–O distances of around 2.05 Å, whereas the larger Ca^{2+} ion, like Na^+ and K^+ , has an irregular coordination geometry, bond angle, bond distance, and coordination number (7–10) with Ca–O distances of 2.3–2.8 Å. In the case of the smaller Mg^{2+} , the central field of the cation dominates the coordination sphere, whereas in the larger cations the second and possibly even the third, coordination spheres, have a more important influence resulting in irregular structures. This also enables Ca^{2+} , unlike Mg^{2+} ion to bind to a large number of centres at once. Further, the kinetics of Ca^{2+} binding are quite different with water exchange rates close to the collision diffusion limits of 10^{10} s^{-1} , unlike much slower rates of 10^6 s^{-1} for Mg^{2+} . Ca^{2+} can interact with neutral oxygen donors, like carbonyls and ethers, unlike Mg^{2+} in aqueous media, as well as with anions, which avoids competition with Na^+ .

THE DISCOVERY OF A ROLE FOR Ca^{2+} OTHER THAN AS A STRUCTURAL COMPONENT

Calcium, together with sodium, potassium, and magnesium, is one of the metals required by living systems in macro-amounts – indeed, it represents 1.5–2% of an adult's total body weight. The biominerals that constitute teeth and bones contain the majority of the body's calcium (about 99%). Yet, the 1% which remains within the cells and tissues has enormous importance in the regulation of a whole series of cellular responses. Like a number of other discoveries, it was made by serendipity, and came far too early for the scientific community to recognise the importance of the discovery. In 1883, the English physiologist Sidney Ringer carried out a rather sloppy experiment, in which he suspended rat hearts in a saline medium made from London tap water (notoriously 'hard' on account of its high calcium content) and observed that they continued beating for a considerable period of time. When he repeated his initial experiments with distilled water, the hearts stopped beating after about 20-min incubation. He subsequently found that the addition of Ca^{2+} to the saline solution of the distilled water allowed prolonged cardiac contraction, establishing unequivocally that Ca^{2+} had a role in a tissue that had neither bones nor teeth. However, we had to wait more than sixty years before the importance of his observation that Ca^{2+} had a real function in cellular biochemistry, totally unrelated to its well-established structural role as a component of bones and teeth, became evident.

We now recognise that most important processes in living cells are regulated by Ca^{2+} . As Ernesto Carafoli has put it, ' Ca^{2+} accompanies cells throughout their entire lifespan, from their origin at fertilisation, to their eventual demise... as a conveyor of doom at the moment of cell death' (Carafoli, 2002). Indeed, Ca^{2+} controls almost

everything else that cells do in the intervening stages of life, including secretion, mobility, metabolic control, synaptic plasticity, as well as the expression of numerous genes (for further details see Berg et al., 2002; Carafoli, 2005; Gurini et al., 2005; Voet and Voet, 2004; Williams, 2006).

Like Na^+ , the extracellular concentration of Ca^{2+} is much higher (20,000-fold) than in the cytosol of the average mammalian cell. This is in sharp contrast with Mg^{2+} , the concentration of which barely differs across the plasma membrane. Since there is such a great discrepancy between the external and internal Ca^{2+} concentrations — cytosolic levels of 100–200 nM Ca^{2+} must be maintained to allow the signalling role of Ca^{2+} fluxes — it is clear that to maintain intracellular Ca^{2+} homeostasis, all cells must have developed mechanisms for regulating both Ca^{2+} uptake and egress. However, there are at least three intracellular compartments which can accommodate much higher Ca^{2+} concentrations — the mitochondria, the endoplasmic reticulum, and the Golgi apparatus. Hence, most of the Ca^{2+} required by cells is not imported, but is released from these storage sites.

AN OVERVIEW OF Ca^{2+} REGULATION AND SIGNALLING

The way proteins function is determined by their shape and their charge. Ca^{2+} binding to proteins triggers changes in both shape and charge. Likewise, phosphorylation of the hydroxyls of Ser, Thr, or Tyr residues by protein kinases (which represent about 2% of eukaryotic genomes) also changes protein charge, introducing a negative charge, and also changes protein conformation. This ability of both Ca^{2+} and phosphoryl groups to alter local electrostatic fields and protein conformations are the two universal tools of signal transduction in biology.

The basic concepts of Ca^{2+} regulation and signalling are summarised in Figure 11.1. Ca^{2+} -binding proteins belong to two broad categories. The first are membrane transporters of Ca^{2+} in the plasma membrane and in the organelles, while the second, known as Ca^{2+} -sensor proteins, decipher the Ca^{2+} signal before transmitting it to enzyme targets.

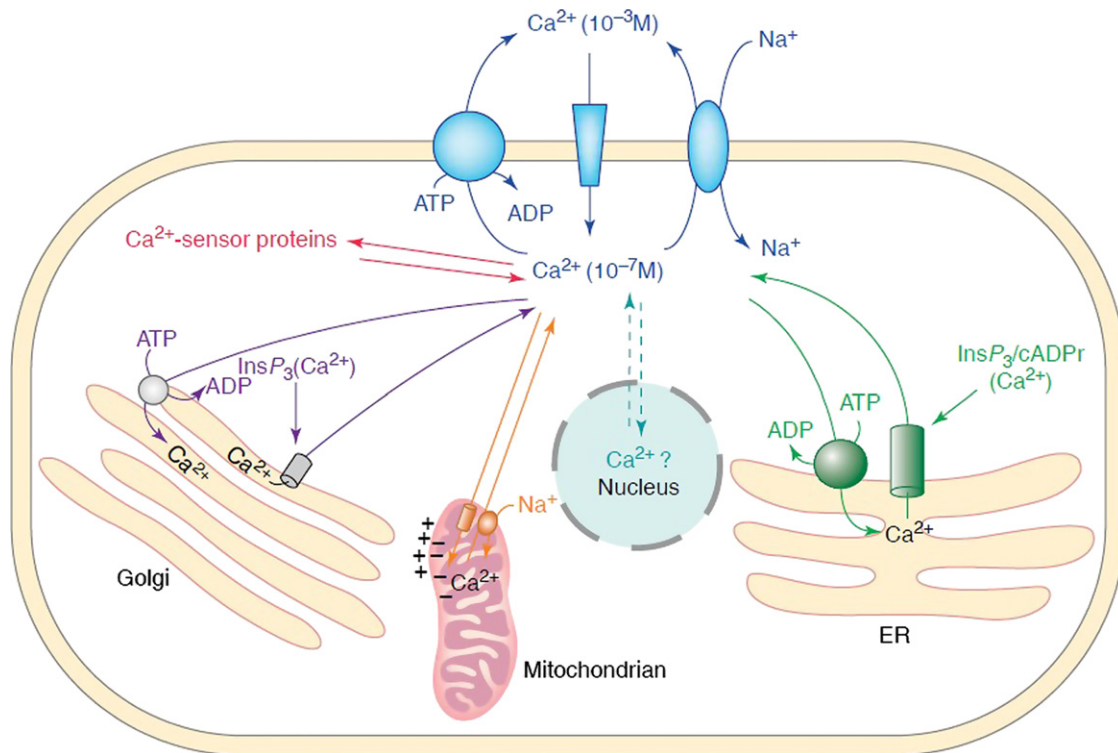


FIGURE 11.1 The basic concepts of Ca^{2+} homeostasis. (From Carafoli, 2004. Copyright 2004, with permission from Elsevier.)

Ca^{2+} enters cells via a number of plasma membrane channels which belong to three families: (i) voltage-gated channels; (ii) ligand-gated channels; and (iii) capacitative, or store-operated, channels. In Figure 11.1 only one Ca^{2+} channel is shown in the plasma membrane, which is representative of all three types.

The voltage-gated Ca^{2+} -selective channels (CaVs), like the corresponding Na^{+} and K^{+} channels (see Chapter 9), consist of a channel-forming α_1 -subunit made up of four six-transmembrane-domain repeats, in each of which the Ca^{2+} pore is formed by the loops which fold within the membrane between transmembrane domains 5 and 6. They also contain a voltage sensor within the transmembrane domain S4 of the α -subunit, rich in polar amino acids, as well as several accessory subunits which influence the properties of the channels. Ten α_1 -subunit genes have been cloned which define four different channel types, three gated by high voltage and one by low voltage. The CAVs are the fastest Ca^{2+} -signalling proteins, each channel conducting roughly a million Ca^{2+} ions/sec. This means that a few thousand channels/cell can increase intracellular Ca^{2+} levels >10-fold within milliseconds.

The ligand gated Ca^{2+} channels can be activated either directly or indirectly. Among the directly activated ligand-gated Ca^{2+} channels are those which are activated by the neurotransmitter glutamate, like the NMDA receptor, activated by the glutamate agonist N-methyl-D-aspartate.

The indirectly activated ligand-gated Ca^{2+} channels act by the interaction of the agonists with G-protein-coupled receptors (Figure 11.2), which produce inositol-(1,4,5)-trisphosphate (IP_3). IP_3 is a ligand for the intracellular IP_3R channel in the ER membrane (Figure 11.2), which then acts to release Ca^{2+} rapidly from the endoplasmic reticulum (ER) stores. The resulting depletion of Ca^{2+} within the lumen of the ER serves as the primary trigger for a message that is returned to the plasma membrane, resulting in the relatively slow (10–100 s)

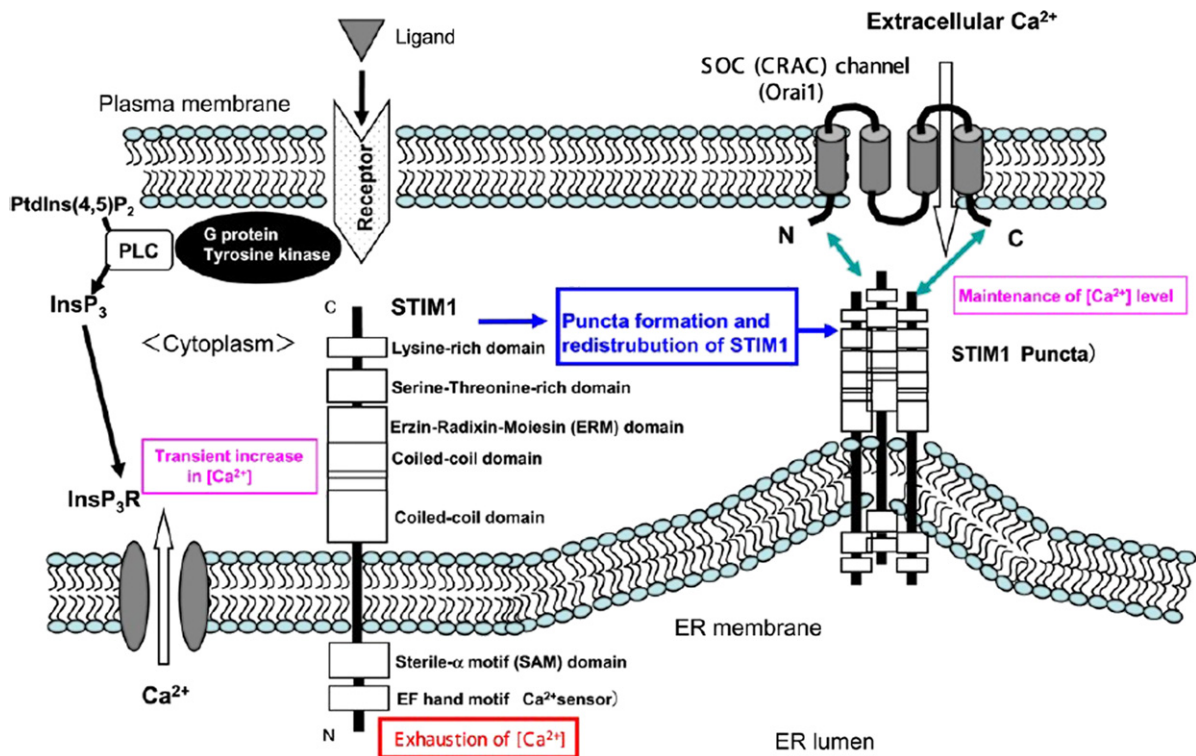


FIGURE 11.2 Formation of puncta structure and redistribution of STIM1. Ca^{2+} store depletion leads to a rapid translocation of STIM1 into puncta and puncta-formed STIM1 migrates from ER sites to the plasma membrane. Thereafter, the CRAC activation domain (CAD) of STIM1 directly binds to the N- and C-termini of Orai1 to open the SOC (CRAC) channel. (From Kurosaki & Baba, 2010. Copyright 2010, with permission from Elsevier.)

activation of the third type of Ca^{2+} channels, the capacitative or store-operated channels (SOCs). It was clear for a long time that a feedback mechanisms existed between the ER and the plasma membrane, and studies in the late 1980s and 1990s established that the depletion of ER Ca^{2+} , but not the resulting rise in cytosolic Ca^{2+} , is the initiating signal which, following InsP_3 -induced release of ER Ca^{2+} , triggers SOC entry (SOCE) through Ca^{2+} channels in the plasma membrane. The best-characterised SOC current is the Ca^{2+} release-activated Ca^{2+} (CRAC) current in lymphocytes and mast cells. However, the molecular mechanism remained undefined until recently. The key breakthrough came from RNAi¹ screening, which first identified STIM proteins (Cahalan, 2009) as the molecular link from ER Ca^{2+} store depletion to SOCE and CRAC channel activation in the plasma membrane, and then identified Orai (CRACM) proteins that comprise the CRAC channel pore-forming subunit. The interaction between STIMs and ORAI is a crucial element of calcium homeostasis in nonexcitable cells and leads to the formation of complexes visible in fluorescent microscopy as so-called “puncta” (Figure 11.2). Calcium entry into the cytoplasm is replenished in the ER by the activity of the Ca^{2+} adenosine triphosphatase (ATPase) of sarco/endoplasmic reticulum (SERCA) pump, which refills emptied ER stores.

The cytoplasmic Ca^{2+} level is low in resting cells. Cytoplasmic $[\text{Ca}^{2+}]$ is maintained at ~ 100 nM by extrusion from the cell via the plasma membrane Ca^{2+} ATPase (PMCA) and into the endo(sarco)solic reticulum by the smooth endoplasmic reticular Ca^{2+} ATPase (SERCA) transporters (Figure 11.3). The Na/Ca exchanger (NCX) is a major secondary regulator of cytosolic $[\text{Ca}^{2+}]$. NCX is electrogenic, exchanging three Na ions for one Ca^{2+} . The NCX, which is particularly important in excitable cells, exports Ca^{2+} with a higher transport capacity than PMCA. Intracellular Ca^{2+} hyperpolarises many cells by activating K^+ channels, and in some cells, Cl^- channels. This decreases CaV channel activity but increases the driving force across active Ca^{2+} -permeant channels.

As we pointed out above, there are at least three intracellular stores of Ca^{2+} , which accumulate Ca^{2+} using energy-driven systems and release Ca^{2+} through coupled transporters or ligand-gated channels. The sarco(endo)plasmic reticulum takes up Ca^{2+} using a sarco(endo)plasmic reticulum Ca^{2+} ATPase (SERCA) pump, and releases it through a channel that is activated by an inositol-(1,4,5)-triphosphate receptor, or via a calcium release channel called the ryanodine receptor (Figure 11.3). The Golgi also imports Ca^{2+} from the cytosol using a secretory pathway Ca^{2+} ATPase (SPCA) and releases it through a channel sensitive to inositol-(1,4,5)-triphosphate receptor (Figure 11.1). The third store is the mitochondrion, which imports Ca^{2+} using an electrophoretic uniporter, not yet identified in molecular terms. Ca^{2+} is continuously released via a $\text{Na}^+/\text{Ca}^{2+}$ antiporter, although a $\text{H}^+/\text{Ca}^{2+}$ release exchanger and the permeability transition pore may also mediate Ca^{2+} efflux from the mitochondria. In the mitochondrial matrix, two tricarboxylic acid dehydrogenases and pyruvate dehydrogenase are regulated by cycling of Ca^{2+} across the inner membrane.

As was pointed out above, inside the cell Ca^{2+} levels are not usually transmitted directly to targets, but are first processed by sensor proteins. Many of them, like calmodulin (described later), bind Ca^{2+} to characteristic EF-hand motifs undergoing in the process a conformational change, which is a prerequisite for their subsequent interaction with their respective target enzymes. However, some of these Ca^{2+} sensors, like protein kinase C, calpains, and calcineurin, are themselves Ca^{2+} -sensitive enzymes, while others like gelsolin and the annexins do not contain EF hands.

We discuss now in greater detail the three Ca^{2+} ATPase pumps (SERCA, PMCA, and SPCA), particularly SERCA for which a vast amount of structural information has been amassed in the course of the last decade. We then present a more detailed description of the intracellular pools of Ca^{2+} and their exchanges with the cytosol.

Calcium Pumps

Like the figure of Greek mythology Sisyphus,² ATPase pumps are condemned to push Ca^{2+} uphill for eternity into the endoplasmic reticulum (ER) (via sarcoendoplasmic reticular Ca^{2+} ATPases; SERCA pumps) or out of the cell (via plasma membrane Ca^{2+} ATPases; PMCA pumps). There is also a family of Ca^{2+} ATPases (pumps), located in the membranes of the Golgi network (the SPCA pumps). All three belong to the family of P-type ATPases,

1. Small non-coding RNAs, present in all organisms, which mostly function as regulators of translation and mRNA stability.

2. Sisyphus was condemned to repeat forever the same meaningless task of pushing a boulder up a mountain, only to see it roll down again.

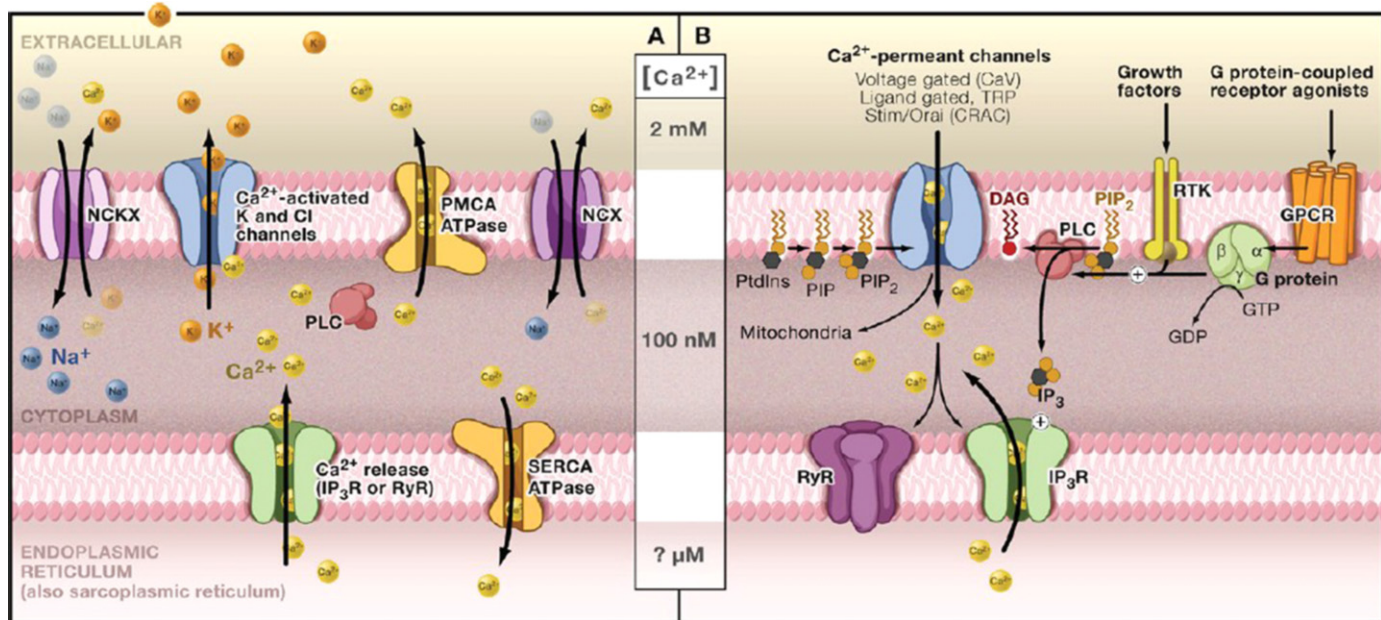


FIGURE 11.3 (A) The cytoplasmic Ca^{2+} is maintained at low levels in resting cells. Cytoplasmic $[Ca^{2+}]$ is maintained at ~ 100 nM by extrusion via plasma membrane Ca^{2+} ATPase (PMCA) and smooth endoplasmic reticular Ca^{2+} ATPase (SERCA) transporters. The Na/Ca exchanger (NCX), a major secondary regulator of $[Ca^{2+}]$, is electrogenic, exchanging three Na ions for one Ca^{2+} . Intracellular Ca^{2+} hyperpolarises many cells by activating K^+ channels, and in some cells, Cl^- channels. This decreases CaV channel activity but increases the driving force across active Ca^{2+} -permeant channels. (B) In excitatory Ca^{2+} signalling, plasma membrane ion channels are triggered to open by changes in voltage, or extra- or intracellular ligand binding. When open, ~ 1 million Ca^{2+} ions/s/channel flow down the 20,000-fold $[Ca^{2+}]_i$ gradient ($E_{Ca} \sim +150$ mV), maintained by elements shown in (A). Initial increases in $[Ca^{2+}]$ trigger more release, primarily from ER via Ca^{2+} -sensitive ryanodine receptors (RyR). G-protein-coupled receptor (GPCR) or receptor tyrosine kinase-mediated activation of PLC cleaves PIP₂ into inositol(1,4,5)-trisphosphate (IP₃) and diacylglycerol (DAG). IP₃ is a ligand for the intracellular IP₃R channel spanning the membrane of the ER. GPCRs catalyse the exchange of guanosine diphosphate (GDP) for GTP on $G\alpha$ subunits, releasing active $G\alpha$ and $G\beta\gamma$ subunits that in turn activate PLC β . RTKs dimerise upon ligand binding, autophosphorylate, and interact with other signalling proteins to activate PLC γ . (From Clapham, 2007. Copyright 2007, with permission from Elsevier.)

characterised by the presence of a phosphorylated intermediate (hence the name P-type), bound to an invariant Asp residue in a highly conserved sequence SDKTGT[L/I/V/M][T/I/S]. We have already briefly discussed the Na^+/K^+ -ATPase in Chapter 9, and in Figure 11.4a the architecture of the α -subunit of the Ca^{2+} ATPase of rabbit

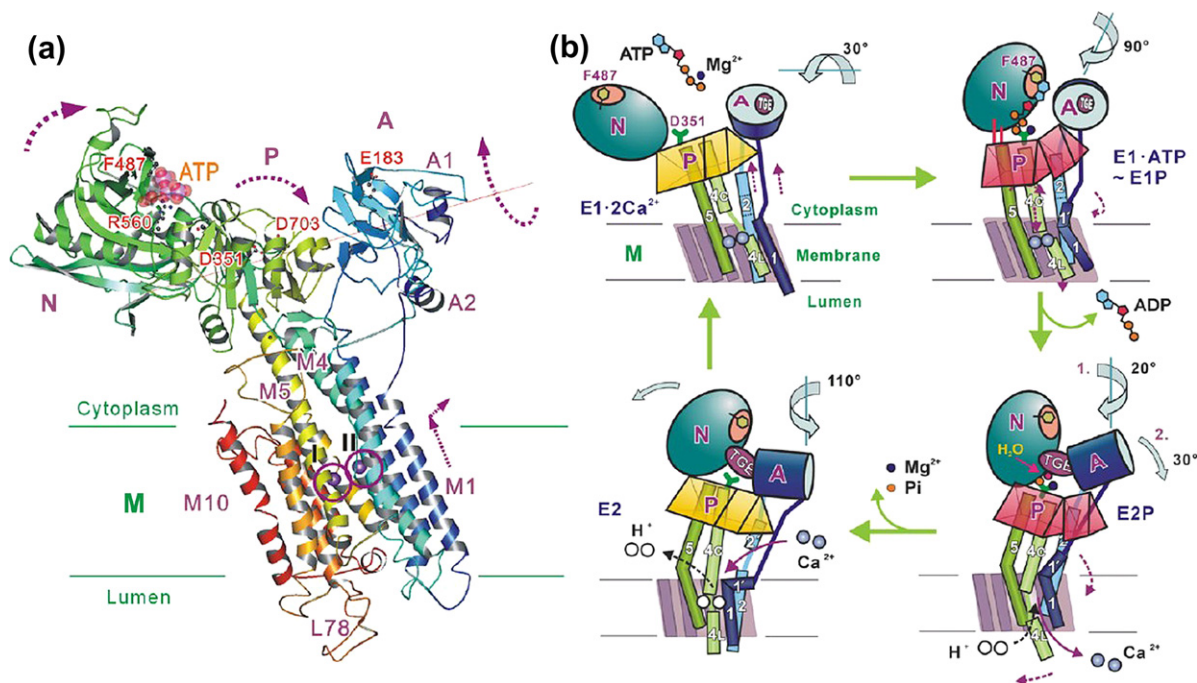


FIGURE 11.4 Architecture of Ca^{2+} -ATPase and its ion pumping mechanism. (a) A ribbon representation of Ca^{2+} -ATPase in the $\text{E1} \cdot 2\text{Ca}^{2+}$ state, viewed parallel to the membrane plane. Colours change gradually from the amino terminus (blue) to the carboxy terminus (red). Purple spheres (numbered and circled) represent bound Ca^{2+} . Three cytoplasmic domains (A, N, and P), the α -helices in the A-domain (A1–A3), and those in the transmembrane domain (M1–M10) are indicated. M1' is an amphipathic part of the M1 helix lying on the bilayer surface. Docked ATP is shown in transparent space fill. Several key residues – E183 (A), F487 and R560 (N, ATP binding), D351 (phosphorylation site), D627 and D703 (P) – are shown in ball-and-stick. Axis of rotation (or tilt) of the A-domain is indicated with a thin orange line. PDB accession code is 1SU4 ($\text{E1} \cdot 2\text{Ca}^{2+}$). (b) A cartoon illustrating the structural changes of the Ca^{2+} -ATPase during the reaction cycle, based on the crystal structures in 7 different states. (From Toyoshima, 2009. Copyright 2009, with permission from Elsevier.)

white skeletal muscle (SERCA1a) is presented. In addition to the ion transport domain, embedded in the membrane, there are three cytoplasmic domains, the N-domain (nucleotide binding), the P-domain (phosphorylation) in which many highly conserved residues are clustered, and the A-domain (actuator³), which together confer the ATP hydrolysing activity. The N-domain recognises and positions the γ -phosphoryl of ATP for nucleophilic attack, while the conserved Asp in the P-domain accepts the phosphoryl group and forms a high-energy aspartyl-phosphate intermediate. A Glu residue in the signature sequence ¹⁸¹TGES motif in the A-domain positions a water molecule for subsequent hydrolysis, leading to release of the phosphoryl group. The cytoplasmic domains are connected to the transmembrane (TM) segment by five linker regions (Figure 11.4) that form the crucial structural connection between the two-step release of energy on the cytoplasmic side and its conversion into physical translocation of ions through the membrane.

In muscle contraction, Ca^{2+} is released from sarcoplasmic reticulum (SR) into muscle cells via a Ca^{2+} -release channel. Ca^{2+} -ATPase then pumps back the released Ca^{2+} into the SR to cause relaxation. SERCA1a is both

3. Actuate – to put into action or motion.

structurally and functionally the best-characterised member of the P-type (or E1/E2-type) ion-translocating ATPases. According to the classical E1/E2 theory (summarised in the cartoon of Figure 11.5), the transmembrane

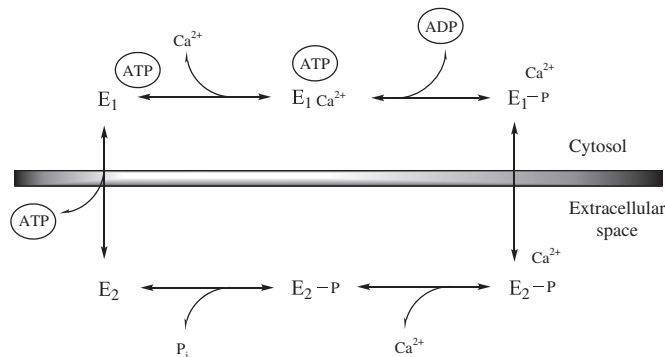


FIGURE 11.5 The reaction cycle of Ca^{2+} -ATPase pumps. In the E_1 conformation of the pump, Ca^{2+} is bound with high affinity at the cytoplasmic side of the plasma membrane. In the E_2 configuration, the binding site exposes Ca^{2+} to the external site of the plasma membrane, where its lower affinity for Ca^{2+} favours its release. (Adapted from Di Leva *et al.*, 2008. Copyright 2008, with permission from Elsevier.)

Ca^{2+} -binding sites have high affinity and face the cytoplasm in E_1 , and have low affinity and face the lumen of the SR (or extracellular side) in E_2 . Actual transfer of bound Ca^{2+} is thought to take place between two phosphorylated intermediates, E_1P and E_2P .

More than 20 crystal structures have been reported for SERCA1a in 9 different states that approximately cover the entire reaction cycle. The entire reaction cycle can be described essentially with the 4 principal structures depicted in Figure 11.4b, including a fairly detailed scenario of ion pumping, a description of how the affinity of the transmembrane Ca^{2+} -binding sites is altered, and how the luminal gate is opened and closed by events that occur around the phosphorylation site more than 50 Å away.

The E_2 state, formed subsequent to the release of Ca^{2+} into the lumen and hydrolysis of aspartyl-phosphate, is considered to be the ground state of the enzyme. The cytoplasmic headpiece composed of the A, P, and N domains is compact, as M5 is bent towards M1 to bring the P-domain underneath the $^{181}\text{TGES}$ loop of the A-domain (Figure 11.4b). The P-domain is free from distortion by bound phosphate or Mg^{2+} . The transmembrane Ca^{2+} -binding cavity is filled with water molecules and all the carboxyl groups there are predicted to be protonated to compensate for the space and charge imbalance created by the release of Ca^{2+} . This structure can only be maintained at low pH, and thermal agitation results in the opening of the headpiece, releasing the bound protons into the cytoplasm, placing most of the ATPase molecules into the E_1 state. In this state, the carboxyl groups in the Ca^{2+} -binding cavity are not protonated and, therefore, have high affinity for Ca^{2+} .

Ca^{2+} binding straightens the M5 helix and breaks the closed configuration of the headpiece by separating the P-domain from the A-domain. This allows delivery of ATP to the phosphorylation site, which can bind to the N-domain in the absence of Ca^{2+} and facilitate the opening of the headpiece, but it cannot reach Asp351, the phosphorylation residue. Straightening of the M5 helix moves the P-domain and the M4 helix towards the cytoplasm and allows two Ca^{2+} ions to enter the high-affinity sites through the gating residue Glu309 on M4 (not shown). ATP binds near the hinge between the P- and N-domains, causing the P-domain to bend, and in the process it tilts the A-domain by $\sim 30^\circ$, bringing the three cytoplasmic domains again closer.

In the next step, the M1 helix is pulled up and bent so that the amphipathic N-terminal part ($\text{M1}'$) lies on the membrane surface. This brings the top of the transmembrane part of M1 to occupy the space around Glu309 and, thereby, fixes the conformation of the Glu309 side chain, and closes the cytoplasmic gate of the Ca^{2+} -binding sites, occluding the two Ca^{2+} ions in the transmembrane binding sites. The M1 and M2 helices form a V-shaped

structure, which moves as a rigid body until the end of the reaction cycle, and transmits the movements of the A-domain to other transmembrane helices, primarily the luminal half of M4.

Phosphoryl transfer from the γ -phosphate to Asp351 fixes the N-domain in an inclined position so that a mechanical couple is formed between the N- and A-domains in preparation for the next main event, a 90° rotation of the A-domain in the E1P–E2P transition. Phosphoryl transfer also triggers the opening of the N- and P-domain interface. The A-domain rotates 90° around an axis $\sim 25^\circ$ inclined from the membrane normal and brings the $^{181}\text{TGES}$ loop of the A-domain deep into the gap between the N- and P-domains above the aspartyl-phosphate. This positions the TGES loop to make the resident time in this state long enough to release the bound Ca^{2+} into the lumen of the SR. This A-domain rotation causes a drastic rearrangement of the transmembrane helices M1–M6, including a large downward movement of M4, bending of M5 towards M1, and rotation of M6, which completely destabilises the Ca^{2+} -binding sites. The lower sections of M1 and M2 push against M4L, opening the luminal gate, thereby releasing the bound Ca^{2+} into the lumen, allowing protons and water molecules to enter and stabilise the empty Ca^{2+} -binding sites, thereby restoring the resting E2 state.

For fuller details on the mechanism of the SERCA1a pump, see the recent reviews by Toyoshima (2008, 2009).

The PMCA pump was isolated and purified using a calmodulin column, which exploited the observation that it was a target for calmodulin regulation. Two conformational states of the phosphorylated PMCA have been described. At the beginning of the transport cycle it is in the E_1 state, which, in contrast to its sister protein SERCA, only binds one Ca^{2+} with high affinity on the cytoplasmic side of the plasma membrane, and releases it from the E_2 form, which has low affinity for Ca^{2+} at the exterior of the cell. However, an important aspect of PMCA is that it has a long C-terminal tail, which contains a binding site for the Ca^{2+} -binding protein, calmodulin. This means that the plasma membrane Ca^{2+} -ATPase is autoregulated by Ca^{2+} itself (a more detailed description of calmodulin and its role in Ca^{2+} signalling follows below). In the absence of Ca^{2+} and calmodulin the pump is inactive, whereas when calcium-saturated calmodulin binds to the C-terminal tail, the pump is activated.

The Ca^{2+} pump of the secretory pathway (SPCA) is the newest member of the family of Ca^{2+} -transporting ATPases, and has the distinctive property that all SPCA pumps also efficiently transport Mn^{2+} . This may be related to the fact that the Golgi has a number of Mn^{2+} requiring enzymes, notably glycosyltransferases.

Intracellular Ca^{2+} Compartments

As was mentioned earlier, there are three intracellular compartments which are able to store substantial amounts of Ca^{2+} , namely the endoplasmic reticulum, the Golgi apparatus, and the mitochondria. Most of the Ca^{2+} required by cells is liberated from these three stores, rather than by importation from the exterior (Figure 11.1).

The endoplasmic reticulum takes up Ca^{2+} using the sarco(endo)plasmic reticulum ATPase (SERCA) pump (Figure 11.4). The SERCA pump of many types of muscle is regulated by a protein called phospholambin, which binds to SERCA both in its cytosolic and its transmembrane regions, maintaining the pump in an inactivated state when in its nonphosphorylated form, but detaches from the pump upon phosphorylation, presumably due to a conformational change. In this sense, the SERCA pump is like the PMCA pump, except that Ca^{2+} -saturated calmodulin activates PMCA, whereas kinase-dependent phosphorylation is involved in SERCA activation (perhaps also dependent on calmodulin).

Once within the endoplasmic (or sarcoplasmic) reticulum, Ca^{2+} is stored complexed to a number of low-affinity Ca^{2+} -binding proteins, the most important of which is called calsequestrin.

Release of Ca^{2+} from the reticulum occurs through two types of specific ligand-gated channels (Figure 11.3), both of which require Ca^{2+} itself in order to be opened. The first, in cells other than striated muscle, requires inositol-1,4,5-trisphosphate (IP_3), which together with diacylglycerol and Ca^{2+} itself, are the second messengers of the so-called phosphoinositide cascade, described in greater detail later in this chapter. The IP_3 -binding site is located in the long cytosolic amino-terminal tail of the protein, whereas the Ca^{2+} channel itself is in the C-terminal part of the molecule, consisting of the characteristic 6-transmembrane domain, with the loop connecting helices 5 and 6 folding back into the membrane to form the walls of the channel, just as it is found in plasma membrane voltage-gated channels.

The other ligand-gated channel is commonly referred to as the ryanodine receptor, after the alkaloid ryanodine which can induce opening or closing of the channels as a function of Ca^{2+} concentration. Ryanodine receptors (RyRs) are located in the sarcoplasmic/endoplasmic reticulum membrane and are responsible for the release of Ca^{2+} from intracellular stores during excitation–contraction coupling in both cardiac and skeletal muscle. Like the IP_3 channel, it has a very large N-terminal cytosolic component, with the Ca^{2+} channel proper localised in the C-terminal part of this very large protein (<5000 amino acids per subunit of the tetrameric receptor). Again, the classical 6-transmembrane helical structure with the channel formed by the loop between helices 5 and 6 found in voltage-gated plasma membrane channel is present. RyRs are the largest known ion channels (>2MDa) and exist as three mammalian isoforms (RyR 1–3), all of which are homotetrameric proteins which interact with, and are regulated by, phosphorylation, redox modifications, and a variety of small proteins and ions. Most RyR channel modulators interact with the large cytoplasmic domain. The ryanodine receptor, like the InsP_3 receptor, is activated by Ca^{2+} , although the precise nature of the native messenger is unclear. A prominent candidate is the metabolite of NAD^+ , cyclic ADP-ribose (cADPr). More recently, nicotinic acid adenine dinucleotide phosphate (NAADP) has been found to be an extremely potent calcium-mobilising messenger. While some evidence suggests that NAADP may act on acidic cellular compartments rather than on the endoplasmic reticulum, other studies indicate that it may also act on the ryanodine receptor. Cardiac ryanodine receptor (RyR2) controls Ca^{2+} release, which is essential for cardiac contractility.⁴

The Golgi apparatus also appears to be an important regulator of intracellular Ca^{2+} homeostasis. It has a SERCA pump, as well as a family of Ca^{2+} -ATPases (SPCA) which can transport Ca^{2+} and Mn^{2+} with high affinity for Ca^{2+} uptake. Ca^{2+} release is mediated by a channel which is modulated by InsP_3 , similar to that in the endoplasmic reticulum. However, it does not seem to have ryanodine-type channels.

The third important storage compartment for intracellular Ca^{2+} is the mitochondria (Figure 11.6). The original observations that mitochondria could actively accumulate Ca^{2+} in the 1950s and 1960s (reviewed in Carafoli, 2003) led both to the clarification of the uptake mechanism and to the seemingly predominant role of the mitochondria in cellular Ca^{2+} homeostasis. The Ca^{2+} uptake pathway relies on an as-yet-unidentified electrophoretic uniporter which gets its energy from the negative membrane potential inside the mitochondrial inner membrane maintained by the respiratory chain (see Chapter 5). Ca^{2+} release is mediated by a $\text{Na}^+/\text{Ca}^{2+}$ exchanger, which in some types of mitochondria, is replaced by a $\text{H}^+/\text{Ca}^{2+}$ exchanger. These uptake and egress pathways constitute a mitochondrial energy-dissipating Ca^{2+} cycle (Carafoli, 1979).

However, it was apparent that the affinity of the mitochondrial uptake system for Ca^{2+} is too low compared to cytosolic Ca^{2+} concentrations (apparent K_m in the 10–15- μM range, compared with sub- μM cytoplasmic Ca^{2+} concentrations) to effectively concentrate Ca^{2+} within the mitochondria. Further, the affinity of the endoplasmic reticulum system Ca^{2+} uptake system is at least one order of magnitude higher than that of the mitochondria (apparent K_m well below 1 μM). Together with the later discovery of the IP_3 -gated channels, this seemed to imply that the endoplasmic reticulum played the principal role in the regulation of cellular Ca^{2+} homeostasis.

The role of the mitochondria in cellular Ca^{2+} homeostasis was saved from oblivion by several important observations. Firstly, it became clear using indicators, notably aequorin, which can sense Ca^{2+} changes within microdomains of the cell rather than in the bulk cytoplasm, that the increase in cytosolic Ca^{2+} induced by the opening of InsP_3 -gated channels was paralleled by the rapid and reversible increase in mitochondrial Ca^{2+} . This activation of mitochondrial uptake results from the proximity of mitochondria and ER: the release of large amounts of Ca^{2+} by the ER creates local ‘hotspots’ of Ca^{2+} concentration in the vicinity of the mitochondrial uptake channels attaining levels of 20–30 μM , thereby activating the low-affinity mitochondrial uniporter. This constitutes the so-called ‘ Ca^{2+} microdomains’ concept (Rizzuto et al., 1993), illustrated in Figure 11.7. Mitochondria are able to sense localised hotspots of Ca^{2+} concentration, whether penetrating from the plasma

4. The American Heart Association estimates that the United States will spend close to \$39 billion in 2010 to treat over five million Americans suffering from heart failure. Advances in ryanodine receptor (RyR2)/calcium release channel research have led to the development of novel compounds targeting RyR2 for treating heart failure and for preventing lethal arrhythmias.

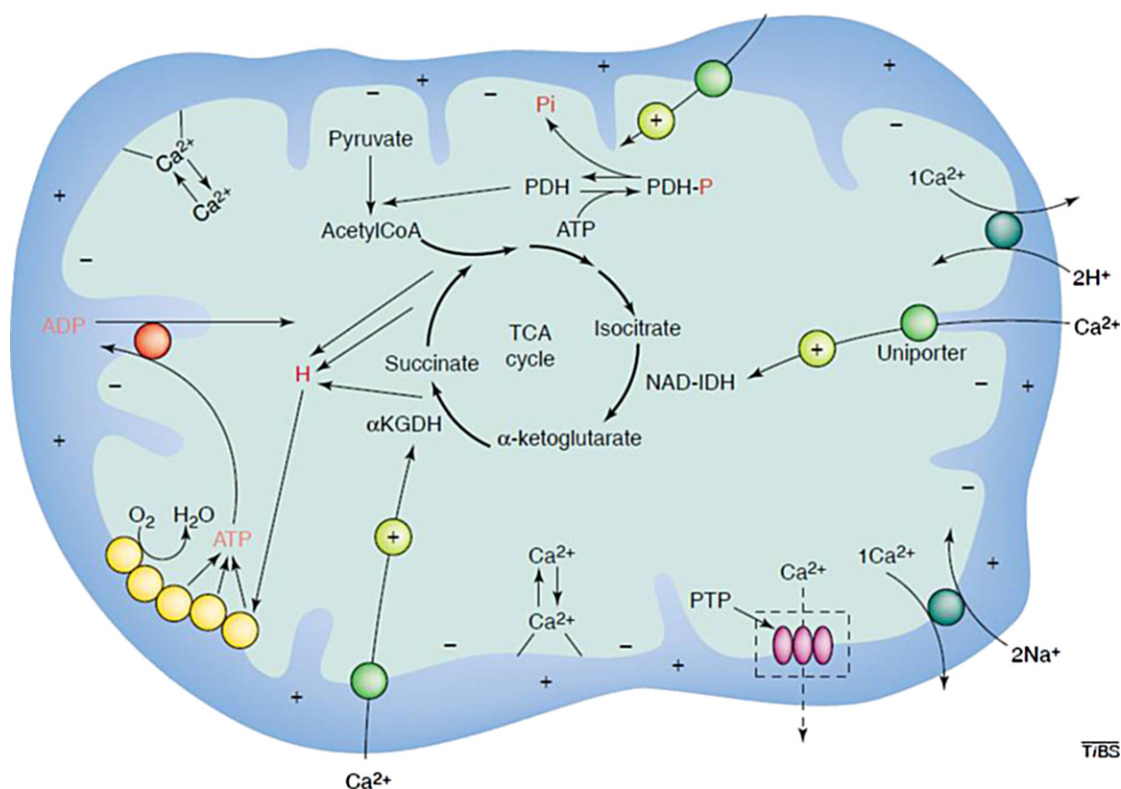


FIGURE 11.6 A schematic representation of the transport of Ca^{2+} in and out of mitochondria. The cartoon shows all the Ca^{2+} transporters, and stresses the activation of matrix dehydrogenases. The permeability transition pore (PTP) is enclosed in a dashed box because its role in Ca^{2+} release is not established. Abbreviations: AcetylCoA, acetyl-coenzyme A; α KGDH, α -ketoglutarate dehydrogenase; NAD-IDH, NAD^{+} -dependent isocitrate dehydrogenase; PDH, pyruvate dehydrogenase; TCA cycle, tricarboxylic acid cycle. (From Carafoli, 2003. Copyright 2003, with permission from Elsevier.)

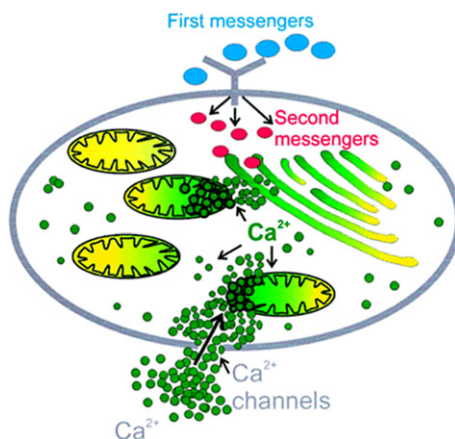


FIGURE 11.7 The microdomain concept of mitochondrial Ca^{2+} transport. Ca^{2+} penetrating from outside or released from the ER generates restricted domains of high Ca^{2+} concentration (20 μM or more), adequate to activate the low-affinity Ca^{2+} uptake system of neighboring mitochondria. The Ca^{2+} -releasing agonist shown is InsP_3 ; however, other agonists acting on different channels (e.g., cADPr) also generate the Ca^{2+} hotspots. (From Carafoli, 2002. Copyright, 2002, National Academy of Sciences, USA.)

membrane or from the ER. The rapid uptake of Ca^{2+} by mitochondria stimulates mitochondrial metabolism, as shown much earlier, by activation of three Ca^{2+} -sensitive matrix dehydrogenases (isocitrate dehydrogenase, α -ketoglutarate dehydrogenase, and pyruvate dehydrogenase).

It was also observed in earlier studies that mitochondria not only accumulate Ca^{2+} as an alternative to phosphorylation of ADP (Ca^{2+} uptake uncouples phosphorylation from electron transport), but that they could also accumulate much larger amounts of Ca^{2+} if phosphate was also taken up, resulting in precipitation of Ca^{2+} within the matrix as insoluble hydroxyapatite, visible as electron-dense granules by EM. An unusual feature of these hydroxyapatite deposits is that they fail to become crystalline, and remain amorphous even over protracted periods of time. Their presence in mitochondria in a number of disease conditions underlines the role for mitochondria as a sort of safety device, which can enable the cell to survive, if only for a limited period of time, situations of cytoplasmic Ca^{2+} overload. Finally, the nucleus may also play a role in Ca^{2+} homeostasis: this matter is controversial – whether the nuclear envelope, which is a prolongation of the endoplasmic reticulum, is a genuine Ca^{2+} store. It contains a Ca^{2+} pump, identical to that of the ER, and channels sensitive to IP_3 and cADPr.

Ca^{2+} AND CELL SIGNALLING

As we mentioned earlier, Ca^{2+} is a component of a number of intracellular signal-transducing pathways, including the phosphoinositide cascade. We also mentioned that in order to prevent the precipitation of phosphorylated or carboxylated calcium complexes, many of which are insoluble, it is essential to keep the cytosolic levels of Ca^{2+} in unexcited cells extremely low, much lower than that in the extracellular fluid and in intracellular Ca^{2+} stores. This concentration gradient gives cells a superb opportunity to use Ca^{2+} as a trigger – the cytosolic Ca^{2+} concentration can be abruptly increased for signalling purposes by transiently opening Ca^{2+} channels in the plasma membrane or in an intracellular membrane. These increases in intracellular free Ca^{2+} concentration can regulate a wide range of cellular processes, including fertilisation, contraction, secretion, learning and memory, and ultimately cell death, both apoptotic and necrotic.

Extracellular signals often act by causing a transient rise in cytosolic Ca^{2+} levels, which, in turn, activates a great variety of enzymes through the action of Ca^{2+} -binding proteins like calmodulin, as we will discuss in detail later: this triggers such diverse processes as glycogen breakdown, glycolysis, and muscle contraction. In the phosphoinositide cascade (Figure 11.8), binding of the agonist to the surface receptor R activates phospholipase C, either, as shown, through a G protein (which uses the energy of GTP hydrolysis to liberate a subunit capable of activating the next partner in the cascade) or alternatively by activating a tyrosine kinase. This results in the activation of phospholipase C, which hydrolyses phosphatidylinositol-4,5-bisphosphate (PIP_2) to InsP_3 (IP_3 in the figure) and diacylglycerol (DG). IP_3 , as we saw above, stimulates the release of Ca^{2+} , sequestered in the endoplasmic reticulum, and this in turn activates numerous cellular processes through Ca^{2+} -binding proteins, such as calmodulin. The membrane-associated DG activates protein kinase C to phosphorylate and activate other enzymes, like glycogen phosphorylase. This step also requires Ca^{2+} .

Ca^{2+} -binding proteins, which bind to their target sites in their Ca^{2+} -activated form, have been specifically designed to bind Ca^{2+} . They do so using a number of structural motifs, the best known of which is the helix–loop–helix EF-hand motif (Figure 11.9). This consists of two helices inclined at approximately 90° , flanking a 12-amino-acid loop which coordinates Ca^{2+} via side chain and carbonyl oxygens of five invariant residues. Calmodulin is the best-characterised member of the Ca^{2+} -binding protein family, and consists of two globular domains, each of which has two high-affinity Ca^{2+} -binding sites, linked by a seven-turn α -helix. In all EF-hand proteins each calcium is seven-coordinate, with three monodentate Asp or Asn residues, one bidentate Glu residue, one peptide carbonyl group, and one bound water molecule (Figure 11.10). Binding of Ca^{2+} to the globular domains of the dumbbell-like calmodulin molecule (Figure 11.9) results in a first change in conformation, which does not alter its overall dimensions, but opens up its two Ca^{2+} -binding lobes, exposing hydrophobic residues (essentially Met – unusually calmodulin is rich in Met, having 6% of this residue compared to about 1% in the average protein). Then, a second, and much more dramatic conformation change occurs, which collapses the elongated structure of

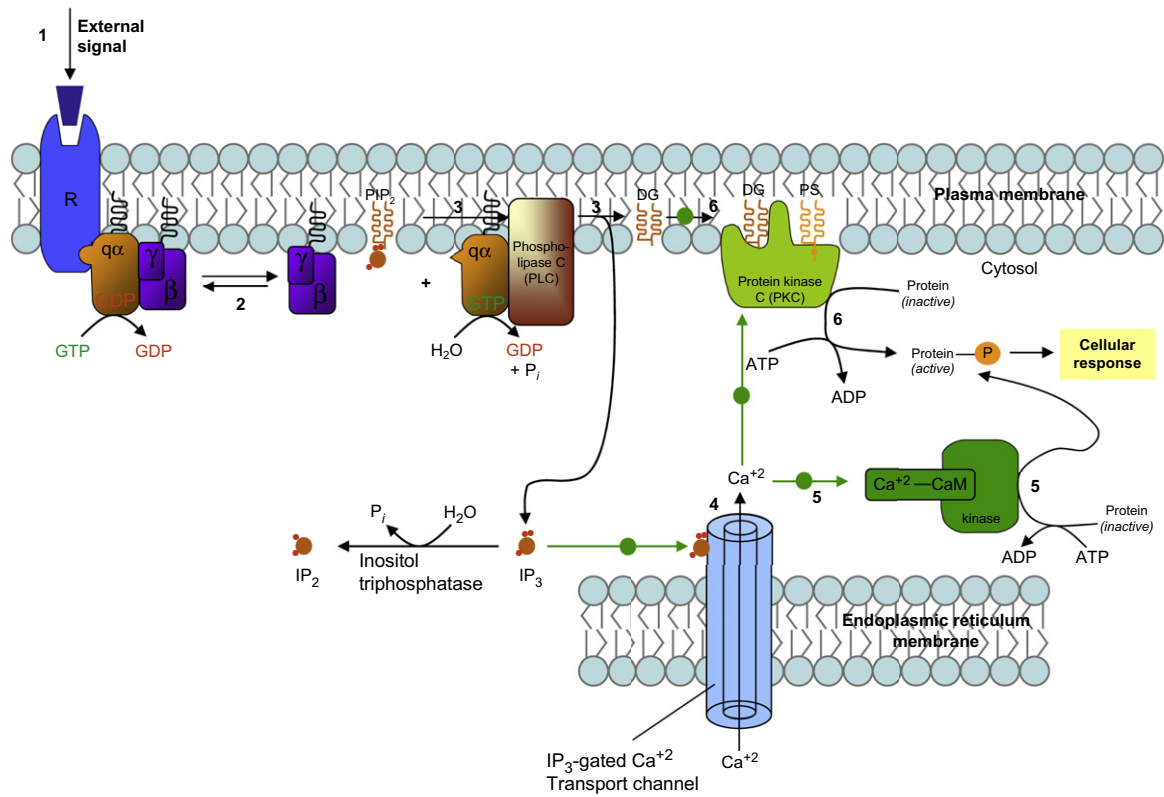


FIGURE 11.8 The phosphoinositide cascade.

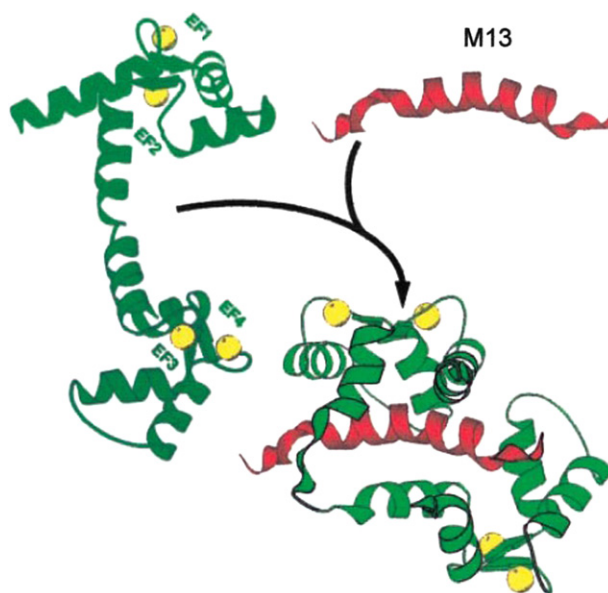


FIGURE 11.9 Decoding of the Ca^{2+} signal by conformational changes in EF hand proteins (CaM). CaM interacts with a 26-residue binding domain (red peptide, top right) of a skeletal muscle myosin light chain kinase termed M13. CaM (left) has bound Ca^{2+} (yellow spheres) to its four EF hands. It has already undergone the change that has made its surface more hydrophobic, but it still is in the fully extended conformation. The interaction with M13 collapses it to a hairpin shape that engulfs the binding peptide. (From Carafoli, 2002. Copyright (2002) National Academy of Sciences, USA.)

calmodulin protein to a hairpin conformation, which wraps around the binding domain of the target enzyme (Figure 11.9).

Binding of Ca^{2+} to calmodulin transmits changes in intracellular Ca^{2+} to the state of activity of a number of pumps, enzymes, including protein kinases, NAD kinase, phosphodiesterases, and other target proteins. Two targets are particularly interesting, one of which propagates the signal, while the other abrogates it. Calmodulin-dependent protein kinases (CaM kinases) phosphorylate many different proteins, which regulate fuel metabolism, ionic permeability, neurotransmitter synthesis and release. Binding of Ca^{2+} -calmodulin to these CaM kinases

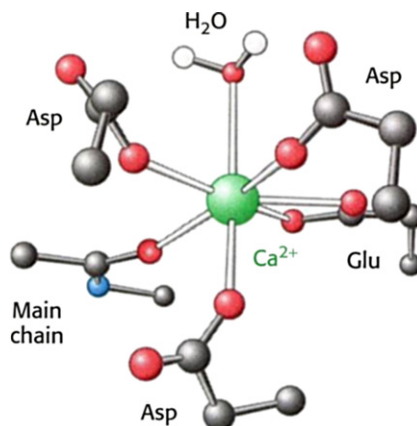


FIGURE 11.10 The Ca^{2+} -binding site of calmodulin.

activates them and allows them to phosphorylate target proteins (Figure 11.8). In addition, the activated enzyme phosphorylates itself, and thus remains partly active even after the Ca^{2+} concentration falls and calmodulin is released from the enzyme. In contrast to the CaM kinases, another important target of Ca^{2+} -calmodulin is the plasma membrane Ca^{2+} -ATPase pump, as we saw earlier, whose activation drives down the Ca^{2+} concentration within the cell, helping to terminate the signal.

One unusual feature of calmodulin is that, unlike other EF-hand proteins, which are usually committed, i.e., only interact with a specific target protein, it interacts with a wide range of targets. Comparisons of amino acid sequences of calmodulin-binding domains of target proteins suggest that calmodulin principally recognises positively charged amphipathic helices. It is interesting to note that the binding affinity of ~ 20 segments of these helices bind to Ca^{2+} -calmodulin as tightly as the target proteins themselves. The dramatic conformation change upon binding the target peptide (compare the central and right images of Figure 11.9) shows how the long central helix of uncomplexed calmodulin has unwound and bent to form a globular structure enclosing the helical target polypeptide within a hydrophobic tunnel.

REFERENCES

- Berg, J. M., Tymoczko, J. L., & Stryer, L. (2001). *Biochemistry* (5th ed.). New York: Freeman. 974.
- Cahalan, M. D. (2009). STIMulating store-operated Ca^{2+} entry. *Nature Cell Biology*, 11, 669–677.
- Carafoli, E. (1979). The calcium cycle of mitochondria. *FEBS Letters*, 104, 1–5.
- Carafoli, E. (2002). Calcium signalling: a tale for all seasons. *Proceedings of the National Academy of Sciences of the United States of America*, 99, 1115–1122.
- Carafoli, E. (2003). Historical review: mitochondria and calcium: ups and downs of an unusual relationship. *Trends in Biochemical Sciences*, 28, 175–181.
- Carafoli, E. (2004). Calcium-mediated cellular signals: a story of failures. *Trends in Biochemical Sciences*, 29, 371–379.
- Carafoli, E. (2005). Calcium – a universal carrier of biological signals. *FEBS Journal*, 272, 1073–1089.
- Clapham, D. E. (2007). Calcium signaling. *Cell*, 131, 1047–58.
- Di Leva, F., Domi, T., Fedrizzi, L., Lim, D., & Carafoli, E. (2008). The plasma membrane Ca^{2+} ATPase of animal cells: structure, function and regulation. *Archives of Biochemistry and Biophysics*, 476, 65–74.
- Guerini, D., Coletto, L., & Carafoli, E. (2005). Exporting calcium from cells. *Cell Calcium*, 38, 281–289.
- Kurosaki, T., & Baba, Y. (2010). Ca^{2+} signaling and STIM1. *Progress in Biophysics and Molecular Biology*, 103, 51–58.
- Rizzuto, R., Brini, M., Murgia, M., & Pozzan, T. (1993). Microdomains with high Ca^{2+} close to IP_3 -sensitive channels that are sensed by neighboring mitochondria. *Science*, 262, 744–7.
- Toyoshima, C. (2008). Structural aspects of ion pumping by Ca^{2+} -ATPase of sarcoplasmic reticulum. *Archives of Biochemistry and Biophysics*, 476, 3–11.
- Toyoshima, C. (2009). How Ca^{2+} -ATPase pumps ions across the sarcoplasmic reticulum membrane. *Biochimica et Biophysica Acta*, 1793, 941–946.
- Voet, D., & Voet, J. G. (2004). *Biochemistry* (3rd ed.). New York, Chichester: John Wiley and Sons.
- Williams, R. J. P. (2006). The evolution of calcium biochemistry. *Biochimica et Biophysica Acta*, 1763, 1139–1146.

Zinc – Lewis Acid and Gene Regulator

Introduction	229
Mononuclear Zinc Enzymes	230
Multinuclear and Cocatalytic Zinc Enzymes	238
Zinc Fingers DNA- and RNA-Binding Motifs	244

INTRODUCTION

Zinc has a highly concentrated charge in comparison to its relatively small ionic radius (0.65 Å) and binds modestly to anions such as carboxylates and phosphates. Its second characteristic is its high affinity for electrons, making it a strong Lewis acid, similar to copper and nickel. However, unlike the other two transition metal ions, it does not show variable valence, which might lead to it being preferred quite simply because it does not introduce the risk of free radical reactions.

After iron, zinc is the second most abundant trace element in the human body. An average adult has about 3 g of Zn, corresponding to a concentration of zinc of about 0.6 mM, most of which (some 95%) is intracellular. Zinc is essential for growth and development in all forms of life, has been proposed to have beneficial therapeutic and preventative effects on infectious diseases, including a shortening of the length of the common cold in man.

Zinc is found in more than 300 enzymes, where it plays both a catalytic and a structural role. It is the only metal to have representatives in each of the six fundamental classes of enzymes recognised by the International Union of Biochemistry: **oxidoreductases** like alcohol dehydrogenase and superoxide dismutase; **transferases** like RNA polymerase and aspartate transcarbamoylase; **hydrolases** like carboxypeptidase A and thermolysin; **lyases** like carbonic anhydrase and fructose-1,6-bisphosphate aldolase; **isomerases** like phosphomannose isomerase; and **ligases** like pyruvate carboxylase and aminoacyl-tRNA synthases. Zinc is not only involved in enzymes, where it plays both a catalytic and a structural role. There are growing numbers of nucleic acid binding proteins with essential Zn atoms, demonstrating the extensive role that Zn plays in the regulation of the transcription and translation of the genetic message (for more information concerning the content of this Chapter see [Auld, 2001](#); [Brown, 2005](#); [McCall et al., 2000](#); [Voet and Voet, 2004](#)).

The bioinorganic chemistry of zinc is dominated by a number of factors, the most pertinent of which are summarised here. The divalent zinc ion is redox inactive, in contrast, for example, to manganese, iron, and copper. Its d^{10} configuration means that not only does it have no $d-d$ transitions, and therefore no absorption spectroscopy, but also its complexes are not subject to ligand field stabilisation effects such that Zn^{2+} has no ligand field constraints on its coordination geometry. Coordination number and geometry are therefore dictated only by ligand size and charge. This means that zinc can, in principle, adopt highly flexible coordination geometry. However, in most zinc proteins, there is a strong preference for tetrahedral coordination, frequently slightly distorted, which enhances both the Lewis acidity of the zinc centre and the acidity of a coordinated water molecule. Only Cu(II) is a better Lewis acid. A few cases of zinc in five coordinate distorted trigonal bipyramidal geometry have been

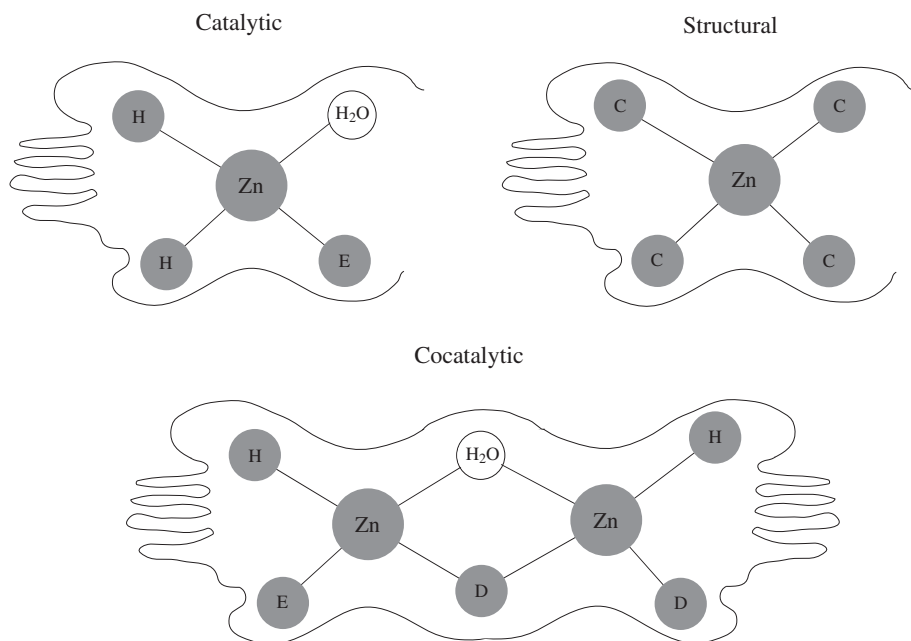


FIGURE 12.1 Zinc-binding sites in enzymes can be catalytic, structural, or cocatalytic. The protein ligands are indicated by smaller filled circles.

reported. Since zinc is of borderline hardness, it can bind oxygen (Asp, Glu, H₂O), nitrogen (His), and sulfur (Cys) ligands.

Three types of zinc-binding sites have been recognised in zinc enzymes (Figure 12.1), – catalytic sites, structural sites, and cocatalytic sites. Many of these zinc enzymes are peptidases and amidases, involved in the cleavage of amide bonds – they include peptidases such as thermolysin and carboxypeptidases, β -lactamases, which destroy the four-membered β -lactam rings in penicillins, and matrix metalloproteinases, which degrade extracellular matrix components such as collagen. Zinc enzymes also participate in the cleavage of the phosphodiester bonds in both DNA and RNA, and their role extends beyond catalysis of hydrolytic reactions to include the important lyase, carbonic anhydrase, and the oxidoreductase, alcohol dehydrogenase.

We consider successively the catalytic role of several classes of mononuclear Zn^{2+} enzymes and then discuss enzymes with di- and trinuclear cocatalytic zinc centres, some of which include a metal ion other than zinc. We conclude with a presentation of some of the zinc-based motifs found in proteins involved in the regulation of nucleic acid and protein synthesis.

MONONUCLEAR ZINC ENZYMES

The first zinc enzyme to be discovered was carbonic anhydrase in 1940, followed by carboxypeptidase A some 14 years later. They both represent the archetype of mono-zinc enzymes, with a central catalytically active Zn^{2+} atom bound to three protein ligands, and the fourth site occupied by a water molecule. Yet, despite the overall similarity of catalytic zinc sites with regard to their common tetrahedral $[(\text{XYZ})\text{Zn}^{2+}\text{-OH}_2]$ structure, these mononuclear zinc enzymes catalyse a wide variety of reactions, as pointed out above. The mechanism of action of the majority of zinc enzymes centres around the zinc-bound water molecule, which is best represented as $\text{Zn}^{2+}\text{-OH}_2$. What determines the catalytic properties of each enzyme is not only the nature of the donor ligands, but also the distance that separates them in the amino acid sequence of the protein. Typically (Table 12.1), two of the ligands are separated by only 1–3 amino acids, whereas the third ligand is separated by a longer spacer of between 5 and 196 residues.

TABLE 12.1 Coordination Motifs in Catalytic Sites of Some Typical Mononuclear Zinc Enzymes

Carbonic anhydrase	His-X-His-X ₂₂ -His
β-lactamase	His-X-His-X ₁₂₁ -His
Thermolysin	His-X ₃ -His-X ₁₉ -Glu
Carboxypeptidase	His-X ₂ -Glu-X ₁₂₃ -His
Alcohol dehydrogenase	Cys-X ₂₀ -His-X ₁₀₆ -Cys
Alkaline phosphatase	Asp-X ₃ -His-X ₈₀ -His
Adenosine deaminase	His-X-His-X ₁₉₆ -His

The mechanism of action of mononuclear zinc enzymes depends on the $\text{Zn}^{2+}\text{-OH}_2$ centre, which can participate in the catalytic cycle in three distinct ways (Figure 12.2) – either by ionisation, to give zinc-bound hydroxyl ion (in carbonic anhydrase), polarisation by a general base (in carboxypeptidase), or displacement of

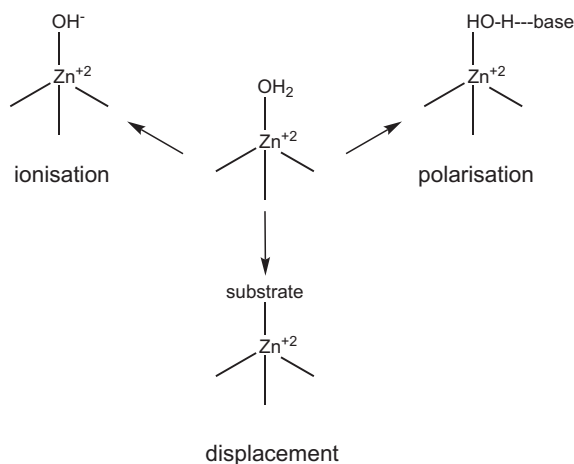


FIGURE 12.2 The zinc-bound water can either be ionised to zinc-bound hydroxide, polarised by a general base to generate a nucleophile for catalysis or displaced by the substrate.

the -OH_2 ligand by the substrate (in alkaline phosphatase). In the first two examples of mononuclear zinc enzymes which we consider, the lyases (carbonic anhydrase) and the hydrolases (carboxypeptidase), the zinc ion functions as a powerful electrophilic catalyst by providing some or all of the following properties: (i) an activated water molecule for nucleophilic attack, (ii) polarisation of the carbonyl of the bond to be cleaved, and (iii) stabilisation of the negative charge which develops in the transition state.

Carbonic Anhydrase

The carbonic anhydrases of mammalian erythrocytes have been the object of extensive study for the last 66 years, and can be considered as the prototype of zinc enzymes which use the hydroxyl ion generated by ionisation of the

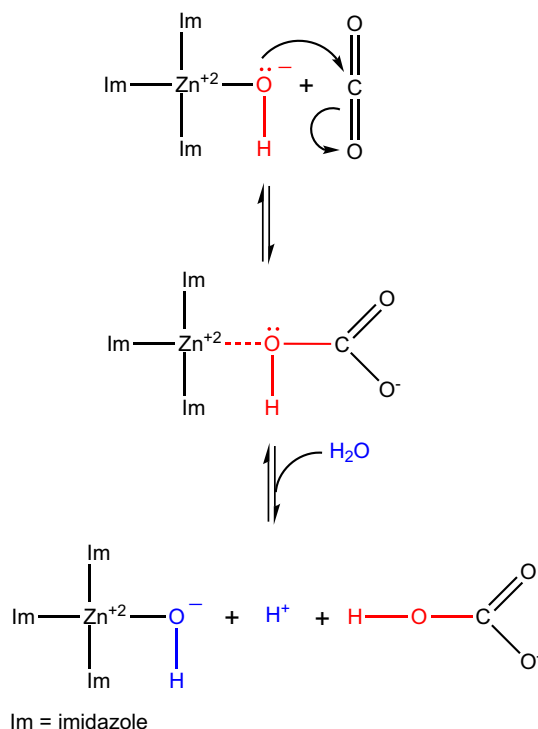


FIGURE 12.4 The main features of the mechanism of carbonic anhydrase.

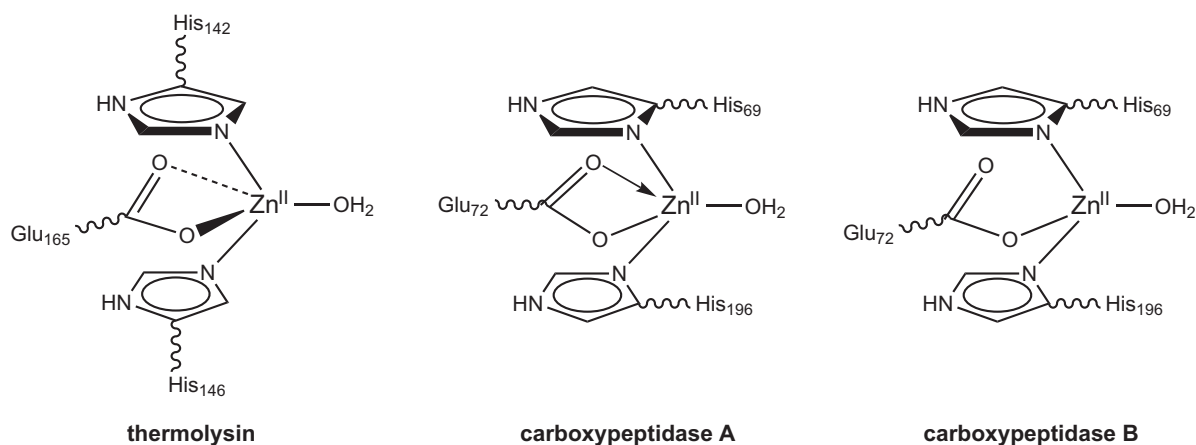


FIGURE 12.5 Active sites of thermolysin and carboxypeptidases A and B.

Bovine carboxypeptidase A was only the third protein, after myoglobin and lysozyme, to have its three-dimensional structure solved at high resolution. The active site zinc is bound to His-69, Glu-72, and His-196 (Figure 12.5), and to a water molecule. The zinc-bound water molecule is itself hydrogen bonded to Glu-270. Despite extensive experimental data, the mechanism of carboxypeptidase still remains controversial. Two major

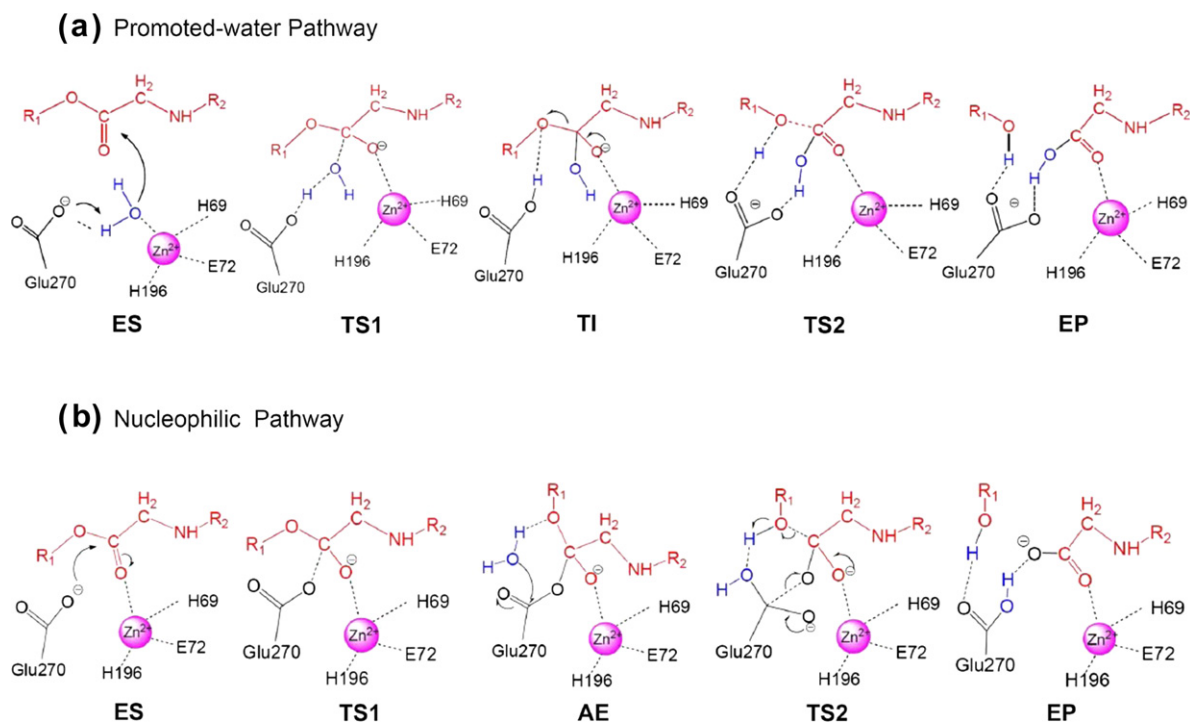


FIGURE 12.6 Two possible reaction pathways for carboxypeptidase A. (Adapted from Wu *et al.*, 2010.)

pathways have been proposed, which are depicted in Figure 12.6. The so-called promoted-water pathway (Figure 12.6a) assigns a dual role to Glu-270. In the initial nucleophilic addition step, it serves as a general base to facilitate the attack of the Zn-bound water on the scissile carbonyl carbon by transferring a proton from water to a carboxylate oxygen. In the second elimination step, it acts as a general acid to transfer this proton to the leaving nitrogen group. The alternative nucleophilic pathway (Figure 12.6b) envisages a direct nucleophilic attack by the carboxylate side chain of Glu-270 at the scissile carbonyl carbon, resulting in an acyl-enzyme (AE) intermediate, which can subsequently be hydrolysed by water. A recent investigation using hybrid quantum mechanical/molecular mechanical methods leads to the conclusion that the prevailing mechanism is the promoted-water pathway (Wu, Zhang, Xu, & Guo, 2010).

The MMPs (matrix metalloproteinases) are another important group of zinc-dependent metalloproteinases, which constitute a separate family within the metzincin clan of metalloproteinases. They were discovered 47 years ago as the agents responsible for the loss of the tails in the morphogenesis of tadpoles to frogs (Gross, 2004). MMPs are the main processors of extracellular matrix components, participating in tissue turnover and repair, embryogenesis, and angiogenesis. If they are not subjected to exquisite control, both spatial and temporal, they can cause pathologies such as arthritis, inflammation, and cancer. There are 23 MMPs present in humans, and to date the catalytic domains of 13 MMPs have been structurally characterised. The targeting of the active site and its associated hydrophobic pocket has enabled the design of a third generation of highly specific inhibitors to target selected MMPs, unlike the first and second generation, which failed in clinical trials because of their inability to distinguish between different MMPs.

The common structural elements in the metzincin superfamily are illustrated in Figure 12.7, for the catalytic domain of human MMP-8 (Phe79–Gly242) shown in standard orientation (PDB 1JAN). The repetitive secondary structure elements (orange arrows for β -strands, β I– β V; cyan ribbons for α -helices, α A– α C) and the four cations

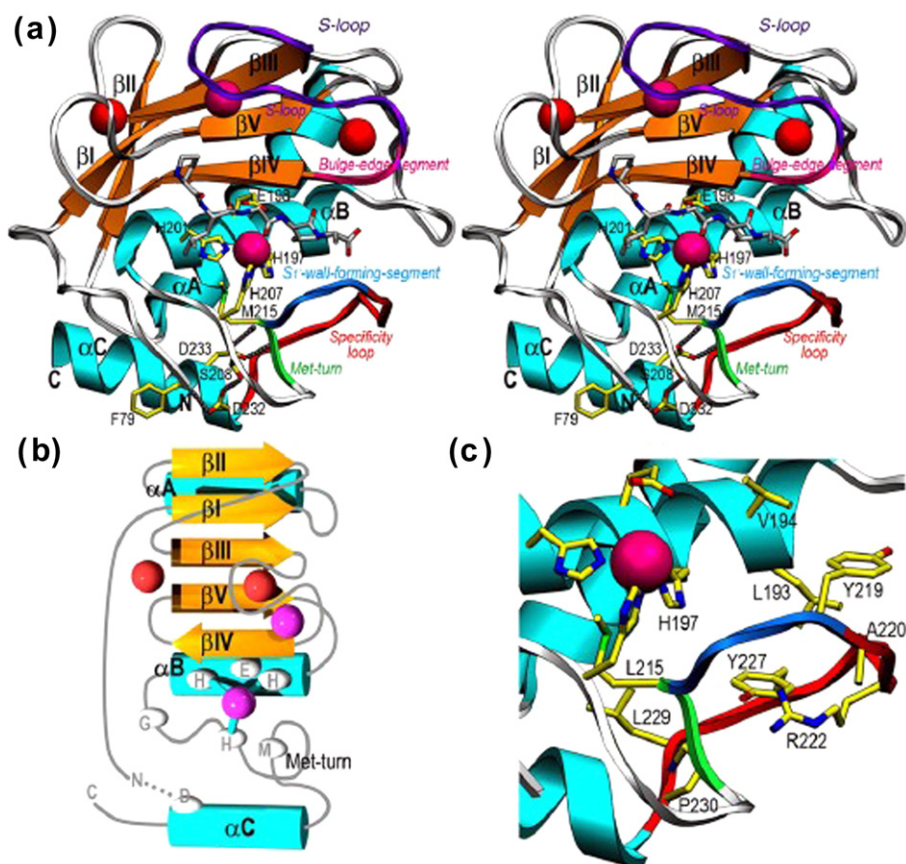


FIGURE 12.7 MMP catalytic domain structure. (a) Stereographic Richardson plot of the catalytic domain of human MMP-8 (Phe79–Gly242) shown in standard orientation (PDB 1JAN). The repetitive secondary structure elements (orange arrows for β -strands, β I– β V; cyan ribbons for α -helices, α A– α C) and the four cations (two zinc ions in magenta and two calcium ions in red) are depicted. The side chains of the zinc-binding histidines, the general base/acid glutamate, the Met-turn methionine, and residues engaged in key electrostatic interactions (grey dots) within the C-terminal subdomain are shown as stick models with yellow carbons and labeled. A substrate of sequence Pro–Leu–Gly–Leu–Ala, modeled based on published inhibitor structures, is shown as a stick model with grey carbons. Additional relevant chain segments are shown in distinct colours and labeled (Met-turn in green; specificity loop in red; S_1 -wall-forming segment in blue; S-loop in purple; and bulge-edge segment in magenta). (b) Topology scheme of MMP-8 in the same orientation as in (A). (c) Close-up view of (A) depicting the side chains engaged in zinc-binding and those shaping the specificity pocket, which are labeled. (From Tallant, Marrero, & Gomis-Rüth, 2010. Copyright 2010 with permission from Elsevier.)

(two zinc ions in magenta and two calcium ions in red) are depicted, as are the side chains of the zinc-binding histidines, the general base/acid glutamate, the Met-turn methionine, and residues engaged in key electrostatic interactions. The catalytic mechanism, based mainly on studies on thermolysin and carboxypeptidase A, is presented in Figure 12.8. This comprises the nucleophilic attack of a catalytic solvent molecule, polarised by the general base/acid glutamate and the catalytic zinc ion, on the scissile peptide bond at close-to-neutral pH values. For this to happen, a substrate must be bound and form a Michaelis complex (Figure 12.8). Binding occurs in an extended conformation through the S_1 -wall-forming segment and the bulge-edge segment on the primed side and through upper-rim strand β IV on the nonprimed side of the active site cleft. The scissile carbonyl group coordinates the catalytic zinc ion, which further ligands the three protein histidines of the zinc-binding consensus sequence and a solvent molecule in a pentameric fashion. The glutamate base abstracts a proton from the water,

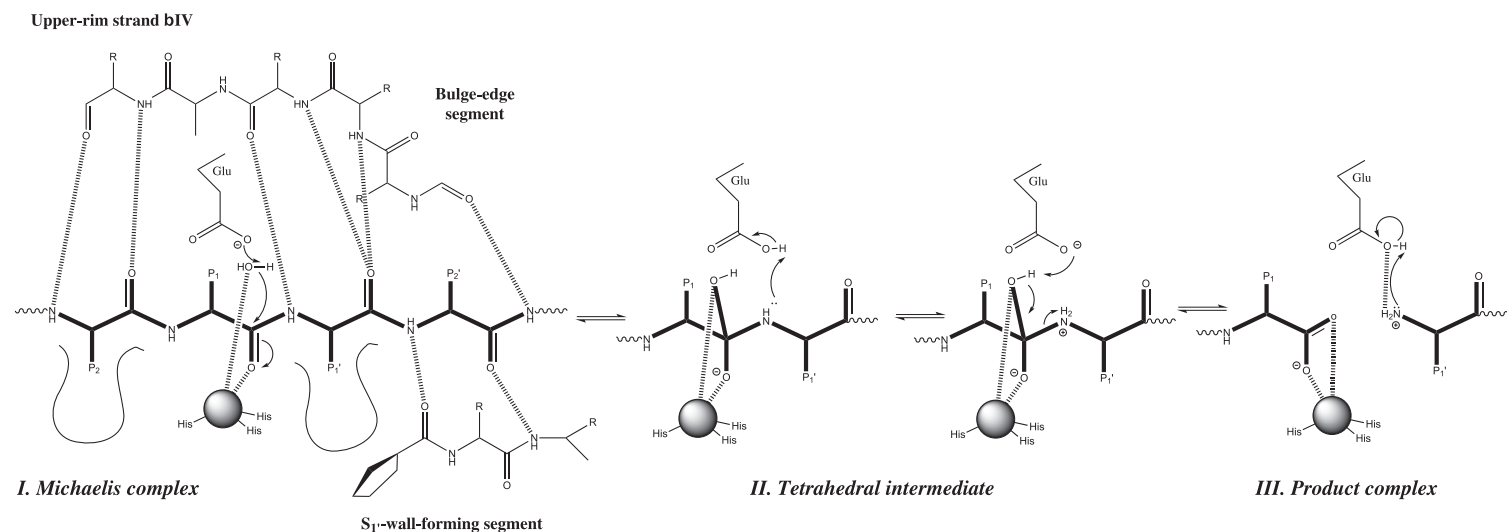
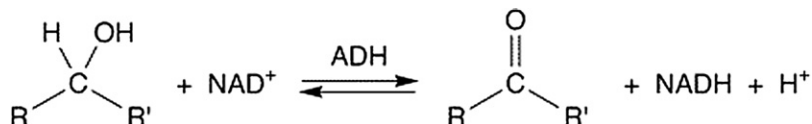


FIGURE 12.8 Catalytic mechanism of MMPs. Scheme for the cleavage mechanism proposed for MMPs, with the catalytic zinc ion as a sphere and hydrogen bonds as dashed lines. The three histidine ligands are represented by sticks. One conceivable alternative is that the second proton is transferred directly from the *gem*-diolate to the leaving amine in II and not *via* the general base/acid glutamate. This proton transfer could hypothetically occur before or after scissile-bond cleavage. (Adapted from Tallant *et al.*, 2010.)

giving rise to a hydroxide that attacks the scissile carbonyl carbon, with formation of a tetrahedral intermediate. The latter interacts in a bidentate manner with the zinc ion, with one of its hydroxyls occupying the position of the catalytic solvent in the substrate-depleted enzyme. The glutamate subsequently acts as a general acid catalyst, delivering the proton captured from the solvent to the scissile-bond nitrogen, which becomes a secondary ammonium function.

Alcohol Dehydrogenases

Alcohol dehydrogenases are a class of zinc enzymes which catalyse the oxidation of primary and secondary alcohols to the corresponding aldehyde or ketone by the transfer of a hydride anion to NAD^+ with release of a proton.



They are part of a very large family of short- and medium-chain dehydrogenases/reductases, which account for about 82 and 25 genes, respectively, in the human genome. The diversity of reactions catalysed by members of the SDR family are summarised in [Figure 12.9](#). By far, the most extensively studied alcohol dehydrogenases are those of mammalian liver. They are dimeric proteins, with each subunit binding two Zn^{2+} ions, only one of which is catalytically active. This catalytic Zn^{2+} ion has distorted tetrahedral geometry, coordinated to one histidine and two cysteine residues. The noncatalytic zinc plays a structural role and is coordinated tetrahedrally to four cysteine residues. The essential features of the catalytic cycle are summarised in [Figure 12.10](#). After binding of NAD^+ , the water molecule is displaced from the zinc atom by the incoming alcohol substrate. Deprotonation of the coordinated alcohol yields a zinc alkoxide intermediate, which then undergoes hydride transfer to NAD^+ to give the zinc-bound aldehyde and NADH. A water molecule then displaces the aldehyde to regenerate the original catalytic zinc centre, and finally NADH is released to complete the catalytic cycle.

Thus, the role of zinc in the dehydrogenation reaction is to promote deprotonation of the alcohol, thereby enhancing hydride transfer from the zinc alkoxide intermediate. Conversely, in the reverse hydrogenation reaction, its role is to enhance the electrophilicity of the carbonyl carbon atom. Alcohol dehydrogenases are exquisitely stereospecific and, by binding their substrate via a three-point attachment site ([Figure 12.11](#)), they can distinguish between the two methylene protons of the prochiral ethanol molecule.

Other Mononuclear Zinc Enzymes

We have already seen the diversity of function in the lyases, hydrolases, and oxidoreductases. Several other types of zinc coordination are found in a number of other enzymes, illustrated in [Figure 12.12](#). These include enzymes with the coordination motif $[(\text{His})_2(\text{Cys}) \text{Zn}^{2+}\text{-OH}_2]$, found in the lysozyme of bacteriophage T7, or $[(\text{Cys})_3 \text{Zn}^{2+}\text{-OH}_2]$ which occurs in 5-aminolaevulinate dehydratase (or porphobilinogen synthase). This latter enzyme catalyses the condensation of two molecules of 5-aminolaevulinate to form the pyrrole precursor of the porphyrins (haem, chlorophyll, and cobalamines), and its inhibition by Pb^{2+} is the cause of lead poisoning (saturnism), frequently observed among inner city children (Chapter 1).

Tetrahedral structural sites typically only involve coordination by the protein, frequently by cysteine residues, as illustrated by the structural $[\text{Cys}_4\text{Zn}^{\text{II}}]$ site in liver alcohol dehydrogenase. However, a class of zinc proteins and enzymes with tetrahedral “non-aqua” functional zinc sites have emerged in which the activity centres upon the reactivity of a zinc thiolate linkage rather than of a zinc-bound water molecule. The first to be discovered was the Ada DNA repair protein ([Figure 12.12](#)) which has a $[(\text{Cys})_4\text{Zn}]$ motif, and whose function is to repair damage to DNA due to methylation. The Ada protein achieves the repair by undergoing sacrificial alkylation of one of its zinc cysteine thiolate ligands ([Figure 12.13](#)). Thus, Ada does not act as an enzyme, but rather as a reagent (hence its

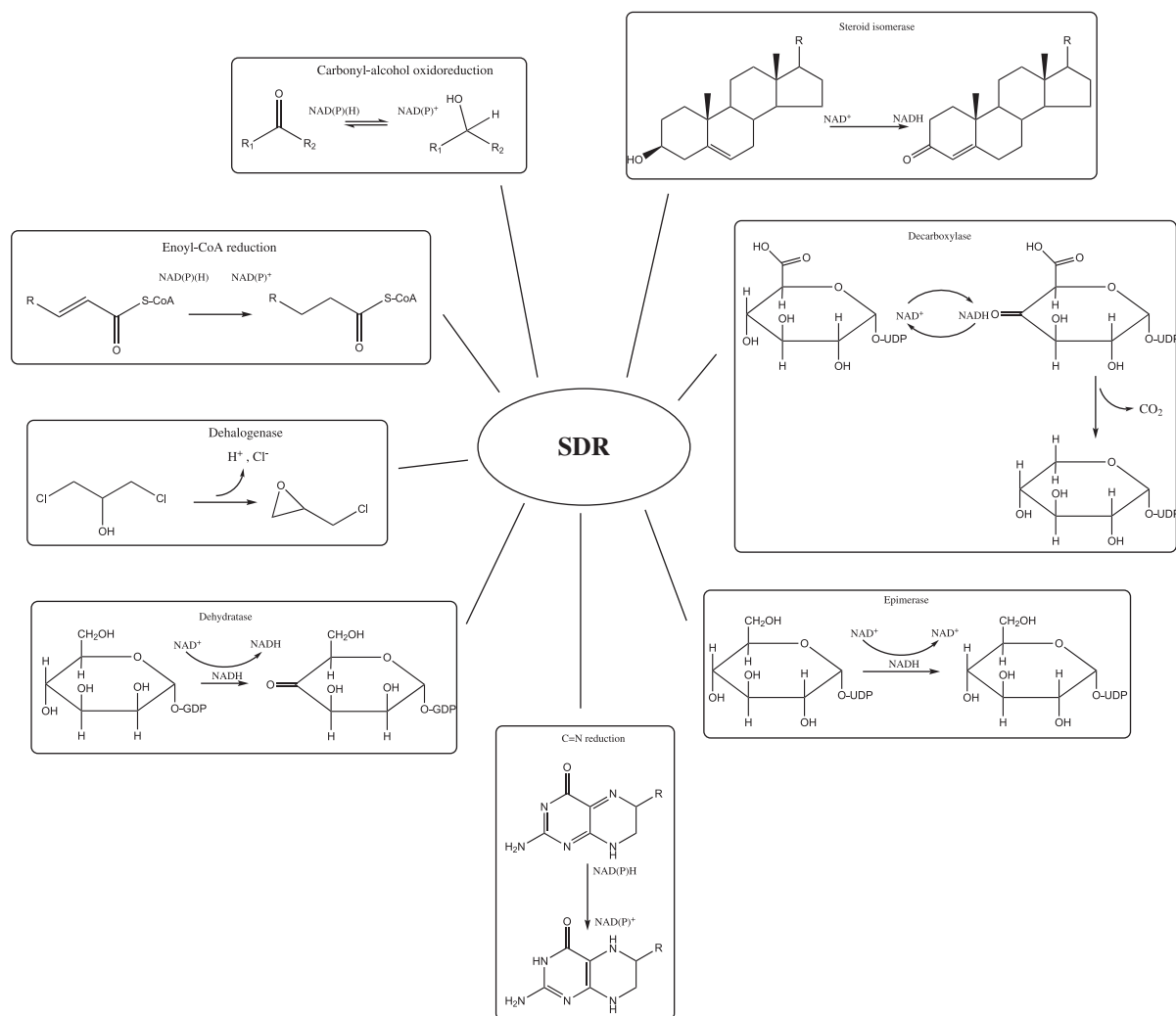


FIGURE 12.9 Reactions catalysed by SDR enzymes. (Adapted from Kavanagh, Örnvall, Persson, & Oppermann, 2008.)

description as a DNA repair *protein*). Other examples which involve reactivity of zinc cysteine thiolate linkages include methionine synthase, and the farnesyl- and geranylgeranyl-transferases, which participate, respectively, in the transfer of farnesyl and geranylgeranyl groups to target proteins.

MULTINUCLEAR AND COCATALYTIC ZINC ENZYMES

A number of zinc enzymes require two or more metal ions for full activity, but in the absence of X-ray structural data the location of these metal centres with regard to one another was often uncertain. When the first three-dimensional structures began to appear, it became clear that the metals were in close proximity. A particular feature of many of these enzymes was the presence of a bridging ligand between two of the metal sites, usually an Asp residue of the protein, which is occasionally replaced by a water molecule. Whereas some of the sites contain only Zn ions, several contain Zn together with Cu (in cytosolic superoxide dismutases), Fe (in purple acid phosphatases), or Mg (in alkaline phosphatase).

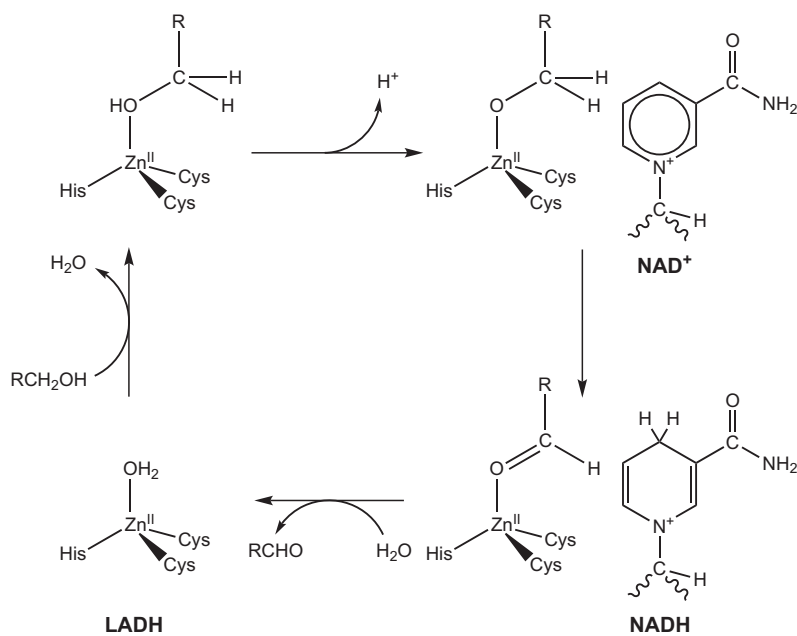


FIGURE 12.10 The essential features of the catalytic cycle of liver alcohol dehydrogenase. (Adapted from *Parkin, 2004*.)

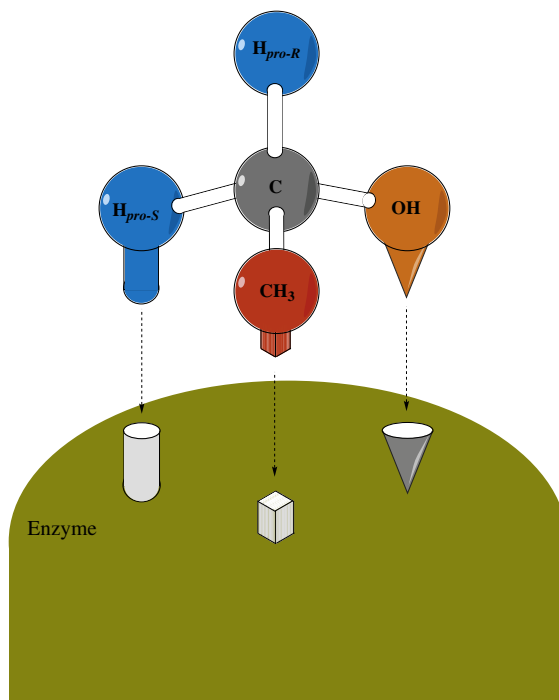


FIGURE 12.11 Specific attachment of a prochiral centre to an enzyme-binding site enables the enzyme to distinguish between prochiral methylene protons in ethanol. (Adapted from *Voet & Voet, 2004*.)

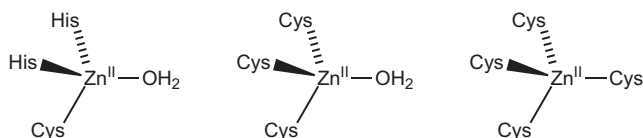


FIGURE 12.12 Some other active site coordination motifs in mononuclear zinc enzymes: from left to right bacteriophage T7 lysozyme, 5-aminolaevulinate dehydratase, Ada DNA repair protein. (Adapted from *Parkin, 2004*.)

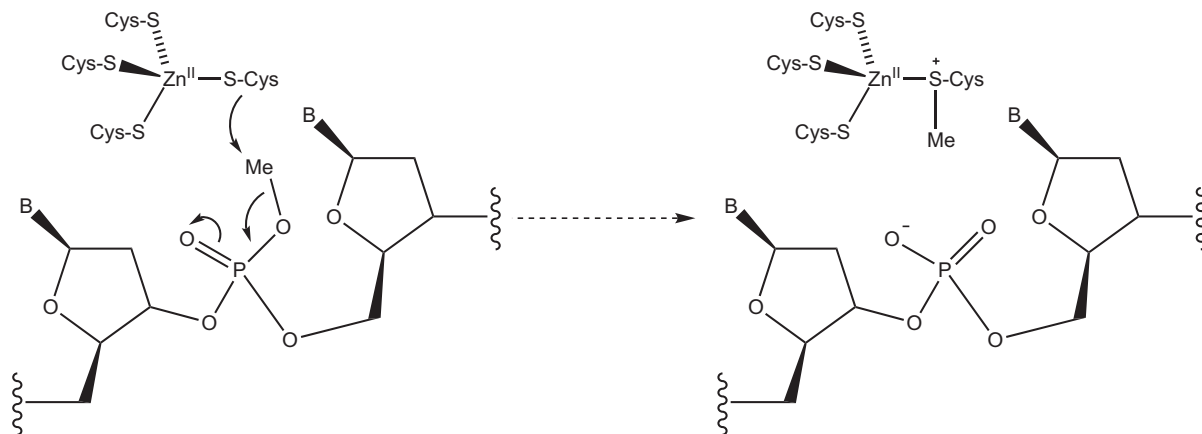


FIGURE 12.13 Repair of damaged DNA by sacrificial alkylation of one of the zinc cysteine thiolate ligands of the Ada DNA repair protein. (Adapted from *Parkin, 2004*.)

Cu–Zn superoxide dismutases will be discussed in greater detail in Chapter 14. Suffice to say here that this is the only cocatalytic site to have a bridging His ligand, and that the role of the Zn ion is thought to be uniquely structural, whereas the Cu undergoes redox cycling during catalysis. The importance of the Zn atom is underlined by the observation that the zinc-deficient enzyme is thought to participate in both the sporadic and familial forms of the neurodegenerative disease, amyotrophic lateral sclerosis, which is discussed in Chapter 21.

An important strategy employed by bacterial strains to resist β -lactam antibiotics (the structural ‘leitmotif’ of the penicillin class of antibiotics) is the expression of Zn-dependent β -lactamases. Many zinc β -lactamases have been described in recent years, and a growing number of pathogens have been shown to synthesise these enzymes, which have a broad activity profile and cleave the four-membered β -lactam ring not only of penicillins and cephalosporins, but also of carbapenems. Three different subclasses of metallo- β -lactamases have been characterised (B1, B2, and B3), which all have two potential Zn^{2+} -binding sites (Figure 12.14). In the B1 enzymes, one zinc atom has tetracoordinate geometry with a $[(\text{His})_3\text{Zn}(\mu\text{-OH})]$ motif in which the hydroxide ion serves as a bridge to the second Zn site, which has trigonal bipyramidal geometry with a $[(\text{His})(\text{Asp})(\text{Cys})\text{Zn}(\text{OH}_2)(\mu\text{-OH})]$ motif. In the B3 family, the ‘histidine’ site is the same as in B1 enzymes, while the second zinc ion is ligated by two His and one Asp. The Cys is replaced by a Ser, which, however, does not interact with the Zn ion. Whereas B1 and B3 β -lactamases have maximum activity with both Zn sites occupied, the B2 β -lactamases are fully active with only one Zn site occupied, but binding of a second zinc atom inhibits the enzyme. EXAFS and X-ray crystallography confirm that first zinc ion is in the ‘cysteine’ site. The mechanism of β -lactamases remains unknown, but it is thought to be analogous to that described above for carboxypeptidases, with the presence of one

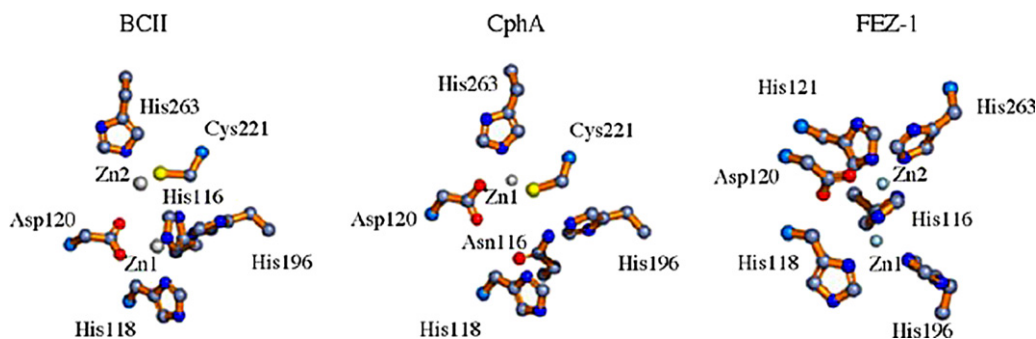


FIGURE 12.14 The zinc-binding sites of subclass B1 (BCII from *B. cereus*), B2 (CphA from *A. hydrophila*), and B3 (FEZ1 *L. gormanii*) β -lactamases. (From Bebrone, 2007. Copyright 2007 with permission from Elsevier.)

Zn^{2+} ion which has the characteristics of a catalytic zinc site, while the role, and even the essentiality of the second zinc atom, is not clear.

Aminopeptidases are counterparts to carboxypeptidases, removing N-terminal amino acids. However, unlike the carboxypeptidases, they contain dinuclear zinc sites. They fall into two groups, the first of which includes the leucine aminopeptidase from bovine lens, while the second includes the leucine aminopeptidases AAP from *Aeromonas proteolytica* and SAP from *Streptomyces griseus* (Figure 12.15). The mechanism of the AAP enzyme has been well studied, and may well represent a general catalytic mechanism for peptide hydrolysis by metalloproteases with a cocatalytic active site.

The proposed general mechanism is represented in Figure 12.16. After the binding of the carbonyl oxygen atom of the incoming substrate to Zn_1 , which polarizes the carbonyl group, rendering it susceptible to nucleophilic attack, the bridging water/hydroxide becomes terminal and is coordinated to Zn_1 . The breaking of the $\text{Zn}_2\text{-OH(H)}$ bond is probably assisted by N-terminal amine binding in aminopeptidases and C-terminal carboxylate binding in carboxypeptidases to Zn_2 whose role is simply to position the substrate correctly in the active site. Next, a glutamic acid residue (or a histidine) located near the catalytic active site assists in the deprotonation of the terminal water molecule, giving a nucleophilic hydroxo moiety similar to that of Glu270 in carboxypeptidase A. Once the metal-bound hydroxide has formed, it can attack the activated carbonyl carbon, forming a gem-diolate intermediate that is stabilized by coordination of both oxygen atoms to the co-catalytic Zn(II) site. The amide nitrogen must also be stabilized, via a hydrogen bond, to make it a suitable leaving group. This hydrogen bond would also facilitate the collapse of the transition state. The active site glutamate (histidine) probably supplies the additional proton to the penultimate amino nitrogen, returning it to its ionized state. Finally, the co-catalytic Zn(II) site releases the cleaved peptides and adds a water molecule that bridges the two metal ions. Thus, both metal ions are required for full enzymatic activity, but their individual roles appear to differ markedly.

Several zinc enzymes which catalyse the hydrolysis of phosphoesters have catalytic sites which contain three metal ions in close proximity. These include (Figure 12.17) alkaline phosphatase, phospholipase C and nuclease P1. In phospholipase C and nuclease P1, all three metal ions are Zn^{2+} . However the third Zn^{2+} ion is not directly associated with the dizinc unit. All three Zn^{2+} ions are pentacoordinate. Alkaline phosphatase shows structural similarity to phospholipase C and nuclease P1; however the third metal ion is Mg^{2+} . One of the Zn^{2+} sites shares a common Asp ligand with the Zn^{2+} site, which is typically hexacoordinate.

Finally, we should briefly mention the purple acid phosphatases, which, unlike the alkaline phosphatases, are able to hydrolyse phosphate esters at acid pH values. Their purple colour is associated with a Tyr to Fe(III) charge transfer band. The mammalian purple acid phosphatase is a dinuclear Fe(II)-Fe(III) enzyme, whereas the dinuclear site in kidney bean purple acid phosphatase (Figure 12.13) has a Zn(II) , Fe(III) centre with bridging

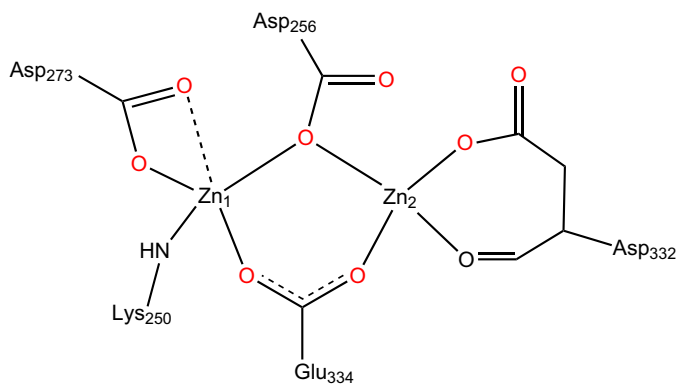
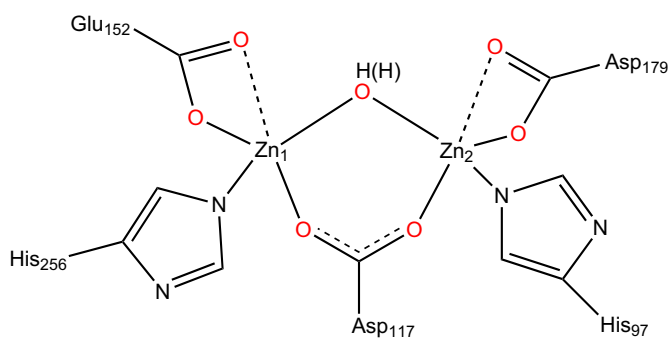
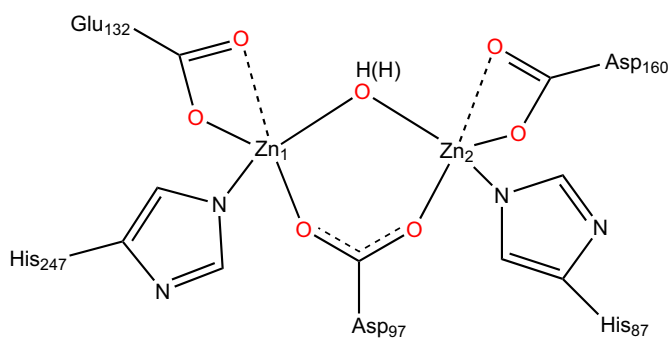
**BILAP****AAP****SAP**

FIGURE 12.15 Drawings of the active sites of the leucine aminopeptidases BILAP (Protein Data Bank [PDB]: 1LAM), AAP (PDB: 1AMP), and SAP (PDB: 1CP7) based on X-ray crystallography. (Adapted from Holz, Bzymek, & Swierczek, 2003.)

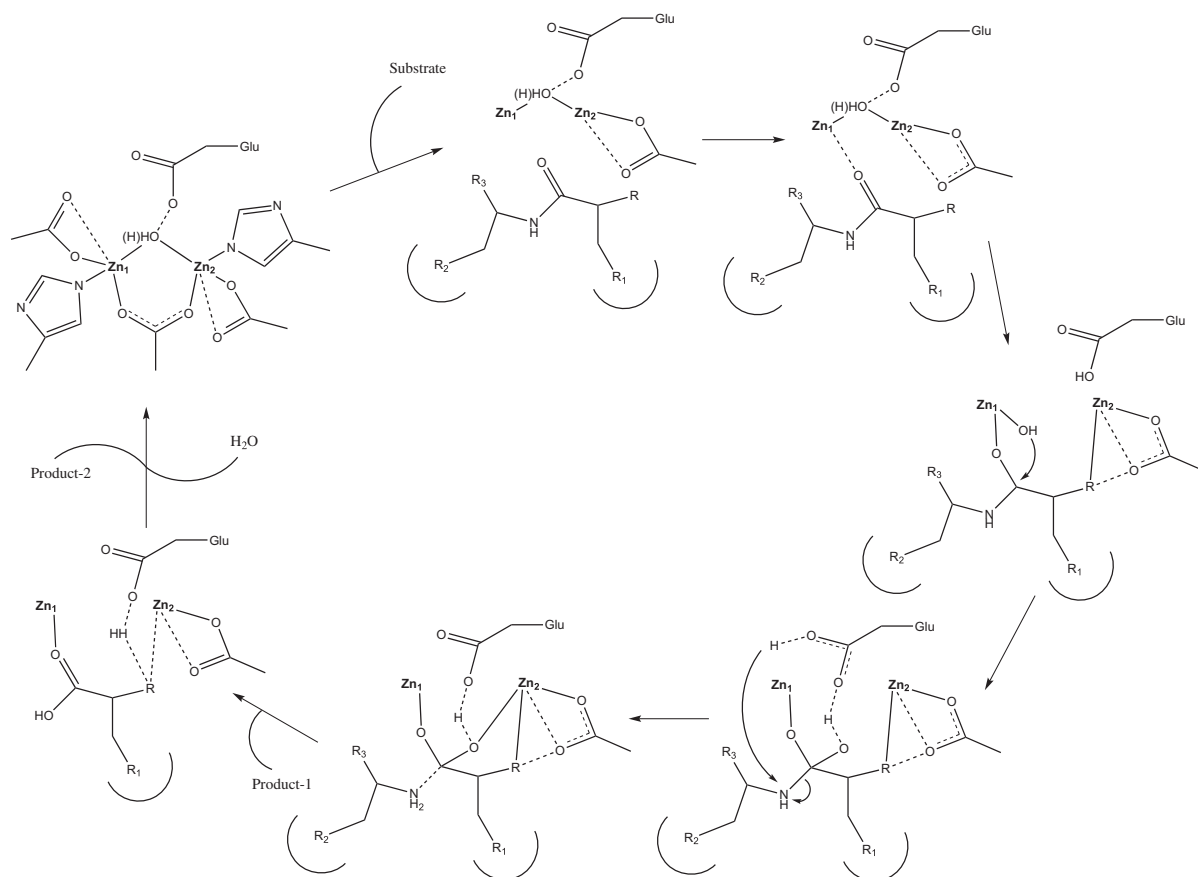


FIGURE 12.16 Proposed general mechanism for the hydrolysis of a peptide, catalysed by a metalloprotease with a cocatalytic active site where R₁, R₂, R₃ are substrate side chains and R is an N-terminal amine or a C-terminal carboxylate. This mechanism is based on the proposed mechanism for the aminopeptidase from *Aeromonas proteolytica*. (Adapted from Holz *et al.*, 2003.)

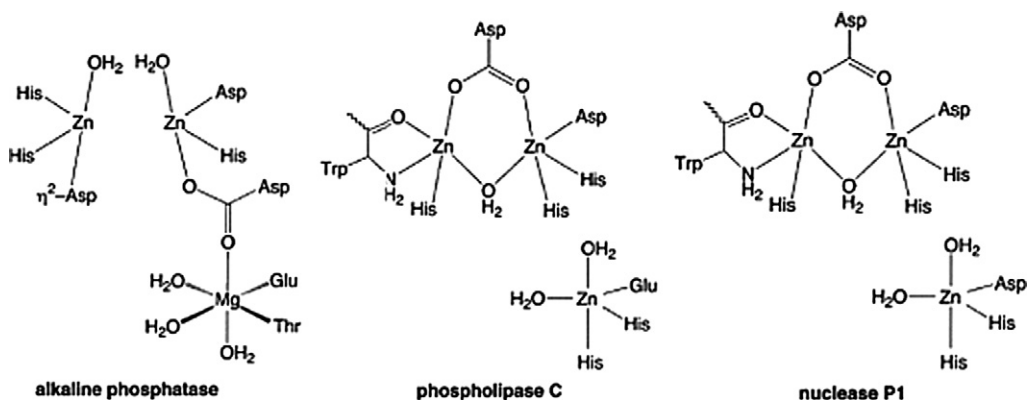


FIGURE 12.17 Metal coordination sites in trinuclear zinc enzymes. (Adapted from Parkin, 2004.)

hydroxide and Asp ligands. It is postulated that the iron centre has a terminal hydroxide ligand, whereas the zinc has an aqua ligand. We do not discuss the mechanism here, but it must be different from the alkaline phosphatase because the reaction proceeds with inversion of configuration at phosphorus (Figure 12.18).

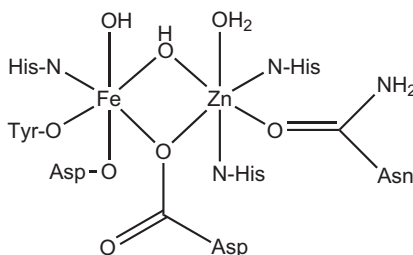


FIGURE 12.18 Coordination of the dinuclear site in kidney bean purple acid phosphatase. (Adapted from *Parkin, 2004*.)

ZINC FINGERS DNA- AND RNA-BINDING MOTIFS

Aaron Klug discovered the first of the eukaryotic DNA-binding motifs in *Xenopus* transcription factor IIIA (TFIIIA), a protein which binds to the 5S rRNA gene. The resulting complex subsequently binds two other transcription factors and RNA polymerase III, which leads to the initiation of transcription of the 5S rRNA gene. The TFIIIA molecule contains 9 similar ~30-residue-long, tandemly repeated modules. Each of these modules contains two invariant Cys residues, two invariant His residues, and several conserved hydrophobic residues (Figure 12.19), and a Zn^{2+} ion, which is tetrahedrally coordinated by the invariant Cys and His

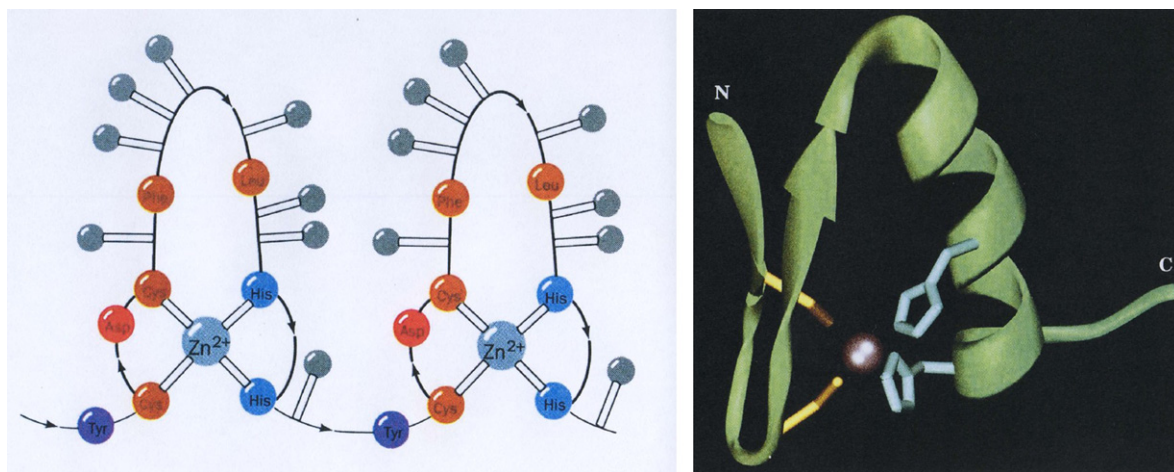


FIGURE 12.19 (Left) Schematic representation of tandemly repeated zinc finger motif with their tetrahedrally coordinated Zn^{2+} ions. Conserved amino acids are labeled and the most probable DNA-binding side chains are indicated by balls. (Right) A ribbon diagram of a single zinc finger motif in a ribbon diagram representation. (From *Voet & Voet, 2004*. Copyright 2004 with permission from John Wiley and Sons.)

residues. These so-called $\text{Cys}_2\text{--His}_2$ Zinc Fingers (*Klug and Rhodes, 1987*) occur from 2 to at least 37 times each in a family of eukaryotic transcription factors. In some zinc fingers, the invariant His residues are replaced by Cys residues ($\text{Cys}_2\text{--Cys}_2$ Zinc Fingers), while in others six Cys residues bind two Zn^{2+} ions (Dinuclear Cys_6 Zinc Fingers). Structural diversity is a hallmark of zinc finger proteins, and it appears that the

Zn^{2+} ion(s) allow(s) formation of a relatively compact globular DNA-binding domain, precluding the requirement for a much larger hydrophobic core. The zinc finger proteins constitute a superfamily, and ~1% of all mammalian proteins contain this motif. The global structural details of how zinc fingers bind to double-stranded DNA are well understood. One isolated $\text{Cys}_2\text{--His}_2$ zinc finger, consisting of two β -strands joined by a β -bend followed by an α -helix (Figure 12.14) held together by a tetrahedrally coordinated Zn^{2+} ion, can span three or four consecutive base pairs of the DNA sequence. The multiple zinc fingers follow a right-handed helical path as they wrap around the double helix, with multiple contacts being made with particular nucleotide bases in the major groove. The contacts are frequently made by the side chains of amino acid residues at positions -1 , $+2$, $+3$, and $+6$ of the α -helix (Figure 12.19).

Among the strong preferences which have been observed, it seems that Arg prefers binding to guanosine, Asp to adenosine and cytosine, and Leu to thymidine. However, we are not yet sufficiently advanced to define a set of coding rules (i.e., to define the amino acid sequence of one or more zinc fingers which would bind to a specific DNA sequence).

The *Xenopus* transcription factor IIIA not only acts as an essential RNA polymerase transcription factor for the expression of the 5S rRNA gene, it also binds to the 5S rRNA to form a 7S ribonucleoprotein particle which stabilises the RNA until it is required for ribosome assembly and facilitates nuclear export of the 5S rRNA. Indeed, it was originally shown to be the protein component associated with 5S rRNA in the 7S particle in *Xenopus* oocytes before it was recognised as a transcription factor. How, we may ask, can this protein not only recognise specific DNA sequences in the 5S rRNA gene upstream region, but also recognise different, but equally specific, sequences in 5S rRNA?

Both biochemical and X-ray crystallographic data show that binding of TFIIIA to the 5S rRNA gene internal control region utilises all but the fourth and sixth of the nine zinc fingers of the transcription factor (Figure 12.20).

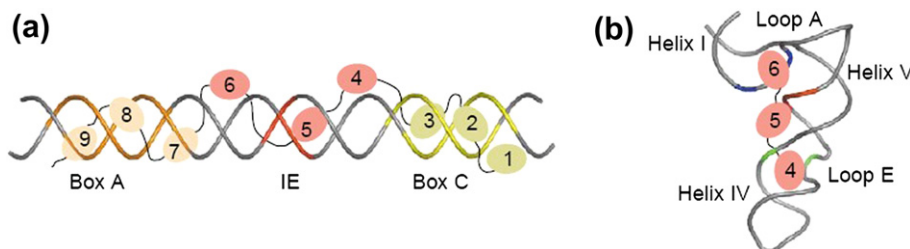


FIGURE 12.20 (a) TFIIIA binds to 5S rRNA promoter sequences using zinc fingers 1–3, 5, and 7–9 which recognise respectively box C (green), the IE sequences (red), and box A (orange). (b) TFIIIA binds to 5S rRNA using primarily zinc fingers 4–6. Finger 4 binds to sequences in loop E, finger 5 to backbone atoms in helix V, and finger 6 binds to sequences in loop A. (From Hall, 2005. Copyright 2005 with permission from Elsevier.)

Fingers 1–3 bind to a 10-base-pair ‘box C’ sequence, wrapping around the major groove of the DNA. Finger 5 binds to a 3-base-pair ‘intermediate element’ (IE) sequence. Fingers 4 and 6 act as non-DNA-binding spacers to allow recognition of the separated elements. This allows fingers 7–9 to interact with an 11-base-pair ‘box A’ sequence (Figure 12.20).

By using a very clever strategy, Klug and his colleagues were able to design a truncated 5S rRNA which binds to zinc fingers 4–6. The resulting X-ray structure shows that finger 4 binds to sequences in loop E, finger 5 binds to backbone atoms in helix V, while finger 6 binds to sequences in loop A. The three fingers are associated with identical sequences in their DNA and RNA complexes, but in quite different ways. This is illustrated in Figure 12.21, which compares the binding of the unique member of the three zinc fingers, finger 5, which binds to both DNA and RNA, in its complexes, respectively, with the 5S rRNA promoter DNA and with the 5S rRNA. Whereas in the DNA structure the interactions are mostly in the major groove and include both specific

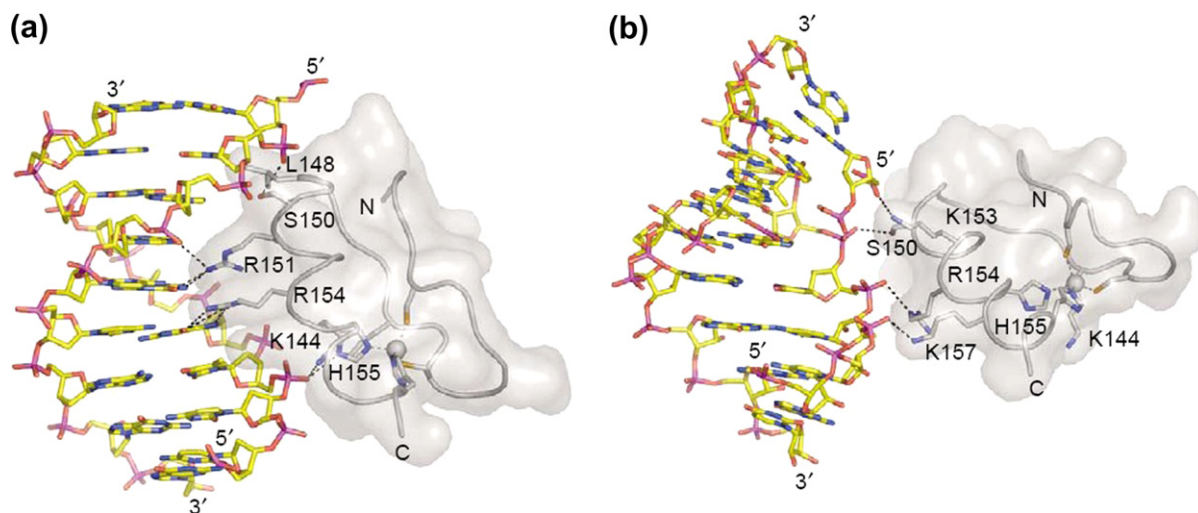


FIGURE 12.21 DNA and RNA recognition by the fifth zinc finger of TFIIIA. (a) The zinc finger recognises bases in the major groove of 5S rRNA promoter DNA (b) The finger recognises the phosphate groups of 5S rRNA. (From Hall, 2005. Copyright 2005 with permission from Elsevier.)

interactions with bases of the DNA (for example, Leu 148 with a thymine residue of the DNA, in the RNA interactions there are no direct interactions with the bases, and the interactions are essentially with the phosphate groups of the 5S rRNA). Some residues in finger 5, such as Ser 150, Lys 144, Arg 154, and His 155 bind to both RNA and DNA, but to different sites in each case. This is in marked contrast to the zinc finger 4 in which a His binds directly to a guanosine and possible also to a second guanosine, and finger 6 in which a Trp stacks onto an adenosine.

REFERENCES

- Auld, D. S. (2001). Zinc coordination sphere in biochemical zinc sites. *BioMetals*, 14, 271–313.
- Bebrone, C. (2007). Metallo-beta-lactamases (classification, activity, genetic organization, structure, zinc coordination) and their superfamily. *Biochemical Pharmacology*, 74, 1686–1701.
- Brown, R. S. (2005). Zinc finger proteins: getting a grip on RNA. *Current Opinion in Chemical Biology*, 15, 94–98.
- Gross, J. (2004). How tadpoles lose their tails: path to discovery of the first matrix metalloproteinase. *Matrix Biol.*, 23, 3–13.
- Hall, T. M. (2005). Multiple modes of RNA recognition by zinc finger proteins. *Current Opinion in Chemical Biology*, 15, 367–373.
- Holz, R. C., Bzymek, K. P., & Swierczek, S. I. (2003). Co-catalytic metallopeptidases as pharmaceutical targets. *Current Opinion in Chemical Biology*, 7, 197–206.
- Kavanagh, K. L., Jörnvall, H., Persson, B., & Oppermann, U. (2008). Medium- and short-chain dehydrogenase/reductase gene and protein families: the SDR superfamily: functional and structural diversity within a family of metabolic and regulatory enzymes. *Cellular and Molecular Life Sciences*, 65, 3895–3906.
- Klug, A., & Rhodes, D. (1987). 'Zinc fingers': a novel protein motif for nucleic acid recognition. *TIBS*, 12, 464–469.
- McCall, K. A., Huang, C.-C., & Fierke, C. A. (2000). Function and mechanism of zinc metalloenzymes. *Journal of Nutrition*, 130, 1437S–1446S.
- Parkin, G. (2004). Synthetic analogues relevant to the structure and function of zinc enzymes. *Chemical Reviews*, 104, 699–767.
- Tallant, C., Marrero, A., & Gomis-Rüth, F. X. (2010). Matrix metalloproteinases: fold and function of their catalytic domains. *Biochimica et Biophysica Acta*, 1803, 20–28.
- Voet, D., & Voet, J. G. (2004). *Biochemistry* (3rd ed.). New York, Chichester: John Wiley and Sons p. 1360.
- Wu, S., Zhang, C., Xu, D., & Guo, H. (2010). Catalysis of carboxypeptidase A: promoted-water versus nucleophilic pathways. *Journal of Physical Chemistry B*, 114, 9259–9267.

Iron: Essential for Almost All Life

*GOLD is for the mistress — silver for the maid —
Copper for the craftsman cunning at his trade.
“Good!” said the Baron, sitting in his hall,
“But Iron — Cold Iron — is master of them all.”*

Rudyard Kipling ‘Cold Iron’.

Introduction	247
Iron Chemistry	248
Iron and Oxygen	248
The Biological Importance of Iron	250
Biological Functions of Iron-Containing Proteins	250
Haemoproteins	251
Other Iron-Containing Proteins	267
Dinuclear Nonhaem Iron Enzymes	272

INTRODUCTION

Human prehistory is conveniently divided into three consecutive periods, the **Stone Age**, the **Bronze Age**, and the **Iron Age**, each defined by the materials out of which tools and weapons were manufactured. The Stone Age began about 2.5 million years ago, with the evolution of humans in sub-Saharan Africa who made tools and weapons out of stone. As the climate gradually grew warmer, the nomadic hunter-gatherer way of life of the Paleolithic Age made its transition to the settled agricultural life of the Neolithic Age. The Stone Age was superseded by the Bronze Age, during which metals, initially copper, began to be used to make metal tools and weapons. The use of copper spread from Anatolia through Mesopotamia and the Middle East from 4000 to 3000 BC. True bronze (an alloy of copper and tin) was used only rarely initially, but during the second millennium BC the use of true bronze increased greatly. The Bronze Age was also marked by important inventions, such as the wheel and the ox-drawn plough. However, by around 1200 BC the ability to heat and forge another metal, iron, brought the Bronze Age to an end. Thus began the Iron Age, when iron replaced bronze in implements and weapons. This shift occurred because iron, when alloyed with a small amount of carbon (0.2–0.8%, absorbed from the charcoal used in its extraction from iron ores), is harder, more durable, and maintains a sharper edge than bronze. For over three thousand years, until its replacement by steel in the middle of the 19th century, iron formed the material basis of human civilisation in Europe, Asia, and Africa. However, while we have many relics from both the Stone and the Bronze Ages, little remains of the Iron Age on account of the poor stability of iron in the face of oxygen and water (rust is not a very practical way of preserving historical relics!).

In this chapter we describe selected aspects of the biological chemistry of iron, with particular reference to iron-containing enzymes. It would be difficult to underestimate the biological importance of iron for almost all

living organisms, but it can be illustrated by three simple examples. *E. coli* has almost fifty genes for proteins involved in iron uptake — six distinct siderophore-mediated Fe^{3+} transport systems, one for iron uptake from ferric citrate, and one Fe^{2+} transport system, yet it synthesizes only one siderophore, enterobactin (as we saw in Chapter 7). When blue-green algal blooms occur in lakes, the determining factor in which algal species takes over is the efficacy of its capacity to chelate iron. And when a clinician wishes to determine the potential for growth of a mammalian tumor, he measures the density of transferrin receptors, which are required for iron uptake and hence cellular growth and division.

IRON CHEMISTRY

Iron, element 26 in the periodic table, is the fourth most abundant element of the earth's crust and, after aluminium, the second most abundant metal. In the middle of the first transition series, iron has the possibility of existing in various oxidation states (from $-\text{II}$ to $+\text{VI}$), the principal being II (d^6) and III (d^5), although a number of iron-dependent monooxygenases generate high valent Fe(IV) or Fe(V) intermediates during their catalytic cycle. The suitability of iron for catalysis in living organisms comes from the extreme variability of the $\text{Fe}^{2+}/\text{Fe}^{3+}$ redox potential, which can be fine-tuned by an appropriate choice of ligands, to encompass almost the entire biologically significant range of redox potentials, from about -0.5 V to about $+0.6$ V.

Fe^{3+} is quite insoluble in water ($K_{\text{sp}} = 10^{-39}$ M and at pH 7.0, $[\text{Fe}^{3+}] = 10^{-18}$ M) and significant concentrations of water-soluble Fe^{3+} species can be attained only by strong complex formation, whereas in contrast, Fe^{2+} is extremely water soluble. Fe(III) with an ionic radius of 0.067 nm and a charge of $3+$ is a “hard” acid, as was pointed out in Chapter 2 (Table 2.1). Fe^{3+} will therefore prefer “hard” oxygen ligands like phenolate and carboxylate rather than imidazole or thiolate. In contrast, Fe^{2+} is intermediate between a « hard » and a « soft » acid, and can accommodate both the « hard » oxygen-based ligands and the « soft » ligands such as those containing nitrogen and sulfur: examples are histidine, protoporphyrin, cysteine, and inorganic sulfur. The distribution of the donor atoms which ligate the metal, and their geometry, will thus determine the functional properties of the metal centre. In the case where one of the coordination spheres is unoccupied, the possibility exists of binding a 6th nonprotein ligand. The aqueous solution chemistry of iron is dominated by forms of Fe^{2+} and Fe^{3+} whose complexes readily undergo electron transfer and acid–base reactions. This explains the wide range and variety of catalytic and other functions of which the element is capable and underlines the importance of iron in biological systems. Another feature of iron which makes it so important is its abundance, although as was pointed out before, since the advent of oxygen into the earth's atmosphere, iron bioavailability has been seriously compromised. When we invoke the extensive range of redox potentials available to the metal by varying its interaction with coordinating ligands, and add to that its capacity to participate in one electron transfer (i.e. free radical) reactions, it is easy to see why iron is virtually indispensable for life.

IRON AND OXYGEN

When life began on earth, with its essentially reducing atmosphere, the natural abundance and bioavailability of iron (mostly in the ferrous state) and its redox properties predisposed it to play a crucial role in the first stages of evolution. However, with the appearance of photosynthetic cyanobacteria about 10^9 years ago, dioxygen was evolved into the earth's atmosphere. It probably required 200–300 million years for oxygen to attain a significant concentration in the atmosphere, since at the outset the oxygen produced by photosynthesis would have been consumed by the oxidation of ferrous ions in the oceans. Once dioxygen had become a dominant chemical entity, iron became poorly bioavailable due to the precipitation of ferric hydroxides as is clearly indicated by the Precambrian deposits of red ferric oxides laid down in the geological strata at that time. In parallel with the loss of iron bioavailability, copper became more available as the oxidation of insoluble Cu(I) led to formation of soluble Cu(II) . The aerobic world now required a new redox active metal with $E_o\text{M}^{n+1}/\text{M}^n$ from 0 to 0.8 V. Copper was ideally suited for this role, and, as we will see in the next chapter, began to be used in enzymes with higher redox

potentials (such as the di-copper centre in laccase and the mixed iron–copper centre in cytochrome oxidase) to take advantage of the oxidising power of dioxygen. The interaction of iron (and copper) centres and oxygen is of paramount importance in biological inorganic chemistry, and we have summarized some of the main features in Figure 13.1.

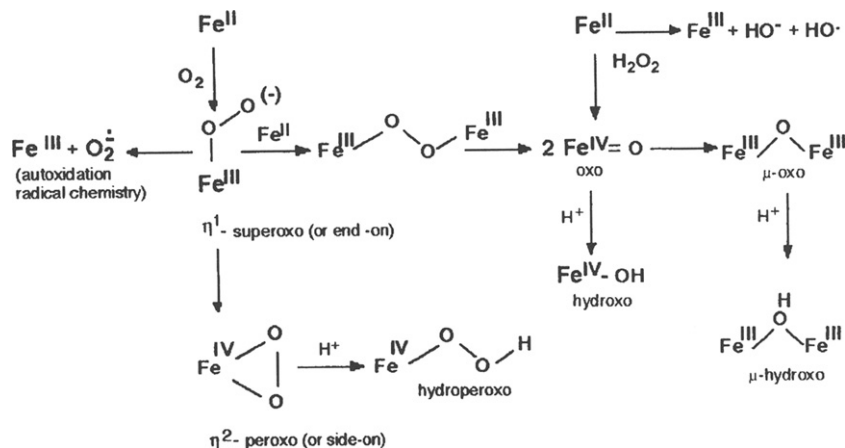


FIGURE 13.1 Iron–oxygen chemistry. (Adapted from Crichton & Pierre, 2001.)

When a single electron is accepted by the ground-state O_2 molecule, it will form the superoxide radical, O_2^- . Addition of a second electron to O_2^- gives the peroxide ion O_2^{2-} with no unpaired electrons. At physiological pH, O_2^{2-} will immediately protonate to give hydrogen peroxide, H_2O_2 . The third reactive oxygen species found in biological system is the hydroxyl free radical. In 1894 James Fenton observed that a simple mixture of H_2O_2 and an Fe(II) salt could oxidize tartaric acid (Fenton, 1894). We now know that this is due to generation of the $\cdot OH$ radical in a reaction which is named after him (1):



In the presence of trace amounts of iron, superoxide can then reduce Fe^{3+} to molecular oxygen and Fe^{2+} (2). The sum of this reaction (2) plus the Fenton reaction (1) produces molecular oxygen, hydroxyl radical, and hydroxyl anion from superoxide and hydrogen peroxide. This is the Haber–Weiss reaction (3), originally described by Haber and Weiss (1934), but manifestly impossible from thermodynamical considerations in the absence of catalytic amounts of redox metals like iron or copper:



This capacity of iron (and copper) to transform oxygen into highly toxic products is the origin of the so-called **oxygen paradox**. As we saw in Chapter 5, the advent of respiratory pathways instead of fermentation represented an almost 20-fold increase in the energetic yield of intermediary metabolism, which enabled organisms with access to such pathways to flourish. The downside — everything which brings advantages inevitably has disadvantages — was that the utilisation of the burning capacity of oxygen came along with a serious fire warning, namely the potential havoc that reactive oxygen species would wreak. We will return to the toxicity of reactive oxygen species particularly in neurodegenerative diseases in Chapters 22 and 23 (Metals in brain function and Metals and Neurodegeneration).

THE BIOLOGICAL IMPORTANCE OF IRON

While iron readily undergoes electron transfer and acid–base reactions, it also has the capacity to participate in one electron transfer (i.e. free radical) reactions. One such free radical reaction, essential for DNA synthesis, is the reduction of ribonucleotides to the corresponding deoxy-ribonucleotides, catalysed by ribonucleotide reductases (RNRs), all of which are radical metalloenzymes (Nordlund & Reichard, 2006; Stubbe et al., 2001). Since all known cellular life forms store their genetic information in DNA, RNRs must be present in all growing cells of all living organisms. They all catalyse the conversion of adenine, uracil, cytosine, and guanine nucleotides to deoxynucleotides, cleaving a 2' carbon–hydroxyl bond with formation of a 2' carbon–hydrogen bond (Figure 13.2).

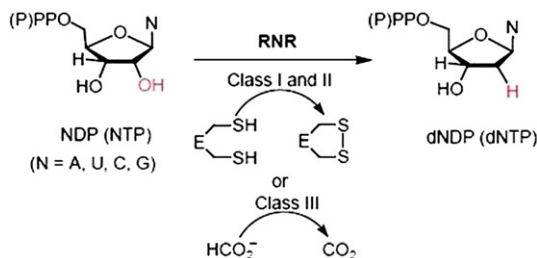


FIGURE 13.2 The reaction catalysed by ribonucleotide reductases (RNRs). (From Stubbe, Ge, & Yee, 2001. Copyright 2001, with permission from Elsevier.)

The hydrogen is derived from water and replaces the hydroxyl with retention of configuration. All RNRs share a common catalytic mechanism involving activation of the ribonucleotide by abstraction of the 3'-hydrogen atom of the ribose by a transient thiyl radical of the enzyme (Figure 13.2). Ribonucleotide reductases (RNRs) can be divided into three classes, largely based on their interaction with oxygen and the way in which they generate the thiyl radical required for ribonucleotide reduction. Class I RNRs contain two nonidentical dimeric subunits (R1 and R2) and require oxygen to generate a stable tyrosyl radical through a Fe–O–Fe centre in the smaller R2 subunit. During catalysis, the radical is continuously shuttled to a cysteine residue, some 30 Å away in the larger R1 subunit where it generates the thiyl radical (Figure 13.3). Almost all eukaryotes, from yeast to man, have Class I RNRs, as do a great many eubacteria and a few archaebacteria. Class II RNRs (for example, in *Lactobacillus* species¹) are different to oxygen, contain a single subunit, and generate their thiyl radical using the Co(III) containing cofactor adenosylcobalamine, probably via formation of a deoxyadenosyl radical. Class III RNRs are anaerobic enzymes, inactivated by oxygen, which generate a glycyl radical, the counterpoint to the tyrosyl radical in Class I RNRs, through a FeS cluster and S-adenosylmethionine. Whereas RNRs of class I and II use electrons from redox-active cysteines of small proteins like thioredoxin or glutaredoxin, class III enzymes use formate as electron donor (Figure 13.2).

BIOLOGICAL FUNCTIONS OF IRON-CONTAINING PROTEINS

Iron-containing proteins can be classified according to a number of criteria – for example the functional role of the metal ion, defined as (i) structural, (ii) metal storage and transport, (iii) electron transport, (iv) dioxygen binding, and (v) catalytic – the latter being extremely large and diverse. As in the previous edition we have chosen here a classification of iron metalloproteins based on the coordination chemistry of the metal. This has the advantage of allowing the reader to more easily appreciate the diversity of biochemical functions in which iron can participate, viewed through the ligands which bind it to the protein. We consider successively:

1. This may explain why this family of bacteria are found in dairy products, where the presence of lactoferrin makes iron availability problematic. Class II RNRs are also found in some archaebacteria.

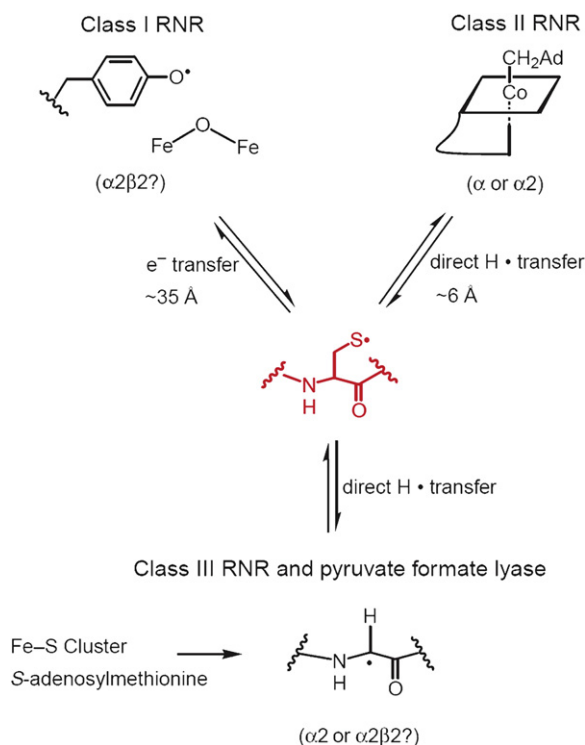


FIGURE 13.3 The three classes of RNRs utilize their metallo-cofactors to generate an active-site thiyl radical (S^\bullet). The diferric-tyrosyl radical in class I enzymes is on the R2 subunit, at best 35 Å from the thiyl radical (on subunit R1). (From Stubbe *et al.*, 2001.)

1. haemoproteins in which an iron porphyrin is incorporated into different apo-proteins to give O_2 carriers, O_2 activators, or alternatively electron transfer proteins.
2. iron-sulfur proteins, many of which are involved in electron transfer.
3. non-haem, non-iron-sulfur, iron-containing proteins, which include proteins of iron storage and transport, already described in Chapter 8.

Since the roles played by iron are so diverse, we clearly cannot cover all of them, so we have chosen only to give a small sample of selected illustrations. The incorporation of iron into porphyrins and Fe-S clusters has already been discussed in Chapter 4.

HAEMOPROTEINS

Oxygen Transport

Oxygen transport and storage in multicellular organisms, whether they are mammals, insects, or worms, are assured by haemoglobins and myoglobins. These were the first proteins to have their X-ray crystal structures determined by John Kendrew and Max Perutz, for which they received the Nobel Prize for Chemistry in 1962; shortly after, when the structures of insect and lamprey haemoglobins were determined, it became clear that all these oxygen-binding proteins share a common tertiary structure, known as the globin fold. This is illustrated in Figure 13.4 by sperm whale myoglobin. However, whereas the monomeric myoglobin with a single haem has a hyperbolic oxygen-binding curve, the tetrameric haemoglobin with four haeme groups has a sigmoidal oxygen-binding curve (Figure 13.4). This reflects the cooperativity of oxygen binding — the fourth O_2 molecule binds with 100-fold greater affinity than the first. We know that, like other allosteric proteins haemoglobin exists in two

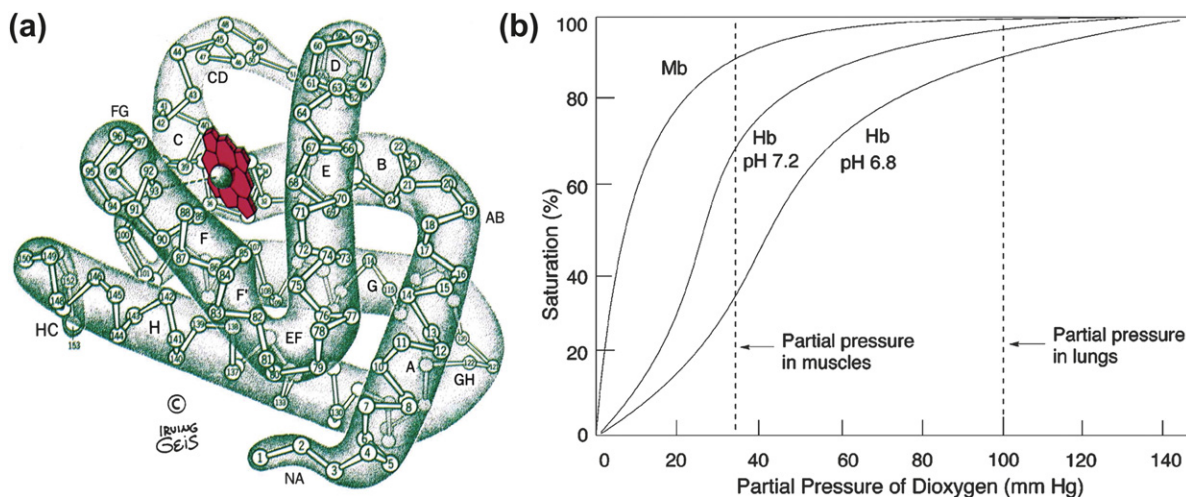


FIGURE 13.4 (a) The structure of sperm whale myoglobin (from Voet & Voet, 2004) and (b) the oxygen binding curves of myoglobin and haemoglobin. (Adapted from Collman *et al.*, 2004.)

distinct and different conformations, corresponding to the T (deoxy) and R (oxy) states. Indeed, the differences between the conformations of oxy- and deoxy-haemoglobins are so great that crystals of deoxy haemoglobin break when oxygen is introduced. But since the haem groups are so far apart in the haemoglobin structure, the positive cooperativity must be transmitted by the protein itself. What might be the trigger that would signal to a neighbouring subunit that oxygenation had taken place?

The haem is tightly bound to the protein in a hydrophobic pocket formed principally by helices E and F and by a single coordinate bond between the imidazole of His F8, termed the **proximal** histidine (Figure 13.5) and the

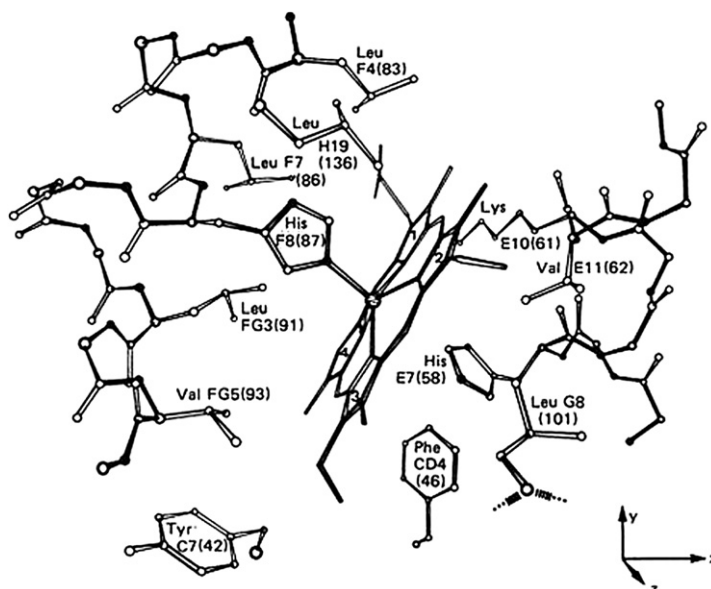


FIGURE 13.5 The haem group and its environment in the deoxy form of the human haemoglobin α -chain. Only selected side chains are shown and the haem 4 propionate is omitted for clarity. (From Gelin & Karplus, 1977.)

ferrous iron, which is some 0.6 \AA out of the plane of the domed porphyrin ring. A second His residue, His E7 (the **distal** histidine), is too far away from the iron atom to coordinate with it in the deoxy state.

A comparison of the deoxy- and oxy-haemoglobin structures reveals a number of important differences. Whereas in the T (deoxy) state the Fe atom is out of the haem plane, on oxygenation it moves into the plane of the now undomed porphyrin, pulling the proximal His F8 and the F-helix, to which it is attached, with it (Figure 13.6),

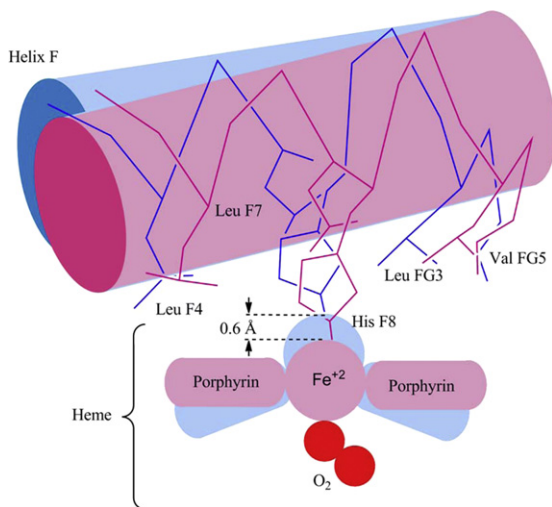


FIGURE 13.6 The triggering mechanism for the T to R transition in haemoglobin.

as we will see shortly, thereby triggering the T to R transition. The major differences between R and T conformations are at the α_1 – β_2 (and the corresponding α_2 – β_1) subunit interfaces which consist of the C helix of α -subunits and the FG interface of the β -subunits. These fit to one another in two distinct conformations, which correspond to a 6 \AA relative shift at the interface. In the T state His FG4 is in contact with Thr C6, whereas in the R state the same His is in contact with Thr C3, one turn further back along the C helix (Figure 13.7). Another series of very important differences concern a network of salt bridges at subunit–subunit interfaces which stabilize the T state, but are broken in the more relaxed R state.

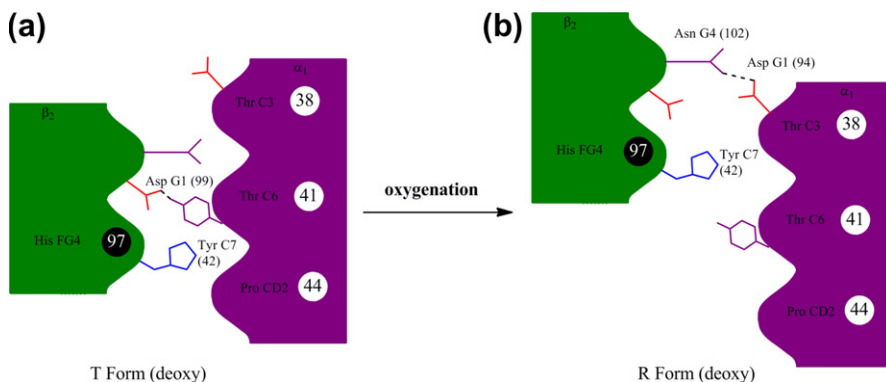


FIGURE 13.7 The α_1 – β_2 interface in (a) human deoxy haemoglobin and (b) oxy-haemoglobin. (Adapted from Voet & Voet, 2004.)

In oxy-myoglobin and oxy-haemoglobin, the N–H proton of the distal histidine E7 in the O₂-binding pocket (Figure 13.6) forms a hydrogen bond with the iron-coordinated dioxygen molecule and imposes an angular bend on the dioxygen molecule. In carbon monoxide adducts of myoglobin and haemoglobin, the steric hindrance caused by the distal histidine results in a less favourable binding geometry (CO prefers a linear coordination). Thus, CO, a poison present both in tobacco smoke and in automobile exhausts, but also produced in the normal biological degradation of haem, binds only about 250 times more tightly than O₂ to both myoglobin and haemoglobin, whereas the affinity of free haem for carbon monoxide is much greater.

What is responsible then for the change in coordination geometry at the iron atom upon oxygenation? Resonance Raman spectroscopy of oxyhaemoglobin shows an O–O stretching band at $\sim 1105\text{ cm}^{-1}$ which is characteristic of coordinated superoxide ion. This implies electron transfer from iron (II) to dioxygen, such that we could consider oxy-haemoglobin and oxy-myoglobin as ferric superoxide complexes, in which the superoxide is stabilized by hydrogen bonding to the distal histidine proton. In deoxy haemoglobin Fe(II) is high spin, and its covalent radius is too large to allow it to fit into the plane of the tetrapyrrole, which explains both the doming of the porphyrin and the out-of-plane location of the iron. The hexacoordinate Fe(III) superoxo is low spin, with a decreased covalent radius, and the iron atom can now move into the plane of the porphyrin. Through the movement of the proximal His F8 and the F helix, the T to R transition is set in motion, perhaps first involving rupture of intersubunit salt bridges and progressively the high-affinity R state predominates. In this mechanism the salt bridges play three roles – (i) they stabilize the T quaternary structure relative to R; (ii) they lower the oxygen affinity in the T state because of the energy required to break them on oxygen binding; (iii) they release protons when they are broken, which explains the almost century-old effect discovered by the physiologist father of the atomic physicist Niels Bohr, Christian, namely that the affinity of haemoglobin for oxygen is lowered when the pH decreases (Figure 13.4).

Activators of Molecular Oxygen

Haem enzymes include cytochrome oxidase, peroxidases, catalases, and cytochrome P-450's. They are characterized by a penta-coordinate geometry in which the sixth site of the metal centre can either bind molecular oxygen and hydrogen peroxide, or, in the case of cytochrome P-450's, even form iron–carbon bonds with the substrate. For all of them, the high-spin iron-porphyrin system can go to the radical cation state at a redox potential close enough to that of the couple Fe(IV)/Fe(III) to allow a ferryl type of iron to participate in chemical reactions such as the activation of oxygen or the oxidation of molecules at the expense of hydrogen peroxide. The highly activated ferryl oxygen of the redox cofactor, $\text{P}^+\text{Fe}^{\text{IV}}=\text{O}$, is the so-called compound I intermediate, in which the $\text{Fe}^{\text{IV}}=\text{O}$ centre resides in a porphyrin cation radical P^+ .

The first illustration of this class of enzymes is the haem-copper cytochrome *c* oxidase (CcO), the terminal component of the respiratory chain in aerobic organism. These membrane-bound enzymes catalyse the reduction of molecular dioxygen to water (Reaction (4)) at the rate of up to 250 molecules of O₂ per second:



We already encountered the respiratory electron transfer chain in Chapter 5, and in the present context, Figure 13.8 serves as a reminder that the structures of many of the components have been determined (Hosler, Ferguson-Miller, & Mills, 2006). Electrons flow from NADH/NAD⁺ and succinate (Complexes I and II) via Coenzyme Q to the cytochrome *bc*₁ complex (Complex III) and are then transferred via cytochrome *c* to cytochrome *c* oxidase (CcO) (Complex IV). We will discuss the electron transport cytochromes in the next section.

In common with Complexes I and III, CcO couples the energy released in this process to the translocation of protons, which contributes to the chemiosmotic gradient required for ATP synthesis. The primary oxygen-binding site involves a haem iron, haem *a*₃, together with a copper ion, Cu_B (Figure 13.9). This dinuclear metal site is where dioxygen is reduced. Electron input to this site comes from cytochrome *c* through a second haem iron, haem *a* together with a second dinuclear copper centre, Cu_A. Over the past decade, the crystal structures of *aa*₃-type

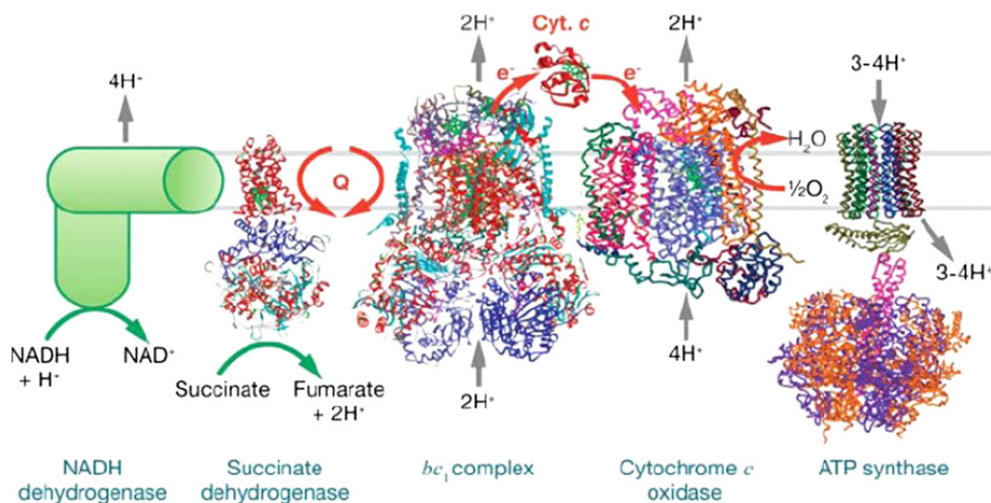


FIGURE 13.8 Complexes of the respiratory chain. These include NADH dehydrogenase, succinate dehydrogenase (PDB code 1NEN), bc_1 complex (PDB code 1PP9), cytochrome c oxidase (PDB code 1V54), and cytochrome c (PDB code 1HRC). (From Hosler *et al.*, 2006. Copyright 2006 with permission from Annual Reviews.)

CcOs from bovine heart mitochondria and bacteria (*Rhodobacter sphaeroides* and *Paracoccus denitrificans*) have been determined, culminating in the 2.0 Å resolution structure of CcO from *Rhodobacter sphaeroides* which contains only the two catalytic subunits — subunit I with 3 redox-active centres, haem a , and the catalytic site made up of haem a_3 and Cu_B , and subunit II with the Cu_A redox centre made up of 2 copper ions, together with two other subunits (Qin, Hiser, Mulichak, Garavito, & Ferguson-Miller, 2006).

CcO catalyses the oxidation of four molecules of cytochrome c^{2+} and uses these electrons to reduce molecular oxygen to water. The electrons are taken from one side of the membrane while the protons are taken from the other side. This topographical arrangement results in a charge separation that is equivalent to moving one positive charge across the membrane for each electron transferred to O_2 . Part of the free energy available from O_2 reduction is conserved in the form of an electrochemical proton gradient, while part of the free energy is used to pump, on average, one proton across the membrane per electron transferred to O_2 . Since electrons and protons are taken up from opposite sides of the membrane, the CcO reaction results in a net charge separation across the membrane. This coupled proton pumping results in an overall translocation of two positive charges across the membrane for each electron transferred to O_2 , from the negative (N) side to the positive (P) side of the membrane (Figure 13.9(a)).

Electrons from cytochrome c are donated to the dinuclear copper centre Cu_A , and then transferred consecutively one at a time to haem a , and from there to the dinuclear haem-copper (haem a_3 - Cu_A) catalytic centre. A tyrosine residue, Y(I-288), which is covalently cross-linked to one of the Cu_B ligands (His 240), is also part of the active site. The structure of the four-subunit CcO from *R. sphaeroides* is presented in Figure 13.9(a), while a more detailed view of the redox-active cofactors and amino acid residues involved in the proton transfer pathways is given in Figure 13.9(b) (Brzezinski & Johansson, 2010).

The individual steps of oxygen binding and its subsequent reduction have been followed spectroscopically in a time-resolved manner using flash-flow techniques. The catalytic cycle for oxygen reduction by CcO is presented in Figure 13.10 (Brzezinski & Johansson 2010). During Cyt c O turnover, electrons and protons are added one by one to the catalytic site and in each step one proton is pumped across the membrane (Figure 13.10). Oxidized CcO is designated O^{40} . The superscript indicates the number of electrons transferred to the catalytic site — both haem a_3 and Cu_B are oxidized, i.e. $Fe_{a_3}^{3+}$ and Cu_B^{2+} . Transfer of the first and second electrons to the catalytic site results in

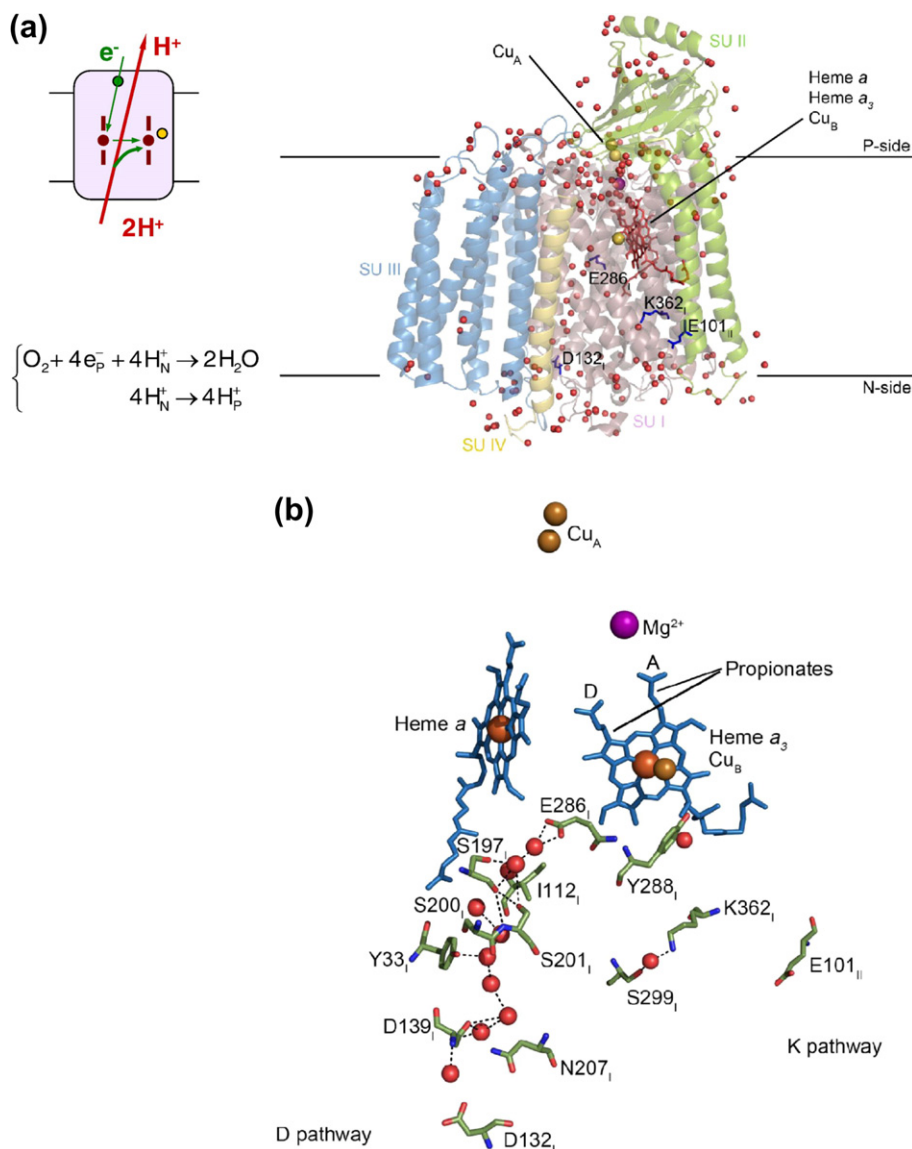


FIGURE 13.9 (a) The structure of cytochrome *c* oxidase from *R. sphaeroides* (PDB code 1M56). The four subunits of the enzyme are coloured as indicated in the figure. Haems *a* and *a*₃ are shown in red and the copper centres Cu_A and Cu_B in yellow. The red spheres are water molecules resolved in the structure. Residues Glu286, Asp132, Lys362, all in SU I, and Glu101 in SU II, are shown in the figure (the subscript indicates the subunit number). The approximate position of the membrane is indicated by the solid lines, where the p- and n-sides are the more positively and negatively charged sides of the membrane, respectively. The purple sphere is a non-redox-active Mg²⁺ ion found in the structure. The schematic picture to the left shows the reaction in each step of the cycle (see Figure 13.10) and the formula describes the reaction catalysed by the Cyt cO, where the lower part signifies proton pumping. (b) The D and K proton pathways shown in more detail. Also, the haem *a*₃ propionates discussed in the text are indicated. (From Brzezinski & Johansson, 2010. Copyright 2011, with permission from Elsevier.)

the formation of states **E**¹ and **R**² (Fe_{a3}²⁺ and Cu_B⁺), respectively, each associated with proton uptake to the catalytic site and pumping. O₂ binds to haem *a*₃ in the **R**² state within 10 μs. In the next step, the O—O bond is broken, forming an oxo-ferryl state on haem *a*₃, Fe_{a3}⁴⁺ = O₂²⁻ (Fe_{a3}²⁺ → Fe_{a3}⁴⁺ donates two electrons) and a hydroxide ion at Cu_B (Cu_B⁺ → Cu_B²⁺ donates one electron), respectively. This state denoted **P**² is formed within 50 μs. This reaction

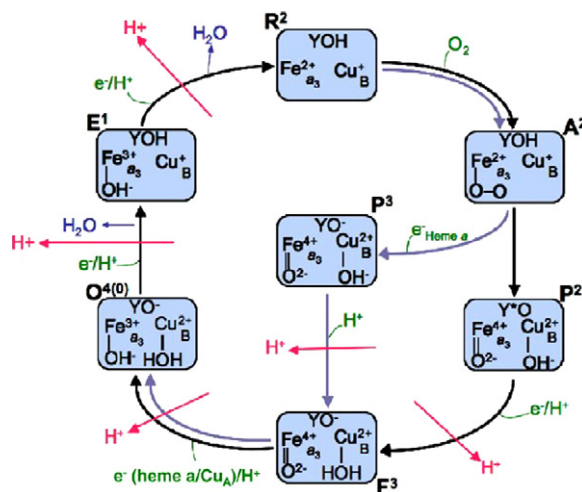


FIGURE 13.10 The catalytic cycle of Cyt cO. The superscript indicates the number of electrons transferred to the catalytic site. The electrons (e^-) and protons at the arrows (in green) are those transferred to the catalytic site, while the protons indicated by arrows (in red) perpendicular to the reaction arrows indicate pumped protons. Y is Tyr288 (see text) where Y^{\bullet} indicates a tyrosyl radical. The oxidized state is $\text{O}^{4(0)}$ (see text). When both haem a_3 and Cu_B are reduced (R^2), O_2 binds to form state A^2 after which the reaction proceeds as described in the text. The pathway along the black arrows indicates the reaction during turnover of the enzyme when electrons are added one by one to the catalytic site. The reaction pathway along the blue arrows is that observed during reaction of the fully reduced Cyt cO (with four electrons) with O_2 . Here, after binding of O_2 to haem a_3 (to form state A^2), an electron is transferred to the catalytic site (to form P^3) before the proton is transferred to the catalytic site (to form F^3). Note that in state P^3 there is an excess negative charge as compared to the other states. (From Brzezinski & Johansson, 2010. Copyright 2011, with permission from Elsevier.)

is not linked to any proton uptake from solution and, protons and electrons are only relocated locally within the catalytic site resulting in oxidation of haem a_3 and Cu_B . In addition, one electron (and a proton) is transferred from residue Tyr288, located within the catalytic site, which forms a tyrosyl radical, Tyr288 $^{\bullet}$, and structural changes occur in the vicinity of the catalytic site. In the next step an electron is transferred to the Tyr radical, accompanied by proton uptake from the n -side to form state F^3 and proton pumping with a time constant of 100 μs . In the final step, with a time constant of ~ 1.2 ms, the last electron is transferred to the catalytic site, also accompanied by proton uptake from the n -side forming state O^4 and proton pumping. When considering the oxidation state of the catalytic site, the O^4 state is equivalent to O^0 as the enzyme becomes fully oxidized when four electrons have been transferred to O_2 .

Part of the energy released in the redox reaction is conserved by vectorial transfer of protons across the membrane from the N -side to the P side, thereby maintaining an electrochemical proton gradient that is used for the synthesis of ATP. Two proton transfer pathways leading from the N -side surface toward the binuclear centre have been identified (Figure 13.9(b)). In cytochrome c oxidase from *Rhodobacter sphaeroides*, one of the pathways (D-pathway) starts with Asp132 and leads to Glu286. Since the D-pathway is used both for the substrate protons, which are transferred to the catalytic site, and pumped protons, which are transferred to a proton-accepting group in the exit pathway, there must be a branching point within the pathway from where protons can be transferred either toward the dinuclear centre or toward the output side of the enzyme. This is thought to be at Glu288. The other pathway (K-pathway) starts at the N -side surface at Glu101 and leads via a highly conserved Lys362 and Tyr288 to the dinuclear centre.

Figure 13.9(b) also illustrates analogies between CcO and peroxidases and catalases, which we discuss next, in terms of both oxygen–oxygen bond cleavage chemistry and the nature of the products of the reactions. In CcO, the enzyme extracts three electrons from metals in the active site – two from haem a_3 as it goes from the $+2$ to the $+4$ state and one from Cu_B as it is oxidized from cuprous to cupric – and one electron from a redox-active protein side

chain. The oxy-intermediate is reduced in one step to O= and OH[−]. Both products are at the level of water, but further protonation and release only occur in later steps of the reaction.

Both catalases and peroxidases can oxidize a variety of organic substrates (peroxidatic activity) (Reaction (5)):

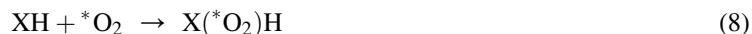
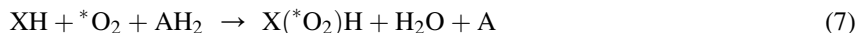


Catalases, unlike peroxidases, can use H₂O₂ both as an electron acceptor and donor, thus catalysing the disproportionation reaction (catalatic activity) (Reaction (6)):

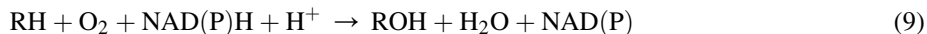


In peroxidases and catalases, the enzyme extracts one electron from haem iron in the active site and a second electron from an organic moiety to reduce H₂O₂ in one step to O= and OH[−]. The immediate product of this chemistry is Compound I, which contains a ferryl-oxo-species and an organic radical, analogous to the $a_3^{4+}=\text{O}/\text{radical}$ found in intermediate *P* in CcO. The organic radical in Compound I is reduced in a subsequent step to produce Compound II, which maintains the ferryl-oxo structure, and exactly the same chemistry is found in the oxidase to produce the *F* intermediate. This similarity in the chemistry catalysed by these oxygen-activating haem proteins may extend further to other enzymes involved in activating and reducing oxygen and peroxides.

Enzymes that incorporate oxygen atoms from molecular oxygen can be classified into two categories, monooxygenases (Reaction (7)) and dioxygenases (Reaction (8)), depending on whether one or both oxygen atoms from dioxygen are incorporated into the substrate, where XH and AH₂ represent substrate and an electron donor respectively:



Cytochrome P450s represent an important class of monooxygenases which play important roles in the hydroxylation of endogenous physiological substrates as well as a vast range of drugs and other compounds foreign to the organism (xenobiotics²). Exposure to such xenobiotics results in the induction of particular families of P450 protein. Cytochrome P450s are found in almost all mammalian tissues and organs, as well as in plants, bacteria, yeast, insects, etc., where they catalyse a panoply of different reactions. Cytochrome P450s are mostly membrane-bound, associated with either the inner membrane of the mitochondria or the membrane of the endoplasmic reticulum. When functioning as a monooxygenase, cytochrome P450 requires a two-electron donor, which transfers electrons, derived from either NADH or NADPH, via electron transport systems (Reaction (9)):



Cytochrome P450s have as fifth, axial ligand to the haem iron a cysteinyl residue of the protein (which accounts for their characteristic 450 nm absorption when bound to CO). Like many of the enzymes involved in oxygen activation, they have a proton transfer network³ disposed orthogonally to the haem redox cofactor. The haem environment of cytochrome P450 (Poulos et al., 1986, 1987) clearly reveals a hard-wired water channel above the haem (Figure 13.11(a)) along which the proton transfer is directed. The peroxo-shunt mechanism of mono-oxygenases is represented in Figure 13.11(b).

The catalytic cycle of cytochrome P-450, typical of monooxygenases, is presented in Figure 13.12 (Johnston, Ouellet, Podust, & Ortiz de Montellano, 2011). This substrate hydroxylation reaction is mediated by the “Compound I”-like ferryl species formed during the catalytic turnover of P450 enzymes. The Fe(IV) haem iron

2. Xenos, as Michael Flanders remarked in the Flanders and Swann recording ‘At the Drop of a Hat’, is the Greek word for stranger or guest; as in xenophobia — fear and hatred of guests!

3. For a recent review of proton-coupled electron transfer, see Reece et al., 2006.

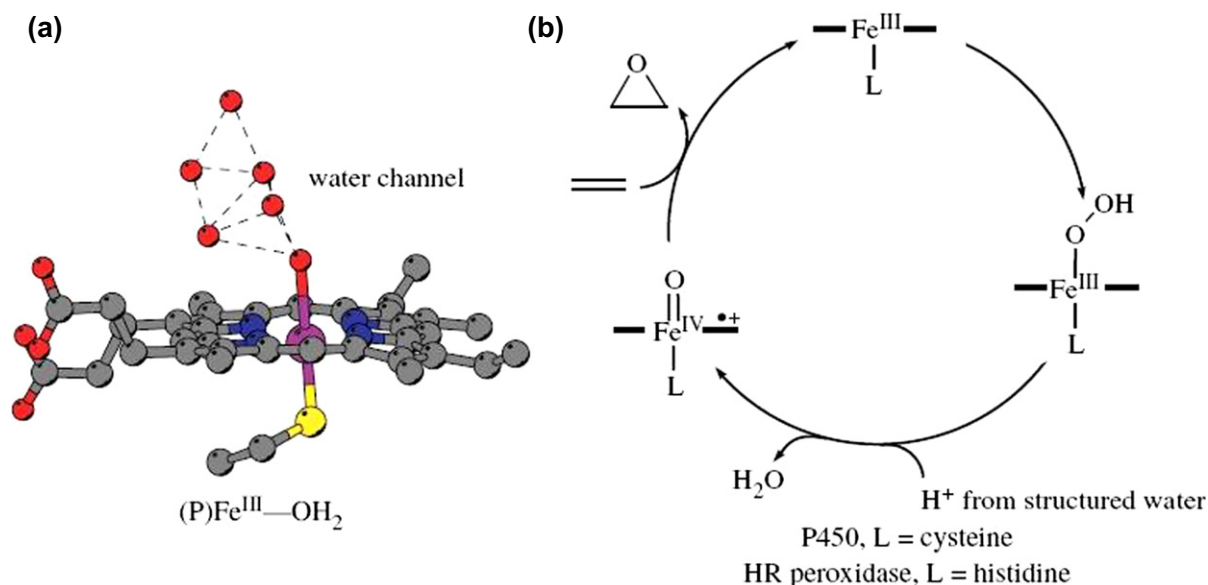


FIGURE 13.11 (a) High-resolution structure of cytochrome P450 from *Pseudomonas putida* displaying a water channel above the haem. (Adapted with permission from Poulos *et al.*, 1986, Copyright (1986) American Chemical Society). (b) The peroxo-shunt mechanism of monooxygenases produces compound I ($P^{+}Fe^{IV}=O$), which oxidizes substrates by their nucleophilic attack on the electrophilic oxo of the (P^{+}) $Fe^{IV}=O$ core. (Reproduced with permission from Dempsey, Esswein, Manke, *et al.*, 2005, Copyright (2005) American Chemical Society.)

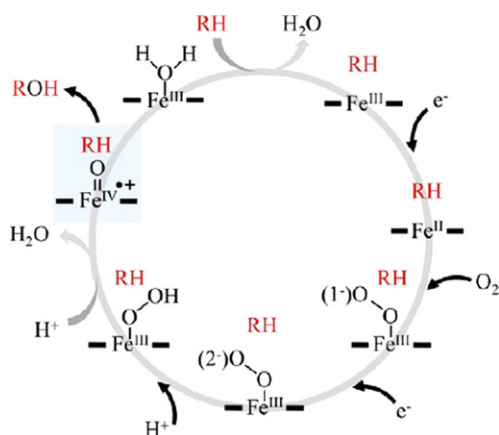


FIGURE 13.12 Catalytic cycle of cytochrome P450. The cytochrome P450 catalytic cycle with the compound I-like ferryl species highlighted by a blue square. The haem is represented by the iron between two bars, which stand for the porphyrin framework. RH is a hydrocarbon substrate and ROH its alcohol product. (From Johnston *et al.*, 2011. Copyright 2011, with permission from Elsevier.)

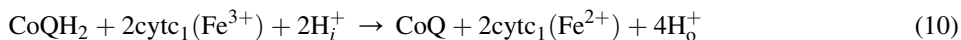
atom in this ferryl species is paired with a radical cation delocalized over the haem porphyrin ring, so the enzyme is two oxidation equivalents higher than the resting enzyme.

Electron Transport Proteins

The third class of hemoproteins are the cytochromes. They were first discovered by C.A. McMunn, a rural physician in Wolverhampton, who identified their characteristic absorption bands, and by manipulating their oxidation and

reduction, realized they were involved in respiration. His observations were published (McMunn, 1884), but treated with contempt by the great German physiologist of the time, Hoppe Seyler. Fortunately, they were rediscovered in 1925 by David Keilin (Keilin, 1925), who coined the name cytochrome. Using a hand spectroscope, he observed the characteristic absorption (Soret) bands of the three cytochromes *a*, *b* and *c* in respiring yeast cells, which disappeared upon oxygenation. Like McMunn, he correctly concluded that they transferred electrons from substrate oxidation to the terminal oxidase, cytochrome *c* oxidase as we know it today, and which we have discussed in the section above. The cytochromes vary in the nature of their haem group — *b*-type haems have protoporphyrin IX, as in haemoglobin, *c*-type cytochromes have protoporphyrin IX in which the vinyl groups form covalent thioether bonds with cysteine residues of the protein, while *a*-type haems contain a long hydrophobic tail of isoprene units attached to the porphyrin, as well as a formyl group in place of a methyl substituent (Figure 13.13(a)). The axial ligands of haem iron vary with cytochrome type (Figure 13.13(b)). In cytochromes *a* and *b*, both ligands are usually His residues, whereas in cytochrome *c*, one is His and the other is often Met. They have a wide cellular and biological distribution, functioning as electron transporters in mitochondria, chloroplasts, endoplasmic reticulum, as well as in bacterial redox chains. The iron in all cytochromes can alternate between an oxidised Fe(III) low-spin state with a single unpaired electron and a formal charge of +1 and a reduced Fe(II) low-spin form with no unpaired electrons and a net charge of zero. Since the iron remains low spin, electron transfer is greatly facilitated.

Cytochromes, as components of electron transfer chains, must interact with the other components, accepting electrons from reduced donor molecules and transferring them to appropriate acceptors. In the respiratory chain of the mitochondria, the ubiquinol:cytochrome *c* oxidoreductase, QCR or cytochrome *bc*₁ complex, transfers electrons coming from Complexes I and II to cytochrome *c*. The *bc*₁ complex oxidises a membrane-localised ubiquinol: the redox process is coupled to the translocation of protons across the membrane, in the so-called proton-motive Q cycle, which is presented in a simplified form in Figure 13.14. This cycle was first proposed by Peter Mitchell 30 years ago and substantially confirmed experimentally since then. The Q cycle in fact consists of two turnovers of QH₂ (Figure 13.14). In both turnovers, the lipid-soluble ubiquinol (QH₂) is oxidized in a two-step reoxidation in which the semiquinone CoQ is a stable intermediate, at the intermembrane face of the mitochondrial inner membrane. It transfers one electron to the Rieske iron–sulfur protein (ISP), one electron to one of the two cytochrome *b* haems (*b*_L), while two protons are transferred to the intermembrane space. In both of the Q cycles, the cytochrome *b*_L reduces cytochrome *b*_H while the Rieske iron–sulfur cluster reduces cytochrome *c*₁. The cytochrome *c*₁ in turn reduces the water-soluble cytochrome *c*, which transfers its electrons to the terminal oxidase, cytochrome *c* oxidase, described above. In one of the two Q cycles, reduced cytochrome *b*_H reduces Q to the semiquinone, which is then reduced to QH₂ by the second reduced cytochrome *b*_H. The protons required for this step are derived from the matrix side of the membrane. The overall outcome of the two CoQ cycles (10) (*i* – matrix: *o* – intermembrane space) is



The cytochrome *bc*₁ complex in eukaryotes is a homodimeric, multi-subunit entity (Figure 13.15(a)). Each monomer has three catalytic subunits: a cytochrome *b*, with two *b*-type haems, one Rieske iron–sulfur protein (ISP) containing a Fe₂–S₂ cluster, and one cytochrome *c*₁, with a *c*-type haem shown in a schematic representation in Figure 13.15(b). The Rieske protein is anchored with its transmembrane helix in one monomer, while the extrinsic domain forms a functional unit with the catalytic subunits of the other monomer. Qo sites are depicted as diamonds and Qi sites as circles. The orientation of cofactors, substrate, and inhibitor molecules in yeast QCR are shown in Figure 13.15(c). Monomers A and B are colour coded in red and blue, respectively. The extrinsic domain of the protein is mobile and the Fe₂–S₂ cluster can be found in different orientations with the maximal positions either close to haem *b*_L (*b*-position) or close to haem *c*₁ (*c*-position). The latter orientation is found in a bovine QCR structure (X, PDB entry: 1BE3) and the Fe₂–S₂ cluster of the superimposed model is coloured in green in Figure 13.15(c). In yeast QCR stigmatellin specifically binds to the Qo site stabilising the *b*-position and inhibiting enzyme activity. Electron transfer and proton uptake are indicated with straight arrows. The curved arrow represents the movement of the Fe₂–S₂ cluster, which most likely precedes oxidation of the cluster by cytochrome *c*₁.

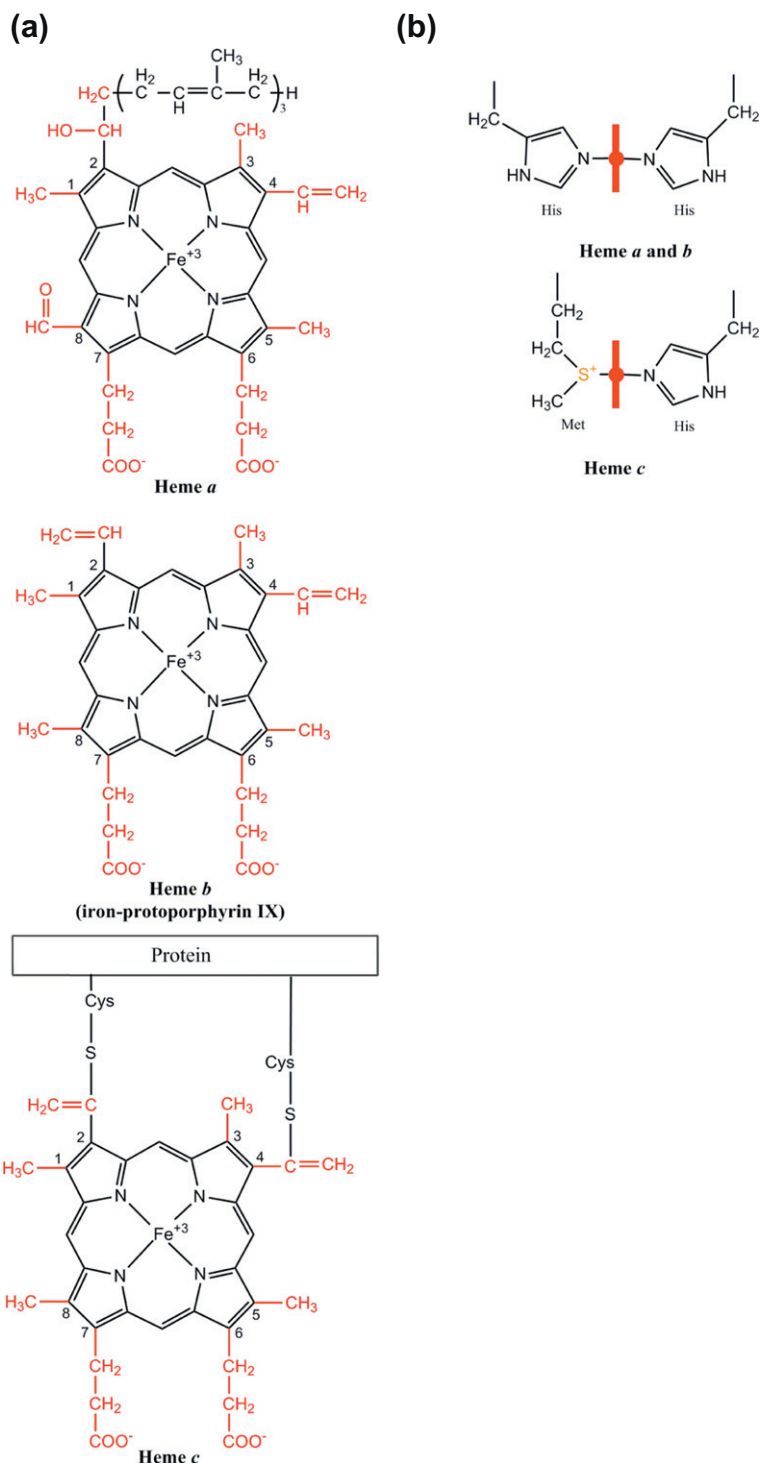


FIGURE 13.13 (a) Chemical structures to the haem groups in cytochromes *a*, *b* and *c*. (b) Axial ligands to the haem groups in cytochromes *a*, *b* and *c*. (Adapted from Voet & Voet, 2004.)

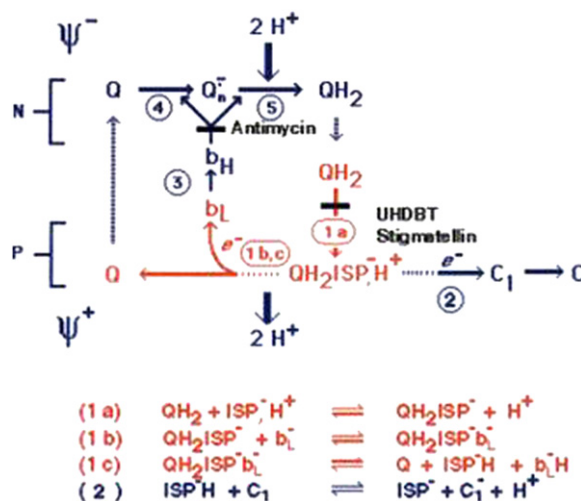


FIGURE 13.14 The proton-motive Q cycle. Electron transfer reactions are numbered and circled. Dashed arrows designate movement of ubiquinol or ubiquinone between centres N and P and of the ISP between cytochrome *b* and cytochrome *c*₁. Solid black bars indicate sites of inhibition by antimycin, UHDBT, and stigmatellin. (From Hunte, Koepke, Lange, Rossmanith, & Michel, 2000. Copyright 2000 with permission from Elsevier.)

The spatial arrangement of the cofactors allows fast electron transfer. The central domain of the complex is formed by eight transmembrane helices of cytochrome *b* per monomer. Both cytochrome *c*₁ and the Rieske protein have their catalytic domains located in the intermembrane space as shown in Figure 13.15(b).

A functionally similar but structurally much simpler version of the *bc*₁ complex is found in the plasma membrane of many bacteria, where it participates among other processes in respiration, denitrification, nitrogen fixation, and cyclic photosynthetic electron transfer.

Iron–Sulfur Proteins

For the first billion years of evolution the environment was anaerobic, which meant that, since iron and sulfur were abundant, proteins containing iron–sulfur (Fe–S) clusters were probably abundant and, therefore, were among the first catalysts that Nature had available to it (Huber and Wächtershäuser 2006).⁴ Although they are distributed in virtually all living organisms, their recognition as a distinct class of metalloproteins only occurred after the observation of their characteristic EPR spectra in the oxidized state in the 1960s. This second class of iron-containing proteins contains iron atoms bound to sulfur, either bound to the polypeptide chain by the thiol groups of cysteine residues, or else with both inorganic sulfide and cysteine thiols as ligands. The biochemical utility of these Fe–S clusters resides not only in their possibility to easily transfer electrons but also in their tendency to bind the electron-rich oxygen and nitrogen atoms of organic substrates.

Iron–sulfur proteins contain four basic core structures which have been characterized crystallographically both in model compounds and in iron–sulfur proteins (Rao and Holm, 2004). These are (Figure 13.16), respectively, (a) rubredoxins found only in bacteria, in which the [Fe–S] cluster consists of a single Fe atom liganded to four Cys residues – the iron atom can be in the +2 or +3 valence; (b) rhombic two iron–two sulfide [Fe₂–S₂] clusters – typical stable cluster oxidation states are +1 and +2 (the charges of the coordinating cysteine residues are not considered); (c) cuboidal three-iron–four sulfide [Fe₃–S₄] clusters – stable oxidation

4. While a passionate enthusiast for evolutionary theories, and their experimental testing, Günther Wächtershäuser was in his professional life a patent lawyer.

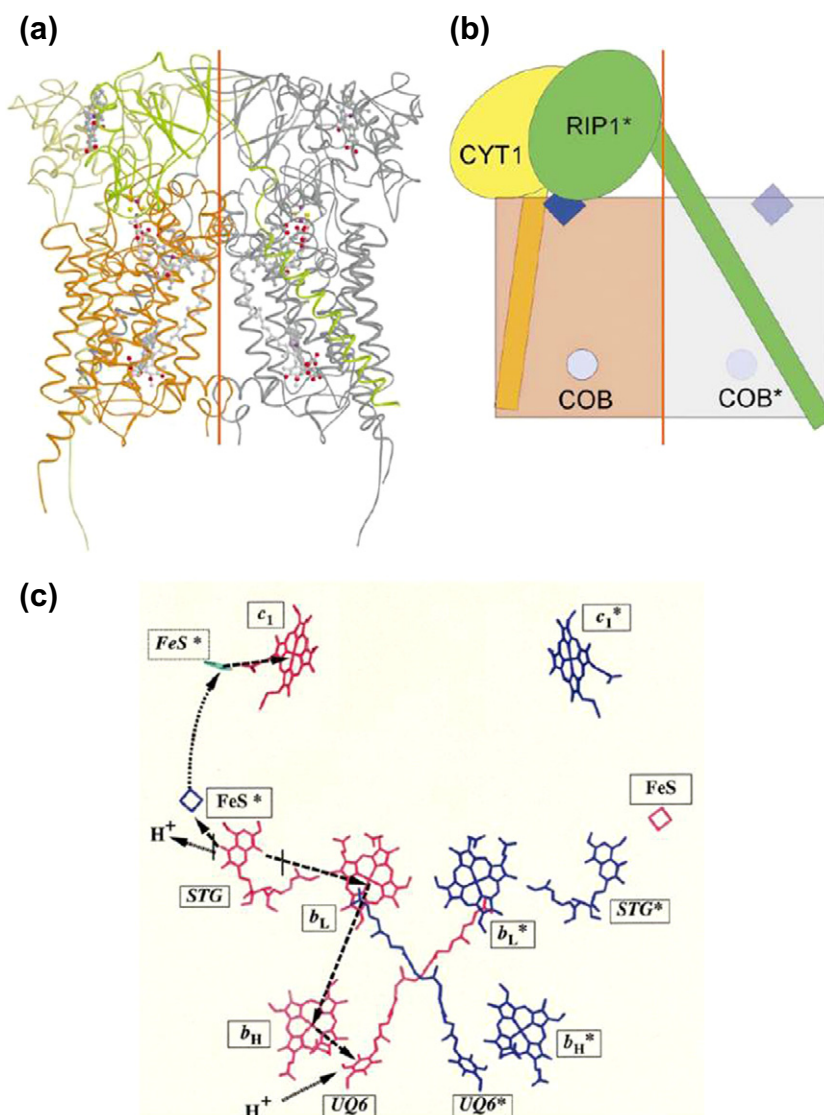


FIGURE 13.15 The yeast ubiquinol-cytochrome *c* oxidoreductase, QCR, or cytochrome *bc*₁ complex. (a) the homodimeric complex of the catalytic subunits cytochrome *b*, orange, Rieske protein, green, and cytochrome *c*1, yellow. The second functional unit is coloured in grey. (b) Schematic representation of one functional subunit. The Rieske protein is anchored with its transmembrane helix in one monomer, while the extrinsic domain forms a functional unit with the catalytic subunits of the other monomer. Qo sites are depicted as diamonds, Qi sites as circles. (c) Orientation of cofactors, substrate, and inhibitor molecules in yeast QCR. Monomers A and B are colour coded in red and blue, respectively. The extrinsic domain of the protein is mobile and the Fe₂-S₂ cluster can be found in different orientations with the maximal positions either close to haem b_L (b-position) or close to haem c₁ (c-position). The latter orientation is found in a bovine QCR structure (X, PDB entry: 1BE3) and the Fe₂-S₂ cluster of the superimposed model is coloured in green. In yeast, stigmatellin specifically binds to the Qo site stabilising the b-position and inhibiting enzyme activity. Electron transfer and proton uptake are indicated with straight arrows. The curved arrow represents the movement of the Fe₂-S₂ cluster, which most likely precedes oxidation of the cluster by cytochrome *c*1. The spatial arrangement of the cofactors allows fast electron transfer. (From Hunte, 2001. Copyright 2001 with permission from Elsevier.)

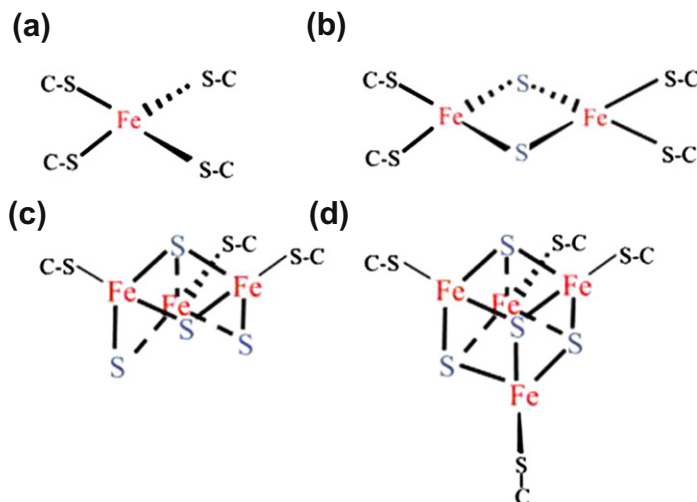


FIGURE 13.16 Structures of iron–sulfur clusters.

states are 0 and +1; and (d) cubane four iron–four sulfide [$\text{Fe}_4\text{-S}_4$] clusters – stable oxidation states are +1 and +2 for ferredoxin-type clusters and +2 and +3 for “HIP” clusters. Electrons can be delocalized, such that the valences of individual iron atoms lie between ferrous and ferric forms. Low-molecular-weight proteins containing the first and the last three types are referred to as rubredoxins (Rd) and ferredoxins (Fd), respectively. The protein ligands are frequently Cys residues, but a number of others are found, notably His, which replaces two of the thiol ligands in the [$\text{Fe}_2\text{-S}_2$] Rieske proteins. In addition to these discrete Rd and Fd electron transfer proteins which are often found in electron transfer chains and as electron donors to enzymes, such centres are often found within redox enzymes where they act as wires (Figure 13.17), delivering electrons one at a time between redox couples which are physically separated. In the *E. coli* quinol-fumarate reductase (Figure 13.17) which transfers electrons from a membrane-bound quinone to cytosolic fumarate, the electrons are transferred to a covalently bound flavin adenine nucleotide at the active site through three distinct iron–sulfur clusters and ultimately are used to reduce fumarate. More complex structures are found in specialized redox enzymes, including hybrid or mixed metal clusters, through metal substitution and/or bridges between simpler clusters (Rees, 2002).

However, the biological activity of Fe–S proteins is not restricted to one-electron transfer reactions. A completely different role for Fe–S clusters is found in a family of dehydratases, of which the best known is aconitase. They all have a [$\text{Fe}_4\text{-S}_4$] cluster (Figure 13.18). However, only three of the four iron atoms have thiolate ligands; the fourth is solvent exposed in the active site pocket and has a water molecule loosely bound in its fourth coordination site. Binding of the substrate (citrate in the case of aconitase) occurs by smooth switching of the iron from tetrahedral to octahedral (six-coordinate) geometry, binding the substrate by both a carboxylate residue and the hydroxyl group to be abstracted. An adjacent base then deprotonates a methylene group simultaneously with the removal of the hydroxyl group by the cationic iron atom, acting as a Lewis acid, accomplishing the net dehydration of the substrate. The iron–sulfur cluster does not function to transfer electrons, but rather to assist in substrate binding and to provide a local positive charge to effect the catalysis.

Studies on three different iron–sulfur enzyme systems which all require S-adenosylmethionine (SAM) – lysine 2,3-aminomutase, pyruvate-formate lyase, and anaerobic ribonucleotide reductase – have led to the identification of SAM as a major source of free radicals in living cells (for a recent review, see Atta et al., 2010). As in the dehydratases, these systems have a [4Fe-4S] centre chelated by only three cysteines with one accessible coordination site. The cluster is active only in the reduced state [4Fe-4S] $^{1+}$ and appears to combine the two roles described previously, serving both as a ligand for substrate binding and as a redox catalyst (Figure 13.19). Their mechanism again requires that the exposed iron atom of the cluster shifts towards octahedral geometry as it binds

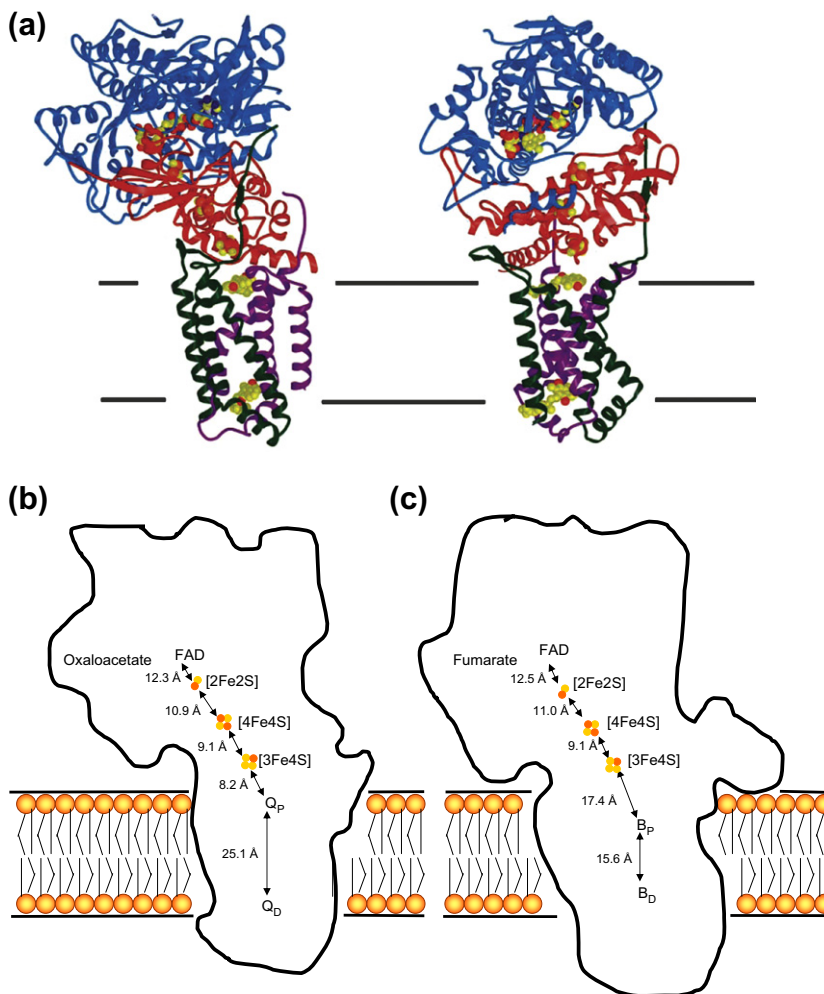


FIGURE 13.17 (a) Polypeptide fold; (b) electron transfer distances in *E. coli* quinol-fumarate reductase; and (c) inter-cofactor distances in the *W. succinogenes* enzyme. (From Iverson et al., 2002. Reproduced by permission of American Society for Biochemistry and Molecular Biology. Copyright 2002.)

both the amino and carboxylate group of SAM. An electron is then transferred from the low potential reduced cluster onto SAM generating the adenosyl radical and possibly also coordinating the liberated thiolate. The binding of the liberated sulfur atom to the remaining coordination site of the iron may help to drive the energetically unfavourable electron transfer step. The highly reactive 5'-deoxyadenosyl radical then initiates the enzyme reaction by abstracting a hydrogen atom from the substrate RH to generate the free radical R^\bullet and 5'-deoxyadenosine. These radical SAM enzymes, as they are now called, constitute a large family involved in many metabolic pathways, including biotin synthase and lipoate synthase. These enzymes catalyse the insertion of sulfur atoms into aliphatic substrates. After activation of the organic substrate by the adenosyl radical, a second Fe—S cluster is the source of the sulfur atoms for insertion into the dethioprecursor.

Finally, we remind our reader that in its apoform, cytoplasmic aconitase is active as an iron regulatory protein (Chapter 8), binding to iron regulatory elements in the mRNAs of ferritin and transferrin receptor and regulating their translation.

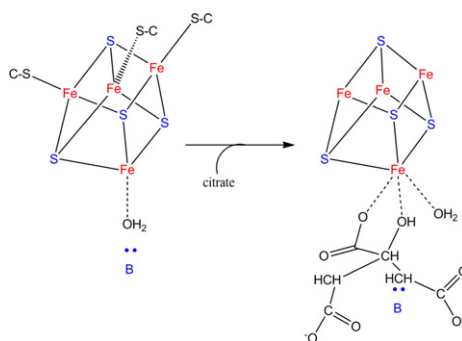


FIGURE 13.18 Role of clusters in substrate binding — in aconitase the cluster geometry shifts from four- to six-coordination on substrate binding. The coordinating iron atom abstracts the hydroxide anion during dehydration. (Adapted from Voet & Voet, 2004.)

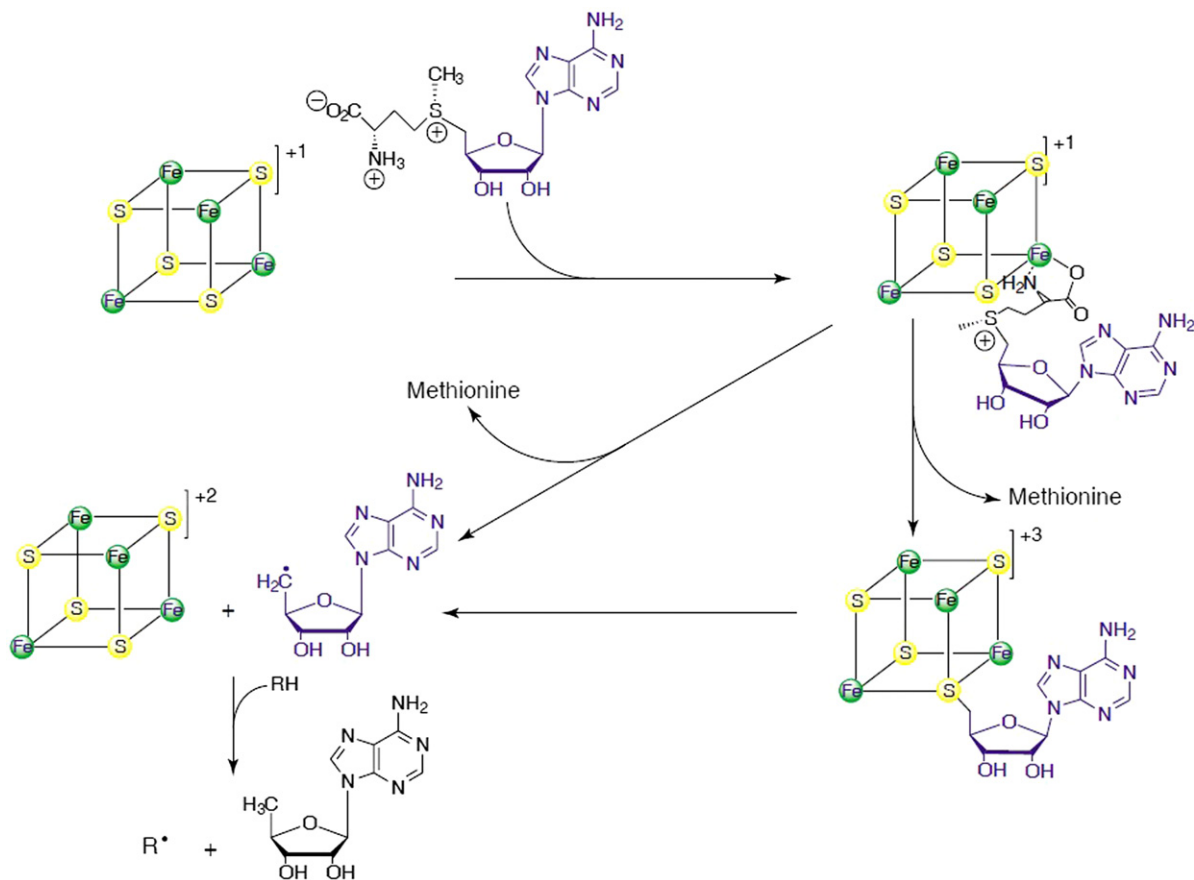


FIGURE 13.19 S-adenosylmethionine (SAM) is a source of 5-deoxyadenosyl radicals. SAM binds to the subsite iron (in blue) of the reduced [4Fe-4S] cluster via its α -aminocarboxylate group. The 5-deoxyadenosine radical is then formed by electron transfer with release of methionine. (From Fontecave, Atta, & Mulliez, 2004. Copyright 2004 with permission from Elsevier.)

OTHER IRON-CONTAINING PROTEINS

There are many other proteins that contain iron in a form which is neither in haem nor in iron–sulfur clusters. We have already encountered the iron-storage and transport proteins, ferritin and transferrin (Chapter 8). We propose to discuss here two other classes of iron-containing proteins, those with mononuclear nonhaem iron centres and those with dinuclear nonhaem iron centres. The mononuclear nonhaem iron enzymes include a large number of enzymes involved in oxygen activation and insertion into organic substrates. We can distinguish between enzymes with a mononuclear high-spin Fe(II) centre and those with a mononuclear Fe(III) centre.

The mononuclear Fe(II) enzymes catalyse a wide variety of reactions and have been classified into five families (Figure 13.20).

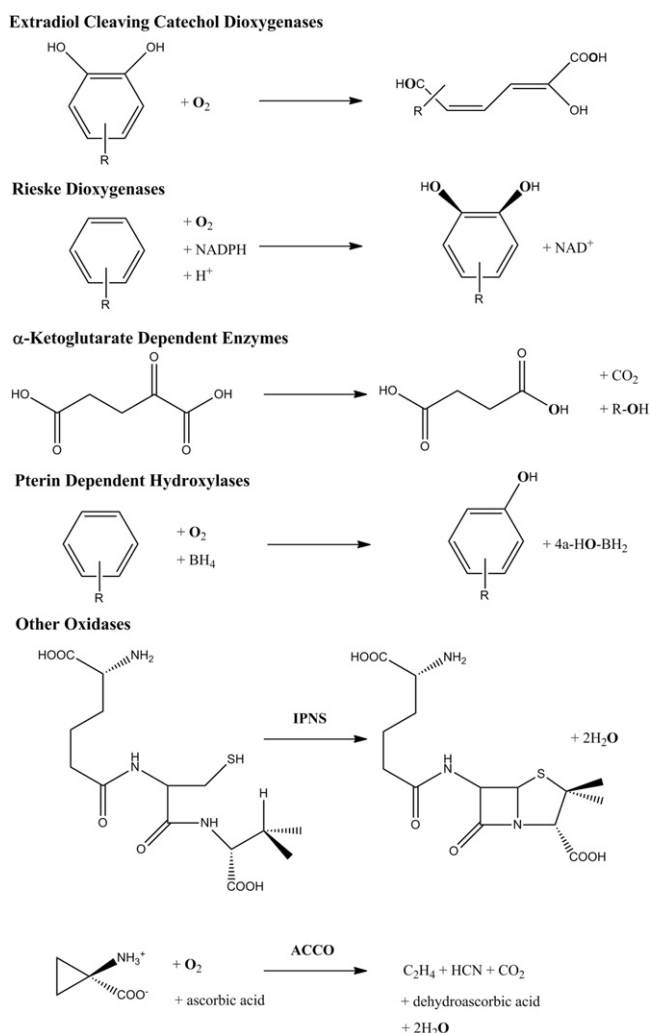


FIGURE 13.20 Reactions catalysed by each of the five families of mononuclear nonhaem iron enzymes with a 2-His-1-carboxylate facial triad. Dioxygen is labelled to indicate the fate of each oxygen atom. (Adapted from Koehntop, Emerson, & Que, 2005.)

The **catechol dioxygenases** are part of nature's strategy for the degradation of aromatic compounds in the environment. They are found in soil bacteria and catalyse the final ring-opening step in the biodegradation of catechols, transforming aromatic precursors into aliphatic products. Whereas the extradiol-cleaving enzymes use Fe(II), the intradiol-cleaving enzymes use Fe(III). Extradiol-cleaving catechol dioxygenases catalyse oxidative aromatic ring cleavage of catechols at the C–C bond adjacent to the enediol group in a four-electron oxidation and incorporate both atoms of dioxygen into the product.

The **Rieske dioxygenases** (so-called because they contain a Rieske [2Fe–2S] cluster in addition to the mononuclear iron centre) catalyse *cis*-dihydroxylation of arene double bonds using NADH as the source of two electrons; again, both dioxygen atoms are incorporated into the *cis*-diol product.

The **α -keto acid-dependent enzymes** are distinguished from other nonhaem iron enzymes by their absolute requirement for an α -keto acid cofactor, usually α -ketoglutarate and ascorbate as well as Fe(II) and O₂ for activity; the α -ketoglutarate is decarboxylated and one oxygen atom introduced into the succinate formed. This group of enzymes carries out hydroxylation of C–H bonds, oxygen atom transfers, heterocyclic ring formation, or desaturation reactions. Examples of these enzymes include proline 4-hydroxylase, prolyl and lysyl hydroxylase (which hydroxylate specific prolyl and lysyl residues in collagen⁵ important in its maturation, clavamate synthase, a key enzyme in bacterial antibiotic resistance, since it is involved in the synthesis of clavulanic acid, an important β -lactamase inhibitor; and 4-hydroxyphenylpyruvate dioxygenase, which converts 4-hydroxyphenyl-pyruvate into homogentisate, an important step in the catabolism of phenylalanine and tyrosine in mammals.

The fourth class, the **pterin-dependent hydroxylases**, includes the aromatic amino acid hydroxylases, which use tetrahydrobiopterin as cofactor for the hydroxylation of Phe, Tyr, and Trp. The latter two hydroxylases catalyse the rate-limiting steps in the biosynthesis of the neurotransmitters/hormones dopamine/noradrenaline/adrenaline and serotonin, respectively.

Finally, there are a mixed bag of oxidases, catalysing ethylene formation in plants and many other diverse reactions, illustrated in Figure 13.20, by isopenicillin N-synthase, IPNS, which catalyses the cyclisation of the heterocyclic β -lactam ring. The importance of penicillin- and cephalosporin-related antibiotics in clinical medicine cannot be underestimated and has stimulated the study of their biosynthetic pathways. A key step in the biosynthesis of these antibiotics involves oxidative ring closure reactions of δ -(L- α -aminoadipoyl)-L-cysteinyl-D-valine (ACV) to form isopenicillin N, the precursor of penicillins and cephalosporins, catalysed by IPNS (Figure 13.20). The overall reaction utilizes the full oxidative potential of O₂, reducing it to two molecules of H₂O. As discussed earlier, these enzymes are technically oxidases and the four electrons required for dioxygen reduction come from the substrate.

Although these oxygen-activating mononuclear nonhaem ferrous enzymes catalyse a diverse range of chemical reactions, structural studies show that they all have a common structural motif in their catalytic centre. This canonical structural motif for coordination of nonhaem ferrous iron in metal-dependent oxygenases is a facial triad of two histidine residues and one aspartate or glutamate residue, which coordinate the iron in a facial triad arranged at the vertices of one triangular face of an octahedron (Figure 13.21(a)). This 2-His-1-carboxylate facial triad motif is used in more than 20 families of enzymes. The metallocentre is often accommodated in a double-stranded beta-helix fold with the iron-coordinating residues located in the rigid core structure of the protein. At the sequence level, the metal ligands are arranged in a HXD/E...H motif, with a variable distance between the conserved histidine residues.⁶ In contrast to haem enzymes, which have a fourth equatorial ligand, the great advantage of the facial triad-binding motif stems from the fact that the 2 His and 1 Asp or Glu residues which bind the metal ion occupy only one face of the coordination sphere (Figure 13.21(a)). This leaves three coordination

5. This of course goes a long way to explaining the association of scurvy with vitamin C deficiency, and the successful utilisation by the British navy of lime juice as a means of prevention of the disease — hence the expression *limey* for British sailors.

6. Interestingly, cysteine dioxygenase, among a growing number of other iron(II) oxygenases, has the carboxylate residue replaced by another histidine.

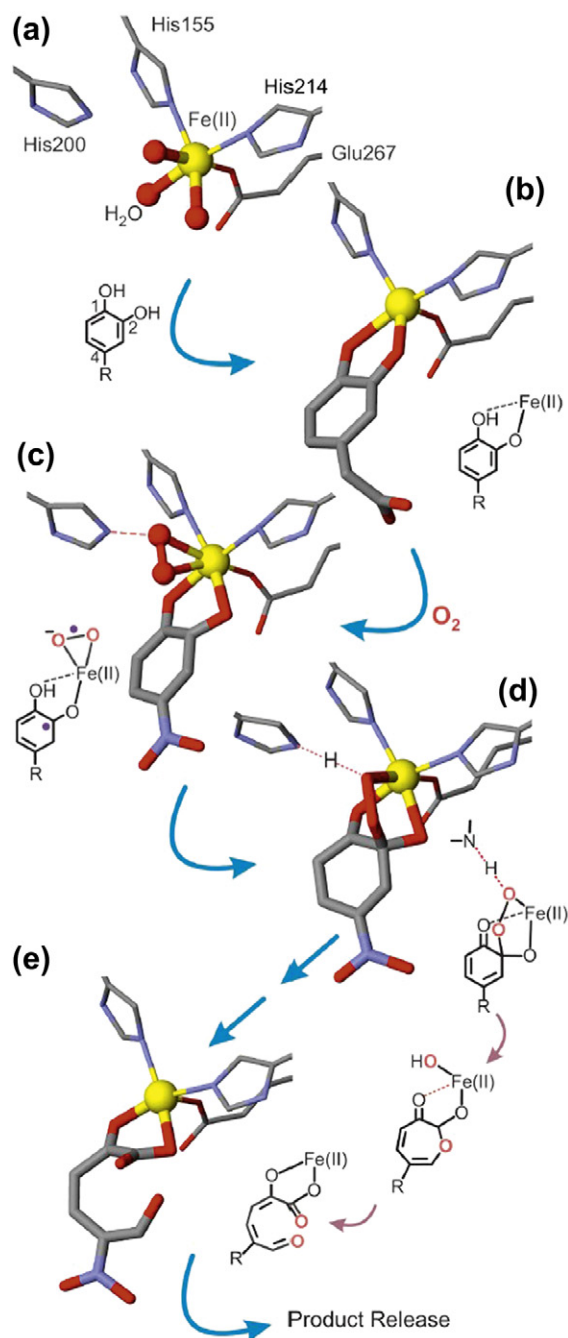


FIGURE 13.21 Proposed mechanism for extradiol aromatic ring-cleaving dioxygenases, illustrated for HPCD. Where known, the X-ray crystal structures of the active site metal centres are shown: (a) resting enzyme, PDB21G9; (b) HPCA complex, PDB1Q0C; (c–e) the semiquinone substrate radical-Fe(II)-superoxo, Fe(II)-alkylperoxo, and product complexes found in subunits C,D, and A, respectively, of a single crystal when using 4NC as the substrate, PDB21GA. The chemical figures provide additional detail for proposed electron distribution or proposed steps for which intermediates have not been structurally characterized. (Colour scheme: yellow, Fe(II); red, oxygen; grey, carbon; blue, nitrogen). (From *Lipscomb, 2008*. Copyright 2008 with permission from Elsevier.)

sites occupied by displaceable water molecules on the opposite site of the facial triad available to bind exogenous ligands, such as O₂, substrate, and/or cofactor, thus giving the protein the flexibility with which to tune the reactivity of its Fe(II) centre, giving rise to the extraordinary range of catalytic versatility that we have seen above.

Figure 13.21 presents a possible mechanism for the extradiol aromatic ring-cleaving dioxygenases (Lipscomb, 2008), illustrated by homoprotocatechuate 2,3-dioxygenase (HPCD). The active site structure with three solvent molecules occupying the opposite side of the metal-binding triad (Figure 13.21(a)) is unreactive to dioxygen. Binding of homoprotocatechuate to the resting form of the enzyme through the hydroxyl oxygens of the catechol substrate results in the formation of a five-coordinate Fe(II) centre, which is primed for dioxygen binding (Figure 13.21(b),(c)). This has two important mechanistic consequences. First, the O₂ and the substrate are juxtaposed and presumably oriented for reaction, and second since both substrates are electronically linked through the metal, this will facilitate electron transfer from the catechol to the oxygen. This would give both reactants radical character, allowing rapid recombination to form the alkylperoxo intermediate (Figure 13.21(c),(d)) in a spin-allowed reaction. Once this intermediate is formed, fission of the O—O bond and C—C bond cleavage could occur to form a 7-membered lactone. The lactone would undergo hydrolysis by the second oxygen atom from O₂, present bound to the metal ion, to form the open-ring product ready for release from the enzyme (Figure 13.21(e)). While the mechanism shown in Figure 13.21 is widely accepted,⁷ other possibilities exist, including the formation of a dioxetane intermediate and the formation of a high-valent metal-oxo species such as Fe(IV)=O, as proposed for other members of the facial triad family (Krebs, Fujimori, Walsh, & Bollinger, 2007).

With an ever-increasing number of protein structures now solved, it has become clear that the 2-His-1-carboxylate signature can be replaced by alternative metal coordination to Fe(II) or Mn(II) in a number of other mononuclear nonhaem Fe(II) oxygenases.

There are also mononuclear nonhaem Fe(III) enzymes, including the intradiol-cleaving catechol dioxygenase and protocatechuate 3,4-dioxygenase (PCD). PCD converts 3,4-dihydroxybenzoate (protocatechuate) to β -carboxy-*cis,cis*-muconate, and is the best characterized of the catechol dioxygenases. The Fe(III) centre in the isolated enzyme lies in a trigonal bipyramidal environment coordinated by two Tyr and two His residues together with a bound solvent molecule, probably a hydroxide. The steps in the catalytic cycle have been identified by the crystallographic determination of the structures of PCD complexed with substrate and substrate analogs (as in the case of HPCD (Figure 13.22)). In the enzyme—substrate complex, Tyr447 removes the second substrate proton and is displaced as the chelated substrate complex is formed. The ternary enzyme—substrate—dioxygen complex then forms. All the structures presented, except for the peroxo-model (Figure 13.22(e)), were generated from X-ray crystal structures.

Lipoxygenases (LOXs), which catalyse the oxidation of unsaturated fatty acids containing the *cis,cis*-1,4-pentadiene moiety to the corresponding 1-hydroperoxy-*trans,cis*-2,4-diene, are widely distributed in plants and animals. The mammalian enzymes typically act on arachadonic acid to produce hydroperoxides that are precursors of leukotrienes and lipoxins, both classes of compounds which are mediators of inflammation. The iron active site metal is a nonhaem iron that is octahedrally coordinated by five amino acid side chains and a water or hydroxide ligand (Figure 13.23). In plant LOXs, these residues are always three histidines, one asparagine, and the carboxy group of the carboxy-terminal isoleucine. In mammalian LOXs, however, the iron is coordinated by four histidines and again the carboxy-terminal isoleucine (Andreou and Feussner, 2009).

Another class of mononuclear nonhaem Fe(III) enzymes are the microbial superoxide dismutases, which have a coordination geometry reminiscent of protocatechuate 3,4-dioxygenase, with four endogenous protein ligands, three His and one Asp residues, and one bound water molecule (Figure 13.24; Lim et al., 1997).

7. An important advance in support of the mechanism was that HPCD remains catalytically active in the crystals, and using a poor substrate at low O₂ concentrations, 3 different intermediates of the reaction cycle were found at high occupancy (the structures shown in Figure 13.22(c)–(e)).

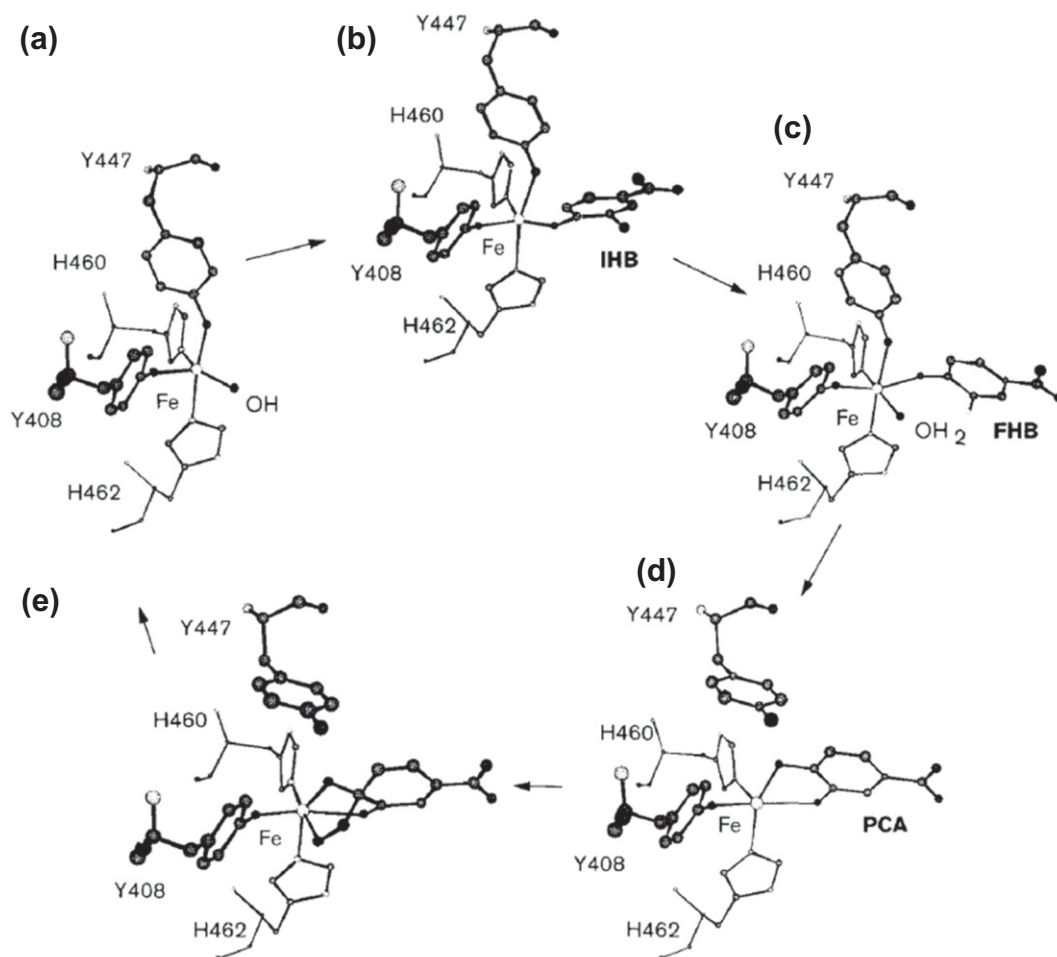


FIGURE 13.22 Iron site of PCD complexed with substrate and substrate analogs. (a) PCD as isolated. (b) PCD complexed with 3-iodo-4-hydroxybenzoate: because the large iodo group does not fit well in the active site, this is proposed to represent an early stage of subunit binding. (c) 3-Fluoro-4-hydroxybenzoate: the smaller fluoro group results in a substrate that fits the active site better. (d) The enzyme-substrate complex (PCA = 3,4-dihydroxybenzoate): Y447 removes the second substrate proton and is displaced as the chelated substrate complex is formed. (e) Hypothetical model for the tertiary enzyme-substrate-dioxygen complex. (From Lange & Que, 1998. Copyright 1998 with permission from Elsevier.)

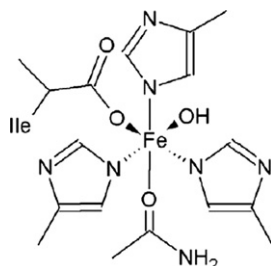


FIGURE 13.23 Active site coordination geometry of plant LOXs. (Adopted from Andreou & Feussner, 2009.)

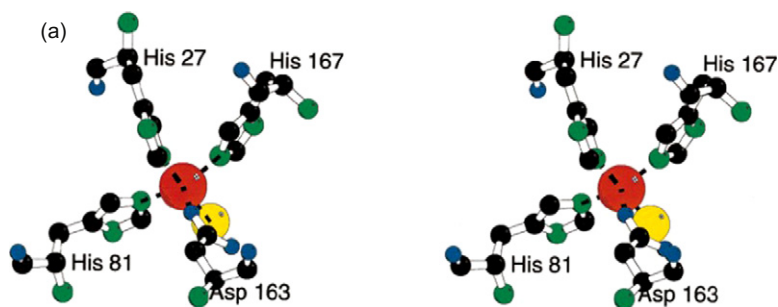


FIGURE 13.24 Coordination of Fe(III) ligands in *Asuifex pyrophilus* SOD. Fe ion (red) and water molecule (yellow) are not labelled. (From Lim *et al.*, 1997. Copyright 1997 with permission from Elsevier.)

DINUCLEAR NONHAEM IRON ENZYMES

The final class of iron proteins that we consider here are a large family of proteins containing nonhaem, nonsulfur, di-iron sites, often known collectively as di-iron proteins. The common link in all of these 'di-iron-oxo' proteins is that they react with dioxygen as part of their function. A more apt structural description of metal sites of this class of proteins would be « (μ -carboxylato)di-iron » (Nordlund and Eklund, 1995). They all contain a four-helix-bundle-protein fold, surrounding a (μ -carboxylato) di-iron core with the two iron atoms separated by 0.4 nm or less, one or more bridging carboxylate ligands, with terminal carboxylate and/or histidine ligands, and often a bridging oxo, hydroxo, or aqua ligand, at least at the di-iron (III) oxidation level (Kurz, 1997). The dimetallic centre is incorporated into a four-helix bundle domain (Figure 13.25), which seems to represent a preferred

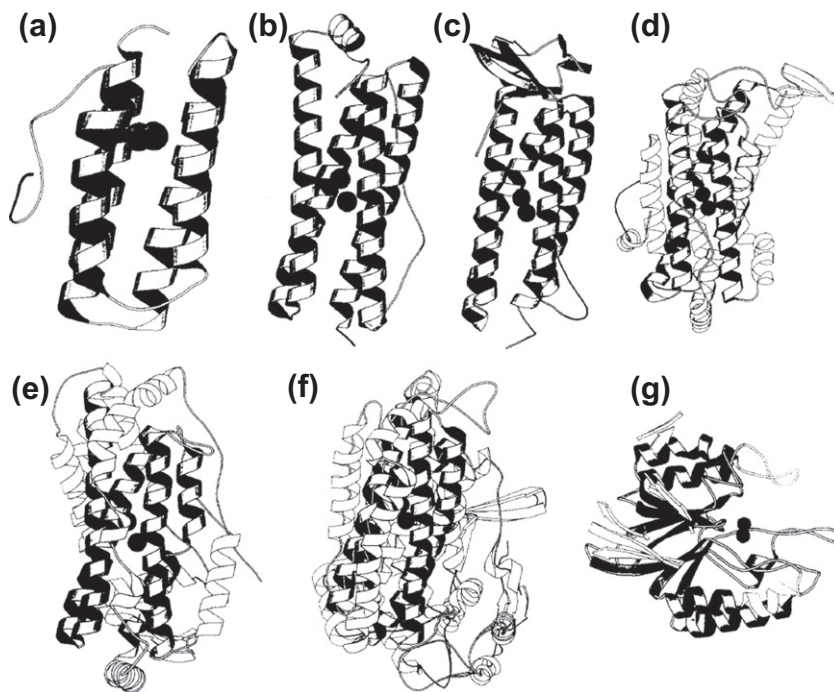


FIGURE 13.25 Three-dimensional structures of di-iron proteins. The iron-binding subunits of (a) haemerythrin, (b) bacterioferritin, (c) rubrerythrin (the FeS centre is on the top), (d) ribonucleotide reductase R2 subunit, (e) stearoyl-acyl carrier protein Δ^9 -desaturase, and (f) methane monooxygenase hydroxylase α -subunit. (From Nordlund & Eklund, 1995. Copyright 1995, with permission from Elsevier.)

biological scaffold for the binding and activation of dioxygen. In many members of the family, four of the iron-binding ligands are provided by two E(D/H)XXH motifs. Among their diverse functions, we find (i) ferritins, which store iron — mammalian H-chains have such a di-iron centre, as do the ferritins found in bacteria; (ii) haemerythrins, which transport O_2 in a number of marine invertebrates (although the protein has also been identified in an archaeobacteria); (iii) the RNR-R2 protein of Class I ribonucleotide reductases: here, the di-iron centre is required to generate a tyrosyl radical, which, in turn, is used to produce the active centre thiyl radical nearly 35 Å distant from the tyrosyl radical; (iv) rubreythrins (a contraction of rubredoxin and hemerythrin, reflecting the presence of both a rubredoxin-type $[Fe(Cys)_4]$ and a di-iron type of iron site) found in air-sensitive bacteria and archaeobacteria, where it is thought to function as a peroxide scavenger; (v) the stearoyl-acyl carrier protein Δ^9 desaturases which introduce double bonds into saturated fatty acids; and (vi) bacterial multicomponent monooxygenases, which catalyse hydroxylation of a variety of hydrocarbon substrates, including alkanes, alkenes, and aromatics. Members of the family include methane monooxygenase (MMOH) and toluene monooxygenase hydroxylase (ToMOH) which transform methane and toluene to their corresponding alcohols. We will discuss the mechanism of action of methane monooxygenases and of Class I ribonucleotide reductases shortly, while postponing a detailed discussion of ferritin function till Chapter 19.

The iron ligands in the dinuclear sites of these proteins are very similar — the structures of the (μ -carboxylato) di-iron cores found for MMOH, ToMOH, RNR-R2, rubreythrin, stearoyl-acyl carrier protein Δ^9 desaturases, bacterioferritin, and methaemerythrin are presented in Figure 13.26. They all have the same three-amino-acid structural motif on one side of the di-iron site, made up of a bridging Glu and two His residues, coordinated in

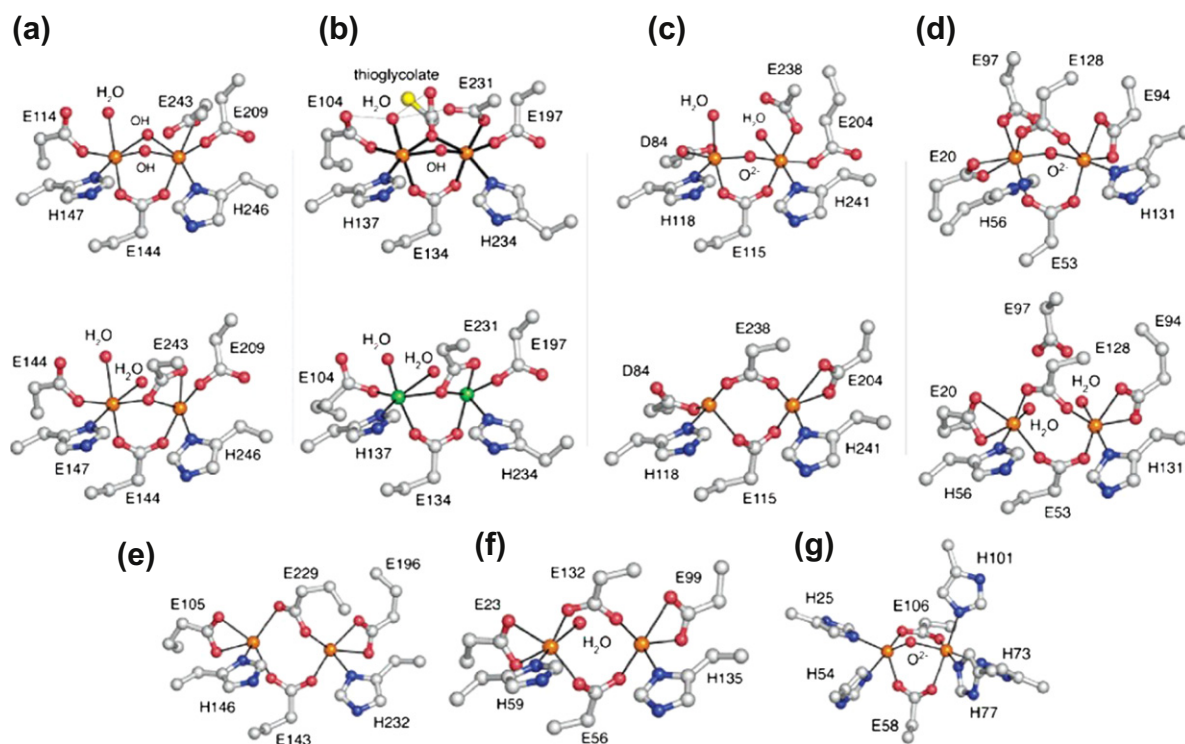


FIGURE 13.26 Dioxygen-utilising carboxylate-bridged di-iron centres. (a) Oxidized (top) and reduced (bottom) MMOH; (b) oxidized (top) and Mn^{II}-reconstituted ToMOH (bottom); (c) oxidized (top) and reduced (bottom) RNR-R2; (d) oxidized (top) and reduced (bottom) rubreythrin; (e) reduced stearoyl-acyl carrier protein Δ^9 -desaturase; (f) reduced bacterioferritin; and (g) methaemerythrin. Fe1 is on the left and Fe2 on the right. (From Sazinsky & Lippard, 2006. Copyright (2006) American Chemical Society.)

positions distal to the active site pocket. The remaining ligands in the two hydroxylases, MMOH and ToMOH, are quite different from those in the other five. In the resting state, Fe1 is coordinated by a monodentate Glu and a water molecule and Fe2 by two monodentate Glu, with bridging hydroxide ions completing the octahedral geometry around the iron atoms. In RNR-R2, Δ^9 desaturase, bacterioferritin, and rubrerythrin, the flanking carboxyl ligands on the opposite side of the di-iron centre are all quite different. The very varied chemistry carried out by these proteins, no doubt, is reflected in the active site geometry, but we are as yet unable to predict what changes in ligands might have what consequences for biological activity.

We consider briefly the structure and mechanism of action of soluble MMO (sMMO), the best characterized of the BMMs (bacterial methane monooxygenases) (Figure 13.27), which is able to activate the inert C–H bond of

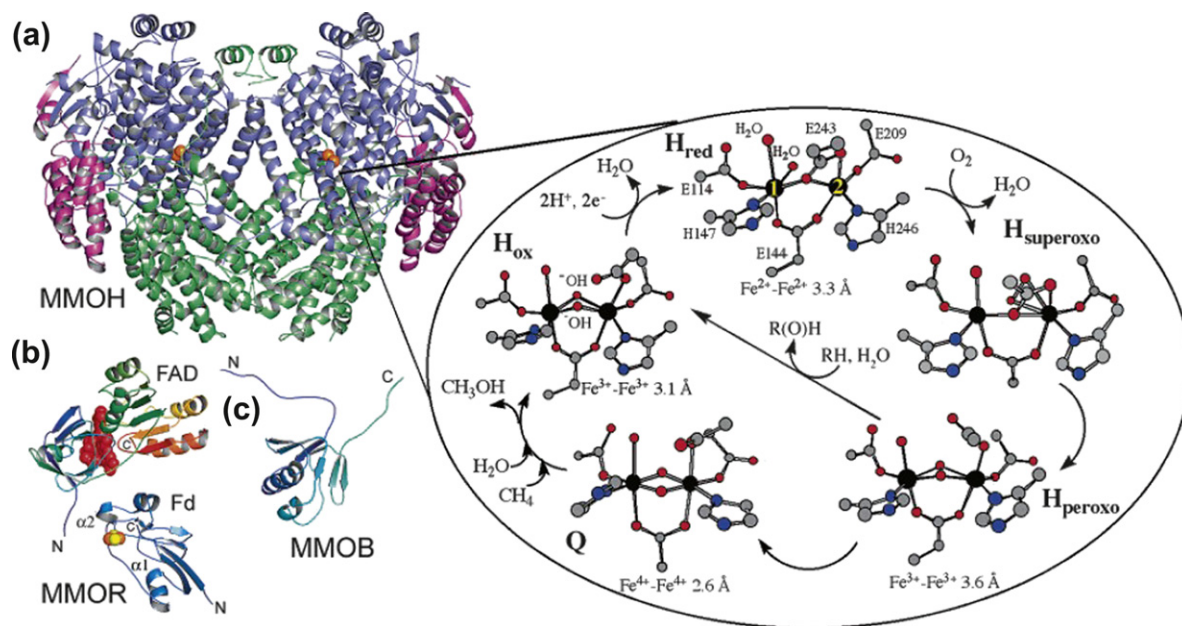


FIGURE 13.27 Structures of sMMOH components and proposed reaction cycle. (a) MMOH; (b) the MMOR FAD and ferredoxin (Fd) domains; and (c) MMOB. In MMOH, the α , β , and γ subunits are coloured blue, green, and purple, respectively. Iron, sulfur, and FAD are coloured orange, yellow, and red, respectively, and are depicted as spheres. The MMO reaction cycle is shown on the right., with atoms coloured [Fe (black), C (grey), O (red), and N (blue)]. (From Sazinsky & Lippard, 2006. Copyright (2006) American Chemical Society.)

methane and catalyse its transformation to methanol. sMMO contains three protein components, the hydroxylase, MMOH, which contains the carboxylate-bridged di-iron centre, a regulatory protein MMOB, and a [2Fe–2S]- and FAD-containing reductase (MMOR) which shuttles electrons from NADH to the di-iron centre. The hydroxylase component (MMOH) is composed of an $\alpha_2\beta_2\gamma_2$ -heterodimer, with the di-iron centre located within a characteristic four-helix bundle made up of helices B, C, E, and F of the α -subunit. Helices E and F are on the surface of the hydroxylase, forming part of the rim of a cleft, with the di-iron centre some 12 Å beneath the rim. In the proposed reaction cycle for MMOH, the resting enzyme, with both iron atoms in the ferric state, is reduced by the MMOHR to the di-iron(II) form. The bridging hydroxyls are expelled and Glu 243 shifts to become a bridging ligand while remaining bound to Fe2, while a water molecule coordinates weakly to Fe1. The Fe–Fe distance lengthens, and the open coordination position which forms on Fe2 facing the active site pocket can now bind dioxygen, forming an intermediate designated as $H_{superoxo}$. This rearranges to a peroxo-intermediate designated H_{peroxo} , which can itself carry out oxygen insertion reactions with some substrates. However, the key intermediate in MMOHs is Q,

which has been characterized spectroscopically, and proposed to have a diamond-shaped $\text{Fe}_2^{\text{IV}} (\mu\text{-O})_2$ core, and a Fe—Fe distance of only 2.6 Å, in marked contrast to the distance of 3.6 Å in H_{peroxo} . Q then reacts directly with methane at a rate which depends on methane concentration.

Finally, we discuss Class I ribonucleotide reductases, in which the role of the di-iron centre is to generate the diferric tyrosyl radical (Y122) cofactor in the R2 subunit, which initiates nucleotide reduction by generating a transient thiyl radical (C439) in the enzyme active site located in R1 (Stubbe and Riggs-Gelasco, 1998). From the crystal structures of the R1 and R2 subunits, a docking model, which places the Y on R2 at a distance greater than 35 Å, has been proposed (Uhlin and Eklund, 1994). Radical transfer across this distance is thought to occur by a proton-coupled electron transfer (PCET) radical hopping pathway, involving radical intermediates of the aromatic amino acid residues illustrated in Figure 13.28 (Stubbe, Nocera, Yee, & Chang, 2003). The radical is thought to

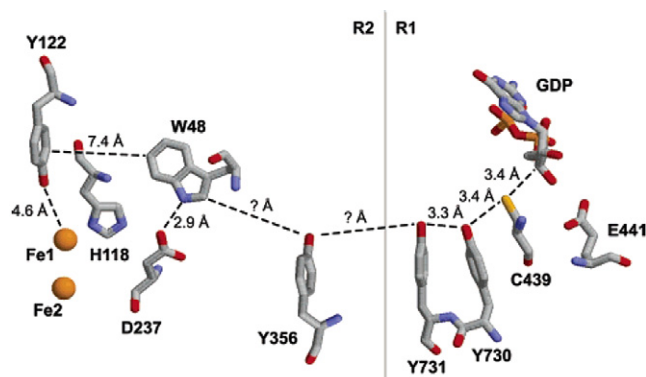


FIGURE 13.28 Conserved residues in Class I RNR, which compose the putative PCET pathway for radical transport from Y122 in R2 to C439 in the R1 active site. (Seyedsayamdost, Yee, Reece, Nocera, & Stubbe, 2006. Copyright (2006) American Chemical Society.)

transfer along the pathway $\text{Y122} \rightarrow \text{W48} \rightarrow \text{Y356}$ in R2 to $\text{Y731} \rightarrow \text{Y730} \rightarrow \text{C439}$ in R1. The pathway begins at the cofactor, where an orthogonal proton transfer (PT) between Y122 and the di-iron oxo/hydroxo cofactor establishes the need only for the transfer of an electron through the span of R2. Oxidation of the proposed gate-keeper for radical transport between R2 and R1, Y356, requires a PCET reaction; this also appears to involve PT orthogonal to the electron transfer pathway between W48 and D236. By moving the protons at Y122 and Y356 off pathway, the radical transport in R2 involves a long distance electron transfer (ET) coupled to short PT hops at the tyrosine endpoints. A collinear PCET pathway through R1 has been suggested, in which both the proton and the electron may be transferred between $\text{Y731} \rightarrow \text{Y730} \rightarrow \text{C439}$. Thus, in contrast to most other biological systems, RNR seems to incorporate all possible variations of PCET mechanisms in the transport of the radical over 35 Å across two protein subunits (Reece, Hodgkiss, Stubbe, & Nocera, 2006).

REFERENCES

- Andreou, A., & Feussner, I. (2009). Lipoxygenases — structure and reaction mechanism. *Phytochemistry*, 70, 644–649.
- Atta, M., Mulliez, E., Arragain, S., Forouhar, F., Hunt, J. F., & Fontecave, M. (2010). S-Adenosylmethionine-dependent radical-based modification of biological macromolecules. *Current Opinion in Structural Biology*, 20, 684–692.
- Brzezinski, P., & Johansson, A. L. (2010). Variable proton-pumping stoichiometry in structural variants of cytochrome c oxidase. *Biochimica et Biophysica Acta*, 1797, 710–713.
- Collman, J. P., Boulatov, R., Sunderland, C. J., & Fu, I. (2004). Functional analogues of cytochrome c oxidase, myoglobin, and hemoglobin. *Chemical Reviews*, 104, 561–588.
- Crichton, R. R., & Pierre, J.-L. (2001). Old iron, young copper: from Mars to venus. *Biometals*, 14, 99–112.

- Dempsey, J. L., Esswein, A. J., Manke, D. R., Rosenthal, J., Soper, J. D., & Nocera, D. G. (2005). Molecular chemistry of consequence to renewable energy. *Inorganic Chemistry*, 44, 6879–6892.
- Fenton, H. J. H. (1894). *Transactions of the Chemical Society*, 65, 899–910.
- Fontecave, M., Atta, M., & Mulliez, E. (2004). S-adenosylmethionine: nothing goes to waste. *TIBS*, 29, 243–249.
- Gelin, B. R., & Karpus, M. (1977). Mechanism of tertiary structural change in hemoglobin. *Proceedings of the National Academy of Sciences of the United States of America*, 74, 801–805.
- Haber, F., & Weiss, J. (1934). The catalytic decomposition of hydrogen peroxide by iron salts. *Proceedings of the Royal Society of London – Series A*, 147, 332–351.
- Hosler, J. P., Ferguson-Miller, S., & Mills, D. A. (2006). Energy transduction: proton transfer through the respiratory complexes. *Current Opinion in Structural Biology*, 17, 444–450.
- Huber, C., & Wächtershäuser, G. (2006). α -Hydroxy and α -amino acids under possible Hadean, volcanic origin-of-life conditions. *Science*, 314, 630–632.
- Hunte, C., Koepke, J., Lange, C., Rossmann, T., & Michel, H. (2000). Structure at 2.3 Å resolution of the cytochrome bc1 complex from the yeast *Saccharomyces cerevisiae* with an antibody FV fragment. *Structure*, 8, 669–684.
- Hunte, C. (2001). Insights from the structure of the yeast cytochrome bc1 complex: crystallization of membrane proteins with antibody fragments. *FEBS Letters*, 504, 126–132.
- Iverson, T. M., Luna-Chavez, C., Croal, L. R., Cecchini, G., & Rees, D. C. (2002). Crystallographic studies of the *Escherichia coli* quinol-fumarate reductase with inhibitors bound to the quinol-binding site. *Journal of Biological Chemistry*, 277, 16124–16130.
- Keilin, D. (1925). On cytochrome, a respiratory pigment, common to animals, yeast, and higher plants. *Proceedings of the Royal Society of London – Series B: Biological Sciences*, 98, 312–339.
- Koehntop, K. D., Emerson, J. P., & Que, L., Jr. (2005). The 2-His-1-carboxylate facial triad: a versatile platform for dioxygen activation by mononuclear non-heme iron(II) enzymes. *Journal of Biological Inorganic Chemistry*, 10, 87–93.
- Krebs, C., Fujimori, D. G., Walsh, C. T., & Bollinger, J. M., Jr. (2007). Non-heme Fe(IV)-oxo intermediates. *Accounts of Chemical Research*, 40, 484–492.
- Kurz, D. M., Jr. (1997). Structural similarity and functional diversity in diiron-oxo proteins. *The Journal of Biological Inorganic Chemistry*, 2, 159–167.
- Johnston, J. B., Ouellet, H., Podust, L. M., & Ortiz de Montellano, P. R. (2011). Structural control of cytochrome P450-catalyzed ω -hydroxylation. *Archives of Biochemistry and Biophysics*, 507, 86–94.
- Lange, S. J., & Que, L., Jr. (1998). Oxygen activating nonheme iron enzymes. *Current Opinion in Chemical Biology*, 2, 159–172.
- Lim, J. H., Yu, Y. G., Han, Y. S., Cho, S., Ahn, B. Y., Kim, S. H., et al. (1997). The crystal structure of an Fe-superoxide dismutase from the hyperthermophile Aquifex pyrophilus at 1.9 Å resolution: structural basis for thermostability. *Journal of Molecular Biology*, 270, 259–274.
- Lipscomb, J. D. (2008). Mechanism of extradiol aromatic ring-cleaving dioxygenases. *Current Opinion in Structural Biology*, 18, 644–649.
- McMunn, C. A. (1884). On myohaematin, an intrinsic muscle-pigment of vertebrates and invertebrates, on histohaematin, and on the spectrum of the suprarenal bodies. *The Journal of Physiology*, 5, XXIV.
- Nordlund, P., & Eklund, H. (1995). Di-iron-carboxylate proteins. *Current Opinion in Structural Biology*, 5, 758–766.
- Nordlund, P., & Reichard, P. (2006). Ribonucleotide reductases. *The Annual Review of Biochemistry*, 75, 681–706.
- Poulos, T. L., Finzel, B. C., & Howard, A. J. (1986). Crystal structure of substrate-free *Pseudomonas putida* cytochrome P-450. *Biochemistry*, 25, 5314–5322.
- Qin, L., Hiser, C., Mulichak, A., Garavito, R. M., & Ferguson-Miller, S. (2006). Identification of conserved lipid/detergent-binding sites in a high-resolution structure of the membrane protein cytochrome *c* oxidase. *Proceedings of the National Academy of Sciences of the United States of America*, 103, 16117–16122.
- Rao, P. V., & Holm, R. H. (2004). Synthetic analogues of the active sites of iron-sulfur proteins. *Chemical Reviews*, 104, 527–559.
- Reece, S. Y., Hodgkiss, J. M., Stubbe, J., & Nocera, S. G. (2006). Proton-coupled electron transfer: the mechanistic underpinning for radical transport and catalysis in biology. *Philosophical Transactions of the Royal Society B: Biological Sciences*, 361, 1351–1364.
- Rees, D. C. (2002). Great metallocusters in enzymology. *Annual Review of Biochemistry*, 71, 221–246.
- Stubbe, J., Ge, J., & Yee, C. S. (2001). The evolution of ribonucleotide reduction revisited. *TIBS*, 26, 93–99.
- Sazinsky, M. H., & Lippard, S. J. (2006). Correlating structure with function in bacterial multicomponent monooxygenases and related diiron proteins. *Accounts of Chemical Research*, 39, 558–566.

- Seyedsayamdost, M. R., Yee, C. S., Reece, S. Y., Nocera, D. G., & Stubbe, J. (2006). pH rate profiles of $F_nY356-R2s$ ($n = 2, 3, 4$) in *E. coli* ribonucleotide reductase: evidence that Y356 is a redox active amino acid along the radical propagation pathway. *Journal of the American Chemical Society*, 128, 1562–1568.
- Stubbe, J., Nocera, D. G., Yee, C. S., & Chang, M. Y. C. (2003). Radical initiation in the class I ribonucleotide reductase: longrange proton-coupled electron transfer? *Chemical Reviews*, 103, 2167–2202.
- Stubbe, J., & Riggs-Gelasco, P. (1998). Harnessing free radicals: formation and function of the tyrosyl radical in ribonucleotide reductase. *TIBS*, 23, 438–443.
- Uhlen, U., & Eklund, H. (1994). Structure of ribonucleotide reductase protein R1. *Nature*, 370, 533–539.
- Voet, D., & Voet, J. G. (2004). *Biochemistry* (3rd ed.). Hoboken, N.J.: John Wiley and Sons.

This page intentionally left blank

Copper – Coping with Dioxygen

Introduction	279
Copper Chemistry and Biochemistry	279
Copper-Containing Enzymes in Oxygen Activation and Reduction	282
Mars and Venus – The Role of Copper in Iron Metabolism	295

INTRODUCTION

Whereas, on account of the solubility of its ferrous form, iron was widely available in the reducing environment of the early Earth, copper which was present as highly insoluble cuprous sulfides must have been poorly bioavailable. In contrast, once photosynthetic *Cyanobacteria* set off the first major irreversible pollution of our environment with the production of dioxygen, copper became much more bioavailable in its cupric form. Whereas the enzymes involved in anaerobic metabolism were designed to act in the lower portion of the range of redox potentials, the presence of dioxygen created the need for new redox systems with standard redox potentials in the range from 0 to 0.8 V, and copper proved eminently suitable for this role. For aerobic metabolism, enzymes and proteins with higher redox potentials came to be utilised, to take advantage of the oxidising power of dioxygen. However, whereas the early evolution of life was the ‘iron age’, it is clear that the subsequent ‘copper age’ was in reality an ‘iron–copper age’, where both metals were involved together. This is well illustrated by ceruloplasmin, the principal copper-binding protein in serum, which plays an important role in iron metabolism, and by the terminal oxidase of the mitochondrial respiratory chain, cytochrome *c* oxidase, which requires both haem iron and copper for its activity.

Copper is present in a large number of enzymes, many involved in electron transfer, activation of oxygen and other small molecules like oxides of nitrogen, methane and carbon monoxide, superoxide dismutation, and even, in some invertebrates, oxygen transport (for further details see [Granata et al., 2004](#); [Hatcher and Karlin, 2004](#); [Messerschmidt et al., 2001](#); [Rosenzweig and Sazinsky, 2006](#); [Solomon, 2006](#)).

COPPER CHEMISTRY AND BIOCHEMISTRY

The routinely encountered oxidation states are Cu(I) and Cu(II), and as with iron, the reduced form can catalyse Fenton chemistry with hydrogen peroxide. Cu(I) can form complexes with coordination number 2, 3, or 4, while Cu(II) prefers coordination numbers 4, 5, or 6. Whereas four-coordinate complexes of Cu(II) are square-planar, the corresponding Cu(I) complexes are tetrahedral. Among the divalent elements of the transition series, Cu(II) forms the most stable complexes. In terms of the HSAB classification Cu(II) is ‘hard’, while Cu(I) is soft underlined by its preference for sulfur ligands. Both forms have fast ligand exchange rates. It appears that throughout the living world, intracellular concentrations of ‘free’ copper are maintained at extremely low levels, most likely because intracellular copper metabolism is characterised by the use of copper chaperone proteins (discussed in Chapter 4) to transport copper toward their target proteins (cytochrome oxidase, superoxide dismutase, and the multicopper oxidases whose copper is inserted in the Golgi apparatus).

In Cu-containing proteins, three types of Cu centres are found, classified on the basis of their visible, UV, and EPR spectra, as originally proposed by one of the pioneers of Cu biochemistry, Bo Malmström (Malkin and Malmström, 1970). Types 1 and 2 centres have a single Cu atom which has an intense blue colour in Type 1 centres, but the single Cu atom in Type 2 centres is almost colourless. In contrast, Type 3 centres have a di-Cu centre which is EPR-silent. More details of the three types are given below:

Type 1 Cu(II): intense blue optical absorption band ($\lambda_{\text{max}} \sim 600 \text{ nm}$; $\epsilon > 3,000 \text{ M}^{-1} \text{ cm}^{-1}$); EPR spectrum with an uncommonly small hyperfine splitting in g|| region

Type 2 Cu(II): weak absorption spectrum; EPR spectrum characteristic of square-planar Cu(II) complexes

Type 3 Cu(II): di-copper centre; strong absorption in the near UV ($\lambda_{\text{max}} \sim 330 \text{ nm}$); no EPR spectra, the two coppers are antiferromagnetically coupled.

The Type 1 copper ions are normally coordinated in a distorted tetrahedral centre (Figure 14.1) by three strong ligands, a cysteine and two histidines, and one weaker ligand such as methionine sulfur or a nitrogen or oxygen

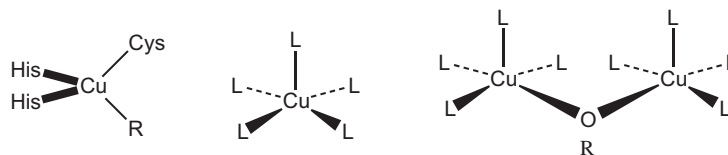


FIGURE 14.1 Classification of Cu sites. From left to right: Type 1; Type 2, Type 3.

donor. Type 2 centres have typically a square-planar or tetragonal geometry around the Cu with nitrogen or oxygen ligands. Type 3 coppers are usually each coordinated by three histidines, with a bridging ligand such as oxygen or hydroxyl anion.

Type 1 Blue Copper Proteins – Electron Transport

The blue copper proteins are so called on account of their intense blue colour which is derived from the strong Cys—Cu²⁺ charge transfer band at around 620 nm in the electronic absorption spectrum. The type 1 Cu centres, function, like cytochromes, exclusively as electron transport proteins. They are found in mobile electron transfer proteins like azurin and plastocyanin, as well as in more complex enzymes which contain multiple functional sites, where they serve to deliver to or take up electrons from the catalytic site. An intriguing question is how Cu can function in rapid electron transfer reactions¹ when Cu(I) and Cu(II) have such drastically different preferences in coordination geometry. As we pointed out above, four-coordinate Cu(II) complexes are square-planar, while the corresponding Cu(I) complexes tend to be more tetrahedral. When the type I copper centre in plastocyanin was first characterised by X-ray crystallography (Figure 14.2(a),(b)), it revealed a copper-binding site which was virtually the same in the apoprotein and in the copper-containing protein, whether the copper was Cu(I) or Cu(II). In other words, the protein imposes a binding site geometry on the metal, which is in reality closer to that of Cu(I) than of Cu(II), such that Cu(II) has no possibility to rearrange² toward its preferred geometry. The copper-coordination site (Figure 14.2(b)) is highly distorted with two His nitrogen and one Cys

1. An important concept in enzymology is that while catalysis involving bond cleavage and formation requires conformational change, and is relatively slow (maximum $\sim 10^8 \text{ s}^{-1}$), electron transfer is much more rapid (10^{12} s^{-1}), which does not allow much time for conformational change!

2. Whereas enzyme catalysis invariably involves movement and conformational change, in electron transfer, which is orders of magnitude faster, there is no time for movement.

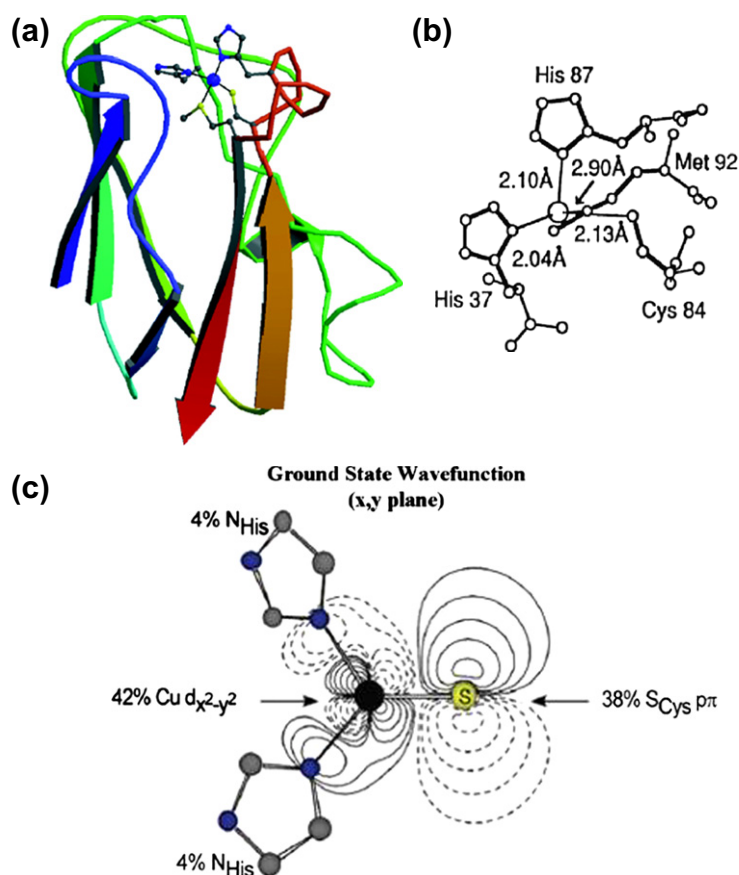


FIGURE 14.2 (a) X-ray structure of poplar plastocyanin from poplar leaves, as a ribbon diagram with its ligands highlighted. PDB code 1PLC. (b) X-ray structure of the Cu site in poplar plastocyanin. (c) Contour of plastocyanin ground-state wave function (RAMO) calculated by SCF-X α -SW adjusted to spectroscopic data. (b and c From Solomon, 2006. Copyright 2006 by permission of American Chemical Society News.)

sulfur donors lying almost in a plane with the metal ion, together with a long, out of the plane axial bond, between the sulfur of a Met residue and the Cu atom. This structure in many ways is the convincing proof of the idea that proteins can fine-tune the properties of bound metal centres, imposing what Vallee and Williams called the ‘entatic state’, which is ‘closer to a transition state than to a conventional, stable molecule’ (Vallee and Williams, 1968). The entatic state, or strain induced by metal binding to proteins, both on the metal and the protein itself, is a useful concept for explaining the generation of metal sites in electron transfer proteins, like the blue copper proteins, which are designed for rapid electron transfer. The trigonal pyramidal structure with three strong equatorial ligands (one Cys and two His) which the protein imposes provides a favorable geometry for both cuprous and cupric oxidation states, and facilitates rapid electron transfer.

Initially, application of molecular orbital theory gave description of the ground state of the blue Cu site which is shown in Figure 14.2(c) in the xy plane defined by Cu, Cys S, and the two His N. Modern DFT calculations give the same description of the ground state of the blue Cu site, highly covalent with the covalency delocalised into the $p\pi$ orbital of the thiolate sulfur.

A number of other Cu electron transfer proteins which contain type-1 Cu centres (azurin, ceruloplasmin, laccase, nitrite reductase, rusticyanin, and stellacyanin) are known. They all have three coordination positions contributed by 2 His and one Cys, similar to the copper coordination chemistry in plastocyanin – yet they span

a range of redox potential from less than 200 mV to at least 800 mV. One of the challenges for the future will be to determine what programmes this fine-tuning of redox properties of type 1 copper centres.

COPPER-CONTAINING ENZYMES IN OXYGEN ACTIVATION AND REDUCTION

There has been enormous activity in the field of Cu(I)-dioxygen chemistry in the last 25 years, with our information coming from both biochemical/biophysical studies and to a very important extent from coordination chemistry. This has resulted in the structural and spectroscopic characterisation of a large number of Cu dioxygen complexes, some of which are represented in Figure 14.3 (Himes and Karlin, 2009). The

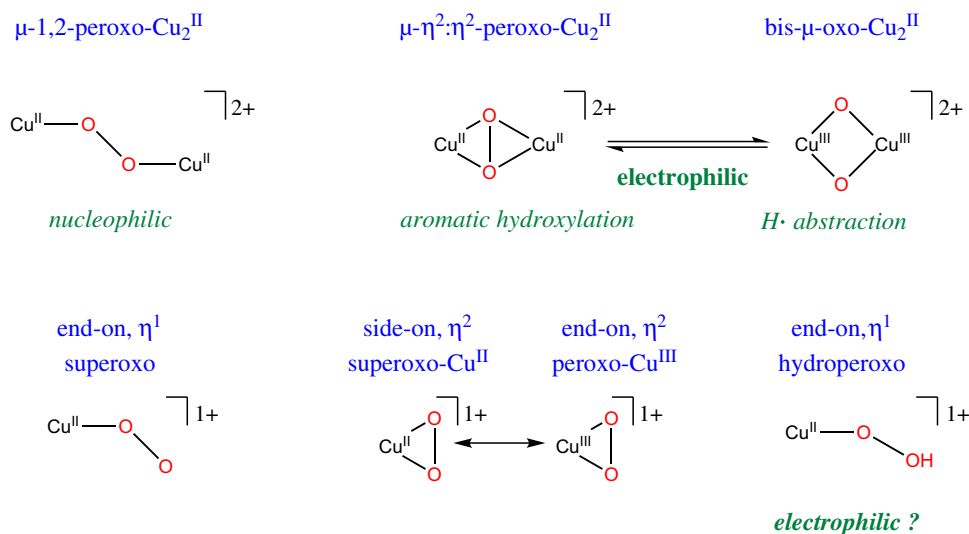


FIGURE 14.3 Crystallographically or spectroscopically characterised Cu—O₂ adduct structures found in small molecule ligand—Cu complexes, with characteristic reactivity patterns (green). (Adapted from Himes & Karlin, 2009.)

O₂-reactive centres in Cu enzymes can be either mononuclear (type 2), dinuclear (type 3), or trinuclear (Type 2 and 3). We will discuss each in turn: the trinuclear sites will be included in our discussion of multicopper oxidases.

Type 2 Copper Proteins

A number of X-ray structures are available for oxidases and oxygenases containing Type 2 copper sites including amine oxidases, galactose oxidase, lysyl oxidase, dopamine β -hydroxylase, and peptidyl-glycine α -hydroxylating monooxygenase. However, there is a paradox concerning type 2 mononuclear Cu sites which bind dioxygen. In order to activate O₂, unless they go to the unlikely Cu(III) state, they cannot supply the 2nd electron which is required to convert the cupric-superoxo complex to the more likely oxygen donor, the cupric-peroxo complex. There are two possible solutions to this dilemma.

The first is best illustrated by galactose oxidase which converts galactose + O₂ to the corresponding aldehyde + H₂O₂. Originally this enzyme was thought to involve Cu(III). However, galactose oxidase turns out to be a free radical metalloenzyme (Rogers and Dooley, 2003) and solves the problem via a novel metallo-radical complex comprising a tyrosine radical coordinated to a Cu ion in the active site (Figure 14.4). The unusually stable

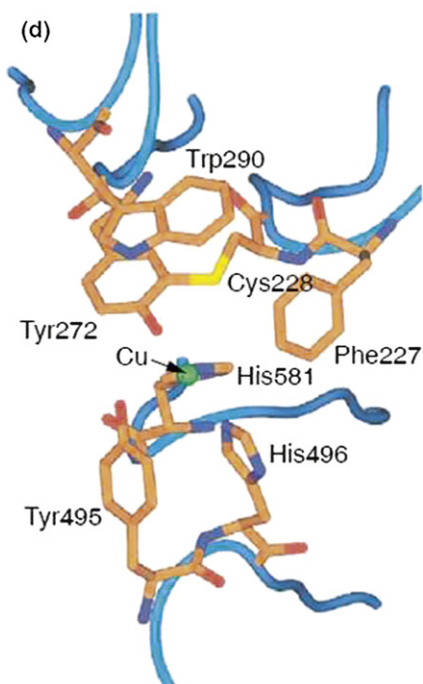
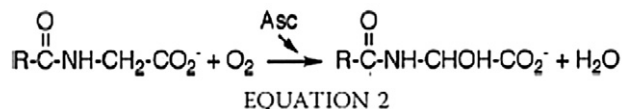
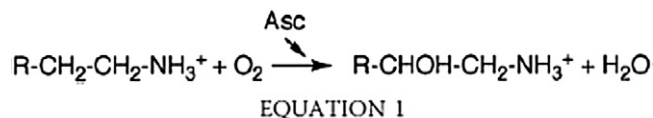


FIGURE 14.4 The Cu ligands of galactose oxidase (Tyr 272, Tyr 495, His 496 and His 581), the Cys228 which forms the thioether bond to Tyr 272, the tryptophan that stacks over it (Trp 290) and Phe 227. (From Rogers & Dooley, 2003. Copyright 2003, with permission from Elsevier.)

protein radical is formed from the redox-active side chain of a cross-linked tyrosine residue (Tyr-Cys). As we saw in Chapter 13 and will discuss later in this chapter, this strategy is also adopted by cytochrome *c* oxidase, which also uses a tyrosine radical.

The second strategy is utilised by two other enzymes with a type 2 Cu centre, which in addition require ascorbate. Peptidyl-glycine α -hydroxylating monooxygenase (PMH), which converts C-terminal glycine-extended peptides to their α -hydroxylated products (Equation 1), and dopamine β -hydroxylase (D β H), which converts dopamine to noradrenaline³ (Equation 2):



Both enzymes contain two Cu atoms and in the case of PMH (Figure 14.5) it has been established that dioxygen binds to one of the two type 2 copper atoms in an ‘end-on mode’. A copper–dioxygen complex has been

3. For our American readers, this corresponds to norepinephrine.

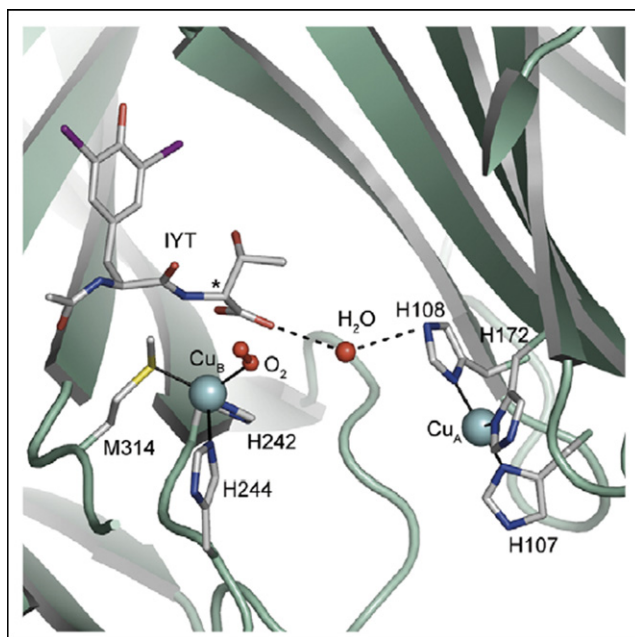


FIGURE 14.5 Active site of PHM with coordinated O_2 . The Cu_A and Cu_B sites are linked by a water molecule and the substrate analog IYT. The position of the hydroxylated α is denoted by an asterisk. (From Rosenzweig & Sazinsky, 2006. Copyright 2006, with permission from Elsevier.)

trapped by freezing crystals of the enzyme which had been soaked with a slowly reacting substrate, N-acetyl-diiodo-tyrosyl-D-threonine (IYT), in the presence of oxygen and ascorbate. Electron density was observed that was best modeled as O_2 within coordinating distance of the catalytic Cu in the precatalytic complex (Figure 14.5), replacing the solvent molecule observed in all other PHM structures. Bound substrate has been proposed to mediate electron transfer between the two Cu centres, each of which contributes one electron for O_2 reduction.

Figure 14.6 presents a possible mechanism for PHM and D β H. Substrate and O_2 bind to the reduced enzyme, triggering initial O_2 activation involving electron transfer from the type 2 Cu atom, to form the Cu-superoxo intermediate. A second electron is then transferred from the other Cu site, followed by-product release and reduction of the two Cu sites by ascorbate. The question of the exact mechanism of long-range electron transfer between the two Cu sites remains to be established.

(i) Dinuclear Type 3 copper proteins

Haemocyanin, tyrosinase, and catechol oxidase all belong to the type 3 Cu protein family which are characterised by two closely spaced antiferromagnetically coupled copper ions. However, while haemocyanin is an O_2 carrier protein, catechol oxidase, which converts catechols to the corresponding *o*-quinones, and tyrosinase, which, in addition to converting catechols to quinones, also hydroxylates monophenols (e.g., tyrosine), are both *enzymes*. They have very different structures and sequences (Figure 14.7). Yet, as we will see shortly, despite this, they have very similar active sites. Figure 14.7 presents the arrangements of the domains within the subunit structures of two haemocyanins from the haemolymph of the horse shoe crab (*Limulus polyphemus*) and the North Pacific giant octopus (*Octopus dofleini*), a streptococcal tyrosinase and catechol oxidase from sweet potato. The location of the copper centres are shown as are the amino acid residues which block access to the catalytic site (blocking residues).

The structures of the oxy forms at high resolution confirms, as predicted from model compounds, that the dioxygen molecule is bound in a peroxo-dicopper(II) complex, corresponding to the $\mu-\eta^2:\eta^2$ -peroxo, illustrated

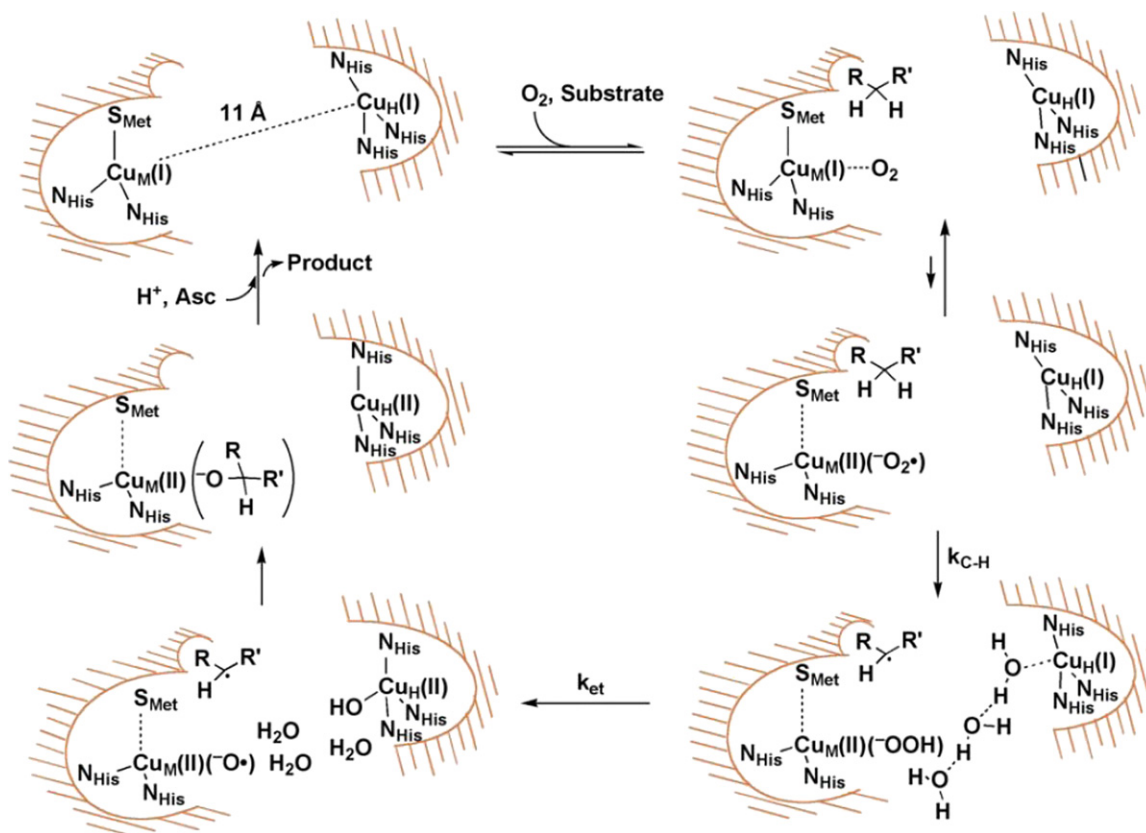


FIGURE 14.6 Copper superoxo mechanism for DβM and PMH. (Adapted from Klinman, 2006.)

in Figure 14.3. Each copper atom is ligated to the protein matrix by three histidine residues (Figure 14.8). Oxygen binding induces a change in the valency of the copper atoms, which are in the Cu (I) state in the deoxy form, but become Cu (II) upon oxygen bonding. This change results in the characteristic blue colour developed by all type 3 copper proteins upon oxygenation. The active sites of catechol oxidase, tyrosinase, and haemocyanins with oxygen bound to the copper atoms exhibit similar spectroscopic properties with respect to UV-resonance Raman, X-ray absorption, and UV/VIS spectroscopy.

This similarity in spectral properties implies that haemocyanins should also have catalytic activity. From the available body of experimental data, it is clear that the distinction between the two major functions – oxygen transport and enzymatic activity – is determined by the presence or absence of a protein domain covering the active site. In the case of tyrosinase and catechol oxidase, inactive pro-enzyme forms are activated by removal of an amino acid which blocks the entrance channel to the active site (indicated by the black bar in Figure 14.7). Haemocyanins behave as silent inactive enzymes but can be activated in the same way if the blocking amino acid is removed. In arthropods, like crabs, this is located in the N-terminal domain of a subunit whereas in molluscs, like octopus, it is in the C-terminal domain of a functional unit.

Figure 14.8(a) shows the initial configuration of the substrate after approach to the active site, based on the crystal structure of *Streptomyces* tyrosinase, while Figure 14.8(b) shows the shift of the substrate to Cu_A. Based on structural and other considerations, a mechanism for tyrosine hydroxylation is presented in Figure 14.9 (for a detailed account see Decker, 2006).

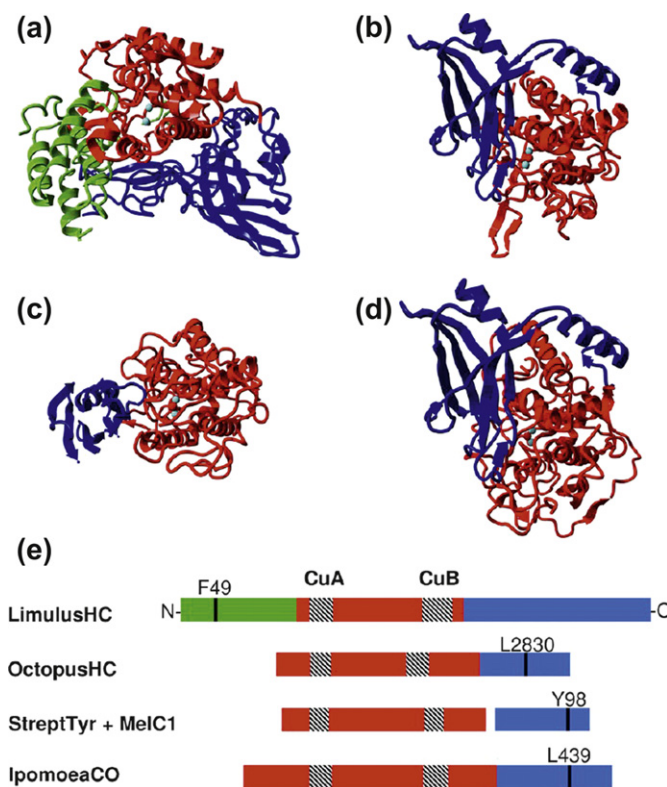


FIGURE 14.7 Arrangement of the domains within the subunit structures of different type 3 copper proteins. (a) *Limulus polyphemus* haemocyanin, (b) *Octopus dofleini* FU g haemocyanin, (c) *Streptomyces castaneoglobisporus* tyrosinase, (d) *Ipomoea batatas* catechol oxidase, (e) Sequence comparison (same colour code: domain I (green), domain II (red), domain III (cyan); copper centres are indicated by the hatched blocks, the blocking residues are shown as black bars). In all cases, the domains are parts of the subunit with the exception of *Streptomyces* tyrosinase, where an associated caddie protein (MelC1) provides Y98. (From Decker, Schweikardt, Nillius, Salzbrunn, Jaenicke, & Tuczek, 2007. Copyright 2007, with permission from Elsevier.)

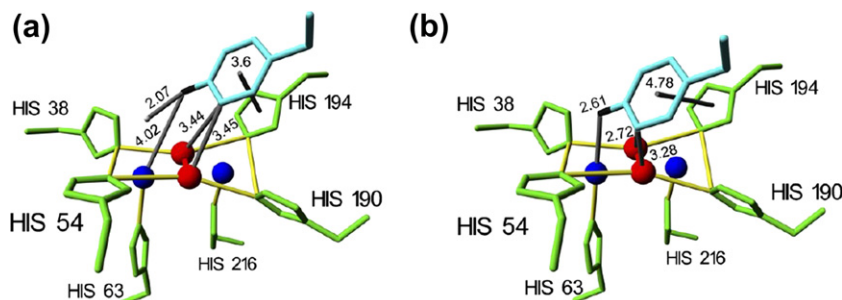


FIGURE 14.8 Dioxygen binding and (hypothetical) coordination of the substrate at the active site of *Streptomyces* tyrosinase. The distances are given to indicate whether a reaction may be possible or not. In (a) the distance between the hydroxyl group and Cu_A is too large for any reaction. After movement to the coordination point (grey) above Cu_A, the distance is shortened reasonably to allow a reaction. (a) shows the initial configuration after approach to the active site, based on the crystal structure of *Streptomyces* tyrosinase; (b) shows the shift of the substrate to Cu_A; Coppers: blue, histidines: green, dioxygen molecule: red, monophenolic substrate: cyan (its oxygen black), equatorial coordination of Cu_A and Cu_B: yellow frame, axial coordination of Cu_A and Cu_B: yellow lines; trans-axial coordination of Cu_A: grey dot. (From Decker et al., 2007. Copyright 2007, with permission from Elsevier.)

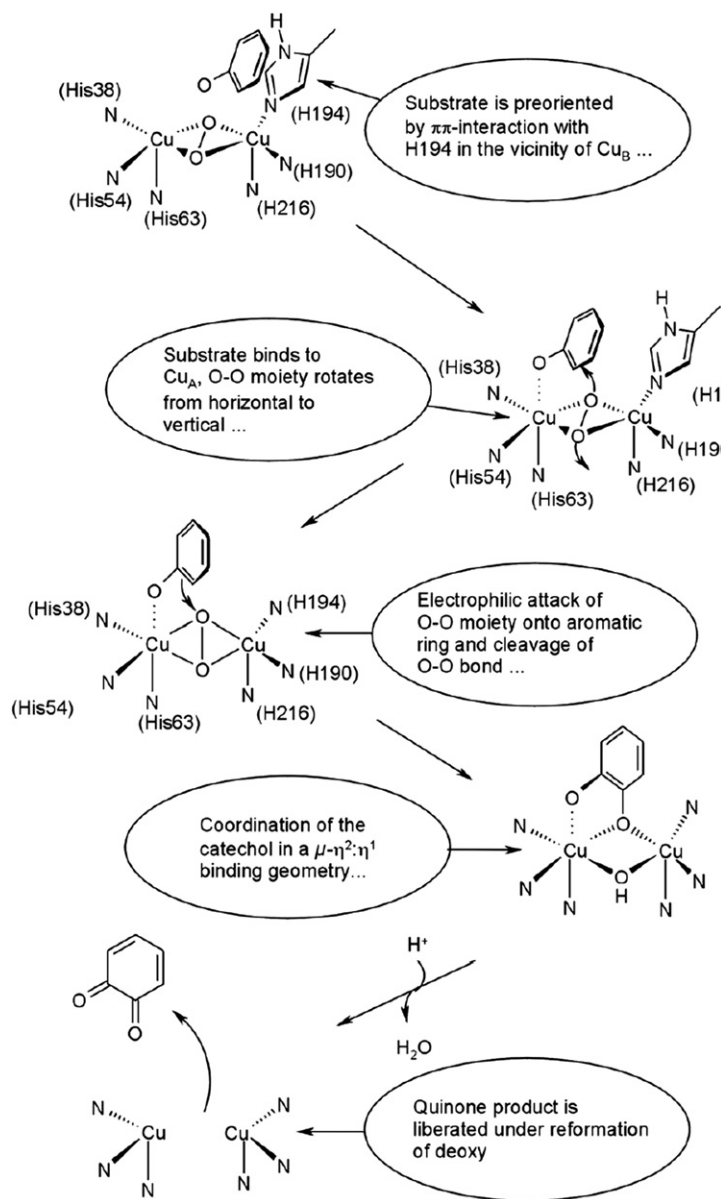


FIGURE 14.9 A mechanism for tyrosine hydroxylation. (From Decker *et al.*, 2007. Copyright 2007, with permission from Elsevier.)

(ii) Multicopper oxidases

An important family of multicopper enzymes couple the reduction of O_2 to H_2O with substrate oxidation. They include ascorbate oxidase, ceruloplasmin, Fet3, hephaestin, and laccase, and contain at least four copper ions. The four Cu ions are distributed between one type 1 blue copper site, one type 2 site, and one type 3 copper site. The blue Type 1 site is usually located some 12–13 Å distant from a trinuclear site which has the two Type 3 coppers, linked by a bridging oxygen and one Type 2 copper. We illustrate this class of oxidases with laccase which catalyses the four-electron reduction of O_2 to water, coupled with the oxidation of small organic

(generally aromatic) substrates. Laccases are functionally diverse, thermostable, and environmentally friendly catalysts: they occur naturally, use air and produce water as a by-product, and have therefore become the object of enormous interest to biotechnologists on account of their potential applications in ‘green chemistry’ (Riva, 2006). Over 100 fungal laccases have been characterised, and to date 10 X-ray structures from nine fungal species determined.

Figure 14.10(a) shows a ribbon diagram of the X-ray structure of *T. versicolor* laccase with the Cu atoms labeled by type and the substrate-binding cleft highlighted in red (Rodgers, Blanford, Giddens, Skamnioto, Armstrong, & Gurr, 2009). The detailed architecture of the four Cu sites is presented in Figure 14.10(b) for three different laccases. There is a variation in the redox potential of the type 1 Cu between the upper structure in Figure 14.10(b) where the ligand is Phe and the lower, where it is Met of 110 mV (hence the idea of ‘designer laccases’).

It is suggested that dioxygen binds to the Type 3 Cu atom of the trinuclear centre. In this ‘resting state’ all of the coppers will be in the oxidised +2 state (the blue colour of this intermediate confirms that the Type 1 copper is certainly oxidised). Two electrons are then transferred from the substrate molecules through the Type 1 Cu to the Type 3 coppers of the trinuclear site, where dioxygen is reduced to give a peroxo intermediate. The Cu in the type 1 site is rapidly re-oxidised by long-range intramolecular electron transfer, via a conserved His–Cys–His motif to the trinuclear Cu cluster. Two further electrons are then assimilated in a similar manner and result in splitting of the peroxo intermediate into two hydroxyl groups. Subsequent addition of protons, provided by acidic residues in exit channels, results in the successive release of two molecules of water. O₂ binds between the two Type 3 Cu atoms and is reduced to water without release of reactive oxygen intermediates. In the complete catalytic cycle, the Type I Cu must be oxidised and reduced four times. Whereas the Type 3 coppers are involved in oxygen binding and electron transfer to the dioxygen and peroxo intermediate, the role of the Type 2 copper is postulated to be to help to anchor the dioxygen molecule to the trinuclear cluster prior to reduction, and to temporarily bind the hydroxyl groups arising from the reduction of the peroxo intermediate prior to their release as water molecules in the exit channel.

(iii) The role of Cu in Cytochrome *c* Oxidases

We have already discussed the terminal oxidase of the respiratory chain, cytochrome *c* oxidase (CcOx) in the previous chapter. Here, we focus on the role of copper in this key metabolic enzyme. The disposition of the different redox metal centres of bovine heart CcOx with their relative distances are represented in Figure 14.11. The dimetallic Cu_A site receives electrons directly from cyt *c*, and is located in a globular domain of subunit II which protrudes into the intermembrane space (the periplasmic space in bacteria). This centre, which was originally believed to be mononuclear is in fact a di-copper site (Figure 14.12) in which the coppers are bridged by two cysteine sulfurs: each copper in addition has two other protein ligands. In the one electron reduced form, the electron is fully delocalised between the two Cu atoms, giving rise to a [Cu^{+1.5} ... Cu^{+1.5}] state. The Cu_A centre then rapidly reduces the haem *a*, located some 19 Å away (metal–metal distance) by intramolecular electron transfer. From haem *a*, electrons are transferred intramolecularly to the active site haem *a*₃ and Cu_B, where oxygen binds. The Cu_B centre (Figure 14.13) involves coordination of the copper atom to three His ligands and the Fe–Cu_B distance in the oxidised enzyme is 4.5 Å, with one of the His ligands covalently linked to a nearby Tyr residue. The mechanism of oxygen reduction has been discussed in Chapter 13.

As we saw, oxygen binds to the Fe of haem *a*₃, and after cleavage of the O–O bond, the oxidised Cu_B centre binds a hydroxide ion, which is subsequently protonated, before being the first of the two water molecules to be released from the enzyme. The coordination of the copper atom of the Cu_B centre (Figure 14.13) involves three His ligands and the Fe–Cu_B distance in the oxidised enzyme is 4.5 Å, with one of the His ligands of Cu_B covalently linked to a nearby Tyr residue. This His–Tyr crosslink was first identified in the crystal structures of the *Paraccocus denitrificans* and bovine heart CcO (Figure 14.13), and it is the source of the 4th electron for the reduction of molecular oxygen to water by the dinuclear haem *a*₃/Cu_B centre. The His–Tyr crosslink appears to modulate the properties of the tyrosine residue, via reduction of the phenol p*K*_a, facilitating proton delivery as well as by tyrosyl radical formation.

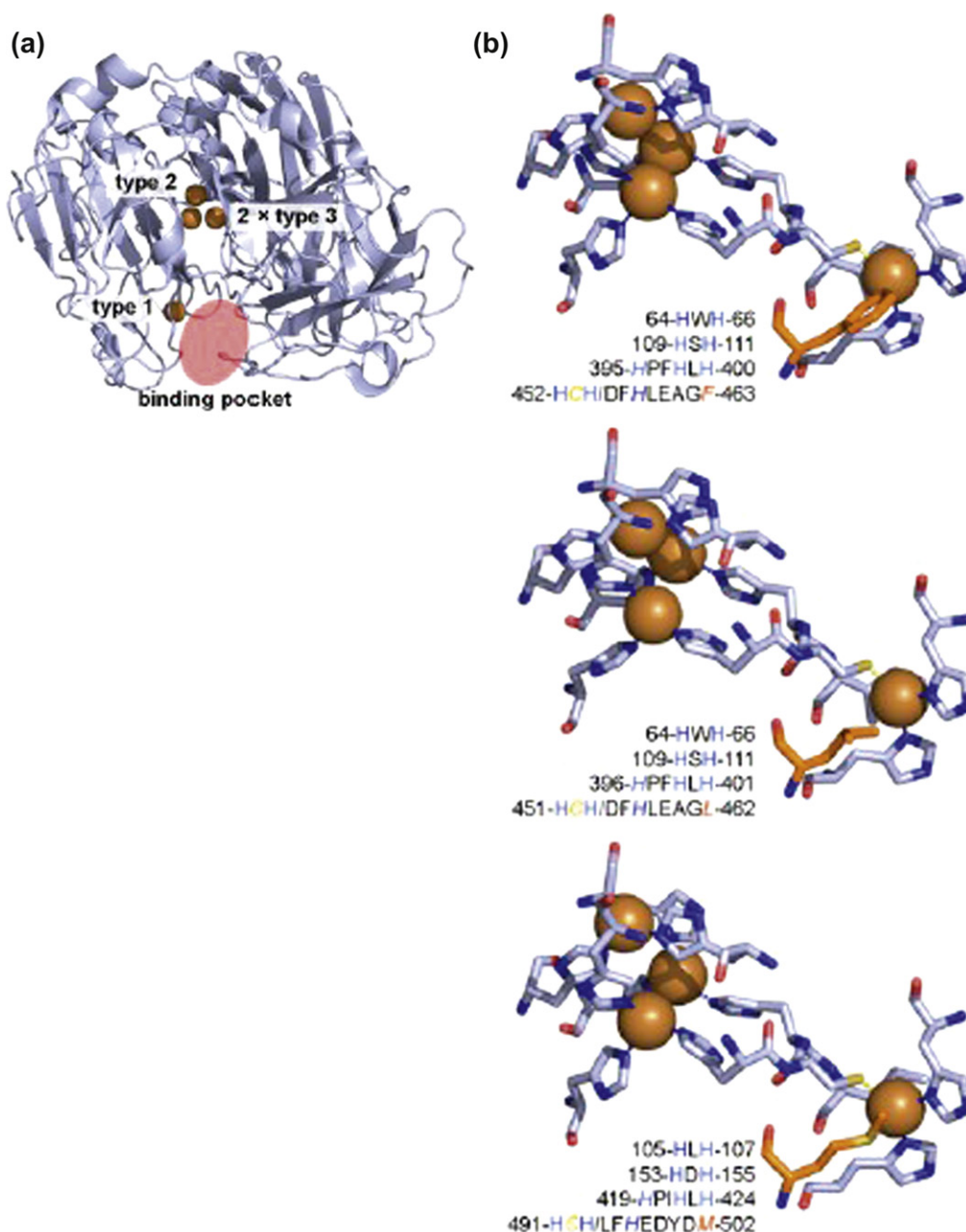


FIGURE 14.10 Structural insight into laccases from X-ray crystallography. (a) A ribbon model of the X-ray crystal structure from *T. versicolor* Lac1 (PDB 1kya) with the coppers (orange circles) labeled by type and the organic substrate-binding cleft highlighted in red. (b) A comparison of the architecture and sequence conservation between laccases from (top) *T. versicolor* Lcc1 (axial Phe in orange, PDB 1kya), (middle) *Rigidoporus microporus* laccase (axial Leu in orange, PDB 1v10), (bottom) *B. subtilis* CotA (axial Met in orange, PDB 1gsk). Coloured residue codes in the sequence alignment comprise the coordination spheres of the coppers; those around the type 1 copper are in italics. (From Rodgers *et al.*, 2009. Copyright 2007, with permission from Elsevier.)

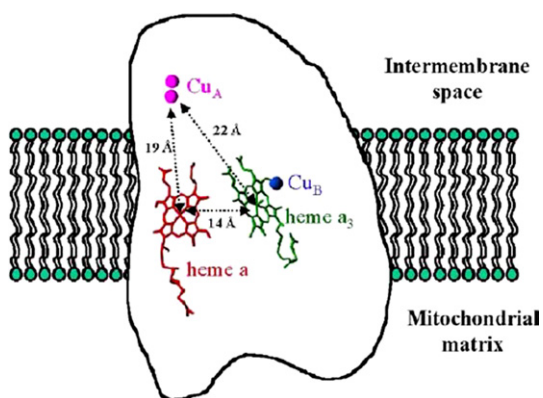


FIGURE 14.11 Schematic representation of the redox metals in beef heart CcO with their relative distances. (From Brunori, Giuffrè, & Sarti, 2005. Copyright 2005, with permission from Elsevier.)

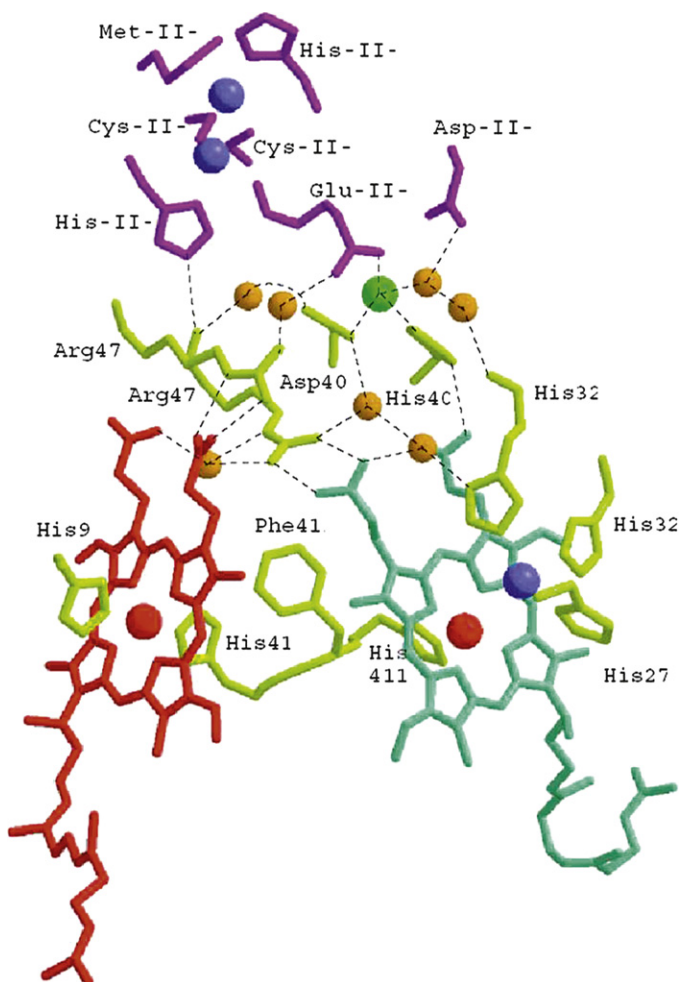


FIGURE 14.12 The metal-binding sites in cytochrome oxidase. Cu is in blue, FeE in red, and Mg in green.

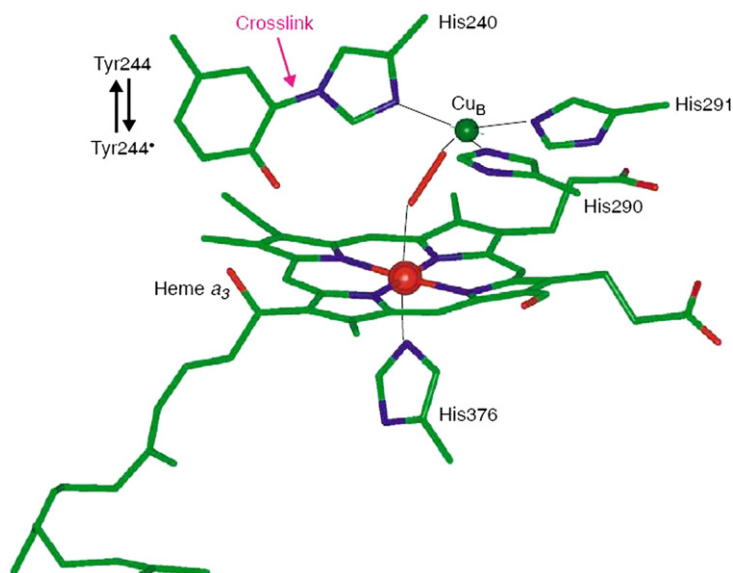
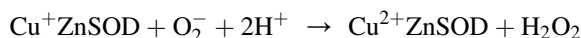
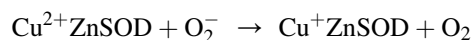
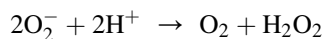


FIGURE 14.13 Crystal structure of the fully oxidised binuclear site in bovine heart CcO at 2.3 Å resolution, showing the His–Tyr crosslink and indicating the putative Tyr. A peroxy species is seen between Fea3 and Cu_B. Adapted from PDB 2OCC using Insight. (From *Rogers & Dooley, 2003*. Copyright 2003, with permission from Elsevier.)

(iv) Superoxide dismutation in health and diseases

Superoxide is generated by a number of enzymes in the course of their reaction cycles, but by far the greatest production of superoxide anion and the reactive oxygen species that can be derived from it is the respiratory chain within the mitochondria. Superoxide dismutases (SODs) lower the levels of superoxide by catalysing the transformation of two superoxide ions into dioxygen and hydrogen peroxide. CuZnSOD is widely distributed, located in the periplasmic space in bacterial cells and in both the cytosol and the mitochondrial intermembrane space in eukaryotic cells. The reaction is a two-step process in which a molecule of superoxide reduces the oxidised (Cu²⁺) form of the enzyme to give dioxygen and the reduced (Cu⁺) enzyme, which subsequently reduces a second molecule of superoxide, giving hydrogen peroxide and restoring the oxidised form of the enzyme:



The human CuZnSOD, SOD1, is a 32-kDa homodimer, each subunit made up (Figure 14.14), as we saw in Chapter 3, of an eight-stranded β-barrel with one Cu and one Zn site, and contains an intra-subunit disulfide. The Cu site is a typical Type 2 site with four His ligands (Figure 14.14) with His44 and His46 in *trans* positions of the distorted square-planar CuN₄ coordination sphere. The tripeptide His44–Val45–His46 completely blocks access to the Cu from one side of the CuN₄ plane, while the other side is solvent accessible via a conical channel some 4 Å wide lined by positively charged residues. The active site channel leading to the copper atom is constructed ideally for small anionic species such as superoxide, allowing nearly diffusion-controlled rates of enzyme catalysis (rate constants $\sim 2 \times 10^9 \text{ M}^{-1} \text{ s}^{-1}$). The Zn ion is also coordinated by one Asp and three His ligands, one of which, His61, bridges the two metal ions – a structural feature that had not been seen previously in coordination geometry. We discuss in greater detail in Chapter 21 mutations in SOD1 associated with amyotrophic lateral sclerosis (ALS) (Potter and Valentine, 2003).

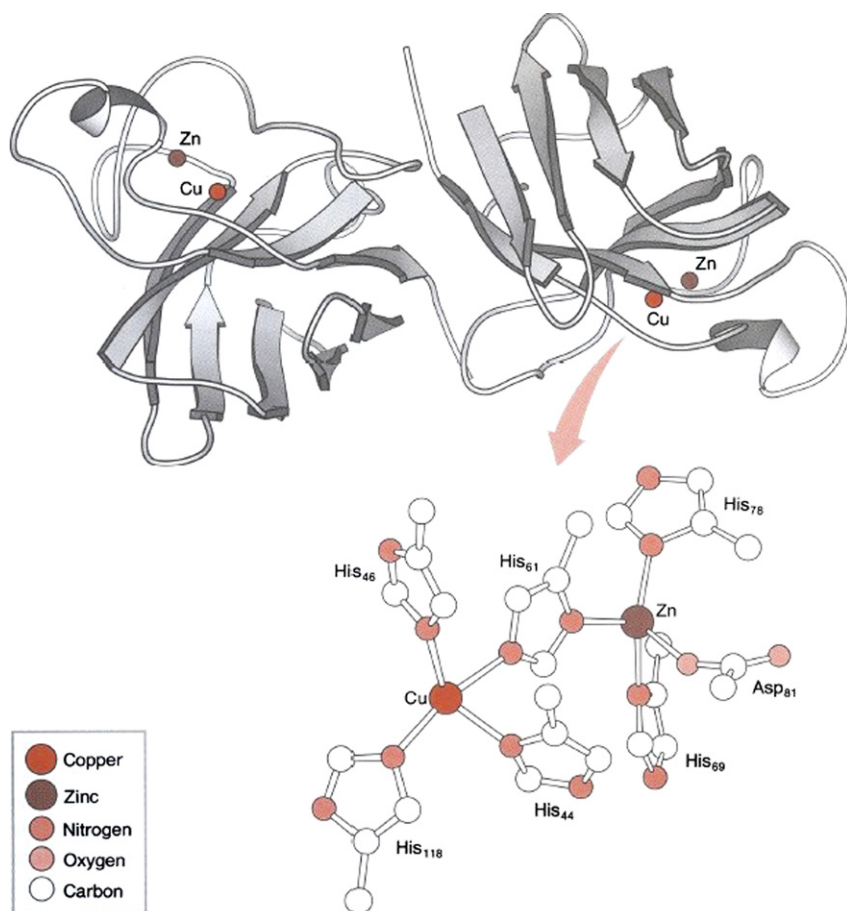


FIGURE 14.14 Human SOD1 showing the disulfide bond in blue in the β -strand which forms the bulk of the dimer interface (in blue) with the Cu and Zn ions as blue and green spheres. In the right monomer, MBr mutations are shown as yellow spheres. (From Hart, 2006. Copyright 2006, with permission from Elsevier.)

Copper enzymes are involved in reactions with a large number of other, mostly inorganic, substrates. In addition to its role in oxygen and superoxide activation described above, copper is also involved in enzymes which activate methane, nitrite, and nitrous oxide.

There are vast reserves of methane gas in the world, which are currently underutilised as a feedstock for the production of liquid fuels and chemicals because of the lack of economical and sustainable strategies for the selective oxidation of methane to methanol. Current processes require high temperatures, are costly and inefficient, and produce waste, yet throughout nature methanotrophic bacteria perform this reaction under ambient conditions using methane monooxygenases (MMOs). We already encountered the soluble di-iron MMO in Chapter 13, expressed by several strains of methanotroph under copper-limited conditions. All methanotrophs produce membrane-bound particulate MMO (pMMO). Yet, in spite of 20 years of research and the availability of two crystal structures, the metal composition and location of the pMMO metal active site were still not known until very recently. In 2010, the structure of particulate methane monooxygenase from the methanotrophic bacteria *M. capsulatus* was determined at a resolution of 2.8 Å (Figure 14.15). It is a trimer with an $\alpha_3\beta_3\gamma_3$ polypeptide arrangement. Two metal centres, modeled as mononuclear and dinuclear copper are located in the soluble part of each β -subunit, which resembles

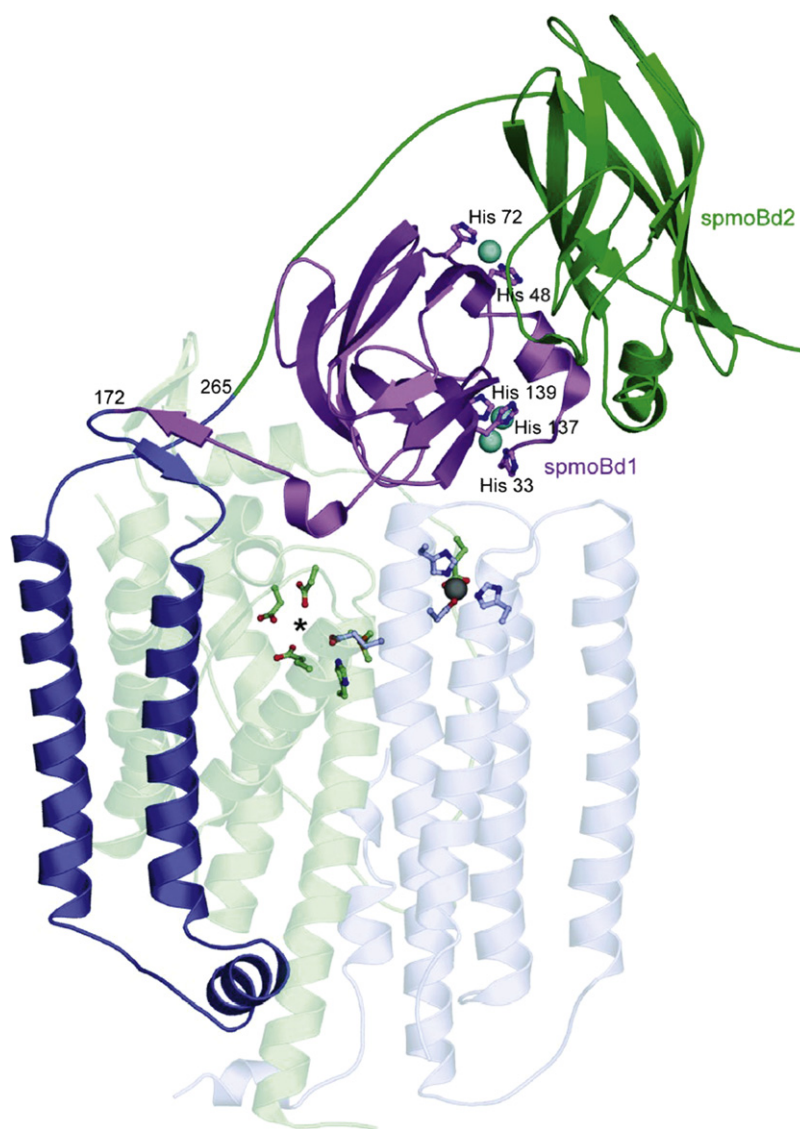


FIGURE 14.15 Structure of *M. capsulatus* (Bath) pMMO protomer (PDB accession code 1YEW). The N-terminal cupredoxin domain of pmoB (spmoBd1) is shown in purple, the C-terminal cupredoxin domain of pmoB (spmoBd2) is shown in green, and the two transmembrane helices are shown in blue. In the recombinant spmoB protein, spmoBd1 and spmoBd2 are connected by a GKLGGG sequence linking residues 172 and 265 instead of the two transmembrane helices. Copper ions are shown as cyan spheres and ligands are shown as ball-and-stick representations. The pmoA (transparent light green) and pmoC (transparent light blue) subunits are composed of transmembrane helices. The location of the zinc ion (grey sphere) has been proposed to house a di-iron centre. A hydrophilic patch of residues marked with an asterisk is the site of a proposed tricopper centre. (From Balasubramanian *et al.*, 2010. Copyright 2010 with permission from Nature.)

cytochrome *c* oxidase subunit II. A third metal centre, occupied by Zn in the crystal, is located within the membrane (Balasubramanian, Smith, Rawat, Yatsunyk, Stemmler, & Rosenzweig, 2010).

While nitrite reductases in many bacteria are haem proteins, some are copper-containing homotrimers which bind three type I and three type II copper centres. The type 1 copper centre serves to transfer electrons from donor proteins to the type 2 centre which has been proposed to be the site of substrate binding.

Nitrous oxide reductases, which catalyse the final step in the denitrification⁴ process, reducing N_2O to N_2 are particularly interesting. Organisms which carry out denitrification use oxidised forms of nitrogen instead of oxygen as the terminal electron acceptors for anaerobic respiration, which is coupled, via proton pumping, to ATP synthesis. N_2O reductase is also of environmental interest, since not only is N_2O the third most important greenhouse gas (after CO_2 and CH_4), it is a potentially attractive oxo-transfer reagent to oxidise organic substrates in a green reaction where the only by-product is N_2 . Nitrous oxide reductase contains two copper sites designated Cu_A and Cu_Z . The Cu_A site is the well-characterised mixed-valence dinuclear electron transfer site with two coppers bridged by two Cys ligands which we already encountered in cytochrome oxidase (and which is also found in NO reductase). The structure of the Cu_Z proved to be quite unusual, namely a μ_4 -sulfide bridged tetranuclear copper cluster (Figure 14.16). The Cu_Z centre is located in the N-terminal domain of the dimeric

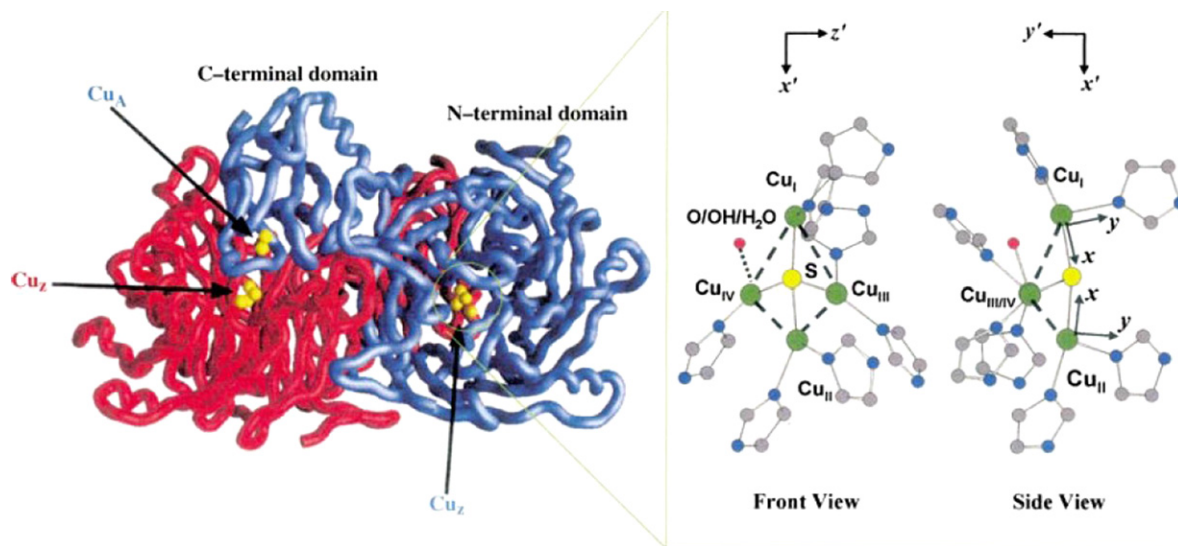


FIGURE 14.16 Structure of the subunits of the homodimer nitrous oxide reductase (red and blue) and of the Cu_Z site. (From Chen, Gorelsky, Ghosh, & Solomon, 2004. Copyright 2004 with permission from Nature publishing.)

enzyme whereas the Cu_A centre is located in the C-terminal domain of each subunit. Thus, in the dimeric protein structure the neighboring Cu_A and Cu_Z sites are contributed by different subunits. While the $[\text{Cu}_4\text{S}]$ cluster has approximate two-fold symmetry, with very similar $\text{Cu}-\text{S}$ bond lengths, the $\text{Cu}-\text{Cu}$ distances are very different with three copper centres, designated as Cu_II , Cu_III , and Cu_IV , closer to one another, with Cu_I further away. The entire $[\text{Cu}_4\text{S}]$ cluster is coordinated by seven His ligands to the protein, with an additional as-yet unidentified oxygen ligand at the $\text{Cu}_\text{I}/\text{Cu}_\text{IV}$ edge. This $\text{Cu}_\text{I}/\text{Cu}_\text{IV}$ edge is thought to be the substrate-binding site. The catalytically relevant form of the Cu_Z is the fully reduced state with Cu^I at each of the four coppers. In the proposed mechanism (Figure 14.17), the reduction of N_2O to N_2 is assumed to involve binding of the N_2O substrate at the $\text{Cu}_\text{I}/\text{Cu}_\text{IV}$ edge where it could interact with Cu_I and Cu_IV in a bridged binding mode. Simultaneous donation of electrons from Cu_I and Cu_IV would allow the two-electron reduction of N_2O . Good electron transfer pathways exist from the neighboring Cu_A centre in the second subunit of the dimeric protein to Cu_II and Cu_IV to allow rapid re-reduction of the Cu_Z centre.

4. In denitrification, part of the biological nitrogen cycle, nitrate in the soil is converted stepwise via four enzymatic reactions to nitrite, nitric oxide, and nitrous oxide to finally yield gaseous nitrogen (see Chapter 18).

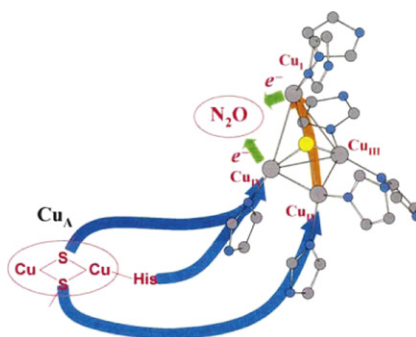


FIGURE 14.17 Reduction of N_2O at the Cu_Z site. (From *Chen et al.*, 2004. Copyright 2004 with permission from Nature publishing.)

MARS AND VENUS – THE ROLE OF COPPER IN IRON METABOLISM

Very early studies established that copper deficiency is associated with anemia in a number of animals. However, the key to understanding the interaction between copper and iron came from the observations that in yeast, mutations affecting copper metabolism blocked the high affinity iron uptake system. Whether the mutations were in the plasma membrane copper transporters or in the copper chaperone P-type ATPase Atx1, which inserts iron into the Fet3 oxidase, the outcome was the same, and for the same reason — a multicopper oxidase is required for high affinity iron uptake into yeast. It then came as no surprise to find that in the rare human neurological disease aceruloplasminaemia, iron accumulated in brain and liver, indicative that Chapter 7) a key role of ceruloplasmin was in tissue iron mobilisation. This was convincingly shown by studies in which the yeast Fet3 oxidase was shown to restore iron homeostasis in aceruloplasminemic mice (*Harris et al.*, 2004). The likely mechanism is shown in *Figure 14.18*, in which the export of iron via the Fe^{2+} transporter ferroportin is thought to require the ferroxidase activity of ceruloplasmin to ensure its incorporation into apotransferrin. For further details see *Crichton & Pierre*, 2001; *Crichton & Ward*, 2006; *Crichton*, 2009; *Hellman & Gitlin*, 2002.

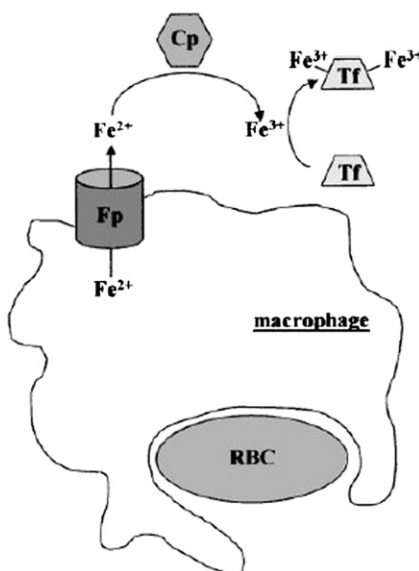


FIGURE 14.18 Representation of the role of ceruloplasmin in mobilising iron from reticuloendothelial cells. (From *Hellman & Gitlin*, 2002. Copyright 2002 with permission from Annual Reviews.)

REFERENCES

- Balasubramanian, R., Smith, S. M., Rawat, S., Yatsunyk, L. A., Stemmler, T. L., & Rosenzweig, A. C. (2010). Oxidation of methane by a biological dicopper centre. *Nature*, *465*, 115–119.
- Brunori, M., Giuffrè, A., & Sarti, P. (2005). Cytochrome *c* oxidase, ligands and electrons. *Journal of Inorganic Biochemistry*, *99*, 324–336.
- Chen, P., Gorelsky, S. I., Ghosh, S., & Solomon, E. I. (2004). N₂O reduction by the μ_4 -sulfide-bridged tetranuclear Cu₄ cluster active site. *Angewandte Chemie International Edition*, *43*, 4132–4140.
- Crichton, R. R. (2001). *Inorganic biochemistry of iron metabolism: From molecular mechanisms to clinical consequences*. Chichester: John Wiley and Sons. pp. 326.
- Crichton, R. R., & Pierre, J.-L. (2001). Old iron, young copper: from Mars to Venus. *BioMetals*, *14*, 99–112.
- Crichton, R. R., & Ward, R. J. (2006). *Metal-based neurodegeneration from molecular mechanisms to therapeutic strategies*. Chichester: John Wiley and Sons. p. 227.
- Decker, H. (2006). A first crystal structure of tyrosinase: all questions answered? *Angewandte Chemie International Edition*, *45*, 4546–4550.
- Decker, H., Schweikardt, T., Nillius, D., Salzbrunn, U., Jaenicke, E., & Tuczek, F. (2007). *Gene*, *398*, 183–191.
- Granata, A., Monzani, E., & Casella, L. (2004). Mechanistic insight into the catechol oxidase activity by a biomimetic dinuclear copper complex. *Journal of Biological Inorganic Chemistry*, *9*, 189–196.
- Hart, P. J. (2006). Pathogenic superoxide dismutase structure, folding, aggregation and turnover. *Current Opinion in Chemical Biology*, *10*, 131–138.
- Harris, Z. L., Davis-Kaplan, S. R., Gitlin, J. D., & Kaplan, J. (2004). A fungal multicopper oxidase restores iron homeostasis in aceruloplasminemia. *Blood*, *103*, 4672–4673.
- Hatcher, L. Q., & Karlin, K. D. (2004). Oxidant types in copper-dioxygen chemistry: the ligand coordination defines the Cu_n-O₂ structure and subsequent reactivity. *Journal of Biological Inorganic Chemistry*, *9*, 669–683.
- Hellman, N. E., & Gitlin, J. D. (2002). Ceruloplasmin metabolism and function. *Annual Review of Nutrition*, *22*, 439–458.
- Himes, R. A., & Karlin, K. D. (2009). Copper-dioxygen complex mediated C–H bond oxygenation: relevance for particulate methane monooxygenase (pMMO). *Current Opinion in Chemical Biology*, *13*, 119–131.
- Klinman, J. P. (2006). The copper-enzyme family of dopamine beta-monooxygenase and peptidylglycine alpha-hydroxylating monooxygenase: resolving the chemical pathway for substrate hydroxylation. *Journal of Biological Chemistry*, *281*, 3013–3016.
- Malkin, R., & Malmström, B. G. (1970). The state and function of copper in biological systems. *Advances in Enzymology and Related Areas of Molecular Biology*, *33*, 177–244.
- Messerschmidt, A., Huber, R., Poulos, T. & Weighardt, K. (Eds.). (2001). *Handbook of metalloproteins* (p. 227). Chichester: John Wiley and Sons.
- Potter, S. Z., & Valentine, J. S. (2003). The perplexing role of copper-zinc superoxide dismutase in amyotrophic lateral sclerosis (Lou Gehrig's disease). *Journal of Biological Inorganic Chemistry*, *8*, 373–380.
- Riva, S. (2006). Laccases: blue enzymes for green chemistry. *TIBS*, *24*, 219–226.
- Rodgers, C. J., Blanford, C. F., Giddens, S. R., Skamnioto, P., Armstrong, F. A., & Gurr, S. J. (2009). Designer laccases: a vogue for highpotential fungal enzymes? *Trends in Biotechnology*, *28*, 63–72.
- Rogers, M. S., & Dooley, D. M. (2003). Copper-tyrosyl enzymes. *Current Opinion in Structural Biology*, *7*, 131–138.
- Rosenzweig, A. C., & Sazinsky, M. H. (2006). Structural insights into dioxygen-activating copper enzymes. *Current Opinion in Structural Biology*, *16*, 729–735.
- Solomon, E. I. (2006). Spectroscopic methods in bioinorganic chemistry: blue to red to green copper sites. *Inorganic Chemistry*, *45*, 8012–8025.
- Vallee, B. L., & Williams, R. J. (1968). Metalloenzymes: the entatic nature of their active sites. *Proceedings of the National Academy of Sciences of the United States of America*, *59*, 498–505.

Nickel and Cobalt: Evolutionary Relics

Introduction	297
Nickel Enzymes	297
Methyl-coenzyme M Reductase	302
Cobalamine and Cobalt Proteins	303
B ₁₂ -dependent Isomerases	303
B ₁₂ -dependent Methyltransferases	306
Noncorrin Co-containing Enzymes	308

INTRODUCTION

When one examines the kinds of reactions catalysed by nickel and cobalt enzymes and their evolutionary distribution, one arrives at the conclusion that these two elements were particularly important in the metabolism of chemicals particularly abundant in the pre-oxygen evolutionary era, like methane, carbon monoxide, and hydrogen. This is reflected in the high levels of both elements in a number of anaerobic bacteria. In contrast, the level of both metals in mammalian serum is less than 100-fold that of zinc, iron, or copper. Nonetheless, cobalt, through its involvement in a number of important vitamin B₁₂-dependent enzymes continued to be used in higher organisms, including mammals. In contrast, with the exception of the plant enzyme urease, nickel proteins are virtually unknown in higher eukaryotes.

Both nickel and cobalt, together with iron, have the characteristic that they are electron rich. Furthermore, in lower oxidation states some of their 3d electrons are forced into exposed σ -(or π -) orbitals: the outcome is that tetragonal Co(II) or Ni(III) are reactive free radicals, able to give or take a single electron, in the same way as σ -organic free radicals. So, cobalt functions in free-radical reactions, such as the transformation of ribonucleotides into their corresponding deoxy derivatives, just like iron. The participation of cobalt or nickel in acid–base chemistry could easily be replaced by zinc, while any redox functions in a post-oxygen world could readily be substituted by iron, copper, or manganese, all of which were much more bioavailable. So nickel, in particular, but also cobalt became the lost leaders of the post-photosynthetic supermarket shelf of bio-metals.

We begin by considering nickel enzymes, and then move on to cobalt, concentrating on enzymes with cobalamine cofactors, including also some noncorrin cobalt enzymes. For reviews, see Bannerjee and Ragsdale, 2003; Brown, 2005; Hegg, 2004; Kobayashi and Shimizu, 1999; Mulrooney and Hausinger, 2003; Ragsdale, 1998, 2004, 2006, 2009.

NICKEL ENZYMES

Seven of the eight known Ni enzymes (Table 15.1) are involved in the use and/or production of gases (CO, CO₂, CH₄, H₂, NH₃, and O₂) which all play important roles in the global cycles of carbon, nitrogen, and oxygen (Ragsdale, 2007, 2009) (Chapter 18). Urease, the first Ni enzyme to be discovered, produces NH₃, acireductone dioxxygenase (ARD) produces CO, SOD generates O₂ from superoxide, hydrogenase rather generates or utilises

TABLE 15.1

Nickel-containing enzymes

Enzyme	Reaction
Glx I (EC 4.4.1.5)	Methylglyoxal \rightarrow lactate + H_2O (Reaction 1)
ARD (EC 1.13.11.54)	1,2-Dihydroxy-3-oxo-5-(methylthio)pent-1-ene + $\text{O}_2 \rightarrow \text{HCOOH}$ + methylthiopropionate + CO (Reaction 2)
Ni-SOD (EC 1.15.1.1)	$2\text{H}^+ + 2\text{O}_2^- \rightarrow \text{H}_2\text{O}_2 + \text{O}_2$ (Reaction 3)
Urease (EC 3.5.1.5)	$\text{H}_2\text{N-CO-NH}_2 + 2\text{H}_2\text{O} \rightarrow 2\text{NH}_3 + \text{H}_2\text{CO}_3$ (Reaction 4)
Hydrogenase (EC 1.12.X.X)	$2\text{H}^+ + 2\text{e}^- \rightleftharpoons \text{H}_2$ ($\Delta E^\circ = -414$ mV) (Reaction 5)
MCR (EC 2.8.4.1)	$\text{CH}_3\text{-CoM} + \text{CoBSH} \rightarrow \text{CH}_4 + \text{CoM-SS-CoB}$ (Reaction 6)
CODH (EC 1.2.99.2)	$2\text{e}^- + 2\text{H}^+ + \text{CO}_2 \rightleftharpoons \text{CO} + \text{H}_2\text{O}$ ($E^\circ = -558$ mV) (Reaction 7)
ACS (EC 2.3.1.169)	$\text{CH}_3\text{-CFeSP} + \text{CoASH} + \text{CO} \rightarrow \text{CH}_3\text{-CO-SCoA} + \text{CFeSP}$ (Reaction 8)

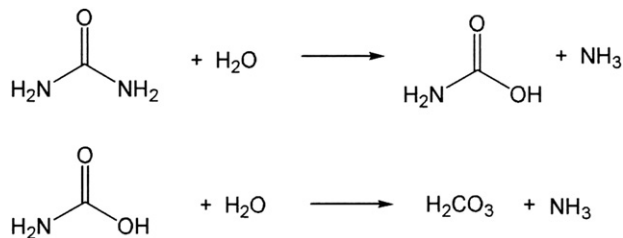
H_2 , CO dehydrogenase (CODH) interconverts CO and CO_2 , acetyl-CoA synthetase (ACS) in concert with CODH converts CO_2 and a methyl group to acetyl-CoA and methyl-CoM reductase (MCR) generates methane.

The remaining Ni enzyme, glyoxylase (GlxI), catalyses the conversion of toxic methylglyoxal, (it can readily form covalent adducts with DNA) to lactate. Its single octahedrally coordinated Ni^{2+} acts as a Lewis acid, without changing valency, which presumably explains why it can be replaced by Zn^{2+} , for example, in man.

Ni sites in enzymes show considerable adaptability, both in terms of Ni coordination and redox chemistry. The Ni centre in SOD must be able to span redox potentials from +890 to -160 mV, whereas in MCR and CODH, it must be able to reach potentials as low as -600 mV. This implies that Ni centres in proteins can carry out redox chemistry over a potential range of ~ 1.5 V. The low levels of available Ni in natural environments has necessitated the development of high-affinity Ni uptake systems, together with metallochaperones and regulators of Ni homeostasis.

(i) Urease

Historically, the earliest Ni-containing enzyme to be described was urease from jack bean meal, which was crystallised by James Sumner in 1926.¹ However, analytical techniques did not allow urease to be recognised as a Ni-containing enzyme until 50 years later. Urease catalyses the hydrolysis of urea to ammonia and carbamate, which spontaneously hydrolyses to give carbonic acid and a second molecule of ammonia. It plays a key role in nitrogen metabolism in plants and microbes whereas land-dwelling animals excrete urea



as the end product of their nitrogen metabolism; clearly, they do not have urease. The active site (Figure 15.1) contains two Ni ions, ~ 3.5 Å apart which are bridged by a carbamylated lysine residue. Both Ni ions are coordinated by two His nitrogen atoms, an oxygen from the bridging carbamyl group, and an oxygen from bound water. One of the Ni atoms in addition has an oxygen ligand from an Asp residue. CO_2 is required for formation of the carbamylated Lys bridge between the two Ni atoms, and mutation of this Lys results in loss of activity. The

1. James Sumner received the Nobel prize for chemistry in 1946 for the crystallisation of proteins. Richard Willstätter, the 1915 chemistry prizewinner, had proposed that proteins were not enzymes, and that the protein in urease was simply a scaffold for the veritable catalyst. Since urease is inactive without Ni, he was not so far wrong!



FIGURE 15.1 The dinuclear Ni active site of urease. Ni atoms are shown in green, metal-bound water as red spheres; the carbamylated Lys is K217*. (From Mulrooney & Hausinger, 2003. Copyright 2003 with permission from Elsevier.)

large kinetic barrier to urea hydrolysis is presumed to be lowered by (i) coordination of the carbonyl group of urea to Ni 1, making the carbonyl more electrophilic, (ii) binding of water to Ni 2 to generate an activated hydroxyl species, and (iii) hydrogen bonding interactions of all four of the protons of urea with electrophilic groups of the protein. Attack of the metal-activated hydroxyl would generate a tetrahedral intermediate. Protonation of this intermediate would eliminate ammonia, leaving carbamate bridged between the two Ni atoms. Dissociation of carbamate from the dimetallic site would be followed by spontaneous hydrolysis to carbonate and a second molecule of ammonia, with a protonated His residue acting as a general acid to promote ammonia release.

(ii) Ni–Fe–S proteins

Three of the eight Ni enzymes, hydrogenase, CO dehydrogenase (CODH), and acetyl-CoA synthase (ACS), are Ni–Fe–S proteins. Hydrogenases play an important role in microbial energy metabolism by catalysing the reversible oxidation of hydrogen:



In some anaerobic microorganisms, production of hydrogen serves as a mechanism to get rid of excess reducing potential, while in many others hydrogen consumption is coupled to the reduction of carbon dioxide, oxygen, sulfate, or other electron acceptors and at the same time used to generate a proton gradient for use in ATP production. Three kinds of hydrogenases have been described, namely, the [NiFe] hydrogenases, [FeFe] hydrogenases, and iron hydrogenases. Under conditions of nickel limitation, some methanogens synthesise a nickel-independent [Fe]-hydrogenase, thereby reducing their nickel requirement. The [Fe]-hydrogenase has a unique iron–guanylylpyridinol cofactor (FeGP cofactor), in which a low-spin iron is ligated by two CO, one COCH_2- , one $\text{S}-\text{CH}_2-$, and a sp(2)-hybridised pyridinol nitrogen (Thauer, Kaster, Goenrich, Schick, Hiromoto, & Shima, 2010). The formation of methane from 4H_2 and CO_2 catalysed by methanogenic archaea could represent an efficient way to store H_2 .

The [NiFe] hydrogenases are characterised by a quite unusual Ni–Fe active site (Figure 15.2). It required a combination of spectroscopic and crystallographic studies to identify the three non-protein diatomic ligands to the Fe as one CO and two CN^- molecules, which are thought to maintain iron in its low-spin ferrous state. In *D. norvegicum* one of the Ni ligands is a selenocysteine (Figure 15.2), whereas in most other Ni–Fe hydrogenases, the four protein ligands to the Ni atoms are all Cys residues. Two of them are bridging ligands to the iron atom. (Figure 15.2). The NiFe hydrogenase seems to require activation, involving prolonged treatment with H_2 to generate the $\text{Ni}_a\text{-C}^*$ state. This may involve replacement of an OH^- ligand with a hydride bridge (in red) between the nickel and iron sites (Figure 15.2), and heterolytic H–H bond cleavage. Catalysis ensues upon conversion of $\text{Ni}_a\text{-C}^*$ to a Ni(I) oxidation state ($\text{Ni}_a\text{-R}^*$) by a hydride transfer or proton-coupled electron transfer reaction, allowing productive binding of H_2 . H–H bond cleavage during the catalytic cycle is proposed to occur by an oxidative addition mechanism that would generate the

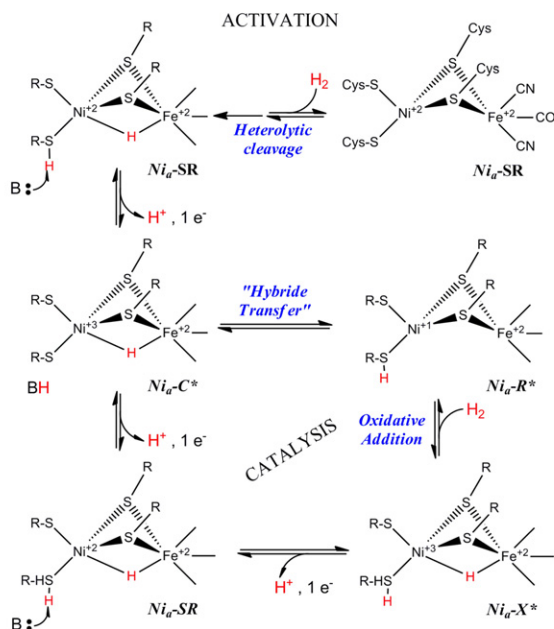
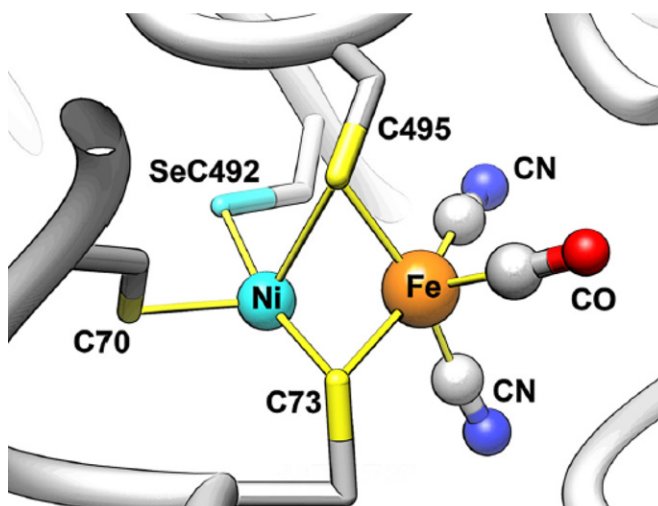


FIGURE 15.2 Structure of the NiFe active site and mechanism of hydrogenase. The structure is based on PDB code ICC1, while the mechanism of hydrogenase activation and catalysis is based on the work of Lill and Siegbahn (2009). The asterisks indicate an EPR-active state. (Adapted from Ragsdale, 2009.)

$\text{Ni}_a\text{-X}^*$ intermediate, which undergoes two successive proton-coupled electron transfer steps to regenerate $\text{Ni}_a\text{-C}^*$ (Lill and Siegbahn, 2009). The Ni–Fe hydrogenases also contain multiple Fe–S clusters which channel electrons to the catalytic site.

‘Conceptually, the simplest way to synthesize an organic molecule is to construct it one carbon at a time’ (Ragsdale and Pierce, 2008). The Woods–Ljungdahl pathway (Figure 15.3) does just that, synthesising acetyl-CoA from CO_2 . Carbon monoxide dehydrogenase, CODH and acetyl-CoA synthase, ACS are responsible for the reduction of CO_2 to CO and the subsequent formation of acetyl-CoA (Drennan et al., 2004). CODH/ACS

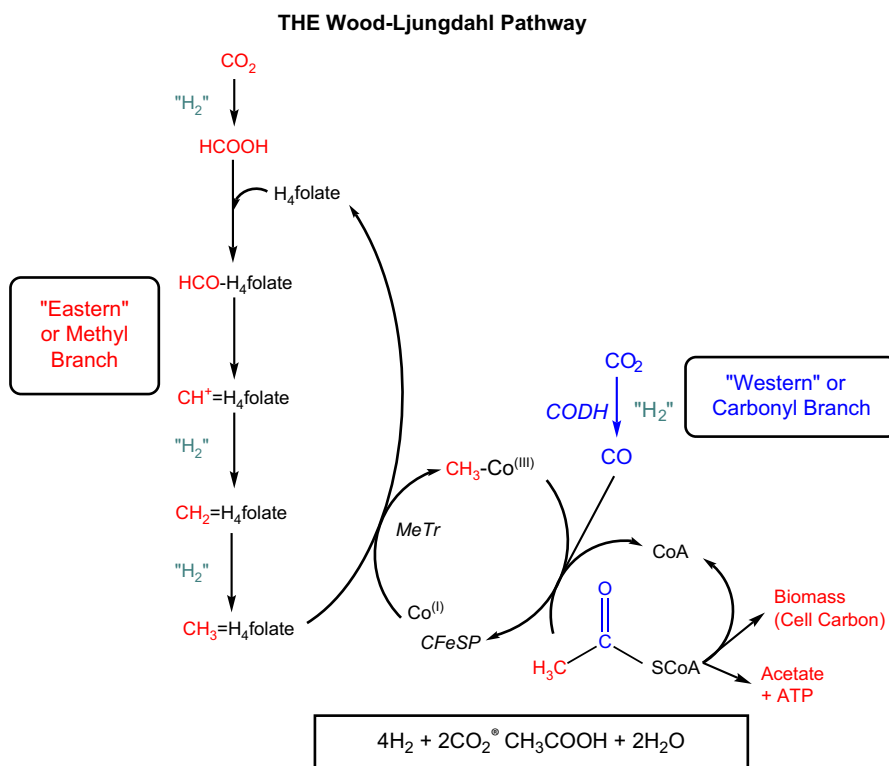


FIGURE 15.3 The Wood–Ljungdahl pathway. “ H_2 ” is used in a general sense to designate the requirement for two electrons and two protons in the reaction. (From Ragsdale & Pierce, 2008. Copyright 2008 with permission from Elsevier.)

are both thought to be ancient enzymes, which possibly allowed primitive organisms to live in the anaerobic, CO_2 -rich atmosphere. In this pathway, carbon dioxide is reduced to carbon monoxide by CODH , which is then converted to acetyl coenzyme A by ACS , using a methyl group which is itself derived from CO_2 . The methyl group is then transferred from methyltetrahydrofolate by a methyltransferase (MeTr) to a corrinoid iron–sulfur protein (CFeSP), which in turn transfers the methyl group to the A-cluster of ACS .

Microorganisms which contain CODH/ACS enzymes are found in all locations where anaerobic metabolism is the only means of survival, from peat bogs to the rumen of the cow, to the human intestine.² The so-called C-cluster of CODHs allow organisms to use CO as a source of energy and carbon, while other acetogenic and methanogenic bacteria use bifunctional CODH/ACS enzymes to convert the greenhouse gas CO_2 to acetyl-CoA. Collectively, CODH/ACS enzymes play a key role in the C1 metabolism of anaerobic organisms and represent a major component of the global carbon cycle.

CODHs catalyse the oxidation of carbon monoxide in a reversible, two-electron process. They are homodimeric enzymes with five metal clusters, two C-clusters which catalyse the oxidation of CO to CO_2 and three typical $[\text{Fe}_4\text{S}_4]$ cubane clusters (Figure 15.4). In *R. rubrum*, electrons are transferred from the D-cluster to a membrane-associated Fe–S protein designated CooF , which transfers electrons to a hydrogenase, coupling CO oxidation with H_2 production.

2. Where it is supplied by the microbial ‘guest workers’ who profit from our prolific source of food, and, in return, perhaps inadvertently, return the hospitality with a few vitamins and other essential nutrients that we are unable to make.

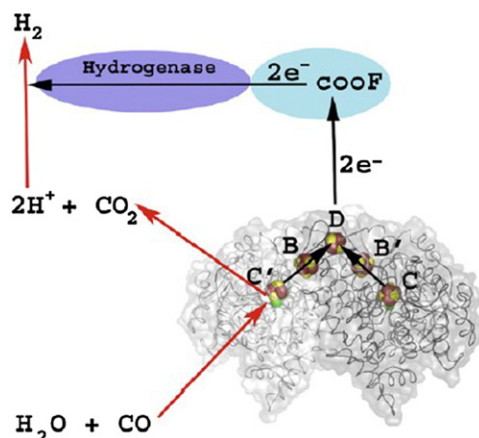


FIGURE 15.4 The coupling of CODH activity with hydrogenase activity in *R. rubrum*. The two subunits of CPDH are shown with light and dark wire tracings. Electrons generated by the oxidation of CO at the C and C' clusters are transferred to the internal redox chain in CODH, consisting of B (and B') and D Fe-S clusters. The D-cluster, located at the interface between the two subunits, is proposed to transfer electrons to the electron transfer protein (Coof), which is coupled to hydrogenase. (From Ragsdale & Pierce, 2008. Copyright 2008 with permission from Elsevier.)

The C-cluster of CODH reduces CO_2 to CO, which is then converted by the A-cluster of the ACS to acetyl-CoA (Figure 15.3). The C-cluster is an unusual Fe-Ni-Fe $_3\text{S}_4$ -5, which can be best viewed as a [Fe $_3\text{S}_4$] cluster bridged to a dinuclear Ni-Fe centre (Figure 15.5). The catalytic efficacy of the C-cluster from *C. hydrogenoformans* is remarkable — for the oxidation of CO the turnover number is $39,000 \text{ s}^{-1}$ and the k_{cat}/K_m greater than $10^9 \text{ M}^{-1} \text{ s}^{-1}$.

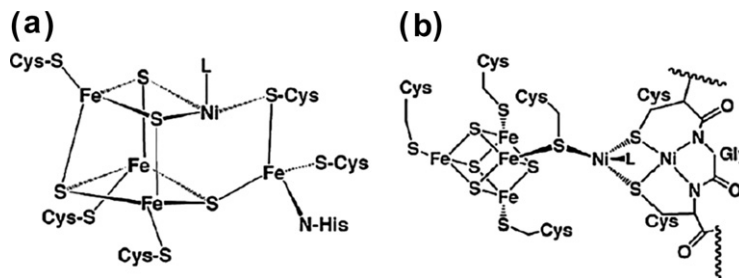


FIGURE 15.5 The C-cluster of CODH and the A-cluster of ACS. (From Ragsdale, 2007. Copyright 2007 with permission from Elsevier.)

The active site A-cluster of the ACS is unusual in that it consists of a [4Fe-4S] cubane unit linked via a bridging cysteine residue to a proximal metal ion which, in turn, is connected to a square-planar distal Ni via two cysteine bridges as shown in Figure 15.5. The identity of the catalytically active metal ion in the proximal site has been the subject of some debate, but it now seems to be agreed that the catalytically active form of the enzyme has Ni in this site (Svetlitchnyi et al., 2004). Cluster-A binds both CO, the methyl group from CoFeSP and CoA. Two mechanisms of acetyl-CoA synthesis at cluster-A have been proposed. In the mononuclear mechanism, both CO and the methyl group bind at the proximal Ni, generating an acetyl group; subsequent attack of the carbonyl carbon by deprotonated CoA-S $^-$ then gives acetyl-CoA. In the binuclear mechanism, CO binds at the proximal Ni and the methyl group at the distal Ni.

METHYL-COENZYME M REDUCTASE

It is estimated that more than 10^9 tons of methane per year are generated by methanogenic archaeobacteria functioning in anaerobic environments, all of which is derived from the catalytic activity of MCR (Shima et al.,

2002; Thauer et al., 2008). MCR converts methyl-CoM (methyl-SCoM) and N⁷-mercaptoheptanoylthreonine phosphate (CoBSH) to methane and the CoB-SS-CoM heterodisulfide (Table 15.1, Reaction 6), with a turnover number of $\sim 100 \text{ s}^{-1}$ and a k_{cat}/K_m (methyl-SCoM) of $\sim 1 \times 10^5 \text{ m}^{-1} \text{ s}^{-1}$. The structure of the enzyme from *M. thermoautotrophicum* has been determined at high resolution in two states with substrate bound. Ni is present in the enzyme in a corrinoid cofactor designated F₄₃₀ on account of its absorption maximum at 430 nm (Figure 15.6). The enzyme is a heterotrimer with two active sites, each with a Ni-containing tetrapyrrole. The cofactor F₄₃₀, which is active in the Ni(I) state, is non-covalently, but tightly bound, deeply buried in the protein, but connected to the surface by a 30 Å long channel through which the substrates enter. The reaction involves the substrates, methyl-S-coenzyme M (CH₃-S-CoM) and N-7-mercaptoheptanoylthreonine phosphate, or coenzyme B (CoB-SH), which are converted into methane and the heterodisulfide CoB-S-S-CoM. Two mechanisms have been proposed, one involving an organometallic methyl-Ni intermediate and the other a methyl radical (Figure 15.6).

COBALAMINE AND COBALT PROTEINS

Vitamin B₁₂, identified as the antipernicious anemia factor in 1925, is a tetrapyrrole cofactor in which the central hexacoordinate cobalt atom is coordinated by four equatorial nitrogen ligands donated by the pyrroles of the corrin ring (Figure 15.7). The fifth Co ligand is a nitrogen atom from a 5,6-dimethylbenzimidazole nucleotide (Dmb) covalently linked to the corrin D ring. The sixth ligand in vitamin B₁₂ is —CN. In the coenzyme B₁₂ (AdoCbl) this ligand is 5'-deoxyadenosine, while in the other biologically active alkylcobalamine (MeCbl), it is a methyl group. This sixth ligand is unusual in that it forms a C—Co bond — carbon—metal bonds are rare in biology. The free cofactor can exist in the base-on or base-off conformations (Figure 15.8), with the Dmb-on form predominant at physiological pH. In some B₁₂-dependent enzymes, an active site His residue replaces the dimethylbenzimidazole (the so-called His-on form). In the corrinoid iron—sulfur protein (CFeSP involved in the CODH/ACS system described earlier), the cofactor is in the Dmb-off conformation and a protein ligand does not appear to occupy the lower axial position. The reactive C—Co bond participates in all three classes of enzymes which use cobalamine cofactors, namely the adenosylcobalamine-dependent isomerases, the methylcobalamine-dependent methyl-transferases and the reductive dehalogenases. We will discuss the first two classes in greater detail here in addition to a number of noncorrin-cobalt-containing enzymes.

B₁₂-DEPENDENT ISOMERASES

Isomerases are the largest subfamily of B₁₂-dependent enzymes found in bacteria, which play important roles in fermentation pathways. The only exception is methylmalonyl-CoA mutase, an enzyme required for the metabolism of propionyl-CoA in man as well as in bacteria. The general reaction mechanism (Figure 15.9) for AdoCbl-dependent isomerases involves homolytic formation of a 5'-deoxyadenosyl radical (step 1) followed by H abstraction to generate a substrate radical (step 2). Once the substrate radical has been formed, it can undergo 1,2 rearrangement (step 3) to generate the product radical. Hydrogen abstraction will then result in the product and the 5'-deoxyadenosyl radical (step 4), which can revert to the initial B₁₂ coenzyme (step 5). As pointed out in Chapter 13, some microorganisms, such as *Lactobacillii*, have B₁₂-dependent Class II ribonucleotide reductases, where a thiyl radical is generated rather than a substrate radical by the deoxyadenosyl radical. The thiyl radical is common to both the diiron-tyrosyl radical-dependent and the B₁₂-dependent ribonucleotide reductases, and is responsible in turn for generating the substrate radical. It is interesting to point out that unlike the other B₁₂-dependent isomerases, the B₁₂-dependent Class II ribonucleotide reductase has a different fold for binding B₁₂, which is similar to the corresponding structural elements used in the Class I diiron-tyrosyl ribonucleotide reductases.

The Co—carbon bond in AdoCbl is stable in water, but is inherently labile, with a bond dissociation energy of around 30–35 kcal mol^{−1}. This instability is exploited by the AdoCbl-dependent isomerases to effect radical-based rearrangements which, as pointed out above, are initiated by homolytic cleavage of the Co-carbon bond. In the absence of substrate, the homolysis products are not observed, yet in their presence the homolytic cleavage

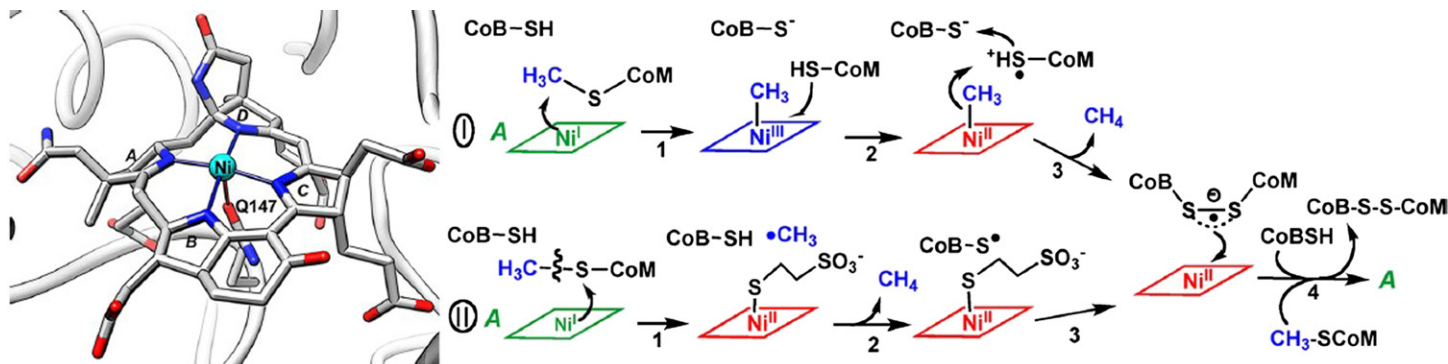


FIGURE 15.6 Structure of P₄₃₀ at the MCR active site and mechanism of methane formation. The structure was derived from PDB code 1HBN. The bound CoM was omitted from the structure to focus on the tetrapyrrole. (From *Ragsdale, 2009*. Copyright 2009 with permission from Elsevier.)

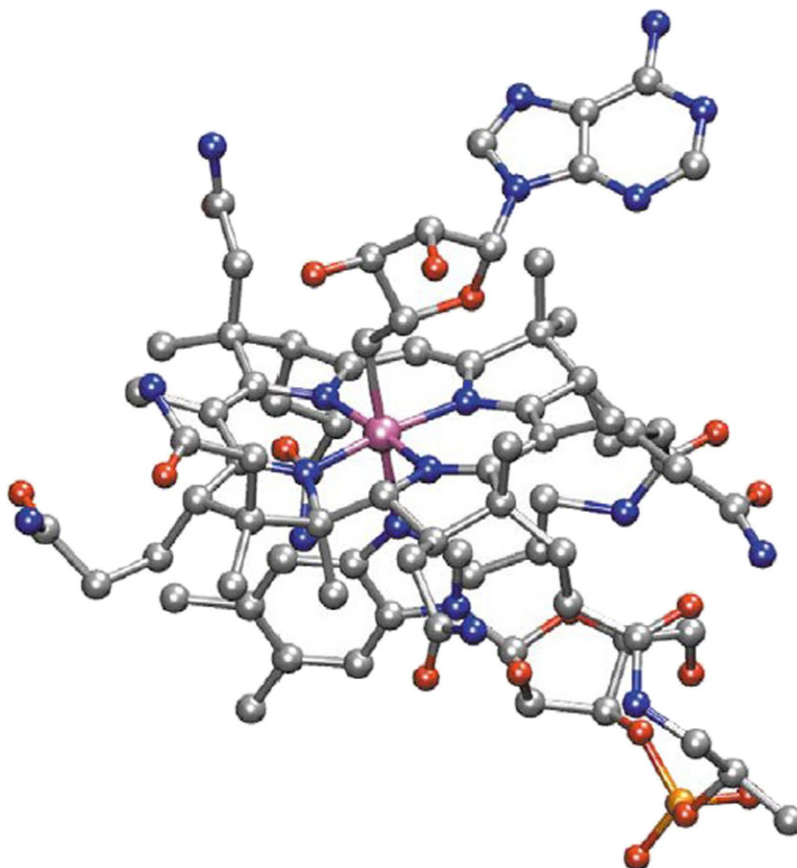


FIGURE 15.7 Ball and stick representation of adenosylcobalamin. (From Reed, 2004. Copyright 2004 with permission from Elsevier.)

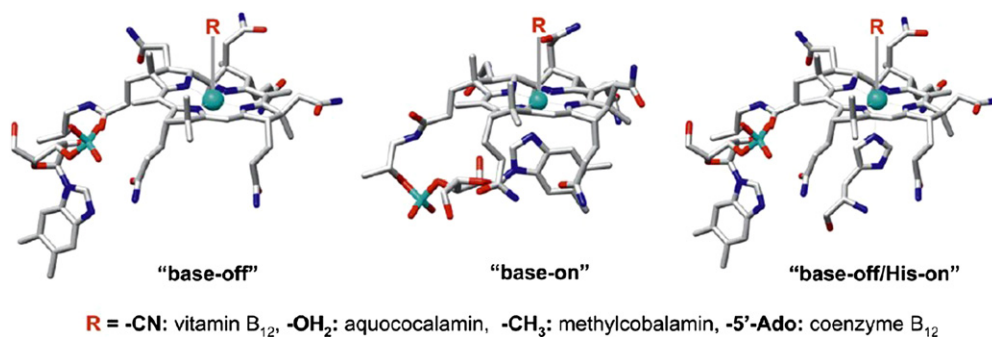


FIGURE 15.8 Structures of cobalamin derivatives and the various ligation states. (From Banerjee, Gherasim, & Padovani, 2009. Copyright 2009 with permission from Elsevier.)

rate is considerably accelerated. It is proposed that the homolysis equilibrium favours recombination, whereas in the presence of substrate, the high-energy **dAdo·** abstracts a hydrogen atom from the substrate to generate a more stable substrate-centred radical intermediate. This has the net effect of shifting the overall homolysis equilibrium from recombination to radical propagation.

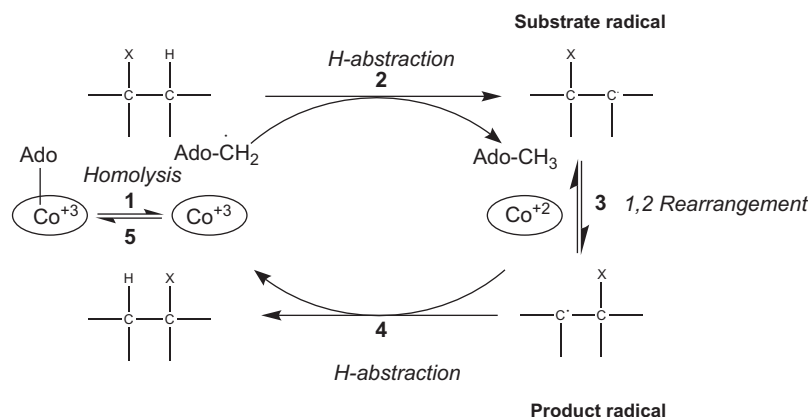


FIGURE 15.9 General reaction mechanism for AdoCbl-dependent isomerases. (From *Banerjee & Ragsdale, 2003*. Reprinted with permission from *Annual Reviews*.)

B₁₂-DEPENDENT METHYLTRANSFERASES

B₁₂-dependent methyltransferases are involved in C1 metabolism and, as we saw earlier, in anaerobic microorganisms, in CO₂ fixation. They also play an important role in amino acid metabolism in many organisms, including humans. They catalyse the transfer of methyl groups from a methyl donor to a methyl acceptor (Figure 15.10(a)), with a B₁₂-containing protein acting as the intermediate carrier of the methyl group. The

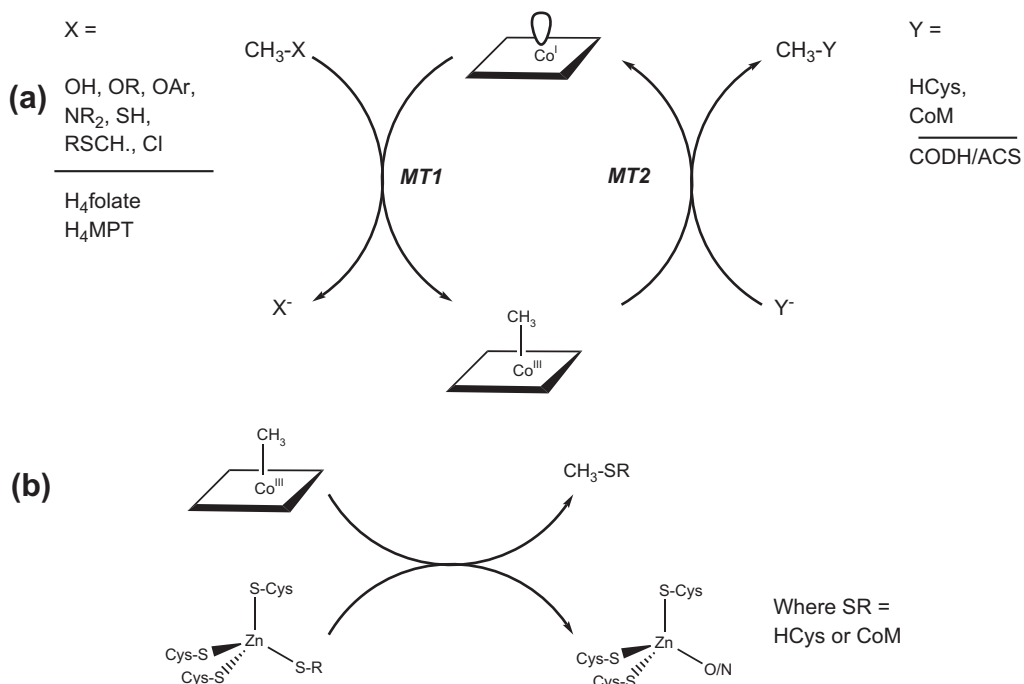


FIGURE 15.10 (a) The three components involved in the B₁₂-dependent methyltransferases. (b) The MT2 enzymes have a thiol group which activates the thiol acceptor. (From *Banerjee & Ragsdale, 2003*. Reprinted with permission from *Annual Reviews*.)

methyltransferases involve three protein components, each of which is localised on a different polypeptide or domain. The first, (MT1) binds the methyl donor ($\text{CH}_3\text{-X}$) and transfers it to the B_{12} -containing protein, leading to the formation of an organometallic methylcobalt intermediate. The third component (MT2) catalyses the transfer of the Co-bound methyl group to the acceptor Y^- . The methyl donor can be any one of a number of molecules like methyltetrahydrofolate, while the methyl acceptor can be, for example, homocysteine to give methionine, or the CODH/ACS bifunctional complex to form acetyl-CoA. The MT2 enzymes all appear to contain Zn, which both coordinates and activates the thiolate methyl acceptor (Figure 15.10(b)). However, in the transfer of a methyl group within the CODH/ACS system, a different type of reaction is involved in which the methyl group is transferred from Co to Ni.

The best characterised B_{12} -dependent methyltransferase is methionine synthase (Figure 15.11) from *E. coli*, which catalyses the transfer of a methyl group from methyltetrahydrofolate to homocysteine to form methionine

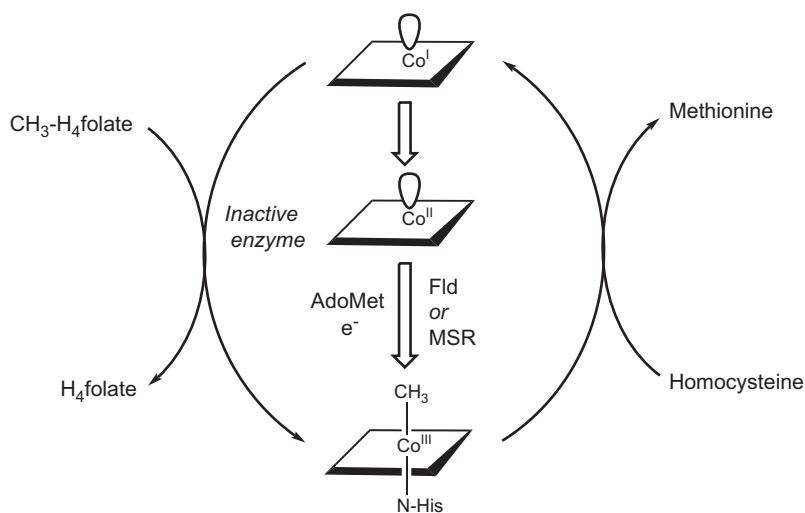


FIGURE 15.11 Reactions catalysed by cobalamin-dependent methionine synthase. (From Banerjee & Ragsdale, 2003. Reprinted with permission from Annual Reviews.)

and tetrahydrofolate. During the catalytic cycle, B_{12} cycles between $\text{CH}_3\text{-Co(III)}$ and Co(I) . However, from time to time, Co(I) undergoes oxidative inactivation to Co(II) , which requires reductive activation. During this process, the methyl donor is S-adenosylmethionine (AdoMet) and the electron donor is flavodoxin (Fld) in *E. coli*, or methionine synthase reductase (MSR) in humans. Methionine synthase is a modular enzyme, with separate domains for binding of homocysteine, methyltetrahydrofolate, B_{12} , and AdoMet (Figure 15.12). The B_{12} domain in its different oxidation states must interact with each of the other three domains: the Co(I) form with methyltetrahydrofolate, the inactive Co(II) form with the AdoMet binding domain, and the $\text{CH}_3\text{-Co(III)}$ form with the homocysteine-binding domain. When cobalamin binds, the lower axial Dmb ligand is replaced by His to generate the His-on conformation (Figure 15.8B). This His residue is part of a catalytic triad which controls the coordination state of cobalt (His-on/His-off) by modulating the protonation state of the histidine.

As pointed out earlier, a third class of B_{12} -dependent enzymes, present in anaerobic microbes, carry out reductive dehalogenation reactions, which play an important role in the detoxification of chlorinated aliphatic and aromatic compounds, among which are many important man-made pollutants (El Fantroussi et al., 1998). The role of B_{12} in this class of enzymes is not clear — possibly by formation of an organocobalt adduct, as in the case of methyltransferases or alternatively by the corrinoid serving as an electron donor.

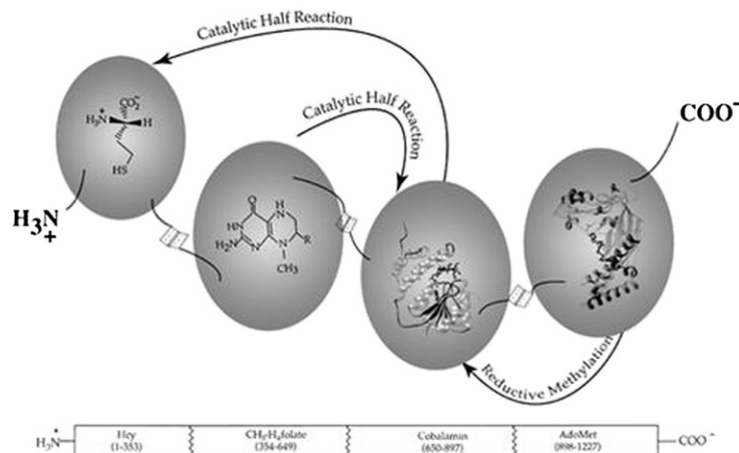


FIGURE 15.12 The modular structure of methionine synthase. The four domains are connected by flexible hinges which allow the $\text{CH}_3\text{tetrahydrofolate-}$, AdoMet-, or homocystein-binding domains to alternatively access the B_{12} -binding domain. (From Banerjee & Ragsdale, 2003. Reprinted with permission from Annual Reviews.)

NONCORRIN CO-CONTAINING ENZYMES

Noncorrin cobalt has a number of interesting applications in the chemical industry, for example, in the hydroformylation (OXO) reaction between CO , H_2 , and olefins. A number of noncorrin Co-containing enzymes have been described, including methionine aminopeptidase (Met-APs), X-Pro aminopeptidase, prolidase, and nitrile hydratase (Lowther and Matthews, 2002). These enzymes cleave a restricted subset of N-terminal peptide bonds, suggesting a role in the regulation of biological processes rather than in general protein degradation. In the case of the ubiquitous Met-APs, which cleave N-terminal methionine from newly translated polypeptide chains, the removal of the N-terminal Met from proteins seems to primarily occur co-translationally. Trimming at the amino-terminus is required for biological activity, subcellular localisation, and the eventual degradation by other enzymes. The importance of MetAP activity is underlined by the lethality of the gene knock-outs in *E. coli*, *S. typhimurium*, and yeast.

Figure 15.13 shows the *E. coli*, *P. furiosus*, and human Met-APs. With their characteristic ‘pita-bread’ fold³ that contains a metal centre flanked by two well-defined substrate-binding pockets. The active site of the enzyme (Figure 15.14) contains two Co(II) ions which are coordinated by the side-chain atoms of five conserved amino acid residues: Asp97, Asp108, His171, Glu204, and Glu235 (*E. coli* MetAP numbering). The distance between the two Co^{2+} is similar to that between the two Zn^{2+} atoms in leucine aminopeptidase, and indeed the catalytic mechanism of methionine aminopeptidase shares many features with other metalloproteases, in particular, leucine aminopeptidases.

Prolidases are widespread in bacteria, and specifically cleave Pro-containing dipeptide sequences, where the Pro residue is C-terminal. They appear to process bioactive peptides involved in the cardiovascular and pulmonary systems and degradation products of collagen. The enzyme from the hyperthermophilic archaeobacteria *P. furiosus* has one tightly bound Co^{2+} , but requires a second Co^{2+} for catalytic activity, suggesting that it may have a similar mechanism of action as methionine aminopeptidase. Nitrile hydratase catalyses the hydration of nitriles to amides and is used industrially on the kiloton scale for the production of acrylamide and nicotinamide from the corresponding nitriles. It has an obligate requirement for Co, which appears to be bound to three Cys residues in a similar motif to that found in iron-containing nitrile hydratases from other microorganisms.

3. Pita bread is a round pocket bread, widely consumed in Middle Eastern, Mediterranean, and Balkan cuisines. The “pocket” is created by steam, which puffs up the dough; as the bread cools and flattens, it leaves a pocket in the middle.

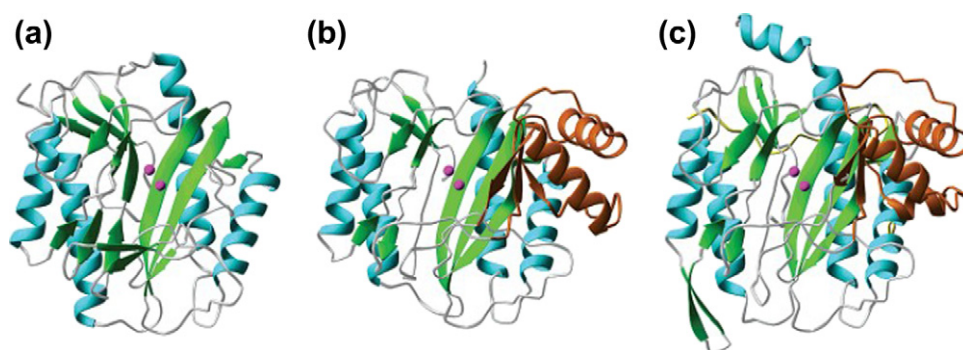


FIGURE 15.13 Type 1 and type 2 MetAPs (“pita-bread” enzymes). (a) *E. coli* MetAP-1; (b) *P. furiosus* MetAP-2; (c) human MetAP-2. In contrast to the type 1 enzymes, type 2 MetAPs contain an α -helical subdomain (orange) inserted within the catalytic domain (cyan and green α -helices and β -strands, respectively). (From Lowther & Matthews, 2002. Reprinted with permission of the American Chemical Society.)

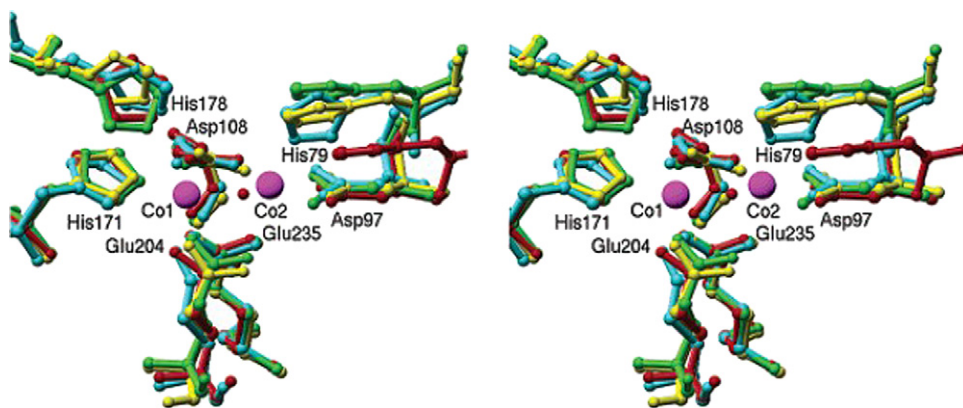


FIGURE 15.14 Comparison of the dinuclear metal centres and flanking His residues of *E. coli* MetAP-1 (red) and its relatives. (From Lowther & Matthews, 2002. Reprinted with permission of the American Chemical Society.)

REFERENCES

- Banerjee, R., & Ragsdale, S. W. (2003). The many faces of vitamin B₁₂: catalysis by cobalamin-dependent enzymes. *The Annual Review of Biochemistry*, 72, 209–247.
- Banerjee, R., Gherasim, C., & Padovani, D. (2009). The tinker, tailor, soldier in intracellular B₁₂ trafficking. *Current Opinion in Chemical Biology*, 13, 484–491.
- Brown, K. L. (2005). Chemistry and enzymology of vitamin B₁₂. *Chemical Reviews*, 105, 2075–2149.
- Drennan, C. L., Doukov, T. I., & Ragsdale, S. W. (2004). The metalloclusters of carbon monoxide dehydrogenase/acetyl-CoA synthase: a story in pictures. *The Journal of Biological Inorganic Chemistry*, 9, 511–515.
- El Fantroussi, S., Naveau, H., & Agathos, S. N. (1998). Anaerobic dechlorinating bacteria. *Biotechnol Progress*, 14, 167–188.
- Hegg, E. L. (2004). Unravelling the structure and mechanism of acetyl-coenzyme A synthase. *Accounts of Chemical Research*, 37, 775–783.
- Kobayashi, M., & Shimizu, (1999). Cobalt proteins. *European Journal of Biochemistry*, 261, 1–9.
- Lill, S. O., & Siegbahn, P. E. (2009). An autocatalytic mechanism for NiFe-hydrogenase: reduction to Ni(I) followed by oxidative addition. *Biochemistry*, 48, 1056–1066.
- Lowther, W. T., & Matthews, B. W. (2002). Metalloaminopeptidases: common functional themes in disparate structural surroundings. *Chemical Reviews*, 102, 4581–4607.
- Mulrooney, S. B., & Hausinger, R. P. (2003). Nickel uptake and utilisation by microorganisms. *FEMS Microbiology Reviews*, 27, 239–269.

- Ragsdale, S. W. (1998). Nickel biochemistry. *Current Opinion in Chemical Biology*, 2208–2215.
- Ragsdale, S. W. (2004). Life with carbon monoxide. *Critical Reviews in Biochemistry and Molecular Biology*, 39, 165–195.
- Ragsdale, S. W. (2006). Metals and their scaffolds to promote difficult enzymatic reactions. *Chemical Reviews*, 106, 3317–3337.
- Ragsdale, S. W. (2007). Nickel and the carbon cycle. *Journal of Inorganic Biochemistry*, 101, 1657–1666.
- Ragsdale, S. W. (2009). Nickel-based enzyme systems. *Journal of Biological Chemistry*, 284, 18571–18575.
- Ragsdale, S. W., & Pierce, E. (2008). Acetogenesis and the Wood-Ljungdahl pathway of CO(2) fixation. *Biochimica et Biophysica Acta*, 1784, 1873–1898.
- Reed, G. H. (2004). Radical mechanisms in adenosylcobalamin-dependent enzymes. *Current Opinion in Chemical Biology*, 8, 477–483.
- Shima, S., Warkentin, E., Thauer, R. K., & Ermler, U. (2002). Structure and Function of enzymes involved in the methanogenic pathway utilising carbon dioxide and molecular hydrogen. *Journal of Bioscience and Bioengineering*, 93, 519–530.
- Svetlitchnyi, V., Dobbek, H., Meyer-Klaue, W., Meins, T., Thiele, B., Römer, P., et al. (2004). A functional Ni-Ni-[4Fe-4S] cluster in the monomeric acetyl-CoA synthase from Carboxydotherrmus hydrogenoformans. *Proceedings of the National Academy of Sciences of the United States of America*, 101, 446–451.
- Thauer, R. K., Kaster, A. K., Seedorf, H., Buckel, W., & Hedderich, R. (2008). Methanogenic archaea: ecologically relevant differences in energy conservation. *Nature Reviews Microbiology*, 6, 579–591.
- Thauer, R. K., Kaster, A. K., Goenrich, M., Schick, M., Hiromoto, T., & Shima, S. (2010). Hydrogenases from methanogenic archaea, nickel, a novel cofactor, and H₂ storage. *The Annual Review of Biochemistry*, 79, 507–536.

Manganese – Oxygen Generation and Detoxification

Introduction: Mn Chemistry and Biochemistry	311
Photosynthetic Oxidation of Water – Oxygen Evolution	311
Mn ²⁺ and Detoxification of Oxygen Free Radicals	314
Nonredox di-Mn Enzymes – Arginase	317

INTRODUCTION: MN CHEMISTRY AND BIOCHEMISTRY

Manganese has access to three oxidation states of relevance to biology, Mn(II), Mn(III), and Mn(IV). A major difference with other redox active metals, like iron, is that manganese has less reducing potential than iron under most biological conditions. Whereas Fe³⁺ is stabilised with respect to Fe²⁺, Mn²⁺ is stabilised relative to Mn³⁺ – this is because, in both cases, the half-filled *d*⁵ shell of both Fe³⁺ and Mn²⁺ confers thermodynamic stability. Two important consequences of this redox chemistry are that, not surprisingly, Mn²⁺ can participate in useful redox catalysis on many similar substrates to Fe³⁺, whereas the higher redox potential of Mn²⁺ makes free Mn²⁺ innocuous under conditions where free Fe²⁺ would wreak havoc through the generation of hydroxyl radicals. This means that cells (notably bacterial cells) can tolerate very high cytoplasmic concentrations of Mn²⁺ with no negative consequences, which is certainly not the case with other biologically important redox metal ions, like iron and copper.

The other property of Mn²⁺ which has important biochemical consequences is that it is a close, but not exact, surrogate of Mg²⁺. As we saw in Chapter 10, Mg²⁺ is confined to a strict octahedral coordination geometry, with ligand bond angles close to 90°, making it an ideal ‘structural’ cation, particularly for phosphorylated biological molecules. Mn²⁺, with its relatively similar ionic radius, readily exchanges with Mg²⁺ in most structural environments and exhibits much of the same labile, octahedral coordination chemistry. However, since Mn²⁺-ligand bonds are generally much more flexible than Mg²⁺-ligand bonds, when Mn²⁺ replaces Mg²⁺ in a catalytic environment, its flexibility is better at lowering the activation energy. It can more easily accommodate the distortions in coordination geometry in progressing from the substrate-bound to the transition state and from there to the bound product. Thus, substituting Mn²⁺ in the active site of a Mn²⁺-enzyme often results in improved enzyme efficacy.

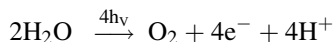
The major role of manganese in biology is in oxygen production by photosynthetic plants, algae, and cyanobacteria. It is also involved in a number of mammalian enzymes like arginase and mitochondrial superoxide dismutase and it also plays an important role in microbial metabolism. Most of manganese biochemistry can be explained on the one hand by its redox activity and on the other by its analogy to Mg²⁺.

PHOTOSYNTHETIC OXIDATION OF WATER – OXYGEN EVOLUTION

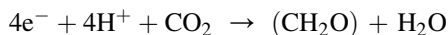
Somewhere around 2.5Ga¹ ago, an enzyme activity emerged which dramatically changed the chemical composition of the earth’s atmosphere forever, resulting in a veritable explosion of biological activity. The enzyme,

1. Geologists use the designations of Ga for a billion years before present time (“G” stands for “giga”) and Ma for million years before.

which we now know as photosystem II, used solar energy to carry out the thermodynamically demanding and chemically challenging reaction of water splitting:



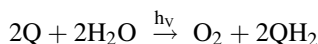
This provided an unlimited supply of reducing equivalents to convert CO_2 to carbohydrates, and subsequently to the other organic molecules of life:



Prior to this bonanza of hydrogen/electron donors, biology had been restricted to H_2S , NH_3 , some organic acids, Fe^{2+} , and the like, which were in short supply when compared with the unlimited oceans of water on the surface of our green planet. However, there were two other consequences of the arrival of oxygenic photoautotrophs.² Firstly, the by-product of the water-splitting reaction, molecular oxygen, transformed our planet from being anaerobic to aerobic, which increased the efficiency of cellular energy production by around 20-fold, and most likely drove the subsequent evolution of eukaryotes and multicellular organisms. The second consequence, which took a bit longer, was the formation of the ozone layer. This provided a shield against harmful UV radiation, allowing the exploitation of new habitats, including, most importantly, the terrestrial environment.

The combination of X-ray crystallography and a wide range of biochemical, biophysical, and molecular biological techniques has provided very exciting new results on the molecular properties of PSII. Indeed, as we will see, we are now very close to understanding the precise chemical mechanism of the water-splitting reaction. For more information see Barber, 2008; Barber and Murray, 2008; Ferreira et al., 2004; Goussias et al., 2002; Iverson, 2006; Rutherford and Boussac, 2004.

Photosystem II (PSII), also known as the water-plastoquinone photo-oxidoreductase, is a multienzyme complex, embedded in the thylakoid membrane of plants, algae, and cyanobacteria, which uses solar energy to power the oxidation of water to dioxygen by a unique tetra-manganese oxygen-evolving cluster (OEC):



We begin by considering how the light-harvesting system of PSII, which varies widely both between organisms and as a function of growth conditions, absorbs the solar energy and transfers it to the reaction centre (RC). It became clear from early structural studies that the PSII core complex of plants and cyanobacteria is dimeric and contains as light-absorbing pigments only chlorophyll *a* and β -carotene molecules bound mainly to the proteins CP43 and CP47. The RC is composed of the proteins D1 and D2, together with all of the redox active cofactors involved in the energy conversion process. The antenna chlorophylls of the CP47 and CP43 subunits collect the energy of photons and transfer this to the special pair of chlorophylls, P_{D1} and P_{D2} (Figure 16.1) in the reaction centre. The excitation of P (Barber, 2008) converts it to a strong reducing agent (P^*). P^* reduces a nearby pheophytin molecule (Pheo) within a few picoseconds, forming the radical pair state $\text{P}^{\bullet+}\text{Pheo}^{\bullet-}$. Within a few hundred picoseconds, $\text{Pheo}^{\bullet-}$ reduces a firmly bound plastoquinone molecule (Q_A) to produce $\text{P}^{\bullet+}\text{PheoQ}_\text{A}^-$. $\text{P}^{\bullet+}$ is a powerful oxidant (redox potential >1 V), and it oxidises a tyrosine residue (TyrZ) to form $\text{TyrZ}^{\bullet+}\text{PheoQ}_\text{A}^-$ on a nanosecond time scale. Oxidation of TyrZ is dependent on deprotonation of its phenolic OH group to generate a neutral radical (TyrZ^{\bullet}). In a millisecond time scale, Q_A^- reduces a second plastoquinone (Q_B) to form $\text{TyrZ}^{\bullet+}\text{PheoQ}_\text{A}\text{Q}_\text{B}^-$. At about the same time, the TyrZ^{\bullet} extracts an electron from the OEC (Mn_4Ca) cluster, to which two substrate water molecules are bound. A second photochemical turnover reduces Q_B^- to Q_B^{2-} . This is protonated to give plastoquinol, QH_2 , which is released into the lipid bilayer to be re-oxidised by photosystem I. Two further photochemical turnovers provide the four oxidising equivalents required to oxidise two water molecules and thereby generate dioxygen.

2. O_2 producing photosynthetic organisms which require only simple inorganic substances to fulfill their nutritional requirements and CO_2 as sole carbon source.

Electron transport cofactors

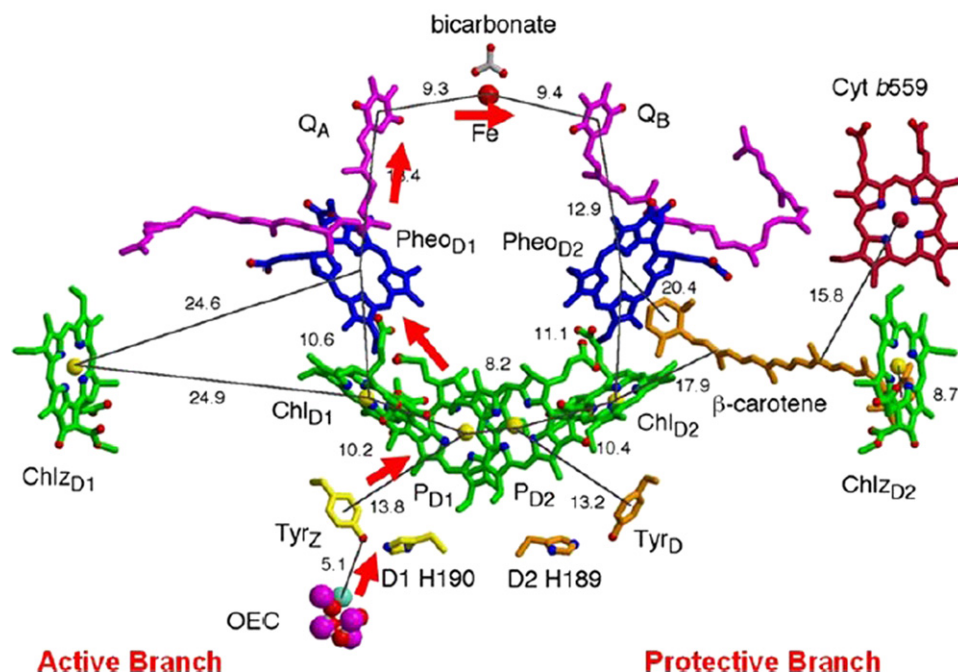


FIGURE 16.1 Cofactors in electron transport in PSII, as determined by X-ray crystallography (Ferreira et al., 2004) (PDB 1S5L). With the exception of the metal-cluster of the oxygen evolving centre (OES), the haem of cyt b559 and a redox active β -carotene molecule, all the cofactors are arranged around a pseudo-2-fold axis passing between the chlorophylls P_{D1} and P_{D2} and the nonhaem iron. Side chains of the D1 and D2 proteins are in yellow and orange, respectively, chlorophyll in green, pheophytin blue, plastoquinones Q_A and Q_B in magenta, haem of cyt b559 red. The phytol tails of the chlorophylls and pheophytins have been removed for clarity. The atoms of the water splitting catalyst are manganese (magenta), calcium (blue-green), and oxygen (red). Also shown are the nonhaem iron (red) and its bicarbonate ligand. Distances are in Ångströms. Red arrows indicate electron pathway of the active branch while cyt b599, a carotenoid (brown), and ChlZ_{D2} form a protective branch. (From Murray & Barber, 2007. Copyright 2007 with permission from Elsevier.)

In classic experiments using an oxygen electrode and short flashes of light, it was established that four photochemical turnovers were required for every molecule of oxygen that was released, and the features of this were rationalised into a kinetic model, known as the S-state cycle (Figure 16.2). In this model, five states, designated S_n , of the enzyme are proposed to exist, with n 0–4, where each state corresponds to a different level of oxidation of the tetra-Mn centre. When S_4 is generated, it reacts in less than a microsecond to release dioxygen and return to the reduced form of the enzyme, S_0 . The stable state of the enzyme in the dark is S_1 , which corresponds to $Mn(III)_2Mn(IV)_2$, so that only three photochemical turnovers are required before O_2 is released.

The location, structure, and protein environment of the Mn_4Ca^{2+} cluster, which catalyses the light-driven, water-splitting reaction of photosystem II, has been elucidated by X-ray crystallography (Figure 16.3). However, owing to the low resolutions of the crystal structures reported to date, and the possibility of radiation damage at the catalytic centre, the precise position of each metal ion remains unknown. To some extent, these problems have been overcome by applying spectroscopic techniques like extended X-ray absorption fine structure. Taking into account the most recent results obtained with these two X-ray-based techniques, Barber and Murray (2008) have attempted to refine models of the structure of the Mn_4Ca^{2+} cluster and its protein environment. Figure 16.3(a) shows the Mn_4Ca^{2+} cluster positioned within the Mn-anomalous difference map of Ferreira, Iverson, Maghlaoui, Barber, and Iwata (2004), while Figure 16.3(b) is a schematic of the amino acid ligation pattern for the model in

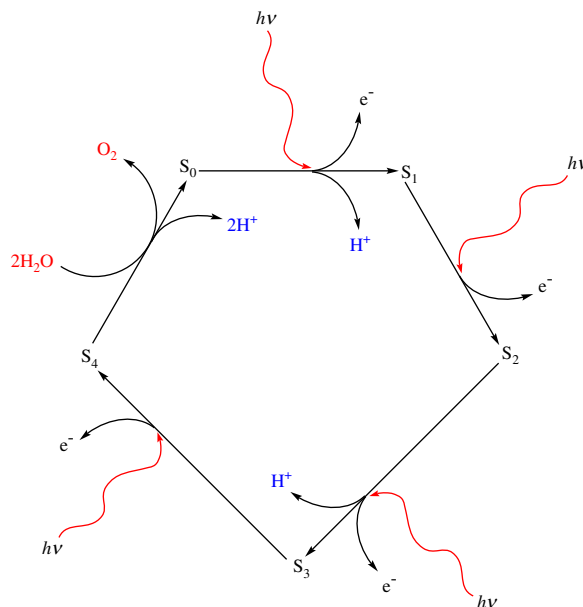


FIGURE 16.2 The S-state cycle model of O_2 generation. (Adapted from Voet & Voet, 2004: pp. 1591.)

(a) with distances less than 3 Å shown by connecting lines. Figure 16.3(c,d) presents a remodelling of the water-splitting site using the native electron density maps of Ferreira et al. (2004) and Loll, Kern, Saenger, Zouni, and Biesiadka (2005) and the Mn-anomalous difference map of Ferreira et al. (2004), keeping the $Mn_3Ca^{2+}O_4$ cubane of Ferreira et al. but with Mn_4 linked to it via a single 3.3 Å mono- μ -oxo bridge.

Although the precise geometry of the Mn_4Ca cluster is not yet known precisely, these models provide a basis for developing chemical mechanisms for water oxidation and dioxygen formation. The location of one Mn ion (Mn_4 or dangler Mn) adjacent to the Ca^{2+} and their positioning towards the side chains of several key amino acids, including the redox active TyrZ, suggests that they provide the ‘catalytic’ surface for binding the two substrate water molecules and their subsequent oxidation. Two mechanisms are presented in Figure 16.4. In the first, it is proposed that the substrate water associated with Mn_4 is deprotonated during the S-state cycle and that Mn_4 is in a high-oxidation state (Mn(V)) by the time the cluster reaches the S_4 -state just prior to O–O bond formation. The other three Mn ions are also driven to high-valency states (Mn(IV)) by S_4 and act as an oxidising battery for the oxo- Mn_4 complex. In this way, the oxo is highly electrophilic, making it an ideal target for a nucleophilic attack by the oxygen of the second substrate water bound within the coordination sphere of the Ca^{2+} (Figure 16.4(a)). The second mechanism (Figure 16.4(a)) proposes that the deprotonated water molecule on Mn_4 forms an oxyl radical which attacks an oxygen atom linking Ca^{2+} with a Mn or the oxygen of the water molecule coordinated to the Ca^{2+} to form the O–O bond.

Mn^{2+} AND DETOXIFICATION OF OXYGEN FREE RADICALS

Manganese is the cofactor for catalases, peroxidases, and superoxide dismutases which are all involved in the detoxification of reactive oxygen species (SOD). We consider here the widely distributed Mn-SOD and then briefly describe the dinuclear Mn catalases.

Mn superoxide dismutases are found in both eubacteria and archaebacteria as well as in eukaryotes, where they are frequently localised in mitochondria. They (Figure 16.5) have considerable structural homology to Fe-SODs: both are monomers of ~200 amino acid and occur as dimers or tetramers and their catalytic sites are also very

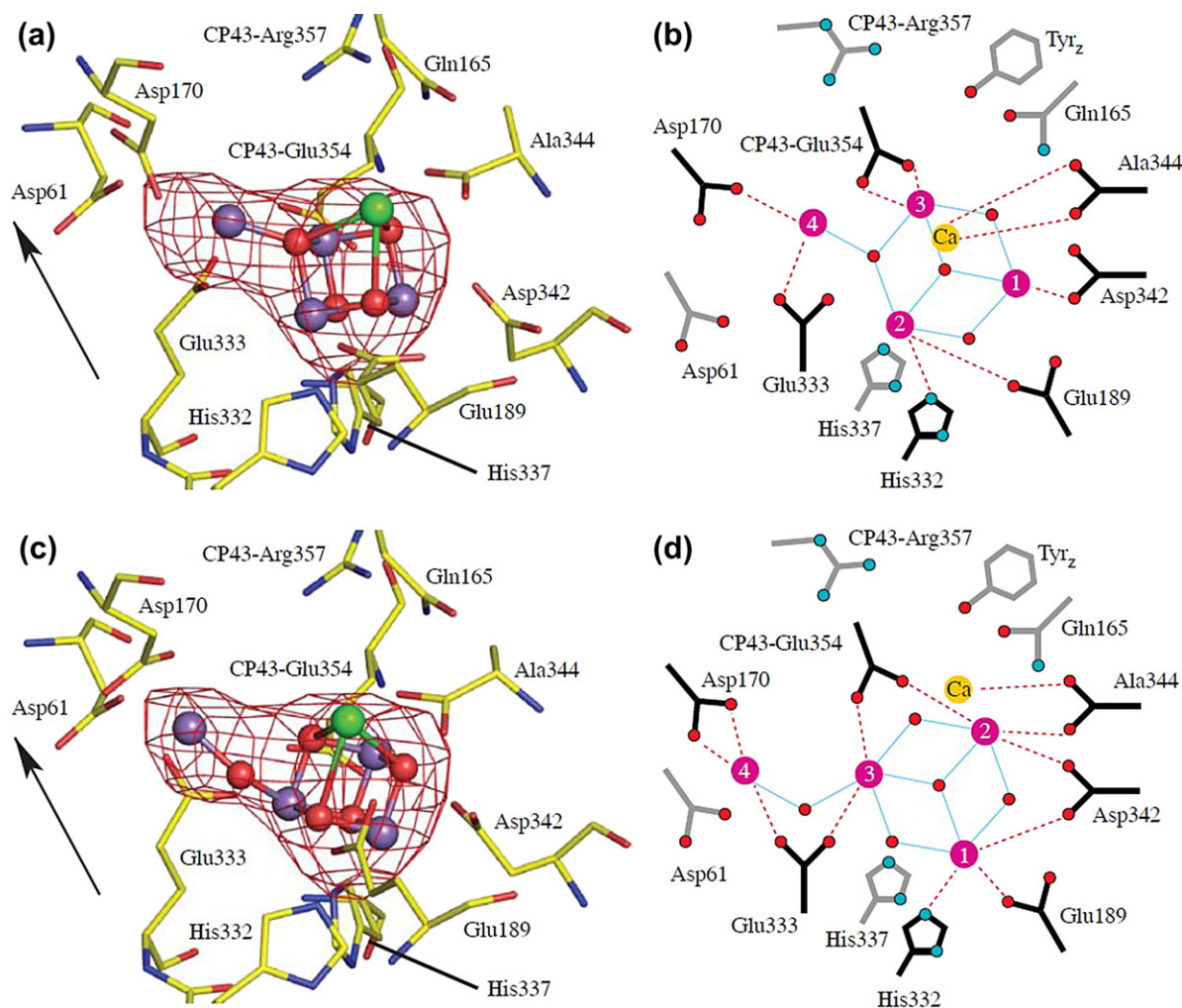


FIGURE 16.3 (a,b) The water-splitting site as reported by Ferreira et al. (2004). (a) The $\text{Mn}_4\text{Ca}^{2+}$ cluster positioned within the Mn-anomalous difference map with amino acid side chains. (b) Schematic of the amino acid ligation pattern for the model in (a) with distances less than 2.8 Å shown by connecting lines. (c,d) Remodelling the water-splitting site using the native electron density maps of Ferreira et al. (2004) and Loll et al. (2005) and Mn-anomalous difference map of Ferreira et al. (2004), keeping the $\text{Mn}_3\text{Ca}^{2+}\text{O}_4$ cubane of Ferreira et al. but with Mn_4 linked to it via a single 3.3 Å mono- μ -oxo bridge. (c) Structure of the water-splitting site, assuming a single mono- μ -oxo bridge between Mn_4 (dangler Mn) and Mn_3 of the $\text{Mn}_3\text{Ca}^{2+}\text{O}_4$ cubane fitted into the Mn-anomalous difference map by real-space refinement. (d) Schematic of the amino acid ligation pattern for model in (c) with distance less than 3 Å shown by connecting lines. The Mn-anomalous difference map is shown in red and contoured at 5 sigma. The arrow indicates the direction of the normal to the membrane plane. (From Barber & Murray, 2008. Copyright 2008 with permission from the Royal Society.)

similar. They both catalyse the two-step dismutation of superoxide anion, and like the CuZn-SODs, they avoid the difficulty of overcoming electrostatic repulsion between two negatively charged superoxide anions by reacting with only one molecule at a time. As in the case of CuZn-SOD, a first molecule of superoxide reduces the oxidised (Mn^{3+}) form of the enzyme, releasing dioxygen, and the reduced (Mn^{2+}) form of the enzyme then reacts with a second superoxide anion and two protons, to give hydrogen peroxide, regenerating the oxidised form of the enzyme.

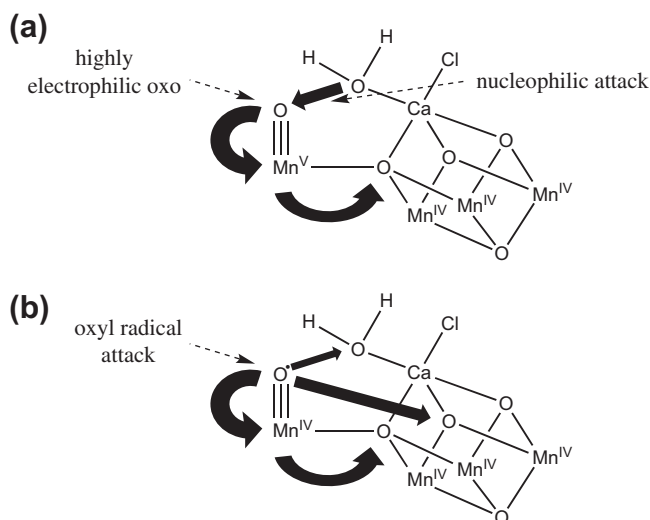


FIGURE 16.4 (a,b) Possible mechanisms for formation of dioxygen during the S4-S0 transition. (Adapted from Barber, 2008.)

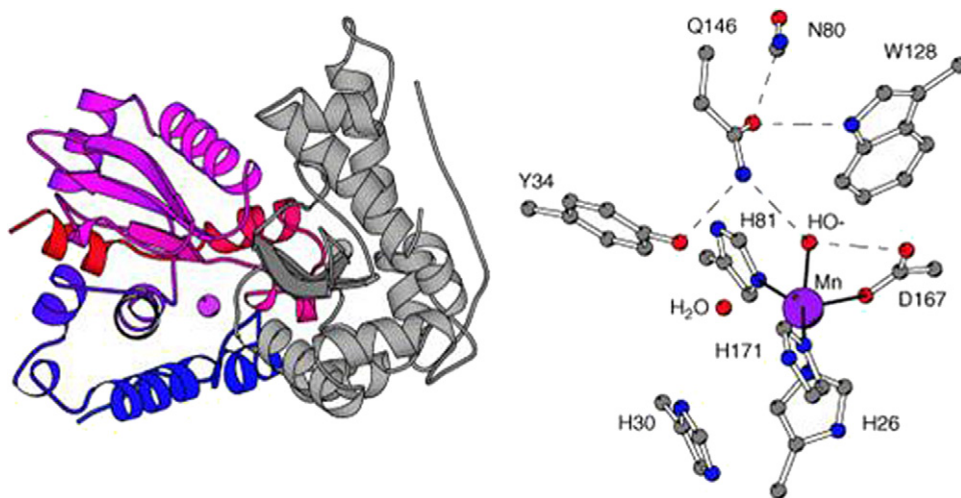


FIGURE 16.5 The protein fold of Mn- or Fe-SODs (left) and the active site (right). (From Miller, 2004. Copyright 2004 with permission from Elsevier.)

Catalases play an important protective role, catalysing the disproportionation of toxic hydrogen peroxide into O₂ and H₂O. In contrast to the haem-containing catalases, which are ubiquitous in aerobic organisms, a broad range of microorganisms, living in microaerophilic (almost oxygen-free) environments, including the lactic acid bacteria,³ have catalases which have a dinuclear manganese centre in their active site (Figure 16.6) (Wu et al., 2004). These 'alternative' catalases are 4-helix bundle proteins, with the di-Mn centre located in the middle of the α helical bundle.

The disproportionation of hydrogen peroxide is thermodynamically favourable; however, rapid reaction requires a two-electron catalyst. For haem catalases, this is achieved by cycling between Fe^{III} and Fe^{IV} porphyrin

3. We mentioned earlier that this family of bacteria has adapted to its environment to function without iron, using Co and Mn instead.

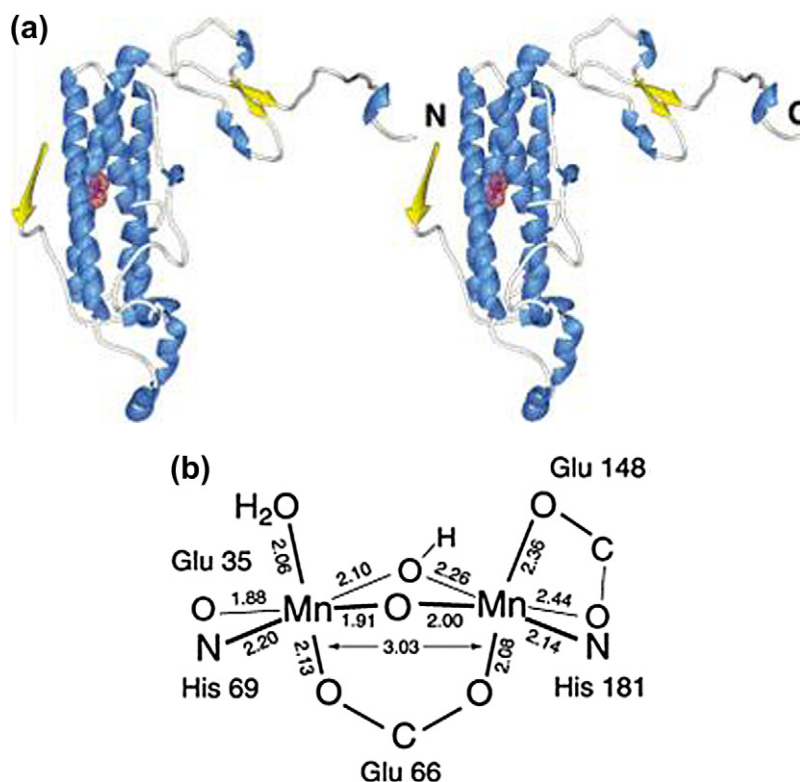


FIGURE 16.6 *Lactobacillus plantarum* Mn catalase: (a) stereo view of the secondary structure — the di-Mn unit as red spheres and (b) the detailed geometry of the di-Mn centre. (From Barynin et al., 2001. Copyright 2001 with permission from Cell Press.)

δ -cation. With two Mn ions, each of which can operate between Mn^{II} and Mn^{IV} , there are five possible oxidation states for Mn catalases. A combination of spectroscopic techniques has shown that at least four of these are observed — a reduced Mn_2^{II} state, a mixed-valence $\text{Mn}^{\text{II}}\text{Mn}^{\text{III}}$ state, an oxidised Mn_2^{III} state, and a superoxidised $\text{Mn}^{\text{III}}\text{Mn}^{\text{IV}}$ state. There is no evidence to date for a Mn_2^{IV} state.

A catalytic mechanism based on the structure of the active site has been proposed (Figure 16.7) involving distinct pathways of reactivity in the oxidised and reduced half reactions. H_2O_2 binds terminally to the oxidised cluster of the oxidative half reaction, replacing the water molecule bound to one of the Mn ions (Figure 16.7); this is also the site at which azide binds in the catalase crystals. Two-electron oxidation of the H_2O_2 by the dinuclear Mn(III) results in release of the dioxygen product, facilitated by the oxygen bridges which electronically couple the Mn ions, allowing them to function as a unit. Glu 178 is proposed to transfer the peroxide protons to active site bases, most likely the solvent bridges between the metal ions. In the reductive half reaction, H_2O_2 is proposed to bind in a bridging position, to give a symmetric μ -bridging peroxide complex which will be activated to O—O bond cleavage and reoxidation of the di-Mn core. Glu 178 could serve to protonate the nonbridging oxygen of the bound substrate. This mechanism results in replacement of one of the oxygen bridges of the cluster during each turnover cycle, with retention of a substrate oxygen atom between successive reactions.

NONREDOX DI-MN ENZYMES — ARGINASE

In addition to the redox di-Mn catalases, there are a number of other enzymes with di-Mn centres, of which the best characterised are arginases, which catalyse the divalent cation-dependent hydrolysis of L-arginine to form L-ornithine (Ash, 2004) and urea.

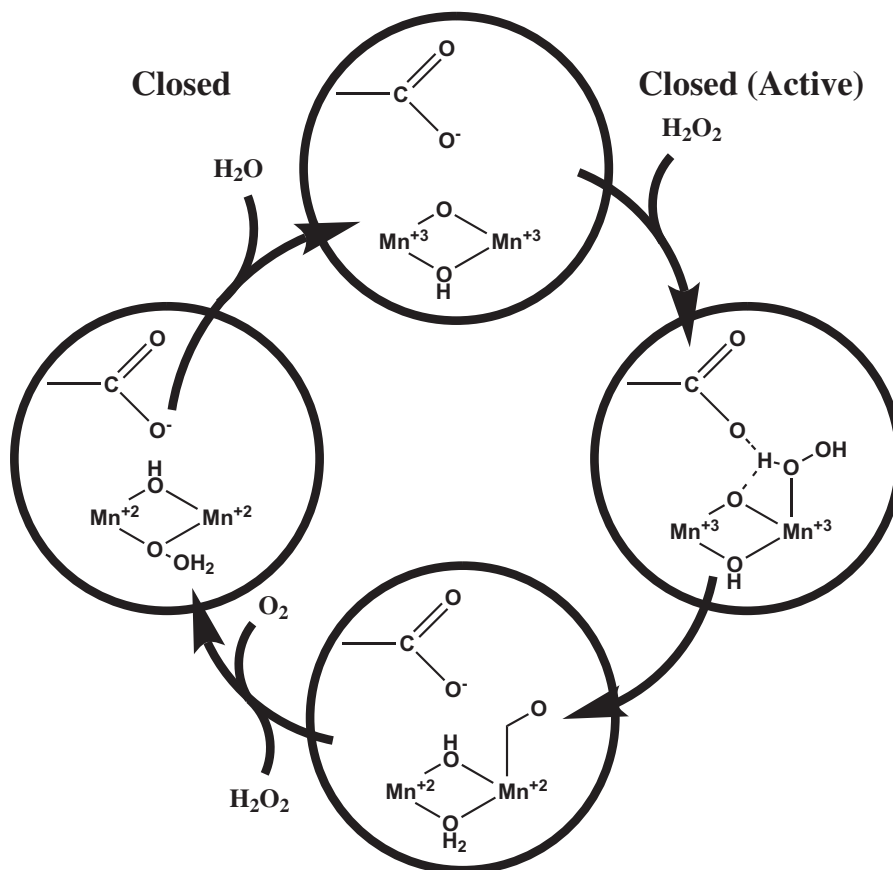
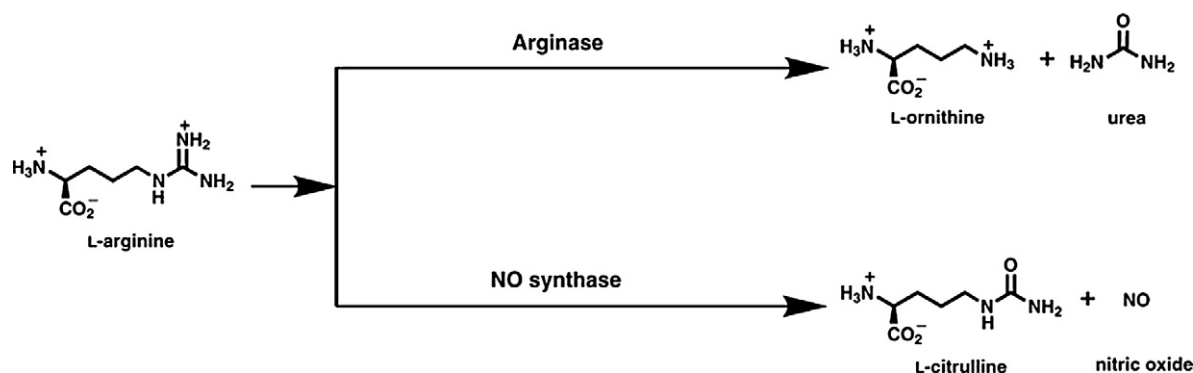


FIGURE 16.7 Catalytic reaction cycle for manganese catalase turnover. (Adapted from Whittaker, Barynin, Igarashi, & Whittaker, 2003.)

In mammals, hepatic arginase is the terminal enzyme of the urea cycle, which represents the major end-product of nitrogen metabolism — the average adult human excretes some 10 kg of urea per year. The enzyme is not restricted to the liver, since ornithine is a precursor of the nonessential amino acid proline, and a biosynthetic precursor of polyamines, required for rapidly dividing tissues. Arginine is also the precursor of the important messenger in many vertebrate signal-transduction pathways nitric oxide, NO (Scheme 16.1), of which more shortly.

A common feature of arginases, whether eukaryotic or prokaryotic, is the requirement of divalent cations for activity, and in almost all arginases, they have 2 spin-coupled Mn(II) /subunit, which are some 3.3 Å apart. Figure 16.8a presents a ribbon plot of the arginase trimer. The dinuclear Mn(II) centre is located at the bottom of a 15 Å-deep active site cleft. Figure 16.8b shows the dinuclear cluster of arginase. Mn_A^{2+} is coordinated with square pyramidal geometry, leaving a vacant coordination site that permits octahedral coordination geometry as a means of transition state stabilisation in catalysis. Mn_B^{2+} is coordinated with octahedral geometry. An interesting feature is the hydrogen bond donated by a metal-bridging hydroxide to the noncoordinating oxygen of Asp 128: residues analogous to Asp 128 are found in the active sites of a large number of other dimetallic hydrolases.

A mechanism which is consistent with biochemical, enzymological, and structural data is outlined in Figure 16.9 and the steps are detailed here. (a) The first step involves binding of the substrate L-arginine to the enzyme in which the side chain of Glu 277 plays an important role; the substrate guanidium group does *not* coordinate to the manganese ions, (b) Nucleophilic attack of metal-bridging hydroxide at the substrate guanidinium group leads to formation of a neutral, tetrahedral intermediate which is stabilised by the dinuclear



SCHEME 16.1 L-arginine catabolism by arginase and NO synthase.

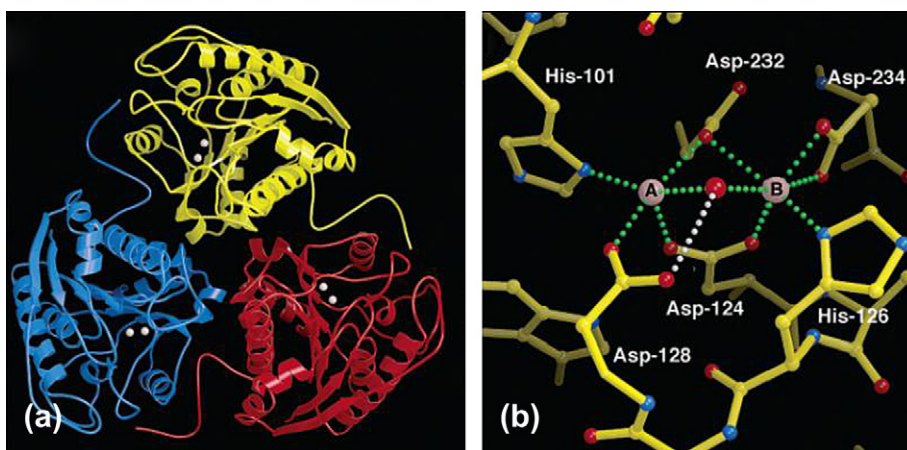


FIGURE 16.8 (a) A ribbon plot of the arginase trimer. The binuclear manganese cluster is represented by a pair of spheres in each monomer. (b) The binuclear manganese cluster of arginase. Metal coordination interactions are indicated by green dotted lines, and the hydrogen bond between the metal-bridging hydroxide ion (red sphere) and Asp 128 is indicated by a white dotted line. Mn_A^{2+} is coordinated with square pyramidal geometry, leaving a vacant coordination site that permits octahedral coordination geometry as a means of transition state stabilisation in catalysis. Mn_B^{2+} is coordinated with octahedral geometry. (Reprinted with permission from Kanyo, Scolnick, Ash, and Christianson, 1996. Copyright 1996 Nature Publishing Group.)

Mn(II) centre (c, d) Following a proton transfer to the leaving amino group mediated by Asp 128, the tetrahedral intermediate collapses to yield the products L-ornithine and urea. (e) A water molecule enters to bridge the binuclear Mn^{2+} cluster, causing the urea product to move to a terminal coordination site on Mn_A^{2+} . Product dissociation facilitates ionisation of the metal-bridging water molecule to yield the catalytically active hydroxide ion. Proton transfer from the metal-bridging water to the bulk solvent is mediated by His-141, followed by the release of the two products.

Arginase can regulate L-arginine bioavailability to the other key enzyme mentioned above which utilises arginine, namely nitric oxide synthase, by depleting the substrate pool for NO biosynthesis. Therefore, arginase inhibitors can enhance the substrate pool for NO biosynthesis. Accordingly, arginase inhibition can enhance NO-dependent physiological processes, such as the smooth muscle relaxation required for sexual arousal: administration of arginase inhibitors *in vitro* and *in vivo* enhances erectile function and engorgement in the male and female genitalia (Christianson, 2005). Therefore, arginase is a potential therapeutic target for the treatment of sexual arousal disorders in men and women. Not quite Viagra, but a step in the same direction!

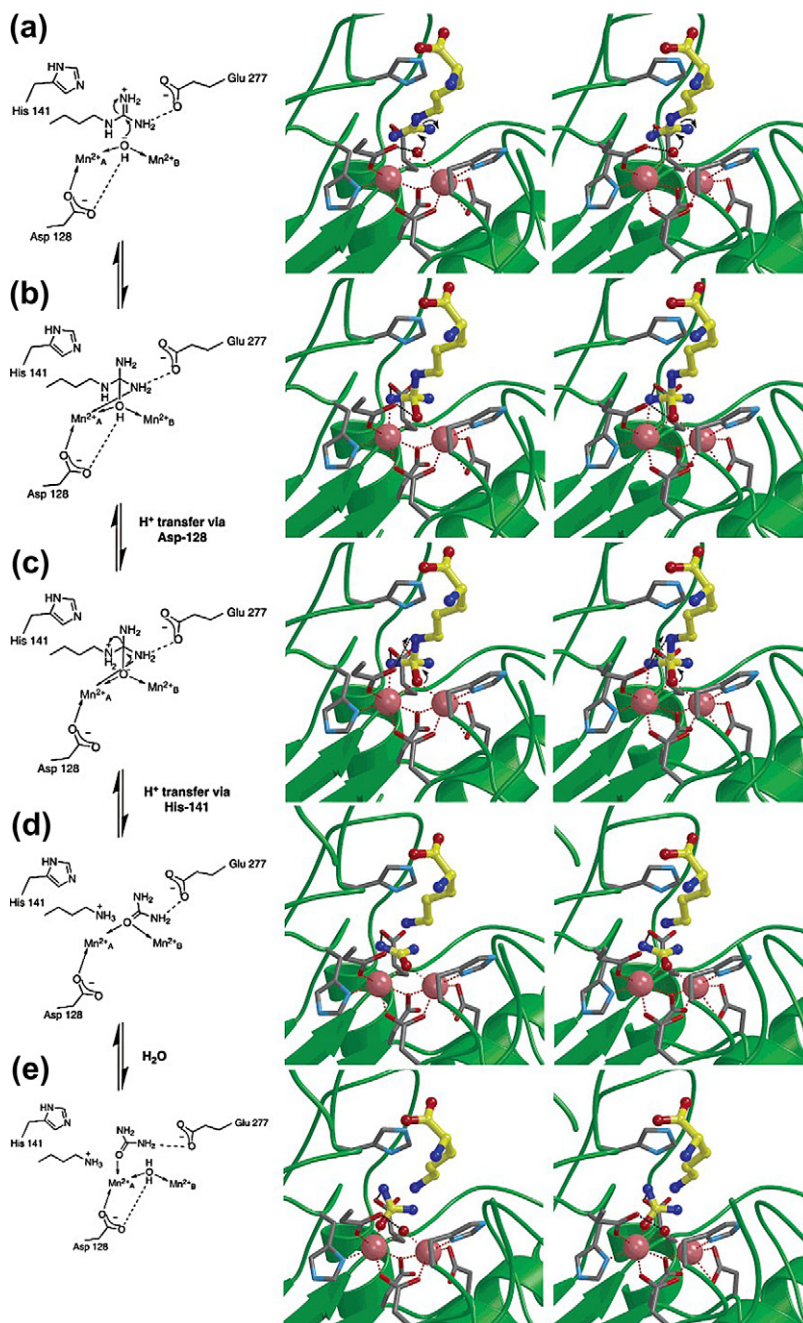


FIGURE 16.9 Structure-based arginase mechanism. (Left) Schematic representation of the arginase mechanism; R-amino and R-carboxylate substrate groups are omitted for clarity. (Middle, right) Stereo view of the arginase mechanism. Protein atoms are colour-coded as follows: C) gray, O) red, and N) blue; ligand atoms are colour-coded the same with the exception: C) yellow; water molecules appear as red spheres. Manganese coordination interactions are designated by red dashed lines and hydrogen bonds by black dashed lines. (From Cox *et al.*, 2001. Copyright 2001 with permission from the American Chemical Society.)

REFERENCES

- Ash, D. E. (2004). Arginine metabolism: enzymology, nutrition and clinical significance. *Journal of Nutrition*, 134, 2760S–2764S.
- Barber, J. (2008). Photosynthetic generation of oxygen. *Philosophical Transactions of the Royal Society B: Biological Sciences*, 363, 2665–2674.
- Barber, J., & Murray, J. W. (2008). The structure of the $\text{Mn}_4\text{Ca}^{2+}$ cluster of photosystem II and its protein environment as revealed by X-ray crystallography. *Philosophical Transactions of the Royal Society B: Biological Sciences*, 363, 1129–1138.
- Barynin, V. V., Whittaker, M. M., Antonyuk, S. V., Lamzin, V. S., Harrison, P. M., Artymiuk, P. J., et al. (2001). Crystal Structure of Manganese Catalase from *Lactobacillus plantarum*. *Structure*, 9, 725–738.
- Christianson, D. W. (2005). Arginase: structure, mechanism, and physiological role in male and female sexual arousal. *Accounts of Chemical Research*, 38, 191–201.
- Cox, J. D., Cama, E., Colleluori, D. M., Pethe, S., Boucher, J.-L., Mansuy, D., et al. (2001). Mechanistic and metabolic inferences from the binding of substrate analogues and products to arginase. *Biochemistry*, 40, 2689–2701.
- Ferreira, K. N., Iverson, T. M., Maghlaoui, K., Barber, J., & Iwata, S. (2004). Architecture of the photosynthetic oxygen-evolving center. *Science*, 303, 1831–1838.
- Goussias, C., Boussac, A., & Rutherford, A. W. (2002). Photosystem II and photosynthetic oxidation of water: an overview. *Philosophical Transactions of the Royal Society B: Biological Sciences*, 357, 1369–1381.
- Iverson, T. M. (2006). Evolution and unique bioenergetic mechanisms in oxygenic photosynthesis. *Current Opinion in Chemical Biology*, 10, 91–100.
- Kanyo, Z. F., Scolnick, L. R., Ash, D. E., & Christianson, D. W. (1996). Structure of a unique binuclear manganese cluster in arginase. *Nature*, 383, 554–557.
- Loll, B., Kern, J., Saenger, W., Zouni, A., & Biesiadka, J. (2005). Towards complete cofactor arrangement in the 3.0 Å resolution structure of photosystem II. *Nature*, 438, 1040–1044.
- Miller, A.-F. (2004). Superoxide dismutases: active sites that save, but a protein that kills. *Current Opinion in Chemical Biology*, 8, 162–168.
- Murray, J. W., & Barber, J. (2007). Structural characteristics of channels and pathways in photosystem II including the identification of an oxygen channel. *Journal of Structural Biology*, 159, 228–237.
- Rutherford, A. W., & Boussac, A. (2004). Water photolysis in biology. *Science*, 303, 1782–1784.
- Voet, D., & Voet, J. G. (2004). *Biochemistry* (3rd ed.). Hoboken: John Wiley and Sons.
- Whittaker, M. M., Barynin, V. V., Igarashi, T., & Whittaker, J. W. (2003). Outer sphere mutagenesis of *Lactobacillus plantarum* manganese catalase disrupts the cluster core. Mechanistic implications. *European Journal of Biochemistry*, 270, 1102–1116.
- Wu, A. J., Penner-Hahn, J. E., & Pecoraro, V. L. (2004). Structural, spectroscopic, and reactivity models for the manganese catalases. *Chemical Reviews*, 104, 903–938.

This page intentionally left blank

Molybdenum, Tungsten, Vanadium, and Chromium

Introduction	323
Mo and W Chemistry and Biochemistry	323
Molybdenum Enzyme Families	324
The Xanthine Oxidase Family	325
The Sulfite Oxidases and DMSO Reductases	328

INTRODUCTION

In this last chapter to consider particular metal ions, we have regrouped four metals, which, together with manganese and nickel, are used as alloys to produce specialist steels.¹ However, this is not on account of their capacity to confer particular properties on steel, but rather for their biological chemistry. For further details see [Brondino et al., 2006](#); [Crans et al., 2004](#); [Enemark et al., 2004](#); [Mendel and Bittner, 2006](#); [Vincent, 2000a](#). Molybdenum is the only second row transition element that is essential for most living organisms, and the few species that do not need molybdenum use tungsten, which is molybdenum's third row homologue. In the case of vanadium, the close similarity between its chemical properties and those of molybdenum has led to its replacement in the FeMo-cofactor in some bacterial nitrogenases. However, it is also involved in the activity of haloperoxidases, and four-coordinate vanadate can mimic cellular metabolites via its analogy with phosphate. All three of these metal ions play important roles in enzymes. In contrast, chromium (Cr), a little like Pirandello's *Six Characters in Search of an Author*, is an element which may be biologically necessary, but for which we have yet to find a function or a protein to which it binds.

MO AND W CHEMISTRY AND BIOCHEMISTRY

While it is relatively rare in the earth's crust, Mo is the most abundant transition metal in seawater. When we consider that the oceans are the closest we get today to the primordial soup in which life first arose, it is not surprising that Mo has been widely incorporated into biological systems, and the only organisms which do not require Mo use W instead. The biological versatility of Mo and W result not only from their redox-activity, ranging through oxidation states VI to IV, but because the intermediate V valence state is also accessible, they can act as interfaces between one- and two-electron redox systems, which allows them to catalyse hydroxylation of carbon atoms using water as the ultimate source of oxygen ([Figure 17.1](#)). This contrasts with systems in which O₂ is the ultimate source of the hydroxyl oxygen incorporated into the product. These monooxygenase systems range from

1. Steel is an alloy of iron and carbon, containing typically up to 2% carbon. The addition of other metals in alloys can give special properties such as superior strength, hardness, durability, or corrosion resistance.

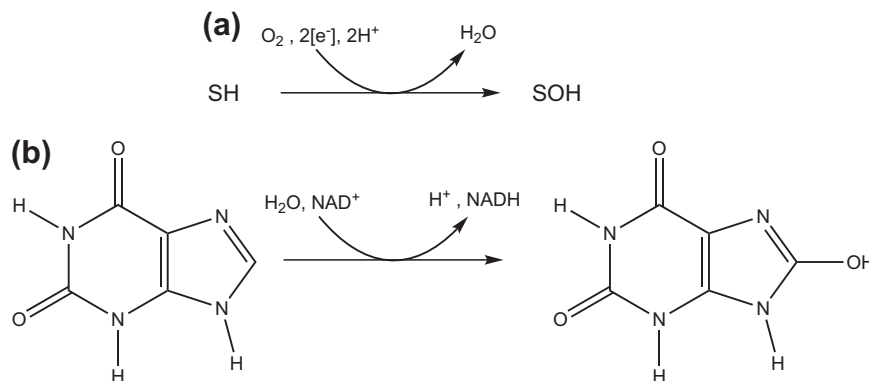


FIGURE 17.1 Reaction stoichiometries for the monooxygenases (a) and molybdenum hydroxylases (b). (Adapted from Hille, 2005.)

the flavin-containing *p*-hydroxybenzoate hydroxylase to the copper-containing dopamine- β -monooxygenase, the haem-containing cytochromes P-450, and the nonhaem iron-containing methane monooxygenase, which we have encountered in previous chapters.

If we assume that the early conditions on our planet were not only anaerobic, but hot, tungsten would have been much better adapted than molybdenum, since low-valent tungsten sulfides would have been more soluble in aqueous solutions, their tungsten-sulfur bonds more stable, and their reduction potentials lower than their molybdenum equivalents. As the earth's crust cooled, and cyanobacterial photosynthesis transformed the atmosphere from anaerobic to aerobic, the oxygen-sensitivity of tungsten compounds, together with the greater water-solubility of high-valence molybdenum oxides, and the dramatically different redox balance, would have pushed the scales in favour of molybdenum. This hypothesis (Hille, 2002) is supported by the distribution of the two; molybdenum enzymes are present in all aerobes and tungsten enzymes only in obligate anaerobes (often thermophiles). A few anaerobes can use either metal, depending on availability.

Another factor which characterises Mo (and W) enzymes is that, with the exception of bacterial nitrogenase, the FeMo-cofactor of which will be discussed later, instead of using the metal itself directly coordinated to amino acid side chains of the protein, they contain a molybdenum pyranopterindithiolate cofactor (MoCo), which is the active component of their catalytic site. The cofactor (pyranopterindithiolate) coordinates the metal ion via a dithiolate side chain.

The biosynthetic pathway for this pterin cofactor, which was described in Chapter 4, appears to be universally conserved in biology, underlining its importance. Interestingly however, baker's yeast, a much used 'model' eukaryote, is the only organism known which does not contain Mo enzymes (it is also one of the few organisms which does not contain ferritin). The MoCo cofactor can exist in the fully oxidised (Mo^{VI}) and fully reduced (Mo^{IV}) forms, with some enzymes generating the (Mo^{V}) form as a catalytic intermediate.

MOLYBDENUM ENZYME FAMILIES

Molybdenum-containing enzymes can be divided into three families, the xanthine oxidase (XO), sulfite oxidase (SO), and the DMSO reductase (DMR) families. They each have a characteristic active site structure (Figure 17.2(a)) and catalyse a particular type of reaction (see below). Whereas in eukaryotes, the pterin side chain has a terminal phosphate group, in prokaryotes, the cofactor (R in Figure 17.2(b)) it is often a dinucleotide.

Of the three members of the XO family, xanthine oxidase/dehydrogenases and aldehyde oxidoreductases catalyse the hydroxylation of carbon centres, whereas the third family member, the CO dehydrogenase from *Oligotropha carboxidovorans*, converts CO to CO_2 . This latter enzyme is a structural exception, in that it has a dinuclear heterometal [CuSMoO_2H] cluster, with the sulfido ligand coordinated by the Cu^{I} centre (for the structure of this, see Chapter 4, Figure 4.12).

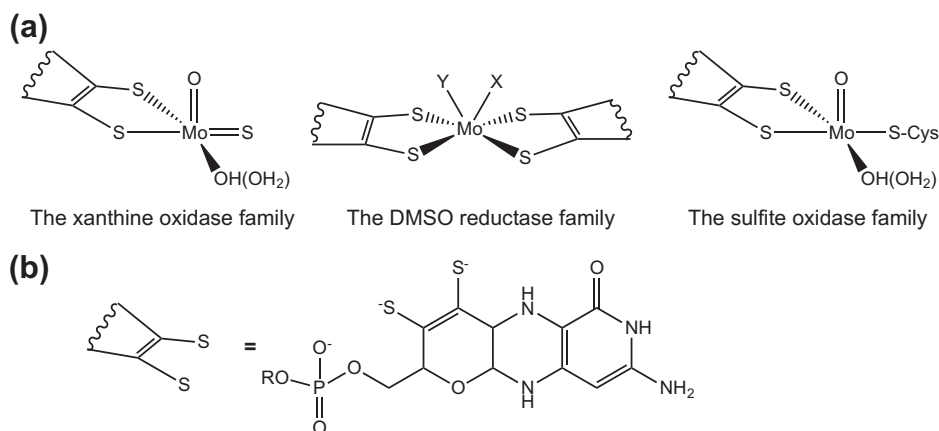


FIGURE 17.2 Active site structures of the three families of mononuclear Mo- and W-enzymes. (a) Coordination around Mo. X and Y represent ligands such as oxygen (oxo, hydroxo, water, serine, aspartic acid), sulfur (cysteine), and selenium atoms (selenocysteine). (b) Structure of the pyranopterin molecule. R=H in eukaryotic enzymes and GMP, AMP, CMP or IMP in bacteria. (Adapted from *Brondino, Romao, Moura, & Moura, 2006.*)

The second SO family sulfite oxidase, which is widely distributed in all phyla, also includes the plant, algal, and yeast nitrate reductases. Like XOs, SOs contain one equivalent of the cofactor, this time with a cysteine ligand provided by the protein.

Finally, the third DMR family catalyses diverse reactions, including DMSO reduction, dissimilatory nitrate reduction, and formate dehydrogenation. All members of this third family have two cofactor molecules bound to a single molybdenum ion. The coordination sphere is completed by a single M=O group and a sixth ligand, which is a serine residue in DMSO reductase (in other members of the family it can be a cysteine, a selenocysteine or a hydroxide). As we will see later in the chapter, all tungsten enzymes which have been structurally characterised contain two pyranopterinindithiolate ligands per tungsten atom.

THE XANTHINE OXIDASE FAMILY

Xanthine oxidoreductases are complex metalloflavoenzymes, present in a wide range of organisms, from bacteria to man, and catalyse the hydroxylation of a wide variety of purine, pyrimidine, pterin, and aldehyde substrates. They all have similar molecular weights and composition of redox centres. The mammalian enzymes, which catalyse the hydroxylation of hypoxanthine and xanthine to the more water-soluble uric acid, are synthesised as the dehydrogenase form xanthine dehydrogenase (XDH) and exist mostly as such in the cell but can be readily converted to the oxidase form xanthine oxidase (XO) by the oxidation of sulfhydryl residues or by proteolysis. XDH shows a preference for NAD⁺ reduction at the flavin adenine dinucleotide (FAD) reaction site, whereas XO fails to react with NAD⁺ and exclusively uses dioxygen as its substrate. This results in the formation of superoxide anion and hydrogen peroxide.

The LMo^{VI}OS(OH) core of the XO family in the oxidised state has a distorted square-pyramidal coordination geometry (Figure 17.2(a)) with the Mo=O group in the apical position. The bidentate enedithiolate ligand of the cofactor lies in the equatorial plane together with the Mo=S and the Mo-OH groups.

Mammalian XO is a homodimer of around 1330 amino acids which binds a number of electron transfer centres — an FAD, two spectroscopically distinct [2Fe-2S] clusters, and the Mo-cofactor. The structure of the bovine xanthine dehydrogenase (XDH), bound to the competitive inhibitor salicylic acid, and presented in Figure 17.3(a), consists of four domains, two Fe/S domains (I and II) in the N-terminal portion of the molecule, followed by the central FAD domain and the molybdenum-binding domain in the C-terminal part of the molecule.

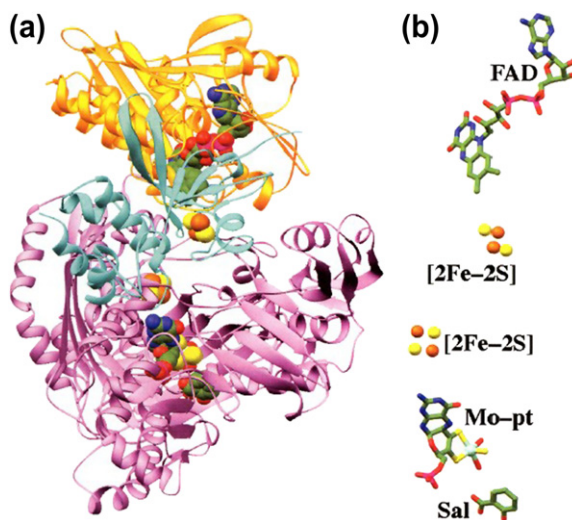


FIGURE 17.3 (a) Ribbon diagram of the XDH subunit with its three major domains and two connecting loops. From N- to C-terminus, the domains are: iron/sulfur domain (residues 3–165; cyan), FAD domain (residues 226–531; gold), and Mo-cofactor domain (residues 590–1,331; lavender). The redox cofactors and the bound competitive inhibitor salicylic acid are shown in space-filling form with C green, N blue, O red, S yellow, P magenta, Fe orange and Mo light blue. The two loops connecting the iron/sulfur domain with the central FAD domain and the FAD domain with the Mo-cofactor domain are disordered and highly flexible. (b) The redox cofactors and salicylate (Sal) are drawn in stick form with the S, Fe and Mo atoms represented by spheres. Based on the X-ray structure in Enroth, Eger, Okamoto, Nishino, Nishino, & Pai, 2000, PDB 1FIQ. (From Voet & Voet 2004. Copyright 2004 with permission John Wiley and Sons.)

Figure 17.3(b) shows that the two [2Fe–2S] clusters are interposed between the FAD and the molybdopterin complex, forming a mini-electron-transport chain. Although the salicylic acid does not contact the Mo-cofactor, it binds to XO in such a way that it blocks the approach of substrates to the metal centre.

The crystal structures of two other molybdenum hydroxylases are known: aldehyde oxidoreductase from *Desulfovibrio gigas* and xanthine dehydrogenase from *Rhodobacter capsulatus*. In addition, the structure of CO dehydrogenase from *Oligotropha carboxidovorans*, an enzyme that catalyses CO oxidation to CO₂ without the cleavage of a C–H bond, yet bears strong structural homology to the molybdenum hydroxylases, has also been reported. All of these enzymes possess the same overall architecture (Figure 17.4), with a pair of [2Fe–2S] clusters in separate domains at the N-terminus, the FAD binding site in a central domain (this FAD binding domain is absent in the *D. gigas* enzyme), and the molybdenum-binding portion of the protein at the C-terminus.

The substrate binding sites of these xanthine-utilising enzymes (Figure 17.5) consist of several highly conserved amino acid residues: Phe 914 (bovine enzyme numbering), Phe 1009, Glu 802, Glu 1261, and Arg 880. On the basis of crystal structures of inhibitors, it is clear that upon binding, the substrate intercalates between the two Phe's. The two Glu's lie on opposite sides of the substrate binding cleft defined by the Phe's: Glu 802 is within hydrogen-bonding distance of the substrate and Glu 1261 within a similar distance to the Mo centre itself (see below). Arg 880 lies on the same side of the substrate binding cleft as Glu 1261, but is further removed from the molybdenum centre. Like Glu 802, it appears positioned to interact with substrate. In the aldehyde-oxidising enzymes, one or both of the Phe's may be a Tyr, but they still define the substrate binding cleft. Neither Glu 802 nor Arg 880 are conserved in the aldehyde oxidases, but Glu 1261 is universally conserved, and its central catalytic role is discussed later.

The mechanism by which xanthine oxidase brings about hydroxylation must take into account the fact that water, rather than O₂ is the ultimate source of oxygen incorporated into the product. In a single-turnover experiment using H₂¹⁸O, the radioisotope is not incorporated into the product, whereas, when the enzyme from that experiment is incubated with substrate in unlabelled water, 8-¹⁸O-uric acid is produced. It follows that

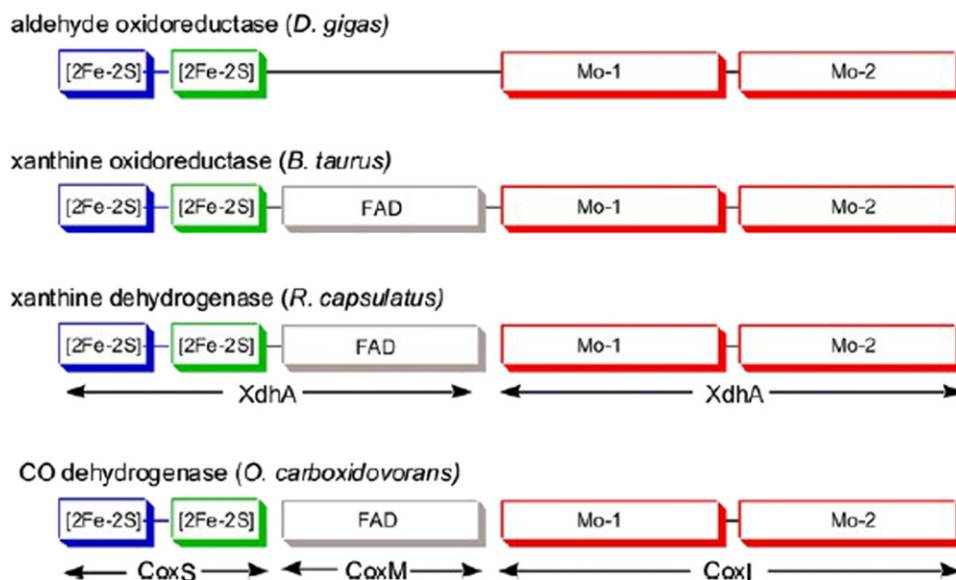


FIGURE 17.4 The topology of xanthine oxidoreductase. Schematic representation of the homologies that exist among the molybdenum hydroxylases. (From Hille, 2005. Copyright 2005 with permission from Elsevier.)

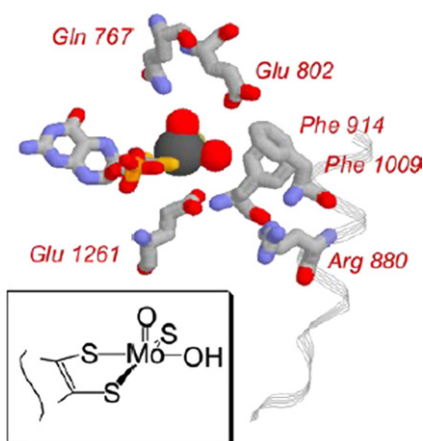


FIGURE 17.5 The active site structure of xanthine oxidoreductase. (A) The LMoOS(OH) core, with an approximately square-pyramidal coordination geometry, with the Mo=O group in the apical position. L represents the bidentate enedithiolate ligand contributed by the pterin cofactor, and lies in the equatorial plane along with the Mo=S and Mo-OH groups. (From Hille, 2005. Copyright 2005 with permission from Elsevier.)

a catalytically labile site on the enzyme is the proximal oxygen donor, and all the evidence points to the Mo-OH group of the molybdenum centre. A mechanism, involving base-assisted nucleophilic attack on the substrate by the Mo-OH group (the catalytically labile oxygen) with concomitant hydride transfer to the Mo=S group, is presented in Figure 17.6. The product (P) is bound in an end-on manner to the molybdenum, via the newly introduced hydroxyl group. Glu 1261 is thought to act as a general base catalyst, initiating the reaction.

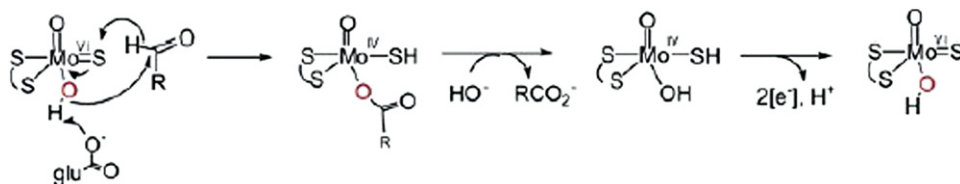


FIGURE 17.6 A reaction mechanism for the aldehyde oxidase group of molybdenum hydroxylases. As with hydroxylation of heterocycles, the conversion of aldehydes to the corresponding carboxylic acids has been proposed to proceed via bases-assisted nucleophilic attack of the Mo—OH on the substrate carbonyl, with concomitant hydride transfer to the Mo=S. (From Hille, 2005. Copyright 2005 with permission from Elsevier.)

THE SULFITE OXIDASES AND DMSO REDUCTASES

Sulfite oxidising enzymes (SOEs) are found in plants, animals, and bacteria. In animals, SO catalyses the oxidation of toxic sulfite to sulfate as the final step in the catabolism of the sulfur-containing amino acids, Met and Cys, and in humans, sulfite oxidase deficiency is an inherited recessive disorder producing severe neonatal neurological problems that lead to early death.² Plant SOs also play an important role in sulfite detoxification and, in addition, serve in the assimilatory reduction of sulfate. Based on their ability to transfer electrons to molecular oxygen, two types of molybdenum-containing SOEs are usually distinguished: sulfite oxidases (SO) that can use molecular oxygen as an electron acceptor and sulfite dehydrogenases (SDH) that use other electron acceptors such as cytochrome *c*. Sulfite occurs naturally in the environment, and due to its highly reactive nature, the sulfite anion can react with vital cell components such as DNA and proteins. Therefore, both pro- and eukaryotic cells that can become exposed to externally or internally generated sulfite need to be able to detoxify it efficiently, which can occur either via reduction to the level of sulfur or sulfide, or, more commonly by oxidation to sulfate.

The structure of chicken sulfite oxidase is shown in Figure 17.7(b). The Mo domain (in blue) is some 36 Å from the haem *b* domain (in red) to which it is tethered by a flexible 13 residue peptide, which appears to be important in docking the two domains for electron transfer. The proposed catalytic mechanism of SO involves two intramolecular one-electron transfer (IET) steps from the Mo-cofactor to the iron of the integral *b*-type haem. A similar mechanism is proposed for SDH, involving its Mo-cofactor and *c*-type haem. However, PSO, which lacks an integral haem cofactor, uses molecular oxygen as its electron acceptor. The oxo-transfer chemistry of molybdenum in sulfite oxidase is probably the best characterised, in terms of synthetic models, structural, and mechanistic data, of all the metals we have described up till now. The reaction cycle (Figure 17.8) starts with the enzyme in the fully oxidised, resting Mo^{VI}/Fe^{III} state, with both metal centres oxidised. Binding of sulfite to the oxidised Mo^{VI} is followed by the primary oxo-transfer reaction, which involves direct atom transfer between the substrate and the metal centre via a covalently bound intermediate. The metal centre is then reduced in two successive one-electron steps. One of the major difficulties of synthetic model compounds was to prevent the usually irreversible μ -oxo dimerisation reaction between Mo^{VI}O₂ and Mo^{IV}O centres to form the stable dinuclear Mo^VO species with an [Mo₂O₃]⁴⁺ core (which can be easily avoided in the enzymatic systems).

Structures of representative Mo- and W-containing enzymes are presented in Figure 17.7. The structure of the DMSO reductase from *Rhodobacter sphaeroides* is given in Figure 17.7(c). In the DMSO reductase family, the metal centre is bound to two molecules of the cofactor. DMSO reductase itself catalyses the reduction of dimethyl sulfoxide to dimethylsulfide with incorporation of the oxygen atom of DMSO into water. The active site of the

2. In 2010, a baby girl was diagnosed with molybdenum cofactor deficiency at 6 days old. After treatment with purified cyclic pyranopterin monophosphate (cPMP), the precursor of MoCo whose synthesis was defective, starting at 36 days old, all urinary metabolites of sulfite oxidase and xanthine oxidase deficiency returned to almost normal values and has remained constant for more than one year.

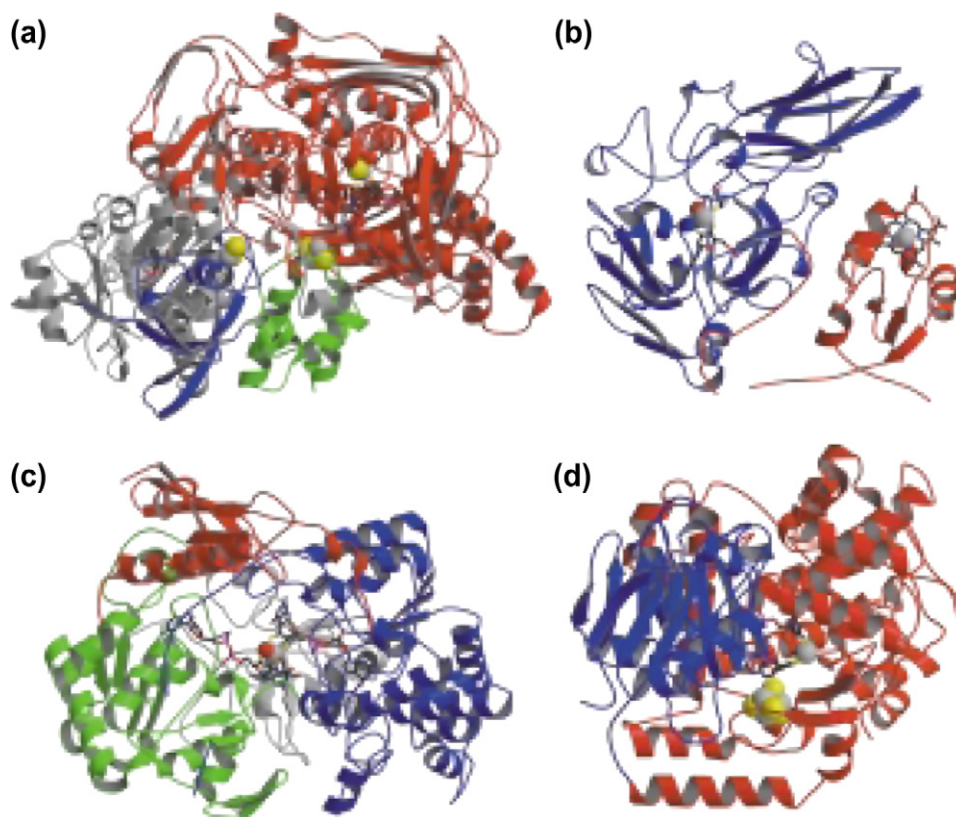


FIGURE 17.7 Structures of representative Mo- and W-containing enzymes. (a) Bovine xanthine oxidase, (b) chicken sulfite oxidase, (c) dimethyl sulfoxide (DMSO) reductase from *Rhodobacter sphaeroides*, and (d) formaldehyde-ferredoxin oxidoreductase from *Pyrococcus furiosus*. For xanthine oxidase (a), the domains are indicated as follows (from the N-terminus): blue and green, [2Fe-2S]; gray, FAD; red, Mo. The Mo centre sits at the interface of two subdomains and is rendered in CPK, with the metal in gray. The [2Fe-2S] centres are rendered in space-filling mode, the FAD and pterin as colour coded in CPK. For sulfite oxidase (b), the haem domain is in red and the Mo domain in blue; each redox-active centre is rendered in CPK with metals shown in gray. For DMSO reductase (c), which possesses only a Mo centre the four identifiable domains of the protein fold are rendered in green, blue, red and gray (the last at the rear of the structure as shown). The two pterin cofactors are rendered in CPK and the Mo in gray. For the W-containing formaldehyde-ferredoxin oxidoreductase (d), the identifiable domains are shown in red, green and blue, with the W centre rendered in CPK (with the W in gray) and the [4Fe-4S] cluster in space-filling mode. In all cases, only one subunit of the oligomeric enzymes is shown. (From Hille, 2002. Copyright 2002 with permission from Elsevier.)

oxidised enzyme is an $L_2Mo^{VI}O(O-Ser)$ centre, which, upon reduction, loses the $M=O$ ligand to give a $L_2Mo^{IV}(O-Ser)$ centre. In the catalytic mechanism (Figure 17.9), the reduced enzyme $L_2Mo^{IV}(O-Ser)$ reacts with DMSO to give the oxidised form $L_2Mo^{VI}O(O-Ser)$ of the enzyme with the oxygen of the DMSO now incorporated into the $M=O$ group of the oxidised enzyme. In the second phase of the catalytic mechanism, the oxidised enzyme is reduced by a cytochrome to release the oxygen derived from DMSO as water (this reaction can also be carried out by a water-soluble phosphine R_3P to give the phosphine oxide $R_3P=O$).

Tungsten Enzymes

As mentioned above, tungsten enzymes are found in place of molybdenum enzymes in thermophilic bacteria and hyperthermophilic archaeobacteria. Like the molybdenum enzymes, they can be classified into three broad families, all of which contain two pterin cofactor molecules per Mo. In this respect, they are similar to the DMSO reductase

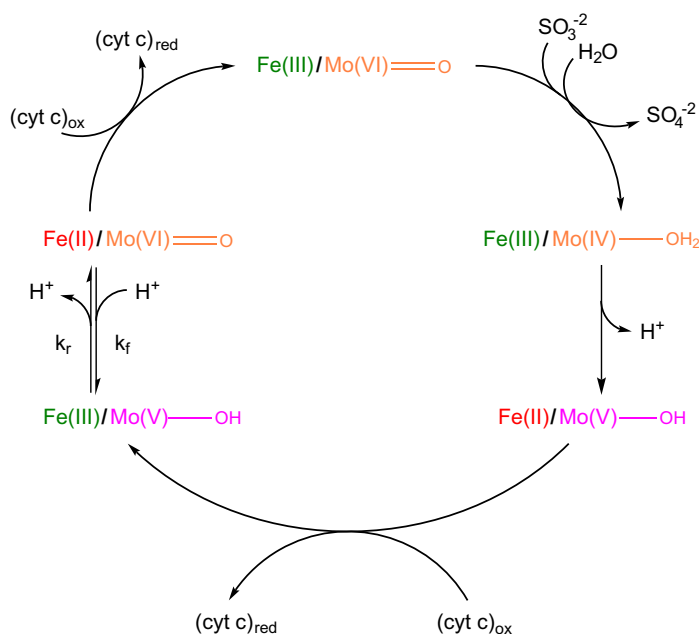


FIGURE 17.8 Proposed oxidation-state changes occurring at the Mo and Fe centres of animal SO during the catalytic oxidation of sulfite and the concomitant reduction of (cyt c)_{ox}. (Adapted from Johnson-Winters, Tollin, & Enemark, 2010.)

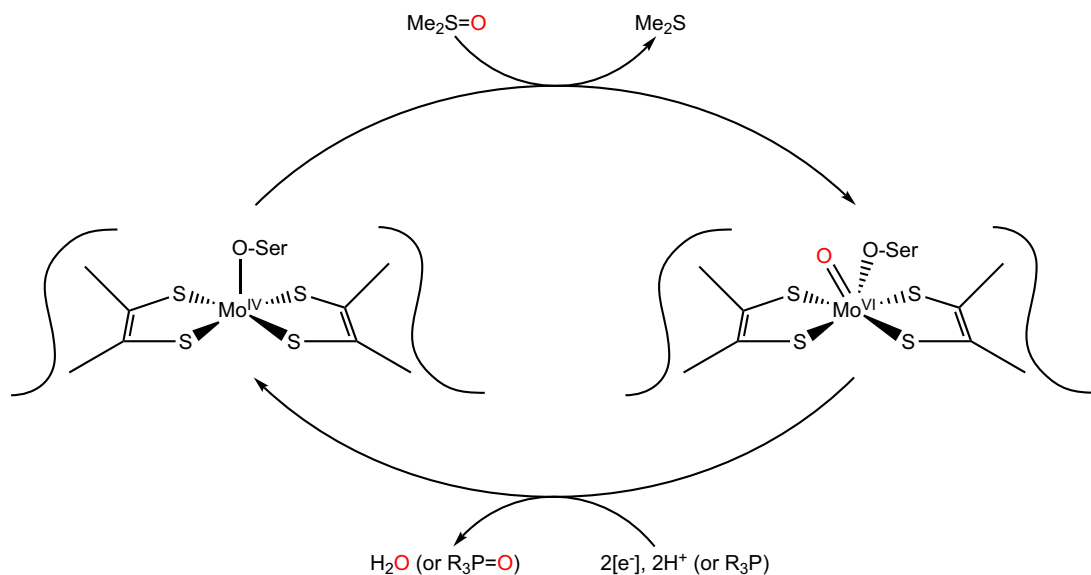


FIGURE 17.9 The catalytic cycle of dimethyl sulfoxide (DMSO) reductase. A minimal catalytic cycle for DMSO reductase involves the reaction of a reduced $\text{L}_2\text{MoIV(OR)}$ enzyme (left) with DMSO ($\text{Me}_2\text{S=O}$) to give the oxidised $\text{L}_2\text{MoVIO(OR)}$ enzyme (right). The oxidised enzyme is subsequently reduced by reaction with either a cytochrome or a water-soluble phosphine (R_3P) to give the phosphine oxide $\text{R}_3\text{P=O}$. The transfer of an oxygen atom during this reaction is indicated by the passage of label (red) from the DMSO source. (Adapted from Hille, 2002.)

family of Mo enzymes. The structure of the formaldehyde–ferredoxin oxidoreductase from *Pyrococcus furiosus* is shown in Figure 17.7(d). Members of the first two families catalyse redox reactions. The first, the aldehyde oxidoreductase family, catalyses the oxidation of aldehydes to carboxylic acids. The reducing equivalents are transferred to a [4Fe–4S] centre. While there is still some ambiguity, it is likely that, in addition to the four ligands from the cofactor, the oxidised enzyme contains the group $W^{VI}O(OH)$ (Figure 17.10): the reduced form probably

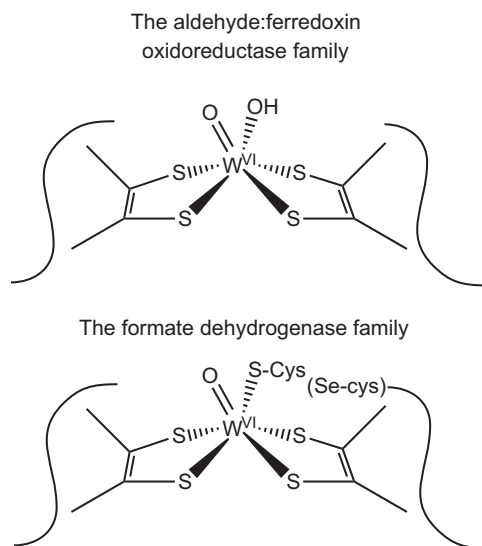


FIGURE 17.10 Active site structures of W-containing enzymes. (Adapted from Hille, 2002.)

has a single $W^{IV}-OH$. As in the xanthine oxidase family of Mo enzymes, there appear to be no ligands contributed by the protein. The second family consists of enzymes which function to reductively fix CO_2 . They have amino acid sequence homologies with the DMSO reductase family of Mo enzymes, with cysteine or selenocysteine as a ligand from the protein coordinating the metal in the oxidised enzyme as $L_2W^{VI}OX$ (Figure 17.10). The third family, with only one member, is made up by acetylene hydratase, which adds water to the double bond of acetylene forming acetaldehyde. Although it contains a [4Fe–4S] centre, this does not appear to participate directly in the catalysis, unlike the situation in aconitase (Chapter 13). Instead, it seems from model studies and observation that the enzyme as isolated, requires activation by a strong reductant, and that the catalysis of acetylene hydration involves the participation of a W^{IV} site.

A number of organisms appear to be able to use either molybdenum or tungsten, as a function of their bio-availability, as mentioned earlier.

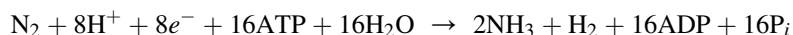
Nitrogenases

In the biological nitrogen cycle (Chapter 18), an important role is played by a relatively limited number of anaerobic microorganisms capable of converting about one-third of atmospheric dinitrogen into ammonia, which can subsequently be incorporated into glutamate and glutamine, and from there into other nitrogen containing molecules. This represents about 10^8 tons/year, about the same as is produced by the Haber–Bosch industrial process — albeit that the latter functions at both high pressures (150–350 atm) and high temperatures (350–550 °C). The microorganisms which fix nitrogen include the bacterium *Rhizobium*, involved in the symbiotic fixation of nitrogen in the root nodules of leguminous plants. Since this enzyme is extremely

sensitive to oxygen,³ the plant roots produce a haemoglobin with a high affinity for oxygen, leghaemoglobin (like haemoglobins from insect larvae or lamprey, it has the classic ‘globin fold’ found in mammalian haemoglobins and myoglobins — see Chapter 3), which maintains an anerobic environment around the enzyme (Downie, 2005).

All nitrogenases consist of two types of subunit, one of which contains a special Fe—S cluster, known as the P-cluster, and a second, which contains an iron and sulfur-containing cofactor which includes a different metal. This metal is usually Mo, hence, the cofactor is known as FeMoCo. However in some species, and under conditions of particular metal bio-availability, Mo can be replaced by V or even by Fe. When Mo levels are low and V is available, these “alternative” nitrogenases contain V. When both Mo and V levels are low, a third nitrogenase is produced, which contains only Fe. However, by far the greatest advances in our understanding of the structure and mechanism of nitrogenases have come from studies on the MoFe-nitrogenases from free living nitrogen-fixing bacteria like *Azotobacter*, *Clostridium*, and *Klebsiella*.

The overall reaction catalysed by nitrogenase is



As we can see, the process of nitrogen fixation is extremely energy intensive, requiring both large amounts of ATP and of reducing equivalents. The nitrogenase is made up of two proteins (Figure 17.11), termed the MoFe protein and the Fe protein. The $\alpha_2\beta_2$ heterotetrameric MoFe protein contains both the FeMo-cofactor and the P-cluster, with the functional unit constituted by an $\alpha\beta$ dimer, containing one FeMo-cofactor and one P-cluster. In contrast, the Fe protein is a homodimer, which binds a single [4Fe—4S] cluster at the interface between the two

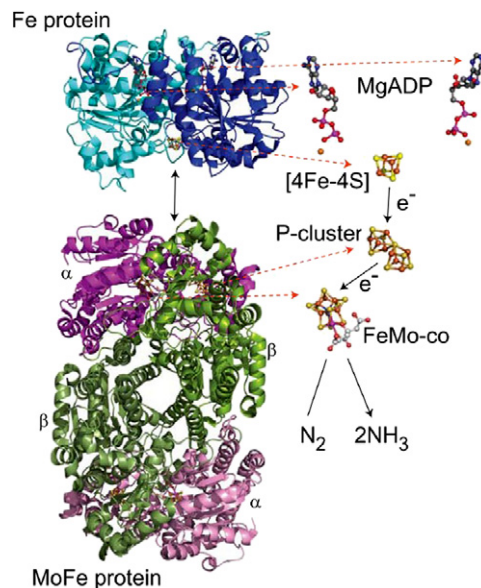


FIGURE 17.11 Structures of the nitrogenase MoFe and Fe proteins. The MoFe protein is an $\alpha_2\beta_2$ tetramer, with the alpha subunits shown in magenta and the beta subunits shown in green. The Fe protein is a γ_2 dimer, with each subunit shown in blue. A MoFe protein binds two Fe proteins, with each $\alpha\beta$ unit being a catalytic unit. One Fe protein is shown associating with one $\alpha\beta$ -unit of the MoFe protein. The relative positions and structures of two bound MgADP molecules, the Fe protein [4Fe—4S] cluster, and MoFe protein P-cluster (8Fe-7S), and FeMo-cofactor (7Fe-Mo-9S-homocitrate-X) are shown. Each is highlighted to the right. The flow of electrons is from the [4Fe—4S] cluster to the P-cluster to the FeMo-cofactor. The element colour scheme is C gray, O red, N blue, Fe rust, S yellow, and Mo magenta. Structures from PDB files 1M1N for the MoFe protein and 1FP6 for the Fe protein. (From Seefeldt, Hoffman, & Dean, 2009. Copyright 2009, with permission from Annual reviews, Inc.)

3. All known nitrogenases are irreversibly inhibited by molecular oxygen. So, if you cut into the root nodules of a common legume like pea or bean, you will see that it has a blood-red colour due to the high levels of leghaemoglobin.

subunits. Unlike many other multiple electron transfer reactions in biochemistry, each individual electron transfer between the Fe-protein and the MoFe protein requires the binding and hydrolysis of at least two ATP molecules. The catalytic cycles of the Fe-protein and the MoFe protein are presented in Figure 17.12. In the first of the

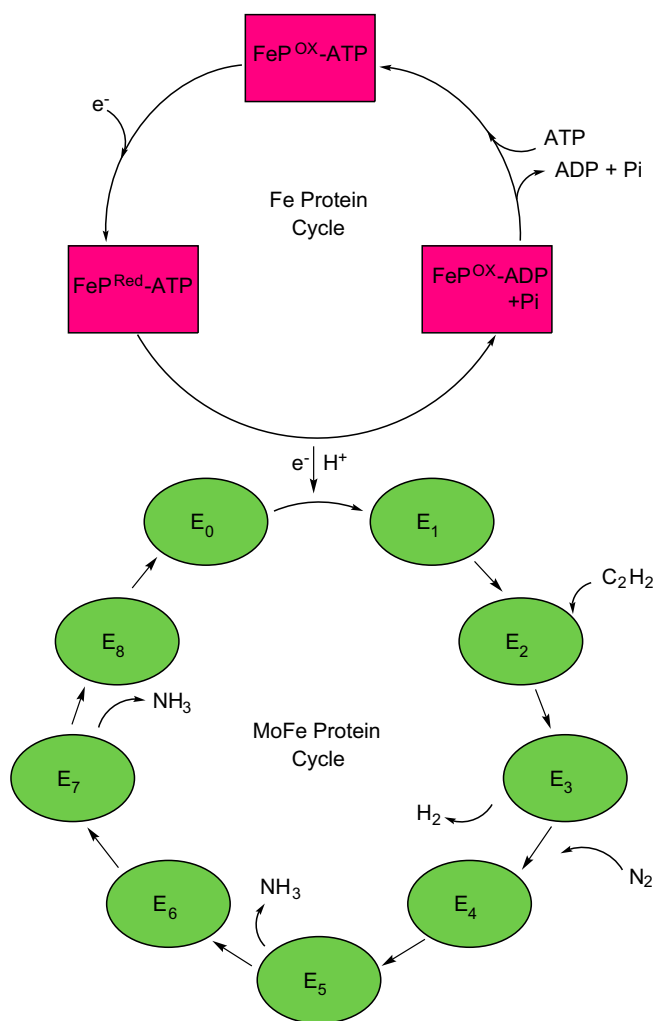
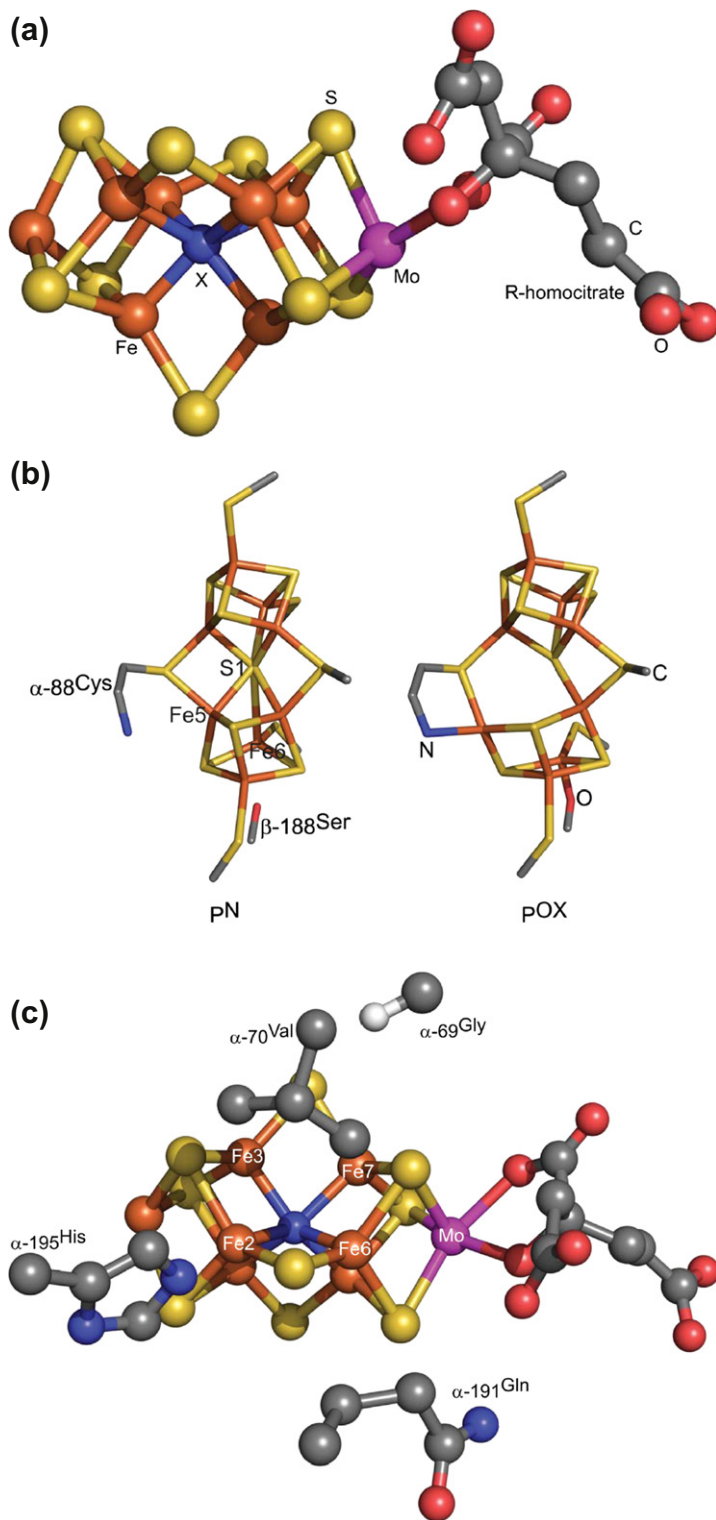


FIGURE 17.12 Fe and MoFe protein catalytic cycles. Shown is a three-state cycle for the Fe protein (top) and an eight-state cycle for the MoFe protein (bottom). For the Fe protein (abbreviated FeP), the $[4\text{Fe}-4\text{S}]$ cluster can exist in the +1 reduced state (Red) or the 2+ oxidised state (Ox). The Fe protein either has two MgATP molecules bound (ATP) or two MgADP with two P_i ($\text{ADP} + \text{P}_i$). The exchange of an electron occurs upon association of the Fe protein with the MoFe protein at the bottom of the cycle. In the MoFe protein cycle, the MoFe protein is successively reduced by one electron, with reduced states represented by E_n , where n is the total number of electrons donated by the Fe protein. Acetylene (C_2H_2) is shown binding to E_2 , while N_2 is shown binding to E_3 and E_4 . N_2 binding is accompanied by the displacement of H_2 . The two ammonia molecules are shown being liberated from later E states. (Adapted from Seefeldt *et al.*, 2009.)

three-state cycle of the Fe protein, the reduced Fe protein ($[4\text{Fe}-4\text{S}]^{1+}$), with two MgATP molecules bound, associates transiently with the MoFe protein. The two MgATP molecules are hydrolysed and a single electron is transferred from the Fe protein $[4\text{Fe}-4\text{S}]$ cluster to the MoFe protein. The oxidised Fe protein ($[4\text{Fe}-4\text{S}]^{2+}$) with two bound MgADP molecules then dissociates from the MoFe protein. This is the overall rate-limiting step for nitrogenase catalysis. The released Fe protein is then regenerated in two steps. The MgADP molecules are



replaced by MgATP, and the $[4\text{Fe}-4\text{S}]^{2+}$ cluster is reduced back to the 1+ oxidation state. Repetition of this cycle of association, reduction, ATP hydrolysis, and dissociation transfers one electron at a time to the MoFe protein. In the eight-state MoFe protein cycle, the MoFe protein is reduced successively by one electron, with the eight states represented by E_n . Usually, when 8 reducing equivalents have been accumulated, and 16 molecules of ATP hydrolysed, the enzyme can bind and reduce the very stable triple bond of a dinitrogen molecule to two molecules of ammonia. Concomitantly, two protons and two electrons are converted to gaseous hydrogen. Electrons derived from photosynthesis or from the mitochondrial electron transport chain are transferred to the Fe-protein.

The structure of both the MoFe-cofactor and of the P-cluster became apparent when the structures of nitrogenases were determined by high-resolution X-ray crystallography. The MoFe-cofactor (Figure 17.13a) consists of a $[4\text{Fe}-3\text{S}]$ cluster connected to a $[3\text{Fe}-\text{Mo}-3\text{S}]$ cluster by a previously undetected central atom (possibly a nitrogen) at one corner and three bridging inorganic sulfides. (R)-homocitrate is coordinated to the Mo atom through its 2-hydroxy and 2-carboxyl groups. The MoFe-cofactor is linked to the protein by only two residues, Cys $\alpha 273$ and His $\alpha 442$, which coordinate Fe1 and the Mo atom respectively, at opposite ends of the extended cluster. This is in marked contrast to other iron-sulfur clusters, which typically have one protein side-chain ligand per metal ion. In order to complete the coordination sphere of the eight metal centres, there are a number of additional inorganic sulfides together with bidentate coordination of the Mo atom to a molecule of homocitrate,⁴ completing its octahedral coordination.

In the dithionite-reduced state (Figure 17.13(b)) P^N , the P-cluster can be considered as two $[4\text{Fe}-3\text{S}]$ clusters bridged by a hexacoordinate sulfur. In the P^{Ox} state, which is oxidised by two electrons relative to P^N , two of the iron atoms Fe5 and Fe6 have moved away from the central sulfur atom, and are now coordinated by the amide nitrogen of Cys $\alpha 87$ and the hydroxyl of Ser $\alpha 186$, maintaining the irons in a four-coordinate state.

The Fe-protein has the protein fold and nucleotide-binding domain of the G protein family of nucleotide-dependent switch proteins, which are able to change their conformation dependent on whether a nucleoside diphosphate (like GDP or ADP) is bound instead of the corresponding triphosphate (GTP or ATP). However, nucleotide analogues which induce the conformational switch of the Fe-protein do not allow substrate reduction by the MoFe protein, nor does reduction of the MoFe protein by other electron transfer reagents (whether small proteins or redox dyes) drive substrate reduction. Only the Fe-protein can reduce the MoFe protein to a level that allows it to reduce substrates like nitrogen.

Electrons arriving at the Fe-protein are transferred to the P-cluster and from there to the MoFe protein, which is the site of interaction with dinitrogen or any of the other substrates which are reduced by nitrogenase. The redox chemistry of nitrogen reduction, on the basis of model reactions first proposed by Chatt, involves nitrogenous species at the level of diazene (N_2H_2) and hydrazine (N_2H_4) before the final release of two molecules of ammonia. Recent evidence for a diazene-derived species bound to the FeMo-cofactor supports this view, as does evidence that hydrazine (N_2H_4) is a substrate for nitrogenase. A binding site for N_2 and for alkyne substrates has been localised on the iron-sulfur face of the FeMo-cofactor defined by the Fe atoms 2, 3, 6, and 7 (Figure 17.13(c)), and ENDOR spectroscopy has shown that the alkene product of alkyne reduction is probably bound end-on to a single Fe atom of the FeMo-cofactor.

A starting point for the nitrogenase reaction pathway can be proposed from the mechanisms of N_2 reduction catalysed by organometallic complexes. A series of model studies initiated in the early 1960s by the groups of Chatt

FIGURE 17.13 (a) Structure of the FeMo-cofactor of nitrogenase. The element colours are as described in the legend to Figure 11. (b) P-cluster structures. Shown are the structures of the P-cluster $[8\text{Fe}-7\text{S}]$ in the oxidised (P^{Ox}) and reduced (P^N) states. MoFe protein amino acid ligands are also shown with β -188^{Ser} and α -88^{Cys} labelled. The central S atom is labelled S1. The PDB files used were 2MIN for the P^{Ox} state and 3MIN for the P^N state. (c) Substrate binding location on FeMo-cofactor. Shown is the FeMo-cofactor with Fe atoms 2, 3, 6, and 7 labelled. The view is from the top looking down on the Fe face that binds substrates. Carbon alpha and the side chain are shown for α -69^{Gly}, α -70^{Val}, α -195^{His}, and α -191^{Gln}. PDB file 1M1N. (From Seefeldt et al., 2009. Copyright 2009, with permission from Annual reviews, Inc.)

4. A homologue of citrate (see Chapter 5) with an additional CH_2 group.

and Hidai (Chatt, 1978; Hidai, 1999) demonstrated that dinitrogen could be bound and reduced to ammonia at a single metal centre by Mo and W complexes. However, although examples of virtually all of the proposed intermediates in a “Chatt” cycle were isolated, no catalytic reduction of N_2 to NH_3 was ever achieved. Catalytic reduction of dinitrogen to ammonia at a single molybdenum centre has now been achieved by the group of Richard R. Schrock⁵ using the HITP [3,5-(2,4,6-*i*-Pr₃C₆H₂)₂C₆H₃] ligand (Yandulov and Schrock, 2003; Schrock, 2005). The essential intermediates in the Chatt mechanism for N_2 reduction on a mononuclear Mo metal complex as elaborated with the recent observation of catalytic reduction by Mo complexes by the Schrock group are shown in Figure 17.14 (left). N_2

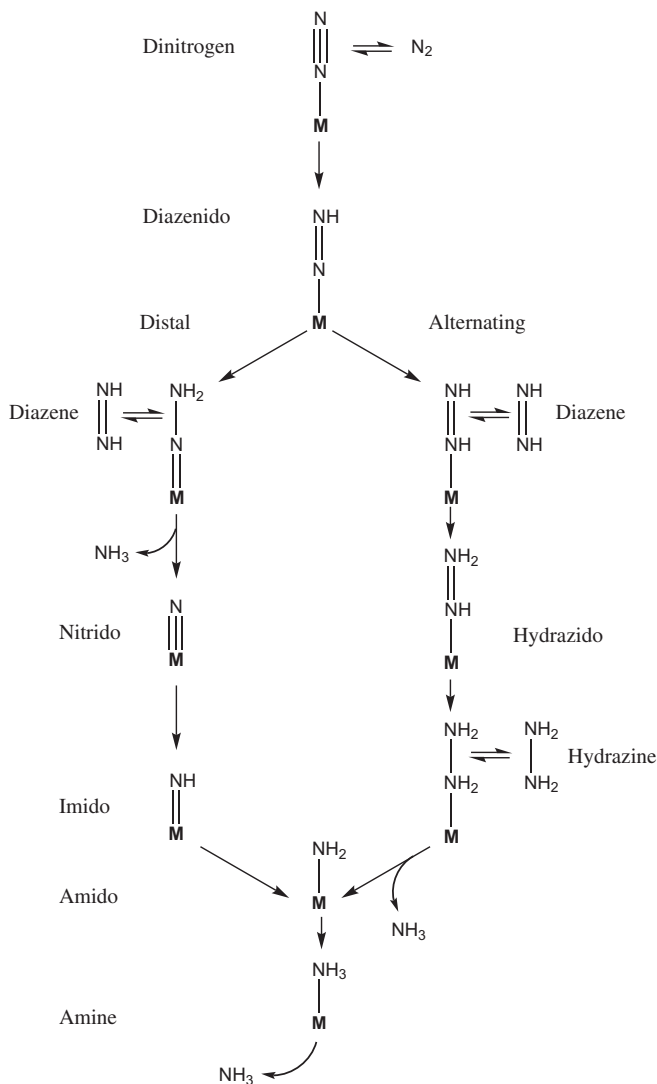


FIGURE 17.14 Possible reaction mechanisms for nitrogenase. Shown are two possible reaction mechanisms for nitrogenase. On the left is shown the distal mechanism and on the right the alternating mechanism. FeMo-cofactor is abbreviated as M and the names of different bound states are shown. Possible points of entry for diazene and hydrazine are shown. (Adapted from Seefeldt et al., 2009.)

5. Who shared the 2005 Nobel prize in chemistry with R.H. Grubbs and Y. Chauvin.

is bound to Mo (represented as M) followed by stepwise reduction and proton addition, with each intermediate remaining bound to the metal. N_2 is successively hydrogenated at a single ('distal') N until the N—N bond is cleaved after the addition of $3 e^-/H^+$, with release of the first ammonia. The second ammonia is released following further reduction of the bound nitrido species by $3 e^-/H^+$. This has been denoted the distal (D) pathway because as drawn, the distal N atom is protonated first and also released first as NH_3 . In an alternative reaction pathway for nitrogenase (Figure 17.14, right), the two N atoms are reduced alternately, with cleavage of the N—N bond occurring only later in the reaction. While both pathways involve the stepwise reduction of the N_2 bound to a metal, the alternating one provides for the addition of protons to both N atoms in turn, delaying cleavage of the N—N bond and release of the first ammonia molecule until after the addition of $5 e^-/H^+$.

The catalytic reduction of the dinitrogen triple bond by single-site metal nitrogen intermediates raises the question of why Nature goes to the trouble of using the complex 7Fe:9S:Mo:homocitrate cluster of the FeMo-cofactor in biological nitrogen fixation. One might have expected that a simpler one- or two-metal centre for nitrogen fixation would have been dominant in evolution if it had been biologically functional. Yet, over more than a billion years, evolutionary pressures have retained this complex cofactor-based nitrogenase system, despite the requirement for the unusual metabolite, homocitrate, and at least twenty additional proteins for its assembly and insertion. Indeed, even the "alternative" nitrogenases are thought to be minor variations on the cofactor, with V or Fe replacing Mo. As Howard and Rees (2006) pointed out at the end of their overview of biological nitrogen fixation, entitled "How many metals does it take to fix N_2 ?", (the number of metal atoms required is 20, corresponding to the metal composition of the FeMo-cofactor, the P-cluster, and the Fe protein) — they all seem to be required, and to date no one has found a way to simplify the system. Perhaps, after all, this simply underlines the Jeremy Knowles affirmation⁶ '*enzyme catalysis — not different, just better!*'.

Vanadium

Vanadium is beneficial and possibly essential for humans. It is certainly essential for a number of other organisms. Vanadate (oxidation state V) and its derivatives are phosphate analogues, showing both ground state and transition state analogy (both structural and electronic) with phosphorus compounds. The analogy of five-coordinate vanadium compounds with the transition state of phosphate ester hydrolysis is well documented and explains why so many vanadium compounds are potent inhibitors of phosphatases, ribonucleases, and ATPases.

Haloperoxidases represent the first, and best characterised class of vanadium enzymes, capable of catalysing the two electron oxidation of a halide by hydrogen peroxide (Butler and Carter-Franklin, 2004). The chloroperoxidases, found in many algae, in seaweed, lichens and fungi, can oxidise both Cl^- and Br^- , whereas bromoperoxidases, found in many marine extracts, can only oxidise Br^- . The X-ray structures of a number of vanadate-dependent haloperoxidases have been reported, and in Figure 17.15, the X-ray structure and the active site of the vanadium site of bromo-peroxidase from the marine algae *C. pilulifera* is shown. On the basis of spectroscopic evidence, it is now thought that the oxidation state of the vanadium remains at V throughout catalysis, and that the mechanism for both types of vanadium haloperoxidases are the same, as indicated in Figure 17.16. The reaction proceeds by the initial binding of H_2O_2 followed by protonation of bound peroxide and addition of the halide. NMR spectroscopy confirms the presence of the VO_2-O_2 and there is no evidence for direct binding of halide to the vanadium ion. The rate-limiting step in the catalysis is the nucleophilic attack of the halide on the protonated protein—peroxide complex, generating an " X^{+} " species, which reacts directly with organic substrates (RH) to halogenate them (RX). In the absence of RH, this step will generate singlet oxygen.

The halide specificity of vanadium-dependent bromoperoxidase from *C. pilulifera* has been changed by the single amino acid substitution of Arg 379 by either Trp or Phe (Ohshiro et al., 2004). Both mutant enzymes R379W and R379F showed significant chloroperoxidase, as well as bromoperoxidase activity, supporting the existence of a specific halogen binding site within the catalytic cleft of vanadium haloperoxidases.

6. Attributed to the Amory Houghton Professor of Chemistry and Biochemistry at Harvard University, Jeremy R. Knowles.

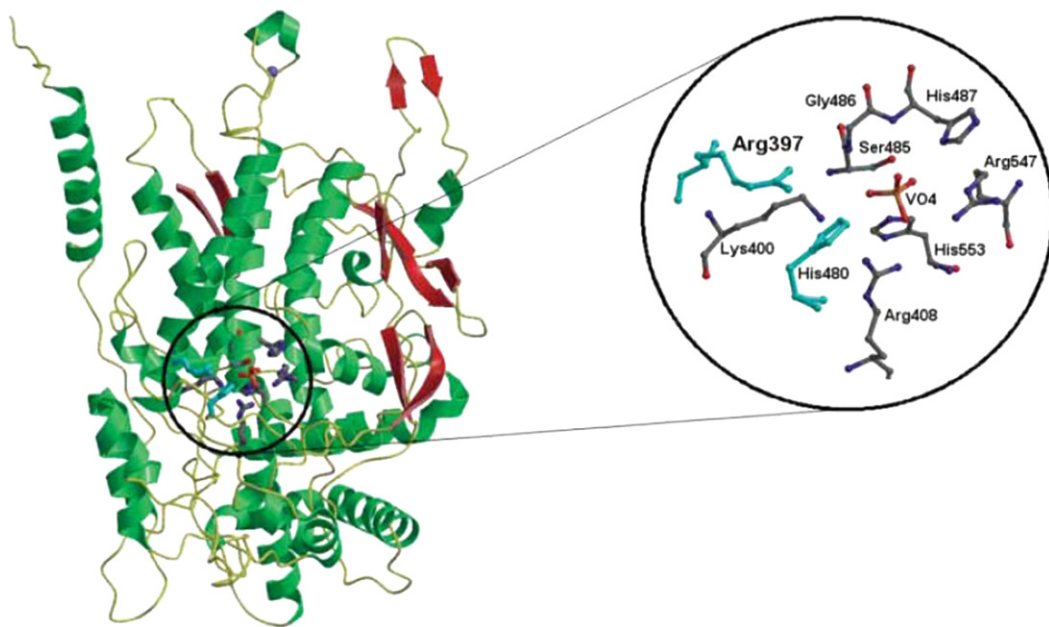


FIGURE 17.15 The structure and active site of the bromoperoxidase subunit from *C. pilulifera*. Residues conserved in all vanadium bromo- and chloroperoxidases are in gray, those that vary in cyan. (From Ohshiro *et al.*, 2004. Copyright 2004 The Protein Society.)

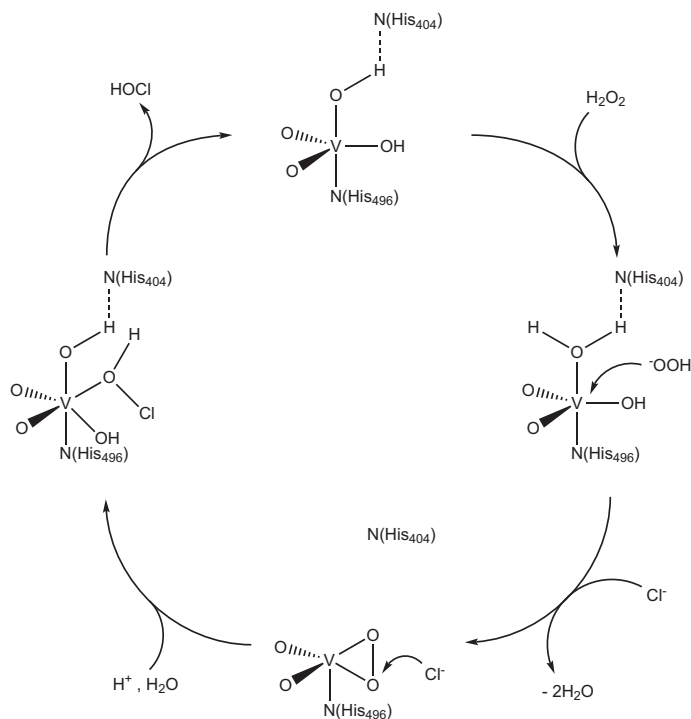


FIGURE 17.16 Proposed mechanism for the vanadium chloroperoxidase oxidation of chloride by hydrogen peroxide. (Adapted from Ligtenbarg, Hage, & Feringa, 2003.)

It is interesting to point out that the amino acid sequence and structure of the active site of vanadium haloperoxidases is conserved within several families of phosphatases, with conservation of the amino acids involved in vanadate binding in the one and phosphate binding in the other.

Information, particularly structural, concerning vanadium-dependent nitrogenases, is relatively limited. The consensus is that they resemble the molybdenum nitrogenase in most aspects, except for the presence of a FeV cofactor, and they will not be discussed further.

High levels of vanadium are found in the mushroom *Amanita muscaria* and in marine tunicates (sea-squirts). In the former organism, a siderophore-like ligand which binds vanadium(IV) called amavidine is found. Amavidine is a metal complex containing one equivalent of vanadium and two equivalents of the ligand S,S-2,2'-hydroxyiminopropionic acid (Figure 17.17). The complex is very stable to hydrolysis, and has reversible one-electron redox properties, suggestive of a possible role in biology as a one-electron redox mediator.

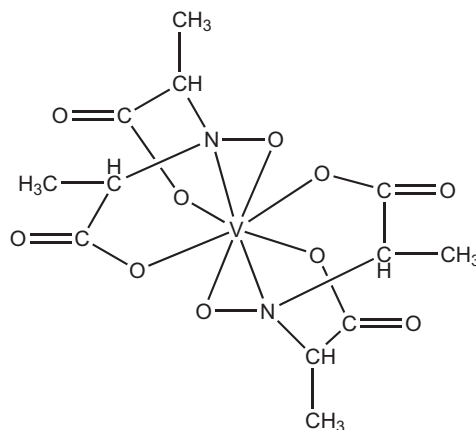


FIGURE 17.17 Structure of amavidine.

Vanadium, as VOSO_4 , has been found to interfere with siderophore-mediated iron transport in bacteria and plants. This seems to imply that vanadium can be transported by siderophores, and a number of studies focussing on applications of hydroxamate V-complexes in biology have been initiated.

Tunicates (ascidians or sea-squirts) are invertebrate marine organisms which can accumulate vanadium at concentrations approaching 350 mM (the concentration of vanadium in seawater is ~ 35 nM!). This vanadium is taken up as V(V) from seawater (Figure 17.18), reduced to oxidation state III or IV and stored in a soluble form in the blood cells within very acidic vacuoles at concentrations a million fold higher than in their external surroundings. Vanadium seems to be bound in the cytoplasm to vanadium binding proteins (vanabins, of molecular weights 12–16 kD). However, the precise role of vanadium in these marine organisms remains unknown. A V transporter of the DMT1 family of membrane metal transporters has been recently cloned from an ascidian (Ueki, Furano, & Michibata, 2011).

Finally, we briefly consider the insulin-like effect of vanadium compounds. As was pointed out in Chapter 5, the regulation of intermediary metabolism is a very complex phenomenon, and there are few examples less complicated than the action of insulin, which through interaction with its receptor in a large number of target tissues initiates a series of signalling cascades, which affect carbohydrate and lipid metabolism, but also have many other metabolic repercussions. Vanadium compounds have been shown to enhance the effect of insulin by stimulating the phosphorylation of the insulin receptor (*in vitro*!) and inhibiting protein phosphatases. They also seem, particularly in the case of the vanadyl cation, to bind to transferrin, thereby facilitating their entry into cells

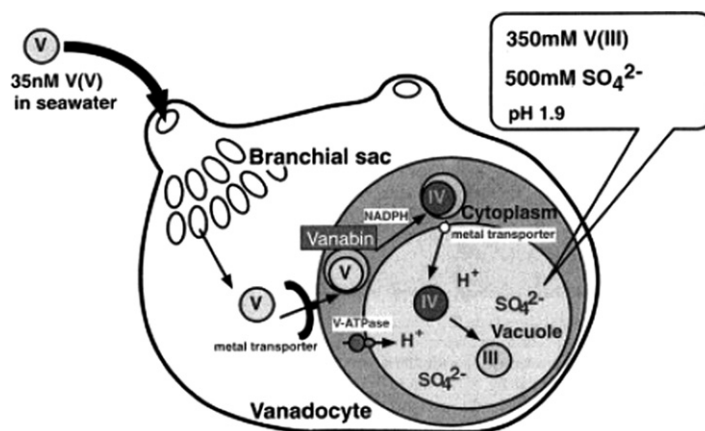


FIGURE 17.18 Model of the pathway for reduction and accumulation of vanadium in ascidian vanadocytes. (From Michibata, Yamaguchi, Uyama, & Ueki, 2003. Copyright 2003 with permission from Elsevier.)

via the transferrin/transferrin receptor pathway (although how they dissociate from the receptor inside the cell remains unclear). They may also influence the redox balance of cells, interacting with the glutathione system. However, despite their potential beneficial effects, failure to bring the use of vanadium salts into therapeutic practice is due on the one hand to their toxicity, and on the other to their limited window of therapeutic action — while they may target some parts of the complex insulin signalling cascade, they cannot exert the exquisite specificity of the natural hormone both to activate, and to ensure the extinction of its activation cascade once its objectives have been achieved.

Chromium

As was pointed out in Chapter 1, chromium has become immensely popular as a nutritional supplement, for promotion of muscle development, and as a weight-loss agent (Vincent, 2003, 2004), second only to calcium as a mineral supplement (Nielsen, 1996). However, while there are indications that Cr administration may be useful as an adjuvant therapy in type 2 diabetes as well as in the regulation of diabetes during pregnancy, the precise biochemical mode of action of chromium remains unclear (Lau et al., 2008). The biologically relevant form, the trivalent Cr^{3+} ion, seems to be required for proper carbohydrate and lipid metabolism in mammals. However, chromium deficiency is difficult to achieve. It has recently been reported that a diet with as little Cr as was reasonably possible to achieve had no effect on body composition, glucose metabolism, or insulin, when compared to a Cr “sufficient” diet. The authors, who include the principal protagonist of Cr essentiality over the last decade, conclude that, ‘together with the results of other recent studies these results clearly indicate that chromium can no longer be considered an essential element’ (Di Bona, 2011).

No Cr-dependent enzymes or Cr-binding proteins have been identified to date. However, one chromium-binding peptide, chromodulin, with the putative sequence pEEEEGDD (where pE is pyroglutamate) has been characterised (Chen, Watson, Gao, Sinha, Cassady, & Vincent, 2011), and found to bind 4 chromic ions per peptide. It is proposed that the chromium-loaded chromodulin may function in the amplification system for insulin signalling (Vincent, 2000b) for transporting Cr^{3+} to tissues in an insulin-responsive manner.

While there are obvious similarities between both the name, and the proposed mechanism of action of chromodulin and the Ca^{2+} -binding protein calmodulin, much remains to be done to establish unequivocally the mechanism of chromodulin action at the molecular level, and I personally remain extremely sceptical regarding the reputedly magical properties of dietary supplementation with chromium.

REFERENCES

- Brondino, C. D., Romao, M. J., Moura, I., & Moura, J. J. G. (2006). Molybdenum and tungsten enzymes: the xanthine oxidase family. *Current Opinion in Chemical Biology*, 10, 109–114.
- Butler, A., & Carter-Franklin, J. N. (2004). The role of vanadium bromoperoxidase in the biosynthesis of halogenated marine natural products. *Natural Product Reports*, 21, 180–188.
- Chatt, J., Dilworth, J. R., & Richards, R. L. (1978). Recent advances in the chemistry of nitrogen fixation. *Chemical Reviews*, 78, 589–625.
- Chen, Y., Watson, H. M., Gao, J., Sinha, S. H., Cassady, C. J., & Vincent, J. B. (2011). Characterization of the organic component of low-molecular-weight chromium-binding substance and its binding of chromium. *Journal of Nutrition*, 141, 1225–1232.
- Crans, D. C., Smees, J. J., Gaidamauskas, E., & Yang, L. (2004). The chemistry and biochemistry of vanadium and the biological activities exerted by vanadium compounds. *Chemical Reviews*, 104, 849–902.
- Di Bona, K. R., Love, S., Rhodes, N. R., McAdory, D., Sinha, S. H., Kern, N., et al. (2011). Chromium is not an essential trace element for mammals: effects of a “low-chromium” diet. *The Journal of Biological Inorganic Chemistry*, 16(3), 381–390.
- Downie, J. A. (2005). Legume haemoglobins: symbiotic nitrogen fixation needs bloody nodules. *Current Biology*, 15, R196–198.
- Enemark, J. H., Cooney, J. J. A., Wang, J.-J., & Holm, R. H. (2004). Synthetic analogues and reaction systems relevant to the molybdenum and tungsten oxotransferases. *Chemical Reviews*, 104, 1175–1200.
- Enroth, C., Eger, B. T., Okamoto, K., Nishino, T., Nishino, T., & Pai, E. F. (2000). Crystal structures of bovine milk xanthine dehydrogenase and xanthine oxidase: structure-based mechanism of conversion. *Proceedings of the National Academy of Sciences of the United States of America*, 97, 10723–10728.
- Hidai, M. (1999). Chemical nitrogen fixation by molybdenum and tungsten complexes. *Coordination Chemistry Reviews*, 185–186, 99–108.
- Hille, R. (2002). Molybdenum and tungsten in biology. *TIBS*, 27, 360–367.
- Hille, R. (2005). Molybdenum-containing hydroxylases. *Archives of Biochemistry and Biophysics*, 433, 107–116.
- Howard, J. B., & Rees, D. C. (2006). How many metals does it take to fix N₂? A mechanistic overview of biological nitrogen fixation. *Proceedings of the National Academy of Sciences of the United States of America*, 103, 17088–17093.
- Johnson-Winters, K., Tollin, G., & Enemark, J. H. (2010). Elucidating the catalytic mechanism of sulfite oxidizing enzymes using structural, spectroscopic, and kinetic analyses. *Biochemistry*, 49, 7242–7254.
- Lau, F. C., Bagchi, M., Sen, C. K., & Bagchi, D. (2008). Nutrigenomic basis of beneficial effects of chromium(III) on obesity and diabetes. *Mol Cell Biochem*, 317, 1–10.
- Ligtenberg, A. G. J., Hage, R., & Feringa, B. L. (2003). Catalytic oxidations by vanadium complexes. *Coordination Chemistry Reviews*, 237, 87–101.
- Mendel, R. R., & Bittner, F. (2006). Cell biology of molybdenum. *Biochimica et Biophysica Acta*, 1763, 621–635.
- Michibata, H., Yamaguchi, N., Uyama, T., & Ueki, T. (2003). Molecular biological approaches to the accumulation and reduction of vanadium by ascidians. *Coordination Chemistry Reviews*, 237, 41–51.
- Nielsen, F. (1996). Controversial chromium: does the superstar mineral of the mountebanks receive appropriate attention from clinicians and nutritionists? *Nutrition Today*, 31, 226–233.
- Ohshiro, T., Littlechild, J., Garcia-Rodriguez, E., Isupov, M. N., Iida, Y., Kobayashi, T., et al. (2004). Modification of halogen specificity of a vanadium-dependent bromoperoxidase. *Protein Science*, 13, 1566–1571.
- Peters, J. W., & Szilagyi, R. K. (2006). Exploring new frontiers of nitrogenase structure and function. *Current Opinion in Chemical Biology*, 10, 101–108.
- Rees, D. C., Tezcan, F. A., Haynes, C. A., Walton, M. Y., Andrade, S., Einsle, O., et al. (2005). Structural basis of biological nitrogen fixation. *The Philosophical Transactions of the Royal Society*, 363, 971–984.
- Schrock, R. R. (2005). Catalytic reduction of dinitrogen to ammonia at a single molybdenum center. *Accounts of Chemical Research*, 38, 955–962.
- Seefeldt, L. C., Hoffman, B. M., & Dean, D. R. (2009). Mechanism of Mo-dependent nitrogenase. *The Annual Review of Biochemistry*, 78, 701–722.
- Ueki, T., Furano, N., & Michibata, H. (2011). A novel vanadium transporter of the Nramp family expressed at the vacuole of vanadium-accumulating cells of the ascidian *Ascidia sydneiensis samea*. *Biochimica et Biophysica Acta*, 1810, 457–464.
- Vincent, J. B. (2000a). The biochemistry of chromium. *The Journal of Nutrition*, 130, 715–718.
- Vincent, J. B. (2000b). Elucidating a biological role for chromium at a molecular level. *Accounts of Chemical Research*, 33, 503–510.
- Vincent, J. B. (2003). The potential value and potential toxicity of chromium picolinate as a nutritional supplement, weight-loss agent and muscle development agent. *Sports Medicine*, 33, 213–230.

- Vincent, J. B. (2004). Recent advances in the nutritional biochemistry of trivalent chromium. *Proceedings of the Nutrition Society*, 63, 41–47.
- Voet, D., & Voet, J. G. (2004). *Biochemistry* (3rd ed). Hoboken: John Wiley and Sons. p. 1591.
- Yandulov, D. V., & Schrock, R. R. (2003). Catalytic reduction of dinitrogen to ammonia at a single molybdenum center. *Science*, 301, 76–78.

Non-metals in Biology

Introduction	343
The Major Biogeochemical Cycles	343

INTRODUCTION

In a departure from the first edition we include here a brief account of selected non-metals and their multiple and various activities in biological systems. We pointed out in Chapter 1 that *organic chemistry is the chemistry of hydrocarbons*, but that if we restricted ourselves to just hydrogen and carbon, it would be impossible to construct the molecules we know to be essential for life as we know it. To construct proteins, nucleic acids, carbohydrates, and lipids, we also need oxygen, nitrogen, phosphorus, and sulfur. Indeed, we also require, as we saw in Chapter 1, a number of other elements, notably a not-inconsiderable number of metals.

We begin this overview of the role of non-metals in biology by focusing on these six essential elements, H, C, N, O, S, and P, which constitute the building blocks of all biological macromolecules. As we will see in the next section, the fluxes of these elements constitute what is called the earth's biogeochemical cycles, that is the pathways by which these chemical elements move through the biotic compartment (the *biosphere*) and the abiotic compartments (the *lithosphere*, the *atmosphere*, and the *hydrosphere*) of the Earth. A good example of such a cycle is the *water cycle*, which is illustrated in [Figure 18.1](#). Water undergoes evaporation, condensation, and precipitation, falling back to the surface of the planet clean and fresh. There are also places where it can be held for long periods of time (reservoirs), which in the case of water are the oceans and lakes, in the ice and snow of the mountains, in the clouds in the atmosphere, and in the ground as ground water storage.

THE MAJOR BIOGEOCHEMICAL CYCLES

We have already pointed out that there are two compartments which constitute the theatre within which the biogeochemical cycles take place, the biotic and the abiotic. Whereas the vast majority of abiotic geochemical reactions are based on acid–base chemistry, the chemistry associated with the biosphere is based on redox reactions. The fluxes of protons and electrons associated with the six major elements, H, C, N, O, S, and P can be combined to construct a global metabolic map of the Earth ([Falkowski, Fenchel, & Delong, 2008](#)). [Figure 18.2](#) presents this generalised model of the biosphere showing the major inputs and outputs of energy and materials. The geochemical (abiotic) transformations are represented by the atmospheric, diagenetic,¹ tectonic, and geothermal compartments, while microbially driven biochemical processes are represented by the biospheric compartment and the sediments. Biological cycling of the elements is not completely closed due to losses through sedimentation of organic carbon and nitrogen, carbonate, metal sulfides, sulfate, and phosphate, and losses to the

1. Diagenesis — the physical and chemical changes occurring in sediment during its deposition and after its compression and transformation into rock.

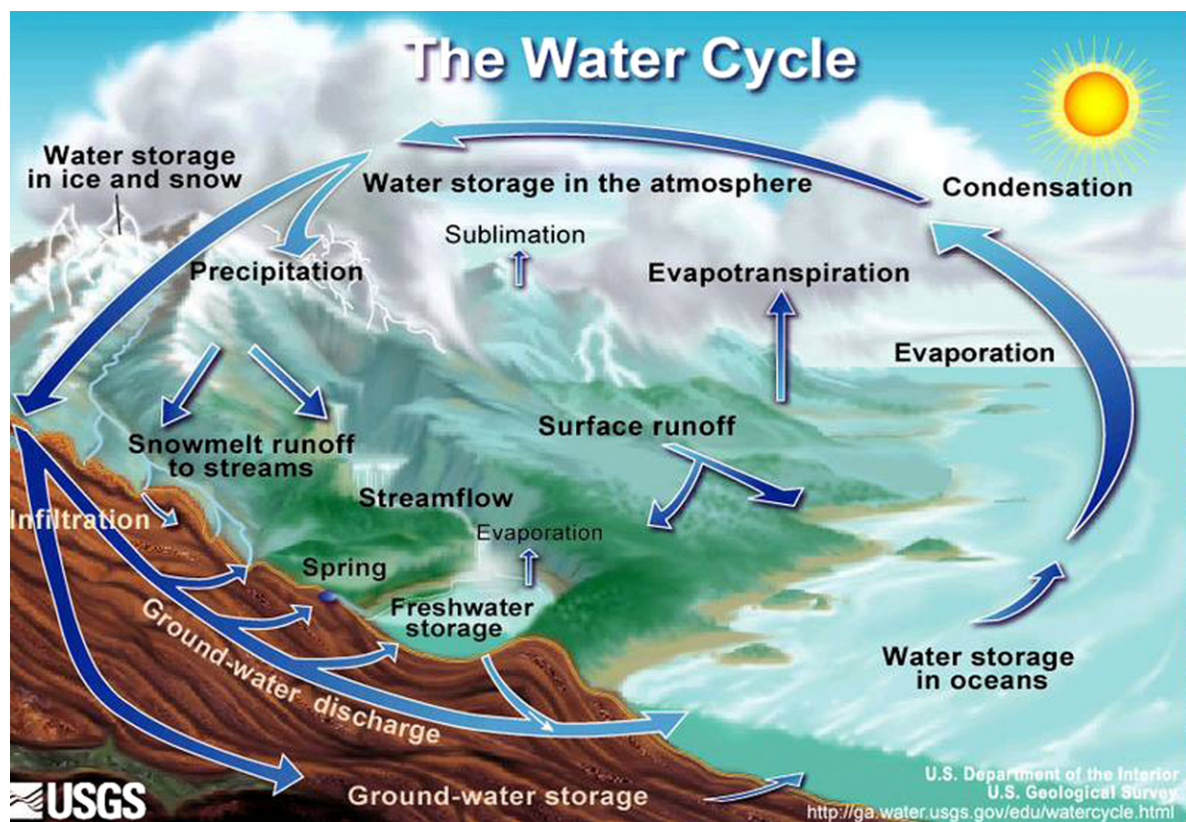


FIGURE 18.1 The water cycle. (Courtesy of the U.S. Geological Survey.)

atmosphere via denitrification. Regeneration of available forms of some of these elements (C, S, and P) is contingent on the geological processes of erosion and geothermal activity.

Carbon, Hydrogen, Oxygen, and Phosphorus

The carbon cycle is perceived by most people as the contrasting yet complementary activities of respiration and photosynthesis. While the first consumes oxygen and generates carbon dioxide, the other carries out the reverse process. This is of course a simplification, since there are reservoirs of carbon which are interconnected by pathways of exchange. These are the atmospheric pool, the terrestrial pool, comprising the biosphere (including fresh water systems) and the pedological pool (the soil), the oceans, and the fossil fuels (Figure 18.3).

Arrhenius (1896) was the first to recognise the importance of the atmospheric concentration of CO_2 on global temperature more than a century ago. Global surface temperatures have increased by 0.8°C since the late nineteenth century, and 11 out of the 12 warmest years on record have occurred since 1995 (IPCC, 2007). These and other observed climate changes are reportedly caused by emission of greenhouse gases (GHGs) through anthropogenic activities including land-use change, deforestation, biomass burning, draining of wetlands, soil cultivation, and fossil fuel combustion. The concentration of atmospheric GHGs have increased in parallel with the increase in the human population, particularly since the onset of the industrial revolution around 1850. The concentration of CO_2 has increased by 31% from 280 ppmv in 1850 to 380 ppmv in 2005, and is currently increasing at 1.7 ppmv yr^{-1} (IPCC, 2007; WMO 2006), as are the concentrations of the other two principal GHGs, CH_4 and N_2O (IPCC, 2007; WMO 2006). We need to understand the global C cycle and the ways in which it might

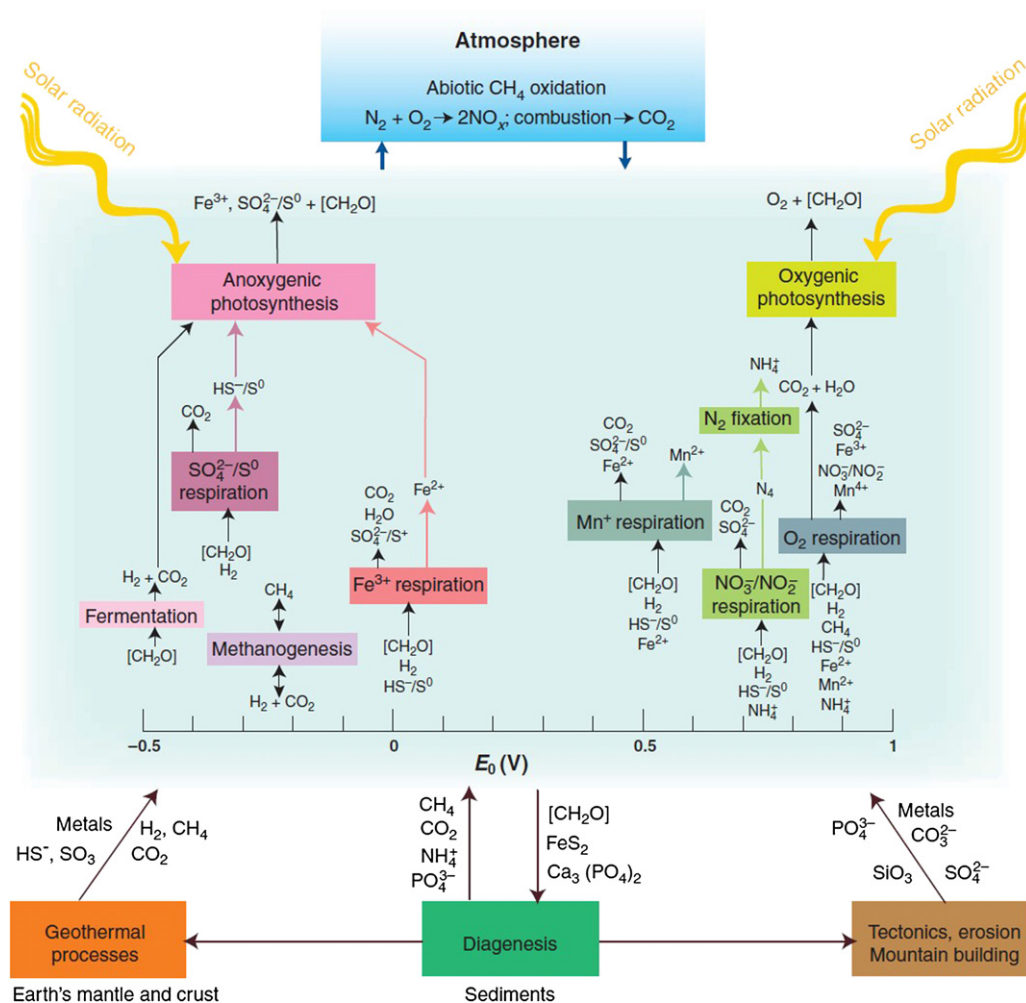


FIGURE 18.2 A generalised biosphere model showing the basic inputs and outputs of energy and materials. Geochemical (abiotic) transformations are represented at the top (atmospheric) and bottom (tectonic and geothermal) compartments, while microbially driven biochemical processes are represented in the middle, biospheric compartment (in blue) and the sediments. Biological element cycling is not completely closed due to losses through sedimentation of organic carbon and nitrogen, carbonate, metal sulfides, sulfate, and phosphate, and losses to the atmosphere via denitrification. Regeneration of available forms of these elements is contingent on geological processes: erosion and geothermal activity. Electron acceptors (oxidants) in the respiratory processes have been arranged from left to right according to increasing capacity to accept electrons. The redox couples (at pH 7) for the reactions are approximate; the exact values depend upon how the individual reactions are coupled. (From *Falkowski et al., 2008*. Copyright 2008 with permission of the American Association for the Advancement of Science.)

be perturbed by anthropogenic activities in order to develop viable strategies for dealing with climate change. The rate of any increase in atmospheric CO_2 concentration in the future will depend not only on anthropogenic activities, but on the interaction of biogeochemical and climate processes on the global carbon cycle and interaction among the principal carbon pools. There are five global pools (Figure 18.3), of which the largest, the oceanic pool, is estimated at 38000 Gt (giga tons) and is increasing at the rate of 2.3 Gt (giga tons of Carbon)/y (Figure 18.3). The geological carbon pool, comprising fossil fuels, is estimated at 4130 Gt, of which 85% is coal, 5.5% is oil, and 3.3% is gas. Proven reserves of fossil fuel include 678 Gt of coal (production 3.2 Gt/y), 146 Gt of oil (production 3.6 Gt/y), and 98 Gt of natural gas (production 1.5 Gt/y). Coal and oil each account for

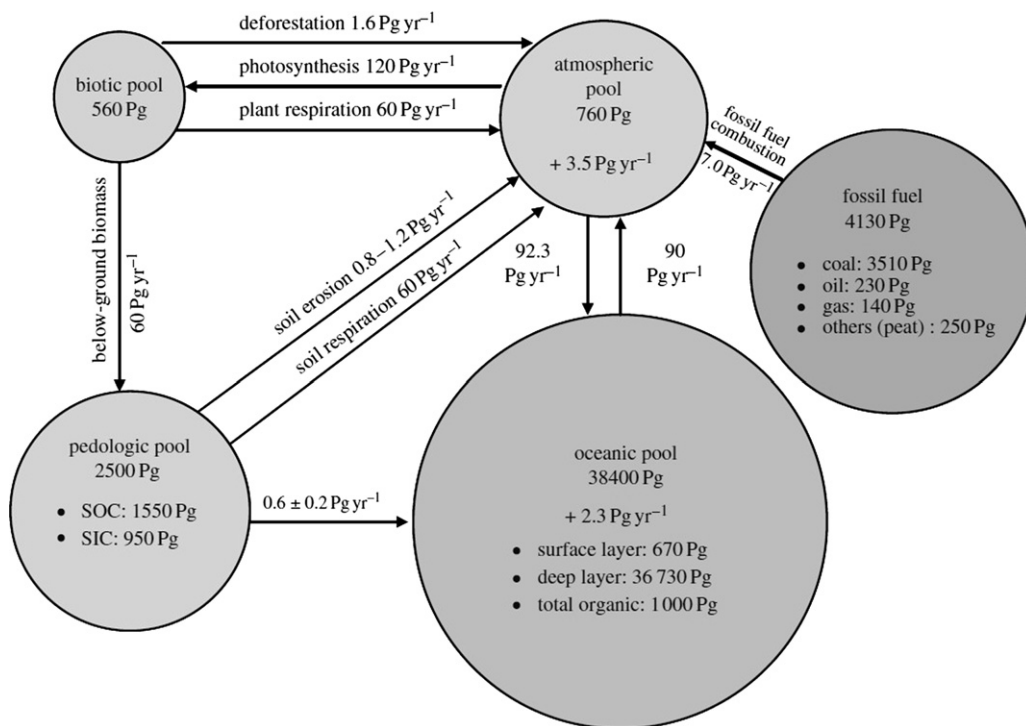


FIGURE 18.3 Principal global C pools and fluxes between them. (From Lal, 2008. Copyright 2008 with permission from the Royal Society.)

approximately 40% of global CO₂ emissions, so, the geological pool is being depleted at the rate of 7.0 Gt C/y due to fossil fuel combustion. The third largest pool is in the soil (the pedologic pool), estimated at 2500 Gt to a depth of 1 m. It consists of two distinct components, the soil organic carbon (SOC) pool (1550 Gt) and soil inorganic carbon (SIC) pool (950 Gt). The SOC pool includes highly active humus and relatively inert charcoal, made up of a mixture of plant and animal residues at various stages of decomposition, whereas the SIC pool includes elemental carbon and carbonate minerals. The fourth largest (atmospheric) pool consists of 760 Gt of mostly CO₂, which is increasing at the rate of 3.5 Gt/y or 0.46%/y. The smallest is the biotic pool estimated at 560 Gt. The pedologic and biotic C pools together constitute the terrestrial C pool (together about 2860). The atmospheric pool is connected to the oceanic pool absorbing 92.3/y and releasing 90/y with a net positive balance of 2.3/y. The oceanic pool is expected to absorb approximately 5⁻¹/y by 2100. The total dissolved inorganic carbon in the oceans is approximately 59 times that in the atmosphere. On the scales of millennia, it is the oceans which determine the atmospheric CO₂ concentration, not the opposite. The exchange between fossil fuel and the atmospheric pool is unidirectional, corresponding to approximately 7.0/y from fossil fuel consumption to the atmosphere. There are hopes that the rate of fossil fuel consumption may peak by about 2025. The annual rate of photosynthesis is 120 Gt, most of which is returned to the atmosphere through plant and soil respiration.

In the atmosphere, carbon is mostly present as CO₂, where it only represents a small percentage of the atmosphere (0.04% on a molar basis). Most of the terrestrial carbon in the soil and above the ground is stored in the forests, while the oceans contain the largest active pool of carbon near the Earth's surface, although the much larger deep ocean part of this pool does not exchange rapidly with the atmosphere.² Most carbon released to the

2. It can, however, contribute as a result of external influences like hydrothermal vents in locations where two tectonic plates are moving apart, or by uncontrolled deep-water oil well leaks.

atmosphere from the biosphere is through respiration, although substantial amounts can also be released by burning of biomass.

It is clear that, as well as carbon, hydrogen is enormously important in biology. We already saw in Chapter 5 that it has a primordial role to play in energy transduction, through the generation of proton gradients across biological membranes. These, in turn, are used to drive the rotary ATPase molecular machine, to generate ATP. As we inferred in Chapter 5, the protonation/deprotonation of redox transporters in their oxidised and reduced forms can contribute to the generation of proton gradients. As we also pointed out there, not only do many biological electron transfer reactions involve two electron transfers, this is often accompanied by the transfer of two hydrogen atoms, e.g., the numerous dehydrogenases involved in intermediary metabolism.

It has been inferred from carbon and sulfur dating that the concentration of oxygen in the Earth's atmosphere was less than 1 part per million volume (ppmv) prior to around 2.4 billion (Ga) years ago, whereas methane would have been present at levels of around 10^2 to 10^3 ppmv (compared with its present value of around 1.7 ppmv). Methane is generated in significant amounts by the anaerobic decomposition of organic matter in modern marine sediments, but is oxidised by sulfate under the ocean sea floor and never reaches the atmosphere. Prior to the watershed constituted by the appearance of oxygenic photosynthesis, the ocean had little sulfate to support anaerobic oxidation of methane, but as atmospheric oxygen and seawater sulfate levels rose, the consequent anaerobic oxidation of methane would have steadily reduced the net release of methane.

With the advent of an oxidising atmosphere through oxygenic photosynthesis, the modern Earth's atmosphere and life was born. In its turn, this created the biogeochemical oxygen cycle (Figure 18.4), the driving force of

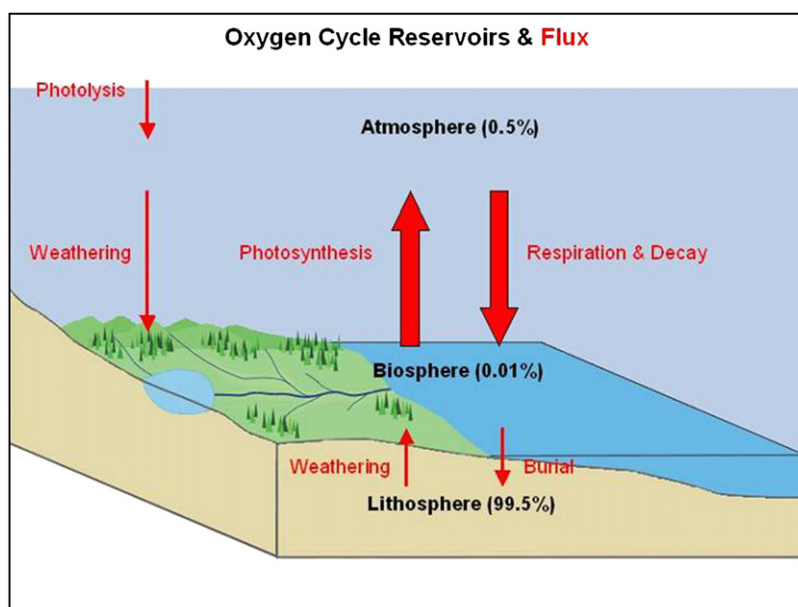
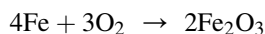


FIGURE 18.4 Oxygen cycle reservoirs and fluxes.

which was photosynthesis. This cycle describes the movements of oxygen between the atmosphere, the biosphere, and the lithosphere (the Earth's crust). By far the largest reservoir of oxygen (99.5%) resides in the silicate and mineral oxides of the lithosphere. Only a tiny amount is found as free oxygen in the biosphere (0.01%) with a somewhat larger amount in the atmosphere (but still only 0.36%).

Photosynthesizing organisms include, of course, green plants on land, but also the phytoplankton, notably the cyanobacteria, in the oceans, generating the air we breathe. An additional source of atmospheric oxygen is

photolysis of water and N₂O to their component elements in the atmosphere by high-energy UV radiation, Oxygen is consumed via respiration and decay, mechanisms by which animal and bacteria return carbon dioxide to the atmosphere. Oxygen can also be lost because of chemical weathering of minerals at the surface of exposed rocks. A good example is the formation of rust:



Oxygen can also cycle between the biosphere and the lithosphere — when marine organisms with calcium carbonate (CaCO₃) shells die, the shells are buried on the shallow waters of the sea floor, becoming the limestone of the lithosphere. A small amount of atmospheric oxygen is transformed to ozone, O₃, and the ozone layer in the stratosphere plays an important role in shielding our planet from harmful ultraviolet radiation.

The flux of oxygen through these three pools are as follows. Photosynthesis accounts for about 300,000 Gt per year, of which 55% is generated on land and 45% in the oceans. The contribution of photolysis is tiny (0.005%). Respiration accounts for 94% of the total annual losses of around 300,000 Gt., with some 4% attributable to the combustion of fossil fuel.

Phosphorus, the only one of the six major elements not to be involved in redox chemistry, is also unable to access the atmosphere, since phosphorus itself and most phosphorus-based compounds are usually solids at typical temperatures and pressures found on earth (only under highly reducing conditions is it found as the gas phosphine, PH₃). In a biological context, its principal roles are in the nucleotide di- and triphosphates like ATP, involved in cellular energy transfer and in the nucleic acids DNA and RNA. It is also found in membranes as a component of phospholipids, in bone, teeth, and insect exoskeleton, and it functions as an important buffering agent in many biological fluids. And, we should not forget the important role played by phosphorylation/dephosphorylation reactions in the regulation of intermediary metabolism.

Phosphorus is usually found in biological systems as the phosphate ion, which transits rapidly through plants and animals, but moves much more slowly through the soil and the oceans, making the phosphorus cycle overall one of the slowest biogeochemical cycles. The major mineral with an important phosphorus content is apatite [Ca₅(PO₄)₃OH], but this is not a major source, and many organisms rely on soil-derived phosphorus released from dead organic matter for their phosphorus requirements.

The Nitrogen Cycle

Because of its presence in both proteins and nucleic acids, the biological requirements for nitrogen, the 5th most abundant element in the solar system, are enormous. For every 100 atoms of carbon incorporated into cells, between 2 and 20 atoms of nitrogen are needed, depending on the organism (Canfield, Glazer, & Falkowski, 2010). Nitrogen biogeochemistry is almost entirely dependent on redox reactions, mostly catalysed by metalloenzymes. The nitrogen cycle, together with its associated enzymes, is shown in Figure 18.5. The only reaction that makes the extremely inert gas N₂ accessible for the synthesis of proteins and nucleic acids is catalysed by nitrogenase, usually referred to as N₂ fixation. This highly conserved multi-enzyme complex converts N₂ to NH₄. As we saw in Chapter 17, nitrogenase is made up of two proteins, the α₂β₂ heterotetrameric MoFe-protein containing both the FeMo-cofactor and the P-cluster, and the homodimeric Fe-protein which binds a single [4Fe-4S] cluster at the interface between the two subunits. Unlike most multiple electron transfer reactions, each of the eight individual electron transfers between the Fe-protein and the MoFe-protein requires the binding and hydrolysis of two ATP molecules. We know that some nitrogen fixers have alternative nitrogenases where Mo is replaced by V or Fe, and that these less efficient forms are expressed when Mo is unavailable. Given the abundant availability of soluble Fe²⁺ at the low atmospheric oxygen levels on the early Earth and the lack of soluble Mo under these conditions, it is likely that the Fe form dominated at that point in evolution. Indeed, the more efficient Mo form may not have become widely distributed until some 500–600 million years ago, when oxygenation of the deep ocean led to an increase in soluble Mo concentration (Canfield et al., 2010). NH₄⁺ can then be incorporated into amino acids and purine and pyrimidine bases, and be assimilated by higher organisms from organic nitrogen in their food.

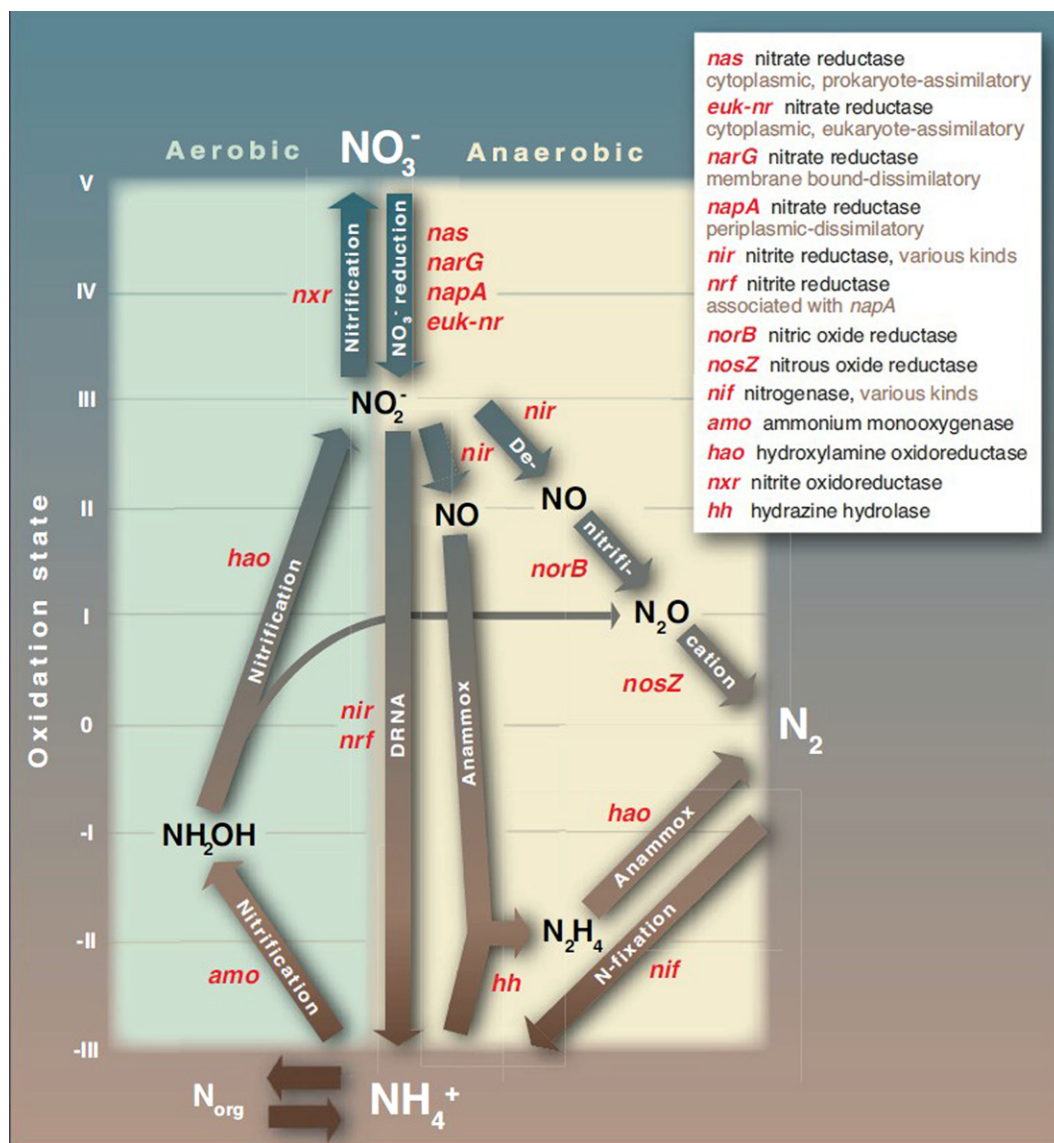


FIGURE 18.5 The major biological nitrogen transformation pathways are linked by their associated enzymes. Genes encoding enzymes that conduct the important transformations include those for various nitrate reductases (*nas*, *euk-nr*, *narG*, *napA*), nitrite reductases (*nir*, *nrf*), nitric oxide reductase (*norB*), nitrous oxide reductase (*nosZ*), nitrogenase (*nif*), ammonium monooxygenase (*amo*), hydroxylamine oxidoreductase (*hao*), nitrite oxidoreductase (*nxr*), and hydrazine hydrolase (*hh*). (From Canfield et al., 2010. Copyright 2010 with permission from AAAS.)

When organisms die, their nitrogen is returned to the environment as NH_4^+ , the fate of which depends on whether oxygen is available or not. In the presence of oxygen, NH_4^+ can be oxidised to nitrate (nitrification), primarily by soil-living bacteria in a two-stage pathway. Initially NH_4^+ is oxidised to NO_2^- by bacteria such as *Nitrosomonas* species. In the first step, ammonium monooxygenase, a copper/iron enzyme oxidises NH_4^+ to hydroxylamine, which is then oxidised to NO_2^- by the haem enzyme, hydroxylamine oxidoreductase. NO_2^- is subsequently oxidised to NO_3^- by a different group of nitrifying bacteria (*Nitrosobacter*), via the haem enzyme nitrite reductase. All of the nitrifiers use the protons and electrons generated in the oxidation of NH_4^+ and NO_2^- to

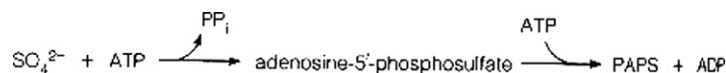
reduce CO_2 to organic matter in the absence of light (i.e., they are chemoautotrophs). N_2O , a greenhouse gas,³ is a by-product of this process, and nitrification by marine and terrestrial organisms is an important source of atmospheric N_2O .

In the *absence of oxygen*, a third set of opportunistic microbes uses NO_3^- and NO_2^- as electron acceptors in the anaerobic oxidation of organic matter. Nitrate reduction is coupled to the anaerobic oxidation of organic carbon producing either NH_4^+ in a process known as dissimilatory nitrate reduction to ammonium (DNRA) or, more commonly, N_2 gas during *denitrification* (Figure 18.5). Organisms which carry out denitrification include representatives of many bacteria and archaea, as well as some eukaryotes. Four metalloenzymes are involved in denitrification: nitrate reductase, nitrite reductase, nitric oxide reductase, and nitrous oxide reductase. N_2O is an obligate intermediate (Figure 18.5), and some ultimately escapes to the atmosphere, making denitrification another important source of this greenhouse gas from both marine and terrestrial environments.

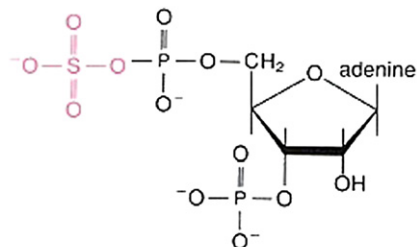
An alternative bacterial route from NO_3^- to N_2 , where NH_4^+ oxidation is coupled to NO_2^- reduction in a process called anammox (anaerobic ammonium oxidation), dominates N_2 production in many marine environments, but, unlike classical denitrification, it does not lead to the production of N_2O . Together, denitrification and anammox close the nitrogen cycle by returning N_2 gas back to the atmosphere.

Sulfur and Selenium

Since the early atmosphere of our planet was essentially characterised by low redox potentials, it is highly probable that sulfur was a very important element. Hydrogen sulfide was likely present at mM concentrations in aqueous solution, and transition metal sulfides were probably among the first biocatalysts. Although some bacteria can synthesise sulfur-containing organic compounds directly from elemental sulfur or from sulfite, most organisms acquire sulfur from sulfate. Just as CO_2 and N_2 must undergo fixation in order to be utilised, sulfate utilisation requires metabolic activation to a form that can readily undergo reduction. In plants and bacteria, this involves the condensation of sulfate with ATP to form APS (adenosine-5'-phosphosulfate), which is further phosphorylated to give PAPS, which has an additional



phosphate in the 3'-position (Figure 18.6). PAPS is then used in bacteria both as an activated form of sulfate, both for sulfation reactions and as a substrate for sulfate reduction. It is initially reduced to sulfite (SO_3^{2-}) in a reaction



3'-Phosphoadenosine-5'-phosphosulfate

FIGURE 18.6 Structure of PAPS.

3. N_2O is currently the third of the 'greenhouse gases', after carbon dioxide and methane in importance. While not as abundant as carbon dioxide, it is 300 times more potent in its ability to warm the planet.

involving thioredoxin. Sulfite is subsequently reduced by sulfite reductase, a large and complex enzyme which involves NADPH, FAD, FMN, and Fe–S centre and the porphyrin sirohaem, and catalyses the six-electron reduction directly to H₂S. In plants, APS is the substrate for reduction rather than PAPS.

The oxidation state of sulfur is +6 in sulfate and –2 in H₂S or RSH. An interesting feature of sulfur chemistry is that the amino acid cysteine, as its RS[–] (cysteinate) form, acts as a base, binding H⁺, but also a number of transition metals, including Fe, Zn, Mo, and Cu.

Hydrogen sulfide can be oxidised to elemental sulfur, for example, by green and purple sulfur bacteria. Further oxidation of elemental sulfur by sulfur oxidising bacteria can produce sulfate.

Selenium, positioned between sulfur and tellurium in group 16 of the Periodic Table (Figure 1.3), was first discovered by Jöns Jacob Berzelius in the reddish mud with the unpleasant smell of black radish from the lead chambers of a Swedish sulfuric acid factory. Berzelius positioned it just between sulfur and tellurium⁴ but with rather more of the character of sulfur than of tellurium.

We will not enter here into the convoluted history of the discovery of the biochemical importance of Se, which has been splendidly summarised recently (Flohé, 2009). Suffice it to say that from being an ugly-smelling nuisance, and then the cause of chronic intoxication in farm animals, selenium was found to be essential for rats and subsequently for other mammals including man. The first selenoenzyme to be identified was glutathione peroxidase, followed in quick succession by two more from *Clostridia*, a component of the glycine reductase system and a formate dehydrogenase. It was quickly recognised that the Se atom was incorporated into the protein in the form of a selenocysteine (Sec) residue. As we will see shortly, the cost for living organisms of synthesising and incorporating a single Sec into selenoproteins is tremendously costly. What might be the advantages of Sec over Cys, which could explain this extravagance? The different chemical and physical properties of the two elements have been recently summarised (Wessjohann, Schneider, Abbas, & Brandt, 2007). While it had long been thought that the key factor might be the significantly lower pK_a of Sec (5.2) compared to Cys (8.5), it now is suggested that the inherent high nucleophilicity of Sec and its higher chemical reaction rate with electrophiles, compared to Cys, is the truly unique property of Sec that cannot be mimicked by the basicity of Cys (Arnér, 2010).

The putative catalytic mechanisms of three mammalian selenoenzymes are shown in Figure 18.7. In Figure 18.7a, the mechanism of thioredoxin reductase is illustrated. This enzyme reduces oxidised thioredoxin (Trx), the electron donor for the ribonucleotide reductase-catalysed conversion of ribonucleotides to deoxyribonucleotides. The proposed mechanism involves electron transfer from NADPH to FAD via the N-terminal active site of one subunit to the Cys–Sec selenenylsulfide bond within the C-terminal active site of the opposite subunit and finally to the substrate Trx. In Figure 18.7b, the catalytic redox cycle of glutathione peroxidase (GpPx) is shown. This enzyme plays a crucial role in protection against oxidative stress by removing hydrogen peroxide and organic hydroperoxides: Sec is oxidised to selenenic acid, which is reduced back to the selenolate anion form by the glutathione/glutathione reductase (GSH/GR) system. Iodothyronine deiodinases (DIOs) catalyse the deiodination of T₄, the major thyroid hormone secreted by the thyroid gland, into the active hormone T₃ (see next section), and their mechanism is illustrated in Figure 18.7c. This involves generation of an oxidised DIO–Sel intermediate, which is reduced by thiol-containing reductants with concomitant liberation of iodine.

Finally, we briefly consider the way in which Sec is generated and co-translationally incorporated in selenoproteins. There are 25 selenoprotein genes in humans, and Sec has been found in the active site of those to which a function has been attributed. Sec does not occur as the free amino acid, and the biosynthetic pathway of Sec from serine on tRNA^{Sec} in eukaryotes requires four enzymes, as illustrated in Figure 18.8. The specific tRNA^{Sec} is aminoacylated with serine by the conventional Seryl-tRNA synthetase (SerRS); and the

4. He gave it the name selenium after the moon goddess Selene. Tellurium, named after the Roman god of the earth, had been isolated a few years earlier.

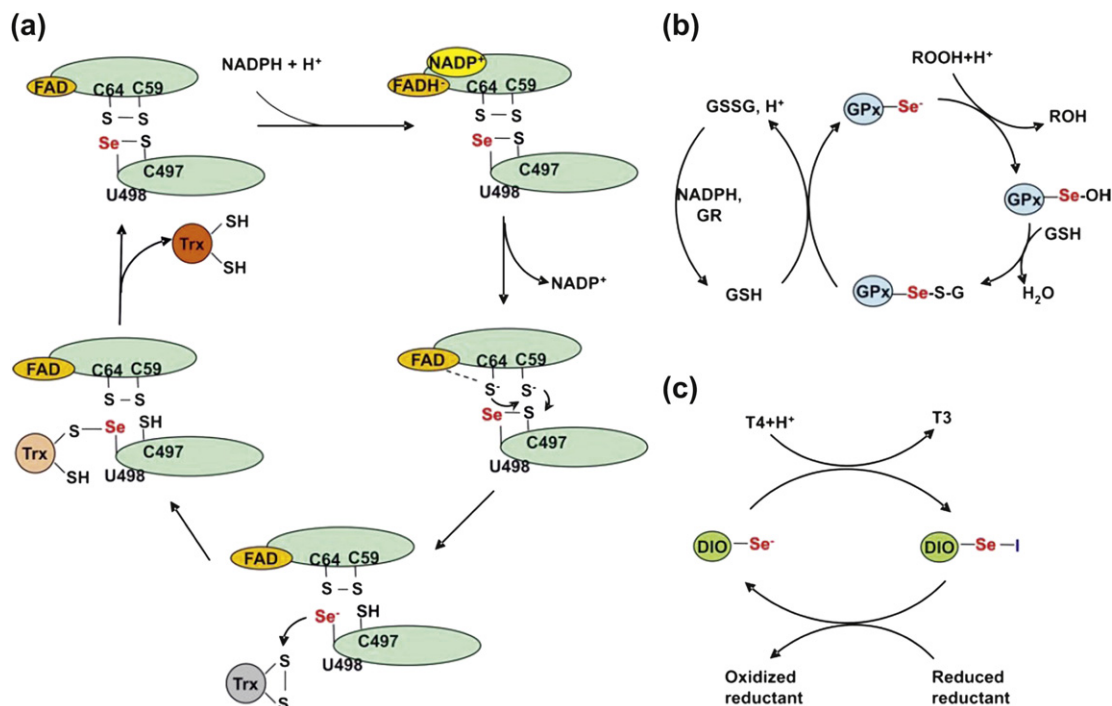


FIGURE 18.7 Putative catalytic mechanism of some mammalian selenoproteins. (a) the proposed mechanism of TrxR-dependent reduction involves electron transfer from NADPH to FAD via the N-terminal active site of one subunit to the Cys–Sec selenenylsulfide bond within the C-terminal active site of the opposite subunit and finally to the substrate Trx. (b) the catalytic redox cycle of GPxs involves the oxidation of Sec to selenenic acid by hydrogen peroxide and organic hydroperoxides and reduction to the selenolate anion form by the GSH system. GR, glutathione reductase. (c) the proposed deiodination mechanism of DIOs involved in the generation of the oxidised DIO–SeI intermediate is shown, and thus, the intermediate is reduced by thiol-containing reductants and releases iodide. (From Lu & Holmgren, 2009. Copyright 2009 with permission of ASBMB.)

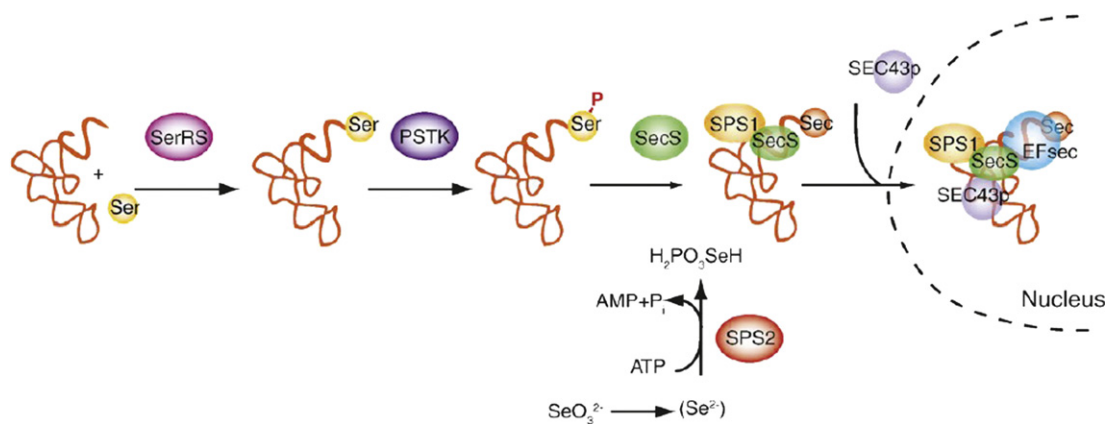


FIGURE 18.8 The selenocysteine biosynthesis pathway in eukaryotes. In the first step, a specific tRNA^{Sec} is aminoacylated with serine by the conventional Seryl-tRNA synthetase (SerRS); the seryl residue of Ser-tRNA^{Sec} is phosphorylated by the O-phosphoryl tRNA^{Sec} kinase (PSTK). Selenocysteine synthase (SecS) converts the Ser-tRNA^{Sec} to Sec-tRNA^{Sec}, using monoselenophosphate (H₂PO₃SeH) as the substrate. This selenium donor is the product of selenophosphate synthetase (SPS2). The biological selenium source is an unknown form of selenide (Se²⁻), likely originating from selenite (SeO₃²⁻). The protein SEC43P has been shown to redirect the complex constituted by SPS1/SecS/ Sec-tRNA^{Sec} to the nucleus. (From Allmang et al., 2009. Copyright 2009 with permission from Elsevier.)

seryl residue of Ser-tRNA^{Sec} is then converted to Sec-tRNA^{Sec}. From sequencing of selenoproteins and cloned DNAs, it was clear that Sec in selenoproteins was coded by the codon TGA (UGA in the corresponding mRNA). How Sec is incorporated in response to an in-frame UGA codon, which should normally signal termination of translation, informing the ribosomes not to stop at this position on the mRNA has been progressively deciphered, first in bacteria and then in eukaryotes. This involves a complex recoding machinery, involving a stem-loop in the 3'-untranslated region of all selenoprotein mRNAs, the selenocysteine insertion sequence, or SECIS, SECIS-binding proteins (SBPs), and a number of other factors. Figure 18.9 presents

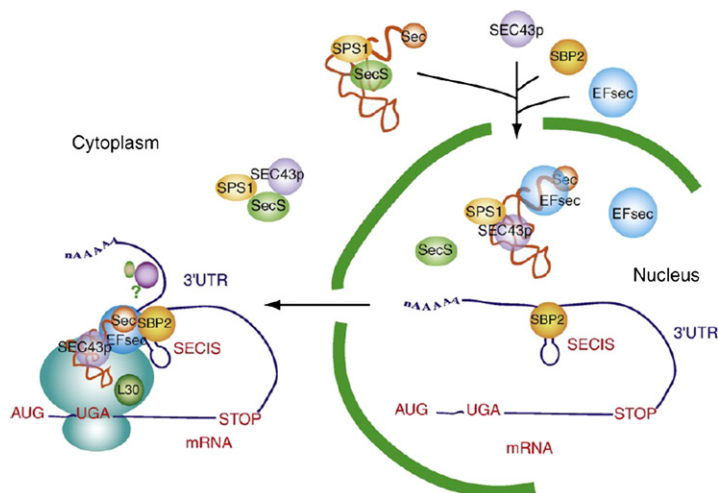


FIGURE 18.9 A model for nucleocytoplasmic trafficking of SBP2. Shuttling of the SPS1/SEC43p/EFsec/Sec-tRNA^{Sec} complex into the nucleus and association with SBP2 and the SECIS element are depicted. Cytoplasmic export of the SECIS-bound complex is shown on the left. (From Allmang et al., 2009. Copyright 2009 with permission from Elsevier.)

a model of how the SPS1/SEC43p/EFsec/Sec-tRNA^{Sec} complex depicted in Figure 18.8 is shuttled into the nucleus where it associates with SBP2 and the SECIS element on a selenoprotein mRNA before being re-exported to the cytosol.

In summary, the codon TGA, which normally codes for termination of protein synthesis is programmed from a distance to encode the “21st amino acid” selenocysteine: a special tRNA is loaded in a unique and unorthodox way, incorporating a selenocysteine residue which is synthesised de novo at the tRNA level by special enzymes; highly specialised proteins are required to recognise and bind the secondary mRNA structures and the tRNA^{Sec}; specialised elongation factors have to compete with canonical ones and with release factors. No wonder that chemists and biochemists ask what are the unique properties of selenocysteine compared to cysteine (Arnér, 2010) to justify the involvement of so many molecular partners (Allmang, Wurth, & Krol, 2009).

Chlorine and Iodine

The halogens as a group in the Periodic Table are characterised by their presence in the biological system as the halide anions F[−], Cl[−], Br[−], and I[−]. We have already briefly discussed F[−] and Br[−] in Chapter 1 and we discuss Cl[−] and I[−], here. The concentration of Cl[−] in biological systems is, in general, quite high. It is the principal ionic component of seawater (Cl[−] 55% compared with Na⁺ 30%, SO₄^{2−} 7.7%, Mg²⁺ 3.7%, Ca²⁺ 1.2%, K⁺ 1.1%) – this

corresponds to a Cl^- concentration of 0.55 mM. In extracellular fluids the Cl^- concentration is 103 mEq/l⁵ (compared with 142 mEq/l Na^+ and 27 mEq/l HCO_3^-). In contrast intracellular Cl^- concentration is extremely low (2 mEq/l), as is that of HCO_3^- (8 mEq/l). Intracellular anionic strength is accounted for predominantly by inorganic and organic phosphates (140 mEq/l) and protein (55 mEq/l). This leads to the logical conclusion that anion channels that selectively allow the passage of Cl^- must exist in the plasma membrane of cells. Since the Cl^- ion is the only halogen ion which is abundantly used in biological systems (the abundance of Br^- and I^- is low), Cl^- transport proteins are faced with the relatively modest challenge of selecting Cl^- over phosphate, sulfate, bicarbonate, and anionic proteins.

CIC Cl^- channels are part of a large family of anion channels, which are widely distributed throughout both eukaryotes and prokaryotes. In vertebrate skeletal muscle, CIC Cl^- channels stabilise the resting potential and regulate electrical excitability, while in kidney, they operate to produce transepithelial fluid and electrolyte

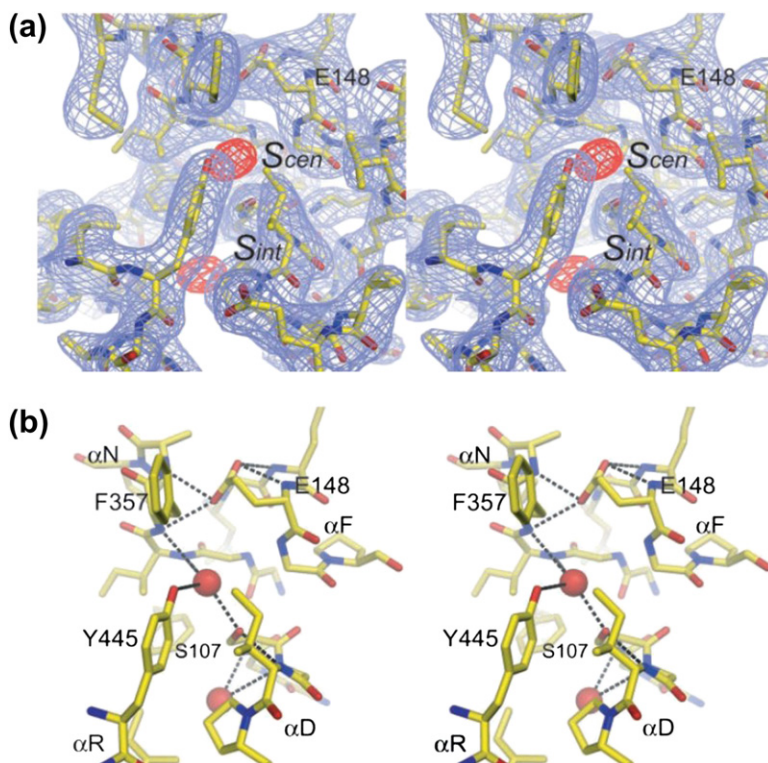


FIGURE 18.10 The two central Cl^- binding sites in a mutant CIC Cl^-/H^+ exchanger (PDB code 1OTU). Stereo view of the ion-binding sites. Selected residues in the vicinity of the bound chloride ions are shown. Hydrogen bonds between the protein and chloride ions (red spheres) as well as between the side chain of Glu¹⁴⁸ and the rest of the protein are shown as black dashed lines. (From Dutzler *et al.*, 2003. Copyright 2003 with permission from AAAS.)

transport. In contrast to cation channels (eg K^+ channels), where selective conduction and gating are mediated by separate structural elements, in CIC Cl^- channels, the selectivity and gating seem to be intimately related. There are two halogen ions bound in the selectivity filter of wild-type bacterial CIC Cl^- channel (Figure 18.10a). In one,

5. Eq/l = milliequivalents per litre

S_{cen} (central site), the Cl^- ion is coordinated by main-chain amide nitrogen atoms from the end of helix αN and from the side chains of Ser¹⁰⁷ and Tyr⁴⁴⁵ (Figure 18.10B). The second, S_{int} (internal site), located at the interface where the aqueous intracellular solution meets the selectivity filter is coordinated on one side by main-chain amide nitrogen atoms from the end of helix αD , and on the other side it is exposed to the intracellular solution (Figure 18.10B). At the opposite end of the selectivity filter, the side chain of Glu¹⁴⁸ obstructs the pore with its carboxyl group inserted between the ends of helices αN and αF , bringing the helices together through hydrogen bonding. It is proposed that this is the structure of the closed channel, with Glu¹⁴⁸ as gate. The structure of mutant channels in which Glu¹⁴⁸ has been mutated to Ala or Gln has also been determined, and now a third halogen ion is observed in place of the Glu side chain. It is proposed (Figure 18.11) that in the closed conformation, the ion-binding

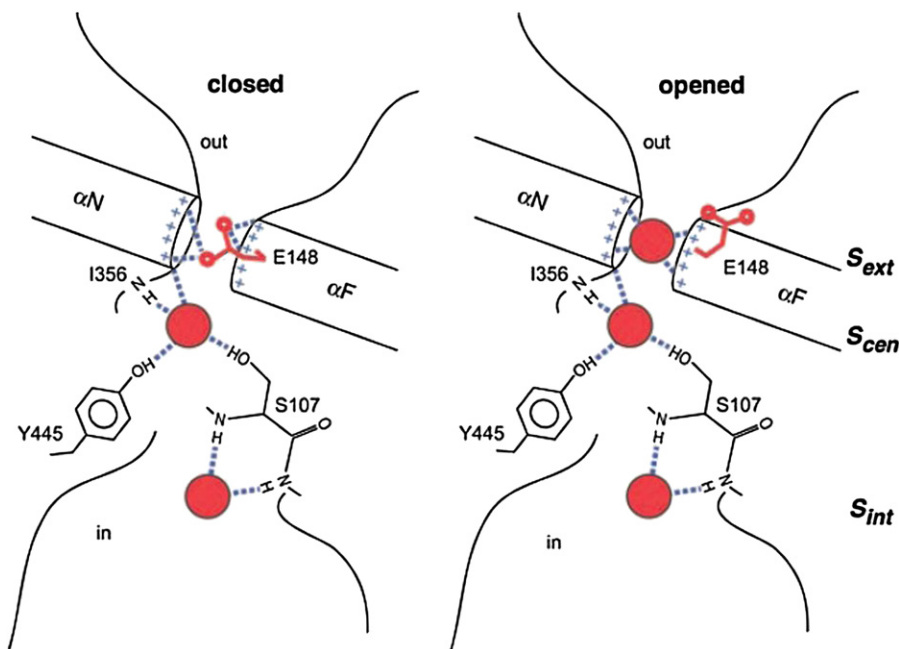


FIGURE 18.11 Schematic drawing of the closed and opened conformation of a CIC chloride channel. In the closed conformation, the ion-binding sites S_{int} and S_{cen} are occupied by chloride ions, and the ion-binding site S_{ext} is occupied by the side chain of Glu¹⁴⁸. In the opened conformation, the side chain of Glu¹⁴⁸ has moved out of binding site S_{ext} into the extracellular vestibule. S_{ext} is occupied by a third chloride ion. Chloride ions are shown as red spheres, the Glu¹⁴⁸ side chain is coloured red, and hydrogen bonds are drawn as dashed lines. (From Dutzler *et al.*, 2003. Copyright 2003 with permission from AAAS.)

sites S_{int} and S_{cen} are occupied by chloride ions, and the ion-binding site S_{ext} is occupied by the side chain of Glu¹⁴⁸. In the opened conformation, the side chain of Glu¹⁴⁸ has moved out of binding site S_{ext} into the outside of the channel; the S_{ext} site is now occupied by a third chloride ion (Dutzler, Campbell, & MacKinnon, 2003).

In contrast to CIC Cl^- channels, CFTR is a plasma membrane cAMP-regulated Cl^- channel which is responsible for transepithelial salt and fluid transport. Genetic defects which cause CFTR hypofunctioning leads to cystic fibrosis (CF), the most common lethal genetic disease in Caucasians affecting approximately 1 in every 2,500 newborns. In contrast, the consequence of the intestinal colonisation by pathogenic microorganisms, results in hyperfunctioning of CFTR, which provokes secretory diarrhea, the leading cause of mortality in early childhood.

Anion flow through this channel is needed for normal function of epithelia such as those lining the airways, the intestinal tract and ducts in the pancreas, testes, and sweat glands. Without anion flow, water movement slows

down, dehydrated mucus clogs the ducts and collects in the lung where it engenders bacterial infections, which are ultimately lethal. When the gene mutated in CF patients was identified by positional cloning in 1989, the expectation was that it would encode a chloride-ion channel. This was because CF epithelia behaved as though they were impermeable to chloride, and chloride channels could be activated by cAMP-dependent protein kinase (PKA) in normal but not in CF airway epithelium. CFTR was found to encode an ABC transporter homologue with several consensus sites for phosphorylation by PKA; it was also shown to be a chloride channel, directly activated by phosphorylation by PKA (Figure 18.12). CFTR is not only a member of the superfamily of ATP-

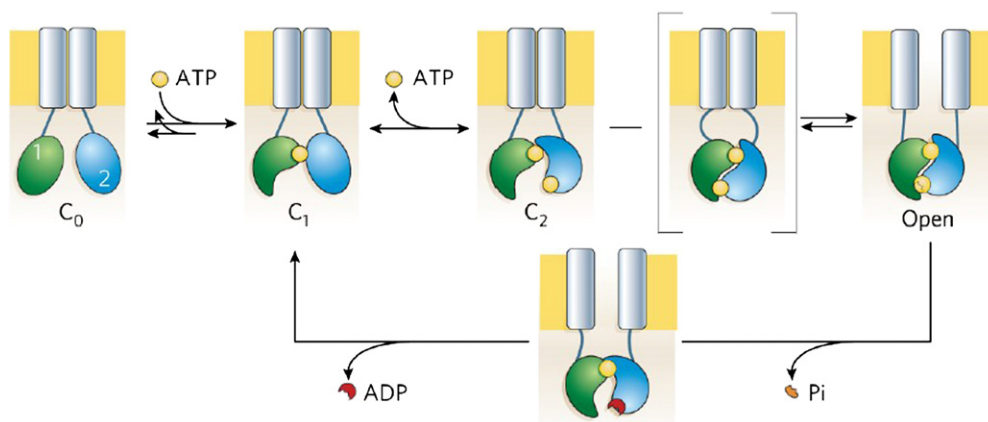


FIGURE 18.12 ATP-dependent gating cycle of phosphorylated CFTR channels. The R domain is omitted. ATP (yellow) remains tightly bound to NBD1 (green) Walker motifs for several minutes, during which time many closed—open—closed gating cycles occur. ATP binding to NBD2 (blue) is followed by a slow channel opening step (C₂-to-Open) that proceeds through a transition state (square brackets) in which the intramolecular NBD1–NBD2 tight heterodimer is formed, but the transmembrane pore (gray rectangles) has not yet opened. The relatively stable open state becomes destabilised by hydrolysis of the ATP bound at the NBD2 composite catalytic site and loss of the hydrolysis product, inorganic phosphate (Pi). The ensuing disruption of the tight dimer interface leads to channel closure. (From Muallem & Vergani, 2009. Copyright 2009 with permission from the Royal Society.)

binding cassette (ABC) transporter ATPases, but among the thousands of ABC family members, CFTR is the only ion channel, linking its enzymatic activity (ATP hydrolysis) with channel gating (opening and closing of the channel). The ATP-dependent gating cycle of phosphorylated CFTR channels is presented in Figure 18.12. Two-thirds of all CF disease cases can be attributed to a single mutation in CFTR, deletion of Phe 508 in nucleotide-binding domain 1, but more than 1000 other disease-related mutations have also been identified.

Iodine is extensively utilised by marine organisms. For example, brown algal kelp species are the most efficient iodine accumulators among all living systems, with an average content of 1.0% of dry weight — representing a ca. 30,000-fold accumulation of the element from seawater. It is used, as we saw in Chapter 17, by vanadium haloperoxidases. But we will focus our attention here on the role of iodine as an absolutely essential trace element for man, and for higher animals, where iodine is required as a component of thyroid hormones. Our need for iodide derives entirely from its requirement for the biosynthesis of the thyroid hormones 3,3',5,5'-tetraiodothyronine (T₄) and 3,3',5-triiodothyronine (T₃) (Figure 18.13). They are first generated in the thyroid and then circulated throughout the body to regulate a wide variety of metabolic processes including the basal rate of metabolism, temperature regulation, and expression of numerous proteins. Iodide is transported and concentrated in the thyroid, attaining levels of iodide within the cell 40-fold greater than that found in plasma. Iodide is sequestered and stored bound to tyrosyl residues of thyroglobulin as mono- and diiodinated tyrosyl residues in reactions catalysed by thyroid peroxidase, which then serve as intermediates in the formation of T₃ and T₄. Proximal diiodotyrosine residues form an iodothyroninyl product, catalyzed by the same thyroid peroxidase responsible for

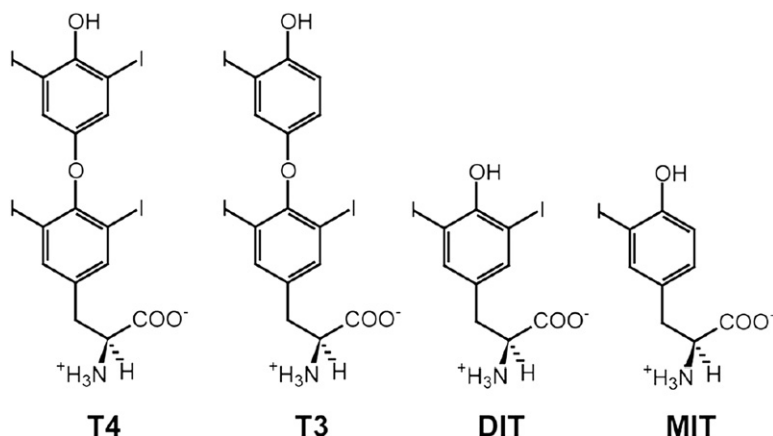


FIGURE 18.13 Thyroid hormones and their side products diiodotyrosine (DIT) and monoiodotyrosine (MIT) formed during their biosynthesis.

the preceding iodination reaction. Ultimately, approximately seven monoiodotyrosines (MIT), six diiodotyrosines (DIT), and one T4 are formed per thyroglobulin molecule. Some thyroglobulin molecules also contain one T3. When thyroid cells are activated by a signal such as thyroid-stimulating hormone, thyroglobulin is taken up from the colloid by endocytosis and hydrolysed to release T4/T3 into the plasma (Figure 18.14). T4 can be considered

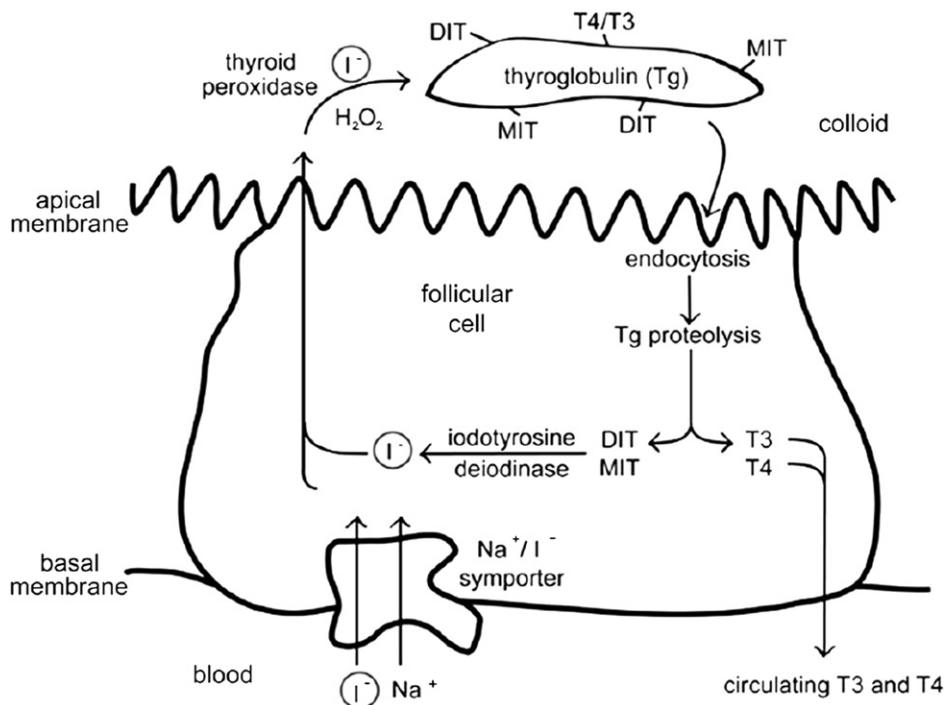


FIGURE 18.14 Iodide uptake, transport, metabolism, and salvage in thyroid follicular cells. (Adapted from Rokita, Adler, McTamney, & Watson, 2010.)

a prohormone, since T3 is 10-fold more potent in metabolic regulation. Peripheral tissues can control the ratio of these derivatives, through the action of iodothyronine deiodinase, which we already encountered earlier in this Chapter, with its essential active site selenocysteine residue (Sec).

REFERENCES

- Allmang, C., Wurth, L., & Krol, A. (2009). The selenium to selenoprotein pathway in eukaryotes: more molecular partners than anticipated. *Biochimica et Biophysica Acta*, 1790, 1415–1423.
- Arnér, E. S. J. (2010). Selenoproteins – what unique properties can arise with selenocysteine in place of cysteine? *Experimental Cell Research*, 316, 1296–1303.
- Arrhenius, S. (1896). On the influence of carbonic acid in the air on the temperature on the ground. *Philosophical Magazine and Journal of Science*, 41, 237.
- Canfield, D. C., Glazer, A. N., & Falkowski, G. T. (2010). The evolution and future of Earth's nitrogen cycle. *Science*, 330, 192–196.
- Dutzler, R., Campbell, E. B., & MacKinnon, R. (2003). Gating the selectivity filter in ClC chloride channels. *Science*, 300, 108–112.
- Falkowski, P. G., Fenchel, T., & Delong, E. F. (2008). The microbial engines that drive earth's biogeochemical cycles. *Science*, 320, 1034–1039.
- Flohé, L. (2009). The labour pains of biochemical selenology: the history of selenoprotein biosynthesis. *Biochimica et Biophysica Acta*, 1790, 1389–1403.
- Intergovernmental Panel on Climate Change. (2007). *Climate change 2007. Climate change impacts, adaptation and vulnerability*. Working Group II. Geneva, Switzerland: IPCC.
- Lal, R. (2008). Carbon sequestration. *The Philosophical Transactions of the Royal SocietyB: Biological Sciences*, 363, 815–820.
- Lu, J., & Holmgren, A. (2009). Selenoproteins. *Journal of Biological Chemistry*, 284, 723–727.
- Muallem, D., & Vergani, P. (2009). Review. ATP hydrolysis-driven gating in cystic fibrosis transmembrane conductance regulator. *The Philosophical Transactions of the Royal SocietyB: Biological Sciences*, 364, 247–255.
- Rokita, S. E., Adler, J. M., McTamney, P. M., & Watson, J. A., Jr. (2010). Efficient use and recycling of the micronutrient iodide in mammals. *Biochimie*, 92, 1227–1235.
- Wessjohann, L. A., Schneider, A., Abbas, M., & Brandt, W. (2007). Selenium in chemistry and biochemistry in comparison to sulfur. *Biological Chemistry*, 388, 997–1006.
- WMO. (2006). *Greenhouse gas bulletin: the state of greenhouse gases in the atmosphere using global observations up to December 2004*. Geneva, Switzerland: World Meteorological Organization.

Biom mineralisation

“For the harmony of the world is made manifest in Form and Number, and the heart and soul and all poetry of Natural Philosophy are embodied in the concept of mathematical beauty.”¹

Introduction	359
Principles of Solid-State Biological Inorganic Chemistry	360
An Overview of the Major Classes of Biom minerals	361

INTRODUCTION

When we survey the living world around us we can only wonder at the diversity of its shapes and forms. The Scottish polymath,² D’Arcy Thompson addressed this subject in his classic book *On Growth and Form*, first published in 1917, and in a revised edition in 1942 (the latter, a mere 1116 pages long) (Thompson, 1942). The central thesis of his book was that biologists placed too much emphasis on the role of evolution, and not enough on the roles of physical laws and mechanics, as determinants of the form and structure of living organisms. He decided that the laws concerned with static and dynamic forces of tension, compression and shear occurred in all living structures and influenced both growth, function and form. The bones of a skeleton in a museum would be a limp heap on the floor without the clamps and rods that pull them together, and Thompson argued that in living animals, tension plays as important role in holding the skeleton together as does weight. In the same way, tension holds together the arches of medieval cathedrals, and steel cables provide the tensile strength on which suspension bridges are hung.

We now recognise that, while much of biology relies on inorganic structures, biom minerals, to supply the tensile strength and the other material properties that we associate with, for example, bone, the diversity of form and shape depends on the organic matrix in which the biom mineral is allowed to form. It is a little like the construction of buildings with reinforced concrete — the mould determines in what shape and form the concrete will set. And it is just so in biom mineralisation — the organic mould is the organic matrix in which the process of selective precipitation of the inorganic mineral to be formed is directed, indeed, one might even say orchestrated, by the organic component.

Calcium is probably the most widely distributed element in biom minerals, particularly in the “hard parts” of organisms, like teeth and bones. With the recognition that numerous minerals based on a great number of cations (among which figure Ba, Ca, Cu, Fe, K, Mg, Mn, Na, Ni, Pb, Sr, and Zn) as hydroxides, oxides, sulfides, sulfates, carbonates, and phosphates, the more restrictive term ‘calcification’ has given way to the more global ‘biom mineralisation’.

1. D’Arcy Wentworth Thompson « On Growth and Form » (1917).

2. Thompson was offered the chair of Classics, Mathematics, or Zoology at the University of Saint Andrews — he chose the latter.

PRINCIPLES OF SOLID-STATE BIOLOGICAL INORGANIC CHEMISTRY

Biomineralisation is the study of processes that lead to the formation of hierarchically structured organic–inorganic materials generated by living organisms, such as shells, bone, and teeth. Over the last few decades, our ability to identify the often large number of macromolecules involved in the process of biomineralisation and the interactions between them has grown and expanded.

As we begin to unravel the mechanisms by which biominerals are produced, more recently efforts have been directed to replicating key fabrication strategies and structural features into materials design. In this introductory section, we present a brief account of the principles involved in the formation of biominerals or if you prefer, the rules of thumb which govern the deposition of solid-state inorganic material.

We can consider three broad classifications of biominerals as a function of their morphology. (i) Amorphous minerals are most morphologically flexible biominerals — since they have no preferred form, they can be readily molded to give the desired shape of product. They are found extensively distributed in the siliceous diatoms and radiolaria. (ii) Polycrystalline biominerals also have a wide range of morphologies, and their small crystalline building blocks can be readily organised to give complex forms. (iii) Single crystals might a priori be expected to be geometric objects defined by regular, planar faces, where the external form is a reflection of the internal symmetry of the crystal lattice. In contrast, biological mineralisation can yield single crystals whose morphologies have no relation to their crystallographic structure.

We can distinguish four parameters which must be carefully controlled to ensure that the outcome of the process is that which is required. These are solubility, level of supersaturation, nucleation, and crystal growth. In all cases, the process involves interaction of the biomineral throughout the course of its formation with biological molecules, particularly proteins and phospholipid-protein ensembles present in biological membranes. To put things simply, biomineralisation begins with precipitation, starting from different ions, and the driving force for the formation of a new phase (the precipitate) is the supersaturation of the solution. Figure 19.1 presents a classical

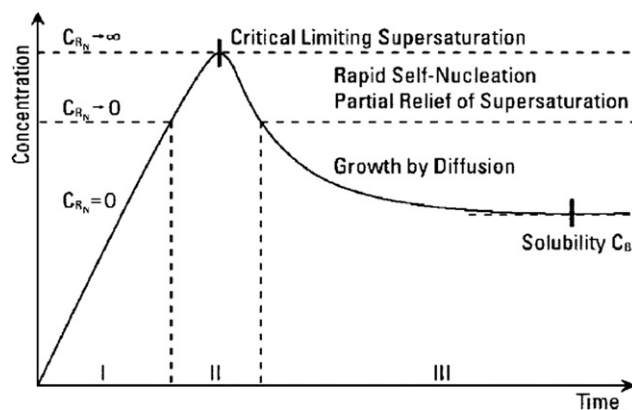


FIGURE 19.1 Schematic representation of the concentration of molecularly dissolved sulfur before and after nucleation as a function of time. C_{RN} is the concentration for a given nucleation rate R_N . (Adapted from Meldrum & Cölfen, 2008.)

curve for the crystallisation of sulfur in ethanol (LaMer & Dinegar, 1950), which can also be considered typical for any precipitation reaction. As the concentration of sulfur increases, a critical supersaturation is reached, and precipitation spontaneously takes place. With time, the sulfur concentration decreases again, and the precipitated particles can grow from the solution provided that they have a nucleus from which to grow. Heterogeneous nucleation proceeds from a starting point which could be a surface (e.g., a protein or a membrane), dust particles, or crystal seeds, whereas in homogeneous nucleation the nucleus forms spontaneously from the solution itself, if

the nucleation burst is short (Figure 19.1), which ensures that all of the nucleated particles have the same size before they grow further by diffusion.

In what follows, we discuss biomineralisation in a number of different systems. We begin with what might seem the simplest, where just one oligomeric protein, ferritin, directs the precipitation, nucleation, and crystal growth of an iron biomineral, all within the same hollow protein shell. We then discuss some of the ways in which the ferritin protein ‘cage’ can be used to generate new functions and properties, before turning to the more complex system represented by the generation of magnetite in the magnetosomes of magnetotactic bacteria, which involves several proteins. Calcium carbonate and calcium phosphate systems are then presented and we conclude with a return to the amorphous silica-based cell walls of plants and diatoms.

AN OVERVIEW OF THE MAJOR CLASSES OF BIOMINERALS

Biominerals can be formed from a number of metal ions, including Ca, Fe, Mg, and Mn with appropriate anions such as carbonate, phosphate, oxalate, sulfate, oxides, and sulfides. More than 60 different biological minerals are known, a few of which are listed in Table 19.1. Calcium carbonates and phosphates alone constitute a major part of

TABLE 19.1 Some Biological Minerals

Calcite	CaCO_3	Ascidians, Molluscs
Aragonite	CaCO_3	Molluscs, Fish
Hydroxyapatite	$\text{Ca}_{10}(\text{PO}_4)_6(\text{OH})_2$	Bones, Teeth, Bony Fish,
Gypsum	CaSO_4	Jellyfish larvae
Barite	BaSO_4	Algae
Silica	$\text{SiO}_2 \cdot n\text{H}_2\text{O}$	Diatoms, Plants, Sponges
Magnetite	Fe_3O_4	Magnetotactic Bacteria, Chitons teeth
Goethite	$\alpha\text{-FeOOH}$	Limpets teeth
Ferrihydrite	$\text{Fe}_{10}\text{O}_{14}(\text{OH})_2$	Mammalian Ferritin cores

the biomineral world, including bones and teeth, most likely easily explained by the high concentrations of Ca^{2+} in extracellular fluids (10^{-3} M) and the low solubilities of its carbonates, oxalates, phosphates, pyrophosphates, and sulfates. The contrast with Mg^{2+} is striking – Mg^{2+} salts are more water-soluble and no simple Mg biominerals are known. Mg^{2+} can, however, be easily accommodated within a calcium lattice.

Iron Deposition in Ferritin

Ferritins (Chapter 8) are widely distributed throughout living organisms. They have a highly conserved structure made up of 24 protein subunits (apoferritin) which assemble to form a roughly spherical hollow shell, with an external diameter of ~ 120 Å and an internal diameter of ~ 80 Å (Figure 19.2). The subunits form a classical four helical bundle, with a short fifth helix at the C-terminal end of the protein. Ferritins are highly symmetrical molecules with two-fold, three-fold, and four-fold axes of symmetry (Figure 19.2). Mammalian ferritins are heteropolymers, made up of variable proportions of two types of subunit, H and L. Tissues involved predominantly in iron storage, like liver and spleen, have a high content of L-chains. In contrast, tissues like heart and brain which require protection from the potential toxic effects of ‘free’ iron, provoking the generation of hydroxyl radicals, have a preponderance of H chains. While both types of subunit have closely similar tertiary structures they have

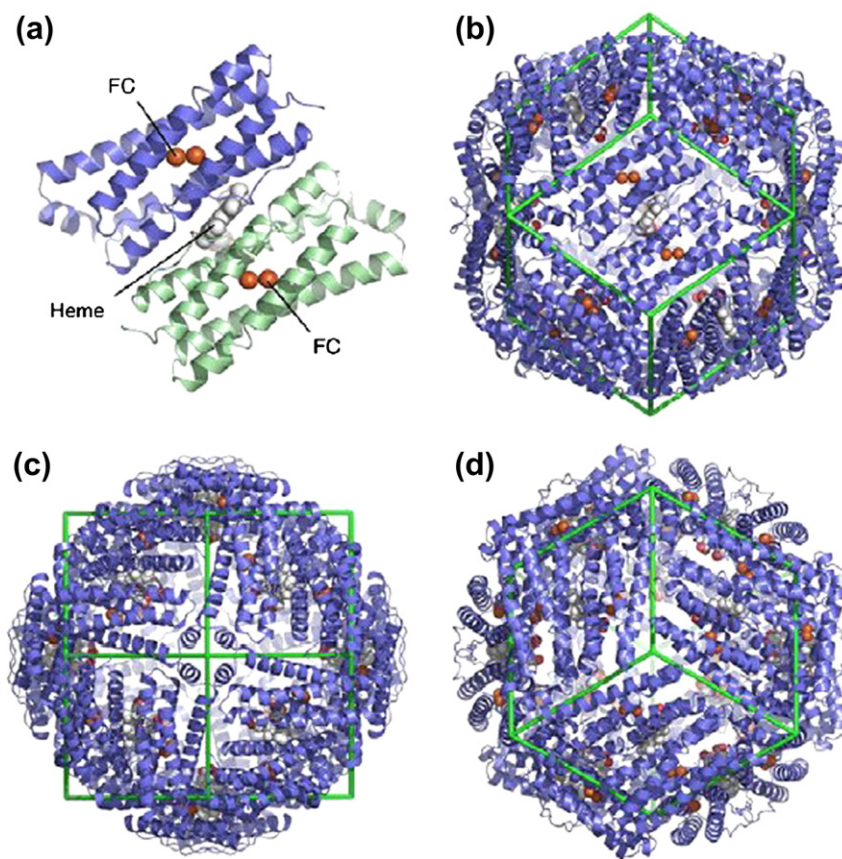


FIGURE 19.2 Structure of BFR. Cartoon representations of (a), the *E. coli* BFR (pdb 3E1M) subunit dimer peptide backbone showing the position of the intra-subunit dinuclear ferroxidase centre and inter-subunit haem site, (b–d), the overall structure of 24 meric *E. coli* BFR looking down a two-fold (b), four-fold (c), and three-fold (d) symmetry axis. (From Le Brun, Crow, Murphy, Mauk, & Moore, 2010. Copyright 2010 with permission from Elsevier.)

only around 50% homology of sequence. There is another important difference between H- and L-chain subunits. In the centre of the four-helix bundle, H-subunits have a dinuclear iron site, the so-called ferroxidase site, which catalyses the oxidation of Fe^{2+} . The ferroxidase site is found in the bacterial ferritins FTN and BFR as well. BFR also has a haem molecule located at the interface between each subunit dimer (Figure 19.2), as we pointed out in Chapter 8. In contrast with H subunits, L-subunits have nucleation sites, at which the iron core of the ferritin molecule is thought to be formed. As we will see shortly, both types of chains are required for optimal iron assimilation (Bou-Abdallah, 2010; Crichton and Declercq, 2010).

Mammalian ferritins can accommodate polynuclear iron clusters containing up to 4,500 atoms of iron, although as isolated they usually contain between 2000 to 3000 iron atoms. This water-soluble, non-toxic, yet bioavailable form of iron is a hydrated ferric oxide mineral core with variable amounts of phosphate. The iron cores of mammalian ferritins are ferrihydrite-like (Figure 19.3) with varying degrees of crystallinity, whereas those from bacterioferritins are amorphous due to their high phosphate content. Ferrihydrite is a ubiquitous nanocrystalline mineral, found in natural sediments as the precursor of haematite, and is often found in areas contaminated by acid mine drainage. Because of its extremely high surface area and reactivity, ferrihydrite plays an important role in sequestering contaminants from groundwater and streams and is used as an industrial sorbent in applications like direct coal liquefaction and metallurgical processing.

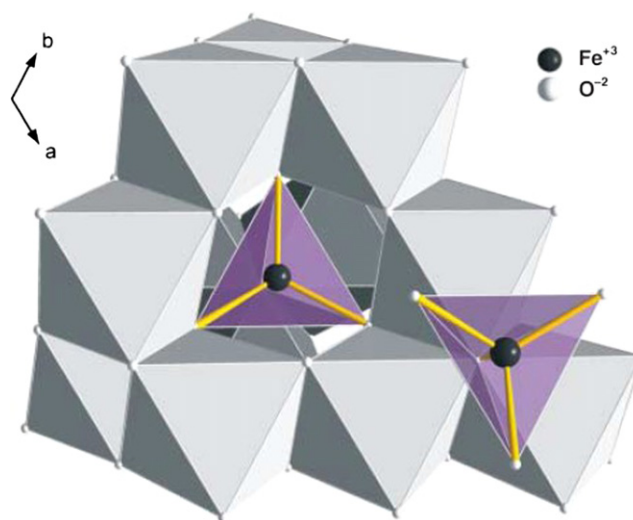


FIGURE 19.3 Polyhedral representation of the ideal ferrihydrite structure viewed along the c axis. The central FeO_4 tetrahedra are surrounded by 12 FeO_6 octahedra. (From Michel *et al.*, 2007. Copyright 2007 with permission from AAAS.)

Iron incorporation into mammalian ferritins is thought to involve the following steps: (1) uptake of Fe^{2+} into the protein shell, most probably through the hydrophilic 3-fold channels, (2) oxidation of ferrous iron by the dinuclear ferroxidase sites situated within the four-helix bundle of H-chain subunits by molecular O_2 , producing H_2O_2 , (3) migration of Fe^{3+} from the ferroxidase sites to nucleation sites on the interior surface of the L-chain subunits of the protein shell, which facilitate mineralisation, and (4) growth of the ferrihydrite mineral crystalline core via iron oxidation and mineralisation on the surface of the growing crystallite itself. The model which best describes the global biomineralisation process in mammalian ferritins is shown in Figure 19.4, and is called the crystal growth mechanism, originally proposed over thirty years ago (Crichton & Roman, 1978).

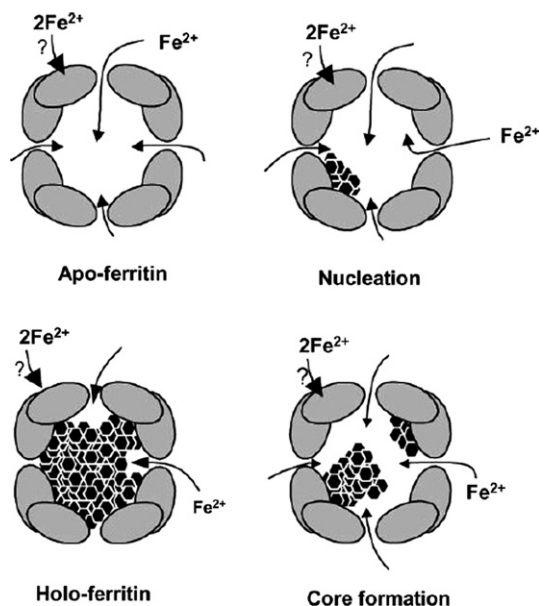


FIGURE 19.4 Representation of the crystal growth mechanism. (Adapted from Lewin *et al.*, 2005.)

The substrates involved in ferritin iron deposition (Fe^{2+} , Fe^{3+} , O_2 .) gain access to the interior of the apoferritin protein shell through the threefold channels. Calculations of electrostatic potential in HuHF show that the negative outer entrance is surrounded by patches of positive potential and that this attracts cations towards the channel entrance. The role of the threefold channel in the entry of divalent cations into the interior of the protein is underlined by our studies on recombinant human H-chain ferritin (rHuH); which show the way Zn^{2+} ions can transit through this channel, using the configurational flexibility of a key cysteine residue to move the ion through the channel (Figure 19.5), in a manner reminiscent of transit through the potassium channel described in Chapter 9. $\text{Zn}(\text{II})$ was used as a redox-stable alternative for $\text{Fe}(\text{II})$.

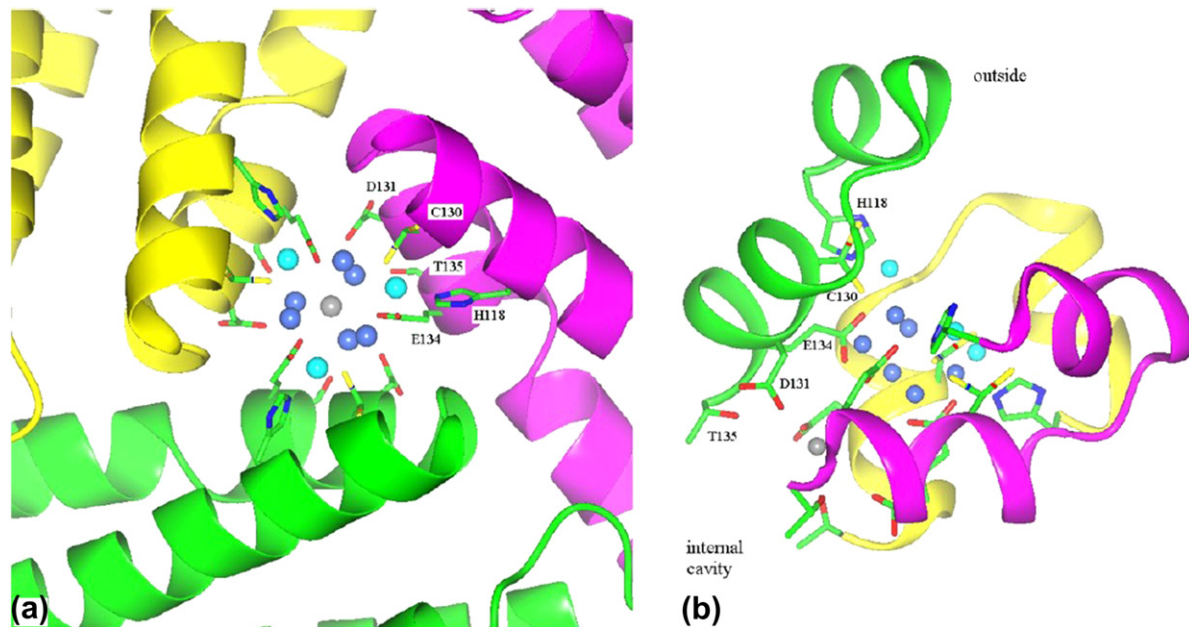


FIGURE 19.5 In the Zn derivative crystal structures, the channel aligned on the 3-fold symmetry axis shows binding to three zinc atoms and their symmetrically related subunits; the first is in the entrance of the funnel-shaped channel (in cyan), the second is in an alternative position (in blue), and the third is aligned on the 3-fold axis (in gray). The two representations are in two different orientations; (a) is aligned on the 3-fold axis and (b) is perpendicular to the axis. (From Toussaint, Bertrand, Hue, Crichton, & Declercq, 2007. Copyright 2007 with permission from Elsevier.)

$\text{Fe}(\text{II})$ must then move from the 12 Å long channel, and traverse a further distance of about 8 Å along a hydrophilic pathway from the inner side of the three-fold channel to the ferroxidase site, and a putative pathway for $\text{Fe}(\text{II})$ is shown in Figure 19.6. The diiron ferroxidase centre is located in the central region of the four-helix subunit bundle and the coordination geometry of the ferroxidase centre of human H-chain ferritin is shown in Figure 19.7. Detailed analysis of the ferroxidase reaction in H-chain ferritin has allowed the identification of a number of intermediates, which are illustrated in Figure 19.8.

While the initial stage of iron incorporation in mammalian ferritins requires the ferroxidase sites of the H-chains, thereafter the inner surface of the protein shell of the L chains provides nucleation sites which supply ligands that can partially coordinate iron but which leave some coordination spheres available for mineral phase anions. This enables the biomineralisation process to proceed, with formation of one or more small polynuclear ferrihydrite crystallites, which can then act as nucleation centres for mineral growth. Most probably, one of these clusters will become the dominant nucleation centre and growth of the mineral would then occur from this centre.

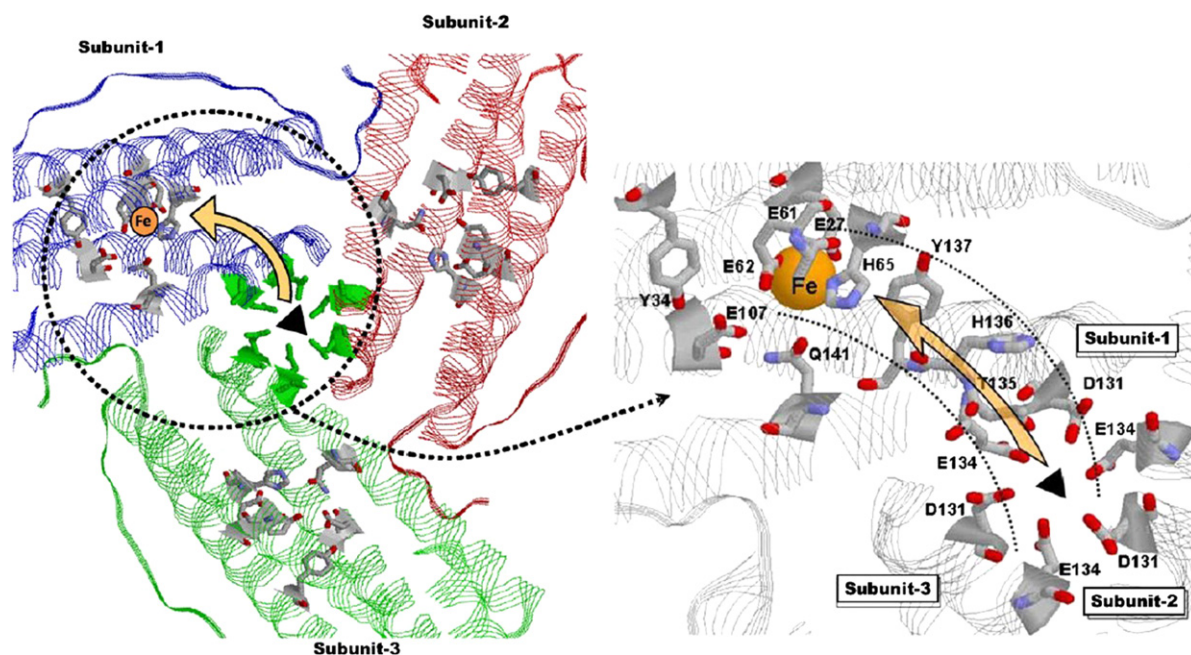


FIGURE 19.6 Internal view of the three-fold channel of ferritin (left panel). The right panel shows a putative Fe(II) pathway from the three-fold channel to the ferroxidase centre of the protein. (From Bou Abdallah, 2010. Copyright 2010 with permission from Elsevier.)

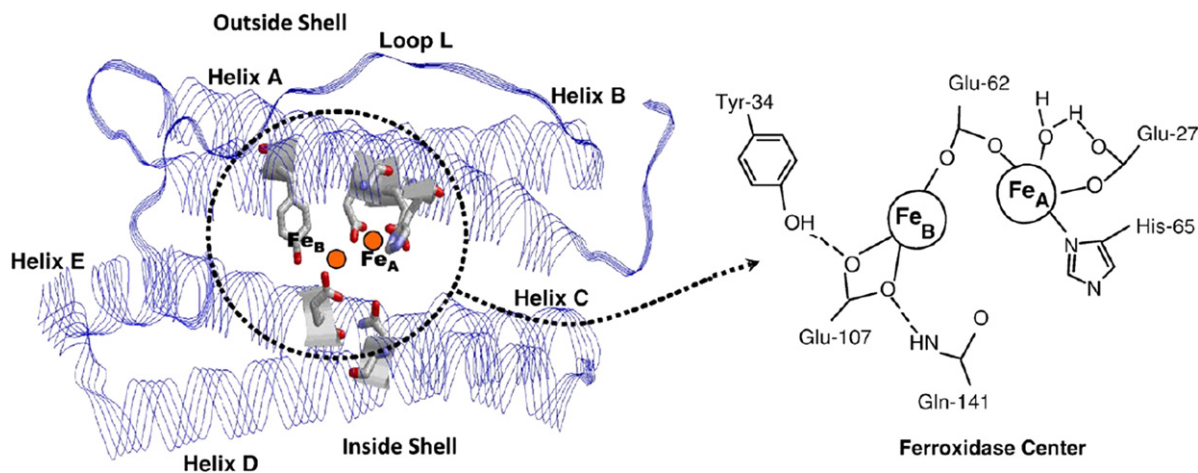


FIGURE 19.7 Schematic view of the di-iron ferroxidase centre on the four-helix of the H-chain ferritin (left panel). Dinuclear ferroxidase centre diagram (right panel) showing the amino acid residues. (From Bou Abdallah, 2010. Copyright 2010 with permission from Elsevier.)

At some stage, oxidation by the protein would cease to be important with essentially all of the oxidation taking place on the surface of the mineral. The role of the protein is to maintain the growing ferrihydrite core within the confines of the protein shell, thus maintaining the insoluble ferric oxyhydroxide in a water-soluble form, while the crystal growth phase of biomineralisation takes place exclusively on the surface of the growing iron mineral crystallite.

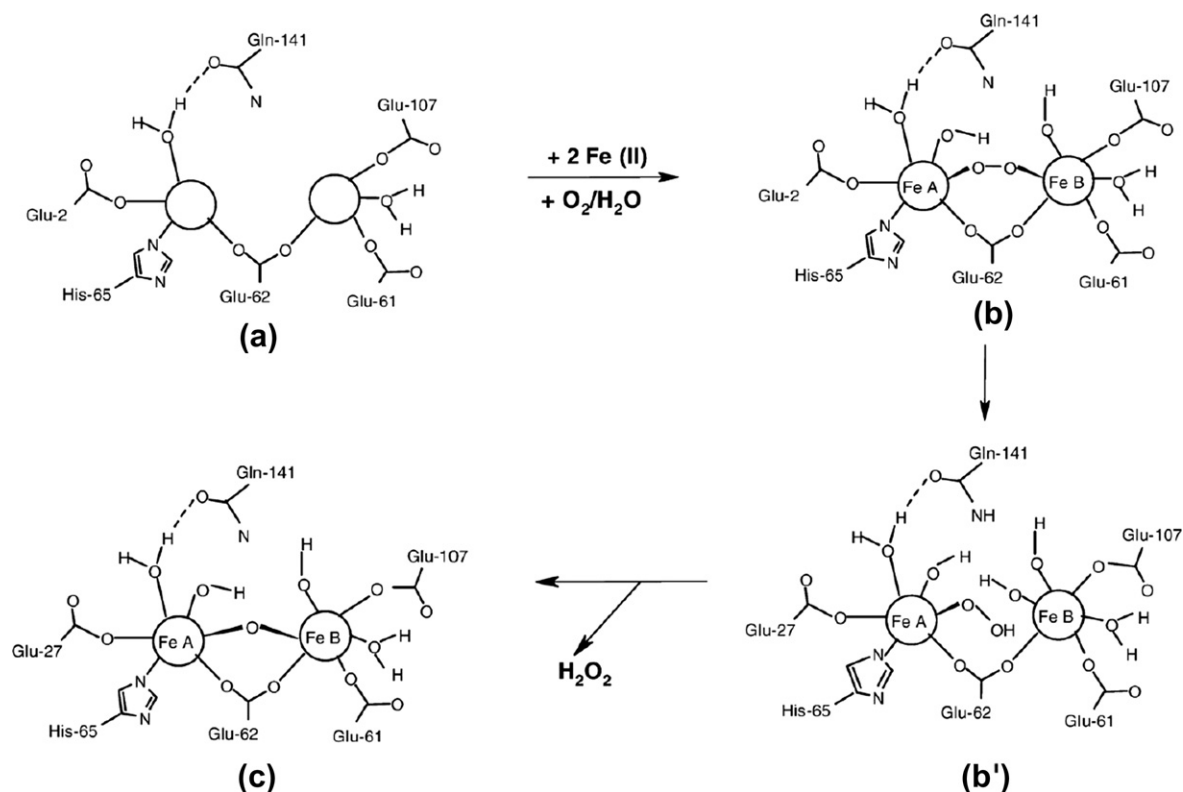


FIGURE 19.8 Ferroxidase centre reaction intermediates in H-chain ferritin. (a) apoprotein, (b) μ -peroxo di-iron(III) complex, (b') μ -hydroperoxo di-iron(III) complex, and (c) μ -oxo di-iron(III) complex. (From Bou Abdallah, 2010. Copyright 2010 with permission from Elsevier.)

While core formation during hydrolysis of Fe(III) produces electrically neutral ferrihydrite, it also produces protons: two per Fe(II) oxidised and hydrolysed, whether due to iron oxidation and hydrolysis at the ferroxidase centre, followed by further hydrolysis and migration to the core nucleation sites or by direct Fe(II) oxidation and hydrolysis on the mineral surface of the growing core. These protons must either be evacuated from the cavity or else their charges must be neutralised by incoming anions, and it seems likely that both mechanisms are employed. In most ferritin molecules, some hydroxyl ions of the core (mostly on the core surface) are replaced by phosphate ions, while electrostatic calculations suggest that expulsion of protons (as well as Fe³⁺ or Fe²⁺ ions) or uptake of orthophosphate (or other anions such as chloride) would be facilitated by the electrostatic field gradient through the four-fold channels in human H-chain ferritin.

Why mammalian ferritin cores contain ferrihydrite-like structures rather than some other mineral phase is less easy to understand, and presumably reflects the way in which the biomineral is built up within the interior of the protein shell together with the geometry of the presumed nucleation sites. The phosphate content in the intracellular milieu can readily be invoked to explain the amorphous nature of the iron core of bacterioferritins and plants. Indeed, when the iron cores of bacterioferritins are reconstituted in the absence of phosphate, they are found to be more highly ordered than their native counterparts, and give electron diffraction lines typical of the ferrihydrite structure. The 12 subunit ferritin-like Dps protein, discussed in Chapter 8, forms a ferrihydrite-like mineral core, which would seem to imply that deposition of ferric oxyhydroxides within a hollow protein cavity (albeit smaller) leads to the production of this particular mineral form.

Ferritin as a Supramolecular Template in Nanotechnology

As one might have anticipated, the extraordinary way in which biological systems manage to control the morphology, the particular form or crystal structure which is selected, and the precise spatial localisation in which it is formed has made biomineralisation processes a focal point for nanotechnology. Understanding the interactions between hard (inorganic) and soft (organic) materials has stimulated the design and application of synthetic biomimetic systems. Ferritin appears as an apparently simple system with only a single protein component, which directs biomineralisation of iron oxide at the protein–solution interface closed shell. Ferritin itself catalyses the transformation of the substrate, possesses a nucleation site for the biomineral, and its architecture defines and imposes the overall morphology of the final product. Add to this that the protein shell maintains the final biomineral product both soluble and mobile, while at the same time being biochemically inert, and one can understand the drive to push ferritin biomineralisation towards biomimetic synthesis.

The potential of some synthetic ferritins in which a non-native inorganic material has been introduced into the cavity or the external shell has been modified, has become a very active area of research. In early studies, the apoferritin protein shell was simply as a ‘nano reactor’ for the formation of a variety of non-native, unusual, mineralised nanoparticles. For example, under conditions of high pH and limited oxygen, it is possible to produce ferritin cores corresponding to the magnetic cores of mixed valence minerals. Thus, magnetite (Fe_3O_4) and/or maghaemite ($\gamma\text{-Fe}_2\text{O}_3$) can be generated *in vitro* which may have potential interest as MRI contrast agents. Cores of amorphous iron sulfide have been produced, containing either 500 or 3000 iron atoms with the iron mostly in the +3 state in FeS_4 tetrahedra with connecting FeS_2Fe bridges. Cores of manganese oxyhydroxide (MnOOH) have been synthesised in both H and L chain homopolymers, and in both mammalian ferritins and *L. innocua* Dps protein, a mineral core of cobalt and oxygen can be generated by the protein-catalysed oxidation of Co^{2+} to Co^{3+} . Ferritins without their iron core can be used to photocatalyse the formation of $\text{Cu}(0)$ colloids from aqueous Cu^{2+} within the protein cavity. Ferritin cores containing Cu and CuFe Prussian Blue derivative nanoparticles (Figure 19.9) have been prepared.

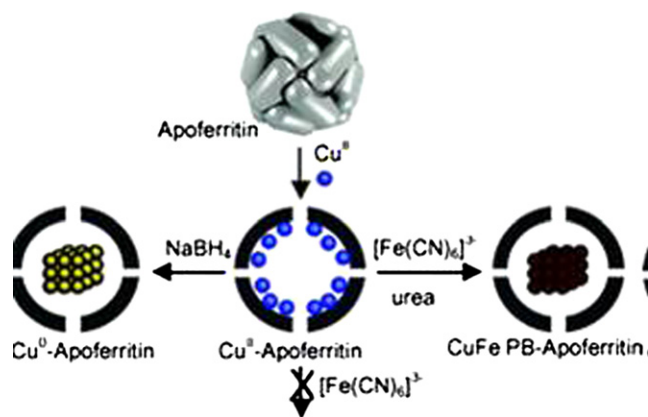


FIGURE 19.9 Cu and CuFe Prussian Blue nanoparticles have been prepared using a Cu(II) loaded apoferritin as a chemically and spatially confined environment for their construction. (from Gálvez *et al.*, 2005. Copyright 2005 with permission from the Royal Society of Chemistry.)

Material scientists have exploited a range of ferritin superfamily proteins as supramolecular templates to encapsulate nanoparticles and/or as well-defined building blocks for fabrication of higher order assembly. For example, the organometallic $\text{Rh}(\text{nbd})$ (nbd = norbornadiene) can be immobilised at specific sites within the apoferritin molecule where it can catalyse the polymerisation of phenylacetylene within the protein shell (Figure 19.10). This is but one example of the quest to develop highly effective ‘artificial metalloenzymes’ by rational design of metal coordination sites within the ferritin molecule.

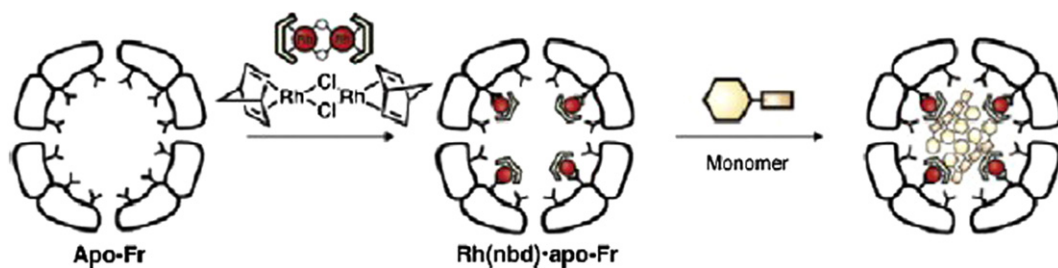


FIGURE 19.10 A schematic illustration of immobilisation of $[\text{Ru}(\text{nbd})\text{Cl}]_2$ complex into apoferritin cage followed by polymerisation of phenylacetylene catalysed by the ferritin. The polymerisation reaction occurs site-specifically inside of the ferritin cage. (From Uchida, Kang, Reichhardt, Harlen, & Douglas, 2010. Copyright 2010 with permission from Elsevier.)

Besides the interior cavity, the exterior surface of the protein cages can be modified without altering the interior characteristics. This allows the protein cages to be delivered to a targeted tissue *in vivo*. The interface between subunits can also be utilised to create chimeric protein cages. Utilizing such ideas, the ferritin superfamily (including the Dps proteins) has been exploited for the development of a broad range of materials with applications from biomedicine to electronics. For example, the two approaches can be combined to target gadolinium-loaded ferritin to tumour cells for use as a contrast agent, as we describe in more detail in Chapter 22.

Formation of Magnetite in Magnetotactic Bacteria

Ferrihydrite is not the only mineral form of iron that is found in nature. Magnetite, the $\text{Fe}^{2+}/\text{Fe}^{3+}$ mineral (Fe_3O_4), is found in magnetotactic bacteria as well as in bees, birds, and fish, where it is believed to function as a navigational magnetic sensor. Some bacteria can form pseudo-single crystals of akaganeite ($\beta\text{-FeOOH}$), many millimetres long in a polysaccharide-template-directed process, and goethite ($\alpha\text{-FeOOH}$) is found in the radular teeth of limpets and in some human haemosiderins.

Magnetotactic bacteria are a group of microorganisms which synthesise nano-sized crystals of magnetite which enable them to use geomagnetic fields for direction sensing. They were discovered by Richard Blakemore in 1975, and at the time were regarded as a kind of curiosity — the idea that bacteria would swim North or South according to some kind of internal compass seemed as absurd as asking if there really was a tRNA to incorporate selenocysteine into proteins (by the way, both turned out subsequently to be correct).

Confronted with the often expensive methods used to synthesise nanomaterials, which involve the use of hazardous chemicals, there is a growing concern to develop environmental-friendly and sustainable methods for the synthesis of nanoparticles of different compositions, sizes, shapes, and controlled dispersity, particularly using a ‘green chemistry’ approach which interconnects nanotechnology and microbial biotechnology.

Magnetic iron oxide particles, such as magnetite (Fe_3O_4) or maghaemite ($\gamma\text{-Fe}_2\text{O}_3$), are widely used in medical and diagnostic applications such as magnetic resonance imaging (MRI), cell separation, and drug delivery. They offer great technological potential since they can be conveniently collected with an external magnetic field. Magnetotactic bacteria synthesise membrane-enveloped magnetic particles (magnetosomes) with well-controlled size and morphology, which can be readily dispersed in aqueous solutions, making them ideal biotechnological materials. They are formed under incredibly mild conditions compared with the usual synthetic methods, and easily outperform artificial materials. Hence, there has been great interest in the formation of magnetite and magnetosomes with a view to their exploitation in biomedical applications, which we review here.

Although magnetotactic bacteria (MTB) have diverse morphologies, they are characterised by the clustering of the genes required for magnetosome formation (Komeili, 2007; Matsunaga and Okamura, 2003), which are

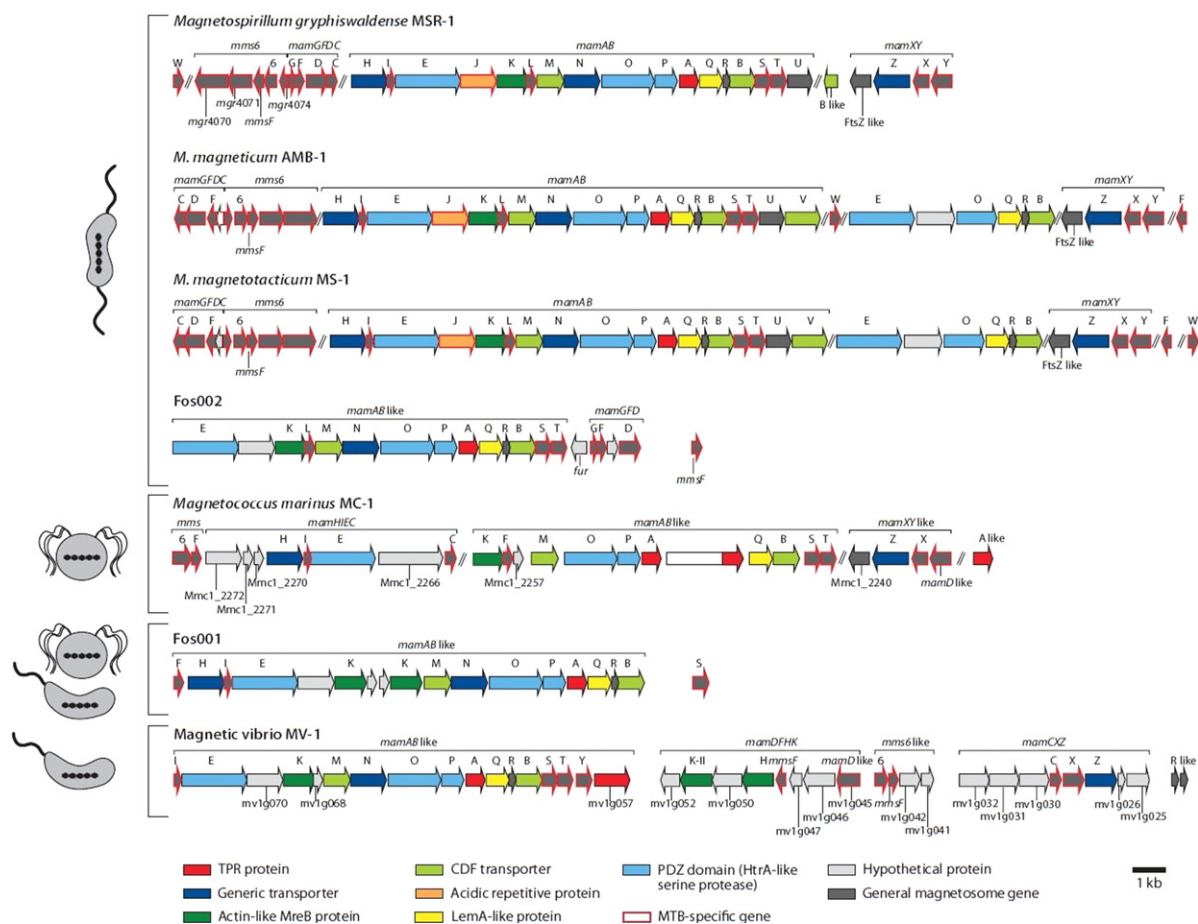


FIGURE 19.11 Molecular organisation of magnetosome genes in the magnetosome island (MAI) of all sequenced magnetotactic bacteria. Different coloured arrows indicate characteristic features of the encoded proteins. The red outline indicates MTB-specific genes, which are shared by all MTB but have no homologues in nonmagnetic organisms. Diagrams of the representative morphologies are shown. (From Jogler & Schüler, 2009. Copyright 2009 with permission from Annual Reviews.)

predominantly located in several operons of a conserved genomic magnetosome island (Figure 19.11). Although a large set of candidate genes has been identified, only a few genes and proteins have been characterised with respect to their function. The small Mms6 protein, which is a tightly bound constituent of the magnetosome membrane, affects magnetite crystallisation *in vitro*. The four small, hydrophobic magnetosome proteins MamG, MamF, MamD, and MamC are specifically involved in the size control of magnetite crystals. MamJ and MamK are cytoskeletal elements involved in the assembly of magnetosome chains.

In most MTBs, the mineral core of the magnetosome consists of magnetite (Fe_3O_4) although a few synthesise magnetosomes containing the magnetic iron sulfide greignite (Fe_3S_4). The biomineralisation of magnetite crystals requires the accumulation of large amounts (>4% by dry weight) of iron which is taken up into precursors which include ferritin and a high-spin ferrous species. The process of biomineralisation involves three steps (Figure 19.12). First, a membrane invagination is derived from the inner membrane, and proteins destined for the magnetosome are sorted away from cell membrane proteins. The vesicle which forms from this invagination serves as the precursor of the magnetosome membrane. In the second stage, ferrous ions are accumulated

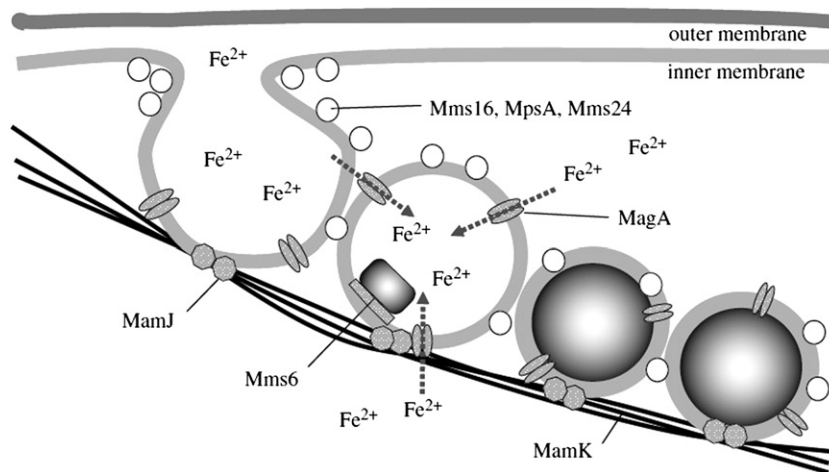


FIGURE 19.12 Model for magnetosome formation.

within the vesicles by transmembrane iron transporters and the invaginations/vesicles are assembled into a chain with the help of MamJ and MamK proteins. In the third and final step, iron is transformed into highly ordered magnetite crystals within the magnetosome membrane with the triggering of magnetite crystal nucleation by a number of tightly bound magnetosome proteins. This requires strict control of iron supersaturation, pH, and redox potentials.

It is striking to see the vast difference in the degree of complexity required to carry out the biomineralisation of magnetite in magnetosomes when we compare it to the relative simplicity of that of ferritin.

Calcium-Based Biominerals – Calcium Carbonates in Ascidians and Molluscs

Biominerals based on calcium carbonate are found in a very large number of organisms. The shells of molluscs are among the most abundant biogenic minerals, and are composed of 95%–99% calcium carbonate crystal and less than 5% organic matrix. Shell layers are formed from calcium carbonate as aragonite or calcite crystals corresponding to different mineral textures (also called microstructures). The organic matrix of the shell is composed of proteins and polysaccharides, which are thought to direct the formation of the calcium carbonate crystal and thus are responsible for the extraordinary properties of the shell. For example, nacre, the aragonite layer of the shell, exhibits a fracture resistance 3000 times higher than that of abiotic aragonite. The different crystal polymorphisms and microstructures of the layers are controlled by proteins secreted from outer epithelial cells in different regions of the mantle. [Figure 19.13](#) shows the molecular correspondence at the inorganic–organic interface in the nacre shell layer of *Nautilus repertus*. There is a close geometric match between the periodicity of the protein β -sheet and the lattice spacings of the aragonite, and it has been suggested that there is molecular complementarity between Ca atoms in the aragonite and aspartic acid residues organised in the sequence Asp-X-Asp (where X = a neutral residue) along the β -sheet.

Ascidians (Tunicates) are a class of marine organisms (including sea squirts) which have a characteristic tough covering, called a tunic. The tunic is composed of cellulose and contains small calcium-containing ‘spicules’ in a wide variety of shapes ([Figure 19.14](#)): they are thought to contribute to the stiffness of the tissues. They are formed in close association with cells called sclerocytes, which secrete a very tough enveloping organic layer as well as in forming the mineralised spicule. The two spicules shown in [Figure 19.7](#) from the tunicate *P. pachydermatina* both contain an unusual and unstable form of calcium carbonate called amorphous calcium carbonate (ACC) together with the organic envelope. The knobbed or “dogbone” tunic spicules also contain an overlay of calcite. Addition of macromolecules extracted from the calcite layer of these spicules speeds up formation of

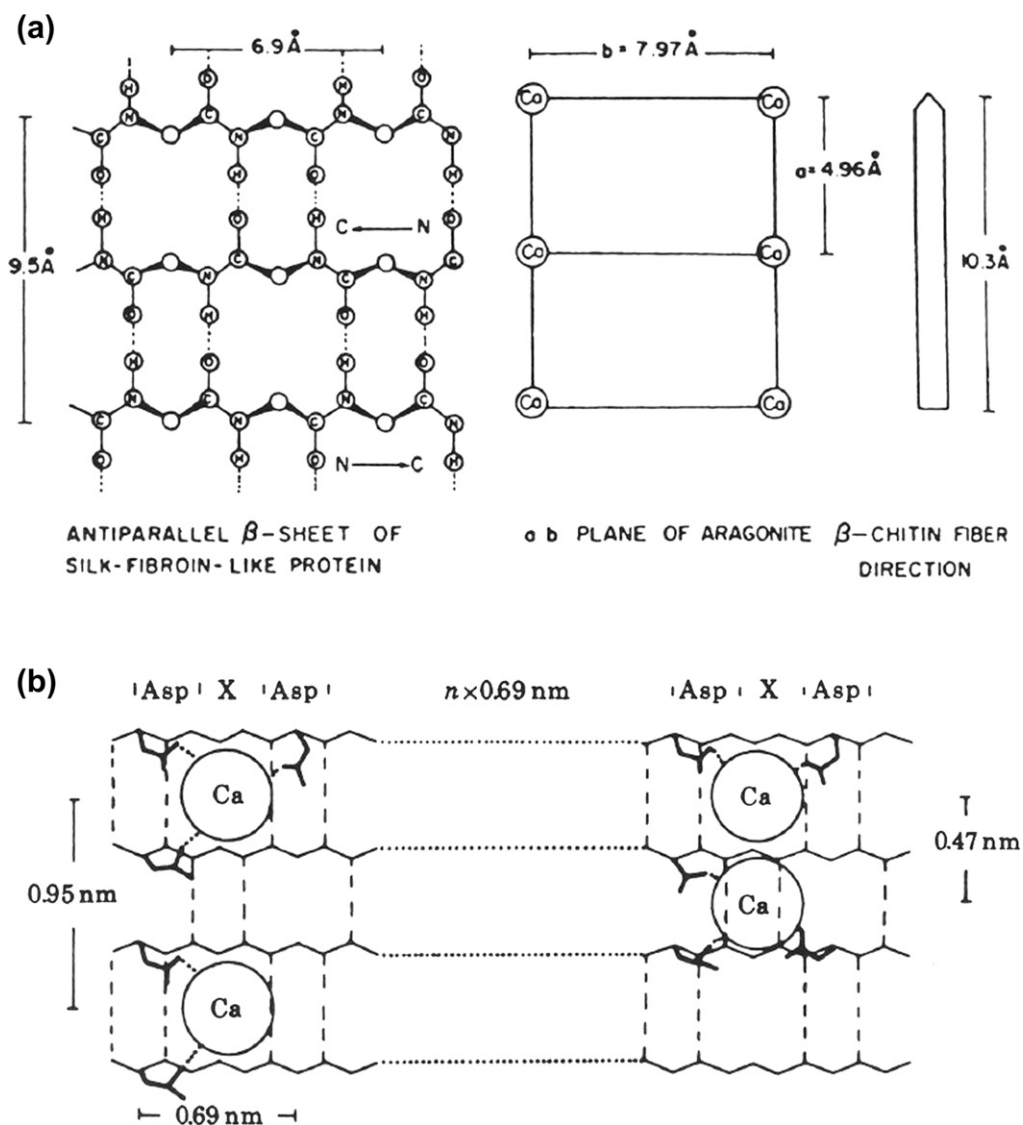


FIGURE 19.13 Molecular correspondence of the inorganic–organic interface in the nacreous shell layer of *Nautilus repertus*. (a) structural relationships between protein sheets, aragonite crystals, and chitin fibres. There is close geometric match between the periodicity of the β -sheet and lattice spacings in the ab plane of aragonite. (b) Possible modes of molecular complementarity between Ca atoms in the aragonite ab face and Asp residues in the sequence Asp-X-Asp along β -sheet matrix interface. (From Mann, Webb, & Williams, 1989: pp. 541.)

calcite crystals, whereas the corresponding extract from the ACC layer inhibits crystal formation. In contrast, macromolecules from antler spicules (composed only of pure ACC) favoured formation of the stable hydrated form of ACC. This clearly shows that the proteins and other macromolecules occluded with the mineral phase play an important role both in stabilisation of unstable forms like ACC and in selection of the polymorphic form which is selected (in this case ACC or calcite).

The shells of molluscs, like clam, oyster, abalone, scallop, and fresh water snail, use CaCO_3 as the principal constituent for an extraordinary array of diverse structures. Several approaches have led, and will lead further in the future, to a greater understanding of how these complex forms are generated.

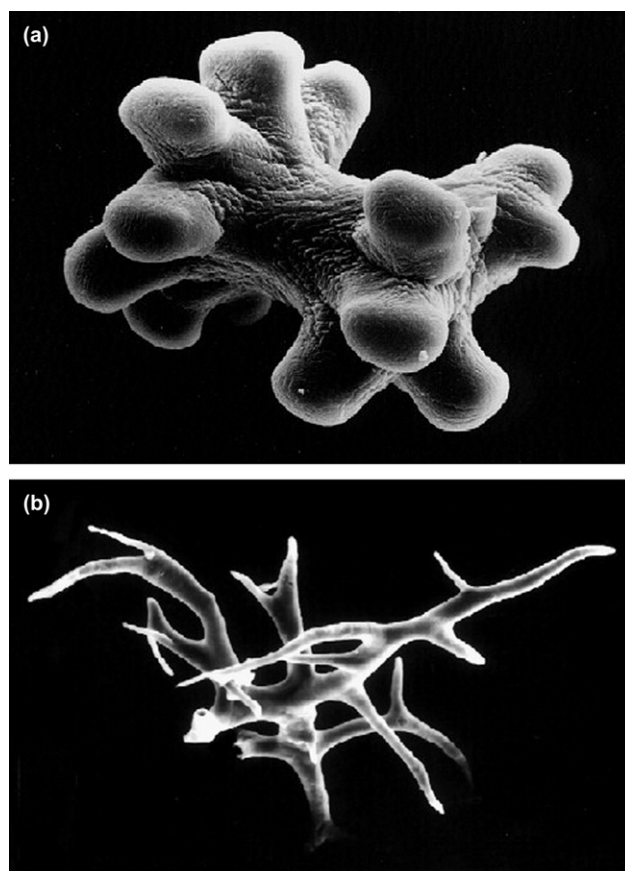


FIGURE 19.14 Scanning electron micrographs of spicules from the tunicate, *P. pachydermatina*. (a) Dogbone spicule from the tunic. (b) Antler spicule from the branchial sac. 10- μm scale bars are shown on the figures. Note the scale differences. (From Wilt, 2005. Copyright 2005 with permission from Elsevier.)

One interesting method is to examine the development of the shell from the larval form of the organism all the way to the adult. The amorphous calcium carbonate (ACC) referred to above has been found together with aragonite in larval shells, and the ACC is gradually transformed into aragonite over a period of hours or days. This novel suggestion that stable crystalline forms of calcium carbonate are formed from an amorphous precursor form, which transforms to the crystal in a slow, regulated way, is becoming increasingly supported by experimental evidence. This is underlined by the observation that the aragonite found in larvae is less crystalline than aragonite obtained from non-biogenic sources, and that the mineral found in embryos was ACC, but showed short-range order similar to aragonite.

Shell formation continues after morphogenesis, and the adult shell may contain either aragonite alone, or a mixture of layers of aragonite and calcite. In species which have a mixture, the layer of calcite, called the prismatic layer, is deposited close to the periostracum, which covers the external surface of the shell (facing the sea water). The inner nacre layer of aragonite is then deposited (Figure 19.15). Shells which have both a prismatic layer of calcite and nacre of aragonite must control the form of CaCO_3 which is deposited. It has been found that soluble molecules of the matrix extracted from the nacre favour aragonite formation *in vitro*, whereas extracts from prismatic layers favour calcite formation *in vitro*. The implication is that the cells which secrete the matrix

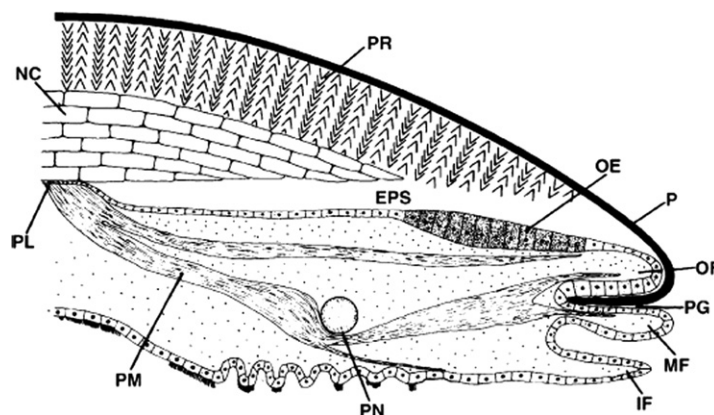


FIGURE 19.15 Diagram of a section through the edge of the shell and attached mantle of a bivalve mollusc. Note the layers of periostracum, prismatic calcite, and aragonitic nacre underlain by the extrapallial space and mantle. EPS, extrapallial space; MF, middle fold of mantle; NC, nacre; OED, outer epithelium of the mantle; OF, outer fold of the mantle; P, periostracum; PG, periostracal groove; PL, pallial line; PM, pallial muscle; PN, pallial nerve, PR, prismatic shell layer. (From Wilt, 2005. Copyright 2005 with permission from Elsevier.)

are programmed to change the composition of the matrix at precise times and places, in order to regulate the change from calcite to aragonite during the transition from prism to nacre.

The final approach is to use a combination of microarray techniques, antisense oligonucleotides, functional tests, and the use of monoclonal antibodies to identify matrix proteins and families of matrix proteins involved in the biomineralisation process, and ultimately to establish their function. The recent publication of the genome of the sea urchin *Strongylocentrotus purpuratus* represents a promising start to the bioinformatic approach to the identification, characterisation, and functional analysis of particular molecules of the matrix involved in biomineralisation.

Biomineralisation in Bone and Enamel Formation

Bone and teeth in mammals and bony fishes all rely on calcium phosphates in the form of hydroxyapatite [$\text{Ca}_{10}(\text{PO}_4)_6(\text{OH})_2$], usually associated with around 5% carbonate (and referred to as carbonated apatite). The bones of the endoskeleton and the dentin and enamel of teeth have a high mineral content of carbonated apatite, and represent an extraordinary variety of structures with physical and mechanical properties exquisitely adapted to their particular function in the tissue where they are produced. We begin by discussing the formation of bone and then examine the biomineralisation process leading to the hardest mineralised tissue known, the enamel of mammalian teeth.

Bone is organised at five hierarchical levels of structure, shown in Figure 19.16: (1) cortical and cancellous (with an open porous structure) bone; (2) osteons (also called Haversian systems), the chief structural component of bone, consisting of lamellae (layer) of bone surrounding a long narrow passage, (the Haversian canal), which are clearly visible in a cross section of a long bone (e.g., the femur); (3) at the micron (μm) level, the lamellae and canals which constitute the osteons; (4) at the sub-micron scale, the mineral matrix embedded in the collagen fibres; and (5) at the nanoscale, mineral crystals, collagen, and water molecules. We will be concerned in what follows by a consideration of the organic matrix, the apatite mineral and the water, which constitute the predominant constituents of bone.

The Organic Matrix, Mineral Phase, and Bone Mineralisation

The organic matrix, which constitutes about 32% of the volume of bone, is made up of 90% type I collagen, with smaller amounts of non-collagenous proteins such as osteocalcin and osteonectin, which assist in the

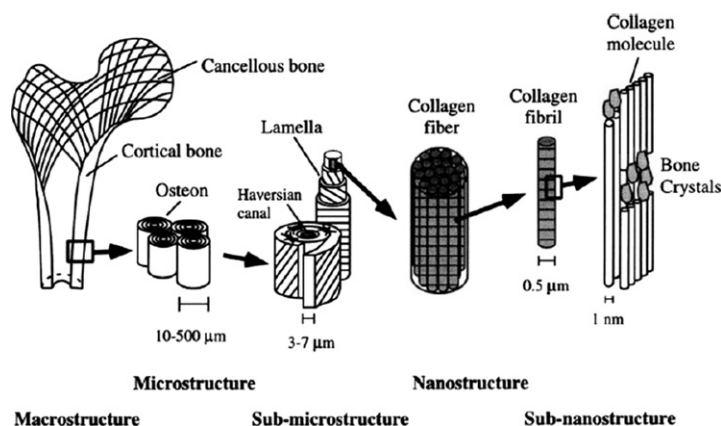


FIGURE 19.16 Hierarchies of structure in the femur. (From Nyman, Reyes, & Wang, 2005.)

biomineralisation process. Collagen is secreted by bone-forming cells, osteoblasts, as a precursor, procollagen, a helical rod made up of three intertwining polypeptide chains (Figure 19.17). It has a typical amino acid

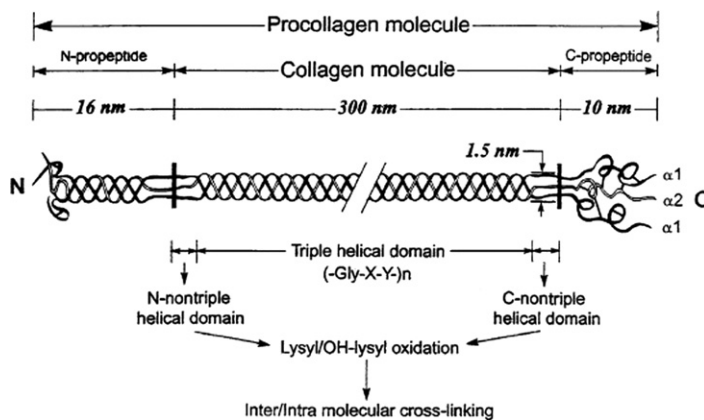


FIGURE 19.17 After cleavage of the terminal ends, the collagen molecule begins to assemble into a fibril via enzymatic cross-links. (From Nyman *et al.*, 2005.)

sequence, with glycine residues in almost every third position, and frequent occupancy of the second and third positions by proline and hydroxyproline, respectively (the latter introduced by the action of the Fe^{3+} - and ascorbate-dependent prolyl hydroxylase). After the amino- and carboxyl-terminal ends have undergone proteolytic cleavage, collagen begins to assemble into a collagen fibril, some 300 nm long and 1.2 nm in diameter, stabilised by cross-links between hydroxylysine residues (introduced by the copper-dependent enzyme lysyl hydroxylase). Other types of cross-link can also be formed.

The mineral phase constitutes about 43% of the volume of bone and mostly contains calcium and phosphate, with small, but highly significant amounts of carbonate (and a few other impurities). The bone mineral is not hydroxyapatite, but rather can be classified as carbonated apatite $[\text{Ca}_5(\text{PO}_4)_3\text{CO}_3]$. Within the mammalian skeleton, bone mineralisation depends on the organisation of the cross-linked collagen network. Initially, water fills the void space within the organic framework of the collagen matrix of the osteoid. Crystal nucleation occurs

first at multiple independent sites within the collagen fibril as well as on the surface of the fibrils. It continues into the zones between collagen molecules, displacing water molecules as it goes, to leave a final water content in bone of up to 25% of the volume. This residual water may help to stabilise collagen by forming inter- and intra-hydrogen bonds with hydrophilic residues, like the hydroxyl group of hydroxyproline and other polar side chains (Figure 19.18).

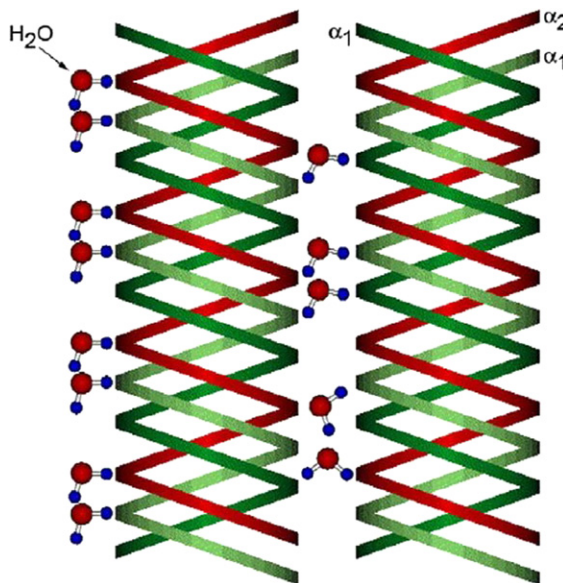


FIGURE 19.18 Water helps to stabilise collagen by forming inter- and intra-hydrogen bonds with hydrophilic residues. (From Nyman *et al.* 2005.)

The enamel of mammalian teeth is much more heavily mineralised than bone, which makes it much harder. In addition, it does not contain collagen, although in its final mature state it does contain small amounts of specialised matrix proteins. Early tooth development is a classical illustration of the interaction between two tissue types (epithelial cells and mesenchymal cells³), whereby a number of signaling molecules are involved in orchestrating reciprocal interactions between the two types of tissue.

Enamel formation is thought to involve the following steps in its assembly: (1) stimulation of cells called ameloblasts, derived from the epithelium, which are responsible for the secretion of enamel matrix proteins and the carbonated apatite of the enamel; (2) self-assembly of matrix proteins, notably amelogenin, which assembles into nanospheres to form “ribbons” of matrix; (3) secretion of saturating levels of Ca^{2+} and of PO_4^- ; (4) nucleation of crystal formation; (5) regulation of crystallite growth by the matrix; and (6) proteolytic degradation of the matrix and rapid filling in with carbonated apatite crystallite. The principal water-soluble protein of enamel is amelogenin, which is degraded as the enamel matures – transient degradation intermediates are found in developing enamel. This 180 residue hydrophobic protein self-assembles into nanospheres *in vitro*, which resemble the matrix ribbons found *in vivo*, and it interacts with carbonated apatite *in vitro* to limit crystallite growth just as it is thought to act *in vivo* to channel accumulation of the mineral crystallite into rods. However, there are other enamel-specific proteins which have been isolated, studied and in some cases cloned. And, to make

3. Mesenchymal tissue is immature, unspecialised tissue, found in the early embryo of animals, whereas epithelial cells are parenchymal cells which line an internal cavity or tube.

matters more complicated, experiments in which there is not complete lack of biomineralisation after particular gene knock-outs of single bone proteins suggest that there is likely to be a redundancy of function, and that many of the actors in this particularly complicated process still need to be identified.

Finally, it is intriguing that in terms of biomineralisation, invertebrates have based their reliance on calcium carbonates, while vertebrates appear to have used almost exclusively calcium phosphate. We say almost, because, while the use of calcium phosphates for biomineralisation is an invention of some vertebrates, they still use calcium carbonate for the formation of otoliths⁴ of the inner ear. It remains to be established if the equivalent of the gene *starmaker* required for otolith formation in zebrafish has homologues among invertebrates.

Silica-Based Biominerals

We saw in Chapter 1 that silicon is an essential element, and that it is particularly found in diatoms, in plants, and in sponges. Diatoms are unicellular algae which produce intrinsically structured cell walls made of nanopatterned silica (SiO_2). There are tens of thousands of diatom species, each forming differently sculpted silica cell walls (Figure 19.19). Diatom biosilica is an inorganic–organic hybrid material composed of inorganic silica attached

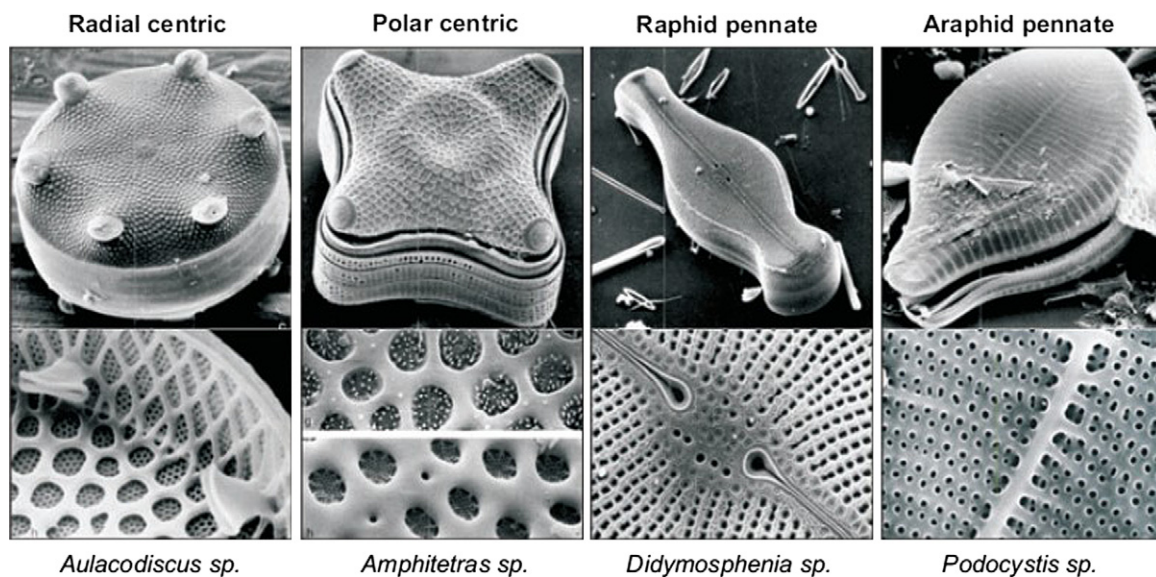


FIGURE 19.19 Scanning electron microscopy (SEM) images of the cell walls of four different diatom species. (From Kröger & Poulson, 2008. Copyright 2008 with permission from Annual Reviews.)

to specific organic macromolecules, including proteins, polysaccharides, and long chain polyamines (LCPA). The monomeric precursor for diatom silica orthosilicic acid $\text{Si}(\text{OH})_4$ is transported into the cell by the SIT family of silicic acid transporter proteins (see Chapter 1). Silica morphogenesis takes place within specialised membrane-bound compartments termed silica deposition vesicles (SDVs). After completion of morphogenesis, the silica is deposited on the cell surface through SDV exocytosis. Each diatom species appears to contain specific silaffin⁵ and LCPA molecules. Both silaffins and LCPA accelerate and control silica morphogenesis

4. Otolith — a tiny bony structure in the inner ear of lower vertebrates.

5. Silaffins (proteins with silica affinity) are a family of phosphoproteins, which are loosely associated with diatom silica; two other families of cell proteins, frustulins, and pleuralins are found bound to the cell walls of diatoms.

from silicic acid, and are believed to be involved in the morphogenesis of the species-specific silica nanopatterns inside the SDVs.

Silica bodies (phytoliths) in plants serve a variety of purposes, including lending the plant structural rigidity by supporting the shoot, preventing it from falling over, and giving mechanical strength and rigidity to leaves. Their hardness deters predators by wearing down tooth enamel, and it has been claimed that the evolution of the teeth of horses correlates with the increased phytolith content of grasses. Silica bodies make some plants distasteful or give their tissues a prickly texture. The hairs that are responsible for the stinging caused by Stinging Nettles, the so-called trichomes, are made of fine hollow needles of silica. They are so sharp that just a gentle brush with the back of the hand is sufficient for them to penetrate the skin and inject a cocktail of inflammatory substances, including the neuro-transmitters serotonin, histamine and acetylcholine, two leukotrienes, and above all the bicyclic octapeptide moroidin, which is the compound responsible for most of the pain and redness of nettle rash.

The sponges polymerise silica enzymatically, depositing hydrated amorphous silica in highly specialised sponge cells, generating massive siliceous skeletal elements (spicules) that range in size from micrometres to metres. The spicules give structural stability to the sponges, deter predators, and transmit light in the same way as optic fibres. Formation of silica nanoparticles is mediated by the enzyme silicatein and starts intracellularly. The resulting nanoparticles fuse and subsequently form concentric lamellar layers around a central protein filament, consisting of silicatein and the scaffold protein silintaphin-1. Once the growing spicule is extruded into the extracellular space, it obtains its final size and shape. Again, this process is mediated by silicatein and silintaphin-1, in combination with other molecules such as galectin and collagen. This is illustrated in Figure 19.20 by the

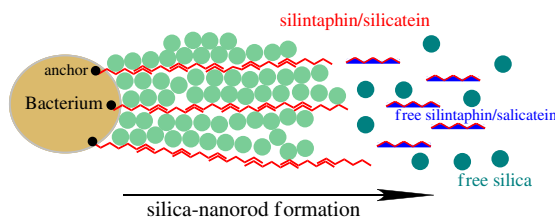


FIGURE 19.20 Proposed formation of light wave guiding biosiliceous nanorods by bacteria, expressing recombinant silicatein and silintaphin-1 proteins. The scaffold protein silintaphin-1 binds and organises molecules of the enzyme silicatein that, after addition of orthosilicate, produces and assembles siliceous nanoparticles to rods. (Adapted from Müller *et al.*, 2009.)

formation of the light wave guiding biosilica nanorods, which confirms very early observations that spicules contain an organic scaffold, which we now know is the structure-providing scaffold, while silicatein is at the basis of the formation of the inorganic matrix.

REFERENCES

- Bou-Abdallah, F. (2010). The iron redox and hydrolysis chemistry of the ferritins. *Biochimica et Biophysica Acta*, 1800, 719–731.
- Crichton, R. R., & Declercq, J. P. (2010). X-ray structures of ferritins and related proteins. *Biochimica et Biophysica Acta*, 1800, 706–718.
- Crichton, R. R., & Roman, F. (1978). A novel mechanism for ferritin iron oxidation and deposition. *J. Mol. Catal.*, 4, 75–82.
- Gálvez, N., Sánchez, P., & Domínguez-Vera, J. M. (2005). Preparation of Cu and CuFe Prussian Blue derivative nanoparticles using the apoferritin cavity as nanoreactor. *Dalton Trans.*, 7, 2492–2494.
- Jogler, C., & Schüler, D. (2009). Genomics, genetics, and cell biology of magnetosome formation. *The Annual Review of Microbiology*, 63, 501–521.
- Komeili, A. (2007). Molecular mechanisms of magnetosome formation. *The Annual Review of Biochemistry*, 76, 351–366.
- Kröger, N., & Poulsen, N. (2008). Diatoms—from cell wall biogenesis to nanotechnology. *Annual Review of Genetics*, 42, 83–107.

- LaMer, V. K., & Dinegar, R. H. J. (1950). Theory, production and mechanism of formation of monodispersed hydrosols. *Journal of the American Chemical Society*, 72, 4847–4854.
- Le Brun, N. E., Crow, A., Murphy, M. E., Mauk, A. G., & Moore, G. R. (2010). Iron core mineralisation in prokaryotic ferritins. *Biochimica et Biophysica Acta*, 1800, 732–744.
- Lewin, A., Moore, G. R., & Le Brun, N. E. (2005). Formation of protein-coated iron minerals. *Dalton Trans.*, 21, 3597–3610.
- Mann, S., Webb, J., & Williams, R. J. P. (1989). *Biomining: chemical and biochemical perspectives*. Weinheim: VCH.
- Matsunaga, T., & Okamura, Y. (2003). Genes and proteins involved in bacterial magnetic particle formation. *Trends in Microbiology*, 11, 536–541.
- Meldrum, F. C., & Cölfen, H. (2008). Controlling mineral morphologies and structures in biological and synthetic systems. *Chemical Reviews*, 108, 4332–4432.
- Michel, F. M., Ehm, L., Antao, S. M., Lee, P. L., Chupas, P. J., Liu, G., et al. (2007). The structure of ferrihydrite, a nanocrystalline material. *Science*, 316, 1726–1729.
- Müller, W. E., Wang, X., Cui, F. Z., Jochum, K. P., Tremel, W., Bill, J., et al. (2009). Sponge spicules as blueprints for the biofabrication of inorganic-organic composites and biomaterials. *Applied Microbiology and Biotechnology*, 83, 397–413.
- Nyman, J. S., Reyes, M., & Wang, X. (2005). Effect of ultrastructural changes on the toughness of bone. *Micron*, 36, 566–582.
- Thompson, D. W. (1942). *On growth and form*. Cambridge University Press Cambridge. pp. 1116.
- Toussaint, L., Bertrand, L., Hue, L., Crichton, R. R., & Declercq, J.-P. (2007). High-resolution X-ray structures of human apoferritin H-chain mutants correlated with their activity and metal-binding sites. *Journal of Molecular Biology*, 365, 440–452.
- Uchida, M., Kang, S., Reichhardt, C., Harlen, K., & Douglas, T. (2010). The ferritin superfamily: supramolecular templates for materials synthesis. *Biochimica et Biophysica Acta*, 1800, 834–845.
- Wilt, F. H. (2005). Developmental biology meets materials science: morphogenesis of biomineralized structures. *Developmental Biology*, 280, 15–25.

Metals in Brain

Introduction	379
The Brain and the Blood–Brain Barrier (BBB)	379
Sodium, Potassium, and Calcium Channels	384
Zinc, Copper, and Iron	388
Concluding Remarks	394

INTRODUCTION

Metal ions are absolutely essential to fulfil a series of important biological functions in the brain, including the transmission of nerve impulses and the synthesis of neurotransmitters. They include spectroscopically silent metal ions like potassium, sodium, calcium, magnesium, and zinc, together with the more spectroscopically accessible iron, copper, manganese, and a few others. The role of some of these metal ions in brain function is particularly important. As we saw in Chapter 9, the alkali metal ions Na^+ and K^+ are involved in the opening and closing of ion channels which generate electrochemical gradients across the plasma membranes of neurons. This plays a crucial role in the transmission of nervous impulses not only within the brain but also in the transmission of signals from the brain to other parts of the body. Calcium and zinc fluxes are also important in regulating neuronal cell function. We will also see that copper and iron play a major role in the brain, particularly in metalloenzymes.

THE BRAIN AND THE BLOOD–BRAIN BARRIER (BBB)

The human brain is complex enough to coordinate the fingers of a concert pianist, and even the fingers, hands, and feet of an organist, all playing on different keyboards; it can create three-dimensional images from light falling on a two-dimensional retina. It constitutes just 2% of the human body mass, yet it consumes 20% of our resting O_2 consumption, varying little between sleep and intense concentration (eg., when we are involved in intensely reading a book on biological inorganic chemistry).

The complexity of the nervous system is staggering, as it regulates all aspects of the functions of our bodies, yet even today, in our post-genomic era, we are still a long way from understanding it. The human brain contains about 10^{12} specialised nerve cells, called neurons, each of which forms as many as 10^3 connections with other neurons. Millions of neurons collect information about our environment (both external and internal), which they transmit to other neurons, where the data is either processed or stored. Millions more respond to this information to regulate the control of muscle contraction, hormone synthesis, etc. In spite of the overwhelming complexity of what we call the central nervous system, we understand the structure and function of neurons quite well. Most neurons contain four distinct regions — the cell body, the axon, the dendrites, and the axon terminals (*Figure 20.1*). The cell body, which contains the nucleus, is the site of synthesis of all neuronal proteins and membranes. Most neurons have one single axon which conducts the electrical impulses, called action potentials, and which terminate in many axon terminals. The extensively branched dendrites receive signals at their interface with

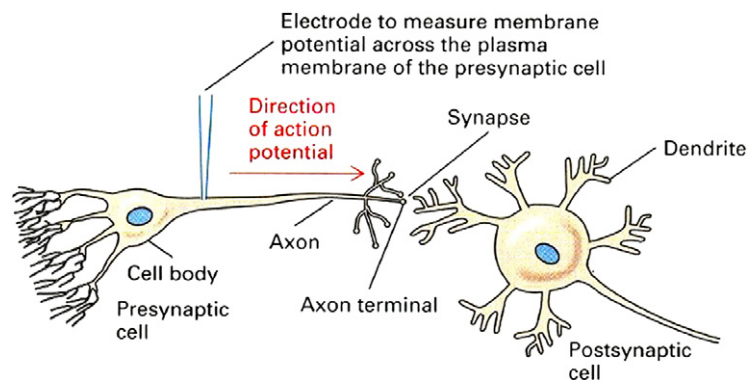


FIGURE 20.1 The typical structure of nerve cells and their synapses. Typical neurons have many axon termini, but only one is shown here. (From Lodish et al., 1995. Copyright 1995 with permission from Scientific American Books.)

several hundred other cells. A single axon in the CNS can interact with many other neurons at synapses and induce responses in all of them simultaneously. The arrival of an action potential at the axon terminal of a presynaptic synapse results in the propagation of the electrical signal to postsynaptic neurons, or other cell types.

We can distinguish three types of neurons. Multipolar neurons have profusely branched dendrites, which receive synaptic signals from several hundred other neurons and transmit them to many other neurons at the lateral branches of its terminals (Figure 20.2(a)). Motor neurons transmit nerve impulses to muscle cells, and their single, often very long, axons extend from the cell body of the neuron to the effector muscle cell (Figure 20.2(b)). Mammalian neurons have an insulating sheath of myelin covering all parts of the axon except for the nodes of Ranvier and the axon terminals at the neuromuscular synapse. Sensory neurons collect all sorts of information, concerning light, smell, sound, pressure, touch, etc. through specialised receptors, and transform this information into electrical signals (Figure 20.2(c)). In sensory neurons, the axon branches when it leaves the cell body. The peripheral branch carries the nerve impulse from the receptor cell to the cell body. The central branch then carries the impulse from the cell body, located in the dorsal root ganglion close to the spinal cord, either to the spinal cord or to the brain.

We will analyse in greater detail the action potential generated by successive cycles of hyperpolarisation/depolarisation, propagated by the opening and shutting of specific ion channels, when we consider the role of Na^+ and K^+ in neurotransmission. An example of what is observed when a microelectrode is inserted into the axonal membrane of a presynaptic neuron is shown in Figure 20.3. The membrane potential observed shows that the neuron is ‘firing’ every 4 ms (i.e., the neuron is generating about 250 action potentials/sec). The axons of larger vertebrate neurons, particularly motor neurons, are sheathed with myelin, a kind of biological insulating tape, which allows them to propagate nerve impulses at velocities of up to 100 m/s. In contrast, in unmyelinated nerves, they travel no faster than 10 m/s.¹

Neurons communicate information in one of two ways, either via chemical signalling or via electrical signalling. At a chemical synapse (Figure 20.4(a)), the axon terminal of the presynaptic cell contains vesicles which are filled with a neurotransmitter, such as adrenaline or acetylcholine, or metal ions such as Zn^{2+} . When the action potential reaches the axon terminal, some of the vesicles fuse with the plasma membrane, releasing their contents into the synaptic cleft. The neurotransmitter diffuses across the synaptic cleft, binds to specific receptors of the postsynaptic cell, and changes the membrane potential of its plasma membrane. If the postsynaptic cell is a neuron, this ultimately induces an action potential, resulting in transmission of the signal, whereas if the postsynaptic cell is a muscle cell, contraction results, and if it is a hormone-producing cell, it will

1. One shudders to imagine the coordination problems of a giraffe if it had to rely on unmyelinated nerves!

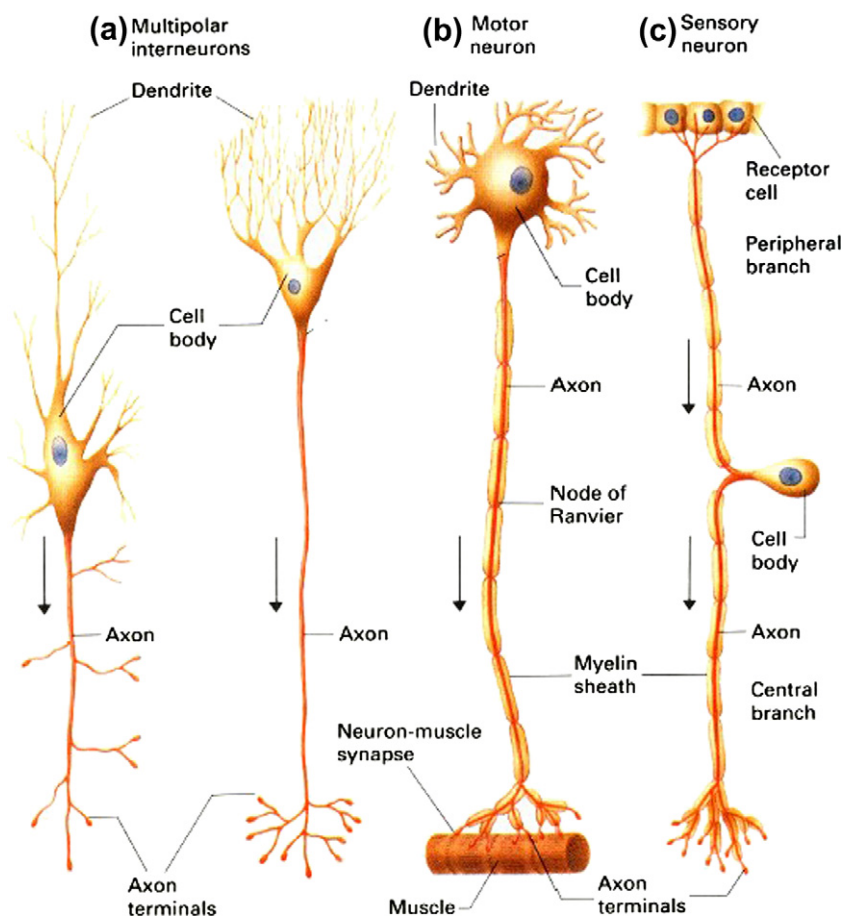


FIGURE 20.2 Structure of typical mammalian neurons. Arrows indicate the direction of conduction of the action potential in the neurons (red). (a) Multipolar interneurons. Each has profusely branched dendrites (which receive signals at synapses with several hundred other neurons) and a single long axon which branches laterally at its terminus. (b) A motor neuron which innervates a muscle cell. Typically, motor neurons have a single long axon extending from the cell body to the effector cell. In mammalian motor neurons, an insulating sheath of myelin covers all parts of the axon except the nodes of Ranvier and the axon terminus. (c) A sensory neuron in which the axon branches when it leaves the cell body. The peripheral branch carries the nerve impulse from the receptor cell to the cell body. The central branch then carries the impulse from the cell body, located in the dorsal root ganglion close to the spinal cord, either to the spinal cord or to the brain. (From Lodish *et al.*, 1995. Copyright 1995 with permission from Scientific American Books.)

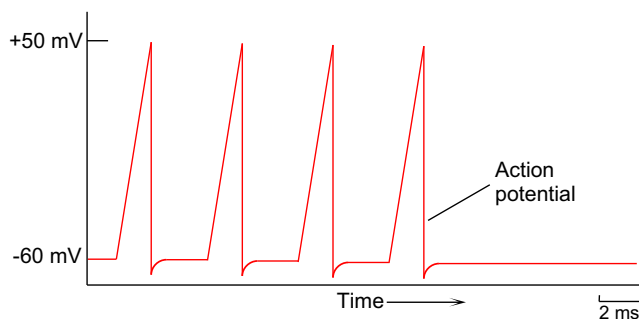


FIGURE 20.3 The observed membrane potential across the plasma membrane of a presynaptic cell.

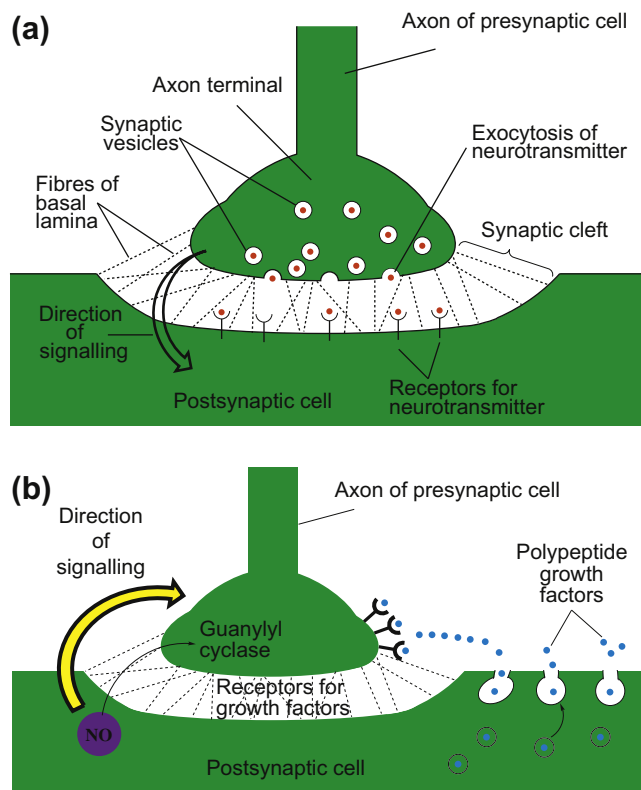


FIGURE 20.4 (a) A chemical synapse. A narrow cleft, the synaptic cleft, separates the plasma membranes of the presynaptic and postsynaptic neurons. Transmission of electrical impulses requires the release of a neurotransmitter by the presynaptic cell, its diffusion across the synaptic cleft, and its binding to specific receptors on the plasma membrane of the postsynaptic cell. (b) An electric synapse. The plasma membrane of the presynaptic and postsynaptic cells are linked by gap junctions. The flow of ions through these channels allows electrical impulses to be transmitted from one cell to the other.

release its hormone. Neurotransmitters must then be cleared out of the synapse efficiently so that the synapse can be ready to function again as soon as possible. Usually neurotransmission by chemical signalling results in amplification of the signal (usually referred to as ‘gain’). In contrast, in an electrical synapse (Figure 20.4(b)), the presynaptic and postsynaptic cell membranes are connected by channels, known as gap junctions, that are capable of passing electrical current. Electrical synapses conduct nerve impulses faster, but unlike chemical synapses they do not have gain. Electrical synapses are often found in neural systems that require very rapid responses, such as defensive reflexes.

The brain is unique among all the organs of the body, hidden behind a relatively poorly permeable vascular barrier, which limits its access to plasma nutrients, such as metal ions. There are three principal barrier sites between blood and brain. These are BBB proper, the blood–CSF barrier (BCSFB), and the arachnoid barrier (Figure 20.5). The BBB is created at the level of the cerebral capillary endothelial cells by tight junction formation. In the adult human, the BBB has a surface area of between 12 and 18 m², and is essentially composed (Figure 20.6) of the cerebral capillary endothelial cells, joined by tight junctions, a basal lamina, pericytes, and astrocyte end-foot processes. The types of cells found at the BBB and their associations are illustrated in Figure 20.6. The endothelial cells form tight junctions which seal the paracellular pathway between the cells such that substances which enter the brain must use dedicated endothelial cell transport systems. The movement of solutes across the BBB may be facilitated by passive or active transporters in the endothelial cell membranes.

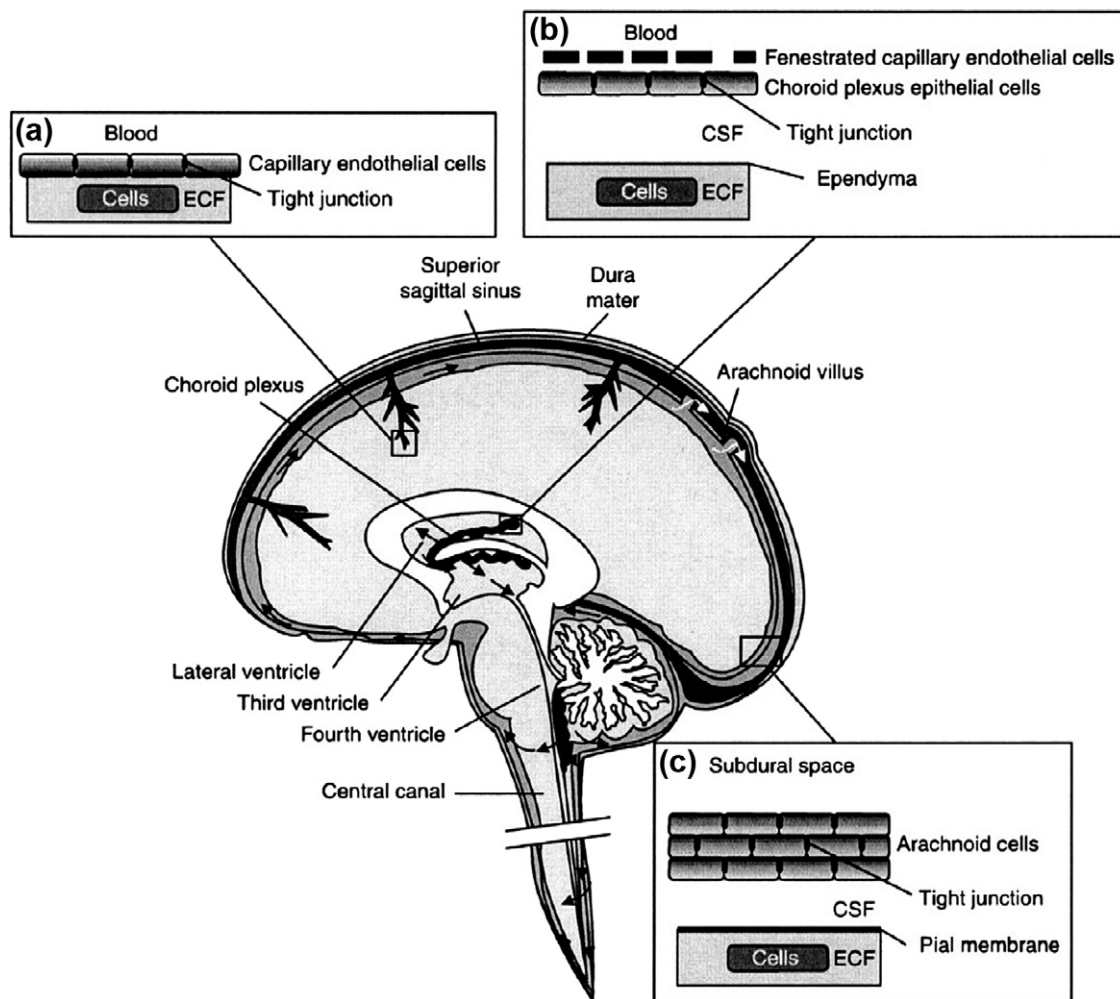


FIGURE 20.5 Barriers of the brain. There are three principal barrier sites between blood and brain. (a) The BBB proper, which is created at the level of the cerebral capillary endothelial cells by tight junction formation. It is by far the largest surface area for exchange and in the adult human is between 12 and 18 m² in surface area. No brain cell is further than about 25 μ m from a capillary, so once the BBB is crossed, diffusion distances to neurons and glial cell bodies for solutes and drugs are short. (b) The blood–CSF barrier (BCSFB) lies at the choroid plexuses in the lateral, third, and fourth ventricles of the brain where tight junctions are formed between the epithelial cells at the CSF-facing surface (apical surface) of the epithelium. (c) The arachnoid barrier. The brain is enveloped by the arachnoid membrane lying under the dura. (From Abbott, Patibandige, Dolman, Yusuf, & Begley, 2009. Copyright 2009 with permission from Elsevier.)

Since no brain cell is further than about 25 μ m from a capillary, once the BBB is crossed, diffusion distances for solutes to neurons and glial cells are short. Unlike other blood vessel epithelia, the BBB epithelia express different receptors at the luminal membrane (facing the circulation) compared to the abluminal membrane, surrounded by astrocyte end-feet, neuronal processes, and interstitial fluid. Pericytes, the connective tissue cells which occur around small blood vessels, are distributed along the length of the cerebral capillaries, partially surrounding the endothelium. Both the cerebral endothelial cells and the pericytes are enclosed by the local basement membrane, forming a distinct perivascular extracellular matrix (basal lamina 1, BL1), different from the extracellular matrix of the astroglial end-feet bounding the brain parenchyma (BL2). Foot processes from astrocytes form a complex network surrounding the capillaries. Astrocytes are the “star-shaped” glial cells which,

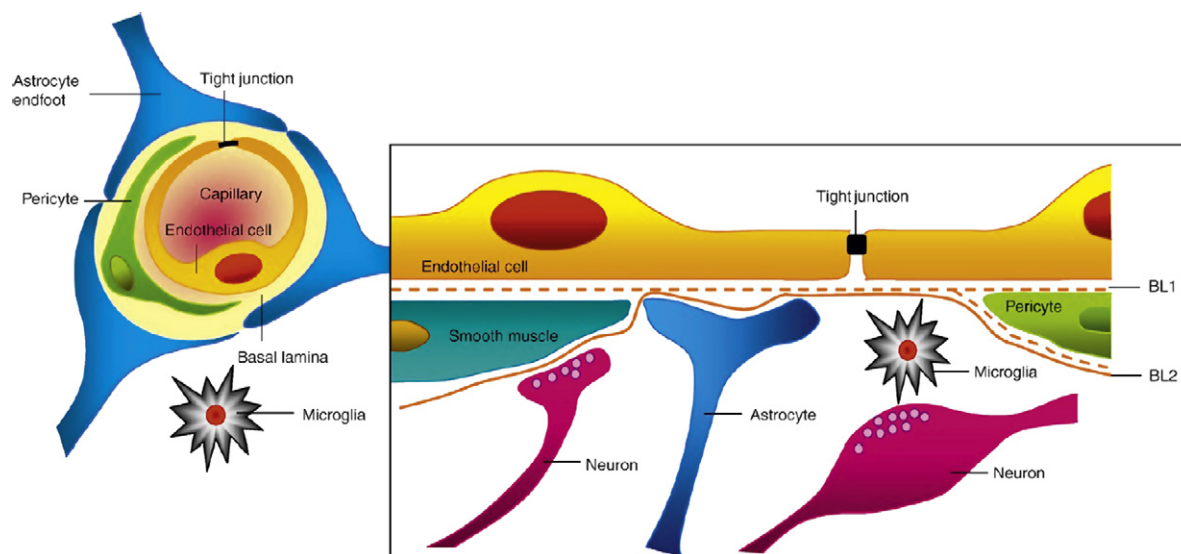


FIGURE 20.6 The cell associations at the BBB. The cerebral endothelial cells form tight junctions at their margins which seal the aqueous paracellular diffusional pathway between the cells. Pericytes are distributed discontinuously along the length of the cerebral capillaries and partially surround the endothelium. Both the cerebral endothelial cells and the pericytes are enclosed by, and contribute to, the local basement membrane which forms a distinct perivascular extracellular matrix (basal lamina 1, BL1), different in composition from the extracellular matrix of the glial end-feet bounding the brain parenchyma (BL2). Foot processes from astrocytes form a complex network surrounding the capillaries and this close cell association is important in induction and maintenance of the barrier properties. Axonal projections from neurons onto arteriolar smooth muscle contain vasoactive neurotransmitters and peptides and regulate local cerebral blood. BBB permeability may be regulated by the release of vasoactive peptides and other agents from cells associated with the endothelium. Microglia are the resident immunocompetent cells of the brain. The movement of solutes across the BBB is either passive, driven by a concentration gradient from plasma to brain, with more lipid-soluble substances entering most easily, or may be facilitated by passive or active transporters in the endothelial cell membranes. Efflux transporters in the endothelium limit the CNS penetration of a wide variety of solutes. (From Abbott et al., 2009. Copyright 2009 with permission from Elsevier.)

with microglia and the oligodendrocytes, are the major cell type in the central nervous system. The network of astrocytic processes forms the infrastructure on which all other CNS cells and vessels are anchored. They have a multitude of functions, including regulation of the ionic milieu in the intercellular space, uptake and/or breakdown of some neurotransmitters, supplying nutrients to the neurons, and formation of the blood–brain barrier. Microglia are also found in the vicinity of the BBB. The microglia are the resident macrophages of the central nervous system, which can communicate with the astrocytes and neurons and with cells of the immune system by a large number of signalling pathways. They are the most susceptible sensors of brain pathology, and when they detect any signs of brain lesions or nervous system dysfunction, they undergo a complex, multistage activation process that converts them into the “activated microglia.” Activated microglial cells have the capacity to release a large number of substances that can act detrimentally, usually causing inflammation, or sometimes beneficially upon surrounding cells; they can also move to the site of injury, proliferate, and phagocytose cells and cellular compartments.

SODIUM, POTASSIUM, AND CALCIUM CHANNELS

Nerve impulses consist of a wave of transient membrane depolarisation/re-polarisation which traverses the nerve cell and is designated an action potential. As we saw in Chapter 9, Alan Hodgkin and Andrew Huxley demonstrated in 1952 that a microelectrode implanted into the giant axon (the long process emanating from the body of

a nerve cell) of the squid² can record such an action potential (Figure 9.1). At the excitation threshold, Na^+ channels begin to open, followed by the subsequent opening of K^+ channels. As Na^+ ions enter, K^+ ions leave the cell. The outcome is that in the first ~ 0.5 ms, the membrane potential increases from the resting potential of around -60 mV to about $+30$ mV. The Na^+ channels now become refractory, and no more Na^+ enters the cell, while K^+ continues to leave the cell, causing a rapid repolarisation, which allows the membrane potential to overshoot the resting potential (hyperpolarisation) before recovering to its initial value. The voltage-gated Na^+ and K^+ ion channels across the axonal membranes create the action potentials (essentially electrochemical gradients) which allow information transfer and also regulate cellular function.

Mammalian neurons express a large repertoire of voltage-dependent ion channels (VDICs), which display a richness of firing behaviours over a wide range of stimuli and firing frequencies, thereby ensuring the intrinsic electrical properties, and rapid processing and transmission of synaptic signals in mammalian neurons. Most of the VDICs are selective for Na^+ , K^+ , and Ca^{2+} ions, and they are located at specific sites in neuronal cell body, dendrites, and axons. The selective placement of specific VDIC types at precise locations in mammalian neurons, and their dynamic regulation through local signalling pathways, allows for the complexity of neuronal function that underlies brain function.

Mammalian potassium VDICs (K_v channels) consist of tetrameric assemblies of six transmembrane α subunits, each associated with an auxiliary β subunit. The human genome contains a total of forty genes encoding potassium K_v channel α subunits. Some of these genes generate messages that are subject to alternative splicing. In mammalian brain, the expression of many of these K_v channel α subunits is restricted to neurons, although glial cells may express a subset of the neuronal repertoire. K_v channels have among the most diverse patterns of subcellular segregation. K_v1 channels are predominantly localised in axons. K_v1 channels are found predominantly on axons and nerve terminals, K_v2 channels on the cell bodies and dendrites, K_v3 channels in dendritic or axonal domains, depending on the subunit and cell type, and K_v4 channels are concentrated in cell body dendritic membranes. The distribution of three K_v channels is illustrated in Figure 20.7.

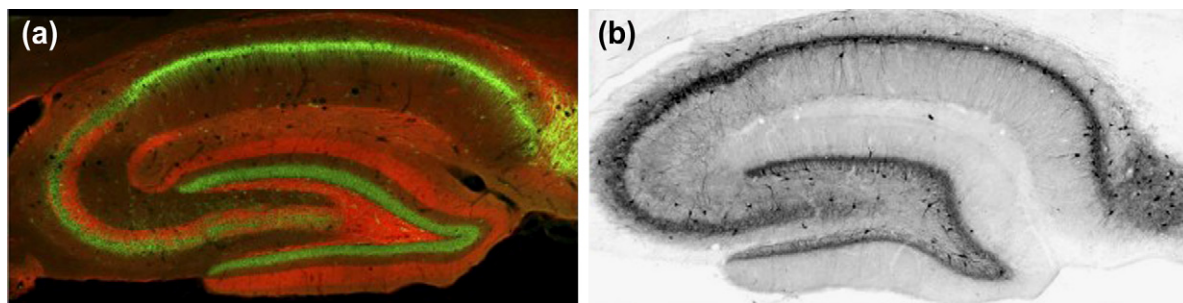
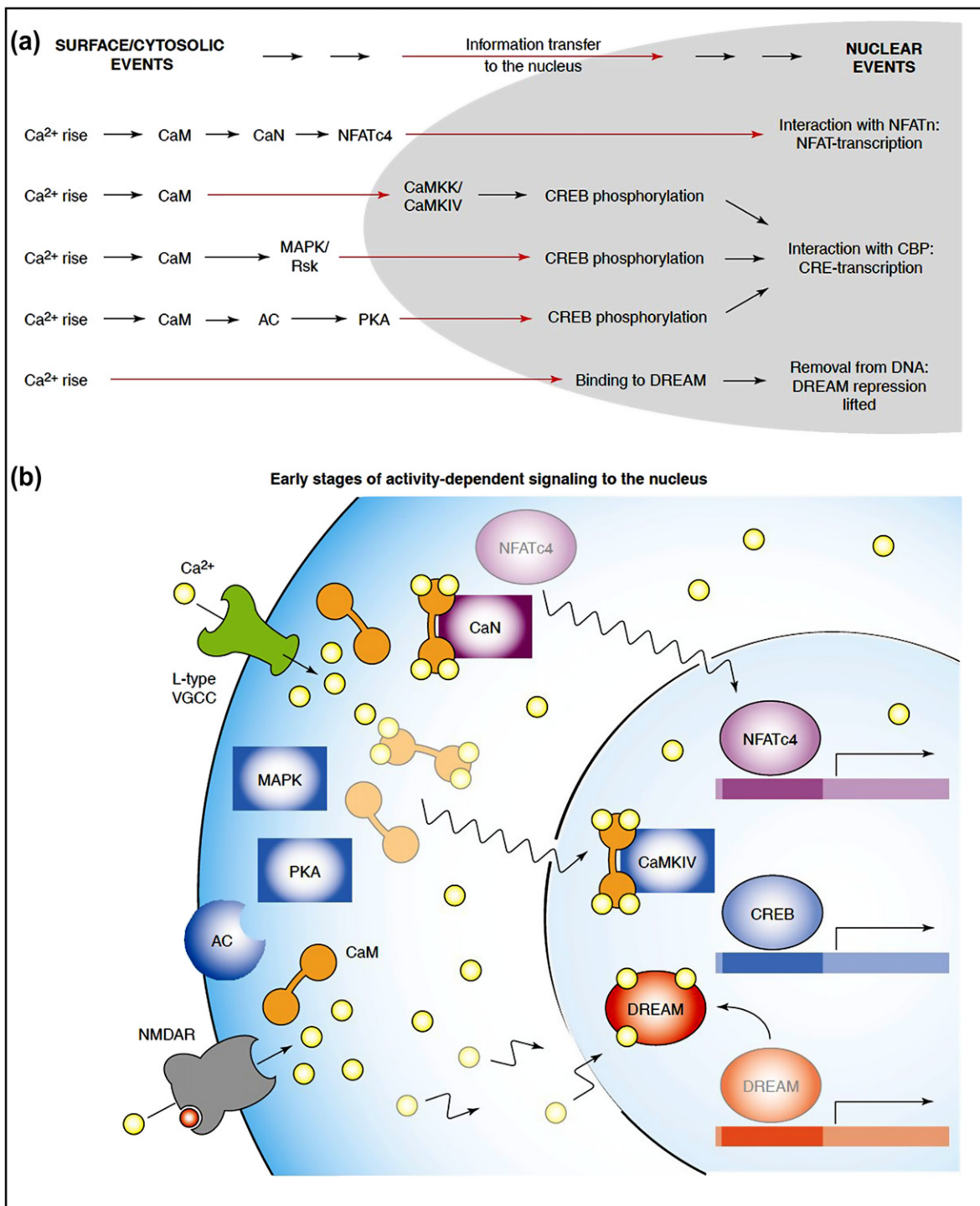


FIGURE 20.7 Cellular and subcellular distribution of K_v channels in adult rat hippocampus. (a) double immunofluorescence staining for $\text{K}_v1.4$ (red) and $\text{K}_v2.1$ (green). Note $\text{K}_v1.4$ staining in terminals fields of the medial perforant path in the middle molecular layer of the dentate gyrus, and mossy fibres axons and terminals in S. lucidum of CA3. (b) Immunoperoxidase staining for $\text{K}_v3.1b$. (From Vacher, Mohapatra, & Trimmer, 2008. Copyright 2008 with permission of the American Physiological Society.)

As we saw in Chapter 9, sodium channels (Na_v channels) consist of a pore-forming α subunit, which is sufficient for functional expression, associated with auxiliary β subunits which modify both the kinetics and the voltage dependence of channel gating of the channel. Nine mammalian Na_v channel isoforms are known, of which $\text{Na}_v1.1$ and $\text{Na}_v1.3$ are predominantly localised in neuronal cell bodies and proximal dendrites, where they control

2. The giant axon of the squid is very large, typically 0.5 mm in diameter, and the conduction velocity is about 25 m/s. During such an action potential, an influx of 3.7 pmol/cm^2 of Na^+ is offset by a subsequent efflux of 4.3 pmol/cm^2 of K^+ .



neuronal excitability, setting the threshold for action potential initiation and propagation to the dendritic and axonal compartments. $\text{Na}_v1.2$ is predominantly expressed in unmyelinated axons, where it conducts action potentials. $\text{Na}_v1.6$ is prominently found at nodes of Ranvier, where it propagates action potentials, and, at axon initial segments where action potentials initiate. Modulation of Na_v1 currents is undoubtedly important *in vivo*, and mutations that subtly alter Na_v1 channel function can lead to human diseases of hyperexcitability such as epilepsy.

Calcium channels (Ca_v channels) mediate calcium influx in neuronal cells in response to membrane depolarisation, mediating a wide range of intracellular processes such as activation of calcium-dependent enzymes, gene transcription, and neurotransmitter exocytosis/secretion. Their activity is an essential requirement for the coupling of electric signals in the neuronal plasma membrane to physiological events within the cells. Biochemical characterisation of native brain Ca_v channels revealed that, in addition to the large principal α_1 subunit, there are also numerous auxiliary subunits. The α_1 subunit is the largest and principal subunit, containing the ion conduction pore, the membrane voltage-sensor, and gating apparatus. A number of different α_1 subunits have been identified and characterised in the mammalian nervous system, each with specific physiological functions and electrophysiological and pharmacological properties.

Calcium and Signal Transduction

Within cells, including nerve cells, fluxes of Ca^{2+} ions play an important role in signal transduction (Chapter 11). Most eukaryotic cells export calcium across the plasma membrane or deposit it in membrane-enclosed storage sites in order to maintain free cytosolic Ca^{2+} levels at 100–200 nM, roughly 10,000 times less than in the extracellular space. This allows calcium to function as a second messenger and also as a carrier of biological signals that guide cells from their origin to their ultimate death. When intracellular Ca^{2+} increases, the ubiquitous eukaryotic Ca^{2+} -binding protein calmodulin binds Ca^{2+} ions (Chapter 11). This causes a major conformation change, exposing a previously buried hydrophobic patch on the calmodulin molecule (Figure 11.9), which can bind to a large number of target enzymes, modifying their activity (Chapter 11).

Ca^{2+} is also involved in signalling from neuronal synapses to the cell nucleus, resulting in neuronal activity-dependent control of neuronal gene expression.³ This synapse-to-nucleus signalling plays a key role in circadian rhythms, long-term memory, and neuronal survival. The transient rise in free Ca^{2+} concentration after neuronal excitation can be transmitted from the cytoplasm to the nucleus in several different ways (Figure 20.8). Following rises in intracellular Ca^{2+} , the nuclear transcription factor downstream regulatory element antagonistic modulator (DREAM) is activated. DREAM is abundant in the nucleus and has three Ca^{2+} -binding motifs, the E–F hands

FIGURE 20.8 Signalling from the membrane to the nucleus: multiple strategies for information transfer. (a) The transcription factors NFATc4, CREB, and DREAM are all activated following increases in intracellular Ca^{2+} , yet each relies upon a different mode of information transfer. At rest, NFATc4 is localised to the cytosol, allowing the transcription factor to be targeted to specific regions of the cell. This would allow for heightened signalling specificity. Indeed, Ca^{2+} entry through L-type calcium channels activates this transcription factor preferentially relative to other voltage-gated Ca^{2+} channels. Yet, this mode of synapse-to-nucleus signalling is limited in both speed and signal amplification. Conversely, DREAM can be activated by general rises in intracellular Ca^{2+} , allowing for rapid information transfer. However, this pathway is limited in regards to signal specificity. CREB activation is typically initiated by nuclear translocation of the calcium sensor CaM or by an activating kinase, providing a combination of the advantages found for both NFATc4 and DREAM signalling. (b) A snapshot image of the early stages (0–5 min) of activity-dependent gene expression. Following rises in intracellular Ca^{2+} , DREAM dissociates from DNA resulting in the lifting of transcriptional repression. Within seconds of Ca^{2+} entry through L-type Ca^{2+} channels and NMDA receptors, CaM translocates to the nucleus, supporting CREB phosphorylation through the activation of CaMKIV. Nearly as rapid, NFATc4 also undergoes translocation to the nucleus following its dephosphorylation by calcineurin (CaN). Other pathways outlined in (a), including the MAPK/PKA pathways, subsequently begin to exert their influence. Abbreviations, VGCC, voltage-gated calcium channel. (From *Deisseroth, Mermelstein, Xia, & Tsien, 2003*. Copyright 2003 with permission from Elsevier.)

3. Synapses are the local sites of communication between neurons.

described in Chapter 11. It is proposed that DREAM remains bound to a downstream regulatory element (DRE) which acts as a gene silencer when nuclear Ca^{2+} is low. When the nuclear Ca^{2+} levels rise, DREAM dissociates from the DNA, causing de-repression of DRE, and activation of downstream genes such as that which codes for dynorphins (which may act as an antidote to the pleasurable effects of cocaine) and attenuation of pain signalling *in vivo*. Within seconds of Ca^{2+} entry into the cytoplasm, through both N-methyl-D-aspartate (NMDA) receptors and L-type voltage-gated Ca^{2+} channels (VGCC), calmodulin (CaM) is activated and translocates to the nucleus where it participates in the activation of Ca^{2+} /cAMP responsive element-binding protein (CREB)-dependent gene expression. Calmodulin also mediates CREB phosphorylation via the adenylyl cyclase/phosphokinase A (AC/PKA) and the MAP kinase (MAPK) pathways, which begin to exert their influence subsequently. Almost as rapidly, CaM activates another target protein in the mammalian brain, calcineurin (CaN), a heterodimeric phosphatase, which dephosphorylates a member of the nuclear factor of activated T-cells (NFAT) family of transcription factors, NFATc4. The NFATc group of transcription factors play a key role in neuronal plasticity as well as vascular development and muscular hypertrophy. NFATc4 is expressed in neurons of the hippocampus, the memory, and learning centre of the brain. Upon dephosphorylation, NFATc4 undergoes translocation from the cytosol to the nucleus.

Synaptotagmins are yet another family of Ca^{2+} -binding proteins, localised on the membranes of synaptic vesicles, where they seem to be involved in the release of neurotransmitters. While the mechanism by which they are involved in Ca^{2+} -mediated synaptic transmission is unclear, it seems likely that the neurotoxicity of heavy metals, such as Pb, is due to a higher affinity of synaptotagmins for Pb^{2+} than for Ca^{2+} .

The Ca^{2+} /calmodulin-dependent protein kinase CaMKII plays a central role in Ca^{2+} signal transduction and is highly enriched in brain tissue, accounting for about 2% of total hippocampal protein and around 0.25% of total brain protein. It is the most abundant protein in the postsynaptic density, the region of the postsynaptic membrane which is physically connected to the ion channels which mediate synaptic transmission. The structural modification of synaptic proteins is thought to be the molecular event which is involved in the memory storage process. The substrates phosphorylated by CaMKII are implicated in homeostatic regulation of the cell, as well as in activity-dependent changes in neuronal function that appear to underlie complex cognitive and behavioural responses, including learning and memory.

Astrocytes can exocytotically release the gliotransmitter glutamate from vesicular compartments. Increased cytosolic Ca^{2+} concentration is necessary and sufficient for this process. The predominant source of Ca^{2+} for exocytosis in astrocytes resides within the endoplasmic reticulum (ER). Inositol 1,4,5-trisphosphate and ryanodine receptors of the ER provide a conduit for the release of Ca^{2+} to the cytosol. The ER store is (re)filled by the store-specific Ca^{2+} -ATPase. Ultimately, the depleted ER is replenished by Ca^{2+} which enters from the extracellular space to the cytosol via store-operated Ca^{2+} entry; the TRPC1 protein has been implicated in this part of the astrocytic exocytotic process. Voltage-gated Ca^{2+} channels and plasma membrane $\text{Na}(+)/\text{Ca}^{2+}$ exchangers are additional means for cytosolic Ca^{2+} entry. Cytosolic Ca^{2+} levels can be modulated by mitochondria, which can take up cytosolic Ca^{2+} via the Ca^{2+} uniporter and release Ca^{2+} into cytosol via the mitochondrial $\text{Na}(+)/\text{Ca}^{2+}$ exchanger, as well as by the formation of the mitochondrial permeability transition pore. The interplay between various Ca^{2+} sources generates cytosolic Ca^{2+} dynamics that can drive Ca^{2+} -dependent exocytotic release of glutamate from astrocytes.

ZINC, COPPER, AND IRON

The brain barrier systems, i.e., the blood–brain and blood–cerebrospinal fluid barriers, ensure that there are adequate supplies of zinc, copper, and iron available for brain function and prevention of neurological diseases. Too much or too little will be detrimental to brain function. Specific transporters present on the BBB will ensure the passage of each of these metals across this barrier.

Another metal ion that has been implicated in brain function is Zn^{2+} , the second most prevalent trace metal in the body after iron. The brain barrier systems, i.e., the blood–brain and blood–cerebrospinal fluid barriers, ensure that

there are adequate zinc supplies for brain function and the prevention of neurological diseases. Zinc bound to albumin within the plasma can be readily transferred to transporter proteins at the BBB. In mammalian brain, the vast majority of zinc is tightly bound within zinc metalloproteins in neurons and glial cells as a structural or as a catalytic cofactor. However, approximately 10% of the total zinc, probably ionic zinc, is less tightly bound and is mainly localised within the synaptic vesicles of the forebrain (Figure 20.8), in a subset of glutamatergic axon terminals. Such vesicular zinc is released into the synaptic cleft during neurotransmission and modulates NMDA-specific postsynaptic receptors in a rapid dose-dependent response that is reversible. Zinc enhances GABA release via potentiation of α -amino-3-hydroxy-5-methyl-4-isoxalolepropionate (AMPA)/ kainate receptors in the CA3 region of the hippocampus, followed by a decrease in presynaptic glutamate release in the same region.

Zinc plays an important role in regulating brain development, particularly during foetal and early postnatal life. During this developmental period, zinc deficiency adversely affects the autonomic nervous system regulation as well as hippocampal and cerebellar development, leading to learning impairment and olfactory dysfunction. Furthermore, the susceptibility to epileptic seizures (which may decrease vesicular zinc) is also enhanced by zinc deficiency in vulnerable individuals. Zinc deficiency may lower the body's adaptability to stress. In this situation, intracellular free calcium concentration may be altered prior to the decrease in zinc concentration in the extracellular fluid. Anxiety-like behaviour, which is observed in animal models of induced zinc deficiency, can be corrected to some extent, by the administration of zinc. This is due to the fact that zinc, which is an antagonist of NMDA receptors, exhibits antidepressant-type activity, by inducing brain-derived neurotrophic factor (BDNF) gene expression, which increases the synaptic zinc levels in the hippocampus. Preliminary clinical studies have also demonstrated the benefit of zinc supplementation in antidepressant therapy.

On the other hand excessive synaptic release of zinc followed by entry into vulnerable neurons contributes to severe neuronal cell death. This is caused by the sequential activation of Akt and GSK-3 β which play an important role in directing hippocampal neural precursor cell death.

Zn²⁺ shows a variety of effects within the nervous system, thereby requiring that levels of zinc are regulated to a very precise level. A fine balance between ion sequestration, intracellular buffering, and extrusion exists in order to maintain cellular zinc homeostasis. A family of proteins known as metallothioneins regulates zinc sequestration and buffering, while zinc uptake and extrusion is mediated by membrane-associated zinc transporters. Mitochondria may serve as the pool of histochemically reactive zinc in neurons and glial cells.

Metallothioneins, MTs, are ubiquitous low-molecular-weight proteins high in cysteine and metal content and devoid of aromatic amino acids, encoded by a multigene family. Human MTs bind up to seven zinc atoms and contain 61–68 amino acids, of which 20 are highly conserved cysteines. In the CNS, MTs show a diverse pattern of expression with MT-1 and MT-2, mainly expressed in astrocytes and spinal glia, but largely absent from neurons, whereas MT-3 is expressed exclusively in neurons and may play an important role in neuronal zinc homeostasis as it is widely distributed in the brain associated with neurons containing synaptic zinc.

Mammalian zinc transporters belong to two gene families (Cousins et al., 2006). Firstly, the ZnT (solute-linked carrier 30 – SLC30) transporters decrease cytosolic zinc bioavailability by facilitating zinc efflux from cells and promoting accumulation into intracellular vesicles. Secondly, the Zip family (solute-linked carrier 39 – SLC39) increases cytosolic zinc by promoting the transport of extracellular and vesicular zinc into the cytoplasm. There are ten human SLC30 genes. ZnT1 and ZnT3 have been co-localised with zinc in the synaptic vesicles. Vesicular zinc concentration is determined by the abundance of ZnT3, and ZnT-3 is required for zinc transport into synaptic vesicles. ZnT-1 is responsible for zinc efflux from the cell. Fourteen Zip genes have been characterised, many of which are located at the plasma membrane, although Zip7 has been identified at the Golgi apparatus.

The mammalian forebrain contains a subset of glutamatergic neurons that sequester zinc in their synaptic vesicles. Zinc-containing axon terminals are particularly abundant in the hippocampus,⁴ the piriform cortex, the neocortex, the striatum, and the amygdala (Figure 20.9). Cytosolic zinc is transported into vesicles by the

4. The hippocampus is a region of the brain important for learning and memory.

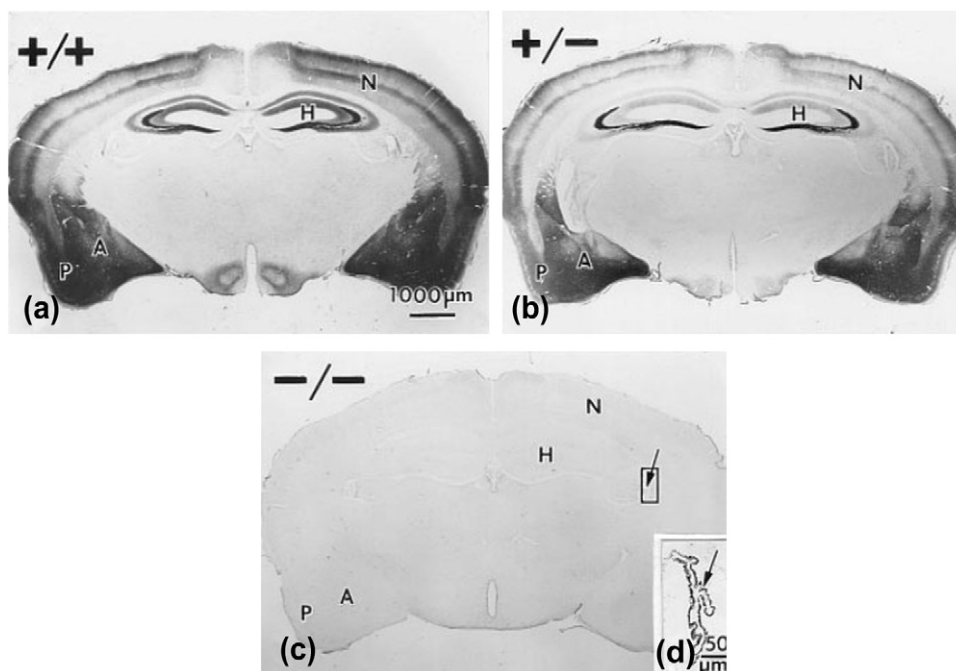


FIGURE 20.9 Coronal sections of rat midbrain. The tan-brown-black staining is the silver staining of zinc by the Timm-Danscher method. With use of the electron microscope, all of the Timm-Danscher staining proves to be in the neuropil, in the presynaptic vesicles of glutaminergic neurons. Timm stain in the hippocampus (H), piriform cortex (P), neocortex (N), and amygdala (A) was conspicuous in the wild type $ZnT3^{+/+}$ brain (a), reduced in the heterogeneous mutant $ZnT3^{+/-}$ brain (b), and undetectable in the brains of homozygous mutant $ZnT3^{-/-}$ mice (c). (d) Higher magnification of the choroid plexus from the lateral ventricle (indicated area in (c)). Timm stain was unperturbed in the $ZnT3^{-/-}$ choroid plexus. (From Cole, Wentzel, Kafer, Schwartzkroin & Palmiter, 1999. Copyright 1999 with permission from US National Academy of Sciences).

neuronal-specific zinc transporter ZnT3, as we saw above, a member of the large family of zinc transporters (the ZnTs), which facilitate zinc efflux from the cytoplasm. ZnT3 and the vesicular glutamate transporter Vglut1 are found in the same vesicle population and the vesicular zinc concentration has been shown to be determined by the abundance of ZnT3 protein. Thus, brains of mice carrying a targeted disruption of the *ZnT3* gene (*ZnT3* KO mice) completely lack “chelatable zinc” (Figure 20.9).

Zinc is released into the synaptic cleft upon neuronal activity. Extracellular zinc has the potential to interact with and modulate many different synaptic targets, including glutamate receptors and transporters. Zinc plays an important role in synaptic plasticity in both the hippocampus and the amygdala, primarily by acting on post-synaptic receptors. In early studies, it was shown that when hippocampal mossy fibres were stimulated, zinc was released from synaptic vesicles into the synaptic cleft during neuronal activity. This release was both calcium and depolarisation dependent. The release of zinc during synaptic transmission makes zinc available for entry into cells through gated zinc channels on neighbouring cells. Since these zinc-releasing neurons also release glutamate, the term “glutaminergic” has been proposed to describe them. The glutaminergic pathways are found almost exclusively in the cerebral cortex and limbic system⁵ (e.g., amygdala, cingulate cortex, hippocampus, and olfactory bulb). While the fate of neuronally released zinc is not totally clear, it appears to modulate the overall excitability

5. The *limbic system* is a set of brain structures located on top of the *brainstem* and buried under the *cortex*. Limbic system structures are involved in many of our emotions and motivations, particularly those that are related to survival. Such emotions include fear, anger, and emotions related to sexual behaviour. The limbic system is also involved in feelings of pleasure that are related to our survival, such as those experienced from eating and sex.

of the brain through its effect on voltage-gated calcium channels as well as on NMDA, γ -aminobutyric acid (GABA), glycine, nicotinic, dopaminergic, and serotonin receptors (Figure 20.10). The zinc which has been stored

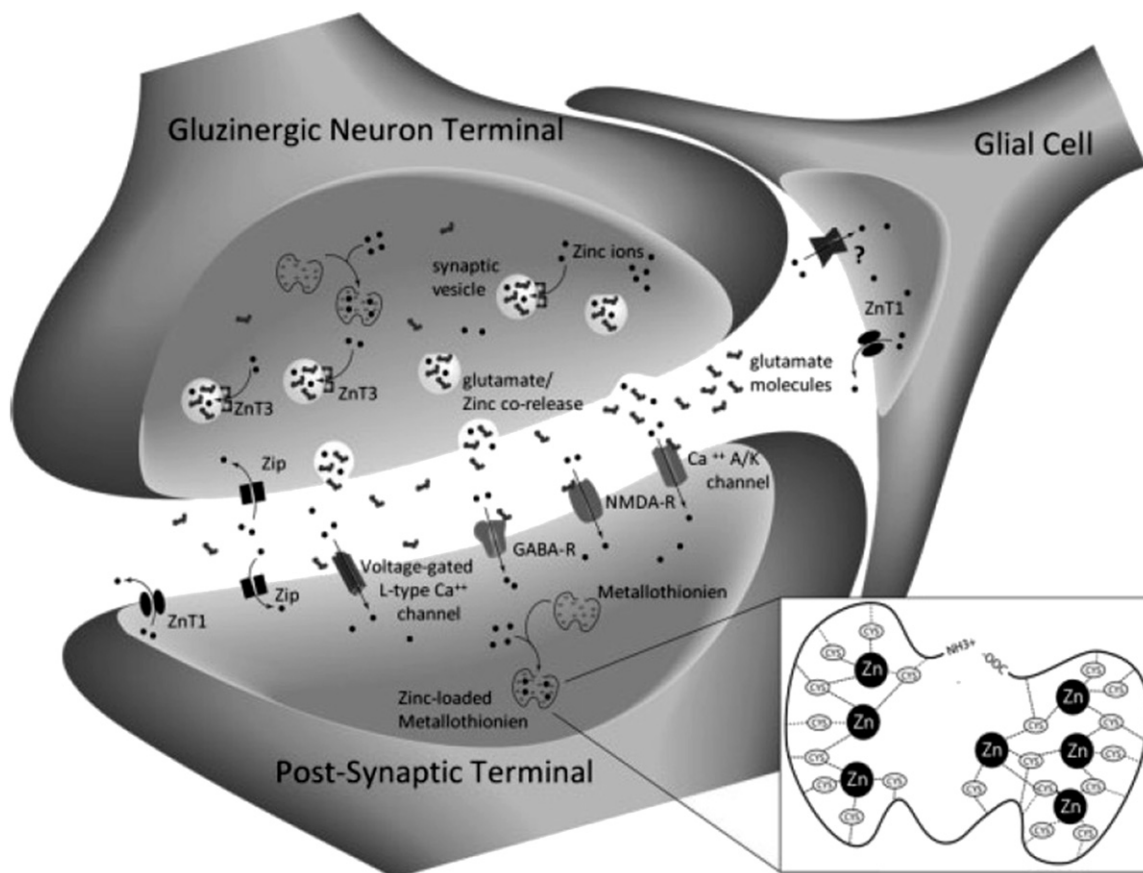


FIGURE 20.10 Zinc trafficking at the gluzineric synapse. Zinc enters synaptic vesicles of gluzineric terminals via the zinc transporter (ZnT-3) and is stored with glutamate. During normal stimulation, zinc is released along with glutamate into the synaptic cleft where it can then act on postsynaptic channel proteins such as GABA receptors, NMDA receptors, voltage-gated channels, or a number of other ion channels to alter their activity, many of which have not been well defined; e.g., the unknown channel illustrated on the glial cell membrane (question mark). Metallothioneins (MTs) are primary intracellular zinc-buffering proteins and they regulate the availability of free zinc in presynaptic terminals and postsynaptic neurons. The metallothionein molecule (inset) consists of two domains, in each of which zinc is bound in a cluster. In one domain, three zinc atoms are bound to nine cysteines (cys), whereas in the other domain, four zinc atoms are bound to eleven cysteines. Each zinc atom is tetrahedrally coordinated to four thiolate bonds with some of the thiolate ligands sharing the zinc atom. (From Bitanhirwe & Cunningham, 2009. Copyright 2009 with permission from John Wiley and Sons.)

together with glutamate in the synaptic vesicles is released during normal stimulation, together with glutamate into the synaptic cleft. There, it can act on postsynaptic channel proteins, such as GABA receptors, NMDA receptors, voltage-gated channels, or a number of other ion channels to alter their activity. Metallothioneins are the primary intracellular buffering proteins, and they regulate the availability of free zinc in presynaptic terminals and postsynaptic neurons. The metallothionein molecule (Figure 20.10) consists of two domains, in each of which zinc is bound in a cluster. In one domain, three zinc atoms are bound to nine cysteines (cys), whereas in the other domain, four zinc atoms are bound to eleven cysteines. Each zinc atom is tetrahedrally coordinated to four thiolate bonds, with some of the thiolate ligands sharing the zinc atom.

Multiple mechanisms by which such extracellular zinc could modulate fast excitatory glutamatergic receptors have been (Paoletti et al., 2009) suggested. Both ionotropic glutamate receptors and glutamate transporters are sensitive to zinc. Zinc selectively inhibits NMDA receptor-mediated responses in cultured hippocampal neurons, by producing a voltage-dependent noncompetitive inhibition, resulting in a decrease in channel opening. Certain NMDA receptor subtypes (those containing the NR2A subunit) appear particularly interesting because they contain allosteric sites which are exquisitely sensitive to extracellular zinc.

Glutamate receptors, which will clear glutamate from the synaptic cleft, are also modulated by zinc. Inhibition of glutamate uptake may be damaging to such activated neurons, although, since zinc will also inhibit the release of glutamate no real change may occur within the synaptic cleft. In addition, high voltage-activated calcium channels that mediate calcium-dependent neurotransmitter release at the central synapses are also inhibited by μM concentrations of zinc. Overall, it can be clearly observed that zinc could act as a critical neural messenger in both health and disease via its ability to regulate NMDA receptor activity. Excessive synaptic release of zinc followed by entry into vulnerable neurons contributes to severe neuronal cell death.

Mutations that cause reduced expression of the full-length Survival Motor Neuron (SMN) protein are a major cause of spinal muscular atrophy (SMA), a disease characterised by the degeneration of the α -motor neurons in the anterior horn of the spinal cord. The severity of SMA may be influenced by the actions of modifier genes. One potential modifier gene is ZPR1, an essential protein with two zinc fingers, present in the nucleus of growing cells which relocates to the cytoplasm in starved cells. ZPR1 p is downregulated in patients with SMA and interacts with complexes formed by SMN. The expression of ZPR1 is suppressed in humans with severe SMA, although the mechanism of its suppression remains unknown.

Copper

Genetic and nutritional studies have illustrated the essential nature of copper for normal brain function. Deficiency of copper during the foetal or neonatal period will have adverse effects both on the formation and the maintenance of myelin (Kuo et al., 2001; Lee et al., 2001; Sun et al., 2007; Takeda and Tamana, 2010). In addition, various brain lesions will occur in many brain regions, including the cerebral cortex, olfactory bulb, and corpus striatum. Vascular changes have also been observed. It is also of paramount importance that excessive amounts of copper do not occur in cells, due to redox mediated reactions such that its level within cells must be carefully controlled by regulated transport mechanisms. Copper serves as an essential cofactor for a variety of proteins involved in neurotransmitter synthesis, e.g. dopamine β -hydroxylase, which transforms dopamine to nor-adrenaline, as well as in neuro-protection via the Cu/Zn superoxide dismutase present in the cytosol. Excess “free” copper is however deleterious for cell metabolism, and therefore intracellular copper concentration is maintained at very low levels, perhaps as low as 10^{-18} M. Brain copper homeostasis is still not well understood.

The major route of copper entry into neuronal cells is via the Cu^+ transporter Ctr1, although a second transporter Ctr2 may also be involved. DMT1 may also contribute to the transport of copper across membranes although its exact role is unknown. Ctr1 is also highly expressed in the choroid plexus. Copper transport to various cuproenzymes from Ctr1 is mediated via metallochaperone pathways which were outlined in Chapter 8. Interestingly, the amyloid precursor protein possesses an N-terminal copper-binding domain which could reduce Cu^{2+} to Cu^+ . The CSF contains non-ceruloplasmin bound copper, although the ligand to which it is bound is not yet identified.

The copper transporters ATP7A and ATP7B transport Cu^+ using energy from ATP hydrolysis to catalyse the transport of copper across membranes. It is thought that such copper is subsequently transported into intracellular vesicles, which then fuse with the plasma membrane and release the copper from the cell. Copper export can be stimulated in response to Ca^{2+} channel activation. ATP7A expression in mouse brain in early postnatal development is in the hippocampus, olfactory bulb, cerebellum, and choroid plexus. This alters with ageing with the highest ATP7A expression found in CA2 hippocampal pyramid cells, cerebellar Purkinje neurons, and choroid plexus. Low levels of ATP7A expression are found in astrocytes, microglia, myelinating oligodendrocytes, and endothelial cells. Copper can be released from synaptic vesicles into the synaptic cleft of glutamatergic synapses

in the cortex and hippocampus following depolarisation, at a concentration of approximately 15 μM . In cultured hippocampal neurons *in vitro*, the efflux of copper involves copper-independent trafficking of ATP7A to neuronal processes via the activation of NMDA receptors. As we will see in Chapter 21, mutations in these two proteins are associated with two neurological disorders, Wilson's and Menkes diseases.

Iron

Iron is critical for a number of basic cellular processes, and in the central nervous system, iron is required as a cofactor for metabolic processes which include oxidative phosphorylation, neurotransmitter production, nitric oxide metabolism, and oxygen transport as well as several neuronal-specific functions, such as dopaminergic neurotransmitter synthesis and myelination of axons. The brain iron content is less than 2% of total body iron content. Nonetheless, while the iron content within different brain regions varies greatly (and is not related to the number of iron transporters present at their cell membrane), significantly higher iron concentrations are found in some brain regions, such as the substantia nigra, the globus pallidus, the dentate gyrus, interpeduncular nucleus, thalamus, ventral pallidus, nucleus basalis, and red nucleus, than in the liver. Regions of the brain associated with motor functions tend to have more iron than non-motor-related regions. This may explain why movement disorders like Parkinson's disease are often associated with brain iron loading.

Numerous advances have been made in the last 10 years in understanding iron homeostasis within the systemic circulation. The mechanism by which iron is transported from the luminal to the abluminal side of the blood capillary endothelial cells remains conjectural. It could be that diferric transferrin binds to transferrin receptors, followed by receptor-mediated endocytosis, with iron released from transferrin within the endosome by the slightly acidic pH. Iron could then be released into the brain, with the recycling of apotransferrin to the luminal side of the endothelial cells and its ultimate release into the plasma. Enormous advances have been made in the last 10 years in understanding iron homeostasis within the systemic circulation (see Chapter 8). However, exactly how the brain regulates fluxes and storage of iron into neurons, oligodendrocytes, astrocytes, and glial cells remains an enigma. Several regulators of intestinal iron absorption have also been localised in the central nervous system, which possibly indicate some similarity with the control of iron homeostasis in the brain.

Transferrin synthesised by the oligodendrocytes in the brain will bind the majority of the iron that traverses the blood–brain barrier after the oxidation of the iron, possibly by a glycoposphoinositide-linked ceruloplasmin found in astrocytic foot processes that surround brain endothelial cells. Neurons acquire iron from diferric transferrin. However, the source of iron within microglia cells is unclear — other phagocytic cells such as macrophages, take up iron via transferrin receptors and release iron via ferroportin.

Ferritins can store excess iron and release it when required for cellular processes. In addition, neuromelanin (NM), which is an organic polymer consisting of dihydroxyindole and benzothiazine units which are products of dopamine metabolism, is also present and is able to bind a number of metals, e.g., copper and iron. In oligodendrocytes, iron is bound to both H- and L-chain ferritin, in microglia to L-ferritin, while neurons contain mostly neuromelanin. In contrast, astrocytes contain hardly any ferritin. As to the movement of iron between different brain regions, this in the main remains unclear. It is thought that transferrin and ferritin may be important, since mRNA receptors for these iron proteins are detectable in grey matter and white matter, respectively. The fate of non-transferrin-bound iron, which may cross the BBB, remains unclear.

Since iron is involved in many central nervous system processes that could affect infant behaviour and development, iron deficiency has adverse effects on brain development, both pre- and post-natal. In various epidemiological studies, it is reported that children with iron-deficiency anaemia have poorer performances on tests of some specific cognitive function. Animal experiments have identified some of the defects of reduced iron availability on brain function, which include post-translational changes (which result in a failure of iron incorporation into protein structures which are subsequently degraded), vulnerability of the developing hippocampus (with loss of the neuronal metabolic marker cytochrome c oxidase), and altered dendritic structure. Iron deficiency will also have a direct effect on myelin, including a decrease in myelin lipids and proteins, as well as neurotransmitter systems, since iron

is essential for a number of enzymes, including tryptophan hydroxylase (serotonin) tyrosine hydroxylase (noradrenaline and dopamine). Long-term follow-up studies of iron deficiency in the human infant brain indicate that such alterations in myelination result in slower conduction in both the auditory and visual systems. Both of these sensory systems are rapidly myelinating during the period of iron deficiency and are critical for learning and social interaction. Together with the reduced energy, impaired glial function, altered activation of monoamine circuits, this may alter experience dependent processes which are critical to brain structure and function during early development.

In contrast, an inevitable consequence of ageing is an elevation of brain iron in specific brain regions, e.g., in the putamen, motor cortex, prefrontal cortex, sensory cortex, and thalamus, localised within H- and L-ferritin and neuromelanin with no apparent adverse effect. However, as we will see in Chapter 21, ill-placed excessive amounts of iron in specific intracellular compartments, like mitochondria, or in specific regions of the brain, such as the substantia nigra and lateral globus pallidus, will lead to neurodegenerative diseases (Friedreich's ataxia, or Parkinson's disease, respectively). Increases in both copper and zinc are also observed in the ageing brain.

CONCLUDING REMARKS

As the reader can appreciate, extremely low concentrations of metal ions are able to orchestrate a multitude of activities in the brain, controlling the opening of various ion channels as well as activating various neurotransmitter receptors. Clearly, changes in the concentrations of such metal ions will induce adverse effects and induce the demise of neurons and other cell types. This will be considered in the next chapter.

REFERENCES

- Abbott, N. J., Patabendige, A. A., Dolman, D. E., Yusof, S. R., & Begley, D. J. (2009). Structure and function of the blood-brain barrier. *Neurobiology of Disease*, 37, 13–25.
- Bitanhirwe, B. K. Y., & Cunningham, M. G. (2009). Zinc: the brain's dark horse. *Synapse*, 63, 1029–1049.
- Cole, T. B., Wenzel, H. J., Kafer, K. E., Schwartzkroin, P. A., & Palmiter, R. D. (1999). Elimination of zinc from the synaptic vesicles in the intact mouse brain by disruption of the ZnT3 gene. *Proceedings of the National Academy of Sciences of the United States of America*, 96, 1716–1721.
- Cousins, R. J., Liuzzi, J. P., & Lichten, L. A. (2006). Mammalian zinc transporters, trafficking and signals. *Journal of Biological Chemistry*, 281, 24085–24089.
- Deisseroth, K., Mermelstein, P. G., Xia, H., & Tsien, R. W. (2003). Signalling from synapse to nucleus: the logic behind the mechanisms. *Current Opinion in Neurobiology*, 13, 354–365.
- Kuo, Y. M., Zhou, B., Cosco, D., & Gitschier, J. (2001). The copper transporter Ctr1 provides an essential function in mammalian embryonic development. *Proceedings of the National Academy of Sciences of the United States of America*, 98, 220–225.
- Lee, J., Prohaska, J. R., & Thiele, D. J. (2001). Essential role for mammalian copper transporter Ctr1 in copper homeostasis and embryonic development. *Proceedings of the National Academy of Sciences of the United States of America*, 98, 6842–6847.
- Lodish, D., Baltimore, D., Berk, A., Zipursky, S. L., Matsudaira, P., & Darnell, J. (1995). *Molecular Cell Biology*. New York: Scientific American Books. p. 1344.
- Paoletti, P., Vergnano, A. M., Barbour, B., & Casado, M. (2009). Zinc at the glutamatergic synapses. *Neuroscience*, 158, 126–136.
- Sun, H. S., Hui, K., Lee, D. W., & Feng, Z. P. (2007). Zn²⁺ sensitivity of high and low voltage activated calcium channels. *Biophysical Journal*, 93, 1175–1183.
- Takeda, A., & Tamana, H. (2010). Zinc signalling through glucocorticoid and glutamate signalling in stressful circumstances. *Journal of Neuroscience Research*, 88, 3002–3010.
- Vacher, H., Mohapatra, D. P., & Trimmer, J. S. (2008). Localization and targeting of voltage-dependent ion channels in mammalian central neurons. *Physiological Reviews*, 88, 1407–1447.

Metals and Neurodegeneration

Introduction	395
Metal-based Neurodegeneration	395
Neurodegenerative Diseases Associated with Metals	401

INTRODUCTION

As actuaries confront life insurance companies in the developed world with their tables of life expectancy over the next decades, some very important positive and negative points emerge from their projections. One of the most striking is that our children's children will live to be centenarians. Bravo, what enormous progress we have made in extending the longevity of the human race! But this progress has been won at what cost? Given the present correlation between the incidence of debilitating neurodegenerative diseases and dementias, like Alzheimer's and Parkinson's disease, with increasing age, it is alarming to contemplate a situation, where we have only extended our life expectancy, in order to confront the probability that we will be struck down by diseases which will virtually reduce our existence to little more than an advanced vegetative state. In stark terms, what this means is that we must be just as concerned about the quality of life of our ageing population as about their life expectancy. The recent statistics published by the WHO of estimates of the incidence of Alzheimer's disease, by far the most frequent form of dementia in Western society do not make for encouraging reading. It is estimated that there are currently about 18 million people worldwide with Alzheimer's disease. This figure is projected to nearly double by 2025 to 34 million. Much of this increase will be in the developing countries, and will be due to the ageing population. While Alzheimer's disease can occur at any age, its occurrence is much more common as the years go by. In fact, the rate of occurrence of the disease increases exponentially with age, which means that it occurs very rarely among those 40–50 years old, increases between 60 and 65 years, and is very common over 80 years. Combining the results of several studies, the rates of occurrence of Alzheimer's disease estimated in the general population in Western societies are shown in [Figure 21.1](#).

METAL-BASED NEURODEGENERATION

Over the last decade, it has become more and more widely accepted that inflammation, associated with dysfunction of metal ion homeostasis (Fe, Cu, and Zn) accompanied by concomitant oxidative stress, is a key factor in a large number of neurodegenerative diseases such as Alzheimer's disease, Parkinson's disease, Huntington's disease, Amyotrophic lateral sclerosis (ALS), multiple sclerosis, Friedreich's ataxia, and others ([Crichton & Ward 2006](#)). Support comes from the observation that AD, PD, and many other neurodegenerative diseases are characterised by increased levels of some of these metal ions in specific regions of the brain.

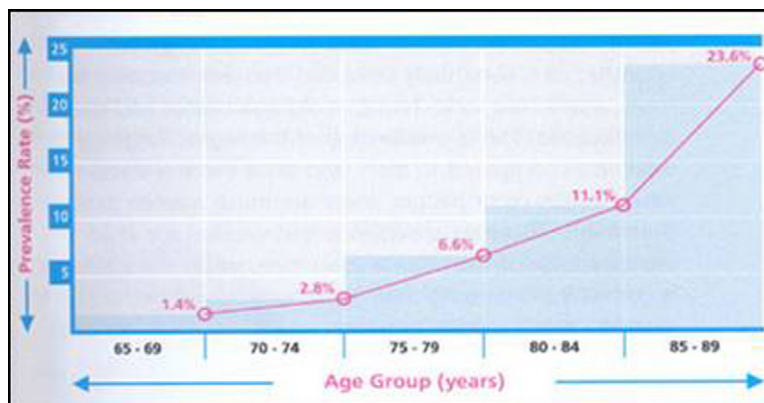


FIGURE 21.1 Estimated rates of occurrence of Alzheimer's disease in the general population in Western societies. (Source WHO regional Office for southeast Asia.)

The '**metal-based neurodegeneration hypothesis**' can be described by the following postulates:

1. Redox-active metal ions (Fe, Cu), present within specific brain regions, can generate oxidative stress by production of reactive oxygen and nitrogen species (ROS, RNS).
2. ROS then cause peroxidation of polyunsaturated fatty acids in membrane phospholipids.
3. This in turn leads to the formation of reactive aldehydes, such as 4-hydroxynonenal.
4. The reactive aldehydes, together with other oxidative processes, interact with proteins to generate carbonyl functions, which damages the proteins, which also undergo modification by reaction with RNS.
5. The damaged, misfolded proteins aggregate, and overwhelm the ubiquitin/proteasome protein degradation system
6. These aggregated, ubiquitinated proteins then accumulate within intracellular inclusion bodies (Figure 21.2).
7. Such intracellular inclusion bodies are found in a great many neurodegenerative diseases.

Although both ROS and RNS are involved in physiologically relevant, and important intracellular signalling pathways, there is considerable evidence that in particular situations of oxidative stress, they are associated with a number of neurodegenerative pathologies. Oxidative stress refers to a situation where elevated levels of ROS are observed, and can result from a variety of conditions that represents either increased ROS production or a decreased level of antioxidant defence. In the case of stimulation of ROS production by macrophages during the innate immune response to bacterial infection, the ROS so generated act in a protective manner. However, dysregulation of ROS levels in a variety of tissues, notably in the brain, has been linked to a growing number of inflammatory and age-associated diseases. During oxidative stress, the oxidation of cellular components results in the modification of DNA, proteins, lipids, and carbohydrates, and the resulting oxidative damage is frequently associated with cell death either by necrosis or by apoptosis (Figure 21.3).

As was pointed in Chapter 13, the most reactive of the ROS is the OH radical generated from H_2O_2 and Fe^{2+} by the Fenton reaction. While ROS play an important role in signal transduction and gene expression, through the activation of nuclear transcription factors, there are some cells in the body which use the cytotoxicity of ROS to attack and kill invading microorganisms. When macrophages and neutrophils encounter a bacterium or other foreign particles, they ingest it and internalise it within an intracellular compartment known as a phagosome. The multicomponent enzyme, NADPH oxidase, is then assembled within the membrane of the phagosome. This enzyme then generates superoxide inside the phagosome, which undergoes dismutation to hydrogen peroxide, and leads to Fe^{2+} -catalysed hydroxyl radical formation. Reactive nitrogen species (RNS) also play an important role as messengers in cells. The first to be discovered, nitric oxide ($\text{NO}\cdot$), is produced by the enzyme nitric oxide

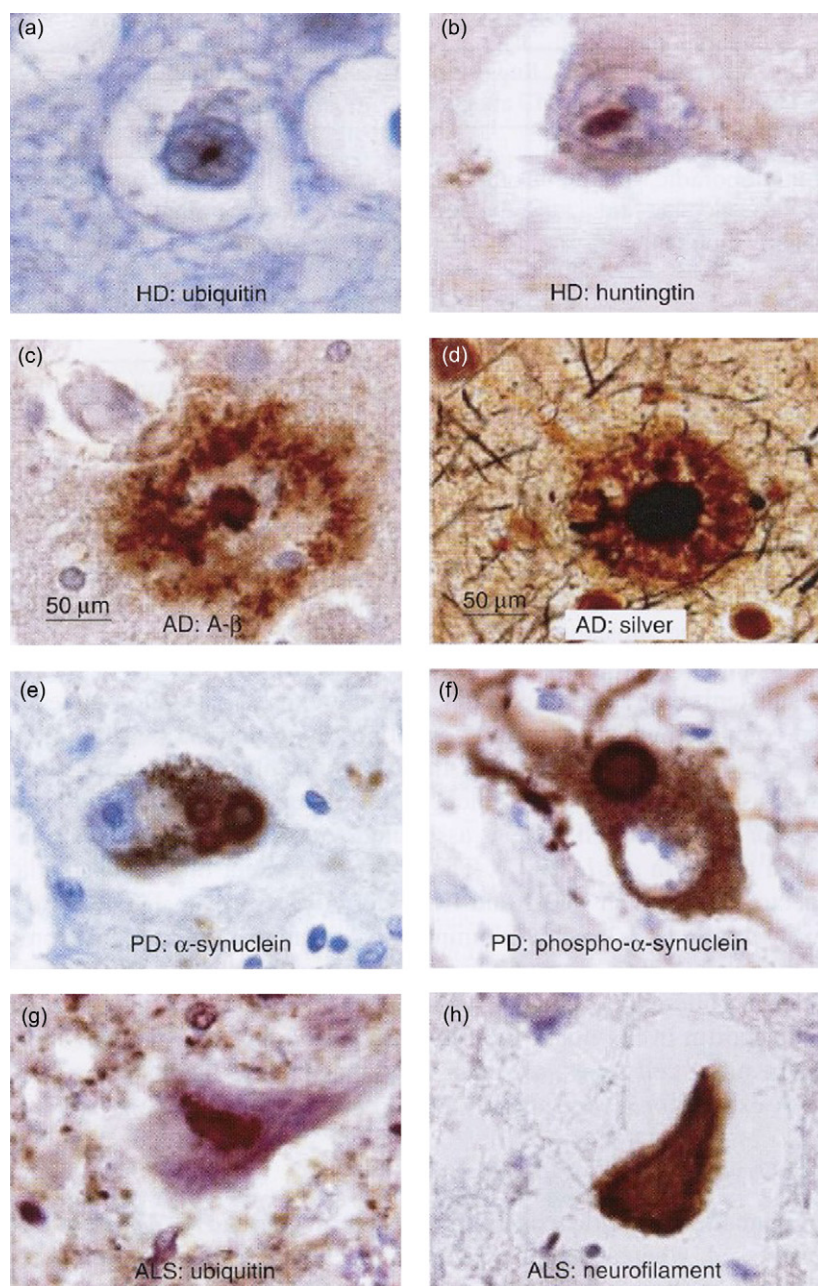


FIGURE 21.2 Characteristic neurodegenerative disease neuropathological lesions involve deposition of abnormal proteins. (From Ross & Poirier, 2004. Copyright 2004 with permission from Nature Publishing Group.)

synthase (NOS), which generates $\text{NO}\cdot$ and citrulline from arginine in a 5-electron oxidation reaction. Once it has been formed, $\text{NO}\cdot$ can diffuse and exert its effects on other cells, but it can also react to form other RNS such as peroxynitrite, ONOO^- , $\text{NO}_2\cdot$, and nitrous anhydride, N_2O_3 . The latter is formed by the autoxidation of $\text{NO}\cdot$ by molecular oxygen, and is a powerful nitrosating agent, thought to be the principal RNS responsible for nitrosative

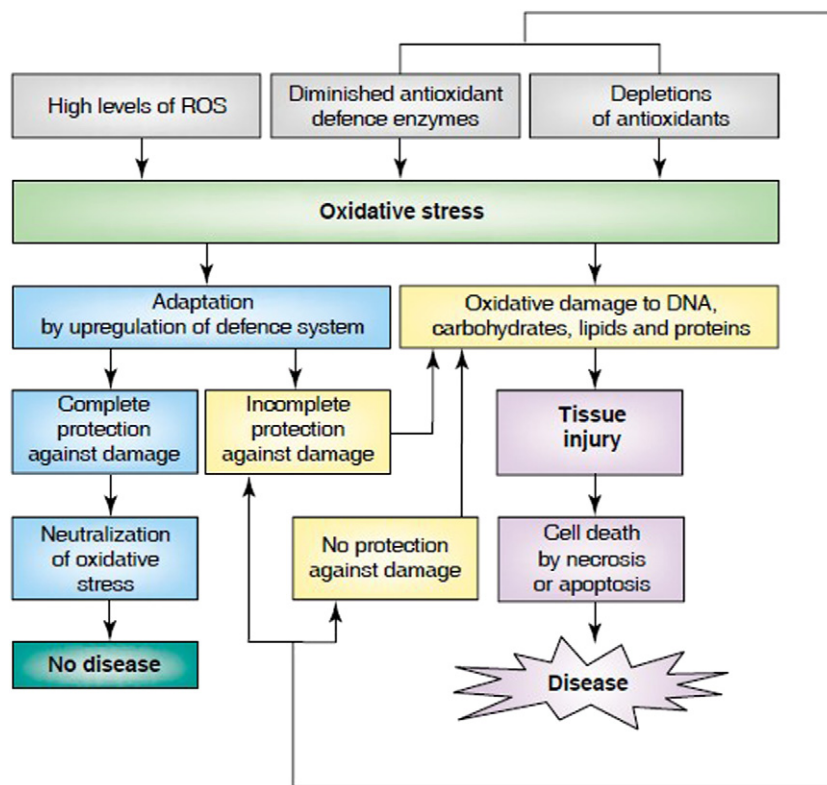


FIGURE 21.3 Origins and consequences of oxidative stress in disease. Reactive oxygen species (ROS) are constantly generated inside cells by oxidase enzymes and by dismutation of the superoxide anion, and their intended functions range from host defence to signal transduction. There are several cellular systems that eliminate ROS, however, endogenous and exogenous triggers can cause the overproduction of ROS or the impairment of antioxidant defence systems, leading to a deleterious condition known as ‘oxidative stress’. Adaptive upregulation of defence systems can protect against damage, either completely or partially, but oxidative-stress-mediated damage to all types of biological macromolecules often leads to tissue injury, and eventually to cell death by necrosis or apoptosis. (From Dalle-Donne, Giustarini, Colombo, Rossi, & Milzani, 2003. Copyright 2003 with permission from Elsevier.)

deamination of nucleobases in DNA. Another nitrogen dioxide radical, $\text{NO}_2\cdot$ is thought to be the agent responsible for nitration of proteins and lipids.

When ROS are generated by redox metals such as iron and copper in proximity to membrane phospholipids, they initiate the peroxidation of polyunsaturated acyl chains of phospholipids or n-6 polyunsaturated fatty acids (PUFA) (Figure 21.4). The lipid hydroperoxides are highly susceptible to breakdown through nonenzymatic Hock cleavage, forming a variety of lipid-derived α,β -unsaturated 4-hydroxyaldehydes of which the most prominent is 4-hydroxynonenal (HNE). 4-Hydroxy-2-nonenal (HNE) is the main aldehyde formed during lipid peroxidation of n-6 polyunsaturated fatty acids, such as linoleic acid C18:2 n-6 and arachidonic acid C20:4 n-6 lipid, whereas peroxidation of n-3 polyunsaturated fatty acids such as α -linolenic acid C18:3 n-3 and docosahexaenoic acid C22:6 n-3 generates a closely related compound, 4-hydroxy-2-hexenal (HHE). The mechanisms by which these 4-hydroxyalkenals might be formed from membrane phospholipid PUFAs has been recently reviewed (Schneider et al. 2008).

HNE was initially recognised as the product of lipid peroxidation with the greatest toxicological potential; it is subsequently considered to be one of the most reliable markers of oxidative stress: it can also trigger signalling events in a physiological context as well acting as a growth-modulating factor. Immunohistochemical

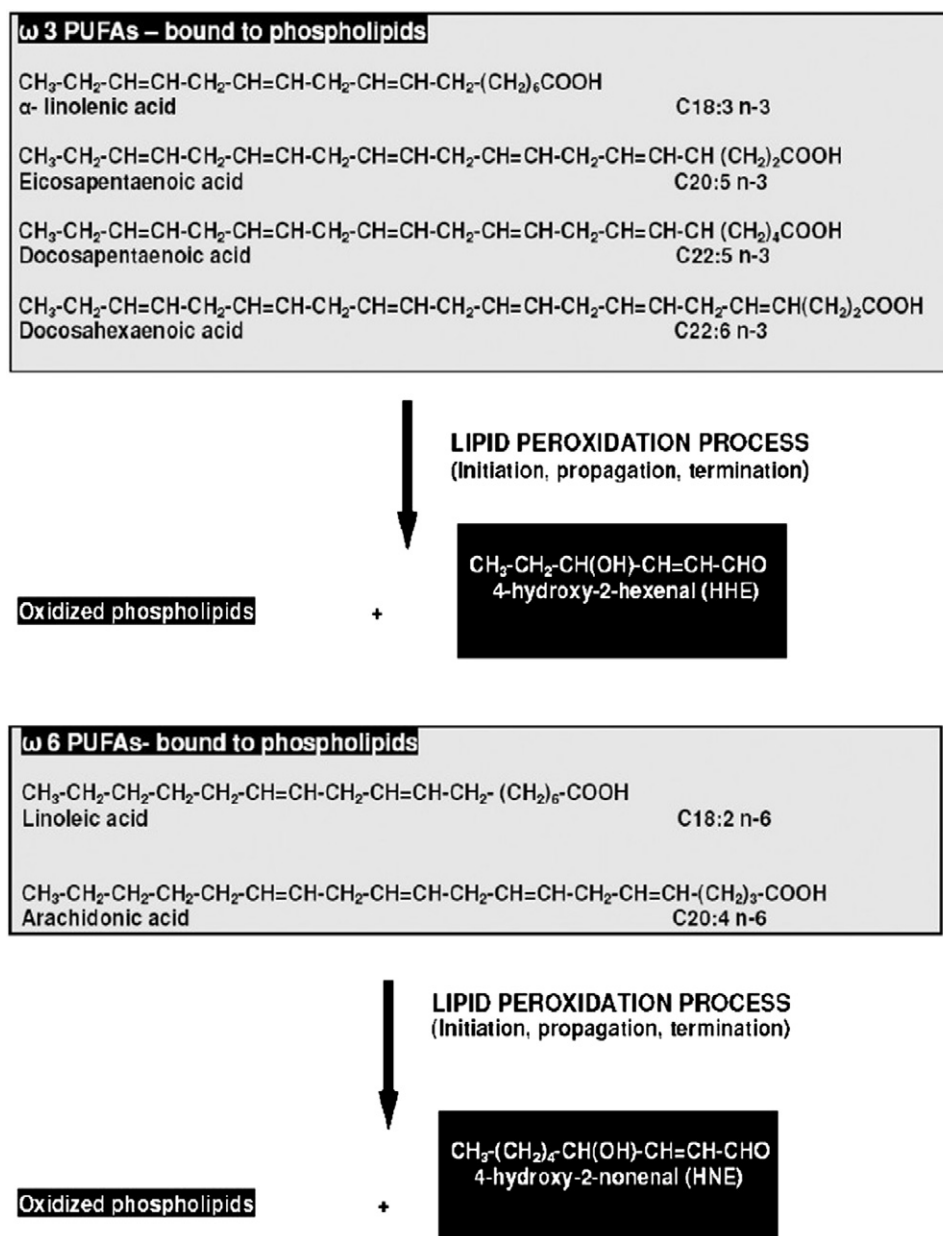


FIGURE 21.4 Schematic diagram of reactive hydroxy-alkenals generated during lipid peroxidation of *n*-3 and *n*-6 polyunsaturated fatty acids. (From Catala, 2009. Copyright 2009 with permission from Elsevier.)

studies show the presence of HNE in neurofibrillary tangles and senile plaques in Alzheimer's disease (AD), in the cytoplasm of the residual motor neurons in sporadic amyotrophic lateral sclerosis (ALS), and in Lewy bodies in neocortical and brain stem neurons in Parkinson's disease (PD). 4-HNE is relatively stable *in vivo*, and has been proposed to be one of the key mediators of the damage resulting from exposure to reactive oxygen and nitrogen species.

During oxidative stress, numerous post-translational modifications of proteins have been characterised resulting either from direct oxidation of amino acid residues by highly reactive oxygen species that are formed during normal metabolism or through the conversion of lipid and carbohydrate derivatives to compounds that react with functional groups on proteins. A significant portion of these ROS-induced post-translational modifications result in the formation of reactive protein carbonyl derivatives, generically termed “protein carbonylation”. The level of carbonyl groups in proteins is widely used as a marker of oxidative protein damage. Direct oxidation of certain amino acid side chains in proteins (proline, arginine, lysine, and threonine) or oxidative cleavage of the protein backbone can lead to the formation of protein carbonyl derivatives (Figure 21.5). Methionine and cysteine

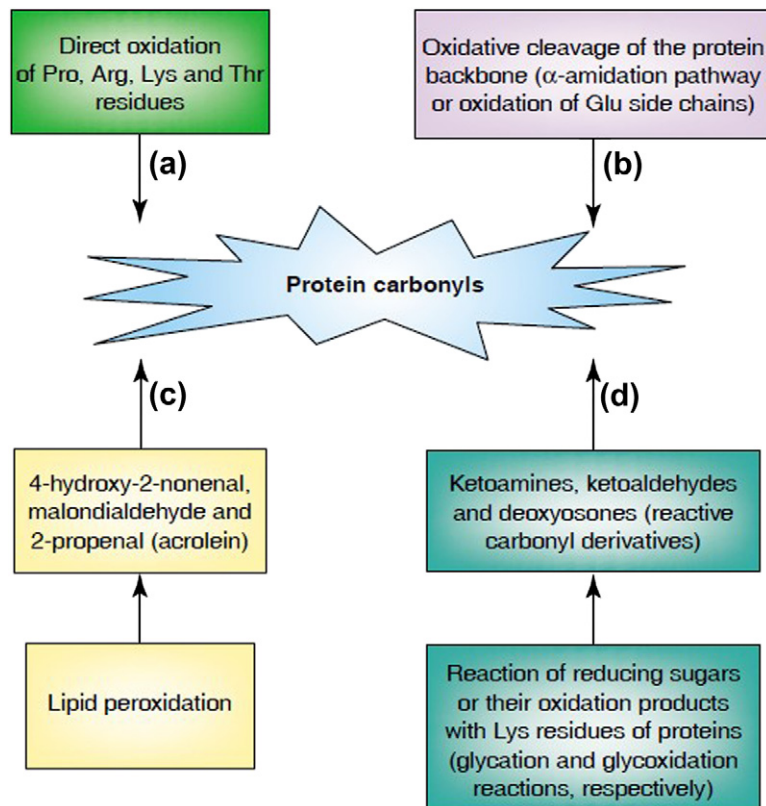


FIGURE 21.5 The production of protein carbonyls. (a) This can arise from direct oxidation of amino-acid side chains (Pro, Arg, Lys, and Thr). (b) Protein carbonyl derivatives can also be generated through oxidative cleavage of proteins, via the α -amidation pathway or through oxidation of glutamine side chains, leading to the formation of a peptide in which the N-terminal amino acid is blocked by an α -ketoacyl derivative. (c) The introduction of carbonyl groups into proteins can occur by Michael addition reactions of α,β -unsaturated aldehydes, such as 4-hydroxy-2-nonenal, malondialdehyde and 2-propenal (acrolein), derived from lipid peroxidation, with either the amino group of lysine, the imidazole moiety of histidine, or the sulfhydryl group of cysteine. (d) Carbonyl groups can also be introduced into proteins by addition of reactive carbonyl derivatives by the reaction of reducing sugars or their oxidation products, with the amino group of lysine residues. (From *Dalle-Donne et al.*, 2003. Copyright 2003 with permission from Elsevier.)

can be directly oxidised. Carbonyl groups can also be introduced into proteins by addition of reactive carbonyl compounds (ketoamines, ketoaldehydes, and deoxyosones) produced by a complex series of reactions between reducing sugars or their oxidation products with the amino groups of lysine residues in proteins, by mechanisms known as glycation and glyoxidation. Because of their electron-withdrawing functional groups, the double bond

of 4-HNE and other α,β -unsaturated aldehydes serves as a site for Michael addition with the sulfur atom of cysteine, the imidazole nitrogen of histidine, and, to a lesser extent, the amine nitrogen of lysine. After forming Michael adducts, the aldehyde moiety may in some cases undergo Schiff base formation with amines of adjacent lysines, producing intra- and/or inter-molecular cross-linking. Recent studies have suggested that such protein carbonylation from lipid-derived aldehydes is more prevalent than that formed via direct amino acid side chain oxidation.

Peroxynitrite is able to oxidise methionine residues and to nitrate tyrosine residues in proteins. Nitration of tyrosine residues may contribute significantly to peroxynitrite toxicity, since nitration will prevent the phosphorylation or nucleotidylation of key tyrosine residues in enzymes which are regulated by phosphorylation/adenylation, thereby seriously compromising one of the most important mechanisms of cellular regulation and signal transduction.

ROS can also readily attack DNA, generating a variety of DNA lesions, such as oxidised bases, abasic sites, and single- and double-strand breaks. If not properly removed, DNA damage can be potentially dangerous, leading to mutagenesis and/or cell death, especially in the case of lesions that block the progression of DNA/RNA polymerases.

NEURODEGENERATIVE DISEASES ASSOCIATED WITH METALS

1. Parkinson's Disease (PD)

PD is the second most common neurodegenerative disease after AD affecting about 1% of the population older than 60. Unlike AD, which affects memory and behaviour centres in the brain, PD is characterised by progressive loss of control over voluntary movement. The characteristic symptoms (bradykinesia, rigidity, tremor, and loss of balance) arise from the progressive loss of dopaminergic neurons (neurons which synthesise and release dopamine) in the substantia nigra pars compacta (SNPC), located in the mid-brain. In PD, there is a two fold increase in the iron content of the substantia nigra and the lateral globus pallidus. This is in marked contrast to other iron storage diseases, like untreated genetic haemochromatosis, and thalassaemia patients, where 10- to 20-fold iron increases in iron stores must be attained before clinical abnormalities occur. The etiology of such iron excesses are unknown although it has been suggested that changes in iron release mechanisms across the BBB, or dysregulation of iron transport across the membranes of specific brain regions may be involved. A second characteristic hallmark of PD is the presence, within dopaminergic neurons, axons, and synapses of the substantia nigra, of intracellular, eosinophilic proteinaceous aggregates called Lewy bodies, which are composed mostly of aggregates of ubiquitinated α -synuclein, but also contain, tyrosine hydroxylase and IRP 2. There are increased levels of iron in both Lewy bodies within cytosolic compartments as well as in dopaminergic neurons of the substantia nigra in PD patients which will cause oxidative damage.

Despite the increased brain iron content in PD, there is no corresponding upregulation of ferritin expression. As we saw earlier, iron regulatory proteins, IRP-1 and IRP-2, act as iron sensors and regulate ferritin synthesis (Chapter 7). IRP2 seems to play the predominant role in post-transcriptional regulation of iron metabolism in brain. Changes in ubiquitination appear to be an important facet of Parkinson's disease; since the degradation of IRP-2 requires its ubiquitination and proteasomal degradation, this may be an explanation for the failure to upregulate ferritin synthesis (which would require the inactivation of IRP2).

Genetically engineered mice, which lack IRP-2 but have the normal complement of IRP-1, develop adult onset neurodegenerative disease associated with inappropriately high expression of ferritin in degenerating neurons. Mice that are homozygous for a targeted deletion of IRP-2 and heterozygous for a targeted deletion of IRP-1 develop severe neurodegeneration with severe axonopathy, and increased levels of ferric iron and ferritin expression, accompanied by degeneration of neuronal cell bodies in the substantia nigra.

The role of iron in PD is outlined in [Figure 21.6](#). In the brain interstitial fluid, iron is transported bound to transferrin (Tf) which is absorbed by neuronal cells via transferrin receptor (TfR1)-mediated endocytosis. Iron

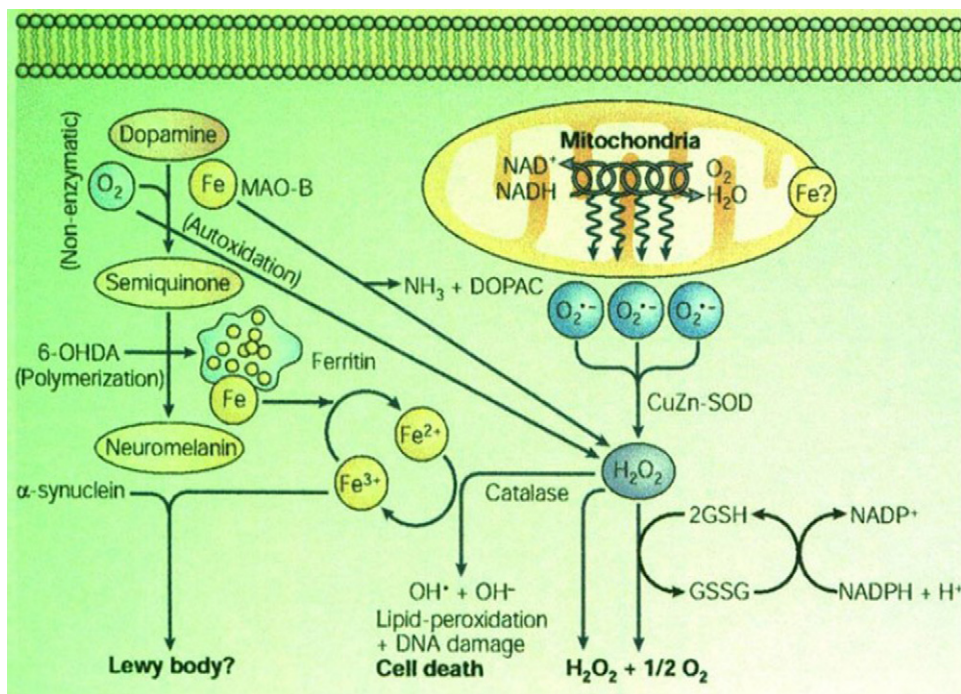
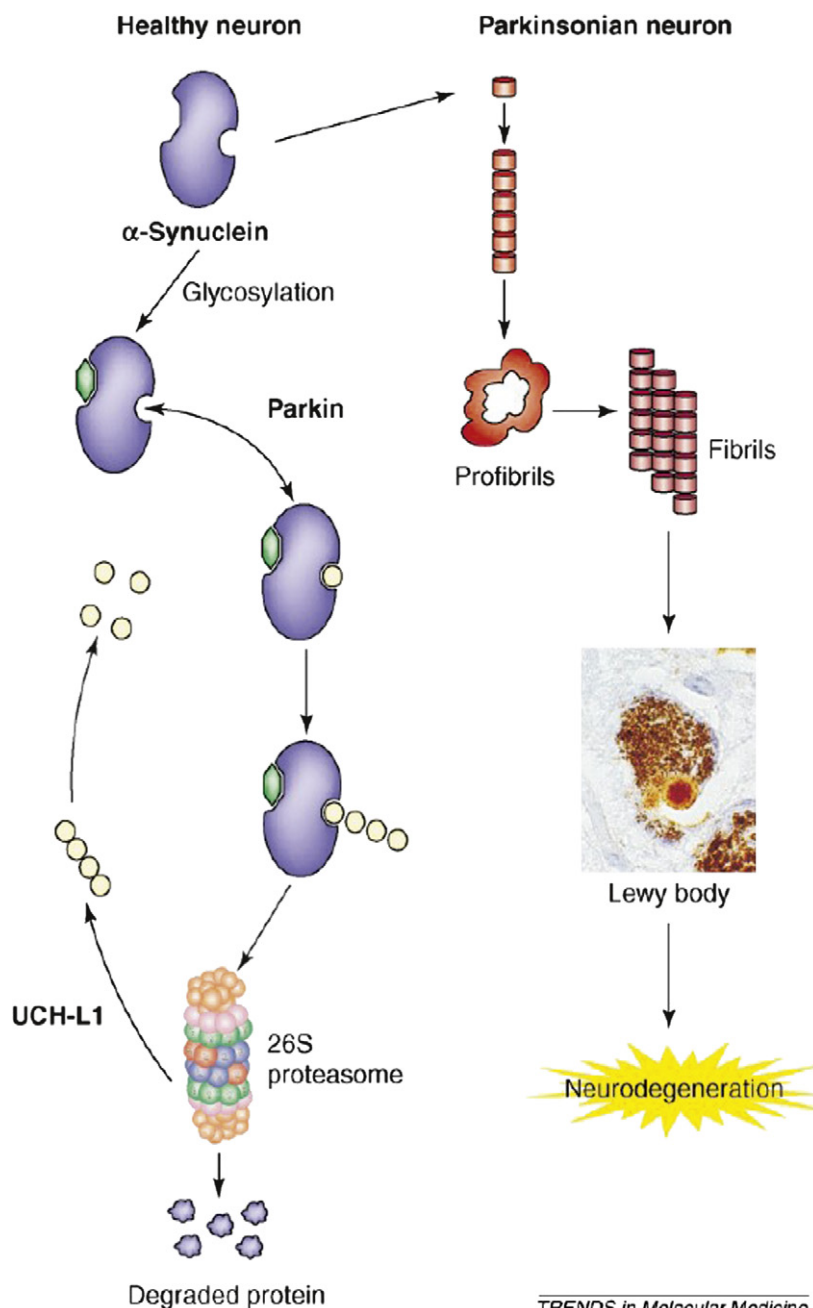


FIGURE 21.6 Oxidative stress in parkinson's disease. (From *Zacca et al., 2004*. Copyright 2004 with permission from Nature.)

levels are elevated in the neurons of the substantia nigra in PD, but whereas iron is normally stored in ferritin, in PD ferritin levels are found to be inappropriately low. Large amounts of iron are normally sequestered in the substantia nigra and the locus coeruleus as neuromelanin—iron complexes in dopaminergic neurons. Neuromelanin, a granular dark brown pigment, is produced in catecholaminergic neurons of the SN and locus coeruleus and is possibly the product of reactions between oxidised catechols with a variety of nucleophiles, including thiols from glutathione and proteins. The function of neuromelanin in the pigmented neurons is unknown but it could play a protective role via attenuation of free radical damage by binding transition metals, particularly iron. Whether the ability of the neurons to synthesis neuromelanin is impaired in PD patients is unknown, although it is reported that the absolute concentration of nigral neuromelanin is less than 50% in PD with respect to age-matched controls. If the capacity of the neurons to store iron is exceeded, potentially toxic free iron will accumulate, which promotes conformational changes within parkin and α -synuclein, causing their aggregation. Iron is also an important cofactor in tyrosine hydroxylase (TH) which is involved in dopamine biosynthesis and of monoamine oxidase (MAO), an enzyme which is involved in dopamine metabolism. Hydrogen peroxide, generated in this reaction, can then be converted to ROS by 'free' iron.

Three proteins, α -synuclein, parkin, and ubiquitin carboxy-terminahydrolase (UCH-L1), have been shown to be linked to inherited forms of PD. A putative model for the role of these proteins is shown in Figure 21.7. In healthy neurons, the cytoplasmic concentration of α -synuclein (blue) is tightly controlled. Glycosylation (green) of α -synuclein is required for its ubiquitination (Ub) (yellow circles), probably by parkin (which is a protein—ubiquitin ligase, the enzyme family responsible for ubiquitination of condemned proteins). Proteasomal degradation of ubiquitylated α -synuclein produces peptide—ubiquitin conjugates, and subsequent recycling of ubiquitin might be controlled by ubiquitin C-terminal hydrolase L1 (UCH-L1). An increase in cytoplasmic α -synuclein concentration, as a result of increased synthesis or via inactivation of parkin, can promote its aggregation. If the gene encoding α -synuclein is mutated, the increased concentration can promote oligomerisation of α -synuclein to form structured



TRENDS in Molecular Medicine

FIGURE 21.7 A putative model of the role of three proteins linked with Parkinson's disease (PD). In healthy neurons, the cytoplasmic concentration of α -synuclein (blue) is tightly controlled. Glycosylation (green) of α -synuclein is required for its ubiquitination (Ub) (yellow circles), probably by parkin. Proteasomal degradation of ubiquitinated α -synuclein produces peptide-ubiquitin conjugates, and subsequent recycling of ubiquitin might be controlled by ubiquitin C-terminal hydrolase L1 (UCH-L1). An increase in cytoplasmic α -synuclein concentration, as a result of increased synthesis or via inactivation of parkin, can promote its aggregation. If the gene encoding α -synuclein is mutated, the increased concentration can promote oligomerisation of α -synuclein, which is eventually converted to Lewy bodies, the pathological hallmark of PD brains. (From Barzilila & Melamed, 2003. Copyright 2003 with permission from Elsevier.)

profibrils, which might be pathogenic in PD. Profibrils are morphologically heterogeneous, and spheres, chains and rings have been identified. These intermediates are eventually converted to fibrils and then to Lewy bodies, which are the pathological hallmark of PD brains.

2. Alzheimer's Disease, AD

As life expectancy in the developed world increases, there is a significant increase in the development of mild cognitive impairment, MCI (dementia), which can progress to AD. Over 24 million people worldwide suffer from some form of dementia, and estimates are that, by 2040, 80 million people will be demented, with AD, accounting for some 60% of all dementias. AD is the most common cause of age-related neurodegeneration, affecting memory and behaviour centres of the brain. This progressive loss of cognitive and behavioural functions is associated with the temporal and frontal lobes of the brain. The classical pathophysiological hallmarks are the presence of toxic insoluble aggregates of amyloid- β peptide (A β) in extracellular senile plaques and of neurofibrillary tangles (NFT) created by the hyperphosphorylation and subsequent aggregation of the microtubule-associated protein, tau, associated with the loss of cortical neurons. Clinical symptoms occur typically between the ages of 60–70 y. This disease, for which no effective treatment is currently available, initially presents with symptoms of memory loss, after which a progressive decline of both cognitive and motor function occurs. Both genetic and environmental factors are implicated in its development. Females are more susceptible than males, which may be attributable to the higher constitutive activity of the synaptic zinc transporter ZnT3 (see Chapter 20). Studies showed that female mice exhibited age-dependent hyperactivity of the ZnT3 transporter which was associated with increased amyloid peptide, A β , deposition.

There is considerable evidence that defective homeostasis of redox-active metals, i.e., iron and copper, together with oxidative stress, contributes to the neuropathology of AD. The characteristic histology of AD is the deposition of both A β , as neurotic plaques, and of the protein tau, as neurofibrillary tangles NFT, predominantly in the cerebral cortex and hippocampus.

A β is derived by the proteolytic cleavage of the amyloid precursor protein (APP), a type 1 transmembrane glycoprotein. APP is cleaved by three types of proteases, the α -, β -, and γ -secretases. The majority of APP is processed in the nonamyloidogenic pathway (Figure 21.8); APP is first cleaved by α -secretase within the amyloid- β protein (A β) domain leading to release of the neuroprotective extracellular soluble sA β PPs α fragment, and precluding A β generation. The membrane-anchored α carboxy terminal fragment (α CTF) is then cleaved by γ -secretase within the membrane, releasing the p3 peptide and the APP intracellular domain (AICD). Alternatively, amyloidogenesis takes place when APP is first cleaved by β -secretase, producing A β PP. A β and AICD are generated upon cleavage by γ -secretase of the β -CTF fragment retained in the membrane. Therefore, stimulation of the α -secretase pathway attenuates A β accumulation in the brain and amyloid formation. The processing of both α - and β -secretases is modulated by furin, a member of the subtilisin-like proprotein convertase family which catalyses the cleavage of precursor proteins into their biologically active forms. Furin is also involved in modulation of systemic iron homeostasis through the production of soluble haemojuvelin (HJV), an antagonist of bone morphogenic protein (BMP)-mediated activation of hepcidin, and an important regulator of iron homeostasis (see Chapter 8). Furin transcription is modulated by cellular iron levels and by hypoxia. Excess iron decreases furin protein levels, and therefore impairs the production of soluble HJV. In contrast, iron deficiency or hypoxia upregulates furin activity, thereby increasing the production of soluble HJV, and blocking hepcidin activation. This has led to the hypothesis, illustrated in Figure 21.8, that iron regulation of furin may play a role in AD. Increased levels of iron in the brain could downregulate furin protein levels, impairing the ability of α -secretase to generate the neuroprotective sA β PPs α fragment, and thereby activating the amyloidogenic pathway, leading to A β production and ultimately neurodegeneration. In addition, the iron-dependent production of ROS could shift the IRP1 to its IRE-binding form, thereby increasing cellular iron uptake via the transferrin receptor, creating a vicious circle which would progressively increase the intracellular iron content, further downregulating furin and shifting the secretase equilibrium in favour of A β production. Furin mRNA levels in the brains of AD patients and the AD animal model, Tg2576 mice, were significantly lower than those in controls. Moreover, the injection of

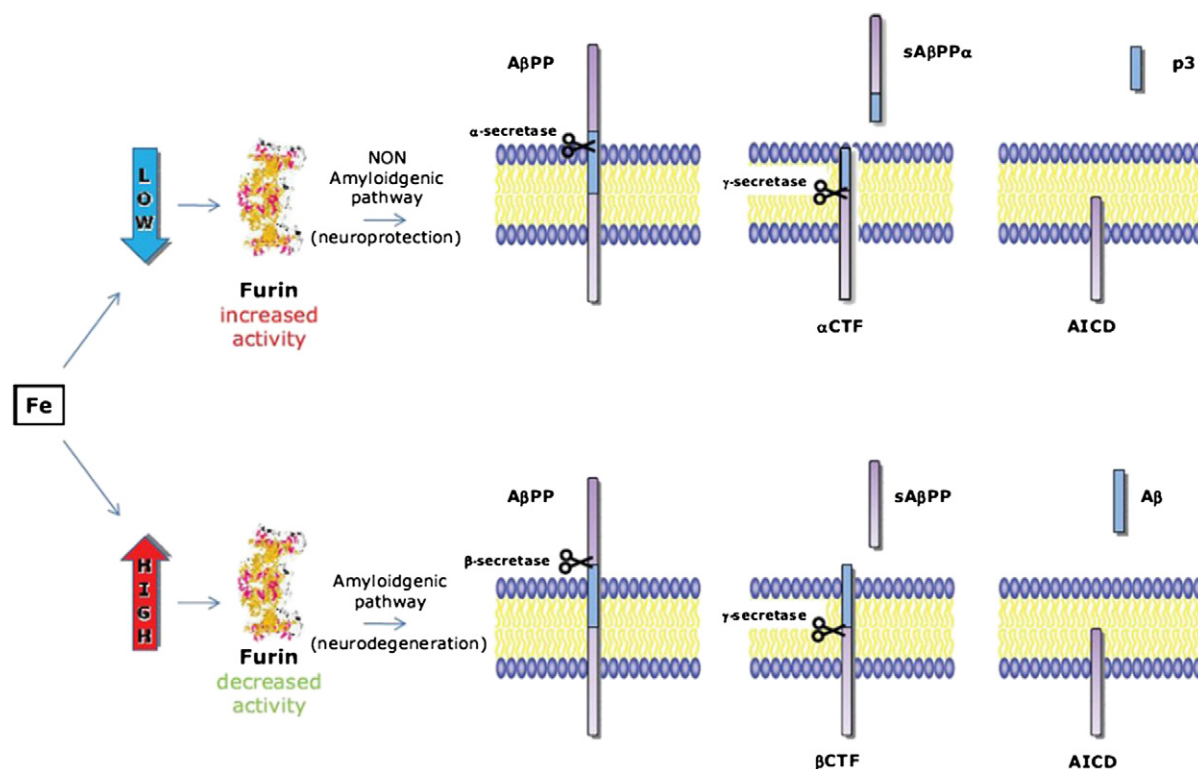


FIGURE 21.8 Furin activity and the fate of AβPP cleavage by α - and β -secretases. Low cellular iron levels are thought to increase furin activity, stimulating the nonamyloidogenic pathway. In contrast, high cellular iron levels decrease furin activity and may activate the amyloidogenic pathway. (From Altamura & Muckenthaler, 2009. Copyright 2009 with permission from IOS Press.)

furin-adenovirus into Tg2576 mouse brains markedly increased alpha-secretase activity and reduced beta-amyloid protein (Aβ) production in infected brain regions. Further support for the connection between iron metabolism and AD comes from the identification of a functional IRE in the 5'-UTR of the amyloid precursor protein mRNA (Rogers et al., 2002). As is the case of ferritin, APP levels increase in the presence of iron and decrease upon addition of an iron chelator in neuroblastoma cells. Increased APP formation in parallel with inhibition of α -secretase activity would favour Aβ deposition.

Aβ has a very effective binding domain for copper in its N-terminal domain and can bind copper in nmol amounts (Figure 21.9). It is unclear whether APP or Aβ, when associated with copper, are in fact neuronal metallo-chaperones. Knock-out and knock-in mice for APP show that in the former, cerebral cortex copper levels are increased, whereas in the latter, reduced copper levels were assayed. Copper was also influential in APP processing in the cell; copper will reduce levels of Aβ and cause an increase in the secretion of the APP ectodomain.

Neurofibrillary tangles, NFTs, contain redox active iron. Accumulation of tau in neurofibrillary tangles is associated with the induction of haem oxygenase 1, HO-1 a potent antioxidant, which plays an important role in metabolising haem released from damaged mitochondria. HO-1 will reduce oxidative damage but Fe^{2+} will be released which may participate in Fenton chemistry to produce hydroxyl radicals. Tau within the neurofibrillary tangles is oxidatively damaged.

It has been suggested that the formation of the β -sheet configuration of Aβ may actually be a protective mechanism, and that the increased synthesis of APP and Aβ is an attempt by the brain cells to detoxify the elevated

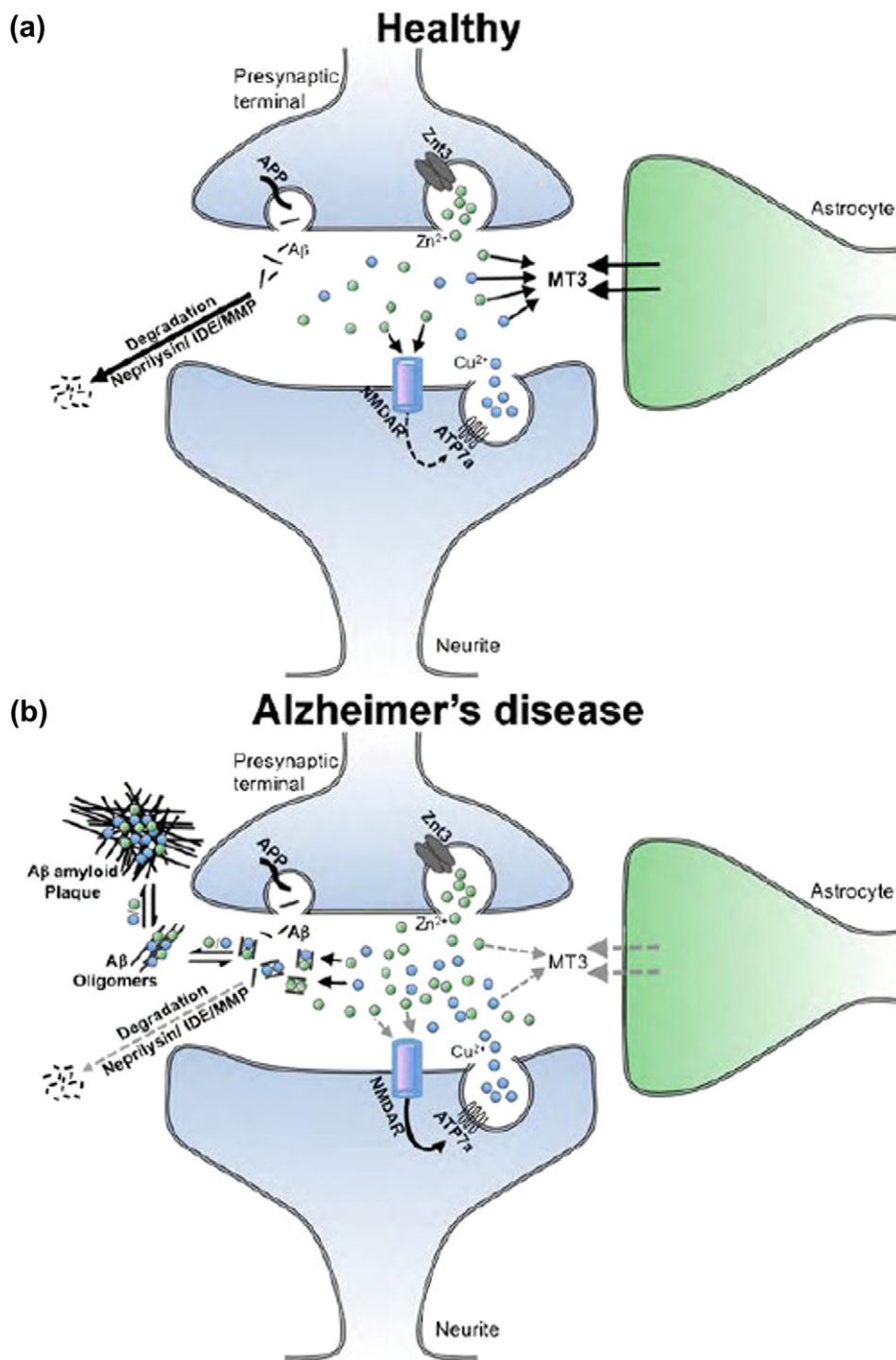


FIGURE 21.9 Models of zinc and copper in the glutamatergic synapse in health and in Alzheimer's disease (a) the healthy synapse (b) Alzheimer's disease synapse. (From *Duce & Bush 2010*. Copyright 2010 with permission from Elsevier.)

levels of redox active metals, copper and iron; other studies suggest that zinc and copper are inhibitory and prevent β -sheet formation.

The possible involvement of copper and zinc in AD is summarised in Figure 21.10 (Duce & Bush, 2010). As we saw in Chapter 20, zinc in the brain is highly enriched in many of the glutamatergic nerve terminals (10–15%),

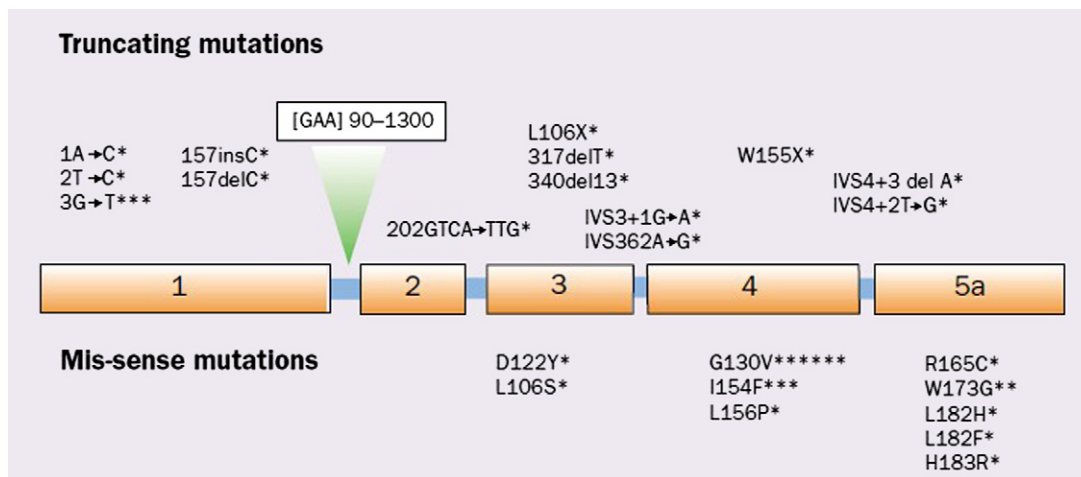


FIGURE 21.10 Frataxin mutations. The commonest mutation is the GAA expansion in the first intron of the frataxin gene (98%). Boxes represent exons and blue bars introns of the frataxin gene. Asterisks indicate the number of families reported with each mutation. (From Dürr, 2002. Copyright 2002 with permission from Elsevier.)

where it is released upon neuronal activation. At healthy synapses, the vesicular zinc transporter ZnT3 transfers zinc into synaptic vesicles. Upon neuronal activation zinc is released, attaining concentrations of 300 μ M within the synaptic cleft. Copper has been reported to be released post-synaptically following NMDA-induced activation, which causes the translocation of ATP7a and its associated copper-laden vesicles to the synaptic cleft. Copper concentrations may reach 15 μ M in the cleft. Both copper and zinc are able to inhibit the NMDA receptor response, which may feedback to prevent further copper from being released into the cleft. Following cleavage of APP, A β can also be released into the synaptic cleft upon neuronal activity, where it may normally act as a ‘zinc sponge’ to lower synaptic levels. A β would typically be cleared by movement into the periphery or degradation by extracellular proteases such as neprilysin and insulin-degrading enzyme (IDE). Despite high concentrations upon neuronal stimulation, the average levels of free synaptic copper and zinc would be kept low over time by a variety of other means, including putative energy-dependent reuptake mechanisms as well as buffering by metallothioneins (e.g., MT3) from neighboring astrocytes. In Alzheimer’s disease, decreased mitochondrial energy production would lead to reduced metal reuptake, causing the average concentration of metals to rise over time. This allows copper and zinc to react with A β released into the synaptic cleft to form oxidised, cross-linked soluble oligomers and precipitated amyloid. A β can bind up to 2.5 moles of metal ions, but becomes more densely aggregated as it becomes loaded with zinc. While the soluble A β monomers are constitutively degraded, zinc-loaded A β oligomers are resistant to degradation. Since MT3 is also decreased in AD, promoting abnormal metal-A β interaction and sequestering of metal ions by A β would permit uncontrolled glutamate activation of the NMDA receptor, leading to the increased release of post-synaptic copper.

Membrane-bound A β may be damaged by metal-induced reactive oxygen species prior to their liberation from the membrane, and consequently precipitated by zinc which is released from synaptic vesicles (Figure 21.10). In vitro, zinc rapidly accelerates A β aggregation, the zinc being associated with the N-terminal region of A β which has an autonomous zinc-binding domain. Zinc induces conformational change of the 1–16 N-terminal region of AP3.

3. Huntington's disease

This is one of a family of diseases in which the expansion of CAG codon repeats resulting in extended polyglutamine (polyQ) tracts in the expressed protein. HD has a frequency of 4 in 10^5 among European populations (less than 1 in 10^6 in Japanese and African populations), and is the most common of the polyQ diseases. It causes movement disorders, cognitive deterioration, and psychiatric disturbances. Symptoms begin appearing insidiously, typically between the ages of 35 to 50: the disease is progressive and fatal some 15–20 years after onset. Motor disturbances include choreiform¹ involuntary movements of proximal and distal muscles and progressive impairment of voluntary movements. In patients with juvenile onset HD, the symptoms include bradykinesia (slowness of voluntary movements and of speech), rigidity, and dystonia (intense irregular muscle spasms); the involuntary movements of the children often take the form of tremor, and they often suffer from epileptic seizures. HD is characterised by a remarkable specificity of neuronal loss. The most sensitive region is the striatum, with the caudate nucleus and the putamen particularly affected; in advanced cases, there is also loss of neurons in the thalamus, substantia nigra, and the subthalamic nucleus. The age of onset of the disease as well as the severity of the symptoms are a function of the length of the glutamine stretches — individuals with 35 CAG repeats or less do not develop the disease; those with 35–39 have an increased risk; while repeats of 40 or over will always lead to the disease in the course of a normal lifespan.

The gene for the protein involved, huntingtin of unknown function, consists of 67 exons, extending over 180 kb of DNA and codes for a protein of 3144 residues (one of the longest polypeptide chains known). The polyQ domain is close to the N-terminus, with the CAG repeat in the first exon. In common with other polyQ diseases, huntingtin with its polyQ repeat is found within aggregates or inclusions within the nuclei of neurons (Figure 21.2). These inclusions in several cases are formed by insoluble amyloid-like fibres, reminiscent of the aggregated forms of proteins found in other neurological diseases. A conformational transition from random coil to β -sheet, which shares most of the features typical of amyloids, takes place during the process of fibre formation.

Alterations in brain iron metabolism have been reported, resulting in increased iron accumulation in Huntington's disease. This was particularly the case in basal ganglia from patients with HD compared to normal controls. In studies in embryonic stem cells, huntingtin was found to be iron regulated, essential for the function of normal nuclear and perinuclear organelles and to be involved in the regulation of iron homeostasis.

4. Friedreich's ataxia

Friedreich's ataxia is the most common hereditary ataxia² and is the most prevalent cerebellar ataxia among children and adults in Europe. It was first described in 1863 by Nikolaus Friedreich. His clinical observations described the essential characteristics of the disease as an adolescent-onset ataxia, particularly associated with clumsiness in walking, accompanied by sensory loss, lateral curvature of the spine, foot deformity, and heart disease. Detailed neuropathological examination showed cerebrosplinal degeneration. Friedreich's ataxia (FRDA) is yet another of the fifteen neurological diseases in man which are known to be caused by the anomalous expansion of unstable trinucleotide repeats. However, unlike Huntington's disease, the trinucleotide expansion occurs in a non-coding region of the gene. The FRDA gene is composed of seven exons spread throughout 95kb of DNA (Figure 21.10), and encodes for the 210 residue protein, frataxin. Frataxin protein levels are severely decreased in FRDA patients, and most FRDA patients are homozygous for the GAA expansion in intron 1. Since the mutation is in the noncoding intron, the consequence of the GAA expansion is to decrease the amount of frataxin mRNA which is synthesised, thereby accounting for the decreased amount of protein. The characteristic pathogenesis of FRDA includes abnormal iron accumulation in mitochondria, hypersensitivity to oxidative stress,

1. Choreiform movements are purposeless, involuntary movements such as flexing and extending of fingers, raising and lowering of shoulders or grimacing.

2. Inability to coordinate voluntary bodily movements, particularly muscular movements.

deficiency of Fe–S enzymes and respiratory chain electron transporters, reflecting the role of frataxin in FeS cluster assembly (Chapter 6).

Amyotrophic Lateral Sclerosis (ALS)

Charcot described amyotrophic lateral sclerosis (ALS, also referred to as motor neuron disease or Lou Gehrig's disease³), a late onset, rapidly progressive neurological disorder, for the first time in 1874. ALS is one of the most common neurodegenerative disorders with an incidence of 4–6 per 100,000. The primary characteristic is the selective degeneration and death of upper (cortico-spinal) and lower (spinal) motor neurons. The disease typically initiates in mid-adult life, and almost invariably progresses to paralysis and death. It is a particularly hideous disease, “in that preservation of cognitive function leaves the victim fully aware of the progressive muscle wasting and loss of motor function, culminating in death within 1–5 years of diagnosis.”

Mutations in SOD1 account for only 2% of ALS, but they represent the best understood. More than 100 different mutations in the gene encoding copper–zinc superoxide dismutase (SOD1) are known cause familial forms of ALS. Aggregation of the SOD1 protein is considered to be the primary mode of pathogenesis, and it appears that these different ALS-associated mutations of SOD1 can increase aggregation of the SOD1 polypeptide for fundamentally distinct reasons (Figure 21.11).

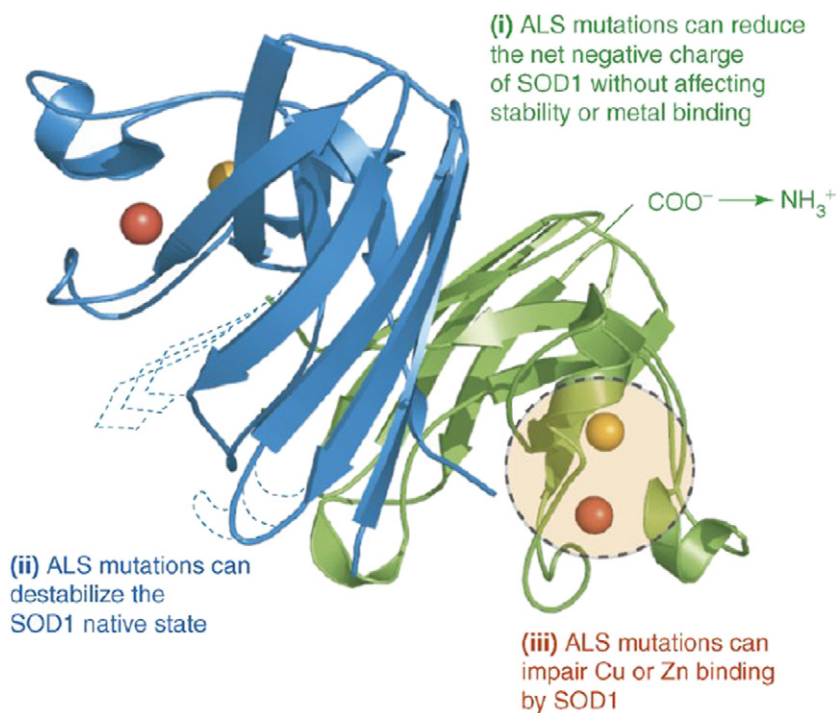


FIGURE 21.11 Different ALS-associated mutations of SOD1 can increase aggregation of the SOD1 polypeptide for fundamentally distinct reasons. (From Shaw & Valentine, 2007. Copyright 2007 with permission from Elsevier.)

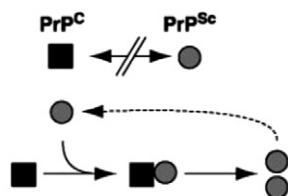
3. **Henry Louis Gehrig**, born **Ludwig Heinrich Gehrig** (June 19, 1903–June 2, 1941), was an American first base man in Major League Baseball who played his entire career for the New York Yankees and was elected to the Baseball Hall of Fame in 1939. His career was prematurely ended by illness, and he retired from the sport later that year after learning he had amyotrophic lateral sclerosis, a degenerative terminal disease so rare that it first became widely known due to him, and is today widely known as “Lou Gehrig’s disease”.

Creutzfeldt–Jakob and Other Prion Diseases

Creutzfeldt–Jakob and other prion diseases have been associated with disorders of copper metabolism. The first cases of Creutzfeldt–Jakob disease in humans were described independently by Creutzfeldt and Jakob over eighty years ago. Although scrapie was known as a fatal neurological disorder of sheep as early as the 1700s, its transmissibility was first demonstrated in 1939. During the 1980s, a bovine spongiform encephalitis epidemic, BSE, occurred in cattle which was attributed to the feeding of BSE-prion-contaminated bone and meat to cattle. More recently, cases of vCJD in vulnerable individuals were thought to be due to their consumption of such BSE-contaminated beef.

The causative agent is known to be the prion protein. There is a considerable body of evidence which indicates that the progression of mammalian prion diseases involves a process in which the normal cellular Prp (PrP^{C}) predominantly α -helical normal form is converted into PrP^{Sc} through a post-translational process during which it acquires a high β -sheet content. This initial event is then followed by the spontaneous formation of a self-propagating aggregate. Finally, the newly formed prion must replicate itself in a process which involves two separate steps: growth of the infectious particle by addition of the aggregate and amplification of the number of infectious particles. Two models have been proposed for the conversion of PrP^{C} to PrP^{Sc} which are illustrated in Figure 21.12. The “**Refolding**” or heterodimer model proposes that the conformational change

A “Refolding” model



B “Seeding” model

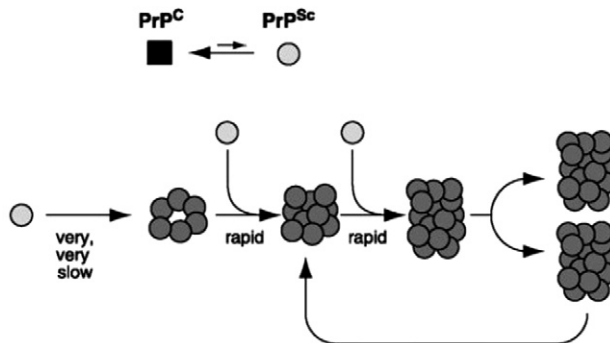


FIGURE 21.12 Models for the conversion of PrP^{C} to PrP^{Sc} . (From Crichton & Ward, 2006.)

involving direct conversion of PrP^{C} to PrP^{Sc} is kinetically controlled, with a high activation energy barrier preventing spontaneous conversion at detectable rates. It is possible that an enzyme or a chaperone could facilitate this reaction. The “**Seeding**” or nucleation model postulates that PrP^{C} and PrP^{Sc} (or a PrP^{Sc} -like molecule, light coloured spheres) are in equilibrium, with the equilibrium largely in favour of PrP^{C} . PrP^{Sc} is only stable when it forms a multimer, hence PrP^{Sc} is stabilised when it adds onto a crystal-like seed or

aggregate of PsP^{Sc} (dark spheres). Seed formation is an extremely rare event: however, once a seed is present, monomer addition ensues rapidly.

It has been well documented that the prion protein binds copper (II) ions and that, among divalent metal ions, PsP^{C} selectively binds Cu(II) . The major copper(II)-binding site has been identified as being within the unstructured amino terminal region (encompassing residues 60–91 of human PsP^{C}). Specifically, copper binds to a highly conserved octapeptide repeat domain, consisting of four sequential repeats of the sequence ProHis-GlyGlyGlyTrpGlyAsn. The Cu(II) to octapeptide-binding stoichiometry is 1:1, i.e., the octapeptide repeat region binds four Cu(II) ions, and copper binding is most favoured at physiological pH, falling off sharply under mildly acidic conditions. While most studies of copper binding have focused on the octapeptide region, evidence has been found for a fifth preferential Cu(II) coordination site, between residues His96 and His111, outside of the octapeptide domain, with a nanomolar dissociation constant. Interestingly, circular dichroism studies show that copper coordination is associated with a loss of irregular structure and an increase in beta-sheet conformation.

Evidence is also growing that PsP^{C} plays an important role in copper homeostasis, in particular at the pre-synaptic membrane; that it may be involved in triggering intracellular calcium signals; and that it may play a neuroprotective role in response to copper and oxidative stress (Figure 21.13). Exposure of neuroblastoma cells to

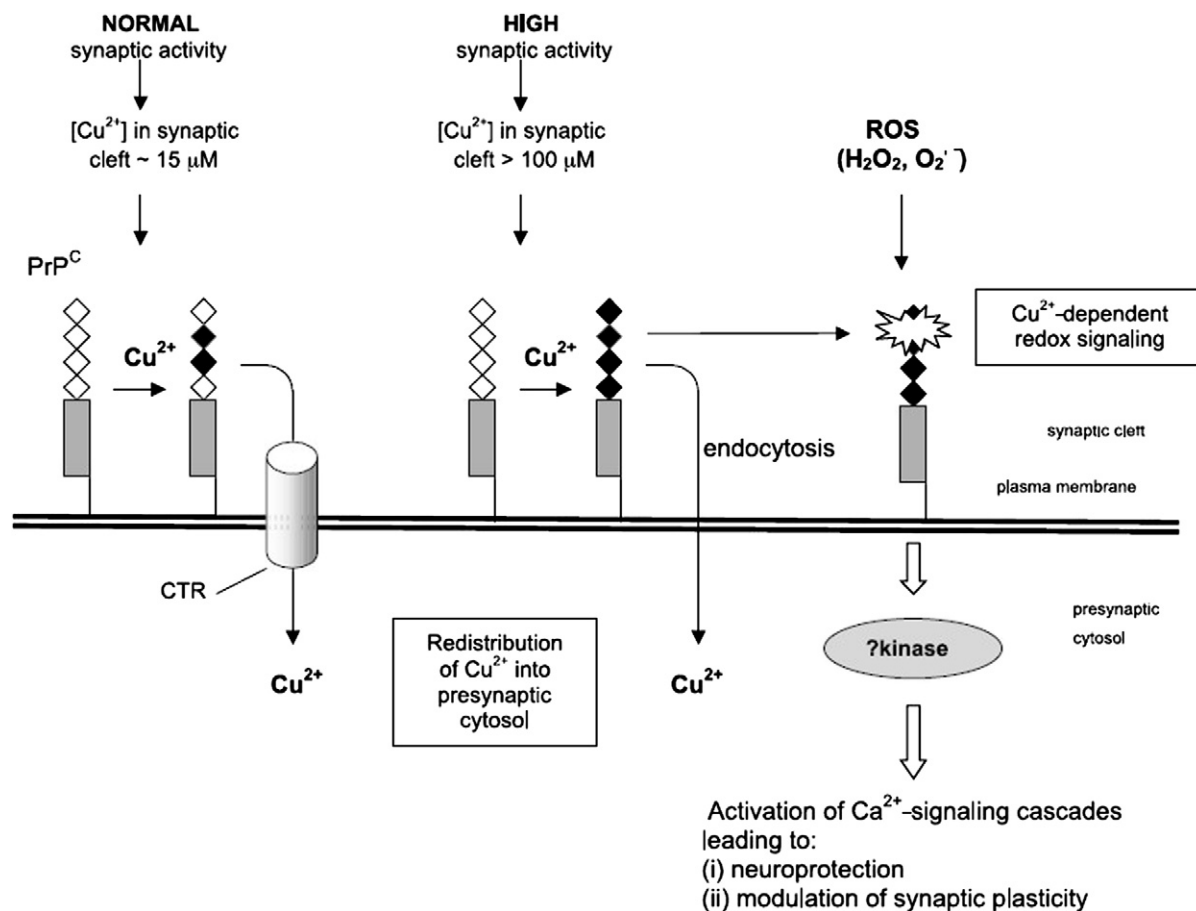


FIGURE 21.13 Schematic representation of the physiological role of prion protein (PrP^{C}) in copper homeostasis and redox signalling. (From Crichton & Ward, 2006.)

high Cu(II) concentrations stimulated endocytosis of PsP^C, whereas deletion of the four octarepeats or mutation of the histidine residues in the central two repeats abolished endocytosis of PsP^C. However, studies at physiological concentrations of copper led to the conclusion that PsP^C does not participate in the uptake of extracellular Cu(II). It has been suggested (Figure 21.13) that in the unique setting of the synapse, PsP^C acts to buffer Cu(II) levels in the synaptic cleft, following the release of copper ions as a result of synaptic vesicle fusion. Cu²⁺ ions released during neurotransmitter vesicle exocytosis are buffered by PsP^C, and subsequently returned to the pre-synaptic cytosol. This can occur either by transfer of copper to copper transport proteins (CTR) within the membrane, or in the case of higher copper concentrations, by PsP^C-mediated endocytosis. Copper-loaded PsP^C may interact with ROS, triggering redox signalling and subsequently activation of Ca²⁺-dependent signalling cascades. These changes in intracellular Ca²⁺ levels lead to modulation of synaptic activity and to neuroprotection.

Disorders of Copper Metabolism – Wilson’s and Menkes Diseases and Aceruloplasminaemia

The neurological diseases caused by disorders of copper metabolism described in 1912 by Samuel Wilson, a young London registrar, and by the Columbia University pediatrician John Menkes 50 years later could hardly be more different. Wilson described a familial nervous disorder, which he called progressive lenticular⁴ degradation, associated with cirrhosis of the liver. Large amounts of copper were present in the brain leading to progressive neurological dysfunction. The disease is characterised by progressive copper accumulation in the brain, liver, kidneys, and cornea. In contrast, in Menkes Disease, first described as an X-chromosome linked fatal neurodegenerative disorder, the transport of copper across the intestinal tract is blocked, resulting in overall copper deficiency (Figure 21.14).

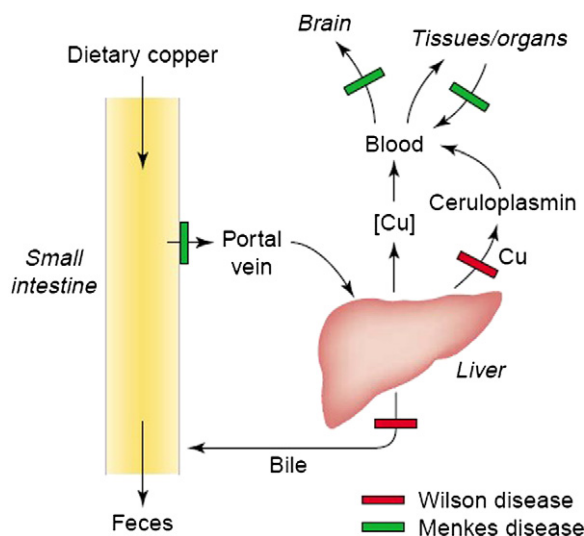


FIGURE 21.14 Pathways of copper which are blocked in Menkes and Wilson's disease. (From Crichton & Ward, 2006.)

Yet in both diseases the mutations are found in copper-transporting P-type ATPases. As we saw in Chapter 8, copper is transported by the chaperone ATOX1 to the P-ATPase ATP7B, located predominantly in the trans-Golgi network, and this is the Wilson's disease protein. The principal function of ATP7B is to transport copper into the

4. Lenticular – pertaining to the lens of the eye.

secretory pathway both for excretion in the bile and for incorporation into ceruloplasmin (Figure 21.15). In Wilson's disease, lack of functional ATP7B results in secretion of Cu-free apoceruloplasmin, which is rapidly

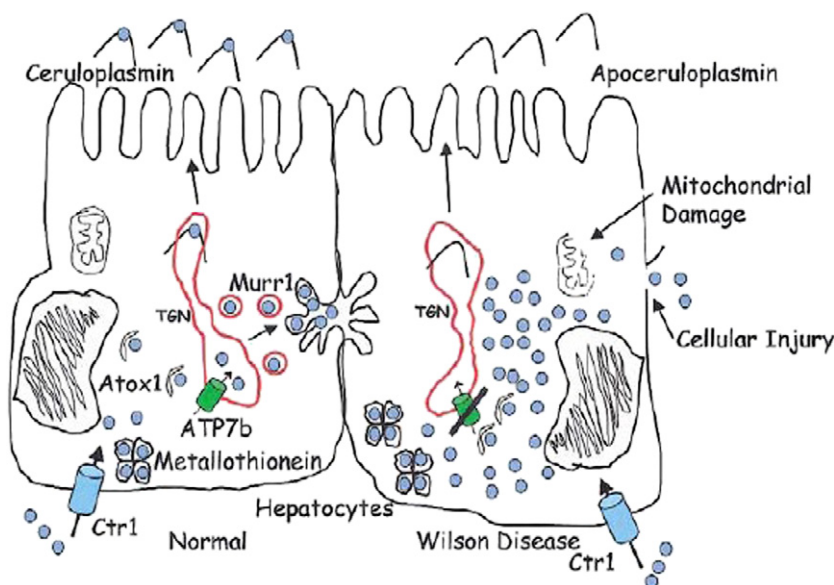


FIGURE 21.15 Proteins involved in copper uptake, incorporation into ceruloplasmin and biliary excretion in normal and Wilson's disease hepatocytes. (From Crichton & Ward, 2006.)

degraded. In normal subjects, when hepatocyte copper content increases, ATP7B cycles to a cytoplasmic compartment near to the bile canicular membrane, where copper is accumulated in vesicles prior to its biliary excretion, most likely associated with Murr1. Murr1 is the product of a gene deficient in canine copper toxicosis, a condition in which affected dogs suffer from defective biliary copper excretion and accumulate massive amounts of lysosomal copper in the liver. In Wilson's disease, mutations in ATP7b result in cytosolic copper accumulation within the hepatocyte, provoking oxidative damage, leakage of copper into the plasma and finally copper overload in most tissues.

Menkes disease is an X-chromosome-linked neurodegenerative disorder of childhood characterised by massive copper deficiency. The boys affected generally die in early childhood, usually in the first decade with abnormalities that can all be related to deficiencies in copper-containing enzymes. The Menkes protein is also a P-type ATPase, known as ATP7A, which appears to play a major role in copper absorption in the gut and in copper reabsorption in the kidney. It has 6 copper-binding motifs in the amino terminal region which also interact with copper chaperones, while 8 transmembrane domains form a channel through which copper is pumped, driven by hydrolysis of ATP. In normal circumstances, the protein is located primarily at the *trans*-Golgi network (TGN), and relocates to the plasma membrane in elevated copper conditions to expel the excess copper from the cell. Copper transport in the brain of Menkes patients is also blocked. Whereas hippocampal neurons release copper in response to activation of NMDA receptors, neurons from animals lacking functional ATP7A do not.

Ceruloplasmin has long been thought to be a ferroxidase and it has been proposed that ceruloplasmin has a custodial role *in vivo*, ensuring that Fe^{2+} released from cells is oxidised to the potentially less toxic Fe^{3+} prior to its incorporation into apotransferrin. Aceruloplasminaemia is a neurodegenerative disease associated with the absence of functional ceruloplasmin due to the presence of inherited mutations within the ceruloplasmin gene. This condition results in disruption of iron homeostasis, with extensive iron accumulation in a number of tissues

such as brain and liver. However, in these patients, as in aceruloplasminaemic mice, both copper transport and metabolism are normal, providing strong evidence against the role of ceruloplasmin as a major copper transporter.

REFERENCES

- Altamura, S., & Muckenthaler, M. U. (2009). Iron toxicity in diseases of aging: Alzheimer's disease, Parkinson's disease and atherosclerosis. *The Journal of Alzheimer's Disease*, 16, 879–895.
- Barzilai, A., & Melamed, E. (2003). Molecular mechanisms of selective dopaminergic neuronal death in Parkinson's disease. *Trends in Molecular Medicine*, 9, 126–132.
- Catala, A. (2009). Lipid peroxidation of membrane phospholipids generates hydroxy-alkenals and oxidized phospholipids active in physiological and/or pathological conditions. *Chemistry and Physics of Lipids*, 157, 1–11.
- Crichton, R. R., & Ward, R. J. (2006). *Metal based neurodegeneration: From molecular mechanisms to therapeutic strategies*. Chichester: John Wiley & Sons. pp. 227.
- Dalle-Donne, I., Giustarini, D., Colombo, R., Rossi, R., & Milzani, A. (2003). Protein carbonylation in human diseases. *Trends in Molecular Medicine*, 9, 164–176.
- Dürr, A. (2002). Friedreich's ataxia: treatment within reach. *The Lancet Neurology*, 1, 370–374.
- Duce, J. A., & Bush, A. I. (2010). Biological metals and Alzheimer's disease: implications for therapeutics and diagnostics. *Progress in Neurobiology*, 92, 1–18.
- Rogers, J. T., Randall, J. D., Cahill, C. M., Eder, P. S., Huang, X., Gunshin, H., et al. (2002). An iron-responsive element type II in the 5'-untranslated region of the Alzheimer's amyloid precursor protein transcript. *The Journal of Biological Chemistry*, 277, 45518–45528.
- Ross, C. A., & Poirier, M. A. (2004). Protein aggregation and neurodegenerative disease. *Nature Medicine*, 10, S10–17.
- Schneider, C., Porter, N. A., & Brash, A. R. (2008). Routes to 4-hydroxynonenal: fundamental issues in the mechanisms of lipid peroxidation. *J Biol Chem.*, 283, 15539–43.
- Shaw, B. F., & Valentine, J. S. (2007). How do ALS-associated mutations in superoxide dismutase 1 promote aggregation of the protein? *Trends in Biochemical Sciences*, 32, 78–85.
- Zecca, L., Youdim, M. B., Riederer, P., Connor, J. R., & Crichton, R. R. (2004). Iron, brain ageing and neurodegenerative disorders. *Nat. Rev. Neurosci.*, 5, 863–873.

Metals in Medicine and Metals as Drugs

Introduction	415
Disorders of Metal Metabolism and Homeostasis	415
Metal-based Drugs	420
Metallotherapeutics with Lithium	425
Contrast Agents for Magnetic Resonance Imaging (MRI)	427

INTRODUCTION

Metals are also found to play an astonishing number and variety of roles in modern medicine. As we saw in Chapter 1, there are around ten metals which are essential for man. These include the four bulk metals, Na^+ , K^+ , Mg^{2+} , and Ca^{2+} , together with the transition metals Mn, Fe, Co, Cu, Zn, and Mo. Genetic disorders involving either their metabolism or their homeostasis, together with dietary insufficiencies either due to genetic or nutritional reasons, will have serious consequences for human health. In addition, at least as many metals again (many of them toxic) are employed as therapeutic and diagnostic agents, or as drugs. Metals, such as arsenic, gold and iron, have been used to treat different human diseases since antiquity. Sometimes, the medical applications use a simple salt of the metal itself, as in the case of the therapeutic use of lithium in bipolar disorders (manic depression). However, there are a constantly growing number of metal-based drugs, involving a broad spectrum of metals, including the widely used anti cancer drug cis-platinum (For further details see Gielen and Tiekink; Hartinger et al., 2006; Sigel and Sigel, 2004; van Rijt and Sadler, 2009).

DISORDERS OF METAL METABOLISM AND HOMEOSTASIS

There are a great number of genetic disorders which affect the metabolism and homeostasis of essential metals in man. While we do not have the space to deal with all of them here, we will briefly discuss a few examples drawn from that almost-ubiquitous transition metal, iron, with which I have what amounts to a life-long association. For most living organisms, iron in excess is toxic, and iron deficiency is also a general problem, particularly in man, which means that iron homeostasis is extremely important, both at the cellular and the systemic level, as we summarised in Chapter 8. Humans, compared to most other mammals, have little capacity to absorb dietary iron, and very little ability to excrete iron. We absorb about 1 mg of dietary iron per day, and excrete roughly the same amount (the figure is slightly higher in women, but the balance remains the same). Therefore it follows, as was originally suggested by McCance and Widdowson (1937), that iron balance in man is primarily determined by iron absorption. The bottom line in any event, is that if we absorb too little iron we suffer from iron deficiency and anaemia, whereas if we absorb too much iron, we become iron-loaded. Needless to say, both conditions are not without important consequences.

Iron deficiency anaemia (IDA) is the most common and widespread nutritional disorder in the world, affecting a large number of children and women in developing countries, but it is also the only nutrient

deficiency which is prevalent in industrialised countries. The WHO estimates that one-third of the world population – some two billion people – are anaemic,¹ and in developing countries every second pregnant woman and around 40% of preschool children are estimated to be anaemic (WHO, 2004). The main cause of IAD is iron deficiency, but this is frequently exacerbated by infectious diseases like malaria, HIV/AIDS, hookworm infestation, schistosomiasis, deficiencies of other important nutrients such as folate, vitamin B12, and vitamin A, or genetically inherited disorders such as thalassaemia which affect red blood cells. IAD has important consequences for human health and childhood development. Both anaemic women and their children are at greater risk of mortality during the perinatal period. The mental and physical development of children is delayed and/or impaired by IAD. The therapeutic management of IDA must include first treatment of the underlying cause, for example, infection, and then correction of the deficiency. Treatment of IDA is rather simple and inexpensive in most subjects and entails oral treatment with ferrous salts. Simple ferrous salts are widely used for oral iron therapy, since these are the cheapest and of these ferrous sulfate is the most common. Clearly, supplementation in developing countries needs to be accompanied by concurrent protection from malaria and other infectious diseases.

Because of our incapacity to excrete significant amounts of iron, referred to above, pathological disorders of iron metabolism associated with excessive iron accumulation, principally in parenchymal tissues, are often observed in man. The term ‘haemochromatose’ was coined by von Recklinghausen in 1889 to describe the dark staining in liver which he (erroneously) attributed to haem,² with accompanying cirrhosis and massive organ damage. It was subsequently shown to be a recessively inherited disease with the gene located on chromosome 6 close to the major histocompatibility HLA-A locus. The term Hereditary Haemochromatosis (HH) is used to describe a number of iron-overload syndromes, all of them characterised by excessive dietary iron absorption. The classical form of HH (HFE or type 1) is an autosomal recessive HLA-linked disease, associated with mutations in the *Hfe* gene. It is the most widely prevalent form of HH, and indeed one of the most frequent genetic disorders in man, more common than cystic fibrosis, muscular dystrophy and phenylketonuria combined, with an estimated carrier frequency of 1 in 200 in Caucasian populations. By far the most common form of HFE is the C282Y homozygote mutation. Several other causes of HH have been identified, constituting the so-called Subtype 1 forms of HH. In addition to HFE mutations, they are associated with rare disorders involving loss of function mutations in the genes for transferrin receptor 2 (*TfR2*), *HAMP* (hepcidin antimicrobial peptide), or haemojuvelin (*HJV*), a co-receptor for bone morphogenic protein (BMP) ligands. Mutations in ferroportin, the iron export protein found predominantly in enterocytes and macrophages, also lead to iron overload (Subtype 2 HH). How then do mutations in any of these four proteins promote dysregulation of systemic iron homeostasis, resulting in an increased absorption of iron from the gastrointestinal tract, which accumulates in parenchymal tissues causing tissue damage, and ultimately death?

For a long time it was thought that the key to understanding the regulation of systemic iron homeostasis resided in the enterocytes of the gastrointestinal tract, which are the sites at which dietary iron is taken up into the body (see Chapter 8 for a detailed account of both iron absorption and systemic iron homeostasis). However, it has recently become clear that the site of action of HFE is not the gastrointestinal tract, but rather the liver, and that, as with all of forms of Subtype 1 HH, the primary defect is in the regulation of hepatic hepcidin synthesis. Two important observations underline this. First, mice with hepatocyte-specific *Hfe* ablation develop systemic iron overload, whereas enterocyte-specific or macrophage-specific disruption of *Hfe* results in a normal iron phenotype. Second, it has been found that in HH patients who have undergone liver transplantation with ‘normal livers’, their iron overload no longer progresses. This underlines the major role of liver hepatocytes as the principal cells controlling systemic iron homeostasis, and we know that they do this through the secretion of hepcidin.

1. Defined as haemoglobin levels significantly below recommended levels.

2. It is in fact due to the heavy deposits of haemosiderin, the lysosomal product of ferritin breakdown.

It has been suggested that haemochromatosis has surprising analogies with diabetes, and might therefore be considered as an endocrine liver disease (Pietrangelo, 2007). Glucose and iron homeostasis are both controlled by negative-feedback systems which are illustrated in Figure 22.1. The levels of both glucose and iron (the latter bound to transferrin) in the circulation are maintained within the normal physiological range by specialised sensors located on the plasma membrane of control centres (pancreatic β -cells and hepatocytes, respectively); the sensor responds to excess glucose or iron by increasing the synthesis and secretion of an effector molecule (insulin or hepcidin), which then acts on target molecules (insulin receptor or hepcidin).

The respective responses are quite similar in their end effect, although their mechanism of action is quite different. Insulin, through its binding to its receptor, initiates a signalling cascade which activates intracellular glucose utilisation, notably for glycogen synthesis, thereby dramatically decreasing the level of glucose in the circulation. The target of hepcidin is ferroportin, and when hepcidin binds to ferroportin it triggers its internalisation and lysosomal degradation (Figure 22.2). Ferroportin degradation results in retention of iron within cells involved in iron exportation like macrophages and in enterocytes of the gastrointestinal tract, where it is stored for future requirements as ferritin, in much the same way as glucose is stored in liver and muscle as glycogen. However, in the enterocytes the ferritin, and the iron that has been stored in it, are lost when the enterocyte is sloughed from the tips of the villi and destroyed, following phagocytosis by macrophages in the intestinal tract.

The way in which the HFE protein might act to regulate systemic iron homeostasis is presented in a simplified form in Figure 22.3. As we pointed out above, mutations in both HFE and Tfr2 cause haemochromatosis. The HFE protein interacts with both Tfr1, Tfr2, and Tfr2 competes with Tfr1 for HFE binding. It is proposed that, under normal homeostatic conditions, HFE is partitioned between Tfr1, Tfr2, and that as Tf saturation increases, Tf displaces HFE from Tfr1. This would shift HFE away from interaction with Tfr1 and towards interaction with Tfr2, as shown in Figure 22.3. Conversely, low iron conditions should favor interaction between HFE and Tfr1. The HFE/Tfr2 complex then propagates a signalling cascade³ resulting in the upregulation of hepcidin, decreased dietary iron uptake and decreased macrophage iron release. Mutations in either HFE or TFR2 would impair this signalling complex, and therefore hepcidin would not be upregulated, resulting in haemochromatosis.

The first step in treatment of haemochromatosis involves diagnosis. Thanks to advances in imaging — which allow noninvasive diagnosis of hepatic iron overload — and molecular genetics — which allow identification of the mutations involved in hereditary iron overload disorders — the task of the clinician confronted with the suspicion of tissue iron excess has been greatly facilitated. The treatment of HH, once it has been diagnosed, is to remove the excess iron by phlebotomy (venesection) at regular intervals. This mobilises iron from the stores for the formation of new red blood cell, and depletes the excedent of storage iron.

There are however a further series of conditions, which are usually classified as secondary haemochromatoses, and which can arise as either inborn or acquired disorders. They all have in common the fact that the patient is anaemic and requires transfusions of erythrocytes. Since one millilitre of red blood cells contains one milligram of iron, the consequence of these transfusions is to almost stoichiometrically increase the body iron burden. In addition, when the anaemia is accompanied by ineffective erythropoiesis, there is also increased dietary iron absorption from the gastrointestinal tract, hence, those patients with ineffective erythropoiesis develop the greatest iron overload. The most common hereditary forms are the thalassaemias, which are due to a reduced rate of synthesis or no synthesis at all of one of the globin chains of haemoglobin. Unlike primary haemochromatosis, where venesection can be used to reduce the iron load, in secondary haemochromatosis this is not possible and management of the iron overloading involves treatment by chelation therapy (Hershko, 2006). Iron chelators are used to remove iron from the body to prevent damage to liver, endocrine organs and, in particular, heart. In thalassaemia major, about 100–200 ml of pure red cells/kg/y are transfused (this corresponds to 0.32–0.64 mg/kg/d of iron). In thalassaemia intermedia, iron absorption is about 5–10 times the normal amount (around 0.1 mg/kg/d).

3. The signalling cascade is much more complex.

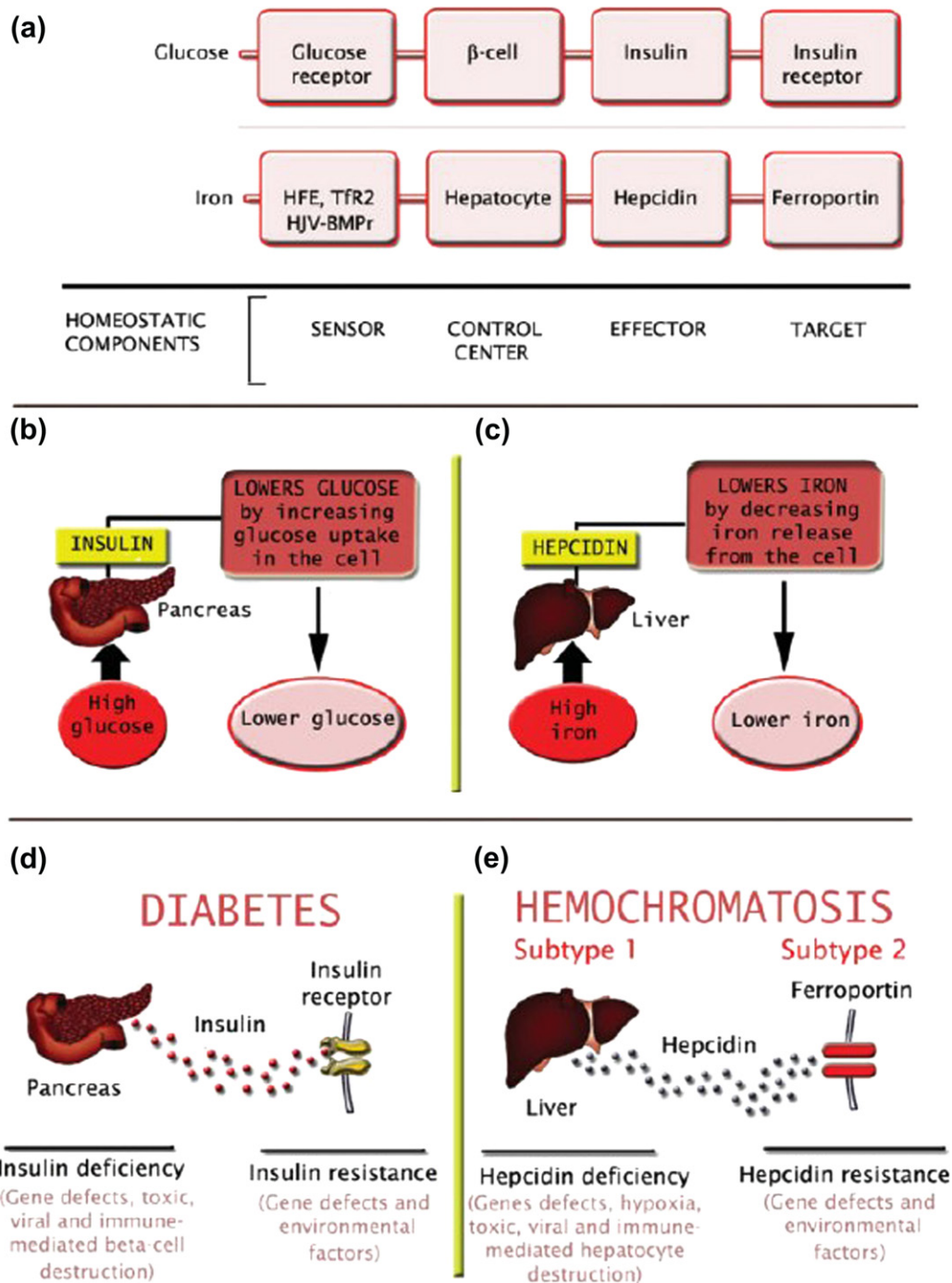


FIGURE 22.1 Negative-feedback systems for the control of glucose and iron homeostasis and their breakdown. (a) Essential components of feedback systems for the maintenance of homeostasis in glucose and iron metabolism. Each component plays a specific role in the process by which an organism regulates its own internal environment. A sensor detects potentially dangerous changes in the internal environment and reports them to a control centre [bone morphogenic protein receptor (BMP)]. The latter responds by activating an effector protein, whose

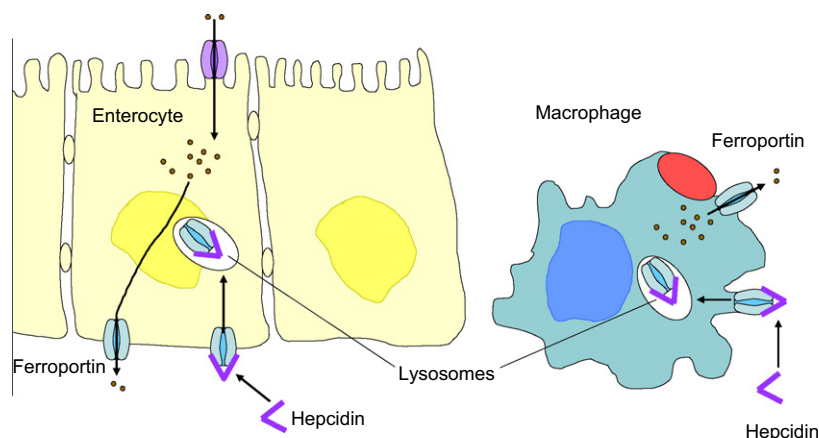


FIGURE 22.2 Hepcidin and haemochromatosis. The activity of hepcidin is depicted, showing ferroportin as a target both on enterocytes and macrophages. Hepcidin binds to ferroportin triggering its internalisation and lysosomal degradation. (Adapted from Andrews, 2008.)

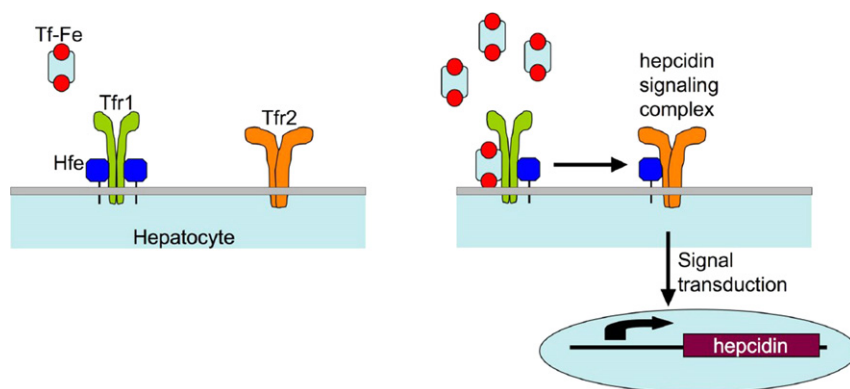


FIGURE 22.3 Model for liver-centred serum iron sensing. (From Schmidt, Toran, Giannetti, Bjorkman, & Andrews, 2008. Copyright 2008 with permission from Elsevier.)

The primary aim of chelation therapy is to remove iron from the body at a rate which is either greater than transfusional iron input (reduction therapy) or equal to iron input (maintenance therapy).

The structures of the three iron chelators which are currently approved for clinical use are presented in Figure 22.4. It is now well established that iron chelation therapy reduces the risk of death and improves patient survival during more than four decades of clinical experience with the current reference standard chelator, desferrioxamine (DFO). DFO is a hexadentate chelator (as we saw in Chapter 2). However, it is not active by oral

function is to restore homeostasis by interacting with a specific target/receptor. (b,c) Homeostatic regulation of glucose and iron metabolism. (d,e) Disruption of homeostasis: diabetes and haemochromatosis. (d) Defective insulin production (caused by immune-mediated or secondary destruction of pancreatic beta cells or genetic defects that impair glucose sensing or insulin synthesis) or reduced insulin sensitivity can cause unchecked increases in blood glucose levels and diabetes. (e) Similarly, defective hepcidin synthesis (caused by a massive loss of hepatocytes or genetic and acquired factors that impair iron sensing or hepcidin synthesis) or reduced hepcidin sensitivity can lead to progressive increases in serum iron levels and haemochromatosis. (From Pietrangelo, 2007. Copyright 2007 with permission from Wiley-Blackwell.)

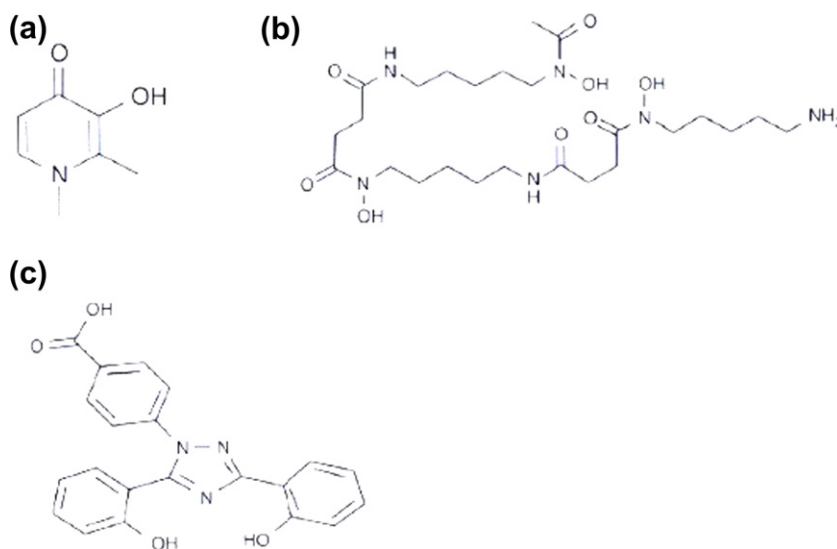


FIGURE 22.4 The iron chelators currently in clinical use.

administration and its effectiveness is further limited by its short half-life (20–30 min). This means that DFO must be administered by slow subcutaneous infusion, using a battery-operated pump over an 8–12 h period, five to seven times per week, at a standard dose of 40 mg/kg/day. This demanding therapeutic regime leads to poor patient compliance and a large number of patients fail to get the full benefits of therapy and die prematurely. The orally active 3-hydroxypyrid-4-one bidentate chelator deferiprone is administered at 75 mg/kg/day fractionated in three doses. Since its half-life is three to four hours, like DFO, it cannot give 24-hour chelation coverage, and levels of the toxic labile plasma iron (LPI) have been shown to rebound between doses. Deferasirox (ICL670) is a once daily, oral iron chelator approved for the treatment of transfusional iron overload in adult and pediatric patients. It can assure continuous 24-hour chelation coverage at comparable therapeutic doses to DFO, thereby eliminating the problems of LPI toxicity, making it in principle the ideal drug. The clinical development of deferasirox represents an investment, the magnitude of which has no precedent in the history of chelator research. Deferasirox has considerable similarities with a tridentate chelator, desferrithiocin, which had been shown to be both orally active and very effective in mobilizing liver iron from an iron-loaded rat model (Longueville & Crichton, 1986; Nick et al., 2003). However, the compound proved to be toxic in animals. Then, in the search for a safe tridentate chelator, the bis hydroxyphenyltriazoles, a completely new chemical class of iron chelators, and more than 40 derivatives were evaluated, together with more than 700 chelators from various other chemical classes, from which ICL670 emerged as the most promising compound, combining oral effectiveness with low toxicity (Nick et al., 2003).

METAL-BASED DRUGS

Despite their prominent place in many biological processes, metal-based drugs are not as extensively developed by the pharmaceutical industry as are purely organic compounds. There have been some notable exceptions — historically salvarsan, an arsenic-based drug, developed by Paul Ehrlich in 1910, has been used against syphilis, bismuth compounds as antiulcer drugs, lithium was used for the treatment of bipolar disorder as early as the 1880s, gold in the treatment of gold complexes (see auranofin, Chapter 1) against arthritis, and perhaps the best known of all are platinum compounds against cancer. In what follows we will outline briefly the drugs based on Pt, Li, Au,

and V, with a brief digression into the important application of paramagnetic metal complexes for magnetic resonance imaging.

Cisplatin, an Anticancer Drug

Cisplatin, $cis\text{-}[\text{PtCl}_2(\text{NH}_3)_2]$, is extensively used for the treatment of testicular and ovarian cancers and increasingly against other types of solid tumours (head/neck, lung, cervical, and bladder), and gives a greater than 90% cure rate in the case of testicular cancer. It was first synthesised by Peyrone in 1845 (known as Peyrone's salt), and its structure was elucidated by Alfred Werner⁴ in 1893. In the 1960s, it was rediscovered serendipitously⁵ when Rosenberg *et al.* investigated the effects of electric fields on bacterial growth. In the presence of NH_4Cl , Pt electrodes and sunlight, *E. coli* cultures grew up to 300 times their normal length but the cells failed to divide. They found that the electric field was not responsible for the arrest of cell division, but that small amounts of certain platinum compounds formed during the electrolysis were responsible. Reasoning that if it inhibited cell division it might be effective as an anticancer drug, they then found that whereas the *trans* isomer was extremely toxic, the *cis* isomer (Figure 22.5) was active against several forms of cancer, although it too had severe side

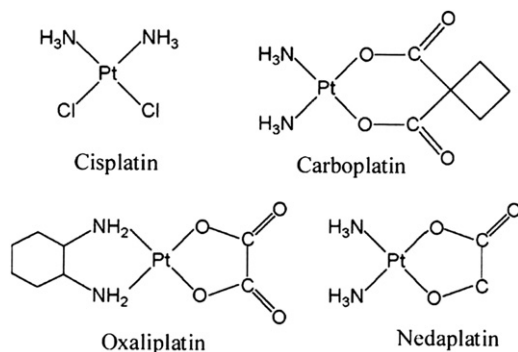


FIGURE 22.5 Platinum complexes currently in clinical use.

effects. Its applicability is still limited to a narrow range of tumours, and some tumours have natural resistance to the drug, or develop resistance after treatment. Drug resistance can occur in several ways: increased drug efflux, drug inactivation, alterations in drug target, processing of drug-induced damage, and evasion of apoptosis. Because of its side effects, limited solubility in aqueous solutions, and intravenous mode of administration, a search for more effective and less toxic analogues has been initiated. Only a few of the thousands of platinum complexes which have been evaluated have achieved routine clinical use. In addition to cisplatin, they include carboplatin, oxaliplatin, and nedaplatin, the latter only approved as an anticancer agent in Japan (Figure 22.5). They all have at least one N–H group, which is responsible for important hydrogen-bond donor properties.

The mechanism of action of cisplatin is relatively well understood. The drug enters cells by passive diffusion, but also by an active transport mechanism. Ctr1, the major copper influx transporter, described in Chapter 8, has

4. Alfred Werner received the Nobel prize in chemistry in 1913 for his research into the structure of coordination compounds.

5. Horace Walpole wrote to his friend Horace Mann in January 28, 1754: "I once read a silly fairy tale, called 'The Three Princes of Serendip' : as their highnesses traveled, they were always making discoveries by accident, and sagacity, of things they were not in quest of: for instance, one of them discovered that a mule blind of the right eye had traveled the same road lately, because the grass was eaten only on the left side, where it was worse than on the right — now do you understand 'serendipity'?" For Walter Gratzer (a regular contributor for many years to *Nature*) serendipity is not that when you drop your buttered toast on the floor that it falls, as it invariably does, buttered side down, but that when you pick it up you discover the contact lens that you lost a few days earlier.

been convincingly demonstrated to transport cisplatin and its analogues, carboplatin, and oxaliplatin. Evidence also suggests that the two copper efflux transporters ATP7A and ATP7B regulate the efflux of cisplatin. The precise role that copper transport proteins play in mediating cisplatin resistance remains enigmatic. The concentration of chloride ions in blood and extracellular body fluids is 100 mM, which is high enough to suppress cisplatin hydrolysis. Once inside the cell, the concentration of chloride ions is much lower (4 mM), resulting in the hydrolysis of the drug to form the mono-aqua $[\text{PtCl}(\text{H}_2\text{O})(\text{NH}_3)_2]^+$ cation, and more slowly the di-aquo $[\text{Pt}(\text{H}_2\text{O})_2(\text{NH}_3)_2]^{2+}$ (Figure 22.6). These positively charged species then cross the nuclear membrane and bind to

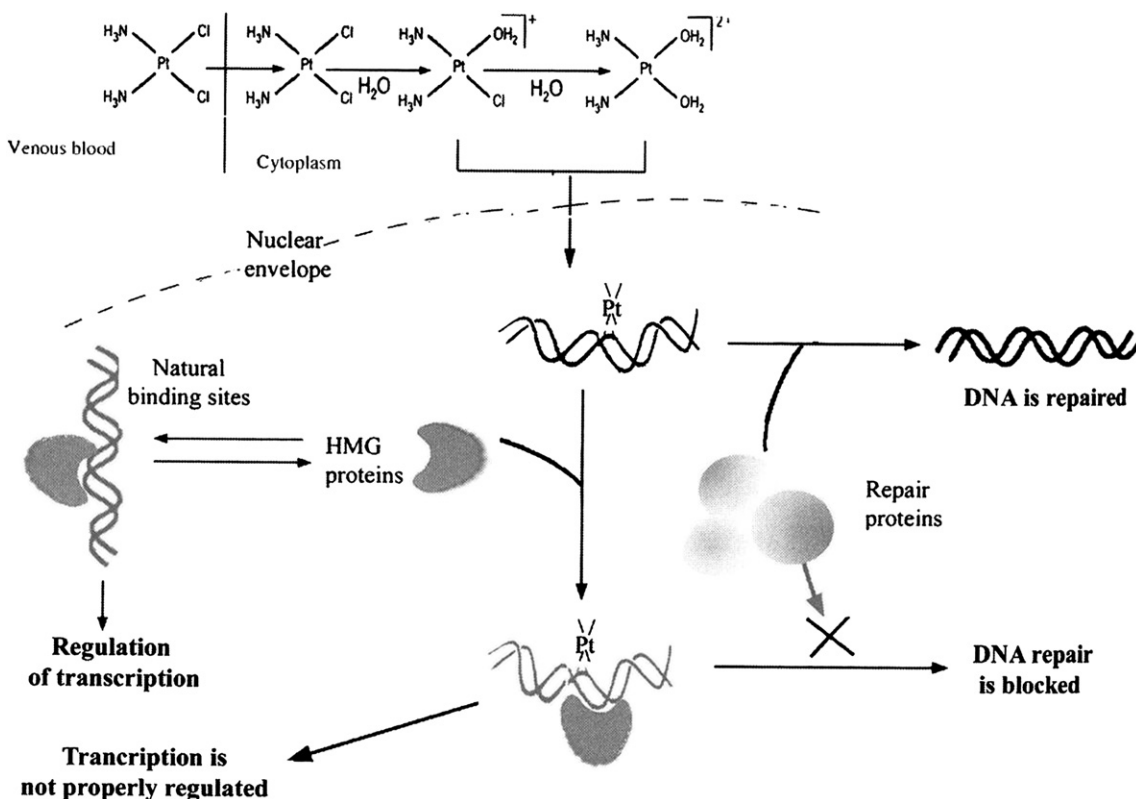


FIGURE 22.6 Mechanism of the anti-tumour activity of cisplatin. (From Brabec & Kasparkova, 2005.)

DNA, although they can also bind to RNA and to sulfhydryl groups in proteins. Bifunctional cisplatin binds to DNA, first forming monofunctional adducts, preferentially at guanine residues, which subsequently form major intrastrand cross-links between adjacent purine residues. In all adducts, the cisplatin is coordinated to the N7 atom of the purine. These cross-links inhibit DNA replication, block transcription, and ultimately trigger programmed cell death (apoptosis). The success of cisplatin in cancer chemotherapy derives from its ability to cross-link DNA and alter the structure. Most cisplatin–DNA adducts are intrastrand d(GpG) and d(ApG) cross-links, which unwind and bend the duplex to facilitate the binding of proteins that contain one or more high-mobility group (HMG) domains. When HMG-domain proteins bind cisplatin intrastrand cross-links, they are diverted away from their natural binding sites on the DNA and shield the adducts from excision repair. This sensitises the cells to cisplatin and contributes to its cytotoxicity. The X-ray structure of the adduct of Pt(II) with the single-stranded

deoxytrinucleotide $\text{cis-[Pt(NH}_3)_2(\text{d(CpGpG)})]$ is shown in Figure 22.7. Figure 22.8 presents the X-ray structure at 2.6-Å resolution of a double-stranded DNA dodecamer containing this adduct.

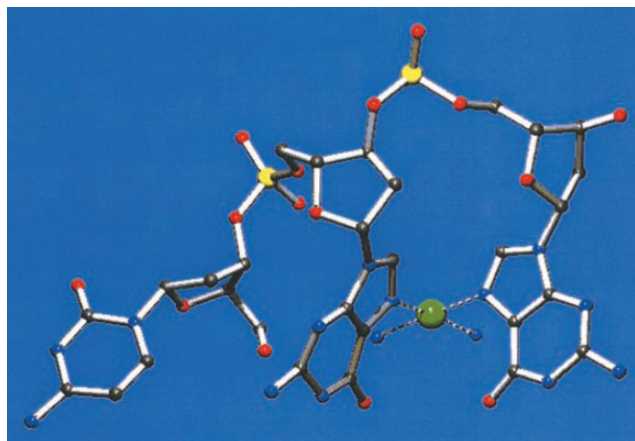


FIGURE 22.7 X-Ray structure of d(CGG) chelated to a cisplatin unit. (From Reedijk, 2003. Copyright 2003 with permission from US National Academy of Sciences.)

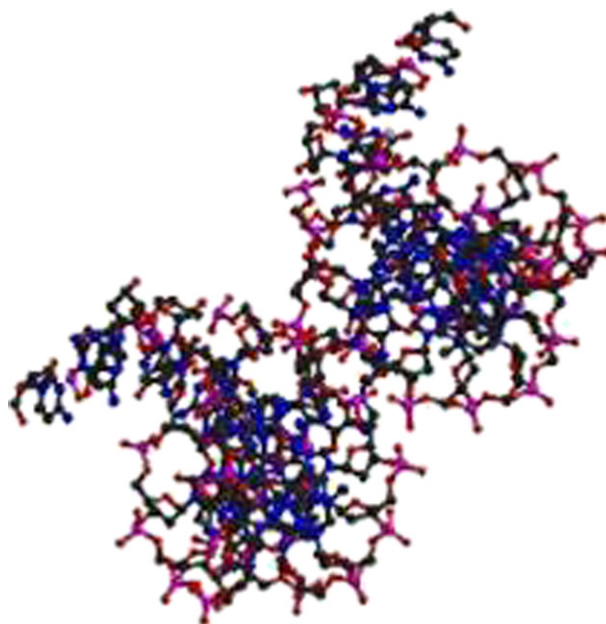


FIGURE 22.8 X-Ray structure showing the kinking of DNA by cisplatin (PDB1AIO).

It seems to be generally accepted that the anti-tumour activity of cisplatin is mediated by the recognition of the platinated adducts by cellular proteins. In particular, HMG (high-mobility group) proteins, which are believed to play a key role in the regulation of gene expression (transcription), have been found to specifically recognise and bind to cisplatin-modified DNA (Figure 22.6). It has been suggested that HMG proteins play a role in the

mechanism of cisplatin toxicity, either by hijacking the proteins away from their natural binding sites or, alternatively, by protecting the cisplatin adducts from DNA repair mechanisms. A number of other proteins have been found to bind to platinated DNA.

Well in excess of 3000 cisplatin analogues have been synthesised in the search for platinum anticancer drugs with broader spectrum of action against different tumours, fewer side effects and activity against cisplatin-resistant tumours. Attention has focused on compounds which only form monofunctional DNA adducts, on *trans*-platinum complexes, polyplatinum compounds, and platinum (IV) analogues, and the search continues. Statistically, for one new clinically active compound to be discovered, 10,000 new compounds need to be synthesised and screened, so high-throughput methodologies are being developed and the search for new cisplatin analogues continues apace.

Other Metals as Anti cancer Drugs

Because of the severe side effects, the restricted tumour spectrum and the acquired or intrinsic resistance, alternative metal-based anticancer drugs are being actively pursued. Ruthenium compounds containing Ru^{II} or Ru^{III} are considered to be suitable candidates: two ruthenium(III) complexes have entered clinical trials, *trans*-[RuCl₄(DMSO)(Im)]ImH (NAMI-A, where Im = imidazole) and *trans*-[RuCl₄(Ind)₂]IndH (KP1019, where Ind = indazole). This is the ruthenium complex, their structures are presented in Figure 22.9. There are two

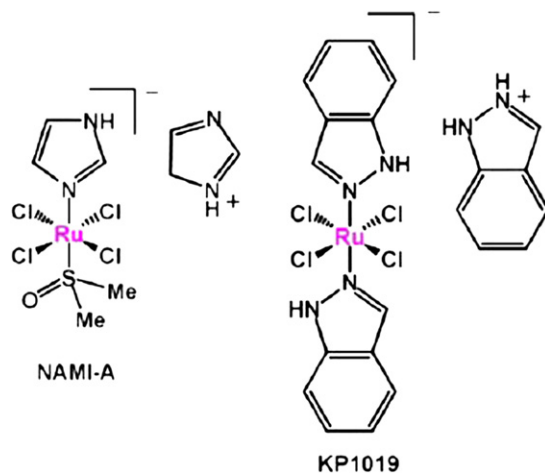


FIGURE 22.9 (a) Structure of NAMI-A. (b) Structure of KP1019.

important differences between KP1019 and most of the Pt-based anticancer drugs; (i) the Ru complexes have octahedral geometry compared to the square-planar Pt(II) drugs and (ii) the Ru complexes can transfer electrons, easily passing from the Ru(II) to Ru(III) form, whereas reduction of Pt(IV) to Pt(II) requires both a change in coordination number and in interatomic bond distance. This may go some way towards explaining why the Ru-based drugs are assumed to have a different mode of action. Another important difference in the mode of action of KP1019 is that it is transported by the serum protein transferrin and its transport into the cell is via the transferrin-cell pathway (see Chapter 7). Since we know that rapidly dividing cells, such as cancer cells, express increased numbers of transferrin receptors, this will effectively target the drug to tumour cells. In addition, the selective activation by reduction in the tumour might contribute to the low side effects observed in *in vivo* studies. These features distinguish it from the established platinum anticancer drugs and suggest that types of cancer which are resistant to Pt drugs might be treatable with this drug.

The anticancer activity of the Pt and Ru drugs described above is attributed to their interaction with DNA to form adducts which cannot be repaired, and therefore interfere with replication and mitosis of the cancer cells. Drugs have also been developed which target cellular signalling pathways which are also over-expressed in cancer cells. Thioredoxin reductase and glutathione reductase are such targets, and phosphole-containing Au(I) complexes are potent nanomolar inhibitors of both enzymes (Figure 22.10(a)). Ga(III) is similar to Fe(III) except that it cannot

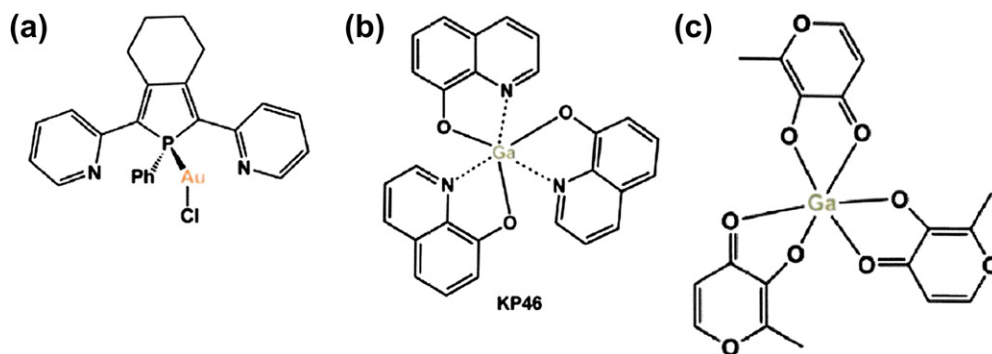


FIGURE 22.10 (a) Gold (I) phosphole complex (b) KP46 (c) Gallium tris-maltolate.

be reduced under physiological conditions, and two Ga(III) compounds, gallium tris-8-quinolinolate (KP46) and gallium tris-maltolate (Figure 22.10(b),(c)), are currently undergoing clinical trials. They are thought to target ribonucleotide reductase, which is of course required to supply deoxyribonucleotides for DNA synthesis. Other potential targets include kinases and cyclooxygenase — the enzyme responsible for the synthesis of the immediate precursor of prostaglandins, prostacyclins and thromboxanes. A Co-alkyne analogue of the anti-inflammatory drug aspirin, itself an inhibitor of cyclooxygenase, is highly active in breast cancer cell lines. Inhibition of cyclooxygenase delays tumour growth and improves response to conventional cancer therapies.

METALLOTHERAPEUTICS WITH LITHIUM

Lithium is the simplest therapeutic agent for the treatment of depression and has been used for over 100 years — lithium carbonate and citrate were described in the British Pharmacopoeia of 1885. Lithium therapy went through periods when it was in common use, and periods when it was discouraged. Finally, in 1949, J.J.F. Cade reported that lithium carbonate could reverse the symptoms of patients with bipolar disorder (manic-depression), a chronic disorder which affects between 1 and 2% of the population. The disease is characterised by episodic periods of elevated or depressed mood, severely reduces the patient's quality of life and dramatically increases their likelihood of committing suicide. Today, it is the standard treatment, often combined with other drugs, for bipolar disorder and is prescribed in over 50% of bipolar disorder patients. It has clearly been shown to reduce the risk of suicide in mood disorder patients, and its socioeconomic impact is considerable.

The molecular basis of mood disorder diseases and their relationship to the effects of lithium remain unknown. How does lithium function? To begin with, we should note that although the hydration shell of Li^+ is similar in size to Na^+ , its ionic radius is much closer to that of Mg^{2+} . This led to the suggestion that lithium ions might exert their action by competing with Mg^{2+} for binding sites on proteins. As we saw in Chapter 10, there are a great many magnesium-dependent enzymes involved in metabolic pathways, not to mention the extensive involvement of Mg^{2+} in nucleic acid biochemistry. It would be difficult to explain the relative specificity of the lithium effect if it interacted with all of these magnesium-binding sites. This suggests that only proteins with rather low affinities for magnesium are targeted by therapeutic concentrations of lithium. As we pointed out in Chapter 1, the

concentration of lithium found in the serum of treated patients is around 1 mM. This is around the concentration of free magnesium within cells.

It is now thought that there are three general targets of lithium in the cell, all involving signal transduction pathways (Figure 22.11). The first of these are the membrane receptors (R_s and R_i), coupled to G proteins (G_s and G_i),

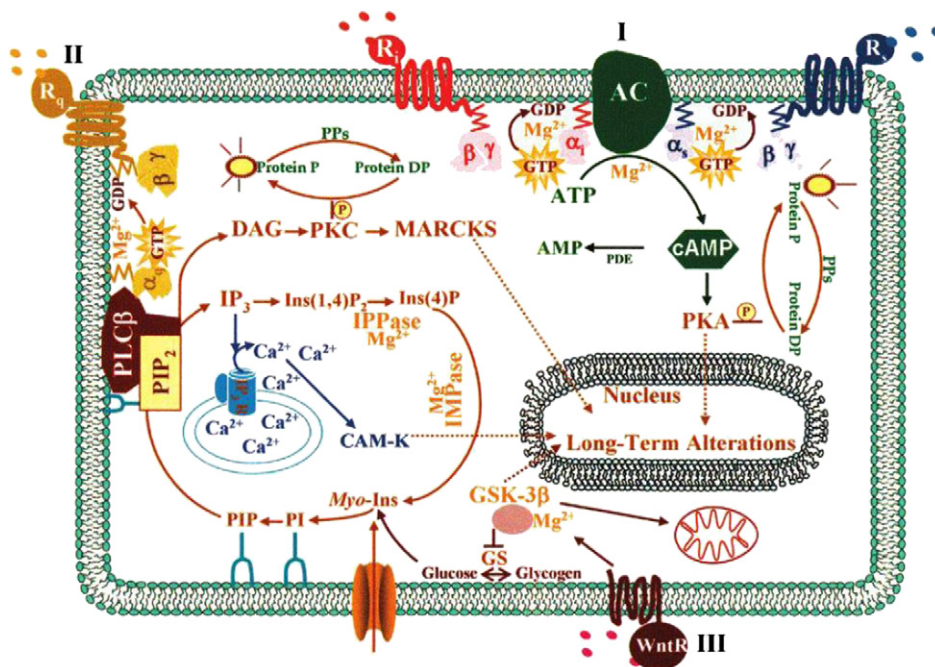


FIGURE 22.11 Adenylyl cyclase (AC), inositol phosphatases (IMPase and IPPase), guanine nucleotide-binding (G) proteins comprised of α , β , and γ subunits, and glycogen synthase kinase-3 β (GSK-3 β) are the main targets for Li^+ action. (From Mota de Freitas, Castro, & Gerales, 2006. Copyright 2006 with permission from the American Chemical Society.)

which activate or inhibit AC-modulating cyclic AMP (cAMP) production (Figure 22.11.I). This in its turn, regulates protein kinase A (PKA) which is able to phosphorylate many substrate proteins. Protein phosphatases (PPs) convert the phosphoproteins back to the dephospho forms, whereas phosphodiesterase (PDE) degrades cAMP to AMP.

The second well-characterised signal transduction pathway (Figure 22.11.II) which is subject to lithium inhibition is the phosphoinositol cascade (see Chapter 11). Activation of G_q induces phospholipase C (PLC β)-mediated hydrolysis of phosphoinositide-4,5-bisphosphate (PIP₂) to diacylglycerol (DAG) and inositol-1,4,5-trisphosphate (IP₃). DAG activates protein kinase C (PKC), an enzyme that phosphorylates many other proteins, including the myristoylated alanine-rich C kinase substrate (MARCKS). IP₃-induced release of intracellular calcium initiates the activation of calmodulin (CAM) and calmodulin-dependent protein kinase (CAM-K). IP₃ is recycled back to PIP₂ via steps catalysed by IPPase and IMPase. It is thought that a number of enzymes of this pathway contain a common amino acid sequence which constitutes a lithium-sensitive Mg^{2+} -binding site, and it has been proposed that lithium exerts some of its effect by affecting phosphoinositol metabolism in as yet uncertain manner.

Binding of the wingless signal to its receptor (WntR) regulates GSK-3 β , which affects cytoskeletal proteins and glycogen synthase (GS) activity (Figure 22.11.III), and this represents the third pathway. GSK-3 is abundant in brain, where it is involved in signal transduction cascades. The phosphorylation of target protein

serine and threonine residues results in the regulation of the cytoskeleton, gene expression via a number of transcription factors, apoptosis, and glycogen synthesis activity. Lithium is a potent and selective inhibitor of the enzyme through competition for Mg^{2+} binding. This inhibition, with its plethora of potential consequences for cellular signalling, may explain to some extent the neuroprotective effects of lithium therapy in bipolar disorders. There are known to be a number of indirect interactions between GSK-3 and phosphoinositide signalling, but clearly much more remains to be uncovered before the mode of action of lithium in the brain is fully understood.

CONTRAST AGENTS FOR MAGNETIC RESONANCE IMAGING (MRI)

While many, often spectacular, advances have been made in our understanding of a great number of diseases at the molecular level, the development of molecular imaging, which allows *in vivo* visualisation of molecular events at the cellular level, is having a revolutionary role in medical diagnosis. Magnetic resonance imaging (MRI) is an important tool for the diagnosis of disease and a noninvasive method of acquiring three-dimensional images of human soft tissue (unlike X-rays which can locate the electron-dense hard tissue, like bone). MRI scanners generate multiple two-dimensional cross-sections (slices) of tissue and three-dimensional reconstructions. MRI utilises the same longer-wavelength radio waves, which are used in nuclear magnetic resonance (NMR) spectroscopy. The samples (or patients) are placed in a powerful magnetic field and exposed to radio-frequency pulses and the relaxation times of excited nuclei (typically protons from water in the tissue) are detected. The contrast in an MRI image is the result of the interplay of numerous factors including the proton density of the tissues being imaged, the relative relaxation times T_1 (spin–lattice relaxation) and T_2 (spin–spin relaxation), and the instrumental parameters. For reviews see [Dzik-Jurasz, 2003](#) and [Terreno, Castelli, Viale, and Aime \(2010\)](#).

The diagnostic power of the technique is illustrated by the MRI scans of patients with two different neurological conditions. [Figure 22.12\(a\)](#) shows the characteristic “eye of the tiger” sign observed in patients with

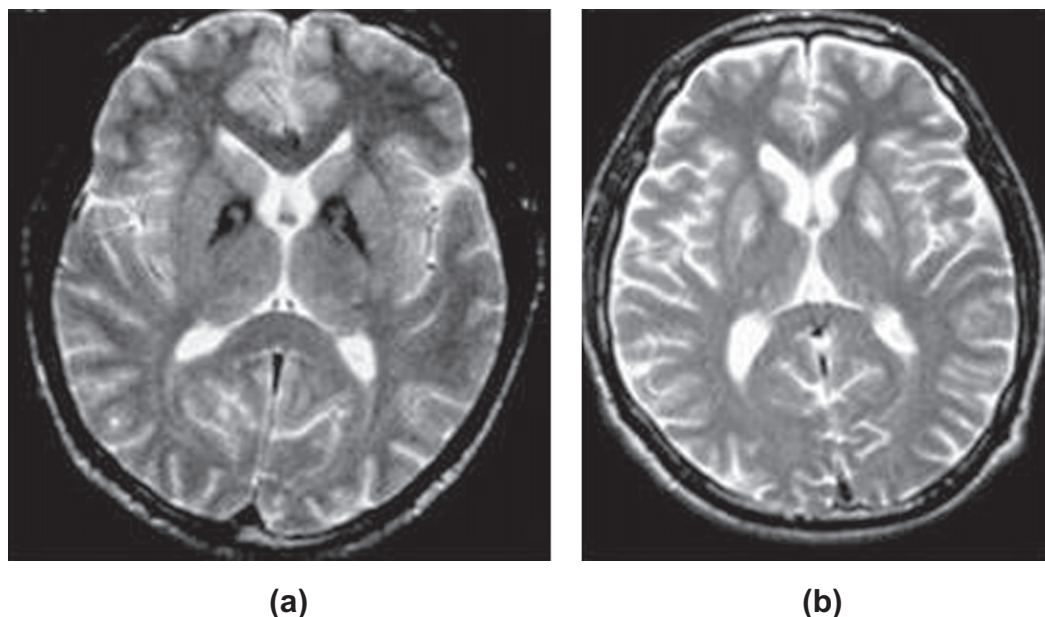


FIGURE 22.12 MRI scans of the brain of a patient with (a) Hallervorden–Spatz syndrome and (b) neuroferritinopathy. (From Crichton & Ward, 2006. Copyright 2006 with permission from John Wiley and Sons.)

Hallervorden–Spatz syndrome (due to a mutation in the gene encoding pantothenate kinase 2). The MRI picture is a T_2 -weighted image which shows diffuse bilateral low signal intensity of the globus pallidus (due to iron deposition) with a region of hyperintensity in the internal segment (the high signal is thought to represent tissue oedema). Neuroferritinopathy is another neurological disorder, in which the insertion of an adenine residue in the gene for the ferritin light chain results in an altered carboxy terminal sequence of the protein. The T_2 -weighted MRI image in Figure 22.12(b) is quite characteristic, with symmetrical degeneration of the globus pallidus and putamen and low signal intensity in the internal capsule.

The use of MRI allows accurate, noninvasive diagnosis of many pathological conditions. However, the use of contrast agents, often in the form of paramagnetic metallochelates, makes the method even more sensitive and the diagnosis more specific. MRI contrast agents are not directly visualised in the resulting image, only their effects are observed. They enhance image contrast as a result of their influence on the relaxation times of nearby water protons, and as a consequence on the NMR signal. Paramagnetic molecules, because of their unpaired electrons, are potent MRI contrast agents, decreasing the T_1 and T_2 relaxation times of nearby proton spins, and enhancing the signal observed. The most extensively studied paramagnetic metal ions are transition metal ions (high-spin Mn(II) and Fe(III), each with five unpaired electrons) and lanthanides (often Gd(III) with its seven unpaired electrons). Since free metal ions are toxic to biological systems they have to be administered in a nontoxic form bound to suitable ligands or chelates. The first contrast agent to be approved for clinical use, Gd-DTPA, which we encountered in Chapter 1, was introduced in the 1980s as a contrast agent for obtaining MR images in humans, and

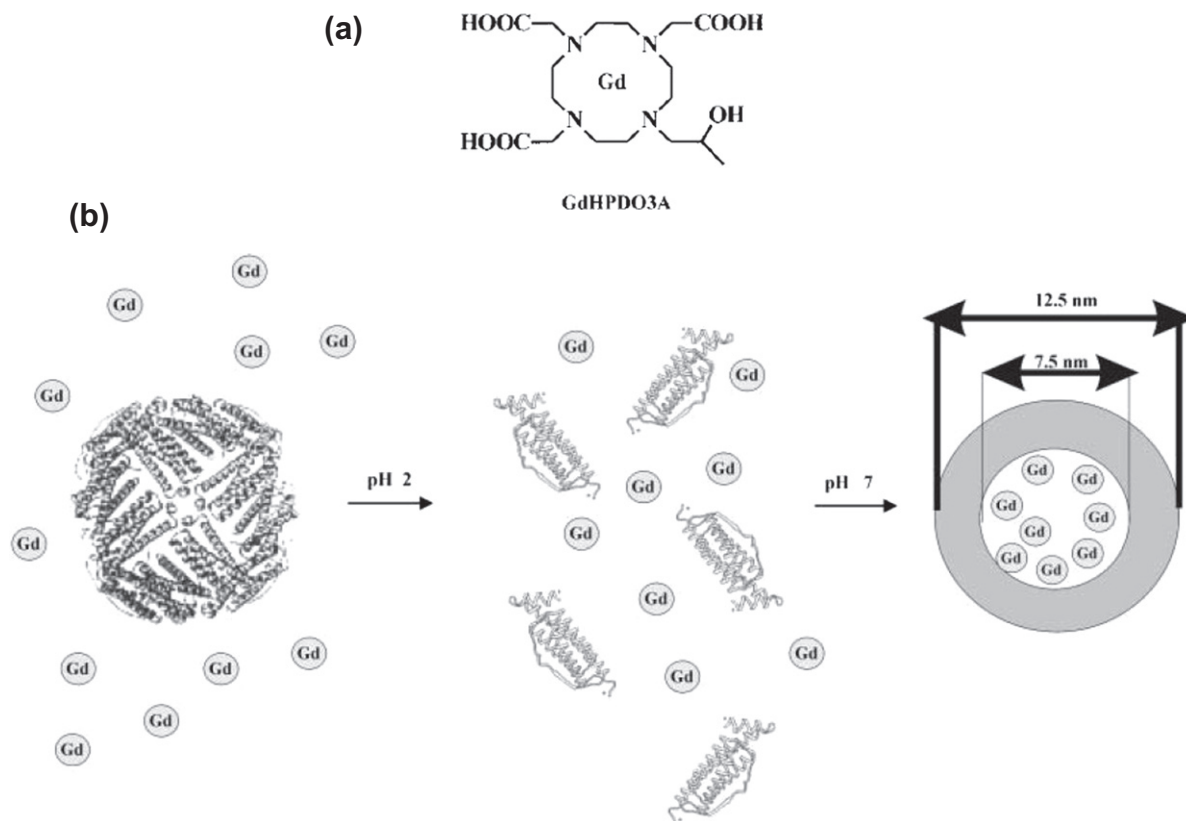


FIGURE 22.13 (a) Structure of Gd-HPDO3A. (b) Schematic representation of the dissociation of apo-ferritin into subunits at pH 2, followed by its reforming at pH 7. In this way the solution components are trapped within its interior. (From Aime, Frullano, & Geninatti Crich, 2002. Copyright 2002 with permission from John Wiley and Sons.)

rapidly became the most extensively used system in the clinic. Gd-DTPA has been administered to more than twenty million patients over a period of 10 years of clinical use. It is a very stable complex which distributes in the blood and in the extravascular regions yet, thanks to its high hydrophilicity, is excreted by the kidneys on the time scale of a few hours. In MR images, Gd-DTPA allows an excellent delineation of tumours.

A major challenge for MRI when the biological targets are present at very low concentrations is to achieve the highest attainable sensitivity. One way to optimize the relaxivity is to use nanoscaffolds, such as dendrimers, proteins, micelles, carbon-based nanosystems and metal-based nanoparticles. Two interesting examples involve apoferritin, the use of which as a supramolecular template in nanotechnology was already discussed in Chapter 19. A remarkably high relaxation enhancement (20-fold) of water protons has been observed for solutions containing apoferritin loaded with Gd-HPDO3A (Figure 22.13). The entrapment of the complex within apoferritin allows an increased number of dipolar interactions with water molecules and exchangeable protons in the protein cavity as carrier for Gd(III) agents. This gadolinium-loaded ferritin can be targeted to tumour cells for use as a contrast agent (Figure 22.14). The imaging procedure consisted of (a) targeting neural cell adhesion molecules with a biotinylated

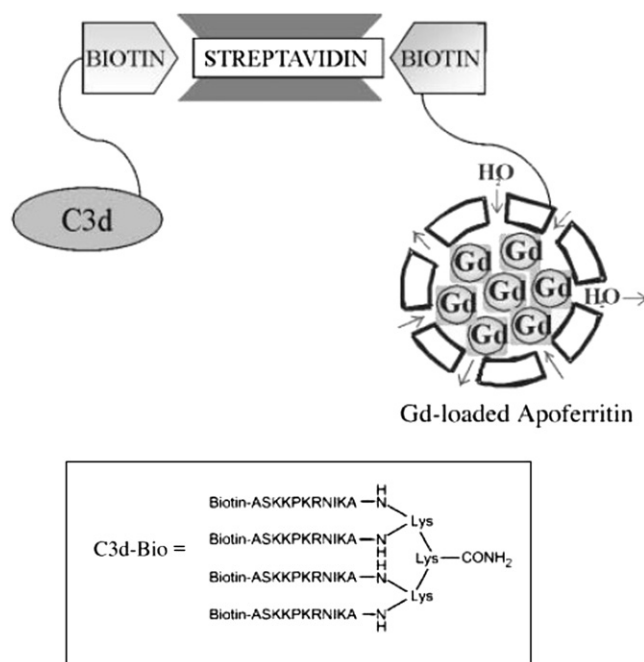


FIGURE 22.14 Schematic representation of the adduct formed by C3d-Bio, streptavidin, and biotinylated Gd-loaded apoferritin (Gd-Apo-Bio). The sequence of the dendrimeric C3d-Bio NCAM mimetic peptide is outlined. (From *Geninatti Crich et al.*, 2006. Copyright 2006 with permission from AACR.)

derivative of C3d peptide, which is known to have high affinity for these epitopes, and (b) delivery of a streptavidin/gadolinium (Gd)-loaded apoferritin 1:1 adduct at the biotinylated target sites. The remarkable relaxation enhancement ability of the Gd-loaded apoferritin system allowed the visualisation of tumour endothelial cells both *in vitro* and *in vivo* when organised in microvessels connected to the mouse vasculature.

Unfortunately, attempts to increase the relaxivity per particle failed, as the preparation method used does not allow the inclusion of more than 8–10 Gd-HPDO3A molecules per apoferritin cavity. The task of internalizing a much greater number of paramagnetic centres inside the apoferritin cavity has been pursued by dissolving the solid β -MnOOH phase that one may create by exposing the protein to a concentrated solution of Mn(II) salts at

basic pH values. The reduction/dissolution processes operated by suitable reducing agents lead to hundreds of Mn^{2+} ions entrapped inside the apoferritin cavity (Figure 22.15). The Mn–apoferritin system shows markedly

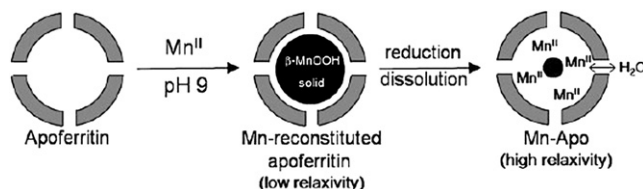


FIGURE 22.15 Mn–Apoferritin preparation. (From Kalman *et al.*, 2010. Copyright 2010 with permission from John Wiley and Sons.)

superior properties as an MRI contrast agent, as its relaxivity per apoferritin particle is almost one order of magnitude higher than that shown by Gd-loaded apoferritin due to accumulation of a large number of manganese ions in its inner cavity.

While the first generation of MRI contrast agents are relatively unspecific, they nonetheless allow the evaluation of physiological parameters such as the status of the blood–brain barrier or renal function. Gd-DTPA-enhanced MRI imaging can assist in the diagnosis and treatment follow-up of many types of cancer. However, in order to improve the diagnostic efficacy of contrast agents, they need to be made target specific so that they accumulate in specific biological locations. Approaches which have been tried include coupling contrast agents to antibodies against membrane receptors, to transferrin in order to image tumour cells, which overexpress the transferrin receptor, or to annexin V, a protein which binds to phosphatidylserine, as a marker of apoptosis. Phosphatidylserine moves from the interior to the exterior of cell membranes when a cell undergoes apoptosis. Several “smart” sensor probes have been designed which are activated only in the presence of their intended target. As one example, a gadolinium-based smart contrast agent has been developed to demonstrate gene transfection (Figure 22.16). When the enzyme β -galactosidase is expressed in

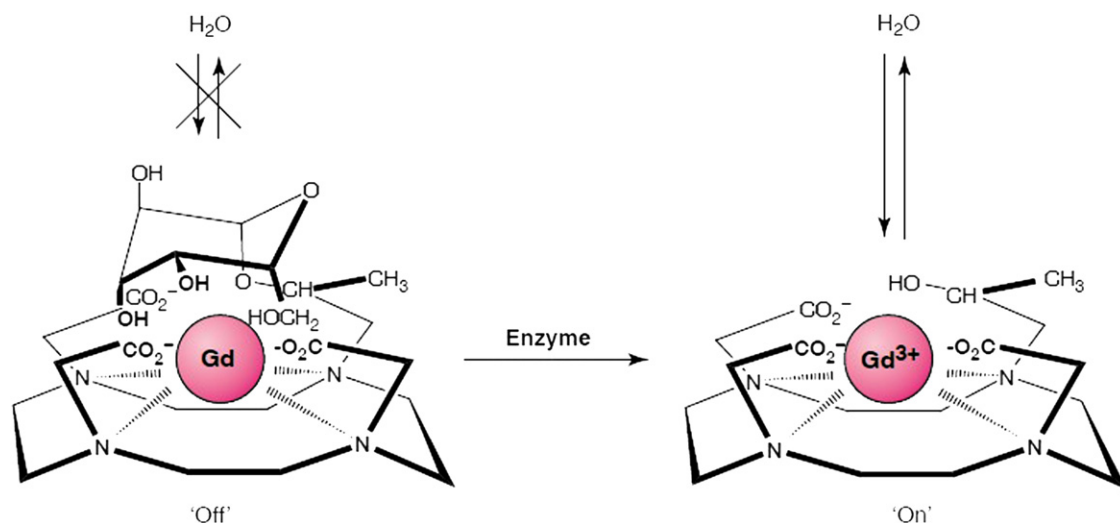


FIGURE 22.16 Enzyme-activated MR contrast agent. Schematic of the transition of methyl substituted Egad (EgadMe) from a weak to a strong relaxivity state. This diagram represents the site-specific placement of the galactopyranosyl ring on the tetraazamacro-cycle (side view). Upon cleavage of the sugar residue by β -galactosidase, an inner sphere coordination site of the Gd^{3+} ion becomes more accessible to water. (From Meade, Taylor, & Bull, 2003. Copyright 2003 with permission from Elsevier.)

engineered cells, the β -galactose ring protecting the Gd^{3+} is cleaved, allowing bulk water access to the paramagnetic gadolinium ion. As we saw in Chapter 11, changes in intracellular Ca^{2+} are important in cell signalling. A gadolinium-based contrast agent capable of specifically detecting Ca^{2+} has been designed which has two distinct conformations as a function of Ca^{2+} concentration (Figure 22.17). In the absence of Ca^{2+} , the

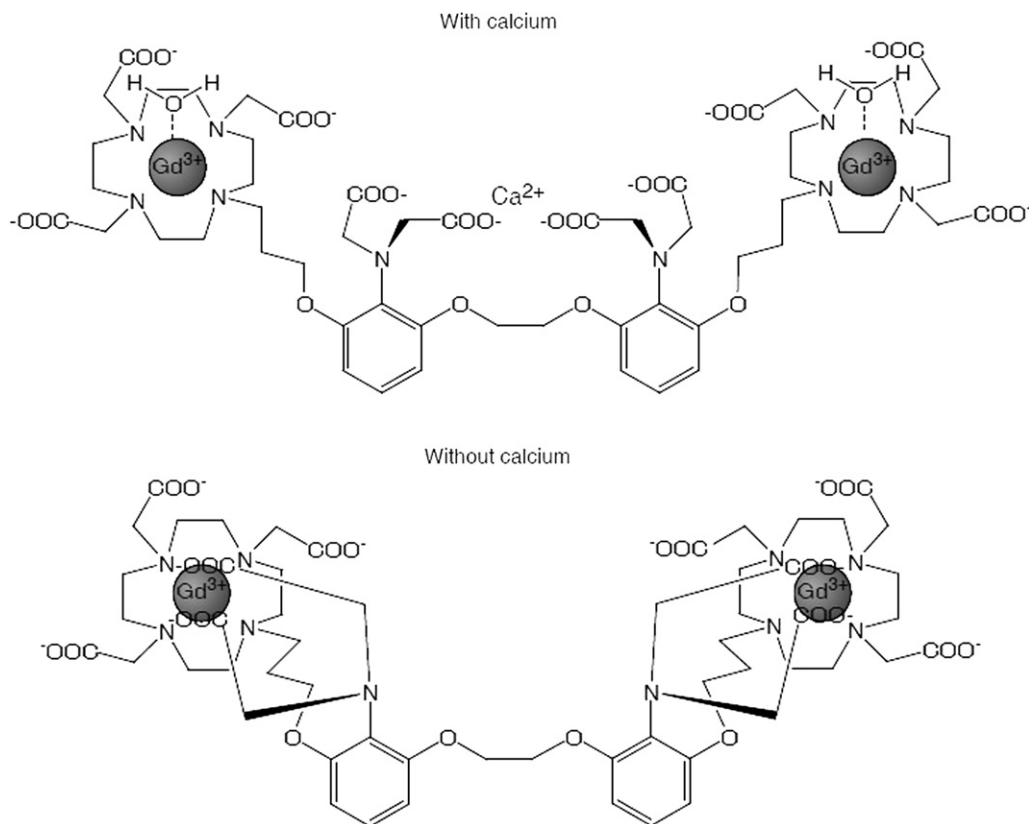


FIGURE 22.17 Calcium-activated MR contrast agent. Proposed conformational change of a Ca^{2+} -activated MR contrast agent. The addition of calcium induces a conformational shift allowing water access to Gd^{3+} , and a change in observed relaxivity. (From Meade *et al.*, 2003. Copyright 2003 with permission from Elsevier.)

aromatic iminoacetates of the ligand interact with the two Gd^{3+} ions. In the presence of Ca^{2+} , the iminoacetates rearrange to bind Ca^{2+} , thereby allowing water to bind directly to Gd^{3+} . This shortens the relaxation time of water protons and results in signal enhancement on T_1 imaging. It should be pointed out that most of the “smart” contrast agents to date have been tested in animal or cellular models, but have not made the ultimate step to clinical applications.

REFERENCES

- Aime, S., Frullano, L., & Geninatti Crich, S. (2002). Compartmentalization of a gadolinium complex in the apoferritin cavity: a route to obtain high relaxivity contrast agents for magnetic resonance imaging. *Angewandte Chemie International Edition*, 41, 1017–1019.
- Andrews, N. C. (2008). Forging a field: the golden age of iron biology. *Blood*, 112, 219–230.
- Brabec, V., & Kasparkova, J. (2005). Platinum-based drugs. In M. Gielen & E. R. Tiekink (Eds.), *Metallo-therapeutic drugs and metal-based diagnostic agents. The use of metals in medicine* (pp. 489–506). Chichester: John Wiley and Sons.

- Crichton, R. R., & Ward, R. J. (2006). *Metal based neurodegeneration: From Molecular Mechanisms to Therapeutic Strategies*. Chichester: John Wiley & Sons. p. 227.
- Dzik-Jurasz, A. S. K. (2003). Molecular imaging *in vivo*: an introduction. *British Journal of Radiology*, 76, S98–S109.
- Geninatti Crich, S., Bussolati, B., Tei, L., Grange, C., Esposito, G., Lanzardo, S., et al. (2006). Magnetic resonance visualization of tumor angiogenesis by targeting neural cell adhesion molecules with the highly sensitive gadolinium-loaded apoferritin probe. *Cancer Research*, 66, 9196–9201.
- Gielen, M., & Tiekink, E. R. (2005). *Metallotherapeutic drugs and metal-based diagnostic agents. The use of metals in medicine*. Chichester: John Wiley and Sons. pp. 598.
- Harterting, C. G., Zorbas-Seifried, S., Jakupiec, M. A., Kynast, B., Zorbas, H., & Keppler, B. K. (2006). From bench to bedside—preclinical and early clinical development of the anticancer agent indazolium trans-[tetrachlorobis(1H-indazole)ruthenate(III)] (KP1019 or FFC14A). *Journal of Inorganic Biochemistry*, 100, 891–904.
- Hershko, C. (2006). Oral iron chelators: new opportunities and new dilemmas. *Haematologica*, 91, 1307–1312.
- Kálmán, F. K., Geninatti-Crich, S., & Aime, S. (2010). Reduction/dissolution of a beta-MnOOH nanophase in the ferritin cavity to yield a highly sensitive, biologically compatible magnetic resonance imaging agent. *Angew Chem Int Ed Engl.*, 49, 612–615.
- Longueville, A., & Crichton, R. R. (1986). An animal model of iron overload and its application to study hepatic ferritin iron mobilization by chelators. *Biochemical Pharmacology*, 35, 3669–3678.
- McCance, R. A., & Widdowson, E. M. (1937). Absorption and excretion of iron. *Lancet*, II, 680–684.
- Meade, T. J., Taylor, A. K., & Bull, S. R. (2003). New magnetic resonance contrast agents as biochemical reporters. *Current Opinion in Neurobiology*, 13, 597–602.
- Mota de Freitas, D., Castro, M. M., & Geraldles, C. F. (2006). Is competition between Li^+ and Mg^{2+} the underlying theme in the proposed mechanisms for the pharmacological action of lithium salts in bipolar disorder? *Accounts of Chemical Research*, 39, 283–291.
- Nick, H., Acklin, P., Lattmann, R., Buehlmayr, P., Hauffe, S., Schupp, J., et al. (2003). Development of tridentate iron chelators: from desferriethiocin to ICL670. *Current Medicinal Chemistry*, 10, 1065–1076.
- Pietrangelo, A. (2007). Hemochromatosis: an endocrine liver disease. *Hepatology*, 46, 1291–1301.
- Reedijk, J. (2003). New clues for platinum antitumor chemistry: kinetically controlled meta binding to DNA. *Proceedings of the National Academy of Sciences of the United States of America*, 100, 3611–3616.
- Schmidt, P. J., Toran, P. T., Giannetti, A. M., Bjorkman, P. J., & Andrews, N. C. (2008). The transferrin receptor modulates Hfe-dependent regulation of hepcidin expression. *Cell Metabolism*, 7, 205–214.
- Sigel, A., & Sigel, H. (2004). Metal ions and their complexes in medication. *Metal Ions in Biological Systems*, 41, 519.
- Terreno, E., Castelli, D. D., Viale, A., & Aime, S. (2010). Challenges for molecular magnetic resonance imaging. *Chemical Reviews*, 110, 3019–3042.
- van Rijt, S. H., & Sadler, P. J. (2009). Current applications and future potential for bioinorganic chemistry in the development of anticancer drugs. *Drug Discovery Today*, 14, 1089–1097.
- WHO (2004). Assessing the iron status of populations. Report of a joint World Health Organisation/Centers for Disease Control and Prevention technical consultation.

Metals in the Environment

Introduction Environmental Pollution and Heavy Metals	433
Aluminium	434
Cadmium	435
Mercury	439
Lead	440
Metals as Poisons	443

INTRODUCTION ENVIRONMENTAL POLLUTION AND HEAVY METALS

We have already seen in earlier chapters that even essential metal ions can be toxic — as the historical father of toxicology, Paracelsus (1493–1541), wrote

“Alle Ding’ sind Gift, und nichts ohn’ Gift; allein die Dosis macht, daß ein Ding kein Gift ist.”

“Everything is poisonous, and nothing is not; only the dose ensures that something is not poisonous.”

This dictum that “The dose makes the poison” is as true today as when it was stated five centuries ago. But it is also applicable to a number of metals which we encounter in our constantly evolving environment, many of which have no biological ‘raison d’être’¹. These include a number of toxic metals which we have introduced into our environment in the course of the industrialisation of our society. Over the past decades, there has been an increasing awareness throughout the world of the health and developmental risks associated with environmental exposure to “heavy metals”², such as lead (Pb), mercury (Hg), and cadmium (Cd). This term has been widely used, often to describe a group of metals and metalloids that have been associated with contamination and potential toxicity or ecotoxicity. At the same time, legal regulations often specify a list of “heavy metals” to which they apply. Such lists differ from one set of regulations to another and the term is sometimes used without even specifying which “heavy metals” are covered. However, there is no authoritative definition to be found in the relevant literature. And while we could agree that all of those mentioned above fall into the category of heavy metals that have been released into the environment by the activity of man, where do we place aluminium, the insidious pollution of which has crept upon us notably as a consequence of acid rain, as we pointed out in Chapter 1.

In what follows, we pass in review aluminium, cadmium, mercury, lead, and chromium toxicity before turning briefly to metals as poisons.

1. Sorry, I of course mean ‘reason to exist’.

2. Perhaps Humpty Dumpty’s definition in “Alice through the looking glass” by Lewis Carrol fits the bill: “*When I use a word, it means just what I choose it to mean — neither more nor less!*”.

ALUMINIUM

Aluminium comprises 8% of the earth's crust; it is the most abundant metal and the third most abundant element after oxygen and silicon. It only occurs naturally in a combined form — as an oxide in bauxite and in complex aluminosilicates (like sands) such as micas and feldspar. Although aluminium has been known to be a toxic metal, it does not usually cause adverse effects on the health of the general population. Biology has managed to avoid using aluminium, despite its natural abundance, although we are not quite sure how it has done so. Despite its abundance in the earth's crust, aluminium concentration in the oceans is less than 40 nM, possibly reflecting the accumulation of aluminium and silicon by diatoms. Until recently, most natural waters contained insignificant amounts of aluminium: any free Al^{3+} usually disappeared into sediment as the insoluble hydroxide.

However, one of the principal consequences of burning fossil fuels has been to generate 'acid rain' which results in the massive acidification of fresh water sources. 'Acid rain' is a broad term referring to a mixture of wet and dry deposited material from the atmosphere containing higher than normal amounts of nitric and sulfuric acids. The precursors of acid rain formation, primarily emissions of sulfur dioxide and nitrogen oxides, are produced by natural sources, such as volcanoes and decaying vegetation, but their recent increases come from man-made sources as a result of fossil fuel combustion. This causes the release of metal ions like aluminium, mercury, and lead from mineral deposits in the soil, leading to aluminium concentrations in fresh water lakes at pH <6 up to μM levels, with disastrous consequences for the plants and animals which come into direct contact with the element (particularly fish, for whom concentrations as low as 5 μM are toxic). In some areas of Europe, like the forests on the mountain slopes of Szklaska Poreba, on the Polish border close to the Czech Republic and Germany, the soil pH values reached less than 3, with disastrous effects on the tree population. There are exceptions, such as the tea plant, which has an extraordinary propensity for accumulating aluminium from acid soils (as much as 3% is found in older leaves). An average tea infusion contains about fifty times as much aluminium as does an infusion of coffee. Tobacco also contains a considerable amount of aluminium, ~500 to 2000 μg /cigarette, although only <0.02 to ~0.075 μg are in the smoke from one cigarette. Another of the effects of acid rain could have been to change the usual association of aluminium in the soil with silicate (predominant above pH 6.5) for phosphate, rendering aluminium more toxic. The greater concentrations of aluminium in fresh water from the effects of acid rain on soils have made this enigmatic element accessible for the first time to living organisms. Despite this, the uptake of aluminium from drinking water does not appear to pose a significant threat to human health. A much more serious cause of aluminium intoxication is the use of aluminium as a phosphate binder in the dialysis fluids used in patients with renal insufficiency. Because of the large volumes of fluid used, the frequency of haemodialysis and the long term nature of the treatment, even small levels of aluminium may become deleterious with time.

Acid soils, with a pH of 5.5 or lower, significantly limit crop production worldwide: approximately 50% of the world's potentially arable soils are acidic, and the production of staple food crops is particularly affected. Twenty percent of the worldwide production of maize and 13% of rice is on acid soils, while 60% of the acid soils in the world are in the tropics and subtropics. Thus, acid soils limit crop yields in many developing countries, while in developed countries such as the United States, the extensive use of ammonia fertilizers causes further acidification of agricultural soils. The primary limitations of acid soils are toxic levels of aluminium and manganese, and suboptimal levels of phosphorous. Acidification of soils leads to acidification of rivers and streams, increasing the solubility of aluminium, with direct consequences on fish populations, and eventually of water supplies to the general population.

The chemistry of aluminium combines features in common with two other groups of elements, namely (i) divalent magnesium and calcium and (ii) trivalent chromium and iron. The toxic effects of aluminium are more related to its interference with calcium-dependent processes, whereas its access to tissues is probably a function of its similarity to ferric iron. Al^{3+} is a much stronger acid than Mg^{2+} and Ca^{2+} , which makes it a powerful competitor for oxygen donor ligands for these two important biological cations, and leads to profound interference with their metabolism. In contrast, Al^{3+} is a weaker acid than Fe^{3+} and therefore causes less interference with iron

metabolism. It has a preference for oxygen ligands, particularly if they are negatively charged, such as carboxylate, catecholate, and phosphate groups. Sulfhydryl groups do not bind Al^{3+} , and amines do not bind strongly except as part of multidentate ligand systems such as NTA and EDTA. The rate of ligand exchange, into and out of the metal coordination sphere, is extremely slow for Al^{3+} . This means that essential metabolic processes involving rapid Ca^{2+} exchange, which is 10^8 -fold slower for Al^{3+} , would be seriously affected by substitution, as would Mg^{2+} -dependent enzymes (10^5 -fold slower with Al^{3+}).

In the extracellular fluids of mammals, the iron-binding protein transferrin is usually only 30% saturated, so that it has 70% of its metal-binding capacity free. If Al^{3+} could get into the circulation, it could certainly occupy those binding sites. The stability constants for the two binding sites on transferrin are similar, $\log K_a$ of 12.9 and 12.3 (Martin, 1994), substantially lower than for iron.

The daily dietary intake of aluminium in man is 2–3 mg/day, but it will not accumulate in the body if the kidneys are functioning normally. In the gastrointestinal tract, less than 0.5% of an ingested dose of aluminium will be absorbed, while the skin and the lungs have also evolved as barriers to aluminium entry into the body. The problem arises when these natural barriers are bypassed by the intravenous administration of aluminium-containing solutions. An example is the use of aluminium hydroxide to treat the high levels of serum phosphate found in end-stage renal disease. Another source is the administration of intravenous solutions used for parenteral nutrition³ which might contain aluminium. The risks from the latter are particularly important in pre-term infants and patients with kidney failure, and have led to the FDA acting to limit the amount of aluminium in such preparations.

Once in the serum, aluminium can be transported bound to transferrin, but also to albumin and low molecular ligands like citrate. However, the transferrin–aluminium complex will be able to enter cells via the transferrin–transferrin-receptor pathway (Chapter 8). Within the acidic environment of the endosome, we assume that aluminium would be released from transferrin, but how it exits from this compartment remains unknown. Once in the cytosol of the cell, aluminium is unlikely to be readily incorporated into the iron storage protein ferritin, since this requires redox cycling between Fe^{2+} and Fe^{3+} (Chapter 13). Studies of the subcellular distribution of aluminium in various cell lines and animal models have shown that the majority accumulates in the mitochondria where it can interfere with calcium homeostasis. Once in the circulation, there seems little doubt that aluminium can cross the blood–brain barrier.

Aluminium toxicity (Verstraeten et al., 2008) is the likely cause of three human disorders arising from long-term dialysis: bone disease, anaemia, and dementia. The first of these conditions is consistent with interference with calcium deposition into bone, and the accumulation of aluminium in the bone matrix. It is also the likely cause of the high frequency of dementia among the natives of certain regions of South East Asia, where the soils are high in Al(III) and low in Mg^{2+} and Ca^{2+} . Al causes a microcytic anaemia, which is not reversible by iron. Elevated levels of Al(III) have been reported in the brains of Alzheimer's patients and the hypothesis that aluminium might exert its toxic effects by interfering with iron homeostasis has been advanced. However, this remains a subject of considerable controversy. Chronic exposure to aluminium results in selective cognitive impairment in rats, with altered calcium homeostasis. Taken together with the demonstration that aluminium causes dementia in dialysis patients, there can be no doubt that aluminium is neurotoxic. The potential therapeutic benefit of long-term chelation therapy to prevent accumulation of both aluminium and iron in brain as a function of ageing could complement a greater understanding of the role of both metal ions in the aetiology and pathogenesis of many neurological diseases.

CADMIUM

That cadmium is a toxic and hazardous product of our industrialised society, manifested itself among inhabitants of the Jinzu River basin in Toyama Prefecture, Japan, in the 1950s, in the form of Itai–Itai disease. It remains the

3. Parenteral – administration of a substance by any other route than via the gastrointestinal tract, particularly by injection.

most severe example of chronic Cd poisoning caused by prolonged oral Cd ingestion. For the first time, Cd pollution was shown to have severe consequences on human health, particularly in women. The most important effects were softening of the bones and kidney failure. The name of the disease is derived from the painful screams (Japanese: 痛い *itai*) caused by the severe pain in the joints and the spine of the victims. Its cause was found to be due to environmental Cd pollution originating from effluent from a zinc mine located in the upper reaches of the river (Figure 23.1). In the Cd-polluted areas, 50%–70% of the amount of Cd ingested orally was derived from

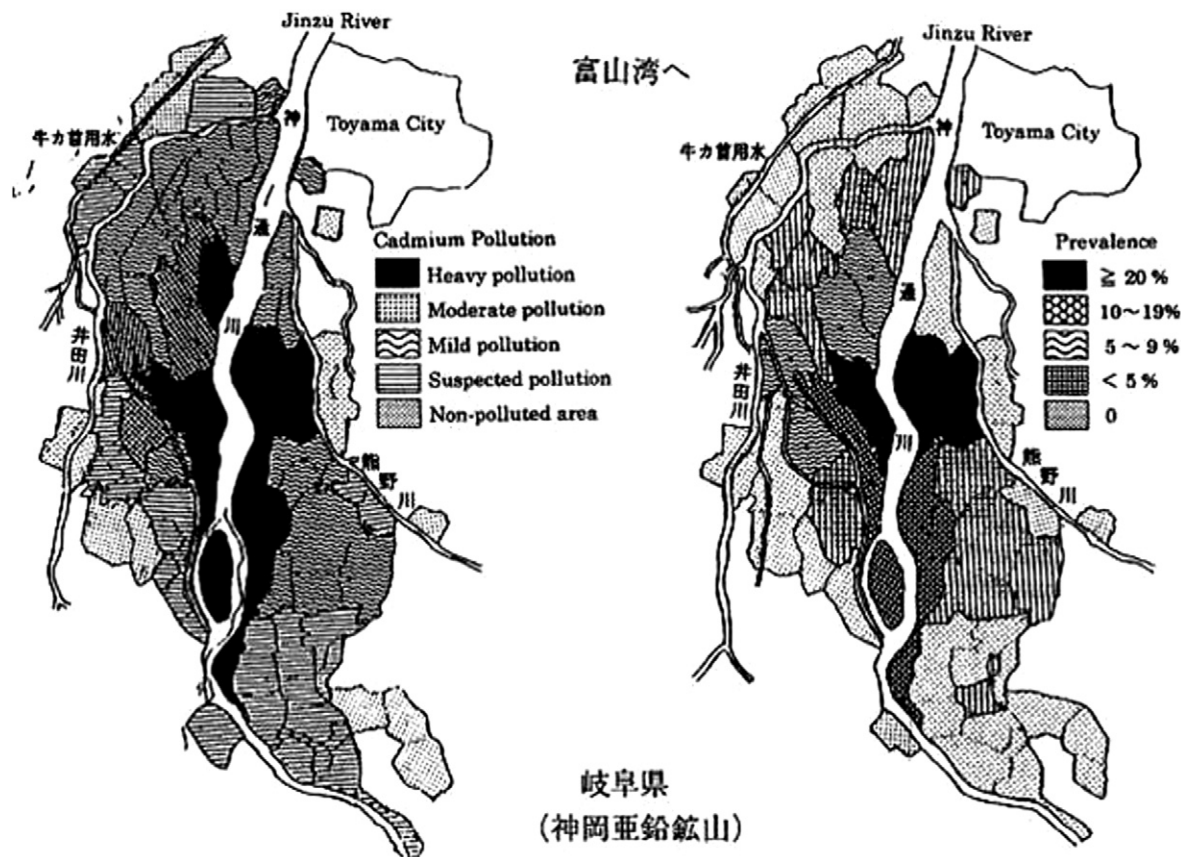


FIGURE 23.1 Itai—Itai disease. (left) the degree of Cd pollution and (right) the presence of the disease in women over 50 years of age.

rice, and in practice a close association was reported between the prevalence of Itai—Itai disease and the Cd concentration in rice.

Although Cd emissions in the air have been constantly decreasing since the 1960s due to improved technology for the production, use, and disposal of Cd and Cd-containing products, industrial Cd consumption in the world has increased steadily (from 18,400 tons in 2003 to 20,400 tons in 2007). Occupational and environmental pollution with cadmium can result from heavy metal mining, metallurgy and industrial use, manufacturing of nickel—cadmium batteries, pigments, plastic stabilizers, and anti-corrosive products. Important sources of human intoxication are cigarette smoke, due to high concentrations of cadmium in cigarettes (smokers on a packet a day can easily double their cadmium intake), as well as food, water, and air contamination. In Europe, the highest Cd levels in soil were found to occur in topsoil and to follow closely the distribution of P_2O_5 , suggesting that the contamination is derived from the use of rock phosphate fertilizer in intensive arable agriculture.

Low levels of chronic exposure to Cd result in completely different human health impacts than those high levels that had caused the 'Itai-Itai' disease. Chronic intoxication is associated with obstructive airway disease, emphysema, irreversible renal failure, bone disorders, and immunosuppression. In humans, cadmium exposure has been associated with cancers of the prostate, lungs, and testes (it is classified as a carcinogen). At the cellular level, cadmium affects proliferation, differentiation, and causes apoptosis. However, since Cd^{2+} is not redox-active, the generation of reactive oxygen species (ROS) and DNA damage must be due to indirect effects. Cadmium also modulates gene expression and signal transduction and reduces the activities of proteins involved in antioxidant defenses. It has also been shown to interfere with DNA repair.

The large and easily polarised Cd^{2+} ion is a soft Lewis acid, with a preference for easily oxidised soft ligands, particularly sulfur, so it would be expected to displace Zn^{2+} from proteins where the zinc coordination environment is sulfur dominated. It is a group 12 element, like Zn^{2+} , with which it shares a full complement of *d* electrons, so it does not change oxidation state in biological environments. However, the close similarities in the ionic radii of Cd^{2+} and Ca^{2+} (0.95 and 1.00 Å respectively) favour exchange of the two metals in calcium-binding proteins. Cadmium can also interfere with iron. A schematic representation of cadmium traffic in animal cells is presented in Figure 23.2. As might be expected, by mimicking other essential metal ions, Cd^{2+} adopts a Trojan

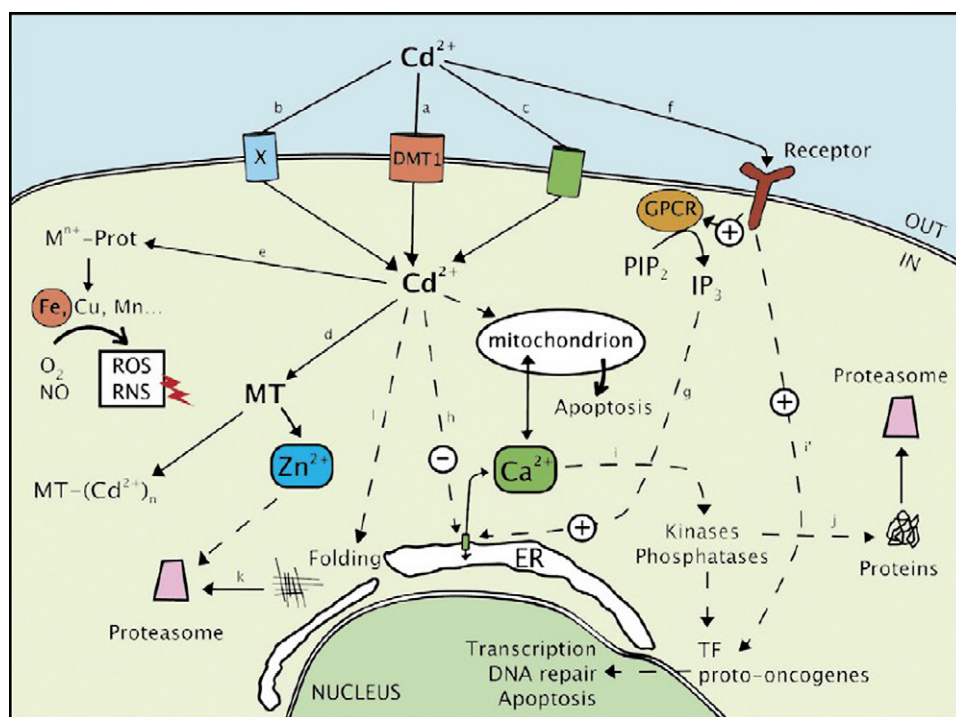


FIGURE 23.2 Schematic representation of cadmium traffic in animal cells. (From Martelli, Rousselet, Dycke, Bouron and Moulis, *et al.*, 2006. Copyright 2006 with permission from Elsevier.)

horse strategy⁴ to be assimilated by cells. In the digestive tract Cd^{2+} is transported by the broad specificity divalent metal transporter, DMT1 (Figure 23.2a), which is the intestinal transporter for nonhaem iron (Chapter 7). Since there is an iron-responsive element (IRE)-containing form of DMT1 which is targeted to the apical membrane of

4. In order to break the ten-year-long siege of Troy, the Greeks constructed an enormous wooden horse, hiding their best warriors in the stomach of the animal.

enterocytes, regulated by iron regulatory protein (IRP) binding, dietary Cd^{2+} uptake and therefore its toxicity will depend on the iron status of the individual. Since women have a higher dietary iron intake than men, because of menstrual blood losses, they are more at risk, and the risk is even greater during pregnancy when DMT1 expression is greatly increased. Cd^{2+} export through the basolateral membrane may not be as efficient as uptake, since Cd^{2+} accumulates in enterocytes on a high Cd^{2+} diet. The iron transporter at the basolateral membrane, ferroportin, may also be involved in transport of Cd^{2+} into the blood stream, as may calcium-ATPases and zinc exporters.

Cd^{2+} enters neurons via voltage-gated calcium channels even in the presence of external calcium, suggesting that these channels are the main cadmium entry pathway in nerve cells (Figure 23.2c). Since Cd^{2+} is able to cross even when these channels are blocked, other calcium channels such as ligand-gated *N*-methyl-D-aspartate (NMDA) receptors or store-operated calcium channels (Chapter 11) may also participate in cellular cadmium uptake. Although there is little evidence that cadmium can enter cells via zinc transporters, recent studies suggest that the zinc transporter ZIP8 is involved in cadmium uptake by mouse testicular cells. Other alternative pathways for cadmium uptake probably also exist (Figure 23.2b).

Once inside the cell the small, cysteine-rich protein, metallothionein (MT, Figure 23.2d), which serves to bind intracellular zinc and copper (Chapter 8), is a major target for cadmium binding. Genes coding for MT are strongly induced by both Zn^{2+} and Cd^{2+} by activation of the cadmium- (and zinc-) sensitive transcription factor MTF-1. The importance of MT in cadmium toxicity is underlined by the observation that mice lacking MT are more sensitive to cadmium exposure than wild-type mice, while MT-overexpressing cells are more resistant. It appears that the abundant intracellular thiol-containing tripeptide, glutathione, may also be involved in the detoxification and excretion of cadmium.

The chemical similarities between cadmium and zinc imply that cadmium could probably exchange with this metal in zinc-binding proteins (Figure 23.2e), although very little concrete evidence has been found in animal cells, with the exception of metallothionein. Cadmium can alter the intracellular concentration of calcium, which is an important and universal intracellular signal messenger (Chapter 11). Acute exposure to cadmium can increase intracellular Ca^{2+} concentration via a poorly characterised cell surface G-protein-coupled “metal-binding receptor,” GPCR (Figure 23.2f), resulting in activation of phospholipase C and IP_3 production by hydrolysis of phosphatidylinositol. This triggers calcium release from intracellular stores, probably from IP_3 -gated Ca^{2+} channels in endoplasmic reticulum (Figure 23.2g). This cadmium-dependent upregulation of the internal concentration of calcium may have consequences for cellular proliferation, differentiation, and apoptosis. Within the cell, cadmium has the opposite effect (Figure 23.2h). It blocks release of stored Ca^{2+} by inhibiting the activity of IP_3 and ryanodine receptors (Chapter 11). Cadmium can also increase intracellular calcium concentration in muscle cells by promoting calcium release from the sarcoplasmic reticulum.⁵

A considerable number of transcription factors have reactive cysteine residues which enable them to respond to the redox conditions in the cell. Since cadmium perturbs redox homeostasis, it can affect this class of transcription factors. If cadmium can displace the tetracoordinate zinc atoms in zinc finger-containing transcription factors, it will affect them as well. Many of the pathways involving activation and inactivation of transcription factors involve kinases and phosphatases, themselves under the intricate control of calcium fluxes. It is therefore no surprise that cadmium will exert effects on the activity of transcription factors, the activation of proto-oncogenes, and thereby on gene expression (Figure 23.2i and i').

Cadmium also appears to be involved in the ubiquitin–proteasome pathway. Ubiquitin binding to proteins is often signalled by post-transcriptional modifications like phosphorylation (Figure 23.2j). Cadmium has also been shown to decrease the solubility of specific proteins, and as we saw in Chapter 18, high concentrations of aggregated proteins can impede the proteasome (Figure 23.2j,k). It can also affect protein folding, again with deficient proteasomal action (Figure 23.2l).

5. The sarcoplasmic reticulum is a fine reticular network of membrane-limited elements which pervades the sarcoplasm of muscle cells.

Although cadmium is not strongly mutagenic, it is known that it causes increased oxidative DNA damage and that it inhibits the DNA repair systems. It has also been found to induce cell death both by necrosis and apoptosis. Since the latter is extremely calcium dependent, it seems likely that the pro-apoptotic effects of cadmium are due to its interference with calcium homeostasis.

MERCURY

The toxicity of mercury (Guzzi La Porta, 2008) was highlighted by Minamata disease, first discovered in Minamata city in Kumamoto prefecture, Japan, in 1956. This is a neurological syndrome caused by severe mercury poisoning, with symptoms including ataxia, numbness in the hands and feet, general muscle weakness, narrowing of the field of vision, and damage to hearing and speech. It was caused by the release of methylmercury in the industrial wastewater from a chemical factory (Figure 23.3). This highly toxic chemical is bioaccumulated



FIGURE 23.3 The Chisso factory, responsible for the methylmercury pollution and its wastewater routes. Instead of discharging its waste into Hyakken Harbour (the source of original contamination), from September 1958 it discharged wastewater directly into Minamata River. The immediate effect was the death of fish at the mouth of the river, and from that point on new Minamata disease victims began to appear in other fishing villages up and down the coast of the Shiranui Sea.

in aquatic food chains reaching its highest concentrations in shellfish and fish in Minamata Bay and the Shiranui Sea, which when eaten by the local population resulted in mercury poisoning. Of the 2265 victims officially recognised, as of March 2001, 1784 died, and it was only in 2004 that the Chisso Corporation was ordered to clean up its contamination. Another major outbreak of MeHg intoxication occurred in rural Iraq in 1971–1972 from seed grain treated with an Hg-based fungicide that was to be used for planting. More than 6500 individuals were hospitalised and 459 died from consumption of Hg-contaminated bread.

Asia has become the largest contributor of anthropogenic atmospheric mercury (Hg), accounting for over half of global emissions, with serious Hg pollutions to the local environment influenced principally by the chemical industry and mercury and gold mining. Studies have shown that in humans and selected Arctic marine mammals and birds of prey there has been an order of magnitude increase in Hg that began in the mid to late 19th century and accelerated in the 20th century (Dietz et al., 2009). The man-made contribution to present-day Hg concentrations was estimated at 92%.

Hg exists essentially in three forms: organic mercury, primarily methylmercury (MeHg), elemental mercury (Hg^0), known as metallic mercury, and inorganic mercury compounds (I-Hg), principally mercuric chloride,

Today the predominant if not the sole source of methylmercury is derived from the methylation of inorganic mercury in aquatic sediments and soils. Methylmercury is well absorbed from the diet and distributes within a few days to all tissues in the body. It is present in the body as water-soluble complexes mainly, if not exclusively, attached to the sulfur atom of thiol ligands, and crosses the blood–brain barrier without hindrance, entering the endothelial cells of the blood–brain barrier as a complex with L-cysteine. The principal target tissue of MeHg is the brain, and its major toxic effects are on the central nervous system. Whereas adult poisoning affects the visual cortex and the cerebellum, in neonatal infants the outcome can be much more serious, ranging in its effects from cerebral palsy to developmental retardation.

Ethylmercury (EtHg) is used in the form of thimerosal as a preservative in vaccines given to children. In recent years, there has been concern that EtHg exposure may induce neurodevelopmental disabilities such as language delay and attention deficit-hyperactivity disorder, but especially autism spectrum disorder. It has been removed from most vaccines in the USA and Europe; but is still used in some developing countries.

Elemental mercury (Hg^0) is a naturally occurring form of the metal that exists uniquely in liquid form at room temperature and quickly turns to vapour when heated. The natural sources of Hg^0 in the environment include the release of Hg gases from volcanic eruptions and the erosion of ores that contain Hg. Several studies over the past 30 years have demonstrated that dental amalgam filling releases mercury vapour into the oral cavity. Mouth breathing carries the vapour to the lung where it is absorbed and distributed to tissues.

Inorganic Hg (I-Hg) compounds (mercury salts) are also a significant source of Hg intoxication in some countries. Inorganic Hg has been used for many years in numerous products, including various medications, germicidal soaps, teething powders, and skin creams, many of which are still in use today. Some skin cream contains as much as 6–10% mercurial chloride or calomel.

In the CNS, MeHg accumulates, particularly in astrocytes. Astrocytic swelling, excitatory amino acid (EAA) release, and uptake inhibition, as well as EAA transporter expression inhibition are known consequences of MeHg exposure. One fairly obvious way in which Hg^{2+} could alter protein functions is by reacting with sulfhydryl groups, thereby inhibiting enzymes containing reactive thiols groups in or near their active site. Potentially of greater importance is the observation that dietary selenium (Se) status is inversely related to vulnerability to methylmercury (MeHg) toxicity. Recent studies have shown that Se-enriched diets not only prevent MeHg toxicity but can also rapidly reverse some of its most severe symptoms. It is now understood that MeHg is a highly specific, irreversible inhibitor of Se-dependent enzymes (selenoenzymes). Selenoenzymes, in particular glutathione peroxidase, thioredoxin reductase and thioredoxin glutathione reductase, are required to prevent and reverse oxidative damage throughout the body, particularly in the brain and neuroendocrine tissues. Inhibition of selenoenzyme activities in these vulnerable tissues appears to be the proximal cause of the pathological effects known to accompany MeHg toxicity (Figure 23.4). Because Hg's binding affinities for Se are up to a million times higher than for sulfur, its second-best binding partner, MeHg inexorably sequesters Se, directly impairing selenoenzyme activities and their synthesis (Figure 23.5).

LEAD

Chronic lead poisoning (saturnism⁶) is a major cause of environmental concern in all countries worldwide. Lead toxicity affects several organ systems, including the nervous, haematopoietic, renal, endocrine, and skeletal. The effect of major concern is the impairment of cognition and behaviour during nervous system development in infants and young children, and the growing body of evidence that exposures to lead in early life may cause neurodegeneration in later life. Low-level exposure to lead from various environmental sources, including lead-based paint, and household dust from surfaces covered with such paints, as well as lead in air, food, and water can

6. Saturn was the alchemist's name for lead. The metal Pb (Latin *plumbum*) was used in domestic plumbing from Roman times on account of it being soft and malleable. Plumbers (lead workers) nowadays rarely use lead, since most modern houses have water pipes in other metals or in plastic. The attraction of lead for young children is that it has a very sweet taste.

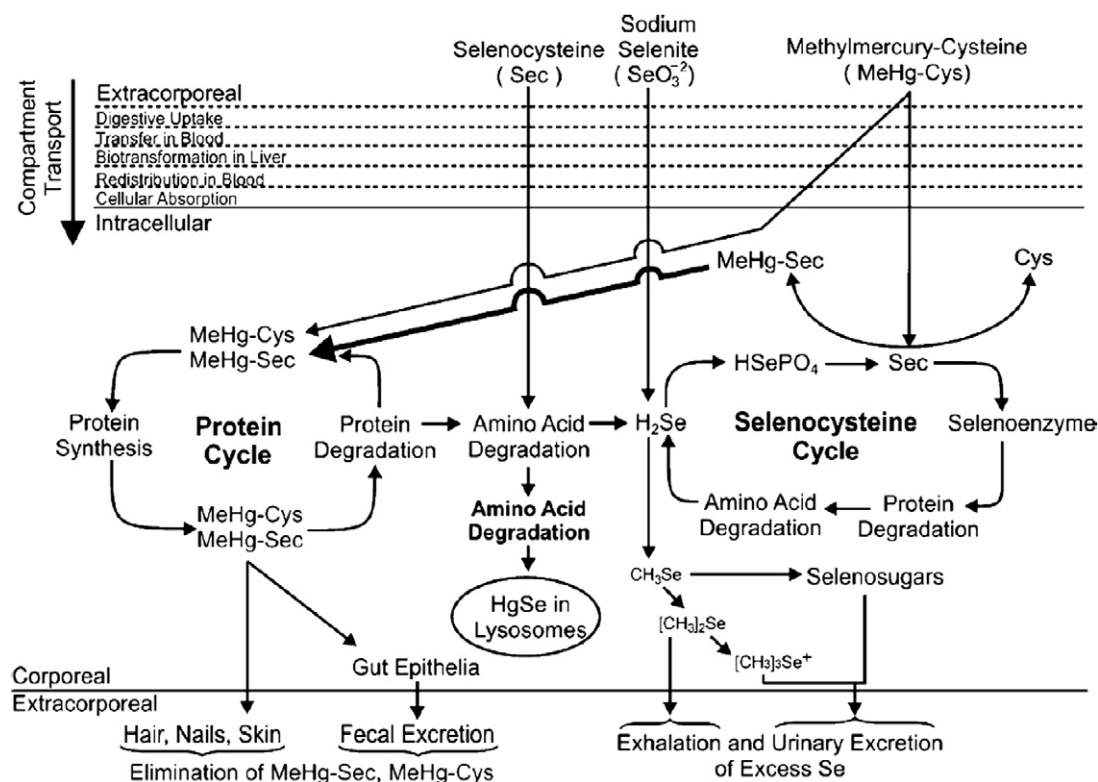


FIGURE 23.4 General scheme of vertebrate Se metabolism and the interactive influences of MeHg. (From *Ralston and Raymond, 2010*. Copyright 2010 with permission from Elsevier.)

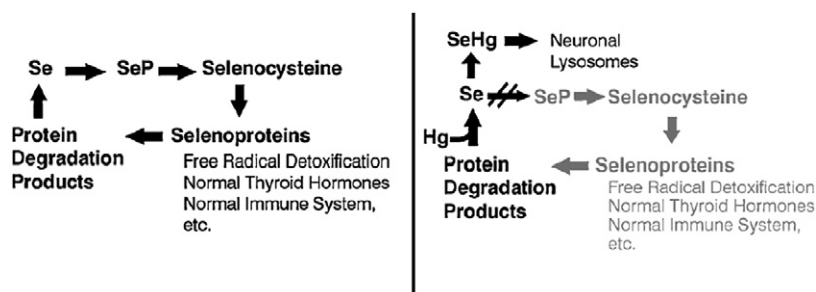


FIGURE 23.5 Schematic of Se sequestration mechanism of Hg toxicity. A simplified portrayal of the normal cycle of selenoprotein synthesis is depicted on the left. Disruption of this cycle by exposure to toxic quantities of Hg (MeHg) is depicted on the right. Selenide freed during selenoprotein breakdown becomes bound to Hg, forming HgSe that accumulates in cellular lysosomes. If Hg is present in stoichiometric excess, formation of insoluble Hg selenides abolishes the bioavailability of Se for protein synthesis (indicated by gray text) and results in loss of normal physiological functions that require selenoenzyme activities. (From *Ralston et al., 2010*. Copyright 2010 with permission from Elsevier.)

be involved. The removal of lead additives from petrol has greatly reduced the levels of the metal in air, food, water, and dust. Lead in water is more efficiently absorbed than lead in food, hence the danger of lead in tap water from solder or pipes in residential plumbing is of particular concern. While lead-based paint remains the most common source of lead exposure for children aged <6 years, 34% of children aged <6 years with lead poisoning in Los Angeles County had been exposed to items containing lead which might include candy, folk and traditional

medications, ceramic dinnerware, and metallic toys and trinkets that had been brought into the home. In Oregon, ingestion of a medallion pendent led to venous blood lead levels in a four-year-old boy of 123 $\mu\text{g}/\text{dl}$ (level of concern: $>10 \mu\text{g}/\text{dl}$). The medallion, purchased from toy vending machines was found to contain 38.8% lead (388 000 mg/kg), leading to a national voluntary recall of more than 1.4 million metal toy necklaces. Because iron deficiency and lead poisoning share common environmental risk factors, it is common practice to supplement the diets of children at risk from lead toxicity with iron, as well as calcium (as might be expected, lead also seriously interferes with cellular calcium metabolism). Lead toxicity correlates with blood lead levels and progresses from biochemical and subclinical abnormalities at levels of around 10 $\mu\text{g}/\text{dl}$ to coma and death at levels in excess of 100 $\mu\text{g}/\text{dl}$. The anaemia of lead poisoning is associated with elevated serum iron levels, which may reflect lower transferrin levels: lead has been shown to suppress human transferrin protein and mRNA levels *in vitro*. Elevated levels of erythrocyte zinc protoporphyrin are found in lead toxicity, together with evidence of increased oxidative stress, as reflected by decreased glutathione peroxidase levels and increased production of thiobarbituric acid reactive substances. Lead has been found to promote lipid oxidation and alterations in physical properties of membranes, while chronic lead intoxication affects the structure of myelin in the central nervous system of rats by targeting myelin glycoproteins. Prolonged exposure to lead in immature rats leads to glial activation with elevation of proinflammatory cytokines. The zinc requiring enzyme δ -aminolaevulinate dehydratase (also known as porphobilinogen synthase, PBGS) catalyses the second step in the haem biosynthetic pathway, forming the pyrrole porphobilinogen by condensation of two molecules of δ -aminolaevulinate (Chapter 7). It is the inhibition of δ -aminolaevulinate dehydratase that is presumed to account for the anaemia of lead poisoning. The zinc-binding site, illustrated in Figure 23.6, with lead bound to the catalytic zinc site of human PBGS (modelled on the

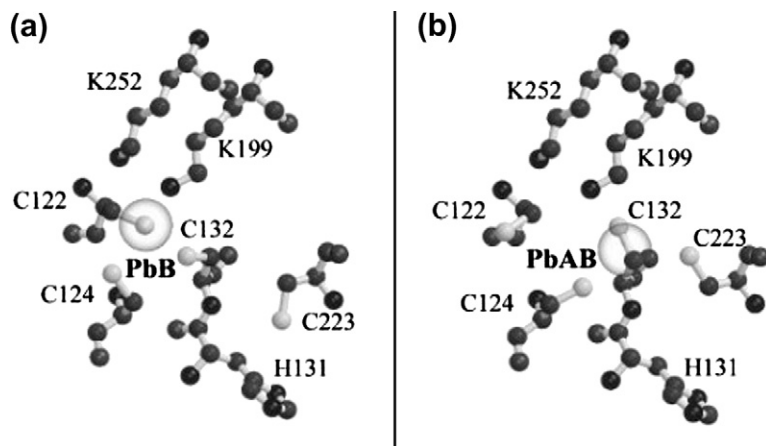


FIGURE 23.6 A model of Pb(II) interactions with human PBGS. (a) a model for Pb(II) (transparent) bound to the PbB site, which is analogous to ZnB. The Pb(II) is slightly more distant from the cysteines than is ZnB and is directly on top of the sulfur of Cys-122 in this representation. (b) an analogous model for Pb(II) (transparent) bound to a hybrid PbAB site. In this model Cys-124, Cys-132, and Cys-223 are the Pb(II) ligands. The cysteines show different rotamer conformations relative to A. (From Jaffe, Martins, Li, Kervinen and Dunbrack, *et al.*, 2001. Copyright 2001 with permission from the American Society for Biochemistry and Molecular Biology.)

published observations of lead bound to yeast PBGS of) is quite unusual for a catalytic zinc site. Most catalytic zinc ligands are not rich in cysteines — and the unusual arrangement of three cysteine ligands all to one side of the metal ion is what makes PBGS a primary target for inhibition by lead, which has unusual stereochemical coordination preference. The inhibition of PBGS, which is an important feature of acute lead poisoning, can be explained by the exceptional affinity of the enzyme for the metal. The enzyme is activated by Zn^{2+} with a K_m of 1.6 pM and inhibited by Pb^{2+} with a K_i of 0.07 pM. It has been suggested that the accumulation in the blood of

δ -aminolaevulinate, which mimics the neurotransmitter γ -aminobutyrate (GABA), and is a potent agonist for GABA receptors, may be responsible for the neurological symptoms and psychosis that often accompanies lead poisoning. Lead is also thought to inhibit ferrochelatase, which may explain the elevated values of zinc protoporphyrin found in lead intoxication.

The effects of Pb^{2+} on human health have been recognised since antiquity — its significant reproductive system toxicity has led to its identification as a potential cause of the fall of Rome, through infertility and abortion. However, it was not until the 1970s that seminal epidemiological studies provided evidence on the effects of Pb^{2+} intoxication on the cognitive function in children. The many and complex effects of Pb^{2+} on neuronal processes that are essential for synaptic plasticity, learning and memory in the mammalian brain, have become much clearer in the last two decades. In particular, the effects of Pb^{2+} on glutamatergic synapses have provided evidence that the N-methyl-D-aspartate type of excitatory amino acid receptor (NMDAR) is a direct target for Pb^{2+} effects in the brain.

METALS AS POISONS

We have not included in this survey of environmentally toxic metals some of the essential metal ions which can also be toxic when present in excessive amounts in the environment. An excellent example is illustrated in Figure 23.7, which shows the Rio Tinto (red river) in Andalucia, south-western Spain, which flows into the



FIGURE 23.7 The blood-red water of the Rio Tinto in Andalucia, south-western Spain.

Atlantic at Huelva. Close to Huelva is Palo de la Frotera from where Columbus departed to discover the New World in 1492. The Rio Tinto is characterised by deep red and highly acidic water which is extremely rich in heavy metals. It can be considered essentially as the birthplace of both the Copper and the Bronze Age. The first mines were developed in 3000 B.C. by the Iberians and Tartessians. Accounts of their fabulous mineral wealth (gold, silver, and copper) drew the Phoenicians followed by the Romans who made some of the first coins from the silver and gold of the Rio Tinto. The mines were also exploited by the Visigoths and the Moors, before being eventually abandoned. They were rediscovered by Spain in 1556 and reopened in 1724, only to be sold to the British in 1871.⁷ They are now one of the most important sources of copper and sulfur in the world. The Rio Tinto

7. The mining company Rio Tinto put on display the medals they have minted for the 2012 London Olympic games just at the moment that I wrote this Chapter.

Bingham Canyon mine is the largest mining operation in the world, positioned upstream of the major population centre, Huelva. According to the EPA database Toxics Release Inventory which follows the release and potential release of chemicals and metals into the environment, the Rio Tinto mine is the largest source of the 650 toxic compounds tracked in this database and emitted into air, soil, and water.

Over 5000 years of mining pollution have contributed to the river becoming an extreme acidic environment (pH 1.7–2.5), in large part due to the presence of chemolithotrophic organisms, such as iron-oxidizing bacteria and sulfur-oxidizing bacteria. The extreme conditions in the river are thought to be analogous to other locations in the solar system which may contain liquid water, such as subterranean Mars. NASA scientists have directly compared the chemistry of the water in which the rocks of Meridiani Planum, a plain located just south of Mars' equator, were deposited in the past, with the Río Tinto. Likewise, Jupiter's moon Europa is thought to contain an acidic ocean of water underneath its ice surface.

However, in addition to their role as environmental toxins, some metals, or compounds containing them, can be molecules of murder — I strongly recommend John Emsley's marvellous book entitled 'Molecules of Murder' (Emsley, 2008). Cinema enthusiasts may recall the Frank Capra film adaptation starring Cary Grant 'Arsenic and Old Lace',⁸ based on Joseph Kesselring's 1939 play — the opening night review in the New York Times reported that the play was "so funny that none of us will ever forget it." The play ran for 1444 performances. We referred in Chapter 1 to the possibility that selenium supplementation of the diet might be an important yet simple way to ameliorate arsenicosis in cases of mass poisoning. This line of thought even provides an intriguing twist on the plot of Dorothy Sayers' detective mystery *Strong Poison*, providing a biochemically believable explanation for the poisoning at the centre of the story (Prince, 2007). Norman Urquhardt poisons the hapless Philip Boyes by feeding both of them an omelette liberally dosed with white arsenic (arsenic trioxide, As₂O₃). According to Sayers, Urquhardt has previously 'trained' himself to eat white arsenic by frequent and increasing doses so that he survives the toxic breakfast while Boyes succumbs. There is a widespread belief that repeated doses of arsenic trioxide lead to habituation.

Arsenic is widely dispersed in the Earth's crust and exists at an average concentration of approximately 5 mg/kg. It exists in many oxidation states, with arsenic (III) and (V) being the most common forms. Because gold- and arsenic-bearing minerals coexist, there is a hazard of mobilizing arsenic during gold mining activities. Many cases of endemic contamination by arsenic with serious consequences to human health are known from areas with high levels of arsenic in their geological formations.

Also in Chapter 1 we briefly mentioned the case of poisoning of the Russian dissident Alexander Litvinenko. Litvinenko, a former officer of the Russian Federal Security Service, FSB and KGB, escaped prosecution in Russia and received political asylum in the United Kingdom. He suddenly fell ill in London on the 1 November 2006, was hospitalised, and died three weeks later, becoming the first confirmed victim of lethal polonium-210-induced acute radiation syndrome. Traces of the polonium-210 were subsequently discovered at various locations in London visited by Mr Litvinenko as well as in Russia and on two British Airways flights.

Po-210 is a naturally occurring radioactive material. It is found in very low concentrations in the environment as a part of the uranium decay chain and can be derived from lead-containing wastes from uranium, vanadium, and radium refining operations — not however in significant quantities. It can also be produced artificially, which requires fairly sophisticated equipment used in the nuclear industry. Po-210 emits α -particles, is 5000 times more radioactive than radium, and has a half-life of Po-210 of 138 days. α -Radiation delivers a large amount of energy to living cells and can cause considerable damage and cell death. However, α -particles lose most of their energy on impact, and cannot move further into matter, hence alpha radiation does not penetrate through surfaces (e.g., paper, human skin, or clothes). Po-210 only represents a radiation hazard if it taken into the body — by inhalation, ingestion, or getting into a wound. This "internal contamination" can cause irradiation of internal organs, which can result in serious medical symptoms or death. The toxicity of Po-210 is much higher than that of

8. The 'murderous old lady' plot line was probably inspired by actual events that occurred in a house in Windsor, Connecticut, where a woman took in elderly boarders and poisoned them for their pensions.

cyanides, for example. Nevertheless, it does not represent a risk to human health as long as it remains outside the body. Most traces of it can be eliminated through careful hand washing and showering.

REFERENCES

- Dietz, R., Outridge, P. M., & Hobson, K. A. (2009). Anthropogenic contributions to mercury levels in present-day Arctic animals—a review. *Science of the Total Environment*, 407, 6120–6131.
- Emsley, J. (2008). *Molecules of murder. Criminal molecules and classic cases*. RSC Publishing.
- Guzzi, G., & La Porta, C. A. (2008). Molecular mechanisms triggered by mercury. *Toxicology*, 244, 1–12.
- Jaffe, E. K., Martins, J., Li, J., Kervinen, J., & Dunbrack, R. L., Jr. (2001). The molecular mechanism of lead inhibition of human phorbilinogen synthase. *Journal of Biological Chemistry*, 276, 1531–1537.
- Martelli, A., Rousselet, E., Dycke, C., Bouron, A., & Moulis, J.-M. (2006). Cadmium toxicity in animal cells by interference with essential metals. *Biochimie*, 88, 1807–1814.
- Martin, R. B. (1994). Aluminium: A Neurotoxic Product of Acid Rain. *Acc Chem Res*, 27, 204–210.
- Prince, R. C., Gailer, J., Gunson, D. E., Turner, R. J., George, G. N., & Pickering, I. J. (2007). Strong poison revisited. *Journal of Inorganic Biochemistry*, 101, 1891–1893.
- Ralston, N. V., & Raymond, L. J. (2010). Dietary selenium's protective effects against methylmercury toxicity. *Toxicology*, 278, 112–123.
- Verstraeten, S. V., Aimo, L., & Oteiza, P. I. (2008). Aluminium and lead: molecular mechanisms of brain toxicity. *Archives of Toxicology*, 82, 789–802.

This page intentionally left blank

Note: Page numbers followed by *f* indicate figures and *t* indicate table.

A

- A β , 404–405
 - copper and, 405
 - zinc and, 407
- ABC. *See* ATP-binding cassette
- ABS. *See* Electronic absorption spectroscopy
- Absorption, 120, 122, 124
- AC. *See* Adenyl cyclase
- ACC. *See* Amorphous calcium carbonate
- Aceruloplasminemia, 412–414
 - CP and, 413–414
- Acetaldehyde, 92
- Acetyl-CoA, 107–108
 - methyl group to, 297–298
 - phosphopantetheine group in, 108f
- Acetyl-CoA synthetase (ACS), 297–298, 299, 302
- N-acetyl-diiodo-tyrosyl-D-threonine (IYT), 283–284
- N-acetylglucosamine, 53–54, 56
- Acid rain, 434
- Acireductone dioxygenase (ARD), 297–298
- A-cluster, 302
- ACP. *See* Acyl-carrier protein
- AC/PKA. *See* Adenyl cyclase/phosphokinase A
- ACS. *See* Acetyl-CoA synthetase
- Action potentials, 379–380
- Activated microglia, 379–380
- Active transport, sodium and, 187–190
- ACV. *See* δ -(L- α -aminoadipoyl)-L-cysteinyl-D-valine
- Acyl-carrier protein (ACP), 107–108
 - phosphopantetheine group in, 108f
- AD. *See* Alzheimer's disease
- Ada, 237–238, 240f
- Adaptor hypothesis, 64f
- Adenine, 49, 250
- Adenosine, 94–95
- Adenosine diphosphate (ADP), 198
- Adenosine triphosphate (ATP), 1, 2–3, 91–92, 95f
 - amino acids and, 62–64
 - to AMP, 94–95
 - anabolism and, 105
 - CcO and, 254–255
 - central role of, 94–95
 - CFTR and, 355–356
 - enzymes and, 112–114
 - glycolysis and, 100–102
 - hydrogen and, 7–9
 - hydrogenases and, 299
 - hydrolysis of, 94f, 187–188
 - magnesium and, 10–11, 197, 198
 - for nitrogen fixation, 332–335, 348
 - OMTs and, 140–141
 - phosphorus and, 348
 - respiration and, 13, 110
- Adenosylcobalamin, 305f
- S-adenosylmethionine (SAM), 80, 264–265, 266f
- Adenyl cyclase (AC), 426f
- Adenyl cyclase/phosphokinase A (AC/PKA), 387–388
- Adipocytes, 57
- ADP. *See* Adenosine diphosphate
- Aequorin, 223–225
- Aerobactin, 137f
- Aeromonas proteolytica*, 241
- AICD. *See* APP intracellular domain
- Alanine, 38t
- Albumin, 173
 - zinc and, 388–389
- Alcohol, 55f
- Alcohol dehydrogenase, 92, 237, 239f
- Aldehyde, 53–55
 - alcohols with, 55f
 - PUFA and, 398
 - zinc and, 237
- Aldehyde oxidase (AO), 82
 - of molybdenum, 328f
- Aldol, 99f
- Aldose, 54f
- Alkali earth metals, 9
- ALS. *See* Amyotrophic lateral sclerosis
- Alterobactins, 137f
- Aluminum, 17, 434–435
 - AD and, 435
 - lithium with, 9
 - toxicity of, 435
- Alzheimer's disease (AD), 395–401, 396f, 404
 - aluminum and, 435
 - copper and, 406f, 407
 - HNE and, 398–399
 - zinc and, 406f, 407
- Amanita muscaria*, 339
- Amine oxidases, 282
- Amino acids
 - ATP and, 62–64
 - as ligands, 69
 - oxidation of, 97–98
 - proteins, 38t
 - residues of, 69–72
 - tRNA and, 65–66
- α -amino acids, 37–39, 39f
- Amino groups, 9f
- α -amino-3-hydroxy-5-methyl-4-isoxalolepropionate (AMPA), 388–389
- Aminoacyl-tRNA synthetases, 37–39, 65–68
- δ -(L- α -aminoadipoyl)-L-cysteinyl-D-valine (ACV), 268
- γ -aminobutyric acid (GABA)
 - lead and, 440–443
 - zinc and, 388–391, 391f
- Aminopeptidases, 241
- Aminotransferase, 105–106
- Ammonia, 331–332
- Ammonium ions, 97–98
- Amorphous calcium carbonate (ACC), 370–372
- AMP. *See also* Cyclic AMP
 - ATP to, 94–95
 - hydrolysis of, 94–95
- AMPA. *See* α -amino-3-hydroxy-5-methyl-4-isoxalolepropionate
- Amphiphilic marine siderophores, 136f
- Amphiphilic molecules, 57–58

- Amyloid precursor protein (APP), 404–405
- Amylopectin, 55–56
- Amyotrophic lateral sclerosis (ALS), 291, 395–401, 409
- HNE and, 398–399
- SOD and, 409f
- Anabolism, 91, 105–106
- Anaplerotic reactions, 105–106
- Anfinsen, Christian B., 41–42
- Φ angle, 43, 43f
- Ψ angle, 43, 43f
- Annexin V, 430–431
- Antibodies, 48
- Antidepressants, 389
- Antimony, 15
- MIPs and, 16–17
- Antiparallel β -pleated sheets, 46
- AO. *See* Aldehyde oxidase
- Apo ferritin, 121–122, 361–362, 364
- copper and, 367f
- MRI and, 429, 430f
- Apoptosis, 437
- APP. *See* Amyloid precursor protein
- APP intracellular domain (AICD), 404–405
- Arabidopsis thaliana*, 15–16, 147, 150
- BHLH in, 163–165
- copper in, 151, 166, 166f
- zinc in, 151
- Arachnoid barrier, 382–384, 383f
- Archaea
- ISC in, 79
- manganese and, 314–315
- ARD. *See* Acireductone dioxygenase
- Arginase, 319f, 320f
- L-arginine and, 319
- divalent cations and, 318
- manganese and, 311
- Arginine, 38t, 400–401
- L-arginine, 317–319
- arginase and, 319
- Argon, 18
- Arsenic, 7, 15
- MIPs and, 16–17
- poisoning with, 444
- selenium and, 17
- for syphilis, 420–421
- Arthritis, 420–421
- Ascidians, 339, 340f
- calcium carbonate in, 370–376
- Ascorbic acid. *See* Vitamin C
- Asparagine, 38t
- Aspartate, 38t. *See also* N-methyl-D-aspartate
- carboxylate ligands and, 69–70
- α -keto acids and, 105–106
- Atmosphere, 343
- ATP. *See* Adenosine triphosphate
- ATP synthase, 111–112, 112f, 113f, 114f, 115f
- ATP7, 392–393
- cisplatin and, 421–423
- ATPase, 160, 355–356
- cadmium and, 437–438
- calcium pumps and, 218–220, 220f, 221f
- Menkes disease and, 413
- PMCA, 218, 222
- P-type ATPases, 218–220
- SERCA, 186–187, 217–218, 221, 222
- sodium-potassium and, 184–187, 186f
- vanadium and, 337
- ATP-binding cassette (ABC), 139, 141–142, 355–356
- Auranofin, 14, 14f
- Azotobacter*, 332
- Azurin, 281–282
- B**
- B. subtilis*, 78f
- Bacillus brevis*, 129f, 130f, 131
- Bacteria. *See also specific bacteria types*
- copper in, 158
- in enzymes, 143, 158–159
- iron and, 138
- metal assimilation in, 137–144
- metal ions in, 155–161
- zinc and, 144, 158
- Bacterioferritins (BFR), 273–274, 273f, 361–362, 362f
- Barium, 10–11
- β -barrel, 47–48, 47f, 141f
- Basal lamina (BL), 384f
- Basic helix-loop-helix (BHLH), 163–165
- BCSFB. *See* CSF barrier
- BDNF. *See* Brain-derived neurotrophic factor
- Bernal, J.D., 128–129
- Beryllium, 10
- Berzelius, Jöns Jacob, 351
- Bethe, Hans, 29–30
- BFR. *See* Bacterioferritins
- BHLH. *See* Basic helix-loop-helix
- BILAP, 242f
- Bioavailability, 4
- Biogeochemical cycles, 343–358
- Biological membranes, 57–59
- Biom mineralization
- in bone, 373
- classes of, 361–377, 361t
- in enamel, 373
- principles of, 360–361
- silicon and, 376–377
- Biopolymers, 2–3
- Biosphere, 343, 345f
- Bipolar disorder, 420–421, 425
- Bis hydroxyphenyltriazoles, 419–420
- Bismuth, 420–421
- BL. *See* Basal lamina
- Blood brain barrier (BBB), 379–384, 383f, 384f, 388–389
- aluminum and, 435
- iron and, 393
- PD and, 401
- Blood clotting cascade, 71
- Blue copper proteins, 280–282
- BMP. *See* Bone morphogenic protein
- π -bonds, 31–32, 33f
- σ -bonds, 31–32
- Bone, 373
- Bone morphogenic protein (BMP), 404–405, 416, 418f–419f
- Boric acid, 15–16
- Boron, 7, 15
- rhamnogalacturonan and, 15–16
- Bovine spongiform encephalitis (BSE), 410
- Boyer, Paul, 112–114
- Boyes, Philip, 444
- Bradykinesia, 408
- Brain. *See also* Blood brain barrier
- calcium channels in, 384–388
- copper in, 388–394
- iron in, 388–394
- potassium channels in, 385f
- sodium channels in, 384–388
- zinc in, 388–394, 390f
- Brain-derived neurotrophic factor (BDNF), 389
- Bromine, 4, 18
- vanadium haloperoxidases and, 7
- Bronze Age, 247
- BSE. *See* Bovine spongiform encephalitis
- b*-type cytochrome, 110–111
- Buckminsterfullerene, 2, 2f
- Bulk elements, 3
- C**
- C. pilulifera*, 337, 338f
- C pools, 344–346, 346f
- CAD. *See* CRAC activation domain
- Cade, J.J.F., 425
- Cadmium, 11, 435–439, 436f
- toxicity of, 1, 14–15, 433
- zinc and, 438
- cADPr. *See* Cyclic ADP-ribose
- Caesium, 9–10
- Calcineurin (CaN), 387f
- Calcium, 3, 10, 216–225, 216f, 219f, 359, 373f
- aluminum and, 435

- binding sites for, 10f
- cadmium and, 437–438
- cation properties, 197t
- cell signaling and, 225–228
- for cellular metabolism, 10–11
- α -helices and, 225
- in intracellular compartments, 222–225
- magnesium and, 215
- manganese and, 314, 315f
- in mitochondria, 223, 224f
- MRI and, 430–431, 431f
- in muscle contraction, 220–221
- NCX, 218, 219f
- phosphatases and, 203f
- pumps for, 218–220, 220f, 221f
- signal transduction and, 387–388
- as structural component, 215–216
- Calcium carbonate, 348
 - in ascidians, 370–376
- Calcium channels, 384–388
- Calcium pump of the secretory pathway (SPCA), 218–220, 222
- Calcium release-activated calcium (CRAC), 217–218
- Calcium/calmodulin-dependent protein kinase (CaMKII), 388
- Calmodulin (CaM), 225, 227f, 387–388, 426
- Calmodulin-dependent protein kinases (CaM kinases), 227–228, 426
- Calsequestrin, 222
- Calvin cycle, 91
- CaM. *See* Calmodulin
- CaM kinases. *See* Calmodulin-dependent protein kinases
- CaMKII. *See* Calcium/calmodulin-dependent protein kinase
- cAMP. *See* Cyclic AMP
- CaN. *See* Calcineurin
- Cancer
 - cisplatin for, 1, 421–424, 422f
 - gallium for, 425
 - platinum for, 420–421, 424
 - ruthenium for, 424
- Candida albicans*, 146
- Carafoli, Ernesto, 215–216
- Carbanions, 96
- Carbapenems, 240–241
- Carbohydrates, 53–56
 - chromium and, 340
- Carbon, 2, 3, 4, 344–348
 - with hydrogen, 7–9
 - palladium and, 14
- Carbon cycle, 344
- Carbon dioxide, 344–346
 - glucose and, 98
 - α -keto acid and, 102–104
- magnesium and, 210
- methanotrophs and, 143–144
- from photosynthesis, 133–134
- vitamin B₁₂-dependent
 - methyltransferases and, 306–307
- zinc and, 135
- Carbon monoxide, 5–7, 31
- Carbonated apatite, 374–375
- Carbon-carbon bonds, 99f
- Carbonic anhydrase, 231–232, 232f
- β -carbons, 39–40
- Carbonyl, 35–37, 36f
 - proteins and, 400–401, 400f
- α carboxy terminal fragment (α CTF), 404–405
- γ -carboxyglutamate residues, 24
- γ -Carboxyglutamic acid, 71–72
- Carboxyl groups, 9f
- Carboxylates, 24, 37–39
 - aspartate and, 69–70
 - zinc and, 229
- Carboxypeptidase, 231, 233–234, 233f, 234f
- Cartesian system, 29–30
- Catabolism, 91, 97–98, 100f
- Catalases, 254, 258
 - manganese and, 316, 317f, 318f
- Catalytic domain, 64–65
- Catechol dioxygenases, 268
- Catechol oxidase, 284
- CaVs. *See* Voltage-gated
 - calcium-selective channels
- C-cluster, 302, 302f
- CcO. *See* Cytochrome *c* oxidase
- CD. *See* Circular dichroism
- Cell signaling, 225–228
- Cellobiose, 54–55, 55f
- Cellulose, 56
- Cephalosporins, 240–241
- Cerebrospinal fluid (CSF), 392
- Ceruloplasmin (CP), 151, 281–282, 295, 295f
 - copper and, 173
 - iron and, 413–414
- CF. *See* Cystic fibrosis
- CFeSP. *See* Corrinoid iron-sulfur protein
- CFT. *See* Crystal field theory
- CFTR, 355, 356f
- Channels. *See specific channels*
- Charge cloud model, 26
- Chelate
 - iron in, 78f
 - tetrapyrroles and, 77–79, 77f
- Chelate effect, 24–26
- Chelators
 - iron, 147f, 417–419
 - zinc, 389–390
- Chlorine, 1, 4, 353–358, 355f
 - binding sites for, 10f
- Chlorine anion, 7
- Chloroperoxidases, 337, 338f
- Chlorophyll, 210–211, 211f
 - in chelate, 77–78
- Chromatium vinosum*, 126
- Chromium, 12–13
 - in biology, 340
 - enzymes and, 340
 - proteins and, 340
- Chromodulin, 340
- Circular dichroism (CD), 118t, 126, 127f
- cis-aconitate, 102–104
- Cisplatin, 14, 423f
 - for cancer, 1, 421–424, 422f
 - DNA and, 423f
- Citrate, 162
- Claisen ester condensation, 99f, 102–104
- Clostridium*, 332, 351
- Cobalamine, 143–144, 303, 305f
- Cobalt, 1, 5, 13, 303
 - enzymes and, 308
 - for metabolism, 5–7
 - vitamin B₁₂ and, 13
- Cobalt dehydrogenase (CODH), 297–299, 301, 302f, 324
- CoBSH. *See N*⁷-
 - mercaptoheptanoylthreonine phosphate
- CODH. *See* Cobalt dehydrogenase
- Codons, 62–64
- Coenzyme F, 77–78
- Coenzyme Q, 111
- Cofactors, 72–76, 75f
 - with PSII, 313f
- Collagen, 373–374
 - silicon and, 16
 - water and, 375f
- Complexes, 23, 110
 - proton pumping by, 111
- Complex I, 110
- Complex II, 110–111
- Complex III, 111
- Complex IV, 111
- Complex lipids, 57–58
- Conjugate acid-base pair, 28
- Conjugate redox pair, 28
- Contrast agents, 427–431
- Coordinate bonds, 22, 22f
- Coordination geometry, 26–27, 27t
 - of iron, 254
 - of magnesium, 198
- Copper, 5, 13, 283f, 286f
 - A β and, 405
 - AD and, 404, 406f, 407
 - apoferritin and, 367f

- Copper (*Continued*)
 in *Arabidopsis thaliana*, 151, 166, 166f
 in bacteria, 158
 in brain, 388–394
 CcO and, 288, 290f
 CP and, 173
 Creutzfeldt-Jakob disease and, 411, 411f
 cysteine and, 69–70
 dioxygen and, 14, 279, 282–294, 286f
 in *Enterococcus hirae*, 158–159, 160f
 enzymes and, 282–294
 in fungi, 167, 169
 in Gram-positive bacteria, 158–159
 histidine and, 69–70, 173
 iron and, 295
 ligands, 24
 in mammals, 153, 173, 174
 methanotrophs and, 143–144
 neurodegeneration and, 395–401, 412–414
 NMDA and, 407
 in plants, 161, 162f, 163
 plasma membrane and, 168
 proteins and, 280
 regulation of, 175f
 in *S. cerevisiae*, 170
 site classification for, 280, 280f
 SOD and, 76–77, 76f, 291
 in yeast, 150
 Copper chaperones, 76–77, 76f, 160
 NMR and, 124
 Copper transport proteins (CTR), 411–412
 Corey, Robert, 42
 Correlation spectroscopy (COSY), 124
 Corrins, 24, 25f
 cofactors in, 72
 Corrinoid iron-sulfur protein (CFeSP), 300–301
Corynebacterium diphtheriae, 157
 Covalent bonding, 22–23
 CP. *See* Ceruloplasmin
 cPMP. *See* Cyclic pyranopterin monophosphate
 CRAC. *See* Calcium release-activated calcium
 CRAC activation domain (CAD), 217f
 CREB, 387f
 Creutzfeldt-Jakob disease, 410–412
 Crick, Francis, 50–52, 62–64
 Crowfoot, Dorothy, 128–129
 Crystal field theory (CFT), 29–34, 30f
 CSF. *See* Cerebrospinal fluid
 CSF barrier (BCSFB), 382–384, 383f, 388–389
 C-terminal thiocarboxylate, 72
 α CTF. *See* α carboxy terminal fragment
 CTR. *See* Copper transport proteins
 Cubane iron-sulfur, 74, 74f, 262–264
 Cuboidal iron-sulfur, 74, 74f, 262–264
 Curie, Marie, 10–11, 17
 Cyanobacteria, 133–135, 138
 manganese and, 311
 photosynthesis and, 347–348
 zinc in, 160–161
 Cyclic ADP-ribose (cADPr), 223
 Cyclic AMP (cAMP), 426
 Cyclic pyranopterin monophosphate (cPMP), 80–82
 Cysteine, 38t, 40f, 400–401
 copper and, 69–70
 disulfide and, 40f
 iron and, 69–70
 tRNA and, 62–64
 Cystic fibrosis (CF), 355
 Cytochromes, 13, 125, 126f, 259–260, 261f
 Cytochrome *c* oxidase (CcO), 111, 168, 254, 255, 256f
 ATP and, 254–255
 copper and, 288, 290f
 iron and, 393–394
 Cytochrome P-450, 254, 258, 259f
 heme and, 323–324
 Cytoplasmic aconitase, 265
 Cytosine, 49, 250
 Cytosol, 106–107
 iron and, 142–143
 SOD in, 392
 zinc in, 160–161
D
D. norvegicum, 299–300
d orbitals, electrons in, 31
 Daughter molecules, 59
 D β H. *See* Dopamine β -hydroxylase
 D-block elements, 11
 D-cluster, 301
 DdBfr. *See* *Desulphovibrio desulfuricans*
 Deferasirox (ICL670), 419–420
 Dehydrogenase, 92
 Denitrification, 350
 Deoxymugineic acid (DMA), 149f
 Deoxynucleotides, 250
 Depolarization, 380
 copper and, 392–393
 Depression, 1
 Desferrioxamine (Desferal, DFO), 24, 25f, 86–87, 419–420
Desulphovibrio desulfuricans (DdBfr), 127–128, 128f
 DFO. *See* Desferrioxamine
 DG. *See* Diacylglycerol
 DHB. *See* 2,3-dihydroxybenzoid acid
 Diabetes, 417
 Diacylglycerol (DG), 225
 Diamond, 2
 Diatoms, 376–377
 Diazotroph, 84
 Dicoumarol, 71–72
 Diethylene triamine penta-acetic acid, 12f
 Diferric-transferrin, 151, 152f, 174f
 Diglyceride, 57–58
 Dihydroxyacetone, 54f
 2,3-dihydroxybenzoid acid (DHB), 87–89
 Dihydroxybenzoyl, 86–87
 Dimethyl sulfoxide (DMSO), 329f. *See also* DMSO reductase
 Dinuclear nonheme iron enzymes, 272–275
 Diodotyrosines (DIT), 356–358, 357f
 DIOs. *See* Iodothyronine deiodinases
 Dioxygen, 7–9, 316f
 copper and, 14, 279, 282–294, 286f
 Diphtheria toxin regulator (DtxR), 157
 Disaccharides, 54–55, 55f
 Distal histidine, 252–253
 Disulfide, 40f
 DIT. *See* Diodotyrosines
 Divalent cations, 318
 DMA. *See* Deoxymugineic acid
 DMR. *See* DMSO reductase
 DMSO. *See* Dimethyl sulfoxide
 DMSO reductase (DMR), 324, 328–329, 329f
 catalytic cycle of, 330f
 tungsten and, 329–331
 DMT1, 392
 cadmium and, 437–438
 DNA
 base composition of, 50–52, 51f, 52f
 cadmium and, 437, 439
 cisplatin and, 421–423, 423f
 Fur and, 158f
 oxygen, 13
 in plants, 147–148
 repair protein, 237–238, 240f
 replication of, 59, 60–62
 ROS and, 396, 401
 structure of, 50f
 transcription of, 62
 zinc and, 14–15
 DNA polymerase, 60, 60f, 61f
 DNA-binding proteins from starved cells (Dps), 129f, 130f, 131
 ferritin and, 366
 in prokaryotes, 155–156
 Dopamine, 393–394
 copper and, 392
 TH and, 401–402
 Dopamine β -hydroxylase (D β H), 282, 283

- Dopamine β -monooxygenase, 323–324
 Downstream regulatory element (DRE), 387–388
 Downstream regulatory element
 antagonistic modulator (DREAM), 387–388, 387f
 D-pathway, 257
 Dps. *See* DNA-binding proteins from starved cells
 DRE. *See* Downstream regulatory element
 DREAM. *See* Downstream regulatory element antagonistic modulator
Drosophila, 180–181
 Drugs, 420–425. *See also specific drugs*
 DtxR. *See* Diphtheria toxin regulator
 Dysprosium, 11
- E**
 EAA. *See* Excitatory amino acids
 EAATs. *See* Excitatory amino acid transporters
 EDTA, 434–435
 Ehrlich, Paul, 420–421
 Electrons
 acceptors, 28
 in *d* orbitals, 31
 donors, 28
 ligands and, 24
 outer shells of, 21–22
 Electron paramagnetic resonance (EPR), 118t, 120–122, 121f
 of ISC, 262
 Electron spin echo envelope modulation (ESEEM), 121
 Electron transfer, 137f, 262f
 IET, 328
 of NADH, 110
 PCET, 275
 with proton pumping, 1–3
 in respiration, 111–112
 Electron transport
 blue copper proteins and, 280–282
 of mitochondria, 111f
 proteins for, 259–262
 Electronegativity, 21–22
 Electronic absorption spectroscopy (ABS), 118t, 125
 Electron-nuclear double resonance (ENDOR), 118t, 121
 Elemental mercury (Hg^0), 440
 Empty-tRNA-synthetases, 66–68
 Emsley, John, 444
 Enamel, 373
 Endoplasmic reticulum (ER), 217–218, 222
 ENDOR. *See* Electron-nuclear double resonance
 Enolase superfamily, 204–205, 206f
 Entatic state, 280–281
 Enterobactin, 86–87
 iron and, 87–89, 88f
 proteins and, 88f
Enterococcus hirae, 143
 copper in, 158–159, 160f
 Enzymes
 ATP and, 112–114
 bacteria in, 143, 158–159
 chromium and, 340
 cobalt and, 308
 copper and, 282–294
 fatty acids and, 107–108
 intermediary metabolism by, 96–97
 iron and, 272–275, 393–394
 magnesium and, 198–199
 manganese and, 317–319
 molybdenum and, 324–325, 325f
 nickel and, 3, 297–302
 nitrogen and, 349f
 nucleic acids and, 205–210
 oxygen and, 258
 proteins and, 3
 redox chemistry and, 5–7
 selenium and, 351
 β -strands and, 48
 sulfur and, 264–265
 tungsten and, 325f, 329–331
 zinc and, 230–244, 230f, 240f, 243f
 EPR. *See* Electron paramagnetic resonance
 ER. *See* Endoplasmic reticulum
Escherichia coli, 80–82, 81f, 140f, 142f, 362f
 cisplatin and, 421
 Fur in, 157–158
 iron and, 87–89, 138, 157
 ISC and, 262–264
 γ -phosphoryl group and, 200–201
 ribosome of, 65–66
 zinc and, 138
 ESEEM. *See* Electron spin echo envelope modulation
 EtHg. *See* Ethylmercury
 Ethylmercury (EtHg), 440
 Eubacteria
 ISC in, 79
 manganese and, 314–315
 Eukaryotes, 5–7, 62, 63f, 135
 ISC in, 79, 79f, 80
 manganese and, 314–315
 protein biosynthesis by, 62
 EXAFS. *See* Extended X-ray absorption fine structure
 Excitatory amino acid transporters (EAATs), 188, 188f
 Excitatory amino acids (EAA), 440
 Extended X-ray absorption fine structure (EXAFS), 127–128, 118t
- F**
 FAD. *See* Flavin adenine dinucleotide
 FADH, 93f
 Fats, 2
 Fat globules, 57
 Fatty acids
 biosynthesis of, 106–108, 109f
 enzymes and, 107–108
 oxidation of, 97–98
 Fatty acid synthase, 107–108
 FdxR. *See* Ferredoxin reductase
 FeEnt. *See* Ferric-enterobactin
 FeMo-cofactor, 83–85, 83f, 85f
 Fenton reaction, 13
 Fe-protein, 82–83
 Feroxidase sites, 361–362
 Ferredoxin oxidoreductase, 329–331, 329f
 Ferredoxin reductase (FdxR), 80
 Ferric oxyhydroxide, 364–365
 Ferric-enterobactin (FeEnt), 142f
 Ferrihydrite, 362, 363f, 368
 Ferritin, 365f
 iron in, 361–368, 363f, 393
 as supramolecular nanotechnology template, 367–368
 Ferroportin disease, 173, 417
 cadmium and, 437–438
 Ferroxidase, 365f, 366f
 FIT, 163–165, 164f
 Flavin adenine dinucleotide (FAD), 92, 95f, 326
 NADPH and, 352f
 XDH and, 325
 Flavin mononucleotide (FMN), 92, 95f
 Fluorine, 7, 18
 FMN. *See* Flavin mononucleotide
 N-formalMet, 66–68
 Francium, 9–10
 Frataxin, 407f
 FRDA. *See* Friedreich's ataxia
 Free radicals, 5–7, 314–317
 Friedreich, Nikolaus, 408–409
 Friedreich's ataxia (FRDA), 394, 395–401, 408–409
 D-fructose, 53–54
 Fuller, Richard Buckminster, 2
 Fullerenes, 2
 Function, 5, 5t
 Fur, 157, 157f
 DNA and, 158f
 in *E. coli*, 157–158

G

- G protein, 225, 335, 426f
lithium and, 426
- GABA. *See* γ -aminobutyric acid
- Gadolinium, 11–12
MRI and, 430–431
- D-galactose, 53–54
- Galactose oxidase, 282, 283f
- β -galactosidase, 430–431, 430f
- Gallium, 1, 17
for cancer, 425
- Gallium tris-8-quinolinolate (KP46), 425
- GAP. *See* Glyceraldehyde-3-phosphate
- Gated channels, 177, 178
- Gd-DTPA, 428–429, 428f
- Genome-sequencing, 138
- Geobacter sulfurreducens*, 135–136
- Germanium, 15, 17
- GHGs. *See* Greenhouse gases
- Giant axon, 384–385
- Globin fold, 48–49
- Gluconeogenesis, 101f, 106–108
- Glucose, 97–98, 418f–419f
carbon dioxide and, 98
chromium and, 340
hemochromatosis and, 417
hexokinase with, 199f
phosphoryl group transfer kinases and, 199–200
sodium and, 188f
water and, 98
- α -D-glucose, 53–54
- β -D-glucose, 53–54
- D-glucose, 53–54
- Glucose-6-phosphate, 102
- Glutamate, 38t–39t
calcium and, 217
 α -keto acids and, 105–106
nitrogenases and, 331–332
zinc and, 234–237, 390–391, 392
- Glutamine, 38t–39t
nitrogenases and, 331–332
- Glutathione peroxidase (GpPx), 351
- Glutathione/glutathione reductase (GSH/GR), 351
- Gluzineric, 390–391
- GlxI. *See* Glyoxylase
- Glyceraldehyde, 53–54
- D-glyceraldehyde, 54f
- Glyceraldehyde-3-phosphate (GAP), 102, 103f
- Glycerol, 57
- Glycerophospholipids, 57–58, 58f
- Glycine, 38t–39t, 373–374
- Glycogen, 55–56, 56f, 57f
- Glycogen synthase (GS), 426–427
- Glycolysis, 91, 101f
- tricarboxylic acid cycle and, 100–105
- Glycosidic bonds, 54–55, 57f
- α -glycosidic linkage, 54–55
- Glyoxylase (GlxI), 298
- Gold, 14
for arthritis, 420–421
- Golgi apparatus, 223
- GPCR. *See* G-protein-coupled metal binding receptor
- GpPx. *See* Glutathione peroxidase
- G-protein-coupled metal binding receptor (GPCR), 438
- Gram-negative bacteria, 137–138
iron and, 139f
- Gram-positive bacteria, 137–138
copper and, 158–159
iron and, 142, 143f
- Graphite, 2
- Greenhouse gases (GHGs), 344–346
- Group transfer reactions, intermediary metabolism and, 97, 97t
- GS. *See* Glycogen synthase
- GSH. *See* Sulfhydryl oxidase ALR and glutathione
- GSH/GR. *See* Glutathione/glutathione reductase
- GSK-3, 426–427
- GTP. *See* Guanosine triphosphate
- Guanine, 49, 250
- Guanosine, 245
- Guanosine triphosphate (GTP), 80–82, 106–107, 106f, 225
MoCo and, 81f

H

- HAD. *See* Haloacid dehalogenase
- Haemophilus*, 72
- Haemophilus influenzae*, 138–139
- Hafnium, 12
- Hallervorden-Spatz syndrome, 427–428, 427f
- Haloacid dehalogenase (HAD), 203–204, 203f
- Halogen, 1, 7, 353–354
- Haloperoxidases, 337
- HAMP. *See* Hepcidin antimicrobial peptide
- Hard ligands, 23–26, 23t
- H-clusters, 80–86
- hCTR1, 174
- HD. *See* Huntington's disease
- Heavy metals, 433
- Heck coupling, 14
- α -helices, 41–45
calcium and, 225
CD and, 126
iron and, 186–187
- π -helices, 45–46
- Helicobacter pylori*, 143–144
- Helium, 18
- Heme, 72
in chelataase, 77–78
cytochrome P-450 and, 323–324
iron and, 139
manganese and, 316
NFT and, 405
- Hemiacetal, 53–54, 55f
- Hemiketal, 55f
- Hemochromatosis, 173, 416
glucose and, 417
hepcidin and, 419f
insulin and, 417
- Hemocyanin, 284
- Hemoglobin, 251–252, 252f, 253f
nitrogenases and, 331–332
- Hemojuvelin (HJV), 173, 174f, 404–405
- Hemoproteins, 251–265
- Hepatic arginase, 318
- Hepatocytes, 171
- Hepcidin, 404–405, 416
hemochromatosis and, 419f
- Hepcidin antimicrobial peptide (HAMP), 173, 174f, 416
- Hereditary hemochromatosis (HH), 416
- Hexokinase, 102, 106–107
with glucose, 199f
magnesium and, 198
phosphoryl group transfer kinases by, 200–201, 200f
- Hexoses, 53–54
- HFE, 174f
- Hg⁰. *See* Elemental mercury
- HH. *See* Hereditary hemochromatosis
- HHE. *See* 4-hydroxyl-2-hexenal
- High-mobility group (HMG), 421–424
- High-spin state, 119–120
- His, 237
- Histidine, 38t–39t
copper and, 69–70, 173
distal, 252–253
proximal, 252–253
- HIV/AIDs, 415–416
- HJV. *See* Hemojuvelin
- HMG. *See* High-mobility group
- HNE. *See* 4-hydroxynonenal
- Hodgkin, Alan, 384–385
- Holliday junction resolvases, 209–210
- Homoprotocatechuate 2,3-dioxygenase (HPCD), 269f, 270
- Hookworms, 415–416
- HPCD. *See* Homoprotocatechuate 2,3-dioxygenase
- Huntington's disease (HD), 408

- Huxley, Andrew, 384–385
 Hybridization, 26, 27t
 HydG, ISC and, 86f
 Hydroformylation (OXO), 308
 Hydrogen, 2–7, 344–348
 bonding of, 9f, 35–37, 36f
 carbon with, 7–9
 nitrogen with, 7–9
 Hydrogen peroxide, 316–317, 337, 338f
 SOD and, 396–398
 Hydrogen sulfide, 351
 Hydrogenases, 75f, 299, 300f
 ATP and, 299
 Hydrolases, 229
 Hydrophobic effect, 35–37, 37f, 39–40, 57–58
 Hydrosphere, 343
 Hydroxyiminopropionic acid, 339
 Hydroxyl groups, 9f, 13, 53–54
 4-hydroxyl-2-hexenal (HHE), 398, 399f
 β -hydroxylase, 392
 4-hydroxynonenal (HNE), 398–399, 399f
 Hyperpolarization, 380, 384–385
- I**
 ICL670. *See* Deferasirox
 IDA. *See* Iron deficiency anemia
 IDE. *See* Insulin-degrading enzyme
 IET. *See* Intramolecular one-electron transfer
 I-Hg. *See* Inorganic mercury
 Imidazole (Im), 424
 IMPase. *See* Inositol phosphatases
 Indazole (Ind), 424
 Inorganic mercury (I-Hg), 439–440
 Inositol phosphatases (IMPase), 426f
 Inositol-(1,4,5)-trisphosphate (IP₃), 217–218, 219f, 222
 Insulin, 339–340
 hemochromatosis and, 417
 Insulin-degrading enzyme (IDE), 407
 Intermediary metabolism
 anabolism and, 105–106
 catabolism and, 97–98
 by enzymes, 96–97
 fatty acid biosynthesis and, 106–108
 gluconeogenesis and, 106–108
 glycolysis and, 100–105
 group transfer reactions and, 97, 97t
 redox and, 92
 tricarboxylic acid cycle and, 100–105
 Intramolecular one-electron transfer (IET), 328
 Iodine, 1, 7, 18, 353–358, 357f
 Iodothyronine deiodinases (DIOs), 351
 Iodothyroninyl, 356–358
 Ionic bonding, 21–22
 IP₃. *See* Inositol-(1,4,5)-trisphosphate
 IPNS. *See* Isopenicillin N-synthase
 IRE. *See* Iron-responsive element
 IREG1, 170
 IREs. *See* Iron regulatory elements
 Iridium, 13
 Iron, 5, 7, 13, 164f, 174f, 418f–419f
 AD and, 404
 aluminum and, 434–435
 bacteria and, 138
 BBB and, 393
 binding sites for, 73f
 biological importance of, 250
 in brain, 388–394
 CcO and, 393–394
 in chelataase, 77–78, 78f
 chelators, 147f, 417–419
 chemistry of, 248
 coordination geometry for, 254
 copper and, 295
 CP and, 413–414
 cysteine and, 69–70
 cytosol and, 142–143
 deficiency responses, 165, 165f
 E. coli and, 87–89, 138, 157
 enterobactin and, 87–89, 88f
 enzymes and, 272–275, 393–394
 EXAFS and, 127–128
 in ferritin, 361–368, 363f, 393
 FRDA and, 408–409
 in fungi, 167, 169
 Gram-negative bacteria and, 139f
 Gram-positive bacteria and, 142, 143f
 HD and, 408
 α -helices and, 186–187
 heme and, 139
 in hepatocytes, 171
 lead and, 440–443
 in macrophages, 171
 in mammals, 151, 152f, 171–173
 in mitochondria, 152–153, 167
 Mössbauer spectroscopy for, 117
 neurodegeneration and, 395–401
 NFT and, 405
 nitrogen fixation and, 348
 oxygen and, 248–249, 249f
 PD and, 401–402
 phytoplankton and, 133–134
 in plants, 148, 148f, 161–162, 162f, 163, 163f
 prokaryotes and, 147
 proteins and, 157, 250–251, 267–270
 in *Saccharomyces cerevisiae*, 146f, 167, 169
 siderophores and, 138, 139, 169
 Tf and, 139, 141–142, 152–153, 152f, 393
 uptake of, 171f
 water and, 248
 yeast and, 146
 Iron Age, 247
 Iron cation properties, 197t
 Iron deficiency anemia (IDA), 415–416
 Iron regulatory elements (IREs), 171–173, 172f
 Iron regulatory protein (IRP), 171–173, 437–438
 PD and, 401
 Iron-responsive element (IRE), 437–438
 Iron-sulfur clusters (ISC), 74, 74f, 79–80, 110–111, 262–265, 266f
 in eukaryotes, 79f, 80
 HydG and, 86f
 IRP. *See* Iron regulatory protein
 ISC. *See* Iron-sulfur clusters
 Isocitrate, 102–104
 Isoleucine, 38t–39t, 98f
 Isomerases, 229
 Isopenicillin N-synthase (IPNS), 268
 Itai-Itai disease, 437
 IYT. *See* N-acetyl-diiodo-tyrosyl-D-threonine
- J**
 Juvenile hemochromatosis, 173
- K**
 KcsA potassium channel, 182–183, 182f, 184, 184f
 Keilin, David, 259–260
 Kendrew, John, 251–252
 α -keto acid, 105–106
 carbon dioxide and, 102–104
 α -ketoglutarate and, 102–104
 β -keto acid, 99f
 α -keto acid-dependent enzymes, 268
 Keto groups, 9f
 α -ketoglutarate, 105–106
 α -keto acid and, 102–104
 Ketone, 53–54
 Ketose, 53–54, 54f
Klebsiella, 332
 Klug, Aaron, 244–245
 Knowles, Jeremy, 200
 KP46. *See* Gallium tris-8-quinolinolate
 K-pathway, 257
 Krebs cycle, 102–104, 108
- L**
 Labile plasma iron (LPI), 419–420
 Laccase, 281–282
 β -lactam antibiotics, 240–241
Lactobacilli, 13, 303
Lactobacillus plantarum, 317f

- Lanthanides, 428–429
 Lanthanum, 11
 LCPA. *See* Long chain polyamines
 Lead, 440–443
 toxicity of, 1, 433
 Leading strands, 60–62
 Leghemoglobin, 331–332
 Leitmotif, 2
 Leucine, 38t–39t
 sodium and, 187–188
 Leucine aminopeptidases, 242f
 LeuT, 178–179, 187–188
 Lewis, G.N., 23
 Lewis acid, magnesium and, 198
 Lewy bodies, PD and, 401, 403f
 LFT. *See* Ligand field theory
 Ligands. *See also specific ligands*
 amino acids as, 69
 coordination bonds in, 23
 Ligand binding, 5, 5t
 Ligand field theory (LFT), 29–34
 Ligand-gated channels, 177, 222
 RyR as, 223
 Ligases, 229
 Limbic system, 390–391
Limulus polyphemus, 284, 286f
 Lipid bilayers, 58–59
 Lipids, 57–59
 Lipoate, 92
 Lipoxigenases (LOXs), 270
 Lithium, 9
 with aluminum, 9
 for bipolar disease, 425
 for depression, 1
 in drugs, 425–427
 G protein and, 426
 Lithium carbonate, 420–421
 Lithosphere, 343
 Litvinenko, Alexander, 444
 Long chain polyamines (LCPA),
 376–377
 Lou Gehrig's disease. *See* Amyotrophic
 lateral sclerosis
 Low-molecular-weight inorganic anions,
 72
 Low-spin state, 119–120
 LOXs. *See* Lipoxigenases
 LPI. *See* Labile plasma iron
 Lysine, 38t–39t, 400–401
 Lysyl oxidase, 282
- M**
M. capsulatus, 292–293, 293f
M. thermoautotrophicum, 302–303
 α_2 -macroglobulin, 173
 Macrophages, 171
 MAD. *See* Multiple anomalous scattering
 Magnesium, 3, 4, 10
 ATP and, 10–11, 197
 calcium and, 215
 carbon dioxide and, 210
 coordination geometry of, 198
 enolase superfamily and, 204–205,
 206f
 enzymes and, 198–199
 Lewis acid and, 198
 ligands, 24
 phosphatases and, 203f, 204f
 photoreception and, 210–213
 porphyrins and, 211
 redox and, 211
 Magnesium cation properties, 197t
 Magnetic circular dichroism (MCD), 118t,
 126
 Magnetic resonance imaging (MRI), 1,
 11–12, 12f, 427f
 apoferritin and, 429, 430f
 calcium and, 430–431, 431f
 contrast agents for, 427–431
 gadolinium and, 430–431
 magnetite for, 368
 Magnetic susceptibility, 118t
 Magnetism, 119–120
 Magnetite, 368–370
 Magnetosome island (MAI), 369f,
 370f
 Magnetotactic bacteria (MTB), 368–370,
 369f
 MAI. *See* Magnetosome island
 Major intrinsic proteins (MIPs), 15
 antimony and, 16–17
 arsenic and, 16–17
 Malaria, 415–416
 Malmström, Bo, 280
 Malonyl/acetyl-CoA-ACP transacylase
 (MAT), 108
 Maltose, 54–55, 55f
 Mandelate racemase (MR), 204–205,
 206f
 Manganese, 5, 13
 calcium and, 314, 315f
 catalases and, 317f, 318f
 chemistry and biochemistry of, 311
 enzymes and, 317–319
 in mammals, 318
 oxygen and, 311–314
 oxygen free radicals and, 314–317
 SOD and, 314–315, 316f
 toxicity of, 1
 MAO. *See* Monoamine oxidase
 MAP kinase kinase kinases (MKKKs),
 202
 MAPK. *See* Mitogen-activated protein
 kinases
 MARCKS. *See* Myristoylated alanine-rich
 C kinase substrate
 MAT. *See* Malonyl/acetyl-CoA-ACP
 transacylase
 Matrix metalloproteinases (MMPs), 234,
 235f, 236f
 Maturation, of RNA, 62, 63f
 MCD. *See* Magnetic circular dichroism
 McMunn, C.A., 259–260
 MCP. *See* MoCo carrier protein
 MCR. *See* Methyl-coenzyme M reductase
 MeHg. *See* Methylmercury
 Menkes disease, 412–414
 N⁷-mercaptoheptanoylthreonine
 phosphate (CoBSH), 302–303
 Mercuric chloride, 439–440
 Mercury, 11, 439–440, 439f
 toxicity of, 14–15, 433, 441f
 Messenger RNA (mRNA), 52, 62, 63f
 lead and, 440–443
 translation of, 171–173, 172f
 Metal assimilation. *See also specific
 metals*
 in bacteria, 137–144
 biochemistry of, 133–136
 in fungi, 144–151
 in mammals, 151–153
 in plants, 144–151
 Metal ions. *See also specific metals*
 in bacteria, 155–161
 in fungi, 161–170
 magnetic properties of, 119–120
 in mammals, 170–175
 in plants, 161–170
 Metal-based neurodegeneration
 hypothesis, 396
 Metal-binding pterin molybdopterin
 (MTP), 80–82, 81f
 Metal-ion-binding, 70f. *See also specific
 metals*
 amino acid residues and, 69–72
 chelataase and, 77–79, 77f
 cofactors and, 72–76
 with ISC, 79–80
 low-molecular-weight inorganic anions
 and, 72
 metalloproteins and, 76–77
 in porphyrins, 77–78, 78f
 siderophores and, 86–89
 Metalloenzymes, 60
 Metalloids, 15
 transport systems of, 16f
 Metallopeptidase, 243f
 Metalloproteinases, 232–237
 Metalloproteins, 76–77
 Metallothionein (MT), 174–175
 AD and, 407

cadmium and, 438
 zinc and, 389, 391f

Methaemerythrin, 273–274, 273f

Methane, 5–7, 292–293, 347
 cofactors and, 72
 methanotrophs and, 143–144

Methane monooxygenases (MMOs), 292–293

Methanococcus, 204f

Methanotrophs, 143–144

Methionine, 38t–39t, 400–401
 sulfur of, 69–70
 vitamin B₁₂-dependent
 methyltransferases and, 307

Methionine synthase reductase (MSR), 307, 308f

Methyl group
 to acetyl-CoA, 297–298
 of valine, 64–65

Methyl-coenzyme M reductase (MCR), 297–298, 302–303, 304f

N-methyl-D-aspartate (NMDA)
 cadmium and, 438
 calcium and, 217
 copper and, 407
 VGCC and, 387–388
 zinc and, 388–391

N-methyl-D-aspartate excitatory amino acid receptor (NMDAR), 443

Methylglyoxal, 298

Methylmercury (MeHg), 439–440
 selenium and, 440

N-methylmesoporphyrin, 78f

Mfn. *See* Mitochondrial transport carriers mitoferrin

Michaelis complex, 234–237

Microbial superoxide dismutases, 270

Microglia, 379–380

Minamata disease, 439, 439f

MIPs. *See* Major intrinsic proteins

MIR. *See* Multiple isomorphous replacement

MIT. *See* Monoiodotyrosines

Mitochondria
 aluminum and, 435
 calcium in, 223, 224f
 electron transport chain of, 111f
 FRDA and, 408
 iron in, 152–153, 167
 zinc and, 389

Mitochondrial transport carriers mitoferrin (Mfn), 170

Mitogen-activated kinase (MAPK), 387–388

Mitogen-activated protein kinases (MAPKs), 202, 202f

MKKKs. *See* MAP kinase kinase kinases

MLE. *See* Muconate lactonizing enzyme

MMOH, 273–274, 273f

MMOs. *See* Methane monooxygenases

MMPs. *See* Matrix metalloproteinases

Mobility, 5, 5t

MoCo. *See* Molybdenum cofactor

MoCo carrier protein (MCP), 82

MoFe-protein, 82–83

Molecular orbital theory (MOT), 31–32

Molecular oxygen, 135

Mollusks, 370–376, 373f

Molybdenum, 5–7, 12–13, 74–76, 75f, 329f
 AO of, 328f
 chemistry and biochemistry of, 323–324
 enzymes and, 324–325, 325f
 nitrogen fixation and, 348
 SO and, 330f

Molybdenum cofactor (MoCo), 80–86
 GTP and, 81f

Molybdenum hydroxylases, 326, 328f

Monoamine oxidase (MAO), 401–402

Monocots, 162, 165–166

Monoiodotyrosines (MIT), 356–358, 357f

Monooxygenase, 323–324

Monosaccharides, 53–54

Mood disorders, 425–426

Mössbauer, Rudolf, 122

Mössbauer spectroscopy, 118t, 122–124, 123f
 for iron, 117

MOT. *See* Molecular orbital theory

MR. *See* Mandelate racemase

MRI. *See* Magnetic resonance imaging

mRNA. *See* Messenger RNA

MSR. *See* Methionine synthase reductase

MT. *See* Metallothionein

MTB. *See* Magnetotactic bacteria

MTF1, 174–175

MthK potassium channel, 184, 184f

MTP. *See* Metal-binding pterin molybdopterin

Muconate lactonizing enzyme (MLE), 204–205, 206f

Multicopper oxidases, 287

Multiple anomalous scattering (MAD), 129–131

Multiple isomorphous replacement (MIR), 129–131

Multiple sclerosis, 395–401

Mycobacterium, 157

Myelin, 393–394

Myoglobin, 252f

Myohaemerythrin, 48f

Myristoylated alanine-rich C kinase substrate (MARCKS), 426

N

NAADP. *See* Nicotinic acid adenine dinucleotide phosphate

Na/Ca exchanger (NCX), 218, 219f

NAD⁺. *See* Nicotinamide adenine dinucleotide

NADH-Coenzyme Q oxidoreductase, 110

NADPH. *See* Nicotinamide adenine dinucleotide phosphate

NAFT. *See* Nuclear factor of activated T-cells

Nautilus repertus, 370, 371f

NCX. *See* Na/Ca exchanger

N-domain, 218–220

Neisseria, 72

Neisseria gonorrhoeae, 138–139

Neisseria meningitidis, 73f, 138–139

Neodymium, 11

Neon, 18

Nernst, Walther, 29

Nerve cells, 379–380, 380f, 381f

Neurodegeneration. *See also specific diseases*
 copper and, 395–401, 412–414
 iron and, 395–401
 proteins and, 397f
 zinc and, 395–401

Neurofibrillary tangles (NFT), 404
 heme and, 405
 iron and, 405

Neuromelanin (NM), 393

Neurotransmitters, 380–382
 copper and, 392

NFATc4, 387f

Nfs1, 80

NFT. *See* Neurofibrillary tangles

Nickel, 13, 14, 300f
 enzymes and, 3, 297–302
 for metabolism, 5–7

Nicotianamine, 149f

Nicotinamide, 97

Nicotinamide adenine dinucleotide (NAD⁺), 80, 92, 93f
 anabolism and, 105
 electron transfer of, 110
 glycolysis and, 100–102
 zinc and, 237

Nicotinamide adenine dinucleotide (NAD⁺), 91–92, 93f
 XDH and, 325

Nicotinamide adenine dinucleotide phosphate (NADPH), 91–92
 anabolism and, 105
 FAD and, 352f
 phagosome and, 396–398

Nicotinic acid adenine dinucleotide phosphate (NAADP), 223
 Niobium, 12
 Nitrate, 349–350
 Nitrate reductase (NR), 82
 Nitric oxide (NO), 396–398
 Nitric oxide synthase (NOS), 396–398
 Nitrification, 349–350
 Nitrile hydratase, 308
 Nitrite reductase, 281–282, 293
 Nitrogen, 2, 3, 4
 chlorine and, 354–355
 enzymes and, 349f
 with hydrogen, 7–9
 oxygen and, 349–350
 tyrosine and, 401
 Nitrogen cycle, 348–350
 Nitrogen dioxide, 396–398
 Nitrogen fixation, 82–83, 84f, 348
 ATP for, 332–335
 in plants, 147–148
 Nitrogen oxide, 17
 Nitrogenase, 75f, 331–337, 332f, 336f
Nitrosomonas spp., 349–350
 Nitrous oxidase, 75f
 Nitrous oxide, 86
 Nitrous oxide reductases, 294, 294f
 NM. *See* Neuromelanin
 NMDA. *See* N-methyl-D-aspartate
 NMDAR. *See* N-methyl-D-aspartate
 excitatory amino acid receptor
 NMR. *See* Nuclear magnetic resonance
 NO. *See* Nitric oxide
 Noble gases, 18
 NOESY. *See* Nuclear Overhauser effect
 spectroscopy
 Noncorrin cobalt-containing enzymes, 308
 Nonredox di-manganese enzymes, 317–319
 Norepinephrine, 393–394
 Northrop, John, 3
 NOS. *See* Nitric oxide synthase
 NR. *See* Nitrate reductase
 NTA, 434–435
 Nuclear factor of activated T-cells (NAFT), 387–388
 Nuclear magnetic resonance (NMR), 118t, 124–125
 Nuclear Overhauser effect spectroscopy (NOESY), 124
 Nucleic acids, 2, 62–64. *See also* DNA; RNA
 enzymes and, 205–210
 hydrogen and, 7–9
 phosphoryl group transfer kinases and, 207–208, 207f

secondary and tertiary structures of, 50–68
 structural building blocks of, 49–50, 49f
 Nucleotidyl-transferase family, 209–210

O

Octopus dofleini, 284, 286f
 Okazaki fragments, 60–62
 Olefin, 13
 Oligodendrites, 393
 Oligodendrocytes, 379–380
Oligotropha carboxidovorans, 324, 326
 OMTs. *See* Outer-membrane transporters
 Orbital overlap, 22
 Osmium, 13
 Outer-membrane transporters (OMTs), 140f
 ATP and, 140–141
 Oxaloacetate, 105–107
 pyruvate to, 106f
 succinate to, 108
 Oxidative phosphorylation, 1
 Oxidoreductases, 229
 OXO. *See* Hydroformylation
 Oxygen, 2–4, 344–348. *See also specific oxygen forms and processes*
 aluminum and, 434–435
 enzymes and, 258
 hemoproteins and, 251–265
 iron and, 248–249, 249f
 manganese and, 311–314
 nitrogen and, 349–350
 nitrogenases and, 331–332
 XO and, 326–327
 Oxygen cycle, 347, 347f
 Oxygen free radicals, 5–7
 manganese and, 314–317
 Oxygen paradox, 13, 249

P

P. furiosus, 308
P. pachydermatina, 370–371, 372f
 Palladium, 14
 PAPS. *See* 3'-phosphoadenosine-5'-phosphosulfate
Paracoccus denitrificans, 288
 Parallel β -pleated sheets, 45–46
 Parkin, 402–404, 403f
 Parkinson's disease (PD), 393, 394, 395–401, 403f
 iron and, 401–402
 Pasteur, Louis, 108
 Pauling, Linus, 42
 PBGS. *See* Porphobilinogen synthase
 PBP. *See* Periplasmic-binding protein
 PCD. *See* Protocatechuate 3,4-dioxygenase
 PCET. *See* Proton-coupled electron transfer
 P-cluster, 80–86, 83f, 335
 PD. *See* Parkinson's disease
 PDE. *See* Phosphodiesterase
 Penicillin, 240–241
 Pentoses, 53–54
 PEPCK. *See* Phosphoenolpyruvate carboxykinase
 Pepsin, 3
 X-ray diffraction and, 128–129
 Peptide-bond formation, 67f
 Peptidyl-glycine α -hydroxylating monooxygenase (PMH), 282, 283, 284f
 Peptidyl-tRNA-synthetases, 62, 66–68
 Periplasmic-binding protein (PBP), 139, 141–142, 144
 Peroxidases, 254, 258
 Peroxynitrite, 401
 Perutz, Max, 251–252
 Petrobactins, 137f
 Phagocytosis cells, 379–380
 Phagosome, 396–398
 Phenoxide, 69–70
 Phenylacetylene, 367
 Phenylalanine, 38t–39t
 Phi angle, 42, 43f
 Phosphatases
 magnesium and, 204f
 phosphoryl group transfer kinases by, 203–204, 204f
 vanadium and, 337, 339–340
 Phosphate
 ferritin and, 366
 ligands, 24
 lipids and, 57–58
 phosphorus and, 348
 zinc and, 229
 Phosphatidic acid, 57–58
 Phosphatidylcholine, 241
 Phosphatidylinositol-4,5-bisphosphate (PIP₂), 225
 Phosphatidylserine, 430–431
 Phosphine, 348
 3'-phosphoadenosine-5'-phosphosulfate (PAPS), 350–351, 350f
 Phosphodiesterase (PDE), 426
 Phosphoenolpyruvate, 95f, 106–107, 107f
 pyruvate to, 106f
 Phosphoenolpyruvate carboxykinase (PEPCK), 106–107
 Phosphoesters, 241
 Phosphofructokinase, 106–107
 magnesium and, 198
 3-phosphoglycerate, 102

- Phosphoglycerate kinase, 198
 Phosphoinositide cascade, 226f
 Phosphoinositide-4,5-bisphosphate (PIP), 426
 Phospholamban, 222
 Phospholipase C (PLC), 225, 241, 426
 Phospholipid bilayers, 2, 4
 Phosphopantetheine group, 108f
 Phosphorus, 2, 3, 344–348
 redox and, 348
 γ -phosphoryl group, 200–201, 201f
 Phosphoryl group transfer kinases, 199–202
 by hexokinase, 200–201, 200f
 nucleic acids and, 207–208, 207f
 by phosphatases, 203–204, 204f
 Photoferritins, 163
 Photolysis, 347–348
 Photoreception, 210–213
 Photosynthesis, 311–314, 347
 carbon cycle and, 344
 carbon dioxide from, 133–134
 manganese and, 311
 organisms with, 347–348
 in plants, 147–148
 Photosystem II (PSII), 1, 312
 cofactors with, 313f
 PHOX, 146
 Phytoferritin, 166
 Phytoliths, 377
 Phytoplankton, 133–134
 iron and, 133–134
 photosynthesis and, 347–348
 PIP. *See* Phosphoinositide-4, 5-bisphosphate
 PIP₂. *See* Phosphatidylinositol-4, 5-bisphosphate
 Pitchblende, 10–11
 PKA. *See* Protein kinase A
 PKC. *See* Protein kinase C
 Plasma membrane, 58–59, 59f
 copper and, 168
 of yeast, 168
 zinc and, 168–169
 Plasma membrane calcium ATPase (PMCA), 218, 222
 Plastocyanin, 281f
 Plastoquinone, 312
 Platinum, 29
 for cancer, 420–421, 424
 cisplatin and, 424
 PLC. *See* Phospholipase C
 β -pleated sheets, 41–42, 44–46
 PLP. *See* Pyridoxal phosphate
 PMCA. *See* Plasma membrane calcium ATPase
 PMH. *See* Peptidyl-glycine
 α -hydroxylating monooxygenase
 Poisons, 443–445
 Polonium, 10–11, 17
 poisoning with, 444–445
 Polyglutamine (polyQ), 408
 Polypeptide chains, 37–39, 42f, 43f
 polyQ. *See* Polyglutamine
 Polysaccharides, 2, 55–56, 370, 376–377
 Polyunsaturated fatty acids (PUFA), 398, 399f
 Porphobilinogen synthase (PBGs), 237, 440–443
 Porphyrins, 24, 25f, 316–317
 cofactors in, 72
 magnesium and, 211
 metal-ion-binding in, 77–78, 78f
 Post-transcriptional processing, 62, 63f
 Potassium, 3, 4, 9
 action potential for, 179f
 binding sites for, 10f, 180f
 channels for, 177, 179–180
 in ionic gradients, 9
 pumps for, 177
 selectivity filter, 183f
 vs. sodium, 178–180
 Potassium cation properties, 197t
 Potassium channels, 180–184, 181f
 in brain, 384–388, 385f
 KcsA, 182f, 184f
 MthK, 184, 184f
 PPs. *See* Protein phosphatases
 Primary structure, of proteins, 41–50, 41f
Prochlorococcus, 135
 Prokaryotes, 62
 Dps in, 155–156
 iron and, 147
 Prolidases, 308
 Proline, 37–39, 38t–39t, 400–401
 Proteins. *See also specific proteins*
 amino acids, 38t–39t
 building blocks of, 37–41
 cadmium and, 438
 carbonyl and, 400–401, 400f
 chelate effect in, 26
 chromium and, 340
 copper and, 280
 for electron transport, 259–262
 enterobactin and, 88f
 enzymes and, 3
 hydrogen and, 7–9
 iron and, 157, 250–251, 267–270
 neurodegeneration and, 397f
 selenium and, 351
 structures of, 41–50, 41f
 synthesis of, 67f, 68
 Protein crystallography, 128–129
 Protein kinase A (PKA), 426
 Protein kinase C (PKC), 426
 Protein phosphatases (PPs), 426
 Prothrombin, 71
 Protocatechuate 3,4-dioxygenase (PCD), 270, 271f
 Proton pumping
 by complexes, 111
 electron transfer with, 1–3
 Proton-coupled electron transfer (PCET), 275
 Proton-motive Q cycle, 262f
 Protoporphyrin IX, 77–78, 259–260
 chlorophyll and, 210–211
 Proximal diiodotyrosine, 356–358
 Proximal histidine, 252–253
 PrP, 410–411, 410f
 Pseudoalterobactins, 137f
Pseudomonas aeruginosa, 138–139, 140f, 157
Pseudomonas putida, 204–205
 Psi angle, 42, 43f
 PSII. *See* Photosystem II
 PsP, 411–412, 411f
 Pterin-dependent hydroxylases, 268
 P-type ATPases, 218–220
 PUFA. *See* Polyunsaturated fatty acids
 Pumps. *See also* Proton pumping
 for calcium, 218–220, 220f, 221f
 for potassium, 177
 for sodium, 177
 SPCA, 218–220, 222
 Purine, 49
 Purkinje neurons, 392–393
Pyococcus horikoshii, 189–190
 Pyridoxal phosphate (PLP), 80
 Pyrimidine, 49
 Pyrophosphate, 60
 Pyruvate, 97–98, 100–104
 to oxaloacetate, 106f
 to phosphoenolpyruvate, 106f
 Pyruvate kinase, 198
- ## Q
- Quaternary structure, of proteins, 41–50, 41f
- ## R
- R. rubrum*, 301
 Radium, 10–11
Ralstonia metallidurans, 160–161
 Ramachandran, G.N., 43
 Reactive nitrogen species (RNS), 396–398
 Reactive oxygen species (ROS), 396
 cadmium and, 437
 DNA and, 396, 401
 redox and, 398

- Recoil-free γ -ray resonance absorption, 122
- Redox, 28–34
cadmium and, 438
enzymes and, 5–7
intermediary metabolism and, 92
magnesium and, 211
pairs, 28
phosphorus and, 348
ROS and, 398
- Refolding, 410–411
- Relaxation, 124
- Replication
of DNA, 60–62
of RNA, 59, 60–62
- Resonance Raman spectroscopy, 118t, 126–127
- Respiration
ATP and, 110
carbon cycle and, 344
electron transfer in, 111–112
in plants, 147–148
- Reverse turns, 41–42
- R-groups, 41
- Rhamnogalacturonan, boron and, 15–16
- Rhenium, 13
- Rhizobium*, 331–332
- Rhodium, 13
- Rhodobacter spheroides*, 255, 256f, 257, 328–329
- Rhodospseudomonas viridis*, 211–213
- Rhombic iron-sulfur, 74, 74f, 262–264
- Riboflavin, *See* Vitamin B₁₂
- Ribonucleases, vanadium and, 337
- Ribonucleotide reductases (RNRs), 250, 250f, 251f
- D-ribose, 53–54
- Ribosomal RNA (rRNA), 52, 62
- Ribosomes, 59, 197
of *E. coli*, 65–66
- Ribozymes, 10–11
- Rieske dioxygenases, 268
- Ringer, Sidney, 215
- Rio Tinto River, 443–444, 443f
- RNA. *See also specific RNA types*
base structure of, 52
binding motifs, 244–246
forms of, 52
maturation of, 62, 63f
nucleic acids in, 50
replication of, 59–62
transcription of, 59, 62
translation of, 59, 62–68
- RNR-R2, 273–274, 273f
- RNRs. *See* Ribonucleotide reductases
- RNS. *See* Reactive nitrogen species
- Robertson, J. Monteath, 129–131
- ROH, 241
- Root hairs, 165
- ROS. *See* Reactive oxygen species
- rRNA. *See* Ribosomal RNA
- Rubidium, 9–10
- Rubredoxins, 74, 74f, 262–264
- Rubreythrin, 273–274, 273f
- Rusticyanin, 281–282
- Ruthenium
for cancer, 424
olefin and, 13
- Ryanodine receptor (RyR), 218, 219f
as ligand-gated channel, 223
- ## S
- Saccharomyces cerevisiae*, 144–146
copper in, 170
iron in, 146f, 167, 169
zinc in, 168–169, 169f, 170
- Salicylic acid, 325–326
- Salvarsan, 420–421
- SAM. *See* S-adenosylmethionine
- Sarcoplasmic reticular calcium-ATPase (SERCA), 186–187, 217–218, 221
phospholamban and, 222
- Sarcoplasmic reticulum (SR), 220–221
- Saturnism, 440–443
- Sayers, Dorothy, 444
- SBP. *See* Substrate-binding proteins
- Scandium, 11
- Scanning electron microscopy (SEM), 376f
- Schistosomiasis, 415–416
- Schrock, Richard R., 335–337
- SDH. *See* Sulfite dehydrogenases
- SDR, 237, 238f
- SDVs. *See* Silica deposition vesicles
- Secondary hemochromatosis, 417–419
- Secondary structure, of proteins, 41–50, 41f
- γ -secretase, 404–405
- β -secretase, 404–405
- Secretory diarrhea, 355
- Sedimentation coefficients, 65–66
- Seeding, 410–411
- Selenium, 1, 7, 350–353
arsenic and, 17
enzymes and, 351
MeHg and, 440
proteins and, 351
- Selenocysteine, 37–39, 299–300, 352f
- Selenophosphate synthetase (SPS2), 352f
- SEM. *See* Scanning electron microscopy
- SERCA. *See* Sarcoplasmic reticular calcium-ATPase
- Serine, 38t–39t
tRNA and, 64–65
- Serotonin, 393–394
- Serratia marcescens*, 138–139
- SerRS. *See* Seryl-tRNA synthetase
- Seryl-tRNA synthetase (SerRS), 351–353, 352f
- Sexual disorders, 319
- Seyler, Hoppe, 259–260
- β -sheets
AD and, 405–407
CD and, 126
HD and, 408
pleated, 41–42
- Shewanella oneidensis*, 135–136
- Side-chain hydroxyl group, 64–65
- Siderophores, 76, 86–89, 87f, 135, 136f, 137f
iron and, 138, 139, 169
uptake pathway, 142f
vanadium and, 339
- Silica deposition vesicles (SDVs), 376–377
- Silicon, 7, 15
biomineralization and, 376–377
collagen and, 16
- Silver, 14
- Simple lipids, 57
- SLC30, 389
- SMA. *See* Spinal muscular atrophy
- sMMO, 274–275, 274f
- SMN. *See* Survival Motor Neuron
- SNPC. *See* Substantia nigra pars compacta
- SO. *See* Sulfite oxidase
- SOC entry (SOCE), 217–218
- SOCs. *See* Store-operated channels
- SOD. *See* Superoxide dismutase
- Sodium, 3, 4, 9
action potential for, 179f
active transport and, 187–190
binding sites for, 180f
in calcium channels, 384–388
glucose and, 188f
in ionic gradients, 9
NCX, 218, 219f
vs. potassium, 178–180
pumps for, 177
- Sodium channels, 177, 184
in brain, 384–388
- SOEs. *See* Sulfite oxidizing enzymes
- Soft ligands, 23–26, 23t
- Soil acidification, 434
- Soil organic carbon (SOC), 344–346
- SPCA. *See* Calcium pump of the secretory pathway
- Spectroscopy techniques, 117, 118t
- Spinal muscular atrophy (SMA), 392

- Sponges, 377
 SPS2. *See* Selenophosphate synthetase
 SQUID. *See* Superconducting quantum interference device
 SR. *See* Sarcoplasmic reticulum
 S-state cycle model, 314f
 Standard redox potential, 110
Staphylococci, 86–87
 Staphyloferrin A, 86–87
 Starch, 55–56, 57f
 Stearic acid, 58f
 Stearoyl-acyl carrier protein Δ^9 desaturases, 273–274, 273f
 Stellacyanin, 281–282
 STIM1, 217f
 Stone Age, 247
 Store-operated channels (SOCs), 217–218
 β -strands, 43, 45–46, 48
 SOD and, 292f
 of TIM, 204–205
Streptomyces, 157
Streptomyces griseus, 241
Streptomyces lividans, 181
Strongylocentrotus purpuratus, 373
 Strontium, 10–11
 Substantia nigra pars compacta (SNPC), 401
 Substrate-binding proteins (SBP), 144
 Succinate, 108
 Succinate dehydrogenase, 110–111
 Sugars, 54–55. *See also* Glucose
 sodium and, 187–188
 Sulfhydryl oxidase ALR and glutathione (GSH), 80
 Sulfite dehydrogenases (SDH), 328
 Sulfite oxidase (SO), 82, 324, 328–329
 molybdenum and, 330f
 Sulfite oxidizing enzymes (SOEs), 328
 Sulfite reductase, 350–351
 Sulfur, 2, 4, 350–353, 360f. *See also* Iron-sulfur clusters
 cadmium and, 437–438
 C-terminal thiocarboxylate and, 72
 enzymes and, 264–265
 of methionine, 69–70
 Sulfur dioxide, 17
 Sumner, James, 3
 Superconducting quantum interference device (SQUID), 119
 Superoxide dismutase (SOD)
 ALS and, 409, 409f
 copper and, 76–77, 76f, 291, 392
 in cytosol, 392
 hydrogen peroxide and, 396–398
 manganese and, 311, 314–315, 316f
 β -strand and, 292f
 Survival Motor Neuron (SMN), 392
 Suzuki coupling, 14
 Synapses, 379–380, 380f, 382f
 zinc and, 390–391
 Synaptogmins, 388
Synechococcus, 135
Synechocystis, 160
 α -synuclein, 401–404, 403f
 Syphilis, 420–421
- ## T
- T3. *See* 3,3',5-triiodothyronine
 T4. *See* 3,3',5,5'-tetraiodothyronine
 T7, 237
 Technetium, 1, 13
 Tellurium, 15
 Terbium, 11
 Tertiary structure, of proteins, 41–50, 41f
 Tetraethylammonium, 180–181
 Tetrahydrofolate, 307
 3,3',5,5'-tetraiodothyronine (T4), 356–358
 Tetrapyrroles, 77–79, 77f
 Tetroxide, 13
 Tf. *See* Transferrin
 TFR. *See* Transferrin receptor
 TGES loop, 222
 TGN. *See* Trans-Golgi network
 TH. *See* Tyrosine hydroxylase
 Thalassemia, 24, 415–419
 Thermolysin, 233f
 Thiolate ligand, 126
 Thompson, D'Arcy, 359
 Threonine, 38t–39t, 400–401
 Threonyl-tRNA synthetase, 64–65
 Thymine, 49
 Thyroid peroxidase, 356–358
 TIM. *See* Triose phosphate isomerase
 Timm-Danscher staining, 390f
 Tin, 7, 18
 Titanium, 12
 ToMOH, 273–274, 273f
 Trans Golgi network, 174
 Transcription, 62
 of RNA, 59
 Transcription factors, 387f
 cadmium and, 438
 Transfer RNA (tRNA), 52, 53f, 62–68
 amino acids and, 65–66
 binding sites of, 66–68
 cysteine and, 62–64
 selenium and, 351–353
 serine and, 64–65
 Transferases, 229
 Transferrin (Tf), 72, 73f
 aluminum and, 435
 iron and, 139, 141–142, 152–153, 152f, 393
 oligodendrites and, 393
 PD and, 401–402
 vanadium and, 339–340
 Transferrin receptor (TFR), 173, 174f, 401–402
 Trans-Golgi network (TGN), 413
 Transition metals, 11
 Translation, 62–68
 of mRNA, 171–173, 172f
 of RNA, 59
 Transport proteins
 binding sites in, 10f
 β -strands and, 48
 Tricarboxylic acid cycle, 91, 97–98, 102–104, 104f, 105f
 anabolism and, 105–106
 glycolysis and, 100–105
 Triglycerides, 57, 97–98
 3,3',5-triiodothyronine (T3), 356–358
 Triose phosphate isomerase (TIM), 47–48, 47f
 β -strands of, 204–205
 Trioses, 53–54, 54f
 tRNA. *See* Transfer RNA
 Trojan horse strategy, 437–438
 Trypsin, 3
 Tryptophan, 38t
 Tryptophan hydroxylase, 393–394
 Tungsten, 12–13, 329f
 chemistry and biochemistry of, 323–324
 enzymes and, 325f, 329–331
 Tunicates, 339
 TVGYG, 181
 Tyrosinase, 284, 285, 287f
 Tyrosine, 38t–39t
 nitrogen and, 401
 phenoxide of, 69–70
 Tyrosine hydroxylase (TH), 393–394
 dopamine and, 401–402
- ## U
- Ubiquinone, 92
 Ubiquitin, 402–404, 403f
 cadmium and, 438
 Ubiquitin C-terminal hydrolase L1 (UCH-L1), 402–404, 403f
 Uracil, 250
 Urease, 3, 5–7, 298–299
 8-¹⁸O-uric acid, 326–327
 Uroporphyrinogen III, 77–78
 Urquhardt, Norman, 444
- ## V
- Valine, 38t–39t, 98f
 methyl group of, 64–65

Vanadium, 7, 12, 338f, 340f
 biochemistry of, 337–339
 in biology, 339–340
 Vanadium haloperoxidases, 7
 VDICs. *See* Voltage-dependent ion channels
 Venus fly trap, 72
 VGCC. *See* Voltage-gated calcium channel
 Vibrational spectroscopy, 118t, 125
Vibrio cholera, 138–139
Vibriobactins, 137f
 Viruses, 48
 Vitamin A, 415–416
 Vitamin B₁₂, 93f, 97, 303
 in chelatase, 77–78
 cobalt and, 13
 IAD and, 415–416
 Vitamin B₁₂-dependent isomerases, 303–305
 Vitamin B₁₂-dependent
 methyltransferases, 306–307, 306f
 Vitamin C, 53–54, 97
 Vitamin K, 71–72, 71f
 Voltage-dependent ion channels (VDICs), 385
 Voltage-gated calcium channel (VGCC), 387f
 NMDA and, 387–388
 Voltage-gated calcium-selective channels (CaVs), 217
 Voltage-gated channels, 177, 222

W

Warfarin, 71–72
 Water
 collagen and, 375f
 glucose and, 98
 iron and, 248
 photolysis of, 347–348
 XO and, 326–327
 zinc and, 231f

Water cycle, 344f
 Watson, Jim, 50–52
 Willstätter, Richard, 3
 Wilson's disease, 412–414
 Wingless signal receptor (WntR), 426–427
 WntR. *See* Wingless signal receptor
 Woods-Ljungdahl pathway, 300–301, 301f

X

Xanthine dehydrogenase (XDH), 82, 325, 326f
 Xanthine oxidase (XO), 324–327
 in mammals, 325–326
 Xanthine oxidoreductase, 327f
 XDH. *See* Xanthine dehydrogenase
 Xenopus transcription factor IIIA, 244–245, 245f, 246f
 XO. *See* Xanthine oxidase
 X-ray diffraction, 118t, 128–131, 128f, 129f, 130f

Y

Yeast
 copper in, 150
 iron and, 146
 plasma membrane of, 168
Yersinia, 86–87
Yersinia enterocolytica, 138–139
Yersinia pestis, 138–139
Yersiniabactin, 86–87
 Yttrium, 11

Z

Zinc, 5, 11, 13, 241f
 A β and, 407
 AD and, 406f, 407
 albumin and, 388–389
 alcohol dehydrogenase and, 237
 aldehyde and, 237

ALS and, 409
 in *Arabidopsis thaliana*, 151
 in bacteria, 158
 bacteria and, 144
 in brain, 388–394, 390f
 cadmium and, 438
 carbon dioxide and, 135
 carbonic anhydrase and, 231–232
 carboxylates and, 229
 chelators, 389–390
 cocatalytic enzymes and, 238–244
 in cyanobacteria, 160–161
 in cytosol, 160–161
 deficiency in, 389
 DNA and, 14–15
 E. coli and, 138
 enzymes and, 230–244, 230f, 240f, 243f
 fingers, 244–246, 244f, 246f
 in fungi, 150, 167–170
 GABA and, 388–391, 391f
 glutamate and, 234–237, 390–392
 in mammals, 153, 173–175
 metalloproteinases and, 232–237
 mononuclear enzymes of, 230–238
 MT and, 391f
 multinuclear enzymes and, 238–244
 NADH and, 237
 neurodegeneration and, 395–401
 NMDA and, 388–391
 phosphate and, 229
 in plants, 161–166, 162f, 163f
 plasma membrane and, 168–169
 RNA and, 14–15
 in *Saccharomyces cerevisiae*, 168–169, 169f, 170
 side-chain hydroxyl group of, 64–65
 water and, 231f
 ZIP, 144, 150–151, 150f, 153, 389
 Zirconium, 12
 ZnT3, 389–390
 AD and, 404